D 37787/81

SMITH GJ.

pp

209

OXO-METAL CATALYSED REACTIONS OF UNSATURATED ALCOHOLS

A thesis submitted to the Council for National Academic Awards in partial fulfilment of the requirements for the degree of Doctor of Philosophy.

By

Graham J. Smith

Department of Chemistry

The Polytechnic of North London

March 1981

ACKNOWLEDGEMENTS

I wish to express my sincere thanks to my supervisors, Dr. A.P. Johnson and Dr. P.A. Tasker, for their encouragement and guidance over the past three years.

Thanks are also extended to all those other members of the department who have made my stay an enjoyable one. I would like to thank Miss S.C. Smith for typing this manuscript.

A. C.A.S.E. award from Bush Boake Allen Ltd. is gratefully acknowledged.

Graham Smith

March 1981

OXO-METAL CATALYSED REACTIONS OF UNSATURATED ALCOHOLS

G. J. SMITH

ABSTRACT

The use of oxo-transition metal complexes (particularly molybdenum and vanadium) as catalysts for a number of synthetically important reactions is described.

The ability of alkyl hydroperoxides to epoxidise alkenes in the presence of transition metal catalysts is well known and is reviewed here along with the more conventional methods of preparing epoxides in the laboratory, with particular emphasis on their application in asymmetric epoxidations.

In this work a number of novel oxo-vanadium and oxo-molybdenum complexes containing bulky and/or chiral ligand systems have been prepared and their application as potential catalysts for regio and/or asymmetric epoxidation has been studied.

A synthesis of the oxo-vanadium complex of the known ligand NN′-ethylenebis(iminomethylcamphor) was developed and the complex characterised. The synthesis and structure of oxo-molybdenum complexes containing novel tridentate ligands derived from substituted salicylaldehydes and chiral 2-aminoalcohols are also described along with a D(-)-2,3-butandiol complex of dioxomolybdenum(VI). As in a number of examples recently reported in the literature, epoxidation of geraniol and related compounds in the presence of these catalysts showed regioselectivity with exclusive reaction of the allylic double bond. The latter complex was also found to give low asymmetric induction in epoxidations of geraniol.

In addition to using pre-formed chiral complexes as asymmetric epoxidation catalysts the possibility of using chiral catalysts prepared *in situ* from simple molybdenum complexes and an excess of the chiral ligand has also been studied. Some of these systems appeared to give the highest asymmetric inductions in epoxidations of geraniol.

During the studies of the epoxidation reaction it was found that some of the oxo-vanadium and oxo-molybdenum complexes were very efficient catalysts for the isomerization of allylic alcohols. The scope of rearrangement reactions of this type was examined for ten structurally different allylic alcohols. It was shown that in most cases isomerization leads to an equilibrium mixture and in some cases the position of equilibria differ from that which would be predicted from classical considerations. Several attempts were also made to prepare more reactive isomerization catalysts by synthesising oxo-vanadium complexes with fluorine containing ligands.

The related isomerization of propargylic alcohols to α,β-unsaturated carbonyl compounds in the presence of oxo-vanadium complexes is well known. Attempts have been made here to utilise this isomerization in the synthesis of five and six-membered ring compounds by diverting the normal course of reaction of the proposed intermediate.

CONTENTS

CHAPTER 1

EXISTING METHODS FOR EPOXIDATION OF ALKENES

1.1 Introduction

Ease of preparation and versatile reactivity have made epoxides among the most useful intermediates in organic synthesis. An additional reason for the increasing attention that has been paid to epoxide chemistry in recent years has been the identification of a number of natural products containing the epoxide group and the recognition of its role as an important biosynthetic intermediate[1]. The stereochemical complexity of many natural products makes the asymmetric epoxidation of olefins a highly desirable process[2] but despite the growth of interest in asymmetric reactions[3] little has been achieved by way of asymmetric epoxidation reactions.

In this chapter are discussed some of the more common methods used to prepare epoxides in the laboratory (Section 1.2) and the way in which some of these procedures have been adapted to give asymmetric epoxidation (Section 1.3). In addition,methods of determining the extent of enantiomeric selectivity in asymmetric epoxidation reactions are reviewed, (Section 1.4) and a detailed account of epoxidation by alkyl hydroperoxides in the presence of transition metal catalysts is given (Section 1.5).

1.2 Common Methods of Epoxidation

The most common methods of preparing epoxides in the laboratory are by oxidation of alkenes with peroxyacids

CHAPTER 1

EXISTING METHODS FOR EPOXIDATION OF ALKENES

1.1 Introduction

Ease of preparation and versatile reactivity have made epoxides among the most useful intermediates in organic synthesis. An additional reason for the increasing attention that has been paid to epoxide chemistry in recent years has been the identification of a number of natural products containing the epoxide group and the recognition of its role as an important biosynthetic intermediate[1]. The stereochemical complexity of many natural products makes the asymmetric epoxidation of olefins a highly desirable process[2] but despite the growth of interest in asymmetric reactions[3] little has been achieved by way of asymmetric epoxidation reactions.

In this chapter are discussed some of the more common methods used to prepare epoxides in the laboratory (Section 1.2) and the way in which some of these procedures have been adapted to give asymmetric epoxidation (Section 1.3). In addition,methods of determining the extent of enantiomeric selectivity in asymmetric epoxidation reactions are reviewed, (Section 1.4) and a detailed account of epoxidation by alkyl hydroperoxides in the presence of transition metal catalysts is given (Section 1.5).

1.2 Common Methods of Epoxidation

The most common methods of preparing epoxides in the laboratory are by oxidation of alkenes with peroxyacids

(Scheme 1.1, reaction 1) and by dehydrohalogenation of halohydrins (Scheme 1.1, reaction 2). Newer methods have also been developed[4], such as the reaction of carbonyl compounds with sulphur ylids (Scheme 1.1, reaction 3), and these have greatly increased the accessibility of epoxides.

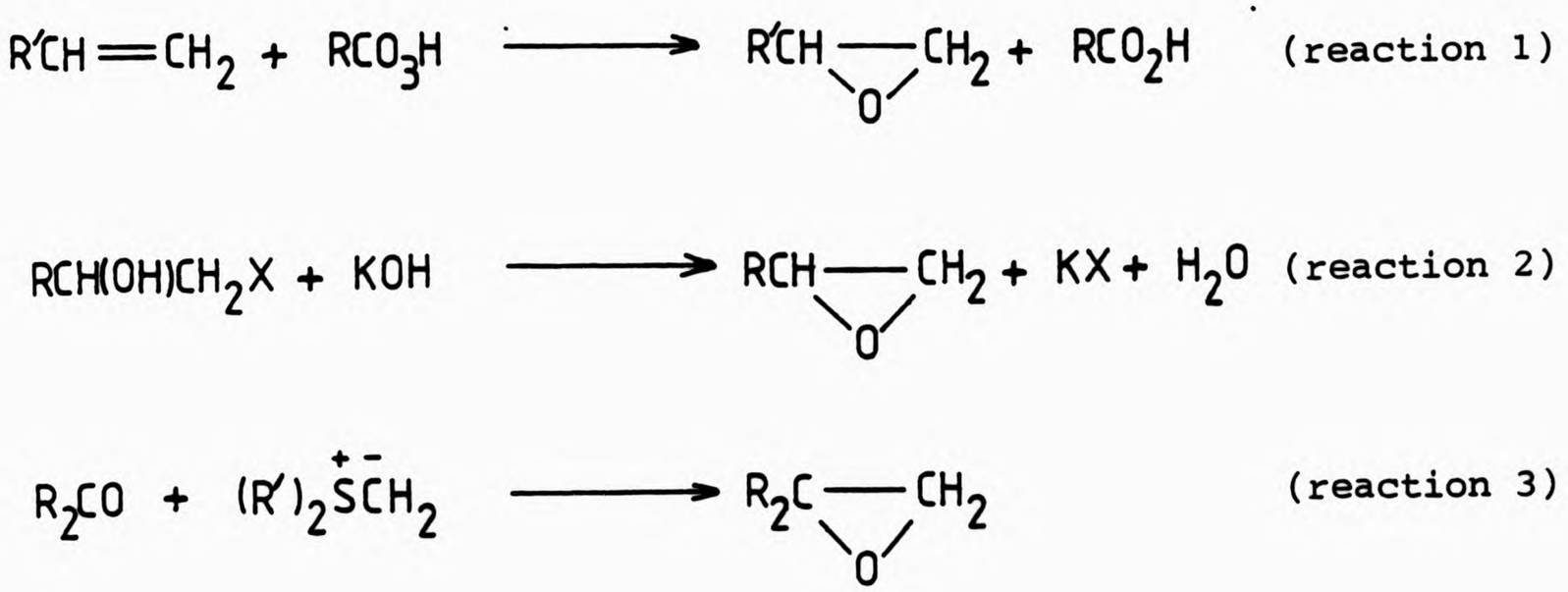

Scheme 1.1

Epoxidation with peroxyacids is usually considered to proceed via an electrophilic attack on the double bond as indicated below (Scheme 1.2).

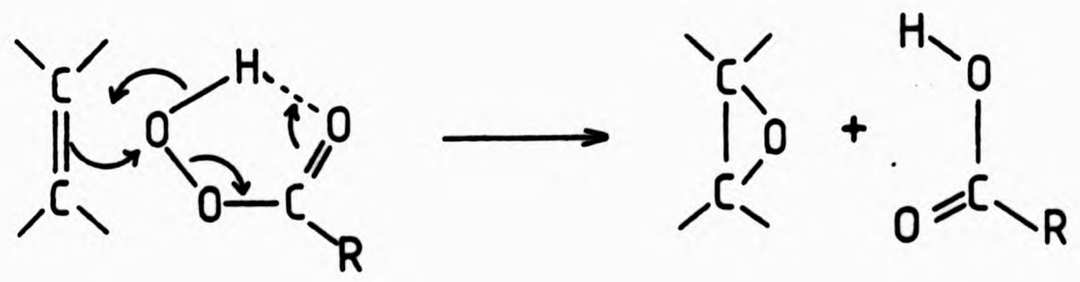

Scheme 1.2

In support of this mechanism it is found that the rate of epoxidation is increased by electron-withdrawing groups in the peracid[5] or electron-donating substituents on the double bond[6,7]. According to the above mechanism the

peroxy oxygen acts as both the electrophile and nucleophile. It therefore differs from other reactions of this type, e.g bromination, in which the initial electrophilic addition is followed by attack of a separate nucleophile. It is also found that the peracid usually attacks the olefin from the less hindered side producing the less hindered epoxide as the major product, although this stereospecificity may be influenced by changes in solvent. In addition, epoxidation is syn-stereospecific, cis-olefins giving cis epoxides and trans-olefins, trans epoxides. To account for this stereospecificity Bartlett[8] proposed the formation of a cyclic transition state (1.1).

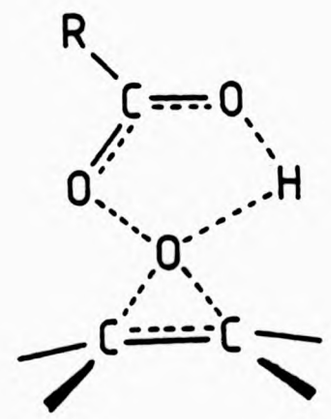

(1.1)

Dehydrohalogenation of halohydrins involves the formation of an alkoxide ion, by treatment of the halohydrin with base, resulting in elimination of the halide ion (Scheme 1.3).

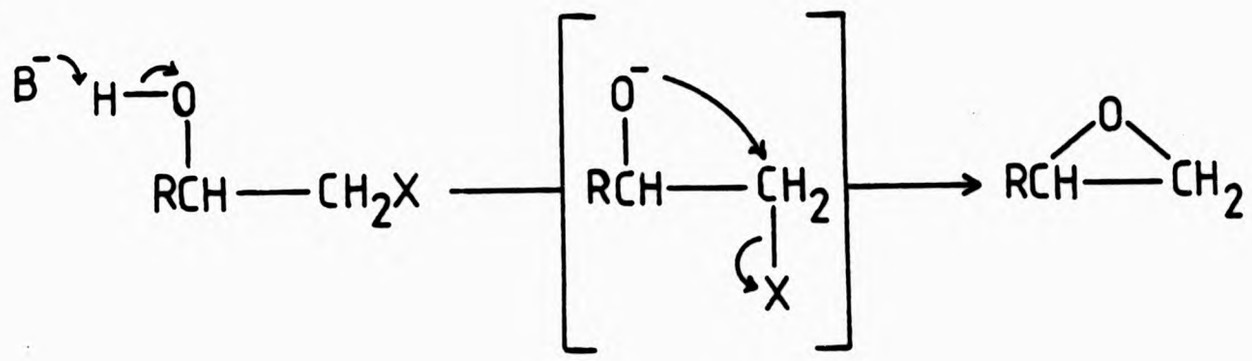

Scheme 1.3

1.3 Asymmetric Epoxidation

When achiral reactants are used in normal chemical synthesis the products are obtained only in racemic form. Although racemic mixtures may sometimes be conveniently separated most separation methods are relatively difficult, requiring large amounts of optically active reagents in relation to the yield of optically active product obtained. It is therefore desirable to prepare optically active compounds more directly with the aid of optically active reagents.

According to modern transition state theory asymmetric induction by an optically active reagent results from formation of diastereoisomeric transition states which react at different rates giving unequal amounts of enantiomeric products.

The success of an asymmetric synthesis is measured in terms of the percent enantiomeric excess (% ee), which is the extent to which one enantiomer is produced over the other.

$$\text{Percent enantiomeric excess} = \frac{[R] - [S]}{[R] + [S]} \times 100$$

Until fairly recently attempts to prepare optically active epoxides could be separated into two types : (a) Asymmetric epoxidation of achiral substrates using chiral epoxidising agents (Section 1.3.1) and (b) Asymmetric epoxidations achieved with achiral reagents under the control of a chiral centre in the substrate (Section 1.3.2). These are discussed in the following sections along with some other methods of obtaining chiral epoxides that have appeared in the literature recently. (Section 1.3.3).

1.3.1 Use of Chiral Reagents

(i) Epoxidising agents

The most common chiral reagent studied is (+)-monoperoxycamphoric acid but other peroxy-acids such as (S)-(+)-peroxyhydratropic acid or (S)-(-)-peroxy-endo-norbornane-2-carboxylic acid have also been used[9]. Epoxidation of achiral alkenes with one of these reagents gives optically active epoxides in yields which are low and solvent dependent. The asymmetric epoxidation of styrene with (+)-monoperoxycamphoric acid has been studied in various solvents[10] and it was found that the maximum optical yield was obtained in chloroform which gave only 4.4% enantiomeric excess of the S-(-)-form. The solvent dependency has been attributed to preferential solvation of one of the competing transition states. The best optical yield obtained so far by this method appears to be a 10% enantiomeric excess achieved when 1,2-dihydronaphthalene was epoxidised with percamphoric acid[11].

Pirkle and Rinaldi have recently[12] re-evaluated the use of peroxycamphoric acid in asymmetric oxidations and have shown that under normal conditions of preparation, the peroxy-acid contains two isomers (1.2) and (1.3) which give opposite stereochemistry in asymmetric synthesis. When one of the isomers (1.2) was obtained in a pure, crystalline form and then used, optical yields were obtained which were 50-100% greater than previously reported.

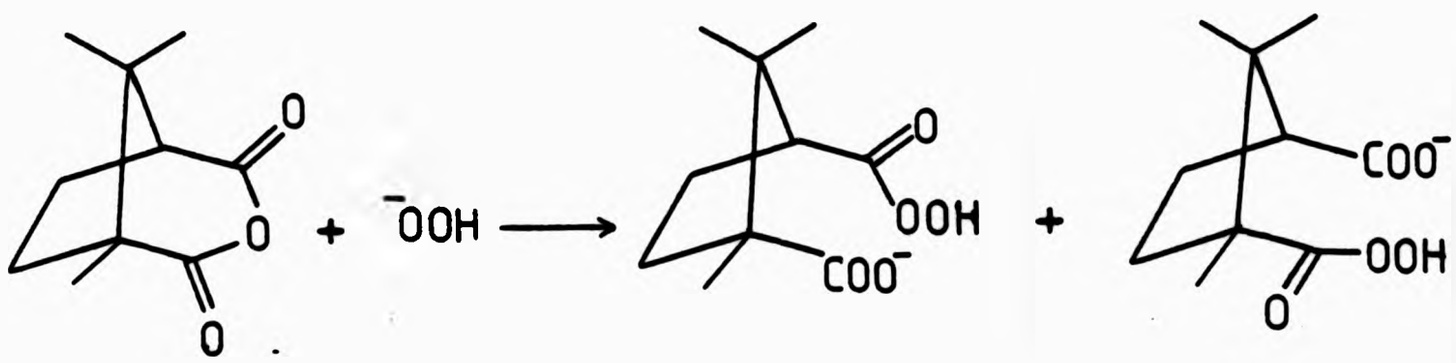

(1.2) (1.3)

Factors governing asymmetric induction in these oxidations are usually interpreted in terms of the effects of small (S), medium (M) and large (L) groups bonded to the asymmetric carbon of the peroxy-acid[13]. The transition state is represented in such a way that the bulkier alkene-bonded group faces the least hindered region of the peroxy-acid, between groups S and M and near S, while the less bulky group faces the medium hindered region, between groups S and L (Scheme 1.4).

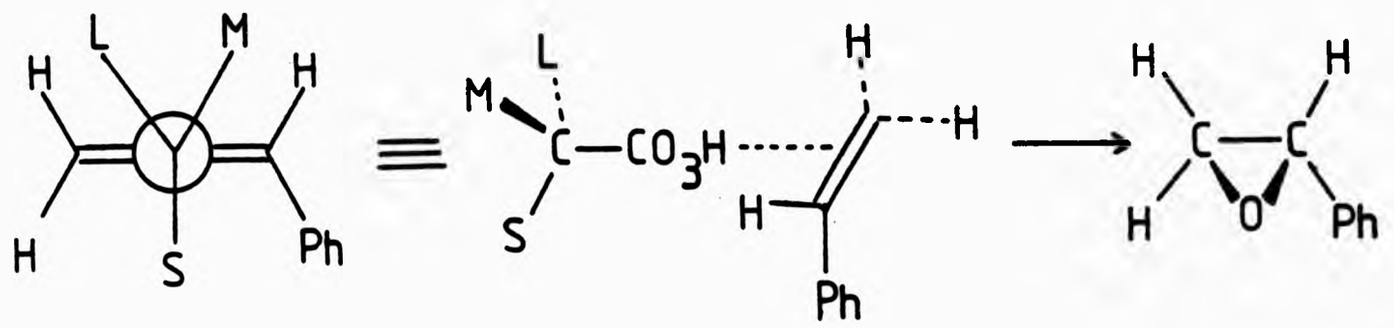

Scheme 1.4

Such a model is valid only when solvation effects and electrostatic interactions can be discounted. In addition asymmetric induction need not necessarily arise from direct steric interactions, indeed it is possible that induction is transmitted through a solvent shell[10].

(ii) Via halohydrins

A procedure for the synthesis of chiral epoxides from racemic halohydrins by 1,2-dehydrohalogenation promoted by alkaloids has been reported recently[14] (Scheme 1.5). Reaction of racemic halohydrins with insufficient (-)-quinine gave the corresponding epoxides (1.4) with an enantiomeric excess in the range 12-35%. The recovered halohydrins were found to be enriched in the less reactive optical isomer and could be converted to epoxides of opposite configuration (1.5) by treatment with an achiral base.

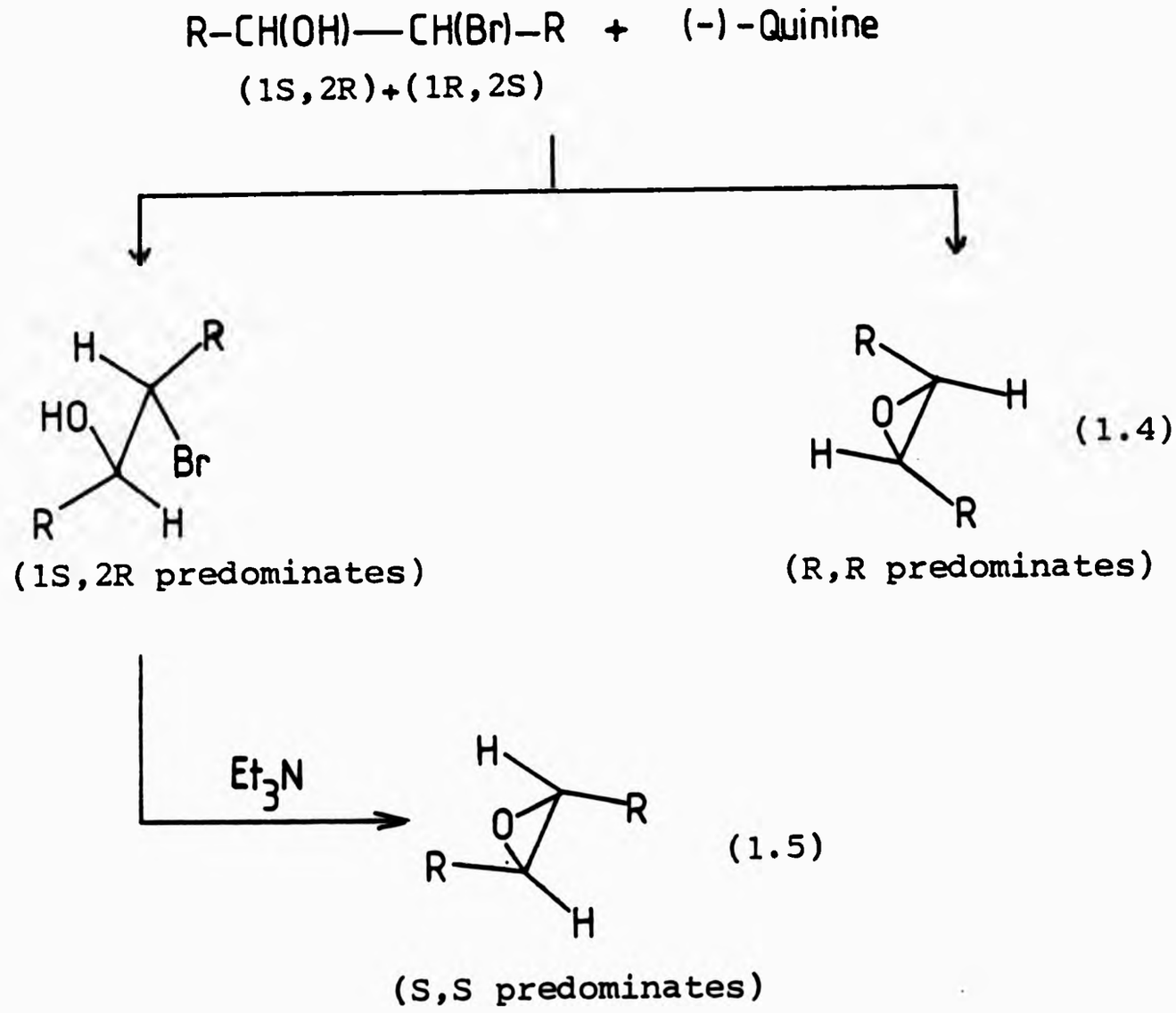

Scheme 1.5

1.3.2 Use of chiral substrate

Asymmetric epoxidation can be achieved with achiral reagents if the substrate contains a chiral centre. An example of this is the epoxidation of optically active linalol with monoperphthalic acid. Following epoxidation, hydrogenation and iodine-catalysed dehydration produces an optically active epoxy product in which the original chiral centre has been removed[15] and a new one generated (Scheme 1.6).

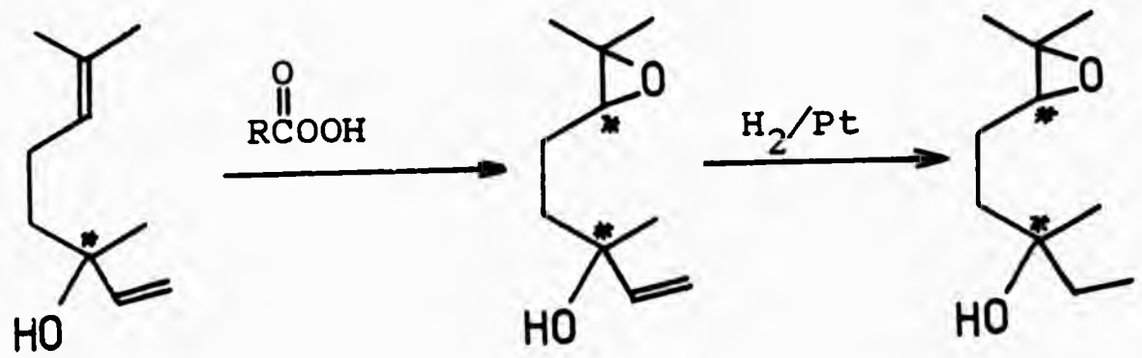

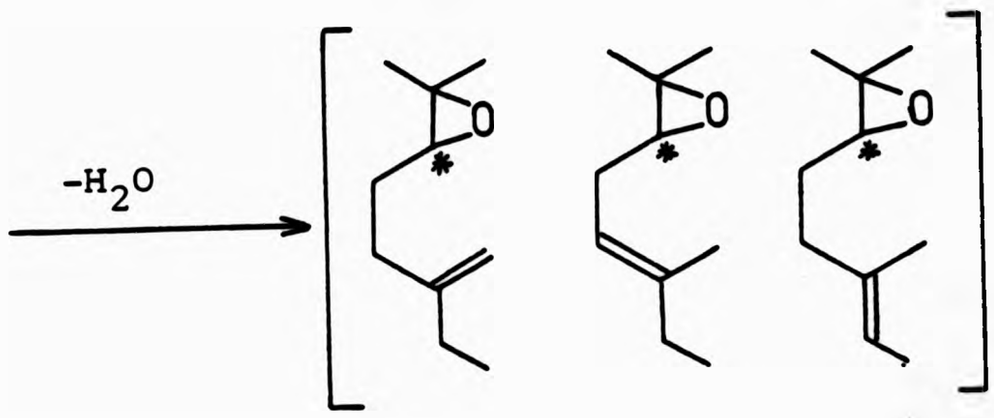

Scheme 1.6

Partial asymmetric synthesis has been achieved when (-)-menthyl alkylidenecyanoacetate was epoxidised with hydrogen peroxide in the presence of base, followed by hydrolysis of the diastereomeric epoxycyanoesters to the epoxy acid[16]. The reaction is thought to involve the Michael addition of a hydroperoxy anion with displacement of hydroxide to form the epoxide (Scheme 1.7).

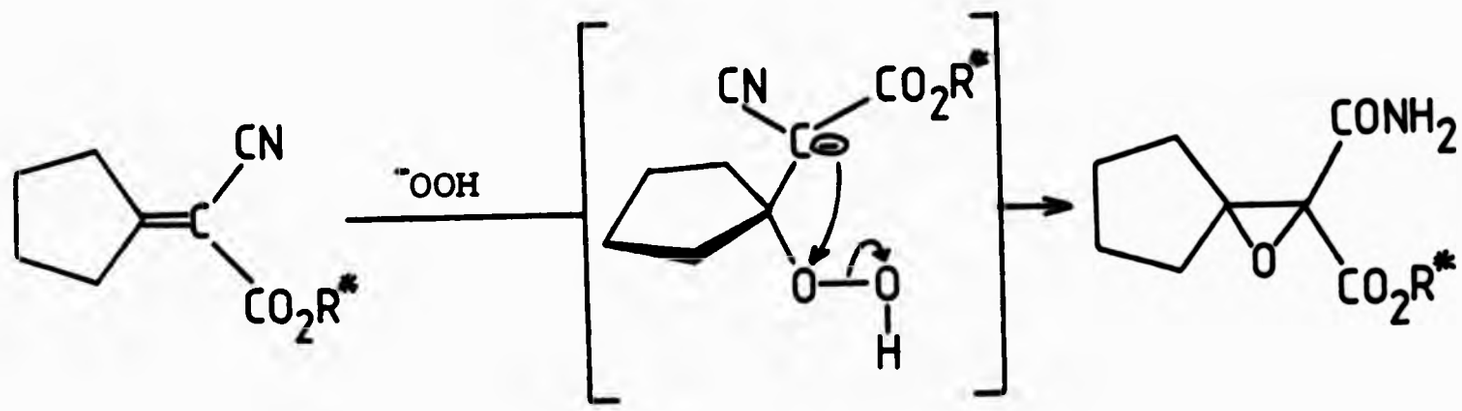

R^*= (-)-menthyl

Scheme 1.7

1.3.3 Other methods

(i) Phase transfer reagents

In the last decade a great deal of attention has been devoted to the study of the phase transfer catalytic properties of quaternary ammonium compounds in two-phase systems[17] and such systems have already been applied to several asymmetric syntheses[18]. Recently, the base-catalysed hydrogen peroxide or t-butyl hydroperoxide asymmetric epoxidation of α,β-unsaturated ketones using quaternary ammonium salts of alkaloids as chiral phase transfer catalysts has been reported[19] (Scheme 1.8). Chemical yields are high (99%) and in one case the enantiomeric excess amounted to 25%.

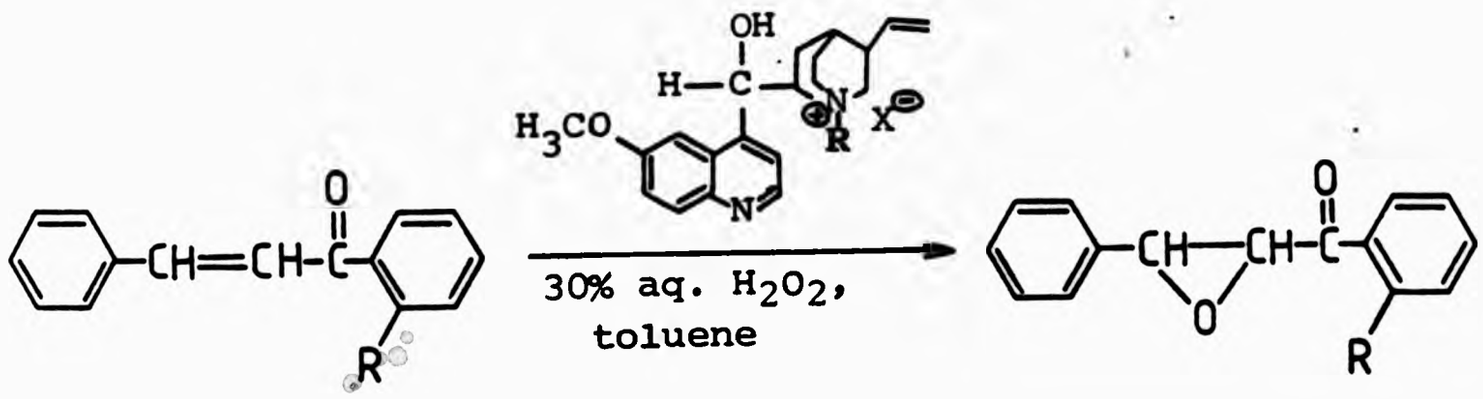

Scheme 1.8

The use of chiral phase-transfer catalysts has been extended to the synthesis of chiral epoxides by other routes[20] (Scheme 1.9):

(a) The epoxidation of α,β-unsaturated ketones by sodium hypochlorite.

(b) The Darzen condensation of chloroketones and aromatic aldehydes.

(c) The dehydrohalogenation of racemic halohydrins.

(d) The addition of cyanide to α-haloketones and α-ketotosylates.

All reactions were conducted under phase-transfer conditions using quininium benzylchloride as catalyst.

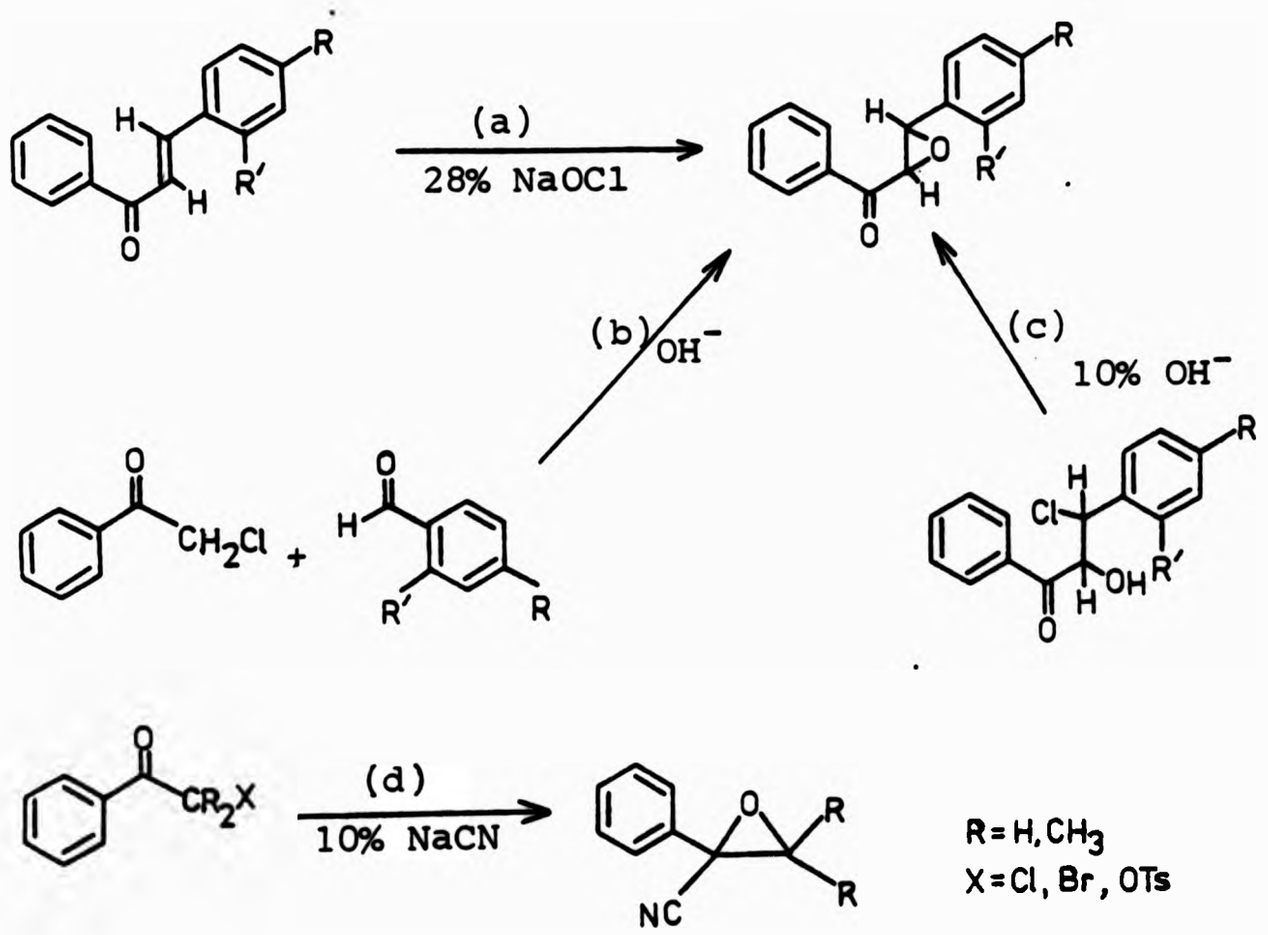

Scheme 1.9

Only (a) gave an enantiomeric excess comparable to that described previously (25% ee), the extent of asymmetric induction in the other methods being much lower (6-8% ee).

(ii) Biological oxidation

The ability of micro-organisms to carry out chemical transformations stereoselectively has been utilised recently in the synthesis of epoxides of long-chain terminal olefins.

(R)-(+)-1,2-epoxyhexadecane was obtained by microbial oxidation of hexadec-1-ene[21]. Although chemical yields were not high (40%) the optical purity of the epoxide was 100%. (R)-(+)-7,8-epoxyoct-1-ene has also been obtained by a similar procedure but with somewhat lower stereospecificity[22].

1.4 Determination of Enantiomeric Composition of Chiral Oxiranes

Reviewed here are physical methods which allow direct determination of the enantiomeric composition of an oxirane mixture. Methods involving chemical conversion of the oxirane to diastereo-isomers prior to separation are not discussed.

If the specific rotation of the pure enantiomer is known, the enantiomeric composition can be determined polarimetrically by determining the optical purity of the mixture. Optical purity is determined by dividing the observed rotation of the mixture, $[\alpha]_{obs}$, by the rotation of the pure enantiomer, $[\alpha]_{max}$, measured under identical conditions.

$$\text{Percent optical purity} = \frac{[\alpha]_{obs}}{[\alpha]_{max}} \times 100$$

Assuming a linear relationship between rotation and composition, the percent optical purity can be equated with percent excess of one enantiomer over the other, % ee (Section 1.3).

A disadvantage of this method is that the presence of impurities in the sample leads to erroneous results,

therefore, a high degree of sample purity is required.

Another widely used method for determining enantiomeric purity involves the use of optically active lanthanide shift reagents (LSR's) in ^{1}H-nmr spectroscopy[23]. Tris(3-(hepta-fluoro-propylhydroxymethylene)-d-camphorato)europium(III)[24] (1.6) and tris(3-(trifluoromethylhydroxymethylene)-d-camphorato)europium(III)[25] (1.7) have been used to distinguish resonances of a number of enantiomorphs.

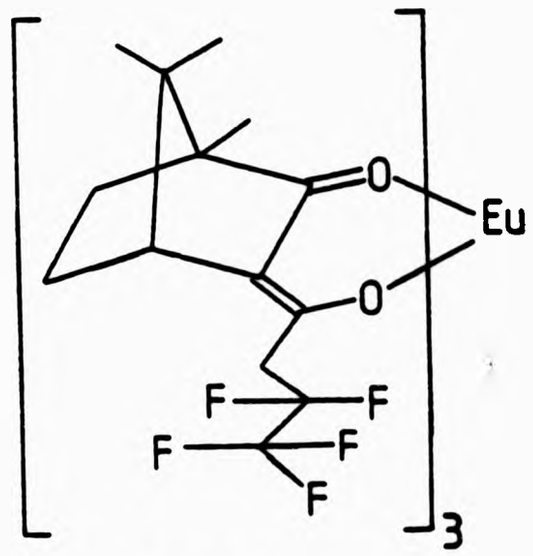

(1.6)

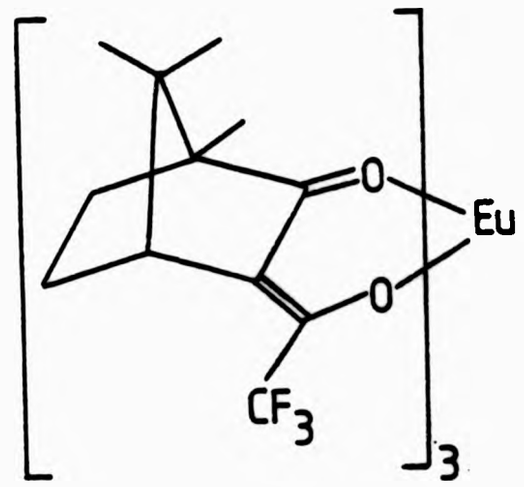

(1.7)

These LSR's are assumed to distinguish between enantiomorphs by forming diastereoisomeric complexes which have either different stability constants[23] or a different magnetic environment[25].

Unlike polarimetric methods this technique is not affected by the presence of impurities in the sample.

There have recently been some developments in the use of gas-liquid chromatography as a technique for determining the enantiomeric composition of oxiranes by incorporating an enantioselective material into the stationary phase. Golding et al have described the separation of R- and S-epoxypropane and 1,2-epoxybutane by glc in which the lanthanoid complex

therefore, a high degree of sample purity is required.

Another widely used method for determining enantiomeric purity involves the use of optically active lanthanide shift reagents (LSR's) in ^{1}H-nmr spectroscopy[23]. Tris(3-(hepta-fluoro-propylhydroxymethylene)-d-camphorato)europium(III)[24] (1.6) and tris(3-(trifluoromethylhydroxymethylene)-d-camphorato)europium(III)[25] (1.7) have been used to distinguish resonances of a number of enantiomorphs.

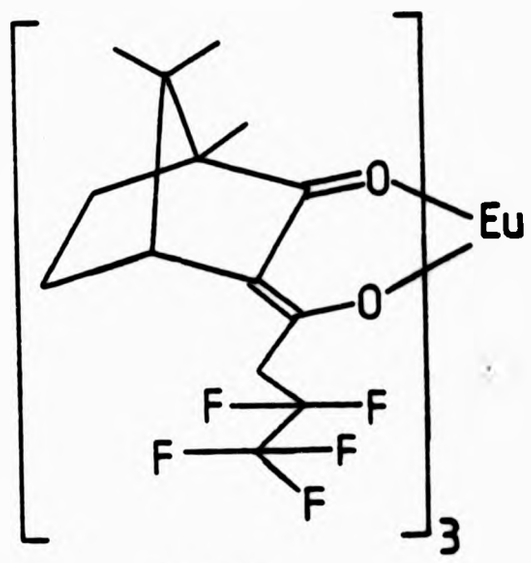

(1.6)

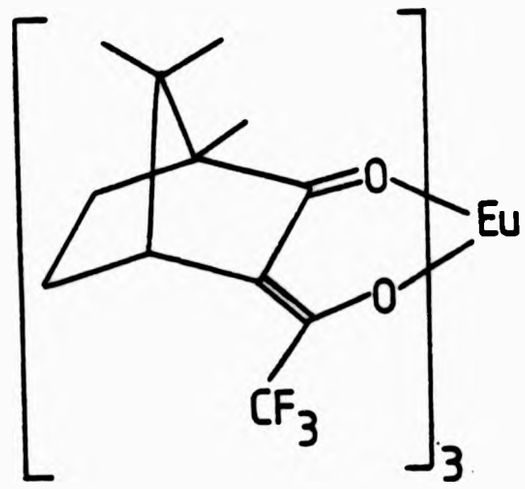

(1.7)

These LSR's are assumed to distinguish between enantiomorphs by forming diastereoisomeric complexes which have either different stability constants[23] or a different magnetic environment[25].

Unlike polarimetric methods this technique is not affected by the presence of impurities in the sample.

There have recently been some developments in the use of gas-liquid chromatography as a technique for determining the enantiomeric composition of oxiranes by incorporating an enantioselective material into the stationary phase. Golding et al have described the separation of R- and S-epoxypropane and 1,2-epoxybutane by glc in which the lanthanoid complex

(1.7), was present in the stationary phase[26].

The enantiomeric composition of oxiranes has also been determined by complexation gas-chromatography on bis(3-(heptafluoropropyl-hydroxymethylene)-d-camphorato)-nickel(II)[27]. However the use of these glc techniques at present appears to be restricted to simple, low molecular weight oxiranes.

1.5 Metal Catalysed Epoxidation of Alkenes by Alkyl Hydroperoxides

The epoxidation of olefins by alkyl hydroperoxides in the presence of transition metal catalysts is well known and has been extensively reported in the patent literature[28]. The most widely used catalysts are compounds of vanadium, molybdenum and tungsten (Scheme 1.10).

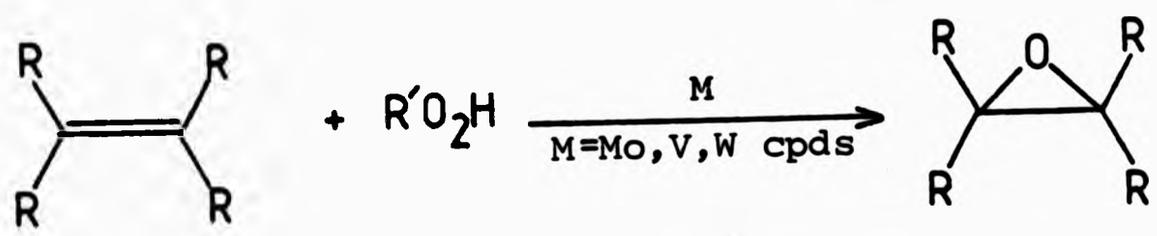

Scheme 1.10

Studies on the mechanism of this reaction are reviewed in Section 1.5.1 while the effect of the nature of the catalyst is discussed in Section 1.5.2. The high stereo- and regio- selectivity of these epoxidation systems is discussed in Section 1.5.3.

1.5.1 Mechanism

The use of oxides of vanadium and chromium to catalyse the oxidation of olefins to diols by hydrogen peroxide was first discovered in 1937[29]. During the investigation of this reaction it was found that the hydroxylation was stereospecific in that trans diols were obtained exclusively. The reaction was believed to involve formation of metal hydroperoxides (known to occur on treatment of the metal with hydrogen peroxide) and the stereospecificity of the reaction was accounted for by postulating intermediate epoxide formation. Failure to isolate an epoxide intermediate was attributed to its high reactivity under the reaction conditions. It was later found that epoxides of various unsaturated compounds could in fact be isolated under favourable conditions (usually involving pH control) using oxides of vanadium, molybdenum and tungsten as oxidation catalysts[30].

Epoxidation of allylic alcohols was found to be particularly successful but epoxidation of simple olefins gave relatively poor yields. These observations led Payne and Williams to suggest the possible formation of an intermediate involving coordination of the allyl alcohol to the metal hydroperoxide[31].

In the first reported epoxidation using an alkyl hydroperoxide in the presence of vanadium pentoxide as catalyst, Hawkins successfully obtained the epoxides of cyclohexene and oct-1-ene but only in poor yield[32].

During investigations into the decomposition of t-butyl hydroperoxide in the presence of olefins,

Indicator and Brill added catalytic amounts of acetylacetonates of vanadium, chromium and molybdenum to the reaction mixture and obtained the epoxides of oct-1-ene and 2,4,4-trimethylpent-1-ene in high yield[33]. In addition they noted that the reaction was stereospecific in that trans alkenes gave trans epoxides and cis alkenes gave cis epoxides and that greater yields of epoxide were obtained for the more highly substituted alkenes. Several possible mechanism were suggested, all of which involve formation of a hydroperoxide-metal complex.

Gould et al[34] carried out a more detailed kinetic study of the epoxidation of cyclohexene catalysed by vanadyl acetylacetonate and although they obtained a rate equation in which the dependency of hydroperoxide and catalyst was different to that established by Indicator and Brill, it was nevertheless consistent with the formation of a hydroperoxide-metal chelate complex.

Gould observed that on addition of hydroperoxide to complexes of vanadium in benzene and cyclohexane solutions, there occured formation of a strongly absorbing red transient species which faded rapidly[35]. Attempts to study the kinetics of formation of these coloured intermediates were unsuccessful but it was possible to establish that the rate of fading was nearly zero order in vanadium and approximately half-order in hydroperoxide. Gould has suggested that the formation of these red intermediates corresponds to the formation of a vanadium(IV)-hydroperoxide complex. Peroxyvanadium complexes of this type have been shown by, esr studies, to be present in ethanolic solutions of vanadyl acetylacetonate treated with t-butyl hydroperoxide[36].

According to Gould the fading of the red species is probably associated with the oxidation of vanadium(IV) to vanadium(V). Oxidation state changes of vanadium from (IV) to (V) can be determined by esr spectrometry, since the signal arising from the d^1 configuration of V(IV) will disappear as the diamagnetic V(V) is produced. Esr studies have been made previously on the oxidation of vanadyl species by hydrogen peroxide in aqueous media and the following steps involving a intermediate $OVOO^{2+}$ radical were proposed[37].

$$VO^{2+} + H_2O_2 \rightleftharpoons OVOOH^+ + H^+$$

$$\longrightarrow [OVOOH^+] \longrightarrow VO_2^+ + \cdot OH \qquad \text{(slow)}$$

The half-order dependency on hydroperoxide found by Gould for the fading of the red intermediate would support a similar oxidation step operating in this reaction. This has recently been investigated further with esr studies carried out on both the red intermediate and the faded yellow solution[38]. No evidence was obtained for any free-radical species in the red intermediate and only a signal arising from a vanadium(IV) species could be observed. However similar studies on the yellow solution indicate that this species is diamagnetic and therefore support the proposal for a rapid and irreversible formation of vanadium(V) as the catalytic species. The proposed mechanism is shown below (Scheme 1.11).

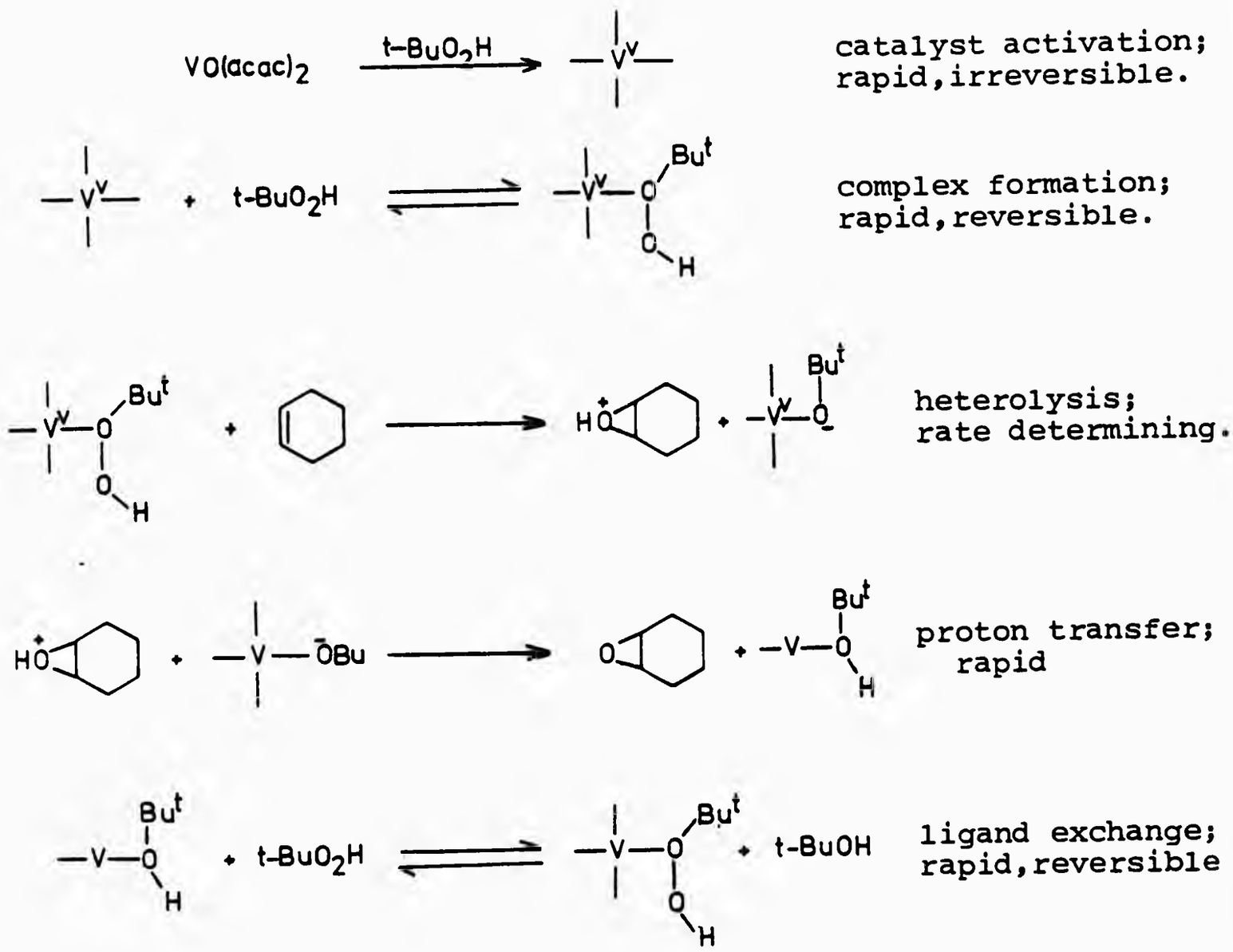

Scheme 1.11

The discovery[39a] that molybdenum(VI) peroxo compounds such as (1.8) stoichiometrically epoxidise olefins under anhydrous conditions in organic solvents, led several groups of workers[39] to suggest that the active oxidants in the catalytic system might also be peroxo species generated <u>in situ</u> by reaction of the alkyl hydroperoxide with a metal oxo compound (Scheme 1.12). Indeed there are reports that molybdenum compounds react with alkyl hydroperoxides to give peroxo complexes, albeit under fairly drastic conditions.

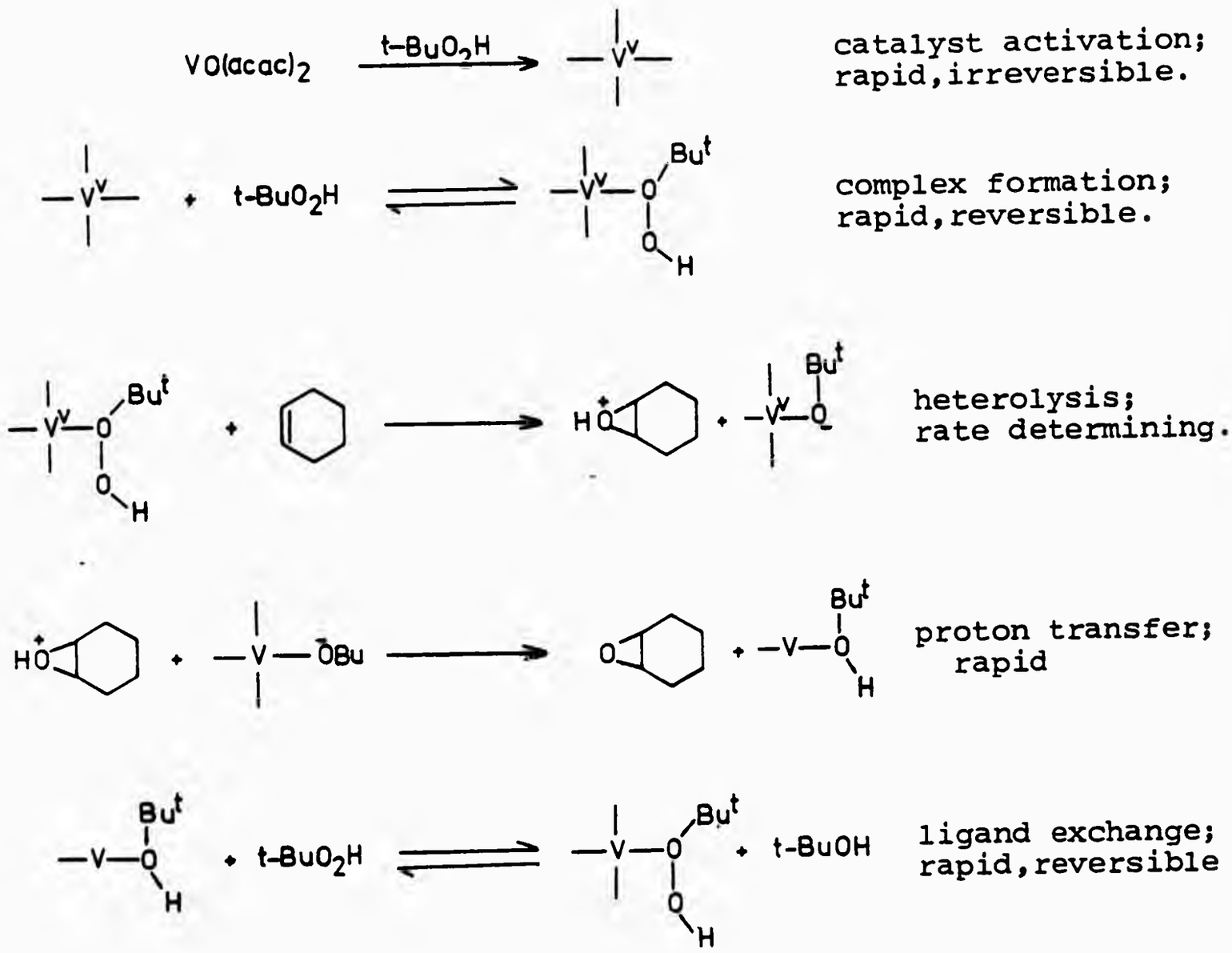

Scheme 1.11

The discovery[39a] that molybdenum(VI) peroxo compounds such as (1.8) stoichiometrically epoxidise olefins under anhydrous conditions in organic solvents, led several groups of workers[39] to suggest that the active oxidants in the catalytic system might also be peroxo species generated in situ by reaction of the alkyl hydroperoxide with a metal oxo compound (Scheme 1.12). Indeed there are reports that molybdenum compounds react with alkyl hydroperoxides to give peroxo complexes, albeit under fairly drastic conditions.

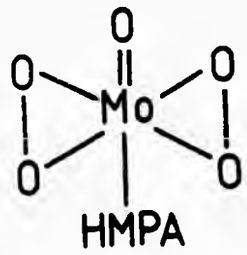

(1.8)

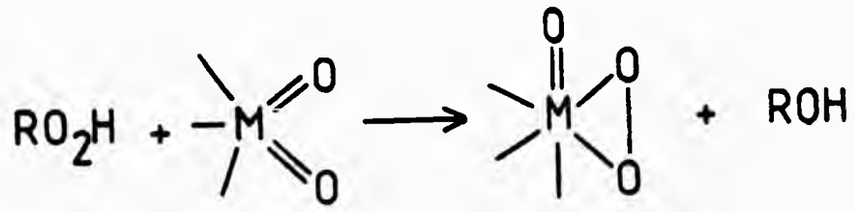

Scheme 1.12

Sheldon has studied the epoxidation of cyclohexene and oct-1-ene by t-butyl hydroperoxide when catalysed by molybdenum(V) and molybdenum(VI) species[40]. Kinetic studies with various molybdenum catalysts indicate that after an initial period, the rate of epoxidation becomes independent of the structure of the molybdenum catalyst used. It was therefore suggested that during the early stages of the reaction the catalyst is modified to the same structure in all cases. Further studies have been carried out to determine the nature of the common species formed during the course of the epoxidation[40a,41]. The resulting catalyst was isolated and found to be a Mo(VI)-1,2-diol complex (1.9).

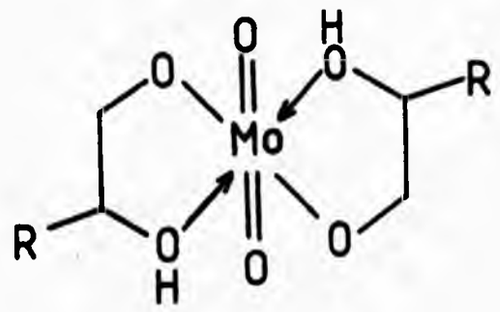

(1.9)

It was suggested that such a complex could be formed if the hydroperoxide was to act as an acid catalyst for the ring opening of the epoxide (Scheme 1.13).

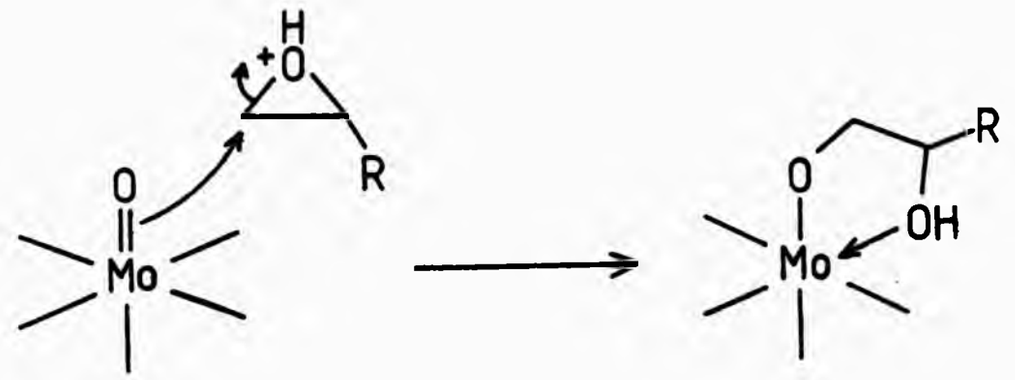

Scheme 1.13

The mechanism favoured by Sheldon for the molybdenum catalysed reaction is similar to that put forward by Gould for that of vanadium. In this case however the proposed catalytic species is a molybdenum(VI)-hydroperoxide complex (Scheme 1.14).

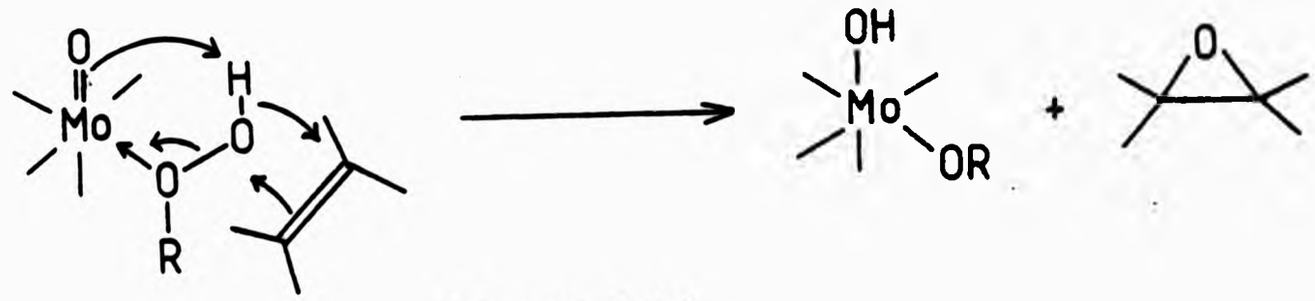

Scheme 1.14

It should be noted here that there are no reports of vanadium compounds degrading to a common species. Indeed although only small differences in reaction rate were observed for a number of vanadium catalysts it has been suggested that the sizable differences in stability constants and activation parameters for the resulting hydroperoxide complexes arise from the catalysts retaining at least in part some of their ligand environment[35].

Gould[35] has carried out kinetic studies using bis(acetylacetonato)dioxomolybdenum(VI) ($MoO_2(acac)_2$) as catalyst and found that the kinetics governing the behaviour of this system are more complicated than for the corresponding vanadium compounds. Although kinetic data point to the existence of a ternary, hydroperoxide-metal-olefin complex, and to a transition state having this composition, epoxidation need not necessarily proceed via such a complex, as a sequence involving reaction of hydroperoxide with a metal-olefin complex or reaction of olefin with a metal-hydroperoxide complex would give similar data. However, the marked resemblance of the $MoO_2(acac)_2$-catalysed epoxidation, not only to epoxidations catalysed by vanadium complexes,but also to those using Mo^{VI}-peroxycomplexes as epoxidising agents,led Gould to favour a mechanism featuring attack by olefin on metal-bound hydroperoxide with formation of a three membered ring in the transition state. (Scheme 1.15).

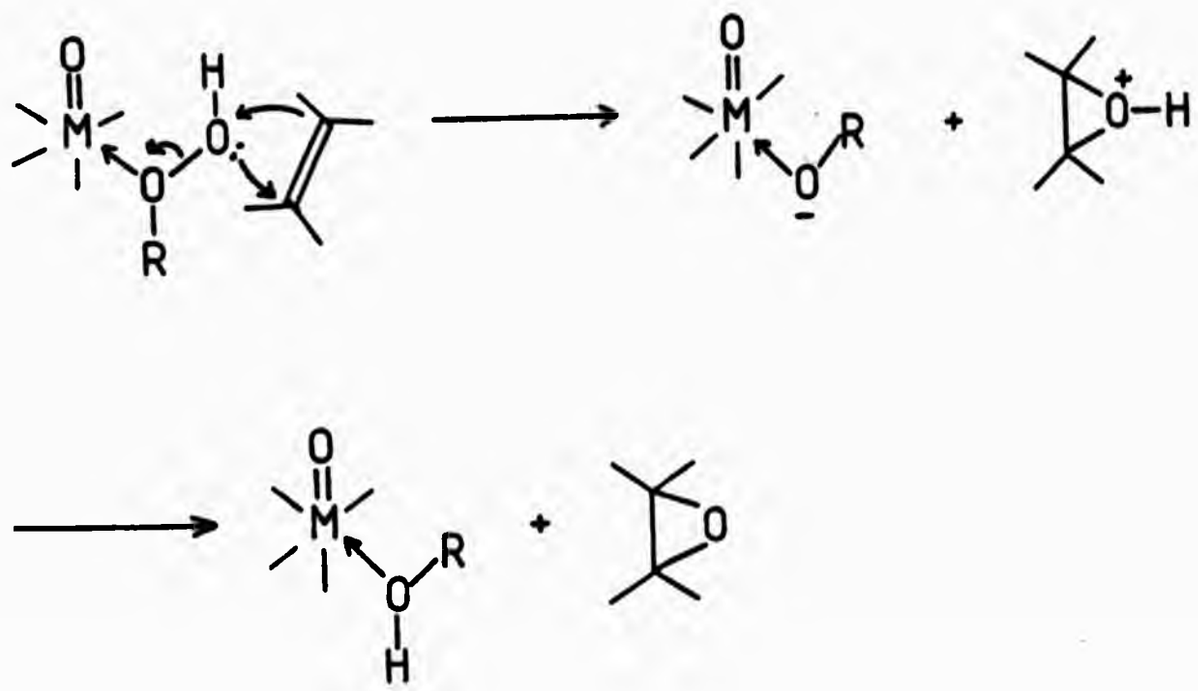

Scheme 1.15

Several groups of workers have recently tried to determine whether the reaction proceeds via a molybdenum-peroxy complex or via an active molybdenum-hydroperoxide complex (as advanced mainly on the basis of kinetic data) by studying the nature of the reaction intermediates more directly.

The epoxidation of cyclohexene by t-butyl and cumyl hydroperoxide in the presence of bis(8-hydroxyquinolinato)-dioxomolybdenum(VI) ($MoO_2(oxine)_2$) has been studied by Trifiro *et al*[42]. In addition to kinetic studies they have observed changes in the electronic spectrum of the catalyst in the presence of reagent and substrate. Addition of hydroperoxide to the catalyst was found to modify the spectrum of the catalyst which reverted back to its original form on addition of the olefin. It was concluded that this change in the electronic spectrum corresponded to formation of the active epoxiding species. Further information about the nature of this species in solution was obtained by evaporating these solutions to dryness. The solid obtained gave an infrared spectrum like that of $MoO_2(oxine)_2$ with no new bonds characteristic of a peroxy group. On the basis of the reversibility of this interaction and the fact that changes in the electronic spectrum were different for the different hydroperoxides, the presence of peroxy groups in the intermediate were excluded and Trifiro concluded the most likely explanation to be formation of a reversible catalyst-hydroperoxide complex.

The above workers have also studied the epoxidation in the presence of other molybdenum catalysts and found that complexes with strongly basic ligands (mostly amines) show no catalytic activity whereas for complexes with ligands that are not strongly bound (such as acetylacetone) epoxidation is accompanied by hydroperoxide decomposition. On the basis of this and spectroscopic evidence these workers have speculated that the active species results from opening of a metal-ligand bond by hydroperoxide and that for epoxidation catalysts to be both active and selective they must have intermediate metal-ligand bond strength.

Sharpless[43] has recently carried out epoxidations catalysed by ^{18}O-labelled oxo-vanadium and oxo-molybdenum complexes. If epoxidation were to proceed via a peroxo-metal intermediate, Sharpless suggests that this would result in incorporation of ^{18}O-label into the epoxide (Scheme 1.16). As no ^{18}O-incorporation occured it was concluded that epoxidation must proceed by a mechanism involving an intact alkyl hydroperoxide.

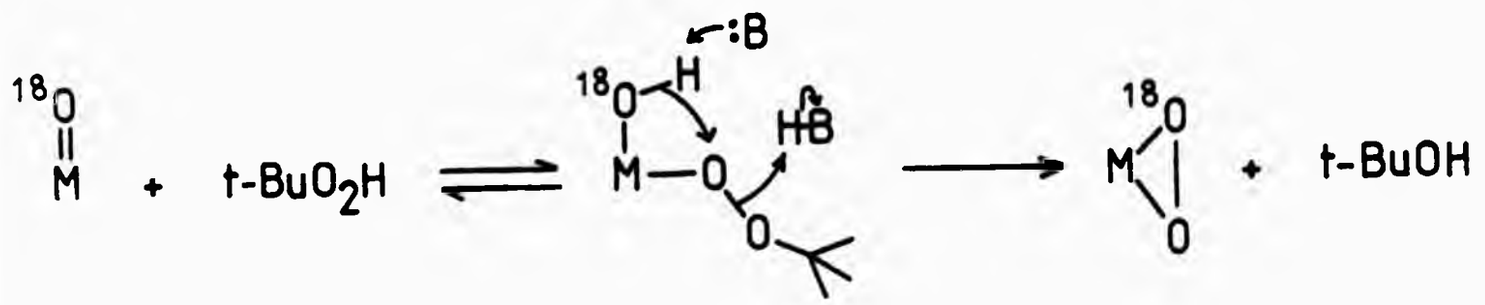

Scheme 1.16

As shown above previous workers have proposed that activation of the hydroperoxide is accomplished by coordination to the metal of the oxygen proximal to the

alkyl group, thereby polarising the O-O bond in the hydroperoxide and facilitating its heterolysis under the action of a nucleophile. According to Sharpless this mechanism does not account for the exceptional reactivity of allylic alcohols as it is apparently geometrically impossible for the double bond of an allylic alcohol to approach the hydroperoxide as suggested and at the same time coordinate to the metal via the hydroxy group. These workers therefore favour coordination of the oxygen distal from the alkyl group as in this case the double bond of the coordinated allylic alcohol would be ideally positioned for oxygen transfer from the oxidant by either routes (1.10) or (1.11).

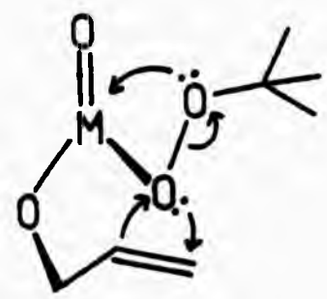

(1.10)

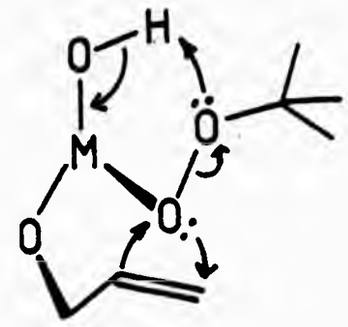

(1.11)

In summarising the above results it can be seen that a metal-hydroperoxide complex is generally accepted to be the catalytic species in solution but the structure and behaviour of such a species remains a matter for spectulation. Little appears to be known about the role or behaviour of the ligand in these reactions except that in the case of molybdenum catalysed epoxidations, complexes having 'weak' ligands are degraded to diol complexes.

1.5.2 Nature of the metal

Transition metal catalysts for peroxide reactions are considered to be of two types. First, metals such as iron and cobalt which have two comparably accessible oxidation states differing by a single unit. These tend to promote homolytic cleavage of the peroxy linkage with subsequent reaction of the free radicals with the hydroperoxide, solvent and/or olefin.

$$M^{n+} + t\text{-}BuO_2H \longrightarrow M^{(n-1)+} + t\text{-}BuO_2\cdot + H^+$$

$$M^{(n-1)+} + t\text{-}BuO_2H \longrightarrow M^{n+} + t\text{-}BuO\cdot + OH^-$$

Second, metals in high oxidation states e.g. Mo(VI), V(V) and Ti(IV) which tend to promote heterolytic cleavage of the 0-0 bond. It is this type that can act as highly selective epoxidation catalysts.

Sheldon[40b] has studied epoxidation in the presence of various metal ions and also concluded that metals which exhibit high Lewis acidity are the most effective epoxidation catalysts. Lewis acidity of transition metal oxides decreases in the order;

$$CrO_3 > MoO_3 > WO_3 > TiO_2,\ V_2O_5,\ UO_3$$

On the basis of its high Lewis acidity Cr(VI) would be expected to be a good catalyst. The fact that it is not has been attributed to the strong oxidising properties of Cr(VI) leading to decomposition of the hydroperoxide.

It has also been pointed out by Sheldon that the Lewis

acidity of the metal would be influenced by the nature of the ligand surrounding the metal although this is clearly only of importance in cases where the original ligand does not undergo destructive oxidation.

Hydrocarbon soluble compounds of molybdenum, vanadium and tungsten are recognised as the best catalysts for epoxidation, but even among these metals differences in activity are evident. Vanadium catalysed reactions proceed at a slower rate than those catalysed by molybdenum. This is due to competitive formation of a complex between the vanadium and alcohol, the reaction co-product[35]. Formation of a vanadium-alcohol complex competes with the formation of a vanadium-hydroperoxide complex and hence retards the rate of reaction with alkene.

The greater tendency of vanadium to co-ordinate alcohol increases its activity in the epoxidation of allylic alcohols, and reactions of these substrates proceed faster with vanadium than with molybdenum catalysts[44].

Other catalysts mentioned in the patent literature include compounds of tungsten[45] as well as titanium, chromium, niobium, zirconium, tellurium, rhenium and other elements[46]. The use of boric esters has been mentioned, with metaborates being the most active[47].

1.5.3 Stereo and Regioselective Metal Catalysed Epoxidation

Sharpless[48] has made use of the exceptionally facile epoxidation of allylic alcohols by t-butyl hydroperoxide in the presence of vanadium catalysts to effect selective epoxidations that were not possible with other reagents.

Thus geraniol (1.12) and linalol (1.13) were selectively epoxidised to the previously unknown mono-epoxides.

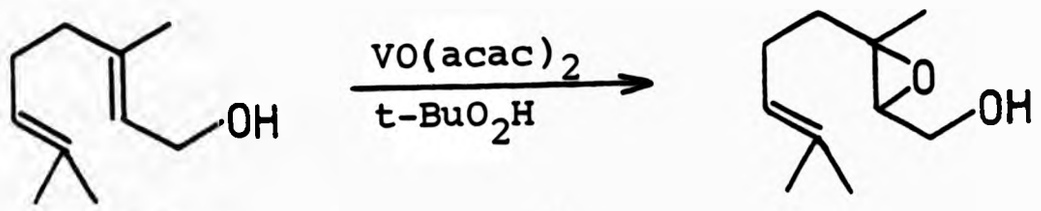

(1.12)

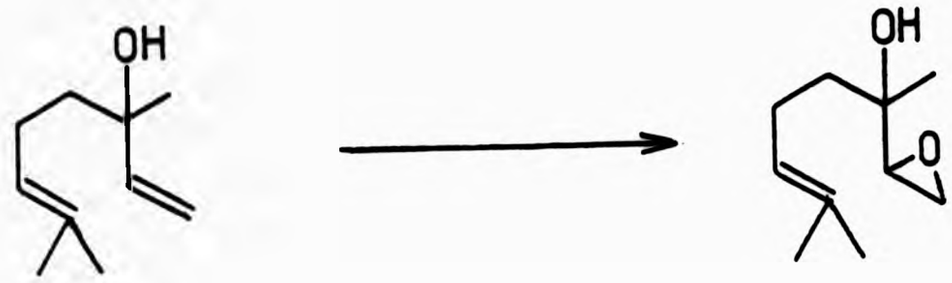

(1.13)

Similarly, the selective epoxidation of the bisallylic alcohol (1.14) to the bis epoxyalcohol (1.15) has been used by Sharpless as the crucial step in the synthesis of juvenile hormone from farnesol[49].

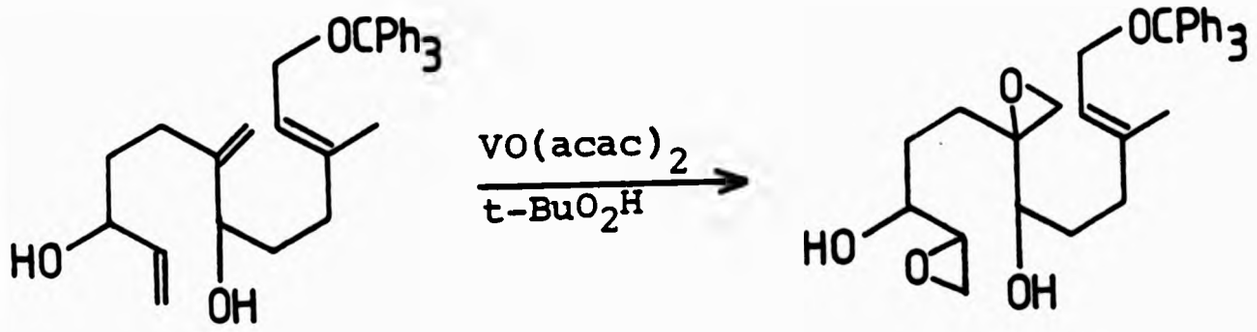

(1.14) (1.15)

Apart from the high regioselectivity exhibited by these metal-hydroperoxide systems, the syn-directive effect of the hydroxyl group has been shown to be more pronounced in the epoxidation of both cyclic and acyclic allylic alcohols than in the previously reported peracid epoxidations

of the same substrate[48,49]. Thus epoxidation of 4β-hydroxycholesterol (1.16) gave only the 5,6-β-oxide (1.17) compared to a 2:1 mixture of β- and α- oxides by peracid epoxidation.

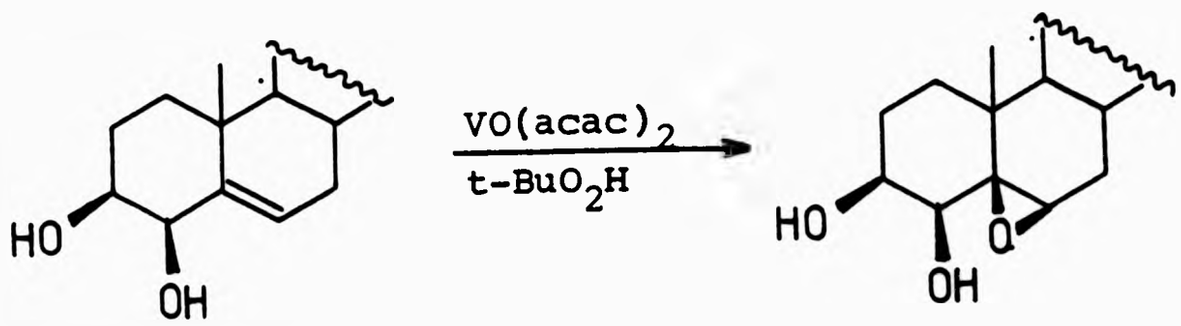

(1.16) (1.17)

Some recent studies have compared the stereochemistry of the epoxidation of cyclic allylic alcohols by vanadium/t-BuO_2H with that obtained using peroxy-acids[50]. Unlike epoxidation by peracids, which show a change from cis to trans stereochemistry in going from common (5-7) to medium (8-12) ring allylic alcohols, it was found that the vanadium catalysed reaction gives consistently cis stereochemistry. Additionally it was found that for the vanadium catalysed epoxidation of conformationally "fixed" allylic alcohols, cis stereochemistry is favoured when the hydroxyl group occupies a quasi-axial position, whereas in peracid epoxidation a quasi-equatorial position is preferred. The effect of ring size on the stereochemistry of epoxidation is therefore explained in terms of the ability of the hydroxyl group to adopt these conformations in the transition state.

CHAPTER 2

DEVELOPMENT OF SELECTIVE METHODS FOR EPOXIDATION OF ALKENES

2.1 Introduction

Although the use of vanadium and molybdenum catalysts for the epoxidation of simple olefins by alkyl hydroperoxides (Scheme 2.1) has been extensively reported in the patent literature[28] it is only recently that Sharpless and his co-workers have shown that the transition metal catalysed epoxidation of allylic alcohols proceeds with a high degree of regio- and stereoselectivity and applied it to the area of complex molecule synthesis[48].

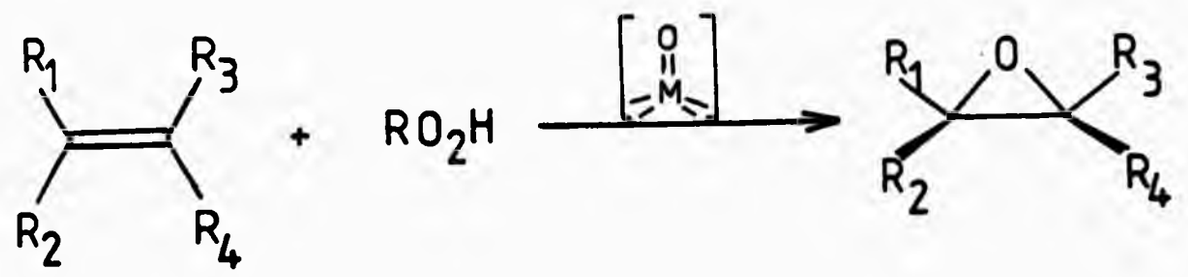

Scheme 2.1

These findings provided a starting point for the proposed investigation which was to be concerned in the first instance with modifying the structure of the catalyst in order to increase regioselectivity and/or stereoselectivity in the epoxidation of a wide range of different olefins. The main modifications envisaged concerned the ligand portion of the catalyst, since it seemed likely that the precise structure and stereochemistry of this ligand could have a marked effect on the orientation of the olefin as it approaches the epoxidising species (believed to be a metal

complex containing the alkyl hydroperoxide as an additional ligand). For example by synthesising a metal complex containing a fairly bulky ligand one might obtain a catalyst which would enable only terminal olefins to be epoxidised. Similarly, a catalyst containing a suitably chosen chiral ligand might be effective in the conversion of prochiral olefins to optically active epoxides.

During the course of these investigations Yamada _et al_[51] and Sharpless _et al_[52] have reported some asymmetric induction in epoxidations in the presence of molybdenum and vanadium complexes having chiral ligands and these are discussed later. However, no work has been reported on the regioselective epoxidation of simple olefins by alkyl hydroperoxides in the presence of metal catalysts.

2.2 Regioselective Epoxidation

As with peracid epoxidation, the relative rate of epoxidation of olefins by alkyl hydroperoxides in the presence of metal catalysts increases as the olefin becomes more substituted with alkyl groups[53]. In polyenes containing two or more nonequivalent double bonds it is, therefore, often possible to epoxidise selectively one of them provided their nucleophilic reactivities are sufficiently different, as is normally the case when the double bonds carry different numbers of substituents.

It was envisaged that by suitable modification of the ligand portion of the catalyst in the metal catalysed epoxidation of polyenes, it may be possible to alter the normal product distribution expected on electronic grounds. For example a metal complex containing a fairly bulky ligand

may give rise to a catalyst which restricts the approach of the polyene to the epoxidising species and enables only less hindered (terminal) double bonds to be epoxidised in the presence of more highly substituted double bonds (Scheme 2.2).

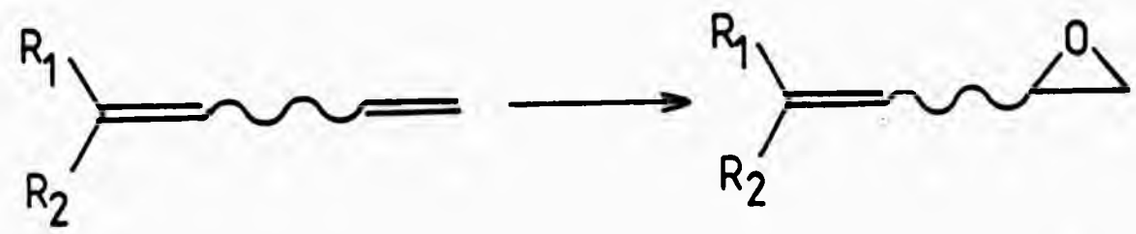

Scheme 2.2

2.2.1 Preparation of some oxo-metal complexes

Since a program aimed at developing regioselective epoxidation catalysts would involve the synthesis of metal complexes having elaborate ligand systems it was desirable, before commencing such a program, to determine the relative reactivities of different double bonds in polyenes since this was likely to have some bearing on the overall feasibility of such a program. For this reason a number of metal complexes having fairly simple ligands were prepared and these are described below.

In addition to their use in reactivity studies and as general epoxidation catalysts these complexes were also seen as useful starting materials for the synthesis of other metal complexes by ligand exchange reactions.

(i) Bis(acetylacetonato)dioxomolybdenum(VI)

An attempt was made to prepare bis(acetylacetonato)-dioxomolybdenum(VI), ($MoO_2(acac)_2$) by the method of Gehrke and Veal[54] in which treatment of a sodium molybdate solution, (adjusted to pH 1 with HCl) with acetylacetone leads to separation of the complex. In several attempts to perform the preparation under these conditions, a yellow solid was obtained in high yield (90%) but the physical data were not entirely compatible with that reported for the complex[54,55]. Although the infrared spectrum showed all the expected absorption bands they appeared to be superimposed on some very broad bands in the regions 1200-1700 cm^{-1} and 2700-3600 cm^{-1} with some additional bands in the 650-800 cm^{-1} region. X-ray powder diffraction showed some additional lines to those expected and elemental analysis was not consistent with that required for the desired complex.

It has been shown by Jones[56], that acidification of sodium molybdate solutions with nitric acid results in formation of molybdic acid at pH values below 3. Performing the previous preparation in molybdate solutions at pH 3 gave a pale yellow solid but in very low yield (>10%). The infrared spectrum, X-ray powder diffraction data and elemental analysis showed the product to be the desired complex in very pure form.

The low yield of complex obtained at pH 3 indicates that this is not the optimum pH for complex formation. It appears probable that at pH 2 pure $MoO_2(acac)_2$ would be obtainable in reasonable yields because at this pH

(i) Bis(acetylacetonato)dioxomolybdenum(VI)

An attempt was made to prepare bis(acetylacetonato)-dioxomolybdenum(VI), ($MoO_2(acac)_2$) by the method of Gehrke and Veal[54] in which treatment of a sodium molybdate solution, (adjusted to pH 1 with HCl) with acetylacetone leads to separation of the complex. In several attempts to perform the preparation under these conditions, a yellow solid was obtained in high yield (90%) but the physical data were not entirely compatible with that reported for the complex[54,55]. Although the infrared spectrum showed all the expected absorption bands they appeared to be superimposed on some very broad bands in the regions 1200-1700 cm^{-1} and 2700-3600 cm^{-1} with some additional bands in the 650-800 cm^{-1} region. X-ray powder diffraction showed some additional lines to those expected and elemental analysis was not consistent with that required for the desired complex.

It has been shown by Jones[56], that acidification of sodium molybdate solutions with nitric acid results in formation of molybdic acid at pH values below 3. Performing the previous preparation in molybdate solutions at pH 3 gave a pale yellow solid but in very low yield (>10%). The infrared spectrum, X-ray powder diffraction data and elemental analysis showed the product to be the desired complex in very pure form.

The low yield of complex obtained at pH 3 indicates that this is not the optimum pH for complex formation. It appears probable that at pH 2 pure $MoO_2(acac)_2$ would be obtainable in reasonable yields because at this pH

appreciable amounts of molybdenyl cations (MoO_2^{2+}) are present in equilibrium with paramolybdate ions[57] ($Mo_7O_{24}^{6-}$), however, this has not been attempted.

(ii) Bis[*trans*-1,2-cyclohexandiolato-O,O^1(1-)]dioxomolybdenum(VI).

This complex was prepared according to the method of Sheldon[41] which involves heating a solution of bis(acetylacetonato)dioxomolybdenum(VI) and *trans*-cyclohexan-1,2-diol in cyclohexane at 80°C for 1 h.

2.2.2 Epoxidation of terminal olefins using transition metal catalysts

Initial studies were concerned with the epoxidation of simple mono-substituted olefins with a number of molybdenum and vanadium catalysts and it was found that the rate of epoxidation is very slow compared to that of more highly substituted olefins. Attempted epoxidation of oct-1-ene by *t*-butyl hydroperoxide in the presence of bis(acetylacetonato)oxovanadium(IV) at 80°C gave no detectable epoxide after 4 h. However bis(acetylacetonato)dioxomolybdenum(VI) gave some conversion to epoxide under similar conditions.

Epoxidation of citronellene (2.1) with *t*-butyl hydroperoxide using bis[*trans*-1,2-cyclohexandiolato-O,O^1(1-)]-dioxomolybdenum(VI) in toluene at 80°C for 3 h gave epoxidation exclusively at the most substituted double bond.

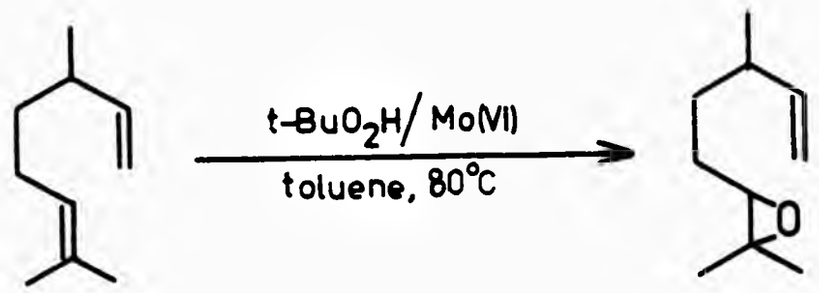

(2.1)

To establish whether it was possible to epoxidise monosubstituted olefins under these conditions methoxycitronellene (2.2) was treated in a similar manner and found to give only a trace of epoxide after 3 h, increasing to 47% after 17 h.

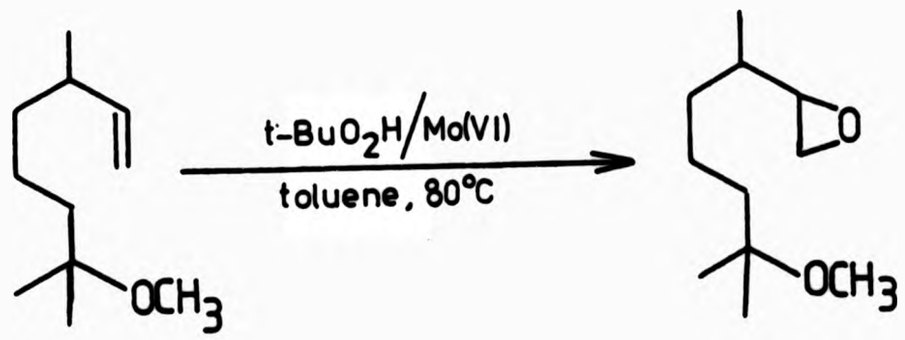

(2.2)

These findings are consistent with those of other workers who have found that epoxidation of all but allylic alcohols proceed at a greater rate with molybdenum than vanadium catalysts and that the rate and selectivity of epoxidation increases as the olefin becomes more substituted with alkyl groups. Thus Sheldon has measured the relative rates of epoxidation of a variety of olefins and found that the rate of epoxidation of 2-methyl-2-heptene is 75 times that of oct-1-ene[40a].

The intrinsically low activity of oxo-metal catalysts in the epoxidation of terminal olefins suggests that the development of catalysts capable of effecting regio-selective epoxidation may be impractical, if this is dependent on increasing the steric bulk at the catalyst active site, as this will further lower the intrinsic activity of the catalyst.

The greater reactivity and regioselectivity of allylic alcohols to epoxidation in the presence of the above catalysts led us to direct our efforts towards developing catalysts capable of effecting asymmetric epoxidation of these substrates since it was expected that attachment of the allylic alcohol substrate to the metal would enhance any asymmetric selection process.

2.3 Asymmetric Epoxidation

Despite studies carried out by other workers on the mechanism of the metal catalysed epoxidation the behaviour of the ligand system in the reaction remains uncertain particularly in the case of the vanadium catalysed reaction where a change in oxidation state of the metal occurs. As discussed previously (Section 1.5.1) Sheldon[40a] found that molybdenum complexes having weakly co-ordinating ligands undergo oxidative degradation during the epoxidation reaction whereas other workers suggest that complexes with ligands having nitrogen donor atoms are stable under the reaction conditions[42]. Furthermore, epoxidation by molybdenum complexes does not involve a change in oxidation state of the metal. For these reasons it was decided to prepare asymmetric epoxidation catalysts based on

molybdenum, however, in cases where the synthesis of the molybdenum complex proved difficult the synthesis of the corresponding vanadium complex was attempted.

The structural requirements of a chiral ligand system for an asymmetric epoxidation catalyst are a matter for speculation and a variety of different ligand systems have therefore been investigated. The first chiral catalysts to be prepared were those with ligands derived from (+)-camphor (Section 2.3.1 and 2.3.2). It was hoped that such ligands would not only give rise to a chiral reaction site but that their steric bulk would also favourably influence the selectivity of the reaction.

Complexes having novel tridentate ligand derived from chiral β-aminoalcohols (Section 2.3.3) have been prepared, so also have complexes with chiral 1,2-diol ligands. (Section 2.3.4).

The results of epoxidation experiments using these catalysts are discussed in Section 2.3.5.

2.3.1 Catalysts derived from (+)-hydroxymethylenecamphor

Scheme 2.3 shows the route employed in the synthesis of the potentially useful quadridentate ligand N,N^1-ethylenebis(iminomethylcamphor) (2.3). Reaction of amyl formate with the sodioketone of camphor in ether gave 3-hydroxymethylene camphor[58] (2.4) which condensed with 1,2-diaminoethane in methanol to give the known Schiff base ligand (2.3)[59].

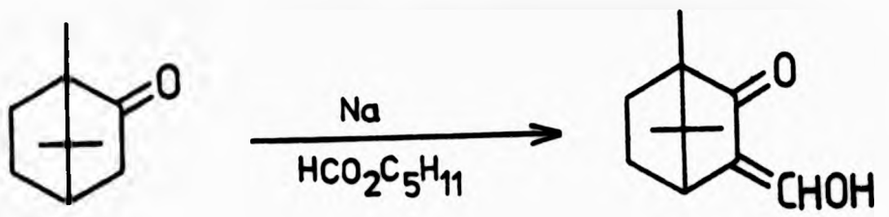

(2.4)

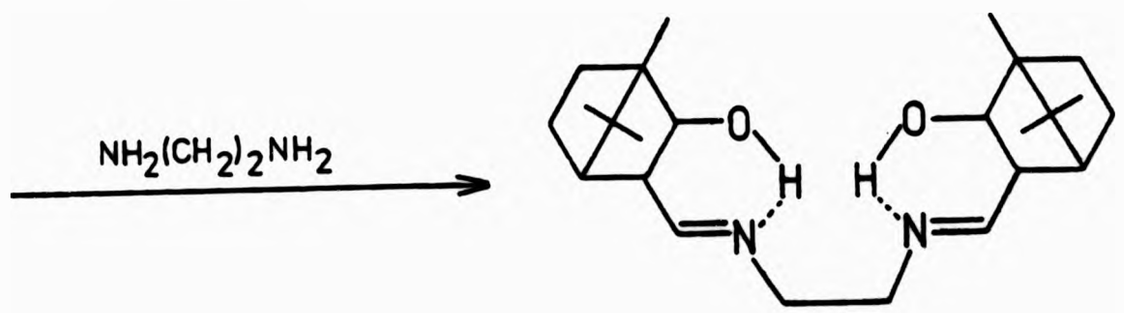

(2.3)

Scheme 2.3

All attempts to prepare the dioxomolybdenum complex of ligand (2.3) have been unsuccessful (Appendix 1). One possible explanation for this could be the preference for <u>cis</u> geometry of the dioxomolybdenum species[60], which would force the ligand to adopt a less favourable non-planar <u>cis</u> geometry.

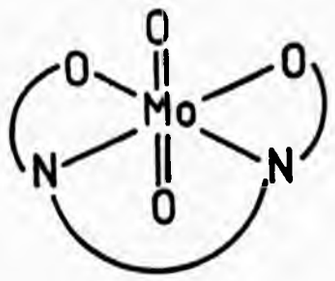

<u>trans</u>-dioxo-complex

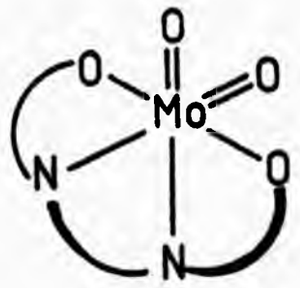

<u>cis</u>-dioxo-complex

Failure to isolate the desired molybdenum complex of NN^1-ethylenebis(iminomethylcamphor) led to attempts to prepare the vanadyl complex in which the ligand would be able to adopt a more or less planar configuration. Dey[61]

has recently reported the preparation of several vanadyl complexes by reaction of bis(acetylacetonato)oxovanadium(IV) with Schiff bases in refluxing toluene. Attempts to prepare the vanadyl complex of ligand (2.3) by this method yielded unchanged starting materials as did the use of higher boiling solvents such as diglyme.

Oxovanadium complexes of β-ketimines (2.5) have been prepared[62,63] by heating an intimate mixture of the ligand and bis(acetylacetonato)oxovanadium(IV) at 230°C under vacuum for 3 h.

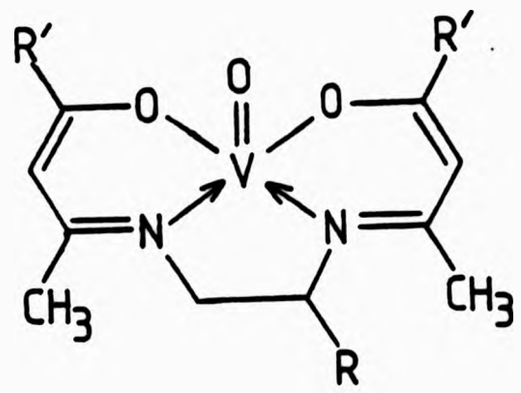

(2.5)

Carrying out this procedure with NN[1]-ethylenebis-(iminomethylcamphor) produced a green sublimate, the infrared spectrum of which showed a strong absorption at 987 cm^{-1} corresponding to the V═O stretching frequency. The N-H stretch present at 3290 cm^{-1} in the ligand had disappeared and the carbonyl stretch at 1695 cm^{-1} in the ligand had shifted to 1605 cm^{-1}. The visible electronic spectrum of the sublimate resembled that for complexes of this type having maxima at 568 nm (ε~80) and 673 nm (ε~100).[63]

Mass spectroscopic analysis of the sublimate showed a parent ion corresponding to that of complex (2.6) as confirmed by accurate mass measurement. The spectroscopic data is therefore consistent with the formation of NN^1-ethylenebis(iminomethylcamphorato)oxovanadium(IV).

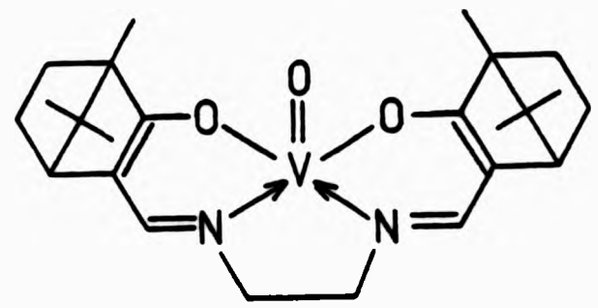

(2.6)

Attempts to prepare NN^1-ethylenebis(iminomethyl-camphorato)dioxomolybdenum(VI) by the above method gave a dark brown solid the infrared spectrum of which showed only a weak band in the region 850-950 cm^{-1} where a strong Mo=O stretching band would be expected. Free ligand was also present as indicated by the presence of C=O and N-H absorptions. Mass spectrometric examination of the crude product however showed the presence of a molybdenum containing parent ion of appropriate m/e value indicating that possibly some of the desired complex was present. The use of less vigorous conditions of temperature and pressure failed to give any reaction.

During our work on the synthesis of the above complexes several groups of workers reported successful metal catalysed asymmetric epoxidations. Yamada *et al* have produced optically active epoxides of the allylic alcohols geraniol and nerol

Mass spectroscopic analysis of the sublimate showed a parent ion corresponding to that of complex (2.6) as confirmed by accurate mass measurement. The spectroscopic data is therefore consistent with the formation of NN^1-ethylenebis(iminomethylcamphorato)oxovanadium(IV).

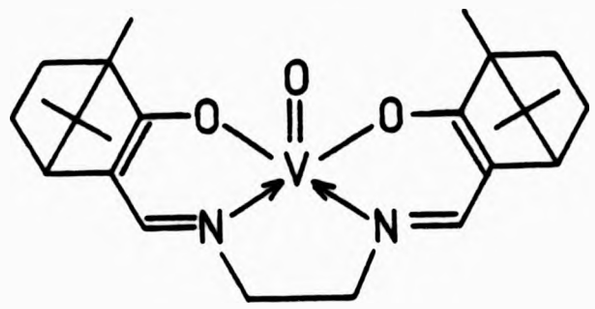

(2.6)

Attempts to prepare NN^1-ethylenebis(iminomethyl-camphorato)dioxomolybdenum(VI) by the above method gave a dark brown solid the infrared spectrum of which showed only a weak band in the region 850-950 cm^{-1} where a strong Mo=O stretching band would be expected. Free ligand was also present as indicated by the presence of C=O and N-H absorptions. Mass spectrometric examination of the crude product however showed the presence of a molybdenum containing parent ion of appropriate m/e value indicating that possibly some of the desired complex was present. The use of less vigorous conditions of temperature and pressure failed to give any reaction.

During our work on the synthesis of the above complexes several groups of workers reported successful metal catalysed asymmetric epoxidations. Yamada et al have produced optically active epoxides of the allylic alcohols geraniol and nerol

using the chiral metal complex (acetylacetonato)[(-)-N-alkylephidrinato]dioxomolybdenum(VI)(2.7) as epoxidation catalyst[51]. The chiral complex was isolated by treating the N-alkylephidrine with $MoO_2(acac)_2$ in cyclohexane at 80°C for 1 h.

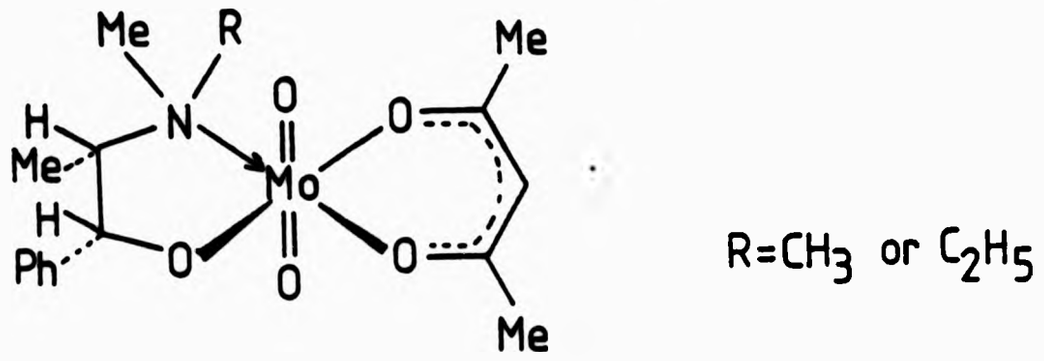

$R=CH_3$ or C_2H_5

(2.7)

According to Yamada the main requirement of an effective chiral epoxidising catalyst is that it should contain a chiral ligand which behaves as a fixed ligand and does not dissociate from the central metal atom during the reaction. In addition the catalyst should contain a labile ligand which can be readily replaced by reactants which would then come under the influence of the fixed chiral ligand. (-)-N-alkylephedrine apparently meets the first criterion and acetylacetone the second.

Sharpless et al have also effected asymmetric epoxidations of allylic alcohols by using chiral hydroxamic acid complexes of vanadium[52]. The chiral complexes were generated in situ by addition of ligand and $VO(acac)_2$ to the reaction mixture. The best induction (50% ee) was achieved in the epoxidation of α-phenylcinnamyl alcohol (2.8) using N-phenylcamphorylhydroxamic acid (2.9) as the chiral ligand.

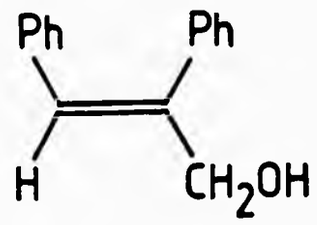

(2.8)

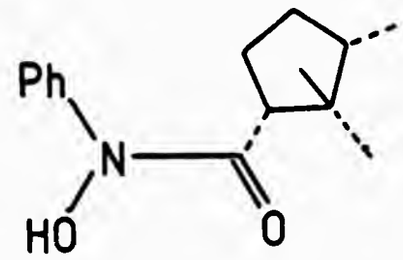

(2.9)

The apparent ease of preparation by Yamada of the N-alkylephidrine complex led us to suppose that complexes with five membered chelate rings may be more stable than the six membered chelate ring complexes we had been attempting to prepare. In addition, the observation by Sharpless that chiral β-diketone complexes give poor results owing to their rapid decomposition under the epoxidising conditions[52] highlights the importance of finding ligand systems stable under the reaction conditions.

2.3.2 Catalysts derived from cis,exo-3-amino-2-hydroxybornane

(i) Cis,exo-3-dimethylamino-2-hydroxybornane

As a result of the observations discussed above, we proposed to synthesise the unsymmetrical complex (2.10) (by the route shown in Scheme 2.4) this complex has one bidentate camphor containing ligand forming a five-membered chelate ring.

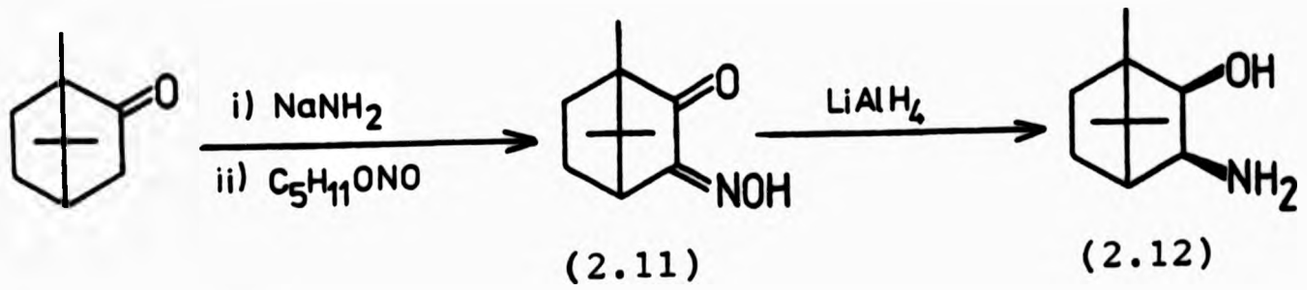

(2.11) (2.12)

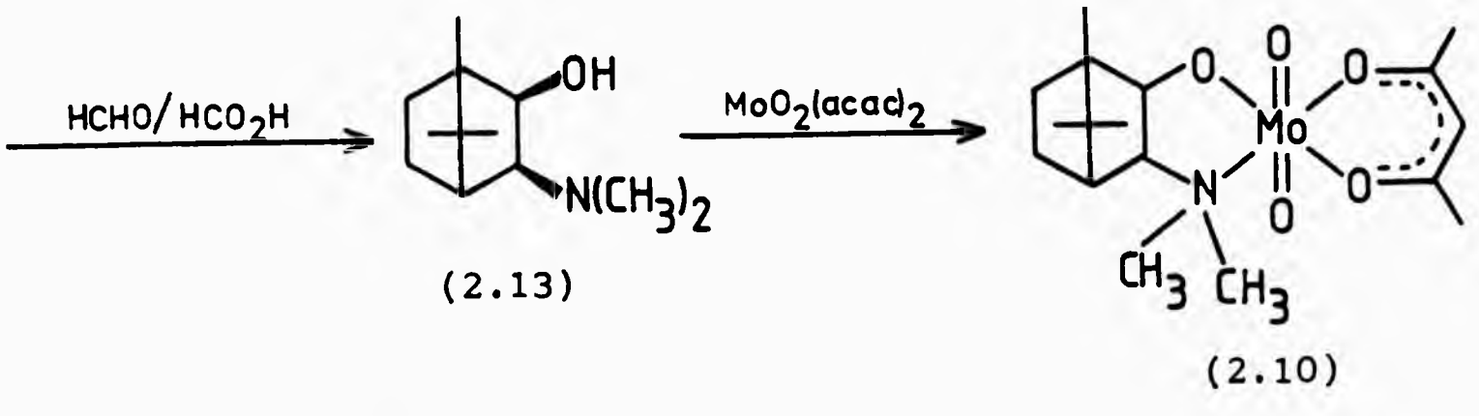

(2.13) (2.10)

Scheme 2.4

3-Hydroxyiminobornan-2-one (2.11) was prepared by the method used by Bredt and Perkin[64] for the nitrosation of epicamphor with amyl nitrite in the presence of sodamide. Reduction of 3-hydroxyiminobornan-2-one with lithium aluminium hydride gave cis,exo-3-amino-2-hydroxybornane (2.12). Provided this reduction is carried out under conditions in which the concentration of reactants is low, the lithium aluminium hydride anion apparently attacks the keto and hydroxyimino functions from the less hindered endo side of the molecule. Increasing the concentration of reactants, however, results in a significant loss in stereospecificity giving a mixture of products[65,66].

Cooper et al[65] have prepared cis,exo-3-dimethylamino-2-hydroxybornane (2.13) in unspecified yield by reductive methylation of cis,exo-3-amino-2-hydroxybornane with formaldehyde and formic acid (Eschweiler-Clark method[67]). In our hands this procedure gave a mixture containing two major components. It is well known that in some cases reductive methylation by this procedure can give rise to complex mixtures resulting from a number of side reactions[68]. Borch and Hassid[69] has reported a mild and efficient

method for amine methylation using a formaldehyde-cyanoborohydride system which is said to yield tertiary methylated amines of high purity in good yield. Using this procedure we obtained a mixture identical to that obtained by the standard Eschweiler-Clark method. Separation of the reaction mixture by column chromatography gave two components one of which was identified as the desired N-dimethyl compound (40%, by nmr of crude product). The ^1H nmr of the other component (60% by nmr) showed in addition to an N-methyl singlet at δ 2.29, two AB doublets at δ 3.67 and δ 4.45 (J = 2.5 Hz) characteristic of the nmr pattern of the C-2 protons in oxazolidines[70,71]. A doublet at δ 3.80 (J = 7.6 Hz) was due to the C-2 proton of the bornane ring. The C-3 doublet was shown to overlap with the N-methyl signal, as irradiation of this region of the spectrum resulted in collapse to a singlet of the C-2 doublet. The infrared spectrum showed no OH or NH stretching bands but three bands at 1067, 1084 and 1139 cm^{-1} characteristic of the oxazolidine ring were observed[72]. The mass spectrum shows a parent ion m/e 195 and accurate mass measurements have confirmed the product to be (2.14).

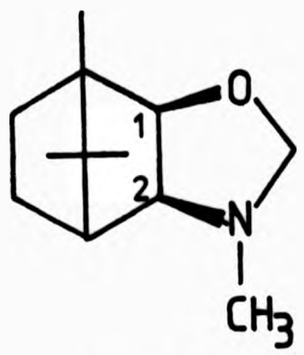

(2.14)

We have since found that Nelson[73] obtained a similar product while attempting to N-methylate cis-3-aminobicyclo-[2,2,2]octan-2-ol by the Eschweiler-Clark method in which only N-methyl-cis-bicyclo[2.2.2]octyl[2.3-d]oxazolidine was isolated. Reduction of the oxazolidine with lithium aluminum hydride was found to give the desired cis-3-dimethylamino-bicyclo[2.2.2]octan-2-ol (Scheme 2.5).

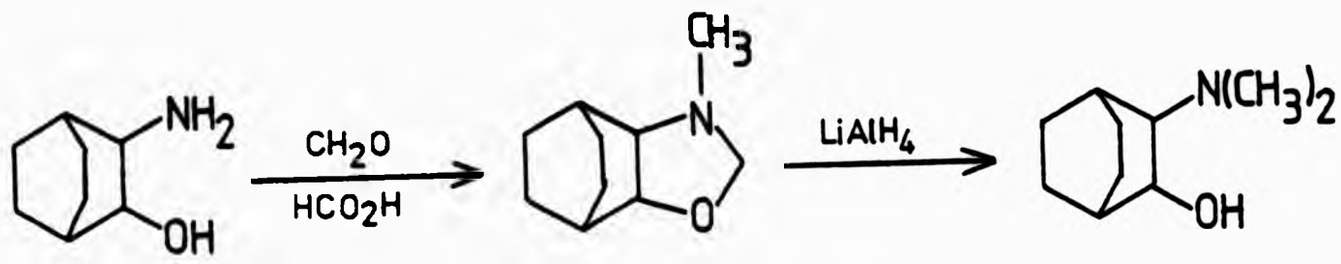

Scheme 2.5

Attempts to prepare the chiral complex by heating cis,exo-3-dimethylamino-2-hydroxybornane with bis-(acetylacetonato)dioxomolybdenum(VI) in cyclohexane according to the procedure adopted by Yamada resulted only in the recovery of starting materials. Failure to isolate this complex made it necessary to look for other ligand systems which form molybdenum complexes fairly easily and which either contain a chiral centre or into which a chiral centre can be introduced.

(ii) Cis,exo-3-amino-2-hydroxybornane-salicylaldehyde complexes.

Although a great deal of work has been published[74,75] on transition metal complexes of N-substituted salicylaldiminates (2.15) it is only relatively recently that dioxomolybdenum(VI) complexes containing ligands of this

type have been reported[76]. These complexes are relatively

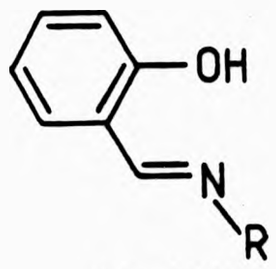

(2.15)

easy to prepare by addition of the appropriate amine to a refluxing suspension of bis(salicylaldehydato)dioxomolybdenum(VI) (2.16) in methanol (Scheme 2.6).

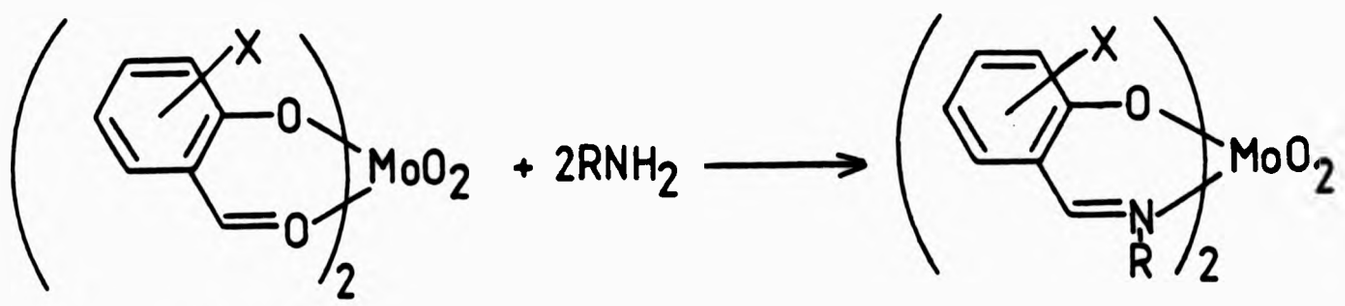

(2.16)

Scheme 2.6

As already discussed (Section 2.3) it has been suggested by other workers that molybdenum complexes with ligands containing nitrogen donor atoms are less likely to undergo oxidative decomposition under the epoxidising conditions[42]. For these reasons we attempted to prepare chiral N-substituted salicylaldiminates using chiral primary amines. In this section derivatives of cis,exo-3-amino-2-hydroxybornane are considered. Related complexes derived from other chiral amino alcohols are included in Section 2.3.3.

When a refluxing methanol suspension of bis(salicylaldehydato)dioxomolybdenum(VI) ($MoO_2(sal)_2$) was treated with cis,exo-3-amino-2-hydroxybornane and allowed to stand

overnight a product was obtained which gave a ^1H nmr spectrum which indicated the presence of one phenyl and one bornane group suggesting the formation of a complex containing a tridentate ligand (2.17a).

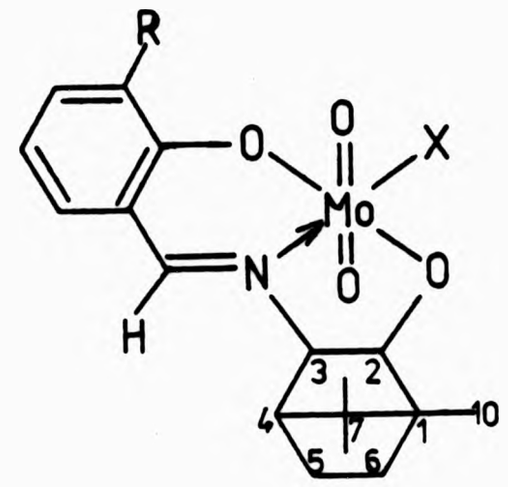

(2.17) (a) R=H (b) R=OMe

In the ^1H nmr spectrum of the product the signals arising from protons C-2 (δ 4.48, J = 7.3 Hz) and C-3 (δ 4.00, J = 7.3 Hz) of bornane were shifted downfield compared with the corresponding signals in the nmr of free cis,exo-3-amino-2-hydroxybornane. In addition the signal arising from the proton at C-3 was coupled with that of the imino proton (δ 8.67, J = 2.5 Hz) which appeared at higher field than the aldehydic proton signal of $MoO_2(sal)_2$. Finally, a signal thought to be due to methanol could not be removed by drying the solid under high vacuum.

The infrared active stretching modes for terminal oxygen (oxo; Mo=O) are found[77] in the region 850-1000 cm^{-1}, the actual value depending on the number of terminal oxygens, the oxidation state of the metal and the nature of the

other ligands present. For dioxomolybdenum complexes the number of infrared active stretching modes depends on whether the terminal oxygens are cis or trans. Species with cis-terminal oxygen atoms show two infrared active bands in this region while comparable trans complexes have only one band[77,78]. Complexes having N-substituted salicylaldiminate ligands are reported[76] to show two or three infrared absorption bands in the region 890-940 cm^{-1}.

The infrared spectrum of the molybdenum complex of the salicylaldimine derived from cis,exo-3-amino-2-hydroxybornane showed several strong bands in the region 850-1000 cm^{-1}, however, the occurence of ligand absorptions in this region makes assignments to the Mo=O stretches difficult. No OH stretching absorption was observed in the infrared spectrum and this along with the shift of the C-2 proton in ^{1}H-nmr spectrum suggests that the deprotonated hydroxyl group of the hydroxybornane is also coordinated to the metal giving a tridentate ligand system.

Mass spectroscopic analysis gave a molybdenum (^{98}Mo) containing molecular ion of m/e 401. This would be in agreement with the five co-ordinate dioxomolybdenum complex (2.17a) containing the N-(cis,exo-2-hydroxybornyl)-3-salicylideniminato ligand and was confirmed by accurate mass measurement.

Although the spectroscopic data were consistent with the structure (2.17a) it was not possible to define the geometry of the complex. Furthermore, it was only possible to establish the occupacy of five of the six coordination sites of the metal and on the basis of the infrared spectrum

the possibility of a binuclear dioxobridged system (2.18) could not be ruled out[79].

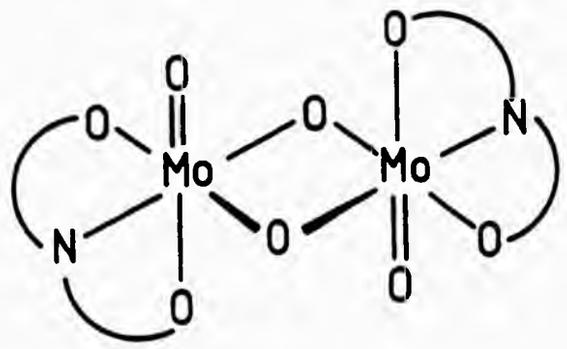

(2.18)

In the hope of improving the organic solubility of the complex and thereby possibly increasing its effectiveness as an epoxidation catalyst the related complex (2.17b) using 3-methoxysalicylaldehyde (o-Vanillin) was prepared. Introduction of the methoxy group did not, however, significantly increase the solubility of the complex. The infrared spectrum of this complex was similar to that described previously as was the ^{1}H-nmr spectrum but with the addition of a methoxy signal at δ 3.78. Mass spectroscopic analysis showed a molybdenum (^{98}Mo) containing molecular ion of m/e 431. Accurate mass measurement again confirmed this to correspond to a five coordinate complex.

In order to establish the geometry of the complex and resolve the question regarding the occupation of the sixth co-ordination site of the metal an X-ray structure determination was carried out on a crystal obtained by recrystallisation from methanol and dimethylformamide. This has confirmed that the complex is mono-nuclear with two terminal oxo-groups in the cis configuration and identified an oxygen bonded dimethylformamide in the sixth co-ordination site of the molybdenum. Before recrystallisation this

co-ordination site was occupied by methanol as judged by the signal at δ 3.28 in the ^{1}H-nmr spectrum.

On the basis of this structural information it is possible to make some additional observations regarding the infrared and mass spectra. In complexes that have been allowed to crystallise from an excess of dimethylformamide the methanol ligand is replaced by dimethylformamide and the infrared spectrum shows an additional absorption band at 1670 cm^{-1} corresponding to the carbonyl stretch of this group. It appears that washing these crystals with methanol, however, can result in exchange of the dimethylformamide ligand by methanol. In all cases the mass spectrum shows only an [M^{+}-solvent] ion.

2.3.3 X-ray structure determination of [N(cis,exo-2-hydroxybornyl)-3-methoxysalicylideniminato(2-)]-(N,N-dimethylformamido)dioxomolybdenum(VI).

Pale yellow crystals were obtained by recrystalisation from a NN-dimethylformamide/methanol mixture.

Intensities were collected on a Philips PW 1100 four-circle diffractometer operating in the ω-2θ scan mode using graphite-monochromated Mo-K_{α} radiation (λ 0.07107 Å). The parameters are summarized in Table 2.1.

co-ordination site was occupied by methanol as judged by the signal at δ 3.28 in the ^{1}H-nmr spectrum.

On the basis of this structural information it is possible to make some additional observations regarding the infrared and mass spectra. In complexes that have been allowed to crystallise from an excess of dimethylformamide the methanol ligand is replaced by dimethylformamide and the infrared spectrum shows an additional absorption band at 1670 cm^{-1} corresponding to the carbonyl stretch of this group. It appears that washing these crystals with methanol, however, can result in exchange of the dimethylformamide ligand by methanol. In all cases the mass spectrum shows only an [M^{+}-solvent] ion.

2.3.3 X-ray structure determination of [N(cis,exo-2-hydroxybornyl)-3-methoxysalicylideniminato(2-)]-(N,N-dimethylformamido)dioxomolybdenum(VI).

Pale yellow crystals were obtained by recrystalisation from a NN-dimethylformamide/methanol mixture.

Intensities were collected on a Philips PW 1100 four-circle diffractometer operating in the ω-2θ scan mode using graphite-monochromated Mo-K_{α} radiation (λ 0.07107 Å). The parameters are summarized in Table 2.1.

Table 2.1 Crystal data

Formula	$C_{21}H_{30}N_2O_6Mo$
M	505.5
Crystal system	Orthorhombic
Space Group	$P2_12_12_1$
a/Å	26.992(8)
b/Å	11.691(6)
c/Å	7.055(6)
U/Å	2 226.3
Z	4
D_c/g.cm^{-3}	1.508
F(000)	1 040
μ(Mo-K_α)/cm^{-1}	5.5
Crystal size/mm	ca. 0.064 x 0.096 x 0.48
Reflections measured	2960
Unique reflections	2816
Scan width(ω)/°	0.64
Scan speed/°s^{-1}	0.05
θ range/°	$3.0 \leqslant \theta \leqslant 30$
R	0.0508
R^1	0.0513
Least-squares parameters	
Average shift-to-error	0.0522
Maximum shift-to-error	0.270

Data was collected for one octant of reciprocal space. Weak reflections were not measured if $[I_p - 2(I_p)^{\frac{1}{2}}] < I_b$ on a preliminary scan, where I_p is the intensity at the top of the reflection profile and I_b the mean of two 5-s background measurements on either side of the peak.

The background measuring time was proportional to I_b/I_i, I_i being the intensity recorded in scanning the reflection. The data was corrected for Lorentz and polarization factors and 2816 reflections were found to be statistically significant with $I \geq 3\sigma(I)$.

To determine accurate cell dimensions the diffractometer procedure "LAT" was used to record accurately the θ values for the more intense reflections down the axes h00, 0k0 and 00ℓ and hence the interplane spacings, d, associated with the crystal axes were obtained. Using these values it is possible to calculate the lengths of the axis a, b, and c. To check the precision of these values they were used to calculate, from simple geometrical formulae, the distance between the planes hh0, h0h and 0kk. These calculated distances were then compared with those determined by measuring reflections from these planes and were found to be in good agreement.

The space group $P2_12_12_1$ was determined unambigously from the systematic absences ; h00 with h even, 0K0 with K even, 00ℓ with ℓ even.

Due to difficulties in measuring the crystal density the number of molecules in the unit cell was estimated as four by assuming a density of 2.0 g cm^{-3} based on values reported for the molybdenum complexes $MoO_2(OCH_2CH_2O)_2$[80], $Mo_2O_4(OCH_2C(CH_3)_2CH_2O)_2(H_2O)_2$[81], $(pyH)_2[Mo_2O_4Cl_4(H_2O)_2]H_2O$[82]. The calculated density for the complex, assuming the molecular formula $C_{21}H_{30}N_2O_6Mo$, is considerably lower (1.508 g cm^{-3}) but is not unreasonable given the presence of a larger organic ligand than in the previously mentioned complexes.

The position of the molybdenum atom was located from a Paterson map. A subsequent difference-Fourier map gave a large number of electron density maxima around the metal atom, many of which could have arisen from donor atoms. Several attempts were made to establish which peaks were most likely to arise from the donor atoms by constructing models to find which occupied the most likely geometry around the metal atom. Substitution of these 'atoms' into the difference-Fourier failed to solve the structure. Finally, a Fourier map was calculated in which only the molybdenum atom had been assigned, and in this case all atoms except one carbon of the benzene ring and the bridgehead methyl of the aminoborneol fragment were found. The remaining ligand not previously identified was immediately identified as NN-dimethylformamide coordinated to the metal via the oxygen. All atoms found were incorporated and the structure refined using full-matrix least-squares procedures, with the metal, oxygen and nitrogen atoms having anisotropic temperature factors. All the hydrogen atoms were inserted into geometrically calculated positions (C-H 1.08A). The final difference-Fourier map showed maxima and minima of electron density of 0.88 and 0.75 eA^{-3} respectively, located near the molybdenum atom. R values are given in Table 2.1 and the refined atomic positional parameters are presented in Table 2.2. Table 2.3 lists interatomic bond lengths and angles in the coordination sphere of the metal. Anisotropic thermal parameters, interatomic bond lengths and angles in the ligand, and final structure factors are given in Appendix 2.

Major computations were performed using the 'SHELX' system of programs[83].

Fig. 2.1 shows the structure of the complex. In addition to identifying the remaining ligand as dimethylformamide and confirming the cis geometry and tridentate nature of the ligand it can be seen that the arrangement of donor atoms is a considerably distorted octahedron.

The Mo=O bond lengths are within the range (1.65-1.82Å) reported in the literature for other oxo-molybdenum(VI) complexes [84-89]. Similarly, the Mo-N(1) and Mo-O(2) bond lengths are comparable to those found[86,88], in complexes having the related salicylaldiminato ligands (2.19) and (2.20).

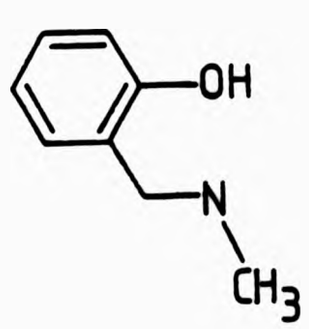

(2.19)

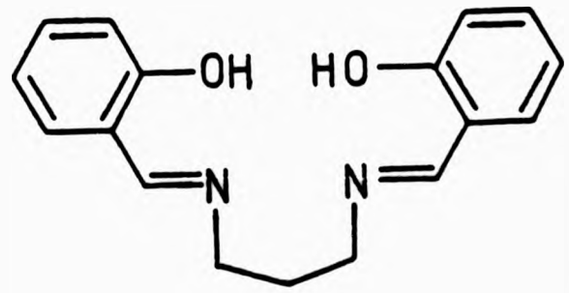

(2.20)

The crystal structure and infrared evidence suggest that exchange of a solvent molecule in the sixth coordination site will occur easily. As discussed previously the presence of an exchangable ligand may be advantageous in the design of asymmetric epoxidation catalysts.

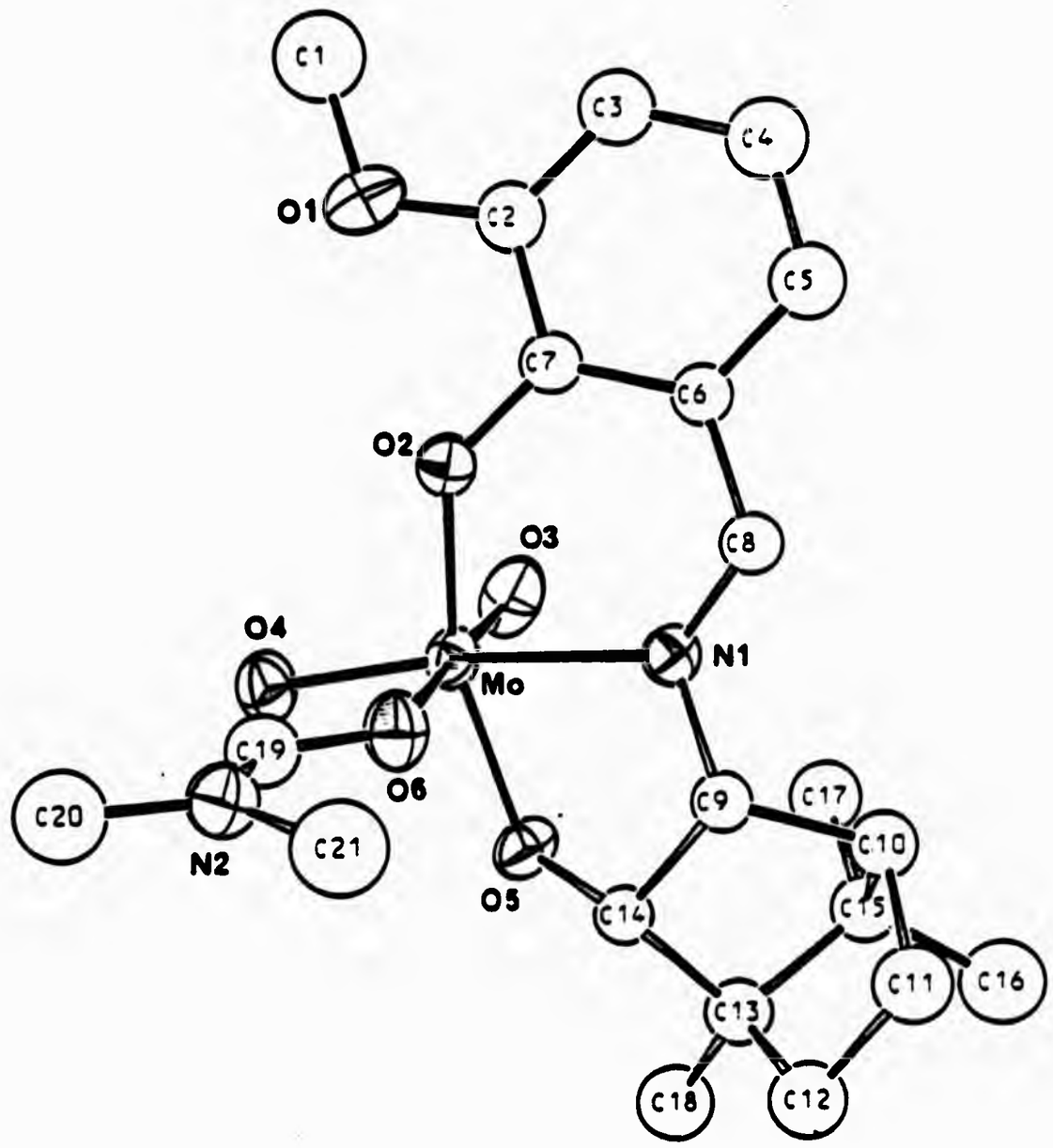

Fig. 2.1 The molecular structure of [N(<u>cis</u>,<u>exo</u>-2-hydroxybornyl)-3-methoxysalicylideniminato(2-)](NN-dimethylformamido)dioxomolybdenum(VI) showing labels used in Tables 2.2 and 2.3.

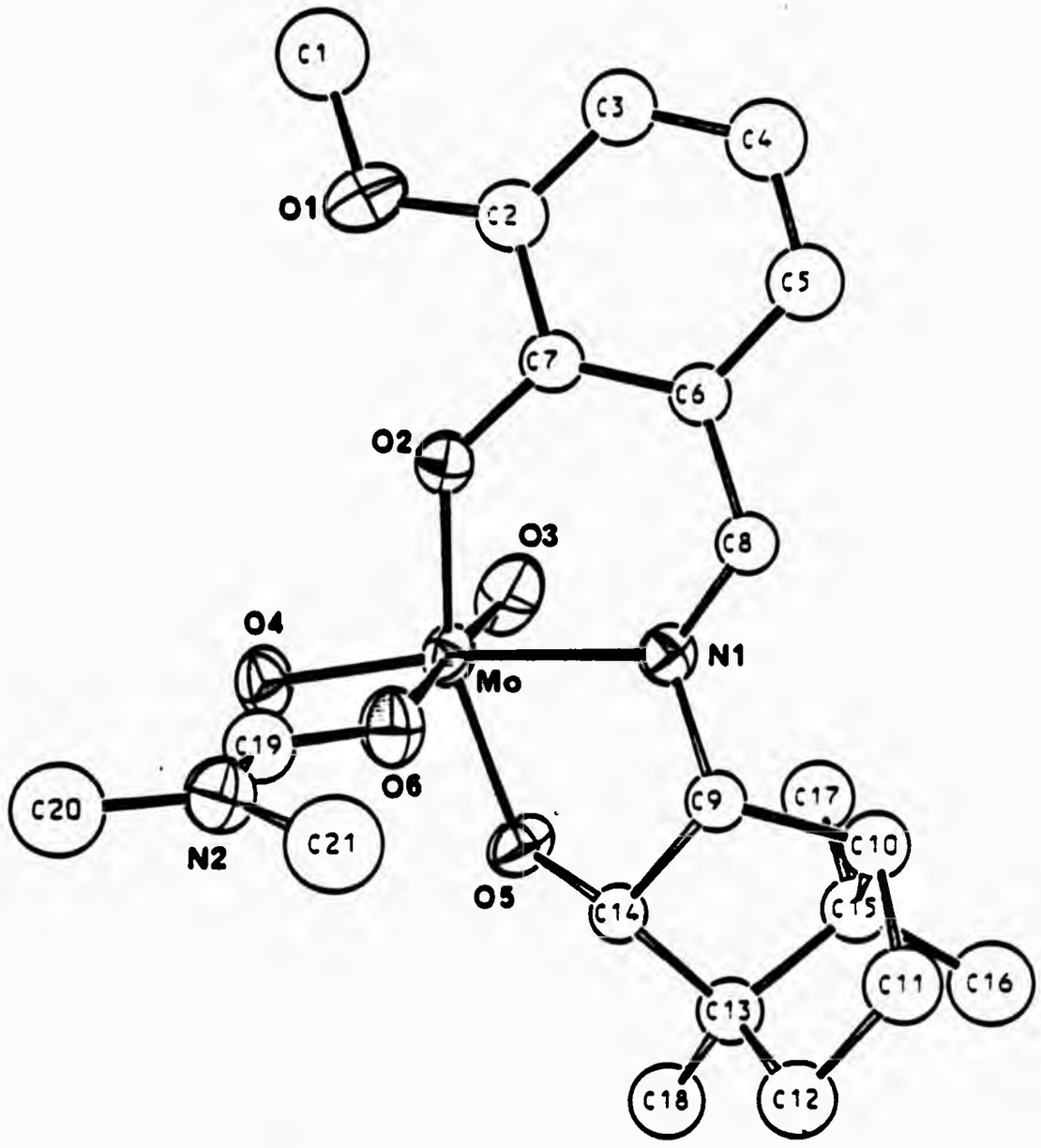

Fig. 2.1 The molecular structure of [N(cis,exo-2-hydroxybornyl)-3-methoxysalicylideniminato(2-)](NN-dimethylformamido)dioxomolybdenum(VI) showing labels used in Tables 2.2 and 2.3.

Table 2.2. Refined atomic positional parameters ($x10^4$) and isotropic thermal parameters ($x10^3$)[a].

Atom	x/a	y/b	z/c	U
Mo	14 035(2)[b]	2 308(1)	1 522(1)	
N(1)	1 283(2)	2 546(5)	4 689(8)	
N(2)	2 929(3)	1 030(6)	2 942(10)	
O(1)	729(2)	-1 063(5)	1 218(10)	
O(2)	1 216(2)	749(4)	2 293(8)	
O(3)	826(2)	2 670(5)	745(8)	
O(4)	1 738(2)	1 984(5)	- 497(7)	
O(5)	1 654(2)	3 797(4)	2 146(7)	
O(6)	2 151(2)	1 743(5)	3 043(7)	
C(1)	457(4)	-2 044(9)	594(15)	64(3)
C(2)	583(3)	- 598(7)	2 896(12)	37(2)
C(3)	216(3)	-1 003(8)	4 069(13)	45(2)
C(4)	102(4)	- 447(8)	5 767(13)	50(2)
C(5)	362(3)	508(7)	6 282(14)	44(2)
C(6)	723(3)	965(7)	5 089(11)	28(2)
C(7)	843(3)	401(6)	3 396(12)	27(1)
C(8)	995(3)	1 967(6)	5 743(12)	29(2)
C(9)	1 601(3)	3 449(7)	5 546(11)	27(2)
C(10)	1 338(3)	4 348(6)	6 801(11)	35(2)
C(11)	1 762(3)	4 954(8)	7 784(13)	46(2)
C(12)	2 022(3)	5 660(8)	6 172(13)	46(2)
C(13)	1 687(3)	5 406(7)	4 448(12)	33(2)
C(14)	1 831(3)	4 159(6)	3 935(10)	26(2)
C(15)	1 167(3)	5 299(7)	5 351(12)	35(2)
C(16)	987(4)	6 378(8)	6 331(14)	58(2)
C(17)	745(3)	4 908(8)	4 023(12)	42(2)
C(18)	1 748(3)	6 259(8)	2 860(13)	46(2)
C(19)	2 501(3)	1 304(7)	2 160(13)	39(2)
C(20)	3 314(4)	482(9)	1 841(16)	65(3)
C(21)	3 034(5)	1 310(11)	4 878(16)	70(3)

(a) The standard deviation of the least significant digit is included in parenthesis in this and subsequent Tables.

(b) The value of x/a for Mo has been multiplied by 10^5.

Table 2.3 Interatomic bond lengths (A) and angles (°) in the co-ordination sphere of the complex.

Atoms	
Mo-N(1)	2.274(6)
Mo-0(2)	1.968(5)
Mo-0(3)	1.706(5)
Mo-0(4)	1.729(5)
Mo-0(5)	1.918(5)
Mo-0(6)	2.379(5)
0(2)-Mo-N(1)	78.8(2)
0(3)-Mo-N(1)	98.9(2)
0(3)-Mo-0(2)	94.8(3)
0(4)-Mo-N(1)	155.6(2)
0(4)-Mo-0(2)	99.1(2)
0(4)-Mo-0(3)	105.4(3)
0(5)-Mo-N(1)	73.4(2)
0(5)-Mo-0(2)	150.2(2)
0(5)-Mo-0(3)	99.8(3)
0(5)-Mo-0(4)	101.8(2)
0(6)-Mo-N(1)	73.2(2)
0(6)-Mo-0(2)	80.6(2)
0(6)-Mo-0(3)	171.5(2)
0(6)-Mo-0(4)	82.4(2)
0(6)-Mo-0(5)	81.3(2)

2.3.4 Catalysts derived from other 2-aminoalcohols.

Attempts to extend the range of chiral complexes of the above type were restricted by the limited number of resolved α-amino alcohols that were available. However, a related complex was synthesised by addition of ℓ(-)-2-amino-1-butanol to bis(methoxysalicylaldehydato)dioxomolybdenum(VI) in refluxing methanol. Unlike the previous preparation the use of excess amino-alcohol gave a 'glassy' product, the spectroscopic properties of which were not consistent with those expected for structure (2.21). However, the use of equimolar amounts of reactants gave the desired complex as a yellow solid.

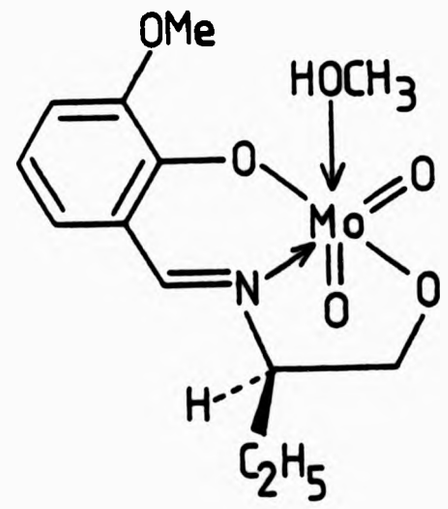

(2.21)

The ^{1}H-nmr spectrum of the product showed the presence of one phenyl and one 2-amino-1-butanol. An upfield shift of the aldehydic proton signal was observed, as with the previously described complex of this type (Section 2.3.2), and was therefore consistent with formation of the tridentate ligand. The normally complex methylene signal of the 2-amino-1-butanol had shifted downfield (δ 4.34) appearing

only as two overlapping signals with the remaining proton in the chelate ring of the amino alcohol appearing as a broad signal (δ 3.81) beneath that of the methoxy group. The infrared spectrum was similar to that of related complexes having a methanol ligand. Mass spectrometry showed a molybdenum containing parent ion m/e 351 (^{98}Mo) consistent with the expected five coordinate complex [M^+-$HOCH_3$]. Accurate mass measurement supports this proposed structure.

2.3.5 Catalysts derived from 1,2-diols

As stressed previously, an important requirement in the design of an asymmetric epoxidation catalyst is that the ligand system should be stable under the reaction conditions. The oxidative decomposition of many molybdenum complexes under the epoxidising conditions (with formation of 1,2-diol complexes which are themselves active catalysts and relatively stable) led us to consider the use of such complexes derived from chiral 1,2-diols as catalysts for asymmetric epoxidation.

Addition of D(-)-2,3-butandiol to a refluxing suspension of bis(acetylacetonato)dioxomolybdenum(VI) in cyclohexane produced a white solid, the infrared spectrum of which exhibited absorption bands characteristic of the oxo-molybdenum group and a co-ordinated hydroxyl group. The ^{1}H-nmr spectrum showed two pairs of overlapping methyl signals suggesting two 2,3-butandiol ligands in different environments, with the signals due to the remaining protons of the chelate ring shifted downfield compared with in the free ligand. The spectroscopic data was therefore consistent

with formation of the expected complex, cis-bis[D(-)-2,3-butandiolato-O,O^1(1-)]dioxomolybdenum(VI) (2.22), and satisfactory analytical data were obtained. It was not possible to obtain a satisfactory mass spectrum of this complex but this may be due to its thermal instability. Heating the complex at 80°C under reduced pressure produced a light-sensitive yellow material with slightly different infrared characteristics.

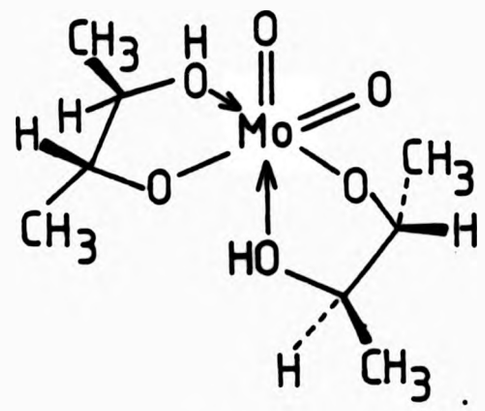

(2.22)

Attempts to prepare a similar complex using L-1-hexadecyl-glycerol (2.23) were unsuccessful, yielding only starting materials, nevertheless in situ epoxidation experiments (Section 2.3.6(ii)) with this ligand indicated that bis(acetylacetonato)dioxomolybdenum(VI) was modified in its presence.

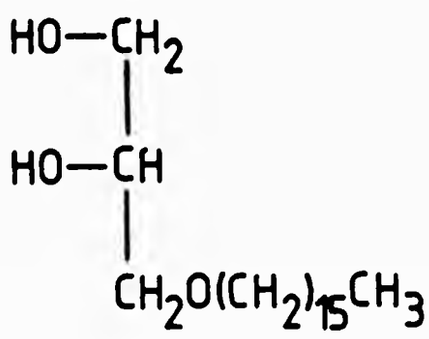

(2.23)

2.3.6 Epoxidation with Chiral Catalysts

Geraniol (2.24) was chosen as substrate for testing all catalyst systems because other workers have determined the specific rotation of 2,3-epoxygeraniol (2.25) thus enabling the optical purity of samples to be determined polarimetrically (Section 1.4) and also to compare the efficiency of our catalysts directly with those of other workers. Alternatively, instead of measuring the optical purity of the epoxide it could be converted to 2,3-epoxygeranyl acetate (2.26), thus permitting the enantiomeric excess to be determined with the aid of chiral nmr shift reagents as well as by polarimetric measurements, Sharpless _et al_[52] having established the specific rotation of the epoxyacetate.

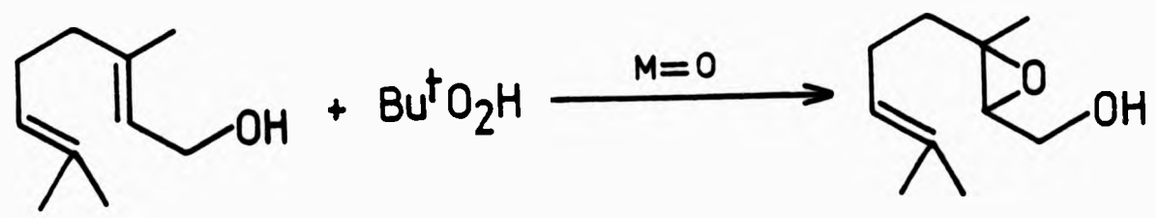

(2.24) (2.25)

(2.26)

Unless otherwise stated, epoxidations were carried out at 40°C in dry benzene in the presence of 1-2% catalyst using t-butyl hydroperoxide as the oxidant.

(i) Epoxidations with pre-formed chiral catalysts.

Epoxidations with vanadium containing catalysts are normally accompanied by the initial formation of a transient red colour on addition of hydroperoxide, associated with the oxidation of vanadium(IV) to vanadium(V) (Section 1.5.1). However, in epoxidations with NN^1-ethylenebis(iminomethyl-camphorato)oxovanadium(IV) (2.6) the original green reaction mixture merely faded to yellow on addition of hydroperoxide. Nevertheless, 2,3-epoxygeraniol was isolated in good yield after purification by column chromatography (Table 2.4, entry i). The product, judged to be pure by tlc, was laevorotatory with an enantiomeric excess of approximately 12%. On further purification by distillation the optical rotation decreased considerably suggesting that the rotation arose from contamination by ligand-containing material. This clearly demonstrates the serious problems involved in attempting to detect small asymmetric inductions in products isolated from catalysts containing ligands having high optical rotations. In this example, although the complex and the free ligand are both dextrorotatory the contaminant is laevorotatory and must therefore arise from decomposition of the catalyst under the reaction conditions.

[N(Cis,exo-2-hydroxybornyl)-3-salyclideniminato(2-)]-(methanolato)dioxomolybdenum(VI) (2.17a) was found to be stable under the epoxidising conditions by treatment of the complex with t-butyl hydroperoxide and epoxycyclohexane in refluxing cyclohexane. Spectroscopic properties of the isolated complex were identical to that of the starting material.

Epoxidation of geraniol in the presence of (2.17a) as catalyst, followed by acetylation and separation by column chromatography gave 2,3-epoxygeranyl acetate in low yield (Table 2.4, entry ii). This lower yield compared with that obtained from use of other complexes probably reflects the much lower solubility of this complex. Polarimetric measurements on the purified product indicated that no detectable asymmetric induction had taken place.

The corresponding complex derived from aminobutanol (2.21) was found to exhibit much greater solubility in benzene (in the presence of hydroperoxide) than the aminoborneol complex, and this is reflected in the increased yield of epoxide (Table 2.4, entry iii). Use of this complex however again failed to show any asymmetric induction in the product.

Cis-bis[D(-)-2,3-butandiolato-O,O^1(1-)]dioxomolybdenum(VI) (2.22) was found to be very soluble in benzene. Epoxidation of geraniol in the presence of this catalyst (Table 2.4, entry iv) followed by acetylation and purification by column chromatography gave laevorotatory 2,3-epoxygeranyl acetate which was judged free from contamination by ligand on the basis of glc and tlc analysis. From duplicate experiments the enantiomeric excess (ee) was determined polarimetrically as 16±1%. An attempt was made to confirm this result by ^1H nmr studies using the chiral nmr shift reagent, $Eu(hfc)_3$. Although some separation of the acetate methyl signal occured on addition of the shift reagent, it was not possible to completely separate the signals of the two enantiomers. Integration of the best separated signals (Fig. 2.2(b)) gave an enantiomeric excess of approximately 16%, which is

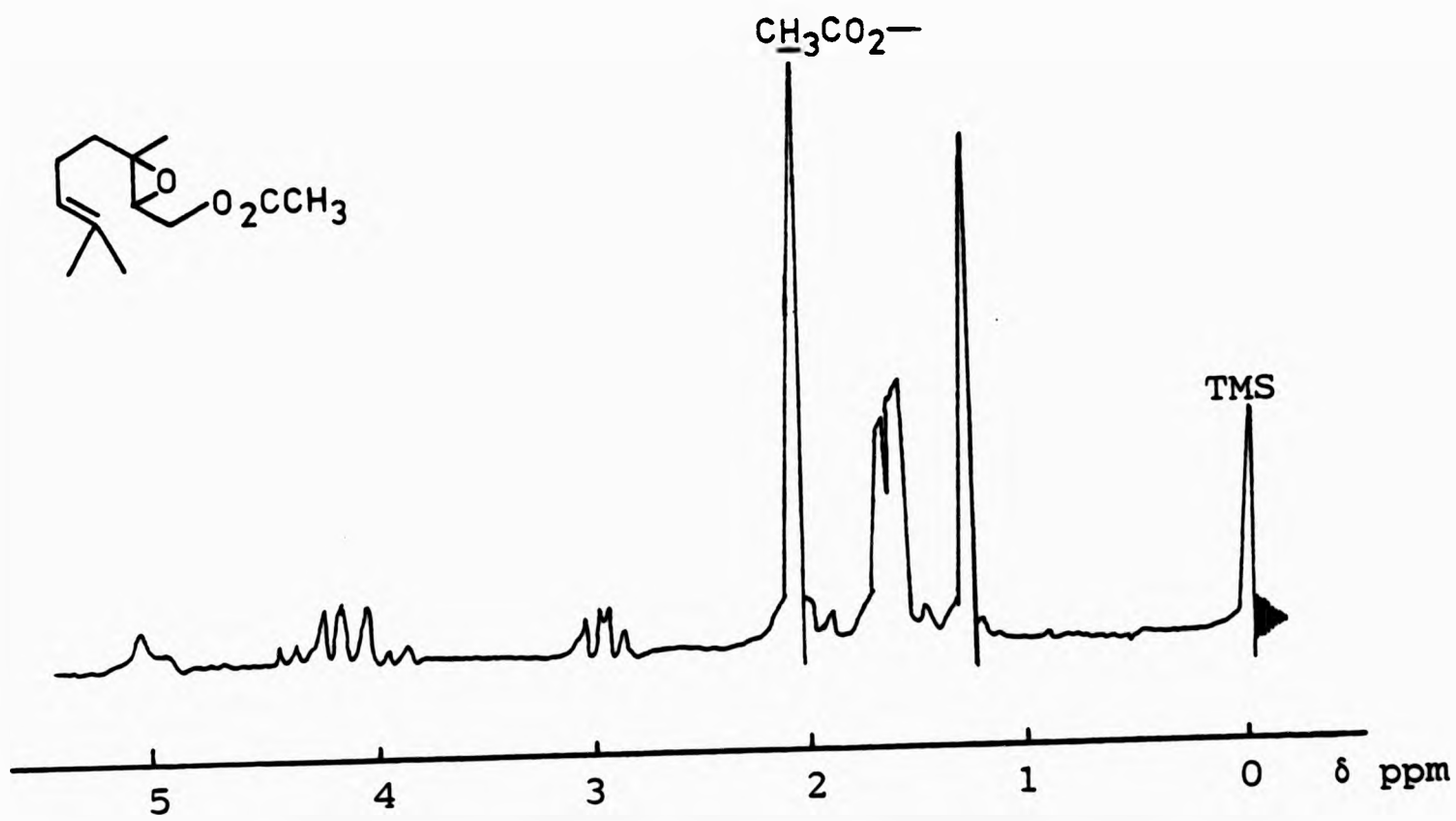

(a)

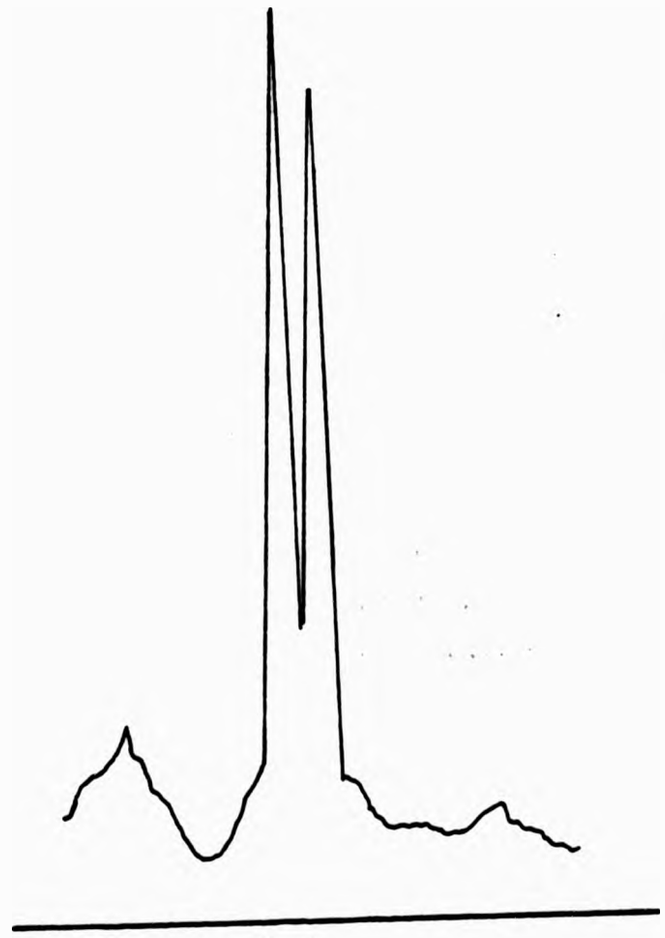

(b)

Fig. 2.2 (a) 60MHz ^1H nmr spectrum of 2,3-epoxygeranyl acetate prepared using MoO_2(D(-)-2,3-butandiol as catalyst.
(b) Acetate signal after addition of the chiral shift reagent, $Eu(hfc)_3$.

consistent with the result obtained by polarimetric methods.

Yamada *et al*[51] have shown, by correlation with R-(-)-linalool that (+)-2,3-epoxygeraniol has the absolute configuration 2(R),3(R). Sharpless *et al*[52] found that hydrolysis of (+)-2,3-epoxygeranyl acetate gives (-)-2,3-epoxygeraniol. From these observations we can conclude that the (-)-2,3-epoxygeranyl acetate obtained in the above process would give (+)-2,3-epoxygeraniol upon hydrolysis and thus has the absolute configuration 2(R),3(R).

(ii) Epoxidation with chiral catalysts prepared *in situ*.

Following the success of Sharpless *et al* in carrying out asymmetric epoxidations using as catalysts, chiral hydroxamic acid complexes of vanadium prepared *in situ* (Section 2.3.1) we have carried out epoxidations using bis(acetylacetonato)-dioxomolybdenum(VI),($MoO_2(acac)_2$) in the presence of chiral coordinating ligands which failed to give isolable complexes.

Epoxidations were carried out with a $MoO_2(acac)_2$: ligand ration of 1:5.

Epoxidation of geraniol catalysed by $MoO_2(acac)_2$ in the presence of the ligand *cis,exo*-3-amino-2-hydroxybornane (2.12) gave 2,3-epoxygeraniol in good yield (Table 2.4, entry v). Isolation of 2,3-epoxygeraniol which was completely free of ligand or ligand derived material presented difficulties. The product isolated from the reaction mixture by short-path distillation appeared by tlc and nmr to be pure and exhibited a significant optical rotation. Further purification by column chromatography however, resulted in a reduction in optical rotation, forcing us to conclude that the optical rotation was due only to trace ligand impurities.

Table 2.4. Epoxidation of geraniol using chiral catalysts

Catalyst	Product	°C	Chem. yield(%)	Opt. yield(%)
(i) 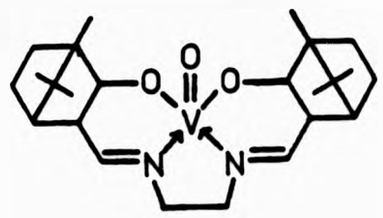 (2.6)	2.25	40	71	0
(ii) 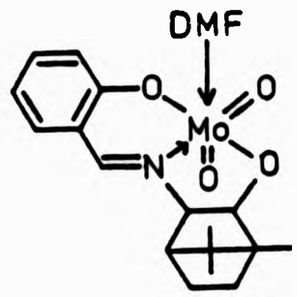 (2.17)	2.26	40	36	0
(iii) 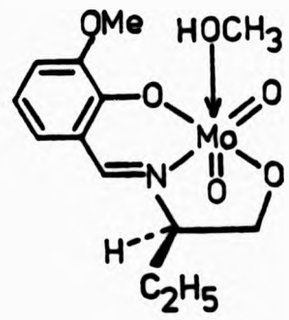 (2.21)	2.25	40	52	0
(iv) 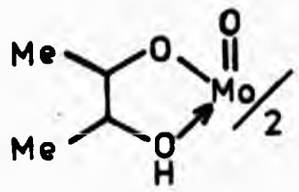 (2.22)	2.26	40	33	16
(v) $MoO_2(acad_2$ 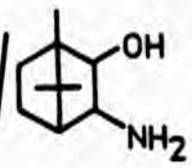	2.25	40 25	77	0
(vi) $MoO_2(acac)_2$ 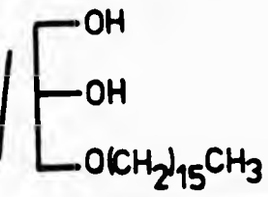	2.26	40	76	25

In general there is a greater chance of asymmetric inductions being obtained at lower reaction temperatures. Carrying out the above epoxidation at 20-25° increased the reaction time considerably but gave similar results.

Replacement of cis,exo-3-amino-2-hydroxybornane by the ligand L-1-hexadecylglycerol (2.23) gave 2,3-epoxygeranyl acetate after epoxidation and acetylation. After purification by column chromatography and preparative thin layer chromatography, the product was found to be laevorotary with an enantiomeric excess of 25% (Table 2.4, entry vi). Attempts to confirm this result using chiral nmr shift reagents were not very successful due to the difficulty of obtaining suitably separated signals for the two enantiomers, however, these results did support the predominance of one enantiomer.

As discussed previously (Section 2.3.1) Yamada et al[51] and Sharpless et al[52] have since reported the metal catalysed asymmetric epoxidation of geraniol, and obtained asymmetric inductions of 18% and 30%.

2.3.7 Epoxidation with chiral hydroperoxide.

In addition to the use of chiral catalysts for asymmetric epoxidation by achiral hydroperoxides, there exists the possiblity of using chiral hydroperoxides, either with achiral catalysts or in conjunction with chiral ones. Although such a process is formally similar to epoxidation by chiral peroxy acids it could provide a useful complementary technique, giving regio- and asymmetric epoxidation of allylic alcohols (Scheme 2.7).

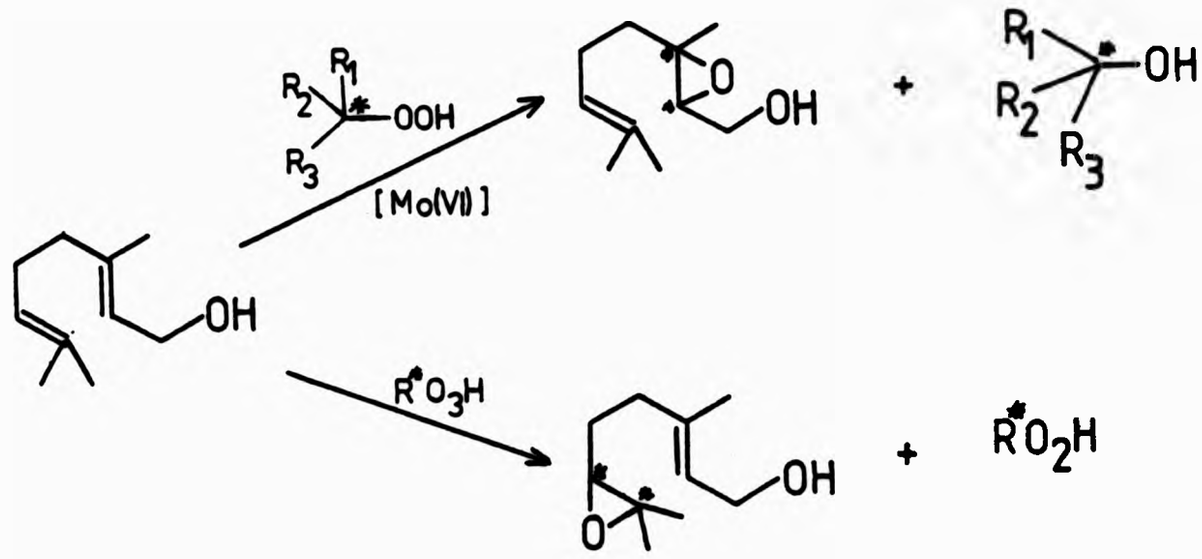

Scheme 2.7

Pinane hydroperoxide (2.27) was chosen as the chiral hydroperoxide since it is readily prepared by atmospheric oxidation of cis-pinane (2.28) at elevated temperatures.

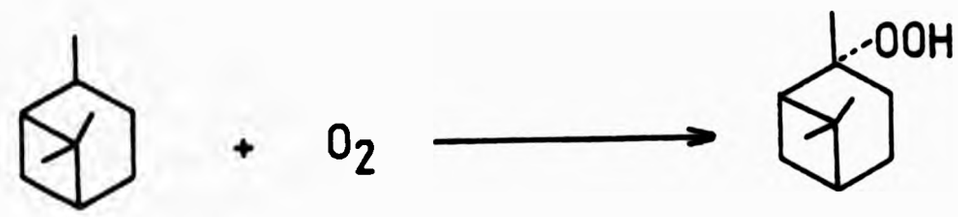

(2.28) (2.27)

Pinane hydroperoxide was used for the epoxidation of geraniol in the presence of the achiral catalysts bis(acetylacetonato)oxovanadium(IV), and bis(1,2-cyclohexandiolato)-dioxomolybdenum(VI) and also in the presence of the chiral [N-(cis,exo-2-hydroxybornyl)-3-methoxysalicylideniminato(2-)]-(methanolato)dioxomolybdenum(VI) (2.17b) and dioxobis-(D(-)-2,3-butandiolato)molybdenum(VI) (2.22) catalysts. Removal of all traces of pinane derived material from the

reaction product proved extremely difficult and in all cases some optical activity was observed. Nevertheless, although the results were not very conclusive, it appeared from the polarimetric measurements, considered in the light of the analytical purity (glc), and also from nmr studies using chiral shift reagents, that in all cases no significant asymmetric induction had taken place.

CHAPTER 3
ISOMERIZATION OF UNSATURATED ALCOHOLS

3.1 Introduction

Our studies of the oxo-metal catalyzed epoxidation of olefins resulted in the observation that these catalysts are capable of affecting the allylic isomerization of allylic alcohols. A detailed study of this reaction was therefore undertaken and is discussed in Chapter 4.

In the course of our investigations into the above isomerization a search of the literature revealed that other workers have extensively studied the rearrangement of tertiary propargylic alcohols to α,β-unsaturated carbonyl compounds in the presence of oxo-metal catalysts (Scheme 3.1). From a consideration of the proposed mechanism of this reaction we envisaged the possibility of developing a procedure for effecting ring closure based on diverting the normal course of reaction of the proposed intermediate. Attempts to obtain a number of cyclized products by this method is discussed in Chapter 5.

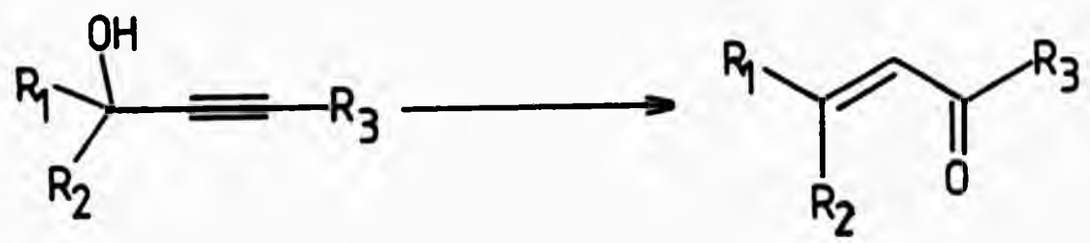

Scheme 3.1

This chapter is therefore devoted to a brief survey of existing methods for the isomerization of allylic (Section 3.2)

and propargylic (Section 3.3) alcohols in order to provide background for the investigations discussed in the subsequent chapters.

3.2 Isomerization of Allylic Alcohols

αβ-Unsaturated alcohols are able to undergo an allylic isomerization[90]. Such isomerizations occur when a functional group migrates from one end of an allylic system to the other (Scheme 3.2).

Allylic isomerizations are often reversible giving an equilibrium mixture of the two isomers.

Scheme 3.2

The allylic isomerization of allylic alcohols (X=OH) and their derivatives occupies a position of considerable importance in synthetic organic chemistry. In a synthesis the most readily accessible allylic isomer is often not the desired one, but if the desired isomer predominates at equilibrium, or is favoured under kinetically controlled conditions, an allylic isomerization may usefully be introduced into the synthetic strategy. The importance of transposing allylic oxygen functionality is reflected in its application to the synthesis of many natural products, notably in the total synthesis of Vitamin A[91]. There are

many other examples in the field of alkaloid,[92] terpene[93] and steroid[94] synthesis.

3.2.1 Equilibria in allylic systems

As mentioned previously, allylic isomerizations are often reversible and in such cases the equilibrium constant(K) between the two allylic isomers depends on the free energy difference (ΔG) between the two isomeric structures as expressed in the equation;

$$\Delta G = -RT \ln K$$

The effect on the equilibrium constant of substituents attached to the C_α, C_β and C_γ positions can be considered in terms of differences in enthalpy between the two isomers. Substituents on the double bond generally have a stabilising effect which is reflected in the heat of hydrogenation or combustion of unsaturated compounds. For mono-olefins the rate of hydrogenation of a double-bond is found to decrease with increasing alkyl substitution, indicating an increase in stability with increasing alkyl substitution. In the isomerization of alkyl substituted allylic systems, it would therefore be expected that the equilibrium would favour the isomer in which the double bond is most substituted. Although this is generally accepted to be the case, there appears to be no systematic experimental information on the position of equilibrium of alkyl substituted allylic systems. Substituents attached to the C_β position should have little effect since they would be expected to stabilize the double bond to the same

extent in the two isomers.

Aryl groups attached to the double bond stabilize it by conjugation. Thus the equilibrium between 1-phenylallyl and cinnamyl compounds (Scheme 3.3) appears to be displaced almost entirely in the direction of the latter isomer[95].

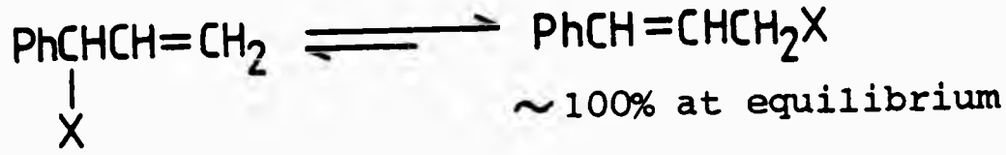

Scheme 3.3

Spectroscopic studies[95b] have indicated that in systems in which phenyl and methyl groups compete for stabilization of the double bond (Scheme 3.4) the equilibrium favours the phenyl group by a factor of at least 10:1. This implies a free energy difference in stabilizing power between the phenyl and methyl groups of at least 1.6 Kcal/mol.

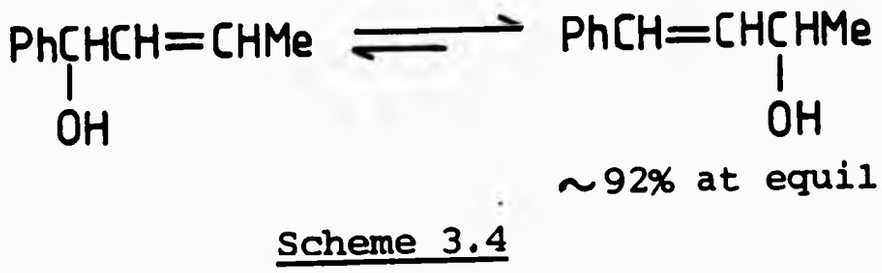

Scheme 3.4

Substitution in the aryl group does not have a very large effect on the position of equilibrium although extension of the conjugated system, for example by a p-nitro group, may displace the equilibrium slightly further in favour of the isomer with the aryl substituent

extent in the two isomers.

Aryl groups attached to the double bond stabilize it by conjugation. Thus the equilibrium between 1-phenylallyl and cinnamyl compounds (Scheme 3.3) appears to be displaced almost entirely in the direction of the latter isomer[95].

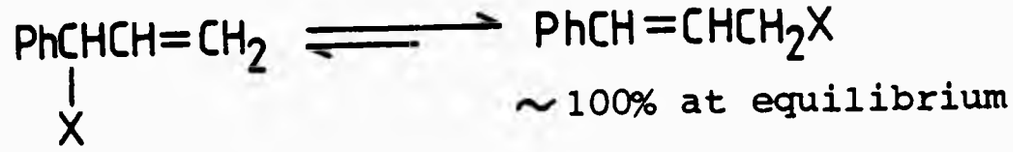

Scheme 3.3

Spectroscopic studies[95b] have indicated that in systems in which phenyl and methyl groups compete for stabilization of the double bond (Scheme 3.4) the equilibrium favours the phenyl group by a factor of at least 10:1. This implies a free energy difference in stabilizing power between the phenyl and methyl groups of at least 1.6 Kcal/mol.

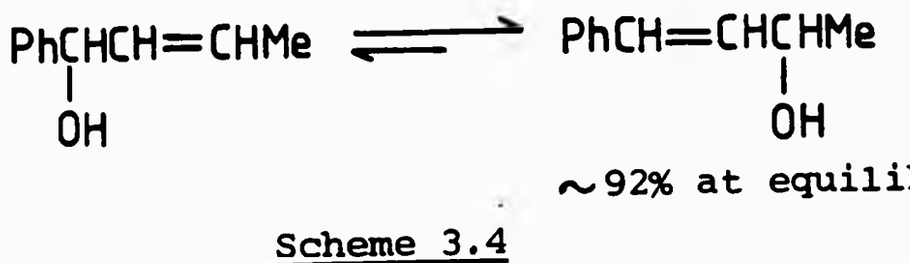

Scheme 3.4

Substitution in the aryl group does not have a very large effect on the position of equilibrium although extension of the conjugated system, for example by a p-nitro group, may displace the equilibrium slightly further in favour of the isomer with the aryl substituent

extent in the two isomers.

Aryl groups attached to the double bond stabilize it by conjugation. Thus the equilibrium between 1-phenylallyl and cinnamyl compounds (Scheme 3.3) appears to be displaced almost entirely in the direction of the latter isomer[95].

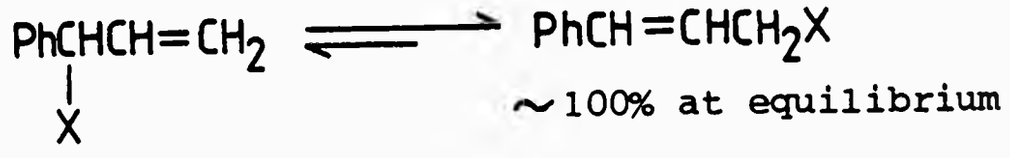

Scheme 3.3

Spectroscopic studies[95b] have indicated that in systems in which phenyl and methyl groups compete for stabilization of the double bond (Scheme 3.4) the equilibrium favours the phenyl group by a factor of at least 10:1. This implies a free energy difference in stabilizing power between the phenyl and methyl groups of at least 1.6 Kcal/mol.

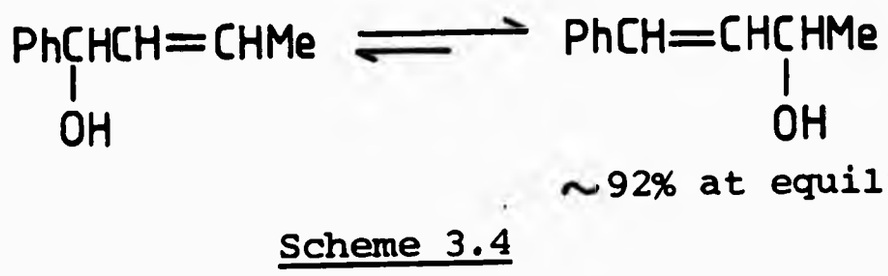

Scheme 3.4

Substitution in the aryl group does not have a very large effect on the position of equilibrium although extension of the conjugated system, for example by a p-nitro group, may displace the equilibrium slightly further in favour of the isomer with the aryl substituent

on the double bond.

Stabilization by conjugation will also occur when the allylic system is substituted with other unsaturated groups. Under equilibrium conditions the allylic double bond will move into conjugation with double and triple bonds[96] and possibly with carbonyl groups[97] (Scheme 3.5) although in the case shown, determination of the position of equilibrium was complicated by cyclization of the product.

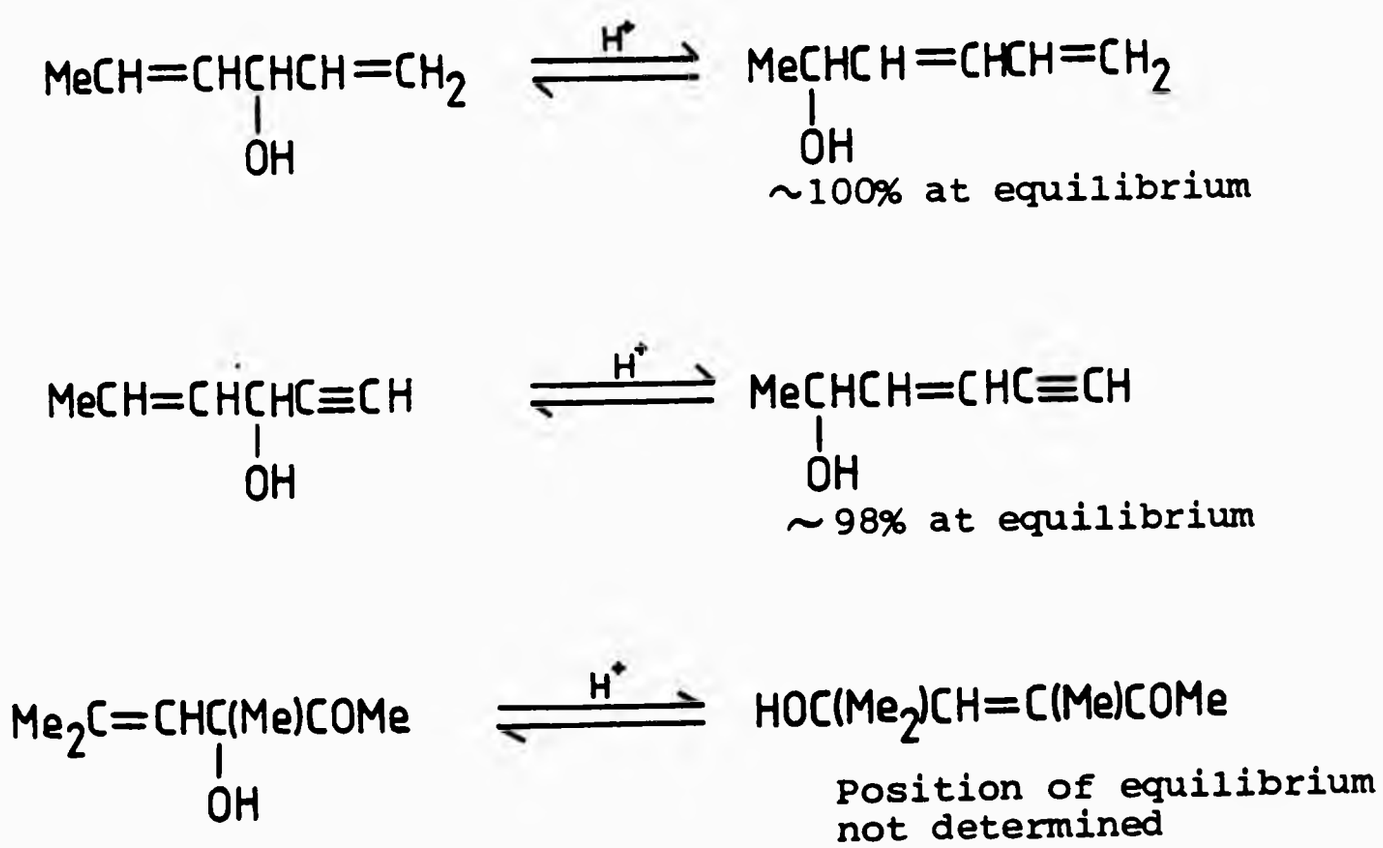

Scheme 3.5

In cyclic systems the structural principles governing the position of equilibrium as discussed above,may be modified by ring strain and conformational preference. Normally, however, conjugation is still a dominant influence[98] (Scheme 3.6).

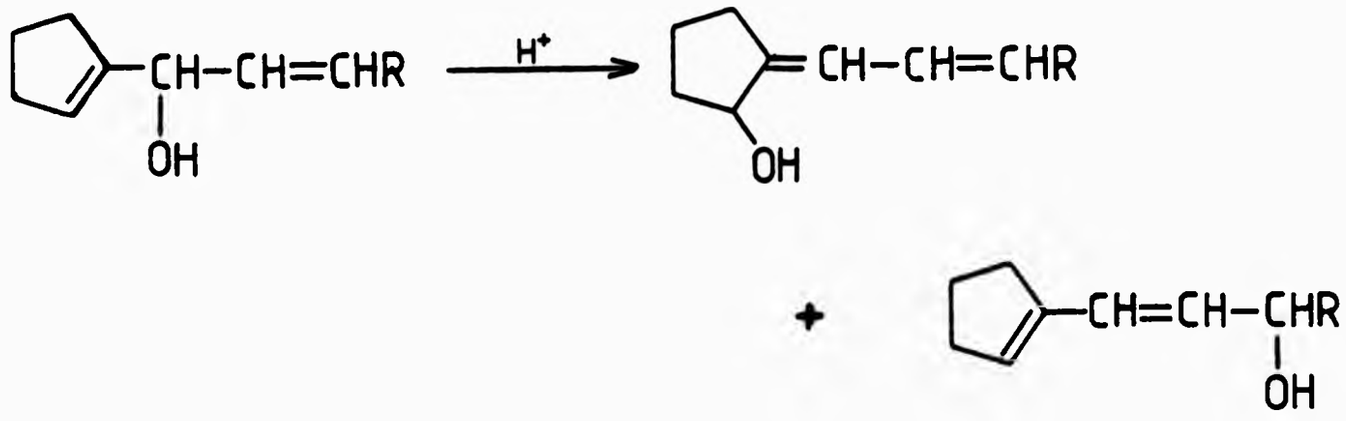

Scheme 3.6

In cyclic systems in which rearrangement would involve migration of an endocyclic double bond to an exocyclic position or vice versa the reaction proceeds in such a manner as to avoid the formation or retention of an exo double bond in a six-membered ring system[99]. Thus the alcohol (3.1) has been shown to be more thermodynamically stable than its isomer (3.2) and rearranges to give only a small amount of the latter[100].

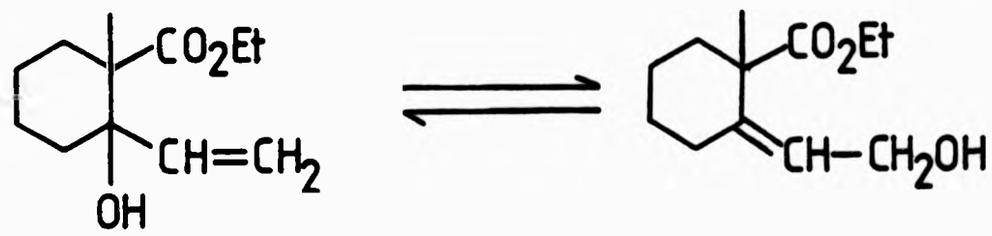

(3.1) (3.2)

3.2.2 Isomerization promoted by acid catalysts

The isomerization of allylic alcohols rarely occurs at a measurable rate in the absence of catalysts and is normally carried out in the presence of strong protic or Lewis acids[90]. The rapid rearrangement of linalol to a

mixture of products which included geraniol was recognized as early as the 1890's by Barbier while investigating the action of acetic anhydride on the former alcohol[101].

The requirement of acid-catalysis in allylic alcohol isomerizations implies the intermediate formation of the conjugate acid of the alcohol (oxonium ion), ROH_2^+. Protonation of the hydroxyl group weakens the carbon-oxygen bond and removes the necessity for the separation of opposite charges in the transition state.

The mechanism of the reaction and the effects of substituents on the rate of acid catalysed isomerization have been extensively reviewed[90]. Three possible mechanisms for the acid-catalysed isomerization of allylic alcohols have been recognized (Scheme 3.7).

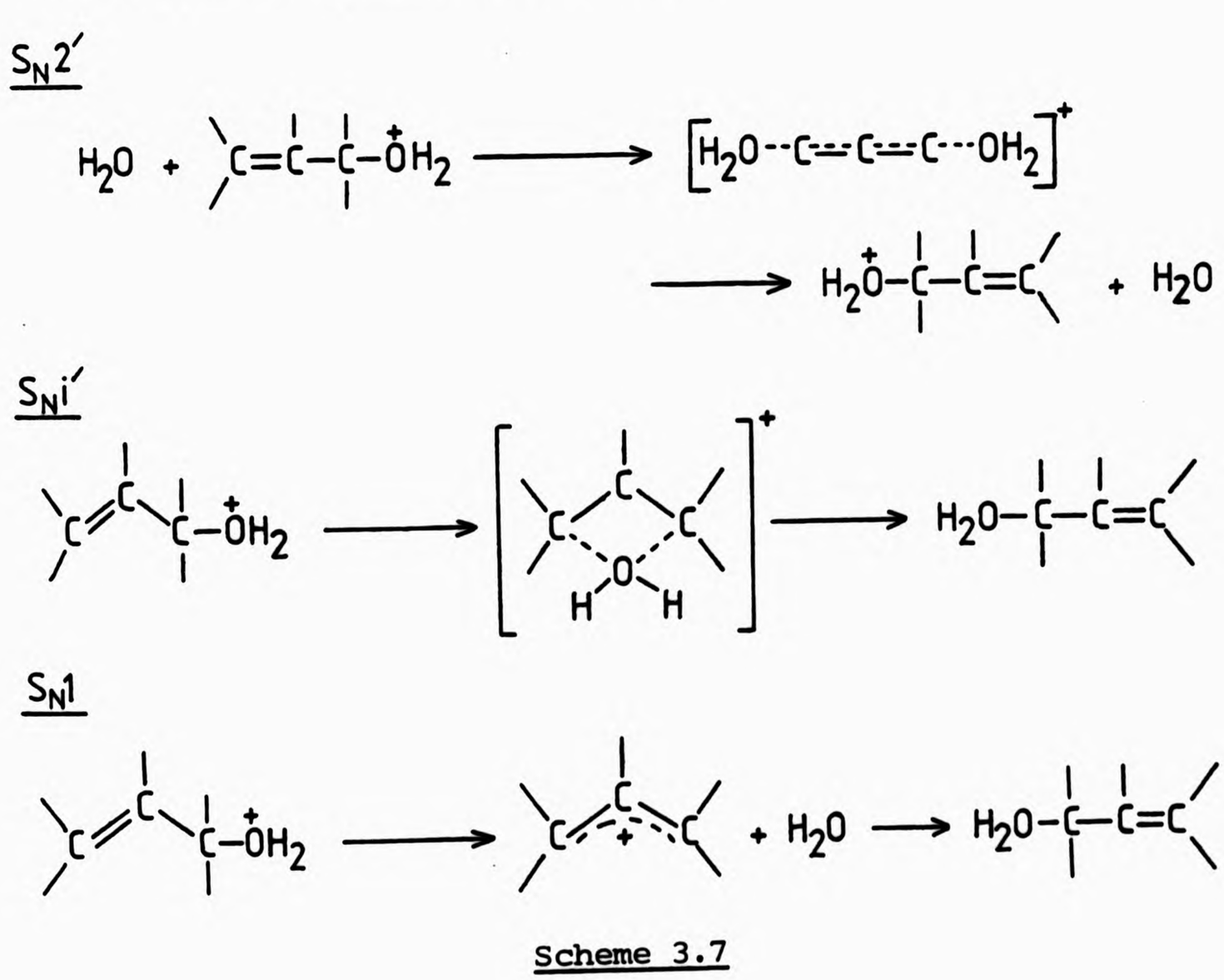

Scheme 3.7

In principle, there is no sharp dividing line between the bimolecular and unimolecular mechanisms since they differ only in the degree of nucleophilic interaction of water with the developing carbonium ion. Similarly, the S_N1 and S_Ni' mechanisms may be viewed as extremes of the bond breaking and bond making process in the transition state. From the data available on allylic alcohol isomerization, particularly that concerned with substituent effects on rates, a unimolecular mechanism is favoured, with considerable carbonium ion character in the transition state.

Allylic alcohols with only one alkyl substituent on the α- or γ- position require prolonged treatment with mineral acids at elevated temperatures to isomerize (conditions which may also cause simultaneous formation of ethers, dienes and carbonyl compounds)[102], whereas α,α- and γ,γ-dialkyl substituted allylic alcohols require less severe conditions, e.g. 1% aqueous sulphuric acid for 60h. at room temperature[103]. Methyl substituents increase the rate of isomerization in the order γ>α>β[96a,97,104]. Unsaturated substituents on the α-carbon atom also increases the rate of isomerization[105], as do aryl substituents which can release electrons into the allylic system[90]. Electron withdrawing substituents, however, decrease the rate of isomerization[90].

Esters of allylic alcohols also undergo acid-catalysed isomerization. These reactions are formally similar to the acid-catalysed allylic alcohol isomerizations in that they are believed to involve alkyl-oxygen cleavage of the protonated ester molecule (Scheme 3.8). In principle, all the mechanistic pathways available in the acid-catalysed

alcohol isomerization are also available to the acid-catalysed ester isomerization. The degree of association of the carboxylic acid molecule and the carbonium ion is dependent on the substrate and the reaction conditions.

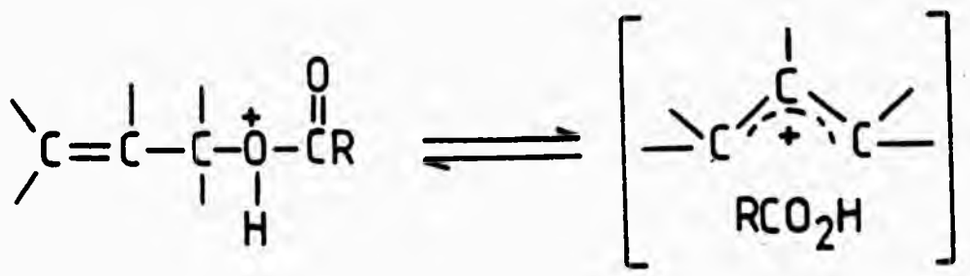

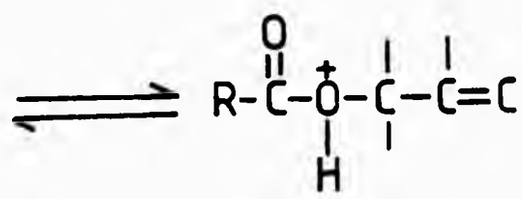

Scheme 3.8

From a synthetic point of view, these procedures often lack selectivity giving low yields of rearranged products. This lack of selectivity results from the ability of the allyl cation (or ion-pair) intermediate to undergo a number of side reactions such as elimination to dienes[90,94a,b,106], skeletal rearrangement[90,107] and cyclization[90,108], and this often leads to the formation of resinous products[90,106a]. Some success in suppressing these side reactions by using more selective protic acid mixtures has been reported. Thus an acetic acid / acetic anhydride / p-toluenesulphonic acid mixture gave the rearranged acetates in 65-90% yield[108c].

In addition to acid-catalysed isomerization, allylic esters undergo thermal allylic isomerization and the mechanism of this rearrangement is discussed in Section 4.3.

3.2.3 Isomerization promoted by catalysts other than acids

Although acid catalysed isomerization has been known for almost a century, it is only relatively recently that there has been development of other catalytic methods which are more specific, often giving no side reactions.

Charbardes et al[109] have reported the isomerization of allylic tertiary alcohols to allylic primary and secondary alcohols usually in low yield (Table 3.1) in the presence of catalytic amounts of oxo-vanadium(V) compounds of the type $(RO)_3VO$, where RO is either an alkoxy or siloxy group. This reaction has not attracted a great deal of interest, unlike the oxo-metal catalysed rearrangement of propargylic alcohols which has been extensively studied (Section 3.3.2). The mechanism of the isomerization (discussed in detail in Section 4.3) is thought to proceed via formation of the vanadate ester of the allylic alcohol.

Overmans' report[110] that mercury(II) salts will promote the rearrangement of trichloroacetimidic esters of allylic alcohols to the corresponding trichloroacetamide (Scheme 3.9) was the first reported mercuric ion catalysed [3,3]-sigmatropic rearrangement.

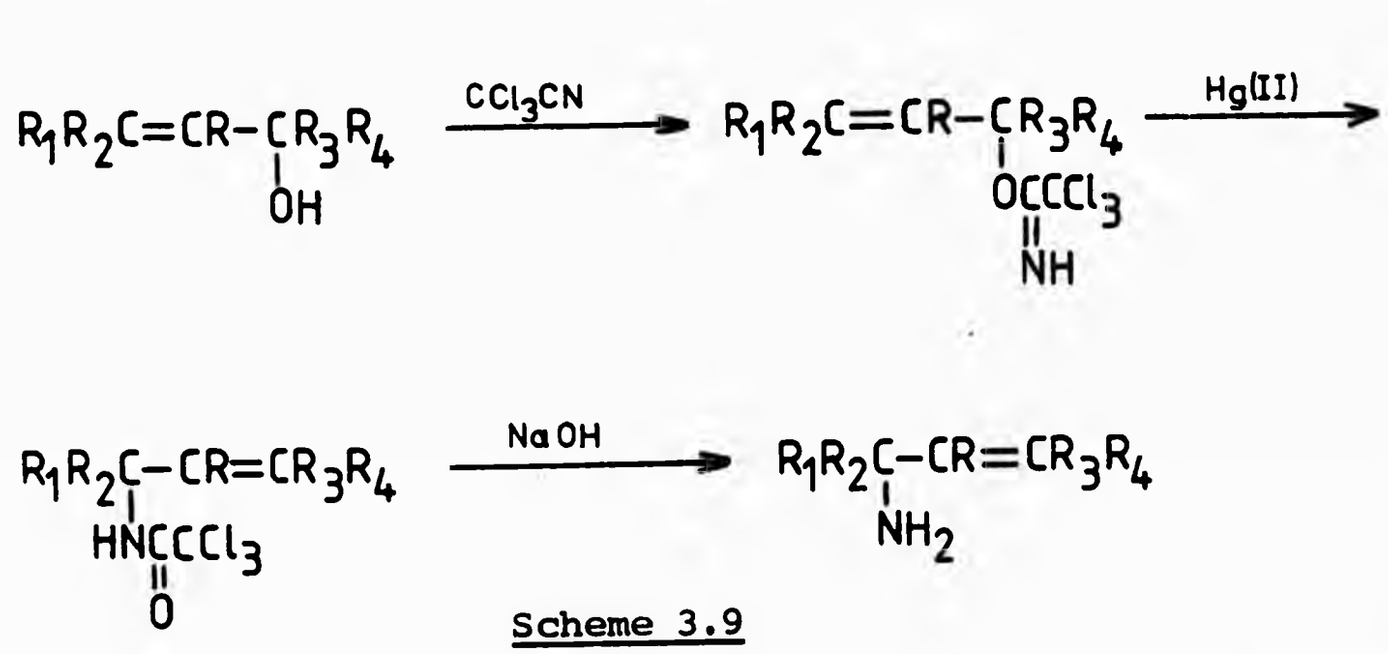

Scheme 3.9

Table 3.1 Vanadate ester catalysed allylic alcohol isomerisation.

Starting alcohol	Isomers obtained	% Conversion
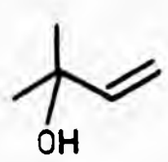	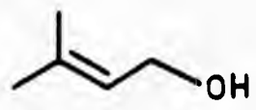	26
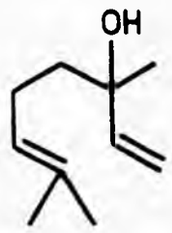	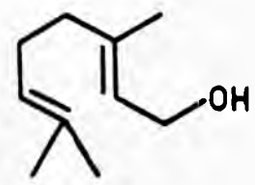	30
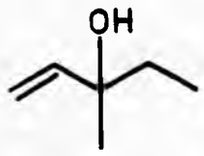	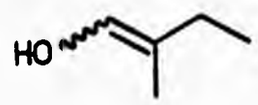	19
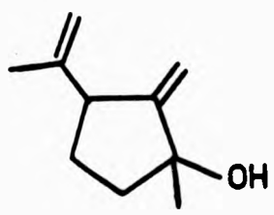	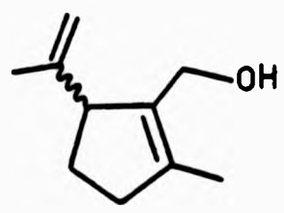	68

Reactions were carried out in the absence of solvent using catalyst concentrations of approximately 1 mol %. Reaction temperatures were 130-160 deg. C and reaction times varied between 30 min and 7h.

Table 3.1 Vanadate ester catalysed allylic alcohol isomerisation.

Starting alcohol	Isomers obtained	% Conversion
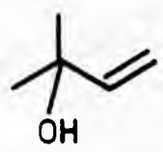	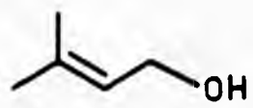	26
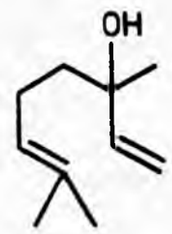	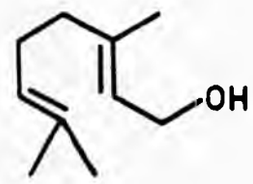	30
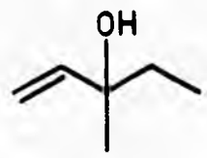	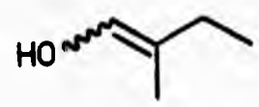	19
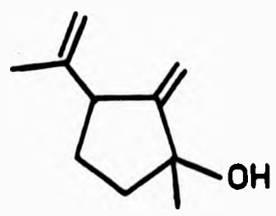	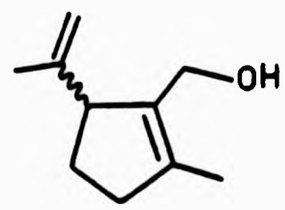	68

Reactions were carried out in the absence of solvent using catalyst concentrations of approximately 1 mol %. Reaction temperatures were 130-160 deg. C and reaction times varied between 30 min and 7h.

Since these transformations were not believed to involve allyl cation or related intermediates it was anticipated that a similar technique applied to the allylic equilibration of oxygen functionality would likely avoid many of the side reactions encountered in the "classical" acid-catalysed methods. Overman et al have, therefore, recently described the equilibration of NN-dimethylcarbamate esters of allylic alcohols in the presence of mercuric trifluoroacetate[111] (Scheme 3.10).

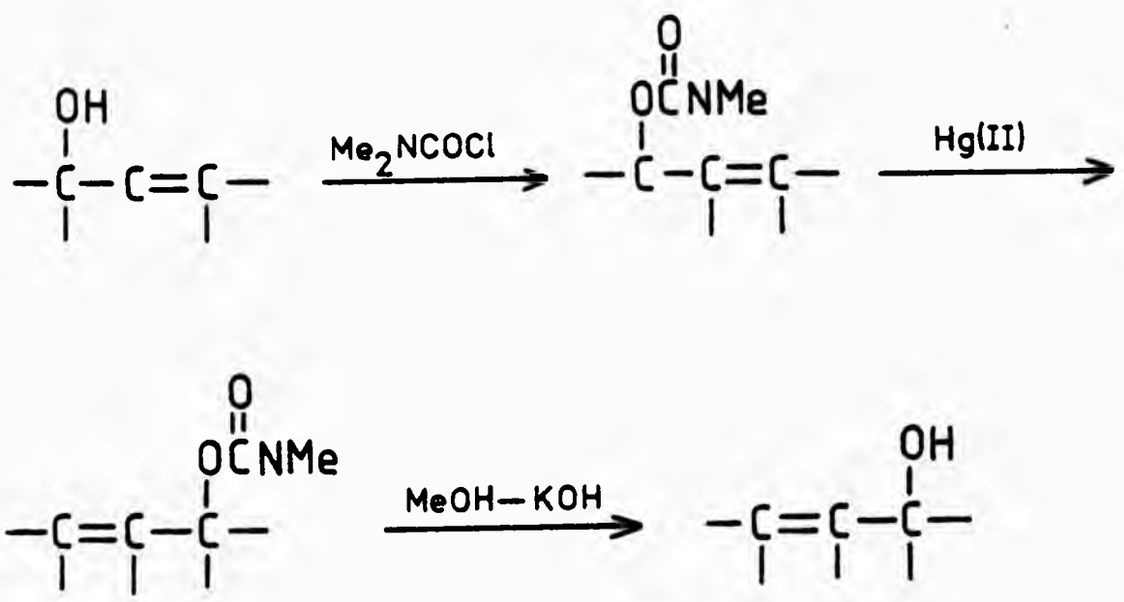

Scheme 3.10

Initial studies with hexenyl carbamate (Scheme 3.11) indicated that oxygen equilibrations were possible in high yield under mild conditions if mercuric trifluoroacetate is employed at low concentrations and the mercuric catalyst is removed by complexation with Ph_3P before product isolation.

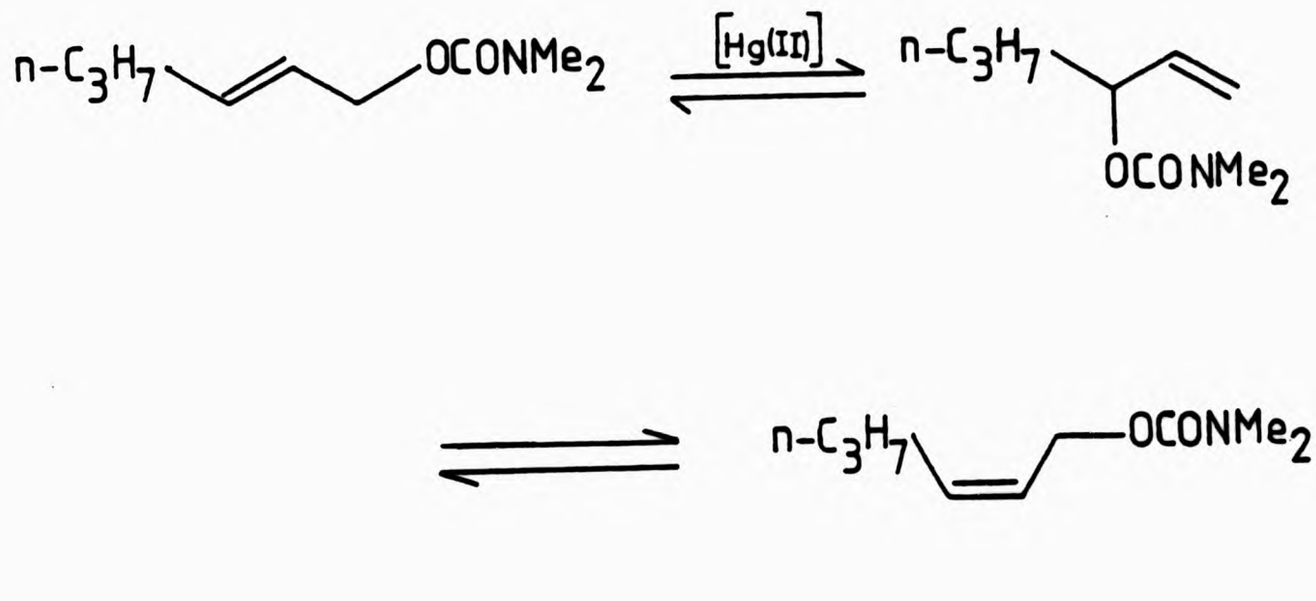

Scheme 3.11

This method was applied to the preparative scale isomerization of a number of tertiary allylic carbamates and these results are summarized in Table 3.2. The starting carbamaic esters were prepared from the corresponding alcohols and dimethylcarbamyl chloride. In all cases isomerization was achieved within a few hours at room temperature. Isolated yields were often greater than 90% and in no case was cyclization or hydrogen, alkyl or aryl migration detected.

The mechanism of the rearrangement was studied and a "cyclisation-induced rearrangement" proposed (Scheme 3.12) in which the mercuric trifluoroacetate interacts with the carbon-carbon π-bond to promote an intramolecular cyclisation to give a cyclic intermediate. Fragmentation of this cyclic intermediate in the alternate sense then gives the rearranged product.

Table 3.2 Mercuric trifluoroacetate catalysed allylic carbamate rearrangement.

Starting carbamate	Products (isolated yield)
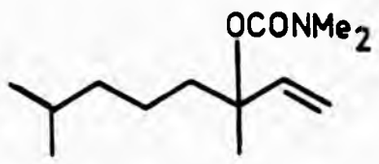	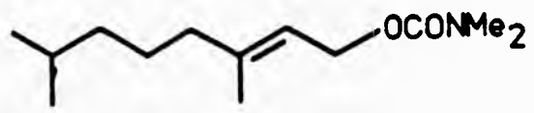 (92%)
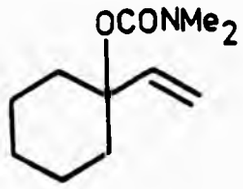	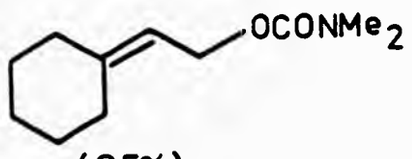 (95%)
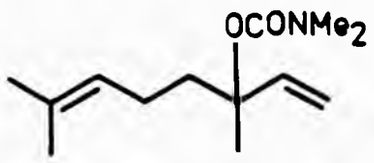	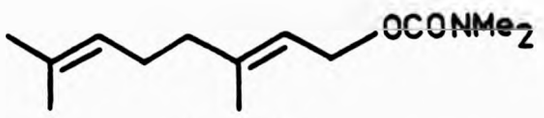 (70%)
	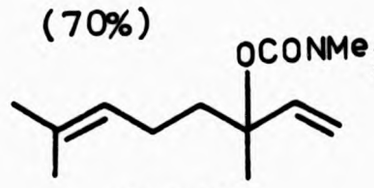 (16%)
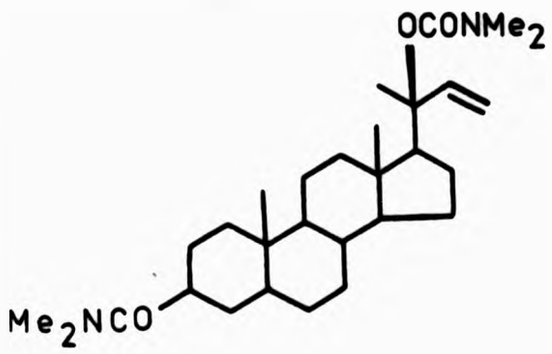	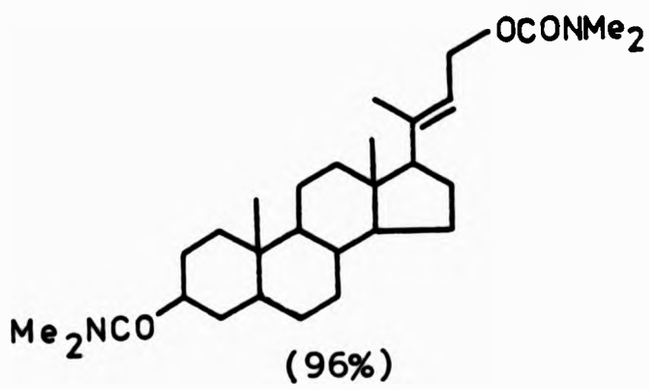 (96%)
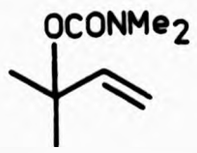	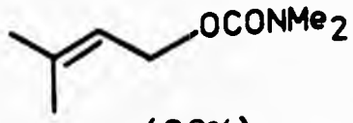 (98%)

Reactions were carried out in THF at room temperature with 0.3 equiv. of catalyst.

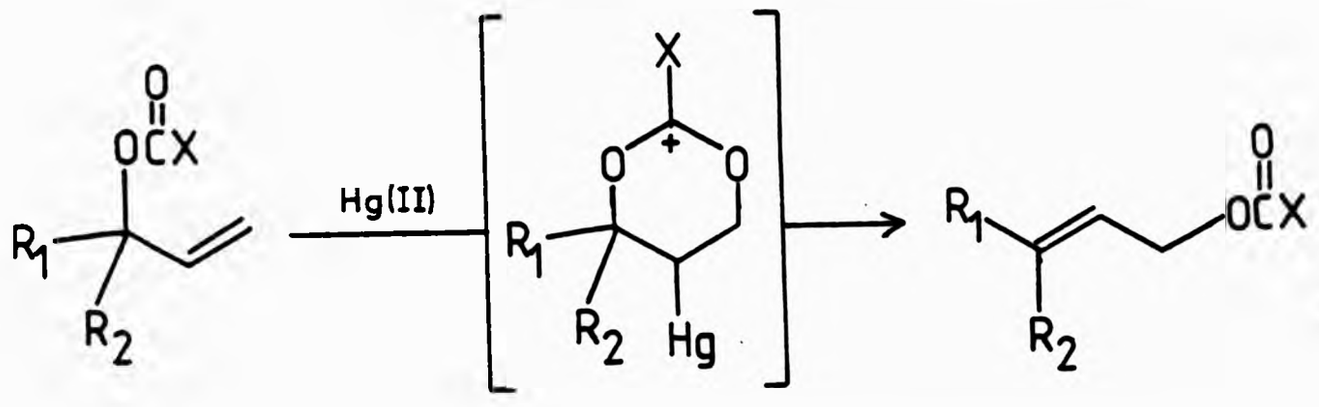

Scheme 3.12

Contrathermodynamic isomerizations were also achieved in a number of cases by using an excess of mercuric trifluoroacetate. The formation constants for covalent alkene-mercuric trifluoroacetate adducts decrease with increasing double bond substitution thus the excess catalyst traps the terminal alkene isomer as a covalent adduct and removes it from the equilibrium. At the end of the reaction the mercury(II)-adduct is destroyed with triphenylphosphine to yield an isomer mixture enriched in the less stable product (Scheme 3.13).

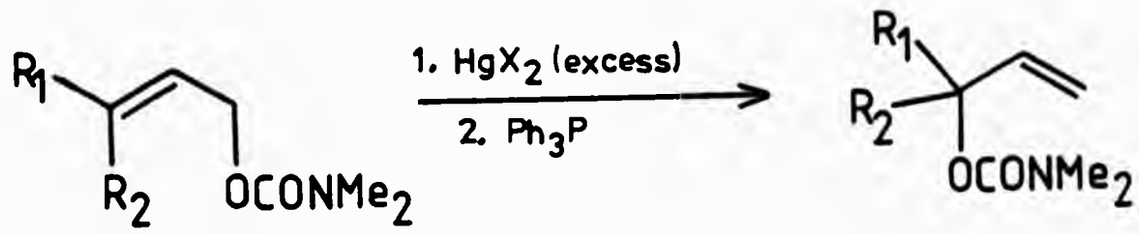

Scheme 3.13

Overmann et al have also studied[112] the equilibration of allylic esters in the presence of metal catalysts and found that soluble palladium(II) salts are more effective than mercuric trifluoroacetate. In particular, catalytic amounts of bis(acetonitrile)palladium(II) chloride were found to cause rearrangement of allylic acetates at room temperature in high yields (Table 3.3) and the reactions are highly E-stereoselective. Thus trans-cinnamyl acetate (3.4) was produced with an isomeric purity of 98%, and the 78:22 E:Z ratio observed for 3,7-dimethyl-2-octen-1-ol (3.3) is higher than would be expected for allylic esters of this type.

As methods for allylic alcohol rearrangement,both the mercury(II)-catalyzed isomerization of carbamate esters and the palladium(II)-catalyzed isomerization of acetate esters are synthetically important, since strongly acidic conditions are not required. However, the disadvantage of both methods is that the ester intermediates must first be prepared and ultimately cleaved. As a result, for allylic alcohols for which acid-catalyzed isomerization succeeds, these more complex and expensive processes offer no practical advantages. However, in cases where skeletal rearrangement, cyclization or elimination can occur or where intramolecular allylic oxygen transfer offers stereochemical advantages, these alternative procedures become the method of choice.

3.3 Isomerization of Propargylic Alcohols

Propargylic systems like allylic ones can undergo rearrangement under a variety of conditions and with various catalysts (Scheme 3.14).

Table 3.3 Palladium(II)-catalysed allylic acetate rearrangements.

Starting acetate	Product	Yield (%)
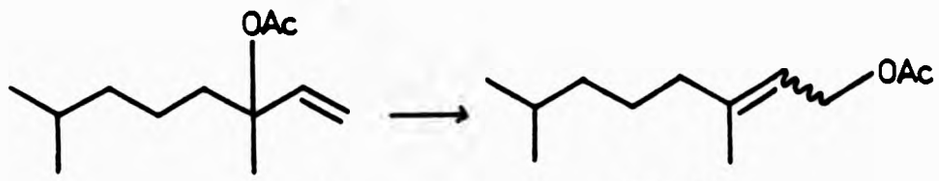	(3.3)	88
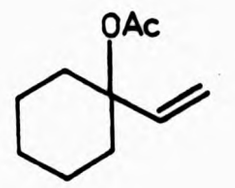	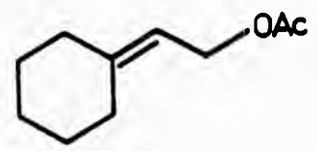	93
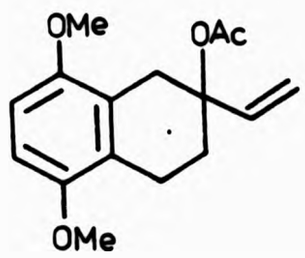	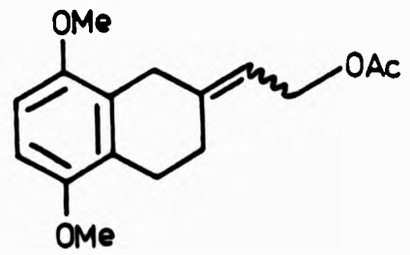	87
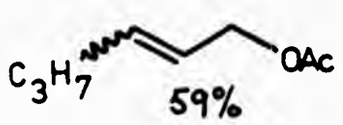	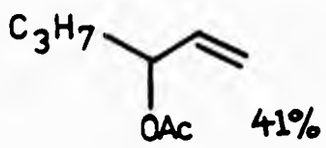	95
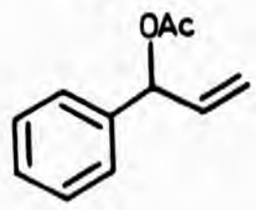	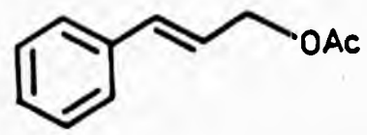 (3.4)	96

Reactions were carried out in THF at room temperature using 0.04 equiv. of catalyst.

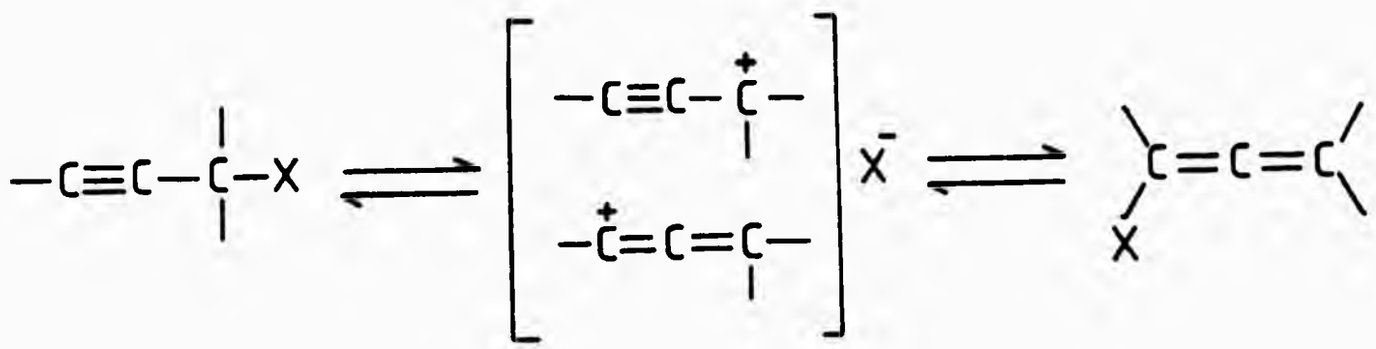

Scheme 3.14

3.3.1 Isomerization by acid catalysts

The acid-catalyzed isomerization of acetylenic tertiary alcohols of α,β-unsaturated carbonyl compounds has been known since the 1920's and a wide variety of acidic catalysts have been employed[113]. However, those most commonly used are formic acid, in concentrations of from 70 to 97%, and mixtures of sulphuric and acetic acid.

Acid-catalyzed isomerization of acetylenic tertiary alcohols may occur by two routes which give different products. In the Rupe rearrangement[114] (Scheme 3.15) a 1,2-oxygen shift occurs. Protonation of the alcohol leads to dehydration with formation of a tertiary carbonium ion which expels a proton from an adjacent carbon atom giving the vinylacetylene intermediate (3.5). Further protonation of this intermediate gives a secondary carbonium ion which on work-up eventually gives the α,β-unsaturated ketone (3.6).

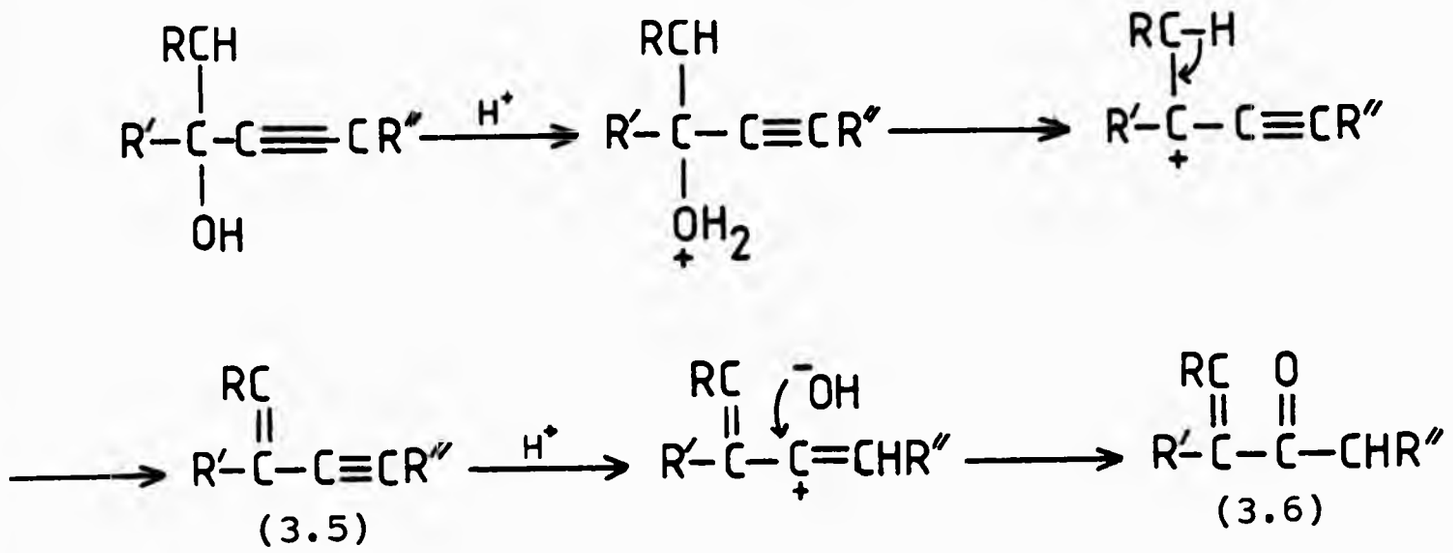

Scheme 3.15

An alternative acid catalyzed rearrangement, the Meyer-Schuster rearrangement involves a 1,3-oxygen shift resulting from a dehydration — hydration sequence with formation of an allene intermediate[114] (Scheme 3.16).

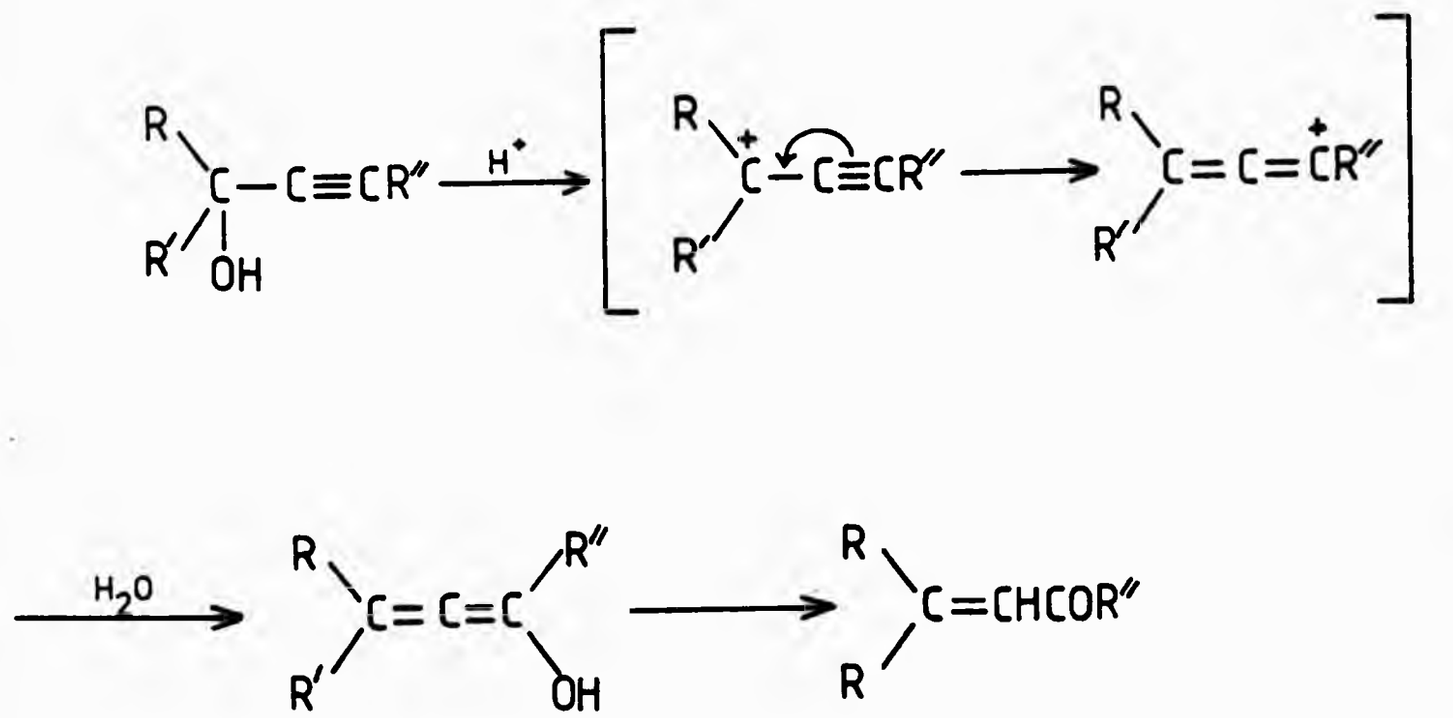

Scheme 3.16

In the Rupe rearrangement the product is always a ketone, whereas in the Meyer-Schuster rearrangement the product can be either an aldehyde or ketone, i.e if the acetylenic group is terminal the product is an aldehyde, otherwise a ketone is produced.

3.3.2 Alternative methods of isomerizing acetylenic tertiary alcohols.

A serious disadvantage of the acid-catalyzed rearrangement of acetylenic tertiary alcohols is that it often leads to formation of complex mixtures of products. Isomerizations in several stages, using various intermediates derived from the alcohol, are often more specific.

Acetate esters of acetylenic tertiary alcohols rearrange on pyrolysis to give allene acetates as the major product. Thus on pyrolysis 1-ethynyl-2,2,6-trimethylcyclohexyl acetate gave the allene acetate (3.7) and the enyne (3.8)[115].

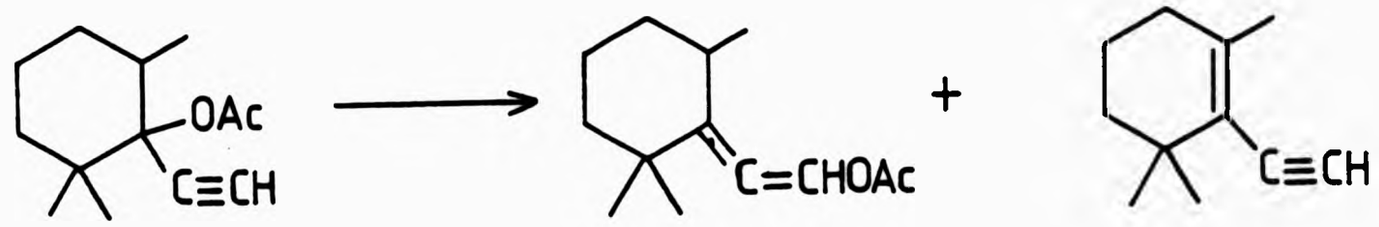

(3.7) (3.8)

The mechanism of the rearrangement of acetate esters of acetylenic alcohols to allenic acetates is thought to involve formation of a six-membered cyclic transition state (3.9)

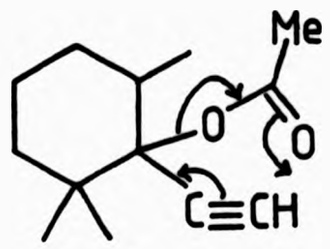

(3.9)

Isler et al[116] have established that such acetates readily undergo rearrangement when heated in glacial acetic acid in the presence of copper powder or salts of copper or silver. The corresponding allene acetates are obtained in almost quantitative yield and give the α,β-unsaturated carbonyl compound on hydrolysis (Scheme 3.17).

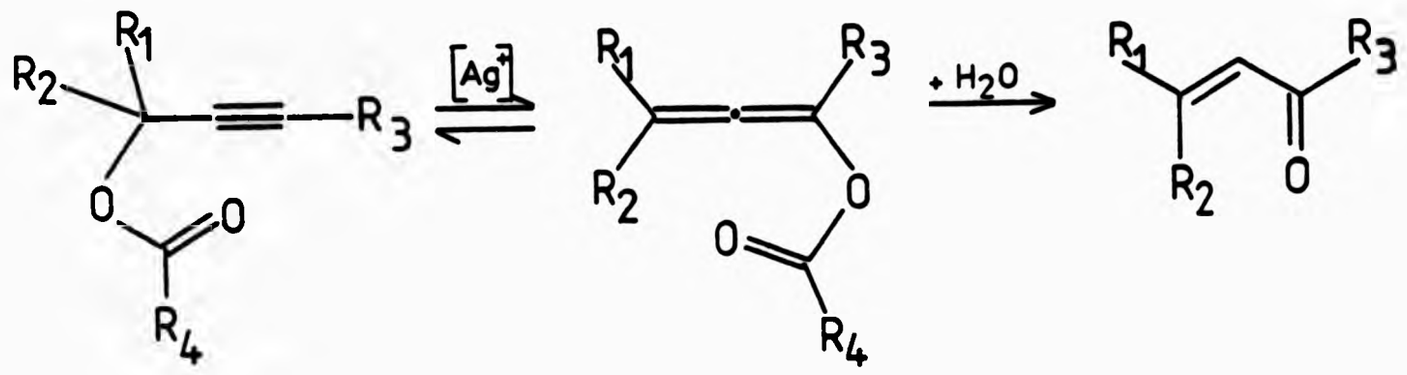

Scheme 3.17

Schmid et al[117] have studied the mechanism of the reversible propargyl ester-allenyl ester rearrangement by silver ions using optically active and diastereoisomeric esters as well as ^{14}C and ^{18}O labelled compounds. From their experiments they concluded that the rearrangement can be described as a [3s,3s]-sigmatropic reaction occuring in a silver(I)-π-complex with the triple bond of the acetylene and a double bond of the allene. As shown in Scheme 3.18, complex formation is thought to occur between the silver ion and the π-bond not directly involved in forming the cyclic transition state.

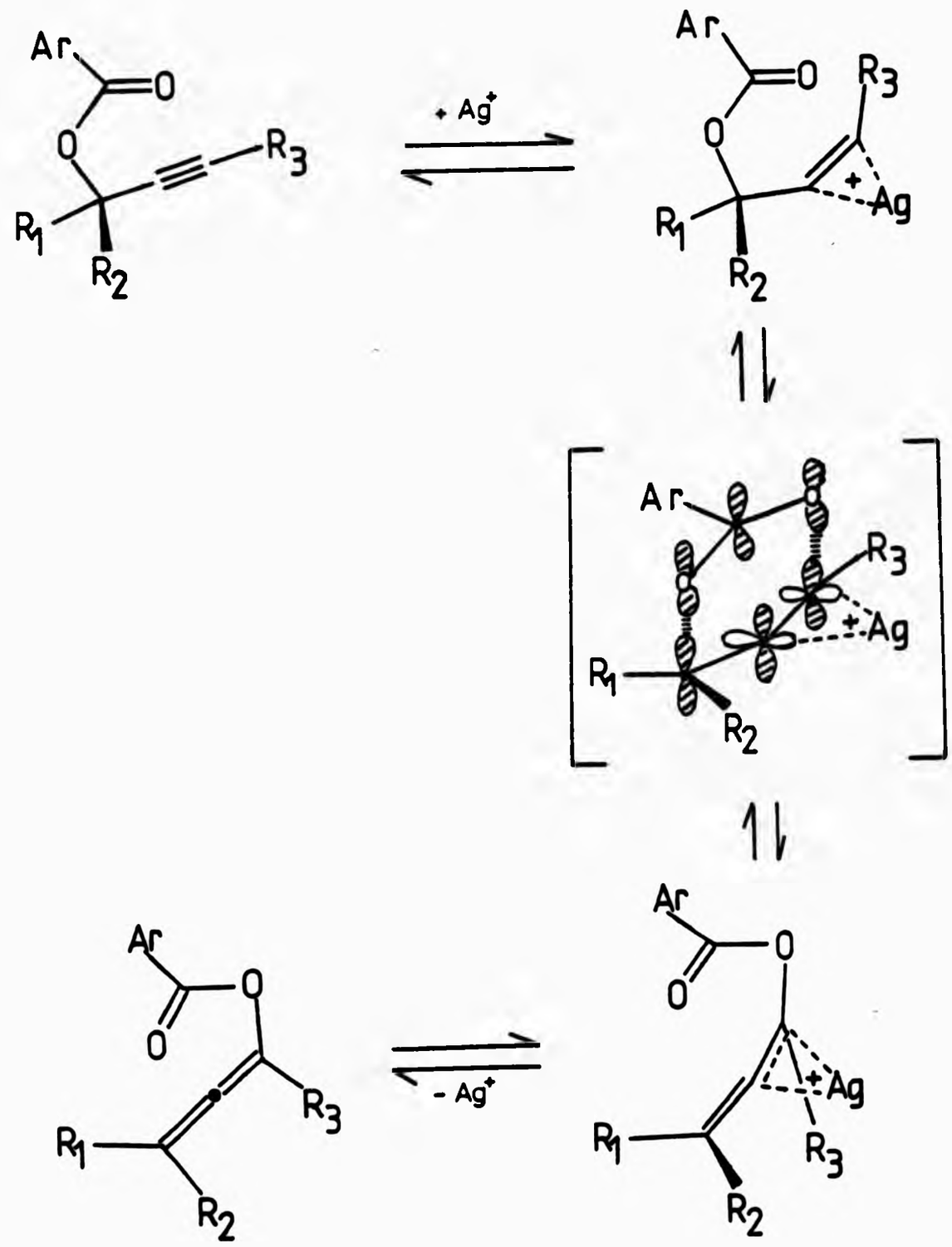

Scheme 3.18

Several groups of workers have recently reported the isomerization of secondary and tertiary acetylenic alcohols to the corresponding α,β-unsaturated carbonyl compounds by heating the alcohol in the presence of a variety of oxo-metal compounds[109b,118]. The most commonly employed catalysts have been oxo-vanadium compounds of the type $O{=}V(OR)_3$ in

which RO is either a siloxy or alkoxy group.

Systematic studies in which RO is a triarylsiloxy group have shown that electron-donating substituents in the aromatic ring result in the formation of a catalyst giving slower rearrangements than the unsubstituted compound while electron-withdrawing substituents give faster rearrangements[118b].

Charbardes et al[109b] have proposed a mechanism for the rearrangement which involves formation of a vanadate ester of the acetylenic alcohols followed by a [3,3]-sigmatropic rearrangement to give an 'allene-vanadate' intermediate which is displaced from the metal in a transesterification step with accompanying protonation and rearrangement to the α,β-unsaturated carbonyl compound (Scheme 3.19).

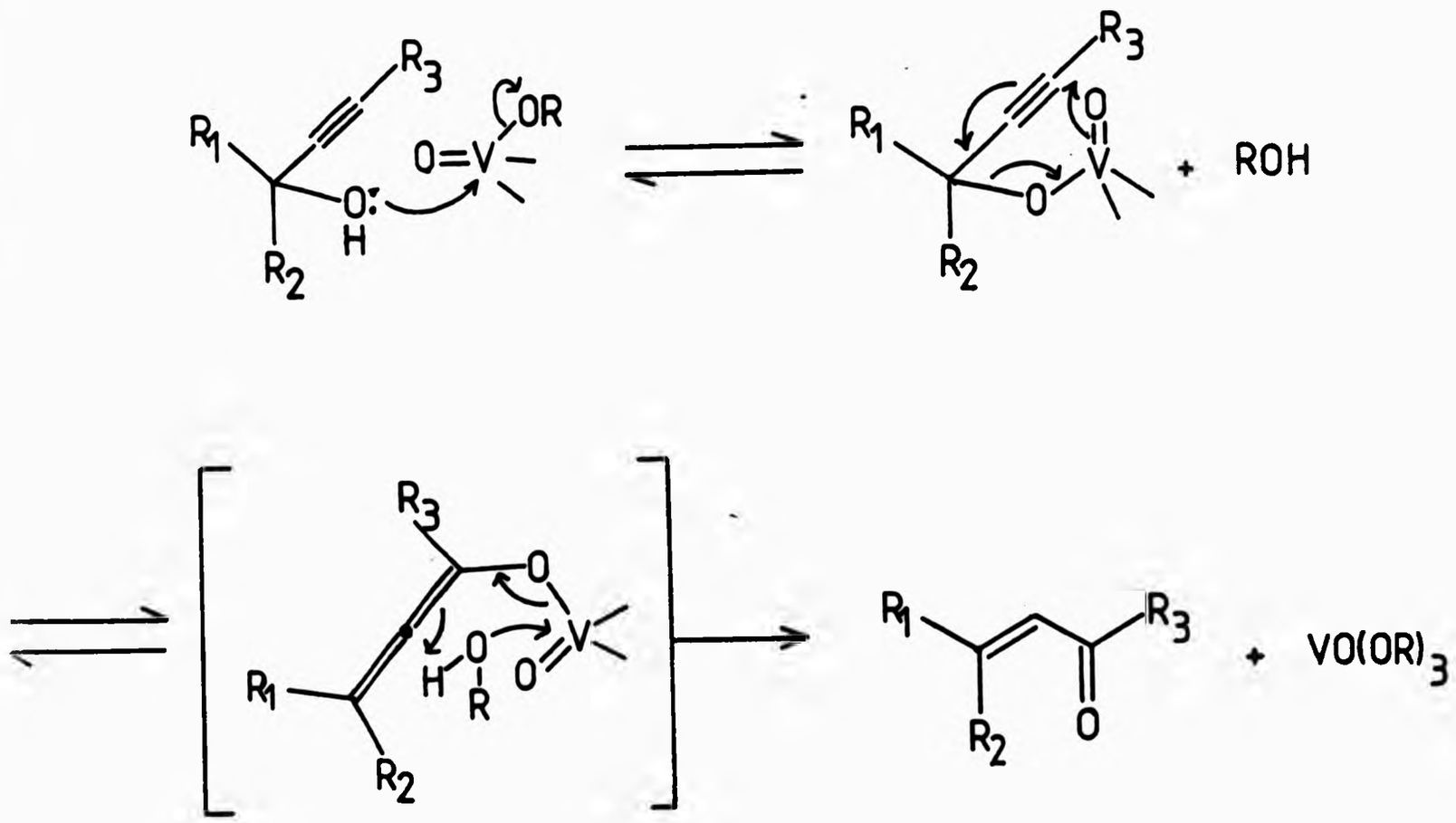

Scheme 3.19

Other workers have reported kinetic studies which apparently support this mechanism[119].

CHAPTER 4

STUDIES OF METAL-ION CATALYSED ISOMERIZATIONS OF ALLYLIC ALCOHOLS

4.1 Introduction

During the course of our investigation aimed at developing oxo-metal catalysts for the regio- and stereoselective epoxidation of olefins (Chapter 2), we observed that when the substrate is an allylic alcohol the epoxidation (Scheme 4.1, reaction 1) may be overshadowed by a competing isomerization reaction (Scheme 4.1, reaction 2).

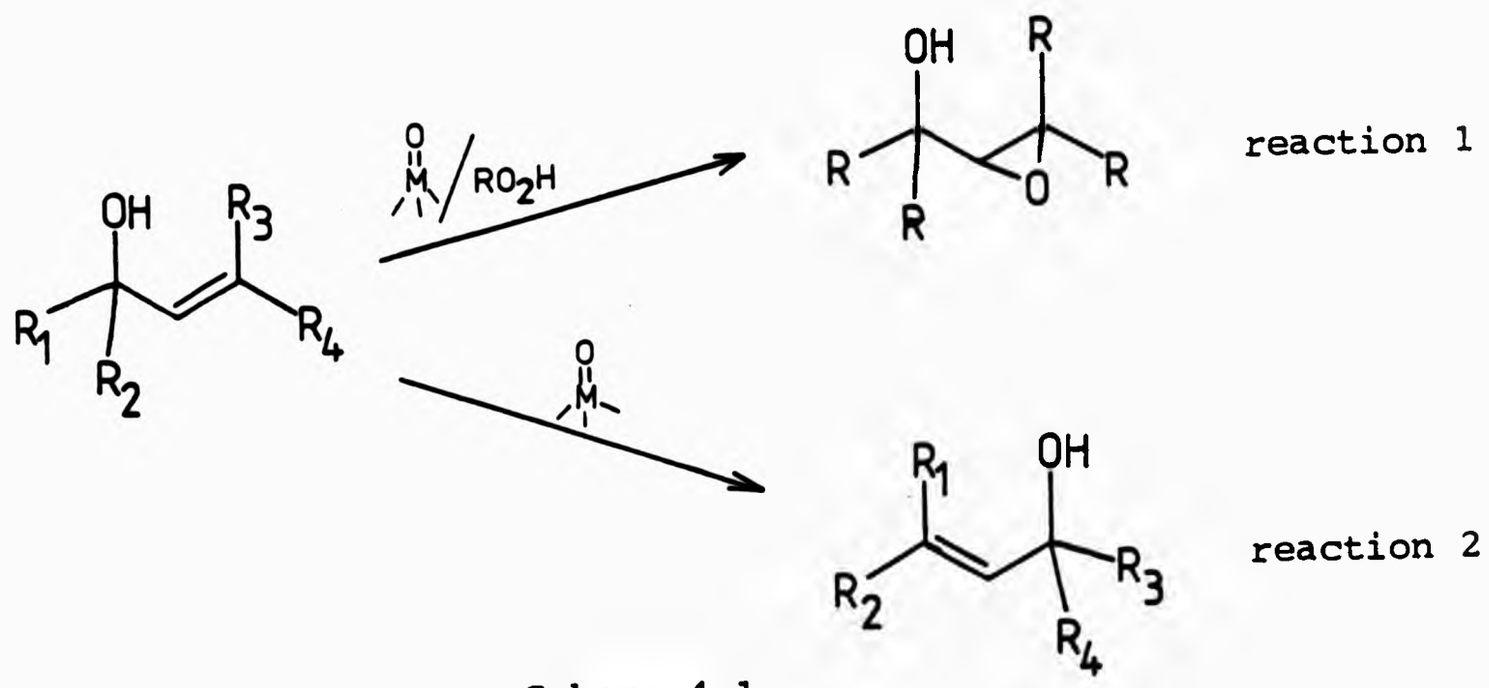

reaction 1

reaction 2

Scheme 4.1

In view of the importance of transposing an allylic oxygen functionality in organic synthesis a study of this oxo-metal catalysed isomerization of allylic alcohols was undertaken. This chapter includes a discussion of the initial observations on the isomerization of geraniol (Section 4.2) as well as the kinetics and mechanism (Section 4.3) and scope of the reaction (Section 4.4). The final section is concerned with attempts to develop more reactive catalysts

by modifying the ligand portion of the oxo-metal catalysts (Section 4.5).

4.2 Oxo-metal catalysed isomerization of geraniol

As part of our study on the metal catalysed epoxidation of olefins it became desirable to compare the catalytic activity of complexes in which the metal is shielded by bulky ligands, with those in which the metal centre is easily accessible to both the epoxidizing reagent and the substrate. An experiment was therefore designed in which olefin epoxidation catalysed by complexes having bulky ligands was to be compared with the rate of olefin epoxidation catalysed by bis(acetylacetonato)dioxomolybdenum(VI), which was arbitrarily chosen as a reference catalyst. The progress of the reaction of geraniol with t-butyl hydroperoxide in benzene at 40°C in the presence of bis(acetylacetonato)-dioxomolybdenum(VI) was monitored by glc, which showed the disappearance of geraniol (4.1) and the formation of a product which, on the basis of retention data, was not the expected 2,3-epoxygeraniol. On removal of the solvent and analysis of the ^{1}H nmr spectrum of the residue the product was easily identified as linalol (4.2).

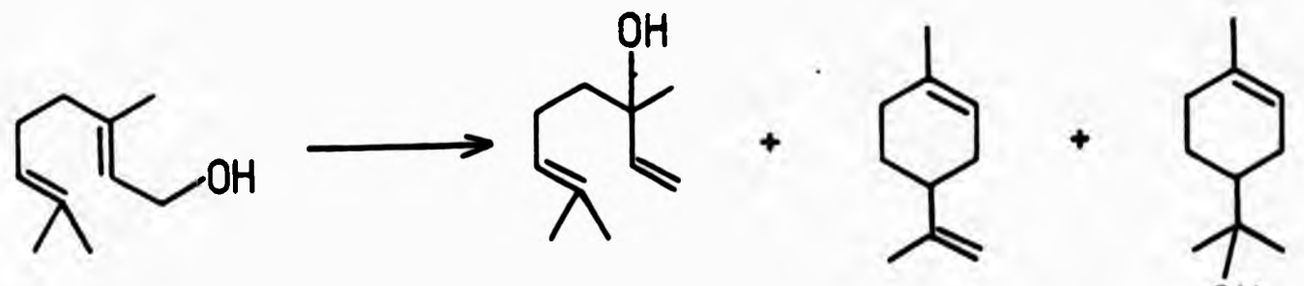

(4.1) (4.2) (4.3) (4.4)

On further investigation of this reaction, glc analysis showed that prolonged heating resulted in the conversion of linalol to other products, identified on the basis of their retention times as the cyclised products dipentene (4.3) and α-terpineol (4.4). Furthermore, it was noted that this conversion of linalol to cyclised products was accompanied by the development of a blue colour in the reaction mixture. At higher reaction temperatures the amount of cyclised products was found to increase at the expense of linalol formation. Similar treatment of linalol also resulted in formation of a blue coloured reaction mixture and formation of cyclised products (Table 4.1). These results support the view that the reaction proceeds largely via initial isomerization of geraniol to linalol followed by further reaction of linalol to give cyclised products.

Cyclisation may be a result of the molybdenum complex acting as a Lewis acid after the initial conversion of geraniol to linalol (Scheme 4.2). This is formally rather similar to the mechanism proposed[120] for the formation of

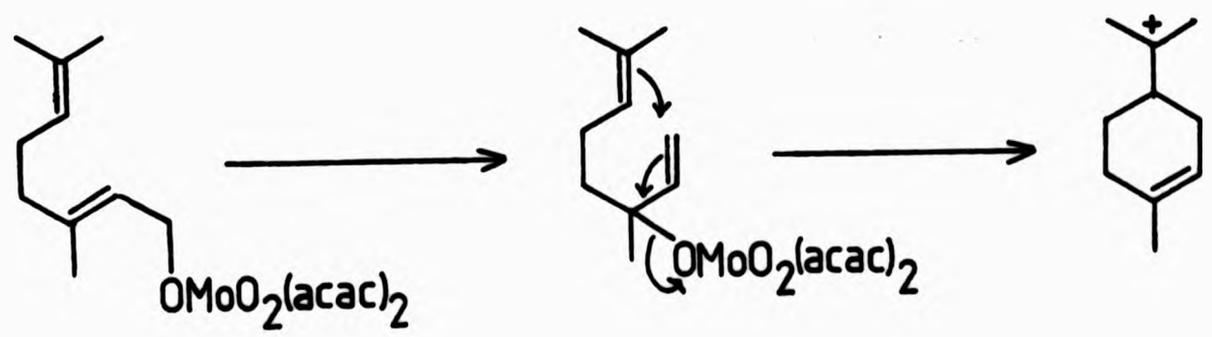

Scheme 4.2

p-menthane monoterpenes from the spontaneous decomposition of geranyl phosphate in inert solvents. In this case it has been

Table 4.1 Isomerisation of geraniol and linalol promoted by $MoO_2(acac)_2$ in benzene.

Substrate	Conditions[a] °C	Product Composition[b], % linalol (4.2)	terpineol (4.4)	geraniol (4.1)	hydrocarbon (4.3)
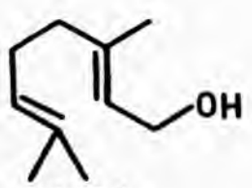 (4.1)	40	31.0	14.6	18.9	35.5
	80	4.5	19.4	0.0	76.1
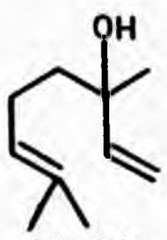 (4.2)	80	17.6	15.8	0.0	66.6

(a) Concentration of substrate and catalyst: 0.05 and 0.001 mol dm^{-3}.
(b) Determined by glc analysis after 1h.

suggested that cyclisation follows an allylic rearrangement of geranyl phosphate to linalyl phosphate.

In an attempt to establish the nature of the blue coloured species produced in the $MoO_2(acac)_2$-catalysed isomerization of geraniol the solvent and volatile products were removed and a deep blue coloured solid isolated. However, the infrared spectrum of this solid was found to be identical to that of $MoO_2(acac)_2$. It is possible that the blue colour arises from an interaction of $MoO_2(acac)_2$ with the dipentene produced during the reaction. This is supported by the observation that treatment of dipentene with $MoO_2(acac)_2$ under the conditions used previously, resulted in the development of a similar blue colour. Use of oct-1-ene instead of dipentene gave similar results, suggesting a general olefin-$MoO_2(acac)_2$ interaction. Attempts to determine the nature of the blue species were again unsuccesful, with no detectable changes in the ir and nmr spectra of either the substrate or catalyst. These observations therefore suggest that the material giving rise to the blue colour is present in only very low concentration.

In view of the importance of transposing allylic functionality in synthetic organic chemistry (Section 3.2), the behaviour of other oxo-transition metal complexes under comparable conditions was examined in the hope of finding one that was more specific for the conversion of geraniol to linalol. Bis(salicylaldehydato)dioxomolybdenum(VI) (4.5) behaved similarly to $MoO_2(acac)_2$. No rearrangement was observed in refluxing benzene or toluene in the presence of dioxomolybdenum(VI) complexes containing nitrogen ligands

suggested that cyclisation follows an allylic rearrangement of geranyl phosphate to linalyl phosphate.

In an attempt to establish the nature of the blue coloured species produced in the $MoO_2(acac)_2$-catalysed isomerization of geraniol the solvent and volatile products were removed and a deep blue coloured solid isolated. However, the infrared spectrum of this solid was found to be identical to that of $MoO_2(acac)_2$. It is possible that the blue colour arises from an interaction of $MoO_2(acac)_2$ with the dipentene produced during the reaction. This is supported by the observation that treatment of dipentene with $MoO_2(acac)_2$ under the conditions used previously, resulted in the development of a similar blue colour. Use of oct-1-ene instead of dipentene gave similar results, suggesting a general olefin-$MoO_2(acac)_2$ interaction. Attempts to determine the nature of the blue species were again unsuccesful, with no detectable changes in the ir and nmr spectra of either the substrate or catalyst. These observations therefore suggest that the material giving rise to the blue colour is present in only very low concentration.

In view of the importance of transposing allylic functionality in synthetic organic chemistry (Section 3.2), the behaviour of other oxo-transition metal complexes under comparable conditions was examined in the hope of finding one that was more specific for the conversion of geraniol to linalol. Bis(salicylaldehydato)dioxomolybdenum(VI) (4.5) behaved similarly to $MoO_2(acac)_2$. No rearrangement was observed in refluxing benzene or toluene in the presence of dioxomolybdenum(VI) complexes containing nitrogen ligands

e.g. (acetylacetonato)[(-)-N-methylephedrinato]dioxomolybdenum(VI) (4.6) and [N(cis,exo-2-hydroxybornyl)-3-methoxysalicylideniminato-(2-)](methanolato)dioxomolybdenum(VI) (4.7). Bis[trans-1,2-cyclohexandiolato-O,O^1(1-)]dioxomolybdenum(VI) (4.8), however, converted geraniol to linalol in high yield without formation of cyclised products. $VO(acac)_2$ was found to be ineffective as a catalyst for the rearrangement under similar conditions.

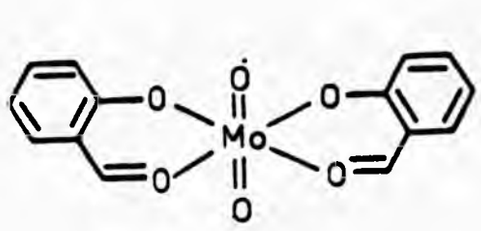

(4.5)

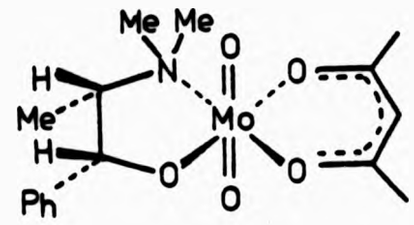

(4.6)

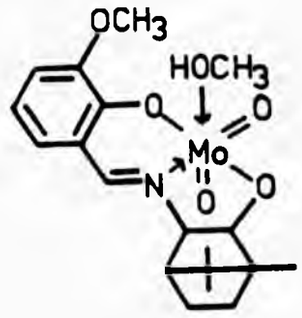

(4.7)

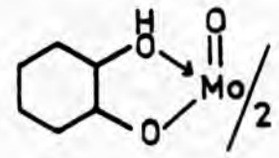

(4.8)

Clearly the nature of the ligand attached to the metal has a marked effect on the ability of the catalyst to promote the isomerization and also on the nature of the products. Why this is so is not clear. The fact that $Mo^{VI}O_2(acac)_2$ in an active catalyst but $V^{IV}O(acac)_2$ is not could point to the Lewis acidity of the metal as an important factor since in the latter the metal is not in its highest available oxidation state. However, as seen above there appears to be considerable variation in activity between the various molybdenum(VI) complexes tested and although these may be attributed partly to variations in Lewis acidity of the metal centre (resulting

from the presence of different ligands) this may not be the only factor involved.

The isomerization of geraniol in the presence of the diol complex (4.8) is of particular interest since the catalytic conversion of geraniol to linalol in high yield has no precedent and would not have been predicted from the classical standpoint that the trisubstituted olefin (geraniol) would be the more thermodynamically stable (Section 3.2.1). Also, other workers have reported that under rather more vigorous conditions a variety of oxo-vanadium compounds will also catalyse the reverse reaction (linalol to geraniol) but give a low yield of geraniol[109b].

We initially thought that the isomerization was irreversible since treatment of linalol with bis(acetylacetonato)-dioxomolybdenum(VI) in benzene at 80°C gave predominantly hydrocarbon with some α-terpineol (identified only by retention data) but no detectable quantity of geraniol. Furthermore, treatment of linalol with bis[trans-1,2-cyclohexandiolato-$O,O^1(1-)$]-dioxomolybdenum(VI) (4.8) under the above conditions at first appeared to give no reaction. Thus in view of the apparent contrathermodynamic and irreversible nature of the isomerization it was initially considered to be a kinetically controlled reaction.

In the initial experiments on the isomerization of geraniol to linalol by bis[trans-1,2-cyclohexandiolato-$O,O^1(1-)$]-dioxomolybdenum(VI) conversions of the order of 65% were obtained after 10-12 h in refluxing benzene. On prolonged heating (18 h) conversions of 75% were obtained, after which no further conversion took place.

In view of the fact that other workers[109b] observed the reverse isomerization in low yield using oxovanadium(V) complexes under rather more vigorous conditions, it was necessary to establish whether these complexes would also promote this apparently contrathermodynamic isomerization observed with dioxomolybdenum(VI) complexes. Tris(triphenylsilyl)oxovanadium(V) was used under the conditions described previously and found to give conversions of geraniol to linalol identical with those obtained using bis[trans-1,2-cyclohexandiolato-O,O^1(1-)]-dioxomolybdenum(VI). In the light of this observation the reverse reaction (linalol to geraniol), which was initially thought not to occur, was again investigated and it was found that both tris(triphenylsilyl)oxovanadium(V) and bis[trans-1,2-cyclohexandiolato-O,O^1(1-)]dioxomolybdenum(VI) did infact promote this isomerization, giving conversions of linalol to geraniol of 25% after 18 h with no further conversion occuring after this time. Furthermore, in experiments with various catalyst concentrations the percentage conversions were found to be unaltered.

Since isomer distributions were independent of catalyst type and concentration and did not alter when either isomer was selected as substrate (see Table 4.2), the isomerization must be an equilibrium reaction and not kinetically controlled as initially thought.

Concentrations of linalol, geraniol and nerol in the equilibrium mixture were found to be 74±2%, 16±1% and 10±1% respectively. In view of the equilibrium nature of the reaction the product distribution must reflect the relative thermodynamic stabilities of the various isomers in toluene

Table 4.2 Isomerization of geraniol and linalol promoted by MoO_2(1,2-cyclohexandiol)$_2$ (A) and $(Ph_3SiO)_3VO$ (B) in toluene at 100°C.

Substrate	Catalyst[a]	Product Composition[b], % terminal isomer (4.2)	internal isomer (4.1)	internal isomer E/Z ratio
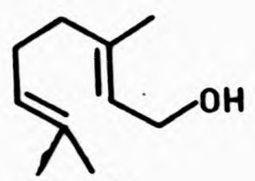 (4.1)	A	75.6	24.3	1:0.56
	B	73.5[c] (72.8[e])	26.4[d] (27.2[e])	1:0.65
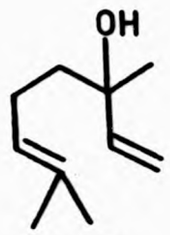 (4.2)	A	73.9	26.0	1:0.64
	B	75.8[c]	24.4[d]	1:0.62

(a) Concentration of substrate and catalyst: 0.05 and 0.004 mol dm^{-3}.
(b) Determined by glc after 24h.
(c) Nmr gives 75%.
(d) Nmr gives 25%.
(e) Concentration of substrate and catalyst: 0.05 and 0.001 mol dm^{-3}. Composition determined by glc after 74h.

at 100°C, hence the formation of linalol as the major product suggests that classical arguments for predicting the relative thermodynamic stabilities of olefins, based on the number of substituents attached to the double bond (Section 3.2.1), cannot necessarily be extended to all allylic systems.

Finally, by monitoring (glc) the progress of the bis[trans-1,2-cyclohexandiolato-O,O^1(1-)]dioxomolybdenum(VI) catalysed isomerization of a 1:1 mixture of geraniol (E-isomer) and nerol (Z-isomer) in toluene at 100°C it was found that nerol is also isomerized at approximately the same rate as geraniol without formation of cyclised products. This is in contrast to the acid-catalysed rearrangement of geraniol and nerol in acetone/0.1N HCl (1:1) at 37°C where it has been shown[121] that nerol is converted mainly to α-terpineol. The greater rate of formation of α-terpineol from nerol under these conditions may be explained by assuming that the intermediate carbonium ion retains the cis configuration to a high degree so that the stereochemistry is favourable to this cyclisation.

4.3 Kinetics and mechanism of oxo-metal catalysed isomerization of allylic alcohols

Charbardes et al[109b] have proposed a mechanism for the oxo-metal catalysed isomerization of tertiary to primary allylic alcohols and this is represented in Scheme 4.3. It is proposed that the first step (step a) involves formation of a vanadate ester of the allylic alcohol by displacement of one of the alkoxy (or siloxy) groups of the catalyst. This is followed by a [3,3]-sigmatropic rearrangement (step b) and a trans-esterification (step c) resulting in displacement of the

at 100°C, hence the formation of linalol as the major product suggests that classical arguments for predicting the relative thermodynamic stabilities of olefins, based on the number of substituents attached to the double bond (Section 3.2.1), cannot necessarily be extended to all allylic systems.

Finally, by monitoring (glc) the progress of the bis[trans-1,2-cyclohexandiolato-O,O^1(1-)]dioxomolybdenum(VI) catalysed isomerization of a 1:1 mixture of geraniol (E-isomer) and nerol (Z-isomer) in toluene at 100°C it was found that nerol is also isomerized at approximately the same rate as geraniol without formation of cyclised products. This is in contrast to the acid-catalysed rearrangement of geraniol and nerol in acetone/0.1N HCl (1:1) at 37°C where it has been shown[121] that nerol is converted mainly to α-terpineol. The greater rate of formation of α-terpineol from nerol under these conditions may be explained by assuming that the intermediate carbonium ion retains the cis configuration to a high degree so that the stereochemistry is favourable to this cyclisation.

4.3 Kinetics and mechanism of oxo-metal catalysed isomerization of allylic alcohols

Charbardes et al[109b] have proposed a mechanism for the oxo-metal catalysed isomerization of tertiary to primary allylic alcohols and this is represented in Scheme 4.3. It is proposed that the first step (step a) involves formation of a vanadate ester of the allylic alcohol by displacement of one of the alkoxy (or siloxy) groups of the catalyst. This is followed by a [3,3]-sigmatropic rearrangement (step b) and a trans-esterification (step c) resulting in displacement of the

rearranged allylic alcohol and regeneration of the vanadate ester, thus completing the catalytic cycle.

Fig 4.1 shows the conversion of geraniol to linalol, as monitored by ^1H nmr, shortly after the addition of various concentrations of $(Ph_3SiO)_3VO$ as catalyst. Initial rates (Table 4.3) appear to show a slightly greater than first order dependence on catalyst. In view of the number of reversible steps in the proposed pathway for the isomerization (e.g. Scheme 4.3), a complex rate equation will be involved, and it is unlikely that support for a particular mechanism will come solely from kinetic studies.

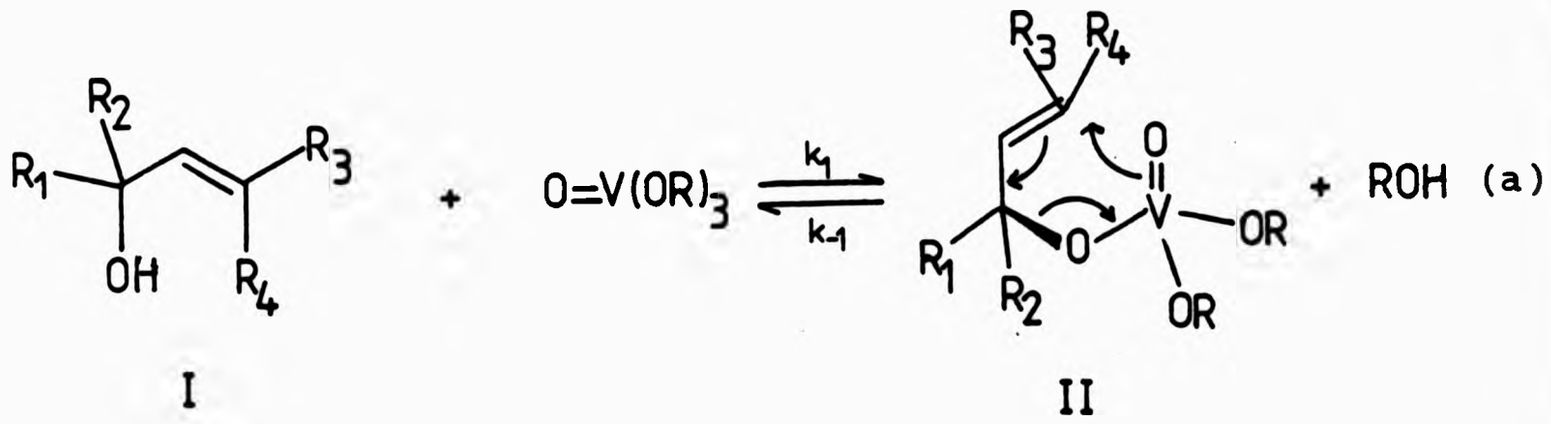

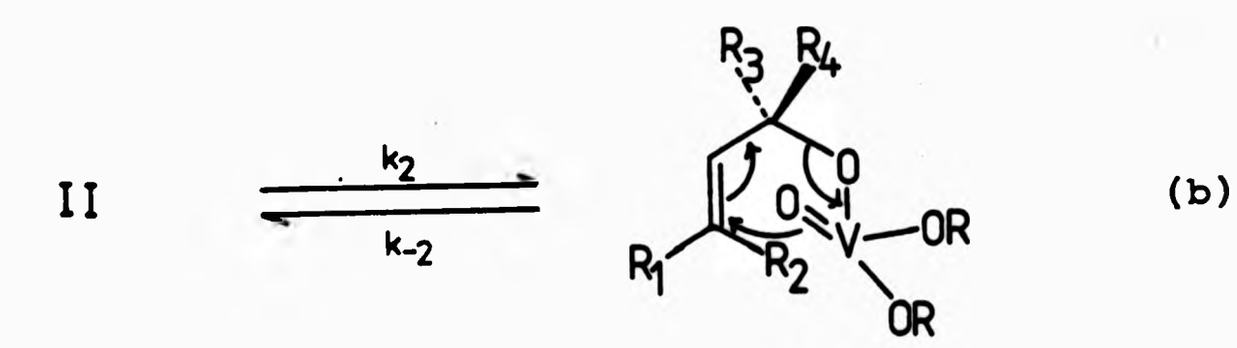

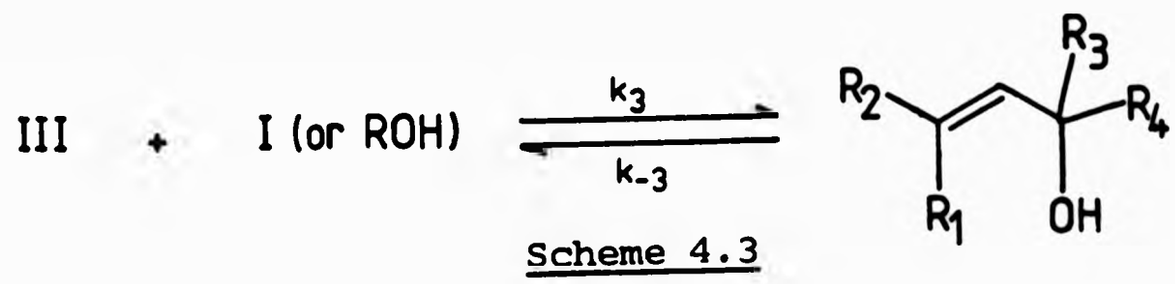

Scheme 4.3

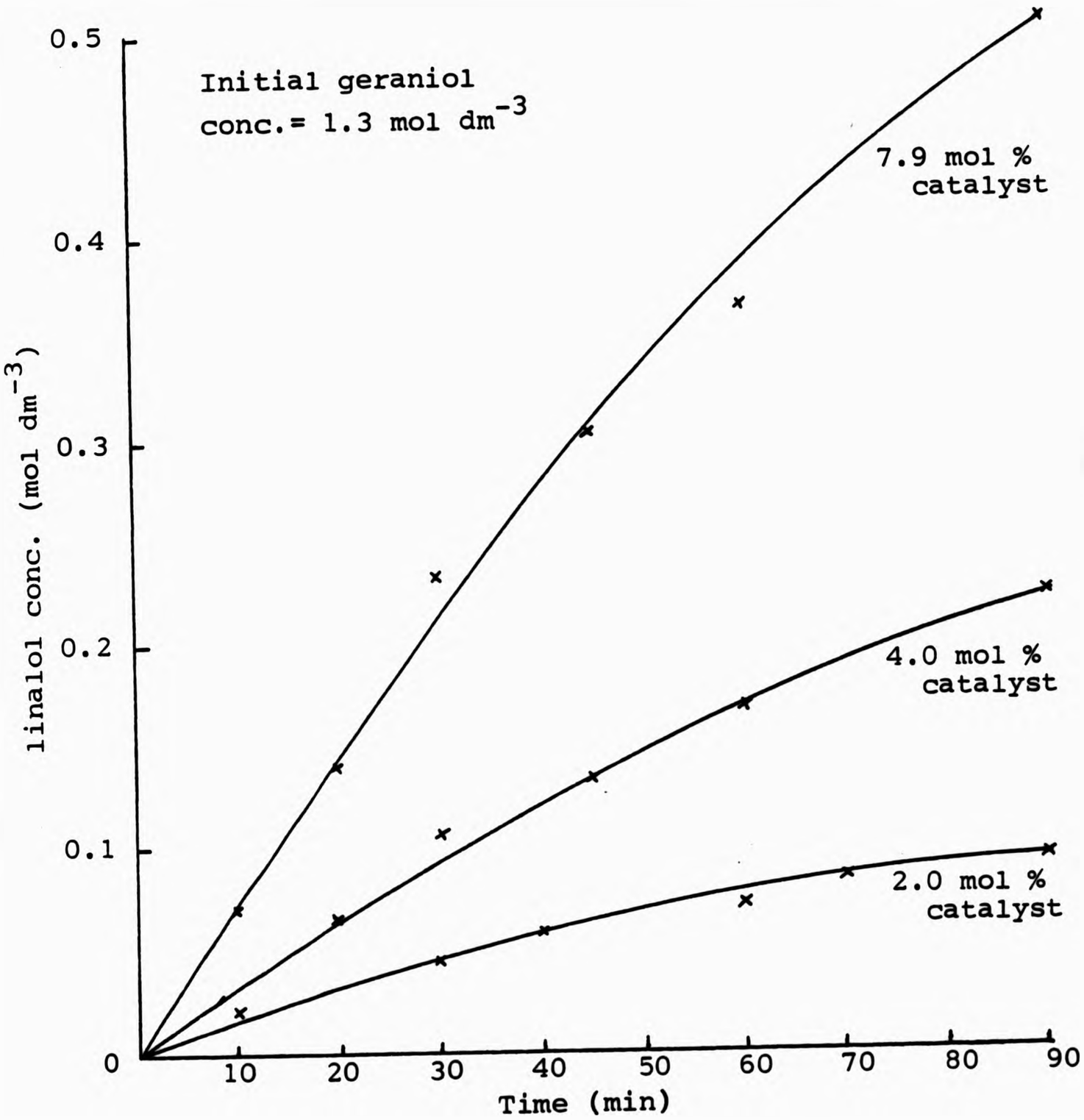

Fig 4.1 Rate of isomerization of geraniol by $(Ph_3SiO)_3VO$ in benzene at 80°C.

Table 4.3 Dependence of initial rate of formation of linalol on the concentration of $(Ph_3SiO)_3VO$.

Catalyst conc./ mol dm^{-3}	0.103	0.052	0.026
Initial rate of formation of linalol/ mol dm^{-3} s^{-1} (x10^{-4})	1.33	0.53	0.25

For the oxo-metal catalysed isomerization of propargylic alcohols to α,β-unsaturated carbonyl compounds[109b] a similar mechanism has been proposed (Section 3.3.2) and this has been supported by kinetic studies[119], the situation there was simplified by the irreversibility of the final step, whereas in the allylic alcohol isomerization it appears from this work that all the steps are reversible. It might be suggested, as was the case with propargylic alcohols[119], that the equilibrium in Scheme 4.3, step (a), is shifted almost completely to the right on account of the large excess of allylic alcohol present. Thus the catalyst $(RO)_3VO$ in its initial form takes no further part in the catalytic cycle which would comprise of step (b) and (c). However, it has not been possible to produce evidence to support such an assumption for reactions of the allylic alcohols in this work. Indeed unchanged tris(triphenylsilyl)-oxovanadium(V) could be recovered in 50% yield by crystallisation from mixtures resulting from the geraniol rearrangement and no allylic alcohol ligands were present in the recovered material. Furthermore, there appeared to be no shift of signals in the ^{1}H-nmr spectrum of geraniol on addition of tris(triphenylsilyl)-oxovanadium(V), as might be expected if transesterification had occured. Probably the geranyl vanadate esters are present in concentrations too low to be detected in these experiments.

The proposed involvement of a vanadate ester in the rearrangement can be compared with mechanistic proposals for uncatalysed rearrangements of allylic esters. It appears to be generally accepted that these latter reactions involve a unimolecular, rate-determining, alkyl-oxygen scission. Such a process could be described, in its two extremes, as a simple

S_N1 mechanism or by a concerted S_Ni' process in which the transition state resembles a rigidly orientated carbonium-carboxylate ion pair (Scheme 4.4).

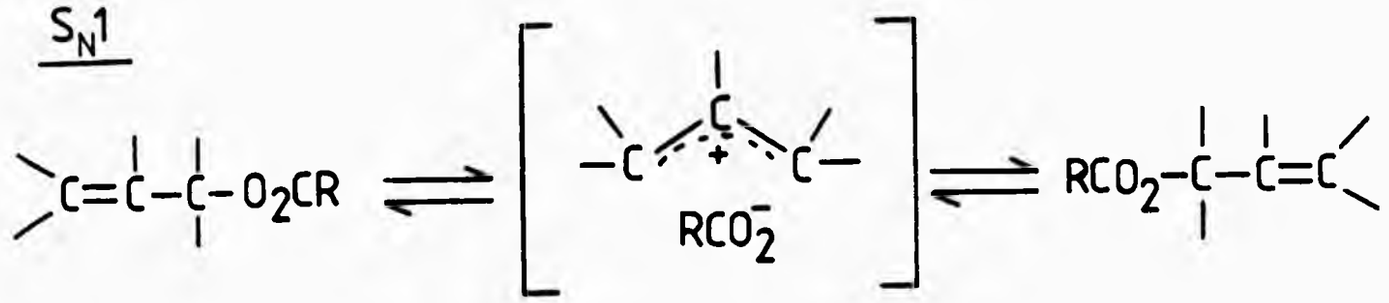

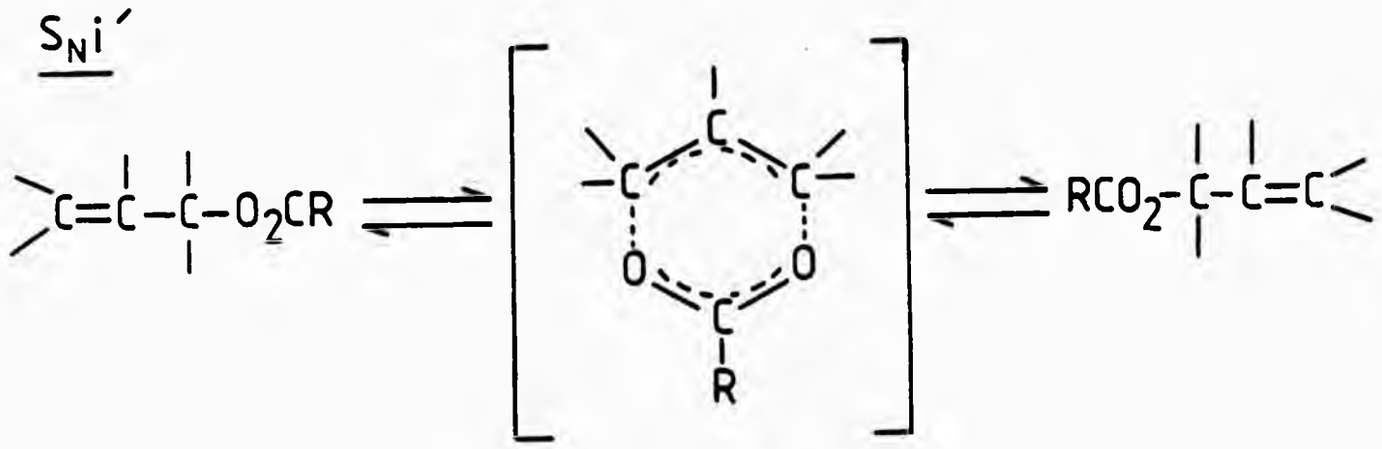

Scheme 4.4

These two mechanisms represent extremes of the bond making and bond breaking processes in the transition state. When bond breaking is more facile than bond making the mechanism tends towards S_N1 but when bond making and bond breaking occur at comparable rates an S_Ni' mechanism is favoured.

The absence of common-ion rate acceleration or exchange in isomerizations accompanying hydrolysis of a number of p-nitrobenzoate esters[122-124] rules out free carbonium ions as intermediates in uncatalysed allylic ester isomerizations. Similarly, in aprotic solvents addition of p-nitrobenzoate to α-phenylallyl p-nitrobenzoate in acetic anhydride and acetonitrile did not give rise to a common-ion rate acceleration[125] and when ^{18}O-labeled α-phenylallyl benzoate was heated with benzoate ion in chlorobenzene, the rates of isomerization and

isotopic exchange showed that only a fraction of the benzoate groups in the resulting cinnamyl benzoate came from the added benzoate salt[126]. These results rule out a classical S_N1 mechanism but do not distinguish between an S_Ni mechanism and internal return from an ion-pair intermediate.

An ion-pair mechanism for the isomerization of labile allylic esters is supported by the observations of Goering et al[123,124]. These workers have investigated the nature of the intermediate in the isomerization of trans-α,γ-dimethylallyl and trans-5-methyl-2-cyclohexenyl p-nitrobenzoates by studying solvolysis, solvent effects, racemization and O^{18} scrambling. In the rearrangement of optically active trans-α,γ-dimethylallyl p-nitrobenzoate (Scheme 4.5) rearrangement resulted in the interconversion of enantiomers (racemization) without geometric isomerization. The sensitivity of the rate of rearrangement to the ionizing power of the solvent suggests that the intermediate has considerable polar character. Studies with the ^{18}O labelled compound showed that ^{18}O equilibration in the two enantiomers occurs at a slower rate than rearrangement. This means the oxygen atoms bond with the nearest carbon atom more rapidly than with the remote one. These results have been interpreted[123] as being consistent with the idea that the intramolecular rearrangement involves an intermediate which is best described as an internal ion pair.

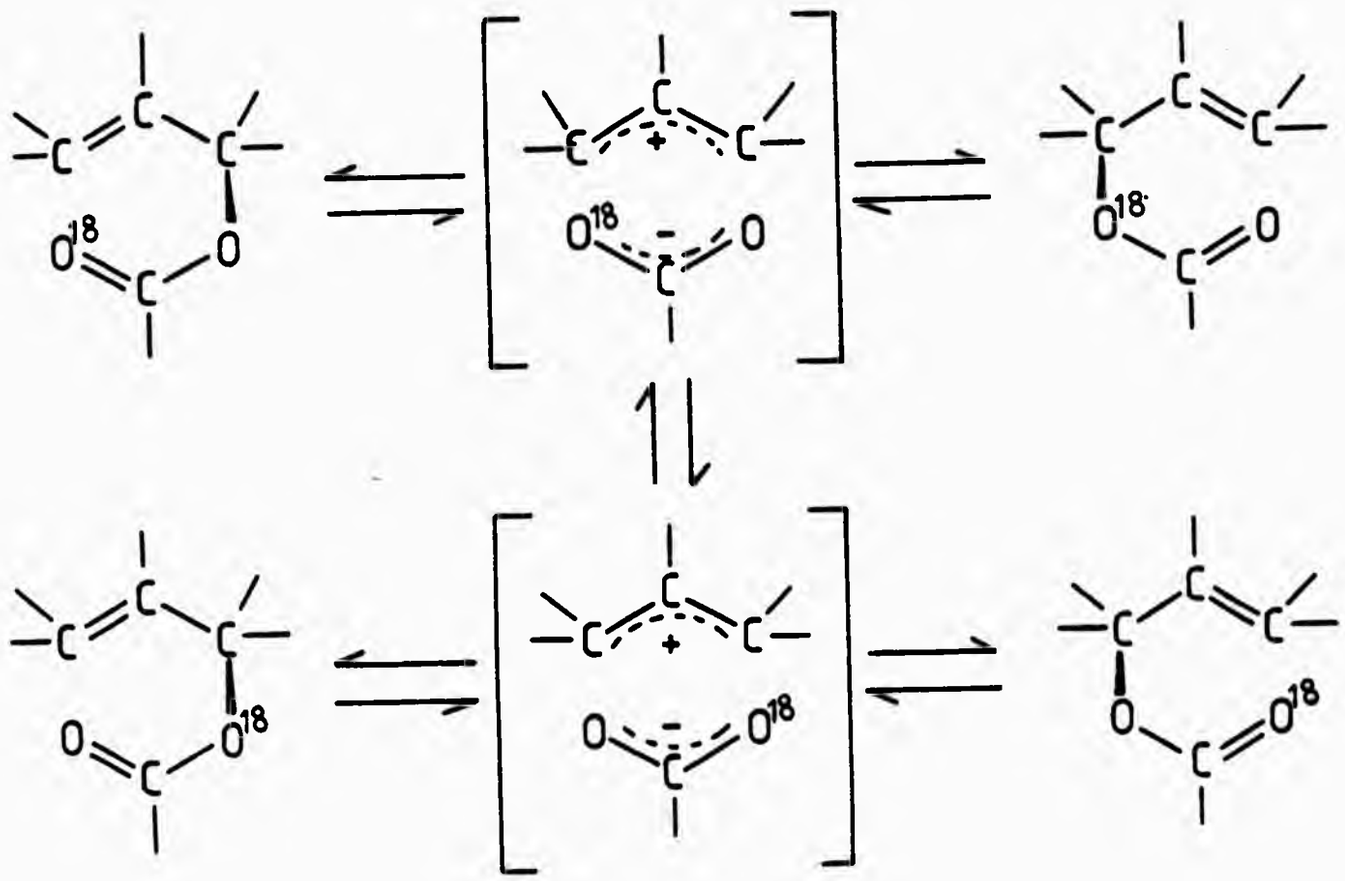

Scheme 4.5

A different situation exists in the rearrangement of the trans-5-methyl-2-cyclohexenyl system. Here oxygen equilibration is found to take place faster than racemization. This is thought to arise from a mechanism involving two ion pair intermediates, one of which is symmetrical (common to both enantiomers) and results in racemization and oxygen equilibration. The second is unsymmetrical giving ^{18}O-scrambling without racemization.

In the vanadate ester catalysed isomerization of allylic alcohols the allylic vanadate esters are present only as transient species in catalytic amounts, this makes attempts to elucidate the mechanism of the reaction much more difficult.

Reactions which involve the creation of charge in the transition state proceed more rapidly as solvent ionizing power (dielectric constant) is increased. Isomerization

of allylic vanadate esters are normally carried out in hydrocarbon solvents and the use of alternative solvents to study the reaction is restricted, as solvents containing heteroatoms with an unshared pair of electrons co-ordinate to the vanadium atoms and hinder the formation of the allylic alcohol ester. However, we have found that the reaction proceeds in chloroform without significant change in reaction rate. This suggests that the reaction does not involve free carbonium ions as intermediates but is not sufficient evidence to rule out the possibility of an intimate ion-pair mechanism, such a (4.9), occuring instead of the concerted mechanism proposed by Charbardes[109b] which involves little separation of charge in the transition state.

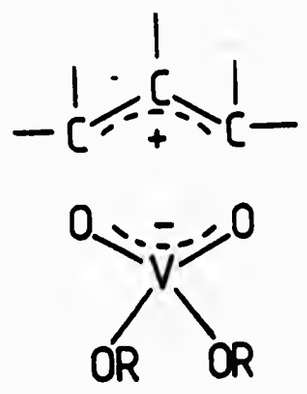

(4.9)

In view of the fact that there is no experimental evidence to support a mechanism involving complete displacement from the catalyst of siloxy or alkoxy ligand by the allylic alcohol, an alternative possibility can be considered in which rearrangement occurs by coordination of the allylic alcohol to the metal without ligand displacement (Scheme 4.6).

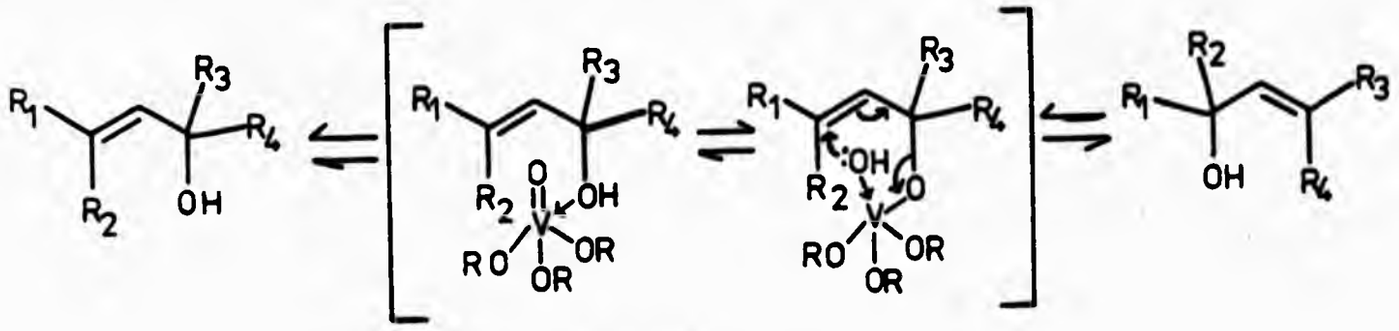

Scheme 4.6

4.4 Scope of isomerization by oxo-metal catalysts

Initially an attempt was made to study the scope of the reaction by treating a variety of allylic alcohols with bis[trans-1,2-cyclohexandiolato-O,O^1(1-)]dioxomolybdenum(VI) (4.8) in refluxing toluene and analysing the reaction mixtures by glc. Although this procedure worked well for a number of substrates, it was less satisfactory in reactions where the boiling points of the substrates and/or products were close to or below the reaction temperature (due to loss of material). An additional complication was that direct injection of the reaction mixture on to the glc column led to a build-up of the molybdenum complex on the column, which resulted in rearrangements taking place on the column during analysis. Although this problem was largely overcome by pre-treatment of the sample by passing it down a short column of alumina which removed the molybdenum complex (tris(triphenylsilyl)-oxovanadium(V) could not be removed in this way), this made the analysis tedious and introduced an additional source of error. The greater solubility of tris(triphenylsilyl)-oxovanadium(V) in benzene enabled isomerizations using this catalyst to be carried out in sealed nmr tubes, this allowed the course of the reaction to be followed easily and the equilibrium composition to be determined directly, and was the preferred method for studying these isomerizations. Table 4.4 summarises the results obtained in the isomerization of a variety of allylic alcohols by this method.

In certain cases higher concentrations of substrate are required in order for the isomerization to occur at an observable rate. For example no isomerization of trans-hex-

Table 4.4 Isomerization promoted by $(Ph_3SiO)_3VO$ in benzene at 80°C.

	Substrate[a]	Product	% Composition at equilibrium[b] Substrate	Product
i)	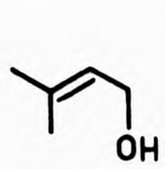 (4.10)	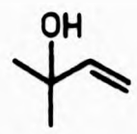 (4.11)	25	75
ii)	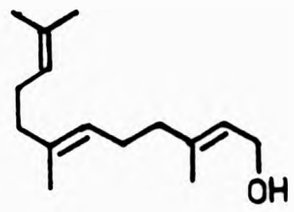 (4.12)	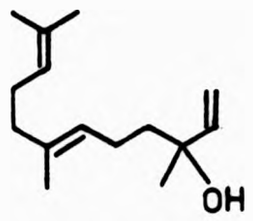 (4.13)	23	77 (68[c])
iii)	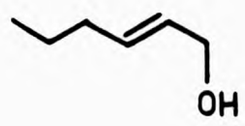	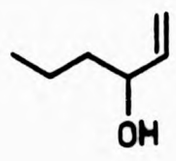	50	50
iv)	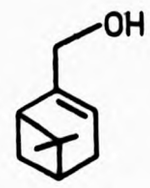 (4.14)	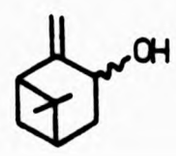 (4.15)	82	18
v)	(4.15)	(4.14)	18	82
vi)	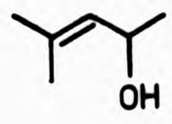	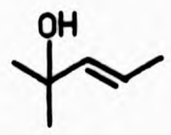	33[d]	66[d]
vii)	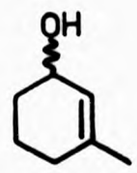	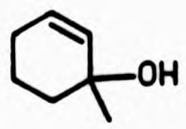	64[d]	36[d]
viii)	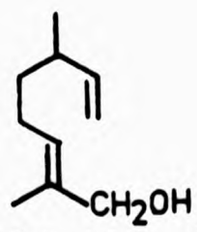 (4.16)	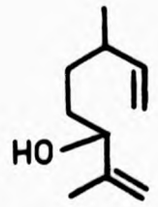 (4.17)	18[e]	82[e]

Table 4.4 cont'd

ix)	(4.17)	(4.16)	82[e]	18[e]
x)	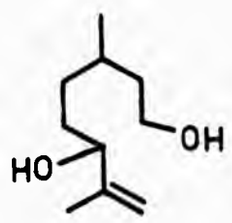	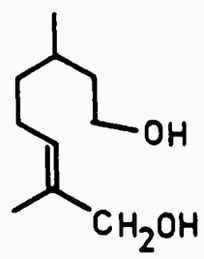	82	18

a) Reactions were carried out in benzene with a substrate concentration of 1.3 mol/l and a catalyst concentration of 8 mol %.

b) Unless otherwise stated this was determined by ^{1}H nmr.

c) Isolated yield.

d) This value was obtained after 3h. Further heating (20h) gave side reactions which appeared to decrease the amount of product.

e) Determined by glc.

2-en-1-ol (Table 4.4, entry iii) or 4-methylpent-3-en-2-ol (Table 4.4, entry vi) appeared to occur when benzene solutions having substrate concentrations of 0.2 to 0.3 mol dm^{-3} were heated at $80^{o}C$ for 16 h. However, when the substrate concentration was increased to 1.0 to 1.5 mol dm^{-3} (as in the nmr experiments) isomerization was observed.

The three primary to tertiary allylic alcohol isomerizations studied involved alcohols with a γ-methyl substituent on the double bond (Scheme 4.7). Within experimental error the equilibrium compositions were the same for all these isomerizations (Table 4.2 and Table 4.4, entries i and ii). Following the initial observation of the isomerization of geraniol to linalol in high yield, it was thought that the position of equilibrium of this reaction may in some way be dependent on the presence of the 7,8-double bond in the molecule, this however is clearly not the case since a similar equilibrium is established when R=CH_3 (Table 4.4, entry i).

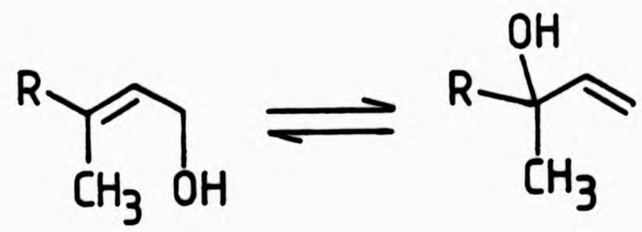

Scheme 4.7

This procedure clearly offers a complimentary technique to the mercuric trifluoroacetate catalysed equilibration of carbamate esters of allylic alcohols and palladium(II)-catalysed rearrangement of allylic acetates (Section 3.2.3) since the equilibrium composition of a pair of isomeric allylic

alcohols is often dramatically different compared with that of the corresponding carbamate or acetate esters; c.f. 25:75 ratio of (4.10) to (4.11) (Table 4.4, entry (i)) compared with the 98:1.5 ratio of the corresponding carbamates[111]. Furthermore this oxo-metal catalysed equilibration offers a useful alternative to the multistep procedures that have been developed in recent years to achieve these interconversions. Yamamoto *et al*[127] have carried out the conversion of geraniol to linalol (4.1) and farnesol (4.12) to nerolidol (4.13) (Table 4.4, entry (ii)) in yields of 82% and 69% respectively by metal catalysed epoxidation of the allylic alcohol followed by mesylation and reductive elimination of the epoxy mesylate by sodium in liquid ammonia (Scheme 4.8). In preparative scale experiments using the oxo-metal catalysed isomerization technique, linalol and nerolidol have been isolated in yields of 60 to 68%.

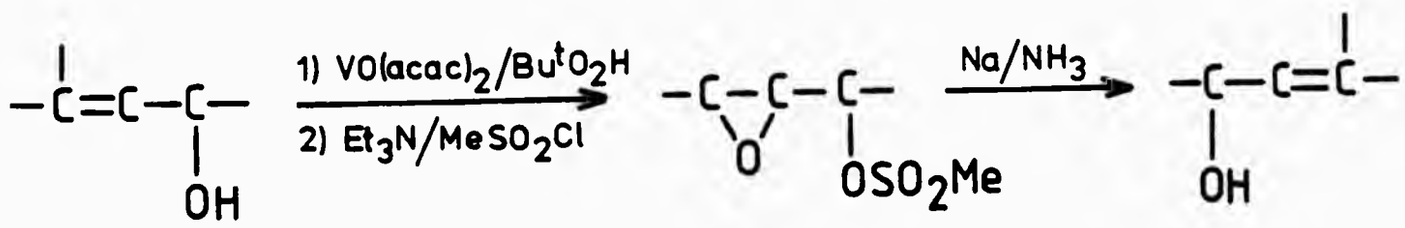

Scheme 4.8

As well as the isomerization of primary allylic alcohols to the corresponding tertiary alcohol, the oxo-metal catalysed isomerization of a number of structurally different allylic alcohols has been investigated and it has been found that the equilibrium does not always favour formation of the product having the less substituted double bond.

Isomerization of 4-methylpent-3-en-2-ol to 2-methylpent-3-en-2-ol (Table 4.4, entry vi) gave an equilibrium mixture in the ratio of 1:2, with decomposition on prolonged heating. Apparently a similar equilibrium mixture is obtained during acid catalysed isomerization of this substrate but under these conditions it is more difficult to avoid accompanying elimination reactions[128].

Trans-hex-2-en-1-ol (Table 4.4, entry iii) isomerized to give an equilibrium mixture containing 50% of the isomer with the less substituted (terminal) double bond. Overmann et al[111] have achieved high conversions (95%) of trans-hex-2-en-1-ol to hexen-3-ol by isomerizing the carbamate esters in the presence of excess (3 equiv.) mercuric trifluoroacetate. The terminal isomer complexes with the mercury(II) thus removing it from the reaction and displacing the equilibrium in favour of this isomer (Section 3.2.3).

The isomerization of myrtenol (4.14) and pinocarveol (4.15) (Table 4.4, entries iv and v) shows that the equilibrium favours the alcohol with the endocyclic double bond (4.14) as would be anticipated on thermodynamic grounds[99]. However, Bassiere et al[129] have recently claimed that in glacial or aqueous acetic acid or HCl/dimethyl sulphoxide the secondary alcoholic function in pinocarveol is favoured over the primary one in myrtenol despite the presence of an exocyclic double bond in the former.

The composition of the equilibrium mixtures obtained from the isomerization of 1-hydroxycitronellene (4.16) and 3-hydroxycitronellene (4.17) (Table 4.4, entries viii and ix) are similar and show that the equilibrium lies well over on

the side of the secondary alcohol (4.17). A comparison of this result with that of trans-hex-2-en-1-ol (entry iii) shows that the introduction of a methyl substituent on the β-carbon has a considerable effect on the position of equilibrium in these primary to secondary alcohol rearrangements. From thermodynamic considerations a substituent on the β-carbon would normally be expected to stabilise both isomers to approximately the same extent. It is therefore surprising that such a large variation in the position of equilibrium was observed in this isomerization.

Similar equilibrium constants were also obtained in the isomerization of 3-hydroxycitronellol (Table 4.4, entry x) and 3-hydroxycitronellene (entry ix) indicating that, under the conditions employed, the oxo-metal catalysed allylic alcohol isomerization is unaffected by the presence of other non-allylic hydroxyl functions in the molecule.

A number of allylic alcohols showed no sign of isomerizing in the presence of oxo-metal catalysts. Damascone (4.18) is a compound of importance to the perfumery and flavour industry and we have investigated the possibility of synthesising it from the readily available α-ionone (4.19) by a route involving an oxo-metal catalysed allylic isomerization (Scheme 4.9).

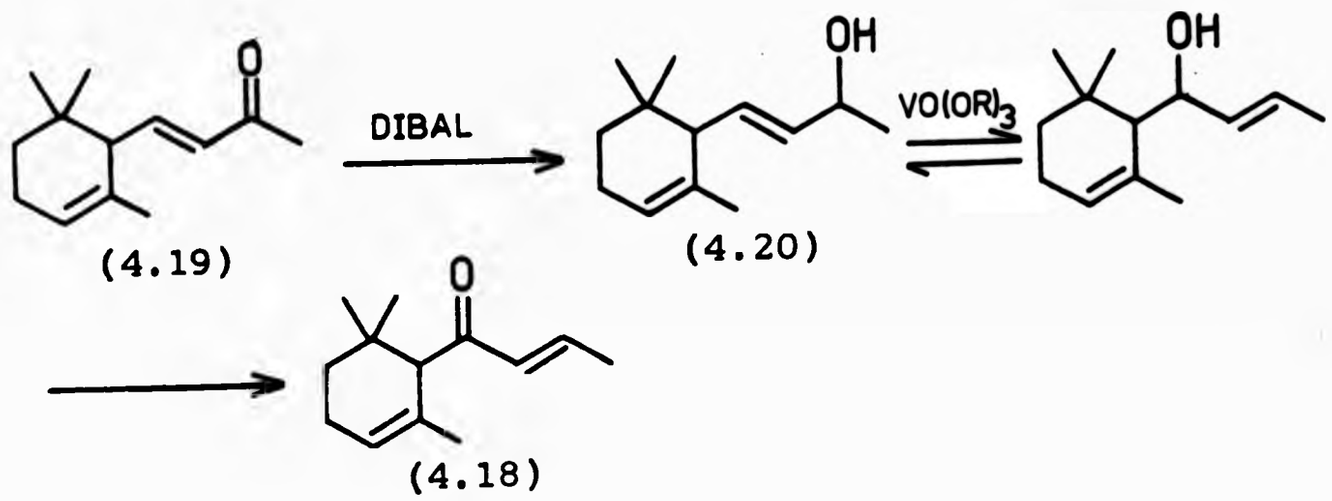

(4.19) (4.20) (4.18)

Scheme 4.9

Treatment of α-ionol (4.20) with either bis[trans-1,2-cyclohexandiolato-O,O^1(1-)]dioxomolybdenum(VI) or tris-(triphenylsilyl)oxovanadium(V) in refluxing benzene or toluene for 4 days failed to give any of the rearranged product. Use of bis(acetylacetonato)dioxomolybdenum(VI) in refluxing benzene resulted in the rapid formation of elimination products e.g. (4.21). Elimination also took place when α-ionol was heated in xylene (130°C) in the presence of bis[trans-1,2-cyclohexandiolato-O,O^1(1-)]-dioxomolybdenum(VI) whereas similar treatment with tris(triphenylsilyl)oxovanadium(V) resulted in the production of a small amount of α-ionone. The ability of oxo-vanadium complexes to oxidise alcohols has been reported by other

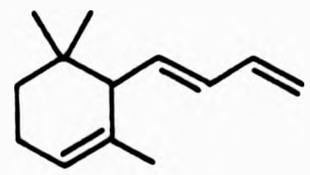

(4.21)

workers[109b], the mechanism is assumed to be as shown below (Scheme 4.10) and is accompanied by a change in oxidation state of the metal.

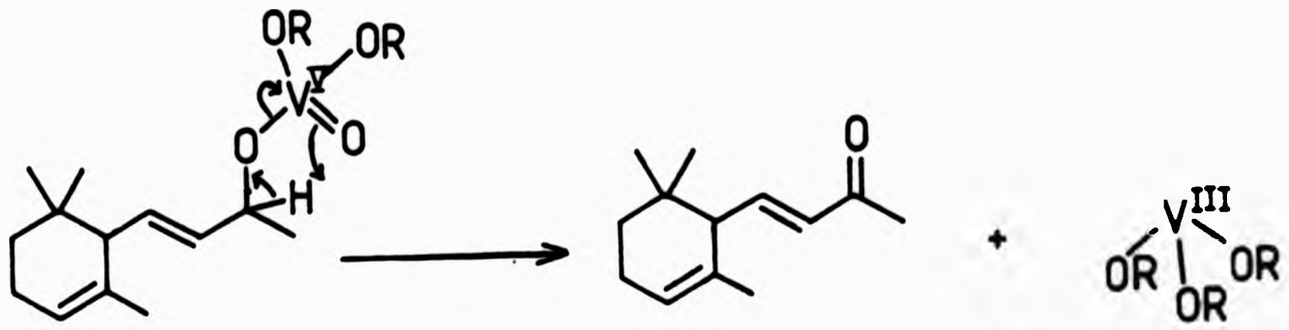

Scheme 4.10

Other workers[130] have carried out an allylic transformation of α-ionol via a Meisenheimer rearrangement by a route which involves a substitution of the bromide with dimethylamine (Scheme 4.11). Substitution apparently occurs without allylic rearrangement and this has been attributed to the shielding of the other allylic position by the substituted cyclohexene ring. The failure of oxo-metal catalysts to isomerize α-ionol may therefore also be due to the steric hindrance at this allylic position.

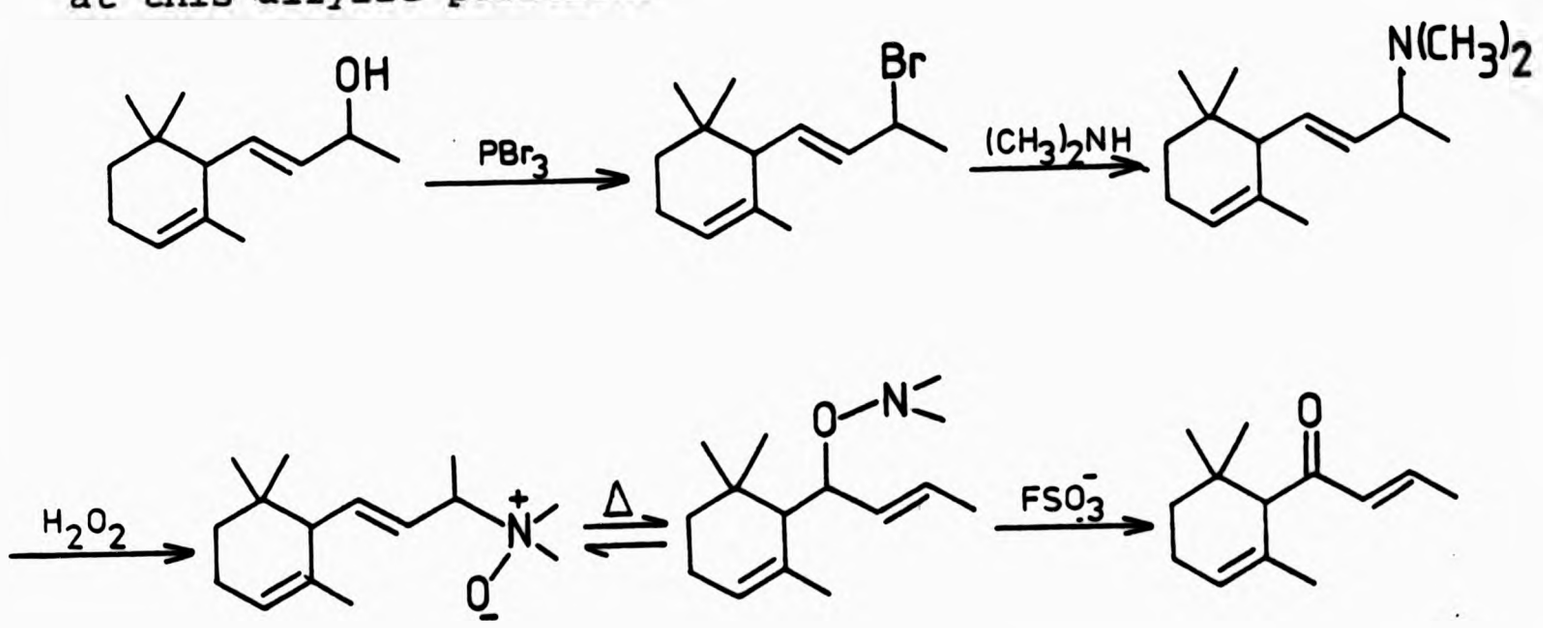

Scheme 4.11

Attempts to isomerize α-ionol acetate by the palladium(II)-catalysed method developed by Overman[112] (Section 3.2.3) also failed to give any rearranged product.

Cinnamyl alcohol (4.22) also failed to rearrange in refluxing toluene in the presence of bis[trans-1,2-cyclohexandiolato-O,O^1(1-)]dioxomolybdenum(VI) or tris(triphenylsilyl)-oxovanadium(V). This is not really surprising since it would require the double bond to move out of conjugation with the benzene ring and this would be highly thermodynamically unfavourable process.

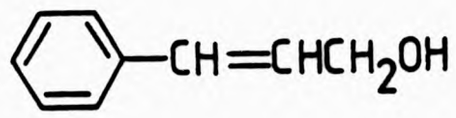

(4.22)

In view of the fact that the cyclopropyl group often exhibits similar behaviour to that of an alkene, the possibility of isomerizing an alcohol containing this group has been investigated. It was thought that isomerization could conceivably occur by a mechanism similar to that for allylic alcohols (Scheme 4.12). However, treatment of cyclopropyl carbinol (4.23) with catalytic amounts of tris(triphenylsilyl)oxovanadium(V) and bis[trans-1,2-cyclohexandiolato-O,O^1(1-)] dioxomolybdenum(VI) in refluxing toluene failed to show any rearrangement.

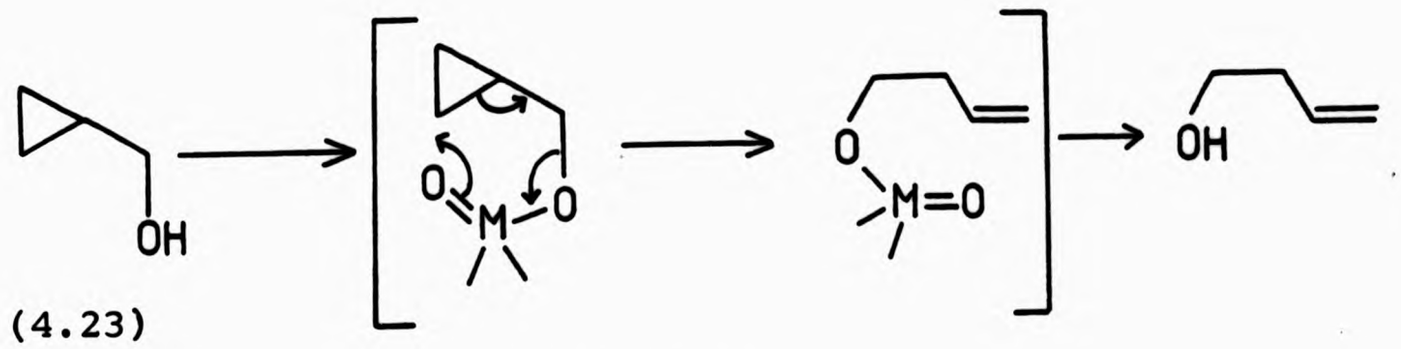

(4.23)

Scheme 4.12

4.5 Development of new isomerization catalysts

Other workers studying the oxo-vanadium catalysed isomerization of propargylic alcohols to α,β-unsaturated carbonyl compounds have investigated the effect of various

substituents on the catalytic activity of substituted triphenylsilyl vanadates and found that the presence of electron-donating groups in the aromatic ring resulted in slower rearrangements while electron-withdrawing groups increased the rate of rearrangement[118b]. In view of the similarity between the isomerization of propargylic and allylic alcohols it was envisaged by us that attachment of strongly electron-withdrawing groups to the metal would enhance the rate of isomerization of the latter. In addition, because of our own interest in the rearrangement of propargylic alcohols (Chapter 5), we wished to develop catalysts more reactive than those used by other workers for this rearrangement. Our attempts to prepare silyl vanadates with strongly electron-withdrawing groups are discussed below along with attempts to prepare other novel complexes of potential interest as isomerization catalysts.

4.5.1 [2-(Hydroxymethyl)-2-methyl-1,3-propandiolato]oxovanadium(V)

Complexes having 2-(hydroxymethyl)-2-methyl-1,3-propandiol (4.24) as ligand were considered to be potentially useful complexes for study as isomerization catalysts. Although the ligand is not electron-withdrawing,and would therefore not increase the Lewis acidity of the metal,it was thought probable that in an oxo-vanadium complex such as (4.25) the metal would be more accessible than in other alkoxy complexes because the alkoxy groups of the ligand would be "held back" from the metal centre and this may be advantageous for the isomerization reaction particularly if the mechanism requires only coordination of the allylic alcohol to the metal centre

(see Section 4.3). On the other hand if the rate of isomerization catalysed by (4.25) is slower than with the silyl-vanadates used previously, this could be indicative of a mechanism involving transesterification since this would be less favourable due to the additional stability resulting from a type of "chelate effect".

An attempt was made to prepare the oxo-vanadium complex of 2-(hydroxymethyl)-2-methyl-1,3-propandiol (4.24) by the method used to prepare tris(triphenylsilyl)oxovanadium(V)[118b] (vanadium pentoxide and the ligand in refluxing xylene). However, only unchanged ligand could be isolated from the reaction mixture.

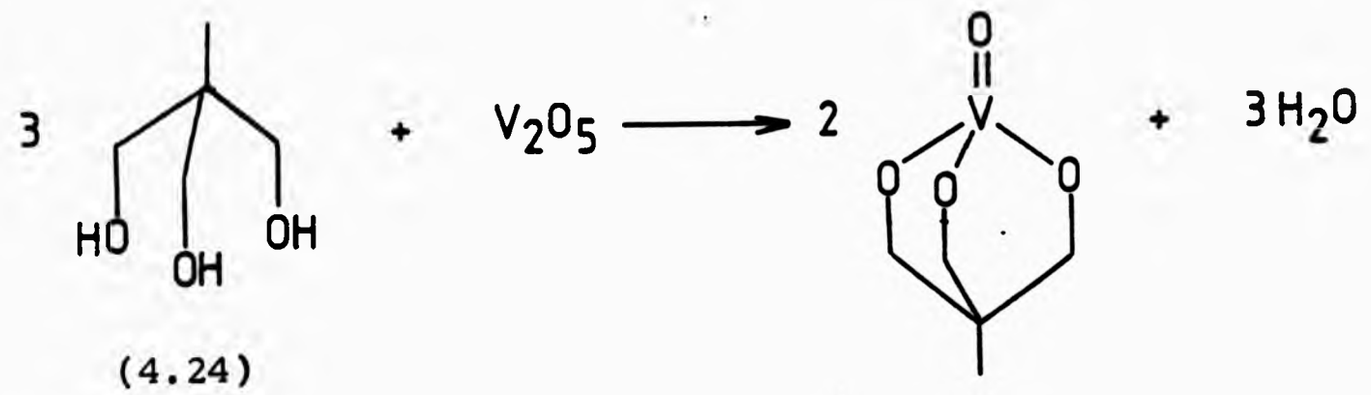

(4.24) (4.25)

4.5.2 Tris(trifluoromethylsilyl)oxovanadium(V)

Because of the very strong electron-withdrawing nature of the ligand, tris(trifluoromethylsilyl)oxovanadium(V) (4.26) is potentially a very reactive isomerization catalyst and it was proposed to synthesise this complex by the route shown (Scheme 4.13).

(see Section 4.3). On the other hand if the rate of isomerization catalysed by (4.25) is slower than with the silyl-vanadates used previously, this could be indicative of a mechanism involving transesterification since this would be less favourable due to the additional stability resulting from a type of "chelate effect".

An attempt was made to prepare the oxo-vanadium complex of 2-(hydroxymethyl)-2-methyl-1,3-propandiol (4.24) by the method used to prepare tris(triphenylsilyl)oxovanadium(V)[118b] (vanadium pentoxide and the ligand in refluxing xylene). However, only unchanged ligand could be isolated from the reaction mixture.

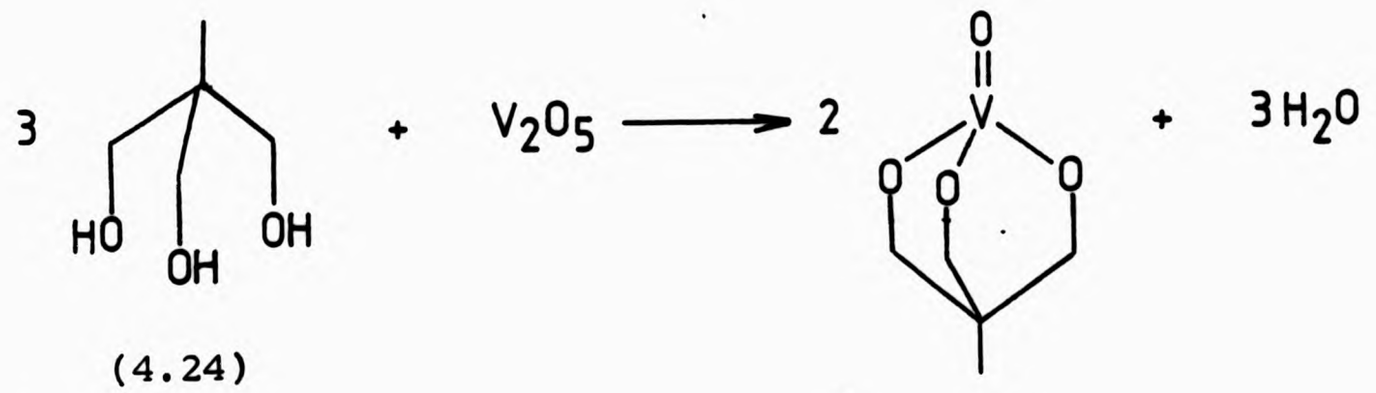

(4.24)

(4.25)

4.5.2 Tris(trifluoromethylsilyl)oxovanadium(V)

Because of the very strong electron-withdrawing nature of the ligand, tris(trifluoromethylsilyl)oxovanadium(V) (4.26) is potentially a very reactive isomerization catalyst and it was proposed to synthesise this complex by the route shown (Scheme 4.13).

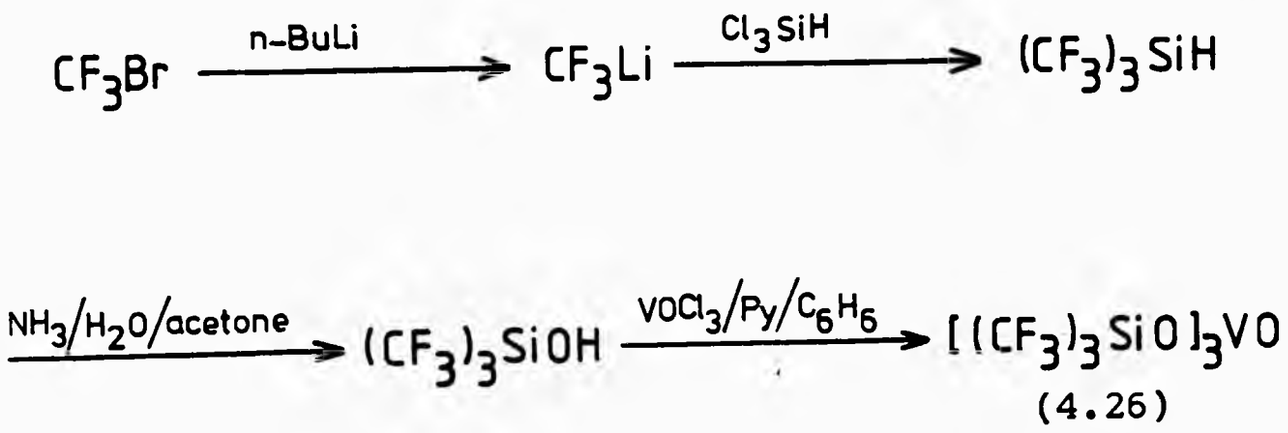

(4.26)

Scheme 4.13

There appear to be no reports in the literature in which trifluoromethyl lithium has been used to introduce the trifluoromethyl group into a molecule. Other workers have demonstrated the existence of heptafluoropropyllithium, produced by interchange with butyl and methyl lithium, but were unable to confirm the existence of trifluoromethyl lithium[131]. However, the production of difluorocarbene ($:CF_2$) in the reaction of bromotrifluoromethane with butyl lithium is thought to occur via trifluoromethyl lithium[132].

Because of the instability of trifluoromethyl lithium, its preparation was attempted at -100°C by metal-halogen exchange between bromotrifluoromethane and butyl lithium. After addition of trichlorosilane and warming to ambient temperature, addition of water gave a white solid, found to result from hydrolysis of unreacted trichlorosilane. The only other product that could be isolated was butyl bromide which clearly indicates that metal-halogen exchange had occurred, but the failure to isolate any fluorinated products suggests that the trifluoromethyl lithium had decomposed,

probably giving gaseous products, e.g. tetrafluoroethylene, as found by other workers[131].

4.5.3 Tris(tripentafluorophenylsilyl)oxovanadium(V)

Finally, the preparation of tris(tripentafluorophenylsilyl)-oxovanadium(V) (4.27) was considered as a possible alternative to tris(trifluoromethylsilyl)oxovanadium(V).

Tris(pentafluorophenyl)silanol (4.28) has been prepared previously by other workers[133] (Scheme 4.14).

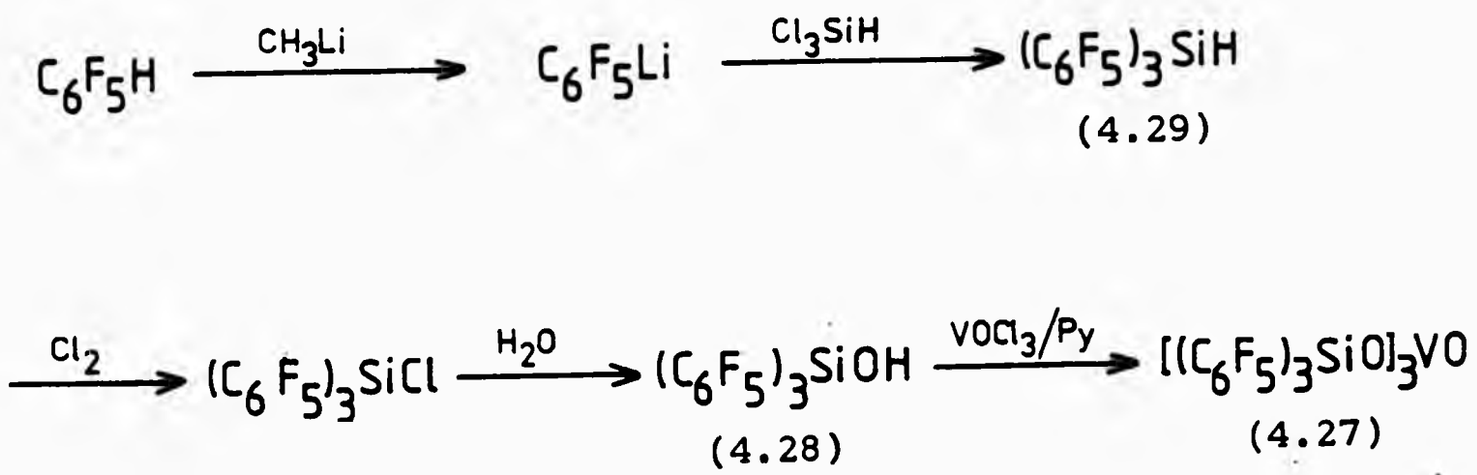

Scheme 4.14

An attempt was made to prepare tris(pentafluorophenyl)silane (4.29) by a similar route except that pentafluorophenyllithium was prepared by a method in which metalation is accomplished by a metal-halogen exchange between pentafluorobromobenzene and n-butyl lithium at -78°C in ether[134]. According to the procedure reported previously[133b], after addition of trichlorosilane to a solution of pentafluorophenyllithium and removal of solvent, tris(pentafluorophenyl)silane was sublimed from the reaction mixture. Attempts to prepare tris(pentafluorophenyl)silane in this way resulted in the precipitation of a white solid and no product could be

sublimed from the reaction mixture. Presumably the precipitated material resulted from the hydrolysis of trichlorosilane despite the use of dry reagents and nitrogen atmosphere. Other workers[134] have found pentafluorophenylmagnesium bromide easier to handle and suitable for most reactions. This could prove to be a useful alternative to pentafluorophenyllithium in the synthesis of this potentially very active rearrangement catalyst.

CHAPTER 5

POTENTIAL APPLICATION OF THE REARRANGEMENT OF PROPARGYLIC ALCOHOLS IN THE SYNTHESIS OF FIVE OR SIX-MEMBERED RING COMPOUNDS

5.1 Introduction

The formation of carbon-carbon bonds is of fundamental importance in synthetic organic chemistry and a great deal of effort has been expended in attempting to develop new and milder methods of effecting this process. Furthermore, the application of these techniques to achieve ring closure is central to the synthesis of many natural products.

During our studies on the oxo-metal catalysed isomerization of allylic alcohols we discovered that the related oxo-metal catalysed rearrangement of tertiary propargylic alcohols to α,β-unsaturated carbonyl compounds had been extensively studied by other workers. The mechanism of this reaction has been discussed previously (Section 3.3.2) and is considered to proceed via an "allene vanadate" which undergoes trans-esterification and rearrangement to form the α,β-unsaturated carbonyl compound. It was proposed by us that a suitably placed reactive group might trap the "allene vanadate" before protonation had had a chance to occur, thus allowing ring closure to take place (Scheme 5.1).

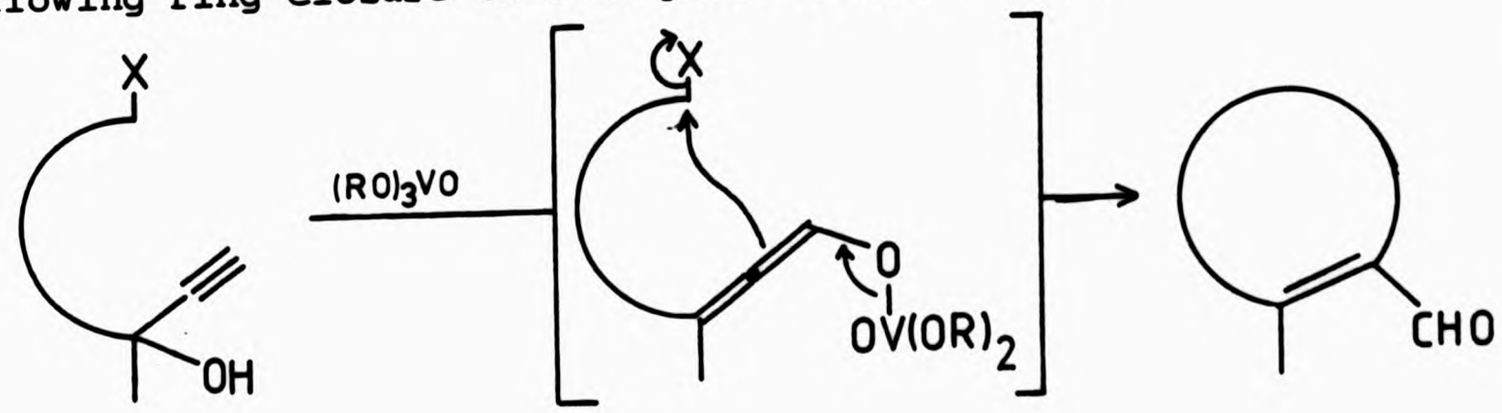

Scheme 5.1

Sections 5.3 and 5.4 discuss several unsuccessful attempts to apply this approach to the synthesis of ring systems in model compounds and in natural products. In addition mention is made of our attempts to rearrange primary propargylic alcohols, a process which has not previously been reported and which would have greatly increased the synthetic application of the proposed method.

5.2 Stereoelectronic requirements in ring closure processes

Baldwin[135] has shown that it is often possible to predict the relative facility of ring forming reactions by considering the stereochemical requirements of the transition states for the ring closure processes. Thus, favoured ring closures are those in which the length and nature of the linking chain enables the terminal atoms involved in the ring closure to follow a line of approach which corresponds to the final ring bond. Disfavoured ring closures are those which require severe distortion of bond angles and distances to achieve the required direction of approach, thus making the desired ring closure difficult. Furthermore it has been shown that for cyclisations resulting from alkylation of an enolate ion, the alkylation requires approach of the electrophile along a line perpendicular to the plane of the enolate[136].

From a study of models of the various allene-vanadate intermediates we have attempted to establish the relative feasibility of the ring closures in the routes discussed in subsequent sections. The types of allene-vanadate intermediates encountered are represented below, (5.1) to (5.4).

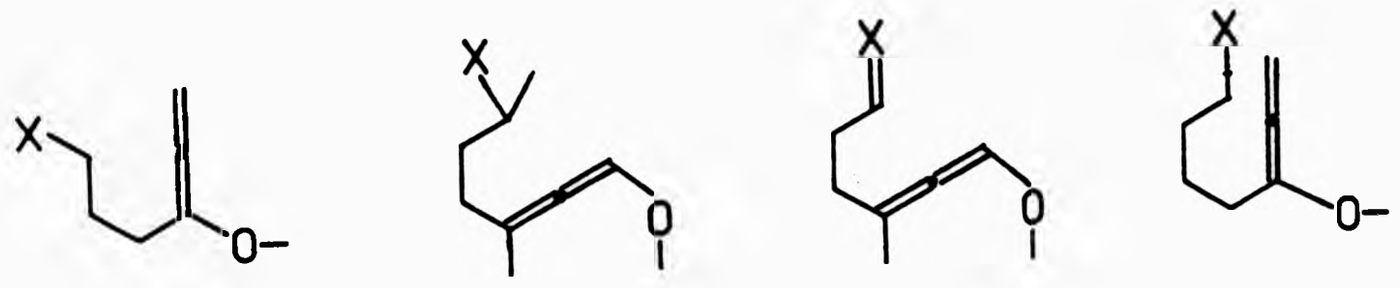

(5.1) (5.2) (5.3) (5.4)

As in the case of enolate ions, cyclisation of these proposed intermediates would presumably result from approach of the electrophile in a direction perpendicular to the plane of the allene-vanadate (Fig. 5.1). In the

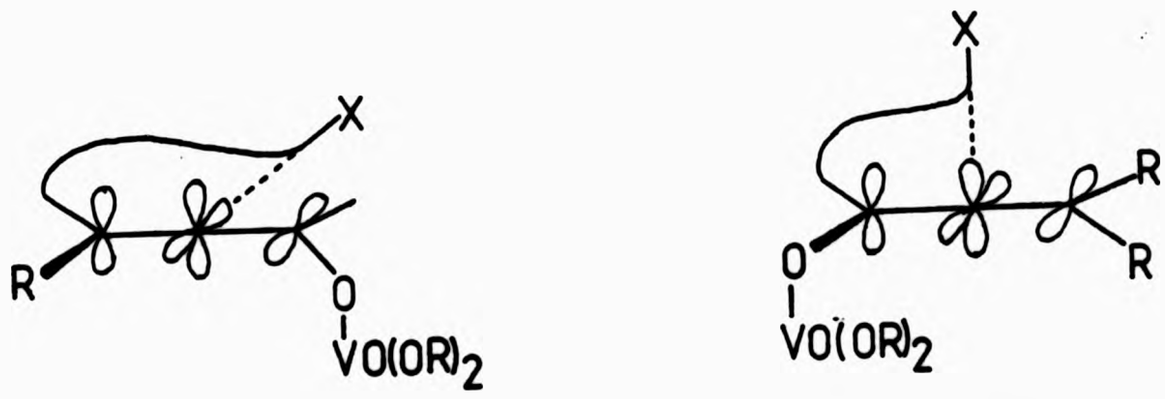

Fig. 5.1 Stereoelectronic requirements for ring closure of allene-vanadate intermediates.

case of intermediate (5.3) it is the p-orbital of the carbon of the C=X bond which must be perpendicular to the plane of the allene-vanadate giving maximum p-orbital overlap during bond formation.

A study of models has shown that (5.2), (5.3) and (5.4) can easily adopt the prefered transition state conformations for ring closure to readily take place.

The feasibility of intermediate (5.4) undergoing ring closure is further supported by the conclusion of Baldwin that the ring closure of the comparable enolate (5.5) is favoured[136].

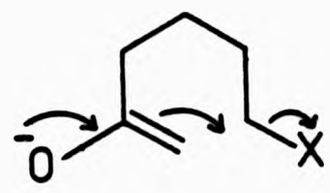

(5.5)

From model studies of the intermediate (5.1) it appears that some distortion of bond lengths and angles would be required to achieve the preferred transition state geometry and ring closure would therefore be less favoured. This is also in agreement with the observation made by Baldwin that formation of a five-membered ring from the comparable enolate (5.6) is sterically difficult[136].

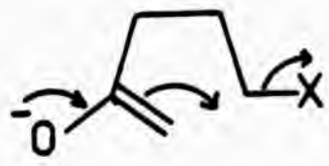

(5.6)

5.3 Synthesis of five-membered rings

5.3.1 Proposed synthesis of 2-methylene-cyclopentanones

Scheme 5.2 shows the proposed route for the synthesis of the methylene-cyclopentanone (5.9). It was anticipated that epoxidation of hex-5-en-2-yn-1-ol (5.7) would give

5,6-epoxyhexan-2-yn-1-ol (5.8) and that after the oxo-metal catalysed rearrangement of this,the allene enolate may open the epoxide ring giving (5.9). Such a process would have some synthetic importance because of the use of compounds such as (5.9) as synthetic precursors of the prostaglandins[137].

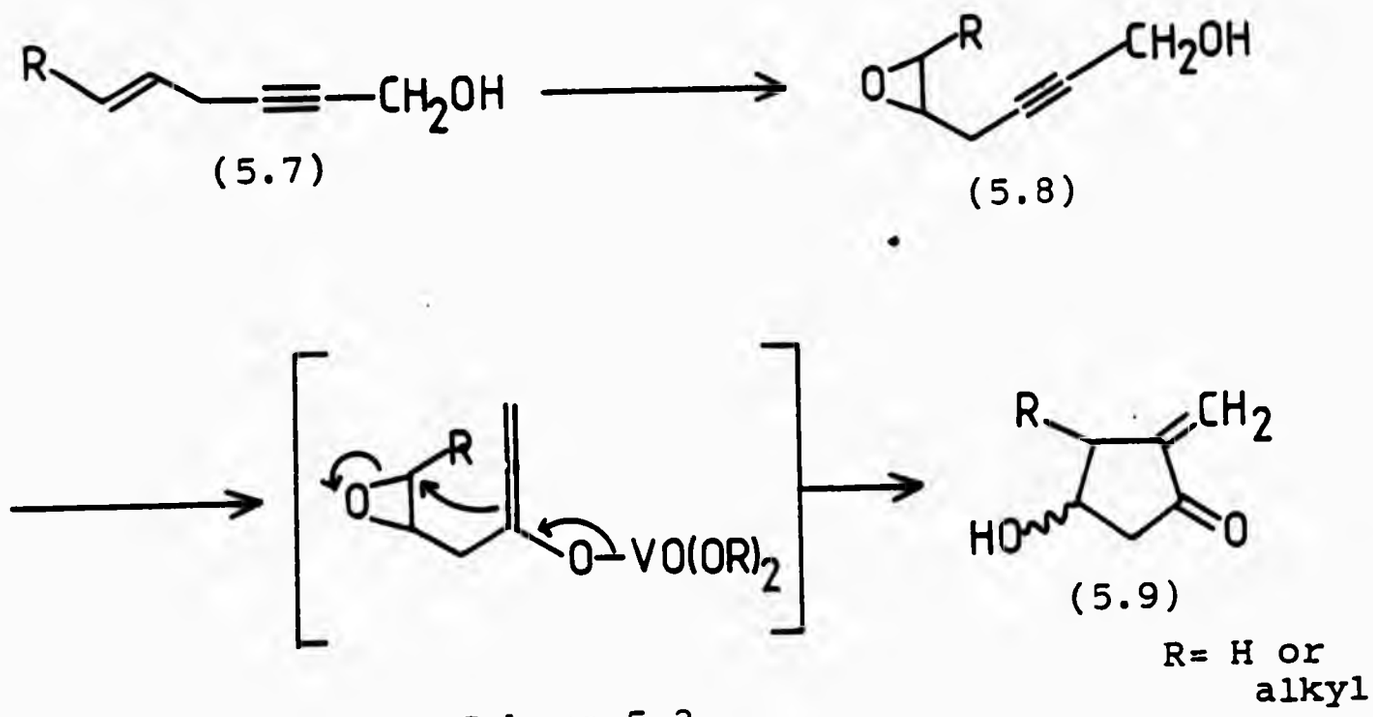

Scheme 5.2

Hex-5-en-2-yn-1-ol (5.7) was prepared as reported in the literature by the coupling of propargyl alcohols with allyl chloride in the presence of a base and a catalytic amount of cuprous chloride[138]. Tlc analysis of the reaction mixture obtained from attempted epoxidation of hex-5-en-2-yn-1-ol with m-chloroperbenzoic acid in dichloromethane showed it to be a mixture of products and although the ^1H nmr spectrum showed no olefinic proton signals (as would be expected), the methylene signal of the CH_2OH group had also decreased in intensity, suggesting some attack on the acetylenic group. Since it was later found that primary acetylenic alcohols could not be made to undergo isomerization in the

presence of the oxo-metal catalysts available,and also because of the complexity of the mixture obtained from the epoxidation, no further attempt was made to isolate and identify the nature of the products from this peracid oxidation.

Other workers[109b] have described only the oxo-metal catalysed rearrangement of secondary and tertiary acetylenic alcohols to α,β-unsaturated carbonyl compounds. Therefore, before pursuing the above synthesis further it was decided to check whether primary acetylenic alcohols will also rearrange since this forms the basis of the proposed route.

Spectroscopic analysis of the material isolated after heating hex-5-en-2-yn-1-ol (5.7) in refluxing toluene in the presence of catalytic amounts of tris(triphenylsilyl)-oxovanadium(V) and bis[trans-1,2-cyclohexandiolato-0,O^1(1-)]-dioxomolybedenum(VI) showed it to be unchanged starting material with no sign of a carbonyl stretching band in the infrared spectrum to suggest the presence of any rearranged product (Scheme 5.3). Similarly, attempts to use more forcing conditions in which the hex-5-en-2-yn-1-ol and catalyst were heated at 160°C using liquid paraffin as solvent resulted in recovery (75%) of unchanged starting material.

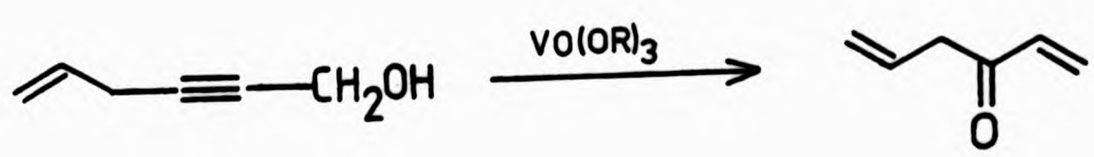

Scheme 5.3

The inability of existing oxo-metal catalysts to isomerize primary acetylenic alcohols led to unsuccessful attempts to prepare more reactive catalysts capable of isomerizing these substrates, and these attempts have been discussed previously (Section 4.5). Failure to synthesise a more reactive catalyst made it necessary to restrict the remainder of this work to syntheses involving rearrangement of a tertiary acetylenic alcohol group.

5.3.2 Proposed synthesis of cyclohexylidene-cyclopentanones

It was proposed to synthesise the cyclohexylidene-cyclopentanone (5.10) from 1-(4-penten-1-ynyl)cyclohexanol (5.11) by the route similar to that discussed above (Section 5.3.1) for the synthesis of methylene-cyclopentanones. The starting material, 1-(4-penten-1-ynyl)cyclohexanol was prepared by coupling the alkyne, 1-ethynyl-1-cyclohexanol, with allyl chloride in the presence of cuprous chloride. However, because of the low water solubility of the alkyne a procedure was adopted in which dimethylsulphoxide was employed as a cosolvent[139].

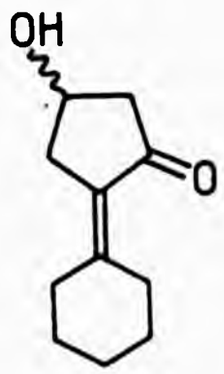

(5.10)

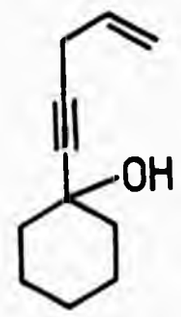

(5.11)

Attempted epoxidation of 1-(4-penten-1-ynyl)cyclohexanol (5.11) with m-chloroperbenzoic acid in dichloromethane gave an oil which was shown to contain four components by tlc analysis. The ^{1}H-nmr spectrum of the crude reaction mixture again suggested some reaction of the acetylene and this was supported by the apparent absence of a C≡C stretching band in the infrared spectrum. Therefore, no attempt was made to isolate and identify the products.

An alternative procedure was proposed (Scheme 5.4) in which the double bond of 1-(4-penten-1-ynyl)cyclohexanol (5.11) is subjected to hydroboration and the resulting alcohol (5.12a) reacted with p-toluenesulphonyl chloride in pyridine to give (5.12b). Rearrangement of (5.12b) in the presence of tris(triphenylsilyl)oxovanadium(V) may then give the cyclohexylidene-cyclopentanone (5.13).

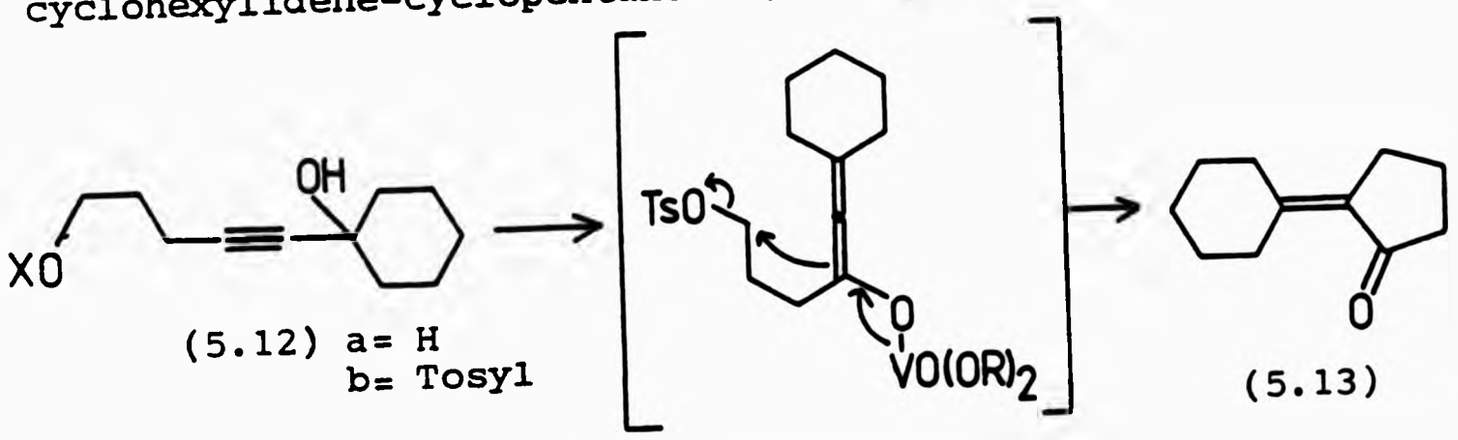

Scheme 5.4

Due to the greater reactivity of triple bonds to addition reactions such as reduction[140], hydroboration[141], and acid-catalysed hydration[142] it is generally difficult to selectively induce double bonds to undergo such additions in the presence of triple bonds. Therefore, not suprisingly attempts to hydroborate the double bond of (5.11) directly were unsuccessful. A method of protecting triple bonds

during addition reactions of the above type has been reported[143]. This involves formation of the corresponding acetylene-dicobalt hexacarbonyl complex which is prepared by stirring dicobalt octacarbonyl and the alkyne in a hydrocarbon solvent[144]. After hydroboration the ligand may be recovered by oxidative degradation of the complex with ethanolic ferric nitrate (Scheme 5.5).

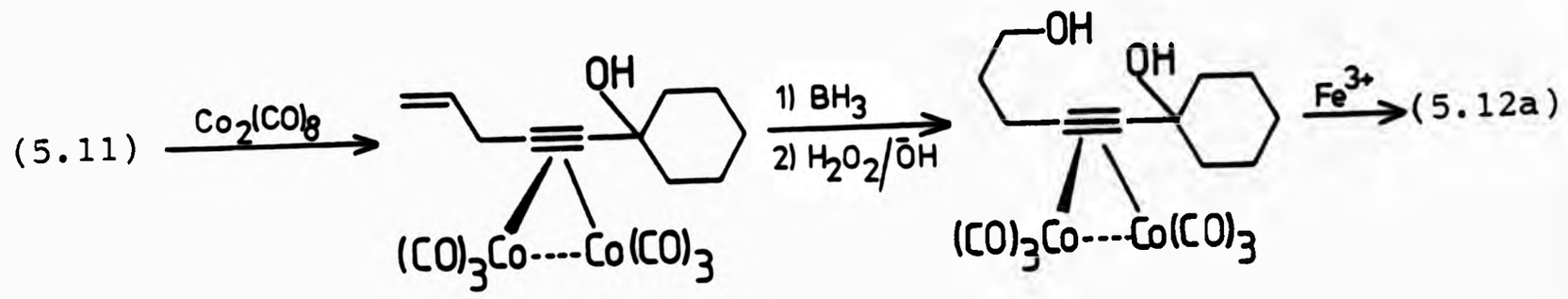

Scheme 5.5

Addition of dicobalt octacarbonyl to a solution of (5.11) in hexane resulted in rapid evolution of carbon monoxide. Removal of the solvent gave a dark red viscous oil which was shown by tlc analysis to contain a number of components. Attempts to purify the product by column chromatography over alumina were unsuccesful.

The infrared spectrum of dicobalt octacarbonyl exhibits four carbonyl absorption bands, the three bands at 2070, 2045 and 2024 cm^{-1} arise from the terminal carbonyl groups while the single band at 1859 cm^{-1} arises from the two bridging carbonyl groups[144]. Formation of the acetylenic-dicobalt hexacarbonyl should result in the disappearance of the band at 1859 cm^{-1} and in our case only a weak absorption band was observed in this position, indicating a small amount of unchanged dicobalt octacarbonyl

in the product. Furthermore the weak absorption band at 2254 cm^{-1}, characteristic of the carbon-carbon triple bond, also appeared to be absent in the infrared spectrum of the product. The observed evolution of carbon monoxide and the infrared data suggest that formation of the acetylenic-cobalt hexacarbonyl complex had taken place.

The crude mixture containing the complex was treated with diborane in tetrahydrofuran and worked up with a sodium hydroxide-hydrogen peroxide mixture in the normal way. After stirring with ethanolic ferric nitrate for several days the mixture was extracted with ether but only a small amount of highly coloured viscous oil could be isolated. The infrared spectrum of this oil showed the reappearance of the carbon-carbon triple bond absorption band and no carbonyl absorptions. However, because the yield was extremely low and insufficient material was isolated to fully characterise the product it was not considered worth while pursuing this route further.

5.3.3 Proposed synthesis of cyclopentenals

It was proposed to synthesise a number of cyclopentenals starting from dehydrolinalol (5.14). Dehydrolinalol was chosen as starting material for a number of reasons. First, the oxo-metal catalysed rearrangement of dehydrolinalol has been extensively studied and forms the basis of an industrial process for the manufacture of citral. Second, dehydrolinalol can itself be readily prepared in high yield from 6-methyl-5-hepten-2-one and sodium acetylide in liquid ammonia[145]. Finally, it was expected that the double bond in

dehydrolinalol, being trisubstituted, would be sufficiently reactive to allow reactions to take place selectively without the accompanying attack on the triple bond as experienced previously (Section 5.3.1 and 5.3.2).

As with the schemes discussed previously, the first route chosen for study involved epoxidation of the double bond followed by an oxo-metal catalysed rearrangement in which the epoxide ring is opened by the allene-vanadate intermediate to give the cyclized product (Scheme 5.6).

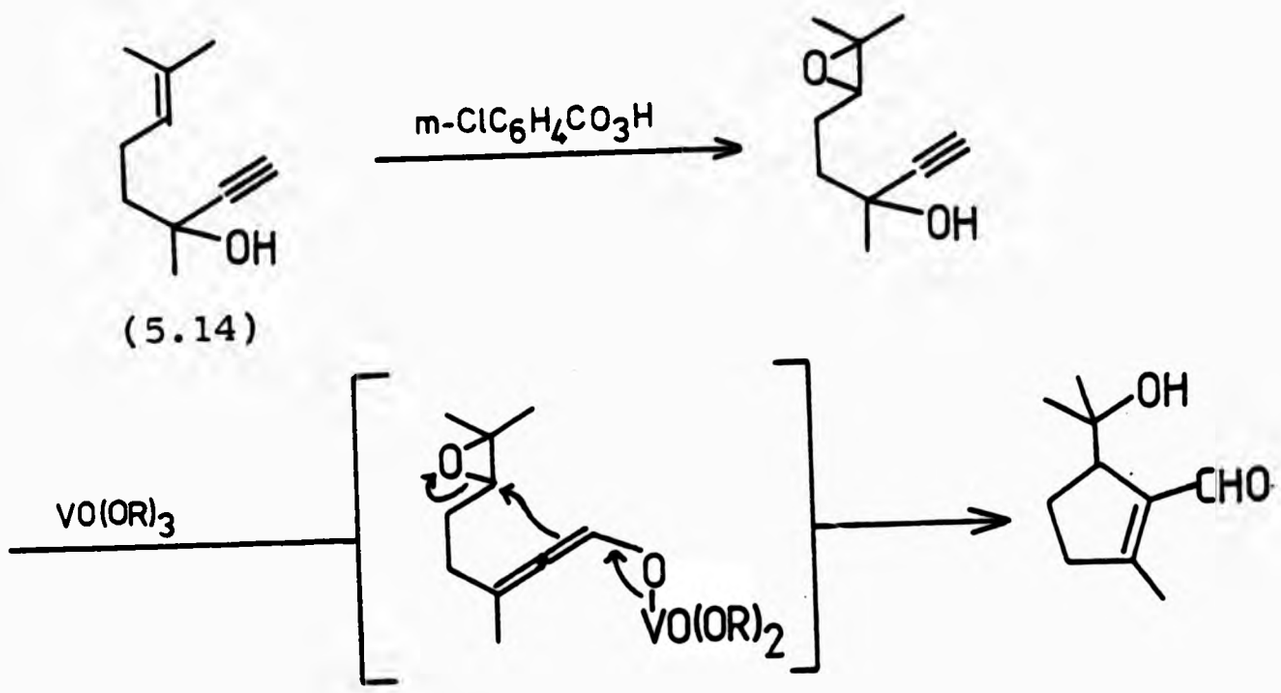

Scheme 5.6

On treatment with m-chloroperbenzoic acid,dehydrolinalol gave a new product containing the intact acetylenic group, as shown by the presence of the carbon-carbon triple bond stretching vibration in the infrared spectrum and the acetylenic proton signal in the ^{1}H-nmr spectrum. Additional features of the ^{1}H-nmr spectrum of the product were the upfield shift and separation of the signals arising from the two methyl groups, and also the upfield shift of what

was formerly the olefinic proton. However the fact that this signal was no longer a triplet but a complex multiplet was surprising.

The mass spectrum of the product did not give a parent ion (M^+) but gave an ion corresponding to loss of a methyl group (M^+-CH_3), which presumably results from α-cleavage of the acetylenic alcohol. Therefore, the above spectroscopic data on the isolated product appears to be consistent with the structure of the desired dehydrolinalol epoxide. However, no rearrangement occured on heating the product with tris(triphenylsilyl)oxovanadium(V) in toluene.

It has been reported[146] that peracid epoxidation of linalol (Scheme 5.7) does not give the expected epoxide but a mixture of the tetrahydrofuran (5.15) as the major product along with the tetrahydropyran (5.16).

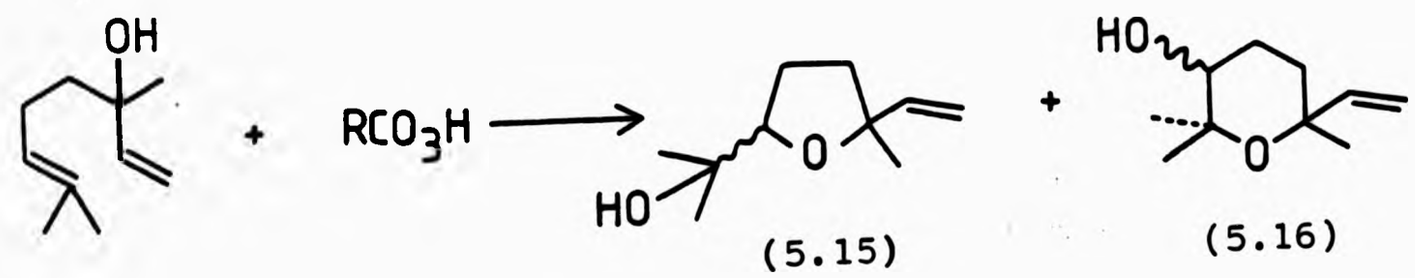

(5.15) (5.16)

Scheme 5.7

It therefore seems most likely that the product isolated from the peracid epoxidation of dehydrolinalol is predominantly the tetrahydrofuran (5.17), since the spectroscopic data would be equally consistent with this structure.

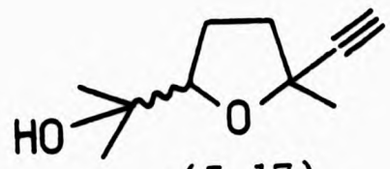

(5.17)

Several attempts were made to effect cyclisation by carrying out metal catalysed epoxidation and rearrangement in the same reaction vessel using tris(triphenylsilyl)oxo-vanadium(V) as catalyst for both reactions. In all cases the tetrahydrofuran (5.17) was the major product with a small amount of citral also being produced.

Because of the difficulty in making the dehydrolinalol epoxide this particular approach was not pursued further. An alternative synthesis was proposed (Scheme 5.8) in which the allene-vanadate intermediate in the oxo-metal catalysed rearrangement of the aldehyde (5.19) undergoes an aldol type addition with the carbonyl group to give the cyclopentenal (5.20).

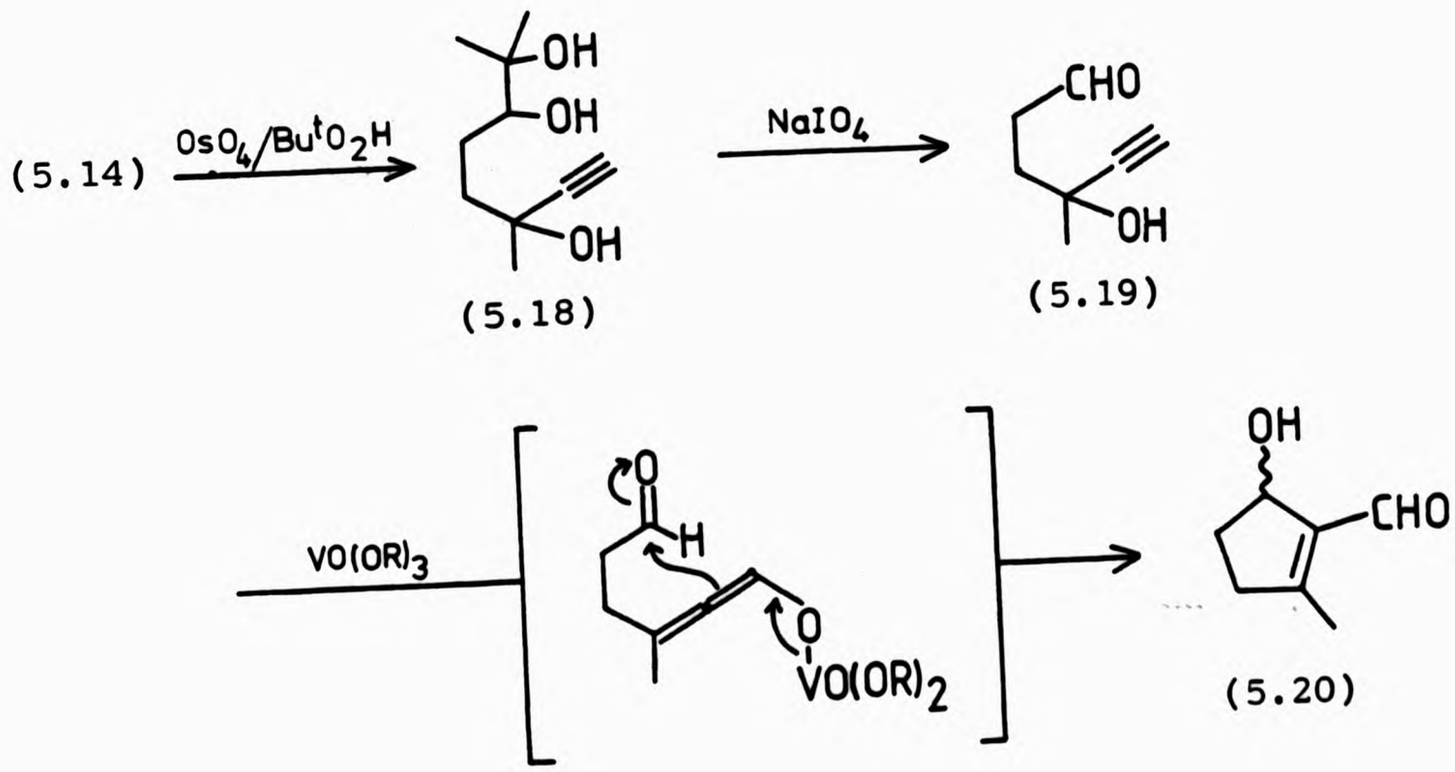

Scheme 5.8

Oxidation of dehydrolinalol with a basic solution of osmium tetroxide and t-butyl hydroperoxide[147] gave the triol (5.18) which was then treated with an aqueous solution of sodium periodate. The ^{1}H-nmr spectrum of the product isolated from the periodate oxidation showed no aldehydic proton and no carbonyl stretching band was observed in the infrared spectrum. Tlc analysis of the product indicated the presence of only one component but the ^{1}H-nmr spectrum showed two separate acetylene signals and two methyl signals suggesting a mixture of two components in approximately equal amounts.

Elemental analysis of the product was consistent with the molecular formula $C_7H_{11}O_2$ and although the mass spectrum showed no parent ion having this formula, the base peak corresponds to a M^+-18 ion which has been shown by accurate mass measurement to result from loss of a water molecule.

The most likely explanation for the above observations is that the hydroxyl group reacts with the carbonyl of the aldehyde (Scheme 5.9) forming the hemiacetal (5.21) and that the two diastereoisomers are distinguishable in the ^{1}H-nmr spectrum.

(5.21)

Scheme 5.9

Although the formation of the hemiacetal was not unexpected, it was hoped that sufficient of the open-chain form would be present in an equilibrium mixture to allow the rearrangement to take place. However, heating with

tris(triphenylsilyl)oxovanadium(V) in toluene resulted only in the recovery of unchanged starting material.

On allowing the hemiacetal to stand at room temperature for 24h, tlc analysis indicated partial conversion to a new product. The mixture was separated by column chromatography and the ^{1}H-nmr spectrum of the new product was also found to have a pair of methyl signals of approximately equal intensities, although the separation between the signals was less than in the hemiacetal. Only one signal was observed for the acetylenic proton, although on integration this was found to correspond to two protons. In addition the signal previously assigned to the methine proton in the hemiacetal had increased in complexity.

In the infrared spectrum the most significant feature was the disappearance of the OH stretch, present at 3440 cm^{-1} in the spectrum of the hemiacetal. Enol ether formation via elimination of water from the hemiacetal can be ruled out on the basis of the ^{1}H-nmr spectrum which shows only one proton in the 4-7 ppm region (originally assigned to the methine proton of the hemiacetal). The most likely remaining possibility is the formation of the acetal (5.22) arising from condensation of two molecules of the hemiacetal.

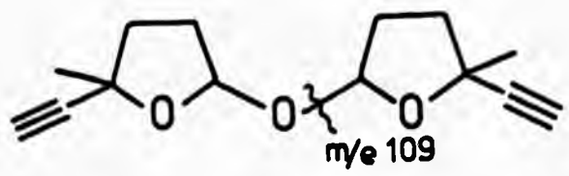

(5.22)

Satisfactory elemental analysis was obtained for this compound and although the mass spectrum showed no parent ion corresponding to the dimer, it did show a $M^{+}-CH_3$ ion and a base peak at m/e 109, arising from cleavage of the C-O ether bond in the dimer.

5.3.4 Proposed synthesis of chrysomelidial

Chrysomelidial (5.24), a physiologically active and biosynthetically important cyclopentanoid monoterpene extracted from the larvae of certain chrysomelid beetles[148], has recently been synthesised[149] from limonene (5.23) by a route involving cleavage of the cyclohexene ring followed by eventual recyclization to the cyclopentanoid (Scheme 5.10).

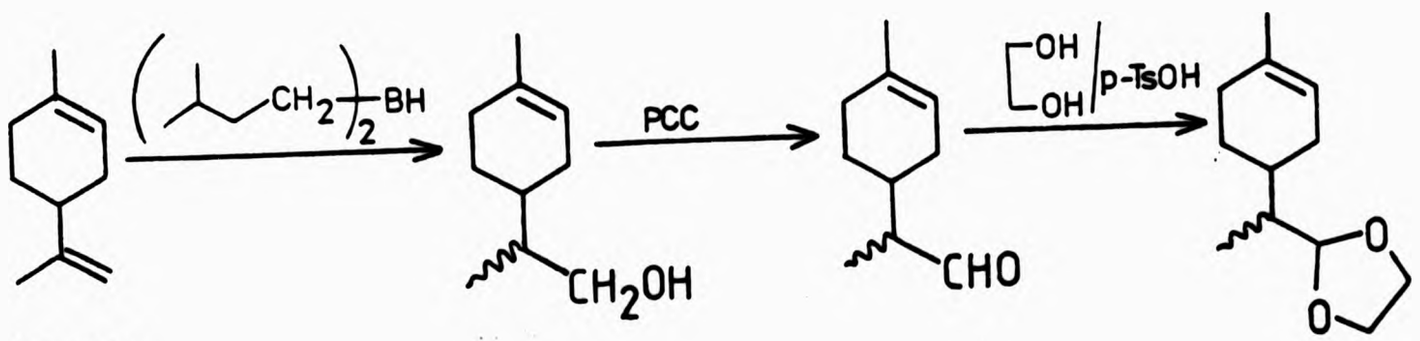

(5.23)

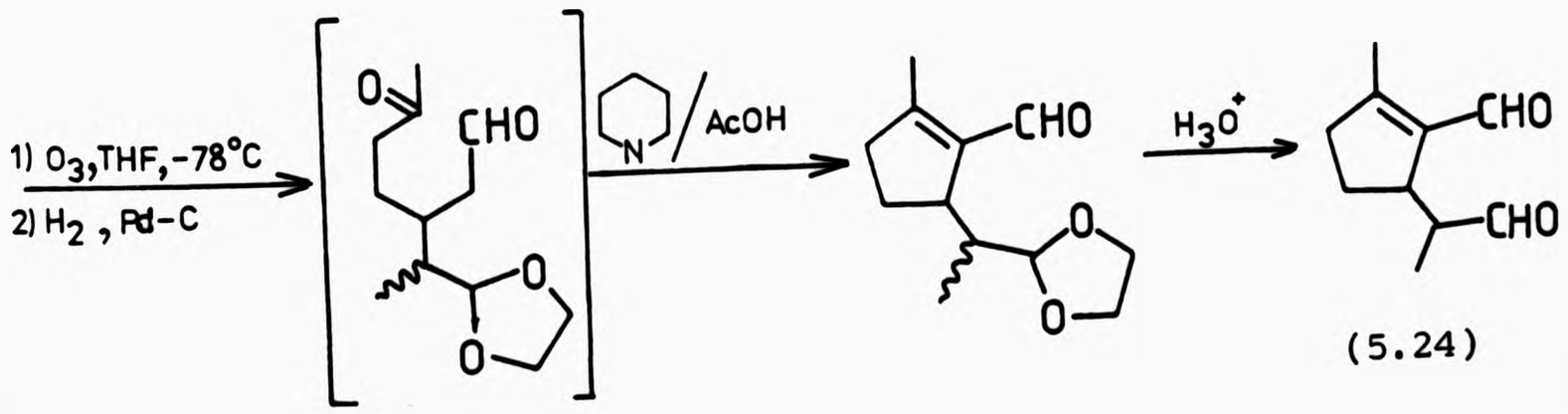

(5.24)

Scheme 5.10

A proposed route to chrysomelidial starting from dehydrolinalol is discussed below (Scheme 5.11). The key step in the synthesis was to be the oxo-metal catalysed rearrangement of the acetylenic alcohol (5.26), as it was hoped that the allene-vanadate intermediate in the rearrangement would undergo a Micheal type addition to effect ring closure giving chrysomelidial (5.24).

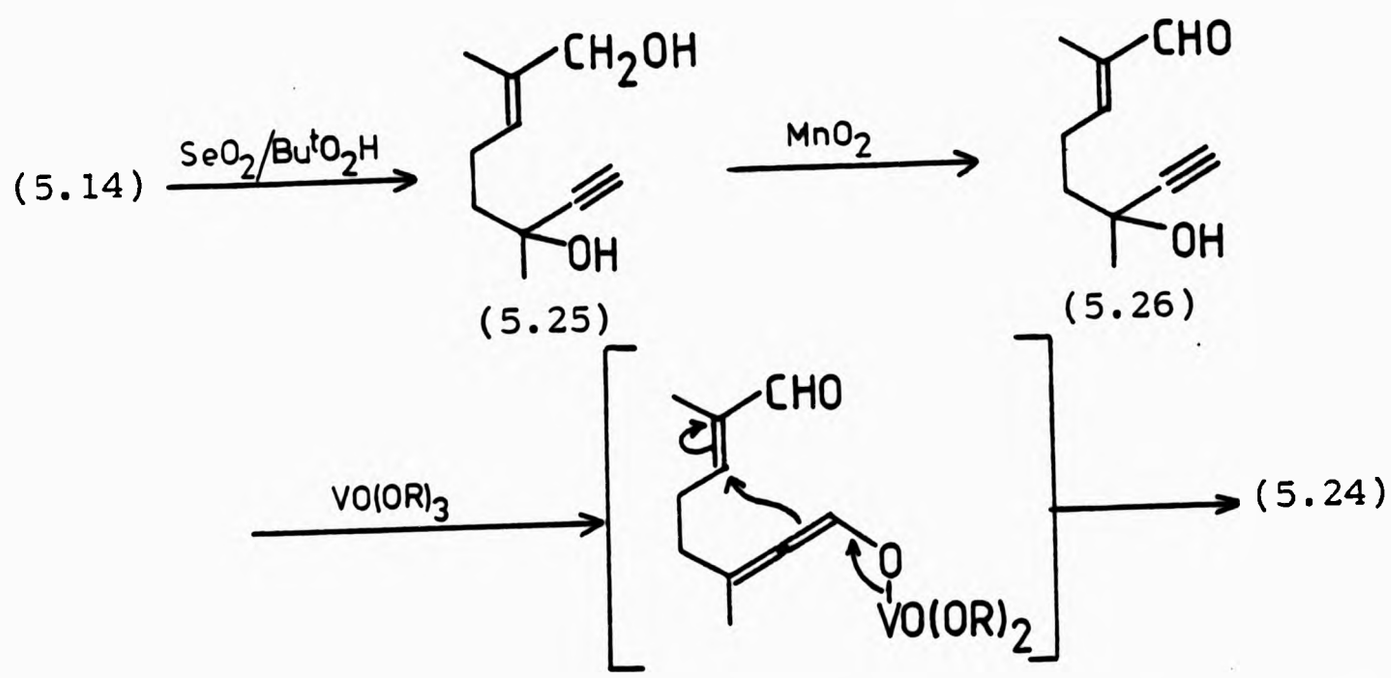

Scheme 5.11

Allylic oxidation of dehydrolinalol by a catalytic amount of selenium dioxide with t-butyl hydroperoxide[150] gave a mixture of the alcohol (5.25) and aldehyde (5.26) in the ration 1:0.3 in 53% yield. After separation of the alcohol by column chromatography, further oxidation with activated manganese dioxide gave the aldehyde (5.26) but recoveries were low (20%).

Tlc analysis of the mixture obtained after heating the aldehyde with tris(triphenylsilyl)oxovanadium(V) in refluxing toluene showed one major product with a number of poorly separated minor products. Separation of the mixture by column chromatography proved difficult and the major product was isolated in only 40% yield. It was not possible

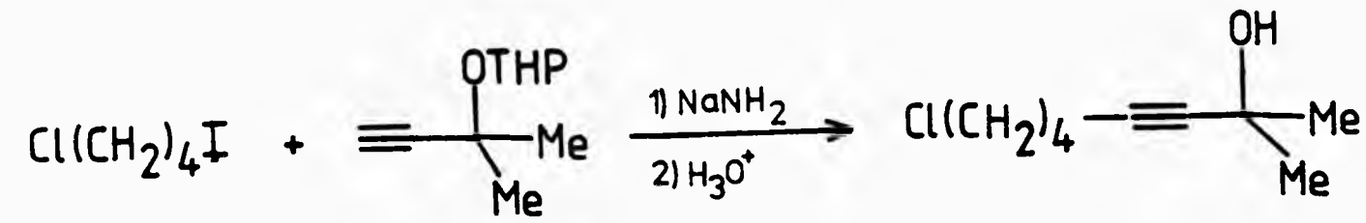

(5.29)

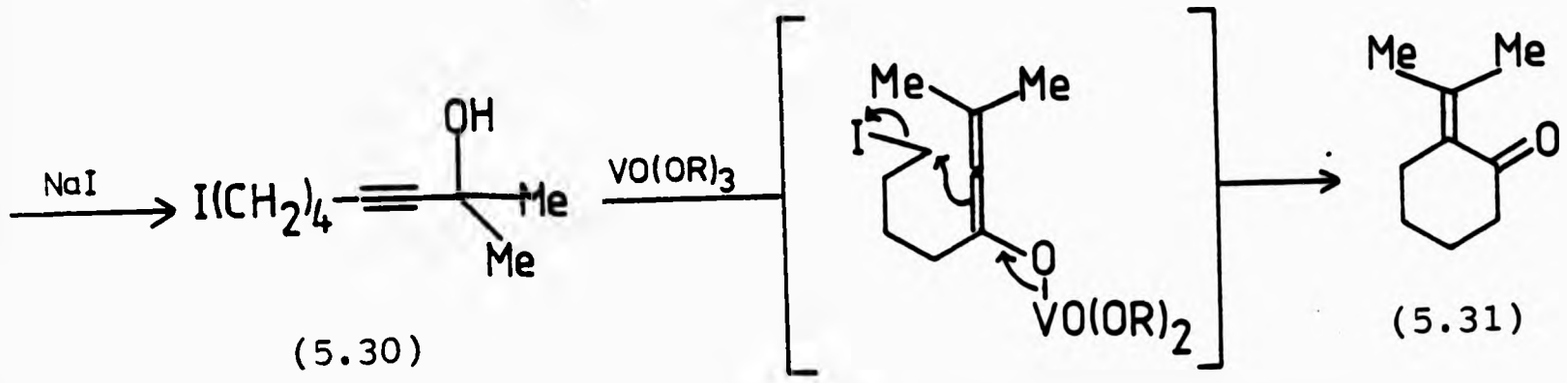

(5.30) (5.31)

Scheme 5.12

1-Chloro-4-iodobutane was prepared from 1,4-dichlorobutane by refluxing in acetone with sodium iodide[152]. Initial attempts to prepare 8-chloro-2-methyl-3-octyn-3-ol (5.29) by addition of 1-chloro-4-iodobutane to the disodium salt of 2-methyl-3-butyn-2-ol in liquid ammonia gave only the O-alkylated product. The hydroxyl group of 2-methyl-3-butyn-2-ol was therefore protected by formation of the tetrahydropyranyl ether,and addition of 1-chloro-4-iodobutane to the lithium acetylide of this ether gave (5.29) in 40% yield after acid hydrolysis.

Treatment of (5.29) with sodium iodide in refluxing acetone[153] gave 8-iodo-2-methyl-3-octyn-2-ol (5.30). On treatment with tris(triphenylsilyl)oxovanadium(V) in refluxing toluene (5.30) was converted almost entirely to a single new compound. The infrared spectrum of this product showed a band at 1690 cm^{-1} corresponding to a

carbonyl stretching vibration of a α,β-unsaturated ketone. The ^{1}H-nmr spectrum indicated that the iodo group was still present in the product molecule and in addition showed an olefinic signal at δ 6.0.

From the spectroscopic evidence it is clear that the acetylenic alcohol (5.30) has rearranged to the α,β-unsaturated ketone (5.32) without cyclization. Satisfactory analytical data was also obtained for this compound.

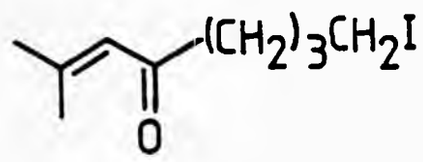

(5.32)

Although the desired cyclised product was not obtained it is perhaps useful to note that the rearrangement can be carried out successfully in a molecule containing an iodo group which may be sensitive to other reagents.

From these experiments it is clear that protonation of the allene-vanadate intermediate must be rapid, resulting in formation of only the α,β-unsaturated carbonyl compound. In an attempt to prevent or slow-down this protonation step, the above rearrangement was carried out in the presence of the base N,N-diisopropylethylamine, however, this only had the effect of slowing down the rearrangement to the α,β-unsaturated carbonyl compound.

An alternative possibility considered for slowing down proton transfer to the allene-vanadate intermediate,thus allowing cyclisation to occur in preference to the normal rearrangement, was to carry out the reaction at high dilution. However, from results of experiments carried out

in the presence of base it seems likely that the proton is held by the ligand and thus easily transferred to the allene-vanadate ester during the reaction. If the reaction does proceed via a proton transfer from the ligand the use of high dilution would have no effect on the nature of the product.

Since we have been unable to obtain cyclised products by the oxo-metal catalysed isomerization of acetylenic alcohols it may be more feasible to devise ring forming reactions using the preformed allene acetates obtained from the silver catalysed rearrangement of the acetate esters of acetylenic alcohols (see Section 3.2.2). Treatment of the allene acetates with reagents such as methyl lithium would cleave the ester, generating the allene enolate under aprotic conditions which may then rearrange with cyclization (Scheme 5.13).

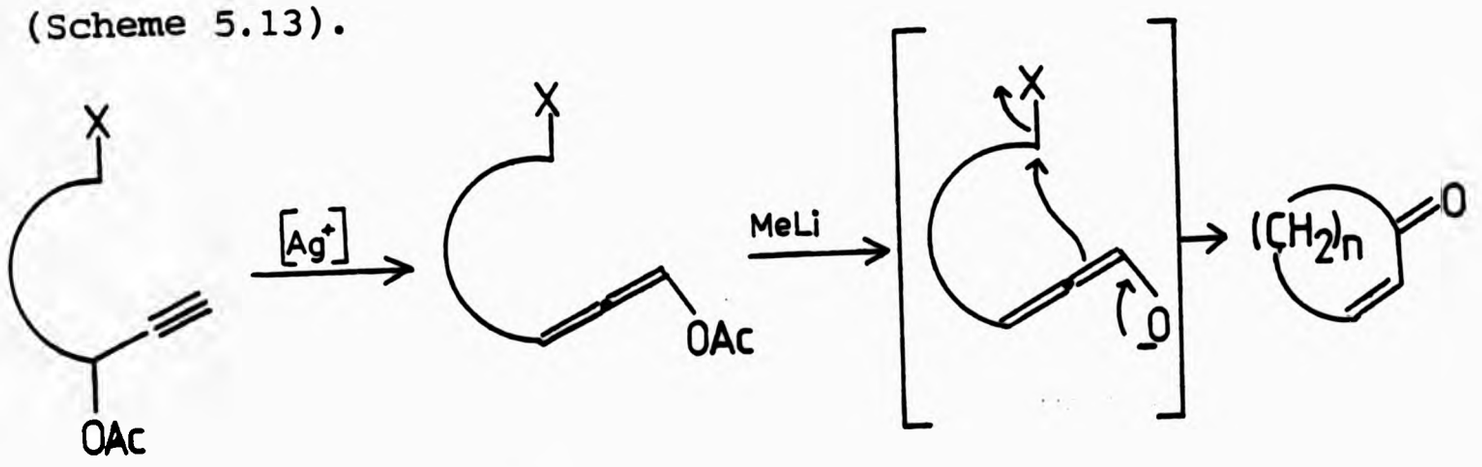

Scheme 5.13

CHAPTER 6

EXPERIMENTAL

Melting points (mp not corrected) were determined on Kofler hot-stage apparatus. Proton nmr spectra were recorded at 60 MHz on a Perkin-Elmer R12B Spectrometer using tetramethylsilane as an internal standard and maintaining the sample at 35°C. Infrared spectra were recorded in the form of liquid films, nujol mulls or as KBr discs using a Pye-Unicam SP2000 spectrophotometer. Uv spectra were obtained on a Pye-Unicam SP1800 spectrophotometer. Mass spectra were recorded at 70 eV on a Hitachi-Perkin-Elmer R.M.S.4 single focus spectrometer, either by distillation or by direct insertion. High resolution mass spectra were measured at the physico-chemical measurements unit, Harwell, on a A.E.I. MS50 spectrometer. Major ion fragments are quoted as percentages of the base peak (100%), which were measured using a Digispec 50SM data system. Elemental analyses were performed by the department microanalyst using a Perkin-Elmer 240 carbon, hydrogen and nitrogen analyser. Optical rotations were measured on a Perkin-Elmer 141 Polarimeter. Glc analyses were performed on a Perkin-Elmer F11 chromatograph using stainless steel columns or on a Pye series 104 chromatograph using glass columns with a flame ionisation detector and nitrogen carrier gas. The following columns were used:-

(A) 4m S.S, 15% carbowax 20M on Chromasorb W.

(B) 1.5m, glass, 10% SP2100 on Supelcoport 80/100 mesh (supplied by Phase Separations Ltd.)

Analytical tlc was carried out using 2 cm x 10 cm glass plates precoated with Merk silica gel $60F_{254}$ (0.25 mm thickness). Spots were visualised by : (a) ultra violet radiation, (b) spraying with potassium permanganate solution, or (c) by exposure to iodine vapour. Column chromatography was carried out with 60-120 mesh silica gel.

Petroleum ether bp 60-80°C was distilled before use. Ether, benzene and toluene where described as dry were distilled over sodium and stored over clean sodium wire. Tetrahydrofuran was distilled from lithium aluminium hydride, under nitrogen, immediately prior to use. Dichloromethane and chloroform were distilled from phosphorous pentoxide. t-Butanol was purified by heating with potassium permanganate for 24 h., filtering, and distilling the filtrate from fresh solid potassium permanganate.

t-Butyl hydroperoxide was purified by dissolving in an approximately equal volume of ether, in a flange flask fitted with a mechanical stirrer, dropping funnel and thermometer. The mixture was cooled to below 5°C in an ice bath and the theoretically required volume of 40% sodium hydroxide solution added dropwise ensuring the temperature does not rise above 10°C. The sodium salt was filtered off, washed with petroleum spirit (30-40°), and dried under suction. The solid was slurried with water and CO_2 bubbled through until two layers separated. The t-butyl hydroperoxide was extracted with ether and the organic layer dried over

sodium sulphate. After removal of the ether under reduced pressure the t-butyl hydroperoxide was distilled (small quantities only) bp 32°C/15mm, and the active oxygen content determined by iodometric titration.

Iodometric determination of hydroperoxide

Solutions of acetic acid (2.5 ml) in isopropanol (25 ml) (solution A) and sodium iodide (2 g) in isopropanol (10 ml) (solution B) were prepared. To an accurately weighed sample of hydroperoxide (ca. 0.7 mmol) in a 100 ml flask was added 25 ml of solution A followed by 10 ml of solution B (N.B. not the reverse procedure). After refluxing for 5 min, 5 ml of water was added and the mixture titrated with standard sodium thiosulphate solution (0.2 mol l^{-1}). The concentration is calculated from the equation:

$$\left[0.5\left(\frac{x}{1000} \times y\right)/M\right] \times 100 = \% \text{ peroxide}$$

where, x=conc. of thiosulphate solution in mol l^{-1}, y = ml of thiosulphate for titration and M=molecular weight of hydroperoxide.

6.1 Experimental relating to chapter 2

Epoxidation of oct-1-ene catalysed by; (i) bis(acetylacetonato)-oxovanadium(IV) and (ii) bis(acetylacetonato)dioxomolybdenum(VI)

(i) Oct-1-ene (1.0 g, 8.9 mmol) in dry benzene (1 ml) was added to a stirred solution of bis(acetylacetonato)oxovanadium-(IV) (26 mg, 0.1 mmol) in dry benzene (3 ml) under a nitrogen atmosphere. The mixture was heated to 80°C and 95% t-butyl hydroperoxide (0.84g, 8.9 mmol) in dry benzene (1 ml) was added over a period of 20 min and the reaction mixture refluxed for a further 4 h. Glc analysis (column A) of the crude reaction mixture showed no 1,2-epoxyoctane.

(ii) Use of bis(acetylacetonato)dioxomolybdenum(VI) as catalyst in the above procedure gave approximately 20% conversion to 1,2-epoxyoctane according to glc analysis (column A) of the crude reaction mixture.

Epoxidation of citronellene (2.1)

Citronellene (0.5g, 3.6 mmol) and bis[trans-1,2-cyclohexandiolato-O,O^1(1-)]dioxomolybdenum(VI) (13 mg, 0.036 mmol) were stirred in dry toluene (10 ml) at 80°C under a nitrogen atmosphere for 15 min. A solution of 80% t-butyl hydroperoxide (0.45 g, 3.96 mmol) in dry toluene (3 ml) was added dropwise to the reaction mixture over a period of 10 min and the reaction stirred at 80°C for a further 3 h. The reaction mixture was cooled to room temperature and shaken with 40% sodium bisulphite solution (20 ml), and the organic layer dried over Na_2SO_4. Removal of toluene under reduced pressure gave an oil (0.46 g) which was shown by

glc analysis (column B) to contain; 2,3-epoxycitronellene (58%), 3,7-dimethyloct-1-en-6,7-diol (6%) and unreacted citronellene (36%).

Epoxidation of methoxycitronellene (2.2)

Methoxycitronellene (0.61 g, 3.6 mmol) was epoxidised according to the procedure described above for the epoxidation of citronellene. Glc analysis (column B) of the reaction mixture after 2 h. showed only slight conversion to methoxycitronellene epoxide and 17 h was required to reach a conversion of 47%.

N,N^1-Ethylenebis(iminomethylcamphorato)oxovanadium(IV) (2.6)

Bis(acetylacetonato)oxovanadium(IV) (0.069 g, 0.26 mmol) and N,N^1-ethylenebis(iminomethylcamphor) (0.1 g, 0.26 mmol) were ground together in a small mortar. The mixture was transfered to a round-bottom flask and heated at 230°C for 2-3 h at a pressure of 0.5 mm. A green solid sublimed up the side of the flask. After cooling to room temperature the product was dissolved in the minimum amount of dry ether (the free ligand is insoluble) and the solution filtered. Removal of the ether gave a dark green solid which was purified further by vacuum sublimation at 180°C/0.5 mm giving N,N^1-ethylenebis(iminomethylcamphorato)oxovanadium(IV) (0.05 g, 42%). It was not possible to obtain a sample of the complex completely uncontaminated by free ligand.

The above complex can be kept for several weeks in a desiccator over calcium chloride but eventually decomposes turning to a black solid. Solutions of the complex in most

common solvents are unstable, usually decomposing in a few hours.

UV-VIS $\lambda_{max}(CH_2Cl_2)$ 568 nm (ε~77) and 637 nm (ε~106)

IR 987(V=0) cm^{-1}

MS m/e (re intensity), 449(M^+)(75), 421(18), 393(15), 205(59), 192(100); calcd m/e for $C_{24}H_{34}N_2O_3V$, 449.2009 (found, 449.1987).

$[\alpha]_D^{20}$(EtOH) +197

3-Hydroxyiminobornan-2-one (2.11)

To liquid ammonia (300 ml) in a flask equiped with a magnetic stirrer and an acetone-dry ice condenser with a soda-lime drying tube, was added the minimum amount of sodium to produce a permanent blue colour. A few crystals of ferric nitrate was added followed by the slow addition of sodium (11.5 g, 0.5 mol). After stirring for a further 1 h the ammonia was allowed to evaporate and replaced with dry ether (200 ml) and the resulting suspension of sodium amide in ether refluxed for 0.5 h to ensure removal of ammonia. After cooling to room temperature a solution of camphor (50 g, 0.33 mol) in dry ether (100 ml) was added dropwise to the sodium amide suspension and the mixture stirred for a further 2 h. To the cooled (0-5°C) reaction mixture was added amyl nitrite (45 g, 0.38 mol) over a period of 4 h. After leaving the reaction at room temperature for 18 h it was poured into an ice-water mixture and the aqueous layer extracted several times with ether to remove unreacted starting material. The aqueous layer was purged with nitrogen to remove traces of ether and acidification

with glacial acetic acid precipitated a solid which was filtered off. The solid was redissolved in ether and insoluble material removed by filtration. Evaporation of the ether and recrystallisation of the solid from toluene/ petroleum ether (60/80) gave a white solid (42 g, 71%) mp 149-150°C.

IR 3360(O-H), 1730(C=O), 1645(C=N) cm^{-1}

NMR ($CDCl_3$) δ 3.27 (1H, m, -C<u>H</u>), 1.4-2.1 (4H, m, 2xC<u>H</u>$_2$), 1.0 and 0.98 (6H, 2xS, C(10)<u>H</u>$_3$ and C(9)<u>H</u>$_3$), 0.86 (3H, S, C(8)<u>H</u>$_3$).

MS m/e (rel intensity), 181(M^+)(6), 150(25), 137(34), 120(100), 110(20), 94(56), 83(28), 70(32).

The spectral data are identical to that reported in the lit.[154]

<u>Cis,exo-3-amino-2-hydroxybornane (2.12)</u>

A solution of 3-hydroxyiminobornan-2-one (8.0 g, 35 mmol) in dry ether (200 ml) was added to a suspension of lithium aluminium hydride (5.6 g, 140 mmol) in dry ether (400 ml) over a period of 1 h. The mixture was heated under reflux for ½ h, cooled to room temperature and the excess lithium aluminium hydride destroyed by the dropwise addition of water (12 ml), 10% NaOH (14 ml) and water (20 ml), added in rapid succession while stirring vigorously. The precipitated solid was filtered off, washed several times with ether and the filtrate extracted with dil. HCl. Basification of the acid solution with dil. NaOH released the base which was extracted with ether (3x20 ml) and the ether extracts dried over anhydrous Na_2SO_4. Removal of the solvent gave a white

solid which was recrystallized several times from petroleum ether (60-80°) giving cis,exo-3-amino-2-hydroxybornane, mp 192-195° (3.27 g, 55%).

Cis,exo-3-dimethylamino-2-hydroxybornane (2.13)

To a solution of cis,exo-3-amino-2-hydroxybornane (0.2 g, 1.2 mmol) and 37% aqueous formaldehyde (0.5 g, 6 mmol) in acetonitrile (4 ml) was added sodium cyanoborohydride (0.12 g, 1.0 mmol). The reaction mixture was stirred for 15 min and glacial acetic acid added dropwise until the solution was neutral when tested with moist pH paper. Stirring was continued for a further 1 h with glacial acetic acid being added as required to maintain the pH near neutrality. The solvent was evaporated off under reduced pressure, and 2N KOH (5 ml) was added to the residue which was extracted with ether (3x5 ml). The combined ether extracts were washed with 0.5N KOH (5 ml) and then extracted with 1N HCl (3x5 ml). The acid extracts were combined and neutralized with solid KOH and extracted with ether (3x10 ml). The combined ether extracts were dried over Na_2SO_4 and the solvent evaporated to give a pale yellow oil (0.2 g, 85%). Tlc analysis (Silica gel;petroleum ether:ethylacetate 3:1) indicated two major components. After separation by column chromatography on a silica gel column eluted with toluene/diethyl ether (1:1), the component with the shortest retention time was identified as N-methyl-cis,exo-bornyl[2,3]oxazolidine (2.14) (0.12 g):

solid which was recrystallized several times from petroleum ether (60-80°) giving cis,exo-3-amino-2-hydroxybornane, mp 192-195° (3.27 g, 55%).

Cis.exo-3-dimethylamino-2-hydroxybornane (2.13)

To a solution of cis,exo-3-amino-2-hydroxybornane (0.2 g, 1.2 mmol) and 37% aqueous formaldehyde (0.5 g, 6 mmol) in acetonitrile (4 ml) was added sodium cyanoborohydride (0.12 g, 1.0 mmol). The reaction mixture was stirred for 15 min and glacial acetic acid added dropwise until the solution was neutral when tested with moist pH paper. Stirring was continued for a further 1 h with glacial acetic acid being added as required to maintain the pH near neutrality. The solvent was evaporated off under reduced pressure, and 2N KOH (5 ml) was added to the residue which was extracted with ether (3x5 ml). The combined ether extracts were washed with 0.5N KOH (5 ml) and then extracted with 1N HCl (3x5 ml). The acid extracts were combined and neutralized with solid KOH and extracted with ether (3x10 ml). The combined ether extracts were dried over Na_2SO_4 and the solvent evaporated to give a pale yellow oil (0.2 g, 85%). Tlc analysis (Silica gel;petroleum ether:ethylacetate 3:1) indicated two major components. After separation by column chromatography on a silica gel column eluted with toluene/diethyl ether (1:1), the component with the shortest retention time was identified as N-methyl-cis,exo-bornyl[2,3]oxazolidine (2.14) (0.12 g):

IR 1067, 1084 and 1139(oxazolidine ring) cm^{-1}

NMR ($CDCl_3$) δ 4.45 and 3.67 (1H, d, J=2.5 Hz, O-C<u>H</u>$_2$-N), 3.80 (1H, d, J=7.6 Hz, CC<u>H</u>O), 2.32 (1H, d, J=7.6 Hz, CC<u>H</u>N), 2.29 (3H, S, N-C<u>H</u>$_3$), 1.16 (3H, S, C<u>H</u>$_3$), 0.98 (3H, S, C<u>H</u>$_3$), 0.79 (3H, S, C<u>H</u>$_3$).

MS m/e (rel intensity), 195(M^+)(50), 180(11), 166(31), 152(68), 137(29), 126(41), 112(58), 98(100); calcd. m/e for $C_{12}H_{21}NO$, 195.1623 (found 195.1636).

The second component isolated by column chromatography was identified as <u>cis</u>,<u>exo</u>-3-dimethylamino-2-hydroxybornane (2.13) (0.06 g). Although the preparation of this compound by an alternative route has been reported by other workers[65] (Section 2.3.2), spectroscopic data is given here since this has not been previously reported.

IR 3400(O-H), 1400(C-N) cm^{-1}

NMR ($CDCl_3$) δ 3.42 (1H, d, J=6.6 Hz, CC<u>H</u>OH), 2.28 (6H, S, N(C<u>H</u>$_3$)$_2$), 2.20 (1H, d, J=6.6 Hz, CC<u>H</u>-N), 1.02 (3H, S, C<u>H</u>$_3$), 0.92 (3H, S, C<u>H</u>$_3$), 0.75 (3H, S, C<u>H</u>$_3$).

MS m/e (rel intensity), 197(M^+)(6), 182(6), 168(14), 149(22), 112(100); calcd. m/e for $C_{12}H_{23}NO$, 197.1780 (found 197.1787).

<u>Attempted preparation of (acetylacetonato)[cis,exo-3-dimethylamino-2-hydroxy-bornanato]dioxomolybdenum(VI) (2.10)</u>

A mixture of bis(acetylacetonato)dioxomolybdenum(VI) (0.16 g, 0.5 mmol) and <u>cis</u>,<u>exo</u>-3-dimethylamino-2-hydroxybornane (0.12 g, 0.6 mmol) in dry hexane (8 ml) was stirred at 70-75°C for 1 h. The solid was filtered off and its infrared spectrum was found to be identical to that of bis(acetylacetonato)-

dioxomolybdenum(VI). Removal of the solvent from the filtrate gave an oil which was found to be unchanged aminoalcohol.

[N-(Cis,exo-2-hydroxybornyl)-3-salicylideniminato(2-)]-(methanolato)dioxomolybdenum(VI) (2.17a)

To a suspension of bis(salicylaldehydato)dioxomolybdenum(VI) (0.11 g, 0.3 mmol) in dry methanol (3 ml) was added cis,exo-3-amino-2-hydroxybornane (0.1 g, 0.6 mmol) and the mixture was refluxed for ½ h under nitrogen. After allowing to stand overnight at ambient temperature the pale yellow solid was filtered off, washed thoroughly with methanol and dried in vacuo to give 2.17a (95 mg, 73%).

IR 1625(C=N) cm^{-1}

NMR (d-DMSO) δ 8.67 (1H, d, J=2.5 Hz, CH=N), 6.7-7.8 (4H, m, aromatic), 4.48 (1H, d, J=7.3 Hz, CH-O), 4.00 (1H, d of d, J=2.5 and 7.3 Hz, CH-N), 3.30 (methanol), 0.89,0.88 and 0.82 (9H, methyls).

MS m/e (rel intensity), 401(M^+)(15), 383(6), 289(23), 275(15), 249(7), 150(18), 134(100), 109(23), 95(44); calcd. m/e for $C_{17}H_{21}O_4N^{98}Mo$, 401.0525 (found 401.0510).

[N-(Cis,exo-2-hydroxybornyl)-3-methoxysalicylideniminato(2-)]-(methanolato)dioxomolybdenum(VI) (2.17b)

This complex was prepared from bis(o-methoxysalicylaldehydato) dioxomolybdenum(VI) according to the procedure described above for the preparation of 2.17a.

IR As for 2.17a.

dioxomolybdenum(VI). Removal of the solvent from the filtrate gave an oil which was found to be unchanged aminoalcohol.

[N-(Cis,exo-2-hydroxybornyl)-3-salicylideniminato(2-)]-(methanolato)dioxomolybdenum(VI) (2.17a)

To a suspension of bis(salicylaldehydato)dioxomolybdenum(VI) (0.11 g, 0.3 mmol) in dry methanol (3 ml) was added cis,exo-3-amino-2-hydroxybornane (0.1 g, 0.6 mmol) and the mixture was refluxed for ½ h under nitrogen. After allowing to stand overnight at ambient temperature the pale yellow solid was filtered off, washed thoroughly with methanol and dried in vacuo to give 2.17a (95 mg, 73%).

IR 1625(C=N) cm^{-1}

NMR (d-DMSO) δ 8.67 (1H, d, J=2.5 Hz, CH=N), 6.7-7.8 (4H, m, aromatic), 4.48 (1H, d, J=7.3 Hz, CH-O), 4.00 (1H, d of d, J=2.5 and 7.3 Hz, CH-N), 3.30 (methanol), 0.89,0.88 and 0.82 (9H, methyls).

MS m/e (rel intensity), 401(M^+)(15), 383(6), 289(23), 275(15), 249(7), 150(18), 134(100), 109(23), 95(44); calcd. m/e for $C_{17}H_{21}O_4N^{98}Mo$, 401.0525 (found 401.0510).

[N-(Cis,exo-2-hydroxybornyl)-3-methoxysalicylideniminato(2-)]-(methanolato)dioxomolybdenum(VI) (2.17b)

This complex was prepared from bis(o-methoxysalicylaldehydato) dioxomolybdenum(VI) according to the procedure described above for the preparation of 2.17a.

IR As for 2.17a.

rom the

hanged

nato(2-)]-

o)dioxo-

anol (3 ml) was

, 0.6 mmol) and

en. After

ature the pale

hly with methanol

., 6.7-7.8 (4H, m,

), 4.00 (1H, d of d,

1), 0.89,0.88 and

6), 289(23), 275(15),

(44); calcd. m/e for

0).

lideniminato(2-)]-

ethoxysalicylaldehydato)

re described above

NMR (d-DMSO) As for 2.17a but in addition δ 3.77 (3H, S, O-CH_3)

MS m/e (rel intensity), 431(M^+)(20), 321(22), 303(14), 150(13), 134(100), 109(18), 95(38), 67(17); calcd. m/e for $C_{18}H_{23}NO_5{}^{98}MO$, 431.0631 (found 431.0627).

The complexes 2.17a and 2.17b were insoluble in most common solvents except pyridine, DMF and DMSO. Recrystallization from a DMF-methanol mixture gave a crystalline product in which the methanol ligand was replaced by a DMF ligand, giving a carbonyl absorption band at 1670 cm^{-1} in the infrared spectrum.

[N-(ℓ(-)-Butan-1-ol)-2-methoxysalicylideniminato(2-)]-(methanolato)dioxomolybdenum(VI) (2.21)

To a suspension of bis(o-methoxysalicylaldehydato)dioxomolybdenum(VI) (0.13 g, 0.3 mmol) in dry methanol (3 ml) was added ℓ(-)-2-amino-1-butanol (0.027 g, 0.3 mmol) and the mixture was refluxed for ½ h under nitrogen. The solvent was evaporated off under reduced pressure and the remaining solid dispersed in dry chloroform, filtered off and dried in vacuo to give (2.21) (82 mg, 72%).

IR 1640(C=N) cm^{-1}

NMR (d-DMSO) δ 8.70 (1H, S, CH=N), 6.6-7.3 (3H, m, aromatic), 4.34 (2H, m, CH_2-O), 3.81 (1H, m, CH-N), 3.75 (3H, S, OCH_3), 3.30 (methanol), 1.69 (2H, q, J=6.6 Hz, CH_3-CH_2-), 0.88 (3H, t, J=6.6 Hz, CH_3-CH_2-).

MS m/e (rel intensity), 351(M^+)(83), 321(88), 302(100), 296(44), 279(54), 264(39), 262(35); calcd. m/e for $C_{12}H_{15}NO_5{}^{98}Mo$, 351.0005 (found 350.9999).

Cis-Bis[D(-)-2,3-butandiolato-O,O′(1-)]dioxomolybdenum(VI) (2.22)

Bis(acetylacetonato)dioxomolybdenum(VI) (0.25 g, 0.75 mmol) was ground to a fine powder and added to a stirred mixture of D(-)-2,3-butandiol (0.19 g, 2 mmol) in dry cyclohexane (1 ml). The reaction was stirred at 80°C under nitrogen for 1 h during which time a white solid was formed which was filtered off, washed with dry hexane and dried *in vacuo* giving (2.22) (0.16 g, 69%), mp 130°C (decomp.), (Found:C, 31.32;H, 5.88. $C_8H_{18}O_6$.Mo requires C, 31.37;H, 5.88).

Attempts to recrystallise (2.22) were unsuccessful since the complex was insoluble and unstable when heated in most common solvents.

IR 930 and 959(O=Mo=O), 2600-3400(broad, co-ordinated O-H) cm^{-1}

NMR ($CDCl_3$) δ 4.63 (4H, m, -C<u>H</u>-), 1.27 and 1.24 (12H, two overlapping doublets, J=6.0 Hz, four C<u>H</u>$_3$-). Due to precipitation accompanying decomposition of the complex in solution, only a poor quality nmr spectrum was obtainable.

Stability of [N-(cis,exo-2-hydroxybornyl)-3-salicylideniminato (2-)](methanolato)dioxomolybdenum(VI) under epoxidising conditions

The complex (20 mg, 0.03 mmol), epoxycyclohexane (30 mg, 0.3 mmol) and 90% t-butyl hydroperoxide (30 mg, 0.3 mmol) were stirred at 80°C in dry cyclohexane (2 ml) for 1 h under a nitrogen atmosphere. After cooling the reaction mixture to room temperature the solid was filtered off and washed with methanol. The infrared spectrum of the isolated solid was identical to that of the starting complex.

Procedure for the epoxidation of geraniol catalysed by pre-formed complexes.

Geraniol (1.0 g, 6.5 mmol) and the catalyst (0.065 mmol) were stirred at 40-45°C in dry toluene (15 ml) under a nitrogen atmosphere for 15 min. t-Butyl hydroperoxide (80%) (0.79 g, 7 mmol) in dry toluene (5 ml) was added dropwise to the reaction mixture over a period of 10 min and the mixture stirred at 40-45°C until tlc analysis showed no further epoxide formation (40-50 h). If the 2,3-epoxygeraniol was required the reaction mixture was shaken with 45% sodium bisulphite solution (4.0 ml) and the organic layer dried over Na_2SO_4. After removal of the solvent under reduced pressure the product was isolated by chromatography on a silica gel column eluted with petroleum ether/acetone (6:1). Alternatively, the epoxyacetate was formed by cooling the reaction mixture to 25°C and adding a solution of acetic anhydride (3 ml) in pyridine (4.5 ml) and stirring for 6 h. The reaction mixture was poured into ice and the organic layer washed with water (3x50 ml), 1N hydrochloric acid (2x50 ml), 45% sodium bisulphite solution (40 ml) and 2% sodium bicarbonate solution (40 ml). After drying the organic layer over Na_2SO_4 and removal of the solvent under reduced pressure the epoxyacetate was isolated by chromatography on a silica gel column eluted with petroleum ether (60-80°)/acetone (40:1).

Procedure for the epoxidation of geraniol catalysed by complexes formed in situ

Geraniol (0.5 g, 3.25 mmol), bis(acetylacetonato)-

dioxomolybdenum(VI) (10.6 mg, 0.0325 mmol) and the ligand (0.16 mmol) were stirred at 40-45°C in dry toluene (10 ml) under a nitrogen atmosphere for 15 min. t-Butyl hydroperoxide (80%) (0.4 g, 3.5 mmol) in dry toluene (5 ml) was added dropwise over a period of 10 min and the reaction stirred until tlc analysis showed no further epoxide formation (24-40 h). The reaction mixture was worked-up and the product isolated according to the procedure described above for epoxidations carried out in the presence of pre-formed catalysts. In the reaction in which cis,exo-3-amino-2-hydroxybornane was the ligand, the 2,3-epoxygeraniol isolated by column chromatography was purified further by short-path distillation.

Preparation of pinane hydroperoxide

Cis-pinane (250 g, 1.8 mol) was heated to 85-90°C and t-butyl hydroperoxide (95%, 2.5 g, 26 mmol) added to initiate the reaction. Air (500 ml min^{-1}) was bubbled into the reaction mixture (85°C) over a period of about 20 h, after which time iodometric titration indicated 25% conversion to pinane hydroperoxide. After cooling to ambient temperature, ether (15 ml) was added to the reaction mixture which was then cooled further in an ice-bath to 5°C. To the stirred reaction mixture was added 40% sodium hydroxide solution (40 ml) at such a rate that the temperature did not rise above 10°C. The sodium salt of pinane hydroperoxide was filtered off, washed with petroleum ether (60-80) and slurried in a small volume of water. Carbon dioxide was bubbled into the slurry to regenerate the pinane hydroperoxide

which was extracted with ether and dried over Na_2SO_4. Removal of the solvent under reduced pressure gave pinane hydroperoxide (61 g, 20%) which was shown to be 81% pure by iodometric titration.

Epoxidations with pinane hydroperoxide

Epoxidations using pinane hydroperoxide were carried out in exactly the same way as those described for t-butyl hydroperoxide.

6.2 Experimental relating to chapter 4

Glc studies on the isomerization of geraniol and linalol

Pre-treatment of isomerization mixtures for glc analysis

The direct injection on the glc column of reaction mixtures obtained from the metal catalysed isomerization of allylic alcohols was found to result in a build-up of metal containing species on the column, leading to isomerization of the substrate on the column. In the case of reactions carried out in the presence of molybdenum catalysts this problem was overcome by passing the reaction mixture down a short (10x0.6 cm) column of basic alumina (activity III) and eluting with ether. After removal of the solvent the molybdenum free sample was injected directly onto the column.

Tris(triphenylsilyl)oxovanadium(V) could not be removed from reaction mixtures by this technique and it was necessary to repack the column when the build-up of vanadium species became sufficient to promote the isomerization.

Quantitative glc analysis

Response factors for geraniol (K_g) and linalol (K_l) were determined relative to the internal standard (2-methylnapthalene) by preparing a calibration mixture containing accurately weighed amounts of geraniol (100 mg), linalol (50 mg) and 2-methylnaphthalene (50 mg) in benzene (15 ml). Removal of the solvent under reduced pressure gave an oil which was chromatographed (column A) and the response factor for each component determined as follows:

$$\frac{A}{A_s} \times \frac{W_s}{W} = K$$

where A = Area of component peak

A_s = Area of internal standard peak

W = Wt. of component

W_s = Wt. of internal standard

In the subsequent analysis of reaction mixtures the percentage of each component was then given by the formula;

$$\% = \frac{A}{A_s} \times \frac{W_s}{K} \times 100$$

Nerol was assumed to have the same response as geraniol.

Isomerization of geraniol and linalol

i) Catalysed by bis(acetylacetonato)dioxomolybdenum(VI)

The allylic alcohol (0.12 g, 0.78 mmol) and bis(acetylacetonato)dioxomolybdenum(VI) (5 mg, 0.015 mmol) were stirred in benzene (15 ml) at 40°C or 80°C (see Table 4.1) under a nitrogen atmosphere for 1 h. 2-Methyl naphthalene (0.1 g) (internal standard) was added to the reaction mixture which was then passed down an alumina column as described above. Removal of the solvent under reduced pressure (15 mm) gave an oil which was analysed by glc (column A).

ii) Catalysed by bis[trans-1,2-cycloheandiolato-0,0′(1-)]-dioxomolybdenum(VI)

The allylic alcohol (0.12 g, 0.78 mmol) and MoO_2-(1,2-cyclohexandiol)$_2$ (20 mg, 0.06 mmol) in toluene (15 ml) were stirred at 100°C under a nitrogen atmosphere for 24 h.

2-Methylnaphthalene (50 mg) (internal standard) was added to the reaction mixture which was then passed down an alumina column. Removal of the solvent under reduced pressure gave an oil which was analysed directly by glc (column A).

iii) Catalysed by tris(triphenylsilyl)oxovanadium(V)

The reaction was carried out as described above in (ii) but tris(triphenylsilyl)oxovandadium(V) (56 mg, 0.06 mmol) was used as catalyst. In reactions using this catalyst, pre-treatment with an alumina column was excluded.

Isomerization of a geraniol/nerol mixture

Geraniol (0.12 g, 0.8 mmol), nerol (0.12 g, 0.8 mmol) and MoO_2(1,2-cyclohexandiol)$_2$ (36.6 mg, 0.11 mmol) were stirred in toluene (15 ml) at 100°C under a nitrogen atmosphere. The progress of the reaction was monitored over 7 h by periodically removing 1 ml aliquots from the reaction mixture. After pre-treatment through an alumina column and reducing the volume of solvent under reduced pressure the samples were analysed by glc (column A) and the relative areas of geraniol and nerol determined.

^{1}H-Nmr studies on the isomerization of allylic alcohols.

Kinetic studies on the isomerization of geraniol (Fig. 4.1)

An accurately weighed sample of tris(triphenylsilyl)-oxovanadium(V) (0.27 g, 0.3 mmol, 7.7 mol%) was dissolved in deutero-benzene (3 ml) and an accurately weighed amount of geraniol (0.6 g, 3.8 mmol) added. Approximately 0.5 ml

of this solution was then placed in six nmr tubes and the stoppered tubes were placed in a thermostated oil bath at 80°C. At intervals of 10,20,30,45,60 and 90 min, a tube was removed from the oil bath and the nmr spectrum recorded. Integration of the $-C\underline{H}_2-O$ signal of geraniol and the $-C(OH)C\underline{H}_3$ signal of linalol enabled the concentration of linalol in each sample to be determined from the formula:

$$M-\left(\frac{x}{y \times 1.5}\right) = \text{Conc. of linalol in mol } l^{-1}$$

where M = initial conc. of geraniol in mol l^{-1}

x = integration of linalol signal

y = integration of linalol signal

Similar experiments were carried out using tris-(triphenylsilyl)oxovanadium(V) at approximately 4 and 2 mol% levels.

<u>General procedure for the ^{1}H-nmr study of allylic alcohol isomerization</u>

Tris(triphenylsilyl)oxovanadium(V) (46 mg, 0.05 mmol, 7.7 mol%) was dissolved with warming in deutero-benzene (0.5 ml). Allylic alcohols (0.65 mmol) was added and the reaction mixture was transferred to an nmr tube. The stoppered tube was placed in a thermostated oil bath at 80°C and the progress of the reaction followed by periodically recording the nmr spectrum. The percentage

composition of the reaction mixture was determined from the integration of suitably separated signals of the two allylic isomers.

Preparative scale isomerization experiments.

Isomerization of farnesol (4.13)

To a stirred mixture of bis(1,2-cyclohexandiolato-0,0^1)-dioxomolybdenum(VI) (64 mg, 0.18 mmol) in dry toluene (30 ml) was added farnesol (0.5 g, 2.25 mmol). The reaction mixture was stirred at 110°C under a nitrogen atmosphere for 15 h. After removal of the solvent the residue was passed down an alumina column, eluted with ether, to remove the complex. Removal of the ether and chromatography of the residue on a silica gel column eluted with ethyl acetate/petroleum ether (60-80) (1:30) gave nerolidol (4.14) (0.34 g, 68%) and unrearranged farnesol (0.12 g, 25%).

Isomerization of geraniol

To a stirred solution of tris(triphenylsilyl)oxo-vanadium(V) (0.46 g, 0.5 mmol) in dry benzene (5 ml) at 80°C was added geraniol (1.0 g, 6.5 mmol) and the reaction stirred for approximately 20 h. After removal of the solvent, the residue was chromatographed on a silica gel column eluted with ethyl acetate/petroleum ether (60-80) (1:15). Short-path distillation of the product gave linalol (0.6 g, 60%), 97.5% pure by glc (column A). Geraniol (0.2 g, 20%) was also isolated from the column.

Reduction of α-ionone to α-ionol (4.21)

To a solution of α-ionone (5 g, 0.026 mol) in dry benzene (40 ml), under a nitrogen atmosphere and cooled to 0-5°C, was added dropwise a solution of di-isobutyl aluminium hydride in hexane (5M) (7.9 ml, 0.039 mol). After stirring the reaction for a further 2 h under nitrogen the aluminium salts were decomposed at 5°C by adding a large excess of methanol. Filtering off the precipitate and removal of the solvent under reduced pressure gave a colourless oil which on distillation gave α-ionol (3.0 g, 60% yield) bp 89°/2 mmHg.

IR 3345(O-H) cm^{-1}

NMR ($CDCl_3$) δ 5.40 (3H, m, olefinic), 4.22 (1H, br.m, -C<u>H</u>(OH)), 1.55 (3H, m, =C-C<u>H</u>$_3$), 1.22 (3H, d, J=6.0 Hz, -C(OH)C<u>H</u>$_3$), 0.87 and 0.80 (6H, 2s, -C(C<u>H</u>$_3$)$_2$).

The spectral data are identical to that reported in the lit[155].

Reduction of mesityl oxide to 4-methylpent-3-en-2-ol

Mesityl oxide was reduced using lithium aluminium hydride in dry ether, according to the method described in the literature[128].

Reduction of 3-methyl-2-cyclohexenone to 3-methyl-2-cyclohexen-1-ol

To a suspension of lithium aluminium hydride (0.5 g, 0.13 mol) in dry ether (10 ml), under a nitrogen atmosphere and cooled to 5°C, was added dropwise a solution of 3-methyl-2-cyclohexenone (3 g, 0.027 mol) in dry ether

(10 ml). After stirring the reaction at room temperature for a further 2 h, excess lithium aluminium hydride was destroyed by the dropwise addition of water (1 ml), 10% NaOH (1.5 ml) and water (10 ml), added in rapid succession while stirring vigorously. The precipitate was filtered off and washed thoroughly with ether. Removal of the ether under reduced pressure gave an oil which on distillation gave 3-methyl-2-cyclohexen-1-ol (1.85 g, 62%) bp 75^{o}/12 mmHg.

IR 3340(O-H) cm^{-1}

NMR ($CDCl_3$) δ 5.43 (1H, m, $=\overset{|}{C}-\underline{H}$), 4.11 (1H, br.S, $-\overset{|}{C}\underline{H}(OH)$), 1.63 (3H, S, $=\overset{|}{C}-C\underline{H}_3$)

The spectral data are identical to that reported in the lit[156].

Preparation of α-ionol acetate

To a solution of α-ionol (0.26 g, 1.3 mmol) in benzene (10 ml) was added acetic anhydride (0.7 ml) and pyridine (0.9 ml) and the mixture stirred at room temperature overnight. The reaction mixture was poured into ice and the organic layer washed with 1N HCl (10 ml), 5% sodium carbonate solution and dried over Na_2SO_3. Removal of the solvent under reduced pressure gave an oil which after chromatography on a silica gel column eluted with ethyl acetate/petroleum ether (60-80) (1:10), gave α-ionol acetate (0.15 g, 50%).

IR 1755(C=O) cm^{-1}

NMR ($CDCl_3$) δ 5.40 (4H, 2m, olefinic and $-\overset{|}{C}\underline{H}Ac$), 1.98 (3H, S, $C\underline{H}_3CO$), 1.52 (3H, m, $=\overset{|}{C}-C\underline{H}_3$), 1.26 (3H, d, J=6.0 Hz, $-\overset{|}{C}(OAC)C\underline{H}_3$), 0.87 and 0.80 (6H, 2S, $-C(C\underline{H}_3)_2$).

Attempted palladium(II)-catalysed isomerization of α-ionol acetate

A solution of α-ionol acetate (0.1 g, 0.42 mmol) and bis(acetonitrile)dichloropalladium(II) (5 mg., 0.02 mmol) (prepared according to the method of Walton[157]) in dry THF (5 ml) was stirred at room temperature under a nitrogen atmosphere for 24 h. Tlc analysis of the reaction mixture suggested that no isomerization had taken place and this was confirmed by the fact that α-ionol acetate was isolated unchanged from the reaction mixture.

Attempted preparation of the oxo-vanadium complex of 2-(hydroxymethyl)-2-methyl-1,3-propandiol (4.26)

The ligand (4.25) (3.6 g, 30 mmol), vanadium pentoxide (1.82 g, 10 mmol) and n-butanol (0.37 g, 5 mmol) were refluxed in xylene (100 ml) for 6 h with continuous removal of water by means of a Dean-Stark trap. The hot reaction mixture was filtered through a celite bed and left to cool overnight. Since no product crystallised from the cooled reaction mixture the solvent was removed under reduced pressure giving a solid which was identified from its infrared spectrum as unchanged ligand.

Attempted preparation of tris(trifluoromethyl)silane

The reaction was carried out in a 500 ml round-bottom flask fitted with a mechanical stirrer, dry-ice/acetone condenser, low temperature thermometer and pressure equalising dropping funnel. The apparatus was purged with argon and a positive pressure of argon maintained

throughout the reaction. The flask was cooled using a dichloromethane/liquid nitrogen cooling bath and bromotrifluoromethane (22 g, 0.15 mol) condensed in the flask. Dry THF (190 ml) was added and the mixture cooled to -80 to -90°C. n-Butyl lithium (0.8 M) in hexane (187 ml, 0.15 mol) was added dropwise over ½ h and the mixture stirred for a further 1 h. Trichlorosilane (5.1 g, 0.037 mol) was added dropwise over 1 h and the mixture stirred for a further 5 h and left to warm slowly to room temperature over a period of about 14 h. The white solid produced was filtered off but appeared to be inorganic material. Removal of solvent from the filtrate gave a colourless oil which was readily identified from its ^{1}H-nmr spectrum as n-butyl bromide.

Attempted preparation of tris(pentafluorophenyl)silane (4.30)

The apparatus employed was similar to that described above but the dry ice/acetone condenser was replaced with an ordinary reflux condenser. Bromopentafluorobenzene (20 g, 0.08 mol) in dry ether (50 ml) was added over a 15 min period, to a stirred solution on n-butyl lithium in hexane (1.5 M) (53 ml, 0.08 mol) at -70°C. After 2 h additional stirring the mixture was warmed to -5 to 0°C and trichlorosilane (3.6 g, 0.026 mol) in dry ether (100 ml) added rapidly over 2-3 min. The mixture was warmed to room temperature and the solvent removed under reduced pressure. Attempts to isolate any tris(pentafluorophenyl)-silane by sublimation from the residue were unsuccessful.

6.3 Experimental relating to chapter 5

Attempted epoxidation of hex-5-en-2-yn-1-ol (5.7)

m-Chloroperbenzoic acid (5.61 g, 32.5 mmol) in dichloromethane (60 ml) was added dropwise to a stirred solution of hex-5-en-2-yn-1-ol[138] (2.4 g, 25 mmol) in dichloromethane (25 ml) at 0-5°C. After stirring for 8 h, the reaction was warmed to room temperature and left overnight. The small amount of m-chlorobenzoic acid that had precipitated was filtered off and the filtrate washed several times with saturated sodium carbonate solution and dried over Na_2SO_3. Removal of the solvent under reduced pressure gave an oil which was shown by tlc analysis to be a multi-component mixture. No attempt was made to isolate and identify the components present.

Attempted rearrangement of hex-5-en-2-yn-1-ol (5.7)

i) Hex-5-en-2-yn-1-ol (0.1 g, 1.0 mmol) and tris(triphenylsilyl)-oxovanadium(V) (7.3 mg, 0.015 mmol) were dissolved in d_8-toluene (0.5 ml) and the mixture heated at 110°C in a closed nmr tube for 72 h. The ^{1}H-nmr spectrum of the mixture showed the hex-5-en-2-yn-1-ol to be unchanged.

ii) Tris(triphenylsilyl)oxovanadium(V) (70 mg, 0.08 mmol), triphenylsilanol (0.2 g, 0.72 mmol), benzoic acid (10 mg, 0.08 mmol) and hex-5-en-2-yn-1-ol (0.4 g, 4 mmol) were mixed in parafin oil (10 g) and heated at 160°C for 4 h under a nitrogen atmosphere. Distillation under reduced pressure (0.1 mmHg) of as much material as possible from

the parafin oil resulted in recovery of unchanged hex-5-en-2-yn-1-ol (0.3 g, 75%) with no other products detectable in the nmr or ir spectrum.

Use of bis[trans-1,2-cyclohexandiolato-O,O^1(1-)]-dioxomolybdenum(VI) as catalyst gave similar results.

Preparation of 1-(4-penten-1-ynyl)cyclohexanol (5.11)

1-Ethynyl-1-cyclohexanol (16.0 g, 0.12 mol) was added to cuprous chloride (1.1 g, 11 mmol) in saturated sodium chloride solution (10 ml) and the mixture stirred at 80°C under a nitrogen atmosphere. The mixture was homogenised by addition of dimethylsulphoxide (40 ml) and the pH adjusted to 9-11 with .88 ammonia solution. Allyl chloride (10 g, 0.13 mol) was added dropwise over a period of 1 h and the pH kept constant throughout. The reaction was stirred at 80°C and the pH continually adjusted with ammonia solution over a period of about 7 h, after which time no further change in pH occurred. The product was steam distilled from the reaction mixture and the distillate extracted several times with ether. After drying the ether layer over Na_2SO_4, removal of the ether and fractional distillation of the residue gave 1-(4-penten-1-ynyl)cyclohexanol (4.0 g, 20%) as a colourless oil bp 126°/16 mmHg. The remainder of the residue was unreacted 1-ethynyl-1-cyclohexanol (8.0 g, 50%).

IR 3410(O-H), 2254(C=C) cm^{-1}

NMR ($CDCl_3$) δ 4.92-6.17 (3H, m, vinyl), 2.97 (2H, m, $-C\underline{H}_2-$), 1.0-2.0 (10H, br.m, ring protons)

Attempted epoxidation of 1-(4-penten-1-ynyl)cyclohexanol

The procedure was the same as that described in the attempted epoxidation of hex-5-en-2-yn-1-ol. Tlc analysis of the crude reaction mixture showed it to be a four component mixture and the infrared and ^{1}H-nmr spectrum showed that the acetylenic group had been attacked. No attempt was, therefore, made to isolated or identify the components of this mixture.

Formation of the dicobalt hexacarbonyl of 1-(4-penten-1-ynyl)-cyclohexanol

Dicobalt octacarbonyl (10 g, 0.03 mol) was added to a solution of 1-(4-penten-1-ynyl)cyclohexanol in petroleum ether (30-40^{o}) (40 ml), rapid evolution of carbon monoxide occured and the mixture was left stirring overnight. Removal of the solvent in a stream of nitrogen gave a dark red viscous oil which was used directly in the following hydroboration.

Attempted hydroboration of the dicobalt hexacarbonyl-acetylene complex

To sodium borohydride (0.27 g, 7.2 mmol) in dry THF was added the above acetylene complex (13.0 g, 0.029 mmol). The mixture was cooled in an ice bath and boron trifluoride etherate (1.37 g, 9.6 mmol) added dropwise. After stirring overnight, water (5 ml) was added to destroy excess sodium borohydride, this was followed by the addition of 2M sodium hydroxide and 30% hydrogen peroxide (10 ml). The solvent was removed under reduced pressure and the residue treated with a solution of ferric nitrate in ethanol for 24 h. Ether extraction of this mixture gave a red oil (0.2 g) which gave

only poor spectra and no attempt was made to characterise the product further.

Attempted preparation of 3,7-dimethyl-6,7-epoxyoct-1-yn-3-ol

A solution of m-chloroperbenzoic acid (1.5 g, 7.26 mmol) in dichloromethane (20 ml) was added over a period of 30 min, to a cooled solution (10°C) of dehydrolinalol (1.0 g, 6.6 mmol) in dichloromethane (10 ml). The reaction was left stirring at room temperature for 18 h and the precipitated solid filtered off. The filtrate was washed several times with saturated sodium bicarbonate solution and the organic layer dried over Na_2SO_4. Removal of the solvent and chromatography of the residue on a silica gel column eluted with petroleum ether (60-80)/ethyl acetate (15:1) gave the tetrahydrofuran (5.17) (0.7 g, 63%).

IR 3475(O-H), 3330(≡C-H), 2122(C≡C) cm^{-1}

NMR ($CDCl_3$) δ 3.91 (1H, m, -C<u>H</u>), 2.39 (1H, S, ≡C-<u>H</u>), 1.52 (3H, S, $C\underline{H}_3C$-), 1.21 and 1.12 (6H, 2xS, $(C\underline{H}_3)_2C$-).

MS m/e (rel intensity), 153(3), 110(20), 95 (15), 79(30), 68(55), 59(100), 43(62).

Attempted simultaneous epoxidation and cyclization of dehydrolinalol

A mixture of tris(triphenylsilyl)oxovanadium(V) (2.5 g, 2.8 mmol), dehydrolinalol (0.5 g, 3.3 mmol) and 95% t-butyl hydroperoxide (0.4 g, 4.2 mmol) in toluene (60 ml) was heated at 110°C for 5 h. Removal of the solvent under reduced pressure and chromatography of the residue on a silica gel column eluted with toluene/ethyl acetate (20:1) gave only

citral (0.14 g, 28%) and the tetrahydrofuran (5.17) (0.26 g, 47%).

Attempted preparation of 4-hydroxy-4-methylhex-5-ynal (5.18)

To a stirred mixture of purified t-butanol (26 ml), 10% tetraethylammonium hydroxide solution (2 ml) and dehydrolinalol (2.0 g, 13.2 mmol), cooled to 0°C in an ice-bath, was added 97% t-butyl hydroperoxide (2.4 ml, 26 mmol) followed by osmium tetroxide catalyst solution (1.3 ml) (prepared from 50 mg OsO_4 and 0.05 ml t-butyl hydroperoxide made up to 10 ml in purified t-butanol). The reaction mixture was stirred for 2 h at 0°C then stored in a refrigerator overnight, and 5% aqueous sodium bisulphite solution (20 ml) added and the mixture allowed to warm to room temperature while stirring. The mixture was concentrated on a rotary evaporator and water (40 ml) added. The aqueous layer was extacted once with ether (20 ml) to remove any impurities and any ether remaining in the aqueous layer was removed on a rotary evaporator. To the stirred aqueous layer was added solid sodium periodate (3.4 g, 16 mmol), and the reaction mixture stirred at room temperature for 5 h, and extracted with ether (3x25 ml). After drying the organic layer over Na_2SO_4 the solvent was removed giving an oil containing a single component (tlc analysis on silica gel plates eluted with a 3:1 mixture of pet. ether/ethyl acetate) identified as the cyclic hemiacetal (5.21) (1.16 g, 69%) (Found:C, 66.70;H, 7.92.$C_7H_{11}O_2$ requires C, 66.67;H, 7.94).

IR 3460(O-H), 3320(≡C-H), 2130(C≡C) cm^{-1}

NMR (Mixture of two diastereoisomers) ($CDCl_3$) δ 5.59 (1H, m, O-C<u>H</u>(OH)), 2.48 and 2.40 (1H, 2S, ≡C-<u>H</u>), 2.11 (4H, m, -(C<u>H</u>$_2$)$_2$-), 1.62 and 1.47 (3H, 2S, -C<u>H</u>$_3$).

MS m/e (rel intensity), 109(100), 79(70), 69(62), 43(56).

On standing at room temperature for 24 h the hemiacetal (5.21) was partially converted (c.a. 50%) to a different compound which was separated by chromatography on a silica gel column eluted with petroleum ether (60-80°)/ethyl acetate (10:1), and was identified as the acetal (5.22). (Found: C, 72.73;H, 7.82.$C_{14}H_{18}O_3$ requires C, 71.79;H, 7.69).

IR 3310(≡C-H), 2122(C≡C) cm^{-1}

NMR (Mixture of two diastereoisomers) ($CDCl_3$) δ 5.49 (1H, m, O-C<u>H</u>(OH)), 2.39 (1H, S, ≡C-<u>H</u>), 2.03 (4H, m, -(C<u>H</u>$_2$)$_2$-), 1.58 and 1.46 (3H, 2S, -CH_3).

MS m/e (rel intensity), 219(1), 177(1), 150(1), 137(2), 109(100), 91(11), 81(23), 79(32), 69(12).

<u>Treatment of 4-hydroxy-4-methylhex-5-ynal hemiacetal (5.21) with $(Ph_3SiO)_3VO$</u>

The hemiacetal (5.21) (25 mg, 0.2 mmol) and tris-(triphenylsilyl)oxovanadium(V) (14.4 mg, 0.016 mmol) were dissolved in d_8-toluene (0.5 ml) and heated at 110°C in a closed nmr tube for 18 h. The ^{1}H-nmr spectrum and tlc analysis of the mixture showed that the hemiacetal remained unchanged.

Preparation of 3,7-dimethyl-6-octen-1-yn-3,8-diol (5.25)

To a stirred suspension of selenium dioxide (75 mg, 0.67 mmol) and salicylic acid (0.23 g, 1.66 mmol) in dichloromethane (6 ml) was added 97% t-butyl hydroperoxide (5.4 g, 58 mmol). The resulting solution was warmed in a water bath at 25°C and dehydrolinalol (2.5 g, 16 mmol) added. After stirring for 27 h, benzene (10 ml) was added and the dichloromethane removed on a rotary evaporator. Ether (30 ml) was added and the organic phase was washed with 10% KOH (4x1 ml) and brine and dried over Na_2SO_4. After removal of the ether the excess t-butyl hydroperoxide was removed by distillation under reduced pressure (1 mmHg). The ^{1}H-nmr spectrum of the crude reaction mixture showed, in addition to some starting material, an aldehyde to alcohol ratio of 1:3.4. The mixture was chromatographed on a silica gel column eluted with petroleum ether (60-80)/ethyl acetate (10:1) giving 3,7-dimethyl-6-octen-3,8-diol (5.28) (1.1 g, 41%) (Found:C, 71.36;H, 9.48.$C_{10}H_{16}O_2$ requires C, 71.43; H, 9.52)

IR 3400(O-H), 3310(≡C-H), 2122(C≡C) cm^{-1}

NMR ($CDCl_3$) δ 5.44 (1H, t, J=7.0 Hz, =C-H), 3.96 (2H, br S, $-CH_2OH$), 2.43 (1H, S, ≡C-H), 1.67 (3H, br S, $=C-CH_3$), 1.46 (3H, S, $-C(OH)CH_3$).

MS m/e (rel intensity), 153(1), 150(6), 135(23), 121(15), 117(15), 107(17), 91(41), 79(50), 69(41), 55(15), 43(100).

Preparation of 2,6-dimethyl-6-hydroxy-2-octen-7ynal (5.26)

To 3,7-dimethyl-6-octen-1-yn-3,8-diol (5.25) (0.9 g, 5.3 mmol) in a mixture of petroleum ether (40 ml) and ethyl acetate (2 ml) was added activated manganese dioxide (9 g) and

the mixture was stirred rapidly at room temperature for 15 h. The manganese dioxide was filtered off and washed thoroughly with ethyl acetate. Removal of the solvents under reduced pressure gave a crude oil (0.5 g, 57%), the ^{1}H-nmr spectrum of which showed only the presence of the aldehyde (5.26). Tlc analysis of the crude oil showed the presence of a small amount of a polar material which did not move on the tlc plate. To obtain an analytically pure sample of the aldehyde, the crude oil was chromatographed on a silica gel column eluted with petroleum ether (60-80)/ethyl acetate (10:1), however, only a small amount of the original aldehyde could be eluted from the column (0.2 g, 23%). (Found:C, 72.53;H, 8.05.$C_{10}H_{14}O_2$ requires C, 72.29;H, 8.43).

IR 3450(O-H), 3218(≡C-H), 2122(C≡C), 1688(C=O) cm^{-1}

NMR ($CDCl_3$) δ 9.31 (1H, S, C<u>H</u>O), 6.50 (1H, t of q, J=1.3 and 6.8 Hz, =C(CH<u>H</u>)-), 2.46 (1H, S, ≡C-<u>H</u>), 1.73 (3H, d, J=1.3 Hz, =C(C<u>H</u>$_3$)-), 1.5 (3H, S, -C(OH)C<u>H</u>$_3$).

<u>Attempted cyclization of 2,6-dimethyl-6-hydroxy-2-octen-7-ynal</u>

The aldehyde (5.26) (0.5 g., 3 mmol) was dissolved in toluene (3 ml) and tris(triphenylsilyl)oxovanadium(V) (0.2 g, 0.24 mmol) added and the mixture stirred at 110°C in a nitrogen atmosphere for 18 h. The solvent was removed under reduced pressure and the bulk of the tris(triphenylsilyl)oxovanadium(V) was removed by passing the residue down a short (10x0.6 cm) column of basic alumina (activity III) eluted with ether. Tlc analysis showed one major component with two or three other components present in only trace amounts. Chromatography of the crude mixture on a silica gel column

eluted with petroleum ether (60-80)/ethyl acetate (15:1) enabled isolation of the major product, 2,6-dimethyloct-2,5-dien-1,8-dial (5.27) and (5.28), in only low yield (0.2 g, 40%).

IR 1690(C=O) cm^{-1}

NMR ($CDCl_3$) δ 9.86 and 9.79 (1H, 2d, J=7.5 Hz, =CHC<u>H</u>O cis and trans isomers) 9.26 (1H, S, =C(CH_3)C<u>H</u>O), 6.33 (1H, br t, J=6.6 Hz, =C-<u>H</u>), 5.82 (1H, d, J=7.5 Hz, =C<u>H</u>CHO)

<u>Preparation of 8-chloro-2-methyl-3-octyn-2-ol (5.29)</u>

In a flask fitted with a dry-ice condenser protected with a sodalime drying tube, was placed liquid ammonia (200 ml) containing a few crystals of ferric nitrate. Lithium (0.7 g, 0.1 mol) was added slowly and the mixture stirred for 1 h. To the resultant suspension of lithamide was added dropwise a solution of the tetrahydropyranyl ether of 2-methyl-3-butyn-2-ol (17.5 g, 0.1 mol) in dry THF (30 ml) and the mixture was stirred for a further 1 h. 1-Chloro-4-iodobutane (15 g, 0.069 mol) in dry THF (100 ml) was added over a period of 45 min and the resulting mixture stirred under reflux for 8 h, after which time ammonium chloride (10 g) was added and the ammonia allowed to evaporate. The residue was poured into a cooled solution of 20% sulphuric acid (100 ml) and the aqueous layer extracted with ether (3x25 ml). The combined organic layers were washed with 5% potassium carbonate solution, water, brine and dried over Na_2SO_4. Removal of the ether and fractional distillation of the residue gave 8-chloro-2-methyl-3-octyn-2-ol (4.7 g, 39%) as a colourless oil bp 74°C/0.1 mmHg. (Found:C, 61.75;H, 8.58. $C_9H_{15}OCl$ requires C, 61.84;H, 8.60).

IR 3458(O-H), 2165(C≡C) cm^{-1}

NMR ($CDCl_3$) δ 3.51 (2H, t, J=6.0 Hz, $-C\underline{H}_2Cl$), 2.23 (2H, t, J=6.0 Hz, $\equiv C-C\underline{H}_2-$), 1.73 (4H, m, $-(C\underline{H}_2)_2-$), 1.46 (6H, S, $2xC\underline{H}_3$).

MS m/e (rel intensity), 159(82), 105(7), 93(11), 79(20), 67(7), 55(11), 43(100).

Preparation of 8-iodo-2-methyl-3-octyn-2-ol (5.30)

8-Chloro-2-methyl-3-octyn-2-ol (5.29) (4.0 g, 22.9 mmol) was added to a refluxing mixture of sodium iodide (7.9 g, 50 mmol) in dry acetone (30 ml) and the mixture stirred under reflux for 18 h. The reaction mixture was poured into water and extracted with ether (3x25 ml). After drying the combined organic layers over Na_2SO_4, removal of the ether and fractional distillation of the residue gave 8-iodo-2-methyl-3-octyn-2-ol (3.7 g, 60%) as a pale yellow oil bp 95-97°C/0.1 mmHg.

IR 3420(O-H), 2255(C≡C) cm^{-1}

NMR ($CDCl_3$) δ 3.16 (2H, t, J=6.0 Hz, $-C\underline{H}_2I$), 2.18 (2H, t, J=6.0 Hz, $\equiv C-C\underline{H}_2-$), 1.75 (4H, m, $-(CH_2)_2-$), 1.43 (6H, S, $2xC\underline{H}_3$).

MS m/e (rel intensity), 266(3)(M^+), 251(76), 160(16), 150(23), 140(19), 129(22), 122(32), 106(11), 96(40), 80(45), 44(100).

Attempted cyclization of 8-iodo-2-methyl-3-octyn-2-ol

8-Iodo-2-methyl-3-octyn-2-ol (0.5 g, 1.9 mmol) was added to a solution of tris(triphenylsilyl)oxovanadium(V) (0.13 g, 0.15 mmol) in toluene (2 ml) and the reaction

mixture heated at 110°C for 3 h. Tlc analysis of the reaction mixture indicated that virtually all the starting material had been converted to a single new product. The toluene was removed under reduced pressure and the residue mixed with ether and passed down a short (10x0.6 cm) column of basic alumina (activity III) eluted with ether to remove most of the metal complex. Chromatography of the crude product on a silica gel column eluted with petroleum ether/ethyl acetate (3:1) enabled isolation of a pure product which was identified as 8-iodo-2-methyl-2-octen-4-one (5.32) (0.33 g, 66%).

(Found:C, 40.76;H, 5.75.$C_9H_{15}OI$ requires C, 40.60;H, 5.64).

IR 1690(C=O) cm^{-1}

NMR ($CDCl_3$) δ 6.01 (1H, m, =C<u>H</u>-), 3.12 (2H, t, J=6.0Hz, -C<u>H</u>$_2$I), 2.39 (2H, t, J=6.0Hz, -COC<u>H</u>$_2$-), 2.11 (3H, 2xS, C<u>H</u>$_3$ cis to carbonyl), 1.85 (3H 2xS, CH_3 trans to carbonyl), 1.61-1.92 (4H, m, -(C<u>H</u>$_2$)$_2$-).

The above reaction was repeated in the presence of N,N-diisopropylethylamine using 2 mol of amine per mol of substrate. Tlc analysis of the reaction mixture showed 8-iodo-2-methyl-2-octen-4-one (5.32) to be the only product.

REFERENCES

1. See A.D. Cross, Quart.Rev., 19(0, 14, 317, for a review on naturally occuring epoxides and their biogenetic relationships with other natural products.

2. See R.M. Bowmann and M.F. Grundon, J. Chem. Soc., C, 1967, 2368 for an example of the use of asymmetric epoxidation in the synthesis of the alkaloid, orixine.

3. J.D. Morrison and H.S. Mosher, "Asymmetric Organic Reactions", Prentice - Hall, Englewood Cliffs, New Jersey, 1971.

4. I.T. Harrison and S. Harrison, "Compendium of Organic Synthetic Methods", Vol. 2, Wiley - Interscience, New York, N.Y., 1974, pp 127-135.

5. B.M. Lynch and K.H. Pausacker, J. Chem. Soc., 1955, 1525.

6. D. Swern, J. Amer. Chem. Soc., 1947, 69, 1692.

7. Y. Ogata and I. Tabushi, J. Amer. Chem. Soc., 1961, 83, 3440.

8. P.D. Bartlett, Record. Chem. Progr., 1950, 47, 11.

9. R.M. Bowmann, J.F. Collins and M.F. Grundon, Chem. Commun., 1967, 1131.

10. (a) H.B. Henbest, Organic Reaction Mechanisms, Special Publication No. 19, The Chemical Society, London, 1965, pp83-92.

    (b) R.C. Ewins, H.B. Henbest and M.A. McKervey, Chem. Commun., 1967, 1085.

11. D.R. Boyd, D.M. Jerina and J.W. Daly, J. Org. Chem., 1970, 35, 3170.

12. W.H. Pirkle and P.L. Rinaldi, J. Org. Chem., 1977, 42, 2080.

13. F. Montanari, I. Moretti and G. Torre, Chem. Commun., 1969, 135.

14. V. Calo, L. Lopez, V. Fiandanese, F. Naso and L. Ronzini, Tetrahedron Letters, 1978, 4963.

15. G.V. Pigulevskir and G.V. Martina, Dokl. Akad. Nauk. SSSR., 1948, 63, 677 ; Chem. Abs., 43, 4628i.

16. M. Igarashi and H. Midorikauva, Bull. Chem. Soc. Japan, 1967, 40, 2624.

17. (a) J. Dockx, Synthesis, 1973, 441
    (b) E.V. Dehmlow, Angew. Chem. Int. Edit., 1974, 13, 170.

18. (a) T. Hiyama, H. Sawaka, M. Tsukanka and H. Nozaki, Tetrahedron Letters, 1975, 3013.
(b) J.C. Fiaud, Tetrahedron Letters, 1975, 3495

19. R. Helder, J.C. Hummelen, R.W.P.M. Loane, J.S. Wienng and H. Wynberg, Tetrahedron Letters, 1976, 1881.

20. J.C. Hummelen and H. Wynberg, Tetrahedron Letters, 1978, 1089.

21. H. Ohta and H. Tetsukawa, J.C.S. Chem. Comm., 1978, 849.

22. S.W. May and R.D. Schwartz, J. Amer. Chem. Soc., 1974, 96, 4031.

23. G.M. Whitesides and D.W. Lewis, J. Amer. Chem. Soc., 1970, 92, 6979 ; ibid, 1971, 93, 5914.

24. R.R. Fraser, M.A. Petit and J.K. Sanders, J.C.S. Chem. Comm., 1971, 1450.

25. H.L. Goering, J.N. Eckenberry and G.S. Koermer, J. Amer. Chem. Soc., 1971, 93, 5913.

26. B.T. Golding, P.J. Sellars and A.K. Wong, J.C.S. Chem. Comm., 1977, 16, 570.

27. (a)V.Schuring, B. Koppenhofer, W. Burkle, Angew Chem. Int. Ed., 1978, 17, 937.
(b)H.B. Kagan, H. Mimoun, C. Mark and V. Schuring, Angew. Chem. Int. Ed., 1979, 18, 485.

28. Review: R. Hiatt in "Oxidation", Vol. 2, R.L. Augustine. Ed., Marcel Dekker, New York, N.Y., 1971, Chapter 3.

29. N.A. Milas, J. Amer. Chem. Soc., 1937, 59, 2342.

30. (a) British Patent 837,464 (1957) ; Chem. Abs., 55, 556.
(b) U.S. Patent 2,786,854 (1957) ; Chem. Abs., 51, 14791.
(c) U.S. Patent 2,833,787 (1958) ; Chem. Abs., 52, 16367.
(d) Z. Raciszewski, J. Amer. Chem. Soc., 1960, 82, 1267.
(e) H.C. Stevens and A.J. Kaman, J. Amer. Chem. Soc., 1965, 87, 735.

31. G.B. Payne and P.H. Williams, J. Org. Chem., 1959, 24, 54.

32. E.G.E. Hawkins, J. Chem. Soc., 1950, 2169.

33. N. Indicator and W.F. Brill, J. Org. Chem., 1965, 30, 2074.

34. E.S. Gould, R.R. Hiatt and K.C. Irwin, J. Amer. Chem. Soc., 1968, 90, 4573.

35. C.C. Su, J.W. Reed and E.S. Gould, Inorg. Chem., 1973, 12, 337.

36. M.C.R. Symons, J. Chem. Soc., A, 1970, 1883.

37. H.B. Brooks and F. Sicilio, Inorg. Chem., 1971, 10, 2530.

38. G.L. Linden and M.F. Farona, Inorg. Chem., 1977, 16, 3170.

39. (a) H. Mimoun, I. Seree de Roch and L. Sajus, Tetrahedron, 1970, 26,37.
(b) J. Kaloustian, L. Lena and J. Metzger, Tetrahedron Letters, 1975, 599.
(c) K.B. Sharpless, J.M. Townsend and D.R. Williams, J. Amer. Chem. Soc., 1972, 94, 295.

40. (a) R.A. Sheldon, Recl. Trav. Chim. Pays-Bas, 1973, 92, 253.
(b) R.A. Sheldon and J.A. Van Doorn, J. Catel, 1973, 31, 427.

41. R.A. Sheldon, Recl. Trav. Chim. Pays-Bas, 1973, 92, 367.

42. F. Trifiro, P. Forzatti, S. Preite and I. Pasquon, J. Less Common Metals, 1974, 36, 319.

43. A.O. Chong and K.B. Sharpless, J. Org. Chem., 1977, 42, 1587.

44. M.N. Sheng and J.G. Zajacek, J. Org. Chem., 1970, 35, 1839.

45. British Patent 1,104,821 (1964) ; Chem. Abs., 64, 11 174.

46. British Patent 1,115 220 (1964) ; Chem. Abs., 64, 19 558.

47. P. Wolf, J. Org. Chem., 1969, 34, 3441.

48. K.B. Sharpless and R.C. Michaelson, J. Amer. Chem. Soc., 1973, 95, 6136.

49. K.B. Sharpless, R.C. Michaelson, J.D. Cutting, S. Tanaka, H. Yamanoto, and H. Nozaki, J. Amer. Chem. Soc., 1974, 96, 5254.

50. T. Itoh, K. Jitsukawa, K. Kaneda, S. Teranishi, J. Amer. Chem. Soc., 1979, 101, 159.

51. S. Yamada, T. Mashiko, S. Teroshima, J. Amer. Chem. Soc., 1977, 99, 1988.

52. R.C. Michaelson, R.E. Palermo and K.B. Sharpless, J. Amer. Chem. Soc., 1977, 99, 1990.

53. M.N. Sheng and J.G. Zajacek, Adv. Chem., 1968, 76, 418.

54. H. Gehrke and J. Veal, Inorg. Chim. Acta. 1969, 3, 623.

55. B. Soptrajanov, A. Nikolovski and I. Petrov, Spectrochimica Acta, 1968, 24A, 1617.

56. M.M. Jones, J. Amer. Chem. Soc., 1959, 81,3188.

57. D.V.R. Rao, Analyt. Chim. Acta, 1957, 17, 538.

58. C.R. Hauser, F.W. Swamer and J.T. Adams, Org. Reactions, 1954, 8, 59.

59. P. Pfeiffer, W. Christeleit, Th. Hesse, H. Pfitzner and H. Thielert, J. prakt. Chem., 1938, 150, 261.

60. F.A. Cotton, J. Less Common Metals, 1974, 36-37, 13.

61. K. Dey, Inorg. Chim Acta, 1976, 20, 197.

62. K. Romaiah and D.F. Martin, J. Inorg. Nuel. Chem., 1965, 27, 1663.

63. L.J. Boucher, E.C. Tynan and T.F. Yen, Inorg. Chem., 1968, 7, 731.

64. J. Bredt and W.H. Perkin, J. Chem. Soc., 1913, 103, 2210.

65. R.A. Chittenden and G.H. Copper, J. Chem. Soc., C, 1974, 49.

66. A.H. Beckett, N.T. Lan and G.R. McDonough, Tetrahedron, 1969, 25, 5689.

67. M.L. Moore, Org. Reactions, 1949, 5, 301.

68. S.H. Pine and B.L. Sanachez, J. Org. Chem., 1971, 36, 829.

69. R.F. Borch and A.I. Hassid, J. Org. Chem., 1972, 37, 1673.

70. M. Tomita, S. Uyeo, Jr., and T. Kikuchi, Tetrahedron Letters, 1964, 1053.

71. T.A. Crabb and R.O. Williams, J. Heterocyclic Chem., 1967, 4, 169.

72. E.D. Bergmann, E. Zimkin and S. Pinchas, Rec. Trav. Chim. Pays-Bas, 1952, 71, 229.

73. W.L. Nelson, J. Heterocyclic Chem., 1968, 5, 231.

74. R.H. Holm, G.W. Everett, Jr., and A. Chakravorty, Progr. Inorg. Chem., 1966, 7, 83.

75. S. Yamada, Coord. Chem. Rev., 1966, 1, 415.

76. K. Yamanouchi and S. Yamada, Inorg. Chim Acta, 1974, 9, 83.

77. P.C.H. Mitchell, Quart Rev., 1966, 20, 103.

78. K. Nakamoto, "Infrared Spectra of Inorganic and Coordination Compounds", Wiley, New York, 1963, p 77.

79. R.M. Wing and K.P. Callahan, Inorg. Chem., 1969, 8, 871.

80. F.A. Schroder, J. Scherele and R.G. Hazell, Acta Cryst., 1975, B31, 531.

81. C.K. Chew and B.R. Penfold, J. Cryst. Mol. Struct., 1975, 5, 413.

82. T. Gowiak and M. Sabat, J. Cryst. Mol. Struct., 1975, 5, 247.

83. G.M. Sheldrick, 1976, SHELX 76 program suite, University of Cambridge.

84. R.H. Fenn, J. Chem. Soc., A, 1969, 1764.

85. R.J. Butcher and B.R. Penfold, J. Cryst. Mol. Struct., 1976, 6, 13.

86. K. Tsukuma, T. Kawaguchi and T. Watanabe, Acta Crystallogr., Sect. B, 1975, 31, 2165.

87. F.A. Cotton and R.C. Elder, Inorg. Chem., 1964, 3, 397.

88. A.C. Villa, L. Coghi, A.G. Manfredotti and C. Guastini, Cryst. Struct. Commun. 1974, 3, 551.

89. K. Yamanouchi, J.H. Enemark, Inorg. Chem., 1979, 18, 1626.

90. (a) E.A. Braude, Q. Rev. Chem. Soc., 1950, 4, 404.
(b) P.B.O. de la Mare, "Molecular Rearrangements", Part 1, Interscience, New York, N.Y., 1963, Chapter 2.
(c) R.H. De Wolf and W.G. Young in "The Chemistry of the Alkenes", E.S. Patai, Ed., Interscience, New York, N.Y., 1964, Chapter 10.

91. (a) O. Isler, W. Huber, A. Ronoco and M. Kofler, Helv. Chim. Acta., 1947, 30, 1911.
(b) O. Isler, A. Ronoco, W. Guex, N.C. Hindley, W. Huber, K. Digler and M. Kofler, Helv. Chim. Acta, 1949, 32, 489.
(c) J. Attenburrow, A.F.B. Cameron, J.H. Chapmann, R.M. Evans, B.A. Hems, A.B.A. Jansen and J. Walker, J. Chem. Soc., 1952, 1094.
(d) G.L. Olson, H.C. Choung, K.D. Morgan, R. Boren and G. Saucy, Helv. Chim Acta., 1976, 59, 557.

92. (a) H.W. Whitlock, Jr, and G.L. Smith, J. Amer. Chem. Soc., 1967, 89, 3600.
(b) R.B. Woodward, M.P. Cava, W.D. Ollis, A. Hunger, H.U. Daeniker and K. Schenker, J. Amer. Chem. Soc., 1954, 76, 4749 ; Tetrahedron, 1963, 19, 247.

93. (a) J.H. Babler, D.O. Olsen and W.H. Arnold, J. Org. Chem., 1974, 39, 1656.
(b) J.H. Babler, Tetrahedron Letters, 1975, 2045.

79. R.M. Wing and K.P. Callahan, Inorg. Chem., 1969, 8, 871.

80. F.A. Schroder, J. Scherele and R.G. Hazell, Acta Cryst., 1975, B31, 531.

81. C.K. Chew and B.R. Penfold, J. Cryst. Mol. Struct., 1975, 5, 413.

82. T. Gowiak and M. Sabat, J. Cryst. Mol. Struct., 1975, 5, 247.

83. G.M. Sheldrick, 1976, SHELX 76 program suite, University of Cambridge.

84. R.H. Fenn, J. Chem. Soc., A, 1969, 1764.

85. R.J. Butcher and B.R. Penfold, J. Cryst. Mol. Struct., 1976, 6, 13.

86. K. Tsukuma, T. Kawaguchi and T. Watanabe, Acta Crystallogr., Sect. B, 1975, 31, 2165.

87. F.A. Cotton and R.C. Elder, Inorg. Chem., 1964, 3, 397.

88. A.C. Villa, L. Coghi, A.G. Manfredotti and C. Guastini, Cryst. Struct. Commun. 1974, 3, 551.

89. K. Yamanouchi, J.H. Enemark, Inorg. Chem., 1979, 18, 1626.

90. (a) E.A. Braude, Q. Rev. Chem. Soc., 1950, 4, 404.
(b) P.B.O. de la Mare, "Molecular Rearrangements", Part 1, Interscience, New York, N.Y., 1963, Chapter 2.
(c) R.H. De Wolf and W.G. Young in "The Chemistry of the Alkenes", E.S. Patai, Ed., Interscience, New York, N.Y., 1964, Chapter 10.

91. (a) O. Isler, W. Huber, A. Ronoco and M. Kofler, Helv. Chim. Acta., 1947, 30, 1911.
(b) O. Isler, A. Ronoco, W. Guex, N.C. Hindley, W. Huber, K. Digler and M. Kofler, Helv. Chim. Acta, 1949, 32, 489.
(c) J. Attenburrow, A.F.B. Cameron, J.H. Chapmann, R.M. Evans, B.A. Hems, A.B.A. Jansen and J. Walker, J. Chem. Soc., 1952, 1094.
(d) G.L. Olson, H.C. Choung, K.D. Morgan, R. Boren and G. Saucy, Helv. Chim Acta., 1976, 59, 557.

92. (a) H.W. Whitlock, Jr, and G.L. Smith, J. Amer. Chem. Soc., 1967, 89, 3600.
(b) R.B. Woodward, M.P. Cava, W.D. Ollis, A. Hunger, H.U. Daeniker and K. Schenker, J. Amer. Chem. Soc., 1954, 76, 4749 ; Tetrahedron, 1963, 19, 247.

93. (a) J.H. Babler, D.O. Olsen and W.H. Arnold, J. Org. Chem., 1974, 39, 1656.
(b) J.H. Babler, Tetrahedron Letters, 1975, 2045.

94. (a) Y. Letourneux, M.M.L. Lo, N. Chaudhuri and M. Gut, J. Org. Chem., 1975, 40, 516.
(b) D.O. Olsen and J.H. Babler, J. Org. Chem., 1975, 40, 255.
(c) P. Morand and A. Van Tongerloo, Steroid, 1973, 21, 47.

95. (a) Y. Pocker, J. Chem. Soc., 1958, 4318.
(b) E.A. Braude, E.R.H. Jones and E.S. Stern, J. Chem. Soc., 1946, 396.
(c) A.G. Catchpole, E.D. Hughes and C.K. Ingold, J. Chem. Soc., 1948, 8.

96. (a) E.A. Braude and E.R.H. Jones, J. Chem. Soc., 1944, 436 ; 1946, 122.
(b) E.A. Braude, J. Chem. Soc., 1944, 443 ; 1948, 794.
(c) E.A. Braude and E.S. Stern, J. Chem. Soc., 1947, 1096 ; 1948, 1982.
(d) J.M. Shackelford and L.H. Schwatzmann, J. Org. Chem., 1962, 27, 1047.

97. E.A. Braude and C.J. Timmons, J. Chem. Soc., 1950, 2007 ; 1953, 3131 and 3138.

98. E.A. Braude and W.F. Forbes, J. Chem. Soc., 1951, 1755.

99. (a) H.C. Brown, J.H. Brewster and H. Schechter, J. Amer. Chem. Soc., 1954, 76, 467.
(b) R.B. Turner and R.H. Garner, J. Amer. Chem. Soc., 1958, 80, 1424.
(c) A.C. Cope, D. Ambras, E. Ciganek, C.F. Howell and Z. Jacura, J. Amer. Chem. Soc., 1960, 82, 1750.

100. C.A. Grab and J.A. Rumpf, Helv. Chim Acta, 1954, 37, 1479.

101. J.L. Simonsen, "The Terpenes", Vol. 1, Cambridge University Press, 1953, pp 58-63.

102. W.G. Young, K. Nozaki and R. Warner, J. Amer. Chem. Soc., 1939, 61, 2564.

103. I.N. Nazarov, I.N. Azerbaev and V.N. Rakcheeva, Izv. Akad. Nauk. SSSR, Otd. Khim. Nauk, 1946, 419.

104. E.A. Braude, J.A. Cole, E.A. Evans and C.J. Timmons, Nature, 1956, 177, 1167.

105. A. Valeur and E. Luce, Bull. Soc. Chim. France, 1920, 27, 611.

106. (a) W.G. Young and I.D. Webb, J. Amer. Chem. Soc., 1951, 73, 780.
(b) G.G. Lyle, E.F. Perlowski and R.E. Lyle, J. Org. Chem., 1956, 21, 423.
(c) T.H. Smith, A.N. Fujiwara, W.W. Lee, H.Y. Wu and D.W. Henry, J. Org. Chem., 1977, 42, 3653.

107. (a) D.F. Morrow, T.P. Culbertson and R.M. Hofer, J. Org. Chem., 1967, 32, 361.
(b) I.M. Heilbron, E.R.H. Jones, D. Smith and B.C.L. Weedon, J. Chem. Soc., 1946, 54.

108. (a) J.F. King and P. DeMayo, in "Molecular Rearrangements", Part 2, Interscience, New York, N.Y., 1964, Chapter 13.
(b) L. Crabalona, Frances et ses Parfums, 1959, 2, 28 ; Chem. Abs., 54, 6037 h.
(c) J.H. Babler and D. Olsen, Tetrahedron Letters, 1974, 351.

109. (a) P. Chabardes, C. Grard and C. Schneider, U.S. Patent 3,925,485, (1975).
(b) P. Chabardes, E. Muntz and J. Varagnat, Tetrahedron, 1977, 33, 1775.

110. L.E. Overman, J. Amer. Chem. Soc., 1976, 98, 2901.

111. L.E. Overman, C.B. Campbell and F.M. Knoll, J. Amer. Chem. Soc., 1978, 100, 4822.

112. L.E. Overman and F.M. Knoll, Tetrahedron Letters, 1979, 321.

113. (a) K.H. Meyer and K. Schuster, Ber., 1922, 55, 819.
(b) H. Rupe and E. Kambli, Helv. Chim. Acta, 1926, 9, 627.
(c) H. Rupe, W. Messner and E. Kambli, Helv. Chim. Acta, 1928, 11, 449.
(d) H. Rupe and Fr. Kuenzy, Helv. Chim. Acta, 1931, 14, 708.

114. S. Swaminathan and K.V. Narayarman, Chem. Rev., 1971, 71, 429.

115. P.D. Landor and S.R. Landor, J. Chem. Soc., 1956, 1015.

116. G. Saucy, R. Marbet, H. Lindlar and O. Isler, Helv. Chim. Acta, 1959, 42, 1945.

117. H. Schlossarczyk, W. Sieber, M. Hesse, H.J. Hansen and H. Schmid, Helv. Chim. Acta, 1973, 56, 875.

118. (a) D.A. Andrews and N.C. Hindley, U.S. Patent, 3,994,936 (1976) ; B.P. 1,409,323.
(b) H. Pauling, D.A. Andrews and N.C. Hindley, Helv. Chim. Acta, 1976, 59, 1233.
(c) M.B. Erman, I.S. Aul'chenko, L.A. Kheifits, V.G. Dulova, Ju. No. Novikov, and M.E. Vol'pin, Tetrahedron Letters, 1976, 2981.

119. M.B. Erman, I.S. Aul'chenko, L.A. Kheifits, V.G. Dulova, Ju. N. Novikov and M.E. Vol'pin, Zh. Org. Khim, 1976, 12, 921.

120. R.C. Haley, J.A. Miller and H.C.S. Wood, J. Chem. Soc.(C), 1969, 264.

121. P. Valenzuela and O. Cori, Tetrahedron Letters, 1967, 3089.

122. R.A. Sheen, J. Amer. Chem. Soc., 1960, 82, 4261.

123. H.L. Goering and M.M. Pombo, J. Amer. Chem. Soc., 1960, 82, 2515.

124. H.L. Goering and J.T. Doi, J. Amer. Chem. Soc., 1960, 82, 5850.

125. A.G. Catchpole and E.D. Hughes, J. Chem. Soc., 1948, 1.

126. Y. Pocker, J. Chem. Soc., 1958, 4323.

127. A. Yasuda, H. Yamamoto and H. Nozaki, Tetrahedron Letters, 1976, 2621.

128. M.E. Cain, J. Chem. Soc., 1964, 3532.

129. Y. Bessiere, E. Resca, F. Chatzopoulos-Ouar and G. Boussac, J. Chem. Research(S), 1977, 302.

130. V. Rautenstrauch, Helv. Chim. Acta, 1973, 56, 2492.

131. O.R. Pierce, E.T. McBee and G.F. Judd, J. Amer. Chem. Soc., 1954, 76, 474.

132. V. Franzen and L. Fikentscher, Chem. Ber., 1962, 95, 1958.

133. (a) M.F. Lappert and J. Lynch, J.C.S. Chem. Comm., 1968, 750.
(b) Abstracted from the D. Phil. dissertation of J. Lynch, University of Sussex, Brighton, England, 1969.

134. P.L. Coe, R. Stephens and J.C. Tatlow, J. Chem. Soc., 1962, 3227.

135. J.E. Baldwin, J.C.S. Chem. Comm., 1976, 734.

136. J.E. Baldwin and L.I. Kruse, J.C.S. Chem. Comm., 1976, 233.

137. G. Stork, J. Amer. Chem. Soc., 1975, 97, 3258.

138. P. Kurtz, Ann., 1962, 658, 6.

139. A. Sevin, W. Chodkiewicz and P. Cadiot, Tetrahedron Letters, 1965, 1953.

140. R.L. Augustine, "Catalytic Hydrogenation", p 70, Marcel Decker, 1965.

141. H.C. Brown, "Hydroboration", W.A. Benjamin Inc., 1962.

142. R.C. Fahey, "Topics in Stereochemistry", Vol. 3, pp 237-342, Interscience, 1968.

143. K.M. Nicholas and R. Pettit, Tetrahedron Letters, 1971, 3475.

144. H. Greenfield, H.W. Sternberg, R.A. Friedel, J.H. Wotiz, R. Markby and I. Wender, J. Amer. Chem. Soc., 1956, 78, 120.

145. W. Kimel, J.D. Surmatis, J. Weber, G.O.Chase, N.W. Sax and A. Ofner, J. Org. Chem., 1957, 22, 1611.

146. E. Klein, H. Farnow and W. Rojahn, Tetrahedron Letters, 1963, 1109.

147. K.B. Sharpless and K. Akash, J. Amer. Chem. Soc., 1976, 98, 1986.

148. J. Meinwald, T.H. Jones, T. Eisner and K. Hicks, Proc. Natl. Acad. Sci. U.S.A., 1977, 74, 2189.

149. J. Meinwald and T.H. Jones, J. Amer. Chem. Soc., 1978, 100, 1883.

150. M.A. Umbreit and K.B. Sharpless, J. Amer. Chem. Soc., 1977, 99, 5526.

151. M. Ohtsuru, M. Teraoka, K. Tori and K. Takeda, J. Chem. Soc.,(B), 1967, 1033.

152. K. Ahmad and F.M. Strong, J. Amer. Chem. Soc., 1948, 70, 1699.

153. A.P. Johnson and A. Pelter, J. Chem. Soc., 1964, 520.

154. K. Tori, Y. Hamashima and A. Takamizawa, Chem. Pharm. Bull, (Tokyo), 1964, 12, 924.

155. C. Kruk, A.A.M. Roof, A. Van Wageningen and H. Cerfontain, Recl. Trav. Chem. Pays-Bas, 1973, 72, 1015.

156. G. Magnusson and S. Thoren, J. Org. Chem., 1973, 38, 1380.

157. R.A. Walton, Spectrochimica Acta, 1965, 21, 1795.

APPENDICES

Appendix 1. Attempts to prepare NN^1-ethylenebis(iminomethylcamphorato)dioxomolybdenum(VI)

i) Reactions in the presence of an organic base.

$$\text{imineH}_2 + \text{MoO}_2\text{Cl}_2 + 2\text{Et}_3\text{N} \longrightarrow \text{MoO}_2(\text{imine}) + 2\text{Et}_3\overset{+}{\text{N}}\text{H}\overset{-}{\text{Cl}}$$

A solution of molybdenum dioxodichloride (51 mg, 0.26 mmol) in dry methanol (10 ml) was added rapidly to a stirred solution of NN^1-ethylenebis(iminomethylcamphor) (2.3) (0.1 g, 0.26 mmol) and triethylamine (52 mg, 0.52 mmol) in dry methanol (10 ml) and the mixture stirred for 1 h under a nitrogen atmosphere. Removal of the solvent under reduced pressure gave a solid, the infrared spectrum of which showed it to be unchanged ligand.

Molybdenum dioxodichloride is known to form complexes of the type $\text{MoO}_2\text{Cl}_2\text{L}_2$ (L = solvent molecule) with donor solvents and it was thought that the formation of such a complex with methanol may be inhibiting the formation of the desired imine complex. The above reaction was, therefore, repeated using dry tetrahydrofuran as solvent, since the donor properties of this solvent would be much weaker than those of methanol. Under these conditions a solid precipitated and was filtered off but its ^1H nmr spectrum showed only signals arising from ethyl groups, suggesting formation of a complex between molybdenum dioxodichloride and trethylamine. Removal of the solvent from the filtrate resulted in the recovery of unchanged ligand.

ii) Reaction in the presence of silver oxide.

$$\text{imine}H_2 + MoO_2Cl_2 + Ag_2O \longrightarrow MoO_2(\text{imine}) + 2AgCl + H_2O$$

NN^1-Ethylenebis(iminomethylcamphor) (0.1 g, 0.26 mmol) was dissolved in dry THF (10 ml) and silver oxide (61 mg, 0.26 mmol) added. Molybdenum dioxodichloride (51 mg, 0.26 mmol) in dry THF (10 ml) was added rapidly and the reaction stirred for 2 h under a nitrogen atmosphere. The reaction mixture was filtered and the solvent removed from the filtrate under reduced pressure. The infrared spectrum of the product showed only the presence of unchanged ligand with no additional absorptions in the 850-1000 cm^{-1} region to indicate the presence of Mo=0 groups.

iii)Reaction of the sodium salt of the imine with MoO_2Cl_2.

$$\text{imine}H_2 + 2NaH \longrightarrow \text{imine}^{-}\,Na^{+}_2 + 2H_2 \xrightarrow{MoO_2Cl_2} MoO_2\text{imine} + NaCl$$

NN^1-Ethylenebis(iminomethylcamphor) (0.1 g, 0.26 mmol) was dissolved in dry THF (20 ml) and sodium hydride (12.5 mg, 0.51 mmol) added and the mixture stirred for 1 h under a nitrogen atmosphere. The mixture was then heated to 50^oC and stirred for a further 1 h, cooled to room temperature and molybdenum dioxodichloride (52 mg, 0.26 mmol) in dry THF (3 ml) added and the mixture stirred for ½ h. After filtering the reaction mixture, removal of the solvent gave a residue with an infrared spectrum showing broad bands of weak intensity which could be assigned to the starting ligand. There were no additional absorptions in the 850-1000 cm^{-1} region to indicate the presence of Mo=0 groups.

iv) Ligand exchange reactions.

Bis(acetylacetonato)dioxomolybdenum(VI) (85 mg, 0.26 mmol) in dry methanol (10 ml) was added to a solution of NN^1-ethylenebis(iminomethylcamphor) in methanol (10 ml) containing a few drops of glacial acetic acid, and the mixture left to stand at room temperature. After three days the orange coloured reaction mixture was evaporated to dryness under reduced pressure giving a green 'gummy' material which on dispersion in ether gave a green solid which was filtered off. The infrared spectrum of this product showed it to be mainly unchanged ligand although a weak absorption at 900 cm^{-1} suggest the presence of a small amount of a molybdenyl containing species.

Appendix 2. The structure determination of $MoO_2(C_{18}H_{23}NO_3)(DMF)$ (Fig 2.1)

Table A2.1 Anisotropic thermal parameters ($x10^3$)

Atom	U_{11}	U_{22}	U_{33}	U_{12}	U_{13}	U_{23}
Mo	32	23	19	1	0	1
N(1)	32(3)	28(4)	19(3)	0(3)	1(2)	1(2)
N(2)	43(4)	38(4)	47(5)	2(3)	5(3)	2(3)
O(1)	67(4)	46(4)	65(5)	19(3)	7(4)	20(4)
O(2)	41(3)	26(3)	35(3)	1(2)	12(2)	3(2)
O(3)	40(3)	48(4)	45(3)	8(3)	7(2)	15(3)
O(4)	46(3)	42(4)	24(3)	0(2)	7(2)	1(2)
O(5)	55(4)	25(3)	18(3)	5(2)	1(2)	0(2)
O(6)	35(3)	44(3)	32(3)	8(3)	0(2)	2(3)

Table A2.2 Interatomic bond lengths/Å in the ligands

Atoms		Atoms	
C(1)-O(1)	1.426(11)	C(10)-C(11)	1.514(11)
O(1)-C(2)	1.363(10)	C(10)-C(15)	1.580(11)
C(2)-C(3)	1.376(11)	C(11)-C(12)	1.571(12)
C(3)-C(4)	1.397(12)	C(12)-C(13)	1.544(11)
C(4)-C(5)	1.368(12)	C(13)-C(14)	1.551(11)
C(5)-C(6)	1.393(11)	C(13)-C(15)	1.547(11)
C(6)-C(7)	1.402(10)	C(13)-C(18)	1.508(11)
C(6)-C(8)	1.458(10)	C(14)-O(5)	1.414(9)
C(7)-C(2)	1.408(10)	C(15)-C(16)	1.519(12)
C(7)-O(2)	1.336(9)	C(15)-C(17)	1.544(11)
C(8)-N(1)	1.272(9)	C(19)-O(6)	1.244(9)
N(1)-C(9)	1.488(9)	C(19)-N(2)	1.320(10)
C(9)-C(10)	1.546(10)	N(2)-C(20)	1.446(11)
C(9)-C(14)	1.539(10)	N(2)-C(21)	1.433(12)

Table A2.3 Interatomic bond angles/^{o} in the ligands

Angles		Angles	
C(1)-O(1)-C(2)	116.3(7)	C(10)-C(11)-C(12)	104.6(7)
O(1)-C(2)-C(3)	126.3(8)	C(10)-C(15)-C(13)	93.3(6)
C(2)-C(3)-C(4)	120.9(9)	C(10)-C(15)-C(16)	112.6(7)
C(2)-C(7)-O(2)	118.8(7)	C(10)-C(15)-C(17)	113.6(7)
C(3)-C(4)-C(5)	119.7(9)	C(11)-C(12)-C(13)	102.0(6)
C(4)-C(5)-C(6)	120.7(9)	C(12)-C(13)-C(14)	102.6(7)
C(5)-C(6)-C(7)	119.7(7)	C(12)-C(13)-C(18)	113.2(7)
C(5)-C(6)-C(8)	118.0(7)	C(13)-C(14)-O(5)	113.9(6)
C(6)-C(7)-C(2)	119.2(7)	C(13)-C(14)-C(9)	103.4(6)
C(6)-C(7)-O(2)	121.8(7)	C(15)-C(13)-C(18)	117.3(7)
C(6)-C(8)-N(1)	123.5(7)	C(15)-C(10)-C(11)	100.8(6)
C(8)-C(6)-C(7)	122.0(7)	C(15)-C(13)-C(12)	102.8(7)
C(7)-C(2)-O(1)	114.1(7)	C(15)-C(13)-C(14)	104.4(7)
C(7)-C(2)-C(3)	119.6(8)	C(16)-C(15)-C(17)	106.6(7)
C(8)-N(1)-C(9)	119.5(6)	C(16)-C(15)-C(13)	114.3(7)
N(1)-C(9)-C(10)	116.8(6)	C(17)-C(15)-C(13)	116.3(7)
N(1)-C(9)-C(14)	108.3(6)	C(18)-C(13)-C(14)	114.8(7)
C(9)-C(14)-O(5)	111.2(6)	O(6)-C(19)-N(2)	123.8(8)
C(9)-C(10)-C(11)	103.5(7)	C(19)-N(2)-C(20)	120.8(8)
C(9)-C(10)-C(15)	104.0(6)	C(19)-N(2)-C(21)	121.0(8)
C(10)-C(9)-C(14)	104.0(6)	C(20)-N(2)-C(21)	118.2(9)

Table A2.4 Observed and calculated structure factors for $MoO_2(C_{18}H_{23}NO_3)(DMF)$.

H	K	L	10FO	10FC
4	0	0	2426	2538
6	0	0	1126	1125
8	0	0	301	283
10	0	0	539	624
12	0	0	123	111
14	0	0	820	319
16	0	0	156	141
18	0	0	670	667
20	0	0	194	200
22	0	0	319	344
26	0	0	439	440
28	0	0	401	390
32	0	0	356	320
4	1	0	846	325
5	1	0	1357	1362
6	1	0	1925	1944
7	1	0	124	170
8	1	0	713	737
9	1	0	377	376
10	1	0	559	569
11	1	0	231	228
12	1	0	1020	1018
13	1	0	329	390
15	1	0	259	288
16	1	0	725	764
17	1	0	272	268
20	1	0	673	680
24	1	0	457	448
26	1	0	374	344
30	1	0	296	280
0	2	0	309	323
1	2	0	33	96
2	2	0	442	439
3	2	0	456	450
4	2	0	1230	1265
5	2	0	909	379
6	2	0	232	210
8	2	0	1058	1036
9	2	0	555	529
10	2	0	857	819
11	2	0	246	257
12	2	0	475	451
13	2	0	151	167
14	2	0	907	884
16	2	0	250	237
18	2	0	720	720
20	2	0	377	385
22	2	0	638	635

H	K	L	10FO	10FC
23	2	0	164	156
24	2	0	373	342
25	2	0	301	314
26	2	0	324	309
32	2	0	210	212
1	3	0	1069	1034
2	3	0	1829	1825
3	3	0	141	150
4	3	0	775	755
6	3	0	538	564
8	3	0	335	352
9	3	0	156	147
10	3	0	351	358
11	3	0	141	113
12	3	0	659	690
13	3	0	510	495
15	3	0	962	934
17	3	0	293	294
20	3	0	343	325
22	3	0	335	324
24	3	0	405	410
25	3	0	208	241
27	3	0	292	306
28	3	0	317	295
30	3	0	292	304
34	3	0	290	277
0	4	0	525	549
1	4	0	480	459
2	4	0	467	432
3	4	0	773	759
4	4	0	1386	1367
5	4	0	344	346
6	4	0	375	386
7	4	0	377	400
8	4	0	845	850
10	4	0	725	749
11	4	0	221	252
12	4	0	371	377
13	4	0	353	333
14	4	0	665	686
15	4	0	311	295
17	4	0	166	157
18	4	0	599	602
21	4	0	247	235
22	4	0	693	650
24	4	0	184	215
25	4	0	564	591
23	4	0	279	238

H	K	L	10FO	10FC
29	4	0	261	244
32	4	0	271	279
1	5	0	490	484
2	5	0	1251	1206
3	5	0	116	74
4	5	0	271	238
5	5	0	1088	1043
6	5	0	1059	1035
7	5	0	274	241
8	5	0	158	170
9	5	0	530	530
10	5	0	572	539
12	5	0	480	461
13	5	0	154	195
14	5	0	327	317
15	5	0	153	145
16	5	0	349	337
17	5	0	181	171
19	5	0	355	373
20	5	0	898	909
21	5	0	180	178
23	5	0	541	526
24	5	0	249	279
26	5	0	297	285
27	5	0	318	259
30	5	0	236	236
0	6	0	1309	1305
1	6	0	610	515
2	6	0	145	132
3	6	0	1107	1099
4	6	0	339	359
6	6	0	280	271
7	6	0	558	520
8	6	0	527	494
10	6	0	552	523
11	6	0	391	370
12	6	0	483	454
13	6	0	152	138
14	6	0	556	571
16	6	0	253	281
17	6	0	396	391
18	6	0	631	636
22	6	0	249	269
24	6	0	221	193
29	6	0	227	187
1	7	0	784	737
2	7	0	639	512
3	7	0	847	788

H	K	L	10FO	10FC
4	7	0	213	197
5	7	0	672	675
6	7	0	846	825
7	7	0	143	149
8	7	0	599	608
9	7	0	597	584
10	7	0	229	240
11	7	0	225	270
12	7	0	449	464
13	7	0	276	261
15	7	0	212	177
16	7	0	202	233
20	7	0	251	236
23	7	0	229	255
27	7	0	191	235
0	8	0	381	371
1	8	0	182	199
2	8	0	167	173
3	8	0	522	488
4	8	0	449	445
5	8	0	210	222
6	8	0	133	122
7	8	0	779	813
8	8	0	231	225
10	8	0	355	361
11	8	0	413	493
13	8	0	293	292
14	8	0	371	333
15	8	0	393	375
17	8	0	171	181
18	8	0	409	393
21	8	0	384	325
25	8	0	269	257
1	9	0	384	411
3	9	0	170	158
5	9	0	533	524
6	9	0	161	123
8	9	0	322	280
9	9	0	565	560
10	9	0	154	144
12	9	0	459	453
13	9	0	501	499
15	9	0	244	276
16	9	0	413	401
17	9	0	381	343
19	9	0	354	397
20	9	0	201	199
23	9	0	179	249

H	K	L	10FO	10FC
27	9	0	301	248
0	10	0	133	203
1	10	0	274	261
3	10	0	455	417
4	10	0	231	256
5	10	0	164	191
6	10	0	146	170
7	10	0	614	611
8	10	0	353	326
9	10	0	171	121
10	10	0	231	236
11	10	0	397	418
13	10	0	171	147
15	10	0	246	252
17	10	0	184	189
21	10	0	373	377
25	10	0	344	328
1	11	0	259	256
2	11	0	247	256
5	11	0	356	359
6	11	0	197	182
9	11	0	450	472
10	11	0	255	269
13	11	0	231	303
17	11	0	336	312
19	11	0	350	373
23	11	0	337	319
1	12	0	214	235
3	12	0	295	313
7	12	0	379	376
11	12	0	357	362
15	12	0	295	272
17	12	0	323	283
21	12	0	201	223
1	13	0	212	171
5	13	0	428	434
9	13	0	455	455
13	13	0	233	333
7	14	0	320	319
11	14	0	353	354
13	14	0	192	130
15	14	0	254	271
5	15	0	217	199
13	15	0	275	232
15	15	0	222	229
7	16	0	213	165
2	0	1	309	313
3	0	1	855	862

OBSERVED AND CALCULATED STRUCTURE FACTORS FOR MD(O)2(C18H23NO3)1(DMF)

H	K	L	10FO	10FC	H	K	L	10FO	10FC	H	K	L	10FO	10FC	H	K	L	10FO	10FC	H	K	L	10FO	10FC
4	0	1	468	475	-5	1	1	1049	1058	-10	2	1	170	140	-16	3	1	334	368	-21	4	1	433	503
5	0	1	781	775	-4	1	1	829	859	-9	2	1	364	341	-15	3	1	509	523	-20	4	1	305	335
6	0	1	259	266	-3	1	1	1232	1241	-8	2	1	922	923	-14	3	1	687	682	-19	4	1	133	174
7	0	1	524	563	-2	1	1	507	520	-7	2	1	1107	1147	-13	3	1	825	806	-18	4	1	257	249
8	0	1	449	446	-1	1	1	1579	1557	-6	2	1	241	205	-12	3	1	427	409	-17	4	1	656	656
9	0	1	337	389	0	1	1	429	395	-5	2	1	820	810	-11	3	1	378	389	-16	4	1	356	336
11	0	1	923	916	1	1	1	1598	1550	-4	2	1	154	175	-10	3	1	606	668	-15	4	1	648	634
12	0	1	735	734	2	1	1	510	517	-3	2	1	1251	1262	-9	3	1	1030	1055	-14	4	1	413	405
13	0	1	755	758	3	1	1	1271	1221	-2	2	1	1338	1902	-8	3	1	319	289	-13	4	1	353	353
14	0	1	221	247	4	1	1	371	838	-1	2	1	832	791	-7	3	1	352	350	-12	4	1	450	465
15	0	1	689	668	5	1	1	1083	1059	0	2	1	455	450	-6	3	1	115	105	-11	4	1	842	835
16	0	1	397	435	6	1	1	765	744	1	2	1	811	806	-5	3	1	667	652	-10	4	1	455	452
17	0	1	293	283	7	1	1	584	571	2	2	1	1948	1816	-4	3	1	765	751	-9	4	1	314	300
18	0	1	170	169	8	1	1	706	692	3	2	1	1271	1249	-3	3	1	963	939	-8	4	1	501	461
19	0	1	433	429	9	1	1	805	805	4	2	1	172	162	-2	3	1	212	227	-7	4	1	466	488
20	0	1	470	484	10	1	1	596	595	5	2	1	859	795	-1	3	1	422	389	-6	4	1	310	323
21	0	1	229	227	12	1	1	342	343	6	2	1	218	229	0	3	1	688	694	-5	4	1	902	847
22	0	1	206	200	13	1	1	828	845	7	2	1	1145	1139	1	3	1	398	423	-4	4	1	239	262
23	0	1	193	156	14	1	1	491	449	8	2	1	950	915	2	3	1	203	234	-3	4	1	337	363
24	0	1	139	221	15	1	1	555	535	9	2	1	847	845	3	3	1	972	940	-2	4	1	473	448
25	0	1	361	359	16	1	1	245	251	10	2	1	160	155	4	3	1	786	740	-1	4	1	585	575
26	0	1	153	192	17	1	1	438	439	11	2	1	872	860	5	3	1	695	627	0	4	1	253	257
30	0	1	224	220	18	1	1	425	407	12	2	1	546	514	6	3	1	110	88	1	4	1	602	564
31	0	1	201	208	19	1	1	508	509	13	2	1	296	286	7	3	1	360	345	-33	5	1	229	196
32	0	1	131	210	22	1	1	299	291	14	2	1	314	296	8	3	1	305	301	-31	5	1	209	153
33	0	1	245	171	23	1	1	292	287	15	2	1	496	527	9	3	1	1040	1043	-24	5	1	234	251
34	0	1	240	250	26	1	1	237	199	16	2	1	453	464	10	3	1	613	659	-23	5	1	259	254
35	0	1	159	139	27	1	1	309	301	17	2	1	582	572	11	3	1	393	382	-21	5	1	216	207
-31	1	1	203	200	28	1	1	214	201	18	2	1	198	178	12	3	1	413	422	-20	5	1	228	249
-28	1	1	338	300	29	1	1	295	253	19	2	1	221	247	13	3	1	809	809	-19	5	1	251	288
-26	1	1	210	201	-34	2	1	209	212	20	2	1	347	363	14	3	1	676	684	-18	5	1	236	208
-24	1	1	197	195	-30	2	1	289	288	21	2	1	441	441	15	3	1	512	513	-17	5	1	409	409
-23	1	1	274	288	-29	2	1	320	319	23	2	1	253	242	16	3	1	335	370	-16	5	1	240	202
-22	1	1	206	279	-25	2	1	177	194	24	2	1	177	203	17	3	1	465	468	-15	5	1	337	372
-21	1	1	177	123	-25	2	1	372	363	25	2	1	337	355	18	3	1	591	599	-14	5	1	409	433
-19	1	1	430	510	-24	2	1	195	214	29	2	1	332	320	19	3	1	396	405	-13	5	1	365	363
-18	1	1	419	412	-23	2	1	202	241	30	2	1	318	291	21	3	1	298	321	-12	5	1	327	313
-17	1	1	433	431	-21	2	1	414	440	34	2	1	197	212	22	3	1	307	314	-11	5	1	405	405
-16	1	1	253	249	-20	2	1	357	364	-28	3	1	302	293	23	3	1	520	503	-10	5	1	250	223
-15	1	1	562	584	-19	2	1	268	239	-27	3	1	354	356	24	3	1	182	185	-9	5	1	517	535
-14	1	1	449	466	-18	2	1	190	185	-25	3	1	164	123	27	3	1	381	353	-8	5	1	447	433
-13	1	1	834	837	-17	2	1	580	572	-24	3	1	165	182	28	3	1	306	296	-7	5	1	608	593
-12	1	1	329	333	-16	2	1	439	468	-23	3	1	507	501	-29	4	1	233	185	-6	5	1	471	410
-10	1	1	510	512	-15	2	1	528	521	-22	3	1	267	315	-28	4	1	237	192	-5	5	1	951	920
-9	1	1	799	812	-14	2	1	314	299	-21	3	1	308	321	-26	4	1	243	243	-4	5	1	1020	953
-8	1	1	697	707	-13	2	1	278	298	-19	3	1	428	407	-25	4	1	254	235	-3	5	1	538	558
-7	1	1	535	566	-12	2	1	533	527	-18	3	1	506	596	-24	4	1	301	314	-2	5	1	534	502
-6	1	1	756	751	-11	2	1	963	954	-17	3	1	467	466	-22	4	1	216	194	-1	5	1	679	631

OBSERVED AND CALCULATED STRUCTURE FACTORS FOR M3(O)2(C18H23N3)(DMF)

H	K	L	10FO	10FC	H	K	L	10FO	10FC	H	K	L	10FO	10FC	H	K	L	10FO	10FC	H	K	L	10FO	10FC
0	5	1	731	744	-3	6	1	588	608	-2	7	1	619	624	0	8	1	290	303	6	9	1	401	392
1	5	1	648	637	-2	6	1	439	449	-1	7	1	474	458	1	8	1	442	455	7	9	1	218	243
2	5	1	514	509	-1	6	1	679	673	1	7	1	511	459	2	8	1	339	331	8	9	1	450	441
3	5	1	524	547	0	6	1	597	609	2	7	1	603	517	3	8	1	356	375	9	9	1	227	243
4	5	1	952	969	1	6	1	666	678	3	7	1	516	503	4	8	1	490	504	10	9	1	219	228
5	5	1	910	916	2	6	1	459	444	4	7	1	178	210	5	8	1	501	509	11	9	1	348	369
6	5	1	434	427	3	6	1	591	601	5	7	1	559	573	6	8	1	200	213	12	9	1	276	254
7	5	1	615	594	4	6	1	770	755	6	7	1	501	506	7	8	1	428	459	15	9	1	304	306
8	5	1	449	441	5	6	1	642	658	7	7	1	453	438	8	8	1	479	479	16	9	1	241	259
9	5	1	541	517	6	6	1	569	570	8	7	1	472	449	9	8	1	447	457	17	9	1	219	201
10	5	1	243	222	7	6	1	714	722	9	7	1	486	495	10	8	1	357	333	19	9	1	232	233
11	5	1	396	408	8	6	1	374	376	10	7	1	444	469	11	8	1	196	222	20	9	1	331	334
12	5	1	330	322	9	6	1	283	294	11	7	1	419	430	12	8	1	425	428	24	9	1	191	189
13	5	1	362	359	10	6	1	293	320	12	7	1	500	524	13	8	1	293	278	25	9	1	173	161
14	5	1	433	436	11	6	1	353	333	13	7	1	284	286	14	8	1	352	361	26	9	1	208	224
15	5	1	333	368	12	6	1	384	402	14	7	1	301	343	16	8	1	247	255	-22	10	1	328	251
16	5	1	209	208	13	6	1	333	344	15	7	1	240	258	17	8	1	245	265	-20	10	1	225	197
17	5	1	391	416	14	6	1	458	507	16	7	1	480	497	18	8	1	296	330	-18	10	1	193	195
18	5	1	192	218	15	6	1	281	258	18	7	1	297	294	19	8	1	230	225	-17	10	1	352	336
19	5	1	237	293	16	6	1	269	278	19	7	1	322	339	20	8	1	164	208	-16	10	1	205	174
20	5	1	258	253	17	6	1	322	325	20	7	1	273	293	21	8	1	191	223	-15	10	1	170	193
21	5	1	242	217	18	6	1	312	337	21	7	1	209	194	22	8	1	235	228	-14	10	1	230	215
22	5	1	220	252	19	6	1	270	278	22	7	1	219	205	23	8	1	191	204	-13	10	1	218	235
23	5	1	257	247	21	6	1	291	281	23	7	1	230	225	28	8	1	167	160	-10	10	1	341	314
24	5	1	154	160	22	6	1	259	271	25	7	1	225	208	32	8	1	182	132	-9	10	1	331	328
26	5	1	216	170	25	6	1	193	212	-29	7	8	217	177	-26	8	8	212	223	-8	10	1	339	338
31	5	1	192	153	25	6	1	252	241	-23	8	8	186	204	-22	8	8	202	194	-6	10	1	157	206
-27	5	1	174	179	-22	6	1	208	220	-22	8	8	254	225	-21	8	8	174	205	-5	10	1	257	254
-25	5	1	235	242	-21	6	1	230	203	-21	8	8	200	218	-20	8	8	347	333	-4	10	1	191	199
-23	5	1	205	214	-21	6	1	204	198	-20	8	8	197	206	-19	8	8	202	234	-3	10	1	237	254
-22	5	1	252	272	-20	6	1	287	235	-19	8	8	247	221	-17	8	8	172	198	0	10	1	213	205
-21	5	1	259	281	-19	6	1	370	339	-18	8	8	350	324	-16	8	8	263	259	3	10	1	329	338
-19	5	1	271	269	-18	6	1	299	299	-17	8	8	253	269	-15	8	8	274	307	4	10	1	219	199
-18	5	1	345	328	-17	6	1	167	129	-16	8	8	242	257	-12	8	8	304	249	5	10	1	234	242
-17	5	1	322	311	-15	6	1	495	485	-14	8	8	373	357	-11	8	8	357	374	6	10	1	193	203
-15	5	1	235	273	-14	6	1	237	248	-13	8	8	277	286	-10	8	8	240	231	8	10	1	279	255
-13	5	1	295	261	-13	6	1	313	351	-12	8	8	440	435	-9	8	8	262	242	9	10	1	160	194
-12	5	1	434	436	-12	6	1	290	277	-11	8	8	218	209	-8	8	8	475	433	10	10	1	337	340
-11	5	1	347	329	-11	6	1	543	521	-10	8	8	346	330	-7	8	8	271	235	13	10	1	299	330
-10	5	1	403	393	-9	6	1	405	430	-9	8	8	425	463	-6	8	8	419	400	14	10	1	318	315
-9	5	1	343	347	-8	6	1	467	471	-8	8	8	501	486	-3	8	8	341	318	15	10	1	195	237
-8	5	1	232	314	-7	6	1	479	499	-7	8	8	461	461	-2	8	8	227	229	16	10	1	204	215
-7	5	1	241	305	-6	6	1	483	449	-6	8	8	215	205	-1	8	8	326	326	18	10	1	196	191
-6	5	1	376	398	-5	6	1	421	442	-5	8	8	522	512	0	8	8	315	294	20	10	1	313	335
-5	5	1	712	729	-4	6	1	511	514	-4	8	8	514	502	1	8	8	325	326	22	10	1	139	197
-4	5	1	543	567	-3	6	1	568	583	-3	8	8	375	383	2	8	8	216	223	24	10	1	307	256
-3	5	1	672	653	-2	6	1	193	208	-2	8	8	348	332	3	8	8	315	327	-26	11	1	202	187
-2	5	1	772	764	-1	6	1	528	507	-1	8	8	494	453	4	8	8	156	179	-24	11	1	218	137

OBSERVED AND CALCULATED STRUCTURE FACTORS FOR M3(O)2(C1M2)3N)3(DMF)

H	K	L	10FO	10FC	H	K	L	10FO	10FC	H	K	L	10FO	10FC	H	K	L	10FO	10FC	H	K	L	10FO	10FC
-20	11	1	235	294	-1	13	1	224	197	-22	1	2	193	174	-33	2	2	194	209	20	2	2	257	254
-16	11	1	314	354	1	13	1	193	135	-21	1	2	540	513	-29	2	2	173	173	21	2	2	270	232
-12	11	1	333	318	2	13	1	372	400	-20	1	2	186	193	-28	2	2	232	195	22	2	2	242	241
-11	11	1	274	278	4	13	1	240	248	-19	1	2	305	311	-27	2	2	305	312	23	2	2	493	489
-10	11	1	130	173	6	13	1	282	277	-17	1	2	533	615	-24	2	2	193	198	24	2	2	213	194
-7	11	1	285	305	7	13	1	255	229	-16	1	2	321	310	-23	2	2	517	492	27	2	2	278	315
-6	11	1	351	391	8	13	1	276	297	-15	1	2	455	501	-22	2	2	225	255	28	2	2	192	195
-3	11	1	321	313	12	13	1	201	205	-14	1	2	194	170	-21	2	2	245	231	-29	3	2	242	223
-2	11	1	342	358	-15	13	1	130	130	-13	1	2	535	544	-20	2	2	253	264	-27	3	2	213	186
-1	11	1	226	183	-14	14	1	215	198	-12	1	2	377	403	-19	2	2	605	613	-26	3	2	243	254
	11	1	205	181	-10	14	1	239	201	-11	1	2	776	812	-18	2	2	169	209	-25	3	2	359	351
	11	1	370	352	-9	14	1	208	175	-10	1	2	580	553	-17	2	2	480	453	-24	3	2	196	177
2	11	1	329	314	-1	14	1	221	181	-9	1	2	251	232	-16	2	2	181	221	-22	3	2	239	302
3	11	1	352	379	0	14	1	221	273	-8	1	2	302	326	-15	2	2	617	595	-21	3	2	572	557
6	11	1	270	306	4	14	1	232	256	-7	1	2	1376	1300	-14	2	2	477	475	-20	3	2	196	209
7	11	1	272	284	2	15	1	190	138	-6	1	2	191	229	-13	2	2	504	514	-19	3	2	331	378
11	11	1	329	318	3	15	1	187	192	-5	1	2	510	530	-12	2	2	270	246	-18	3	2	381	406
12	11	1	154	179	5	15	1	193	164	-4	1	2	217	209	-11	2	2	594	587	-17	3	2	542	559
14	11	1	337	355	8	15	1	509	507	-3	1	2	951	953	-10	2	2	562	563	-16	3	2	312	296
16	11	1	240	298	0	0	2	1184	1173	-2	1	2	290	237	-9	2	2	523	569	-15	3	2	716	692
20	11	1	193	194	1	0	2	815	797	-1	1	2	796	797	-8	2	2	405	400	-14	3	2	256	263
22	11	1	233	246	2	0	2	1290	1257	0	1	2	375	373	-7	2	2	246	258	-13	3	2	647	637
-18	12	1	230	242	3	0	2	257	239	1	1	2	774	804	-6	2	2	131	137	-12	3	2	588	560
-14	12	1	229	234	4	0	2	918	946	2	1	2	243	252	-5	2	2	695	725	-11	3	2	224	281
-13	12	1	313	315	5	0	2	259	244	3	1	2	943	951	-4	2	2	207	184	-10	3	2	331	343
-9	12	1	303	273	6	0	2	596	591	4	1	2	198	203	-3	2	2	1040	1014	-9	3	2	259	272
-8	12	1	322	326	7	0	2	367	356	5	1	2	530	525	-2	2	2	161	174	-8	3	2	523	482
-6	12	1	212	231	8	0	2	1271	1258	6	1	2	244	219	-1	2	2	952	911	-7	3	2	463	496
-5	12	1	256	266	10	0	2	441	426	7	1	2	1405	1385	0	2	2	381	344	-6	3	2	475	469
-4	12	1	408	415	11	0	2	245	284	8	1	2	321	315	1	2	2	899	909	-5	3	2	537	591
-1	12	1	247	244	12	0	2	340	326	9	1	2	240	231	2	2	2	165	171	-4	3	2	432	412
0	12	1	352	386	13	0	2	674	703	10	1	2	644	633	3	2	2	1049	1019	-3	3	2	1040	1004
1	12	1	210	244	14	0	2	322	297	11	1	2	803	804	4	2	2	217	185	-2	3	2	234	218
4	12	1	389	411	17	0	2	460	477	12	1	2	385	372	5	2	2	705	735	-1	3	2	792	813
5	12	1	219	267	19	0	2	395	383	13	1	2	547	536	6	2	2	150	134	0	3	2	177	151
6	12	1	217	229	20	0	2	720	750	14	1	2	173	176	7	2	2	236	258	1	3	2	815	903
8	12	1	321	324	23	0	2	152	112	15	1	2	480	495	8	2	2	384	410	2	3	2	236	219
9	12	1	272	280	26	0	2	403	413	16	1	2	295	317	9	2	2	567	545	3	3	2	1049	1022
10	12	1	314	314	27	0	2	245	253	17	1	2	532	519	10	2	2	526	573	4	3	2	397	419
13	12	1	220	230	31	0	2	293	267	19	1	2	277	310	11	2	2	597	587	5	3	2	593	593
14	12	1	252	247	-35	1	2	325	324	20	1	2	178	191	12	2	2	264	256	6	3	2	445	470
18	12	1	273	251	-33	1	2	219	198	21	1	2	543	518	13	2	2	516	505	7	3	2	476	473
-12	13	1	203	210	-31	1	2	197	185	22	1	2	178	175	14	2	2	465	481	8	3	2	530	490
-8	13	1	322	300	-29	1	2	215	165	24	1	2	141	103	15	2	2	571	593	9	3	2	246	267
-7	13	1	253	231	-23	1	2	266	279	25	1	2	364	377	16	2	2	195	217	10	3	2	318	331
-6	13	1	238	275	-25	1	2	201	181	28	1	2	201	177	17	2	2	429	456	11	3	2	253	272
-4	13	1	270	247	-23	1	2	365	381	29	1	2	275	279	18	2	2	198	202	12	3	2	605	561
-2	13	1	385	402			2	158	148	33	1	2	195	187	19	2	2	614	611	13	3	2	611	634

OBSERVED AND CALCULATED STRUCTURE FACTORS FOR M1(O)2(C18H23N3O3)(DMF)

H	K	L	10FO	10FC
14	3	2	278	265
15	3	2	653	700
16	3	2	247	302
17	3	2	544	557
18	3	2	396	402
19	3	2	339	381
20	3	2	179	202
21	3	2	537	559
22	3	2	253	300
25	3	2	333	349
26	3	2	244	250
29	3	2	248	227
-27	4	2	341	290
-24	4	2	352	354
-23	4	2	457	472
-22	4	2	230	230
-21	4	2	157	149
-20	4	2	295	279
-19	4	2	494	479
-18	4	2	255	246
-17	4	2	394	369
-16	4	2	372	357
-15	4	2	392	411
-14	4	2	287	315
-13	4	2	686	628
-12	4	2	390	409
-11	4	2	421	409
-10	4	2	231	227
-9	4	2	857	846
-8	4	2	249	236
-7	4	2	152	142
-6	4	2	953	935
-5	4	2	719	713
-4	4	2	134	129
-3	4	2	407	380
-2	4	2	330	338
-1	4	2	575	502
0	4	2	329	357
1	4	2	572	591
2	4	2	353	347
3	4	2	391	394
4	4	2	135	143
5	4	2	706	720
6	4	2	982	939
7	4	2	152	143
8	4	2	258	225
9	4	2	808	953
10	4	2	236	222

H	K	L	10FO	10FC
11	4	2	424	397
12	4	2	368	405
13	4	2	629	633
14	4	2	275	307
15	4	2	395	407
16	4	2	356	355
17	4	2	355	372
18	4	2	277	248
19	4	2	465	487
20	4	2	303	277
22	4	2	243	228
23	4	2	452	471
24	4	2	332	350
27	4	2	261	298
33	4	2	223	195
-29	5	2	259	259
-26	5	2	191	188
-25	5	2	335	353
-24	5	2	167	176
-22	5	2	174	173
-21	5	2	356	377
-20	5	2	232	248
-19	5	2	179	223
-18	5	2	305	321
-17	5	2	466	454
-15	5	2	523	500
-14	5	2	341	352
-13	5	2	279	292
-12	5	2	303	311
-11	5	2	762	784
-10	5	2	371	397
-8	5	2	503	527
-7	5	2	549	549
-6	5	2	635	532
-5	5	2	520	495
-4	5	2	447	458
-3	5	2	567	590
-2	5	2	380	340
-1	5	2	587	562
0	5	2	493	481
1	5	2	539	563
2	5	2	350	347
3	5	2	582	579
4	5	2	459	456
5	5	2	530	490
6	5	2	581	595
7	5	2	530	546
9	5	2	503	525

H	K	L	10FO	10FC
10	5	2	405	391
11	5	2	798	739
12	5	2	310	320
13	5	2	320	290
14	5	2	372	348
15	5	2	489	513
17	5	2	452	453
18	5	2	307	324
19	5	2	198	219
20	5	2	248	243
21	5	2	376	375
22	5	2	234	173
25	5	2	323	367
26	5	2	170	131
29	5	2	239	259
-31	6	2	217	202
-27	6	2	196	218
-26	6	2	208	232
-22	6	2	179	170
-21	6	2	187	200
-20	6	2	315	297
-19	6	2	274	293
-17	6	2	393	408
-16	6	2	305	309
-15	6	2	456	459
-14	6	2	263	241
-13	6	2	578	539
-12	6	2	504	493
-11	6	2	359	379
-10	6	2	346	351
-9	6	2	446	427
-8	6	2	401	395
-6	6	2	513	492
-5	6	2	488	482
-4	6	2	392	366
-3	6	2	421	422
-2	6	2	489	483
-1	6	2	596	597
0	6	2	290	266
1	6	2	596	598
2	6	2	456	495
3	6	2	422	410
4	6	2	359	373
5	6	2	462	475
6	6	2	485	488
8	6	2	401	399
9	6	2	416	418
10	6	2	372	349

H	K	L	10FO	10FC
11	6	2	389	380
12	6	2	484	495
13	6	2	594	604
14	6	2	209	248
15	6	2	468	457
16	6	2	284	309
17	6	2	370	413
19	6	2	296	292
20	6	2	307	291
22	6	2	177	165
27	6	2	214	221
30	6	2	194	153
31	6	2	214	202
-31	7	2	193	181
-28	7	2	205	182
-26	7	2	179	135
-24	7	2	214	214
-22	7	2	293	318
-21	7	2	195	200
-20	7	2	156	169
-18	7	2	233	238
-17	7	2	337	332
-15	7	2	249	290
-14	7	2	259	260
-13	7	2	303	304
-12	7	2	244	239
-11	7	2	291	309
-10	7	2	382	369
-8	7	2	585	558
-7	7	2	395	399
-6	7	2	434	427
-5	7	2	350	337
-4	7	2	545	563
-3	7	2	482	493
-1	7	2	483	474
0	7	2	631	605
1	7	2	474	475
3	7	2	495	481
4	7	2	567	561
5	7	2	355	345
6	7	2	417	426
7	7	2	390	394
8	7	2	547	550
10	7	2	380	351
11	7	2	298	302
12	7	2	252	242
13	7	2	305	305
14	7	2	242	251

H	K	L	10FO	10FC
15	7	2	272	285
17	7	2	339	333
18	7	2	240	231
22	7	2	271	312
24	7	2	214	212
25	7	2	213	167
-27	8	2	171	135
-26	8	2	199	169
-24	8	2	232	239
-23	8	2	213	165
-20	8	2	234	262
-19	8	2	232	212
-16	8	2	410	420
-15	8	2	253	229
-13	8	2	231	193
-12	8	2	405	423
-11	8	2	372	367
-10	8	2	339	338
-9	8	2	218	196
-8	8	2	394	393
-7	8	2	305	332
-6	8	2	506	483
-5	8	2	337	369
-4	8	2	415	418
-3	8	2	215	207
-2	8	2	632	608
-1	8	2	354	354
0	8	2	175	141
1	8	2	325	353
2	8	2	616	601
3	8	2	205	208
4	8	2	420	412
5	8	2	339	362
6	8	2	439	472
7	8	2	329	332
8	8	2	357	385
9	8	2	172	194
10	8	2	322	337
11	8	2	343	371
12	8	2	405	405
13	8	2	137	182
15	8	2	244	233
16	8	2	425	415
19	8	2	232	207
20	8	2	257	257
23	8	2	195	184
24	8	2	221	240
-22	9	2	297	247

OBSERVED AND CALCULATED STRUCTURE FACTORS FOR MD(O)2(C18H23N3)(DMF)

H	K	L	10FO	10FC
-21	0	2	169	130
-19	0	2	393	357
-18	0	2	357	359
-17	0	2	209	231
-14	0	2	515	527
-13	0	2	229	241
-12	0	2	217	185
-11	0	2	208	223
-10	0	2	359	412
-9	0	2	348	337
-8	0	2	262	258
-7	0	2	323	325
-5	0	2	134	176
-4	0	2	526	553
-3	0	2	350	348
-2	0	2	171	132
0	0	2	625	506
1	0	2	197	123
2	0	2	194	181
3	0	2	341	352
4	0	2	534	551
5	0	2	150	186
6	0	2	329	314
7	0	2	272	270
8	0	2	329	343
9	0	2	379	402
10	0	2	219	215
11	0	2	135	141
12	0	2	207	238
13	0	2	522	523
14	0	2	199	179
15	0	2	219	224
16	0	2	355	358
17	0	2	232	260
19	0	2	255	244
22	0	2	206	195
-26	1	2	157	153
-22	1	2	210	202
-21	1	2	232	230
-20	1	2	200	186
-17	1	2	342	340
-16	1	2	448	432
-12	1	2	398	396
-10	1	2	218	220
-9	1	2	327	299
-8	1	2	449	460
-6	1	2	171	224
-5	1	2	139	165
-4	1	2	407	391
-2	1	2	291	253
-1	1	2	244	260
1	1	2	393	400
2	1	2	209	223
5	1	2	463	459
6	1	2	252	294
8	1	2	235	222
9	1	2	392	396
10	1	2	435	429
12	1	2	222	204
15	1	2	330	351
16	1	2	197	187
17	1	2	237	239
20	1	2	185	203
21	1	2	211	195
25	1	2	214	243
-19	1	1	288	306
-14	1	1	193	224
-12	1	1	388	375
-10	1	1	372	394
-3	1	1	352	392
-6	1	1	221	240
-4	1	1	173	200
-3	1	1	208	220
-1	1	1	364	367
0	1	1	225	219
1	1	1	210	194
3	1	1	199	239
4	1	1	403	331
6	1	1	351	390
8	1	1	400	377
10	1	1	200	221
11	1	1	225	226
12	1	1	203	208
13	1	1	266	243
14	1	1	212	252
15	1	1	348	331
16	1	1	201	193
17	1	1	208	241
19	1	1	236	250
20	1	1	260	239
22	1	1	353	357
26	1	1	297	358
-32	1	0	226	239
-28	1	0	183	143
-26	1	0	302	248
-24	1	0	201	243
10	1	0	182	199
12	1	0	326	337
16	1	0	257	251
20	1	0	236	216
-14	2	0	255	246
-10	2	0	193	227
-6	2	0	190	189
-4	2	0	262	309
0	2	0	295	312
4	2	0	327	309
10	2	0	219	226
14	2	0	255	244
18	2	0	253	234
-8	2	1	268	249
-2	2	1	301	319
2	2	1	339	317
6	2	1	252	225
8	2	1	258	245
16	2	1	255	229
-4	2	2	244	223
0	2	2	252	206
6	2	2	218	195
10	2	2	226	220
1	2	3	170	169
2	2	3	911	940
3	2	3	150	156
4	2	3	252	239
5	2	3	238	248
7	2	3	1357	1366
8	2	3	758	778
9	2	3	172	187
10	2	3	564	595
11	2	3	195	197
12	2	3	894	892
13	2	3	262	259
14	2	3	181	197
15	2	3	363	372
16	2	3	562	558
17	2	3	289	285
18	2	3	402	442
19	2	3	342	310
20	2	3	223	223
21	2	3	250	263
22	2	3	308	275
23	2	3	219	225
24	2	3	258	226
26	2	3	227	212
28	2	3	252	308
-23	1	3	185	223
-22	1	3	309	340
-20	1	3	266	265
-19	1	3	259	255
-18	1	3	605	632
-17	1	3	371	373
-16	1	3	175	176
-15	1	3	414	420
-14	1	3	590	611
-13	1	3	307	310
-12	1	3	295	287
-10	1	3	883	862
-9	1	3	249	261
-8	1	3	797	809
-7	1	3	284	297
-6	1	3	649	651
-5	1	3	405	408
-4	1	3	1155	1170
-3	1	3	241	259
-2	1	3	192	193
-1	1	3	128	105
0	1	3	299	301
1	1	3	201	185
2	1	3	257	253
3	1	3	155	165
4	1	3	392	399
5	1	3	629	650
6	1	3	275	281
7	1	3	781	811
8	1	3	243	249
9	1	3	825	864
10	1	3	127	152
11	1	3	277	285
12	1	3	293	310
13	1	3	603	604
14	1	3	399	415
15	1	3	163	177
16	1	3	389	372
17	1	3	603	621
18	1	3	257	262
19	1	3	243	262
20	1	3	184	193
21	1	3	314	337
22	1	3	220	231
23	1	3	301	301
24	1	3	200	216
26	1	3	207	230
28	1	3	211	213
-26	2	3	222	247
-24	2	3	314	317
-22	2	3	228	256
-21	2	3	157	197
-20	2	3	646	648
-19	2	3	194	153
-17	2	3	350	375
-16	2	3	757	784
-15	2	3	333	410
-14	2	3	250	252
-13	2	3	253	235
-12	2	3	818	844
-11	2	3	504	524
-10	2	3	627	630
-9	2	3	527	526
-8	2	3	699	712
-7	2	3	392	394
-6	2	3	950	993
-5	2	3	429	421
-4	2	3	134	162
-3	2	3	328	295
-2	2	3	1059	1038
-1	2	3	334	343
0	2	3	837	813
1	2	3	331	334
2	2	3	1037	1043
3	2	3	322	282
4	2	3	155	169
5	2	3	440	414
6	2	3	972	982
7	2	3	420	389
8	2	3	714	713
9	2	3	544	520
10	2	3	528	518
11	2	3	536	524
12	2	3	803	836
13	2	3	240	229
14	2	3	253	248
15	2	3	431	402
16	2	3	750	780
17	2	3	349	371
20	2	3	613	644
21	2	3	178	198
22	2	3	260	255
23	2	3	164	164
24	2	3	320	316
26	2	3	277	241
28	2	3	193	199

OBSERVED AND CALCULATED STRUCTURE FACTORS FOR MO(O)2(C18H23N)3)(DMF)

H	K	L	10FO	10FC	H	K	L	10FO	10FC	H	K	L	10FO	10FC	H	K	L	10FO	10FC	H	K	L	10FO	10FC
30	2	3	207	218	28	3	3	263	256	26	4	3	270	283	-27	6	3	227	202	-11	7	3	454	439
-28	3	3	224	256	32	3	3	245	218	30	4	3	207	199	-26	6	3	195	213	-10	7	3	325	342
-26	3	3	195	186	-26	4	3	305	291	-28	5	3	266	238	-23	6	3	243	243	-8	7	3	393	366
-24	3	3	220	207	-24	4	3	341	354	-26	5	3	165	192	-20	6	3	270	239	-7	7	3	543	518
-23	3	3	186	151	-23	4	3	201	239	-24	5	3	253	248	-17	6	3	205	202	-6	7	3	240	258
-22	3	3	482	494	-22	4	3	318	268	-22	5	3	245	283	-16	6	3	470	503	-5	7	3	310	301
-21	3	3	216	216	-20	4	3	474	457	-21	5	3	314	346	-15	6	3	185	170	-4	7	3	537	550
-19	3	3	153	197	-19	4	3	465	473	-20	5	3	159	190	-14	6	3	243	229	-3	7	3	616	623
-18	3	3	650	677	-18	4	3	194	204	-18	5	3	318	335	-13	6	3	337	370	-2	7	3	211	219
-17	3	3	226	240	-17	4	3	211	231	-17	5	3	364	358	-12	6	3	483	494	-1	7	3	424	389
-15	3	3	311	284	-16	4	3	471	464	-15	5	3	292	291	-11	6	3	189	191	0	7	3	754	797
-14	3	3	751	759	-15	4	3	263	268	-14	5	3	712	730	-10	6	3	364	353	1	7	3	359	393
-13	3	3	192	224	-14	4	3	308	309	-13	5	3	233	239	-9	6	3	466	461	2	7	3	227	210
-12	3	3	517	530	-13	4	3	293	328	-12	5	3	474	457	-8	6	3	239	215	3	7	3	521	534
-11	3	3	193	181	-12	4	3	487	455	-11	5	3	428	431	-6	6	3	415	410	4	7	3	553	552
-10	3	3	654	650	-10	4	3	687	660	-10	5	3	595	580	-5	6	3	695	674	5	7	3	310	307
-9	3	3	430	388	-9	4	3	409	398	-8	5	3	444	457	-4	6	3	239	238	6	7	3	240	248
-8	3	3	910	938	-8	4	3	541	525	-7	5	3	590	554	-3	6	3	525	491	7	7	3	491	521
-7	3	3	327	337	-7	4	3	248	255	-6	5	3	456	455	-2	6	3	681	680	8	7	3	378	370
-6	3	3	405	423	-6	4	3	776	792	-5	5	3	161	195	-1	6	3	574	565	10	7	3	344	345
-5	3	3	516	494	-5	4	3	222	225	-4	5	3	523	529	1	6	3	578	562	11	7	3	453	440
-4	3	3	972	945	-4	4	3	574	544	-3	5	3	218	253	2	6	3	655	682	12	7	3	238	223
-3	3	3	443	441	-3	4	3	672	645	-2	5	3	277	287	3	6	3	531	492	14	7	3	317	333
-2	3	3	351	315	-2	4	3	787	793	-1	5	3	452	425	4	6	3	246	226	15	7	3	427	402
-1	3	3	499	503	-1	4	3	360	373	0	5	3	483	512	5	6	3	685	677	16	7	3	224	233
0	3	3	851	867	0	4	3	125	139	1	5	3	458	440	6	6	3	392	413	17	7	3	244	293
1	3	3	491	503	1	4	3	377	358	2	5	3	281	278	8	6	3	205	225	18	7	3	321	301
2	3	3	343	322	2	4	3	810	787	3	5	3	239	244	9	6	3	469	458	19	7	3	239	214
3	3	3	472	422	3	4	3	643	652	4	5	3	524	535	10	6	3	378	355	21	7	3	287	283
4	3	3	945	946	4	4	3	585	545	5	5	3	199	190	11	6	3	190	196	22	7	3	238	217
5	3	3	495	486	5	4	3	208	208	6	5	3	451	465	12	6	3	490	490	25	7	3	132	194
6	3	3	455	414	6	4	3	780	790	7	5	3	530	553	13	6	3	356	373	-23	8	3	252	269
7	3	3	331	328	7	4	3	265	255	8	5	3	442	454	14	6	3	231	229	-19	8	3	311	328
8	3	3	940	927	8	4	3	549	529	10	5	3	555	592	16	6	3	455	508	-17	8	3	231	260
9	3	3	415	389	9	4	3	395	411	11	5	3	448	436	17	6	3	193	212	-16	8	3	273	276
10	3	3	650	641	10	4	3	657	661	12	5	3	442	458	20	6	3	254	235	-15	8	3	328	371
11	3	3	176	191	12	4	3	489	511	13	5	3	226	238	23	6	3	244	246	-13	8	3	369	349
12	3	3	553	540	13	4	3	326	336	14	5	3	709	741	26	6	3	183	218	-12	8	3	398	392
13	3	3	173	222	14	4	3	343	311	15	5	3	304	299	30	6	3	230	200	-11	8	3	173	167
14	3	3	776	754	15	4	3	241	274	17	5	3	347	354	-25	7	3	203	197	-10	8	3	224	216
15	3	3	299	301	15	4	3	459	472	18	5	3	344	336	-22	7	3	194	219	-9	8	3	403	428
17	3	3	233	236	17	4	3	225	223	20	5	3	170	195	-21	7	3	281	292	-8	8	3	379	349
18	3	3	638	681	19	4	3	195	209	21	5	3	331	350	-19	7	3	206	213	-6	8	3	196	203
19	3	3	210	193	19	4	3	476	475	22	5	3	230	277	-18	7	3	285	304	-5	8	3	433	391
21	3	3	194	213	20	4	3	479	453	24	5	3	265	245	-17	7	3	270	284	-4	8	3	183	215
22	3	3	497	496	22	4	3	290	252	26	5	3	218	193	-15	7	3	395	405	-3	8	3	358	366
24	3	3	203	205	23	4	3	260	232	28	5	3	197	230	-14	7	3	337	328	-2	8	3	595	602
26	3	3	193	190	25	4	3	283	355	32	5	3	208	164	-12	7	3	222	226	-1	8	3	501	520

OBSERVED AND CALCULATED STRUCTURE FACTORS FOR M3(O)2(C13H23N)3)(OMF)

H	K	L	10FO	10FC
0	8	3	194	190
1	8	3	510	510
2	8	3	594	601
3	8	3	344	364
4	8	3	207	211
5	8	3	389	383
6	8	3	192	209
8	8	3	356	352
9	8	3	404	419
10	8	3	213	212
11	8	3	167	167
12	8	3	405	395
13	8	3	354	348
15	8	3	379	367
16	8	3	259	276
17	8	3	244	261
19	8	3	313	326
20	8	3	194	210
21	8	3	137	156
23	8	3	253	268
25	8	3	220	201
-21	9	3	219	201
-17	9	3	303	301
-15	9	3	277	292
-11	9	3	277	286
-10	9	3	421	389
-8	9	3	230	286
-7	9	3	275	241
-6	9	3	253	293
-4	9	3	253	292
-3	9	3	203	235
-2	9	3	458	484
-1	9	3	290	305
0	9	3	474	460
1	9	3	346	355
2	9	3	452	463
3	9	3	317	301
4	9	3	434	470
5	9	3	242	237
6	9	3	251	287
7	9	3	294	290
8	9	3	264	237
9	9	3	249	291
10	9	3	377	380
11	9	3	285	287
13	9	3	253	294
15	9	3	317	300
17	9	3	258	197
21	9	3	226	200
-25	10	3	267	277
-23	10	3	220	218
-13	10	3	363	362
-10	10	3	163	145
-9	10	3	383	418
-8	10	3	217	228
-7	10	3	157	137
-5	10	3	321	313
-5	10	3	349	381
-4	10	3	213	217
-1	10	3	338	337
0	10	3	150	167
1	10	3	315	344
3	10	3	178	176
5	10	3	390	372
6	10	3	297	310
8	10	3	264	226
9	10	3	453	415
13	10	3	329	353
17	10	3	201	174
19	10	3	249	276
23	10	3	244	208
-25	11	3	279	251
-21	11	3	205	259
-17	11	3	209	231
-15	11	3	204	222
-11	11	3	360	355
-7	11	3	400	433
-4	11	3	224	220
-3	11	3	364	334
-2	11	3	185	191
-1	11	3	213	192
1	11	3	189	201
3	11	3	325	333
4	11	3	205	217
6	11	3	191	146
7	11	3	440	437
11	11	3	351	365
15	11	3	209	223
17	11	3	237	230
21	11	3	279	269
25	11	3	242	259
-19	12	3	228	212
-13	12	3	283	302
-9	12	3	331	331
-5	12	3	355	351
-3	12	3	192	147
-1	12	3	315	349
0	12	3	196	181
1	12	3	347	343
5	12	3	314	353
9	12	3	297	334
13	12	3	298	301
17	12	3	181	180
19	12	3	234	208
-17	13	3	199	153
-11	13	3	225	242
-7	13	3	261	309
-3	13	3	297	333
-1	13	3	267	257
3	13	3	276	269
7	13	3	318	332
11	13	3	326	307
13	13	3	252	245
14	13	3	207	138
-15	14	3	279	248
-5	14	3	210	226
-1	14	3	244	223
1	14	3	277	247
5	0	4	506	502
6	0	4	459	471
8	0	4	275	245
10	0	4	177	150
11	0	4	405	410
13	0	4	1097	1080
14	0	4	138	156
16	0	4	299	307
17	0	4	917	890
18	0	4	322	325
19	0	4	298	303
20	0	4	228	235
21	0	4	584	508
22	0	4	172	190
23	0	4	394	400
24	0	4	519	554
25	0	4	199	193
27	0	4	181	221
28	0	4	225	224
31	0	4	373	392
32	0	4	229	224
			336	322
			296	278
			236	246
			225	191
			259	212
-34	1	4	203	170
-30	1	4	257	223
-26	1	4	287	254
-25	1	4	218	242
-24	1	4	218	253
-22	1	4	245	246
-21	1	4	298	301
-20	1	4	418	451
-19	1	4	235	235
-16	1	4	469	461
-15	1	4	394	417
-14	1	4	245	279
-13	1	4	190	173
-12	1	4	426	462
-11	1	4	551	570
-10	1	4	288	304
-9	1	4	325	336
-8	1	4	470	474
-7	1	4	815	835
-6	1	4	480	447
-4	1	4	339	347
-3	1	4	725	698
-2	1	4	531	515
-1	1	4	457	430
0	1	4	161	168
1	1	4	417	438
2	1	4	510	522
3	1	4	691	702
4	1	4	350	345
5	1	4	141	118
6	1	4	452	454
7	1	4	800	830
8	1	4	444	466
9	1	4	319	235
10	1	4	313	305
11	1	4	577	567
12	1	4	450	462
13	1	4	193	167
14	1	4	260	272
15	1	4	387	414
16	1	4	449	458
18	1	4	157	145
19	1	4	182	238
20	1	4	445	449
21	1	4	243	305
22	1	4	244	251
24	1	4	266	253
25	1	4	255	243
26	1	4	244	258
29	1	4	218	207
30	1	4	218	226
34	1	4	252	172
-28	2	4	203	205
-24	2	4	232	235
-23	2	4	257	293
-22	2	4	274	260
-21	2	4	206	217
-20	2	4	153	149
-19	2	4	236	277
-18	2	4	259	282
-17	2	4	427	445
-14	2	4	438	449
-13	2	4	379	410
-12	2	4	232	253
-11	2	4	171	161
-10	2	4	494	493
-9	2	4	528	543
-8	2	4	530	530
-6	2	4	319	321
-5	2	4	503	570
-4	2	4	771	750
-3	2	4	294	297
-2	2	4	133	149
-1	2	4	372	370
0	2	4	550	537
1	2	4	371	364
2	2	4	131	151
3	2	4	274	292
4	2	4	737	745
5	2	4	551	565
6	2	4	314	321
7	2	4	526	533
8	2	4	519	544
9	2	4	457	494
10	2	4	132	165
11	2	4	211	256
12	2	4	417	413
13	2	4	445	444
14	2	4	419	441
15	2	4	312	286
17	2	4	259	264
18	2	4	198	153
19	2	4	221	213
20	2	4	279	264
21	2	4	287	292
23	2	4	241	239

OBSERVED AND CALCULATED STRUCTURE FACTORS FOR MO(O)2(C13H23NO3)(DMF)

H	K	L	10FO	10FC
28	2	4	203	207
32	2	4	213	180
-30	3	4	237	198
-26	3	4	209	182
-25	3	4	231	203
-22	3	4	206	187
-21	3	4	251	237
-20	3	4	230	214
-19	3	4	213	203
-18	3	4	211	226
-17	3	4	272	282
-16	3	4	550	546
-15	3	4	169	239
-14	3	4	159	145
-13	3	4	295	209
-12	3	4	582	508
-11	3	4	439	445
-10	3	4	398	385
-9	3	4	277	298
-8	3	4	328	316
-7	3	4	620	513
-6	3	4	290	603
-5	3	4	239	272
-4	3	4	415	238
-3	3	4	738	423
-2	3	4	210	714
-1	3	4	239	199
0	3	4	190	256
1	3	4	685	201
2	3	4	413	709
3	3	4	254	428
4	3	4	299	267
5	3	4	579	507
6	3	4	609	612
7	3	4	305	318
8	3	4	306	293
9	3	4	375	393
10	3	4	449	438
11	3	4	551	594
12	3	4	311	302
13	3	4	256	231
14	3	4	529	542
15	3	4	295	282
16	3	4	240	223
17	3	4	178	208
18	3	4	223	209
22	3	4	231	188
25	3	4	218	201
26	3	4	193	182
30	3	4	198	193
-23	4	4	174	182
-20	4	4	341	319
-19	4	4	245	242
-18	4	4	363	394
-15	4	4	315	321
-14	4	4	479	475
-13	4	4	533	508
-12	4	4	223	177
-11	4	4	218	220
-10	4	4	453	470
-9	4	4	375	320
-8	4	4	455	447
-7	4	4	390	395
-6	4	4	387	400
-5	4	4	624	607
-4	4	4	466	448
-3	4	4	317	322
-2	4	4	398	423
-1	4	4	484	465
0	4	4	685	679
1	4	4	473	469
2	4	4	405	424
3	4	4	301	315
4	4	4	437	451
5	4	4	582	613
6	4	4	406	395
7	4	4	415	421
8	4	4	472	459
9	4	4	333	395
10	4	4	453	430
11	4	4	241	219
12	4	4	204	183
13	4	4	513	510
14	4	4	437	480
15	4	4	298	322
16	4	4	373	373
17	4	4	232	249
18	4	4	302	317
19	4	4	221	179
20	4	4	205	206
21	4	4	259	215
22	4	4	220	199
23	4	4	228	217
28	4	4	305	295
-19	5	4	206	215
-17	5	4	238	248
-16	5	4	282	295
-15	5	4	411	416
-14	5	4	197	211
-13	5	4	310	281
-12	5	4	384	373
-11	5	4	599	592
-10	5	4	245	262
-9	5	4	339	323
-8	5	4	322	312
-7	5	4	468	458
-6	5	4	494	463
-5	5	4	377	384
-4	5	4	398	404
-3	5	4	377	373
-2	5	4	653	605
-1	5	4	542	545
0	5	4	347	339
1	5	4	532	544
2	5	4	596	512
3	5	4	363	372
4	5	4	412	394
5	5	4	369	384
6	5	4	468	474
7	5	4	458	472
8	5	4	307	321
9	5	4	279	335
10	5	4	265	271
11	5	4	570	598
12	5	4	352	379
13	5	4	248	298
14	5	4	205	220
15	5	4	404	424
16	5	4	276	291
17	5	4	252	253
18	5	4	159	194
19	5	4	211	211
20	5	4	243	291
21	5	4	131	216
22	5	4	252	218
23	5	4	220	233
24	5	4	209	223
25	5	4	242	216
26	5	4	236	219
27	5	4	253	304
28	5	4	290	251
29	5	4	287	258
-14	6	4	205	213
-13	6	4	294	285
-12	6	4	210	201
-11	6	4	308	324
-10	6	4	294	259
-9	6	4	504	494
-8	6	4	477	475
-7	6	4	161	199
-6	6	4	391	373
-5	6	4	579	566
-4	6	4	302	277
-3	6	4	236	185
-2	6	4	405	398
-1	6	4	527	510
0	6	4	494	444
1	6	4	516	503
2	6	4	411	402
3	6	4	187	192
4	6	4	260	295
5	6	4	550	564
6	6	4	388	384
7	6	4	196	200
8	6	4	465	487
9	6	4	498	492
10	6	4	270	269
11	6	4	321	331
12	6	4	175	204
13	6	4	280	284
14	6	4	201	218
15	6	4	307	261
16	6	4	242	245
17	6	4	299	298
18	6	4	202	225
19	6	4	189	219
20	6	4	253	233
21	6	4	207	183
22	6	4	249	211
23	6	4	251	199
24	6	4	279	303
25	6	4	234	234
26	6	4	234	211
27	6	4	266	259
28	6	4	270	265
29	6	4	265	263
30	6	4	212	212
31	6	4	227	207
32	6	4	201	209
33	6	4	360	383
-8	7	4	272	267
-7	7	4	262	270
-6	7	4	204	233
-4	7	4	477	481
-3	7	4	574	584
-1	7	4	250	219
0	7	4	192	203
1	7	4	209	227
3	7	4	554	579
4	7	4	470	489
6	7	4	234	236
7	7	4	231	277
8	7	4	251	267
9	7	4	339	382
10	7	4	200	204
11	7	4	176	208
12	7	4	251	265
13	7	4	278	265
14	7	4	218	252
15	7	4	203	216
16	7	4	257	231
17	7	4	238	303
18	7	4	191	216
19	7	4	202	191
20	7	4	170	221
21	7	4	249	198
22	7	4	251	266
23	7	4	347	321
24	7	4	178	219
25	7	4	271	262
26	7	4	343	365
27	7	4	250	258
28	7	4	207	211
29	7	4	249	202
30	7	4	454	434
31	7	4	205	216
32	7	4	246	290
33	7	4	355	356
34	7	4	334	380
35	7	4	130	195
36	7	4	179	187
37	7	4	347	372
38	7	4	271	358
39	7	4	270	285
40	7	4	206	205
41	7	4	471	439
42	7	4	176	216

OBSERVED AND CALCULATED STRUCTURE FACTORS FOR MO(O)2(C13H23NO3)(DMF)

H	K	L	10FO	10FC
10	8	4	285	257
11	8	4	331	366
12	8	4	232	263
13	8	4	202	222
14	8	4	316	319
15	8	4	230	252
16	8	4	239	266
17	8	4	198	197
20	8	4	202	205
-23	9	4	251	206
-18	9	4	237	235
-16	9	4	135	204
-14	9	4	235	252
-13	9	4	237	270
-11	9	4	159	177
-10	9	4	199	191
-9	9	4	347	348
-8	9	4	213	221
-7	9	4	400	426
-6	9	4	207	218
-5	9	4	249	248
-4	9	4	356	338
-3	9	4	372	378
-2	9	4	370	335
-1	9	4	256	245
0	9	4	154	171
1	9	4	143	213
2	9	4	177	228
3	9	4	186	158
4	9	4	233	176
5	9	4	337	218
6	9	4	288	357
7	9	4	223	272
8	9	4	222	251
9	9	4	240	232
10	9	4	207	212
11	9	4	330	184
12	9	4	255	275
13	9	4	198	187
14	9	4	266	148
15	9	4	173	214
16	9	4	353	267
17	9	4	133	197
18	9	4	364	358
19	9	4	213	144
20	9	4	244	379
21	9	4	269	221
22	9	4	269	269
0	10	4	212	160
1	10	4	300	259
2	10	4	207	222
3	10	4	351	377
7	10	4	359	362
10	10	4	174	193
11	10	4	243	272
15	10	4	261	279
20	10	4	218	213
21	10	4	222	135
-19	11	4	218	198
-14	11	4	208	231
-13	11	4	195	229
-9	11	4	301	252
-8	11	4	184	180
-5	11	4	312	329
-4	11	4	294	297
-3	11	4	284	294
-2	11	4	322	297
-1	11	4	198	203
0	11	4	303	335
1	11	4	215	195
2	11	4	251	258
3	11	4	213	233
4	11	4	236	195
5	11	4	221	175
6	11	4	233	237
7	11	4	223	198
8	11	4	199	237
9	11	4	321	285
10	11	4	189	255
11	11	4	244	220
12	11	4	188	201
13	11	4	196	216
14	11	4	243	244
15	11	4	194	179
16	11	4	275	251
19	11	4	204	222
23	11	4	281	281
27	11	4	195	225
-29	12	4	227	254
-25	12	4	209	200
-21	12	4	251	252
-19	12	4	302	247
-17	12	4	447	441
-15	12	4	682	684
-13	12	4	330	308
-11	12	4	187	190
-9	12	4	634	628
-8	12	4	155	159
-7	12	4	380	403
-6	12	4	300	323
-5	12	4	421	420
-4	12	4	374	391
-3	12	4	372	390
-2	12	4	199	186
-1	12	4	384	396
0	12	4	326	370
1	12	4	195	157
2	12	4	238	222
3	12	4	359	340
4	12	4	424	433
5	12	4	407	389
6	12	4	236	156
7	12	4	224	201
8	12	4	347	330
9	12	4	230	254
10	12	4	227	435
11	12	4	250	281
12	12	4	270	256
13	12	4	625	650
14	12	4	301	318
15	12	4	771	760
16	12	4	331	344
17	12	4	214	179
18	12	4	667	558
19	12	4	641	562
20	12	4	165	179
21	12	4	357	336
22	12	4	752	760
23	12	4	298	322
24	12	4	671	641
25	12	4	218	252
26	12	4	243	276
27	12	4	163	172
28	12	4	400	420
29	12	4	259	254
30	12	4	338	330
31	12	4	218	202
32	12	4	369	388
33	12	4	435	433
34	12	4	325	338
35	12	4	305	309
36	12	4	362	368
37	12	4	329	348
38	12	4	249	181
-17	2	5	331	340
-15	2	5	339	337
-14	2	5	157	144
-13	2	5	202	243
-11	2	5	593	603
-9	2	5	247	261
-7	2	5	809	829
-6	2	5	167	196
-4	2	5	245	213
-3	2	5	817	811
-1	2	5	463	463
0	2	5	133	123
1	2	5	459	453
3	2	5	795	804
4	2	5	221	217
6	2	5	183	200
7	2	5	813	815
8	2	5	274	259
9	2	5	595	605
10	2	5	234	245
11	2	5	203	145
12	2	5	349	326
13	2	5	314	339
14	2	5	163	191
15	2	5	335	350
16	2	5	200	188
17	2	5	390	367
18	2	5	284	307
19	2	5	262	273
20	2	5	285	332
21	2	5	334	255
22	2	5	269	276
23	2	5	194	215
24	2	5	153	204
25	2	5	494	508
26	2	5	751	765
27	2	5	223	222
28	2	5	641	644
29	2	5	313	311
30	2	5	420	424
31	2	5	575	554
32	2	5	165	145
33	2	5	539	553
34	2	5	403	425
35	2	5	322	312
36	2	5	187	188
37	2	5	636	642
38	2	5	221	222
9	3	5	746	770
13	3	5	493	506
14	3	5	195	202
15	3	5	221	214
17	3	5	274	275
19	3	5	326	351
20	3	5	182	188
23	3	5	356	334
27	3	5	274	276
-25	4	5	325	324
-22	4	5	202	197
-21	4	5	327	348
-19	4	5	218	166
-18	4	5	171	161
-17	4	5	288	280
-15	4	5	277	274
-13	4	5	243	237
-11	4	5	418	410
-7	4	5	618	628
-6	4	5	263	267
-4	4	5	312	300
-3	4	5	532	569
-1	4	5	372	371
0	4	5	525	528
1	4	5	351	367
3	4	5	573	565
4	4	5	304	307
6	4	5	219	264
7	4	5	520	527
8	4	5	153	159
10	4	5	175	196
11	4	5	403	411
12	4	5	193	181
13	4	5	239	248
15	4	5	255	277
17	4	5	296	274
18	4	5	175	167
21	4	5	356	347
22	4	5	201	198
25	4	5	253	326
29	4	5	205	203
-24	5	5	245	206
-23	5	5	304	283
-20	5	5	223	241
-19	5	5	251	324
-17	5	5	256	228
-16	5	5	238	247
-15	5	5	257	269

OBSERVED AND CALCULATED STRUCTURE FACTORS FOR MO(O)2(C18H23NO)3(DMF)

H	K	L	10FO	10FC
-13	5	5	313	314
-12	5	5	259	252
-11	5	5	272	292
-10	5	5	185	173
-9	5	5	356	338
-8	5	5	214	214
-6	5	5	400	356
-5	5	5	423	434
-2	5	5	401	405
-1	5	5	392	361
-25	5	5	238	254
-21	6	5	299	304
-18	6	5	317	315
-17	6	5	329	275
-15	6	5	299	262
-14	6	5	252	270
-11	6	5	349	332
-10	6	5	280	299
-8	6	5	244	217
-7	6	5	347	361
-5	6	5	133	162
-4	6	5	574	567
-3	6	5	189	228
-1	6	5	234	220
0	6	5	651	649
2	6	5	198	176
3	6	5	213	243
5	6	5	295	222
6	6	5	253	223
7	6	5	212	200
8	6	5	344	323
9	6	5	326	322
10	6	5	309	315
12	6	5	427	425
13	6	5	279	271
15	6	5	173	148
16	6	5	365	374
17	6	5	302	295
18	6	5	239	241
20	6	5	478	489
23	6	5	190	197
-29	7	5	253	247
-23	7	5	193	158
-20	7	5	237	233
-19	7	5	299	276
-17	7	5	232	339
-16	7	5	309	363
-13	7	5	222	227
-12	7	5	293	278
-9	7	5	331	324
-8	7	5	370	331
-7	7	5	205	232
-6	7	5	513	529
-5	7	5	252	275
-3	7	5	326	340
-2	7	5	197	191
-1	7	5	211	195
0	7	5	309	278
1	7	5	335	343
2	7	5	233	241
3	7	5	472	478
4	7	5	263	255
5	7	5	281	293
6	7	5	250	253
7	7	5	384	422
8	7	5	418	428
9	7	5	210	284
10	7	5	219	242
11	7	5	205	203
12	7	5	309	299
13	7	5	447	406
14	7	5	234	231
15	7	5	270	297
16	7	5	294	246
17	7	5	235	251
18	7	5	248	245
19	7	5	288	298
20	7	5	239	224
21	7	5	213	216
22	7	5	233	225
23	7	5	267	227
24	7	5	221	213
25	7	5	222	233
26	7	5	359	356
27	7	5	515	523
28	7	5	272	250
29	7	5	196	200
30	7	5	174	143
31	7	5	392	381
32	7	5	403	405
33	7	5	312	332
34	7	5	361	387
35	7	5	578	558
36	7	5	438	429
37	7	5	303	277
23	0	5	135	210
27	0	5	220	247
28	0	6	221	204
-24	1	5	224	210
-20	1	6	289	294
-17	1	6	177	143
-16	1	6	474	455
-15	1	6	249	245
-14	1	5	207	197
-12	1	6	518	502
-11	1	6	439	450
-10	1	5	401	405
-9	1	6	177	193
-8	1	6	406	411
-7	1	6	406	383
-6	1	6	379	379
-5	1	6	209	180
-4	1	6	210	216
-3	1	6	467	458
-2	1	6	187	217
-1	1	6	275	238
0	1	6	211	215
1	1	6	275	301
2	1	6	246	257
3	1	6	423	441
4	1	6	345	309
5	1	6	253	250
6	1	6	357	333
7	1	6	345	335
8	1	6	470	472
9	1	6	181	173
10	1	6	411	407
11	1	6	439	442
12	1	6	502	504
13	1	6	202	184
14	1	6	307	279
15	1	6	341	378
16	1	6	546	509
17	1	6	229	200
18	1	6	174	155
19	1	6	281	269
20	1	6	252	255
21	1	6	326	288
22	1	6	251	257
23	1	6	278	254
24	1	6	358	368
25	1	6	242	228
26	1	6	324	319
-8	3	6	246	255
-7	3	6	379	390
-6	3	6	244	232
-5	3	6	492	531
-4	3	6	234	213
-3	3	6	387	374
-2	3	6	573	574
-1	3	6	465	483
0	3	6	450	433
1	3	6	282	236
2	3	6	203	203
-22	4	6	298	274
-18	4	6	193	177
-17	4	6	285	265
-14	4	6	267	264
-12	4	6	395	395
-11	4	6	374	383
-10	4	6	414	421
-9	4	6	381	401
-8	4	6	322	297
-7	4	6	354	343
-6	4	6	415	409
-5	4	6	395	409
-4	4	6	323	324
-3	4	6	275	272
-2	4	6	312	319
-1	4	6	395	405
0	4	6	185	216
1	4	6	295	321
2	4	6	248	241
3	4	6	314	308
4	4	6	172	199
5	4	6	243	210
6	4	6	304	321
7	4	6	367	354
8	4	6	380	379
9	4	6	323	320
10	4	6	261	248
11	4	6	205	201
12	4	6	299	295
13	4	6	465	440
14	4	6	287	297
15	4	6	217	193
16	4	6	248	209
17	4	6	219	222
18	4	6	193	193
19	4	6	297	267
20	4	6	253	280
-13	6	6	273	270
-12	6	5	150	156
-11	6	6	230	239
-10	6	6	318	322
-9	6	5	276	234
-8	6	6	218	226
-7	6	6	226	203
-4	6	5	359	366
-3	6	6	238	229
-2	6	6	184	156
0	6	5	315	320
-19	7	6	243	223
-13	7	6	201	216
-12	7	6	133	211
-10	7	6	229	215
-8	7	6	245	221
-7	7	6	242	246
-6	7	6	270	264
-5	7	6	300	283
-2	7	6	243	261
0	7	6	197	195
22	7	6	232	201
-11	8	6	202	256
-8	8	6	290	211
-7	8	6	202	283
-5	8	6	272	217
-3	8	6	244	288
-1	8	6	235	212
21	8	6	210	179
-15	9	6	244	223
-13	9	6	230	265
-9	9	6	190	280
-6	9	6	290	198
-5	9	6	242	310
-4	9	6	190	219
-3	9	6	245	213
-1	9	6	241	260
-11	10	6	289	243
-7	10	6	244	289
-3	10	6	273	274
-1	10	6	222	241
-5	10	6	217	257
-7	10	6	212	225
3	10	6	175	197
6	11	6	270	220
7	11	6	201	165
12	11	6	374	376
1	12	6	122	130
2	12	6	122	130
6	12	6	66	97

OBSERVED AND CALCULATED STRUCTURE FACTORS FOR MO(O)2(C13H23NO3)2(DMF)

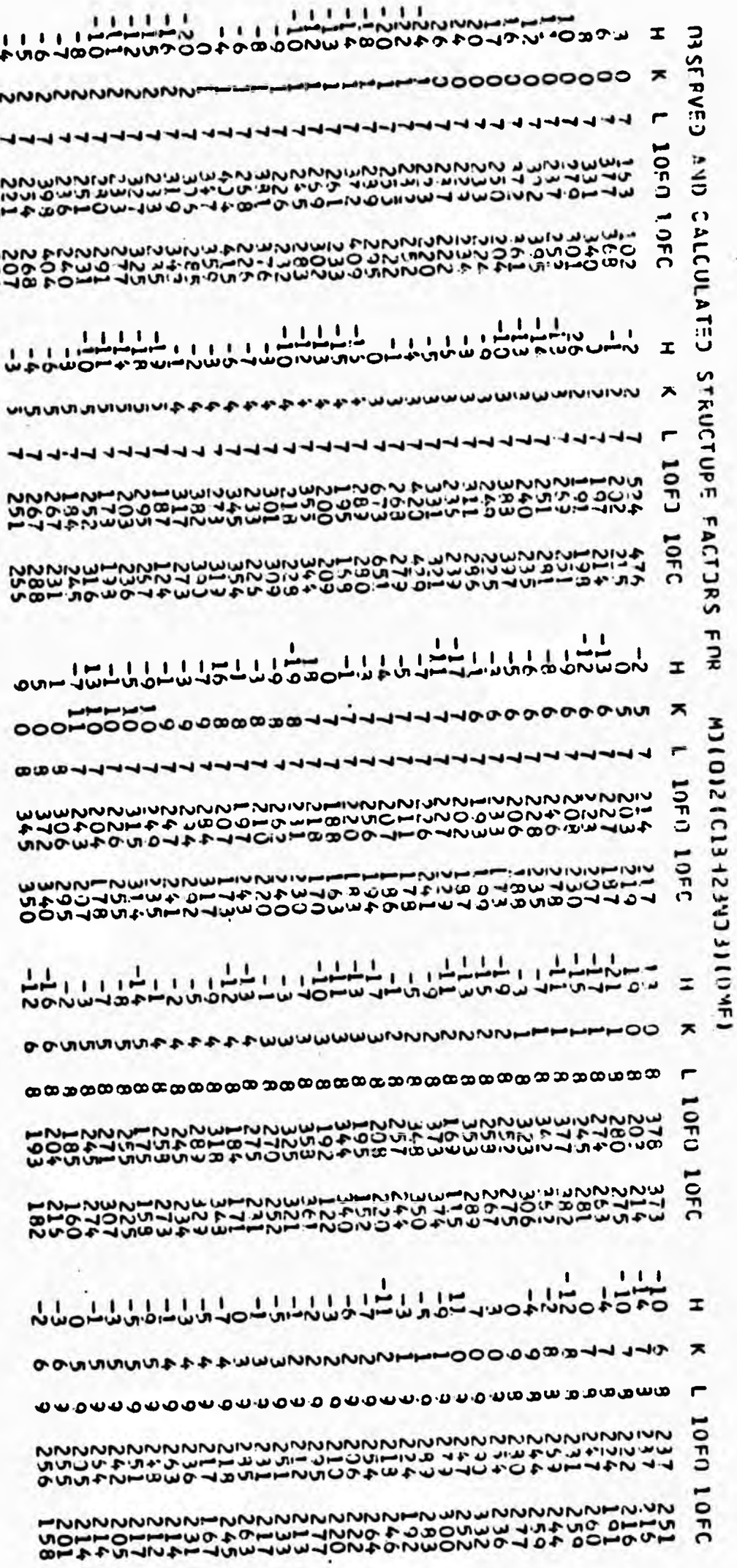

END

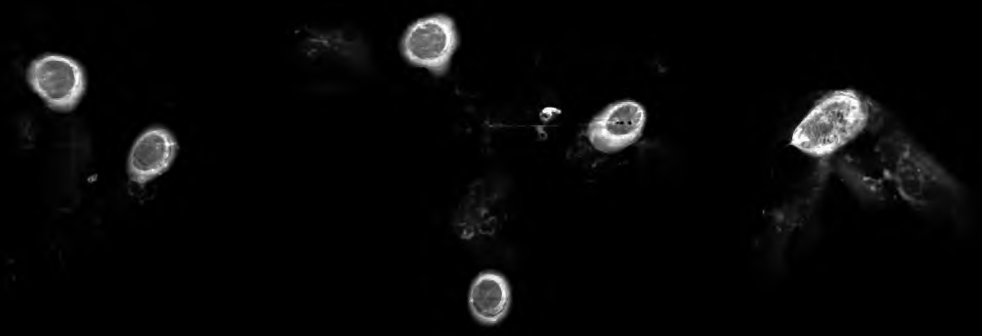

I

*

D 37788/81.

SPRAGGS GK

Vol I

pp 438.

Coloured Plates

Duds

ASPECTS OF SURFACE AND SUBSURFACE SOLUTE DYNAMICS IN A SMALL CATCHMENT : WEST WALK, SOUTH HAMPSHIRE

Gerald Edward Spraggs, B.A., Dip. Hydrol.

Thesis submitted as part of the requirement for the degree, Doctor of Philosophy, of the Council for National Academic Awards.

September 1980

The work was carried out while a Research Assistant in the Geography Department, Portsmouth Polytechnic, with the collaboration of Southern Water Authority.

WEST WALK CATCHMENT LOOKING SOUTH-EAST

(The A.32 is in the foreground; gauging stations shown by dots)

WEST WALK CATCHMENT LOOKING SOUTH-EAST
(The A.32 is in the foreground; gauging stations shown by dots)

WEST WALK CATCHMENT LOOKING SOUTH-EAST

(The A.32 is in the foreground; gauging stations shown by dots)

VOLUME I

Contents

List of Figures

List of Tables

Acknowledgements

Abstract

Chapters 1 - 8

VOLUME I

C O N T E N T S

(VOLUME I)

Chapter 4 (cont'd)

Chapter 5 (cont'd)

Chapter 6 (cont'd)

C O N T E N T S

(VOLUME II)

SECTION 4 (cont'd)

LIST OF FIGURES

LIST OF FIGURES (cont'd)

LIST OF FIGURES (cont'd)

LIST OF FIGURES (cont'd)

LIST OF FIGURES (cont'd)

LIST OF FIGURES (cont'd)

LIST OF FIGURES (cont'd)

LIST OF TABLES

LIST OF TABLES (cont'd)

LIST OF TABLES (cont'd)

LIST OF TABLES (cont'd)

ACKNOWLEDGEMENTS

I am very grateful to Dr D N Mottershead and Mr B F Sprunt, my two supervisors, for guidance during the preparation of this thesis.

Thanks are also due to the many other members of Portsmouth Polytechnic Geography Department, past and present, who assisted with the work at some stage. Other Departments of Portsmouth Polytechnic also co-operated, notably Chemistry, Civil Engineering, Fine Art, Geology, Marine Resources, Mechanical Engineering and Physics.

Assistance with instrumentation was obtained from:

Mr D Fourt and Dr W Binns,	Forestry Commission, Alice Holt Research Station, Farnham
Mr R Gibbs,	Military Engineering Experimental Establishment, Christchurch
Mr M Newson and Mr W Smith,	Institute of Hydrology, Wallingford
Mr M Waylen,	King's College Field Centre, Rogate

Figures 3.1, 3.4, 3.5, 5.7, 5.19 and 5.20 were drawn by the Cartographic Section of Portsmouth Polytechnic Geography Department.

Mr R Homer assisted with photography and photographic reproduction.

Southern Water Authority assisted by loaning equipment and providing hydrological data.

Mr S Rickards and Mr V Cope of the Rooksbury Estate allowed access to the study catchment.

Thanks are due to the painstaking work of typists Judy Hayes, Sheila Ladell (first draft) and Judy Cahill (final draft).

Finally, I wish to acknowledge the encouragement and patience of my family and friends during the completion of this study.

ABSTRACT

ASPECTS OF SURFACE AND SUBSURFACE SOLUTE DYNAMICS IN A SMALL CATCHMENT : WEST WALK, SOUTH HAMPSHIRE

G. E. SPRAGGS

The primary objective of this study was to model the natural, unpolluted water quality in a small clay and sandstone catchment (area 0.6 square km) during the period 1975 - 1977. The investigation was undertaken at (i) the catchment scale, whereby hydrological and water quality data were collected for empirical, lumped-parameter modelling of quality; and (ii) the hillslope scale, whereby soil and soil water physical and chemical parameters were monitored to aid explanation of processes observed at the catchment scale.

Chapters 1 and 2 give research objectives, applications and a literature review of atmospheric and stream solute dynamics. Chapter 3 describes geology, soils, vegetation and climate of the study catchment. Chapters 4 and 5 detail the catchment scale hydrometry and methods of water quality analysis.

In Chapter 6 bivariate and multivariate regression models of solute response are developed using regularly sampled water quality data and hydrometeorological variables. In Chapter 7 storm and regularly sampled quality data are modelled by linear and polynomial regression, and an improvement in the former is achieved using separate autumn and non-autumn periods. Regression models can predict approximate weekly solute levels but fail to reproduce intra-storm variability. In Chapter 8 it is shown that the 1975-1976 drought was a period of net solute accumulation, the post-drought period one of net solute loss. Spatial variation of solute concentrations and loads within the catchment is strongly related to geology and soils. Temporal fluctuation of solute source areas is shown to be strongly influenced by expansion and contraction of the hydrological contributing area.

Chapter 9 presents a theoretical basis to the movement of water and solutes in hillslope soils. Chapter 10 describes the instrumentation of a hillslope to monitor soil water and solute movement. In Chapter 11 soil chemical analyses and laboratory permeability determinations are used to pinpoint potential solute sources and routeways. It is shown that solutes are leached from near-surface, upslope sources and transported in pulse form to the slope base, where they contribute to streamflow recession. Upward water and solute movement was observed during periods of plant growth and high transpiration, near surface solute accumulations being flushed into the stream during subsequent rainfall. The K^+ increase during storms is shown to be due to leaching from near-surface organic-rich horizons close to the stream. Chapter 12 introduces a suite of computer programs which use the theoretical basis of Chapter 9 for processing collected soil water and solute data. Investigation and modelling of soil water processes is seen as an important step towards a physically-based model of catchment solute response which should incorporate the variable contributing area concept.

SECTION 1

RESEARCH BACKGROUND, OBJECTIVES, LITERATURE REVIEW AND INTRODUCTION TO THE STUDY CATCHMENT

CHAPTER 1

SURFACE AND SUBSURFACE SOLUTE DYNAMICS IN A SMALL CATCHMENT: RESEARCH BACKGROUND AND OBJECTIVES

1.1 INTRODUCTORY COMMENTS

In Britain during the past few years there has been a continuously increasing involvement by geographers in the field of hydrology, with major literature contributions from R.C. Ward (1967, 1979), K.J. Gregory and D.E. Walling (1973a) and J.C. Rodda et al (1976). Much of this involvement arose from small catchment studies initiated by universities, and quite naturally some of these developed specialities in particular facets of the subject. Exeter University for example carried out research into sediment and solute dynamics in relatively undisturbed catchments (e.g. Walling, 1974), and urbanising catchments (e.g. Gregory, 1974). At Bristol University research focussed on surface and subsurface runoff processes (e.g. Weyman, 1970, 1974) and karst hydrology (e.g. Atkinson and Drew, 1974), with expertise in the latter being offered for applied studies (e.g. Atkinson and Smith, 1974). Subsequently there has been a flux of geographically trained hydrologists into research institutes (notably the Institute of Hydrology) and decision-making public bodies (especially resource planning units of the national Water Authorities). Contributions have been made to many other aspects of hydrology, for example, mapping evapotranspiration (Foyster, 1973); distributed catchment runoff models (Beven, 1977c; Beven and Kirkby, 1979); the effects of urbanisation on hydrograph parameters (Hollis, 1974); over-exploitation of ground water resources (Burgess and Smith, 1979); urban and highway water quality (Ellis, 1977, 1979).

The use of small catchments for hydrological research is logical in that earth surface boundaries are usually well defined, simplifying the assessment of inputs and outputs when using a systems or budget approach (More, 1969). Furthermore, the catchment may be treated as an outdoor laboratory and detailed investigations carried out into component subsystems such as the solute content of throughfall or solute transport within hillslopes. This approach should ultimately lead to a physically realistic model of catchment hydrology. Two major criticisms have been levelled at the small catchment approach by

W.C. Ackermann (1966); firstly, there is a difficulty in extrapolating results to much larger areas and secondly catchments may be unrepresentative even within a particular region. To answer these criticisms is difficult because generalisations cannot be made, and project objectives should be considered before starting. If there is considerable spatial variation in a regional study then several sample catchments might be required (e.g. Wheater et al, 1978) although cost may then become a decisive factor. By contrast, investigation of fundamental hydrological processes is more convenient in a small catchment (say 1.0 km^2) where the variation of soils and vegetation can be minimised. Even here, however, spatial variability may necessitate replication of experiments in order to develop a spatially distributed catchment model.

To parallel the involvement of geographers in hydrology there has been a recent upsurge of interest in watershed solute dynamics. One reason for this has been the realisation that solutional loss may exceed sediment loss in the total denudation of some catchments (Walling and Troake, 1973; Jaworska, 1968). Relatively simple bivariate concentration/discharge models have been used to synthesise water chemistry (e.g. Steele, 1968) and compute rates of chemical erosion. D.E. Walling and I.D.L. Foster (1978) have recently demonstrated the inability of these simple models to describe adequately solute behaviour and there has been recognition that other environmental controls should be considered. Acknowledgement of the necessity to more precisely model 'background' water quality has directed attention to flow through hillslope soils. ('Background' water quality is a term used by B.W. Webb and D.E. Walling (1974, p. 142) "to refer tc the quality characteristics of those small streams which are themselves essentially unpolluted and particularly to characteristics controlled by natural hydrological processes and which are often termed conservative water quality parameters".) T.P. Burt (1979, p. 266) recognises that conclusions regarding solute transport by throughflow and infiltration 'are still poorly understood'. It is clear that more precise modelling of 'background' water quality depends upon a greater understanding of the processes actually contributing to the stream 'Chemograph'. (The 'chemograph' was a term used by A.W. Davies (1971) to describe the variation of water quality

during a flood hydrograph.) This could eventually lead to an improvement in estimates of the rate and spatial variability of chemical denudation.

K.J. Gregory and D.E. Walling (1973a) stress that values of denudation rates are very generalised and care is required when attempting to extend them in time and space. Temporal variations in climate and vegetation make backward extrapolation hazardous, while averaging the rate of chemical loss over an entire catchment ignores spatial contrasts implied by the variable contributing area concept (Betson, 1964). These points are discussed in the next section.

Besides denudation there are other applications for the study of solute dynamics which have sometimes been given secondary recognition in the geographical literature. These include nutrient budgeting in disturbed and undisturbed ecosystems (e.g. Bormann and Likens, 1970); baseflow separation by hydrochemical methods (e.g. Pinder and Jones, 1969); the inter-catchment transfer of water for supply purposes (Rodda et al, 1976; Birtles and Brown, 1978); the maintenance of river water quality using pumped ground water; the nutrient input to reservoirs used for water supply and river regulation (Rodda et al, ibid). The opportunity to monitor solute variation at a time of very low flow has recently been taken by I.D.L. Foster and D.E. Walling (1978), D.E. Walling and I.D.L. Foster (1978), and M.G. Anderson and T.P. Burt (1978c), while A.W. Davies (1978) has discussed general water quality problems associated with the 1976 drought.

This thesis is divided into four sections. The first presents an introduction to the topic of solute dynamics with some applications; a review of the literature concerning rainfall chemistry (i.e. inputs), catchment solute dynamics and modelling approaches; an introduction to the study catchment including preliminary experimental design. The second section presents results of research carried out at the catchment scale, i.e. hydrometric techniques and general instrumentation; methods of sampling and chemical analysis; details and interpretation of solute dynamics and development of bivariate and multivariate regression models; solute inputs in bulk precipitation and the chemical budget. The third section presents a theoretical basis for

water and chemical movement in hillslope soils (considered as the hillslope scale); the design of an experiment to measure hillslope water and solute dynamics; characteristics of hillslope water and solute movement and model application. An assessment of the results is presented in the fourth section. Firstly, however, the applications of studying solute dynamics are considered in greater detail.

1.2 APPLICATIONS OF THE STUDY OF SOLUTE DYNAMICS

(A) Chemical Denudation

The geomorphologist's most common objectivesin studying solute dynamics have been, firstly, to compute rates of erosion or denudation, expressed in m^3/km^2/year or mm/1000 years and, secondly, to understand the details of earth surface processes. Using the relationship between sampled chemical load (kg/s) (i.e. concentrations x discharge) and discharge (m^3/s) for a drainage basin, it is possible to synthesise the chemical load from the available discharge record. The gross chemical loss can then be computed by integrating the area under the time/load curve, and the total loss expressed as kg/km^2/year. Conversion to depth of material eroded (mm/1000 years) is achieved from a knowledge of the specific gravity, a value which varies with different rock types. Data have been collected from various parts of the world by several authors and can be used to illustrate the relative importance of chemical and suspended sediment loads in the denudation process. K.J. Gregory and D.E. Walling (1973a) quote the work of D.A. Livingstone (1963) and J.N. Holeman (1968) for the world's continents (Table 1.1). With the exception of Europe, suspended sediment discharge exceeds chemical discharge by a factor of 1.1 to 19.6 and it is suggested that the importance of chemical loss over suspended sediment loss in Europe (1.2) may be due to a combination of the relatively moist climate and fine-grained deposits (Gregory and Walling, 1973a). These figures mask considerable inter-continental ranges in concentration, Livingstone (1963) reporting 10 mg/l dissolved solids for the north-western highlands of Victoria, Australia, and 7900 mg/l for the Kalaus River, USSR. Data from F.H. Rainwater (1962) has been adapted by Gregory and Walling (1973a) to plot the spatial variation of mean annual dissolved solids concentration of rivers in the United States. This shows an intra-continental range of <200 to >1800 mg/l dissolved solids, and

water and chemical movement in hillslope soils (considered as the hillslope scale); the design of an experiment to measure hillslope water and solute dynamics; characteristics of hillslope water and solute movement and model application. An assessment of the results is presented in the fourth section. Firstly, however, the applications of studying solute dynamics are considered in greater detail.

1.2 APPLICATIONS OF THE STUDY OF SOLUTE DYNAMICS

(A) Chemical Denudation

The geomorphologist's most common objectivesin studying solute dynamics have been, firstly, to compute rates of erosion or denudation, expressed in m^3/km^2/year or mm/1000 years and, secondly, to understand the details of earth surface processes. Using the relationship between sampled chemical load (kg/s) (i.e. concentrations x discharge) and discharge (m^3/s) for a drainage basin, it is possible to synthesise the chemical load from the available discharge record. The gross chemical loss can then be computed by integrating the area under the time/load curve, and the total loss expressed as kg/km^2/year. Conversion to depth of material eroded (mm/1000 years) is achieved from a knowledge of the specific gravity, a value which varies with different rock types. Data have been collected from various parts of the world by several authors and can be used to illustrate the relative importance of chemical and suspended sediment loads in the denudation process. K.J. Gregory and D.E. Walling (1973a) quote the work of D.A. Livingstone (1963) and J.N. Holeman (1968) for the world's continents (Table 1.1). With the exception of Europe, suspended sediment discharge exceeds chemical discharge by a factor of 1.1 to 19.6 and it is suggested that the importance of chemical loss over suspended sediment loss in Europe (1.2) may be due to a combination of the relatively moist climate and fine-grained deposits (Gregory and Walling, 1973a). These figures mask considerable inter-continental ranges in concentration, Livingstone (1963) reporting 10 mg/l dissolved solids for the north-western highlands of Victoria, Australia, and 7900 mg/l for the Kalaus River, USSR. Data from F.H. Rainwater (1962) has been adapted by Gregory and Walling (1973a) to plot the spatial variation of mean annual dissolved solids concentration of rivers in the United States. This shows an intra-continental range of <200 to >1800 mg/l dissolved solids, and

TABLE 1.1

Mean Dissolved Load, Concentration and Suspended Sediment Concentration for the World's Continents

(Source: Gregory and Walling, 1973a)

Continent	Dissolved Load (Livingstone 1963) tonnes/km^2/yr	Mean Chemical Conc (Livingstone 1963) mg/l	Suspended Sediment Load (Holeman, 1968) tonnes/km^2/yr
N.America	33.0	142	96
Europe	42.6	182	35
Asia	32.2	142	600
Africa	24.4	121	27
Australia	2.3	59	45
S.America	28.3	69	63

also suggests an inverse relationship with runoff and precipitation. Gregory and Walling (1973a) have plotted, for the United States, dissolved solids concentration data from W.H. Durum et al (1960) and W.B. Langbein and D.R. Dawdy (1963) to support the inverse relationship. However, dissolved solids load is shown to increase with annual runoff because any decrease in concentration is countered by an increase in the quantity of runoff (data from Langbein and Dawdy, 1963 ; Livingstone, 1963; and Van Denburgh and Feth, 1965; plotted by Gregory and Walling, 1973a, Figure 6.20B). These general relationships are duplicated at various scales down to the small instrumented catchment (see, for example, A.M.C. Edwards, 1973a, 1973b and D.E. Walling, 1974), although considerable temporal and spatial variations occur. These will be discussed in Chapter 2. There are numerous problems associated with assessing rates of chemical denudation.

The first of these is that computation of net chemical denudation should be based upon the components of dissolved load derived from chemical weathering of rocks and soils, and should exclude input from the atmosphere (Janda, 1971; Goudie, 1970; E.H. Winkler, 1970). R.J. Janda (1971) suggests that some past computations exaggerated the significance of chemical denudation because they were calculated from total dissolved loads. This problem can be overcome by measuring bulk atmospheric solute input in addition to solute output and computing net chemical loss from:

$$J_N = \frac{Q\,C_1}{A} - \frac{P\,C_2}{A} \qquad \text{Weight/Length}^2\text{/Time} \qquad (1.1)$$

where
- J_N = net chemical loss, $W/L^2/T$
- Q = discharge, L^3/T
- C_1 = concentration in discharge, W/L^3
- C_2 = concentration in precipitation, W/L^3
- P = rainfall, L^3/T
- A = catchment area, L^2

The second problem concerns synthesis of the catchment output load using an inadequate predictive model. The model inadequacy may stem from a poor sampling scheme which fails to incorporate the full range of temporal and spatial responses (Walling, 1975; Walling and Foster, 1975).

The third problem is incurred in extrapolation of present day denudation rates into the geological past or future due to natural changes in climate and vegetation cover (Young, 1969). The effects of vegetation change have been examined by ecologists interested in natural resource-management (e.g. Bormann and Likens, 1969). Water quality investigations during present day extreme hydrological events will help in reconstructing palaeohydrological conditions.

The fourth problem involves man's effect on past and present stream and precipitation chemistry (Douglas, 1967). The list of interferences is long, although some studies which monitor the effects are available: ploughing (I.O.H., 1973, p. 17-19); cropping and fertiliser application (Blakemore, 1966; Cooke and Williams, 1970); effluent discharge (Owens and Wood, 1968); industrial pollution (Edwards, 1974); afforestation (I.O.H., 1978, p. 35); deforestation (Bormann et al, 1967); urbanisation (Gregory, 1974); highway runoff (Ellis, 1977, 1979); and quarrying and mining (Ineson and Downing, 1964). Furthermore there may be time lags between cause and effect, exemplified in the pollution of ground water by nitrates and its predicted reappearance in stream baseflow (Young et al, 1976). Increases in the acidity of precipitation in recent years may also influence the final concentration of water quality (Cogbill and Likens, 1974; see Chapter 2).

(B) Nutrient Cycling

The ecosystem* can often be given the watershed boundaries for studying input-output relationships. Nutrient cycle/hydrological

* '<u>ecosystem</u>': defined by Odum (1963) as 'a basic functional unit of nature which includes both organisms and their non-living environment, each interacting with the other and influencing each other's properties, and both necessary for the maintenance and development of the system'

cycle interaction can then be turned to very good advantage in the study of the nutrient cycles and other basic parameters of the system (Bormann and Likens, 1969). According to these authors, there are six good reasons why the study of nutrient cycling is important.

Firstly, there is a need to understand the relatively undisturbed energy nutrient relationships and to develop total chemical budgets of the individual ecosystems.

Secondly, the behaviour of individual ecosystems may be compared.

Thirdly, an assessment may be made of the effect of geomorphological processes such as sediment erosion and deposition, mass movement and weathering on ecosystem dynamics.

Fourthly, meteorological and climatic variations on ecosystem behaviour may be studied.

Fifthly, the chemical budgets of individual ecosystems may be placed in a global context by relating them to the larger biogeochemical cycles of the earth (e.g. Mackenzie and Garrels, 1966).

Sixthly, by comparison with relatively undisturbed ecosystems the effects of managerial practices on the structure and function of individual ecosystems may be determined.

The first and last of these objectives form the basis of much of the research into nutrient cycling in forest ecosystems undertaken in the United States. The classic example is that of Hubbard Brook Experimental Forest, in the White Mountain National Forest of New Hampshire, USA, which has produced studies of atmospheric chemical inputs (Fisher et al, 1968); throughfall and stemflow chemistry (Eaton et al, 1973); modelling of water chemistry (Johnson and Likens (1969); and budgeting of the major cations (Likens et al, 1967). Studies of the more detailed internal processes have also been published, for example, outputs of dissolved organic and fine particulate carbon in streamflow (Hobbie and Likens, 1973); litterfall nutrient content (Gosz et al, 1972); leaching losses from leaves

(Gosz et al, 1969); and nutrient cycling of the herbaceous layer (Siccama et al, 1970). The results of research involving manipulation of the forest ecosystem by clear-cutting and herbicide treatment are described by Bormann and Likens, (1969, 1970), Bormann et al, (1967), and Likens et al, (1970). The effects of forest fires on ionic concentration in streamwater have been studied elsewhere in the USA (Johnson and Needham, 1966; Brown et al, 1973). The objectives in clear-cutting part of Hubbard Brook were fourfold; Firstly, to determine whether or not the ecosystem had the capacity under such circumstances to hold the nutrients accumulating in the available nutrient compartment; secondly, to determine the effect of deforestation on streamflow; thirdly, to examine some of the fundamental chemical relations of the forest ecosystem; fourthly, to evaluate the effects of forest manipulation on nutrient relations and the eutrophication of water (Bormann and Likens, 1970). Continuous monitoring at Hubbard Brook has shown that while increased nutrient and water loss were the first responses to deforestation, after two years particulate matter output rose sharply as biotic control on erodability weakened (Bormann et al, 1974). The loss of dissolved matter subsequently decreased, possibly because of diminution of readily available nutrients stored within the system. Subsequently, nutrient flux and erosion losses began a return to previous levels as the catchment processes were increasingly regulated by biotic factors.

The Hubbard Brook experiment assumed that the chemistry of the disturbed stream would have been identical to that of the undisturbed stream had the disturbance not occurred. However, a study of three adjacent catchments in British Colombia has shown that such an assumption may not always be valid and emphasises caution in interpreting the results of such studies (Feller and Kimmins, 1979). Furthermore, this points to the need for an understanding of the physical processes of solute movement within the undisturbed ecosystem, and a suitable means of modelling undisturbed streamflow and water chemistry for prediction of 'undisturbed' solute dynamics after disturbance has occurred.

(C) Hydrochemical Methods of Flow Separation

Separation of stream baseflow from storm runoff is carried out for a variety of purposes ranging from unit hydrograph analysis (e.g. NERC, 1975) to calibration of a ground water flow model (e.g. A.W.A., 1980a). The techniques used are usually arbitrary by nature; the Flood Studies Report (NERC, ibid) used a separation line joining the start of hydrograph rise to a point on the recession limb four times (distance from total rainfall centroid to total hydrograph centroid) units of time later, see Chapter 4; baseflow from a Chalk catchment in the Great Ouse basin, Cambridgeshire, was successfully synthesised using the multiple regression between present and lagged well levels (independent variables) and baseflow (dependent variable) (A.W.A., 1980a). Other techniques commonly used are semi-logarithmic plotting with back-extrapolation of the recession curve (Barnes, 1939) and time-based separation by drawing a line from the point of hydrograph rise at a gradient of 0.55 $l/s/km^2/hr$ (Hibbert and Cunningham, 1967). A comprehensive review of baseflow separation techniques has been written by F. H. Li (1976).

Hydrochemical methods of flow separation are based upon the principle that waters of different origin have characteristic chemical 'labels'. For example, solute-rich baseflow dominated by a ground water component may be diluted by storm runoff with a much lower solute concentration. It is possible to separate the baseflow from the storm runoff by measuring total stream discharge and its chemistry and applying the mixing model:

$$C_t Q_t = C_1 Q_1 + C_2 Q_2 \qquad (1.2)$$

where C = chemical concentration
Q = discharge
t = total flow
1 = ground water
2 = storm runoff

In a re-arranged form:

$$Q_1 = Q_t \left[\frac{C_t - C_2}{C_1 - C_2} \right] \qquad (1.3)$$

C_1 and C_2 are often assumed to remain constant and are determined from samples of minimum and maximum flow respectively. The technique has principally been used in the United States and Russia.
G.R. Kunkle (1965) determined baseflow from a small stream in Iowa, USA, with specific electrical conductance used as the water quality 'label'. A recording conductance meter at the gauging station gave uniform values of 520 micromhos $\pm$ 1 % for low flow, which compared favourably with the conductance of water from wells in the contributing aquifer, averaging 515 micromhos. A representative conductance value for surface runoff of 160 micromhos was determined from conductance data for peak runoffs, surface detention and drainage from grassed ditches. Working in Nova Scotia, G.F. Pinder and J.F. Jones (1969) determined the concentrations of bicarbonate, nitrate, sulphate, chloride, calcium, magnesium, potassium, sodium, iron and silica for each component, but finally used a combination of ions which showed reasonable and consistentvalues for ground water discharge, i.e. bicarbonate, calcium, magnesium and sodium. R.W. Newbury et al (1969) carried out a threefold separation into storm runoff, leaching interflow and transient ground water and long term "old" ground water components, using sulphate and specific conductance. B.G. Skakalskiy (1966) reported the use of chemically-based hydrograph separation on short term and annual flow records in European Russia. Using different herbicides,applied on a basin segmented into discrete sub-zones,as water quality variables, L.J. Lane et al (1977) have found that contributing areas of a basin as well as the runoff hydrograph from each zone can be determined by systematically analysing the respective herbicide concentrations and the runoff hydrograph at the outlet.

Surprisingly, a literature survey failed to find comparisons of hydrochemical and traditional flow separation techniques. Furthermore, there are drawbacks in using the hydrochemical approach resulting from the complexity of streamflow solute dynamics. Equation (1.3) is usually solved by assuming that the concentration in each flow

component is constant and known. The detailed study of solute dynamics has shown that this assumption is not always valid and D.A. Pilgrim et al (1979) report two complications.

Firstly, solutes are flushed from the soil in subsurface outflow during the early part of storms occurring after long dry periods. The actual physical processes involved have not been studied in detail, although the 'flushing' effect is likely to be displacement of 'old' water by infiltrating rainfall.

Secondly, the solute concentration of infiltrating water increases with increasing residence time in the soil. The dissolution is initially rapid but as the products accumulate in the solvent the rate decreases progressively until there is no further change, when equilibrium is reached (Trudgill, 1977).

Pilgrim et al (1979) employ a semi-quantitative approach which explicitly considers the variation of concentration with contact time. Flow components 1 and 2 in equation (1.2) were termed 'old' and 'new' water respectively and the equation re-arranged to give:

$$C_t = C_o - (Q_n/Q_t)(C_o - C_n) \qquad (1.4)$$

A mixture of soil and pure water was used to determine the dissolution rates for a field plot, and a specific conductance-time relationship computed. The relationship was used with equation (1.4) to compute a family of curves of C_t for various values of the ratio (Q_n/Q_t) at 25°C, with C_o given an equilibrium concentration of 240 μmho/cm. If two storm events coalesced so that there was insufficient time for runoff component concentrations to reach equilibrium then C_o would also be time-dependent. A curve matching procedure was used to estimate the relative contributions of recession flow components with different residence times. However, it is made clear that a good understanding of field solute dynamics is necessary for interpretation of runoff sources and quantitative application of the approach.

(D) Inter-Catchment Transfer of Water

The strategy presented by the now defunct Water Resources Board for future water supplies in England and Wales included the transfer of water between major river systems (W.R.B., 1973). J.C.Rodda et al (1976), who have summarised the proposals, point out that parts of northern and eastern England, England south of the Thames, south-west England and west Wales have adequate resources within their boundaries to meet all anticipated demands until AD 2000. Integrated resource development will be used in these areas for both internal use and export to areas of deficiency.

Inter-catchment transfer of water by pumping over watershed boundaries is one way in which [redacted] deficiencies can be satisfied. In order to provide operational flexibility, a number of different sources may be used, to be drawn upon depending upon their capability to provide the transfer of flow required. Consequently, a complex mixture of waters of different origins is likely to result at the end of the transfer line. Physical, chemical and biological effects of transfer from a donor source to a recipient stream must be studied in order to avoid damage to existing natural or semi-natural ecosystem components. Physical factors to be considered include river stability and siltation, the survival of rooted plants, the survival of the invertebrate food organisms and the suitability of the habitat for different species of fish at various life stages (Allan, 1977). Chemical problems may occur if waters with some degree of domestic and industrial pollution are used, although the extra dilution might offset this problem. Pollution might alter fish susceptibility to diseases and affect the 'homing' reaction of migratory fish to their natal stream. The transfer of water rich in inorganic salts to a nutrient-deficient stream is likely to increase primary production in the recipient. However, if the addition were too great then excessive production of undesirable vegetation such as Cladophora (green filament algae) could occur, with the risk of diminished night-time BOD levels and hindrance to angling. Biological problems might arise from the transfer of biota in the water, in addition to the chemical and physical effects already discussed. Biological factors include the transfer of desirable or undesirable fish and fish eggs; the transfer of phytoplankton, zooplankton, macrophytes and invertebrate fish food

organisms (Allan, 1977; Hancock, 1977). There are several proposed inter-catchment transfers in England and Wales; examples include the Ely-Ouse to the Blackwater in Essex; from Northumberland's Kielder Reservoir in the North Tyne valley to the Tees (Durham) and Swale (Yorkshire); from the Severn to the Thames. An understanding and ability to model the background water quality of both donor and recipient rivers, together with the changes in quality during transfer, is clearly desirable.

A.B. Birtles and S.R.A. Brown (1978) have recently attempted computer prediction of the changes in the River Thames quality regime after receipt of water transferred from the River Severn. Water would be abstracted from the Severn at Haw Bridge just downstream of its confluence with the River Avon and would be discharged to the Thames at a point upstream of the Farmoor Reservoir near Eynsham. Severn flows would be supplemented by releasing water from the Welsh reservoirs Clywedog (Severn catchment) and an enlarged Craig Goch (Wye catchment). Problems identified at the outset included descaling, pitting and corrosion in distribution networks, adverse effects on water treatment works, disruption of the ecological balance in storage reservoirs and the adverse biological effects (noted earlier). The frequency of quality excursions to extreme values, the persistence of concentrations outside certain threshold limits, and the degree of this persistence were considered to be important with regard to river ecology. Recorded concentrations of ortho-phosphate, total nitrogen and chloride were used with river discharge for quality model development based upon division of the river hydrograph into distinct components, viz. sewage effluent returns, two or three aquifer components and surface runoff (Birtles, 1978). Water quality was simulated for the Severn and Thames with 1932 - 1975 streamflows and used to construct quality-duration curves for different values of percentage time that simulated concentration persisted in excess of a specified value. Sets of curves were drawn for situations with and without water transfer. Clear differences were found to result; for example, the five day 95 percentile difference between orthophosphate concentration with transfers and that which would have occurred at the same time in the River Thames was found to be 63 % of the overall mean concentration prior to transfers, or 1.012 mg/l orthophosphate. Interpretation of

the study results was lacking, perhaps emphasising the necessity for collaboration with ecological expertise before assessing environmental impact.

Although in some cases donor and recipient rivers may already be polluted, the study, interpretation and modelling of background water quality and its significance in terms of stream ecology would form a sound basis for research prior to inter-catchment transfer schemes.

(E) Ground water Development and River Regulation Schemes

The integrated use of surface and ground water is now an accepted part of water resource planning in the UK (W.R.B., 1973; Ineson, 1970). In the case of the Ely-Ouse basin this involves regulation of rivers to their natural flow equalled or exceeded 90 % of the time, in order to maintain adequate dilution of effluents, and the supply of water for domestic, industrial, spray irrigation and agricultural purposes. In this scheme (the 'Great Ouse Ground Water Development Scheme') some 345 wells are being drilled in a 2462 km^2 area of Chalk. In addition it is estimated that up to 440 M l/d may be available for inter-catchment transfer to water deficient areas in south Essex (G.O.R.A., 1972). A pilot scheme was carried out on part of the Chalk aquifer in south Norfolk in order to examine the effects of ground water abstraction and river regulation on water quality, river ecology, soil moisture and crop growth, in addition to hydrological responses under operational conditions (i.e. ground water levels, streambed infiltration losses, etc.). Apart from soil moisture depletion in riparian areas the pilot scheme was successful.

More detailed information on temporal and spatial variation in solute levels would have been valuable. The autumn flushing of solutes could cause problems after drought conditions, as the 1975-1976 drought indicated, notably with respect to nitrates from land drainage runcff and ground water (Davies, 1978; Walling and Foster, 1978; Foster and Walling, 1978). Under extreme conditions the extra nitrate load, in addition to that contained in effluents, might place an extra burden upon regulation by ground water, perhaps requiring much higher short term dilution and higher longer term dilution. A further problem is likely to occur in the near future when nitrates leached from the soil

reach the saturated zone and enter wells and streams (Young et al, 1976). Detailed spatial surveys are likely to point out areas of potentially dangerous solute levels.

(F) Reservoir and Lake Eutrophication

There has been an increasing awareness in recent years of the dangers of eutrophication and its effects upon water supplies, freshwater ecology and amenities such as boating and angling (Rodda et al, 1976). Eutrophication is the process of enrichment of water by nutrients. Naturally it takes place at a very slow rate but it can be accelerated by increasing the rate of addition of nutrients, as, for example, when water is polluted by sewage and land drainage (Collingwood, 1977). Excesses of nutrients, notably nitrogen and phosphorus, feed filamentous bacteria and the problem can be particularly serious in lakes and reservoirs because these have a lower assimilative power than highly aerated streams.

Programmes of water quality monitoring to ascertain the proportions of nutrients derived from natural, agricultural, forest, sewage effluents and waste waters have been suggested (Owens and Wood, 1968; Strobel and Silvestro, 1970). Detailed studies of relevant solute dynamics above lakes and reservoirs (present and planned) would be particularly useful, especially where artificial fertilisers were applied or where deforestation was anticipated.

1.3 CONCLUSION

This introductory chapter has reviewed some general applications of water quality studies in geomorphology, ecology and water resources. The approach to writing this thesis which was outlined in 1.1 shows that experimental work has been approached at two scales; the catchment and the hillslope. This rationale reflects a need for greater understanding of the intra-catchment processes of solute transport contributing to total basin solute dynamics. Studies of subsurface water flow and partial area contributions to runoff have laid the foundation for distributed models of catchment streamflow (e.g. Beven and Kirkby, 1979) and subsequently detailed studies of solute transport within the contributing area. It was noted at the

1973 B.G.R.G. symposium on Fluvial Processes in Small Instrumented Watersheds in the British Isles, that:

> "the prospect appeared to be signposted by more detailed work on sediment and solute production comparable in detail to the work already achieved in the study of water discharge, and also by attention directed towards the components of the catchment ..... more fieldwork is obviously required and a subsequent meeting could perhaps be devoted to results from <u>within</u> small instrumented catchments".

(Gregory and Walling, 1973b).

Accordingly, a project was designed with the following objectives:

(i) To gain an understanding of stream solute dynamics and controls in a small woodland catchment.

(ii) To apply traditional techniques of data transformation, bivariate and multivariate regression to model the temporal variation of individual ions in catchment and sub-catchment streamflow (definition of sub-catchments should allow an assessment of spatial variations in solute contributions and the chemical budget).

(iii) To measure and interpret the variation of bulk atmospheric solute input to the catchment ('bulk input' is the solution resulting from rainfall and dry fallout (Whitehead and Feth, 1964)).

(iv) To monitor and describe solute and water movement in the hillslope soil of one sub-catchment, in order to improve knowledge of the mechanisms of solute delivery to the stream under a range of hydrological conditions.

(v) To apply a model of hillslope water and solute flux to the collected data, comparing model and measured outputs (slope base discharge and solute concentration), optimising internal parameters (hydraulic conductivity, solute dispersion coefficients) until 'real' and 'predicted' agree.

(vi) To place 'hillslope' results in the catchment framework and assess the future of spatially distributed modelling of catchment solute response.

(vii) To compute solute budgets for the catchment and sub-catchments and compare net gains or losses with the results of similar studies.

Chapter 2 discusses literature pertinent to solute inputs in precipitation, water quality characteristics and modelling at the catchment scale.

CHAPTER 2
CATCHMENT SOLUTE DYNAMICS: ATMOSPHERIC INPUTS AND SURFACE WATER OUTPUTS - A REVIEW OF THE LITERATURE

2.1 INTRODUCTION

Atmospheric and stream water solute fluxes may be viewed within the framework of the terrestrial watershed ecosystem (Figure 2.1). F.H. Bormann and G.E. Likens (1969, 1970) used a similar rationale to describe nutrient relationships, sites of accumulation, major pathways and origins of chemical losses in stream water from the Hubbard Brook Experimental Forest, New Hampshire. S.T. Trudgill (1977) has recently employed the same approach in discussing the components of soil and vegetation nutrient systems. In this chapter the emphasis will be placed upon literature relevant to stream water solute dynamics and atmospheric chemical inputs, while in Section III solute dynamics of the soil sub-system and inputs from mineral weathering are discussed.

The atmospheric component consists of sea salt aerosol, dissolved gases and dust (dry fallout). The concentration of this input may be increased due to solute pickup during interception and stemflow. Minerals in rocks and soils form an important component, contributing elements at varying rates to the available nutrient store. The available nutrient component itself is composed of nutrients held on the surface of particles of the clay-humus complex of the soil, or in the soil water solution. Cations held in this way may be exchanged for positively charged hydrogen ions produced at the root surface (Keller and Frederickson, 1952), the nutrients then being taken up by roots. This is the input to the biotic component. the products of which are slowly released for subsequent re-uptake by plants. Leaching is the major process of cation removal from the soil nutrient store. This is principally achieved through the exchange of anions derived from rainfall with cations held on the clay-humus complex of the soil. The resulting solution may then be transported to the stream in throughflow, although final nutrient concentrations at the slope/channel interface may differ from the upslope concentrations due to further chemical solution or precipitation en route. The channel component may also show solute gain by exchange with bed or suspended sediment

CHAPTER 2

CATCHMENT SOLUTE DYNAMICS:

ATMOSPHERIC INPUTS AND SURFACE WATER OUTPUTS -

A REVIEW OF THE LITERATURE

2.1 INTRODUCTION

Atmospheric and stream water solute fluxes may be viewed within the framework of the terrestrial watershed ecosystem (Figure 2.1). F.H. Bormann and G.E. Likens (1969, 1970) used a similar rationale to describe nutrient relationships, sites of accumulation, major pathways and origins of chemical losses in stream water from the Hubbard Brook Experimental Forest, New Hampshire. S.T. Trudgill (1977) has recently employed the same approach in discussing the components of soil and vegetation nutrient systems. In this chapter the emphasis will be placed upon literature relevant to stream water solute dynamics and atmospheric chemical inputs, while in Section III solute dynamics of the soil sub-system and inputs from mineral weathering are discussed.

The atmospheric component consists of sea salt aerosol, dissolved gases and dust (dry fallout). The concentration of this input may be increased due to solute pickup during interception and stemflow. Minerals in rocks and soils form an important component, contributing elements at varying rates to the available nutrient store. The available nutrient component itself is composed of nutrients held on the surface of particles of the clay-humus complex of the soil, or in the soil water solution. Cations held in this way may be exchanged for positively charged hydrogen ions produced at the root surface (Keller and Frederickson, 1952), the nutrients then being taken up by roots. This is the input to the biotic component, the products of which are slowly released for subsequent re-uptake by plants. Leaching is the major process of cation removal from the soil nutrient store. This is principally achieved through the exchange of anions derived from rainfall with cations held on the clay-humus complex of the soil. The resulting solution may then be transported to the stream in throughflow, although final nutrient concentrations at the slope/channel interface may differ from the upslope concentrations due to further chemical solution or precipitation en route. The channel component may also show solute gain by exchange with bed or suspended sediment

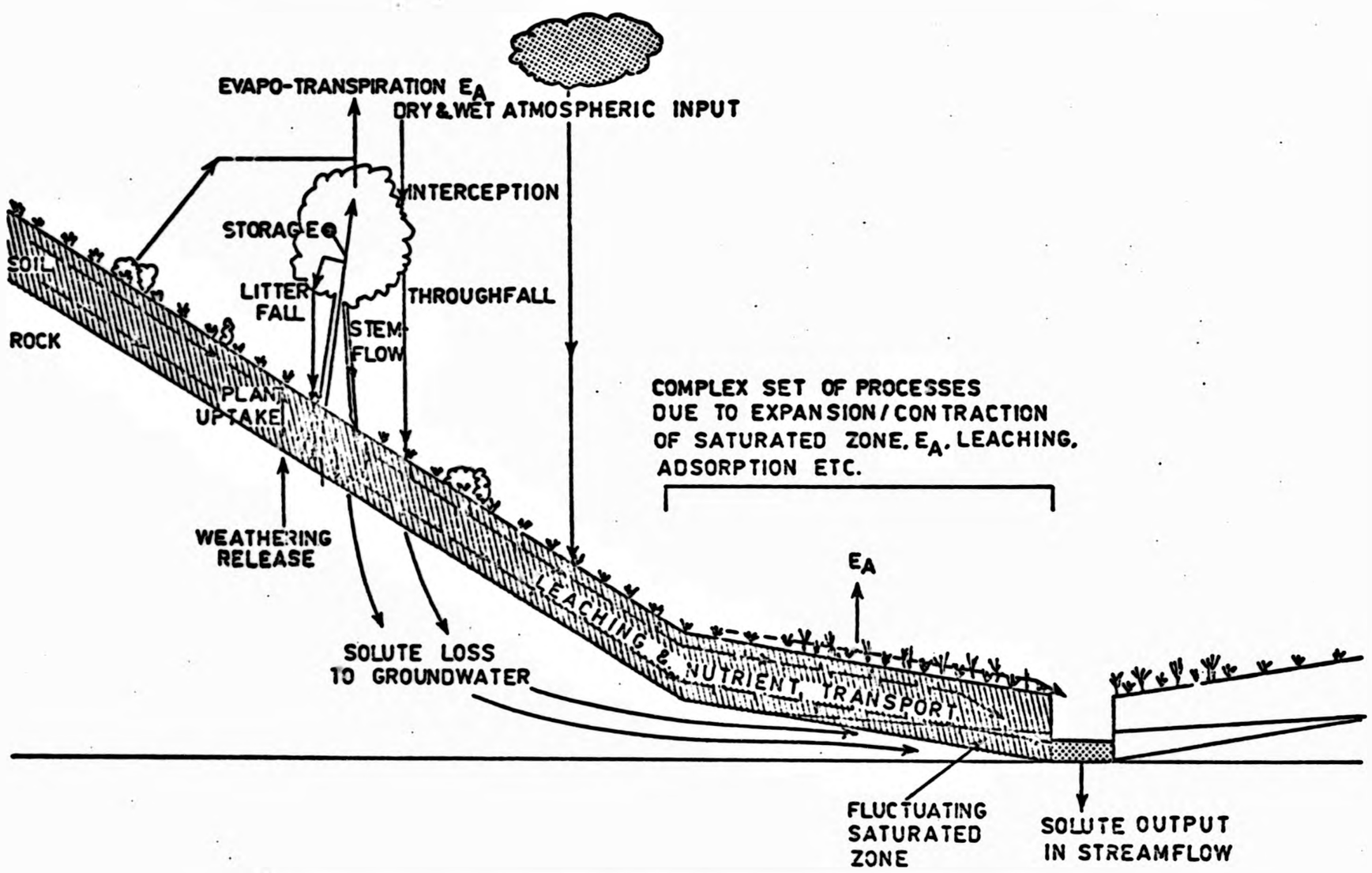

FIGURE 2.1: PRINCIPAL WATER AND SOLUTE COMPONENTS OF THE TERRESTRIAL WATERSHED ECOSYSTEM

(The stippled area is considered in Sections I and II, the shaded area in Section III)

(Kennedy, 1965) or loss due to chemical precipitation (Barnes, 1965) and plant or animal uptake (Wang and Evans, 1969; Edwards, 1973a; Edwards and Liss, 1973). Knowledge of these various components and the links involved lead to an understanding of the inter-relationships within the system and of the ramifications of any manipulation applied at any point in the system. The principal components considered in detail in this thesis are: atmospheric solute inputs to the catchment system, the transfer of solutes through the valley-side soils to the channel and the subsequent transfer along the channel and loss from the catchment. Literature pertinent to the first and third components are discussed below. The transfer of solutes through valley-side soils is treated in Section III.

2.2 ATMOSPHERIC INPUTS TO THE CATCHMENT SYSTEM

The chemistry of atmospheric inputs to the catchment must be studied to determine denudation rates as was pointed out in Chapter 1 (Goudie, 1970; Janda, 1971). However, if water chemistry is to be physically and realistically modelled then the details of input chemistry take on a greater significance than in simple solute budgeting procedures. Study is required of:

(i) chemical sources,
(ii) the spatial and temporal variability of individual elements,
(iii) the interaction of atmospheric chemicals with the vegetation and soils, and
(iv) the effects on stemflow, throughfall, leachates, vegetation 'health' and soil fertility.

Figure 2.2 provides a basis for discussion of these aspects. J.N. Galloway and G.E. Likens (1976) have recently shown that the type of rainfall collector used influences the amounts of chemical caught, while M.P. Paterson and R.S. Scorer (1975) indicate that the quality and consistency of analysis leaves much to be desired. These points must be borne in mind when comparing chemical data presented in the literature.

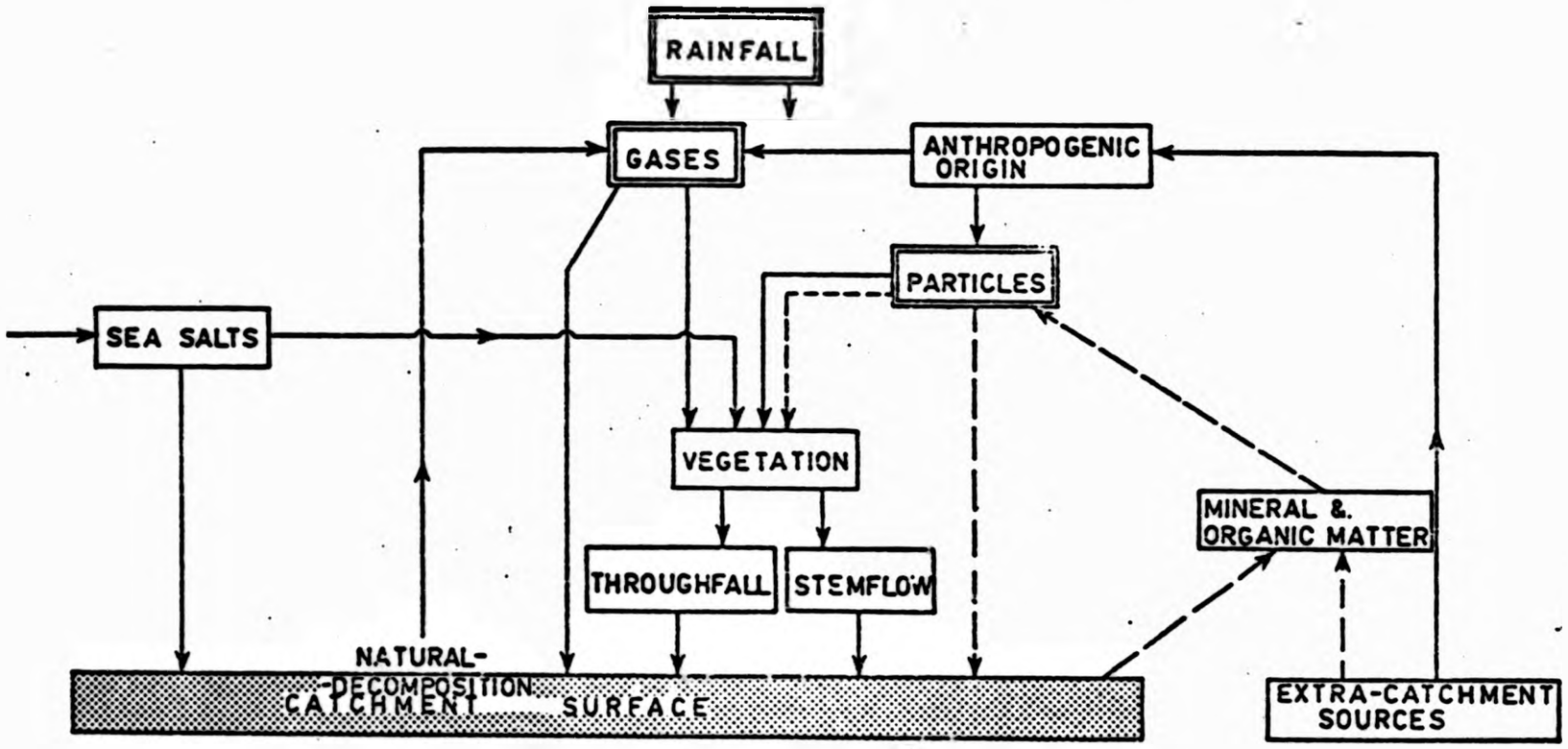

FIGURE 2.2: -WET AND DRY ATMOSPHERIC CHEMICAL INPUTS TO THE CATCHMENT SYSTEM

(Wet inputs shown by solid lines, dry by dashed lines; it is assumed there are no pollution sources within the catchment)

(A) Constituents and Sources

The sources of elements in rainfall are important because they strongly influence the pattern of spatial variability. Atmospheric sources were ably discussed by E. Eriksson in the 1950's (Eriksson, 1955, 1959, 1960; Egner and Eriksson, 1955). The principal gaseous constituents of the atmosphere likely to be of importance are carbon, nitrogen, sulphur and chlorine (Eriksson, 1959).

Carbon is present in the troposphere* as carbon dioxide (CO_2) with a generally accepted concentration of 316 ppm or a partial pressure of 3.16×10^{-4} atmospheres (Reuss, 1976). CO_2 is a product of combustion, animal exhalation and is inhaled by plants. It forms about 0.03 % of the atmosphere, by volume (Critchfield, 1966). Pure rainwater in equilibrium with atmospheric CO_2 at 25°C would have a pH of 5.65 (Reuss, 1976) which N.M. Johnson et al (1972) have called 'geologically normal precipitation' or relatively unpolluted rainfall characteristic of the geological past.

Nitrogen constitutes about 78 % of the troposphere by volume although it does not readily combine with other elements. It occurs as ammonia gas (NH_3) at median concentrations of about 4 $\mu g/m^3$ over Britain but with occasionally much higher levels (Stevenson, 1968). T.V. Healy et al (1970) regarded animal urine as the main source of NH_3 with fertilizer use, coal combustion, ammonia and fertilizer factories, human sweat, and sewage contributing in decreasing order of importance. They considered that NH_3 is converted over several hours into $(NH_4)SO_4$ by reaction with SO_2 and O_2 in mist or cloud droplets and reactions with H_2SO_4 droplets from power station plumes. J.O. Reuss (1976) has illustrated the importance of the NH_4 component in the capacity of rainfall to acidify soils. When NH_4 is taken up by the plant, acidification occurs due to the H^+ given off by the plant in the

* The troposphere is defined as extending from the ground surface to an altitude of 8 - 18 km depending on the latitude (Critchfield, 1966).

(A) Constituents and Sources

The sources of elements in rainfall are important because they strongly influence the pattern of spatial variability. Atmospheric sources were ably discussed by E. Eriksson in the 1950's (Eriksson, 1955, 1959, 1960; Egner and Eriksson, 1955). The principal gaseous constituents of the atmosphere likely to be of importance are carbon, nitrogen, sulphur and chlorine (Eriksson, 1959).

Carbon is present in the troposphere* as carbon dioxide (CO_2) with a generally accepted concentration of 316 ppm or a partial pressure of 3.16×10^{-4} atmospheres (Reuss, 1976). CO_2 is a product of combustion, animal exhalation and is inhaled by plants. It forms about 0.03 % of the atmosphere, by volume (Critchfield, 1966). Pure rainwater in equilibrium with atmospheric CO_2 at 25°C would have a pH of 5.65 (Reuss, 1976) which N.M. Johnson et al (1972) have called 'geologically normal precipitation' or relatively unpolluted rainfall characteristic of the geological past.

Nitrogen constitutes about 78 % of the troposphere by volume although it does not readily combine with other elements. It occurs as ammonia gas (NH_3) at median concentrations of about 4 $\mu g/m^3$ over Britain but with occasionally much higher levels (Stevenson, 1968). T.V. Healy et al (1970) regarded animal urine as the main source of NH_3 with fertilizer use, coal combustion, ammonia and fertilizer factories, human sweat, and sewage contributing in decreasing order of importance. They considered that NH_3 is converted over several hours into $(NH_4)SO_4$ by reaction with SO_2 and O_2 in mist or cloud droplets and reactions with H_2SO_4 droplets from power station plumes. J.O. Reuss (1976) has illustrated the importance of the NH_4 component in the capacity of rainfall to acidify soils. When NH_4 is taken up by the plant, acidification occurs due to the H^+ given off by the plant in the

* The troposphere is defined as extending from the ground surface to an altitude of 8 - 18 km depending on the latitude (Critchfield, 1966).

uptake process. Furthermore, burning of fossil fuels releases large quantities of nitrogen oxides to the atmosphere, which are transformed to nitric acid (HNO_3) (Likens et al, 1972).

Naturally occurring <u>sulphur</u> is only present in very small quantities in the atmosphere. Hydrogen sulphide (H_2S) may be formed by bacterial reduction of sulphate under anaerobic conditions such as bogs, waterlogged soils and in lakes with stable stratification (Eriksson, 1959; Junge and Werby, 1958). Once in the atmosphere, H_2S is probably oxidised to sulphur dioxide (SO_2) which is in turn converted to SO_4^{2-} by photochemical processes and by oxidation in cloud droplets (Junge and Werby, 1958), although it is doubtful whether this source is adequate to account for some of the high sulphate - sulphur (SO_4^{2-}-S) concentrations found in rainfall. Stevenson (1968) found median values of SO_4^{2-}-S to range between 0.9 and 3.9 mg/l in the British Isles from 1959 - 1964; Likens and Bormann (1974) found weighted annual concentrations of SO_4^{2-}-S to range between 2.2 and 3.3 mg/l at the Hubbard Brook Experimental Forest in New Hampshire, USA from 1963 - 1972.

It is clear from published analyses that anthropogenic sources contribute significantly to SO_4^{2-}-S concentrations in rainfall (Junge and Werby, 1958; Cogbill and Likens, 1974; Nordø, 1976; are just a few of the published sources substantiating this statement). The principal source of anthropogenic sulphur is release through industrial processes, particularly the burning of fossil fuels (Likens et al, 1972). SO_2 may be deposited by dry deposition or oxidised and hydrolysed to sulphuric acid (H_2SO_4) and deposited in precipitation.

Free <u>chlorine</u> (Cl_2) is most unlikely to exist in the atmosphere, where hydrogen is present at a fifty times higher pressure, and is more likely to occur as the compounds hydrochloric acid (HCl) and ammonium chloride ($(NH_4)Cl$) (Junge, 1956). Chloride is probably the most commonly reported anion present in rainwater. Its main source is seawater, a fact which emerges from published spatial surveys from various parts of the world (e.g. Scandinavia: Eriksson, 1960, Figs. 6.1, 6.2; British Isles: Stevenson, 1968, Fig. 2; North America: Junge and Werby, 1958, Fig. 1; Australia: Eriksson, 1960, Fig. 7.3;

European Russia: Matveyev and Bashmakov, 1967, Fig. 4), which generally show chloride concentrations decreasing inland. It is thought that wind leads to wave formation on the sea surface with the larger waves breaking and producing foam patches. Surface bubbles burst and shoot up small jets which break into droplets at their tips, some of which are sufficiently small to be swept up into the air, and may evaporate there to form salt particles which are capable of acting as nuclei for cloud and raindrop condensation (Gorham, 1961; Eriksson, 1959). G.K. Yue and V.A. Mohnen (1976) have recently demonstrated that non-precipitating clouds containing NaCl can produce a source of free HCl in the atmosphere. The amount of HCl released is a combined result of the intricate physical and chemical processes occurring inside the cloud and especially temperature, oxidisation rates, ambient concentrations of SO_2, NH_3 and H_2SO, and the liquid water content.

(B) Acid Precipitation

The chemical constituents discussed so far (carbon, nitrogen, sulphur and chlorine) all contribute to rainfall acidity. Rainfall is a naturally weak acid due to the combination of H_2O and CO_2 to form carbonic acid (H_2CO_3) with a pH of 5.7 (e.g. Kennedy et al, 1979). However, there have been a succession of reports since 1970 pointing to excessively acid rainfall with pH values between 3 and 5, notably in the industrial areas of north-west Europe and the north-eastern United States (Likens et al, 1972; Johnson et al, 1972; Cogbill and Likens, 1974; Likens and Bormann, 1974; Likens et al, 1976; Oden, 1976). The excess acid appears to be linked to mounting levels of certain gaseous pollutants such as sulphur and nitrogen oxides, and their conversion to the strong acids H_2SO_4 and HNO_3. Such increases can do considerable damage to man-made structures and equipment and more importantly it has serious implications for solute dynamics and the ecosystem.

Concern over rainfall acidity led the United States Department Agriculture Forest Service to organise the 1st International Symposium on Acid Precipitation and the Forest Ecosystem in 1976, with discussions of atmospheric transport, chemistry and precipitation, aquatic ecosystems, forest soils and vegetation (USDA, 1976). C.O. Tamm and

E.B. Cowling (1976) discuss the potential direct and indirect effects of acidic precipitation on vegetation. Direct effects include interference with normal functioning of guard cells (which would lead to loss of stomatal control and thus alter transpiration rates); alteration of leaf- and root-exudation processes (this might lead to changes in throughfall due to accelerated leaching of mineral elements and organic substances). Indirect effects include alterations in symbiotic relationships such as nitrogen-fixing organisms and increased susceptibility to drought and other environmental stress factors. J. Baker et al (1976) show that acidity in rainfall, throughfall, stemflow and soil solution is related to the emission of SO_2 at nearby industrial sources. The resulting effects on soil chemistry include elevated extractable acidity and aluminium and depressed exchangeable bases, especially Ca and Mg. J.W. Hornbeck et al (1976) give an excellent summary of acidity conditions at Hubbard Brook Experimental Watershed. The stability of stream water pH at Hubbard Brook indicated a uniform buffering action by forest vegetation and soils that reduced the hydrogen ion content by a factor of between 5 and 10. N.M. Johnson (1979) supports this conclusion, and suggests that on a regional basis acidified lakes and streams in New England are confined mainly to low order watersheds. She describes the soil and regolith of the New England landscape as a 'large sump' for the absorption of excess acidity, but finds the contemporary ionic denudation rate of 0.22 eq/m^2 to be 0.16 eq/m^2 below the North American average, despite the added component of strong acids washing out*. T.P. Burt and M.R. Day (1977) obtained similar results near Avonmouth industrial complex, U.K., with little variation of stream pH in response to pollution washout, but a large increase in specific conductance, suggesting leaching of basic soil salts accompanied by pH buffering.

* 'eq' is an abbreviation for 'number of equivalents',

$$\text{eq} = \frac{\text{actual mass of substance}}{\text{equivalent weight}},$$

$$\text{equivalent weight} = \frac{\text{molecular weight}}{\text{net positive valence}}$$

net positive valence = + element x its subscript

(C) Metallic Ions

So far, little has been said of metallic ion inputs from the atmosphere. The most commonly reported are Ca^{2+}, Mg^{2+}, Na^{+} and K^{+}. R. Cryer (1976) gave volume-weighted mean concentrations for the Maesnant Catchment in mid-Wales of Ca^{2+} = 1.41 mg/l (158 %), Mg^{2+} = 0.34 mg/l (53 %), Na^{+} = 2.22 mg/l (68 %) and K^{+} = 0.12 mg/l (63 %). The bracketed values are cations in rainfall expressed as percentages of cations in catchment streamwater and indicate signficant contributions from atmospheric sources (the high value for Ca^{2+} may be due to a consistent analytical error). Fisher et al (1968) reported Si and Al in atmospheric precipitation at Hubbard Brook with concentrations less than 0.1 mg/l. R.P. Betson (1978) measured total Fe, Mn, Pb, total PO_4, Hg, chemical oxygen demand (COD)* and suspended solids in rural and urban rainfall in order to determine the urban impact on streamflow water quality. Total Fe was present at 0.18 mg/l, total PO_4 at 1.1 mg/l, suspended solids at 16 mg/l and COD at 65 mg/l, while Mn, Pb and Hg were all present in concentrations less than 0.1 mg/l. Little difference between rural and urban precipitation quality was found. H.C. Whitehead and J.H. Feth (1964) reported the halogens iodine, fluorine and bromine in rain, dry fallout and bulk precipitation in California, although concentrations were very low.

Dry fallout, collected between rainfall events, often shows strong effects from locally derived materials in the atmosphere, notably mineral or organic dust from quarrying, roadworking or building. If analyses are carried out for catchment budgeting, and the catchment contains potential sources of dry fallout, then both re-circulation and atmospheric output is possible and results must be interpreted with caution. Bulk precipitation is a mixture of rain and dry fallout (Whitehead and Feth, 1964) and is the most commonly reported rainfall quality parameter. It is the geochemically active agent in rock weathering and soil formation on surfaces with minimal vegetation cover.

* COD "provides a measure of the oxygen equivalent of that portion of the organic matter in a water sample that is susceptible to oxidation by a strong chemical oxidant" (A.P.H.A., 1969, p. 510).

An assessment of solute origin, whether it be land surface, industrial pollution or oceanic, is often achieved by comparing measured ion ratios with equivalent standards for seawater. Only sodium and chloride are closely related in atmospheric occurrence in that the major source of both is the sea. They occur in seawater in a Cl-Na ratio of 1.80; if the ratio is greater than 1.80 then a land source of Cl exists; if the ratio is less than 1.80 then a land source of Na exists. E. Eriksson (1960) maps 'excess' amounts of Na, K, Mg and Ca for Europe and North America, the 'excess' being the sample concentration remaining after the subtraction of the concentration of the element in seawater diluted to the sample chloride concentration. Coastal excesses of Na, K and Mg in precipitation over Europe for 1958 were explained by chemical or photochemical separation, although M.P. Paterson and R.S. Scorer (1975) ascribed this to incorrect chemical analysis. Ca excesses in Europe are mainly continental, suggesting primarily land sources of this element. R. Cryer (1976) obtained similar results for mid-Wales, except that Ca excesses were 2 - 3 times larger, perhaps confirming the importance of a terrestrial source for this element, or indicating analytical error.

(D) Temporal Variations and the Influence of Meteorological Variables on Precipitation Chemistry

Detection of significant temporal variations in precipitation on chemistry is dependent, amongst other factors, upon sampling frequency. The most common sampling interval is one week, which rules out meaningful correlation with meteorological conditions, but with a long sampling period may allow analysis of cycles and trends.

(i) Annual trends have been discussed in association with precipitation pH, SO_4, NH_4 and NO_3, HCO_3 and major cations. Likens et al (1976) found significant linear upward trends (5 % level of probability) in H^+ and SO_4^{2-} inputs and significant linear downward trends in Ca^{2+}, Mg^{2+} and K^+ inputs to Hubbard Brook, New England between 1963 and 1974. S. Oden (1976) presents evidence of upward trends in precipitation NO_3-N, NH_4-N, S and excess (mineral) acids, and corresponding downward trends in pH for various stations of the European atmospheric chemical network (which started in Sweden in 1948).

(ii) Seasonal variations are also exhibited in precipitation quality data. Stations situated in New York and Pennsylvania show pH to be maximal in summer, intermediate in spring and autumn and minimal in winter (Hornbeck et al, 1976). Nine year monthly average values of SO_4^{2-} for Hubbard Brook exhibited this cyclic behaviour but to a greater degree, which might be explained by the reduced efficiency of winter snow in capturing sulphur compounds (Fisher et al, 1968). R. Cryer (1976) detected an annual cycle in chemicals in bulk precipitation at Plymlymon, Central Wales. Specific conductance, Mg^{2+}, Na^+ and Cl^- all peaked significantly in February, while pH showed minimum values in May and April respectively. Ca^{2+} and K^+ peaks were not significant. Precipitation sampled simultaneously, at Penglais, a coastal location, only showed a significant Ca^{2+} minimum and K^+ maximum value in February and May respectively. It was suggested that this resulted from a land source of Ca^{2+} and K^+, while seasonal variation in Mg^{2+}, Na^+ and Cl^- at Penglais was "swamped out" by influx and 'sedimentation' of hygroscopic particles from the sea.

(iii) Weekly variations in the concentrations of Ca^{2+}, Mg^{2+}, Na^+, K^+ and Cl^- in bulk precipitation were found from the same experiment. Attempts to explain variation by correlation with simple meteorological variables and synoptic indices was unsuccessful, probably due to the nature of the bulk sample and long sampling interval. E. Gorham (1958) analysed H^+, Na^+, K^+, Ca^{2+}, Cl^-, SO_4^{2-} and NO_3^- in daily precipitation samples collected in the Lake District, and examined correlation of these with precipitation quantity, wind direction, wind velocity and temperature. All solute concentrations were found to decline with increasing rainfall, which represented an initial "flushing" of hygroscopic, saline or acid material from the atmosphere, with a constantly decreasing availability thereafter. Cl^- and $(SO_4^{2-} + NO_3)$ concentrations were significantly related to wind direction, which suggested maritime and industrial sources respectively. Cl^- concentration increased logarithmically with speeds of over 10 km/hour which suggested that wind was important to actually produce the sea spray carried inland. These relationships, together with a negative correlation between temperature and Cl^-, reflect the seasonal distribution of solute concentration noted above.

E. Gorham (1958) and I. Douglas (1968) also sampled intra-storm rainfall, again finding an initial 'flushing' of solutes, with reduced concentrations thereafter. Concentrations through a storm (K^+ apart) were not directly related to rainfall intensity, in contrast to reports by W.A. Mordy (1953), A.H. Woodcock and D.C. Blanchard (1955), R.A. Duce et al (1965), D.F. Gatz and A. Dingle (1971) and V.C. Kennedy et al (1979). Evidence for considerable variation of concentration during one rainstorm was presented by Kennedy et al (1979). They reported variation of Cl^- concentration in San Francisco rainfall by a factor of 2000. E. Gorham (1958) also detected strong antecedent controls, with initial storm concentrations being higher after a period without rainfall.

(E) The Effects of Interception Processes on Precipitation Inputs

Solutes are removed from vegetation and transferred to the forest floor in throughfall and stemflow. Throughfall refers to the precipitation which drips down through the forest and canopy and stemflow refers to the precipitation which reaches the ground by running down the trunks of trees. Chemistry of these two components includes solutes leached from vegetation, solutes washed from the surface of the vegetation and solutes contained in the incident precipitation. The volume of precipitation intercepted depends upon tree species, tree size and structure, antecedent conditions and storm size and intensity (Rutter et al, 1971; 1975). Interception by the canopy may affect the chemistry of throughfall by:

(i) retaining solutes in surface storage;

(ii) leaching solutes from a leaf's surface and either transporting them or depositing them as the water evaporates; and

(iii) absorbing solutes into leaves from the water (Carlisle et al, 1966) or being taken up by leaf and branch microflora (Carlisle et al, 1967; Eaton et al, 1973).

P.M. Attiwell (1966) found that the concentrations of K^+, Na^+, Ca^{2+} and Mg^{2+} in throughfall were inversely related to rainfall intensity, which suggests that a long leaf surface residence time is necessary for maximum solute uptake. Concentrations were found to be highest during the early period of the storm.

Chemical contents of throughfall and stemflow are usually significantly higher than in open plot rainfall (Madgwick and Ovington, 1959; Attiwell, 1966; Carlisle et al, 1966; 1967; Eaton et al, 1973). The studies by Carlisle et al in the Lake District are detailed and interesting. The contents of P, K, Ca, Mg and Na in throughfall were 3.1, 9.5, 2.4, 2.0 and 1.6 times greater than the contents of incident rainfall during 1963 - 1964. Throughfall was shown to be an important contributor of chemicals to the soil surface, giving 37.4 % P, 72.8 % K, 41.9 % Ca, 79.7 % Mg and 97.1 % Na in litter and throughfall. There is general agreement in the literature that the importance of throughfall in comparison to litter fall as a nutrient return mechanism decreases in the order K > Ca = Mg > P = N (Henderson et al, 1977; Carlisle et al, 1966; Eaton et al, 1973). These data are significant since throughfall contains dissolved chemicals, while litter must undergo decomposition and leaching before transport through the soil is possible, Carlisle et al, 1966). Bracken (Pteridium aquilinum) was found to play an important role in the woodland nutrient cycle, its litter and throughfall contributing 31.4 % of the total K falling from all sources and its contribution to total interception being 26 %. Stemflow contributed 3 - 6 % of the total fall of K, Na, Ca and Mg (Carlisle et al, 1967).

Varying throughfall concentrations under different tree species have been reported by A.A.I. Madgwick and J.D. Ovington (1959) and G.S. Henderson et al (1977). The contribution of 'dry fallout' (impaction) to the canopy with subsequent solution by incident rainfall has been recognised by several authors (Carlisle et al, 1967; Eaton et al, 1973), although quantitative data appears scarce.

The importance of hydrogen ion exchange in the removal of cations from the forest canopy was discussed earlier. Low pH precipitation has

been shown to accelerate the intrasystem cycling of nutrients within forested ecosystems (Eaton et al, 1973; Hornbeck et al, 1976).

There appears to have been little research into spatial variation and significance of throughfall and stemflow input to the soil. Stemflow, for example, represents a high solute concentration,point input to the soil, while both throughfall and stemflow might contribute significantly to the chemograph via the hydrological contributing area. Tracer experiments could be used to detect these contributions.

In summary, precipitation, throughfall and stemflow chemistry are important aspects of catchment solute dynamics, although they are topics about which generalisations are difficult. D. Carroll (1962), in reviewing the role of precipitation in rock weathering, suggests that weathering reactions and products are influenced by rainfall chemistry. Again, spatial variations occur. In areas of resistant rock weathering processes may be very slow and rainfall solutes almost balance or form a high proportion of stream solutes (White et al, 1971; Cryer, 1976), while in areas of less resistant rock precipitation solutes account for a small proportion of total stream solutes (Douglas, 1968). These points are further supported by evidence from the North Eastern USA, which suggests that rainfall is a major source of reactants for weathering processes to take place (Fisher et al, 1968). Sedimentary bedrock reacts with acid rainfall to produce solute rich stream water, although processes operating within the soil are not completely understood (Johnson, 1979). Collection and analysis of atmospheric inputs are essential in local studies of catchment solute dynamics to aid interpretation of surface processes, assist modelling procedures and compute overall solute budgets.

2.3 SURFACE WATER SOLUTE DYNAMICS

The behaviour of solutes in streamwater and attempts to model solute response to variations in flow are well documented. A review of the literature indicates a trend away from the more general modelling procedures, for example, W.H. Durum (1953) used daily sampling and a simple inverse hyperbolic relationship between solute concentration and discharge towards attempts to gain a more detailed understanding of the complex fluctuations of solute concentration (e.g. Walling, 1975).

I.D.L. Foster (1978) has used hydrometeorological variables describing conditions prior to and at the time of sampling for multivariate modelling of solute dynamics.

Such modelling is essentially empirical by nature, following observed relationships rather than postulated theory, with little knowledge of the processes actually causing the relationships. Under certain circumstances, this approach may point to the physical and chemical processes which could be given priority for field study as a means of progressing towards a conceptual or spatially distributed model. In this section, attention is given initially to the characteristics of temporal solute response which are of value in improving the empirical modelling approach and isolating the field processes worthy of closer study. Consideration of modelling techniques follows.

(A) Some Characteristic Solute Responses

Standard chemical analyses only tell the gross chemical constitution of a natural water sample, that is, the total amount of calcium, magnesium, chloride, etc., in solution, rather than the concentrations of the individual free ions. Ideally, therefore, as complete an analysis as possible should be carried out to allow computation of the degree of ion association present and the charge balance error, a useful parameter for detecting errors in chemical analysis (computer programs are useful in determining equilibrium speciation of aqueous solutions and the charge balance error, e.g. Wigley, 1977; Plummer et al, 1976; Truesdell and Jones, 1974). The major species usually determined are Ca^{2+}, Mg^{2+}, Na^{+} K^{+} (cations) and Cl^{-}, SO_4^{2-}, HCO_3^{-} and CO_3^{-} (anions), together with pH. For equilibrium speciation calculations, water temperature is also required. Minor species determined are SiO_2, Al, Fe, NO_3, NH_4. Specific conductance and total dissolved solids are also frequently recorded.

As with rainfall, temporal response may be examined at various scales from long term trends to continuous recordings (e.g. specific conductance). The concern here is with detailed response, that is at sampling intervals of one day to 15 minutes, although some mention of longer term changes will be made.

(i) Trends

Time series modelling usually involves consideration of trends, cycles and serial correlation. A.M.C. Edwards and J.B. Thornes (1973) found signficant upward linear trends in mean annual Cl^-, NO_3^--N, non-carbonate hardness and NH_3-N in the River Stour near Langham, England between 1951 and 1970. They attributed this to a combination of increasing intensification of arable agriculture and the increased contribution of fertilizers and sewage effluent, that is essentially anthropogenic factors. P.W. Anderson and J.R. George (1966) and L.T. McCarthy and W.B. Keighton (1964) detected an upward trend in total dissolved solids concentration in the Delaware River, New Jersey, using double-mass curve analysis. The increase was attributed to flow reduction implying a simple ground water dilution model.

(ii) Cycles

Annual cycles in water quality are well documented in the literature. A.M.C. Edwards and J.B. Thornes (1973) detected a strong annual cycle for the River Stour whose peak NO_3 concentration preceded a peak discharge by 1 - 2 weeks and represented a flushing of mineralised nitrogen from the soil. Maximum pH and CO_3 concentrations occurred in September, about two months after the minimum flow. I.D.L. Foster (1977) used harmonic analysis to detect seasonal peak concentrations of specific conductance, Ca^{2+} and Mg^{2+} (July); Na^+ (June); K^+ and Cl^- (November), and NO_3-N (February) in a South Devon catchment. Discharge maxima and minima occurred in December and July respectively. However, R.Cryer (1976), working in mid-Wales, found that peak concentrations of specific conductance, Cl^-, K^+, Mg^{2+} and Na^+ occurred in winter (usually January), corresponding with peak discharge and hence rainfall. The details of other reported seasonal maxima and minima are summarised in Table 2.1. Ground water dilution appears to be a major cause of the correspondence between maximum discharge and minimum concentration (e.g. Johnson and Swank, 1973). The relative timing of the discharge trough and concentration peak varies in response to catchment hydrogeology (compare the Stour (Essex) - Chalk - with the Exe instrumented catchment (South Devon) - Sandstone, Clays and Breccias), although in some ground water catchments alkalinity shows little variation (e.g. River Frome). Potassium and nitrate usually peak at or near maximum discharge. Although explanations for these variations may be tentatively offered at the seasonal time scale,

TABLE 2.1: SUMMARY OF SOME SEASONAL VARIATIONS IN WATER QUALITY REPORTED IN THE LITERATURE

(Q = discharge; Alk = alkalinity; * = uniform all year; Ø = inconsistent peaks; Aut = autumn)

Authors	Locality	Month of Max. Q	Month of Min. Q	Months for which maximum values of concentration occur											
				Ca	Mg	Na	K	pH	Cl	Alk	NO_3	SO_4	SC	TDS	Si
Edwards and Thornes (1973)	River Stour (Essex)	Dec	Jun/Jul	-	-	-	-	Sep	-	Sep	Dec	-	-	-	-
Foster (1979)	Instrumented Catchment of River Exe (South Devon)	Dec	Jun/Jul	Jul	Jul	Jun	Nov	-	Nov	-	Feb	-	Jul	-	-
Cryer (1976), Lewin et al (1974)	Maesnant, Mid-Wales	Dec	Jun/Jul	-	Jan	Jan	Jan	-	Jan	-	-	-	Jan	-	-
Anderson and George (1966)	Various rivers, (New Jersey)	Apr/May	Jun/Jul	-	-	-	-	-	-	-	-	-	-	Jul /Sep	-
Feller (1977), Feller and Kimmins (1979)	Experimental catchments (S.W. British Colombia	Dec/Jan	Jul	Aut	Aut	Aut	*	Aut	-	-	ø	*	-	-	-
Johnson and Swank (1973)	Coweeta Watersheds (N. Carolina)	Jan/Feb	Aug/Sep	Aug/ Sep	Aug/ Sep	Aug/ Sep	Aug/ Sep	-	-	-	-	-	-	-	-

TABLE 2.1 (cont'd)

Authors	Locality	Month of Max. Q	Month of Min. Q	Months for which maximum values of concentration occur											
				Ca	Mg	Na	K	pH	Cl	Alk	NO_3	SO_4	SC	TDS	Si
Kennedy (1971)	Mattole River, Petrolia (California)	Dec	Oct	-	-	-	-	-	-	-	-	-	-	-	May
Casey and Newton (1972; 1973)	River Frome, (Dorset)	Feb	Sep	*	-	-	Oct	-	-	*	Dec	-	-	-	-
Likens et al (1967)	Hubbard Brook (New England)	April	Jul/Oct	ø	ø	ø	ø	ø	ø	-	ø	ø	-	-	ø
Toler (1965)	Spring Creek, (S.W. Georgia)	April	Sep	-	-	-	-	-	-	-	-	-	-	Jun	-
Glancy et al (1972)	Lower Truckee River (Nevada)	June	Dec										Dec		
Gibbs (1972)	Amazon (S. America)	May/Jun	Nov	Jan	Jan	Jan	-	-	-	Jan	-	Jan	-	-	Jan
Imeson (1973)	Hodge Beck (Yorkshire)	Nov	Jun	Jun	Jun	-	Dec	-	-	Jun	-	Dec	-	Jul	-

recourse is best made to detailed chemographs with a sampling interval of one day or less. D.E. Walling (1975) criticised the use of weekly sampling for evaluating fluctuations and controls, except where long periods of records were available, and suggested that 30 minute or even 10 minute sampling might be necessary using automatic equipment.

(iii) Short Term Variations

D.E. Walling (1975) has surveyed the literature on short term temporal solute variations, and illustrated the complex nature of individual ion response with data from South Devon catchments. Much of the recent detailed documentation of solute response in Britain has come from work carried out in South Devon catchments by the University of Exeter (e.g. Walling, 1974; Foster, 1978).

The dilution effect described by various authors in the literature (e.g. Hem, 1970; Anderson and George, 1966) is shown using specific electrical conductance (Walling, 1974; Figure 8A), Ca^{2+}, Mg^{2+} and Na^{+} (Walling and Foster, 1975; Figure 2).

In contrast, K^{+} usually increases during storm hydrographs (Walling and Foster, 1975; Figure 1B; Walling, 1975). Very little is known about the physical processes contributing this extra K^{+} to the stream, although several mechanisms seem possible. K^{+} ions form complex bonds with clay colloid minerals in the soil (Hem, 1970). When suspended sediment is washed into the stream during hydrographs, the colloidal material, if not filtered, might be included in chemical analyses. This would only include K^{+} ions attached to the external colloid surfaces, because those K^{+} ions 'locked' in between crystal units of 2:1 type minerals enter solution very slowly. If suspended sediment is an important source of 'dissolved' K^{+}, then a consistent relationship with the type of response described by D.W. Walling (1974) might be expected, although I.D.L. Foster (1977) found this not be be the case. Walling (1975) attributed increases in K^{+} to the washing of accumulated solutes and fertiliser residue into the stream following a dry period. V.C. Kennedy (1964, 1965) noted that the mineralogy and exchange capacity of stream sediments should be considered in understanding the chemistry of stream waters. Depending upon the conditions, exchange capacity of suspended sediments might act as a

stabilising agent for the chemical composition of stream water. Another possible mechanism of K^+ increase is rapid leaching from the upper soil horizons with the aid of organic acids from surface humus (Kerpen and Scharpenseel, 1967). During a period of baseflow recession K^+ concentration is often seen to decline, probably as a result of its preferential incorporation into some clay-mineral structures. In illite, for example, K^+ ions are incorporated in spaces between crystal layers where they are not removable by further ion-exchange reactions (Hem, 1970).

Anion concentrations in streamflow also exhibit dilution during storms. Edwards (1973a) found that bicarbonate concentrations in the River Yare, Norfolk, decreased during storms, representing a dilution, or more accurately acidification due to the usually lower pH of rainfall, (although hydrogen ion concentrations were not presented). Hendrickson and Kreiger (1960) reported dilutions in bicarbonate, chloride and sulphate with increasing flow, but also noted temporary increases in concentration at the beginning of storms after a period of low flow; this phenomenon will be discussed later. In some catchments sulphate and chloride are poorly represented in rocks and soils, and atmospheric precipitation is the major source (Johnson et al, 1969; Juang and Johnson, 1967; Cryer, 1976). In such cases, there may be a concentration of anions during storms.

Although solutes are often reported to have characteristic dilutions or concentrations during storm discharge, a survey of the literature shows that the behaviour of individual ions is often inconsistent. Seasonal inconsistencies occur in particular catchments in addition to the more predictable spatial changes due to geological, pedological and land use variation.

(B) Seasonal Variations in Discharge/Solute Response

(i) The 'Flushing Effect'

Detailed sampling programmes using automatic devices, such as those reported by W.F. Lester and G.M. Woodward (1972) and D.E. Walling and A. Teed (1971), have picked out seasonal changes in individual ion responses. Most commonly reported is the autumn 'flushing effect' where the decrease in concentration may be followed by a rise, or an

initial drop may be followed by an increase before giving way to a subsequent decrease (Walling and Foster, 1975; Walling, 1974; Edwards, 1973a; Waylen, 1977) (Figure 2.3A). In some cases dilution may be completely replaced by concentration (Figure 2.3B), the magnitude of the concentration decreasing through subsequent storms as available solutes are leached from the soil (Gburek and Heald, 1970). The flushing effect is most pronounced after periods of low flow, during which time the soil moisture deficit increases. The physical processes behind the effect are poorly understood although it would appear that diminution of the hydrological contributing area due to drainage and evapotranspiration is accompanied by an increase in the solute concentration of baseflow. Exchangeable ions may accumulate in the root zone at the same time. The way in which these accumulated salts are transported to the stream is likely to depend, amongst other factors, upon soil structure. Clay soils crack whilst drying to produce a structure not dissimilar to that of fissured Chalk, although on a smaller scale. A tentative analogy can be made between recharge of the Chalk aquifer, that is rapidly through macrofissures and very slowly through microfissures (Young et al, 1976), and flow through a clay soil after a long dry period. Accumulated salts might be leached from the root zone, carried into the fissure system and transported rapidly to the stream.

Another possibility is that after an initial dilution due to a combination of channel precipitation and possibly overland flow, ion-rich water (which represented the pre-storm contributing area) is 'shunted' into the stream as 'piston' or 'displacement' flow (Laidlow et al, 1974).

A further contribution to 'flushing' may come from atmospheric 'washout' of solutes after a long dry spell (Kennedy et al, 1979) together with the high solute concentrations in throughfall and stemflow that would be expected after a lengthy period of dry fallout and leaf exudation.

However, the precise mechanism of solute flushing has not been studied in detail and requires field study.

initial drop may be followed by an increase before giving way to a subsequent decrease (Walling and Foster, 1975; Walling, 1974; Edwards, 1973a; Waylen, 1977) (Figure 2.3A). In some cases dilution may be completely replaced by concentration (Figure 2.3B), the magnitude of the concentration decreasing through subsequent storms as available solutes are leached from the soil (Gburek and Heald, 1970). The flushing effect is most pronounced after periods of low flow, during which time the soil moisture deficit increases. The physical processes behind the effect are poorly understood although it would appear that diminution of the hydrological contributing area due to drainage and evapotranspiration is accompanied by an increase in the solute concentration of baseflow. Exchangeable ions may accumulate in the root zone at the same time. The way in which these accumulated salts are transported to the stream is likely to depend, amongst other factors, upon soil structure. Clay soils crack whilst drying to produce a structure not dissimilar to that of fissured Chalk, although on a smaller scale. A tentative analogy can be made between recharge of the Chalk aquifer, that is rapidly through macrofissures and very slowly through microfissures (Young et al, 1976), and flow through a clay soil after a long dry period. Accumulated salts might be leached from the root zone, carried into the fissure system and transported rapidly to the stream.

Another possibility is that after an initial dilution due to a combination of channel precipitation and possibly overland flow, ion-rich water (which represented the pre-storm contributing area) is 'shunted' into the stream as 'piston' or 'displacement' flow (Laidlow et al, 1974).

A further contribution to 'flushing' may come from atmospheric 'washout' of solutes after a long dry spell (Kennedy et al, 1979) together with the high solute concentrations in throughfall and stemflow that would be expected after a lengthy period of dry fallout and leaf exudation.

However, the precise mechanism of solute flushing has not been studied in detail and requires field study.

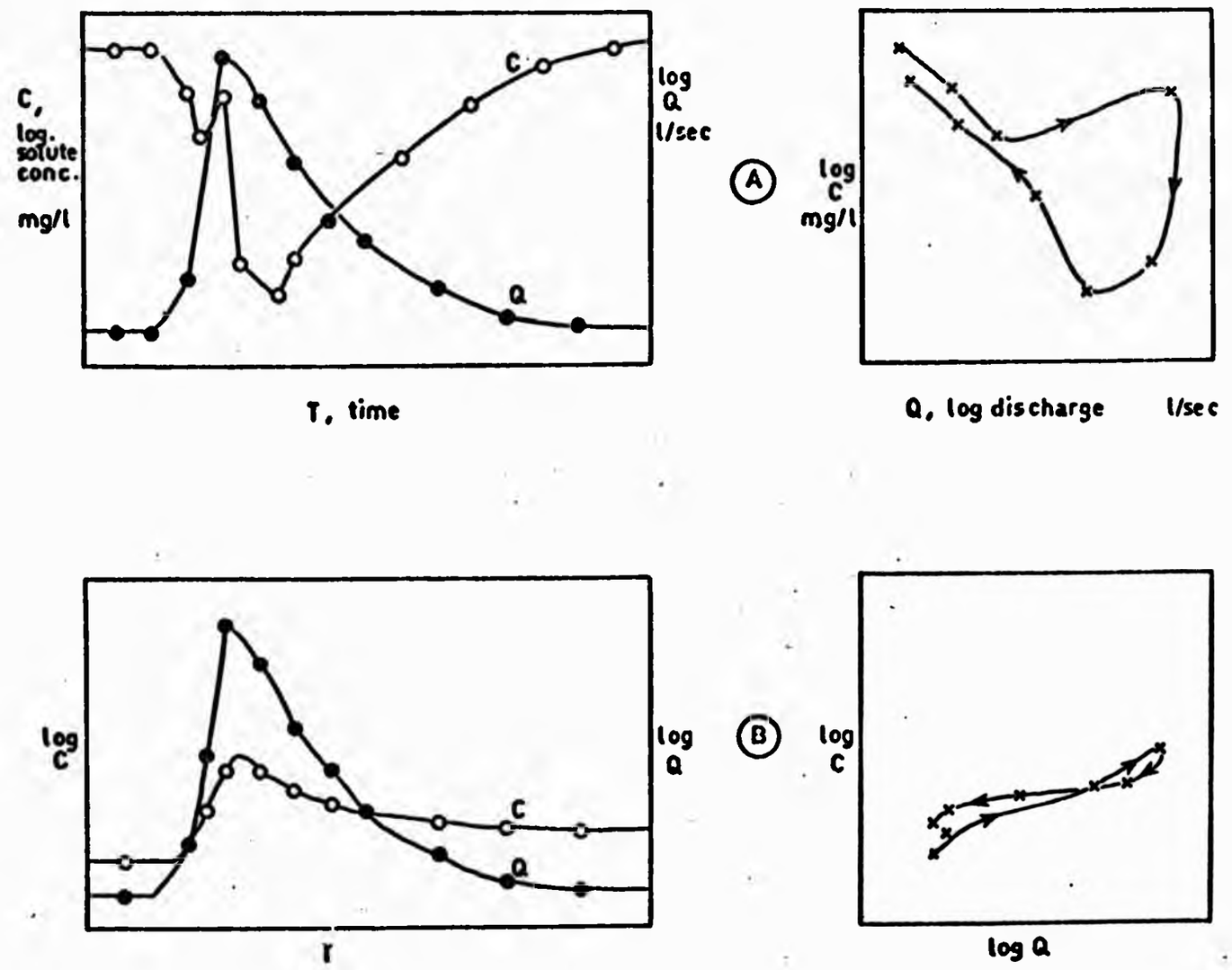

FIGURE 2.3: THE EFFECTS OF AUTUMN FLUSHING ON SOLUTE/DISCHARGE RATINGS

A: DILUTION WITH FLUSHING B: CONCENTRATION ONLY

More intensive sampling through storm hydrographs has also shown that individual ion concentrations fluctuate around a more general response (e.g. Gburek and Heald, 1970; Walling and Foster, 1975; Walling and Foster, 1978). This may be due to random error in sampling or analysis, or it may represent the arrival of solutes from different source areas within the catchment. Such areas might show delayed response due to a longer transport time from a 'new' upslope source as the contributing area expands, or a longer travel time in channel flow, or both.

(ii) Comparing chemographs with hydrographs: lag and lead

The relative timing of the hydrograph peak and chemograph trough is dependent upon several factors. Channel precipitation or overland flow very low in solute concentration is required for the trough to precede the peak (Figure 2.4B). The more common response gives either a trough and peak occurring simultaneously (Figure 2.4A) or a trough lagging behind a peak (Figure 2.4C).

B.J. Glover and P. Johnson (1974) suggested that in large rivers the lag effect was due to solute surface runoff being associated with the mean water velocity, which arrived later than the flood wave. Lag time was also found to be longer for small rises in flow because the speed of travel down the channel was slower. D.E.Walling and I.D.L.Foster (1975) confirmed these results but showed that the lag effect was related to processes operating over the entire catchment in addition to those in the channel. The phenomenon was also demonstrated in catchments two orders of magnitude smaller than the River Tyne, used by Glover and Johnson (1974). Chemograph lag on the River Creedy, Devon, (defined by specific conductance records) was inversely related to the logarithm of hydrograph rise, seasonality and log. preceding flow level by multiple regression. The first parameter confirms the results given by Glover and Johnson (1974) whilst the second two are interpreted in terms of a 'flushing' effect which acts to delay the chemograph trough.

The seasonal variations in ion response described above introduce hysteresis into the simple ratings between concentration and discharge. Hysteresis loops are widely reported in the literature but are rarely

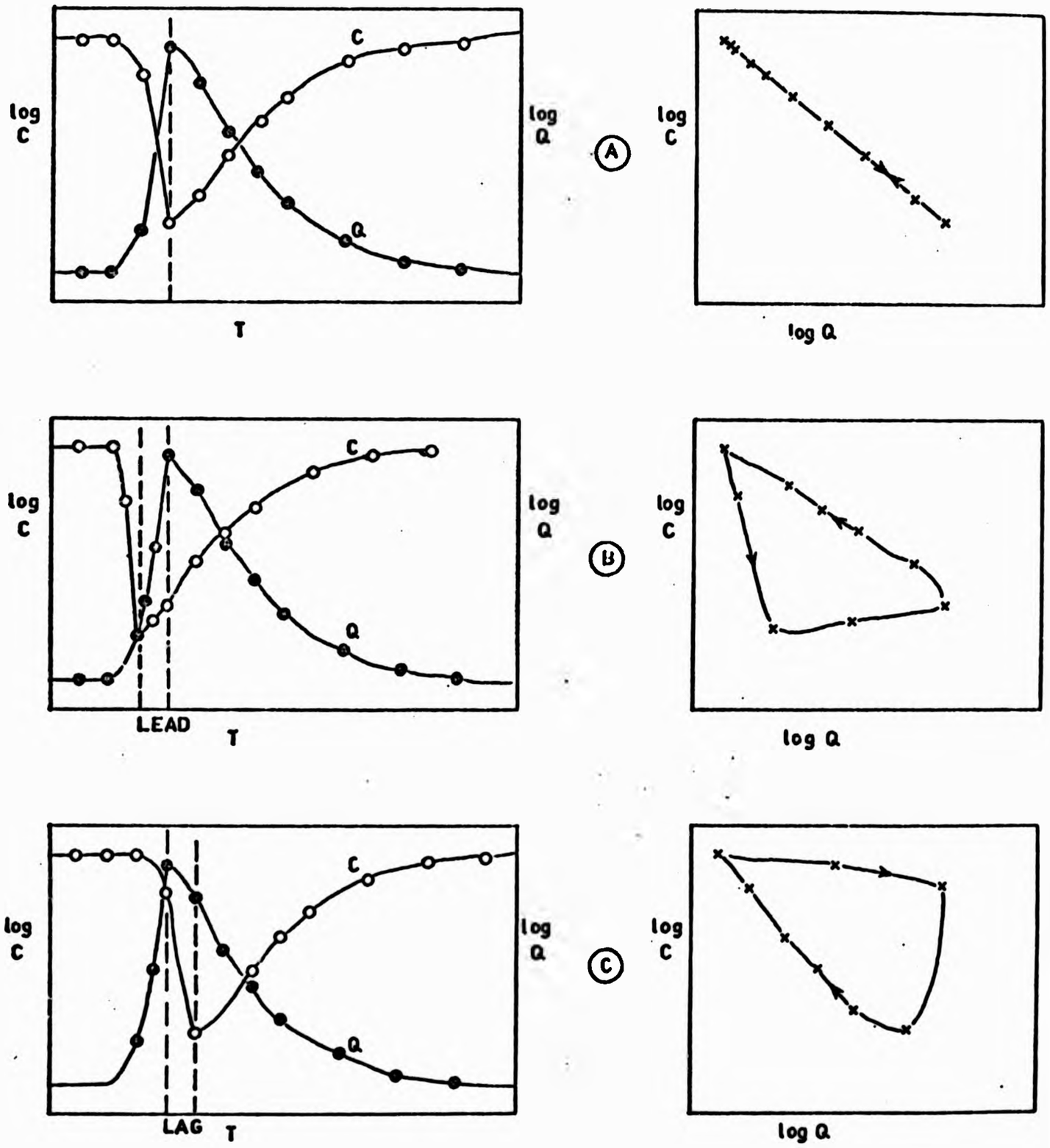

FIGURE 2.4: THE EFFECTS OF LAG AND LEAD ON SOLUTE/DISCHARGE RATINGS

A: SYNCHRONOUS HYDROGRAPHS AND CHEMOGRAPHS

B: C LEADS Q B: C LAGS Q

as simple as those shown schematically in Figures 2.3 and 2.4 (Hendrickson and Kreiger, 1960; Toler, 1965; Gunnerson, 1967; Glancy et al, 1972; Walling, 1974; Balek et al, 1978; Foster, 1978). Hysteresis adds to the problem of modelling water quality described in the next section.

(C) Modelling Water Quality in small Catchments using Bivariate and Multivariate Regression

A model describes the conversion of one phenomenon into another, an 'input' into an 'output' (Clarke, 1973). The model formulation in bivariate regression treats discharge as the input and solute concentration as the output; the physical processes operating within the catchment are treated as a 'black box'. The functional relationship between discharge and solute concentration is usually obtained by sampling over a range of conditions and optimising using least squares regression. Multivariate regression also ignores physical processes, but can incorporate hydrological and meteorological conditions which help to explain the complexity of solute response. Again, optimisation is usually achieved by a least squares computer routine. F.R. Hall (1970; 1971) described several discharge-concentration relationships in the context of mixing models. Some of the more commonly used empirical models fit into the classification by Hall and are discussed below.

The power relationship (usually linear for log. concentration versus log. discharge) is the most frequently reported. This takes the form

$$C = AQ^n \qquad (2.1)$$

where C is concentration
Q is discharge
A is a constant, representing concentration as discharge nears zero
n is also a constant, representing $\frac{dC}{dQ}$

The value of n may be negative in the case of dilution or positive for concentration. The model cannot account for the mixing of different waters as it assumes only one source, the inflow to which has zero concentration. It has, however, been used in many cases as a descriptive equation (e.g. Gunnerson, 1967; Edwards, 1973a) as an estimator of historical water quality (e.g. Steele, 1968; 1976) or to compute solute budgets (e.g. Edwards, 1973b; Hughes and Edwards, 1977). J.O. Ledbetter and E.F. Gloyna (1964) considered that the exponent n (representing rate of change of concentration with discharge) was empirically related to discharge by

$$n = pQ^b \qquad (2.2)$$

where p and b are regression constants. D.E. Walling (1974) used this relationship to describe specific conductance variations with discharge to the Rosebarn catchment, South Devon, but only found a marginal improvement over the use of equation (2.1). In an effort further to improve the prediction of n, Ledbetter and Gloyna incorporated an antecedent flow index, describing the past 30 days flow record,

$$n = f + g.\log.Aq + pQ^b \qquad (2.3)$$

where Aq is an antecedent flow index and f and g are constants. They regard the combination of equations (2.1) and (2.3) as the maximum degree of complication required in predicting quality from quantity.

A large number of possibilities exist when developing empirical models of water quality, due to the range of data transformations and curve fitting procedures available in computer packages. The literature indicates that best-fit functions are sometimes obtained and used both as predictive models and as a means of suggesting the physical processes behind solute production. For example Waylen (1976) used equation (2.1), a semi-logarithmic function and untransformed data to describe individual ion responses at East Twin Brook, Somerset, and to compute solute budgets. I.D.L. Foster (1977) fitted polynomial functions to weekly data from South Devon catchments. There is some merit in taking a unique approach to modelling each ion as this is likely to give better predictive power and understanding of processes.

Some authors have preferred to develop curve fitting procedures from mixing models, notably F.R. Hall (1970; 1971), F.C. Hart et al (1964), N.M. Johnson et al (1969) and D.E. Walling (1974).

N.M. Johnson et al (1969) considered the mass balance equation,

$$C_o V_o + C_\alpha V_\alpha = C(V_o + V_\alpha) \qquad (2.4)$$

where C_o is the concentration of solute per volume in the storage solution
V_o is the volume of the storage solution
C_α is the concentration of solute in the added solution
V_α is the volume of the added solution
C is the resulting solute concentration of the mixed solution

By substituting γD for V_α, where γ is the residence time of water in the system, and D is stream discharge, (2.4) becomes,

$$C_o V_o + C_\alpha \gamma D = C(V_o + \gamma D) \qquad (2.5)$$

Re-arranging and substituting β for γ/V_o and C_δ for $(C_o - C_\alpha)$ gives

$$C = \frac{1}{1 + \beta D} C_\delta + C_\alpha \qquad (2.6)$$

The final equation (2.6) gives concentration as a linear function of the reciprocal of discharge, but incorporates elements of physical reality in its development from equation (2.4). N.D. Turvey (1975) tested the reciprocal and power function models for data from a tropical rain forested catchment and found no significant difference in levels of variance explained. D.E. Walling (1974) followed F.C. Hart et al (1964) in separating flow components and describing the solute response of each by a separate equation. The final mixing model was of the form,

$$C_t = \frac{(C_g . Q_g) + (C_d . Q_d)}{Q_t} \qquad (2.7)$$

where C_t is total specific conductance

Q_t is total discharge

Q_d is delayed flow

C_d is total specific conductance of delayed flow defined by $C_d = aQ_d^{-b}$

Q_q is quickflow

C_q is total specific conductance of quickflow defined by $C_q = eQ_q^{-f}$

Walling (1974) found that this approach gave a better prediction of specific conductance than either equation (2.1) or (2.1) plus (2.2). However, it failed to explain adequately detailed hysteresis loops and flushing effects described in the previous section.

Multivariate models have been used by various authors to explain solute variations and provide information on the relative control of independent variables. Principal components analysis and stepwise multiple regression are the techniques available, although J.L. Mahloch (1974) found difficulty in interpreting factor solutions from the former. Using multiple regression, the model is,

$$C = k + aP_1 = bP_2 + \ldots + zP_n \qquad (2.8)$$

or if log transformed values are used,

$$C = kP_1^{a} * P_2^{b} * \ldots * P_n^{z} \qquad (2.9)$$

where C = total solute concentration

$P_1, P_2 \ldots P_n$ are independent variables

$k, a, b \ldots z$ are constants

This approach has been used by H.B. Pionke and A.D. Nicks (1970) to predict total dissolved solids variation in streamflow with monthly, maximum daily and antecedent precipitation, pan evaporation and distance from the raingauge. H.M. Keller (1970) found discharge, water temperature and a seasonal index explained more than 80 % of the solute variation in three Swiss mountain streams. D.E. Walling (1974) used stepwise multiple regression involving three dependent variables and thirteen independent variables to produce optimum relationships for

where C_t is total specific conductance

Q_t is total discharge

Q_d is delayed flow

C_d is total specific conductance of delayed flow defined by $C_d = aQ_d^{-b}$

Q_q is quickflow

C_q is total specific conductance of quickflow defined by $C_q = eQ_q^{-f}$

Walling (1974) found that this approach gave a better prediction of specific conductance than either equation (2.1) or (2.1) plus (2.2). However, it failed to explain adequately detailed hysteresis loops and flushing effects described in the previous section.

Multivariate models have been used by various authors to explain solute variations and provide information on the relative control of independent variables. Principal components analysis and stepwise multiple regression are the techniques available, although J.L. Mahloch (1974) found difficulty in interpreting factor solutions from the former. Using multiple regression, the model is,

$$C = k + aP_1 = bP_2 + \dots + zP_n \qquad (2.8)$$

or if log transformed values are used,

$$C = kP_1^{a} * P_2^{b} * \dots * P_n^{z} \qquad (2.9)$$

where C = total solute concentration

$P_1, P_2 \dots P_n$ are independent variables

$k, a, b \dots z$ are constants

This approach has been used by H.B. Pionke and A.D. Nicks (1970) to predict total dissolved solids variation in streamflow with monthly, maximum daily and antecedent precipitation, pan evaporation and distance from the raingauge. H.M. Keller (1970) found discharge, water temperature and a seasonal index explained more than 80 % of the solute variation in three Swiss mountain streams. D.E. Walling (1974) used stepwise multiple regression involving three dependent variables and thirteen independent variables to produce optimum relationships for

predicting suspended sediment concentrations in the Rosebarn catchment, South Devon. I.D.L. Foster (1978) has taken a similar approach in developing multiple regression equations for predicting storm period solute behaviour in the Yendacott catchment, South Devon. The dependent variables selected were minimum storm specific conductance, Ca^{2+}, Na^{+}, Mg^{2+} and Cl^{-} concentrations; maximum K^{+} concentration; the concentration range exhibited by each variable during the storm; the rate of change of each solute concentration with increasing discharge. Independent variables used in the stepwise multiple regression were: maximum storm discharge, hydrograph rise, water temperature, Soil Moisture Deficit, antecedent precipitation index, half-hourly rainfall intensity, seasonal (sine) index, hydrograph rise. Most success was obtained for extreme values of all the dependent variables, with the exception of Cl^{-}, and various independent variables, the percentage of explained variance ranging from 67.4 to 87.7. Interpretation of the results in terms of solute sources and operative processes was also attempted.

It has been pointed out by D.E. Walling and I.D.L. Foster (1975) and Foster (1978) that care must be taken in choosing independent variables for multiple regression analysis due to their inter-dependence; e.g. maximum storm discharge and hydrograph rise (Foster, 1978). Residual normality and serial correlation are further important factors to be considered (Johnston, 1978).

This chapter has given detailed consideration to the two major components of a watershed ecosystem, i.e. precipitation solute inputs and streamwater solute outputs. Precipitation constituents and sources, acidity, temporal variations, the influence of meteorological factors, throughfall and stemflow have all been discussed. With respect to streamflow solute dynamics, typical solute responses, e.g. dilution, and seasonal complications in response, e.g. solute flushing, are recognised, and a variety of descriptive or predictive models presented. A preliminary literature survey of this kind is useful in that it allows the strengths and weaknesses of previous experiments to aid

design of that currently under consideration*. For example, the complexity of solute response necessitates sampling streamwater at frequent intervals through storms in addition to regular, but less frequent times, during a long baseflow recession. Consideration of sampling frequency is an important factor if valid comparisons are to be made of different types of model (Hall, 1971).

The following chapter describes the small catchment chosen for studying surface and sub-surface solute dynamics.

* With the obvious exception of some of the later references cited.

CHAPTER 3

WEST WALK CATCHMENT:

PHYSIOGRAPHY, GEOLOGY, SOILS, VEGETATION AND CLIMATE

3.1 INTRODUCTION

During autumn 1973 two small river basins in south-east Hampshire were chosen for hydrological studies. The first of these (Hipley) is approximately 1.0 km^2 in area, mainly underlain by London Clay and used as pasture. It contributes runoff to the River Wallington system. The second (West Walk) is 0.6 km^2 in area, underlain by Bagshot Sand, London Clay and Plateau Gravel and covered by woodland. This contributes to the River Meon system. The two catchments are on opposite sides of the same divide.

West Walk catchment was selected for research into surface and subsurface solute dynamics. It has several advantages over other catchments. Firstly, and most significantly, it is unpolluted by fertiliser application or sewage discharge. Secondly, London Clay catchments in the Portsmouth area were observed to have a wide flow regime, ranging from zero flow during summer 1973 to over bankfull stage in the 1973 - 1974 winter. West Walk flow was maintained during summer 1973 due to baseflow from the Bagshot Sand, Plateau Gravel and interflow from valley-side deposits. Crest-stage recorders showed that high flows during the 1973 - 1974 winter were all below bankfull, probably due to the 'damping' of hydrograph peaks by forest interception and the artificial deepening of natural channels. Thirdly, West Walk has greater relief and is topographically more suitable for the detailed study of subsurface processes than lower angle hillslopes of the clay catchments. Furthermore, areas of free-draining brown earth soils in West Walk were preferable to gleyed soils on clay catchments.

However, it was thought that the spatial diversity of vegetation and soils within West Walk might complicate the explanation of solute response and hence make modelling difficult. The solution to this problem of spatially varying response was a division into subcatchments. However, complexity of soils and vegetation even within a small area was likely to be such that a division into subcatchments would not

completely elucidate the processes controlling stream chemograph response. The solution to this problem might be an instrumented hillslope within one subcatchment, with the aim of monitoring water and solute movement, and using collected data to model inflow to the channel. Soil catenary variations might still exist although vegetation variability could be minimised. The results from such an experiment would probably only be referable to the subcatchment scale at best and would not have general application at the total catchment scale. However, detailed knowledge of solute throughflow processes should provide information upon which physically realistic models of solute response could build.

Figure 3.1 shows how West Walk was firstly divided into three approximately equal sections by a flume and weirs W1 and W2 on the main channel. Two east bank catchments were then defined by weirs 4 and 5. A justification for this division will become apparent in the catchment description which follows.

3.2 PHYSIOGRAPHY

West Walk is a catchment 1.22 km long from divide to main gauging station, and 0.65 km in width at its widest point. It has an area of almost 0.6 km^2 and 57 m relative relief. Table 3.1 gives the areas of other subcatchments.

Table 3.1 Catchment Areas

	Area (km^2)	% West Walk
West Walk	0.598874	100
Subcatchment 1 (above W1)	0.165000	27.55
Subcatchment 2 (above W2)	0.391375	65.35
Subcatchment 3 (above W4)	0.075313	12.58
Subcatchment 4 (above W5)	0.072938	12.18

(Areas planimetered from map surveyed by staff and students of Portsmouth Polytechnic Geography Department)

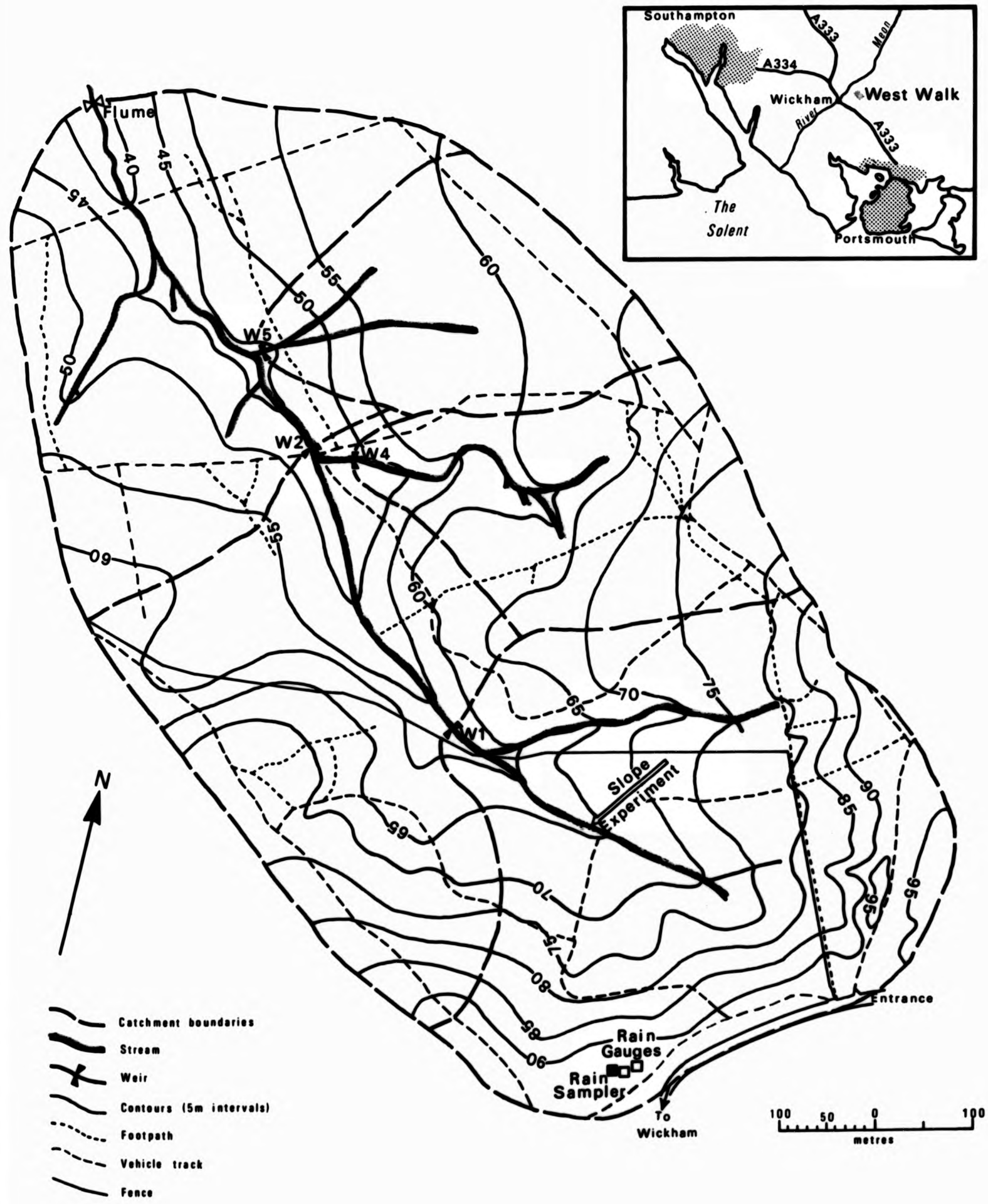

FIGURE 3.1: WEST WALK CATCHMENT
BOUNDARIES, STREAMS, FOOTPATHS AND VEHICLE TRACKS

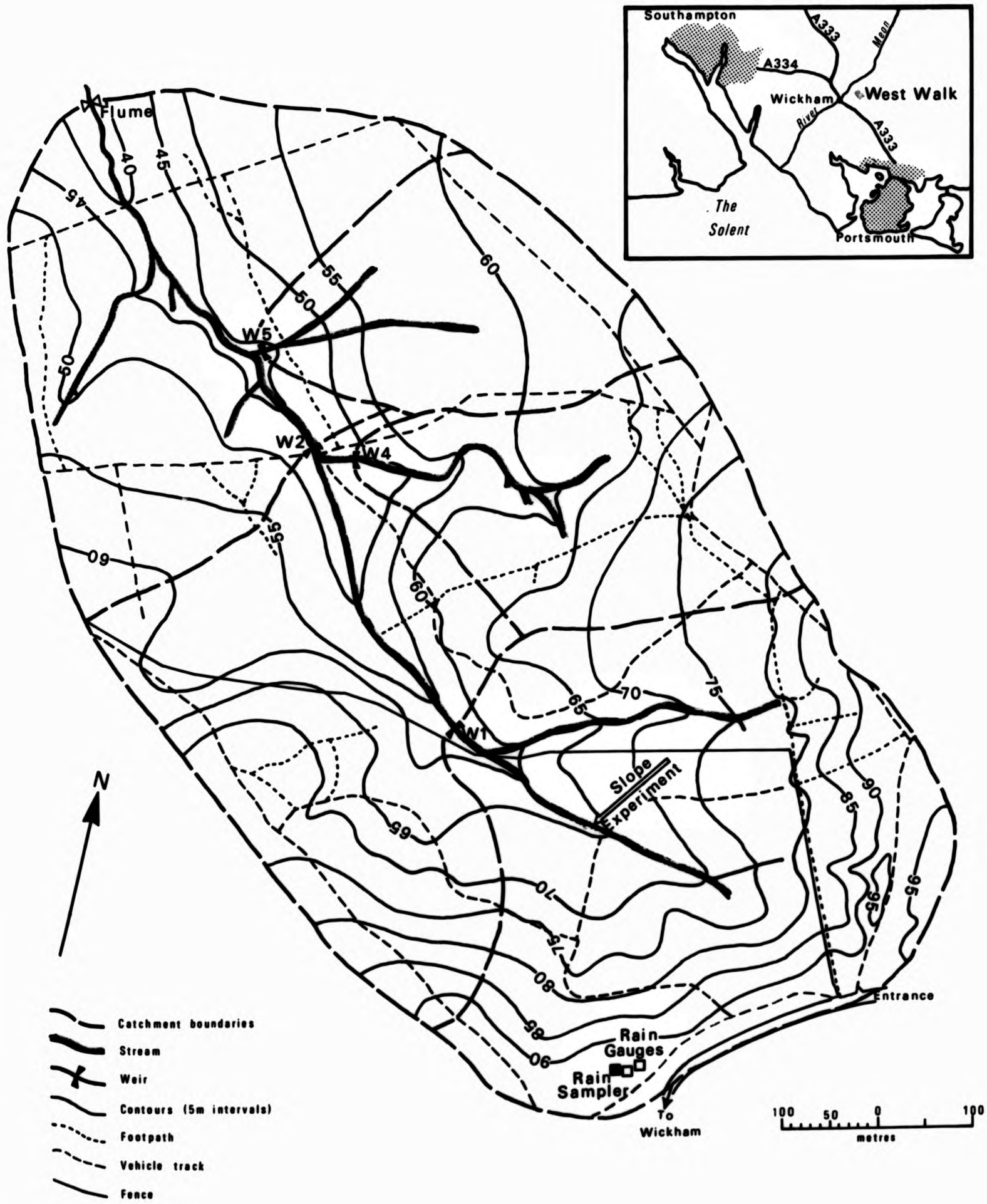

FIGURE 3.1: WEST WALK CATCHMENT
BOUNDARIES, STREAMS, FOOTPATHS AND VEHICLE TRACKS

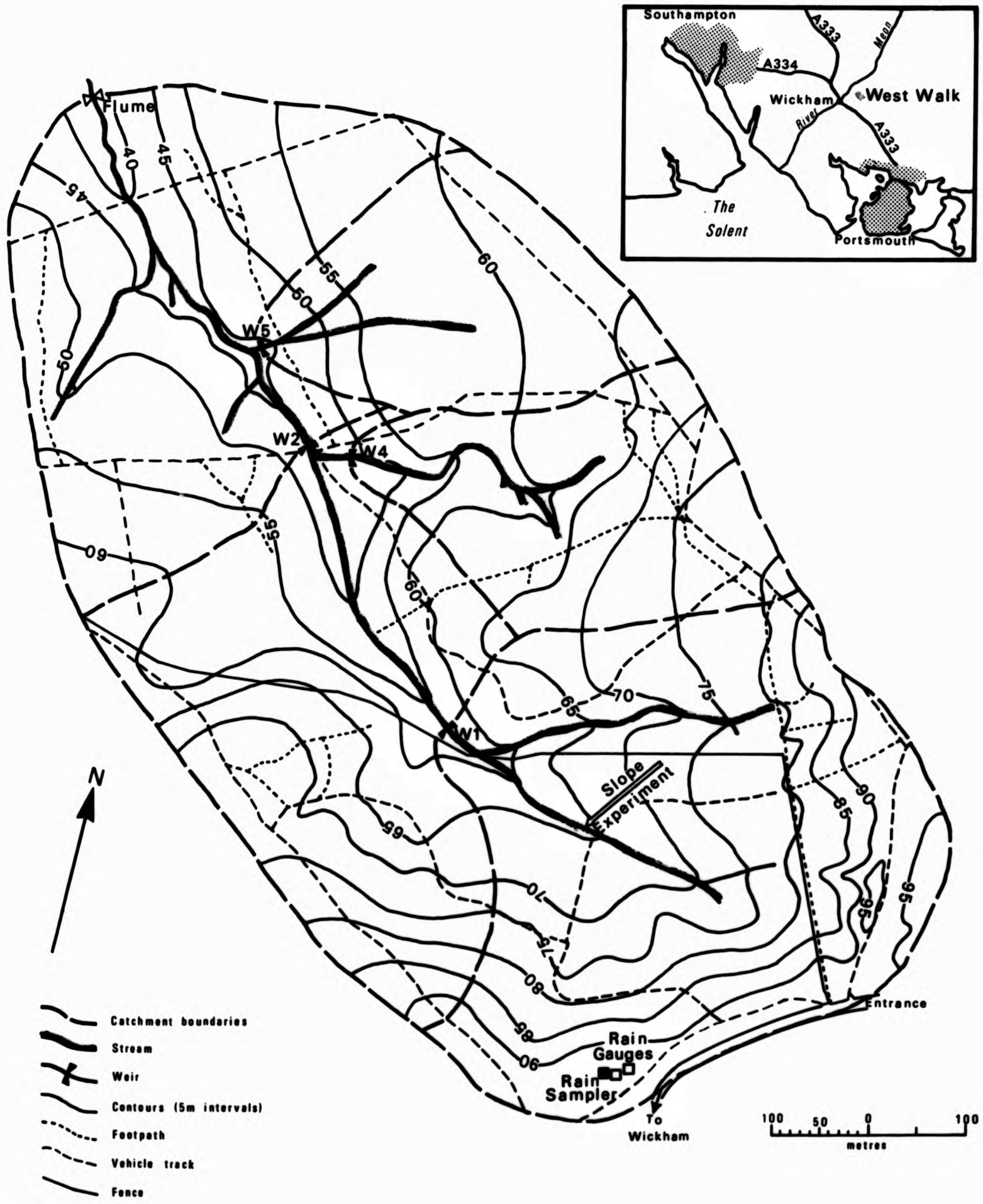

FIGURE 3.1: WEST WALK CATCHMENT
BOUNDARIES, STREAMS, FOOTPATHS AND VEHICLE TRACKS

Catchment boundaries were first defined from the map surveyed in 1975 by staff and students of Portsmouth Polytechnic Geography Department and subsequently checked in the field. The main channel drains north-westwards joining the southward flowing River Meon in about 3 00 metres. Catchment drainage is asymmetrical with all the important tributaries entering from the east bank. In cross section the catchment itself is also asymmetrical, the south-west facing slopes being much gentler than those facing north and north-east.

Figure 3.2 gives slope angle frequency curves for comparing the steepness of subcatchment hillslopes. The data was obtained by laying a grid of 100 metre squares over the catchment map and calculating the slope angle for each intersection. Since the data is map-derived values are not absolutely correct and Figure 3.2 is best used as a comparative tool. Subcatchment 1, at the head of West Walk has 26 % of its slopes greater than 12^{o} as compared to 12.5 % for West Walk, which would give the former a more rapid response if all other factors were equal. Curves for subcatchments 4 and 5 show these to have a high proportion of gentle slopes, with maximum angles of 8.3^{o} and 6.2^{o} respectively. This might reduce the response rate for these two catchments.

Using the same grid point method a rose diagram of slope orientation was constructed (Figure 3.3). This shows that a high proportion of West Walk's slopes face between WNW and SW, while slightly less face between NNW and ENE. Since the prevailing winds are west and south-westerly, south-west and west facing slopes might receive more rainfall than those in the opposing quadrant. Subcatchments 4 and 5 both fall dominantly in the south-west facing category.

3.3 GEOLOGY

The solid geology of West Walk is dominated by Eocene deposits, namely London Clay and Bagshot Sand. River and Plateau Gravel of Pleistocene age cover smaller areas (Figure 3.4). Table 3.2 gives the percentage of catchment areas covered by these deposits.

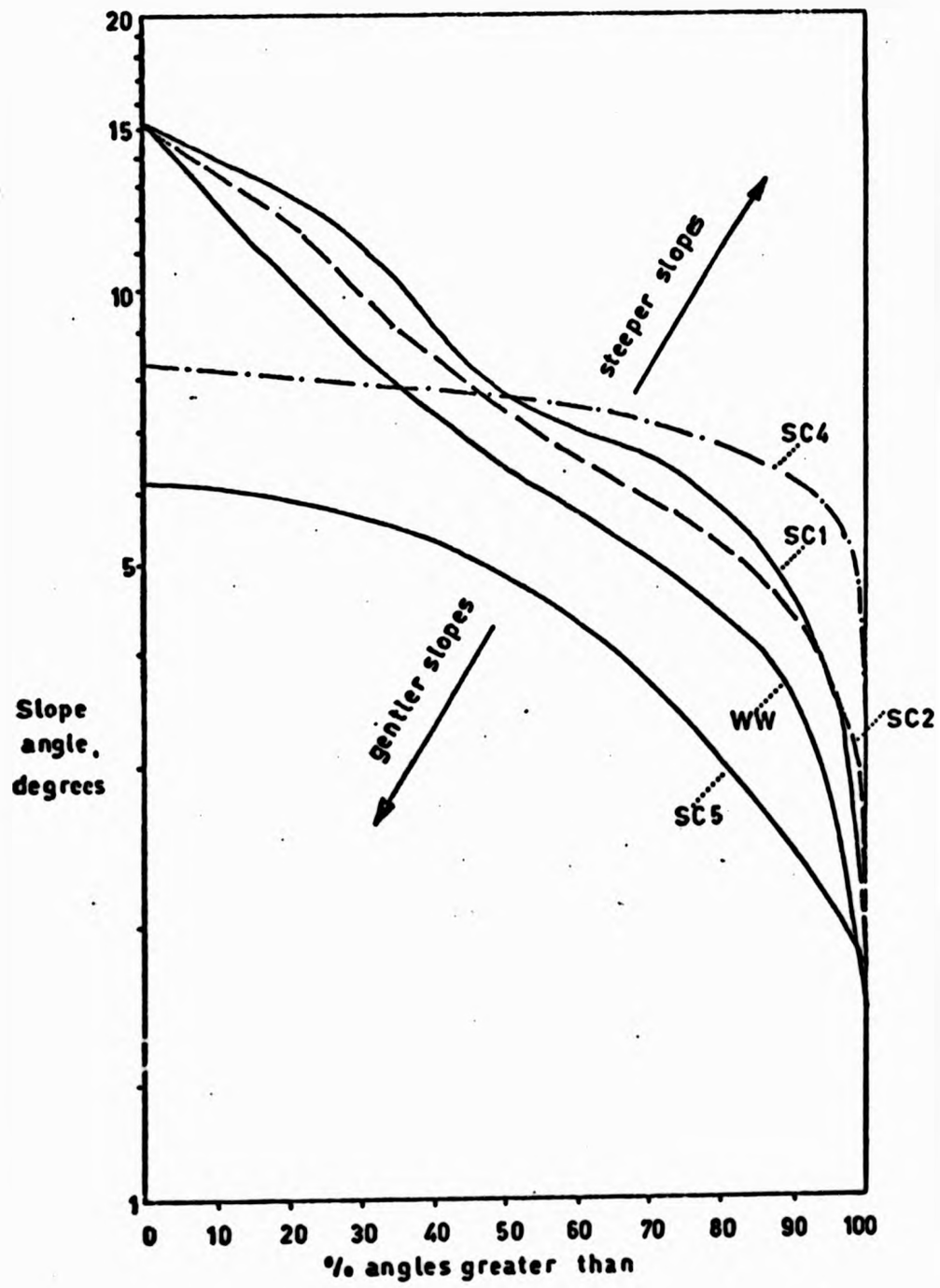

FIGURE 3.2: SLOPE ANGLE FREQUENCY CURVES FOR WEST WALK SUBCATCHMENTS (10^{o} Class intervals used)

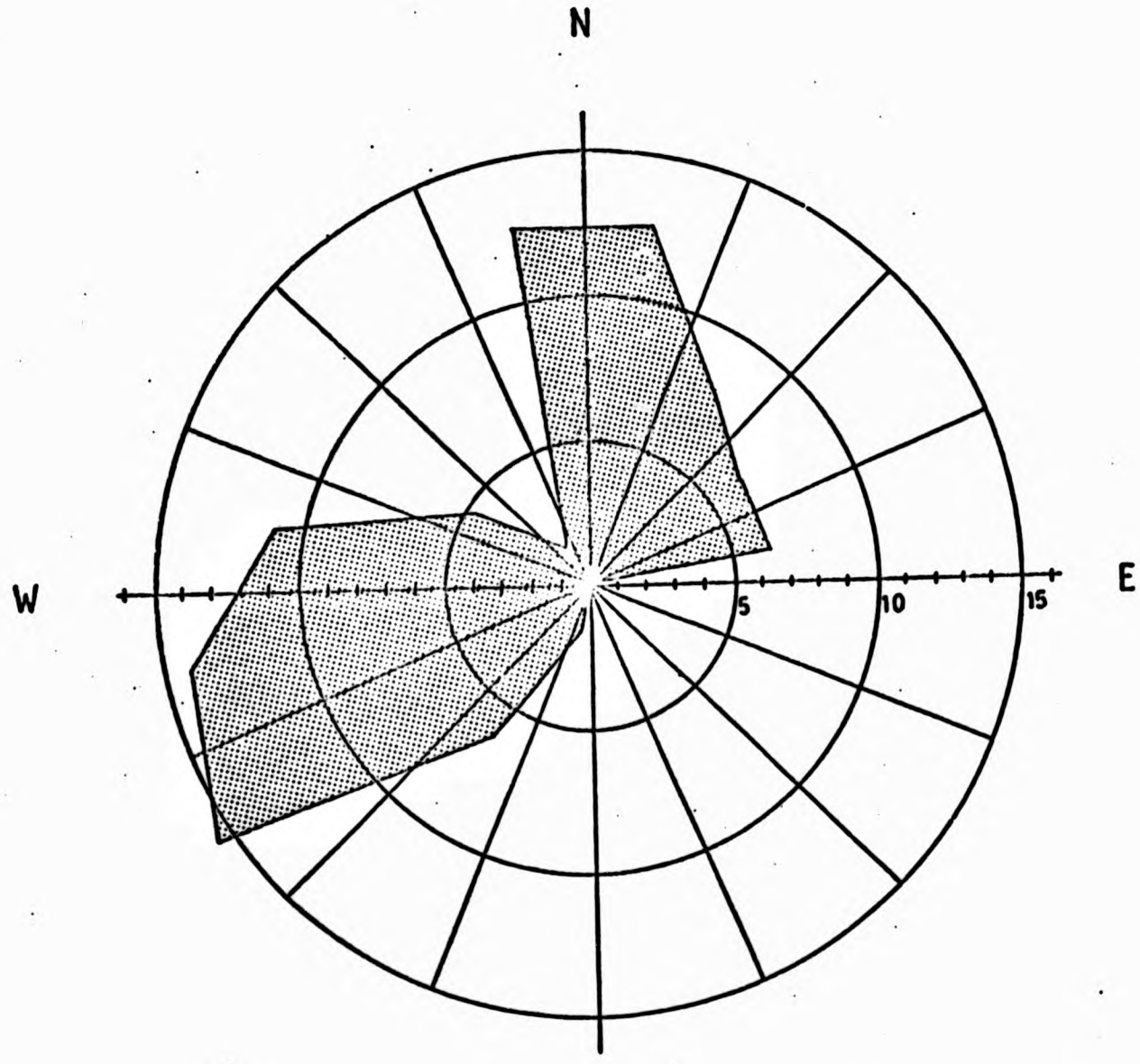

FIGURE 3.3: WEST WALK SLOPE ORIENTATION
(% catchment facing a given direction)

London Clay

This formation is entirely of marine origin and consists of blue, brown and grey clay, yellow and grey sands and sandy loam, interspersed with pebble beds (Chatwin, 1960). Its thickness is difficult to ascertain in the West Walk area, although sandy lenses are apparent in several parts of the catchment as zones of natural seepage. On the whole the London Clay is a poor aquifer, providing a good watertight basement to West Walk.

Bagshot Beds

The transition from London Clay to the overlying Bagshot Beds is gradual and difficult to map. Figure 3.4, based on 1:10560 Geological Survey of Great Britain, represents a simplification of the true picture. The Bagshot Beds thin northwards across the Forest of Bere syncline. Within West Walk they consist of yellow-brown ferruginous sands with thin beds of laminated loam and grey clay. Thin pebble beds are also present in lenses from 0.5 to 1.0 metres thick. The Bagshot Sand is not a good aquifer because of its low transmissivity and the fine-grained nature of the sand.

Plateau Gravel

Plateau Gravel consists of sub-angular flints mixed with flint pebbles and other materials derived from the Eocene deposits. It caps the Bagshot Beds in the uppermost part of the catchment forming a plateau at 90 - 95 metres O.D. The capping is about five metres in thickness and due to its resistance to erosion forms much steeper slopes than either the Bagshot Sand or London Clay.

River Gravel

A small gravel deposit occurs near the catchment exit. It is probably a terrace of the River Meon, formed during the Pleistocene. It is of no great hydrological significance in West Walk.

Table 3.2 West Walk: Percentage Geology

	% London Clay	% Bagshot Beds	% Plateau Gravel	% River Gravel
West Walk	64.73	27.42	7.35	0.50
Subcatchment 1	38.73	42.51	18.761	-
Subcatchment 2	38.00	51.58	10.42	-
Subcatchment 4	79.24	20.76	-	-
Subcatchment 5	100.00	-	-	-

3.4 SOILS

The soils of the catchment are complex owing to the variable lithology of the solid geology, the drift deposits, the variable topographic and drainage conditions, and the great variation in type and age of vegetation. F.F. Kay (1939) published 'A Soil Survey of the Strawberry District of South Hampshire', an area bounded by Southampton in the west, Southampton Water in the south, Wickham in the east, and Swanmore and West End in the north. Although the survey just excludes West Walk some of the soils mapped by Kay are represented there, as shown by the results of a detailed soil survey of the catchment by staff and undergraduates of Portsmouth Polytechnic Geography Department in 1977 and 1978 (about 75 % of the area had been surveyed at the time this was written). After preliminary reconnaissance pits were dug at selected sites and samples taken from each horizon for laboratory analysis. A monolith was also taken from each pit. The following analyses were carried out on selected horizons from each site: particle density; particle size; % organic carbon; exchangeable Na, Ca and Mg; cation exchange capacity; pH and % moisture; Munsell colour was also recorded. Results of the analyses are shown in Appendix 1. These were used, in conjunction with a series of auger holes, to produce the soil map shown in Figure 3.4. The classification is essentially that used by F.F. Kay (1939), i.e. Podsols, Brown Earths and Clays and a description of each type follows.

A. Podsols and Podsolic Soils

These are strongly influenced by geology, i.e. either Plateau Gravel or Bagshot Sand, and a fourfold subdivision has been made. The chief morphological characteristics of the podsols are (after Avery, in Clark, 1940):

(a) the presence of a bleached (grey layer) under the surface raw humus; from which virtually all free iron has been removed by leaching water

(b) the yellow to rusty coloured accumulation layer which follows has a high content of iron and aluminium.

(i) Gravel Podsol

This corresponds with the Southampton Series of Kay (1939) and occurs on the Plateau Gravels (HT: this refers to an example profile given in Appendix 1). Beneath litter (L) and a humus layer about 5 cm deep (H) is the grey eluviated mineral horizon (Ea) comprising gravel and interstitial sand up to about 75 cm depth. Below the Ea horizon is a layer of brown/black translocated organic matter (Bh) 4 to 15 cm deep. Below the Bh horizon is a layer of iron-cemented gravel and sand, orange-brown and grey (B/C) with a gradual transition to yellowish-brown loose sub-angular flints and sand. The whole profile is freely drained, although water may be held up to a certain extent by the indurated B horizons. Acidity is very strong throughout ranging from pH 3.2 to 3.8. The presence of the exchangeable cations is directly related to the quantity of organic matter being highest in the H horizon.

(ii) Sand Podsol

This corresponds with Kay's Shirrell Heath Series and is derived from the Bagshot Beds (LB). The soil is similar to that of the gravel podsol, except in the absence of the sub-angular flints and the weaker induration of the B horizon. In places it contains black rounded flint pebbles inherited from certain pebble beds of the Bagshot Sands. These pebbles are bleached in the A horizons. The dark raw humus H horizon at the surface is underlain by a dark grey humus-stained A_1 layer,

containing bleached sand grains. Below this is a very pale grey sand of variable depth (Ea), although it may reach up to 75 cm. These A horizons tend to be loose and structureless.

Below the E_a lies the dark humus-stained somewhat indurated Bh horizon. It is generally blackish at the top and coffee-coloured below. The humus content is responsible for the cementation but this is not as great as in the gravel podsol. The Bh horizon is undulating in character and generally runs down in pipes into the Bs horizon below. The Bs layer is orange-brown in colour and is somewhat cemented and indurated by the accumulation of sesquioxides from above. Below this lies the parent material, or C horizon, which is generally a coarse yellow-brown sand. The horizons are either strongly acid (pH 4.1 to 4.8) or moderately acid (E_a : pH 5.5). Exchangeable cations are present in highest amounts in the H layer, with signs of Na, Ca and Mg accumulation in the Bh horizon.

(iii) Podsolic Soil with gravel phase

This has features of types (i) and (ii) with a high proportion of fine sand in the upper layers becoming coarser and more gravelly with depth (PP). It corresponds with Kay's Salisbury Gravelly Fine Sand to Fine Sandy Loam derived from the Plateau Gravel.

The L and A_1 horizons are essentially the same as for (ii) except that the A_1 contains fine sand and silt. This fine sand is also present in the Ea layer although gravel has increased to 13 %. The indurated B layer contains 67 % coarse sand and 20 % gravel, the latter increasing to 41 % in the C horizon. Acidity increases down profile from pH 5.6 in the A_1 layer to pH 4.2 in the B layer, falling slightly to pH 4.4 in the C layer. Conversely the quantities of exchangeable cations generally decrease down profile with slight accumulations in the B horizon.

(iv) Podsolic Soil with Fe/sesquioxide accumulation and/or gleying at depth

This is intermediate between the gravel podsol and the podsolic soil with gravel phase. Kay describes this as a podsolised/gley soil derived from Bagshot and Bracklesham Beds. Its nearest equivalent is

the Netley Sand to Fine Sand. The example (NW) showed both the gravel and find sand contents to remain high throughout the profile. However the lower layer, (Eb (B)) browner in colour than the grey Eb (A), showed a decrease in gravel and an increase in fine sand and silt. The major difference between this soil and the other podsols in the catchment is the presence of a clay accumulation in the B horizon, that is between about 40 and 70 cm depth. Bluish mottles indicate occasional gleying. Exchangeable cation contents increase significantly in this Btg layer. The whole profile is strongly acid (pH 4.2 to 4.3) although the upper Eb layer is very strongly acid (pH 3.9).

B. Brown Earth Soils

A fourfold sub-division has been made depending upon the proportions of sand and clay and whether gleying or clay/sesquioxide accumulation occurs at depth. There are three distinct characteristics which form the basic definition of brown earths (Avery, in Clarke, 1940):

(a) the soil has free drainage throughout the profile

(b) there is no vertical differentiation of silica and sesquioxides in the clay fraction

(c) there is no natural free $CaCO_3$ in the soil horizon.

Other morphological and chemical features may vary; thus the soil may be of any colour, but this colour is more or less uniform throughout the profile; the degree of acidity may vary widely. A division is usually made into soils of low and high base status.

(i) Gravel-phase sandy brown earth

This is represented by a small area within SC1. No pits were dug and no detailed sedimentological or chemical information is available.

Its nearest equivalent in Kay's classification is the Warsash Gravelly Loamy Sand which is derived from the Plateau Gravel. In West Walk however the soil is thicker with a layer of grey-brown flinty loamy sand, 30 cm deep, overlying a brown gravel of sub-angular flints.

(ii) Sandy brown earth with gleying at depth

This is equivalent to Kay's Bursledon Fine Sandy Loam (GM) and is derived from non-calcareous sands of the Bagshot Beds. The A horizon is a grey to pale brown fine sandy loam, stoneless and structureless becoming stiffer with depth. It becomes darker brown in the B horizon and shows slight drainage impedance towards the base of the layer, as indicated by occasional grey and reddish-yellow mottlings. Demarcation between horizons is generally very indistinct. The soil appears moderately alkaline (pH 8.5 - 8.8) for the first 3 cm, this probably being due to the presence of bases from leaf litter. The soil is slightly alkaline from 3 to 15 cm, then becoming strongly acid (pH 4.8). Cation exchange capacity contradicts the pH trend, total CEC increasing with depth, and some doubt must be placed upon these chemical analyses.

(iii) Clayey gravel-phase brown earth

This has no direct equivalent in Kay's classification. It occurs on south-west facing slopes at the head of the catchment where gravel and sand has moved downslope from the Bagshot Beds and Plateau Gravel (JA). Below the H humus layer is a dark coloured horizon about 5 cm thick containing humus and mineral matter. From 10 to 23 cm there is an orange-brown layer of coarse sand and gravel. The interstitial sandy material gives way to a higher clay and silt fraction after about 23 cm. Here the gravel comprises angular and sub-angular material from the Plateau Gravel, small black rounded flint pebbles and large pieces of indurated sandstone from the Bagshot Beds. Below about 90 cm the C horizon is an orange-yellow silty-clay loam derived from the London Clay. There is also strong catenary development, the gravel and sand deposits being thickest near the base of the valley side and thinning gradually to the divide. This catenary variation is reflected in the exchangeable contents of the soil. Na, K, Ca and Mg all decrease in availability downslope, reaching minimum values throughout the profile at about 15 m from the slope base. Thereafter cation exchange capacities rise dramatically, showing a considerable reservoir in the hydrological contributing area adjacent to the channel. The soil ranges from moderately acid (pH 5.1) to very strongly acid (pH 3.5) although this masks catenary variation. Acidity is highest throughout the soil depth at 15 m and 75 m upslope which inversely

correlates with the availability of exchangeable cations. In general high acidity and low exchangeable cations are associated with the maximum depth of sand and gravel about 15 m upslope. Conversely, lower acidity and high exchangeable cations are found at the base of the slope in association with higher clay contents.

(iv) Clavey-brown earth with clay-sesquioxide and/or gleying at depth

Again this sub-type has no direct equivalent in Kay's classification. It covers areas of the middle and lower catchment (SB/SC) and has some within-sub-type variability of physical and chemical properties. Below the H layer there is a grey-brown B layer of variable depth composed predominantly of clay and silt, although percentages of fine and coarse sand increase with proximity to the Bagshot Beds. The B/C layer is characterised by either:

(i) reddish-brown and grey mottling, and grey ped faces due to occasional waterlogging; the extent of this gleying depends on the duration of waterlogging;

or, (ii) accumulation of translocated clay and sesquioxides.

Cation exchange capacity depends upon the amount of humus and clay present, usually decreasing with depth, but increasing towards B/C layers.

Acidity follows this trend, increasing slightly with depth (moderately acid, increasing from pH 5.5 to 5.3 in profile SC) but decreasing in the B/C layers (slightly acid, pH 6.6). There is also a general tendency for acidity to decrease away from the Bagshot Beds as the percentage sand decreases.

C. Gleyed Soils

These represent soils in which the profile morphology reflects periodic waterlogging. Where pore or ped spaces are filled by water containing dissolved organic substances, reduction and solution or iron compounds occurs with the aid of anaerobic bacteria. The evidence of gleying is the presence of bluish-grey rusty or yellowish spots or

mottling. Two types of gley soils are present.

(i) Ground Water Gley

This is derived entirely from the upper and more sandy beds of the London Clay or it may occur where there is a wash of Bagshot Sands and/or Plateau Gravels over the London Clay. Drainage is generally free in the upper layers but becomes impeded with depth. This type occurs in the valley bottoms adjacent to the streams and corresponds with Kay's Titchfield Gravelly loam and Swanmore loam to clay-loam, the latter containing a lower percentage of gravel (MJ). The surface soil is a brownish-grey medium to heavy loam, generally rust mottled and structureless with varying proportions of gravel. Below, the soil passes into clay loam and then clay, which is grey and orange-mottled in colour. Exchangeable contents vary with the percentage clay content; that is, relatively high in the A horizon, lower in the Ag, but higher again in the G layer. Acidity increases with depth from pH 5.26 at 6 cm to pH 4.9 at 45 cm.

(ii) Surface Water Gley

This is restricted to a small area of sub-catchment 1 where water appears to seep from a flat area just below the Bagshot Beds. No detailed profile analysis is available.

The ten soil types described are the result primarily of superficial and solid geology, as emerges from Figure 3.4. Past climatic conditions have probably influenced the re-distribution of these deposits, particularly downslope by freeze-thaw processes, and profile development. Vegetation provides varying degrees of shelter and supplies nutrients and organic matter, while topography partly controls aspect and soil drainage.

3.5 VEGETATION

The vegetation of West Walk is mainly represented by planted tree species with considerable variation in age. The oldest trees are Oaks (Quercus robur), the only remnants within the catchment of the post-Napoleonic replanting of the Forest of Bere. These, planted in 1828, are situated near the catchment outlet (see Figure 3.5). Replanting

mottling. Two types of gley soils are present.

(i) Ground Water Gley

This is derived entirely from the upper and more sandy beds of the London Clay or it may occur where there is a wash of Bagshot Sands and/or Plateau Gravels over the London Clay. Drainage is generally free in the upper layers but becomes impeded with depth. This type occurs in the valley bottoms adjacent to the streams and corresponds with Kay's Fitchfield Gravelly loam and Swanmore loam to clay-loam, the latter containing a lower percentage of gravel (MJ). The surface soil is a brownish-grey medium to heavy loam, generally rust mottled and structureless with varying proportions of gravel. Below, the soil passes into clay loam and then clay, which is grey and orange-mottled in colour. Exchangeable contents vary with the percentage clay content; that is, relatively high in the A horizon, lower in the Ag, but higher again in the G layer. Acidity increases with depth from pH 5.26 at 6 cm to pH 4.9 at 45 cm.

(ii) Surface Water Gley

This is restricted to a small area of sub-catchment 1 where water appears to seep from a flat area just below the Bagshot Beds. No detailed profile analysis is available.

The ten soil types described are the result primarily of superficial and solid geology, as emerges from Figure 3.4. Past climatic conditions have probably influenced the re-distribution of these deposits, particularly downslope by freeze-thaw processes, and profile development. Vegetation provides varying degrees of shelter and supplies nutrients and organic matter, while topography partly controls aspect and soil drainage.

3.5 VEGETATION

The vegetation of West Walk is mainly represented by planted tree species with considerable variation in age. The oldest trees are Oaks (Quercus robur), the only remnants within the catchment of the post-Napoleonic replanting of the Forest of Bere. These, planted in 1828, are situated near the catchment outlet (see Figure 3.5). Replanting

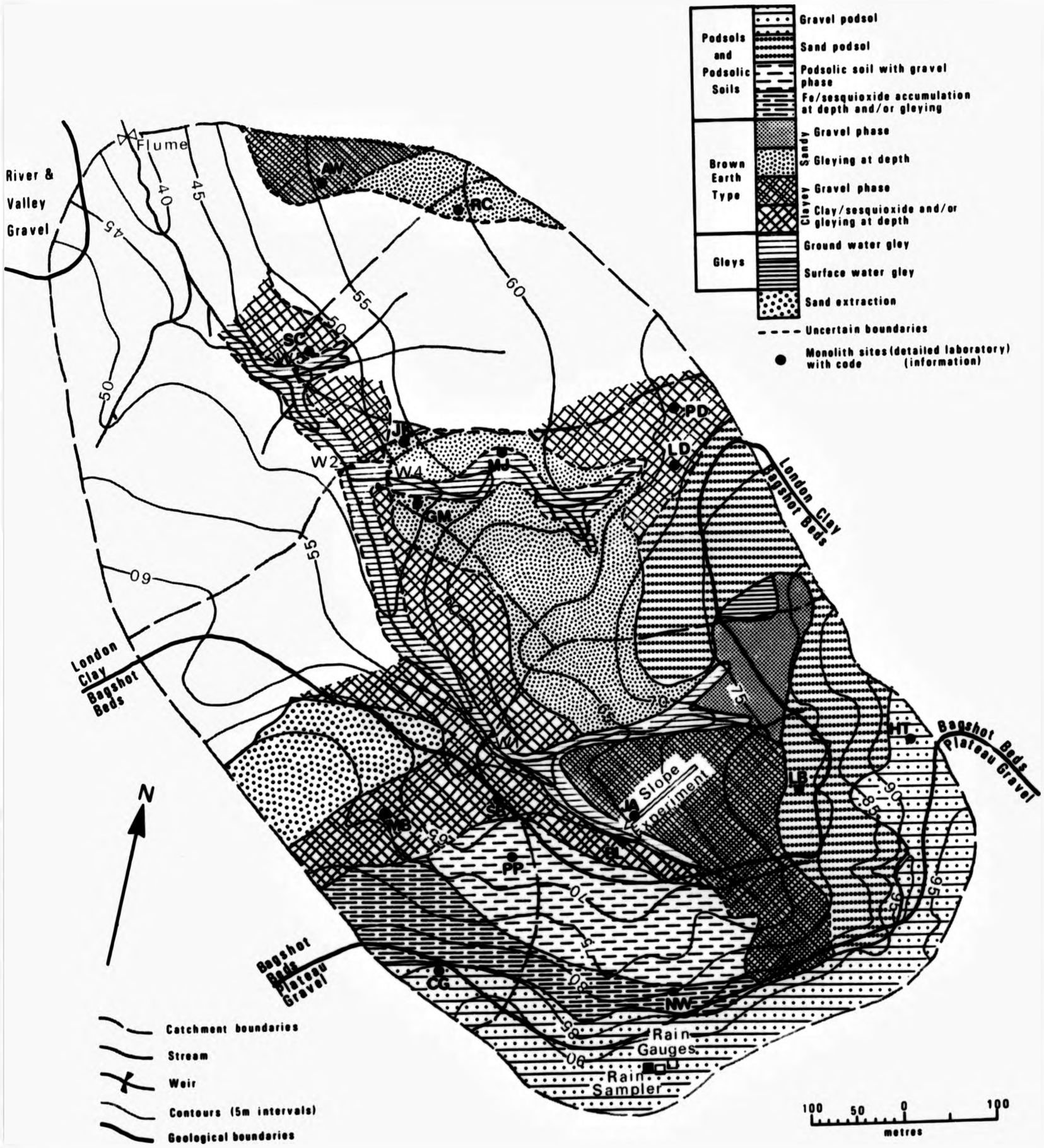

FIGURE 3.4: WEST WALK CATCHMENT GEOLOGY AND SOILS

between 1928 and 1936 is now represented only by isolated stands of Oak, Scots Pine (Pinus sylvestris) and Corsican Pine (Pinus nigra var. corsicana) on the Forestry Commission land. Little change occurred between the mid-1930's and 1969's, apart from the planting of Corsican Pine (1946) and Norway Spruce (Picea abies), Japanese Larch (Larix leptolepis) and Oak (1955) by the Forestry Commission. The period 1960 - 1975 was a time of considerable change in West Walk. Clearance of the mature oak stands and replacement with quicker growing Western Hemlock (Tsuga heterophylla) and Corsican Pine notably in the lower part of West Walk, exemplified the Forestry Commission's accent on economic management. The Rookesbury Estate also placed an emphasis on economic land use at that time, not only replanting but later (1975) leasing part of the catchment for sand extraction. While the private estate maintains a policy of commercial land management, the Forestry Commission have recently begun to place greater emphasis upon planting for recreational and amenity purposes. Large plantations of Oak and Japanese Larch (1972 - 1973), blended with older species in the centre of West Walk, exemplify this policy.

In addition to the planted species, Birch (Betula verrucosa) grows naturally over much of the catchment, although mainly in the valley bottoms. A considerable ground flora also exists with bracken (Pteridium aquilinum), subordinate bramble (Rubus sp.) and grasses (mainly Agrostis sp.) on the drier slopes and rushes (Juncus sp.) near the stream channels.

The age and maturity of the tree species within West Walk can be expected to influence the hydrological and hydrochemical response of West Walk. Clearly the more mature the cover the greater the interception and stemflow times and hence the slower the channel response. This factor also varies seasonally depending on whether the trees are evergreen or deciduous. The amount of evapotranspiration also depends upon the type and maturity of the species and therefore affects the water balance.

The vegetation participates in the circulation of nutrients and hence the hydrochemistry. Nutrients are taken up from the soil in solution and returned in the form of leaf litter, twigs and branches.

As the litter decomposes throughfall leaches the nutrients and carries them into the soil, although the amounts depend upon the intensity of throughfall, which in turn depends upon the density and species. i.e. evergreen or deciduous. Throughfall and stemflow themselves contribute nutrients to the soil surface, the amount of these depending upon the tree species and the time of year (Madgwick and Ovington, 1959). The considerable species diversity at West Walk together with the wide range in age and maturity might be expected to produce considerable spatial and temporal variation in the nutrient content of throughfall and leaf litter. Clearly a simple division into sub-catchments with uniform age and species is difficult.

The age structures for the main tree species at West Walk are shown in Figure 3.6. This shows that Oak is the dominant tree species with 18.33 % planted since 1968. Interception in these young plantations is likely to be low and infiltration higher (Oak matures relatively slowly when compared with, say, Western Hemlock). Western Hemlock covers 14.5 % of the catchment and forms a dense, mature cover over part of the lower catchment. By isolating sub-catchments 4 and 5 as shown in Figure 3.5, catchments with high proportions of a single age and species are identified. Four year old Oak dominates SC4 (50 %) and sixteen year old Western Hemlock dominates SC5 (82.9 %) giving an interesting contrast in type (deciduous/evergreen) and probable interception losses (Figure 3.6). Since definition of other nearly homogenous areas is very difficult there is some benefit in dichotomising into either evergreen or deciduous species when considering seasonal variations in throughfall.

3.6 CLIMATE

Although only rainfall data is available for West Walk considerable climatological data is available for the Portsmouth area and some generalised comments are possible.

The catchment has a near-coastal location which would produce relatively mild temperatures when taken in the British Isles context. The mean annual temperature (1931 - 1960) for Southsea Common (2 m OD) is given as 11.1°C, with equivalent maximum and minimum values of 14.2°C and 7.9°C respectively (Harrison, 1976). Temperature differences

As the litter decomposes throughfall leaches the nutrients and carries them into the soil, although the amounts depend upon the intensity of throughfall, which in turn depends upon the density and species. i.e. evergreen or deciduous. Throughfall and stemflow themselves contribute nutrients to the soil surface, the amount of these depending upon the tree species and the time of year (Madgwick and Ovington, 1959). The considerable species diversity at West Walk together with the wide range in age and maturity might be expected to produce considerable spatial and temporal variation in the nutrient content of throughfall and leaf litter. Clearly a simple division into sub-catchments with uniform age and species is difficult.

The age structures for the main tree species at West Walk are shown in Figure 3.6. This shows that Oak is the dominant tree species with 18.33 % planted since 1968. Interception in these young plantations is likely to be low and infiltration higher (Oak matures relatively slowly when compared with, say, Western Hemlock). Western Hemlock covers 14.5 % of the catchment and forms a dense, mature cover over part of the lower catchment. By isolating sub-catchments 4 and 5 as shown in Figure 3.5, catchments with high proportions of a single age and species are identified. Four year old Oak dominates SC4 (50 %) and sixteen year old Western Hemlock dominates SC5 (82.9 %) giving an interesting contrast in type (deciduous/evergreen) and probable interception losses (Figure 3.6). Since definition of other nearly homogenous areas is very difficult there is some benefit in dichotomising into either evergreen or deciduous species when considering seasonal variations in throughfall.

3.6 CLIMATE

Although only rainfall data is available for West Walk considerable climatological data is available for the Portsmouth area and some generalised comments are possible.

The catchment has a near-coastal location which would produce relatively mild temperatures when taken in the British Isles context. The mean annual temperature (1931 - 1960) for Southsea Common (2 m OD) is given as 11.1°C, with equivalent maximum and minimum values of 14.2°C and 7.9°C respectively (Harrison, 1976). Temperature differences

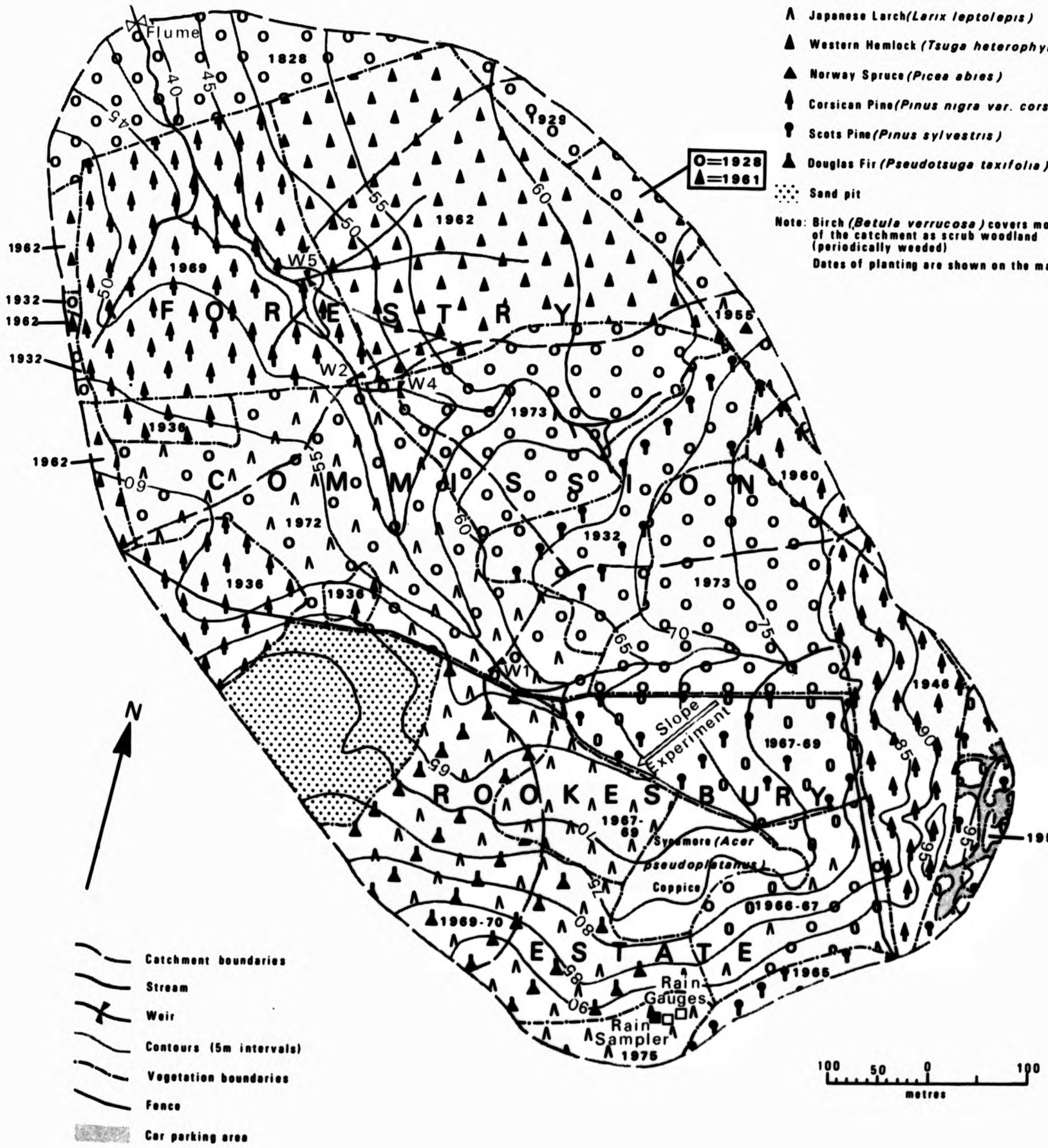

FIGURE 3.5: WEST WALK
MAJOR TREE SPECIES

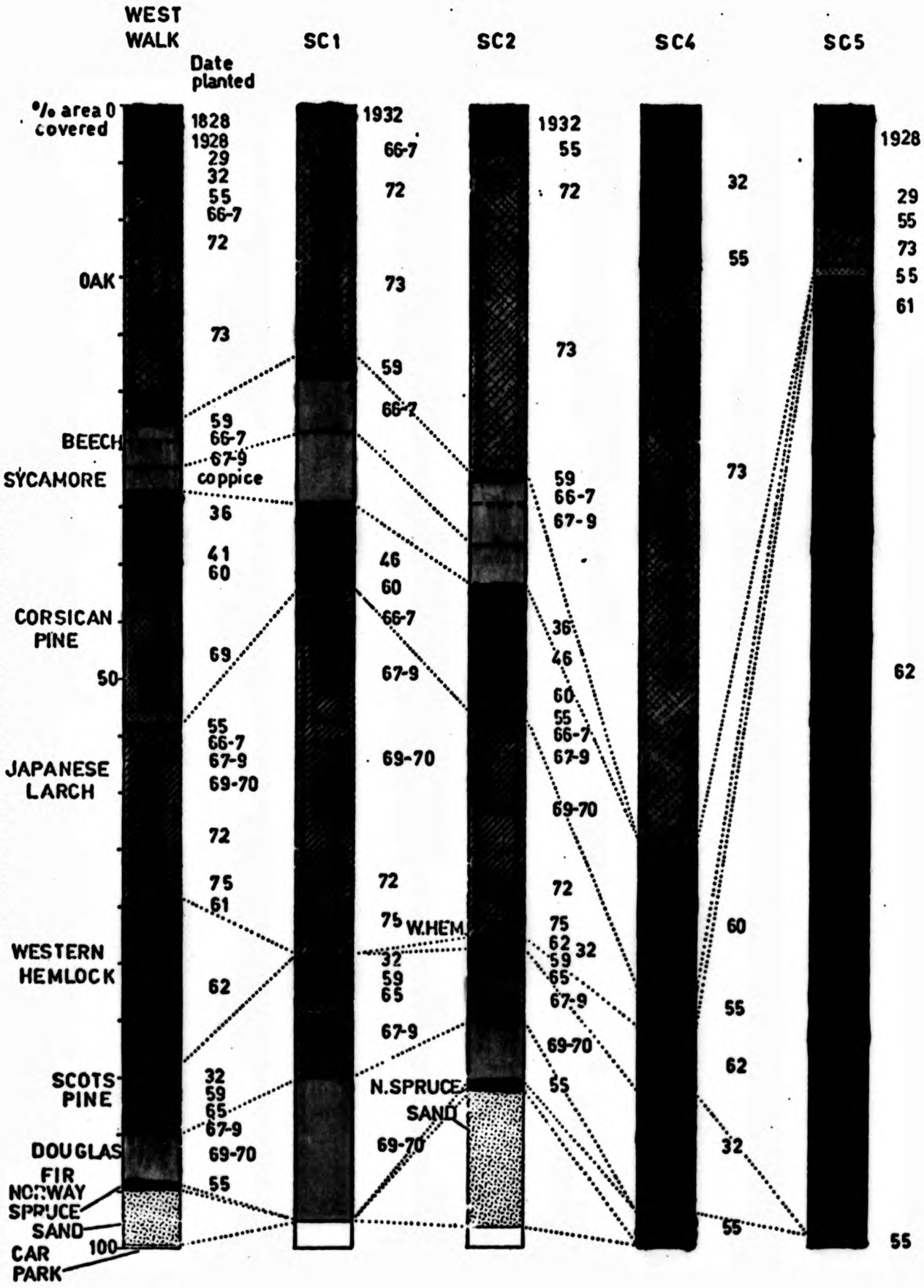

FIGURE 3.6: WEST WALK: LAND USE AND VEGETATION AGE STRUCTURE
(Dark green - greater than 10 years old;
light green - less than 10 years old, in 1976)

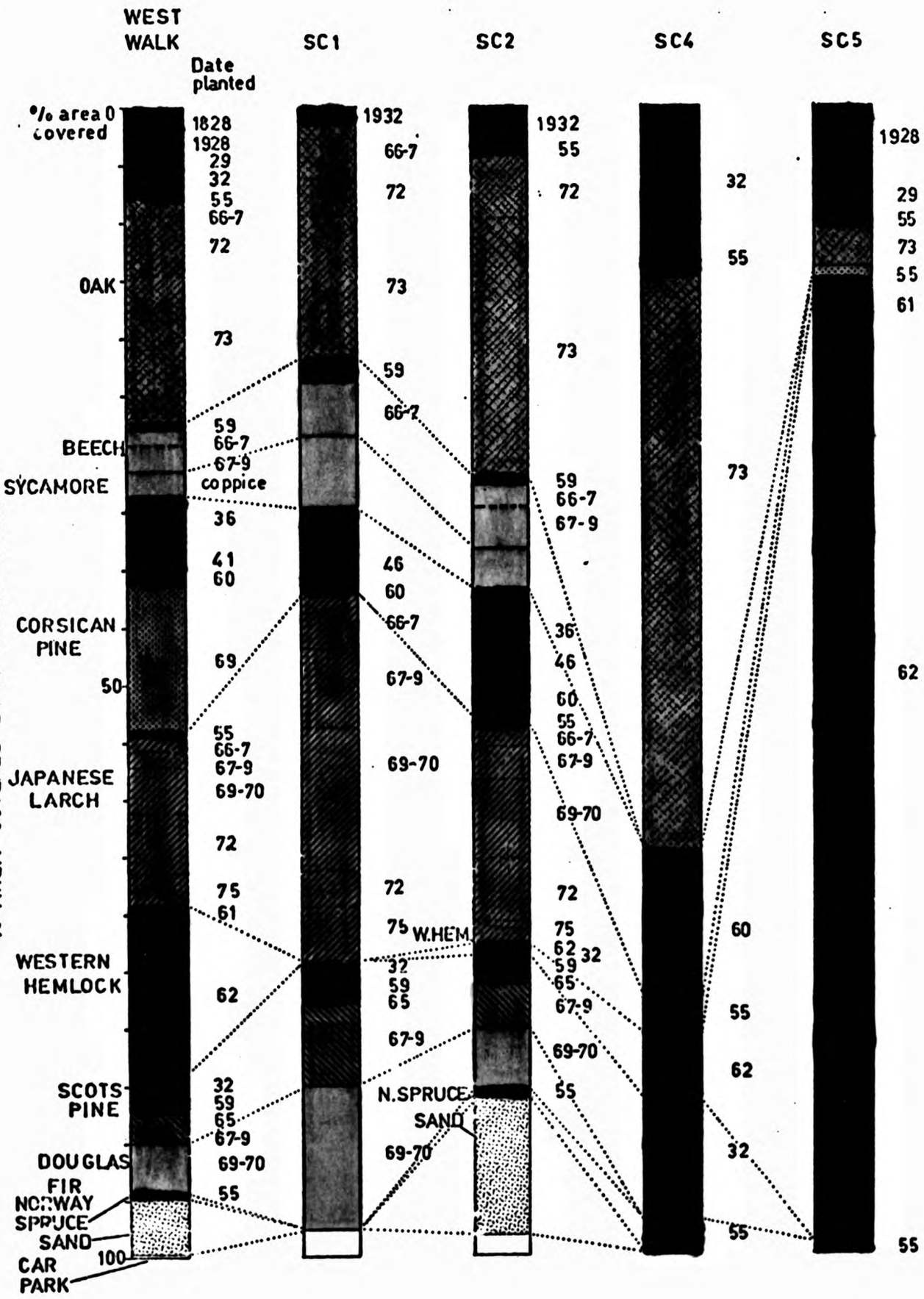

FIGURE 3.6: WEST WALK: LAND USE AND VEGETATION AGE STRUCTURE

(Dark green - greater than 10 years old;
light green - less than 10 years old, in 1976)

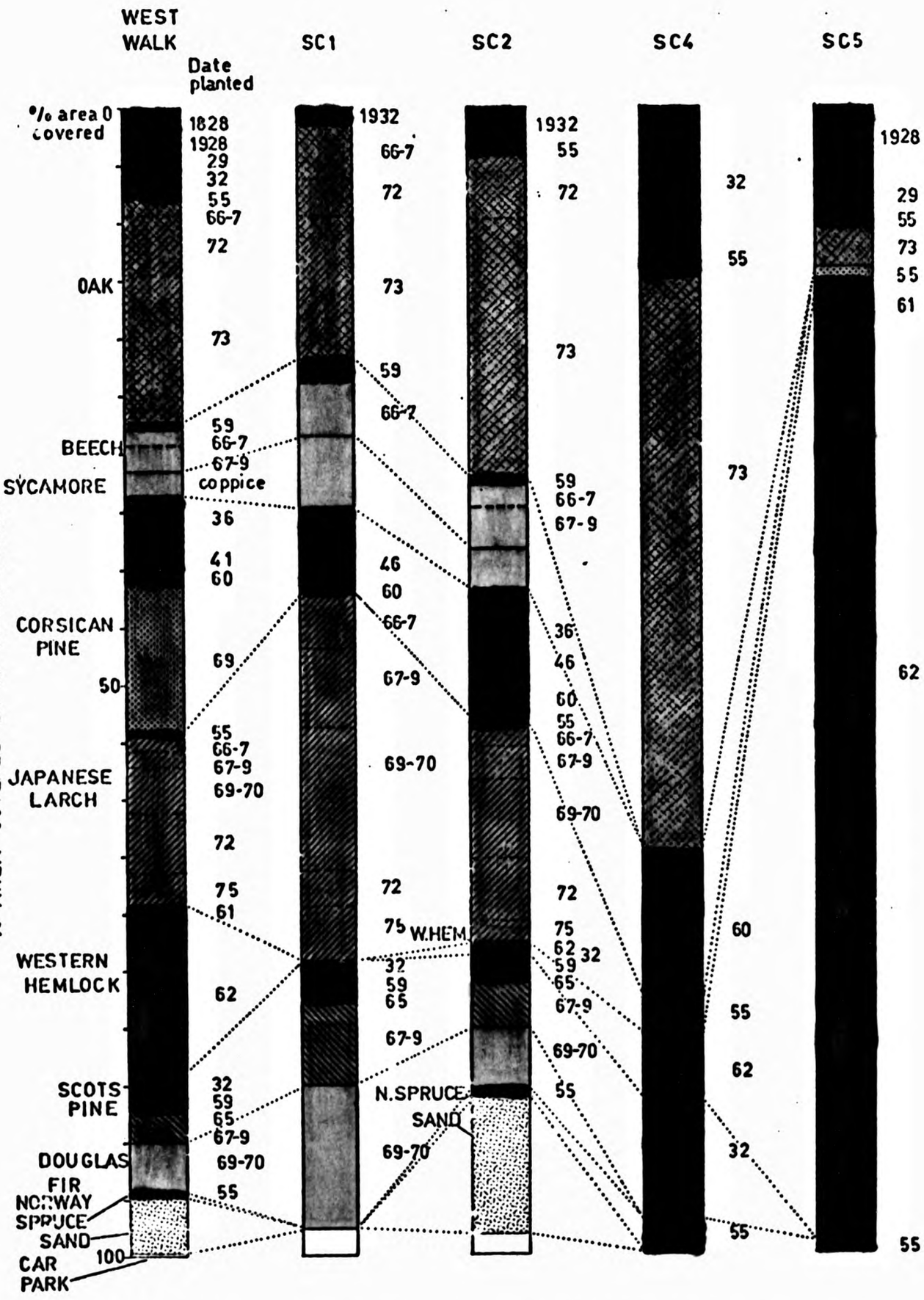

FIGURE 3.6: WEST WALK: LAND USE AND VEGETATION AGE STRUCTURE

(Dark green - greater than 10 years old;
light green - less than 10 years old, in 1976)

have been found between Southsea Common and an inland site (Butser Hill 268 m OD) which suggest mean lapse-rates of 10.5°C and 7.8°C per 1000 m increase in elevation. These are far in excess of the commonly adopted lapse-rate in mean temperature of 6.5°C per 1000 m (Harrison, ibid) and suggest that the mean annual maximum and minimum temperatures for the top of West Walk might be given as 13.3°C and 7.2°C respectively. Such figures could not be expected to apply to the whole catchment, since microclimate would vary with the vegetation cover. Short term differences might also include an inversion effect with higher temperatures at the head of the catchment than at the exit.

Cloudiness is important in calculating evaporation and hence the water balance for a catchment. There is an eastwards decrease in hours of sunshine along the south coast, Southsea having a daily mean of 4.8 hours (1931 - 1960 average) with a monthly maximum of 7.85 hours in June and minimum of 1.78 in December (Harrison, ibid).

The annual distribution of wind direction for Thorney Island immediately east of Southsea shows that 58 % of the recordings at 0900 GMT fall between 200° and 340°, a figure which compares very closely with other south of England stations and emphasises the westerly component of airflow (Atlas of Portsmouth, 1975; Harrison, ibid). This is particularly interesting because a high proportion of the catchment faces between 200° and 315°. The dominance of the westerly winds also serves to increase the amount of sodium chloride in rainfall.

The early 1970's has been a period of drier than average years and this can be shown by reference of annual totals to the long term annual mean for Southsea Common (Table 3.3). Only 1974 and 1977 temporarily reversed the trend towards drier than average conditions.

Table 3.3: Deviation of Annual Rainfall from the 1916 - 1950 Average for Southsea Common (705.6 mm)

	1972	1973	1974	1975	1976	1977
Cumulative Deviation	- 144.2	- 223.2	+ 183.4	- 41.3	- 137	+ 30.2

Rainfall data are available for West Walk between 1975 and 1977, three very dry years which are not representative of long term conditions. Harrison (ibid) suggests that annual rainfall increases by 150 mm for every 100 metres elevation giving West Walk an estimated long term mean annual total of 837.6 mm. The mean annual figure for the period 1975 - 1977 (heavily biased by the 1975 - 1976 drought) is 760.5 mm, and the monthly figures are shown in Figure 4.15 (Chapter 4). This clearly shows how actual monthly rainfall fell below the estimated mean monthly totals from October 1975 until October 1976, when twice the average fell. Low rainfall coupled with high temperatures (from June to August the maximum temperatures for Southsea Common were above 20°C, 79 days out of 92) caused considerable actual evaporation and a high soil moisture to accumulate in West Walk.

West Walk catchment was chosen for research into surface and subsurface solute dynamics in South Hampshire for reasons stated in the introduction. It was hoped that a division into subcatchments would help in studying spatially varying solute response and that an intensively instrumented hillslope experiment would enable modelling of the fundamental mechanisms of solute transport in throughflow. The next chapter outlines the techniques used for water data collection at the catchment scale (rainfall and streamflow), preliminary treatment of the data and describes catchment hydrology during the period of study (July 1975 to June 1977).

have been found between Southsea Common and an inland site (Butser Hill 268 m OD) which suggest mean lapse-rates of 10.5°C and 7.8°C per 1000 m increase in elevation. These are far in excess of the commonly adopted lapse-rate in mean temperature of 6.5°C per 1000 m (Harrison, ibid) and suggest that the mean annual maximum and minimum temperatures for the top of West Walk might be given as 13.3°C and 7.2°C respectively. Such figures could not be expected to apply to the whole catchment, since microclimate would vary with the vegetation cover. Short term differences might also include an inversion effect with higher temperatures at the head of the catchment than at the exit.

Cloudiness is important in calculating evaporation and hence the water balance for a catchment. There is an eastwards decrease in hours of sunshine along the south coast, Southsea having a daily mean of 4.8 hours (1931 - 1960 average) with a monthly maximum of 7.85 hours in June and minimum of 1.78 in December (Harrison, ibid).

The annual distribution of wind direction for Thorney Island immediately east of Southsea shows that 58 % of the recordings at 0900 GMT fall between 200° and 340°, a figure which compares very closely with other south of England stations and emphasises the westerly component of airflow (Atlas of Portsmouth, 1975; Harrison, ibid). This is particularly interesting because a high proportion of the catchment faces between 200° and 315°. The dominance of the westerly winds also serves to increase the amount of sodium chloride in rainfall.

The early 1970's has been a period of drier than average years and this can be shown by reference of annual totals to the long term annual mean for Southsea Common (Table 3.3). Only 1974 and 1977 temporarily reversed the trend towards drier than average conditions.

Table 3.3: Deviation of Annual Rainfall from the 1916 - 1950 Average for Southsea Common (705.6 mm)

	1972	1973	1974	1975	1976	1977
Cumulative Deviation	- 144.2	- 223.2	+ 183.4	- 41.3	- 137	+ 30.2

Rainfall data are available for West Walk between 1975 and 1977, three very dry years which are not representative of long term conditions. Harrison (ibid) suggests that annual rainfall increases by 150 mm for every 100 metres elevation giving West Walk an estimated long term mean annual total of 837.6 mm. The mean annual figure for the period 1975 - 1977 (heavily biased by the 1975 - 1976 drought) is 760.5 mm, and the monthly figures are shown in Figure 4.15 (Chapter 4). This clearly shows how actual monthly rainfall fell below the estimated mean monthly totals from October 1975 until October 1976, when twice the average fell. Low rainfall coupled with high temperatures (from June to August the maximum temperatures for Southsea Common were above 20°C, 79 days out of 92) caused considerable actual evaporation and a high soil moisture to accumulate in West Walk.

West Walk catchment was chosen for research into surface and subsurface solute dynamics in South Hampshire for reasons stated in the introduction. It was hoped that a division into subcatchments would help in studying spatially varying solute response and that an intensively instrumented hillslope experiment would enable modelling of the fundamental mechanisms of solute transport in throughflow. The next chapter outlines the techniques used for water data collection at the catchment scale (rainfall and streamflow), preliminary treatment of the data and describes catchment hydrology during the period of study (July 1975 to June 1977).

SECTION 2

SURFACE WATER SOLUTE DYNAMICS IN WEST WALK

CHAPTER 4: WATER DATA COLLECTION AND PRELIMINARY TREATMENT

CHAPTER 5: TECHNIQUES USED IN THE SAMPLING AND ANALYSIS OF WATER

CHAPTER 6: AN ANALYSIS OF SURFACE WATER SOLUTE DYNAMICS IN WEST WALK CATCHMENT:
I: THE REGULARLY SAMPLED DATA (RSD)

CHAPTER 7: AN ANALYSIS OF SURFACE WATER SOLUTE DYNAMICS IN WEST WALK CATCHMENT:
II: THE STORM SAMPLE DATA (SSD)

CHAPTER 8: THE SOLUTE BUDGET

CHAPTER 4

WATER DATA COLLECTION AND PRELIMINARY TREATMENT

4.1 INTRODUCTION

Rainfall and streamflow are agents of transportation of dissolved substances which form the input to and output from the catchment system. Their continuous measurement through time achieves high importance in the modelling of solute response, understanding of solute behaviour and computation of catchment solute budgets.

4.2 STREAMFLOW GAUGING

The locational requirements for measurements of streamflow have been discussed in the previous chapter (see Figure 3.1). Suitable channel sections were chosen, surveyed and channel roughness assessed. During the winter and early spring of 1973 - 1974 maximum water levels were obtained using crest-stage gauges similar to those described by K.J. Gregory and D.E. Walling (1971).

Table 4.1: Survey Data for Structure Design at West Walk

Structure	Gradient 1 : x	Manning's n	Hydraulic Radius m	Q l/s	*QMAX l/s
SC1	18.88	0.025	0.054	52	116
SC2	37.65	0.035	0.097	130	274
West Walk	26.65	0.035	0.106	134	420
SC4	30.2	0.035	0.058	25	53
SC5	28.17	0.035	0.067	20	51

* See equation (4.1)

These data were used to compute the corresponding approximate channel discharge by the Manning equation as shown in Table 4.1. Inaccuracy may stem from the visual estimation of the value of 'n' (Powell, 1979).

At this stage the probability of these values being exceeded during the period of study was unknown, so a comparison was made with 'peak' discharges computed from the equation,

$$Q_{MAX} = 0.7016\ A \qquad (4.1)$$

where Q = discharge (l/s)
A = catchment area (km^2)

This equation was used by the then Hampshire River Authority for predicting peak flows from small clay catchments; it was likely to over-estimate flows for a forested catchment such as West Walk. Values obtained by the method are much in excess of those estimated by the Manning equation. The ability of a structure accurately to measure the lower range of flows is also very important, since these comprise a high percentage of the flow duration curve. Estimation of low flows was not possible for West Walk due to a lack of data. The high percentage of London Clay however, together with forest cover, seemed likely to produce low flows during late summer and early autumn. This assumption was confirmed during the 1976 drought when flow from the catchment ceased completely. The measurement of channel flows over a large range of discharge was a problem. However it was decided to construct a series of V-notch weirs for the sub-catchments and a critical depth flume for the main catchment outlet.

A. West Walk: Rectangular-throated Flume

(a) Design and Construction

Several types of structure were considered for the complete West Walk catchment. Amongst these the favourites were the trapezoidal and rectangular-throated flumes. The former is particularly suited to large installations where it is desired to measure a wide flow range. The rectangular-throated flume is appropriate for use in small and medium size installations, without a bottom hump where the flow is silt-laden (BS3680, Part 4O, 1974). It was considered that the trapezoidal-throated flume would be more complex to construct and difficult to accommodate in the channel than a rectangular-throated flume.

A rectangular-throated flume without a bottom hump was designed for a Q_{MAX} of 420 l/s and Q_{MIN} of 3.5 l/s. It had the desirable property that large quantities of silt and leaves would not be deposited in the approach section. Design drawings were completed in November 1974 and a decision made to construct the flume from fibreglass reinforced plastic (Figures 4.1, 4.2). This had the advantage of being cheap to build, smooth and hard wearing, and relatively light and easy to install. A male half-mould was constructed from marine-plywood (Figure 4.3); the two halves of the flume were formed separately with a minimum of four laminations. The sides were reinforced with a series of stiffeners (map tubes sliced lengthways) and subsequently glassed in. The halves were bonded at the base and the complete flume cleaned, primed and coated with polyurethane yacht varnish. Eight threaded cross bars were added to the top of the structure to give strength and allow fine width adjustment. The flume was installed in May 1975 together with a Munro vertical drum, continuous chart recorder (modified to take a fibre tip pen) mounted over a concrete stilling-well, with horizontal pipe connection to the flume. Design, construction and installation specifications conform to BS3680 Part 4C, 1974 (see Figures 4.1, 4.2). Concrete was used to seal the upstream join between flume and channel cross-section. The initial zero setting of the recorder was achieved by plumbing the depth from the flume top to the level of the throat and water level, and setting the pen accordingly. Plumbing was undertaken initially at monthly intervals to check for possible settlement and then at intervals of four months.

(b) Discharge Calculation

The basic discharge equation for rectangular-throated flumes is (BS3680 Part 4C, 1974),

$$Q = \left(\frac{2}{3}\right)^{\frac{3}{2}} g\, C_V\, C_D\, b\, h^{\frac{3}{2}} \qquad (4.2)$$

where
$$C_D = \left(1 - 2\,\frac{\delta^*}{L}\,\frac{L}{b}\right)\left(1 - \frac{\delta^*}{L}\,\frac{L}{h}\right)^{\frac{3}{2}} \qquad (4.3)$$

(the coefficient of discharge)

FIGURE 4.1: WEST WALK FLUME: NHE WATER SAMPLER (left), RECORDER BOX ABOVE STILLING WELL (centre), STAGE TRIGGER FOR ACTIVATING NHE SAMPLER (right)

FIGURE 4.1: WEST WALK FLUME: NHE WATER SAMPLER (left), RECORDER BOX ABOVE STILLING WELL (centre), STAGE TRIGGER FOR ACTIVATING NHE SAMPLER (right)

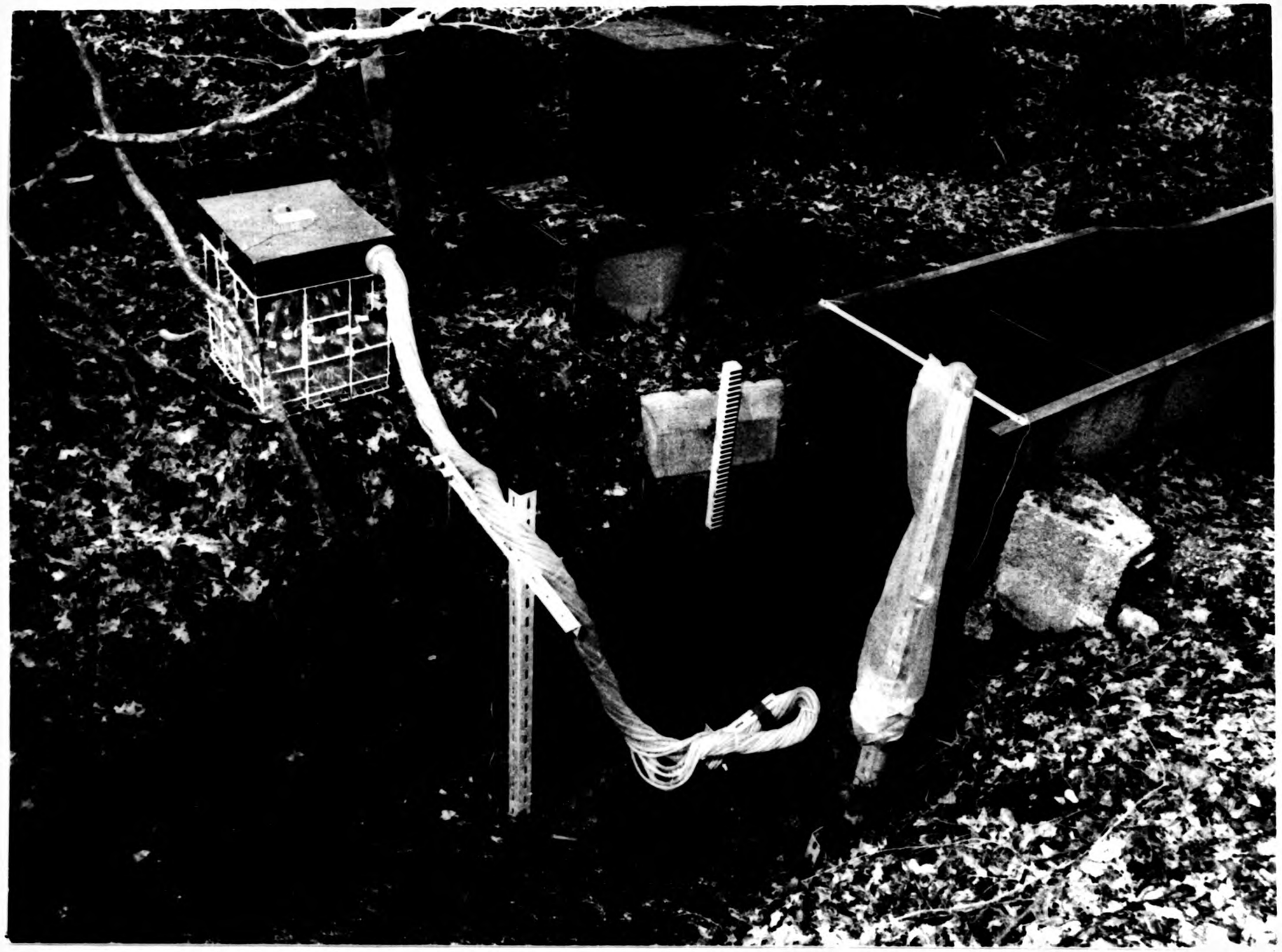

FIGURE 4.1: WEST WALK FLUME: NHE WATER SAMPLER (left), RECORDER BOX ABOVE STILLING WELL (centre), STAGE TRIGGER FOR ACTIVATING NHE SAMPLER (right)

FIGURE 4.2: WEST WALK FLUME: VIEW FROM DOWNSTREAM

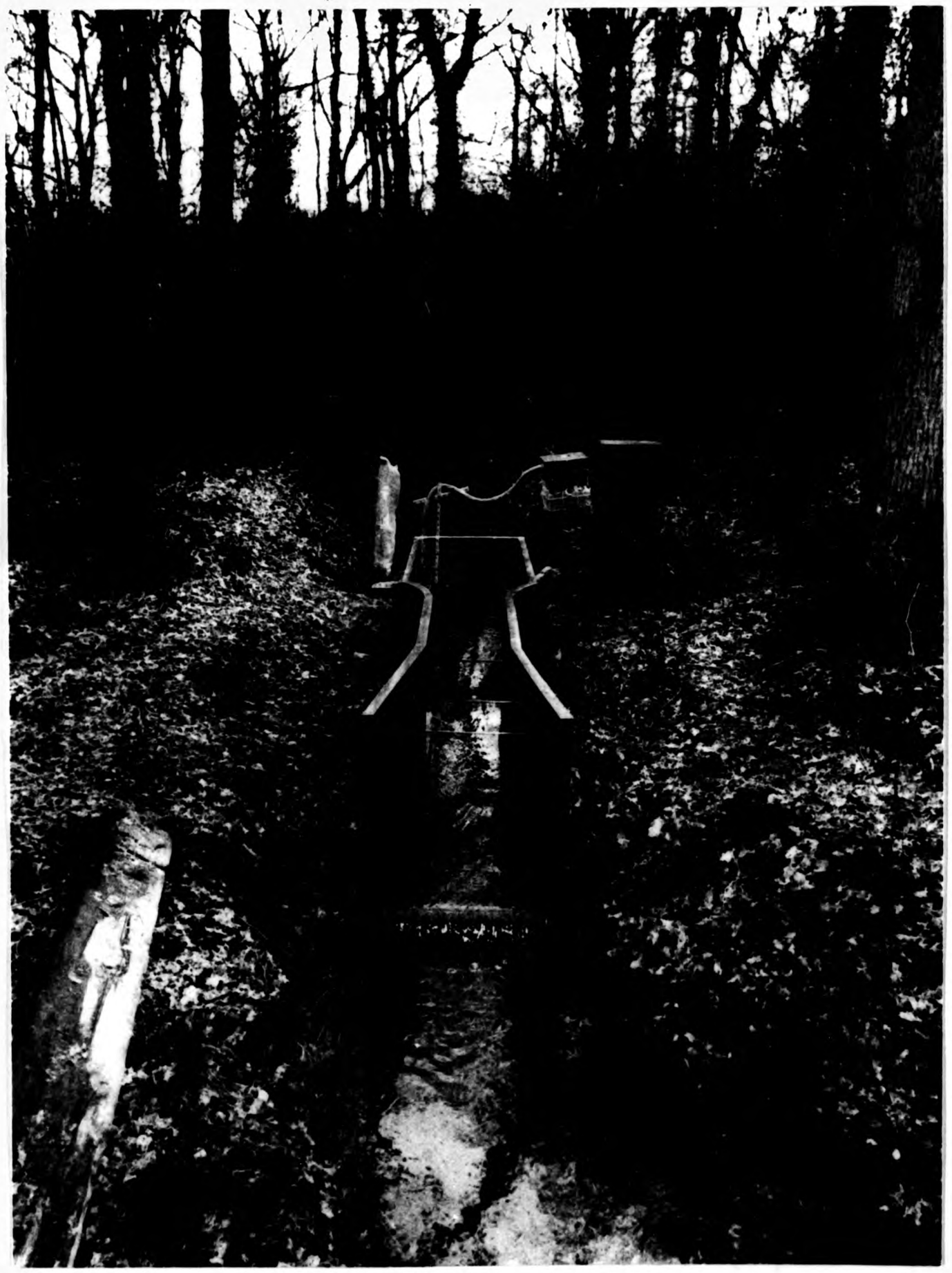

FIGURE 4.2: WEST WALK FLUME: VIEW FROM DOWNSTREAM

FIGURE 4.2: WEST WALK FLUME: VIEW FROM DOWNSTREAM

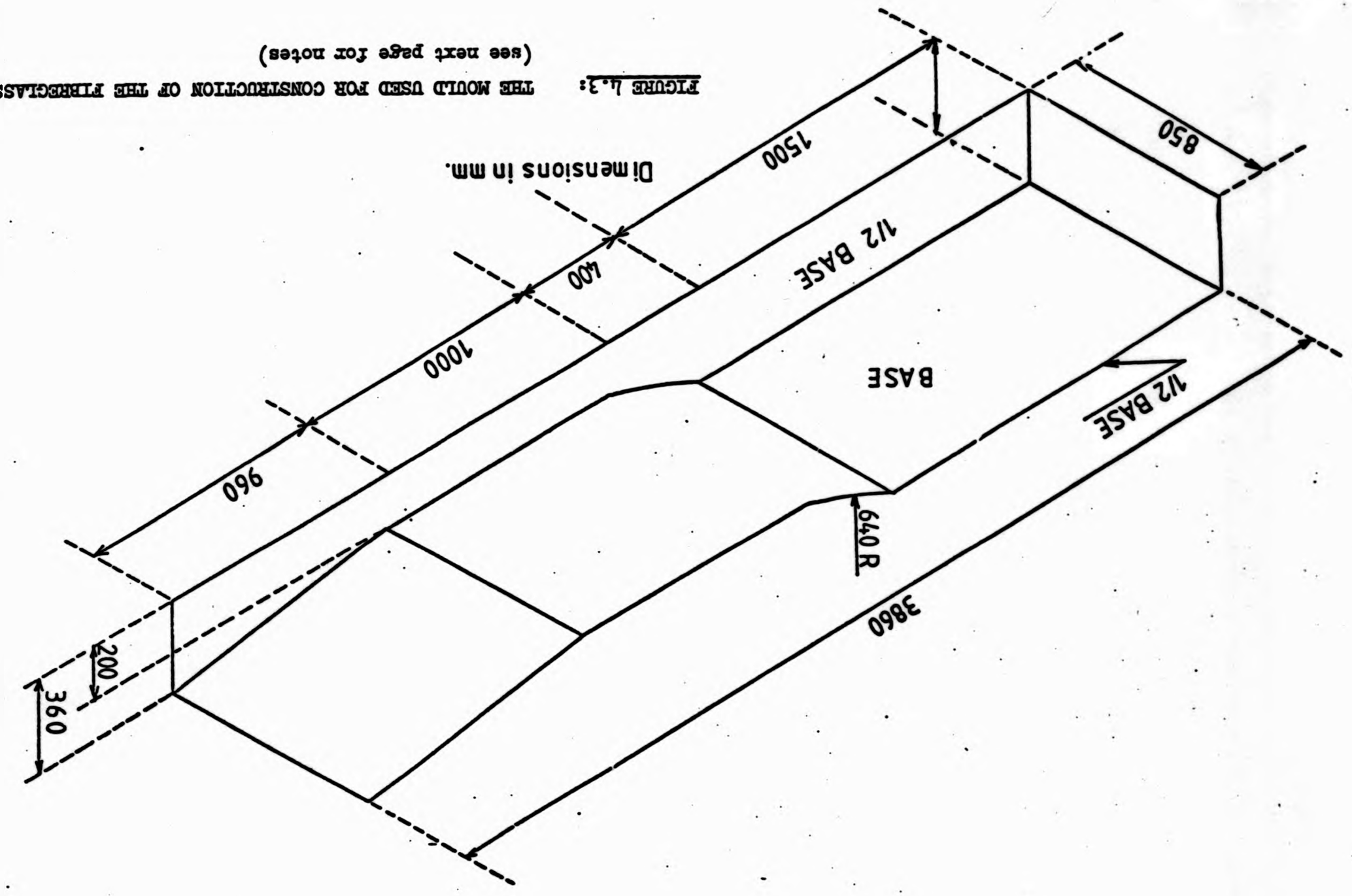

FIGURE 4.3: THE MOULD USED FOR CONSTRUCTION OF THE FIBREGLASS FLUME
(see next page for notes)

FIGURE 4.3

Notes for Figure 4.3

1. Mould: to be manufactured from 9 mm ($\frac{3}{8}$") marine plywood
2. Mould: allow for laying up of left and right hand halves of flume
3. PLY to be screwed to ($1\frac{1}{2}$") sq. pan softwood as necessary
4. Side(s) to be square to base
5. Radii can be laminated to form accurate curve
6. All edges to be kept 'sharp'
7. Half base (one each side) to be kept straight and flat
8. Finished mould to be sanded smooth after filling all joints and screw heads
9. Finished mould to be coated with polyurethane varnish
10. Ends of mould can be filled or left open

where L = length of the prismatic section of the contraction (m)

δ^* = flow boundary displacement due to boundary layer effects (m)

b = width of throat (m)

h = gauged head (m)

g = gravitational acceleration (ms^{-2})

$$(C_V^{\frac{1}{2}} - 1) = \frac{2}{3\sqrt{3}} \frac{(b - 2\delta^*)(h - \delta^*) C_V}{B h} \qquad (4.4)$$

(the coefficient of velocity)

In practice C_V was obtained from Table 1 of BS 3680; with b/B = 0.27 and h/h + p = 1.0, C_V = 1.0169. Particular attention was paid to providing a smooth finish to the flume, achieving a roughness value of K_S = 0.03 mm; thus δ^*/h = 0.003 satisfying the requirement: $10^5 > L/K_S > 4000$, ($L/K_S = 3.3 \times 10^4$) and Reynolds number $> 2 \times 10^5$ (Re = 9.4×10^8 (at 3.5 l/sec) and 2.1×10^9 (420 l/sec) at 20°C); thus,

$$C_D = \left(\frac{b}{b + 0.004L}\right)^{\frac{3}{2}} \cdot \left(\frac{h - 0.003}{h}\right)^{\frac{3}{2}} \qquad (4.5)$$

The theoretical equation for discharge at West Walk flume is therefore,

$$Q = \left(\frac{h - 0.003}{h}\right)^{\frac{3}{2}} \cdot \left\{h\right\}^{\frac{3}{2}} \cdot 0.7308 \quad m^3 s^{-1} \qquad (4.6)$$

Current meter calibration of the flume was undertaken during 1975 and 1976 using an Ott mini-current meter. A stage-discharge relationship is shown in Figure 4.4, with the theoretical line superimposed. During 1976 the flow fell below the design drought of 3.5 l/s and the flow ceased; at these low discharges flow was measured by bolting a $\frac{1}{4}$-90° V-notch weir to the upstream face of the structure (bolts had been built in during construction), recording the head and calculating the discharge by the standard V-notch formula (see later in this chapter). Discharge was also recorded volumetrically, by catching water pouring over the notch in a bucket and making a direct measurement. There

appears to be some deviation from the line in the range 0.04 - 0.06 m, although generally the fit is good; unfortunately no current meter observations were made above h = 0.13 m (36 l/s). To check for a significant difference between field-measured discharges, with the given values of h, and their equivalents calculated by equation 4.6, a Kolmogorov-Smirnov test was used (Siegel, 1956; p. 27). This showed no difference between the two data sets, actual and calculated, thus upholding use of the theoretical equation. The null hypothesis was that no significant difference existed between the two distributions (Ho). A maximum difference, D_{MAX} of at least 10 was required to establish a significant difference at the 1 % level. Since the $D_{MAX} = 3$ the null hypothesis (Ho) was accepted.

(c) Assessment of Errors in gauging

The 'error' is defined as the difference between the actual rate of flow and that calculated in accordance with equation (4.6). 'Tolerance' is defined as the deviation from the true rate of flow within which the measured flow is expected 95 times out of 100 (BS3680 Part 4C, 1974). The tolerance is estimated with a combination of errors from the various sources; full details are given in BS 3680 (ibid).

Tolerance on the flow rate is calculated from,

$$X = \pm (X_c^2 + \gamma^2 X_b^2 + \phi^2 X_h^2) \qquad (4.7)$$

where
X_c = % error in $C_V C_D$
X_b = % error in b
X_h = % error in h
γ = 1.0 for a rectangular throated flume
ϕ = a coefficient

$$X_c = \pm 1 + 20 (C_V - C_D) \% \qquad (4.8)$$

$$X_b = 100 (e_b/b) \qquad (4.9)$$

$$X_h = \frac{100 (e_{h1}^2 + e_{h2}^2 + e_z^2 \ldots + 2\sigma_m)^{\frac{1}{2}}}{h}$$

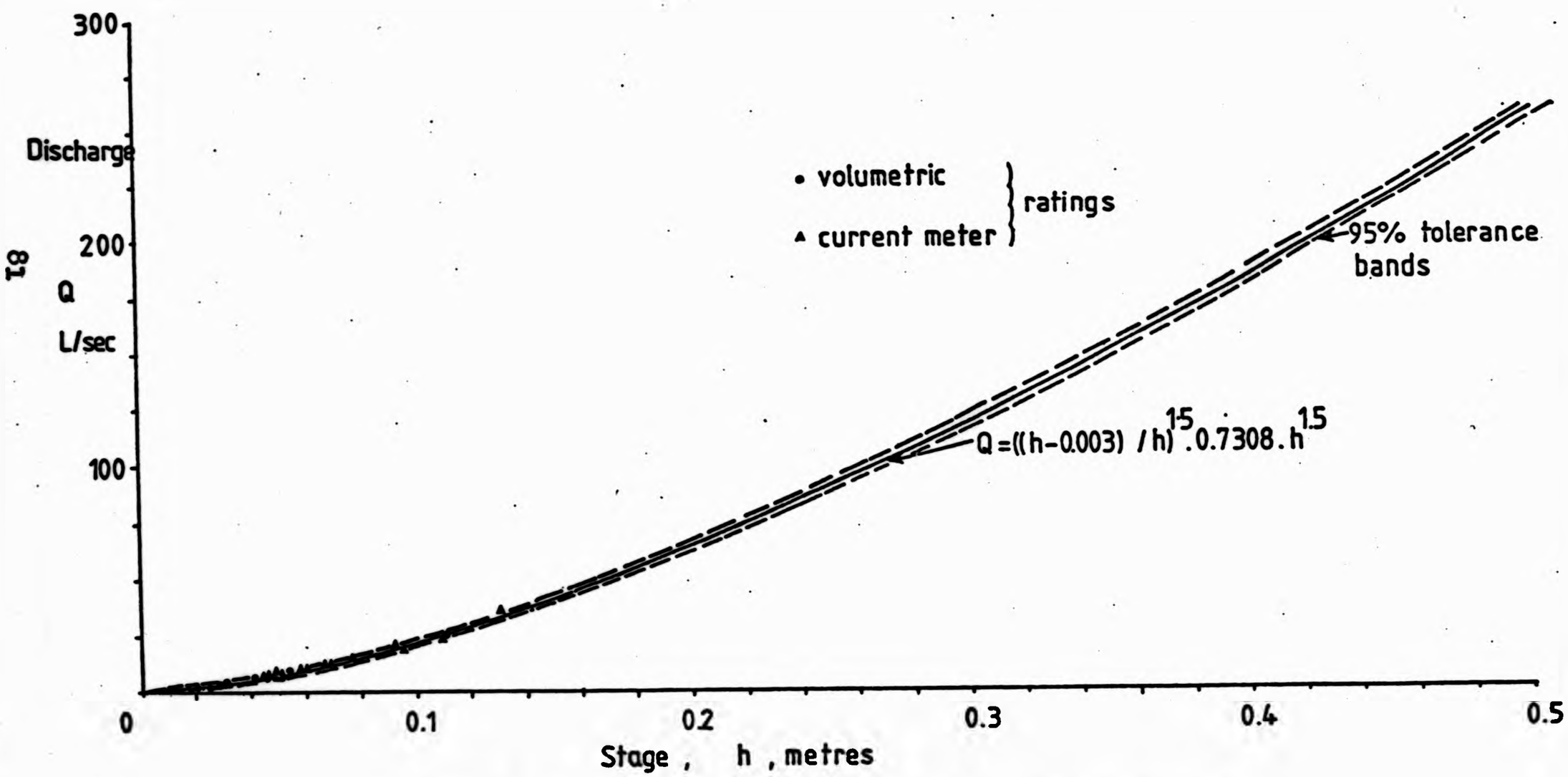

FIGURE 4.4: WEST WALK FLUME: THE STAGE-DISCHARGE RELATIONSHIP

where e_b = error in width measurement

e_z = error in zero setting

e_{h1}, e_{h2} = errors in head measurement

$2\sigma_m$ = error of the mean of a series of the head measurement

Tolerance, X, is not single-valued for a given flume, but varies with discharge. Percentage errors are thus calculated for values of h from 0.01 to 0.75 metres; details are shown in Table 4.2.

Error in the width measurement is assessed as 2 mm, although this may vary slightly with temperature and earth settlement around the flume. The pen is zeroed to within h = 1 mm of its true value. The accuracy of the head series depends upon the type of chart trace (fibre tip pen gives a fine line about 0.2 mm thick) and the method of reading the trace; the latter was by digitisation and the total head measurement error was assumed to be 3.0 mm. It can be seen that the percentage error increases rapidly for flows less than about 7 l/s, decreases rapidly with increasing discharge and stabilises to about 2.0 % above about 40 l/s. It is thus important to realise that gauging errors of around 10 % and possibly higher occurred during low flows in the drought of 1976.

B. V-notch Weirs

(a) Design and Construction

A decision was made to instal V-notch weirs at the remaining four selected sites. These have the advantage of very accurately measuring the lower range of flows, owing to their greater sensitivity. Three 90° V-notch weirs were already available for installation; these were constructed from 3 mm thick mild steel plate, strengthened laterally with steel angle-iron; the notch was bevelled at 60° as described in BS3680, Part 4A (1965). These three plate weirs were to be installed in subcatchments 1, 2 and 5 and a ½-90° V-notch weir specially built for subcatchment 4; here the structure was built specifically for the range of flows expected, while in the other cases availability and economy ruled the decision. Structure dimensions and the range of flows accommodated are given in Table 4.3.

TABLE 4.2

Error Calculations for West Walk Flume

$h^{\neq}$	Q^{*}	C_V	C_D	$\pm X_b\%$	$\pm B_b\%$	$\pm X_h\%$	$\pm X\%$	$h - h_e$	$h + h_e$	$Q - Q_e$	$Q + Q_e$
0.01	0.43	1.0169	0.58	9.70	0.5	0.1	9.71	0.009	0.011	0.34	0.52
0.05	7.45	1.0169	0.90	3.34	0.5	0.02	3.38	0.048	0.052	6.98	7.93
0.1	22.08	1.0169	0.94	2.54	0.5	0.01	2.59	0.097	0.103	21.06	23.11
0.15	41.19	1.0169	0.96	2.14	0.5	0.007	2.2	0.147	0.153	39.93	42.46
0.5	256.06	1.0169	0.98	1.74	0.5	0.002	1.81	0.491	0.509	249.13	263.04
0.75	471.82	1.0169	0.98	1.74	0.5	0.001	1.81	0.736	0.764	458.6	485.15

$\neq$ metres * l/s

Table 4.3: V-notch weirs installed at West Walk

Sub-Catchment	Angle (Deg)	Height* (H_{MAX})m	Maximum Possible Flow (l/s)	Minimum Possible Head (m)	Flow (l/s)≠
1	90°	0.3223	81.31	0.05	0.803
2	90°	0.3063	71.57	0.05	0.803
4	½-90°	0.3820	62.15	0.05	0.406
5	90°	0.2155	29.95	0.05	0.803

* vertical line from apex of V-notch to horizontal top of plate

≠ from BS3680, Part 4A (1965)

There are obvious disparities between the values of maximum discharge expected (Table 4.1) and those that can be accommodated (Table 4.3). This is because, as already stated, weirs 1, 2 and 5 were acquired from another experiment and only weir 4 was specifically designed for its location. In retrospect only weir 2 was overtopped during the period of study, and even then only twice. The maximum values quoted in Table 4.1 have, with the possible exception of weir 2, return periods greater than two years.

The structures were cleaned, de-rusted with 'Jenolite', coated with metal chlorate primer and two coats of bituminous paint before installation. Site conditions were as near as possible to those described in BS3680, Part 4A (1965, p. 13). Slots were dug in the banks at each site and the structures hammered home and well grouted with clay. Paving stones were laid below each weir to eliminate cavitation. It was later discovered (notably during summer 1976) that leaks were occurring due to the shrinkage of clay around the plates, and repairs made.

Table 4.3: V-notch weirs installed at West Walk

Sub-Catchment	Angle (Deg)	Height* (H_{MAX})m	Maximum Possible Flow (l/s)	Minimum Possible Head (m)	Flow (l/s)≠
1	90°	0.3223	81.31	0.05	0.803
2	90°	0.3063	71.57	0.05	0.803
4	½-90°	0.3820	62.15	0.05	0.406
5	90°	0.2155	29.95	0.05	0.803

* vertical line from apex of V-notch to horizontal top of plate

≠ from BS3680, Part 4A (1965)

There are obvious disparities between the values of maximum discharge expected (Table 4.1) and those that can be accommodated (Table 4.3). This is because, as already stated, weirs 1, 2 and 5 were acquired from another experiment and only weir 4 was specifically designed for its location. In retrospect only weir 2 was overtopped during the period of study, and even then only twice. The maximum values quoted in Table 4.1 have, with the possible exception of weir 2, return periods greater than two years.

The structures were cleaned, de-rusted with 'Jenolite', coated with metal chlorate primer and two coats of bituminous paint before installation. Site conditions were as near as possible to those described in BS3680, Part 4A (1965, p. 13). Slots were dug in the banks at each site and the structures hammered home and well grouted with clay. Paving stones were laid below each weir to eliminate cavitation. It was later discovered (notably during summer 1976) that leaks were occurring due to the shrinkage of clay around the plates, and repairs made.

Only in the case of weir 2 was the tailwater level ever high enough to interfere with free-discharge of the nappe. During summer 1976 the flow at all V-notch weirs ceased. During the descent of water levels below 0.05 metres the nappe was seen to cling to the downstream surface of the weir plate, introducing an unavoidable source of error. Volumetric calibrations were made at levels below 0.05 metres, as described later, to help overcome this problem.

In each case a concrete stilling well was sited 4 h_{MAX} upstream of the plate, with a horizontal pipe connection to the channel. Continuous water level measurement was made with recorders built and loaned by the Forestry Commission Research Station at Alice Holt, Farnham, Hampshire (Figure 4.5). These too were fitted with fine fibre tip pens (which lasted $> 2\frac{1}{2}$ years) and a continuous roll of ungraphed paper. The charts were collected weekly. Adjacent to each stilling well was installed a crest-stage gauge. This gave a valuable check upon values of maximum water level during storms; this was considered important, initially, since non-standard level recorders were being used. It also allowed a quick, visual reading of stage during storms without uncovering the recorder box. Zero-setting was made by dropping a pointer from a horizontal beam laid from weir top to the bank adjacent the stilling well. This was deducted from the appropriate height given in Table 4.3. The stage was re-checked in unison with the flume as described earlier.

(b) Discharge Calculation

Since all weirs had fully developed contractions (i.e. the bed and walls of the channel upstream of the weir were sufficiently remote for boundaries to have no significant influence on the contractions of the nappe) the Kindsvater and Carter equation was considered suitable for calculation of discharge (BS3680, Part 4A, 1965, p. 37). This states,

$$Q = \frac{8}{15} \cdot (2g)^{\frac{1}{2}} . C_e . \tan \frac{\theta}{2} \cdot h_e^{\frac{5}{2}} \qquad (4.10)$$

where C_e = discharge coefficient
θ = notch angle
$h_e = h + K_h$

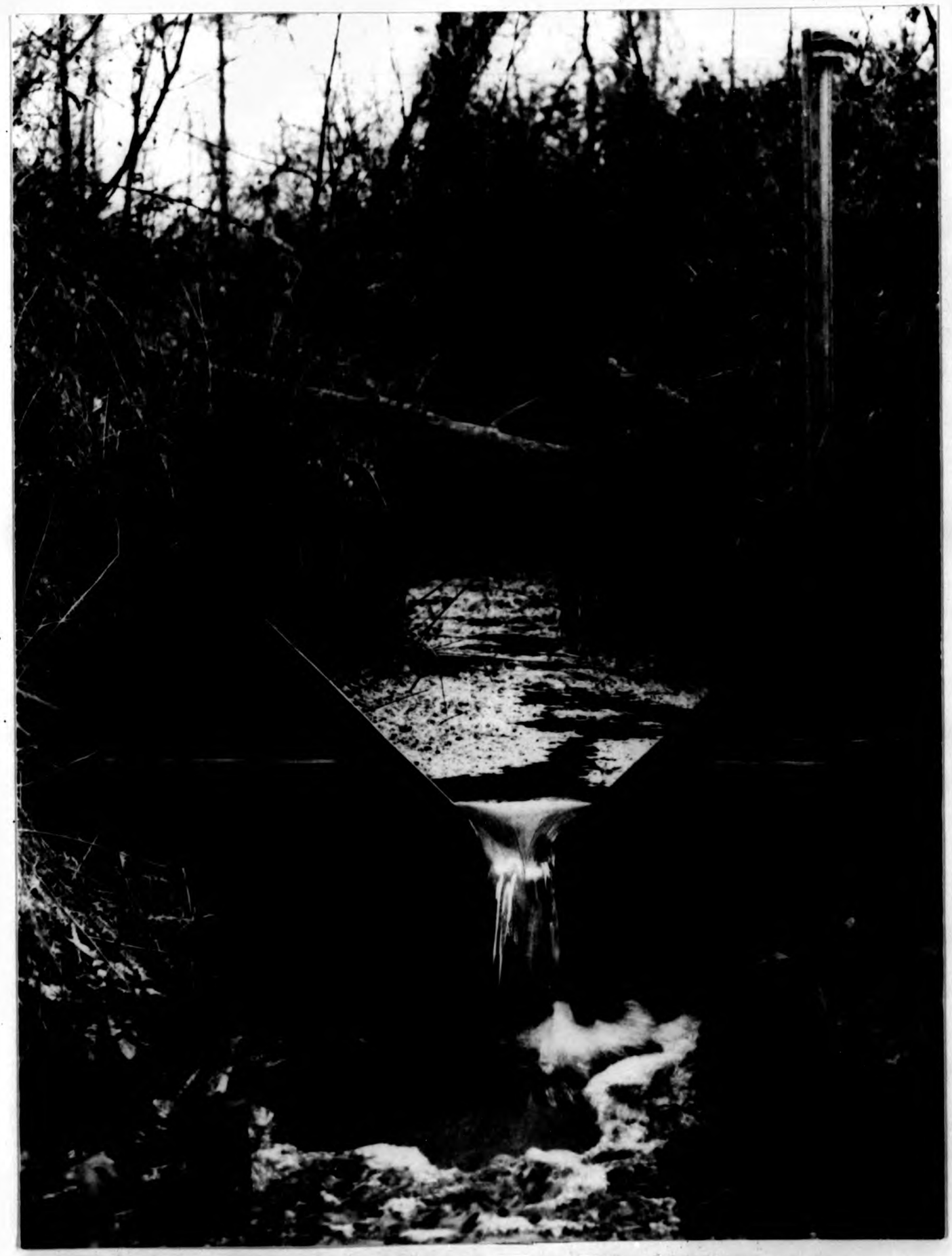

FIGURE 4.5 A: 90° V-NOTCH WEIR AT W2
(Note crest stage recorder, right-background)

FIGURE 4.5 A: 90° V-NOTCH WEIR AT W2
(Note crest stage recorder, right-background)

FIGURE 4.5 A: 90° V-NOTCH WEIR AT W2
(Note crest stage recorder, right-background)

FIGURE 4.5 B: FORESTRY COMMISSION WATER LEVEL RECORDER AT W1
(Weir out of picture on left; note iron-rich, organic precipitate in the stilling pool)

FIGURE 4.5 B: FORESTRY COMMISSION WATER LEVEL RECORDER AT W1
(Weir out of picture on left; note iron-rich, organic precipitate in the stilling pool)

FIGURE 4.5 B: FORESTRY COMMISSION WATER LEVEL RECORDER AT W1
(Weir out of picture on left; note iron-rich, organic precipitate in the stilling pool)

h = head

K_h = empirical constant allowing for the influence of fluid properties

C_e is a function of θ, obtainable from Figure 5 of BS3680; thus C_e = 0.578 (90° notch) and 0.580 (½-90° notch). K_h is also a function of θ, obtainable from Figure 6 of BS3680; thus K_h = 9.0×10^{-4} metres (90° notch) and 1.5×10^{-3} metres (½-90° notch). The discharge equation becomes,

$$Q = 1.3655\ (h + 0.0009)^{2.5} \quad (90^\circ \text{ notch}) \quad (4.11)$$

$$\text{and } Q = 0.6851\ (h + 0.0015)^{2.5} \quad (\tfrac{1}{2}\text{-}90^\circ \text{ notch}) \quad (4.12)$$

where Q is in $m^3 sec^{-1}$ and h in metres.

Since the weirs were installed according to the BS3680 and were within the application limits described on page 37 of the BS3680 calibration was restricted to the lower values of h where Q could be expected to deviate from that calculated theoretically, due to a clinging nappe. Current meter calibration at high discharges was not undertaken because

(i) it was felt that the theoretical equation approximated discharge well for the reason described above, and

(ii) collection of water samples and data from the weirs and experimental slope were given priority.

A portable 'spout' was constructed; this bolted into the 'vee' of the 90° V-notch weirs and directed flow into 12.6 litre bowl; flow was measured very precisely by the volumetric procedure, the mean value of five successive, stable discharge readings being accepted.
Calibrations gave the following results:

(i) Weir 1

Computed Q very slightly under-estimated, actual Q between h = 0.05 m and 0.07 m. Below h = 0.05 m (the BS 3680 minimum gaugeable head for a V-notch weir) the under-estimation progressively

increases. A power function fitted to the manually/directly measured flow data, h <0.05 m gives,

$$Q = 0.6295\ h^{2.2041} \qquad (4.13)$$

Q is in $m^3 sec^{-1}$, h is in m
with n = 6; r = 0.999; r^2 = 99.8 %; t = 44.68;
significance level = 0.1 %; standard error of the
estimate = 0.000169 $m^3 sec^{-1}$.

The difference between Q actual and Q theoretical increases from 0.0558 l/s (6.53 % of actual) at h = 0.05 to 7.659×10^{-6} l/s (31.14 % of actual) at h = 0.01 m. The empirical equation has been used for all calculations of Q where h <0.05 m. The plotted data is shown in Figure 4.6.

(ii) Weir 2

Theoretical Q over-estimates actual Q for h <0.05 m. The difference in trend between this and weir 1 may reflect low flow losses due to leakage at weir 2. Fewer data points were available, but a power function was again fitted,

$$Q = 3.0077\ h^{2.8138} \qquad (4.14)$$

with n = 4; r = 0.996; r^2 = 99.17 %; t = 15.38;
significance level = 1.0 %; standard error of the
estimate = 5.38×10^{-5}.

The difference between Q actual and Q theoretical increase from 0.1063 l/s (13.9 % of actual) at h = 0.05 m to 0.0069 l/s (58 % of actual) at h = 0.01 m. The empirical equation has been used for h <0.05 m.

(iii) Weir 4

No calibration measurements were made for the $\frac{1}{2}$-90° V-notch at weir 4. This was mainly due to problems in constructing a bolt-on 'spout' for the notch and difficulty encountered when current-metering very low flows.

(iv) Weir 5

Q actual and Q theoretical differ very little for 0.036 < h < 0.065 m. For h < 0.036 m Q actual over-estimates Q theoretical. The power function is,

$$Q = 0.1191\ h^{1.741} \tag{4.15}$$

with n = 5; r = 0.998; r^2 = 99.53 %; t = 25.21; significant level = 0.1 %; standard error of the estimate = 5.8×10^{-4}.

The difference between Q actual and Q theoretical increased from 0.0294 l/s (8.0 % of actual) at h = 0.036 m to 0.0255 (65 % of actual) at h = 0.01 m. The empirical equation was used for h < 0.036 m.

(c) Assessment of Errors in Gauging

Tolerance is calculated by,

$$X = \pm\sqrt{X_c^2 + X_{b(e)}^2 + \beta\, X_{h(e)}^2} \tag{4.16}$$

where X_c = % error in C

$X_{b(e)}$ = % error in $\tan \frac{\theta}{2}$

$X_{h(e)}$ = % error in h_e

β = 2.5

$$X_{h(e)} = (100\sqrt{e_{h(1)}^2 + e_{h(2)}^2 + e_{K(h)}^2 + e_z^2 + 2\sigma_m^2})/h \tag{4.17}$$

where $e_{h(1)}$ = errors in head measurement

e_z = error in zero setting (0.001 m)

$e_{K(h)}$ = error in the K_h term

$2\sigma_m$ = Error of the mean of a series of the head measurement.

As in Table 4.2 percentage error is calculated for a range of flow. The percentage error in C_e is given as 1 - 2 (BS3680, 1965); therefore,

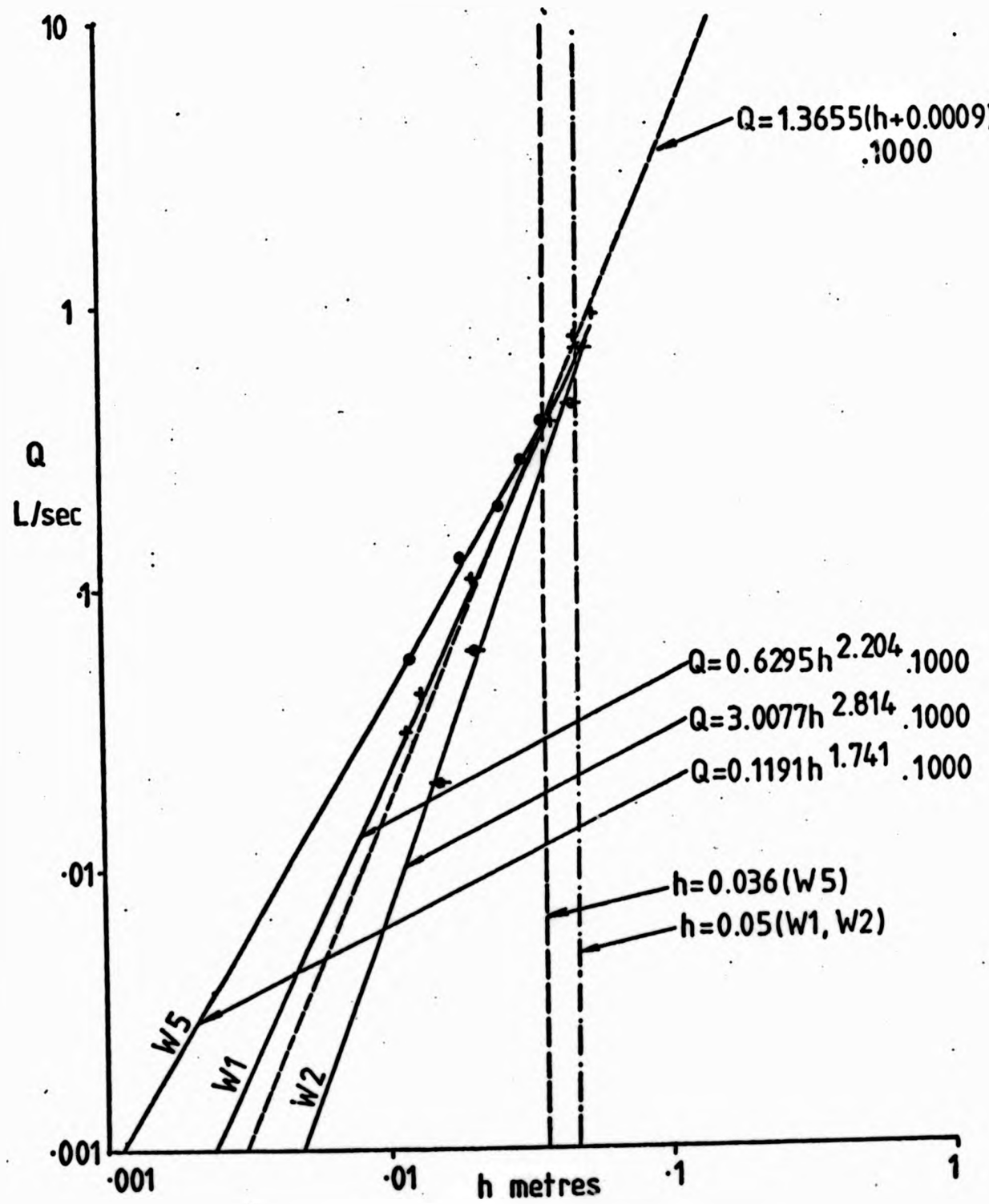

FIGURE 4.6: LOW FLOW STAGE-DISCHARGE RELATIONSHIPS AT THE V-NOTCH WEIRS

(Theoretical equation shown by diagonal dashed line; vertical dashed lines represent upper limit of application for low flow rating)

C_e was made = 1.5 %, although this may increase at low flows. The top widths of the weirs were checked to within 1.0 mm giving the following values of $X_{b(e)}$: W1 = 0.16 %; W2 = 0.16 %; W4 = 0.32 %; W5 = 0.23 %. Percentage error in head measurement was assessed at $\pm$ 3 mm (as for the flume). The error in K_h is given as 3.0×10^{-4} m (BS3680, 1965). The percentage tolerances shown in Table 4.4 apply to all the V-notch weirs, with no more than 0.02 % difference between the sets of values.

Table 4.4: Error Calculations for the V-notch Weirs

h	$\pm$ C %	$\pm X_b$ %	$\pm X_{h(e)}$	$\pm$ X %
0.05	1.5		6.35	6.54
0.1	1.5	Varies -	3.18	3.52
0.2	1.5	see	1.59	2.21
0.3	1.5	text	1.06	1.86
0.35	1.5	above	0.91	1.78

The percentage errors for low h values reflect the high ratio of head measurement error to low flow. Taking W1 as an example, h = 0.05; Q = 0.763 $\pm$ 0.045 l/s. Errors using the calibration equations are given by the standard errors of the estimates quoted earlier.

C. Data Digitisation

During late 1976, a digitising table became available for use with the Geography Department WANG 2200B 12k computer. This had a suitable resolution for digitisation of streamflow traces on an hourly basis ($\frac{1}{100}$ inch or 0.254 mm) with storage on magnetic tape cassettes.

(a) West Walk Flume

Since a weekly Munro recorder with graduated charts was used, the point digitising mode separately digitised successive hourly values of stage. The program used, QUEZEDIG, is given in Appendix 2. Briefly, the following procedure was used.

(i) Stick one end of the chart to the table with drafting tape.

(ii) Digitise end of the chart and continue until Y co-ordinates are equal; stick other end of the chart to the table.

(iii) Digitise base of the chart at the beginning and end; this gives the chart datum.

(iv) Digitise the chart from left to right, incrementing one hour at a time.

On completion the week's data (about 168 co-ordinate values plus two chart-base co-ordinates) are automatically recorded on magnetic tape. Each file was given a unique name; e.g. "12240678", representing 1200 hours (12) on the 24th (24) of June (06) 1978 (78). An immediate visual check on the digitised data was possible with PLOTS which plotted the complete week's values of h on the Tektronix 4006-1 CRT, (see Appendix 2). The program FLUMQ was written to convert head to discharge and print out hourly values of time (hours), h (metres) and Q ($m^3 sec^{-1}$), (Appendix 2).

(b) <u>V-notch Weirs</u>

The digitisation of weekly charts from V-notch weirs was approached differently for two reasons; firstly, the paper was ungraphed; secondly, the clocks driving the paper always lost time over a week. Digitisation was therefore undertaken in the 'stream' mode using the program TRACES (Appendix 2). The procedure was briefly as follows.

(i) Rule lines from the ends of the trace to meet the bottom of the chart at 90^{o}.

(ii) Adjust the chart to give equal Y co-ordinates; the program continues when Y values are equal; both X and Y co-ordinates are retained in memory.

(iii) Enter the time (hours, mins) of the start of the trace start. Enter the total length of time between 'pen on' and 'pen off' (circa 168 hours). The digitising increment, D, is then calculated (line 80 of the program).

(iv) Digitise the trace by running the 'bullseye' along the line; a 'bleep' is emitted each time a point is digitised; if this is done too fast, a point may be missed; the program allows missing points to be searched back and digitised; digitising then continues.

Data are converted to values of h and recorded on magnetic tape. The remaining details are the same as for the flume, except that time, h and Q are printed using the program WEIRQ (Appendix 2).

Digitising is an easy, accurate method of reading and storing data from charts, far superior to any manual method. Errors are possible when digitising (e.g. sudden jumps, due to 'hand-slip', or trends, due to 'paper-slip' on the table) although these can usually be seen by using the visual display program, PLOTS. To check the accuracy of the digitising method a series of twenty digitised stage readings were compared with the same twenty values measured optically using a Coradograph (resolution $\frac{1}{1000}$ th inch or 0.0254 mm by vernier); a Kolmogorov-Smirnov two sample test showed that no significant difference existed between the two data sets, i.e. they were both drawn from the same population (N = 20; required DMAX = 3; Ho (i.e. no difference) upheld at the 1 % probability level). This non-parametric test was used because of its suitability for non-normal data (Siegel, 1956, p. 127).

D. Cross-Correlation between Structures

There was some loss of data due to equipment failure (this ranged from stopping clocks to stilling-well blockage by a nesting animal !). The amount of time lost over two years for each gauging station is shown in Figure 4.7. The most extensive losses were for weirs 4 (15 %) and 5 (10 %), while the flume (2 %) and weir 1 (5 %) were relatively

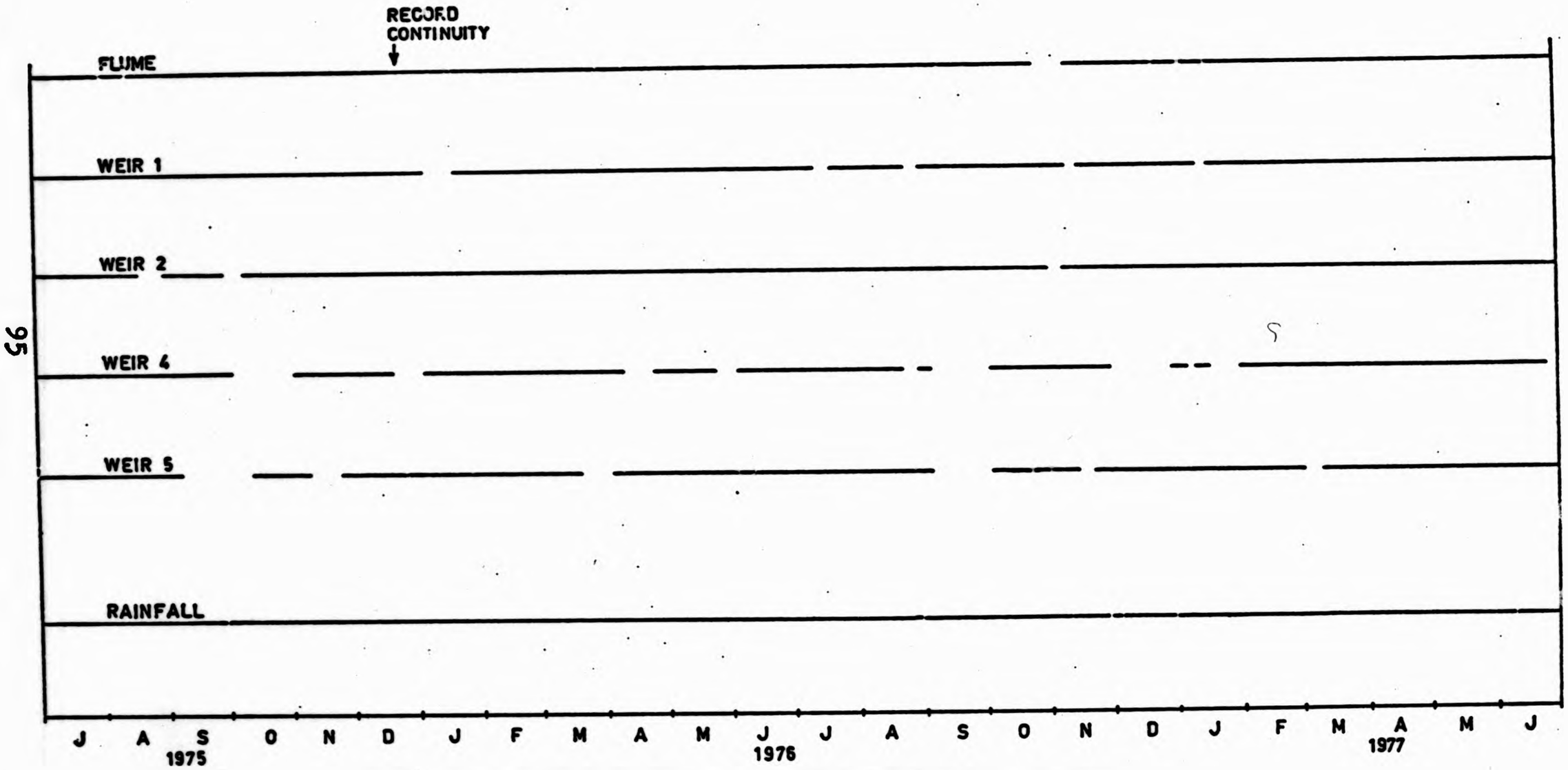

FIGURE 4.7: CONTINUITY OF RECORD FOR THE FLOW GAUGING STATIONS

reliable. The data lost are either:

(a) baseflow, which is relatively easy to synthesise by cross-correlation with another structure;

or, (b) stormflow, which is more difficult to synthesise due to differences in hydrograph parameters, e.g. time to peak, form of recession, etc.

(a) Baseflow

A set of baseflow data from 20.12.76 to 08.08.77 was assembled for all gauging structures (Table 4.5). Low flow data from 1976 was not considered due to the probability of large errors at low h. Regression equations were established for all stations using weir 1 and the flume (i.e. the most reliable stations) as independent predictors. The results of the regression analyses are shown in Table 4.6. The regression equations take the form,

$$Y = bX \pm a \pm SE_{\hat{y}} \qquad (4.18)$$

where X = independent variable (l/sec)
Y = dependent variable (l/sec)
b = slope
a = intercept (l/sec)
SE_y = standard error of the forecast (l/sec)

$SE_{\hat{y}}$ is a combination of the error terms SE_y (standard error of the estimate), $SE_{\bar{y}}$ (SE of the mean) and SE_b (SE of the regression coefficient) (Johnson, R.J., 1978),

$$SE_{\hat{y}} = \sqrt{SE_y^2 + SE_{\bar{y}}^2 + SE_b^2} \qquad (4.19)$$

However, since SE_b varies with x there is no one value for SE_b (see Table 4.6).

There are several reservations associated with the assumptions of the general linear model in applying this method to the available data.

TABLE 4.5

Baseflow Cross Correlation Data
for the West Walk Gauging Stations (l/s)

Date	Time	W1	W2	W4	W5	Flume
20.12.76	12.40	2.40	5.49	1.75	1.84	15.00
03.01.77	14.40	4.33	9.33	2.85	2.11	18.92
22.03.77	10.22	2.18	5.62	2.19	1.16	11.15
05.04.77	09.25	1.42	3.40	1.18	0.53	6.63
13.04.77	09.45	0.89	2.04	0.62	0.19	4.48
19.04.77	10.15	0.68	1.31	0.43	0.17	3.15
26.04.77	10.10	0.68	1.16	0.39	0.14	2.98
03.05.77	09.55	1.84	4.22	0.90	0.81	8.92
10.05.77	10.15	1.71	4.12	1.30	1.11	8.79
17.05.77	10.20	1.21	3.06	1.45	0.36	5.52
24.05.77	10.05	0.64	1.42	0.48	0.14	3.33
31.05.77	10.20	0.32	0.73	0.24	0.05	1.41
14.06.77	09.55	2.04	5.68	2.19	0.90	10.00
21.06.77	09.50	0.28	0.89	0.19	0.04	1.69
29.06.77	09.30	0.20	0.85	0.12	0	1.41
05.07.77	09.40	0.03	0.06	0.05	0	1.02
12.07.77	10.25	0.02	0.03	0.03	0	0.91
19.07.77	09.50	0.02	0.04	0.03	0	0.79
26.07.77	10.15	0.04	0.05	0.05	0	0.91
02.08.77	10.15	0.01	0.01	0.01	0	0.79
08.08.77	11.45	0.03	0.02	0.02	0	0.79

TABLE 4.6

Baseflow Cross Correlations for West Walk Gauging Stations: Regression Analyses

Stations X	Y	n	r	t_r	sig r %	a	b	t_b	sig b %	SE_y	$SE_{\bar{y}}$	$\frac{SE_y}{S_x(\sqrt{N-2})}$
W1	W2	21	0.992	13.36	0.1	0.074	2.29	18.77	0.1	0.316	0.574	0.068
W1	W4	21	0.950	12.97	0.1	0.039	0.743	13.27	0.1	0.263	0.184	0.057
W1	W5	15	0.940	7.31	0.1	-0.147	0.575	10.27	0.1	0.221	0.168	0.047
W1	Flume	21	0.982	19.21	0.1	0.477	4.64	45.49	0.1	0.481	1.162	0.104
Flume	W1	21	0.981	19.19	0.1	0.006	0.201	20.1	0.1	0.210	0.237	0.009
Flume	W2	21	0.982	22.66	0.1	-0.151	0.485	15.65	0.1	0.472	0.546	0.030
Flume	W4	21	0.94	21.69	0.1	-0.027	0.157	17.44	0.1	0.207	0.184	0.002
Flume	W5	15	0.987	18.1	0.1	-0.236	0.127	42.33	0.1	0.052	0.168	0.002

$SE_{\hat{y}} = \sqrt{SE_y^2 + SE_{\bar{y}}^2 + SE_b^2}$

(Discharge in l/sec)

The components of $SE_{\hat{y}}$ are as follows:

$SE_y = S_y(\sqrt{1 - r_{yx}^2})$ (S_y = standard deviation of y)

$SE_{\bar{y}} = S_y/\sqrt{N}$

$SE_b = ((SE_y/(S_x(\sqrt{N-2})))(x_i - \bar{x})^2$ (S_x = standard deviation of x)

(SE_b varies with x_i)

For b, $t_b = b_{yx}/SE_b$

For r, $t_r = \frac{r\sqrt{n-2}}{\sqrt{1-r^2}}$

(i) The requirement that observations are independent of each other is not completely satisfied, i.e. spatial and temporal serial correlation exists.

(ii) Both dependent and independent variables are subject to error. The linear model assigns error to the dependent variable alone; the dependent variable is considered as an observation on a random variable, the independent variable as some known constant associated with this random variable. M.S. Bartlett (1949) suggested a method of overcoming the problem by dividing the n points into three approximately equal groups. The join of the mean co-ordinates $\bar{x}_1$, $\bar{y}$, and $\bar{x}_3$, $\bar{y}_3$ for the two extreme groups is used to determine the slope. The intercept is determined from the intersection point of the co-ordinates $\bar{x}$, $\bar{y}$, as in the least squares method. The confidence interval for b is slightly wider than that obtained by the least squares method, since the assumption of no error in x has been dropped. A simpler method of overcoming the problem is to regress y on x and x on y, and then to use the mean slope of the two best fitting equations, and a re-calculated intercept. This gives the reduced major axis line (RMA).

(iii) Heteroscedasticity exists in some of the relationships, i.e. the residual variance is not independent of x.

In practice little could be done to remove serial correlation or heteroscedasticity without recourse to more sophisticated techniques. Using the RMA regression line was also found to be unwarranted since, in most cases, regression slopes were very similar (although these were not tested for significant differences). Despite the reservations cross-correlation was the simplest method to apply and was used to synthesise hourly values of discharge where gaps in baseflow existed.

(b) Stormflow

A more complex model is required for obtaining hourly flows during missing storm hydrographs. The development of such a model (e.g.

N.H. Crawford and R.K. Linsley's Stanford Watershed Model, 1966) was beyond the scope of the project, especially since there were only a few missing storm sequences. Flows for the entire period were required to compute water and solute budgets and it was therefore decided to infill the record gaps with daily mean flows obtained from cross-correlations with daily mean flows from the flume and weirs. The use of daily mean in place of hourly flows introduces error into the computation of solute budgets (Walling, 1978) but simplifies the infilling of lost stormflow data. The regression equations, similar in form to (4.18), are given in Table 4.7.

E. Hydrograph Separation

A method for the separation of hydrographs into storm run-off ('quickflow' - Hibbert and Cunningham, 1967) and baseflow (comprising interflow, ground water discharge and termed 'delayed flow' by Hibbert and Cunningham, ibid) was required for future work.

An empirical technique used in the Flood Studies Report N.E.R.C., 1975, p. 389) was used on twenty-seven hydrographs from the flume, spanning the entire two years. Reference to Figure 4.8 shows how both hydrographs and hyetographs are used in determining the position at which the separation line intersects the recession curve. Lag is defined as the time between the hydrograph and hyetograph centroids; the intersection point is then defined as 4 x lag after the cessation of rainfall. In comparison with many arbitrary techniques the method is given a degree of reality, employing criteria based upon physical processes involved in hydrological events. However, as it stands the method has the disadvantage that it requires an input in addition to discharge (i.e. rainfall) making it less amenable to computer processing. Slopes of the twenty-seven separation lines determined in this way were plotted as a frequency histogram (Figure 4.9). The median value of 0.602 l/s / km^2/h is the most acceptable description of central tendency, considering the positively skewed distribution. This differs little from the value of 0.55 l/s / km^2/h proposed by Hibbert and Cunningham (1967) for use in a time-based separation technique. The similarity is interesting in that two different methods using different terminology produce almost equivalent results, i.e. "baseflow" approximates to "delayed flow". The proposed

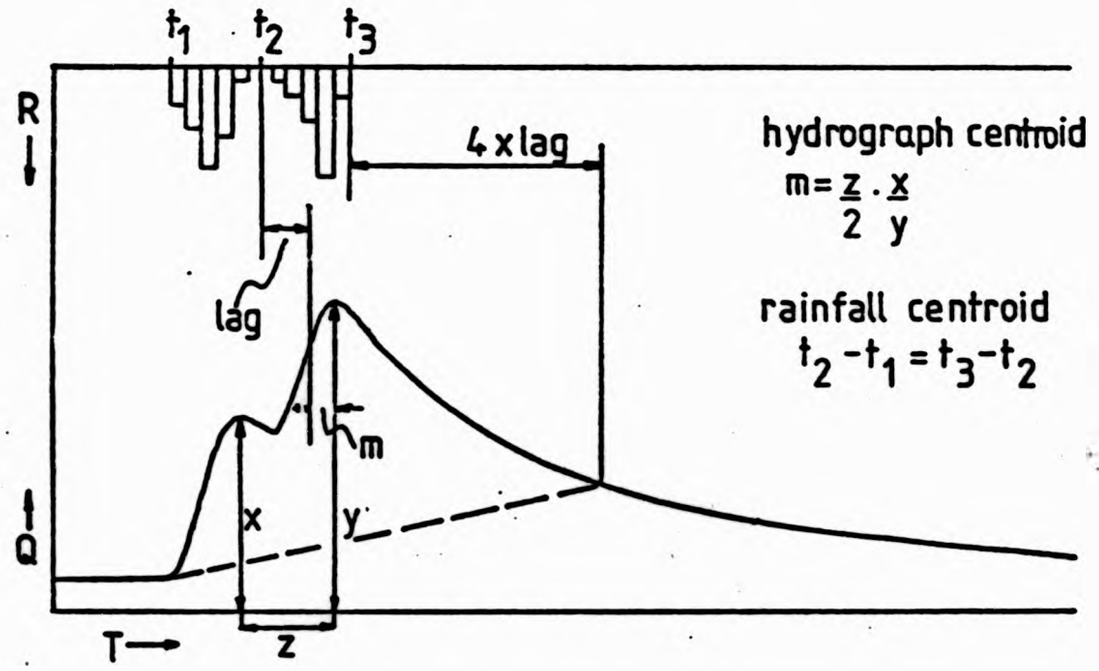

FIGURE 4.8: SUMMARY OF THE FLOOD STUDIES METHOD OF BASEFLOW SEPARATION (top right)

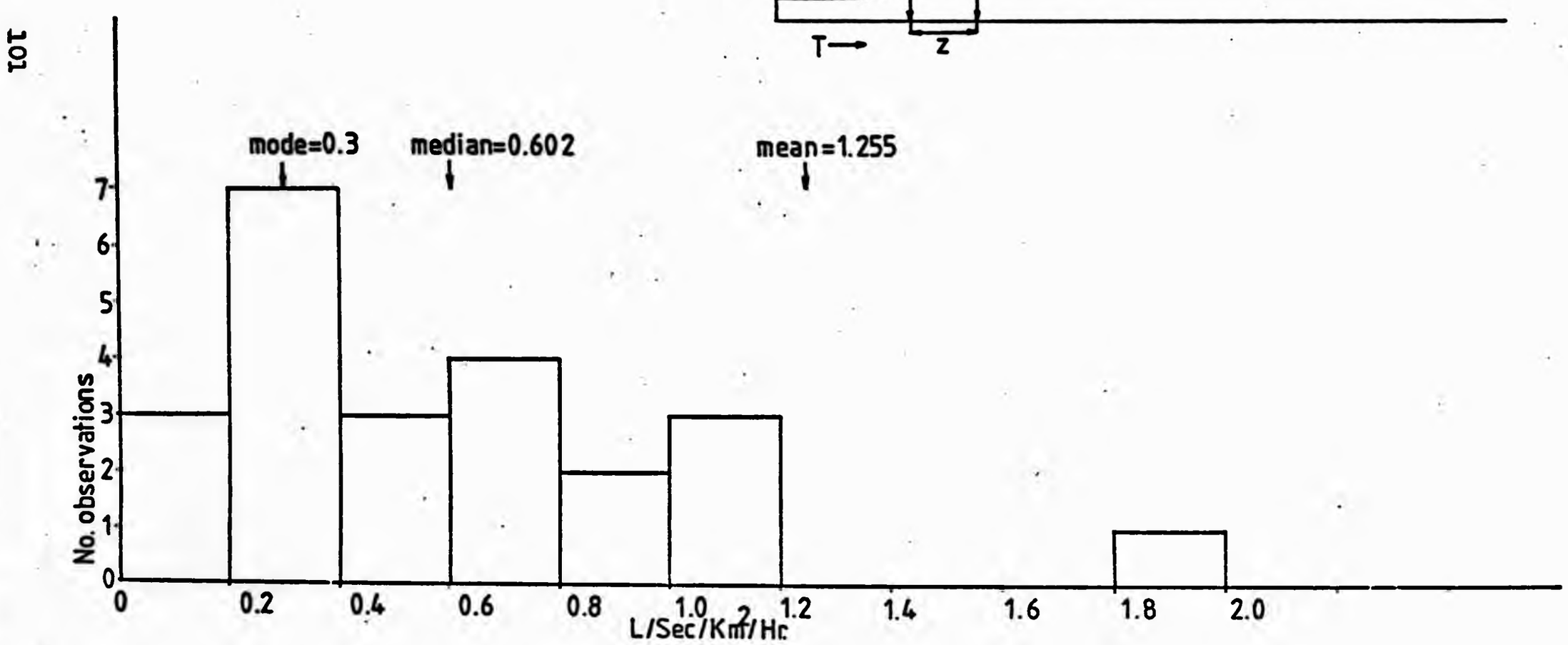

FIGURE 4.9: FREQUENCY HISTOGRAM OF THE SLOPES OF BASEFLOW SEPARATION LINES DETERMINED USING THE FLOOD STUDIES METHOD (bottom left)

TABLE 4.7

Mean Daily Flow Cross Correlations for West Walk Gauging Stations

	Stations X / Y	n	r	t_r	sig r %	a	b	SE_y
	W1/W4	50	0.97		0.1	0.597	0.905	0.244
*	W1/W5	50	0.93		0.1	0.409	1.227	0.745
*	Flume/W1	50	0.93		0.1	2.722	0.986	0.523
*	Flume/W2	50	0.86		0.1	2.135	0.792	0.601
	Flume/W4	50	0.95		0.1	4.937	1.080	0.370
	Flume/W5	50	0.96		0.1	5.160	0.542	0.279

(Discharge in l/sec; logarithmic flows used)

* RMA line used

technique is still arbitrary in nature, but is simple to implement and adequate for the proposed work.

4.3 RAINGAUGING

A. Gauge Installation

Measurement of gross rainfall input to the catchment was required for both water and solute budgeting. Net rainfall will be less than gross rainfall in a forested catchment due to interception by the canopy and subsequent loss by evaporation (recent work has shown the loss by interception to vary between 214 mm and 790 mm in Britain; J.H.C. Gash and A.J. Morton, 1978). No attempt was made to measure net rainfall as it was felt this constituted an entirely separate project. Attention was therefore focussed on accurately measuring gross rainfall.

M.J. Green (1969) states: "It is desirable to design and site raingauges so that the funnel collects the same amount of precipitation that would have fallen on the ground surface had the gauges not been present. If the collecting funnel is raised above ground level there is a wind-eddy effect and subsequent loss of catch, while if the funnel rim is at ground level it is liable to in-splash from the surrounding ground." After substantial field research into the various methods he recommended that gauges should be set with rims at ground level and surrounded by anti-splash grids. The Meteorological Office give recommendations for raingauge siting, the salient features of which are:

(a) the surface should be level;

(b) the distance from every object should be not less than twice the height of the object above the rim of the gauge;

(c) a position sheltered from the wind is preferable to an exposed one;

(d) the surrounding ground should be covered by short grass (Meteorological Office, undated).

The head of the catchment provided a site meeting two of these conditions. The ground was level (i.e. the Plateau Gravel surface) and sparsely covered with a failed plantation of immature Japanese Larch, too small to interfere with catch. Due to the gravel surface all attempts to germinate grass seed failed; exposure was also greater than desirable. Despite these drawbacks the site remained the only really suitable location within the catchment (Figure 4.10).

Two types of raingauge were used during the study period, mainly due to availability. These divide the main period into two sub-periods.

(I) Period One - May 1975 to July 1976

At the beginning of this period two identical Plessey tipping-bucket raingauges were installed, one at ground level, surrounded by a metre square anti-splash grid, the other five yards away, with rim 32 cm above ground level. The gauge orifice was 18.5 cm diameter; thus one bucket tip represented 1.0 mm depth of rainfall. The data was recorded as mm per 15 minutes on a magnetic tape data logger; the tapes were translated accurately by tape recorder to avoid the time delay in sending away for processing. It was necessary to rectify the following faults in the recorders before installation:

(a) Bucket top lodged against the inlet tube when tipping; the tube length was reduced.

(b) Buckets did not measure exactly 1.0 mm and required individual calibration.

(c) Various electronic faults in the data logger. Weekly totals from the translated tape were checked against a digital counter on the logger.

(II) Period Two - July 1976 to July 1977

Due to recurrent faults in the Plessey recorders and the time-consuming nature of data interpretation, a Casella tilting-syphon gauge was installed under the anti-splash grid. This necessitated considerably deepening the pit, strengthening the walls and incising a drainage trench downslope from the pit base. The orifice of this gauge is 27 cm diameter and records on a weekly chart.

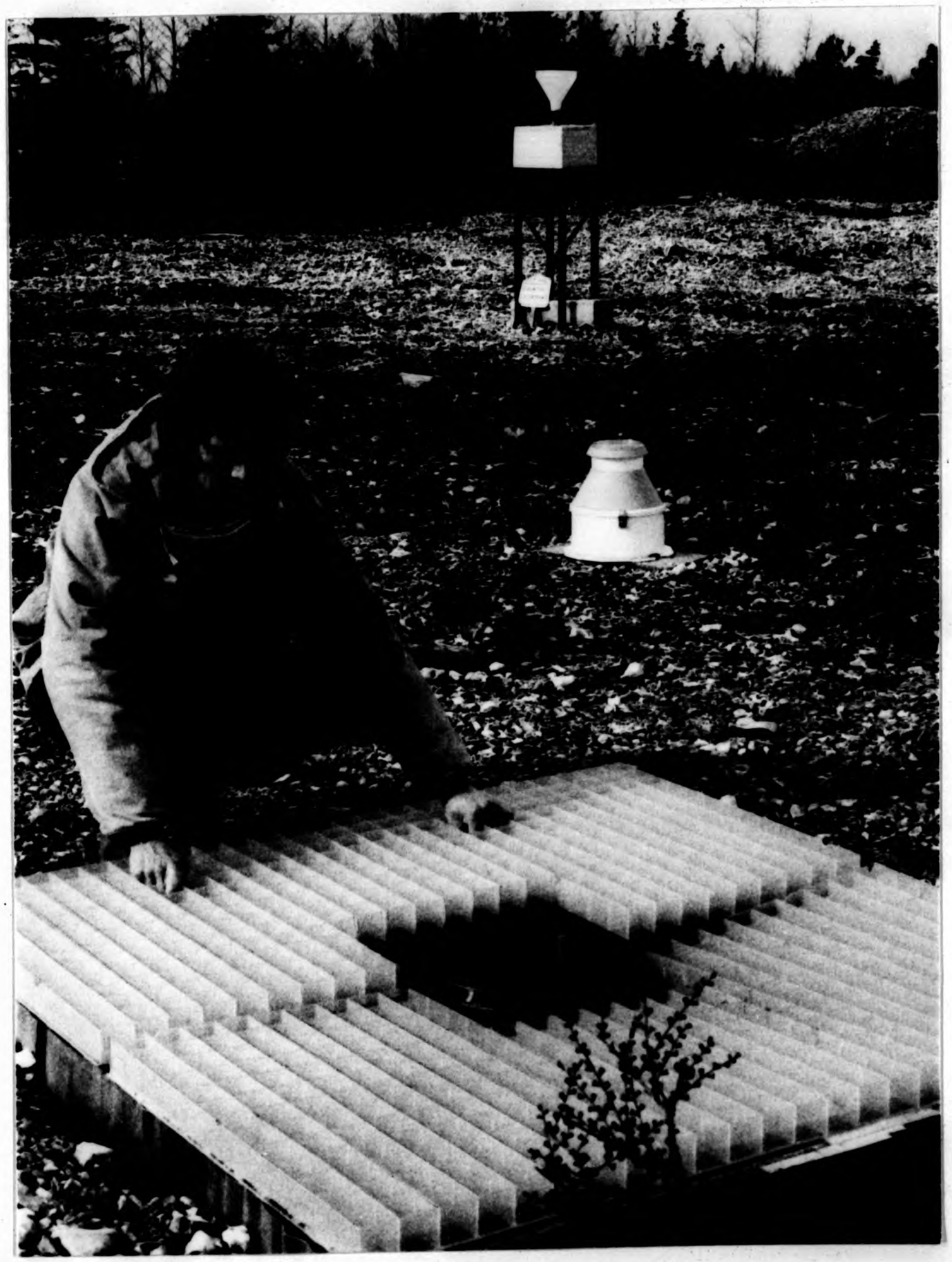

FIGURE 4.10: RAINGAUGING AND SAMPLING SITE: CASELLA GAUGE AND ANTI-SPLASH GRID (foreground); PLESSEY GAUGE (middle ground); SAMPLER (background)

FIGURE 4.10: RAINGAUGING AND SAMPLING SITE: CASELLA GAUGE AND ANTI-SPLASH GRID (foreground); PLESSEY GAUGE (middle ground); SAMPLER (background)

FIGURE 4.10: RAINGAUGING AND SAMPLING SITE: CASELLA GAUGE AND ANTI-SPLASH GRID (foreground); PLESSEY GAUGE (middle ground); SAMPLER (background)

B. Rainfall Data Quality

The above ground level Plessey gauge was retained in its previous position (i.e. above ground level) but modified to only record weekly total on the digital counter. These were used for comparison with weekly totals from the Casella gauge. The relationship between the two was,

$$Y = 0.92\,X + 0.011 \text{ mm} \qquad (4.21)$$

($r > 0.99$; $r^2 > 99\ \%$; $n = 39$; $t = 96$; significance level = 0.1% SE = 1.1 mm).

Y = rainfall recorded in Casella gauge, mm
X = rainfall recorded in Plessey gauge, mm.

This implies that the ground level Casella gauge consistently receives 8 % less than the Plessey gauge. This is surprising since research has shown that a gauge orifice set above ground level under-registers the catch (e.g. Green, 1969, found deficiencies of between 3 and 7.5 %), raindrops being diverted past the orifice by wind-eddying. Ground level gauges suffer from splash-in unless surrounded by a grid, as in the present case. Site over-exposure (the site is at the top of the catchment) is unlikely to be the causative factor, as it would most likely work in the opposite direction. Splash into the Plessey gauge is quite likely, enhanced by a combination of over-exposure (hence higher terminal velocities than in sheltered locations) and a hard pebbly surface (the short grass recommended by the Met. Office cushions impact and reduces splash). A systematic error in either instrument is unlikely, since both were carefully calibrated before installation. However, taking into consideration the Plessey gauge's design faults and the Casella gauge's better resolution, it was felt that the Casella gauge was probably correct and all readings from the Plessey gauge were reduced by 8 % (including those from Period I). In conclusion it is worth pointing out that no truly objective method of measuring absolute point rainfall exists (Rodda, 1967).

C. The Estimation of Missing Rainfall Data

Some data were lost due to blockage in the Casella gauge orifice (caused by wind blown leaves and other organic debris). This amounted to the loss of data for ten individual storms between 10.09.76 and 01.01.77. A linear regression between West Walk and the Casella tilting syphon at Southsea Common (NGR SZ 4064 0990, 2 m AOD) gave,

$$Y = 1.064\,X + 2.175 \qquad (4.22)$$

($n = 26$; $r = 0.986$; $r^2 = 92.2\,\%$; $t = 28.9$; significance level = 0.1 %; SE of the forecast = 1.25 mm).

The relationship was based upon individual storm data, and was used to estimate missing storm totals. Estimated rainfall was given the same hourly temporal distribution as that for Southsea Common, although it was realised that this might incur error due to the rate of storm movement and spatial variability. The linear regression was used in preference to a double mass curve technique (Searcy and Hardison, 1960) because of the good regression relationship and the necessity for estimating individual storm totals.

4.4 ASPECTS OF THE HYDROLOGY OF WEST WALK

The study period (July 1975 to June 1977) covered the 1975-1976 drought, the scientific aspects of which are well described in a recent publication of the Royal Society (O. Gibb, et al, 1978). In the short term a severe depletion of soil moisture probably concentrated solutes in a rapidly shrinking contributing area. Thus during early autumn high concentrations were available for flushing into streams. Salts were also transported to the root zone by plant uptake of water, although it is not certain whether this deposition was higher than average in 1976 because once available water has been used by plants further loss occurs at a reduced rate. It is important to recognise that due to the low return periods associated with the drought extrapolation of results beyond the study period becomes dangerous.

Two aspects of the hydrology of West Walk are considered here as being relevant to solute dynamics. Firstly, a water balance is attempted for the period despite the possible errors incurred in

estimation of evapotranspiration from forested catchments (Clarke and Newson, 1978; Calder, 1979). Secondly, the spatial variability of short term catchment response is shown by the comparison of hydrograph characteristics for two storms.

A. The Water Balance: 1975 - 1977

(a) Climatic Background - the 1975 - 1976 Drought

From May 1975 to September 1976 the pattern of weather over the British Isles was dominated by high pressure that kept most of the country in a dry situation. 1975 proved to be the fifth driest year of the century with less than 70 % of the 1916 - 1950 average rainfall from Devon to Yorkshire and in the east of Scotland. Dry weather continued through February and March 1976 becoming even more severe during the summer. The drought broke at the end of August, autumn rainfall rapidly replenishing soil and ground water.

Southsea Common is the nearest rainfall station to West Walk with a long record; in Table 4.8 the rainfall totals for winter 1975-1976 and the summers of 1975 and 1976 are compared with the 1916-1950 averages. Here the deficit for February and March 1976 reached 73 %.

The term 'drought' is used to determine both the shortage of rainfall and the shortage of river flow, there being a clear difference between the recurrence intervals of each (CWPU, 1976). Below average short term rainfall will not produce as severe an effect on river flow in a Chalk catchment as in a Clay catchment; while long term below average rainfall is likely to severely reduce runoff from both Chalk and Clay catchments and deplete ground water storage in the former.

M.J. Hamlin and C.E. Wright (1978) and CWPU (1976) map the probability of occurrence of various drought lengths of both rainfall and river flow for the 1975 - 1976 drought. The sixteen month period to the end of August 1976 provided an average rainfall over England and Wales of 757 mm which was only 64 % of the average for the period 1916 - 1950; the previous lowest such rainfall was 809 mm for the sixteen months ending in August 1750. The likelihood of such a low rainfall for a sixteen month period ending in August was given as about once in a thousand years (CWPU, 1976, Table 1). South Hampshire was

TABLE 4.8

Comparison of 1975 - 1976 Rainfall with Long Term Averages at Southsea Common

Values in mm. Percentages of Seasonal Means in Brackets

	1916 - 1950	1975	1975 - 1976	1976	1976 - 1977
Summer (April - September)	290.1	184.5 (64)		76.8 (27)	
Winter (October - March)	415.5		290.8 (70)		605.5 (146)

shown to have 50 - 60 % of its long term average sixteen month rainfall; this compares with a figure of 70 - 75 % for the eighteen month drought April 1933 to September 1934. Whereas rainfall drought frequencies can be given in terms of a particular starting date, streamflow droughts cannot, due to the varying delays in runoff in different catchments. Thus, low river flows that occurred during 1975 - 1976 will occur appreciably more often than indicated by the frequency of specified rainfall for a given starting date. CWPU (1976) conclude that in general 1975 - 1976 conditions were comparable with those that occurred during other years within the past half century. Comparison was limited by a paucity of historical records but it was shown that for the Thames at Teddington the July 1975 to September 1976 fifteen month drought was not as severe in its effects on runoff as the earlier periods (notably 1933 - 1934 and 1943 - 1944). However a comparison of the last nine months of each period showed the 1976 period to be more severe than 1933 - 1934 and 1943 - 1944.

Assessment of drought severity for West Walk is difficult due to the absence of long records. However it is possible to show the variation and response of rainfall, runoff and SMD (soil moisture deficit) in the catchment. Potential evaporation (E_p), areal actual evaporation (E_A), effective rainfall and areal SMD were calculated by the Meteorological Office using climatological data from the nearest climate station (Martyr Worthy NGR SU 4151 7338, 61 m AOD) and rainfall from West Walk. The land use classification for the computation was as follows:

Type A: vegetation up to 10 years old - root constant 50.8 mm - 60.2 % catchment area

Type B: vegetation over 10 years old - root constant 203.2 mm - 34.8 % catchment area

Type G: bare soil - 5 % catchment area.

Potential and actual evaporation and SMD are calculated using the Penman equation for West Walk. Recent research has shown that in forested catchments E_A comprises interception and soil moisture

depletion losses (see Calder, 1979, for a 'state of the art' Summary). The Penman model does not include the former component and will introduce errors into the water balance. It is possible that this error was smaller during the drought than in average years, simply because there was less rainfall to be intercepted; that is, soil moisture depletion increased by comparison with interception loss.

Figure 4.11 gives daily rainfall, daily SMD and daily mean flow for subcatchment W1. There was a striking shortage of recharge during the 1975 - 1976 winter, the SMD never disappearing. Consequently, baseflow diminished rapidly during 1975 with channel flow in the catchment ceasing for most of July and August, a period when the SMD was usually above 150 mm, touching 215 mm towards the end of August. The wilting point of some of the shallow-rooted plants and shrubs was reached as evidenced in the field during August 1976. Autumn 1976 represented a period of considerable ground water recharge with the SMD disappearing from November to February. Baseflow reappeared as a substantial componcnt of catchment runoff. The streamflow response to rainfall can be seen to depend heavily upon the state of the soil moisture reservoir at any point in time. Streamflow is higher for a low SMD than for a high SMD, ground level rainfall being equal. In the latter case some soil moisture recharge takes place before runoff occurs, although rapid interflow to the channel may operate through interped fissures near the stream.

(b) Tests for Data Homogeneity

Bcfore a water balance can be attempted the data must be checked for homogeneity. Heterogeneity may be due, in the case of rainfall, to changing a raingauge, or in the case of streamflow, deforesting an area within the catchment. These examples both occurred in West Walk during the study period. The double-mass curve technique (Searcy and Hardison, 1960) is used for the purpose here, and involves plotting the cumulative data in question against cumulative concurrent data from another nearby station or average of several nearby stations. Any inconsistency in the record will show as a break of slope in the curve. V.T. Chow (1964) recommends that at least five years of record are required before any consistent slope can be recognised on a double-mass curve. In the present case this is impossible, so monthly data are used.

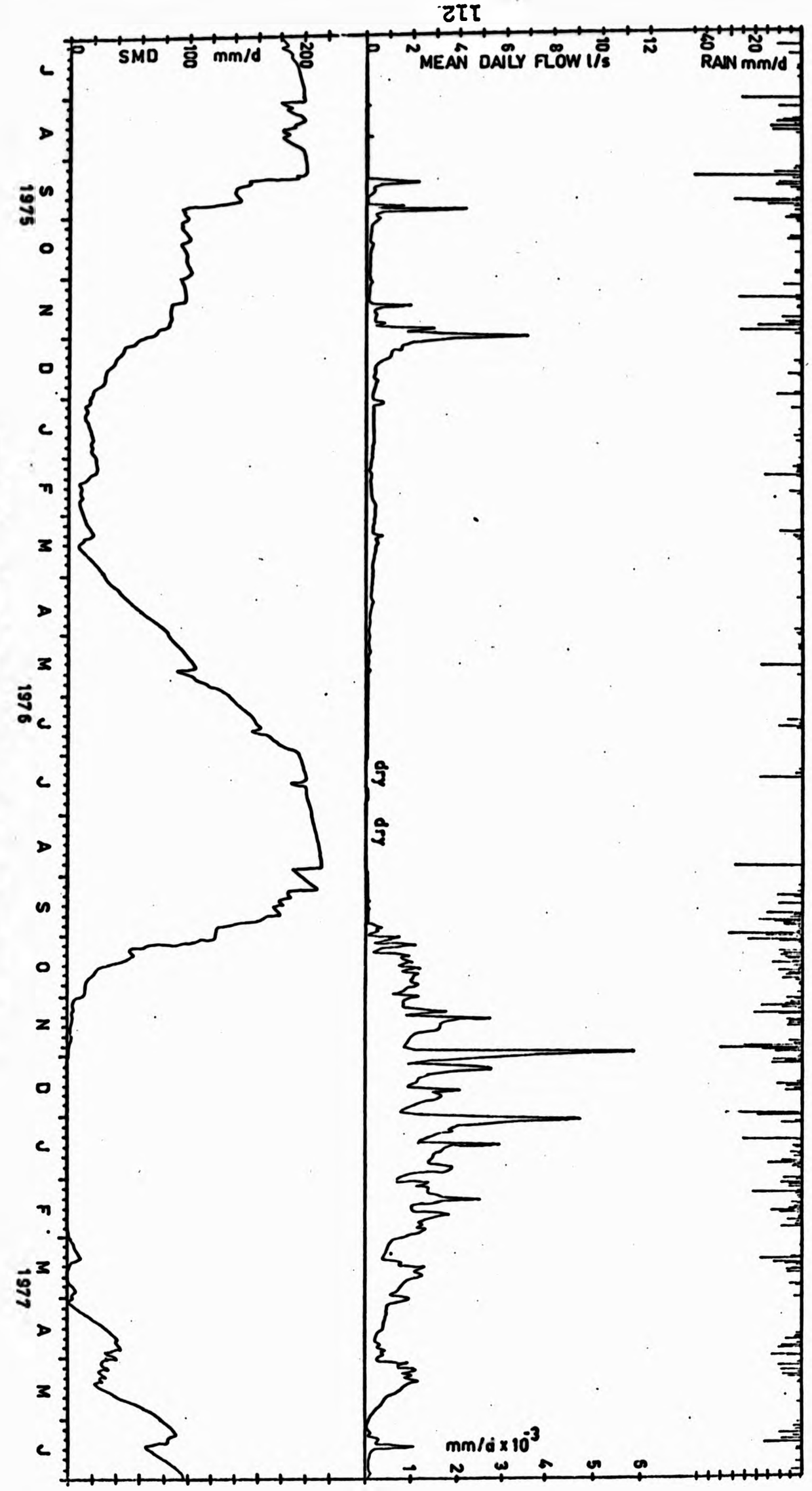

FIGURE 4.11: DAILY RAINFALL, SOIL MOISTURE DEFICIT AND DAILY MEAN FLOW AT W1, 1975/1976 - 1976/1977

(i) Rainfall

In Figure 4.12 cumulative monthly rainfalls for West Walk are plotted against the mean of cumulative monthly rainfalls for Butser Hill (NGR SU 716 202, 262 m AOD) and Southsea Common (NGR SZ 640 990, 2 m AOD). There are some small temporary deviations from this line, indicating single errors rather than trends. In particular, the breaks at August and November 1976 may represent cumulative errors in estimation of data by linear regression where gaps in the record occurred. No attempt was made to improve the data quality.

(ii) Actual Evaporation

Areal E_A for West Walk is double-massed against areal E_A for the River Rhee catchment (Cambridgeshire) (Figure 4.13). The latter data were prepared for a separate water balance by the Meteorological Office and are known to be consistent (G.E. Spraggs, 1979). The temporary deviations from the general line may be due to land use differences between the two catchments (greater E_A is allowed from the forested catchment during summer months) or to regional climatic variations.

(iii) Streamflow

Mean monthly streamflows for West Walk and its subcatchments were double-massed against the nearby River Wallington at North Fareham (NGR SU 587 075). The Wallington catchment is geologically similar to West Walk and is preferable to the predominantly Chalk River Meon catchment into which West Walk drains. However, catchment land use contrasts strongly, West Walk having a much higher proportion of forest than the Wallington, a factor which would produce seasonal deviations from a double mass curve, using monthly data. In Figures 4.14 A - E, double mass curves are plotted for each of the gauging stations at West Walk against the River Wallington on a monthly basis, although October 1976 has been omitted due to instrument failure at North Fareham.

West Walk Flume versus River Wallington (Figure 4.14 A)

The relationship suggests that the gauged flows at West Walk flume generally represent a consistent record. Two deviations from the line occur from July to October 1975 and from October to November 1976, although both deviations gradually return to the double-mass curve.

The earlier deviation is unlikely to be caused by over-estimation for West Walk because corrected values would be less than the sum of discharges from subcatchments 2 and 5. The later deviation may be due to under-estimation of flows at North Fareham during the very wet autumn because flow bypasses the gauging station above about 9.2 cumecs. While it is possible to speculate about the cause of these deviations it is equally likely that they represent seasonal differences in catchment response. Similar seasonal fluctuations around a double mass curve have been detected elsewhere (Spraggs, 1979).

Subcatchment 1 versus River Wallington (Figure 4.14 B)

The gauged record at W1 is consistent until February 1977 when flows begin to under-estimate the predicted value. This suggests a drift in the datum (i.e. setting of the chart pen) until March when the datum was corrected as indicated by the line almost parallel to the double mass curve. It is interesting to note that the start of this deviation corresponds exactly with a change of field technicians. W1 flows were corrected by converting Wallington flows from the double mass curve.

Subcatchment 2 versus River Wallington (Figure 4.14 C)

The relationship is very similar to that of the flume and Wallington, and again seasonal fluctuations in catchment response may explain slight deviations from the line.

Subcatchment 4 versus River Wallington (Figure 4.14 D)

The record is consistent apart from December 1976 and January - February 1977 when there appears to have been a drift in the datum similar to that at W1. During these three months recorded flows were lower than true flows. Between March and June 1977 there is small over-estimation of flow. Monthly mean flows from December 1976 to June 1977 have been estimated using the double mass curve.

Subcatchment 5 versus River Wallington (Figure 4.14 E)

The double mass curve for these data is non-linear, probably due to contrasting catchment land use and hence hydrological response. Subcatchment 5 has a dense forest cover, 95 % of which is more than

fifteen years old, enhancing actual evaporation and interception losses. As a further check on data consistency SC5 is double massed against West Walk flume, which has already been shown to be reasonably consistent. There is fluctuation around the straight line, again probably best explained by differences in seasonal catchment response. In the absence of a nearly identical catchment for comparison the prime record for SC5 was accepted as accurate.

Use of the double mass curve technique suggests that, with a few exceptions, streamflow data for West Walk is consistently reliable. The double mass curve has been used to homogenise data for 1977 at W1 and W4 although apparent inconsistencies during the drought may be due to differential catchment response and no changes were made.

(c) <u>The Water Balance</u>

The equation for the water balance is (values in mm):

$$RF = RO + AE \pm \Delta SMD \pm \Delta Sg \pm U + IL \qquad (4.23)$$

where
- RF = rainfall
- RO = runoff
- AE = actual evaporation
- $\pm\Delta$SMD = change in soil moisture deficit
- $\pm\Delta$Sg = change in ground water storage
- $\pm$ U = underflow from the catchment
- IL = interception loss

Runoff is integrated from the record of hourly discharges for each gauging station using Simpson's rule (see Appendix 2 for computer program: WATLOS). Actual evaporation and soil moisture deficit were calculated for West Walk by the Meteorological Office as described earlier. Subcatchment variations in land use (i.e. tree age) were taken into account when converting potential to actual evaporation. The residual from the water balance represents a combination of $\pm\Delta Sg \pm U + IL$. In the absence of extensive aquifer storage and with a relatively watertight basement $\pm\Delta Sg \pm U$ should be relatively small components of the water balance. It has recently been demonstrated that interception loss can be a highly significant component of the water balance in

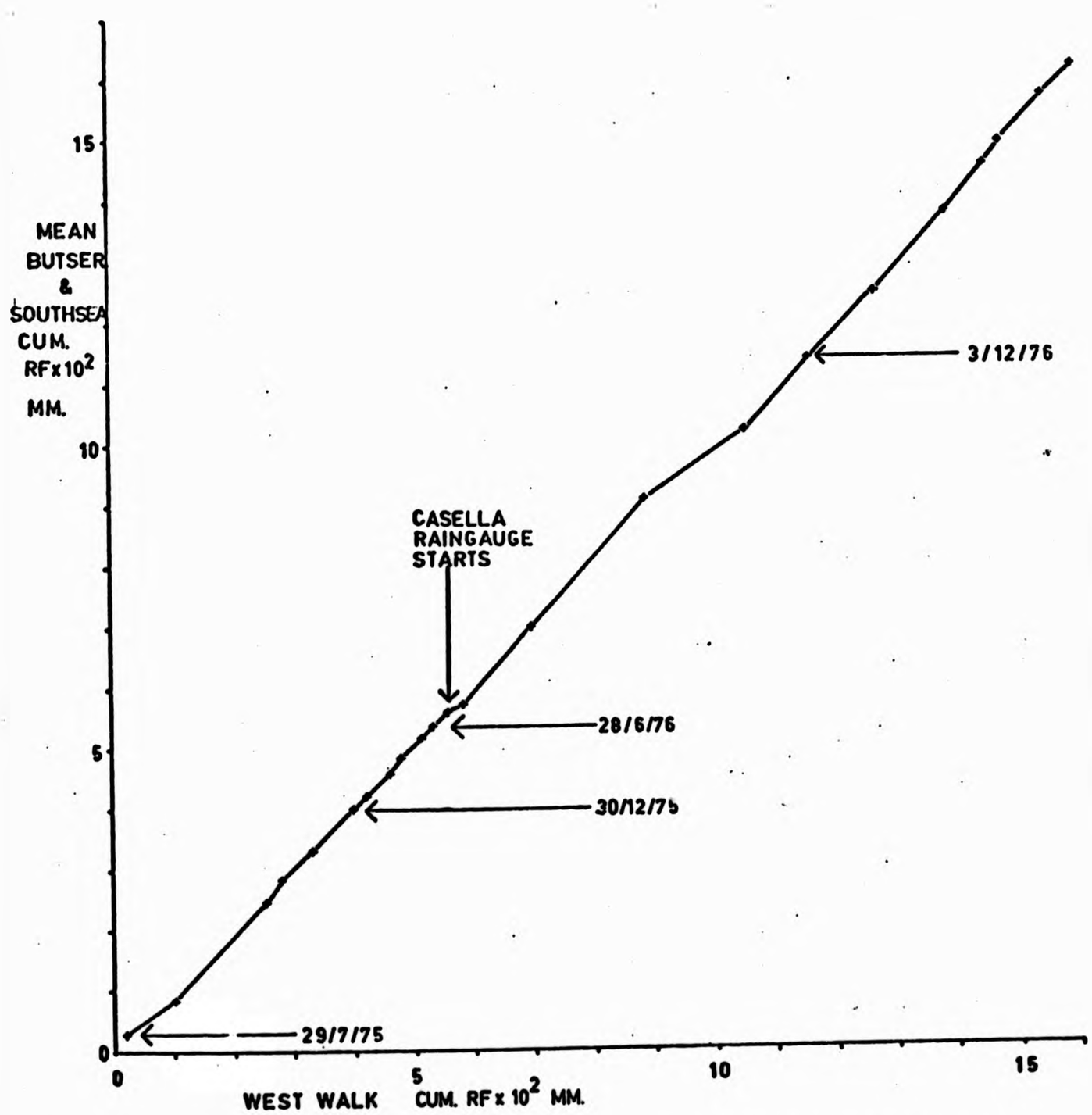

FIGURE 4.12: DOUBLE MASS CURVE FOR CHECKING WEST WALK RAINFALL DATA

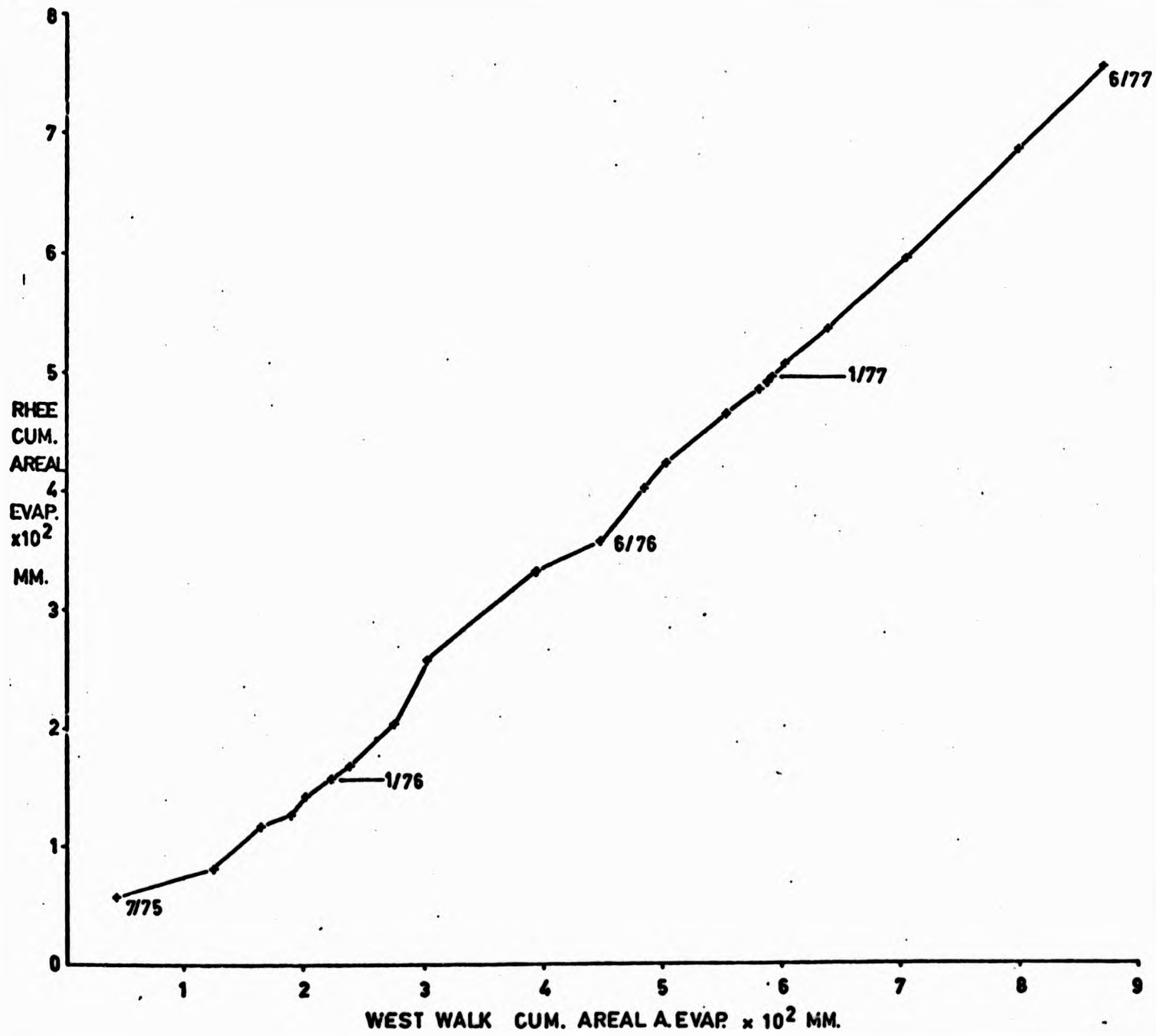

FIGURE 4.13: DOUBLE MASS CURVE FOR CHECKING WEST WALK ACTUAL EVAPORATION DATA

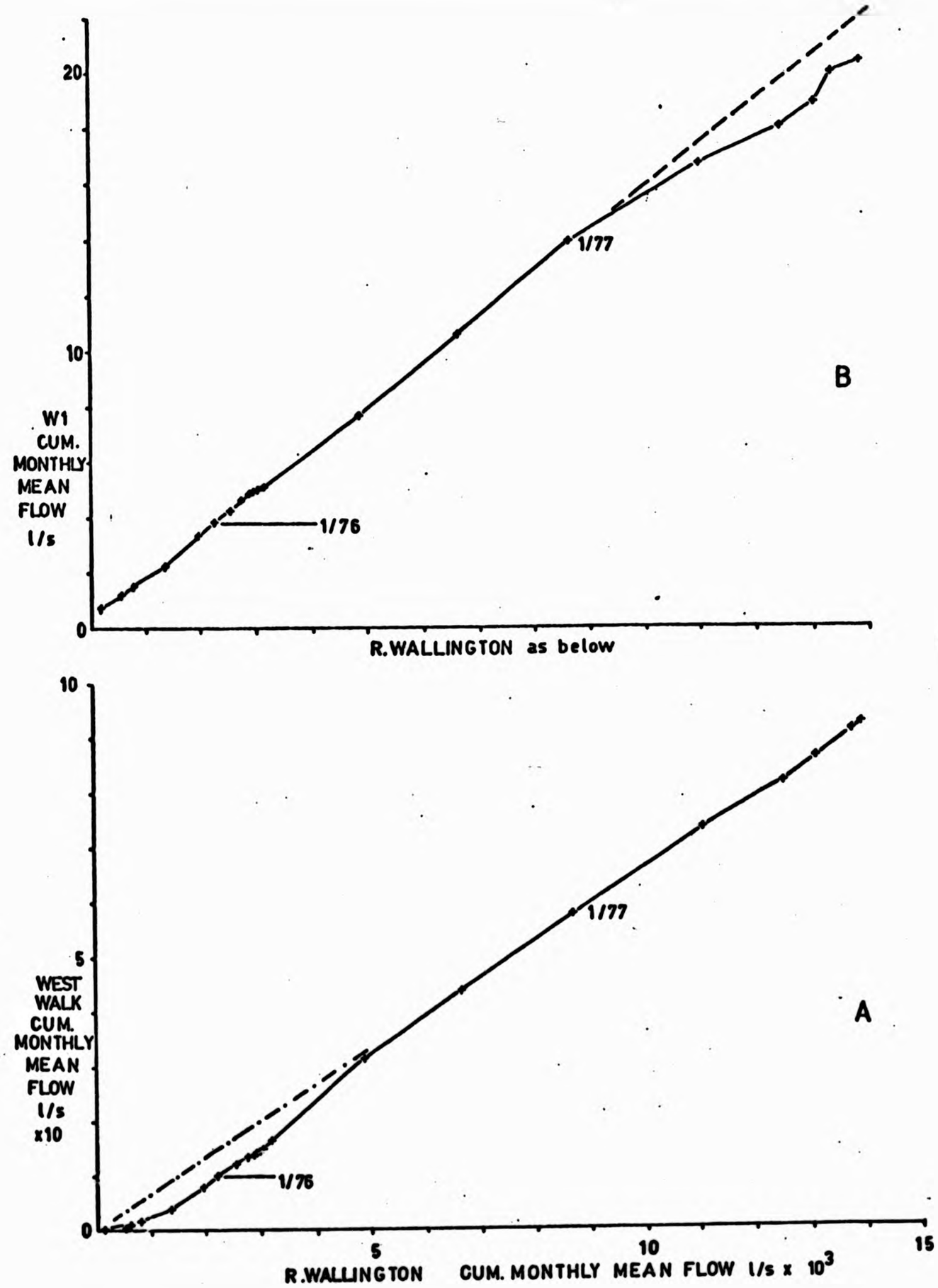

FIGURE 4.14: DOUBLE MASS CURVE FOR CHECKING WEST WALK STREAMFLOW DATA
A: FLUME B: WEIR 1

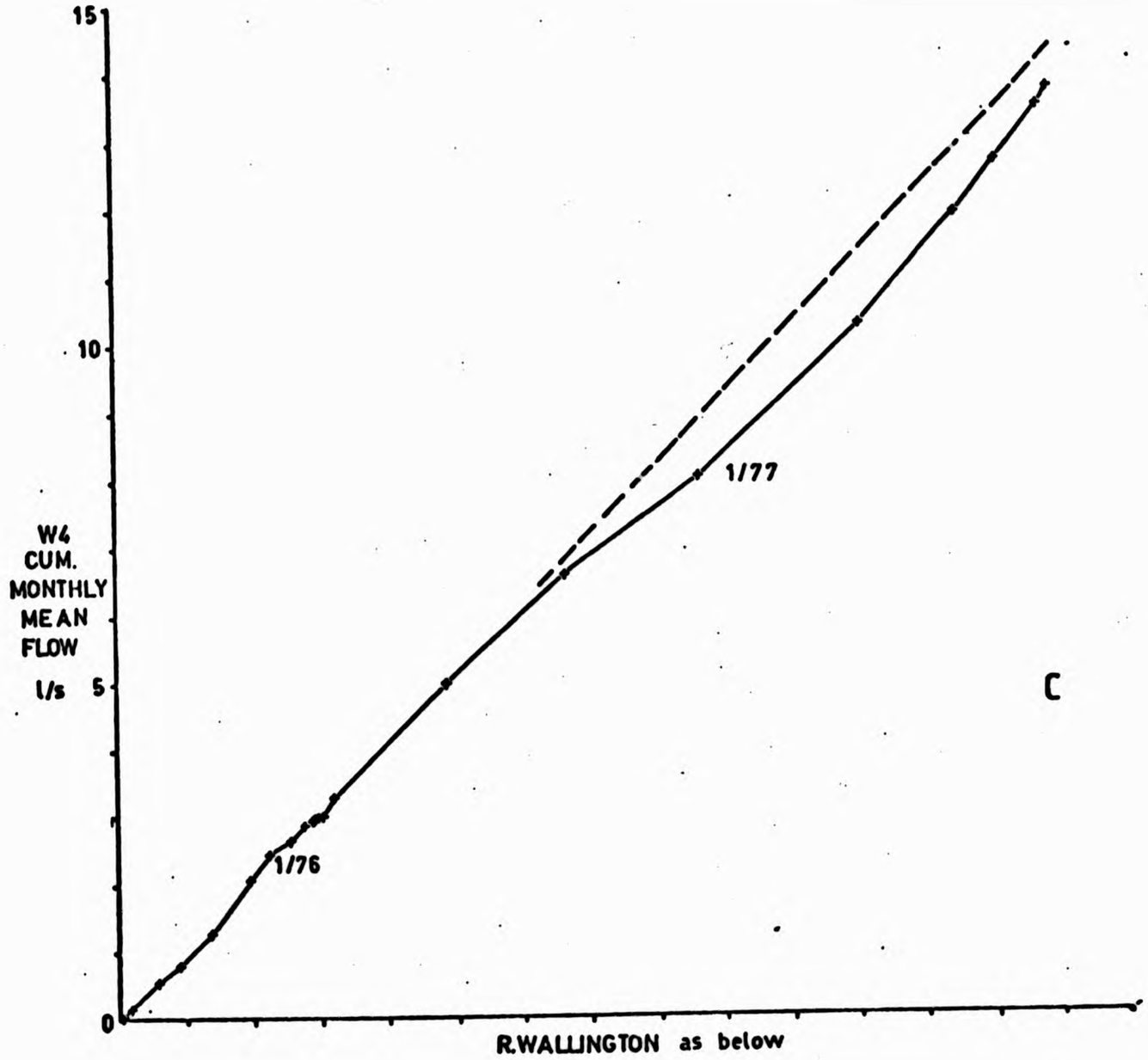

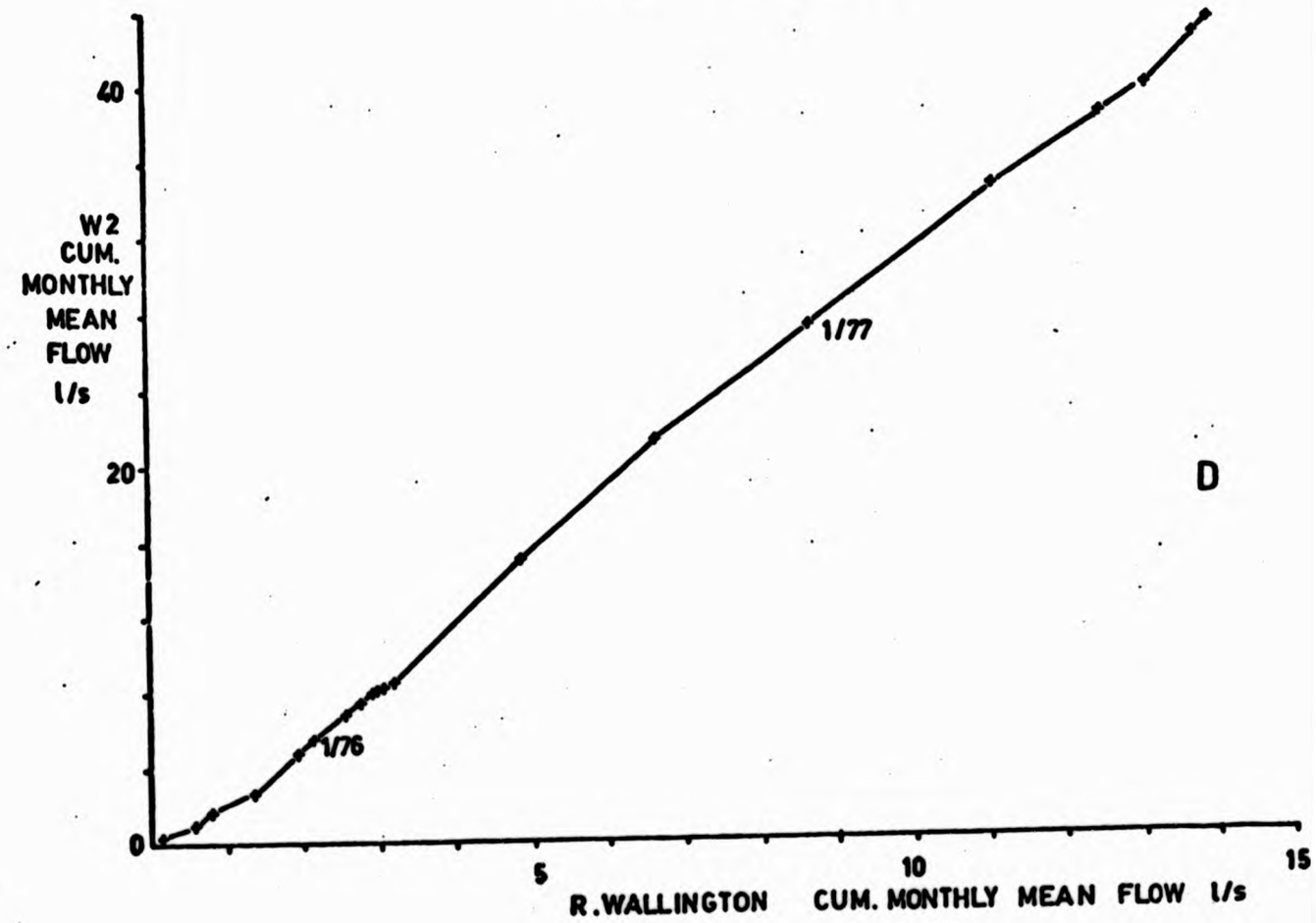

FIGURE 4.14 (cont'd): C: WEIR 4 D: WEIR 2

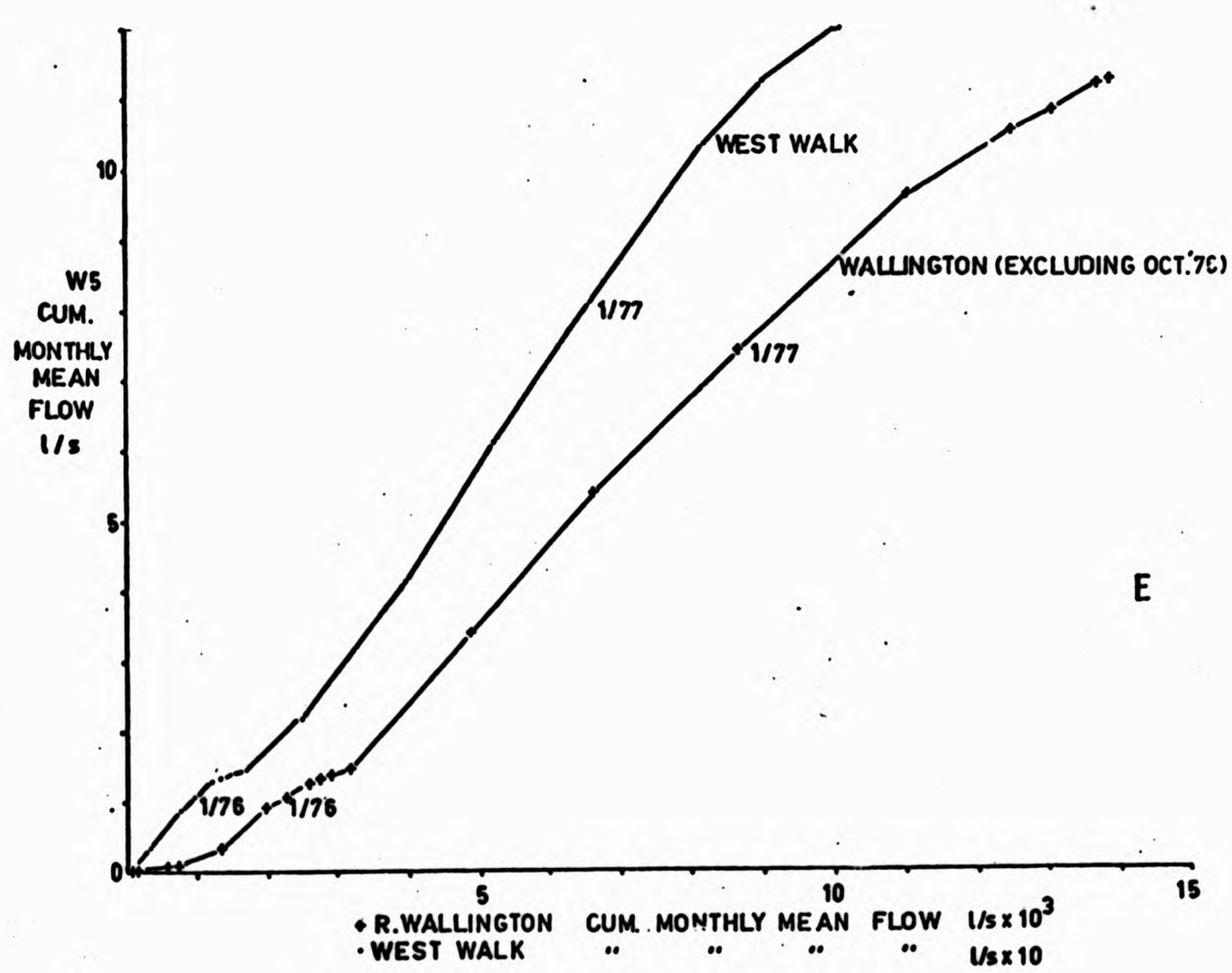

FIGURE 4.14 (cont'd): E: WEIR 5

forested catchments. I.R. Calder (1979) has used a lysimeter experiment to measure interception and evapotranspiration losses from a forest in the upper Severn catchment. The rate of interception loss was shown to be twice that by transpiration. In the present case it is not possible to quantify interception loss, only to speculate as to its possible role in the catchment and subcatchment water balance. Figures 4.15 to 4.19 show the water balance for 1975/1976 to 1976/1977, with Table 4.9 giving the annual summaries.

A combination of low rainfall and high actual evaporation give an overall gain in soil moisture storage during the period for each catchment, this comprising a small loss to storage in 1975/1976 and a large gain in 1976/1977. Seasonal variation is characterised by losses from storage during summer months, gains in September and October, and little change during winter months.

Streamflow is severely depleted during 1975/1976 and only rises as the soil moisture store is filled in September 1976. This is well illustrated by the mean monthly flows for all catchments shown in Figure 4.20 (SC4 is omitted because of virtual coincidence with SC1).

Subcatchment 5 with the high percentage of forest cover greater than 10 years old shows the highest losses by actual evapotranspiration, with streamflow ceasing in July and August 1975 and from June to August 1976. It is also interesting to compare the peak actual evaporation losses in 1975, 1976 and 1977 for each catchment. The equally high values for subcatchment 5 reflect the dominance of older trees with an ability to reach deeper storage. 1976 peak evapotranspiration is lower than in 1975 or 1976 in other catchments, the amount depending upon the proportion of trees more or less than 10 years old.

The water balance residuals are difficult to interpret because of the unknown proportions of interception and changes in ground water storage. However, since there is only a very small Bagshot Sand aquifer there are unlikely to be large ground water storage changes within West Walk or its subcatchments. It therefore seems reasonable to interpret residuals from the water balance as being predominantly interception losses. For West Walk and its subcatchments there is a

good balance from July 1975 to September 1976, the major residuals occurring in October and November 1975 for all areas. The absence of significant negative residuals implies that ground water storage is not greatly depleted and that the large positive residuals which occur during winter 1976/1977 mainly represent interception losses. Larger negative residuals occur in all areas from April - June 1977.

Interception loss may be modelled in terms of both the structure of the forest and the climate in which it is growing by the Rutter model (Rutter et al, 1971; 1975). Structure of the forest is important in terms of its canopy storage capacity, aerodynamic properties for evaporation from the canopy store, stemflow and trunk storage. Climate influences the spatial difference in interception loss due to different durations of rainfall and hence of canopy wetness (Gash and Morton, 1978). Within West Walk there is considerable variation in vegetation species and maturity and hence of interception loss due to canopy structure. Within a stand of 16 year old Western Hemlock in SC5 interception loss has been inferred as varying from circa 10 % under wet canopy conditions to circa 50 % under dry canopy conditions with an average of circa 35 %. Throughfall was also found to be a direct function of rainfall intensity (N. Argent, personal communication, 1979). Table 4.9 shows that there is an overall positive residual for all catchments, this being greatest for SC2 and West Walk. The smallest residuals occur in SC4 and SC5. Negative residuals occur in all catchments, particularly in the autumn of 1975 and 1976, and spring 1977. The smaller residual for SC4 suggests the influence of geology in minimising ground water storage and low interception losses resulting from immature vegetation. Low residuals for SC5 are surprising considering the mature Western Hemlock forest and may reflect the importance of geology. Residuals are expressed as percentages of rainfall in Figures 4.15 to 4.19, mean values ranging from 23 % (SC5) to 36.4 % (SC2). There is a marked similarity between these percentages and inferred interception (Argent, ibid) although true proportions of interception and ground water storage cannot be quantified in this study. There are errors in estimation of the water balance components which places some uncertainty on the conclusions reached. Errors in the measurement of point rainfall have already been discussed; the estimation of actual evaporation by the Meteorological

TABLE 4.9

Summary of West Walk Water Balance 1975/1976 - 1976/1977 (Values in mm)

		RF	RO	AE	± Δ SMD	RESIDUAL (RESID/RF) %
West Walk	1975 - 1976	530	69	449.3	26.4	37.8 (7 %)
	1976 - 1977	1055.4	373.3	416.6	- 52.8	213.6 (20 %)
	TOTAL	1585.4	442.3	865.9	- 26.4	251.4 (16 %)
W1	1975 - 1976	530	69.3	507.1	33.2	- 13.2 (- %)
	1976 - 1977	1055.4	293.4	428.2	- 92.1	241.7 (23 %)
	TOTAL	1585.4	362.7	935.3	- 58.9	228.5 (14 %)
W2	1975 - 1976	530	52.2	425.2	19.4	68.8 (13 %)
	1976 - 1977	1055.4	260	415.6	- 53.1	326.7 (31 %)
	TOTAL	1585.4	312.2	840.8	- 33.7	395.5 (25 %)
W4	1975 - 1976	530	102.5	480.7	25.5	- 27.7 (- %)
	1976 - 1977	1055.4	448.2	451	- 88.5	67.7 (6 %)
	TOTAL	1585.4	550.7	931.7	- 63.0	40 (2.5 %)
W5	1975 - 1976	530	48.4	561.8	43.6	- 43.6 (- %)
	1976 - 1977	1055.4	379.6	434.7	- 123.3	117.2 (11 %)
	TOTAL	1585.4	428	996.5	- 79.7	80.6 (5 %)

Office method is also subject to error (Headworth, 1970). The accuracy of streamflow data is variable with discharge, as discussed earlier.

In conclusion it appears that actual evaporation was the dominant loss process during the drought period of 1975 - 1976; spatial variation occurred within West Walk with highest soil moisture and AE losses and lowest runoff losses from subcatchment 5, with its relatively mature forest and London Clay basement. 1976 - 1977 was a period of increased rainfall, higher interception and streamflow losses, and soil moisture recharge. Subcatchment 4 exhibited the greatest runoff for both periods, with high evapotranspiration and relatively low interception losses; this reflects its mainly London Clay base and lower percentage of mature forest.

B. Spatial Variation in Short Term Catchment Response

Within West Walk catchment hydrological response to rainfall varies both spatially and temporally. Spatial variation can be accounted for in terms of differences in geology, soils, vegetation and, to a lesser extent, topography. There are seasonal variations in the relative importance of each of these factors, together with the natural variability of rainfall quantity and intensity, evapotranspiration, interception and soil moisture. The end result is a highly complex, non-linear, spatially variable hydrological system. Streamflow solute dynamics at the flume will reflect the spatial response of the system and some understanding of the latter is desirable.

(a) Example 1: A Winter Storm

Figures 4.21 and 4.22 show catchment response to a February 1977 rainstorm of 13.75 mm with flows in $l/s/km^2$ and l/s respectively. The soil was at field capacity and actual evaporation almost zero for this period. The temporal relationship of the hydrograph peaks is interesting although travel times must be treated with caution due to

(i) the linear correction of clock time-loss which may in reality be non-linear;

and (ii) errors in extracting data from the charts (e.g. due to line thickness).

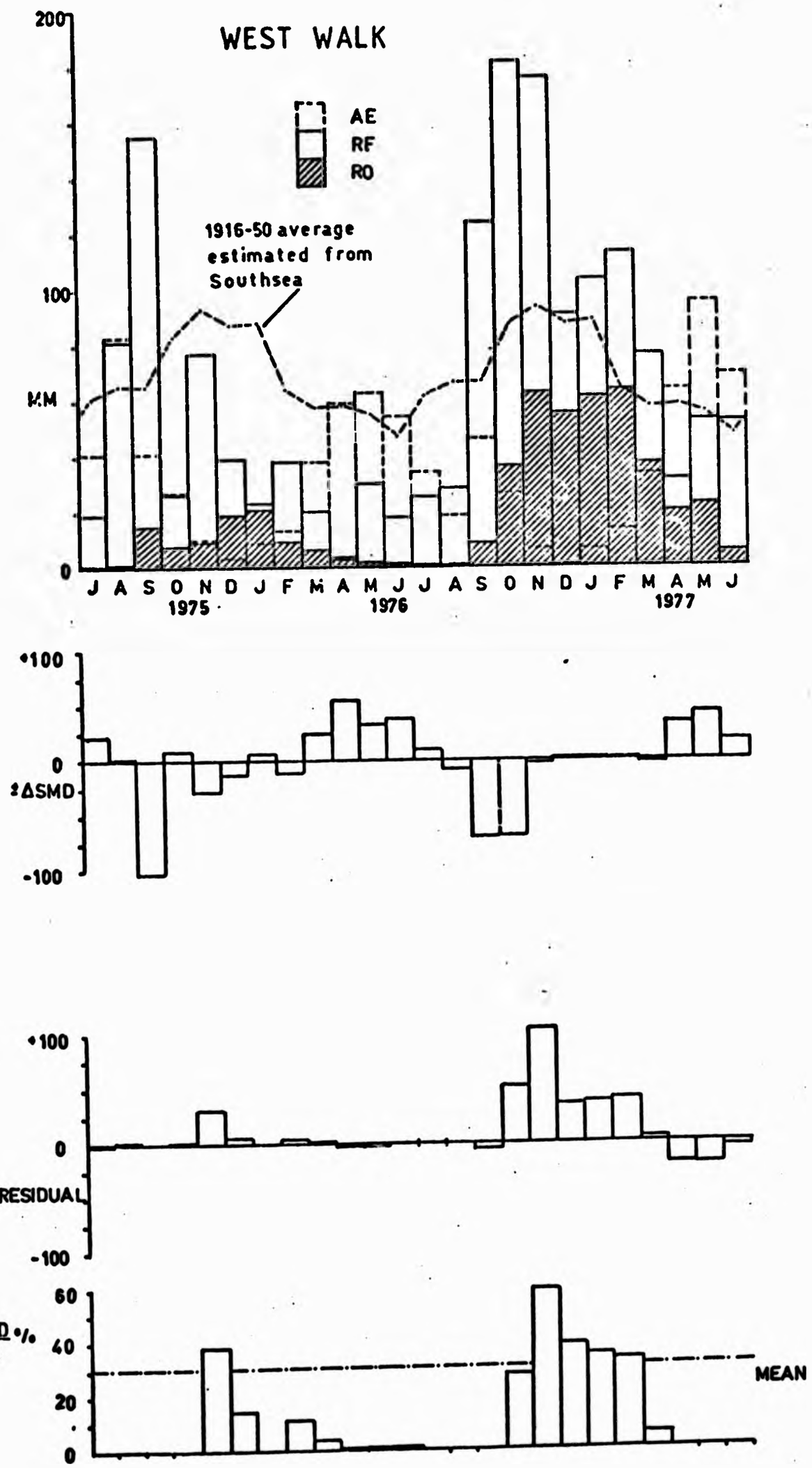

FIGURE 4.15: THE WATER BALANCE FOR WEST WALK
(AE: actual evaporation; RF: rainfall; RO: runoff)

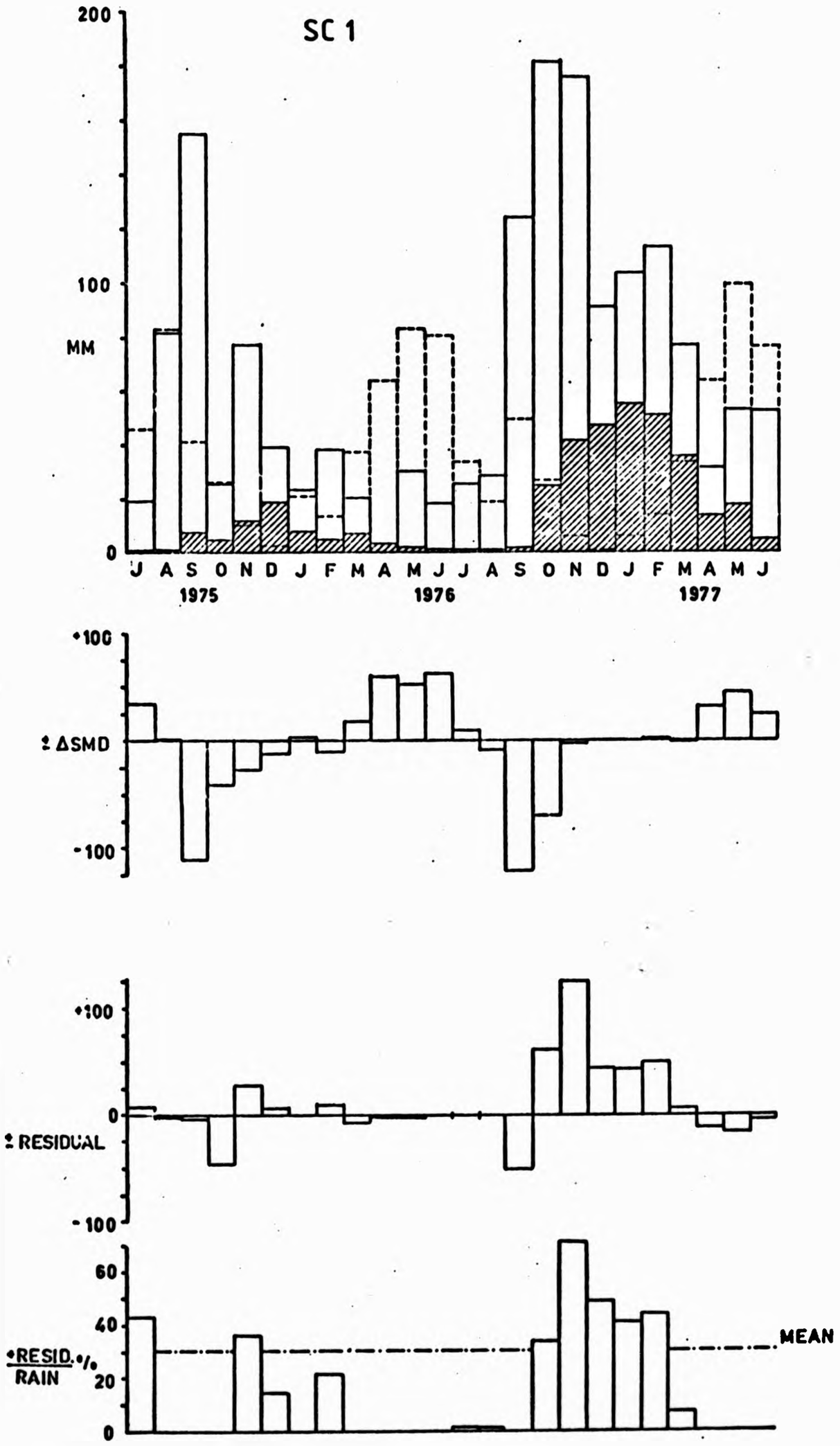

FIGURE 4.16: THE WATER BALANCE FOR SUBCATCHMENT 1
(for Key, see Figure 4.15)

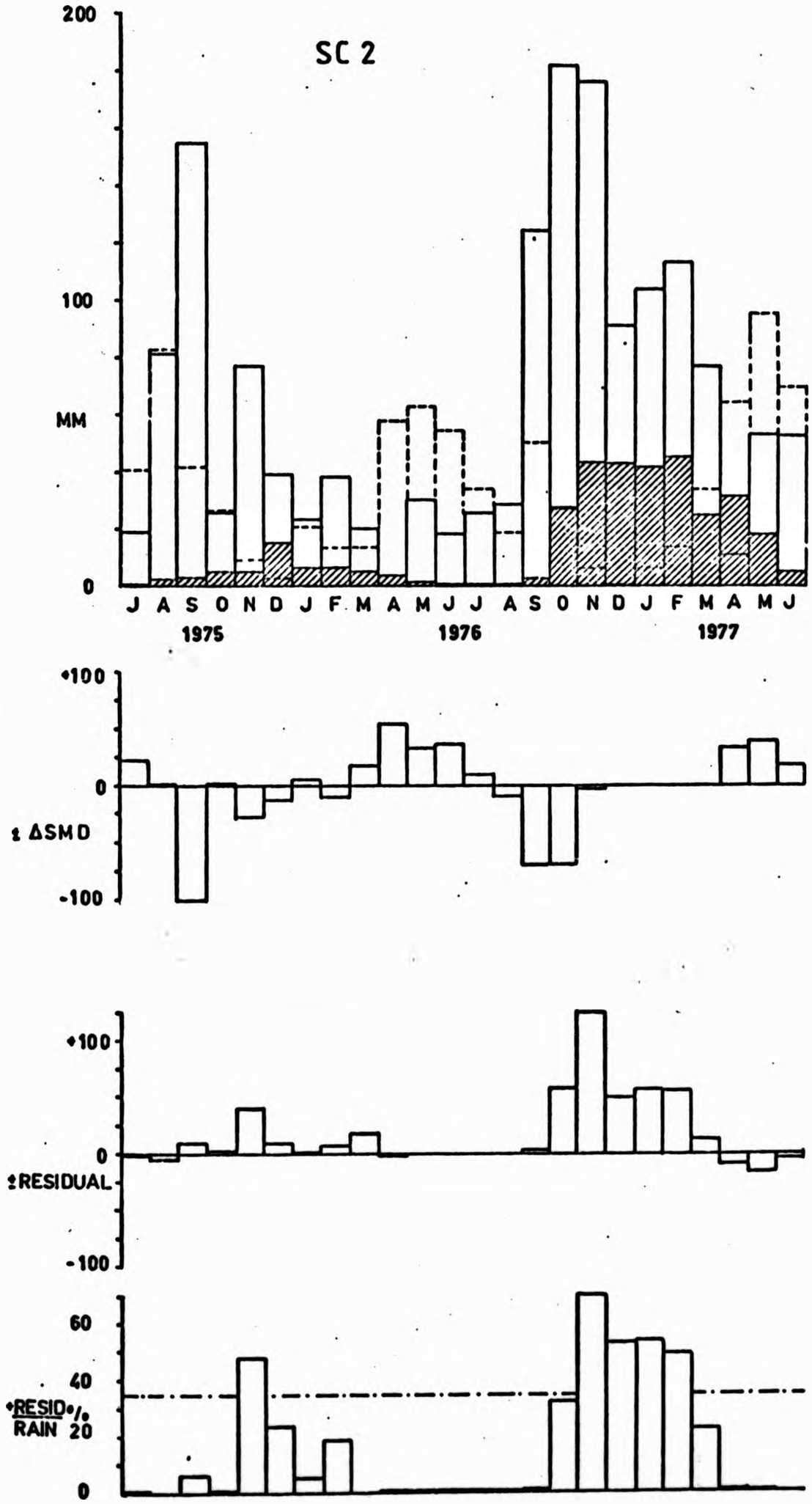

FIGURE 4.17: THE WATER BALANCE FOR SUBCATCHMENT 2
(for Key, see Figure 4.15)

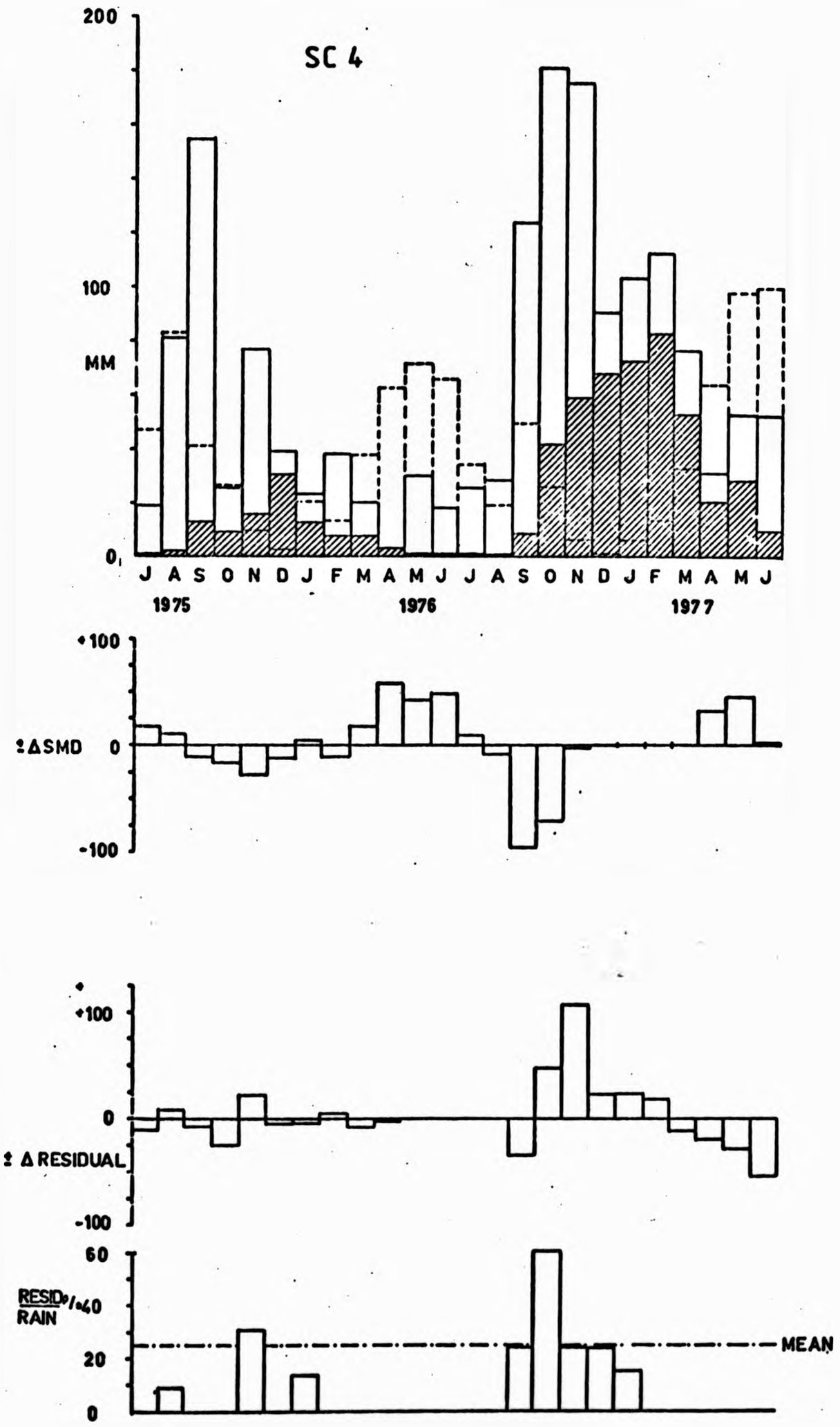

FIGURE 4.18: THE WATER BALANCE FOR SUBCATCHMENT 4
(for Key, see Figure 4.15)

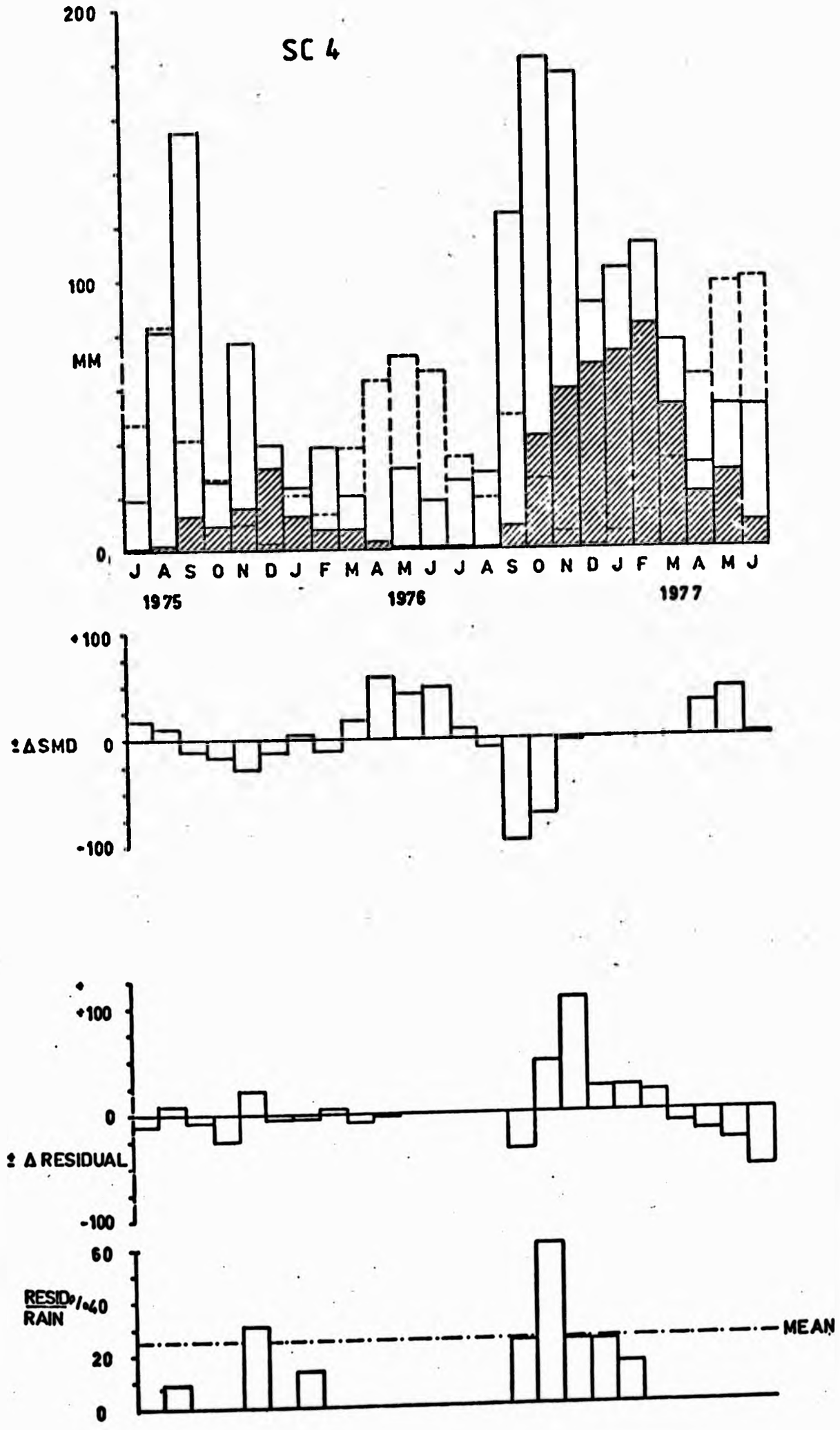

FIGURE 4.18: THE WATER BALANCE FOR SUBCATCHMENT 4
(for Key, see Figure 4.15)

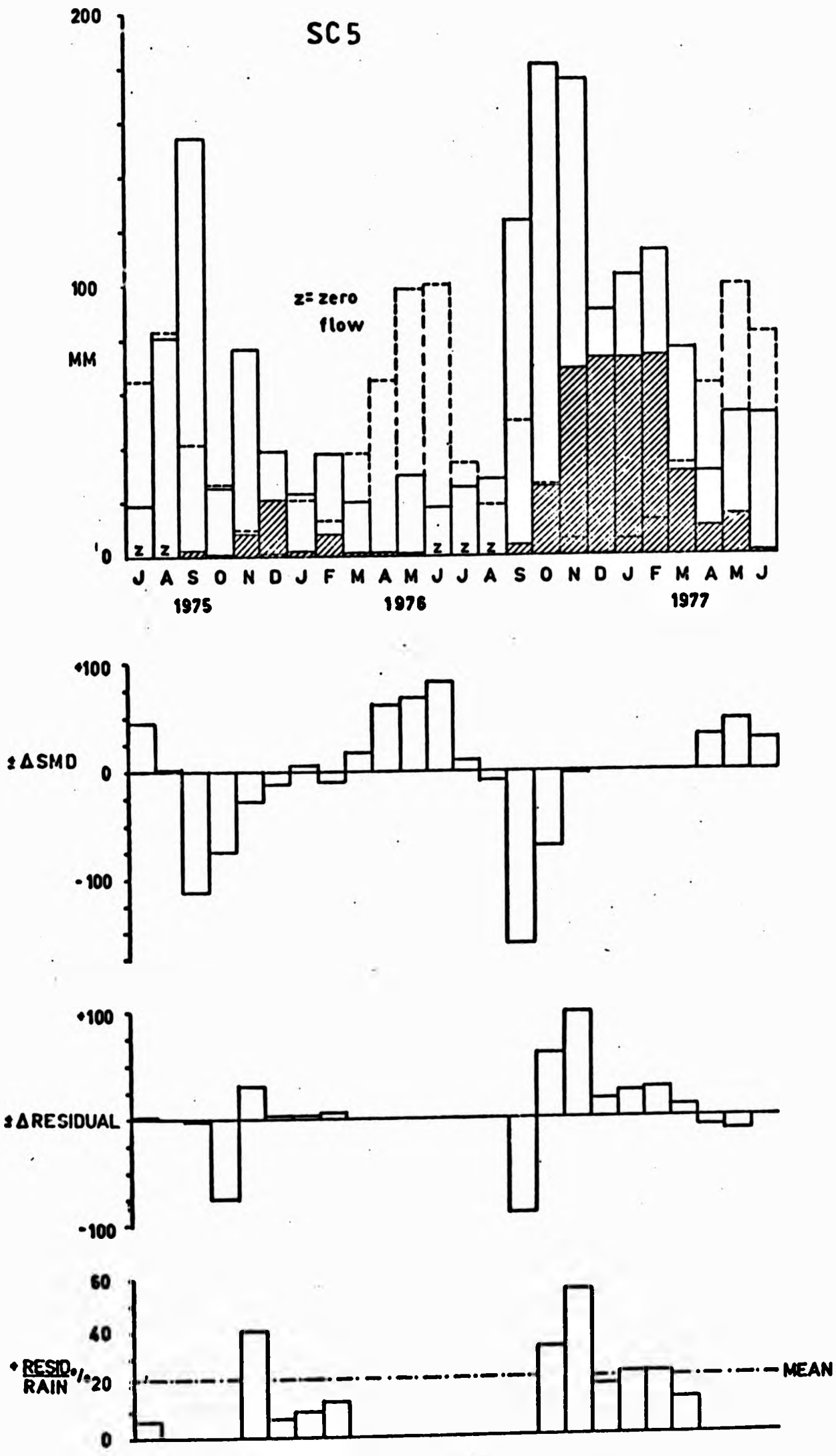

FIGURE 4.19: THE WATER BALANCE FOR SUBCATCHMENT 5
(for Key, see Figure 4.15)

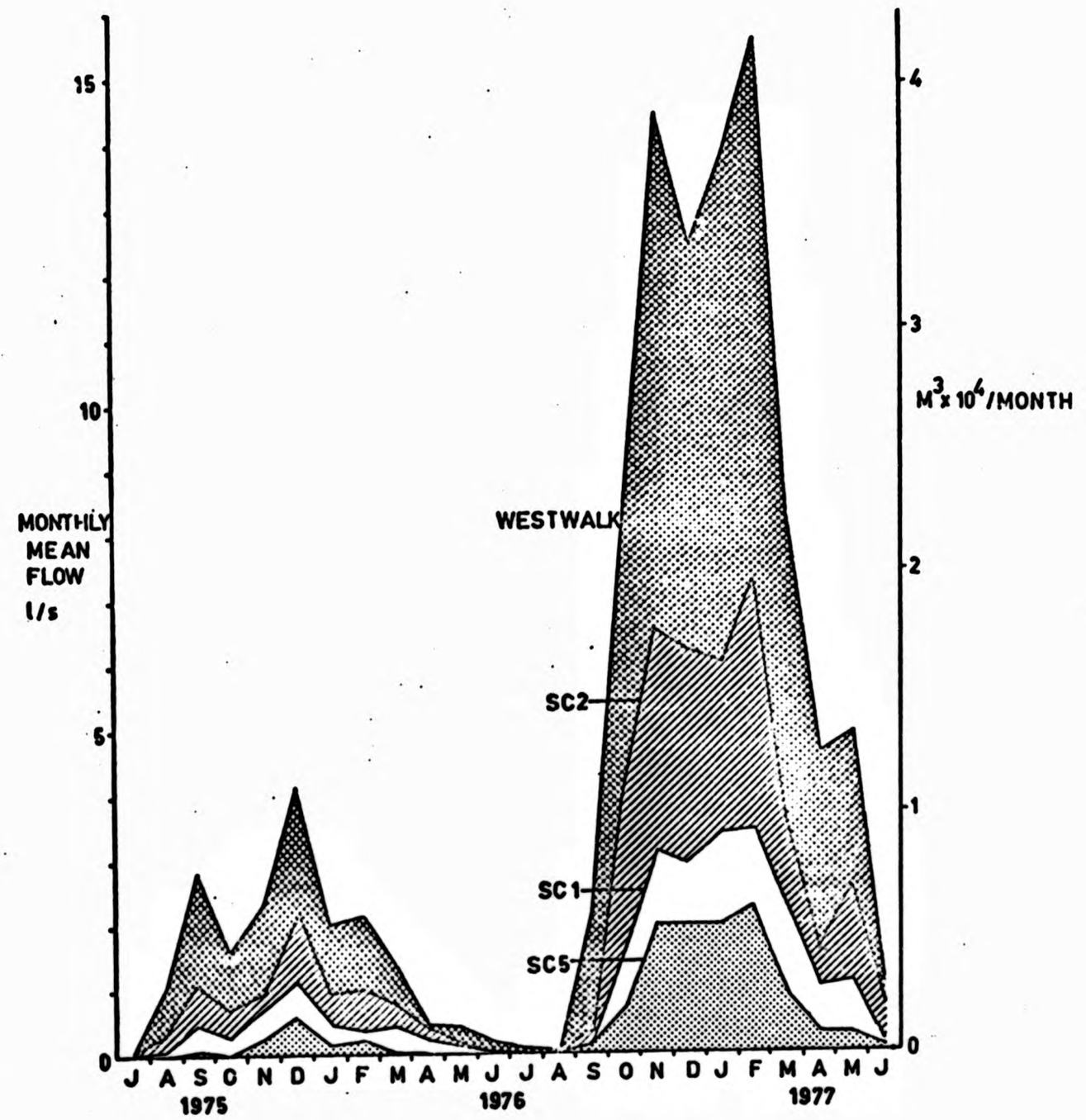

FIGURE 4.20: MEAN MONTHLY FLOWS AT WEST WALK, 1975/1976 - 1976/1977

Table 4.10 gives a comparison of catchment response using several indices. Peak runoff appears to be dominated by geology rather than vegetation age and species during the winter storm. The highest value occurs from SC4 where 80 % is London Clay and 50 % Oak planted in 1973. Total catchment peak runoff is similarly high suggesting the importance of geology over vegetation in the catchment area below W2. The value of 13.41 % for SC5, 85 % of which is evergreen forest more than 15 years old (in 1978) re-affirms this conclusion. It is probably the combination of immature Oak and Beech on London Clay adjacent to the channel which produces a peak runoff of 45.74 $l/s/km^2$ for SC2. The lower peak runoff for SC1 is probably due to a combination of higher percentage Bagshot Beds and Plateau Gravel (61 %) and higher percentage vegetation greater than 10 years old (70 %).

The intensity of hydrograph rise (IR) diminishes up catchment from 7.5 l/s/hr at the flume to 1.3 l/s/hr at W1. This emphasises the influence of geology and soils (i.e. London Clay with ground water gleys) in rapidly converting rainfall to runoff in lower and middle catchment contributing areas. The low IR for SC4 is surprising considering the high peak runoff and vegetation/geological characteristics described earlier.

The peak to mean ratio is a simple measure of hydrograph 'peakedness' (Gregory and Walling, 1973a). Headwater areas produce a more 'peaky' response than at the West Walk flume with the exception of SC5 where the delayed response can be accounted for by interception and throughfall processes. The low peak to mean ratio at the flume is due to attenuation of the hydrograph as storm peaks arrive from various parts of the catchment with different time lags.

Time to peak (i.e. hyetograph centroid to hydrograph peak) increases down the main channel as expected, although SC5 peaks later due to a delayed response. Individual hydrographs are similarly lagged and from these tentative travel times can be calculated The peak from SC4 arrives at the flume first, with an approximate mean velocity of 0.17 m/s; the main channel peak moves between W1 and W2 at 0.08 m/s increasing to 0.4 m/s between W2 and the flume. The flood peak from SC5 arrives at the flume later than the main peak, contributing to the recession curve, although it is not possible to compute a velocity.

The percentage Direct Runoff gives an indication of the quantity of storm rainfall lost from the catchment. Dependence is placed upon an arbitrary method of runoff separation (Hibbert and Cunningham, 1967) discussed in an earlier section. The low percentages for the catchment areas within SC2 suggest the effects of interception and higher infiltration rates, although 5.65 % for SC4 is surprisingly low. The higher percentages for the catchment below W2 can be explained by the lower infiltration rates upon London Clay. The value of 13.41 % for SC5 also implies that a high proportion of rainfall reaches the channel due to limited infiltration, despite delayed response resulting from interception and throughfall.

(b) Example 2: A Summer Storm

An early summer storm is analysed in the same way for comparison. This occurred on 14th - 15th June 1977 when the actual evaporation rate was 2.8 mm/day (still at the potential rate) and the pre-storm SMD 72.1 mm (falling to 58.7 mm after the storm). The total storm rainfall was 15.58 mm and maximum intensity 11.4 mm/hour. The hydrographs for West Walk are given in Figure 4.23 (no data is available for W4 as the clock on the recorder had stopped). Runoff peaks were lower than for the winter storm (with the exception of the anomalous SC1) despite higher total storm rainfall and greater maximum rainfall intensity, and may be attributed to drier soil moisture conditions and higher percentage of intercepting foliage. Intensity of hydrograph rise is higher for the summer storm (with the exception of SC5 where throughfall may significantly delay response) reflecting the increased rainfall intensity and small contributing area. There is very little difference between catchment times to peak, reflecting faster channel travel velocities and low throughflow discharge to the immediate contributing area. The percentage direct runoff is lower for all catchments, indicating a replenishment of soil moisture and canopy storage (i.e. interception). In the summer storm vegetation appears to dominate geological variation as a runoff control due to the increased vegetation cover and fairly uniform SMD.

Overall, periods with a high SMD give short, quick-response hydrographs with a small percentage of direct runoff. This can probably be attributed to the replenishment of soil moisture storage

TABLE 4.10

A Comparison of Hydrograph Characteristics for West Walk Subcatchments (3.2.77 and 14.6.77)

		West Walk	SC1	SC2	SC4	SC5
Peak Runoff (l/s/km^2/hr)	winter	64.61	29.64	45.74	67.72	47.58
	summer	46.35	38.66	34.03	NA	30.71
Intensity of Rise (l/s/hr)	winter	7.54	1.26	3.96	1.53	1.49
	summer	12.07	2.33	5.60	NA	0.77
Peak to Mean Ratio	winter	2.55	3.64	3.86	6.02	2.74
	summer	2.68	2.50	2.86	NA	3.19
Direct Runoff (%)	winter	14.22	2.87	4.55	5.65	13.41
	summer	2.6	2.4	2.1	NA	2.15
Time to Peak (hours)	winter	2.5	1	2.25	1	3.75
	summer	1.5	1.5	1.5	NA	1.5

NOTES:

- Intensity of Rise - hydrograph rise divided by time of rise
- Peak to mean ratio - peak discharge divided by mean discharge during time occupied by direct runoff
- Direct Runoff % - (direct runoff separated by a line of 0.602 l/s/km^2/hr divided by rainfall) x 100
- Time to peak - time between rainstorm centroid and hydrograph peak
- NA - not available

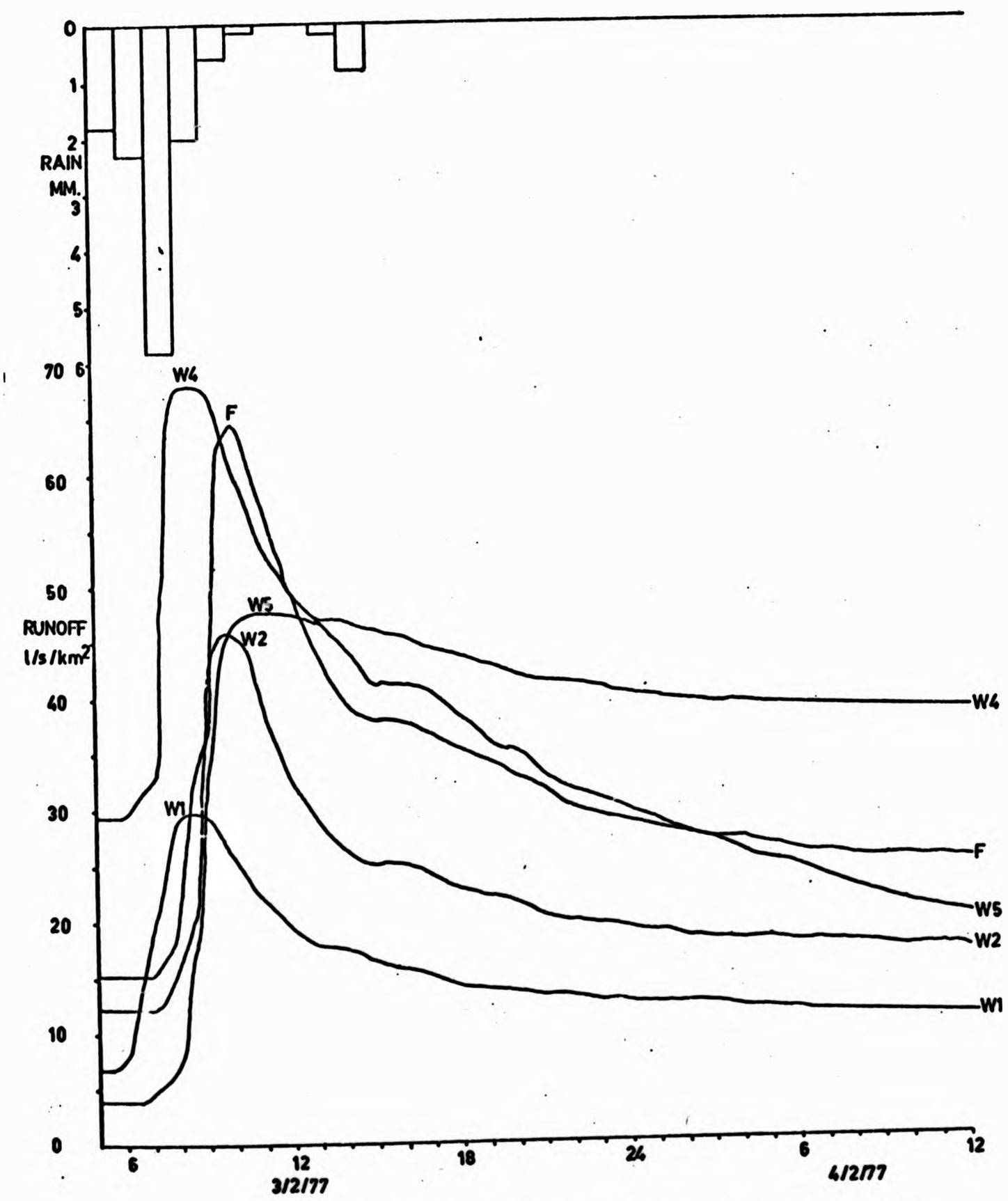

FIGURE 4.21: HYDROGRAPH RESPONSE TO A WINTER STORM AT WEST WALK ($l/sec/km^2$)

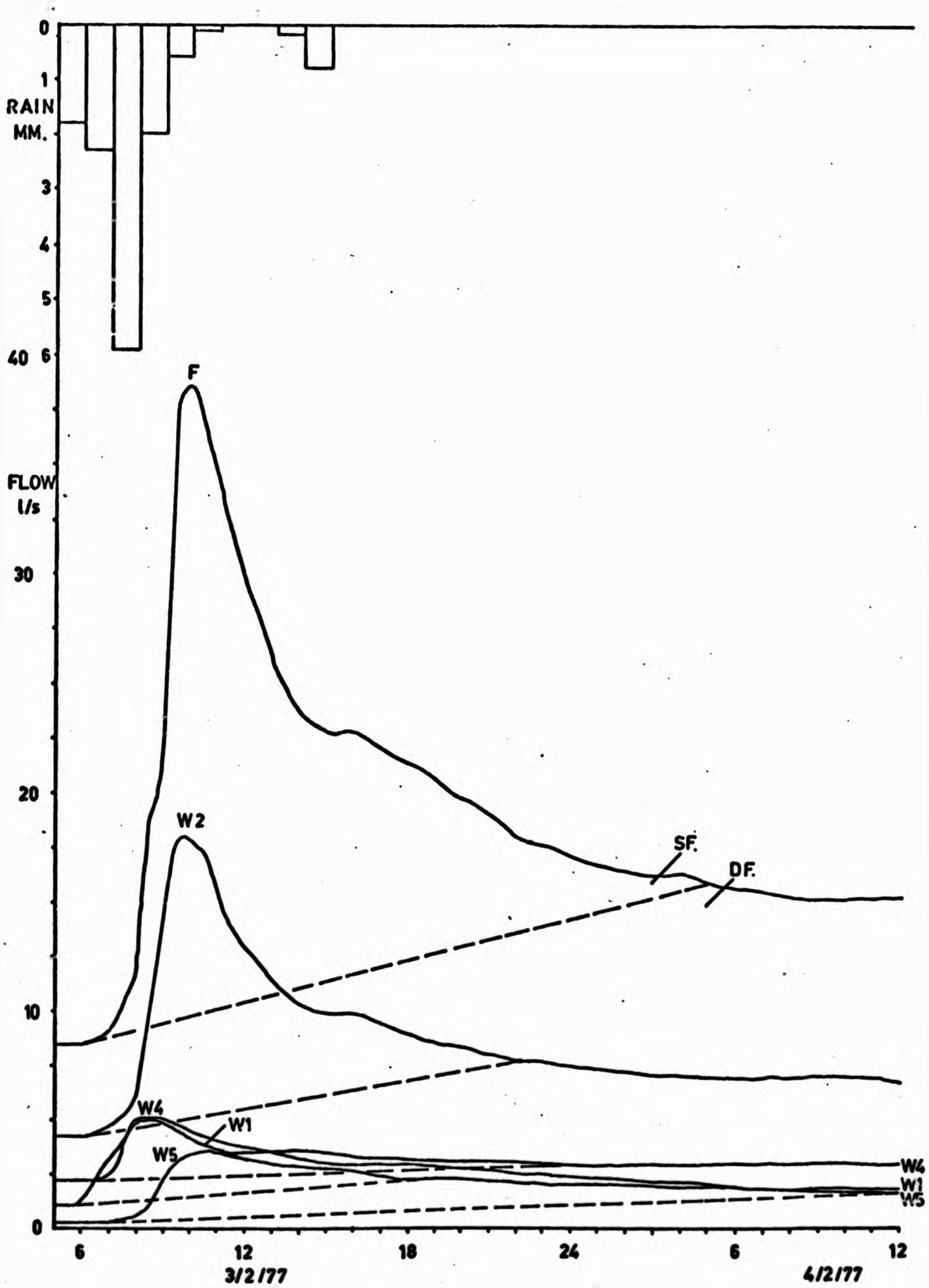

FIGURE 4.22: HYDROGRAPH RESPONSE TO A WINTER STORM AT WEST WALK (l/sec)

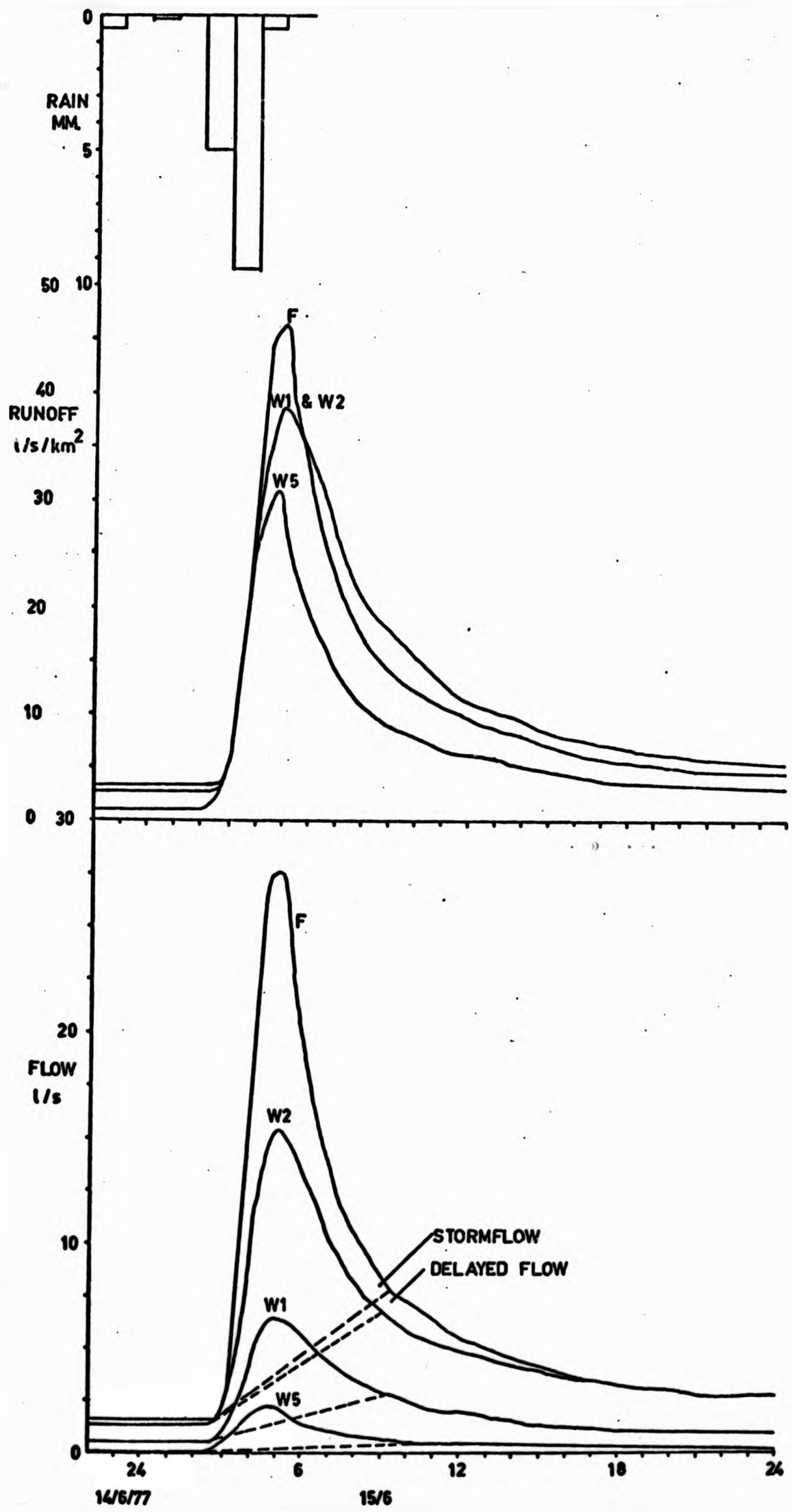

FIGURE 4.23: HYDROGRAPH RESPONSE TO A SUMMER STORM AT WEST WALK

over much of a 'dry' catchment, with a relatively small contributing area adjacent to the channel. Throughflow is likely to be greatly reduced by movement into soil moisture storage and evaporation. These results agree with a comprehensive analysis of unit hydrographs from Clay catchments in the Gloucester region (H.F. Wheater et al, 1978).

This chapter has described the design, construction and installation of West Walk gauging stations; streamflow data collection, processing and storage; errors involved in gauging, estimation of missing data and baseflow separation; rainfall measurement. The data is then used to paint the backcloth to the period of study (July 1975 to June 1977) with a water balance, and to indicate the spatial variation in hydrological responses. The water data are to be utilised in studying solute dynamics, for which the chemical analyses are described in the following chapter.

CHAPTER 5
TECHNIQUES USED IN THE SAMPLING AND ANALYSIS OF WATER

5.1 INTRODUCTION

The aims of this chapter are:

(i) to describe the methods used to sample rainfall and streamwater;

(ii) to outline procedures for sample preparation and storage; and

(iii) to describe the techniques used for the determination of individual ions, specific electrical conductance (SC) and total dissolved solids (TDS).

In chapter 2.3 (A) it was noted that the major species usually determined are Ca^{2+}, Mg^{2+}, Na^{+}, K^{+} (cations) and Cl^{-}, SO_4^{2-}, HCO_3^{-} and CO_3^{2-} (anions), together with pH. Minor species determined are SiO_2, Al, Fe, NO_3^{-} and NH_4^{+}. Determinations of all the major ion species were undertaken with the exception of CO_3^{-} which was present in very low concentrations or totally absent. Problems were encountered in the analysis of some ions due to the lack of instrument availability or instrument breakdown. Neither a direct reading colorimeter nor turbidimeter were available, restricting individual ion analyses to either atomic absorption spectrophotometry (AAS), flame photometry or volumetric titration. Thus the number of SO_4^{-} analyses by indirect atomic absorption were reduced due to the limited loan of a barium lamp. Neither NO_3^{-} nor NH_4 were determined due to lack of suitable equipment, which in retrospect was regrettable in view of the interesting variations in these species during the 1975 - 1976 drought shown by other researchers (e.g. Foster and Walling, 1978; Walling and Foster, 1978). A limited number of Si and Fe determinations were also made. Neither HCO_3^{-} nor CO_3^{-} were present in dissociated form in rainfall, while SO_4^{-} concentrations were too low for accurate use of indirect AAS.

From the project outset it was clear that the analysis of a large number of water samples would be necessary. As standard methods for the determination of ion concentrations by volumetric titration can be tedious and time consuming it was decided, as a basic philosophy, to employ AAS wherever possible. Methods for the analysis of K^+, Na^+, Ca^{2+}, Mg^{2+}, Fe and Si were already available. Problems arise when such a philosophy is applied to the major anions in solution, since AAS is only applicable to metal cations. Indirect methods have been developed for Cl^-, NO_3^- and SO_4^{2-}, although only the latter species was analysed by the technique. Cl^- analysis required the use of a silver AAS lamp, which was not regularly available, while NO_3^- analysis involved the use of organic solvents and hence a separate atomic absorption spectrophotometer to avoid frequent overhauling and cleansing of the equipment. Thus standard methods of titration were used for determining Cl^- and also HCO_3^- concentrations.

The pH of each sample was determined as an essential preliminary to individual ion analysis. The SC of the water sample was determined at the same time as pH. Total dissolved solids were also determined for a number of samples and attempts made to relate TDS to SC. The ions determined in stream and rainwater are cummarised in Table 5.1.

5.2 SAMPLING FREQUENCY AND METHODS

To meet the research objectives outlined in chapter 1, a program was designed which would sample streamwater over a wide range of hydrometeorological conditions. Initially, it was decided to sample at each weir and the flume weekly over a two year period 1st July 1975 to 30th June 1977 and to treat this time series as a water quality data base for developing bivariate regression models of solute response for each subcatchment. In addition, individual storms were to be sampled at intervals of between 0.25 and two hours during the period in order to provide detailed information on the seasonal variability of solute response.

D.E. Walling (1975) placed particular emphasis on sampling frequency when attempting to understand temporal solute variations. Using a continuous record of specific conductance for the River Creedy, South Devon, he showed that weekly samples inadequately described

TABLE 5.1

Stream and Rainwater: Ions Determined

Ion	Streamwater	Rainwater
K^+	AAS	AAS
Na^+	AAS	AAS
Ca^{2+}	AAS	AAS
Mg^{2+}	AAS	AAS
Cl^-	V Titration	V Titration
SO_4^-	IAAS	-
HCO_3^-	P/V Titration	-
pH	Pye Meter	Pye Meter
SC	Conductivity Meter	Conductivity Meter
TDS	Evaporation/ Gravimetric	Evaporation/ Gravimetric
Fe	AAS	-
Si	AAS	-

AAS - atomic absorption spectrophotometry

V - volumetric

I - indirect

P - potentiometric

temporal variability. Ideally, the requirement is for an automatic method of sampling, with the option of sampling interval related to flow volume (e.g. Fredriksen, 1969) and with an on/off switch activated by a given water stage. An automatic 12 bottle vacuum sampler manufactured by North Hants Engineering was already available for use (Figure 5.1) and two 24 bottle NHE vacuum samplers were kindly loaned by the Southern Water Authority (Figure 4.1). These all use 500 ml glass bottles from which air is extracted with a hand vacuum pump, and the vacuum maintained by closing pinch valves on rubber tubing inlets to each bottle. The valves are opened at the required interval by an arm rotating from a clock in the centre of the instrument (Figure 5.1). The samples are taken from the stream through individual plastic tubes to the sample bottles. The sampling intake was located in the centre of the channel, making the reasonable assumption that concentration is uniform across the section (Glover and Johnson, 1974) (Figure 4.1). Switching the sampler on automatically was achieved by dropping the rotating arm into position using a solenoid (Figure 5.2). To switch the solenoid on, two methods of signalling were used. Firstly, a crest stage recorder was converted by glueing a magnet to the top of the float arm. A sliding reed switch outside the crest stage guide tube could be pre-set at any water level, and would be closed by a rise in water level floating the magnet upwards. This sent a signal via an electronic relay to the solenoid to drop the rotating arm. Thus, the technique sampled above a specified flow level (Figure 5.3). Secondly, a Plessey tipping bucket raingauge sited next to the sampling point (normally recording on magnetic tape) sent a signal to the sampler after 1.0 mm of rain had fallen, again closing a reed switch. Thus samples were taken prior to, as well as through, a storm hydrograph. Although these techniques were used on numerous occasions to activate samplers there was always some doubt relating to accuracy of the switch on time. Hence manual switching of instruments was used whenever possible.

NHE vacuum samplers have several disadvantages. During frosty weather vacuum is partially lost due to leakage around the screw caps and pinch valves; on several occasions as many as 4/24 bottles remained empty, while sample size was considerably reduced in others. An increased head created by locating the samplers on the bank above the streambed also reduced the sample taken (Figure 4.1). Algal growth

FIGURE 5.1: A N.H.E. 12 - BOTTLE VACUUM WATER SAMPLER

FIGURE 5.1: A N.H.E. 12 - BOTTLE VACUUM WATER SAMPLER

FIGURE 5.1: A N.H.E. 12 - BOTTLE VACUUM WATER SAMPLER

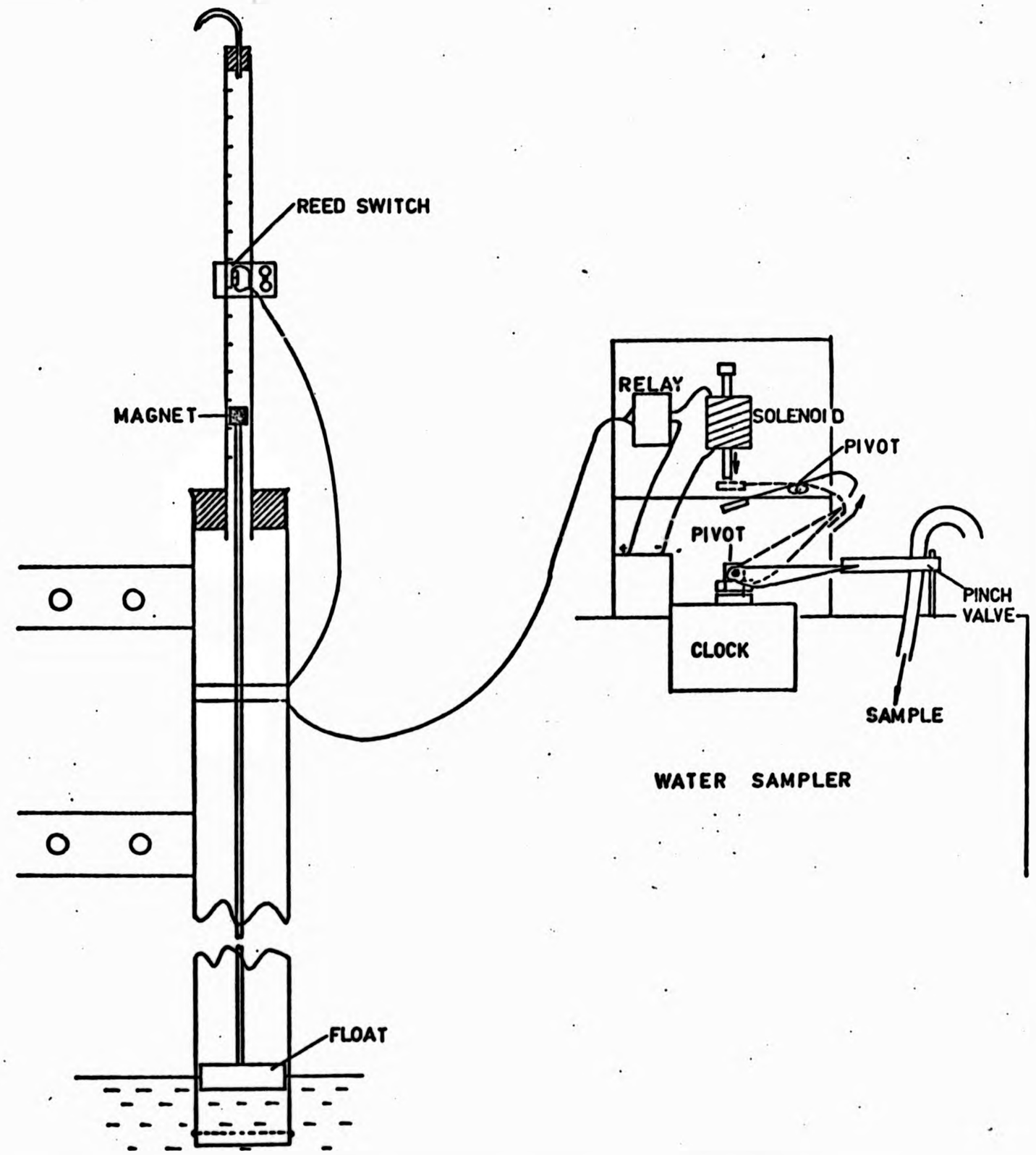

FIGURE 5.2: TRIGGER ATTACHMENT FOR N.H.E. WATER SAMPLER (right)

FIGURE 5.3: CONVERTED CREST STAGE RECORDER FOR TRIGGERING N.H.E. SAMPLER AT A PRE-SET WATER LEVEL (left)

appeared on the walls of the 'bunched' plastic sampling tubes and was difficult to remove without taking them back to laboratory and cleaning. This was done only once during the two year sampling program (by immersing the 'bunch' of tubes in very hot water, hanging from a roof beam and pulling cleaning brushes through each tube), although the effect of algal growth on solute concentrations was thought to be small.

Hand collected samples were taken from upstream of the gauging structures, in the centre of the channel, using 500 ml polythene bottles.

Great care was taken to ensure that glass and plastic sample bottles were free from contamination. They were washed in tapwater, rinsed in concentrated HCl and finally rinsed twice in distilled, de-ionised water. The NHE sampler was cleaned between each period of use by pumping distilled de-ionised water through the system.

Although it was initially decided to take weekly water samples at each gauging structure in West Walk, it became apparent early in 1975 that this would impose severe logistical problems during the two year field program. This was due to the estimated time that the planning, construction of instruments, field installation, data and sample collection and laboratory and computer analysis for the hillslope experiment would take (Section III). The revised scheme involved periodic sampling during two flow recessions: February - August 1975, and February - June 1977; and sampling during storms, particularly those occurring between September and January. This scheme eliminated the possibility of some types of analysis (e.g. time series modelling) but placed emphasis on the times when the most interesting solute variations were likely to occur (i.e. autumn) and gave information on baseflow water quality.

The fact that the sampling program was undertaken during a rare drought has the disadvantages that extrapolation of results to longer time periods is dangerous. However, since this work places greater emphasis on physical processes than on predicting long term erosion, the occurrence of the drought was useful in that it provided a wider range of conditions to sample. The frequent heavy rainfall during the months September - December 1976 allowed sampling of several storms in

sequence. However, there were logistical problems encountered in maintaining the hillslope and surface water sampling schemes and subsequently analysing water samples.

Bulk rainfall samples were taken weekly using a sampling receptacle situated at the catchment raingauge site (Figures 3.1, 4.10). J.N. Galloway and G.E. Likens (1976) have described several types of rainfall collector varying in complexity. In the present experiment the aim was to use an instrument which required a minimum of maintenance, yet took representative samples of bulk atmospheric input. Trials were carried out during late 1974 with the rain collector described by G.E. Likens et al (1967), although this had the disadvantage that the vapour barrier (included to reduce sample evaporation) frequently froze during cold weather. The 6 mm inside diameter inlet tubing became blocked by insects on several occasions. This rain collector was superceded by that shown in Figure 5.4, simply a 2 litre polythene bottle situated under a large polythene funnel. The covering box was built from glass reinforced plastic and covered with aluminium foil to reflect incoming solar radiation, reduce temperature and minimise evaporation. The sampling funnel rim was situated at 1.5 metres to avoid splash in from the ground surface. Some researchers recommend a ring of spikes around the funnel to avoid birds roosting and fouling the sample (e.g. Gambell and Fisher, 1966). In the present experiment this was not considered necessary because of the greater probability of birds roosting on trees; no fouling of the funnel was apparent during the two year period.

Each time a sample was taken, both the 2 litre bottle and a clean funnel were installed. The same methods of cleansing were used as for streamwater sample bottles.

5.3 SAMPLE PREPARATION AND STORAGE

Considerable attention was given to the treatment of water samples between site collection and laboratory analysis. Figure 5.5 shows the preparation and storage routine followed between collection and analysis. Significant changes in chemical concentrations may take place if samples are not stored under suitable conditions. This has been shown by specific projects to determine the effects of different

FIGURE 5.4: THE RAINFALL SAMPLER

FIGURE 5.4: THE RAINFALL SAMPLER

FIGURE 5.4: THE RAINFALL SAMPLER

FIGURE 5.5

FLOW DIAGRAM OF THE VARIOUS STAGES IN SAMPLE PREPARATION STORAGE AND ANALYSIS

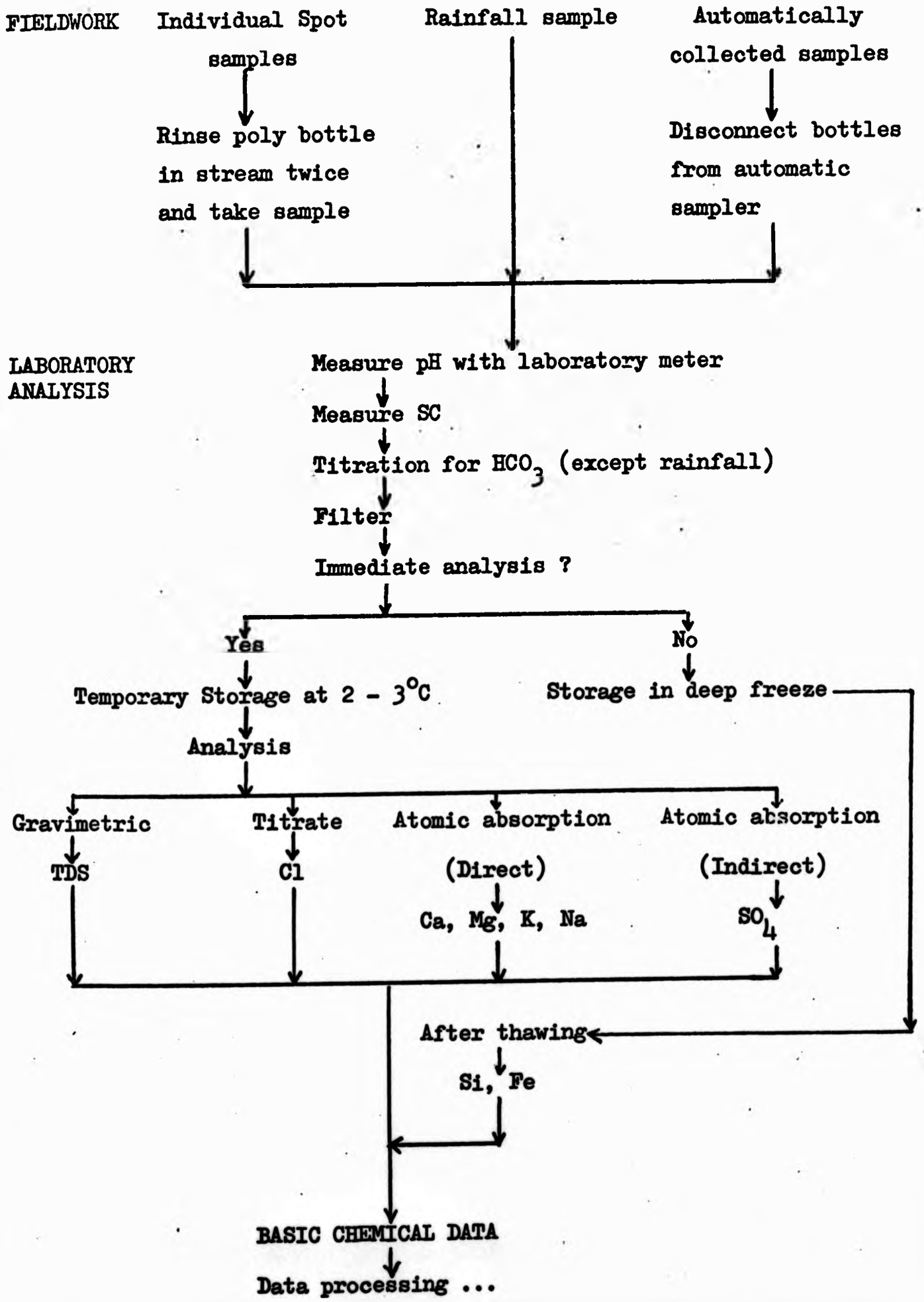

storage methods, as for example that by K.V. Slack and D.W. Fisher (1965). River water samples maintained at 25°C in plastic bottles and exposed to alternating twelve hour periods of darkness and light for three months showed no signficant changes in the major constituents (pH, CO_2, SO_4^{2-}, PO_4^{3-}, Cl^-, Ca^{2+}, Mg^{2+}, Na^+, K^+ and SiO_2).

However, during a subsequent two month period of dark storage both pH and PO_4^{3-} decreased, while free CO_2 and HCO_3^-, SiO_2, Mg^{2+} and SO_4^{2-} all increased. Viable explanations were proposed for all the changes except Mg^{2+}. Such changes resulted from the alteration of only one variable, light, with temperature kept constant.

Thus if samples cannot be analysed within a short time of return to the laboratory an adequate method of storage must be used. In the present work the use of AAS aimed to expedite analysis and so increase the number of ions which could be immediately determined. pH, SC, TDS, Cl^-, HCO_3^-, Ca^{2+}, Mg^{2+}, K^+, Na^+ and SO_4^{2-} were all determined before storage, while Si and Fe were determined later.

H.L. Golterman and R.S. Clymo (1969) suggest three main methods for storing river water samples. Firstly, by the addition of preservatives. The addition of either 0.5 % $CHCl_3$ or 0.5 ml bromine-water/100 ml sample are suggested by B. Aberg and W. Rodhe (1942).

The second method is to acidify the sample with H_2SO_4 or HCl to pH = 1 - 2. This prevents the precipitation of iron and aluminium but has the disadvantage that it can cause changes in the state of the ions in solution.

The third method, and the one used in the present work, is to freeze the filtered sample in a polythene bottle. These can then be kept for a long time before analysis (no more than six months in the present work). It is important to thoroughly mix the solution after thawing. Problems can also arise when, as in the present case, silicates are to be determined after freezing, because silica may precipitate when the sample thaws.

Golterman and Clymo (1969) suggest the storage of both an acid and a neutral solution and prefer the use of borosilicate glassware to plastic, the latter to overcome the absorption of phosphorus by the plastic. In the present work refrigerator space was only available for storing one sample. Samples to be analysed within a few hours after return to the laboratory were maintained at 2 - 3°C in the refrigerator.

5.4 FILTRATION

During sample storage ion exchange between dissolved ions and the surface of particulate matter can occur, so that separation of particulate from dissolved matter must be an early step. Filtration was undertaken after the measurement of pH, SC and titration for HCO_3^-, to avoid alteration of the dissolved gas content of the sample. Prior to the analysis or storage of most samples filtration was carried out using a Whatman No 32 low ash filter circle (mean pore diameter = 0.75 μm). This was done under vacuum in a Büchner funnel and flask, the filtration rate being inversely proportional to the amount of sample which has passed through the filter.

Inevitably, some colloidal particles (taking the colloidal/solute boundary as 0.01 μm) pass through the filter paper, but a balance must be struck between filtration time and purity.

Sample filtration for silicon was an exception to this method. A subsample of 200 ml was passed through an oxoid membrane (mean pore diameter = 0.5 μm) and stored in the deep freeze at - 20°C. This was done to avoid contamination from the glass fibre of the Whatman No 32 filter circle.

5.5 pH MEASUREMENT

Sample pH was measured as an essential preliminary (before filtration) to all other analyses. It was used in several analytical methods, which either directly calculated ionic concentration or standardised calibration and sample solutions. An example of the former is given in the determination of an exact end point pH for HCO_3^- titration, using the initial pH and conductivity of the solution (see 5.12). Large differences in pH between sample and calibration solutions may adversely affect the accuracy of determinations by AAS.

Inconsistent viscosity resulting from the pH differences affects sample uptake in AAS, the size of droplets formed and ultimately the number of atoms entering the radiation beam. Matching of solutions to within 0.5 pH unit helps to overcome this problem.

The first decision necessary was whether to measure pH in the field or after returning to the laboratory. A time lapse of 2 - 3 hours between collection and laboratory determination might allow liberation of dissolved gases and thus changes in pH. A.M.C. Edwards (1971) measured pH in the field and several hours later in the laboratory but found the differences to be negligible. As a result he discontinued field determination. In the present case the time lapse between collection and laboratory determination could be more than 24 hours if an automatic sampler was being used.

The pH of two water samples from weirs 2 and 4 were determined, 2, 26 and 96 hours after collection. The results are shown below:

The pH Change of two Samples through Time

Time after collection (hours)	W2 pH	W2 -ΔpH	W4 pH	W4 -ΔpH
2	7.480	0.000	7.610	0.000
26	7.425	0.055	7.577	0.033
96	7.290	0.135	7.523	0.087

These show increases of only 0.033 and 0.055 pH units between 2 and 26 hours after collection which are acceptable errors, considering the problems of sample collection. Any backward extrapolation to standardise values was ruled out due to probable variations in the rates of change of pH through time, resulting from variable sample chemistry and temperature.

Thus the pH of samples was determined in the laboratory at either two or 26 hours after collection using a Pye Model 290 pH meter (Figure 5.6). This instrument has a pH range of 0 - 14 with 14 ranges

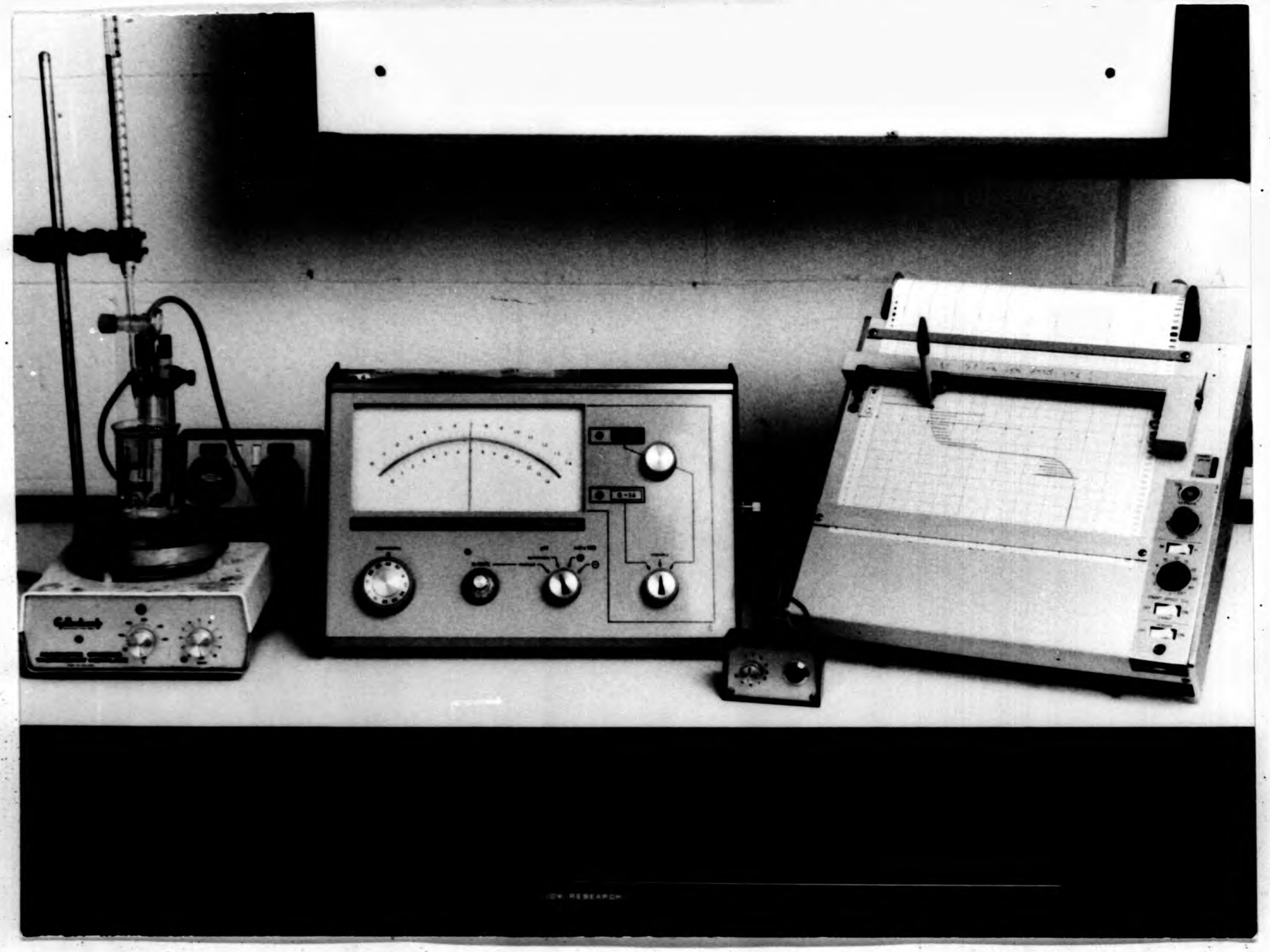

FIGURE 5.6: PYE MODEL 290 pH METER

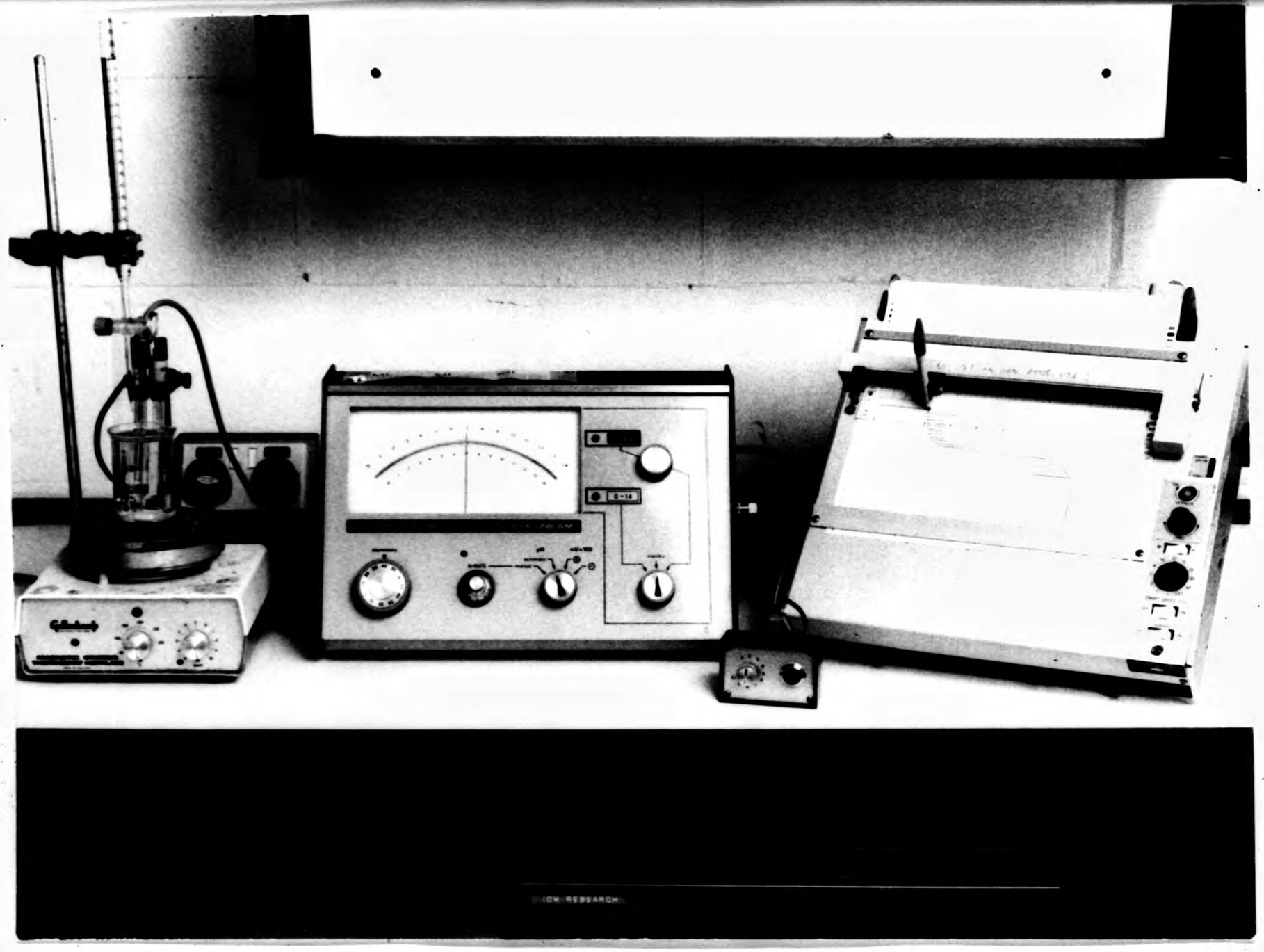

FIGURE 5.6: PYE MODEL 290 pH METER

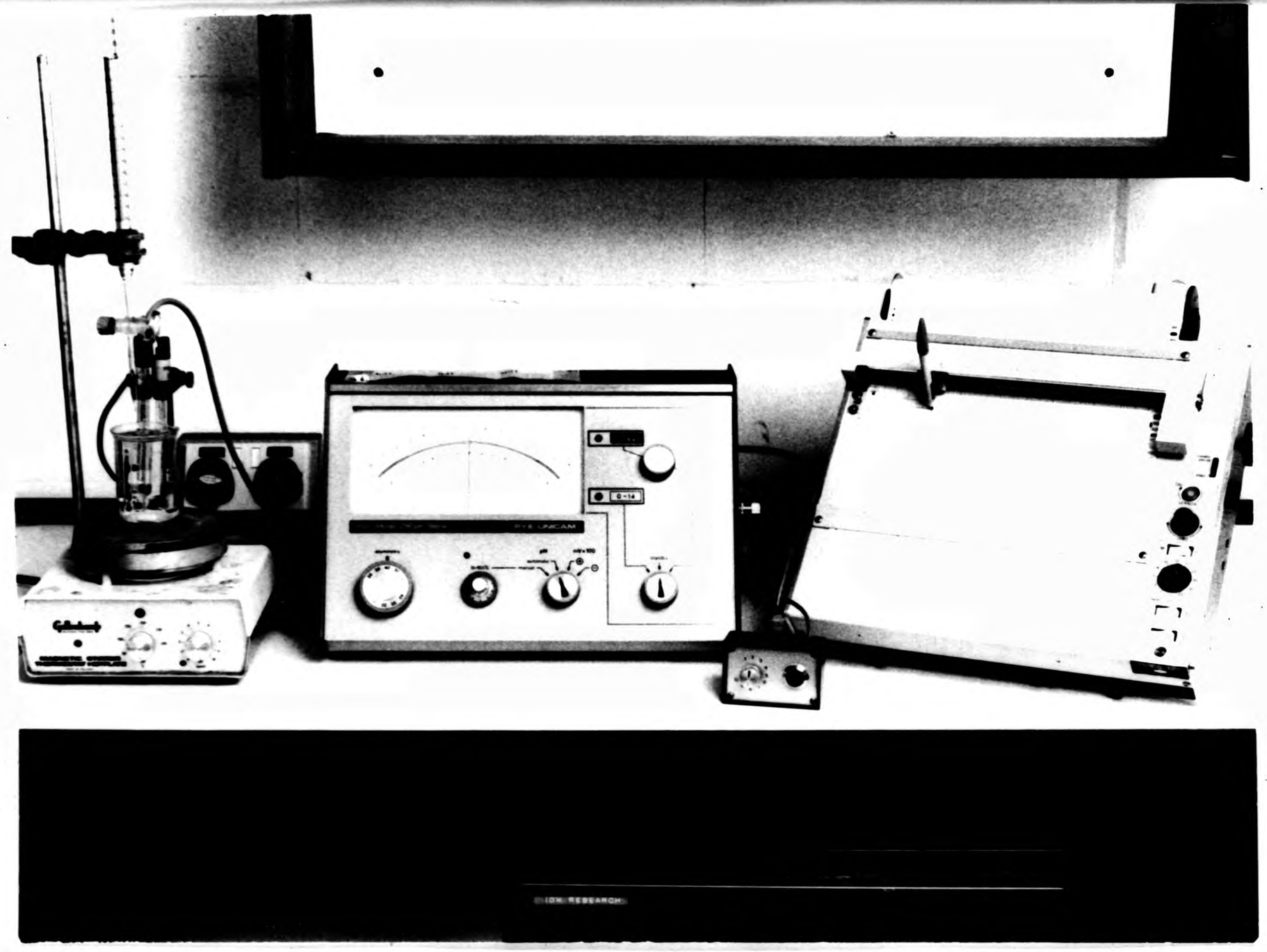

FIGURE 5.6: PYE MODEL 290 pH METER

of 1.4 pH for fine scale determination (allowing a precision of ± 0.0005 pH). The instrument stability is better than 0.002 pH per 24 hours (non-cumulative). Automatic temperature compensation was achieved using a resistance thermometer.

A Pye Ingold 450.E7 combination electrode was used. Three EIL buffer solutions (pH 4, pH 7 and pH 9) were used to calibrate the meter. The electrodes were washed with distilled de-ionised water and immersed in the pH 7 buffer solution. The function switch was turned to automatic and the asymmetry control adjusted until the meter read precisely pH 7; fine adjustment was obtained using the appropriate 1.4 pH range. This procedure was repeated for the other two buffer solutions until calibration was perfect.

Measurements of pH were made by first calibrating the instrument then, with the range selector switch set to standby, the electrode and thermometer probe were immersed in the sample solution. The range selector switch was turned to the 0 - 14 range to estimate the pH; an exact pH reading was obtained by selecting the appropriate 1 - 4 pH range. The electrodes were rinsed in distilled de-ionised water between successive readings. Meter drift was sometimes encountered while finding the pH of a sample. In such cases the electrodes were removed from the solution and gently brushed and rinsed with distilled de-ionised water to remove possible contaminants. If drift was still encountered, then the pH was taken after two minutes on the 1.4 range and DRIFT noted on the method sheet.

5.6 SPECIFIC ELECTRICAL CONDUCTANCE

Specific conductance was measured at the same time as the pH, that is, within 26 hours of sampling.

Conductance is a measure of the ability of a conductor to convey an electric current. In the case of water it is related to the concentration of ions present and to the temperature at which the measurement is made (standardised at 25°C in the present case). Conductance is reported as micromho/cm and abbreviated to μmho. It gives no indication of the nature of the substances in solution but any increase or decrease in their concentration will be reflected in a

corresponding increase or decrease in conductance. By establishing a relationship between SC and the concentration of total dissolved solids (TDS) in a range of solutions it becomes possible to use SC as an estimator of TDS.

Conductivity was measured using a MCl Mk V Electrolytic Conductivity Measuring Set made by Electronic Switchgear Limited. A sample was poured into a measuring cell (with a constant K = 1.0) and the conductivity read from the measuring dial. Sample SC was calculated by multiplying this value by the value of the range selector switch (either 10, 10^2 or 10^3). Temperature compensation was achieved by setting the instrument temperature dial to the temperature of the solution (measured in ^{o}C by thermometer) and adjusting to $25^{o}C$ using the appropriate conversion factor from Golterman and Clymo (1969, Table 3.1).

5.7 TOTAL DISSOLVED SOLIDS

The concentrations of the total dissolved constituents (TDS) of a number of samples were determined in order to establish a relationship between TDS and SC.

The simple oven-evaporation procedure was used. A 50 ml glass beaker was oven dried at $90^{o}C$ and allowed to cool in a desiccator; it was weighed on an analytical balance when cool and the weight recorded. 50 ml of sample solution was added to the beaker and placed in the oven at $90^{o}C$. This temperature (lower than the normally recommended $110^{o}C$) was used in order to reduce possible losses of volatile dissolved organic matter. After evaporation the beaker was placed in a desiccator to cool and then re-weighed. The weight difference was used to calculate the TDS concentration in mg/l. The analytical balance is accurate to 0.0001 g, which converts to 2 mg/l TDS concentrate. A replicate analysis of NaCl solution, concentration 230 mg/l gave the satisfactory results shown in Table 5.2.

TABLE 5.2

Replicate TDS Analysis for a Solution of NaCl

Replicate	Concentration mg/l
1	226
2	230
3	230
4	230
5	240
6	236
	Mean = 232.0
	SD = 5.0596
	CV % = 2.18

5.8 ATOMIC ABSORPTION METHODS

A. Introduction

Atomic absorption methods have become increasingly popular over the past ten years. This popularity results from a number of the advantages of an ideal technique, well summarised by L.L. Lewis (1969). Firstly, it allows the detection of low concentrations. Secondly, more than one element may be determined by preparing a single solution. Thirdly, with direct determination there is usually no lapse time in sample preparation (as there is, for example, in colorimetric methods, where time is required for colour development). Fourthly, data output is in directly readable form. Fifthly, smaller volumes of water are required in comparison with titrimetric determinations.

It is a method ideally suited to the analysis of river water samples, since direct aspiration of the aqueous solution with limited pre-treatment is possible.

These attributes combine to make AAS a versatile and rapid tool for the analyst undertaking routine determinations of a large number of samples.

B. Instrument Background

It is unnecessary here to give the detailed theoretical background of AAS. However, an understanding of the basic system of analysis is useful. In order to be able to make measurements in atomic absorption it is necessary to devise an instrumental assembly which will convert an aqueous solution as efficiently as possible to a population of ground state atoms, and then pass resonance radiation of the element to be measured through that population. Ideally the light-measuring device should "see" only the wavelength which is being absorbed, as the presence of other radiation will lower the proportion of absorbed radiation and thus decrease the sensitivity of the measurement.

The basic layout of the Pye Unicam SP90 atomic absorption spectrophotometer is shown in Figure 5.7. Light from the source lamp generating a sharp line spectrum characteristic of the desired element passes through the flame into which the sample solution is sprayed as a fine mist. The region of the spectrum in the immediate neighbourhood

5.8 ATOMIC ABSORPTION METHODS

A. Introduction

Atomic absorption methods have become increasingly popular over the past ten years. This popularity results from a number of the advantages of an ideal technique, well summarised by L.L. Lewis (1969). Firstly, it allows the detection of low concentrations. Secondly, more than one element may be determined by preparing a single solution. Thirdly, with direct determination there is usually no lapse time in sample preparation (as there is, for example, in colorimetric methods, where time is required for colour development). Fourthly, data output is in directly readable form. Fifthly, smaller volumes of water are required in comparison with titrimetric determinations.

It is a method ideally suited to the analysis of river water samples, since direct aspiration of the aqueous solution with limited pre-treatment is possible.

These attributes combine to make AAS a versatile and rapid tool for the analyst undertaking routine determinations of a large number of samples.

B. Instrument Background

It is unnecessary here to give the detailed theoretical background of AAS. However, an understanding of the basic system of analysis is useful. In order to be able to make measurements in atomic absorption it is necessary to devise an instrumental assembly which will convert an aqueous solution as efficiently as possible to a population of ground state atoms, and then pass resonance radiation of the element to be measured through that population. Ideally the light-measuring device should "see" only the wavelength which is being absorbed, as the presence of other radiation will lower the proportion of absorbed radiation and thus decrease the sensitivity of the measurement.

The basic layout of the Pye Unicam SP90 atomic absorption spectrophotometer is shown in Figure 5.7. Light from the source lamp generating a sharp line spectrum characteristic of the desired element passes through the flame into which the sample solution is sprayed as a fine mist. The region of the spectrum in the immediate neighbourhood

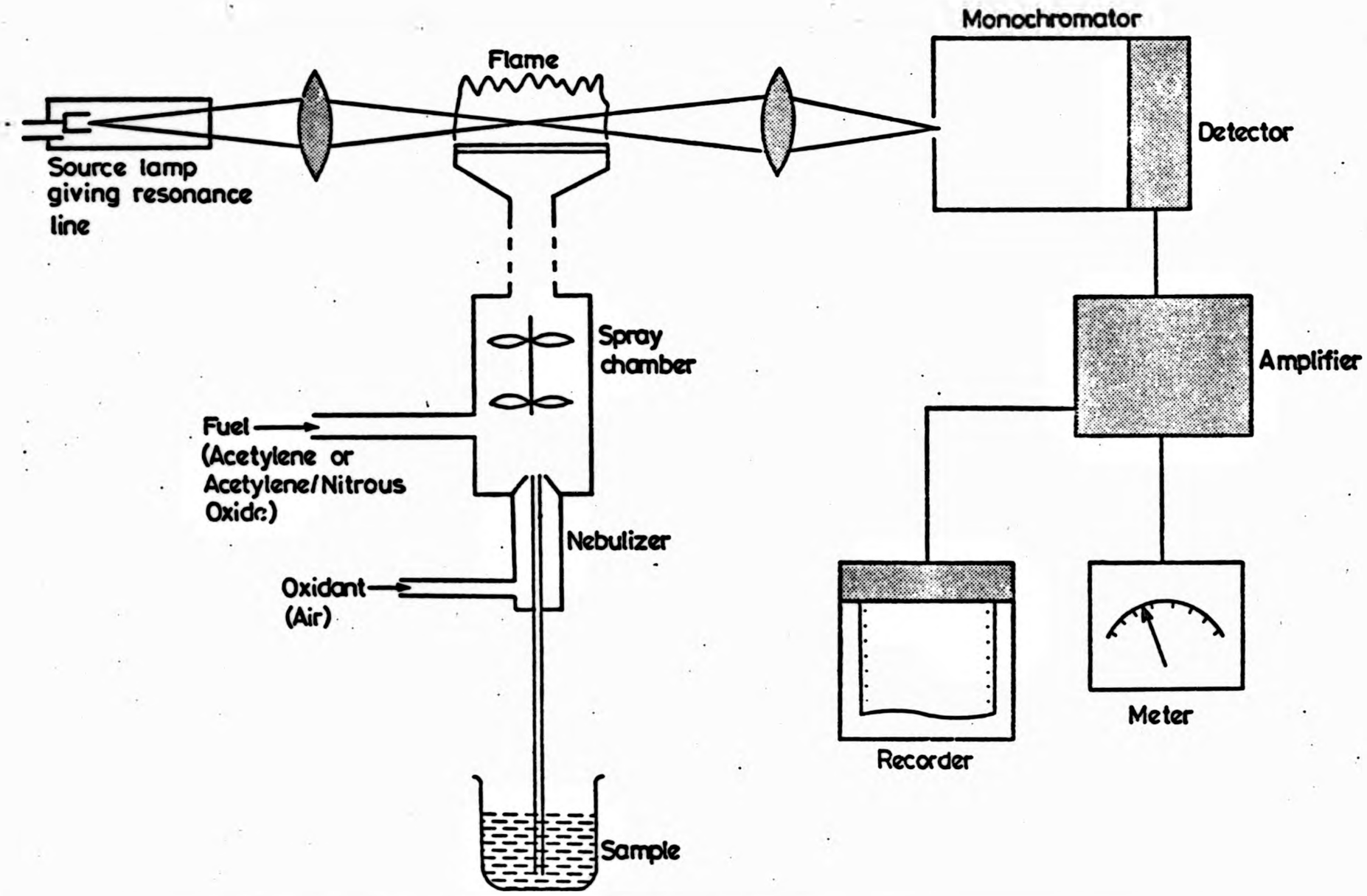

FIGURE 5.7: BASIC LAYOUT OF THE PYE-UNICAM SP 90 ATOMIC ABSORPTION SPECTROPHOTOMETER

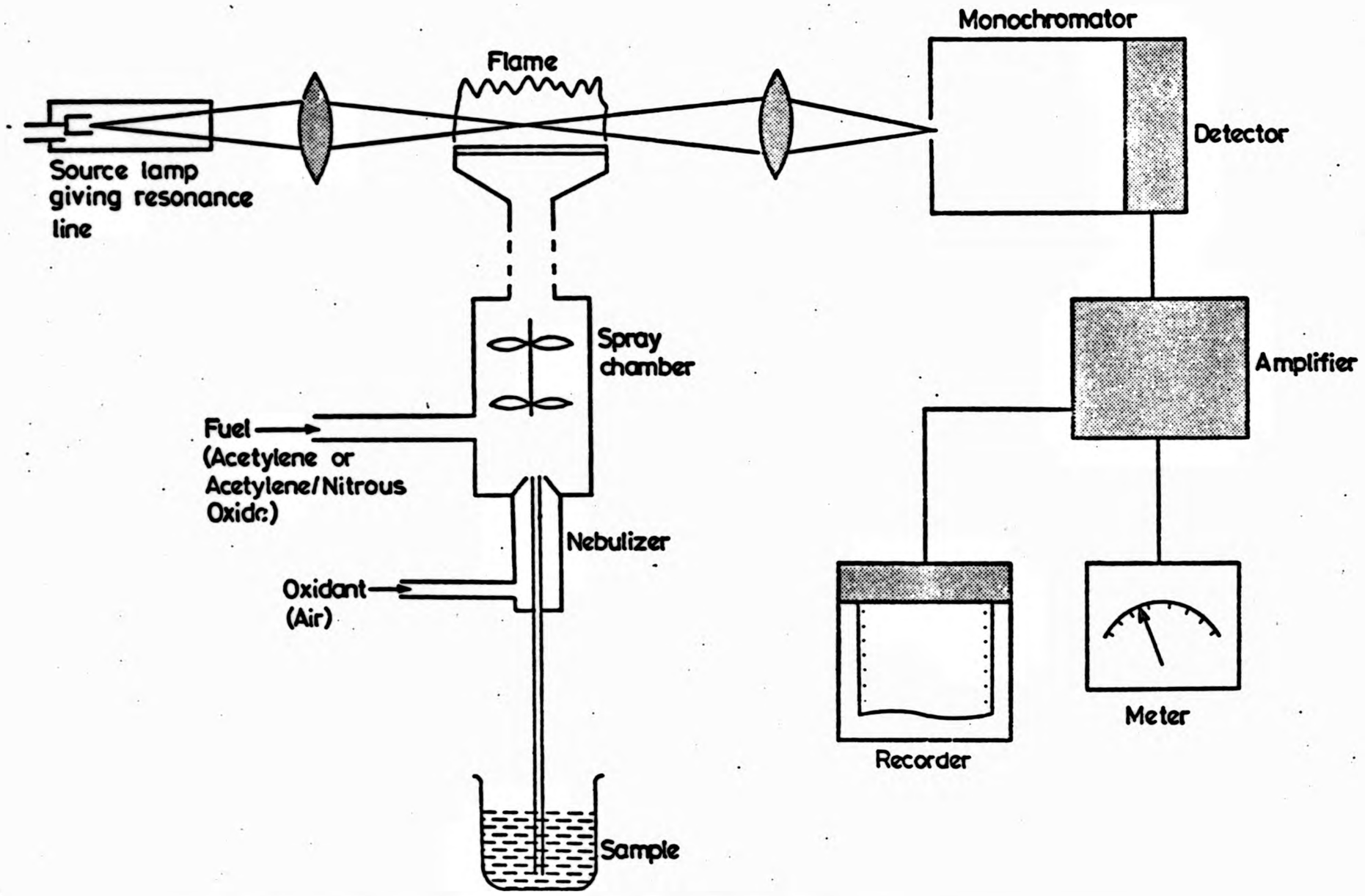

FIGURE 5.7: BASIC LAYOUT OF THE PYE-UNICAM SP 90 ATOMIC ABSORPTION SPECTROPHOTOMETER

of the resonance line to be measured is selected by the monochromator. The isolated resonance line from the lamp falls on to the detector, a photomultiplier, the output of which is amplified and drives either a meter or more usually a chart recorder. The intensity of the resonance line is measured with and without the sample passing into the flame. The difference between these readings is a measure of the absorption and therefore of the amount of the element being determined.

For emission spectroscopy the source lamp is removed, and the flame radiation detected by the monochromator at the desired frequency.

The instrument used for most of the analytical work described below was a Pye Unicam SP90 Series 2 Atomic Absorption Spectrophotometer. The instrument is capable of carrying out high sensitivity, low noise atomic absorption and sensitive emission measurements. It is a compact unit which houses a monochromator, plug-in electronic unit and interchangeable burner heads into which are fed pre-mixed fuel, air and sample (Pye Unicam, Technical Manual). An SP91 Series 2 lamp turret and SP94 Series 2 nitrous oxide system were also fitted. A Mitsui graph recorder was used for most readouts. The salient specifications for the instrument are given in Table 5.3.

C. Analytical Techniques

Instrument operation is straightforward if a basic setting-up routine is followed. Details will not be given here of optical alignment or nebulizer-atomizer adjustment; these may be found in the Pye Unicam Technical Manual, pages 4.15 - 16 and 4.27 - 30 respectively.

The most important instrumental settings for an analysis are lamp current, amplifier gain and damping, scale expansion, slitwidth, damping and recorder expansion. The standard setting-up procedure for the SP90A was as follows (absorbance mode):

I The instrument was set to absorbance

II The mode switch was set to low gain

III The lamp current was adjusted to the appropriate value for the lamp being used and the lamp allowed to warm for 15 minutes

TABLE 5.3

Specifications for the SP90 Series 2 Atomic Absorption Spectrophotometer

Range	:	190 to 852 nm
Sources		Hollow cathode lamps mounted in rapid-focus holders
Slits	:	Gauged slits continuously variable up to 1.5 mm
Monochromator	:	Littrow type with 30°C rear-aluminised high-purity silica prism
Detector	:	EMI 9558QB photomultiplier
Wavelength Stability	:	0.06 nm per °C change in ambient temperature at 300 nm
Scale Expansion	:	Continuous absorbance expansion up to X 10 maximum
Electronic Stability	:	Zero drift less than 1 % per day
Sample Take Up Rate	:	3 to 4 ml/m with an indicated air flow of 5 l/m
Presentation	:	Taut suspension meter calibrated linearly in transmission and absorbance, depending on mode of operation. 10 mV output for recorder
Response Time - Recorder	:	Time constant 3 (damping) : 1.8 sec time constant 4 : 4.3 sec
Fuel Supply	:	Acetylene, pressure regulated between 0.35 - 0.7 bar (kg/cm^2) (5 - 10 psi)
Air Supply	:	Compressed air with a steady pressure of up to 2.1 bar (kg/cm^2) (30 lb/in^2) at up to 10 l/m flow rate

IV The damping control was set to 1

V The shutter control was set to zero energy

VI The scale expansion was set to 5, the meter zeroed, and the SE reset to 1

VII The shutter control was set to absorption and the slitwidth set to the required value (usually between 0.08 - 0.1 mm)

VIII The lamp was correctly aligned

IX The wavelength of the spectral line for the individual lamp was selected using the wavelength control. This was done by adjusting the control to give the minimum absorbance reading

X (i) The acetylene air flame was ignited by:

(a) adjusting the air pressure to 2.1 bar (kg/cm^3) (30 psi) at the compressor and to 4.5 - 5.5 l/m on the instrument gauge

(b) turning on the fuel at the cylinder to give a pressure of 0.7 bar (kg/cm^3) (10 psi)

(c) turning on the gas flow control on the instrument to 1.5 l/m and igniting the flame

(d) the fuel supply was adjusted to provide a non-luminous flame

(ii) The nitrous oxide-acetylene system is used to produce a significantly higher flame temperature than that attainable with air-acetylene mixtures. It allows analysis of additional elements which are not reduced to the atomic state at the lower temperature of the air-acetylene flame. Precautions were taken when using nitrous oxide since there is some risk of flashback (Pye Unicam Tech. Man. SP94 p. 2 et seq). A special nitrous oxide burner head was fitted first. The flame was then ignited by:

(a) turning on the air supply and setting the control switch to 'AIR'; set 5 l/m at 2.1 bar (kg/cm^3) (30 psi)

(b) turning on the N_2O supply switch to 'N_2O' and adjusting the nitrous oxide pressure to 2.1 bar, allowing 5 l/m flow rate

(c) alternating between 'AIR' and 'N_2O' to ensure maintenance of flow rate and pressures

(d) switching to air and allowing the system to flush for one minute

(e) setting 1.5 l/m acetylene at 0.7 bar (10 psi) at the cylinder and lighting the flame

(f) increasing the acetylene flow to 3 l/m

(g) switching to 'N_2O' and adjusting the flame using the acetylene flow only

Having set up the instrument to produce a stable non-luminous flame the next step was to 'tune' the instrument for optimum performance. This involved the minimisation of noise and the linearisation of the calibration curve. Figure 5.8 gives several types of output trace, all influenced by the amount of noise.

D. Noise and Noise Reduction

(a) Flame noise: this arises from refractive index variations in the region between the hot parts of the flame and the cold surrounding atmosphere and from small variations in effective path length of the flame cell. It is apparent that flame noise always exists and it was best minimised by ensuring operation in a draught-free environment, with all doors closed and all panels in position.

(b) Lamp noise:. this has two components:

(i) 'shot' or short term noise due to the quantum nature of the electronic charge

(ii) 'drift' or long term noise

Shot noise was not found to be a major problem with the SP90A. Since shot noise is proportional to the square root of the light intensity then adjustments to reduce shot noise followed the procedure:

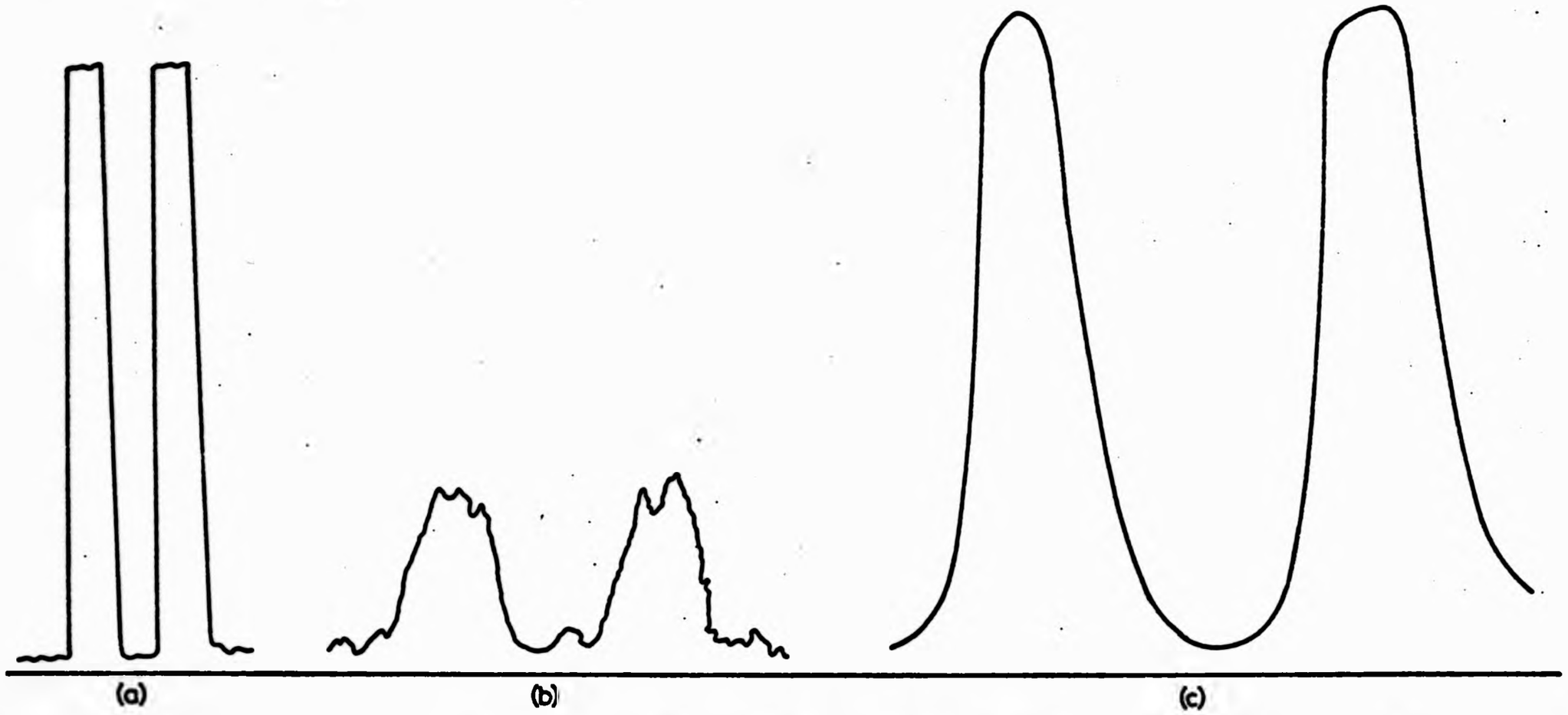

FIGURE 5.8: THREE TYPES OF OUTPUT TRACE USING AAS
(see text for description)

(i) the lamp current increased

(ii) the aperture stop removed

(iii) the slitwidth increased

(iv) the gain control altered to compensate, so that the readout meter was at zero while aspirating a blank solution

This four stage process was continued until a point was reached where the low frequency or drift component predominated. Further increase in light level worsened the detection limit because the signal decreased at a greater rate than the noise.

(c) Electronic noise: this is due to photomultiplier dark currents and amplifier noise but was not a major problem in 'tuning' the SP90A.

E. Curve Linearisation and Concentration Readout

Beer's Law, the theoretically linear relationship between the amount C of the absorbing species in the light path and the absorbance A, is partially followed in AAS. After an almost linear portion the calibration curve usually bends towards the concentration axis (the independent variable is taken as the abscissa). The amount of curvature and point of onset of the curvature depend on the amount of unabsorbable radiation reaching the detector, and on the presence of less sensitive lines within the monochromator. Figure 5.9 shows four possible calibration curves. (a) is the ideal (almost impossible) case where all light reaching the detector is absorbed by the element being determined to the same extent. The normal curve is shown in (b), where Y represents the residual unabsorbed light level and the curve is asymptotic to this value. The cause of the curvature away from the concentration axis, shown in (c), is ionisation. At very low concentrations a higher proportion of the element is ionised. Sodium or potassium in the air-acetylene flame exemplify this effect. Correction is usually by addition of a buffer as will be described later. Many elements give linear calibrations up to about 0.5A and most give only slight curvature to 1.0A, given optimum operational conditions. The following procedure was used to correct the

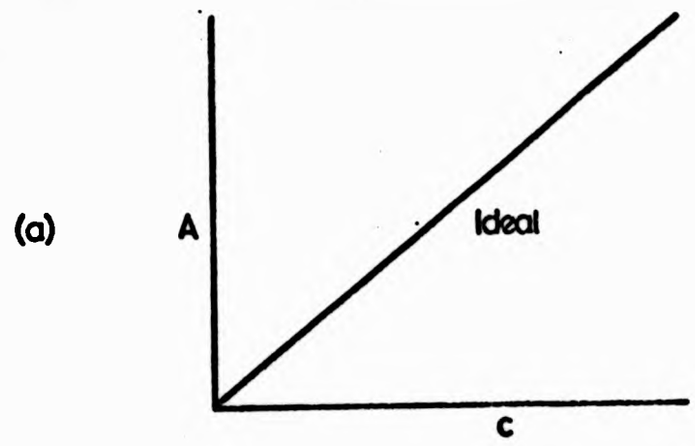

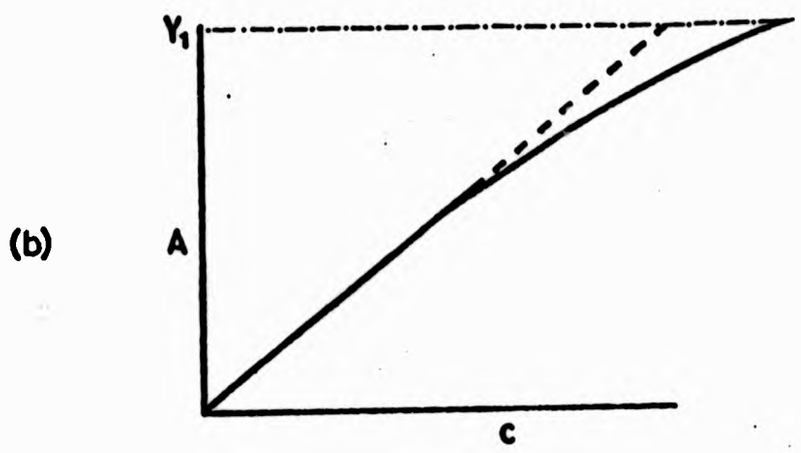

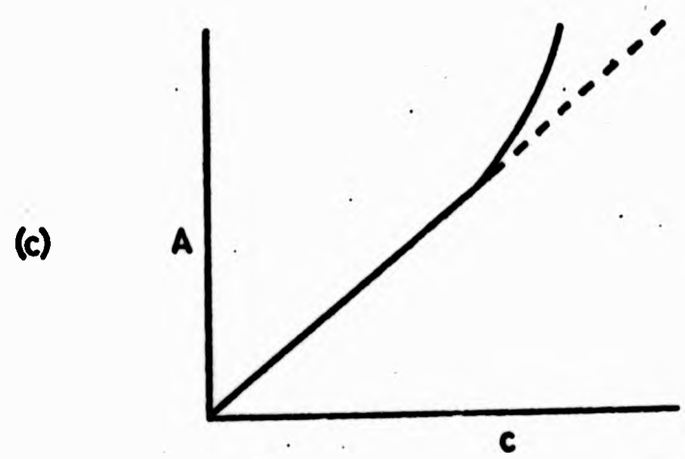

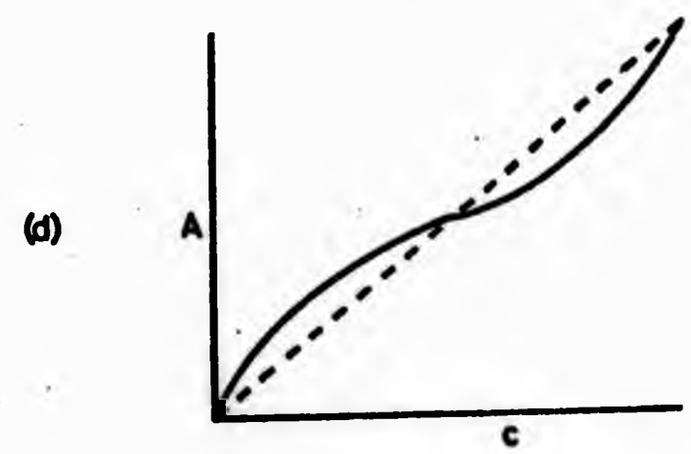

FIGURE 5.9: FOUR TYPES OF CALIBRATION CURVE USING AAS
(see text for description)

non-linearity of calibration curves (Pye Unicam Tech. Manual, p. 4.22 - 4.23).

(a) The instrument was adjusted for conditions of optimum linearity; the most important influences upon linearity here were found to be stray light and non-uniformity.

(i) Stray light: here the photomultiplier detects light of a wavelength that is not absorbed by (or not so strongly absorbed as) the principal resonance wavelength being used in the absorbance measurement. Stray light is usually eradicated by optimising the monochromator to reduce the amount of light detected by the photomultiplier. This adjustment was never found to be necessary while using the SP90A.

(ii) Use of the aperature stop reduces non-uniformity caused by off-axis rays passing through a shorter pathlength in the flame.

Ionic interference or various anionic effects can cause non-linearity of the calibration curve and are treated later.

(b) The absorbance/transmission switch was set to T.

(c) The shutter control was set to zero energy and the transmittance zero control for a zero reading on the readout meter.

(d) The shutter control was set to absorption and the coarse and fine gain controls adjusted until the readout meter read 1.0 (100 % transmittance).

(e) A stock solution of the element being determined was aspirated (giving > 3A). The transmittance zero was adjusted for a zero reading on the readout meter.

(f) The T/A switch was set to absorbance.

(g) While aspirating a blank solution the gain controls were adjusted until the meter read zero.

(h) Readout was changed to the graph recorder and the standard solution aspirated. It was then possible to check visually the linearity of the calibration curve. It was found that the best possible method of achieving curvature correction was to use two solutions, A and B. Solution A was of a concentration giving an absorbance of about 0.5 before curvature correction. Solution B was of a concentration twice that of A. The absorbance of both solutions was measured. If the absorbance of B was less than twice that of Solution A, then the transmittance was increased. If the absorbance of Solution B was more than twice that of A, then the transmittance was decreased. The optimum degree of curvature correction was achieved when the absorbance of solution B was twice that of Solution A. The curve generally approximated to an 'S' as in Figure 5.9 (d), the degree of curvature depending upon the prevalence of other causes of curvature.

Once the calibration had been linearised concentration readout was easily achieved by using the scale expansion facility. If, for example, 50 mg/l was read as 0.4A then the SE expanded the readout to 0.5A; thus, 0.5A = 50 mg/l and multiplication by a factor of 100 gave the concentration. There was some loss of precision using this method due to incomplete linearisation of the calibration. Where this was apparent a separate curve was used for calibration purposes.

F. Interference Effects

These can be divided into chemical and physical interferences (Price, 1972).

(a) Chemical

Both 'enhancing' and 'depressive' interferences are known to occur. In either case the proportion of atoms in the flame available to absorb the resonance radiation is the causative factor.

Stable compound formation is the primary cause of chemical interference. This arises because compounds containing the element being measured are not broken down into individual atoms at the temperature of the flame being used.

In the reaction

$$M\text{-}O\text{-}X \underset{\text{excess oxyacid}}{\overset{\text{heat}}{\rightleftharpoons}} M\text{-}O \underset{\text{low temp flame}}{\overset{\text{heat}}{\rightleftharpoons}} M{+}O \overset{C}{\rightleftharpoons} M{+}CO$$

an equilibrium will be set up between the species M-O and M-O-X. But, in the presence of excess O-X, the equilibrium will tend to the left preventing the formation of free M (Price, 1972). This represents a persistence of the stable oxy-salt and a depression of the metal, M. By adding a releasing agent, the effect is to influence the chemical equilibrium in the desired direction as follows:

$$M\text{-}O\text{-}X + R \overset{\text{excess R}}{\rightleftharpoons} R\text{-}O\text{-}X + M$$

where R is a metal which forms a stable compound with the oxy-salt and, when present in excess, allows the reaction to proceed to the right, producing a higher proportion of atoms.

The releasing agents most frequently used are those metals which form stable oxy-salts, for example, lanthanum. Use of a nitrous oxide-acetylene flame in place of air-acetylene also improves the situation by increasing the temperature and thus the sensitivity.

The degree of ionisation of a metal can be affected by the presence of a second alkali metal. When the second metal is present as an impurity in varying amounts the degree of ionisation varies and an interference effect results. This will cause the calibration curve to move away from the absorbance axis as shown in Figure 5.9(b). These effects are eliminated by adding an ionisation buffer, usually a higher alkali metal, in excess.

(b) Physical

Incomplete volatilisation can be caused by an inadequate flame temperature or speed of the droplets through the flame or both. A likely result is the curvature of the calibration graph. The solution is to increase the temperature of the flame or add a releasing agent such as ammonium chloride.

Matrix effects influence the number of atoms entering the radiation beam rather than their effectiveness once there. They usually arise from physical differences in the solutions being aspirated, such as a difference in acid concentration causing inconsistent viscosity. This in turn affects nebulizer uptake and the size of droplets formed. If both standards and samples are always made up in exactly the same way, i.e. with the same additions, then matrix effects are largely eliminated. Thus, the pH of sample solutions was brought to within 0.5 of the calibration solution pH in all analyses.

G. Preparation of Standard and Reagent Solutions for AAS

(a) Standard Solutions

Relatively concentrated stock solutions were prepared for each element to be analysed. The minimum quality of chemical used was analytical grade. These solutions were as follows.

(i) Barium chloride: 0.1779 g of $BaCl_2.2H_2O$ were dissolved in de-ionised water and diluted to 500 ml. The solution contained 200 mg/l Ba.

(ii) Calcium carbonate: 0.2497 g of dry $CaCO_3$ were dissolved in the minimum amount of HCl and made up to 1 litre. The solution contained 100 mg/l Ca.

(iii) Ferric chloride: BDH $FeCl_3$ solution, concentration 1000 mg/l Fe, was used. This is a solution prepared in N HCl specially for atomic absorption spectroscopy.

(iv) Magnesium chloride: 0.1000 g of oxide free magnesium ribbon was dissolved in the minimum quantity of dilute HCl and made up to 1 litre. The solution contained 100 mg/l Mg.

(v) Potassium chloride: 0.1905 g of dry potassium chloride was dissolved in de-ionised water and made up to 1 litre. The solution contained 100 mg/l K.

(vi) Sodium metasilicate: 7.6 g of $Na_2Si0_3 5H_2O$ was dissolved in de-ionised water and made up to 1 litre. The solution contained 1000 mg/l Si.

(vii) Sodium chloride: 0.2542 g of dry sodium chloride was dissolved in de-ionised water and made up to 1 litre. The solution contained 100 mg/l of Na.

All solutions were stored in polythene bottles with a maximum shelf life of six months. Very dilute standards, e.g. 5 mg/l or less, were prepared fresh and used for one week only.

(b) Reagent Solutions

These were solutions added to standards and samples to overcome the interferences of other ions. It was important that these were of a high degree of purity.

Lanthanum chloride: this was used extensively as a spectroscopic buffer to overcome interference. Special atomic absorption grade lanthanum oxide was used in preference to ordinary grade, since the latter is contaminated by calcium and magnesium. Ca/Mg is as low as 0.1 mg/l in the 'pure' lanthanum oxide. Even so, it was found to be important to add La^{3+} to both standards and samples to obtain uniform results. 4.7 g of AA grade lanthanum oxide was added to a 500 ml beaker. 300 ml of de-ionised water followed by 25 ml of 12N HCl were added. The beaker was heated and the mixture stirred until all the salt had dissolved. After cooling the solution was filtered into a 1 litre flask and made up to the mark with de-ionised water. All stock solutions, wherever possible, were stored at pH 2.0, except $Na_2Si0_3.5H_2O$ which was stored at pH 1.0 and made up freshly every two weeks.

5.9 ELEMENT DETERMINATION BY AAS

Atomic absorption spectroscopy is a highly sensitive technique for determining metals. Sensitivity of an element is defined as the concentration (mg/l of aqueous solution) which will absorb 1 % of the incident resonance radiation of that element.

The detection limit is particularly important when analysing solutions of low concentration. This is the concentration corresponding to twice the standard deviation of a series of not less than ten determinations taken close to the blank.

Sensitivity and detection limit, where available, are quoted for each element determined. These values are from W.J. Price (1972) and were themselves obtained using a Pye Unicam SP90 AAS.

A. Sodium

Sodium may be determined either by atomic absorption or flame emission spectroscopy. The latter allows higher concentrations to be determined without large dilutions. Atomic absorption was used due to its greater sensitivity and the small sample dilution actually required (large dilutions tend to magnify sources of error in the results).

Partial ionisation of sodium may occur in the air-acetylene flame due primarily to high concentrations of calcium. These effects are substantially overcome by addition of an excess (1000 mg/l) of KCl as K^+ to both standards and samples. This addition was made to the first batch of samples analysed but no difference in absorption found. The practice was henceforth discontinued.

Calibration solutions of 1.5, 3.0 and 5.0 mg/l were made from the 100 mg/l stock solution. Sample dilution was always required for Na, ranging from 10 (winter samples) to 25 (summer samples). This was carried out using distilled de-ionised water. Instrument settings were typically as follows.

Wavelength:	589.0 nM
Flame:	Air-acetylene, lean
Slit width:	0.08 mm
Lamp current:	6.5 mA
Gain:	5
Scale expansion:	1.0
Chart speed:	2 cm/min

The sensitivity is approximately 0.02 mg/l at 1 % absorption. Figure 5.10 shows a typical output trace for Na determination with calibration and three sample solutions (chart speed was 2 cm/min). The calibration curve is shown in Figure 5.11. In this case the relationship is only linear to 1.5 mg/l, since curve linearisation was not carried out. The sample shown was diluted by a factor of 10 before aspiration.

Precision is remarkably good using AAS. A replicate analysis for six dilutions of one sample give the results shown in Table 5.4.

Table 5.4 Sodium Replication

Replicate	Absorption %	Concentration mg/l
1	34.5	19.65
2	34.5	19.65
3	34.4	19.6
4	34.4	19.6
5	35	20.1
6	34.5	19.65
		Mean = 19.71 mg/l
		SD = 0.19 mg/l
		CV % = 0.96 %

B. Potassium

Like sodium, potassium may be determined in either the absorption or emission mode. Sample dilution was very rarely required in the case of potassium, justifying the use of atomic absorption.

Potassium may be partially ionised in the air-acetylene flame. The effects can be overcome by the addition of NaCl, with a concentration of 1000 mg/l as Na^+. As with Na, additions of an alkali salt (Na^+) were made to the first batch of samples analysed. No

The sensitivity is approximately 0.02 mg/l at 1 % absorption. Figure 5.10 shows a typical output trace for Na determination with calibration and three sample solutions (chart speed was 2 cm/min). The calibration curve is shown in Figure 5.11. In this case the relationship is only linear to 1.5 mg/l, since curve linearisation was not carried out. The sample shown was diluted by a factor of 10 before aspiration.

Precision is remarkably good using AAS. A replicate analysis for six dilutions of one sample give the results shown in Table 5.4.

Table 5.4 Sodium Replication

Replicate	Absorption %	Concentration mg/l
1	34.5	19.65
2	34.5	19.65
3	34.4	19.6
4	34.4	19.6
5	35	20.1
6	34.5	19.65
		Mean = 19.71 mg/l
		SD = 0.19 mg/l
		CV % = 0.96 %

B. Potassium

Like sodium, potassium may be determined in either the absorption or emission mode. Sample dilution was very rarely required in the case of potassium, justifying the use of atomic absorption.

Potassium may be partially ionised in the air-acetylene flame. The effects can be overcome by the addition of NaCl, with a concentration of 1000 mg/l as Na^+. As with Na, additions of an alkali salt (Na^+) were made to the first batch of samples analysed. No

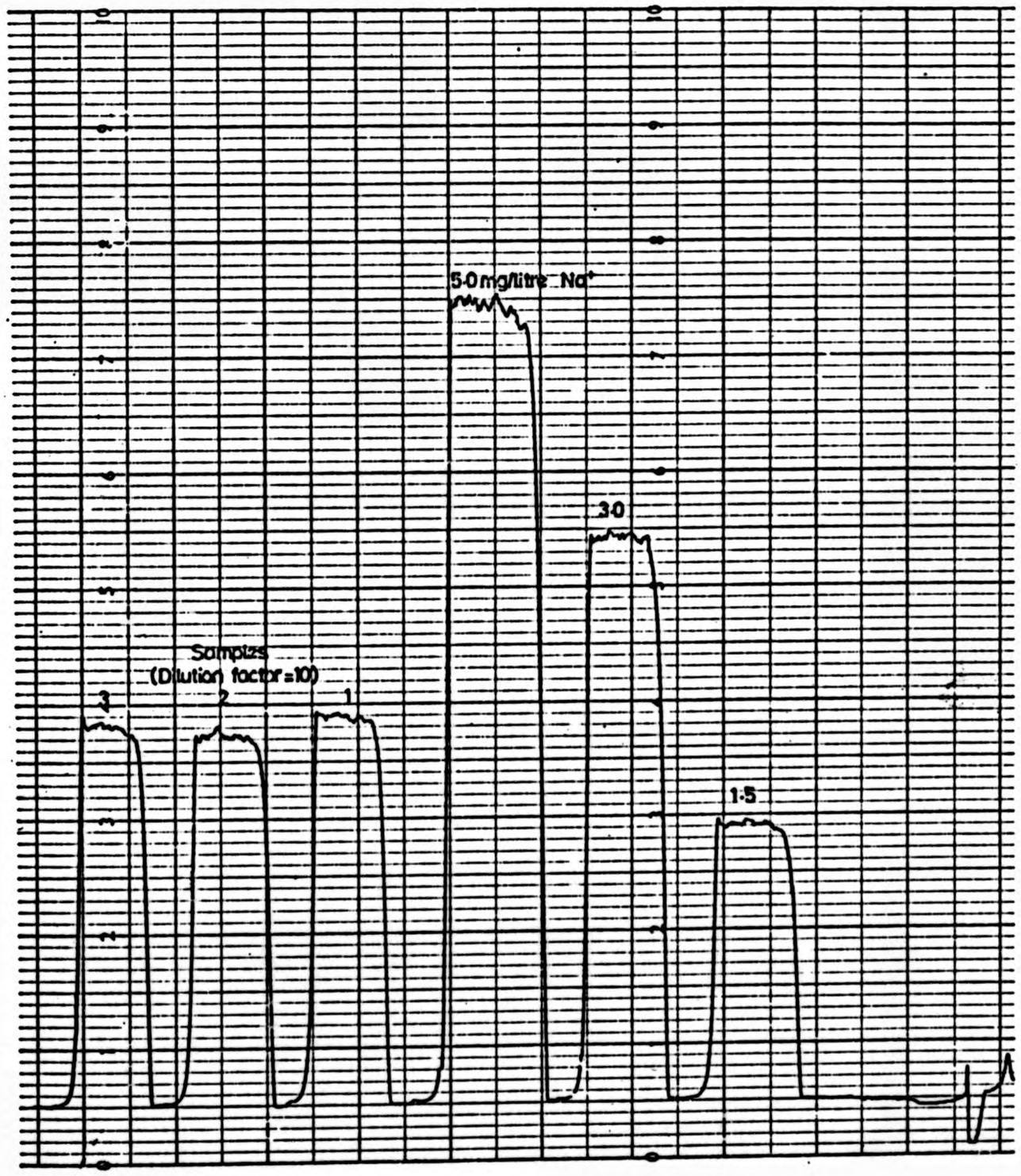

FIGURE 5.10: OUTPUT TRACE FOR SODIUM DETERMINATION BY AAS

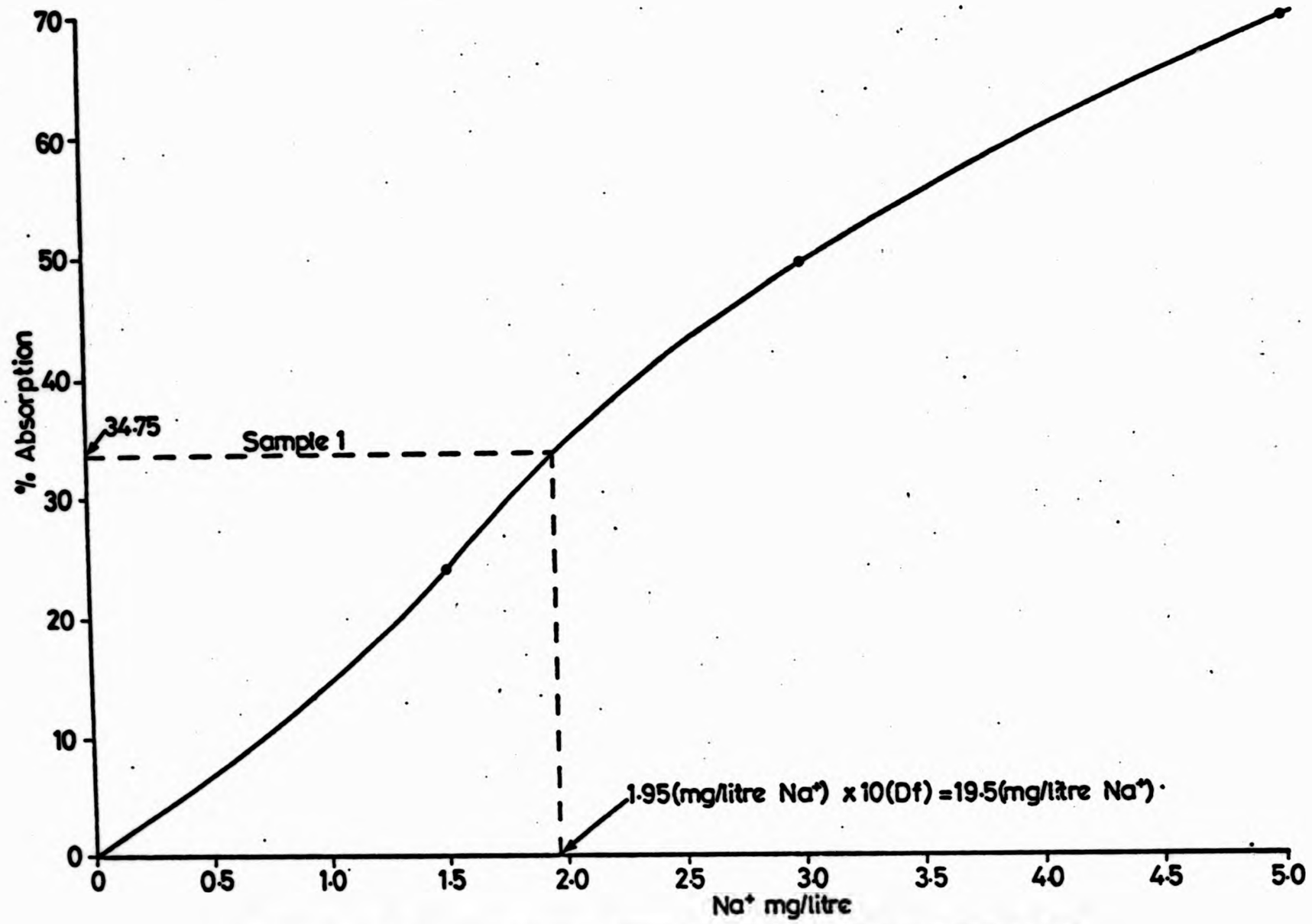

FIGURE 5.11: CALIBRATION CURVE FOR SODIUM DETERMINATION BY AAS

difference was found between those with an addition and those without an addition. Again, the practice of alkali salt addition in large concentrations was discontinued. Calibration solutions of 1.5, 3.0 and 5.0 mg/l K^+ were prepared from the 100 mg/l K^+ stock solution. Sample dilution was rarely necessary; exceptions occurred for early autumn storms when a dilution by 2 - 2.5 was required. Figure 5.12 shows a typical output trace for the three calibration solutions with two samples; Figure 5.13 gives the calibration curve. The calibration curve is linear to approximately 1.75 mg/l K^+. Interference effects are apparent on the trace; the absorption was obtained by averaging the two lowest and the two highest absorption values from the trace.

Instrument details for Figure 5.12 were as follows.

Wavelength:	766.5 nM
Flame:	Air-acetylene, lean
Slit width:	0.1 mm
Lamp current:	4.5 mA
High Gain:	7.0 (with K filter)
Scale expansion:	2.0
Chart speed:	1 cm/min

The sensitivity is approximately 0.1 mg/l K^+ for 1 % absorption. A replicate analysis of one sample gave the results shown in Table 5.5. Despite the noisy output trace precision is again remarkably good.

Table 5.5 Replicate Analysis for Potassium (No Dilution)

Replicate	Absorption %	Concentration mg/l
1	16.5	2.20
2	16.3	2.19
3	16.3	2.19
4	17.1	2.22
5	16.25	2.18
6	16.75	2.21
		Mean = 2.198 mg/l
		SD = 0.015 mg/l
		CV % = 0.68 %

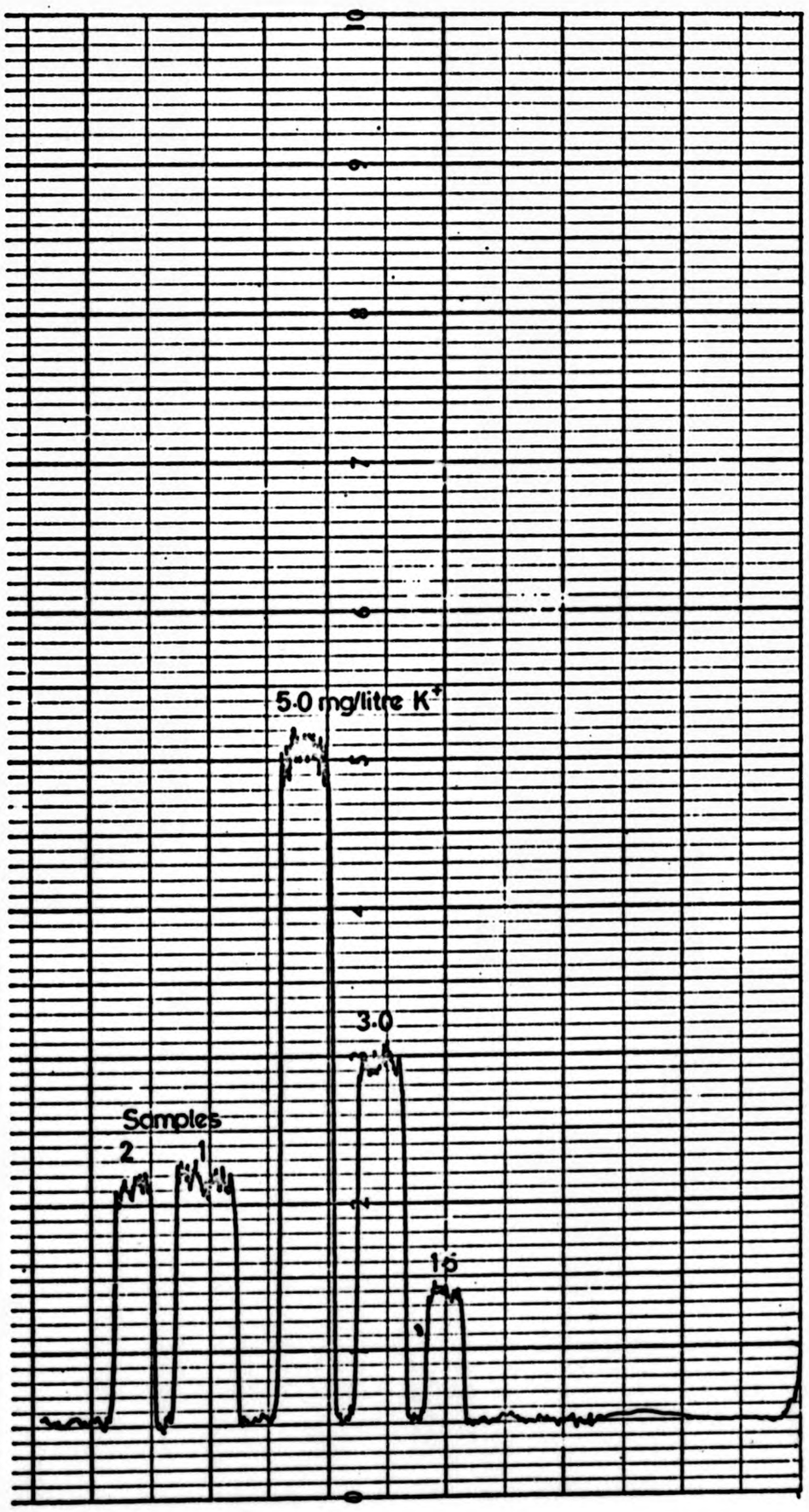

FIGURE 5.12: OUTPUT TRACE FOR POTASSIUM DETERMINATION BY AAS

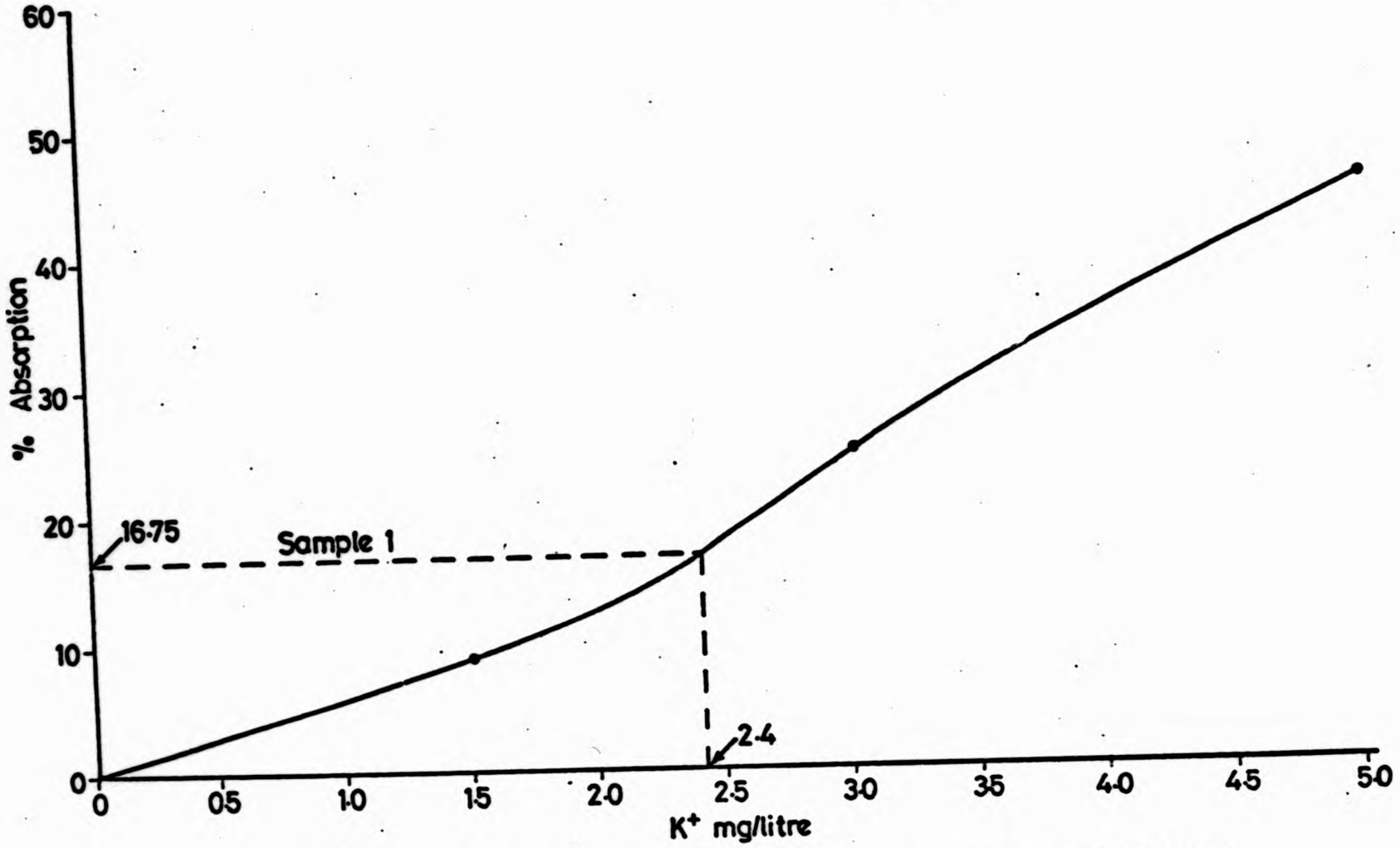

FIGURE 5.13: CALIBRATION CURVE FOR POTASSIUM DETERMINATION BY AAS

C. Calcium

Determination of calcium by atomic absorption is complicated by the fact that several interferences occur in the cooler flames (e.g. air-acetylene). In the air-acetylene flame the oxy-salts of aluminium, phosphorus and silicon are the chief interferents. The result of such interference is a depression of calcium value in the sample solutions, which depends upon the X/Ca ratio (where X is an interferent). The greatest problems arise when this ratio is equal to or greater than 1.0. Unfortunately the most sensitive part of the air-acetylene flame, immediately above the blue cone, is affected strongly by interference (Price, 1972).

Lanthanum chloride solution was added to both samples and standards to overcome the depression of calcium. A comparison of results obtained with and without the addition of La^{+} showed an overall enhancement of absorption, this being greatest at greater concentration of calcium, (Table 5.6).

Table 5.6 Enhancement of Calcium Absorption by Addition of Lanthanum Chloride

% Absorption			
Calcium Concentration mg/l	Without La^{3+}	With La^{3+} 400 mg/l	Differe nce
10	58.5	84	25.5
7	46	69.5	23.5
3	17	32	15
0	2	10.5	8.5

Figure 5.14 shows a typical output trace for calcium standards of concentration 0, 5, 10, 15, 20, 30 mg/l. Each contained lanthanum chloride, concentration 400 mg/l. Equivalent additions of La^{3+} were made to sample solutions, necessitating a slight dilution, usually of 1.11. The calibration curve for Figure 5.14 is shown in Figure 5.15.

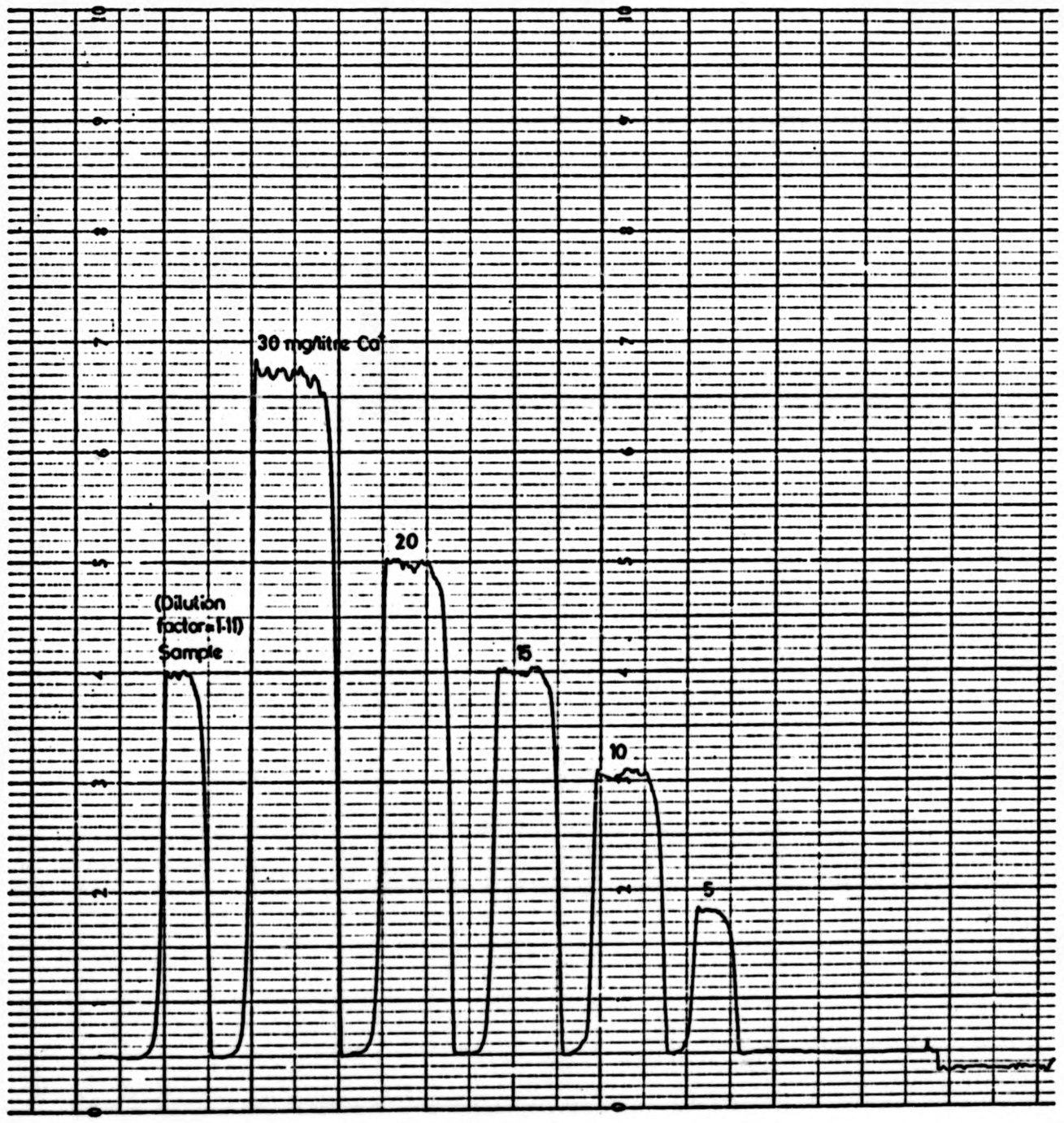

FIGURE 5.14: OUTPUT TRACE FOR CALCIUM DETERMINATION BY AAS

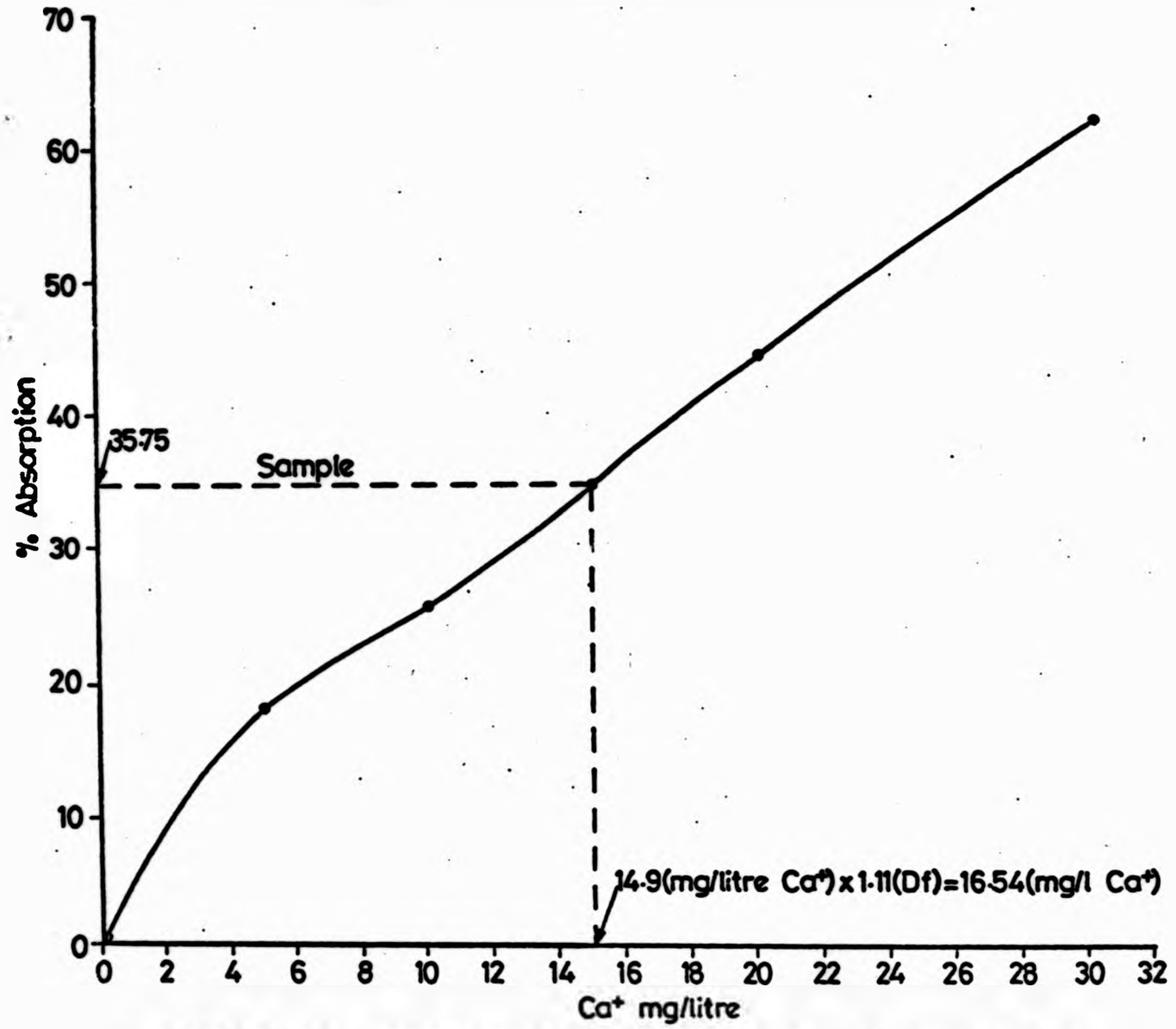

FIGURE 5.15: CALIBRATION CURVE FOR CALCIUM DETERMINATION BY AAS

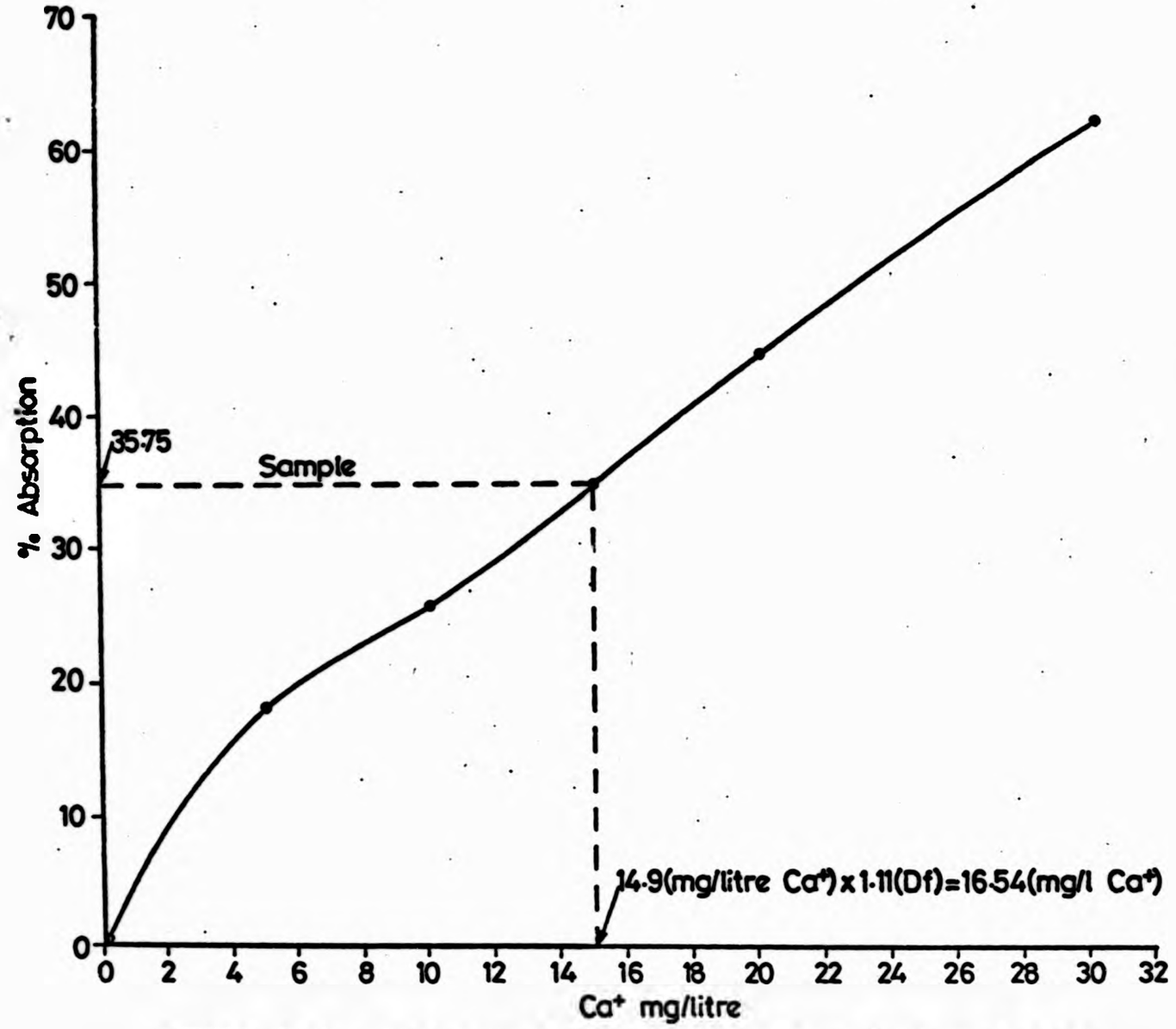

FIGURE 5.15: CALIBRATION CURVE FOR CALCIUM DETERMINATION BY AAS

Instrument details were as follows.

Wavelength:	422.7 nM
Flame:	Air-acetylene, lean
Slit width:	0.08 mm
Lamp current:	5.5 mA
Gain:	1.0
Scale Expansion:	1.0
Chart speed:	2 cm/min

The sensitivity is about 0.06 mg/l for 1 % absorption. A replicate analysis for calcium is given in Table 5.7. Replication is excellent; variation is probably due to calibration drift and dilution error.

Table 5.7 Replicate Analysis for Calcium

Replicate	Absorption %	Concentration mg/l
1	40.1	17.51
2	40.1	17.51
3	41.0	17.59
4	40.4	17.54
5	40.4	17.54
6	40.5	17.55
		Mean = 17.54 mg/l
		SD = 0.027 mg/l
		CV % = 0.15 %

D. Magnesium

Interference has been reported from aluminium, phosphorus and silicon salts (Price, 1972) when determining Mg^{2+} by atomic absorption. As with calcium determination lanthanum chloride was added to both samples and standards to overcome this interference. Magnesium is detectable in low concentrations by atomic absorption; Price (1972) gives an approximate sensitivity of 0.005 mg/l and a detection limit of 0.0005 mg/l. Thus considerable dilutions (usually by a factor of 10 - 15) were required to bring the sample solutions within the

calibration range of the instrument. Figure 5.16 shows a typical output trace for magnesium standards of 0, 0.25, 0.5, 0.75 and 1.0 mg/l with final concentrations of added La^{+} at 400 mg/l. The calibration curve given in Figure 5.17 is slightly curved between 20 and 45 % absorption.

Instrument details were as follows.

Wavelength:	285.2 nM
Flame:	Air-acetylene, stoichoimetric
Slit width:	0.1 mm
Lamp current:	5.5 mA
Gain:	6.0
Scale expansion:	1.0
Chart speed:	2 cm/min

A replicate analysis for magnesium is given in Table 5.8. One ml of the sample solution used for calcium determination (DF = 1.11) was pipetted into a 10 ml volumetric flask and an amount of La^{3+} added which would bring the final concentration up to 400 mg/l La^{3+} (0.9 ml in this case). The volume was then made up to 10 ml with de-ionised water. The dilution factor for the data in Table 5.8 is 11.11.

The multiplication by 11.11 (the DF) causes a twelve-fold increase in the standard deviation. Although this is expected and unavoidable it points to the dangers of dilution, especially when analysing on less sensitive wavelengths and under unfavourable analytical conditions. The replication for magnesium however is highly consistent.

E. Iron

A small number of samples were analysed for iron. The method used was based upon that suggested by Pye Unicam for the determination of iron in igneous silicate rocks (Fe 5). Concentrations of iron were generally low (< 0.1 mg/l Fe) and it was necessary to evaporate 100 ml of sample solution at 90°C and then dissolve the residue salts in 4.0 ml of N HCl, giving a concentration factor of 25.0.

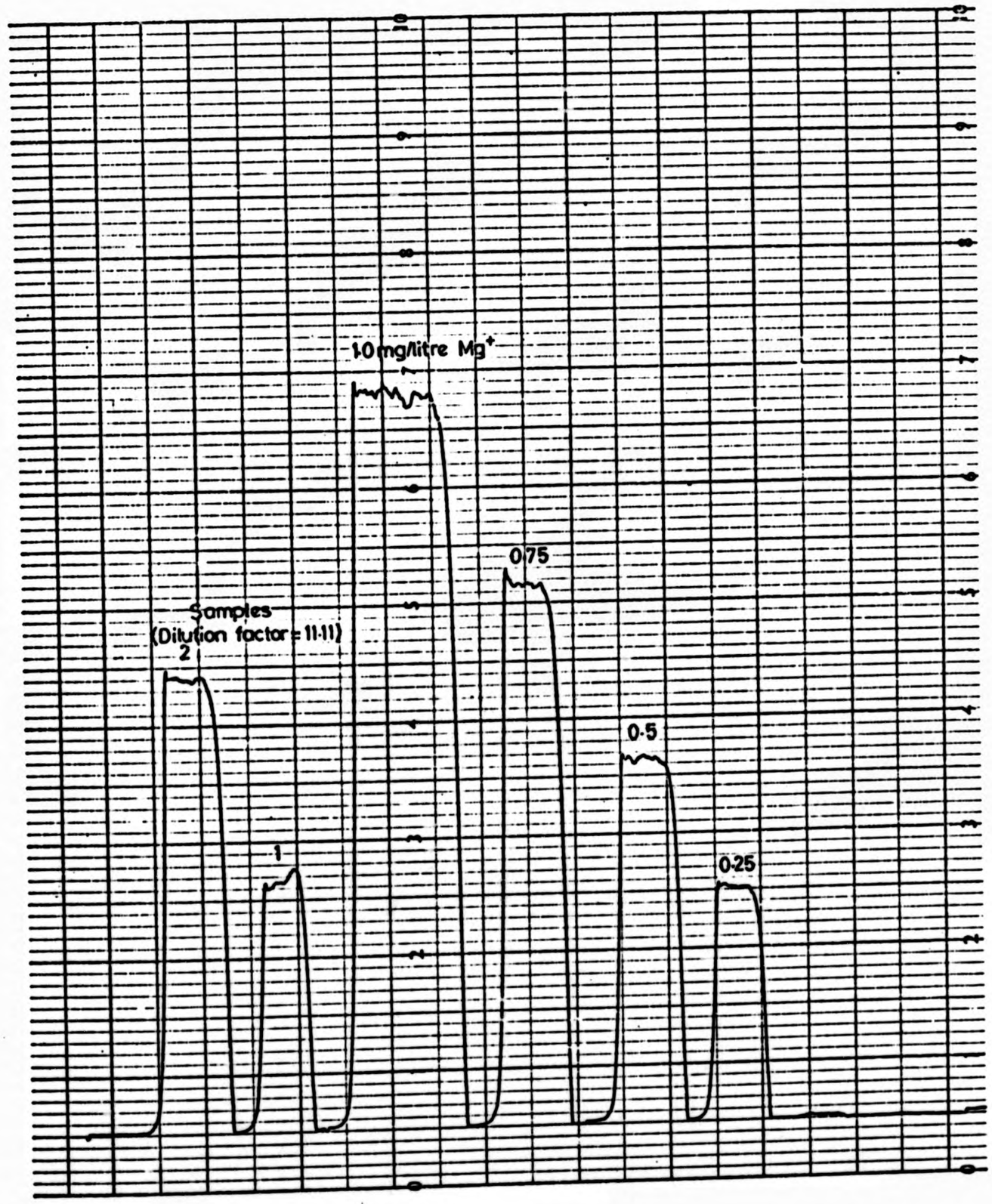

FIGURE 5.16: OUTPUT TRACE FOR MAGNESIUM DETERMINATION BY AAS

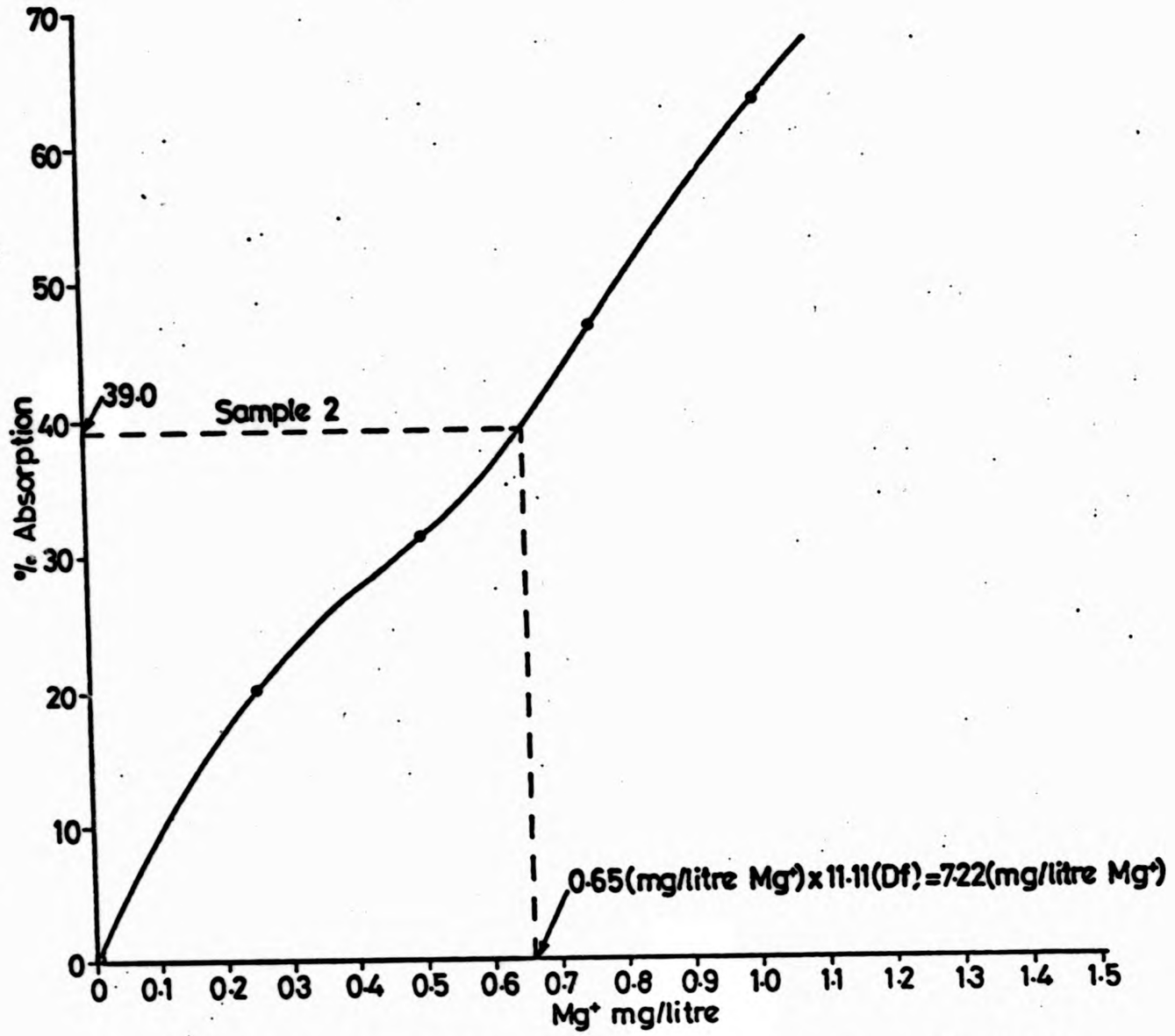

FIGURE 5.17: CALIBRATION CURVE FOR MAGNESIUM DETERMINATION BY AAS

TABLE 5.8

Replicate Analysis for Magnesium

Replicate	Absorption %	Conc. mg/l	Conc. mg/l x DF (11.11)
1	39.9	0.650	7.777
2	39.8	0.645	7.166
3	39.8	0.645	7.166
4	39.8	0.645	7.166
5	38.9	0.638	7.088
6	39.5	0.640	7.110
		$\bar{x}$ = 0.6438	$\bar{x}$ = 7.1530
		SD = 0.004	SD = 0.0476
		CV % = 0.620	CV % = 0.665

TABLE 5.8

Replicate Analysis for Magnesium

Replicate	Absorption %	Conc. mg/l	Conc. mg/l x DF (11.11)
1	39.9	0.650	7.777
2	39.8	0.645	7.166
3	39.8	0.645	7.166
4	39.8	0.645	7.166
5	38.9	0.638	7.088
6	39.5	0.640	7.110
		$\bar{x}$ = 0.6438	$\bar{x}$ = 7.1530
		SD = 0.004	SD = 0.0476
		CV % = 0.620	CV % = 0.665

The stock $FeCl_3$ solution A (prepared by BDH in N HCl: 1000 mg/l Fe or 2859 mg/l Fe_2O_3) was diluted to 100 mg/l Fe_2O_3 for later use in ferric oxide determination in soils. 35 ml of stock solution A was added to a 1000 ml volumetric flask and made up to the mark with de-ionised water, giving solution B. 5, 10, 25 and 50 ml of solution B were added to 100 ml volumetric flasks and made up to the mark with N HCl, giving calibration solutions of 5, 10, 25 and 50 mg/l Fe_2O_3 (1.75, 3.5, 8.74, 17.5 mg/l Fe).

Instrument details were as follows.

Wavelength:	248.3 nM
Flame:	Air-acetylene, lean
Slit width:	0.09 mm
Lamp current:	10 mA
Gain:	3.0
Scale expansion:	2.5
Chart speed:	2 cm/min

Despite concentrations by 25 most sample solutions were still only between 0 - 5 mg/l Fe_2O_3 (0 - 1.75 mg/l Fe). However the calibration curve was linear between 0 - 10 mg/l Fe_2O_3 (0 - 3.5 mg/l Fe) and the output trace showed little noise making interpretation relatively simple and accurate. A replicate analysis showed reasonably consistent results taking into consideration the initial evaporation process (Table 5.9).

F. <u>Silicon</u>

Silicon was determined in a similar way to iron for a small number of samples using a method based upon that described by Pye Unicam for the determination of silicon in cement (Si 1). Again sample concentrations were low (< 6.0 mg/l Si) which, when combined with the low sensitivity of the method, required sample concentration. Accordingly 100 ml of sample solution was evaporated at 90°C in a PTFE beaker; 5 ml of N HCl was added, rinsing around the side of the beaker. When the sample was re-dissolved (except for any precipitated silica) 1.0 ml of HF was added (40 % w/w). After swirling the mixture 25 ml of boric acid solution (4 % w/v) was added and mixed thoroughly. The

TABLE 5.9

Replicate Analysis for Iron

Replicate	*Absorption %	Fe_2O_3 Conc. mg/l	Fe Conc. mg/l	Fe Conc. mg/l x CF (0.04)
1	9.7	3.82	1.34	0.054
2	9.5	3.74	1.31	0.052
3	10.2	4.02	1.41	0.056
4	10.2	4.02	1.41	0.056
5	9.0	3.55	1.24	0.050
6	8.7	3.43	1.20	0.048

$\bar{x} = 0.053$

$SD = 8.9 \times 10^{-6}$

CV % = 0.0169

* Linear calibration, therefore Fe_2O_3 (mg/l) = 0.394 A %

solution was transferred to a 100 ml volumetric flask and 10 ml of lanthanum chloride (5 % La^{3+}) added, and made up to the mark with de-ionised water.

Calibration solutions followed a similar procedure. 0, 10, 15, 25 and 30 ml of the 1000 mg/l Si (2140 mg/l SiO_2) stock solution were added to 100 ml volumetric flasks. These were diluted to about 50 ml with de-ionised water and 5 ml N HCl, 25 ml of boric acid solution (4 % w/v) and 10 ml lanthanum chloride solution (5 % La^{3+}) added. They were then made up to the mark with de-ionised water, representing 0, 100, 150, 250 and 300 mg/l Si or 0, 214, 321, 535 and 643 mg/l SiO_2.

In this preparation PTFE beakers are used throughout to prevent the uptake of impurities (from glassware) by the action of HF. The addition of boric acid complexes the HF before addition to glass volumetric flasks. Lanthanum chloride is added to all solutions in order to compensate for the enhancing effect of aluminium, iron and calcium ions on silicon absorption.

Instrument details were as follows.

Wavelength:	251.6 nM
Flame:	Acetylene/nitrous oxide
Slit width:	0.1 mm
Lamp current:	10 mA
Gain:	2.0
Scale expansion:	3.0
Chart speed:	2 cm/min

The calibration graph over the range 0 - 300 mg/l Si was slightly curved (type (c), Figure 5.9), although most of the samples fell in the range 0 - 150 mg/l Si where the graph was approximately linear. The analysis of six replicates is shown in Table 5.10.

The coefficient of variation is relatively high due to the evaporation/dissolution procedure and noise associated with the silicon wavelength.

TABLE 5.10

Replicate Analysis for Silicon

Replicate	*Absorption %	Si Conc. mg/l	Si Conc. mg/l x CF (0.04)
1	24.0	147.5	5.9
2	26.4	162.5	6.5
3	27.7	170.0	6.8
4	30.1	185.0	7.4
5	24.0	147.5	5.9
6	24.8	152.5	6.1
			$\bar{x}$ = 6.43
			SD = 0.292
			CV % = 4.55

* Calibration linear, therefore Si (mg/l) = 6.15 A %

5.10 SULPHATE

There are several methods available for determining sulphate concentrations. A.I. Vogel (1961) details the colorimetric technique using barium chloranilate; the potentiometric technique with lead nitrate; and the gravimetric method precipitating barium sulphate. Golterman and Clymo (1969) outline in detail the popular turbidimetric technique; a volumetric titration using EDTA; and a potentiometric method using Pt and Ag electrodes. Problems arose in choosing any one of these techniques, either through lack of equipment (e.g. colorimeter) or slowness of method (e.g. turbidimetric with a simple comparator).

A little used indirect atomic absorption method is described by R. Dunk et al (1967). In principle an accurately measured excess of barium chloride solution is added to sulphate solution and the excess barium is determined by atomic absorption. The following reaction occurs.

$$2\ BaCl_2 + Na_2SO_4 = \underset{\text{precipitate}}{\downarrow BaSO_4} + 2\ NaCl + \underset{\text{unreacted - measured by AAS}}{\uparrow (BaCl_2)}$$

The method may be used over the concentration range 0 - 100 mg/l. It has an advantage over volumetric titrations in that the latter are slow and inconvenient when handling large numbers of samples. AAS involves a longer start to finish time but less operator handling.

Reagents

1. Barium chloride, 200 mg/l Ba^{2-}
2. Sodium sulphate, 1000 mg/l $Na_2\ SO_4$
3. HCl, 0.012 N

Method

Reagent (2) was diluted to make standard solutions of 10, 25, 50, 75, 100, 125 and 150 mg/l Na_2SO_4 (corresponding to 7, 17, 35, 51, 68, 85 and 101 mg/l SO_4^{2-}).

5.10 SULPHATE

There are several methods available for determining sulphate concentrations. A.I. Vogel (1961) details the colorimetric technique using barium chloranilate; the potentiometric technique with lead nitrate; and the gravimetric method precipitating barium sulphate. Golterman and Clymo (1969) outline in detail the popular turbidimetric technique; a volumetric titration using EDTA; and a potentiometric method using Pt and Ag electrodes. Problems arose in choosing any one of these techniques, either through lack of equipment (e.g. colorimeter) or slowness of method (e.g. turbidimetric with a simple comparator).

A little used indirect atomic absorption method is described by R. Dunk et al (1967). In principle an accurately measured excess of barium chloride solution is added to sulphate solution and the excess barium is determined by atomic absorption. The following reaction occurs.

$$2\ BaCl_2 + Na_2SO_4 = \underset{\downarrow}{BaSO_4} + 2\ NaCl + \underset{\uparrow}{(BaCl_2)}$$

precipitate — unreacted - measured by AAS

The method may be used over the concentration range 0 - 100 mg/l. It has an advantage over volumetric titrations in that the latter are slow and inconvenient when handling large numbers of samples. AAS involves a longer start to finish time but less operator handling.

Reagents

1. Barium chloride, 200 mg/l Ba^{2-}
2. Sodium sulphate, 1000 mg/l $Na_2\ SO_4$
3. HCl, 0.012 N

Method

Reagent (2) was diluted to make standard solutions of 10, 25, 50, 75, 100, 125 and 150 mg/l Na_2SO_4 (corresponding to 7, 17, 35, 51, 68, 85 and 101 mg/l SO_4^{2-}).

10 ml of sample containing not more than 150 mg/l Na_2SO_4 (100 mg/l SO_4^{2-}) were pipetted into a 25 ml graduated flask. One drop of (3) was added, and again by pipette 10 ml of reagent (1). The solution was made up to 25 ml. The sulphate standards were treated in exactly the same way.

Sample and standard solutions were left overnight (i.e.> 18 hours).

Approximately 5 ml of the supernatant liquid was carefully decanted and the unreacted Ba^{3+} determined by atomic absorption spectroscopy.

The instrument details were ideally as follows.

Wavelength:	455.4 nM
Flame:	Nitrous-oxide acetylene
Slit width:	0.1 mm
Lamp current:	6 mA
Gain:	4
Scale expansion:	1.0
Chart speed:	2 cm/min

Using the wavelength 455.4 nM with a nitrous-oxide flame has the advantage that interference by CaOH is largely obviated. Typical sensitivities and detection limits of 2 mg/l and 1 mg/l respectively are obtained using this wavelength.

A calibration graph of absorption versus SO_4^{2-} was plotted (Figure 5.18) and the sample absorptions read directly in terms of mg/l SO_4^{2-}.

There are two potentially serious sources of error in the above procedure to precipitate $BaSO_4$ (Dunk et al, 1967). Firstly, at low concentrations of Ba and SO_4^{2-}, in the cold, the reaction is relatively slow. Dunk showed that a minimum of 18 hours is required for complete reaction of Ba and SO_4^{2-} (Figure 5.19).

Secondly, at low concentrations the solubility of $BaSO_4$ is significant and very dependent upon acid concentration. It was shown

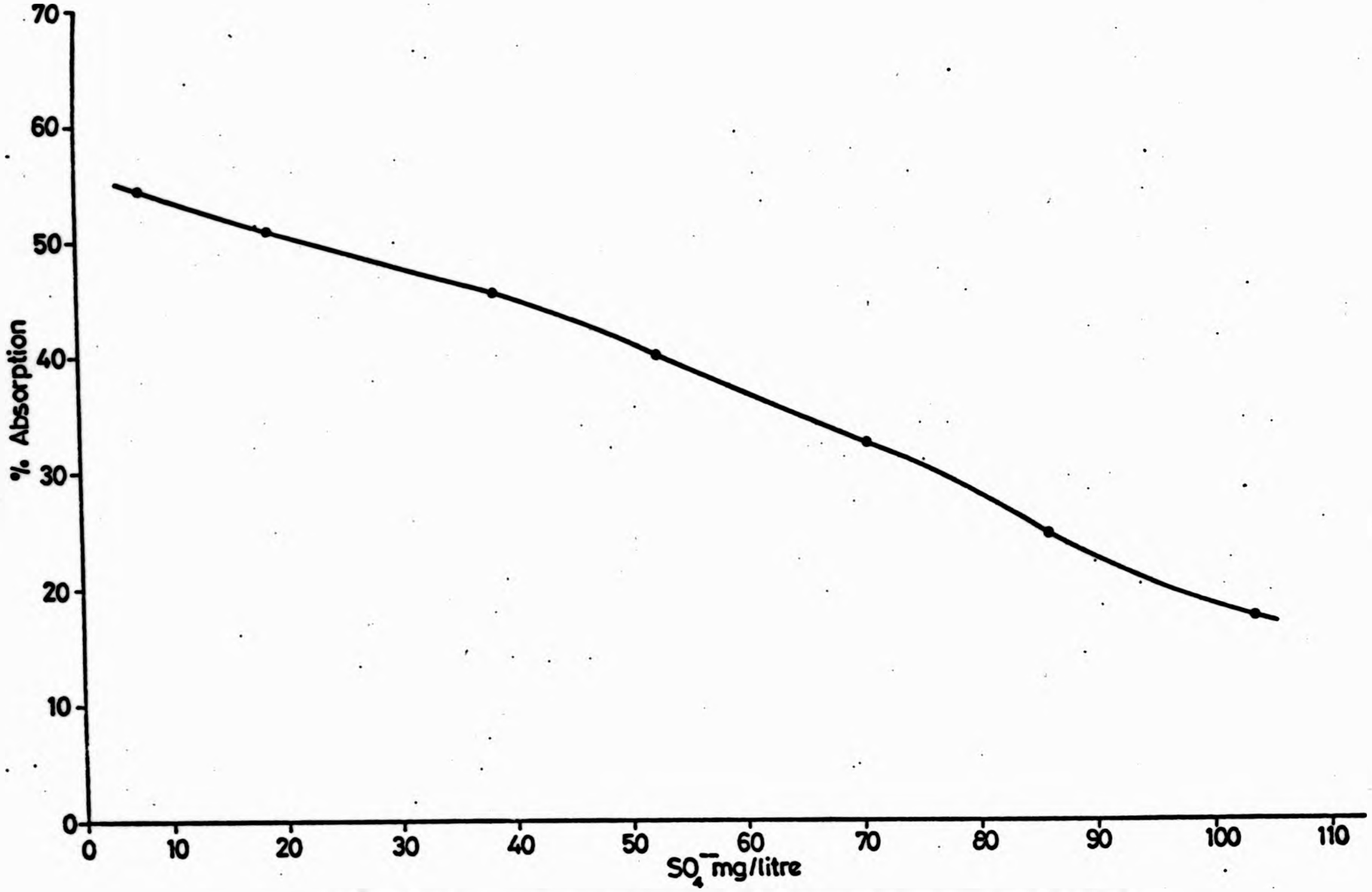

FIGURE 5.18: CALIBRATION CURVE FOR SULPHATE DETERMINATION BY AAS

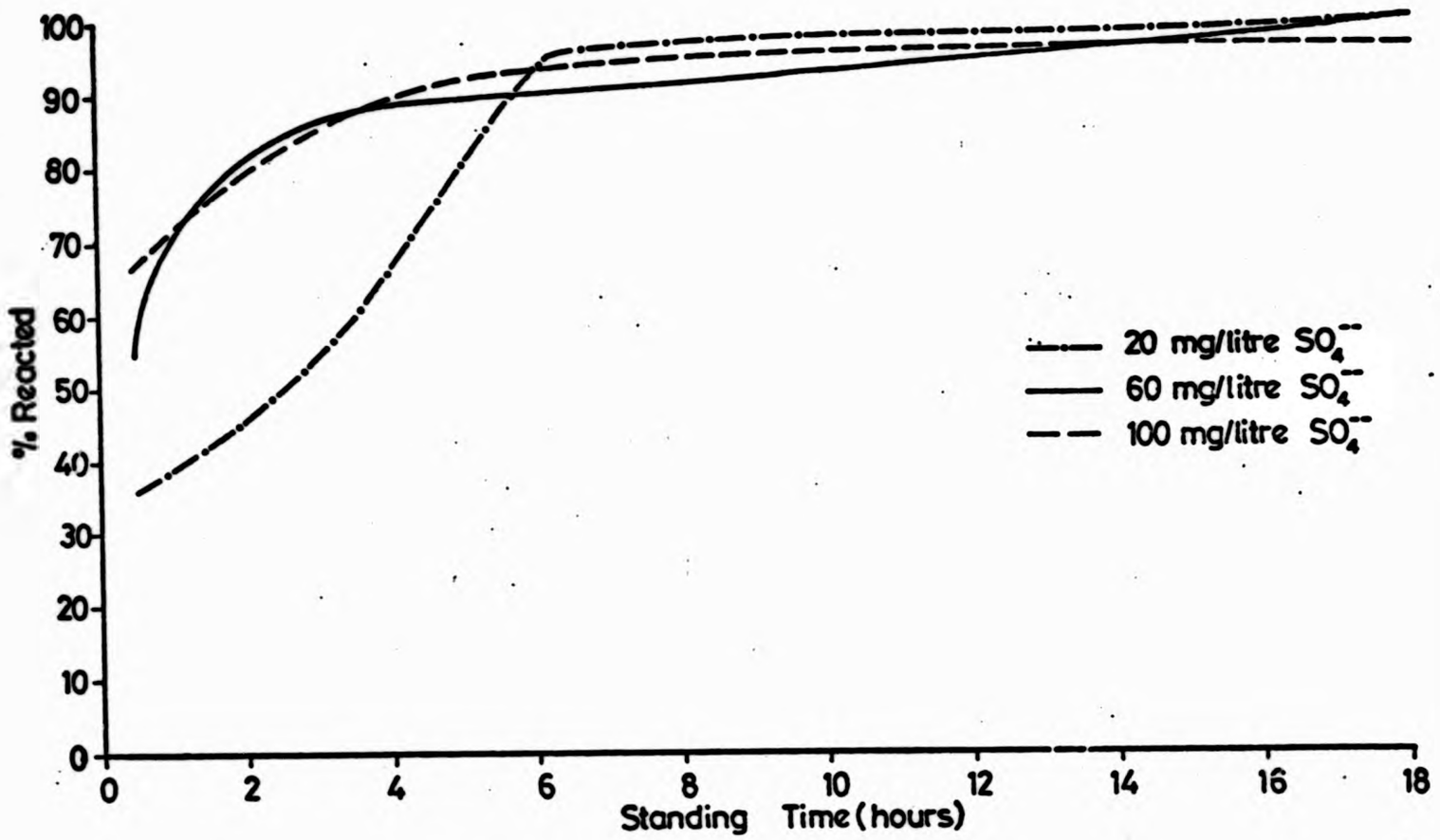

FIGURE 5.19: STANDING TIMES REQUIRED FOR COMPLETE REACTION OF Ba AND SO_4^{2-} (after Dunk et al, 1967)

to be essential to work at low acid concentrations to avoid large errors due to the sclubility of $BaSO_4$. Precipitation must be made in acid solution to avoid errors due to non-selectivity and co-precipitation. A replicate analysis of a known 50 mg/l SO_4^{2-} standard gave a mean value of 48.87 mg/l (Table 5.11).

Table 5.11 Sulphate Replication

Replicate	SO_4^{2-}
1	49.2
2	47.8
3	49.5
4	48.1
5	49.1
6	49.5
	$\bar{x}$ = 48.87 mg/l
	SD = 0.73 mg/l
	CV % = 1.49 %

5.11 CHLORIDE

Chloride, together with bicarbonate, was determined immediately (i.e. within 26 hours) of return to the laboratory. Thus no storage procedure was required.

Several methods are available for determination of the chloride ion. Golterman and Clymo (1969) describe volumetric titrations with both mercuric nitrate and silver nitrate, potentiometric titration using an Ag electrode and conductometric titration using $AgNO_3$. A.I. Vogel (1961) gives a more comprehensive treatment. In addition to the techniques proposed by Golterman, he describes volumetric titrations using Volhard's method (the chloride solution is treated with an excess of standard silver nitrate solution, and the residual silver nitrate determined by titration with standard thiocyanate

to be essential to work at low acid concentrations to avoid large errors due to the sclubility of $BaSO_4$. Precipitation must be made in acid solution to avoid errors due to non-selectivity and co-precipitation. A replicate analysis of a known 50 mg/l SO_4^{2-} standard gave a mean value of 48.87 mg/l (Table 5.11).

Table 5.11 Sulphate Replication

Replicate	SO_4^{2-}
1	49.2
2	47.8
3	49.5
4	48.1
5	49.1
6	49.5
	$\bar{x}$ = 48.87 mg/l
	SD = 0.73 mg/l
	CV % = 1.49 %

5.11 CHLORIDE

Chloride, together with bicarbonate, was determined immediately (i.e. within 26 hours) of return to the laboratory. Thus no storage procedure was required.

Several methods are available for determination of the chloride ion. Golterman and Clymo (1969) describe volumetric titrations with both mercuric nitrate and silver nitrate, potentiometric titration using an Ag electrode and conductometric titration using $AgNO_3$. A.I. Vogel (1961) gives a more comprehensive treatment. In addition to the techniques proposed by Golterman, he describes volumetric titrations using Volhard's method (the chloride solution is treated with an excess of standard silver nitrate solution, and the residual silver nitrate determined by titration with standard thiocyanate

solution), and also with mercurous perchlorate; colorimetric or spectrophotometric with mercuric chloranilate; gravimetric with silver nitrate. W. Westerlund-Helmerson (1966) has described an indirect method using atomic absorption spectroscopy.

The choice of technique was restricted by the laboratory facilities available. The mercuric chloranilate method was ruled out through lack of a spectrophotometer; the rapid potentiometric titration through the lack of an Ag electrode; the indirect atomic absorption method through the lack of a silver lamp. The gravimetric method is considered slow and unsuitable for the analysis of a large batch of samples. Of the remaining methods titration with either mercuric nitrate or silver nitrate seemed most attractive, since both are uncomplicated and accurate to about 1.0 mg/l Cl^-.

The mercuric nitrate titration (Golterman and Clymo, 1969) was chosen because of its simplicity, although there is no particular advantage over the silver nitrate procedure. The chloride ion is titrated with mercuric ion (i.e. with a solution of mercuric nitrate acidified with nitric acid) and follows the reaction:

$$2Cl^- + Hg^{++} = HgCl_2$$

The end point is determined with a mixture of diphenyl-carbazone and bromophenol blue. The bromophenol blue changes from blue (alkaline) to yellow (acid) at circa pH 3.6, which is the acidity recommended for Cl^- concentrations below 10 mg/l. At the equivalence point the yellow colour of the solution becomes blue-violet owing to the reaction of the excess of mercuric ions with diphenylcarbazone (Vogel, 1961):-

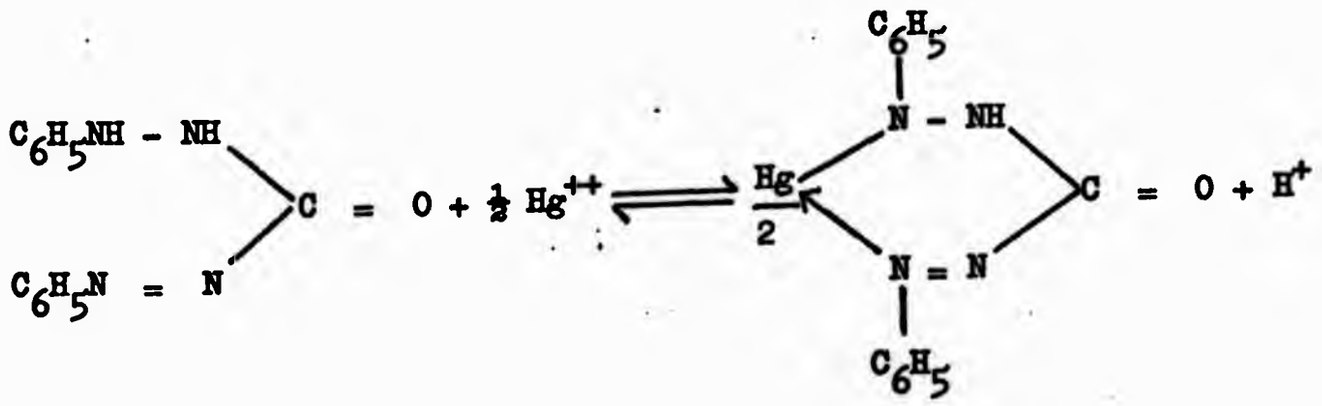

The ions CrO_4^{2-}, Fe^{3+}, Mn^{2+}, Zn^{2+} and Cu^{2+} react with diphenylcarbazone if present in concentrations greater than 10 mg/l. Such interference was not found in the analyses. The method described follows that of Golterman and Clymo (1969).

Reagents

1. Standard NaCl, 0.01 N
2. $Hg(NO_3)_2$, 0.02 N (standardised against NaCl as described in A.I. Vogel (1961, p. 48 - 50) using bromophenol blue as indicator)
3. HNO_3, 0.2 N
4. Diphenylcarbazone-bromophenol blue mixed indicator solution

Method

To 50 ml sample (diluted by 2 - 3) to bring it within approximately 10 mg/l Cl^-) were added ten drops of reagent (4). Reagent (3) was added dropwise until the solution became yellow (pH = 3.6), whereupon five more drops of (3) were added.

Titration with (2) proceeded until the colour changed through orange to blue-violet.

An automatic stirrer was used in the titration. Table 5.12 gives a replicate analysis using the titration.

Table 5.12 Chloride Replication

Replicate	ml titrated	mg/l Cl^-
1	0.90	25.5
2	0.95	27.0
33	0.95	27.0
4	0.93	26.4
5	0.90	25.5
6	0.97	27.5
		Mean = 26.48 mg/l
		SD = 0.84 mg/l
		CV % = 3.17 %

Variation in the results can be attributed to the standard of the equipment used and also variation in burette drop size. A 50 ml burette was used and read to the nearest 0.025 ml (0.71 mg/l Cl^-). As this is the approximate size of a drop from the burette under-estimation of Cl^- occurs when only half a drop forms. This problem was overcome by washing the drop from the burette with a little de-ionised water.

5.12 BICARBONATE

As with chloride, HCO_3^- was determined as soon as possible on return to the laboratory; that is, within a maximum of three hours. Bicarbonate values decrease continuously from sample collection. Golterman and Clymo (1969) showed that an unboiled solution of 0.001 M $NaHCO_3$ increased in alkalinity and decreased in pH over a 24 hour period (pH from 7.2 to 7.94, and CO_2 from 6 mg/l to 1.1 mg/l). The concentrations in a boiled sample remained the same over 24 hours. He suggested that the water became more alkaline due to the uptake of CO_2 by algae. Two samples from West Walk showed the opposite trend in pH, pointing to the necessity of analysing for HCO_3^- (and pH) as soon as possible after sample collection.

Bicarbonate is just one component of the carbonate-bicarbonate system, generally referred to as alkalinity. The alkalinity reaction of water is due to the relative amounts of effective acids and bases present. Carbonate, borate, silicate and phosphate act as strong bases and can be neutralised by titration with a strong acid. In this case carbonate is converted to carbonic acid. $H_3SiO_4^-$, $H_2BO_3^-$ and $H_2PO_4^-$ are not present in large enough quantities to affect the total alkalinity in the waters analysed. Golterman and Clymo (1969) cite four quantities which are commonly reported in alkalinity determinations (Table 5.13). The concentrations of OH^- and H^+ can be neglected because of their small magnitude. The alkalinity due to CO_3^{2-} + OH is determined by titration with acid to pH $\simeq$ 8.3, where the end point can be detected by phenolphthalein. Since the pH of water samples from the catchment rarely rise above 7.5, it is argued that alkalinity is all in the form of HCO_3^- which can be found by titration to an end point of pH 4.5. At this end point virtually all the bicarbonate has been converted to carbonic acid.

TABLE 5.13

Four Quantities commonly reported in Alkalinity Determinations

Quantity	Symbol	Compounds	End Point pH
1. Phenolphthalein alkalinity .	PA	$OH^- + CO_3^{2-}$	8.3
2. Total alkalinity	TA	$OH^- + CO_3^{2-} + HCO_3^-$	4.2 - 5.4
3. Carbonate alkalinity	CA	$CO_3^{2-} + HCO_3^-$	
4. Total CO_2	TC	$CO_3^{2-} + HCO_3^- + CO_2$	

Two methods were considered for the determination of HCO_3^- in the present work. The first method uses either a mixed indicator or methyl orange to identify the titration end point of 4.5. The method is unsuitable for precise work, however, because the exact end point pH of the TA titration depends on the amount of CO_2 in solution and is therefore related to TC. If indicators are to be used an approximate value of TA is found first; from this an estimate is made to TC and then the TA recalculated. This true value of TA will give an end point pH very close to the true value. The method is detailed in Golterman and Clymo (1969).

The second method employs a potentiometric titration. This uses a pH meter with graphical output to monitor the neutralisation of alkalinity as acid is added from a burette. The end point is identified on the graph as the steepest gradient on the pH descent curve (Figure 5.20). A conductometric titration makes this end point much easier to determine. Since the conductivity of the water increases linearly up to the end point, past the end point the increase of conductivity per unit of titrant added is greater, but still linear. The intersection of the two curves gives the titration end point. Conductometric facilities were not available and the end point was of necessity determined from the single pH descent curve. This method has the advantage of being fast and reliable when analysing a large number of samples.

Reagents

1. HCl, 0.012 N, standardised against 0.01 N NaOH
2. Sample, 100 ml

Method

Assemble the apparatus as shown in Figure 5.6. Titrate the sample with HCl from the burette, operating the graphical recorder simultaneously. Read the end point and ml titrant from the trace (Figure 5.20). Calculate bicarbonate by:

$$HCO_3^- = \frac{(\text{ml titrant} \times N) \times 1000 \times 61.018}{\text{ml sample}} \text{ mg/l}$$

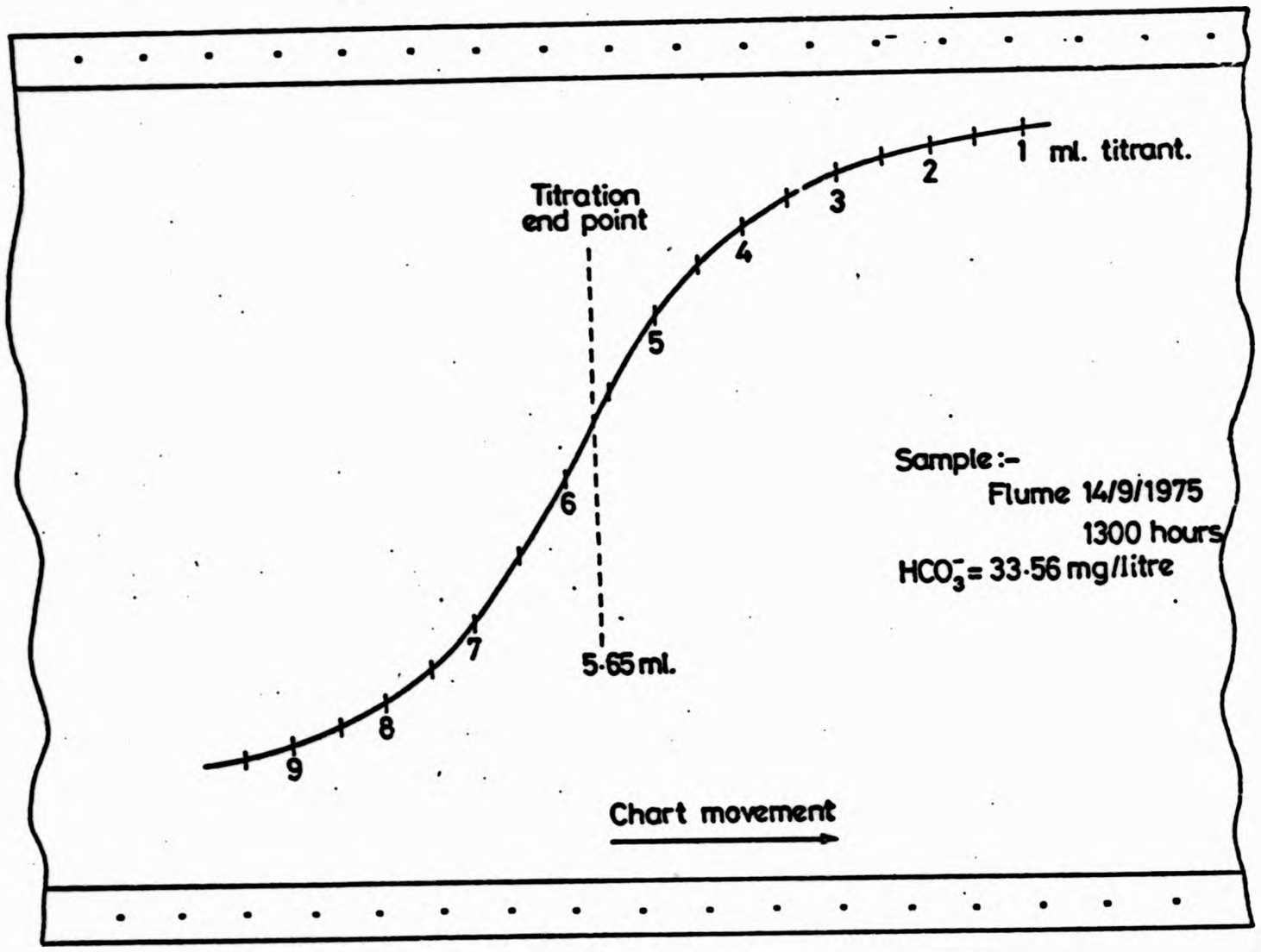

FIGURE 5.20: CHART OUTPUT FROM BICARBONATE DETERMINATION

A set of six samples was checked independently using a more exact method of end point determination suggested by Golterman and Clymo (1969). The pH and conductivity of the sample are recorded first. The sample is then titrated with HCl as described above until the TA end point is almost reached (pH = 5.0 - 5.5) and the burette read.

End point pH is then calculated as follows.

(i) Estimate TA from the expression

$$TA = \frac{(\text{ml titrant} \times N) \times 1000}{\text{ml sample}} \text{ meq/l}$$

(ii) Calculate CA = TA - 0.01 using Table 3.3 in Golterman and Clymo (1969). This gives an easy solution of $CA = TA - 10^{3}(OH^{-})$.

(iii) Calculate TC = from the expression

$TC = CA\,\partial$

where ∂ is obtained from Table 3.4 in Golterman and Clymo (1969), given the initial conductivity and pH of the sample.

(iv) Calculate end point pH by

$pH = -\frac{1}{2} \log (TA\ K_1)$,

where $K_1 = 10^{-6.38}$

Titration then continues to the new pH and the HCO_3^- concentration is calculated as shown previously. The use of a magnetic stirrer keeps CO_2 losses to minimum during the analysis.

Results from the comparison of the two methods are shown in Table 5.14. The Kolmogorov-Smirnov test shows that the two samples were drawn from the same population (Siegel, 1956). Therefore, the potentiometric graphical method was used throughout.

In several cases the determination of HCO_3^- by the usual method was not possible due to instrument failure. A relationship between pH

(determined by field pH meter) and HCO_3^- was established to overcome this problem. It was found that

$$HCO_3^- = (1.32 \times 10^{-9})\ pH^{12.275}$$

(N = 50, r = 0.97, SE_Y = 0.24; significant at 0.1 % level)
This was used to estimate a total of 24 samples.

Table 5.14 Reliability Test for the Potentiometric-Graphical Titration of HCO_3^-

P-G Titration	P Titration with Calculated End Point pH
45.9	46.1
46.1	46.9
9.9	10.0
6.8	6.4
7.1	7.3
3.1	2.8

H_o = No difference between the two samples
H_1 = Signficiant difference between the two samples
DMAX = 1
N = 6

H_o upheld at the 99 % significance level

Table 5.15 gives a replicate analysis of one sample using the potentiometric-graphical procedure, with a surprisingly consistent result. As with all titrations problems occur when half-formed drops remain on the burette. These were washed into sample with a little de-ionised water.

(determined by field pH meter) and HCO_3^- was established to overcome this problem. It was found that

$$HCO_3^- = (1.32 \times 10^{-9})\ pH^{12.275}$$

(N = 50, r = 0.97, SE_Y = 0.24; significant at 0.1 % level)
This was used to estimate a total of 24 samples.

Table 5.14 Reliability Test for the Potentiometric-Graphical Titration of HCO_3^-

P-G Titration	P Titration with Calculated End Point pH
45.9	46.1
46.1	46.9
9.9	10.0
6.8	6.4
7.1	7.3
3.1	2.8

H_o = No difference between the two samples
H_1 = Signficiant difference between the two samples
DMAX = 1
N = 6

H_o upheld at the 99 % significance level

Table 5.15 gives a replicate analysis of one sample using the potentiometric-graphical procedure, with a surprisingly consistent result. As with all titrations problems occur when half-formed drops remain on the burette. These were washed into sample with a little de-ionised water.

(determined by field pH meter) and HCO_3^- was established to overcome this problem. It was found that

$$HCO_3^- = (1.32 \times 10^{-9})\ pH^{12.275}$$

(N = 50, r = 0.97, SE_Y = 0.24; significant at 0.1 % level)
This was used to estimate a total of 24 samples.

Table 5.14 Reliability Test for the Potentiometric-Graphical Titration of HCO_3^-

P-G Titration	P Titration with Calculated End Point pH
45.9	46.1
46.1	46.9
9.9	10.0
6.8	6.4
7.1	7.3
3.1	2.8

H_o = No. difference between the two samples
H_1 = Signficiant difference between the two samples
DMAX = 1
N = 6

H_o upheld at the 99 % significance level

Table 5.15 gives a replicate analysis of one sample using the potentiometric-graphical procedure, with a surprisingly consistent result. As with all titrations problems occur when half-formed drops remain on the burette. These were washed into sample with a little de-ionised water.

Table 5.15 Replicate Analyses for HCO_3^-

Replicate	ml titrated	mg/l HCO_3^-
1	3.5	25.6
2	3.45	25.3
3	3.8	27.8
4	3.5	25.6
5	4.0	29.3
6	3.5	25.6

Mean = 26.5 mg/l HCO_3^-
SD = 1.68 mg/l HCO_3^-
CV % = 6.34 %

5.13 ESTIMATION OF TOTAL DISSOLVED SOLIDS FROM SPECIFIC CONDUCTANCE

Specific conductance (SC) is an easily measured water quality parameter widely used as an estimator of total dissolved solids (TDS). In the present study knowledge of TDS was required for calculating total solute loss and for checking the sum of the individual ion totals of each sample. In the past various models have been used relating SC and TDS and these range from empirical to analytical.

The simplest most widely used empirical model is,

$$C = bK \qquad (5.1)$$

where C = concentration in mg/l
K = specific conductance, μmhos/cm
b = constant.

This model assumes, from theoretical considerations (i.e. C = 0, K = 0), a zero intercept or an intercept which is insignificantly different from zero at some specified level of probabality. The values of 'b' have ranged from 0.55 to 0.75 (Gregory and Walling, 1973); in

the UK 'b' has been found to vary from 0.65 (Walling and Webb, 1975) to 0.91 (Cryer, 1976). The second model, including an intercept, is

$$C = a + bK \qquad (5.2)$$

R. Cryer (1976) used this model separately for precipitation and streamwater, obtaining intercepts of + 3.38 and - 1.11 respectively. He does not state whether these values are significantly different from zero, nor does he recalculate through the origin. The 'b' value of 0.28 obtained for precipitation probably reflects the increasing contribution of H^+ to conductivity at lower pH, accompanied by little increase in TDS (this point will be discussed later). Cryer explains his value of b = 0.91 for streamflow by the assumed presence of uncharged organics which inflate the TDS concentrations. These results are interesting, and re-affirm the conclusions of T.D. Steele (1968) that mixing water bodies with different origins may increase scatter about the regression line and give an intercept which is significantly greater than zero.

Using equation (5.2) the results for West Walk are given in Table 5.16. The plotted data are shown in Figure 5.21. The correlation coefficient for all the data, although significant at the 0.1 % level, is not satisfactory if the model is to be used for the calculation of TDS. Furthermore, the intercept of the line (44.36) is significantly greater than zero (using a 't' test: Brownlee, 1965, p. 345) which suggests that dissolved matter is being included in TDS but not contributing to conductivity (either uncharged paired ions or organic molecules). When individual bodies of water are treated separately there is no improvement, with intercepts increasing in all cases. Although not having a significant individual relationship (the scatter here is probably due to pH variation) the rainfall data clearly acts to pull the overall regression line towards zero. Treatment of individual components was unsuccessful and a quadratic fitted to the complete data set giving,

$$C = 9.52 + 0.96\,K - 0.0012\,K^2 \qquad (5.3)$$

N 160, $r = 0.78$, $r^2 = 61\ \%$, significant at the 0.1 % level,
$SE_Y = 39.5$

TABLE 5.16

Relationships between SC and TDS for West Walk Data

Data Group	Equation	N	r	r^2 %	SE_Y	Significance Level %
All data	C = 44.36 + 0 48 K	160	0.72	52	43.52	0.1
All flow data	C = 89.64 + 0.31 K	123	0.49	24	43.95	0.1
Rainfall data	C = 50.55 + 0.5 K	37	0.08	1	37.59	NS
W1	C = 104.40 + 0.21 K	59	0.35	12	46.08	1.0
W2	C = 54.23 + 0.38 K	11	0.29	8	52.16	NS
Flume	C = 253.95 - 0.36 K	31	- 0.24	6	31.9	NS
W4	C = 67.29 + 0.42 K	11	0.23	5	53.77	NS
W5	C = 107.49 + 0.31 K	11	0.61	37	33.05	5.0

TABLE 5.16

Relationships between SC and TDS for West Walk Data

Data Group	Equation	N	r	r^2 %	SE_Y	Significance Level %
All data	C = 44.36 + 0 48 K	160	0.72	52	43.52	0.1
All flow data	C = 89.64 + 0.31 K	123	0.49	24	43.95	0.1
Rainfall data	C = 50.55 + 0.5 K	37	0.08	1	37.59	NS
W1	C = 104.40 + 0.21 K	59	0.35	12	46.08	1.0
W2	C = 54.23 + 0.38 K	11	0.29	8	52.16	NS
Flume	C = 253.95 - 0.36 K	31	- 0.24	6	31.9	NS
W4	C = 67.29 + 0.42 K	11	0.23	5	53.77	NS
W5	C = 107.49 + 0.31 K	11	0.61	37	33.05	5.0

A 't' test showed the intercept to be significantly different from zero at the 1.0 % level which did not justify forcing the regression line through the origin. This re-affirms the suggestion that dissolved matter is being included in the TDS but is not contributing to conductivity. The percentage variance explained improves over the linear model, from 52 % to 61 %. An unexplained variance of 39 % still leaves room for improvement if the model is to be used for accurate estimation of TDS. Furthermore, the model is a poor predictor of TDS above about 400 um, where TDS declines with increasing SC. A further model was used by T.D. Steele (1968) which related conductivity to individual ion concentration,

$$c_i = a_i + b_i K \qquad (5.4)$$

where c_i = concentration of the ion species, i;
thus TDS is calculated from,

$$C = \sum_{i=1}^{i=n} (c_i) = \sum_{i=1}^{i=n} (a_i + b_i K) \qquad (5.5)$$

where n = number of ions.

Steele found that in most cases the individual c_i was well predicted from K, although with lower r^2 % values than for the TDS/SC relationship (r^2 % = 0.98, N = 70). To satisfy the requirement of a zero intercept (this must be true from theoretical considerations) the data was dichotomised about a specific flow level and each set described by a separate regression. This produced r^2 % values ranging from 4.0 (lower SO_4^{2-} data) to 98.0 (higher Mg^{2+} data). The overall conclusion was that the method could not be applied successfully to all ions, which made it difficult to apply equation (5.5). Scatter diagrams of individual ions plotted against SC for West Walk data suggested that the relationships could not all be fitted by a simple linear model (Figures 5.22 - 5.28). A variety of best-fit functions were therefore employed and these are given in Table 5.17.

Excepting the plots of HCO_3^- and SO_4^{2-} against SC all the regression lines pass very close to the origin. The scatter about the regression line is partly due to the mixing of different bodies of

TABLE 5.17

Relationships between SC and individual Ions for all West Walk Data

Ion	Equation	N	r	r^2 %	Significance Level %	SE	λ_i°
Mg^{++}	$C_i = 0.04\ K - 0.000014\ K^2 - 1.04$	198	0.90	81	0.1	2.18	53.0
Na^+	$C_i = 0.13\ K - 0.00013\ K^2 - 2.0$	173	0.89	80	0.1	4.05	50.1
K^+	$C_i = 0.25 + 0.0032\ K + 0.000022\ K^2$	187	0.86	74	0.1	1.37	73.5
Cl^-	$C_i = 0.44\ K^{0.77}$	177	0.85	73	0.1	2.29	76.4
Ca^{++}	$C_i = 0.069\ K + 0.92$	198	0.51	26	0.1	17.8	59.5
HCO_3^-	$C_i = 0.05\ K + 13.9$	143	0.27	7	0.1	23.2	44.5
$SO_4^=$	$C_i = 21.84 - 0.0025\ K$	108	0.01	-	NS	27.13	80.2

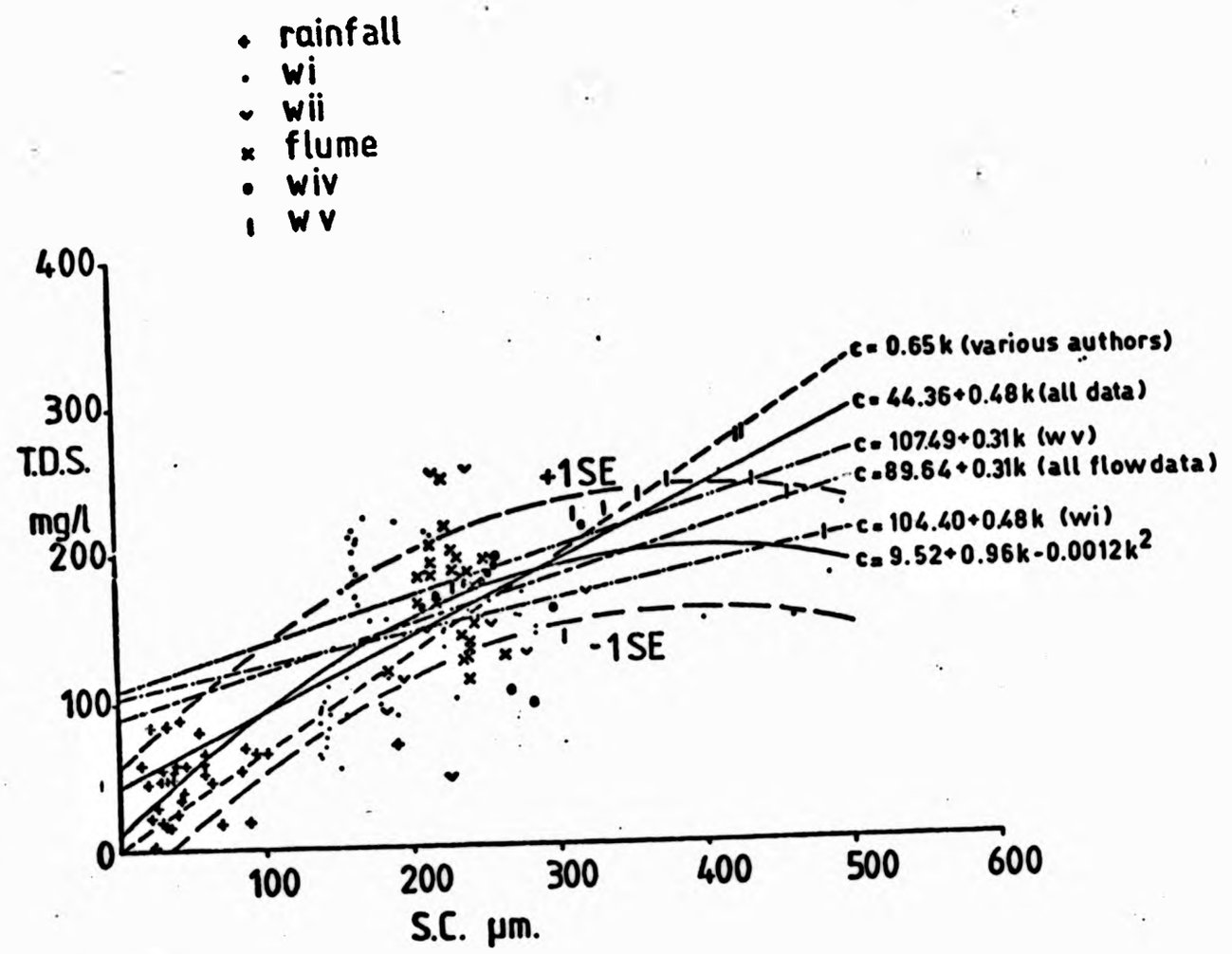

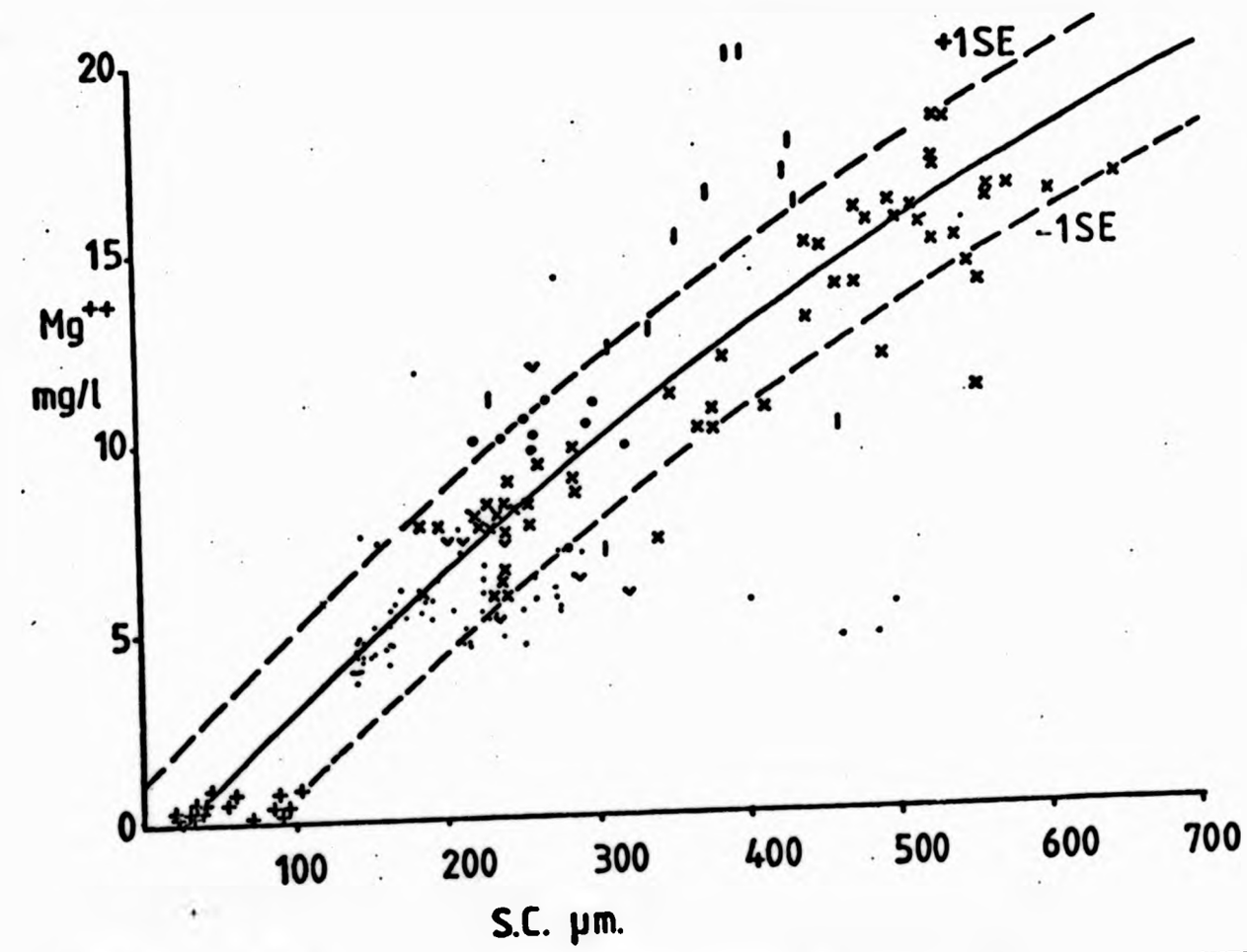

FIGURE 5.21: SPECIFIC CONDUCTANCE/TOTAL DISSOLVED SOLIDS RELATIONSHIP (top)

FIGURE 5.22: SPECIFIC CONDUCTANCE/MAGNESIUM RELATIONSHIP (bottom) (for Key, see Figure 5.21)

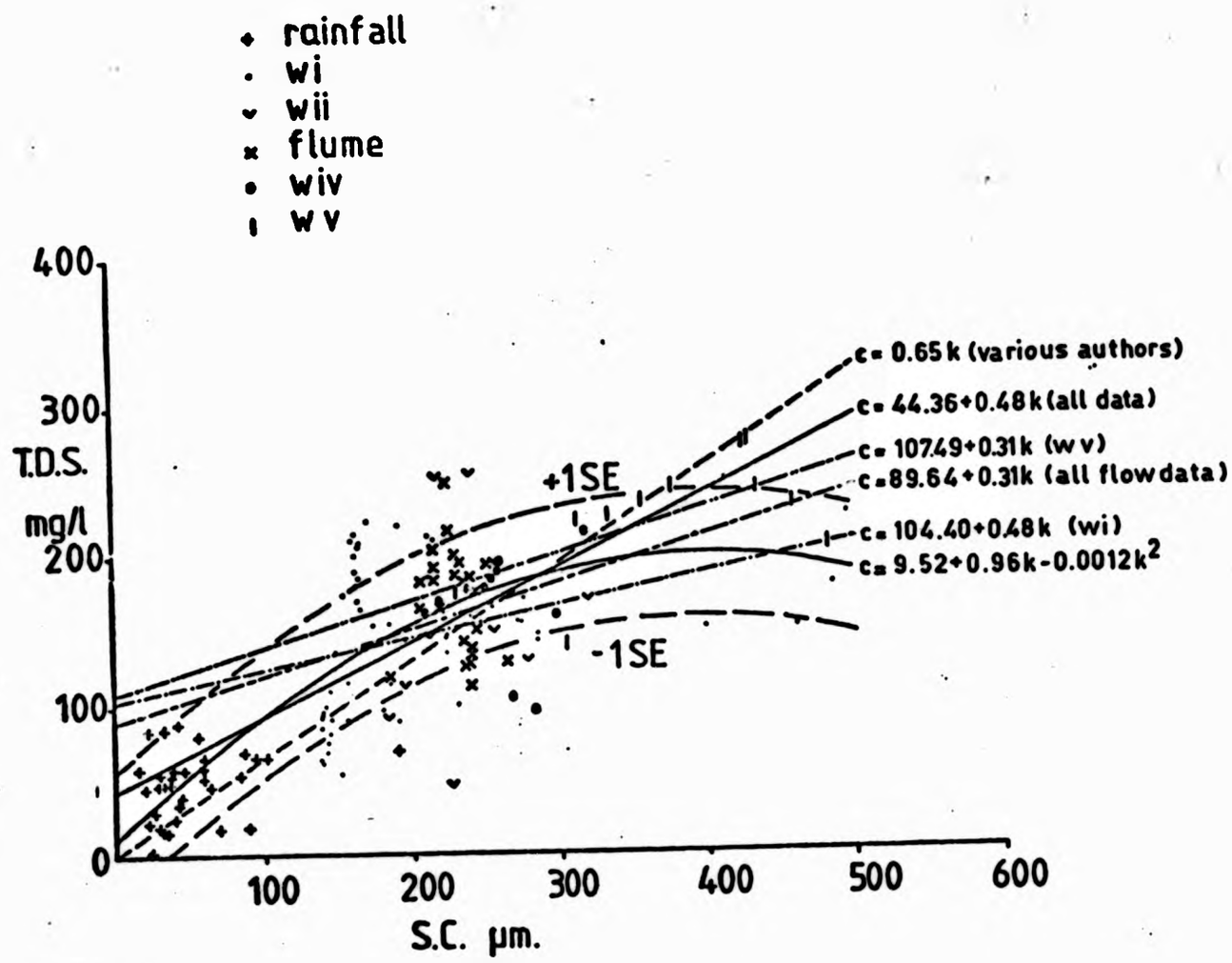

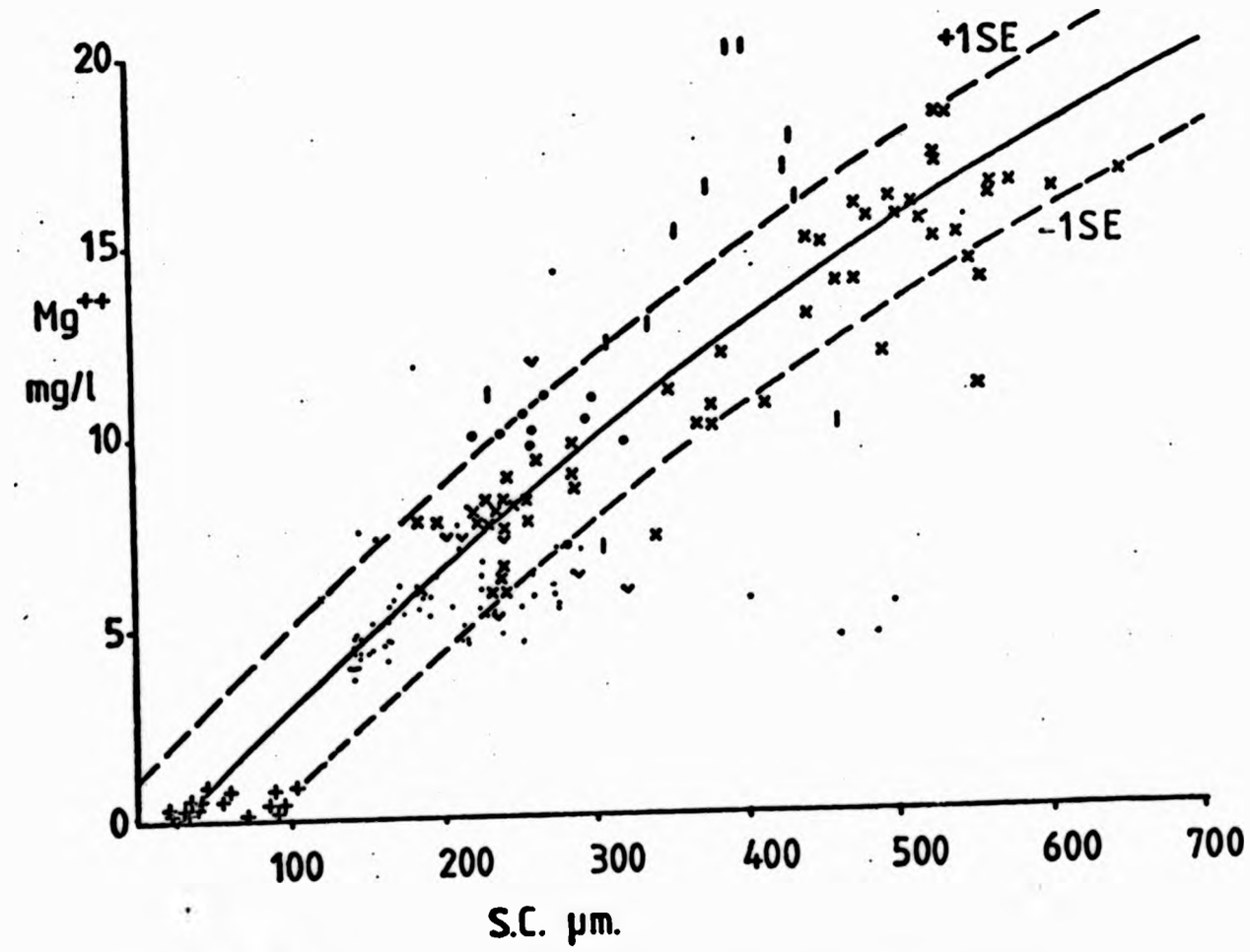

FIGURE 5.21: SPECIFIC CONDUCTANCE/TOTAL DISSOLVED SOLIDS RELATIONSHIP (top)

FIGURE 5.22: SPECIFIC CONDUCTANCE/MAGNESIUM RELATIONSHIP (bottom)

(for Key, see Figure 5.21)

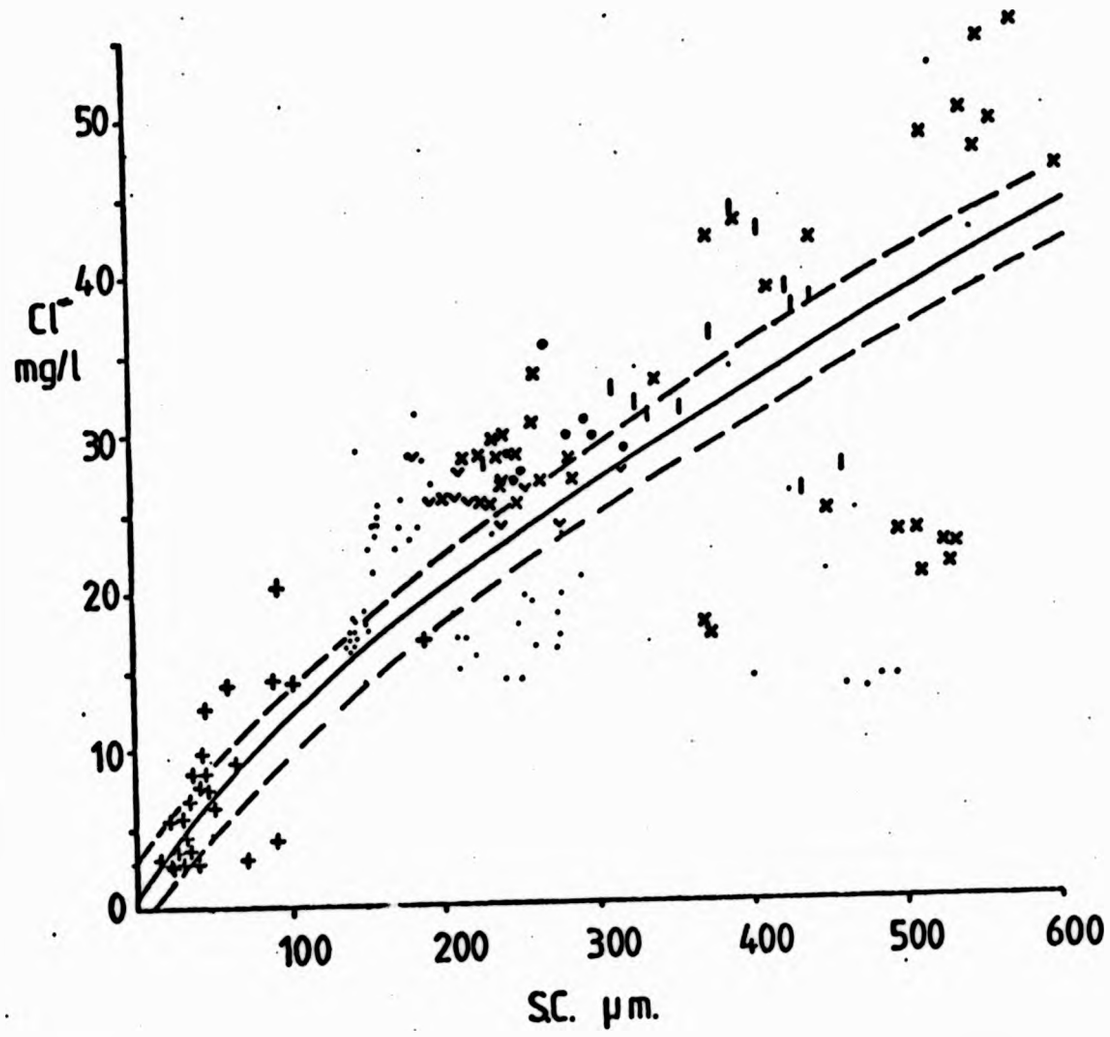

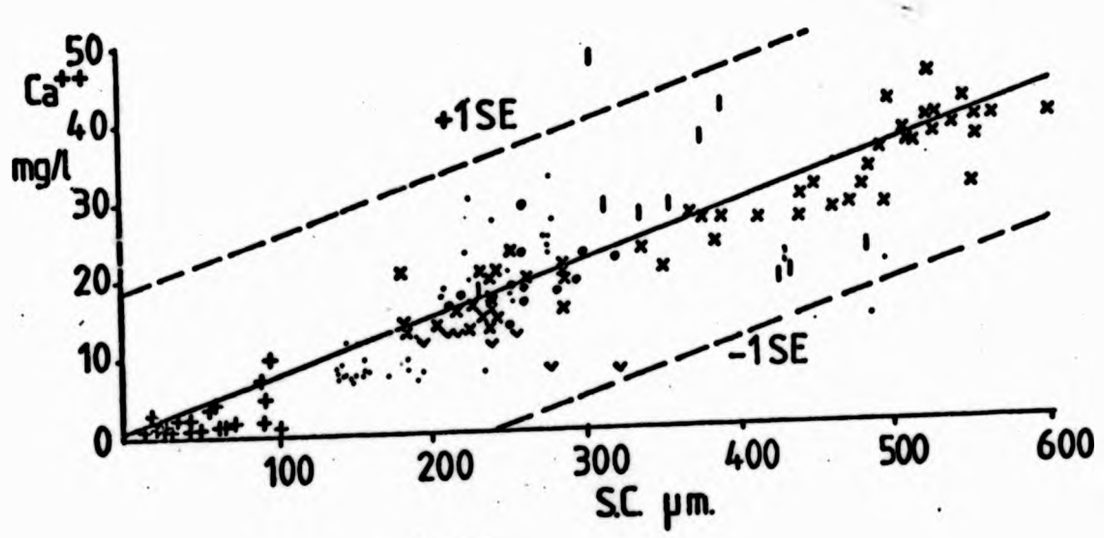

FIGURE 5.23: (top) SPECIFIC CONDUCTANCE/CHLORIDE RELATIONSHIP (for Key, see Figure 5.21)

FIGURE 5.24: (bottom) SPECIFIC CONDUCTANCE/CALCIUM RELATIONSHIP (for Key, see Figure 5.21)

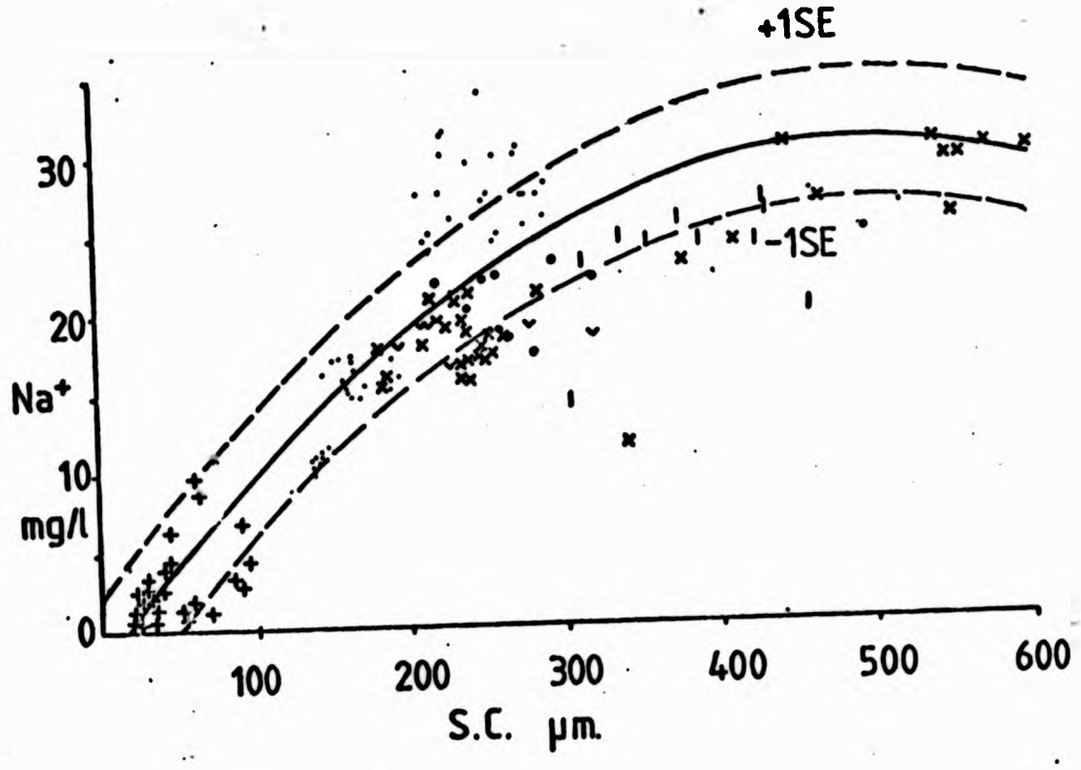

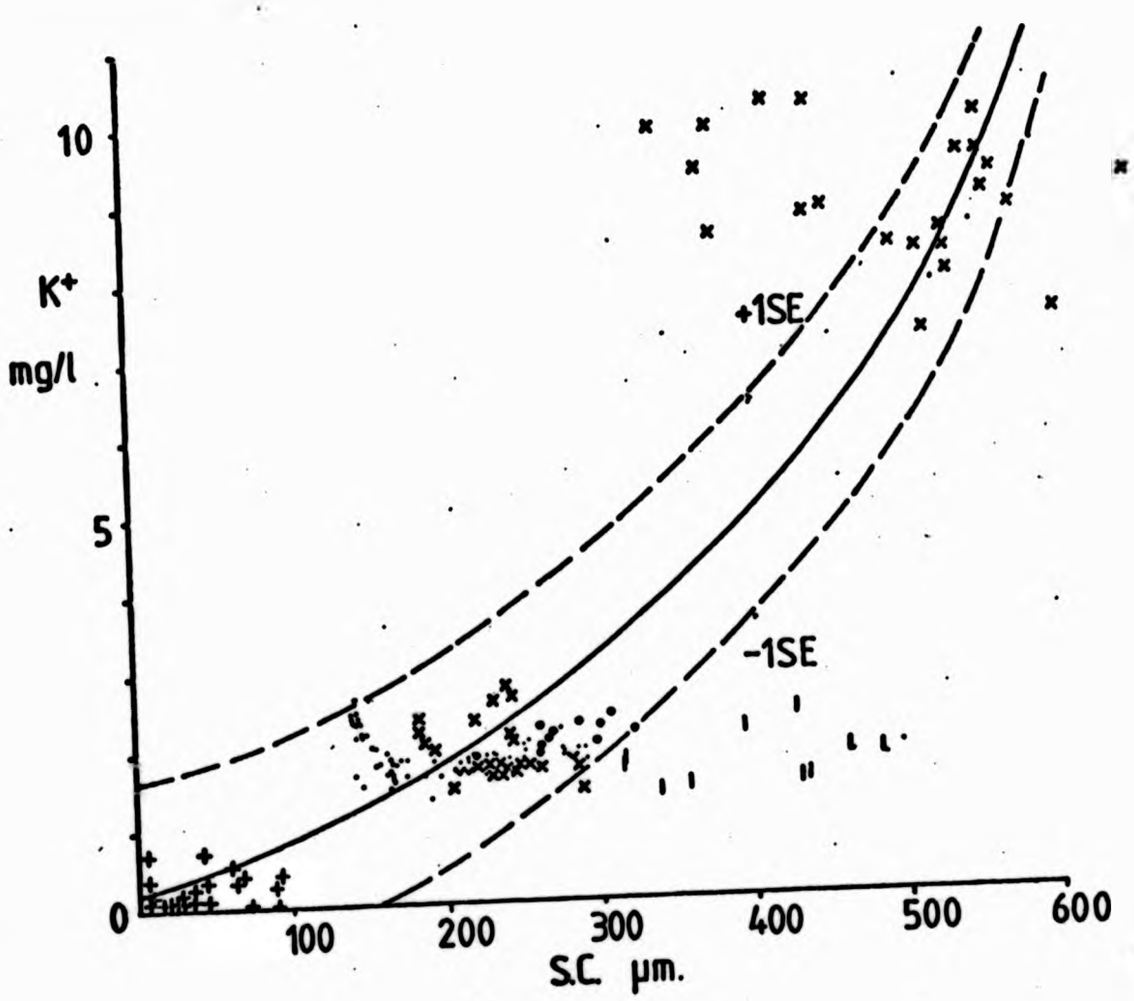

FIGURE 5.25: (top) SPECIFIC CONDUCTANCE/SODIUM RELATIONSHIP (for Key, see Figure 5.21)

FIGURE 5.26: (bottom) SPECIFIC CONDUCTANCE/POTASSIUM RELATIONSHIP (for Key, see Figure 5.21)

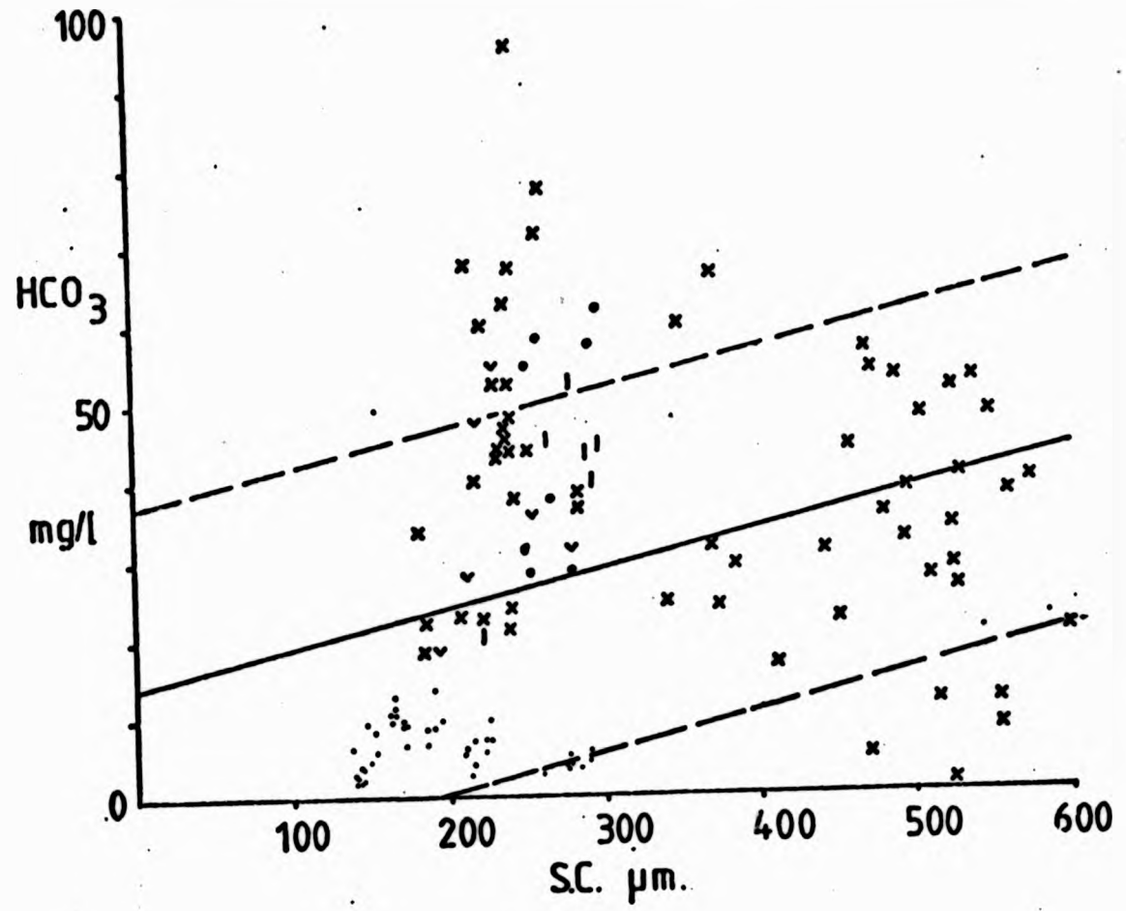

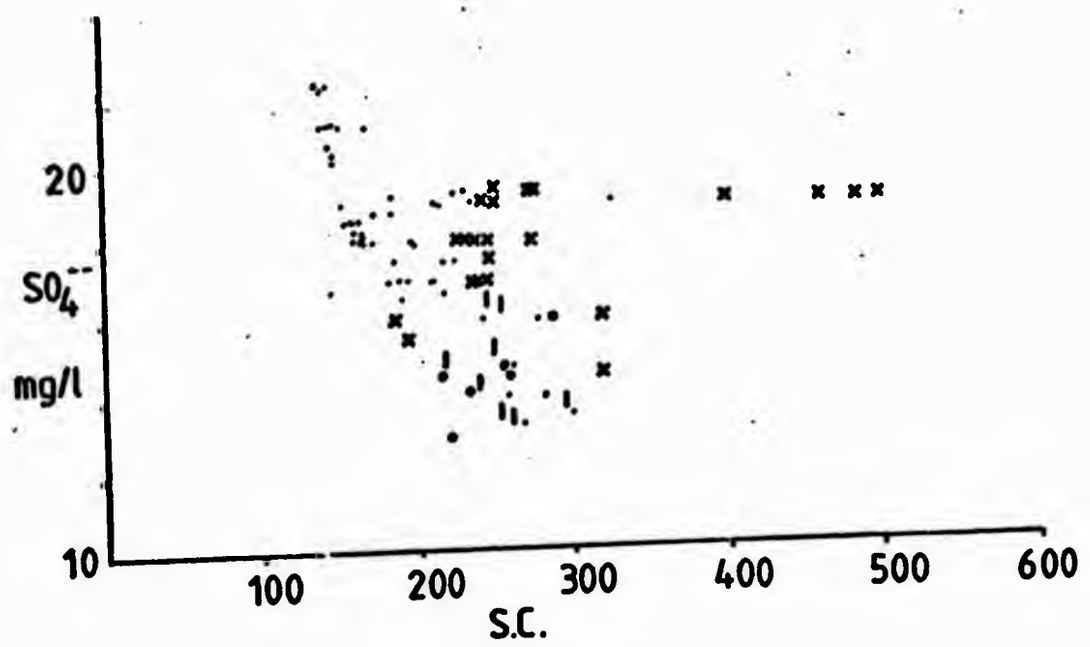

FIGURE 5.27: (top) SPECIFIC CONDUCTANCE/BICARBONATE RELATIONSHIP (for Key, see Figure 5.21)

FIGURE 5.28: (bottom) SPECIFIC CONDUCTANCE/SULPHATE RELATIONSHIP (for Key, see Figure 5.21)

water (i.e. rainfall/streamflow from several different subcatchments) and sampling during highly contrasting seasonal conditions (e.g. summer/autumn, 1976). The plot of K^+ against SC exemplifies the effect of these factors. The winter and spring streamflow data (central group) shows that K^+ concentration changes very little with a change in SC while autumn samples (upper group of points) are 4 - 5 times higher; the rainfall data (lower group), clustering near the origin, pull the regression line towards zero. The wide scatter of HCO_3^-/SC data is due to the inclusion of autumn values (cluster on right of plot) with higher values of SC. M.J. Waylen (1976) comments on the similarity between the ranking of r values for linear regressions (K/C_i) and the limiting ionic conductivities (λ_i^o) given by R.A. Robinson and R.H. Stokes (1965, p. 463). The order of values for λ_i^o (i.e. the conductance of an ion at limiting infinite dilution) reflects ion mobility in a very dilute solution (Robinson and Stokes, 1965). Thus the lack of a similarity in the rankings of λ_i^o and $r(K/C_i)$ for West Walk data could suggest a degree of ion-pairing exists, possibly during autumn storms when concentrations are high (Table 5.17). This interpretation can only be tentative, since ion-pairing is generally of minor importance in surface and soil waters (Waylen, 1976); furthermore, the first four r values themselves differ only slightly. The approach gives an incomplete description of individual ion concentration and was not used for estimation of TDS at West Walk.

K.K. Tanjii and J.W. Biggar (1972) tested a 'simplified, multi-component conductance model' of the form,

$$K = \sum_{i=1}^{i=n} k_i = \sum_{i=1}^{i=n} \lambda_i c_i \qquad (5.6)$$

where k_i = ionic specific conductance (umhos cm^{-1})
λ_i = ionic equivalent conductance (cm^2 Int ohm^{-1} $equiv^{-1}$)
c_i = concentration of the ith ion in meq $litre^{-1}$

For dilute concentration ranges the Kohlrausch equation states that,

$$\lambda_i = \lambda_i^o - ac_i^{\frac{1}{2}}$$

where λ_i° = limiting ionic conductance (cm^2 Int ohm^{-1} $equiv^{-1}$)

a = an adjustable empirical coefficient for the salt concentration and ion association effects, or the slope of the plot of λ_i against $c_i^{\frac{1}{2}}$.

The model satisfactorily predicted conductivity with values of 'a' ranging from 4 to 9. Waylen (1976) re-calculated the value of 'a' from measured conductivity and ion concentration of each sample for East Twin Brook, Mendips, and found that it ranged from 56 to - 2400. He found that the value of the constant increased as pH decreased and concluded that ionic specific conductance for hydrogen should be included in the model if water is particularly acidic (i.e. pH < 4.5). This is calculated from,

$$K_{H^+} = (H^+)\lambda_{H^+}^{\circ}\ 10^3 \qquad \text{(Sjors, 1950)} \qquad (5.7)$$

where (H^+) = H^+ concentration in mg/l

$\lambda_{H^+}^{\circ}$ = 349.8 μmhos cm^{-1} (25°C)

Equation (5.7) gives K_{H^+} = 111.0 μmhos cm^{-1} at pH 3.5 (25°C)

and K_{H+} = 0.11 μmhos cm^{-1} at pH 6.5 (25°C)

Thus the concentration of the hydrogen ion begins significantly contributing to total conductivity at pH 4.5 and becomes rapidly very important down to pH 3.5. For West Walk the measured pH values, calculated K_{H^+} and percentage total measured conductivity, are given in Table 5.18. This confirms the importance of considering pH. The value of 59 % for subcatchment W1 reflects the contribution of organic acids derived from accumulations of surface humus; the influence clearly diminishes downstream. Organic complexes may affect cation concentration by chelation, also reducing the conductivity. No analyses for organic complexes were undertaken for West Walk samples and hence no quantified assessment of chelation effects is possible.

The Tanjii and Biggar model is a compromise between the empirical approach (e.g. Steele, 1968) and the analytical finally used by Waylen (1976). This simply states,

TABLE 5.18

Minimum Values of pH and their percentage contribution to SC

Subcatchment	Min. pH measured	K_{H+} (25°C)	% Total K
W1	3.08	291	59
W2	3.69	111	35
Flume	6.28	0.18	1
W4	4.91	4.3	1.6
W5	3.92	42	9.9

$$K = \sum_{i=1}^{i=n} \frac{a_i \lambda_i^{\circ}}{10^{-3}} \qquad (5.8)$$

where a_i = individual ionic activity.

Furthermore, $a_i = M_i \gamma_i$

where γ_i = activity coefficient of the ith ion

M_i = molality of the ith ion

and $-\log \gamma_i = \frac{A Z_i^2 \sqrt{I}}{1 + \mathring{a}_i B\sqrt{I}}$ (the Debye-Huckel Eqtn) (5.9)

where Z_i = charge of the ith ion

$\mathring{a}_i$ = an empirical value dependent on 'effective ion diameter'

$A = 0.4921 - 0.00079\ (t - 5)$ t = temp °C

$B = 0.3249 - 0.00016\ (t - 5)$

I, the ionic strength of the solution is calculated from,

$$I = \tfrac{1}{2} \sum_{i=1}^{i=n} M_i Z_i^2$$

These equations are treated in greater depth in R.M. Garrels and C.L. Christ (1965). Waylen found close agreement between calculated and measured conductivity using this approach. A computer program was written to process the data for West Walk (Appendix 2: WATQUAL) with the outputs: ionic strength (I), calculated conductivity (K_c), measured conductivity (K_m) and sum of ions (C_s). A plot of K_c against K_m (Figure 5.29) shows there to be a systematic difference between the two values, a difference which increases with conductivity. The first explanation of this discrepancy is that of systematic errors in the analyses of individual ions; secondly the lack of analysis for certain constituents. The former is unlikely with the possible exception of SO_4^{-2}, since great care was taken in ensuring analytical

accuracy. Nitrate (NO_3^-) is the ion which probably contributes the major part of this excess conductivity. If the excess conductivity is used to approximately back-calculate NO_3^- concentrations then,

$$NO_3^- = 19 \text{ mg/l} \quad \text{at} \quad K_c = 150 \text{ umhos cm}^{-1}$$
$$\text{and} \quad NO_3^- = 60 \text{ mg/l} \quad \text{at} \quad K_c = 450 \text{ umhos cm}^{-1}$$

Although rather high these values may be compared with figures quoted by F.H. Bormann et al (1967) for a disturbed forested catchment in New Hampshire, USA. They attributed increases in NO_3^- concentration in leaching waters to clear-cutting and herbicide treatment. Similarly much of West Walk was clear cut in the period 1969 - 1971, periodic thinning was carried out and herbicide ('Casaron G') widely applied in April/May to young oak plantations during the study period.
D.E. Walling and I.D.L. Foster (1978) recorded very high concentrations of NO_3^-N after the 1976 drought (up to 100 mg/l NO_3^-N in a catchment of area 1.6 km^2) which they attributed to the influence of extreme drought conditions on mineralisation and nitrification processes within the soil. Similarly the divergence of the lines $y = x$, and $y = 0.86\ x$, in Figure 5.29 suggests that the concentration of NO_3^- increases dramatically with discharge particularly during the autumn flushing of elements. The plot of TDS (measured) and TDS (sum of ions) reinforces the view that some ions 'escaped' analysis (Figure 5.30). It is possible that a proportion of this unanalysed matter may have been uncharged organics which would support the findings of a high intercept for equation (5.2). However, the samples were evaporated to dryness at a temperature of 90°C (lower than the normal 110°C) in order to reduce the losses of volatile organic matter. Furthermore it is difficult to envisage uncharged organic ions occurring in rainfall.

A further possibility is related to the hygroscopic nature of the salts remaining after evaporating the water. As the salts cool in a moist atmosphere they take back some of the water lost from the crystal structure, thus increasing in weight. This should not have occurred in the analysis of West Walk samples since these were all cooled in a desiccator containing the dehydrant silica gel before weighing. The only time available for uptake of water from the atmosphere was between removal from the oven and insertion in the desiccator, for a short

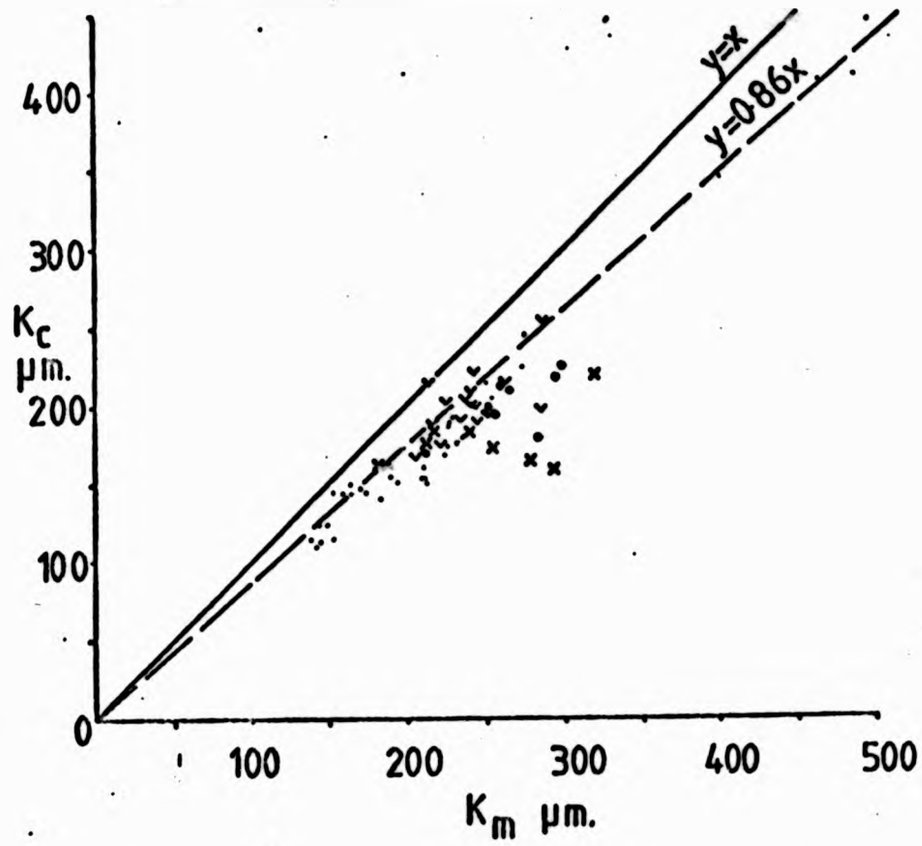

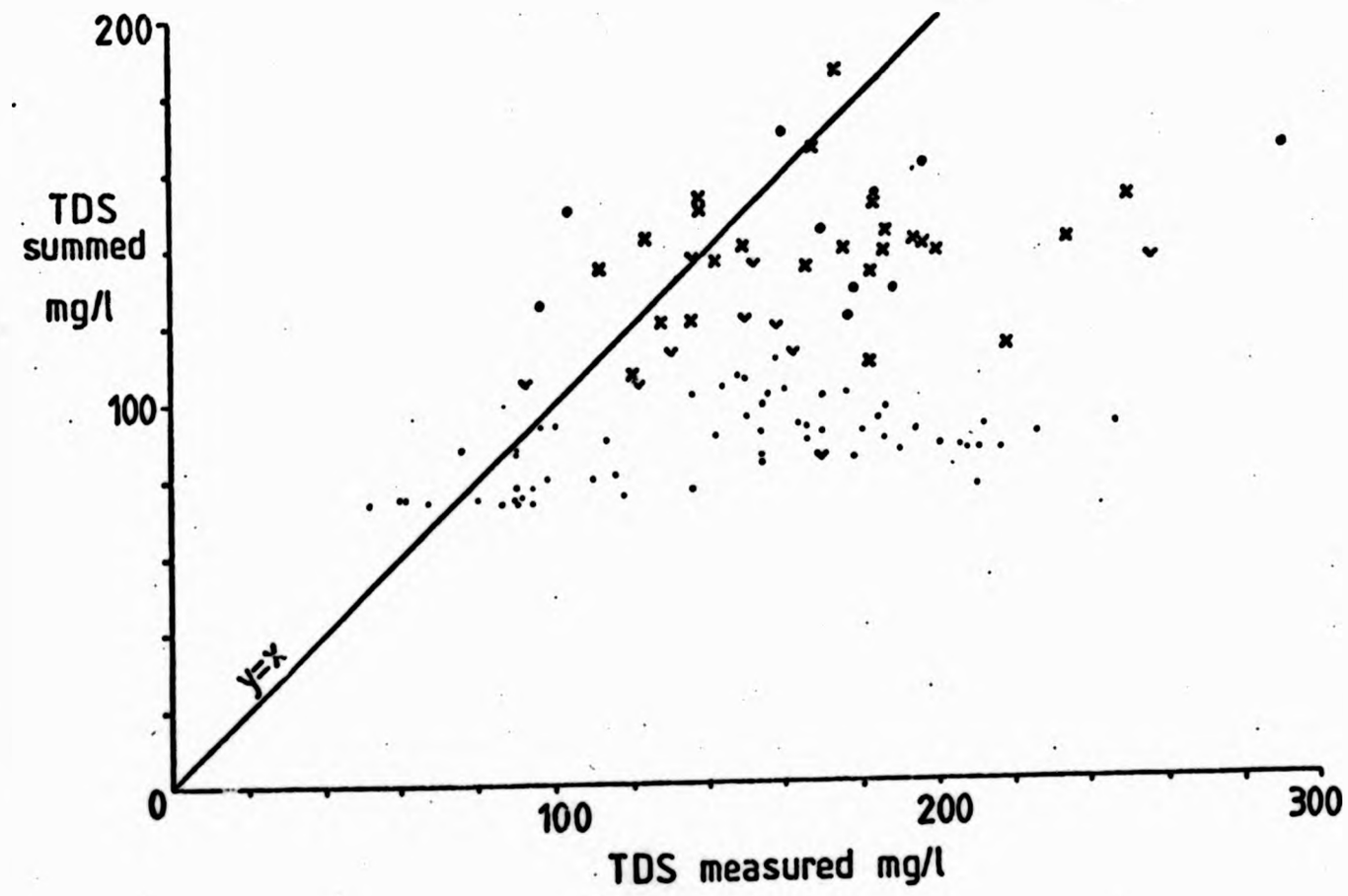

FIGURE 5.29: MEASURED AND COMPUTED SPECIFIC CONDUCTANCE (top)

FIGURE 5.30: MEASURED AND SUMMED TOTAL DISSOLVED SOLIDS (bottom)

period while the desiccator stop-tap was left open to allow for heat expansion, and between removal of each sample for weighing. This might account for the scatter about the regression lines and the positive intercepts in Figure 5.21. The procedural and chemical aspects of TDS determination need more careful examination if these problems are to be overcome.

None of the models discussed is entirely satisfactory for West Walk data, although the analytical model discussed would probably be suitable if NO_3^- data were available. The model evaluation is more time consuming and data intensive than the simple empirical approach of equation (5.1) and cannot be used for checking the ion balance.

The fitted quadratic regression (equation 5.3) is probably the best available means of generating TDS from SC, for SC <400 µmhos. Above 400 µmhos TDS the quadratic predicts an unrealistic decrease in TDS with increasing SC.

Chapter 5 has outlined the methods used for sampling stream and rainfall quality, the procedures of sample preparation and storage, described the techniques for individual water quality parameter determination and discussed the problems in using SC as a predictor of TDS. Chapter 6 draws upon the data generated from Chapters 4 and 5 to examine the characteristics of surface water solute dynamics and to develop bivariate and multivariate regression models of solute response.

CHAPTER 6

AN ANALYSIS OF SURFACE WATER SOLUTE DYNAMICS IN WEST WALK CATCHMENT: I: THE REGULARLY SAMPLED DATA (RSD)

6.1 INTRODUCTION

The previous two chapters outlined the collection and analysis of water samples and hydrometry for West Walk. In this chapter bivariate and multivariate regression analyses are applied to the regularly sampled solute and hydrometeorological data and an assessment made of the spatial variation of solute levels within West Walk. In the light of the regression results factors controlling solute levels are also discussed. In Chapter 7 the regularly sampled data (RSD) are combined with those collected during storms, and further regression analyses are carried out. Thus a similar rationale to that of Chapter 2.3 is used, proceeding from general to detailed analysis, ending up with models for synthesis of solute response from one or more easily measured hydrometeorological variables.

Recapping, the following data are available for use in this chapter.

(i) Approximately weekly concentrations of K^+, Na^+, Mg^{2+}, Ca^{2+}, Cl^-, HCO_3^-, pH and values of SC, sampled synchronously for West Walk and its subcatchments during the first six to eight months of 1975 and 1977;

(ii) A reduced number of concentrations for TDS, SO_4^-, Si and Fe for the first six months of 1977;

(iii) Hourly values of discharge for West Walk and its subcatchments over the period 1975 - 1977;

(iv) Hourly values of rainfall over West Walk for the period 1975 - 1977;

(v) Daily actual evaporation and SMD calculated by the Meteorological Office for the period 1975 - 1977.

This chapter begins with a discussion of the assumptions inherent in using the general linear regression model. It proceeds via a description of solute and hydrometeorological variables, data transformation and preliminary consideration of average solute concentrations to bivariate and multivariate regression analyses. Bivariate model residuals are briefly discussed. The chapter closes by examining predictive accuracy of the models developed.

6.2 STATISTICAL CONSIDERATIONS

The use of bivariate or multivariate regression methods for interpretation and prediction involves assumptions relating to the statistical structure of the basic data. M A Poole and P N O'Farrell (1971) have pointed out that few authors rigorously test the requirements of the general linear regression model which may place limitations on the inferences or predictions made. R T Clarke (1973) has made a similar observation concerning the stochastic structure of residuals in hydrological modelling.

To satisfy the six main requirements of the bivariate model adds considerable time and effort to analysis, although some of these may be relaxed, depending upon the use to which the regression is put. Although it is not always possible to fulfil these for hydrological data, then there should at least be an awareness of model limitations for prediction or inference. The six critical assumptions attached to the model may be summarised as follows (Poole and O'Farrell, 1971; Johnston, 1978):

(i) Measurement Error

Both X and Y in the expression $Y = a + bX + e$ are without measurement error (e represents a stochastic disturbance term). An assessment of errors is possible and this was discussed for stream discharge and solute concentration in Chapters 4 and 5 respectively. If error exists in the independent variable, X, then this may lead to biased estimates of the regression coefficients. However, J Johnston (1963) states that measurement error can be ignored if the sole objective of the regression analysis is to predict the value of Y corresponding to a given set of X values.

(ii) Linearity

The relationship between X and Y is linear when considering the specific function chosen. Serious non-linearity in a relationship can usually be seen by plotting the data pairs on normal axes. It may be removed by applying a specific transform to the data (e.g. logarithmic) or described by a higher order polynomial function.

(iii) Residual Means

The means of the conditional distribution should be zero. Conditional distributions, i.e. residuals, represented by $e = Y_i - \hat{Y}_i$ for each X_i; should be independent of X_i. If little or no correlation exists then the residuals may be considered independent and the assumption valid. If significant correlation exists then the linear model is invalidated.

(iv) Residual Variance (homoscedasticity)

The variances of the conditional distributions should be equal (i.e. they should be homoscedastic). Thus each value of $\sum (Y_i - \hat{Y}_i)^2 / N$ (residual variance) should be independent of X_i. If the variance of e is not constant, but is independent of X_i, then the estimates of the regression coefficients are unbiased and may be used in a predictive but not an inferential model. Correlation of the variance of e with X_i seriously biases the regression coefficients.

(v) Serial Correlation

There should be no serial correlation between the residuals. If the e_i's are not serially independent then :-

(a) autocorrelation exists in the data;

(b) estimates of the regression coefficients have excessive, inaccurate variance; and

(c) statistical inference is impossible.

Autocorrelation may be detected by the Durbin-Watson statistic, d, (Durbin and Watson, 1951), computed from:

$$d = \frac{\sum (\Delta z)^2}{\sum z^2} \qquad (6.1)$$

where $\Delta z = \Delta y - b\Delta x$

$z^2 = (y - \bar{y} - b(x - \bar{x}))^2$

$\Delta y = y_i - y_{i-1}$

and $\Delta x = x_i - x_{i-1}$

The value of d is compared with critical upper and lower bounds d_U and d_L, such that if $d < d_L$ significant serial correlation exists, if $d > d_U$ no significant serial correlation exists, and if $d_L < d < d_U$ the test is inconclusive.

(vi) Normality

If both X and Y are randomly selected from the population, then marginal and conditional distributions of each variable should be normal, although this only applies if the model is to be used for inference, not for prediction. R J Johnston (1978, p.41) points out that:

"...if the conditional distributions are normal, then it is almost certain that the distributions of Y and X (the marginal distributions) are also normal, but the converse is not necessarily the case..."

This creates problems in testing for normality, since the conditional distributions are only known when much of the computational work has been completed. Departure from normality can be tested by examining the skewness and kurtosis of the marginal and conditional distributions. R C Geary (1936) gives the methods for computation of skewness and kurtosis.

Skewness is calculated from:

$$\sqrt{b_1} = \sqrt{n'} \sum_{i=1}^{n'} (x_i - \bar{x})^3 \Big/ \left\{ \sum_{i=1}^{n'} (x_i - \bar{x})^2 \right\}^{3/2} \qquad (6.2)$$

Autocorrelation may be detected by the Durbin-Watson statistic, d, (Durbin and Watson, 1951), computed from:

$$d = \frac{\sum (\Delta z)^2}{\sum z^2} \qquad (6.1)$$

where $\Delta z = \Delta y - b\Delta x$

$z^2 = (y - \bar{y} - b(x - \bar{x}))^2$

$\Delta y = y_i - y_{i-1}$

and $\Delta x = x_i - x_{i-1}$

The value of d is compared with critical upper and lower bounds d_U and d_L, such that if $d < d_L$ significant serial correlation exists, if $d > d_U$ no significant serial correlation exists, and if $d_L < d < d_U$ the test is inconclusive.

(vi) Normality

If both X and Y are randomly selected from the population, then marginal and conditional distributions of each variable should be normal, although this only applies if the model is to be used for inference, not for prediction. R J Johnston (1978, p.41) points out that:

"...if the conditional distributions are normal, then it is almost certain that the distributions of Y and X (the marginal distributions) are also normal, but the converse is not necessarily the case..."

This creates problems in testing for normality, since the conditional distributions are only known when much of the computational work has been completed. Departure from normality can be tested by examining the skewness and kurtosis of the marginal and conditional distributions. R C Geary (1936) gives the methods for computation of skewness and kurtosis.

Skewness is calculated from:

$$\sqrt{b_1} = \sqrt{n'} \sum_{i=1}^{n'} (x_i - \bar{x})^3 \Big/ \left\{ \sum_{i=1}^{n'} (x_i - \bar{x})^2 \right\}^{3/2} \qquad (6.2)$$

where $n' = n + 1$

The value $\sqrt{b_1}$ is compared with a graphical plot of $\sqrt{b_1}$ against $n' - 1$ (Geary, 1936) to obtain the significance of skewness in the sample. Generally, the closer $\sqrt{b_1}$ lies to zero the greater the probability of normality.

Kurtosis is computed from:

$$a = \sum_{i=1}^{n'} (x_i - \bar{x}) \Big/ \left\{ n' \sum_{i=1}^{n^1} (x_i - \bar{x})^2 \right\}^{1/2} \qquad (6.3)$$

The significance of kurtosis is determined by graphical comparison of a, with upper and lower significance bounds on the plot of a against $n' - 1$ (Geary, 1936). The closer a lies to 0.8, the greater the probability of normality.

If departure from normality is significant, then a specific transformation can be applied and the data re-tested until a satisfactory approximation to normality is obtained.

In general it is considered that the normality, measurement error and conditional distribution mean assumptions are all less important than linearity, homoscedasticity and serial independence.

A further assumption applies if multiple regression is being used.

(vii) Collinearity

Collinearity must be absent or insignificant amongst the independent variables, i.e. they should be linearly independent of each other. If this is not the case then the regression coefficients may become uninterpretable, certain independent variables should be omitted, and perhaps others included. Initial computation of a bivariate correlation matrix helps in the selection of independent variables. If correlation coefficients are greater than about 0.8, then pairwise linearity is considered 'serious' (Huang, 1970; Johnston, 1978). However, if the multiple regression equation is to be used for prediction then multicollinearity is not a serious problem, provided that intercorrelations remain unchanged into the future (Johnston, 1963).

Clearly, such an assumption is hazardous when dealing with data collected during 1975 and 1976.

6.3 ANALYSIS OF THE REGULARLY SAMPLED DATA (RSD)

In the belief that solute response is dependent upon more than stream discharge, variables describing catchment moisture status and seasonality were included in correlation matrices with solute data for each subcatchment. A similar approach has been used in association with storm solute levels (Foster, 1978) and storm sediment concentrations and loads (Walling, 1974). Information on collinearity between independent variables can also be obtained from the correlation matrix for multiple regression analysis.

A. The Variables

The dependent variables (X1 - X8) are represented by the individual solute concentrations (see Figures 6.1 - 6.10). The following independent variables were selected.

(i) Instantaneous Discharge at the time of Sampling (Q l/sec): X9

This is a standard parameter used in solute models and represents the current level of catchment outflow (Figures 6.11A and 6.13C).

(ii) Antecedent Precipitation Index (API, mm) : X10 - X13

An API calculated for any day provides information on the amount of rainfall which has fallen over a preceding period of T days, and hence catchment moisture conditions. The individual API's are usually weighted so rainfall exerts progressively less influence the further back in time the API is calculated. One method of calculating the API for any preceding period T (the API.T) employs a decay function, K (Gregory and Walling, 1973).

$$API.T = \sum_{t=1}^{t=T} P.K^t \qquad (6.4)$$

where K is fixed at a value from 0.85 - 0.98

P = precipitation on a day t before the point of calculation.

A second, similar approach employs a reciprocal decay function, 1/t (Osborn and Lane, 1969; Weyman, 1974).

$$API.T = \sum_{t=1}^{t=T} P.t^{-1} \qquad (6.5)$$

The second method was employed for its simplicity; it also obviated the need to estimate a decay function, K. The use of progressively greater values of T gives the API.T's longer 'memories' and such an approach could be useful where long throughflow times are considered to be important. Thus API.T's were calculated for T = 5, 10, 15, 20, 25, 30 and 60 days for West Walk, using daily rainfall 1975 - 1977 (see Appendix 2 for program APIPROG). To avoid excessive use of computer storage in correlation matrix programming API.5, 15, 30 and 60 were selected for use. Figures 6.11B and C and 6.13A and B show API 5 and API 60 for 1975 and 1977 respectively. 6.11 clearly shows how API 60 for the end of June 1975 includes the effect of heavy rainfall in May, while for API 5 this effect 'dies' well before the end of May, and API 5 at 30th June is zero.

(iii) Soil Moisture Deficit (SMD, mm) : X14

Soil moisture deficit represents the cumulative excess of rainfall over evaporation and was calculated for West Walk by the Met. Office as described in Chapter 4. Figure 6.12C shows that the SMD rose from 20 mm in May to about 150 mm in August 1975 as actual evaporation increased and streamflow decreased. To some extent, therefore, the SMD duplicates information contained in the API's although it represents a more direct index of catchment moisture status. The SMD took longer to accumulate in 1977 due to frequent heavy rainfall and lower evapotranspiration (Figure 6.13D).

(iv) Season Index (SI, dimensionless) : X15

The seasonal variation of solute concentration was discussed earlier and some of the reported details summarised in Table 2.1. The data collected from West Walk are not susceptible to time series or harmonic analysis (e.g. Edwards and Thornes, 1973) due to their discontinuity and brevity of record. Seasonal variation can be detected, however, by correlation with a simple sine or cosine curve

(e.g. Walling, 1974; Walling and Foster, 1975). D E Walling (1974) points out that the sine function:

$$\text{SINE INDEX} = \text{SIN (RAD)} \frac{2\pi D}{365} \qquad (6.6)$$

where D = day of year numbered from 1st January, has its maximum at 31st March and minimum at 30th September, closely approximating the water year. This is considered more appropriate for hydrological analyses than a cosine function of the same form, which closely approximates the calendar year. However, the use of an unlogged sine index does not allow precise definition of annual maxima and minima in solute concentrations. By introducing a lag, L, into equation (6.7):

$$\text{S I} = \text{SIN (RAD)} \frac{2\pi (D - L)}{365} \qquad (6.7)$$

firstly, approximate solute maxima and minima may be determined and, secondly, the concentration/SI relationships optimised (e.g. Cryer, 1976). A computer program was written for this purpose, correlating SI with solute concentration for each catchment, increasing L from 1 to 183 (Appendix 2 : SINDAY). The program gave the optimum correlation between solute concentration and SI $\pm$ 5 days (L was incremented by 5.0 to save computer time). It should be noted that in the correlation matrices which follow, the value of L is kept constant for each solute in each catchment, i.e. other independent variables are not optimised in the same way.

B. <u>The Transformation of Variables</u>

Linearity was given priority over normality when transforming the variables, as suggested by Poole and O'Farrell (ibid). The simplest method of determining whether linearity had been achieved in this x/y relationship was to plot the data. A reduced number of plots were made to determine the best functional relationships. These were usually found to involve a logarithmic transformation of the basic data (the logarithmically transformed plots of solute concentration against discharge are given in Figures 7.1 to 7.5).

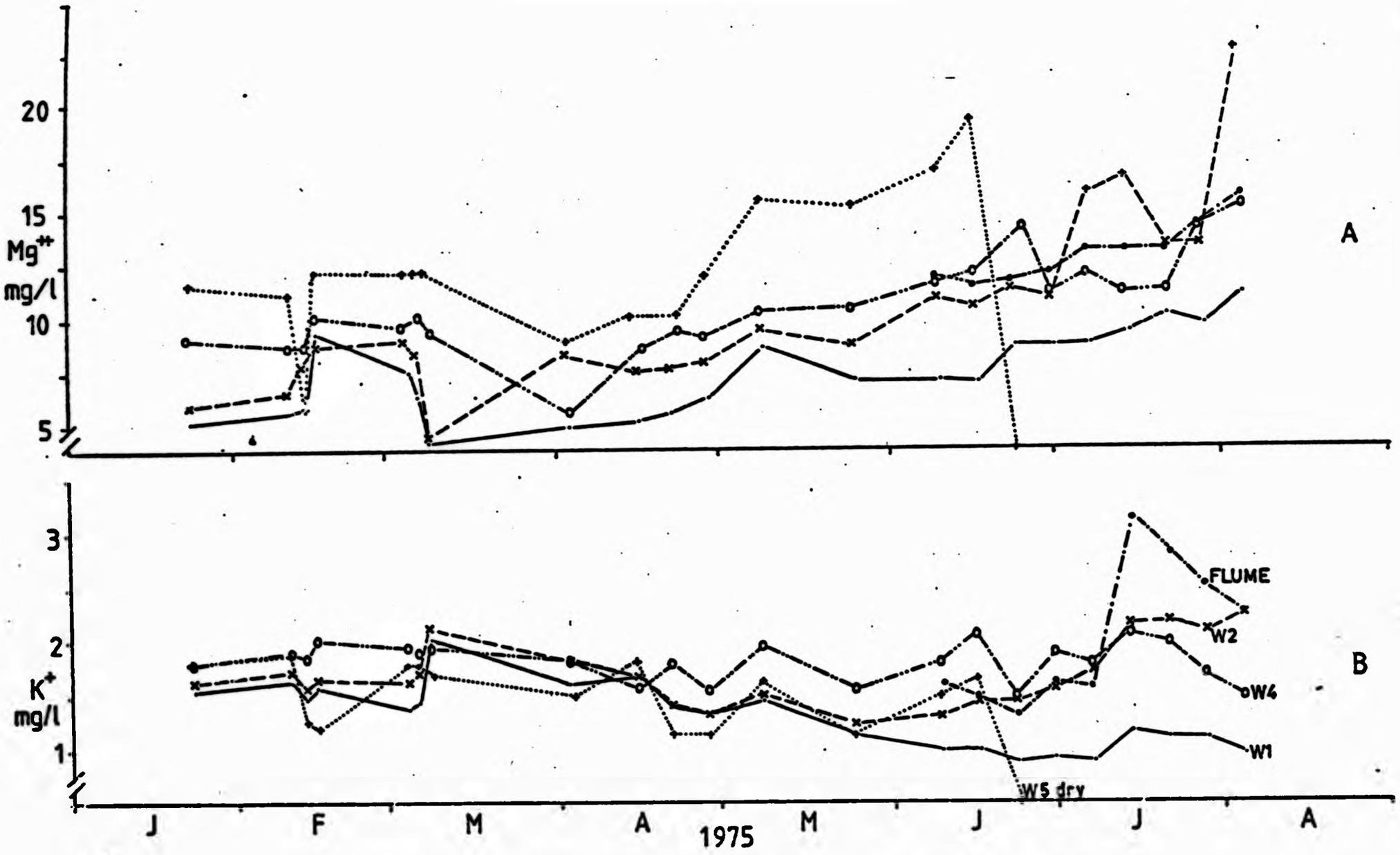

FIGURE 6.1: VARIATION OF MAGNESIUM AND POTASSIUM CONCENTRATIONS IN STREAMFLOW, 1975

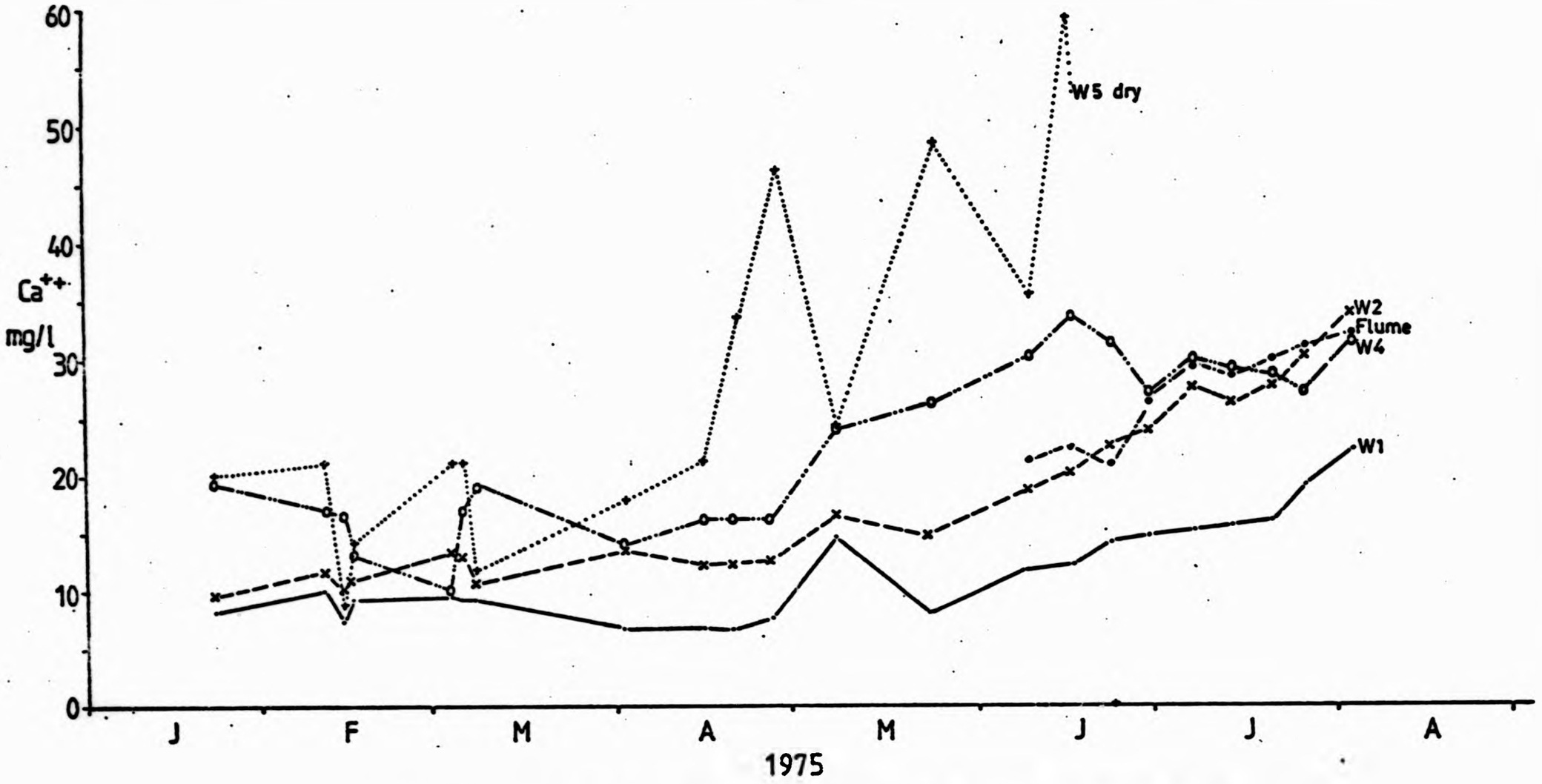

FIGURE 6.2: VARIATIONS OF CALCIUM CONCENTRATION IN STREAMFLOW, 1975

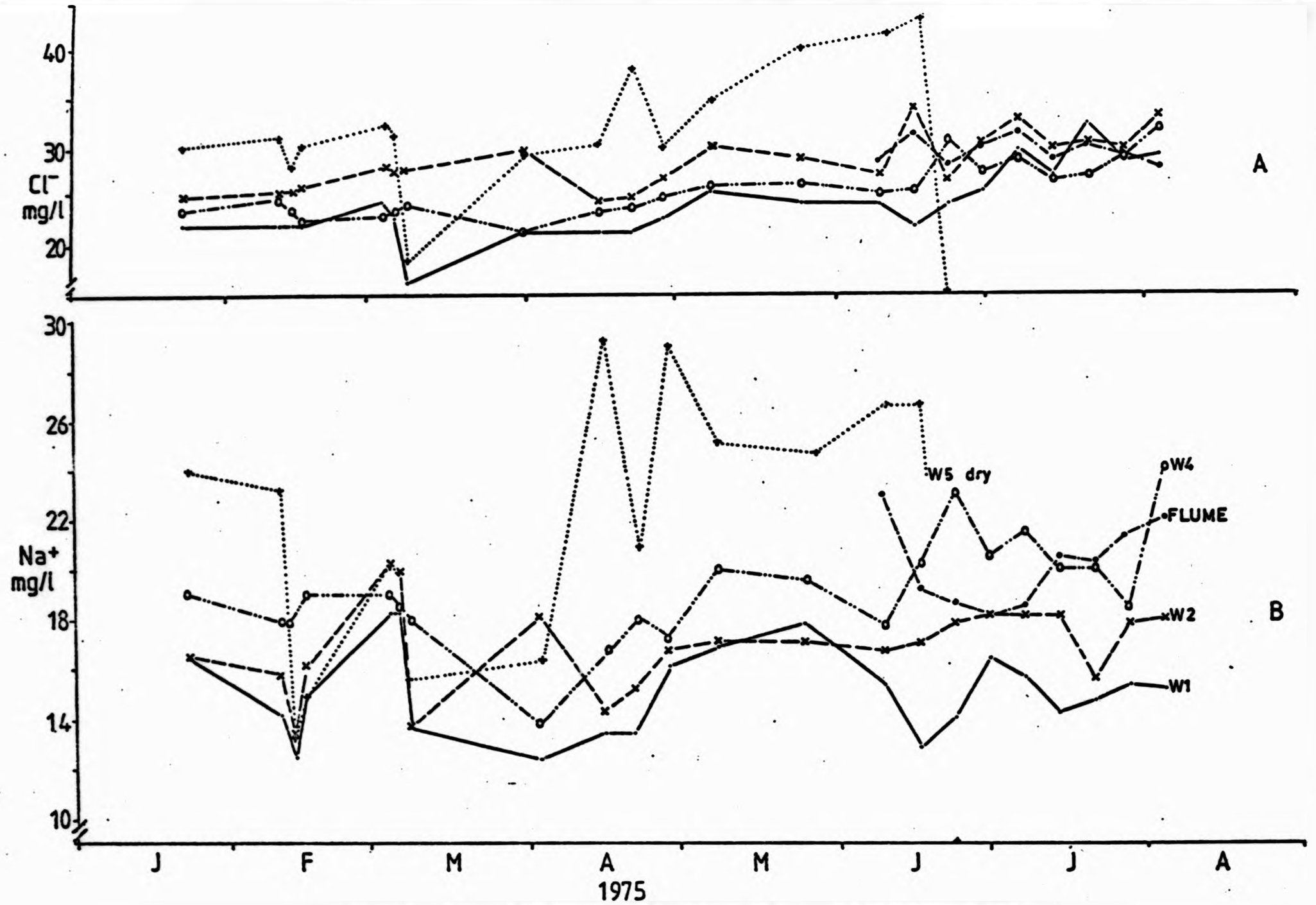

FIGURE 6.3: VARIATIONS OF CHLORIDE AND SODIUM CONCENTRATIONS IN STREAMFLOW, 1975

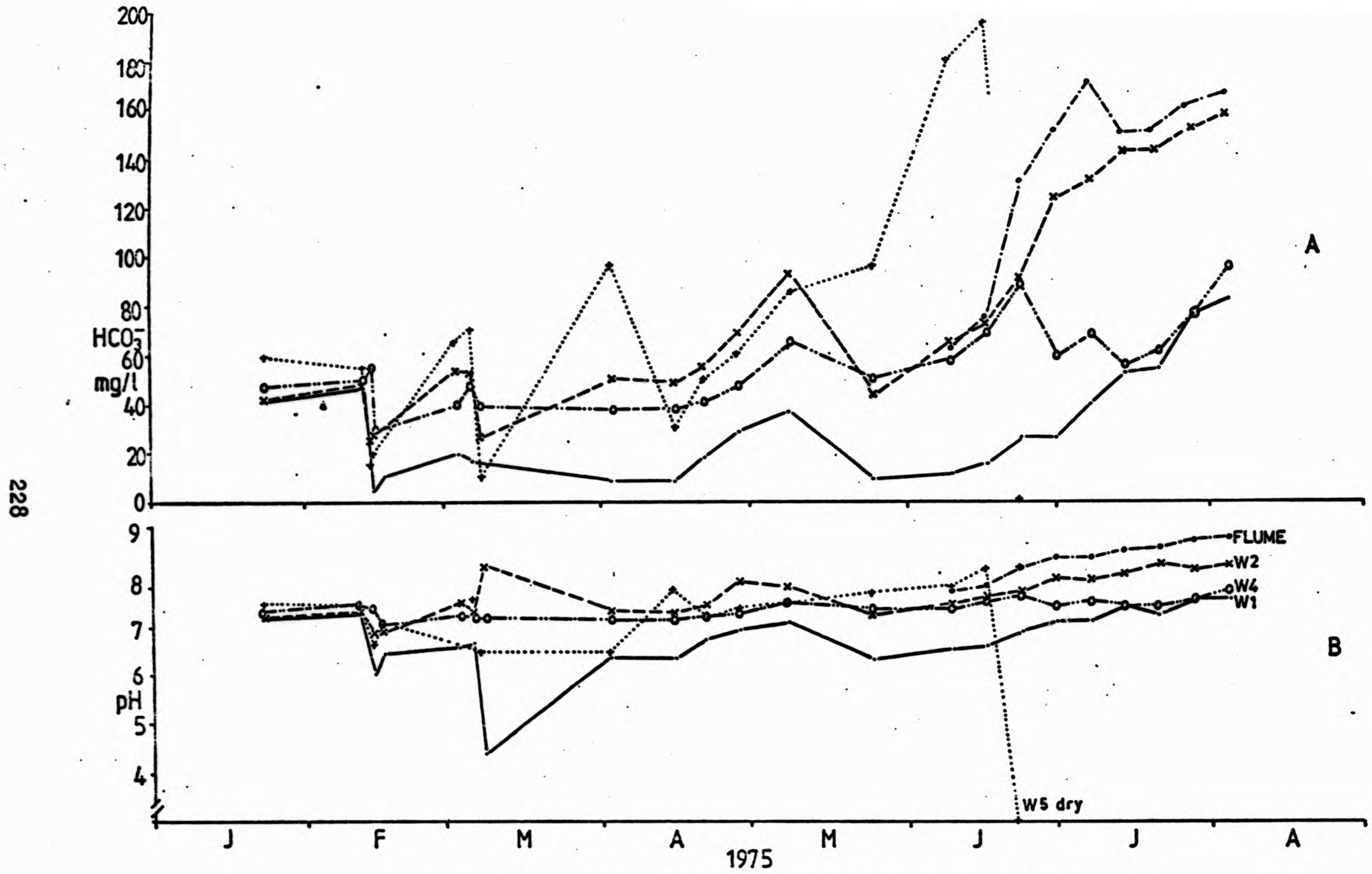

FIGURE 6.4: VARIATIONS OF BICARBONATE CONCENTRATION AND pH IN STREAMFLOW, 1975

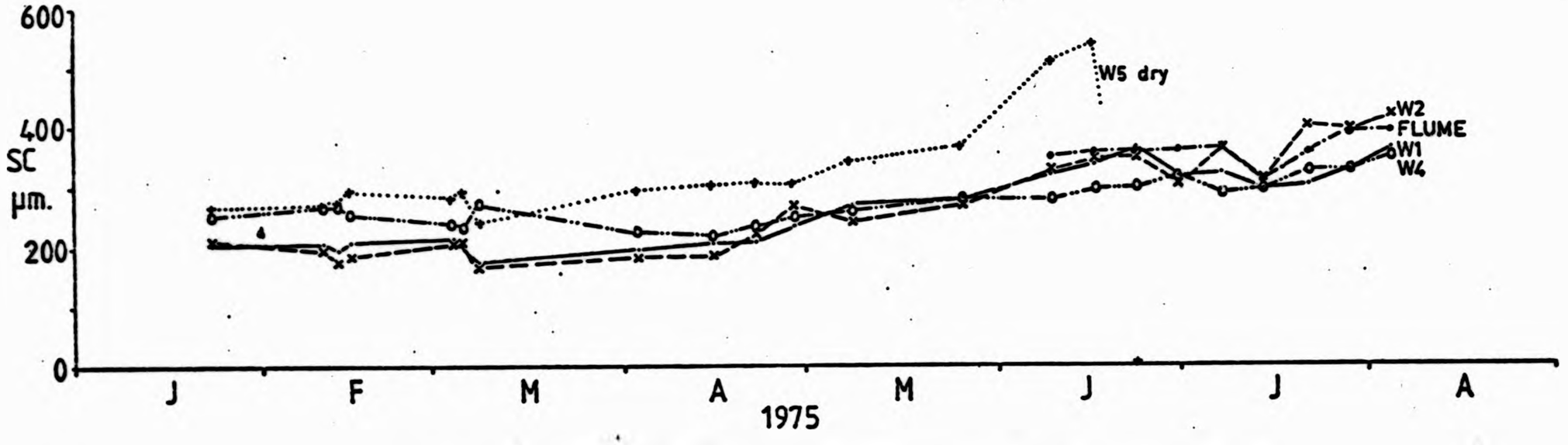

FIGURE 6.5: VARIATIONS OF SPECIFIC CONDUCTANCE IN STREAMFLOW, 1975

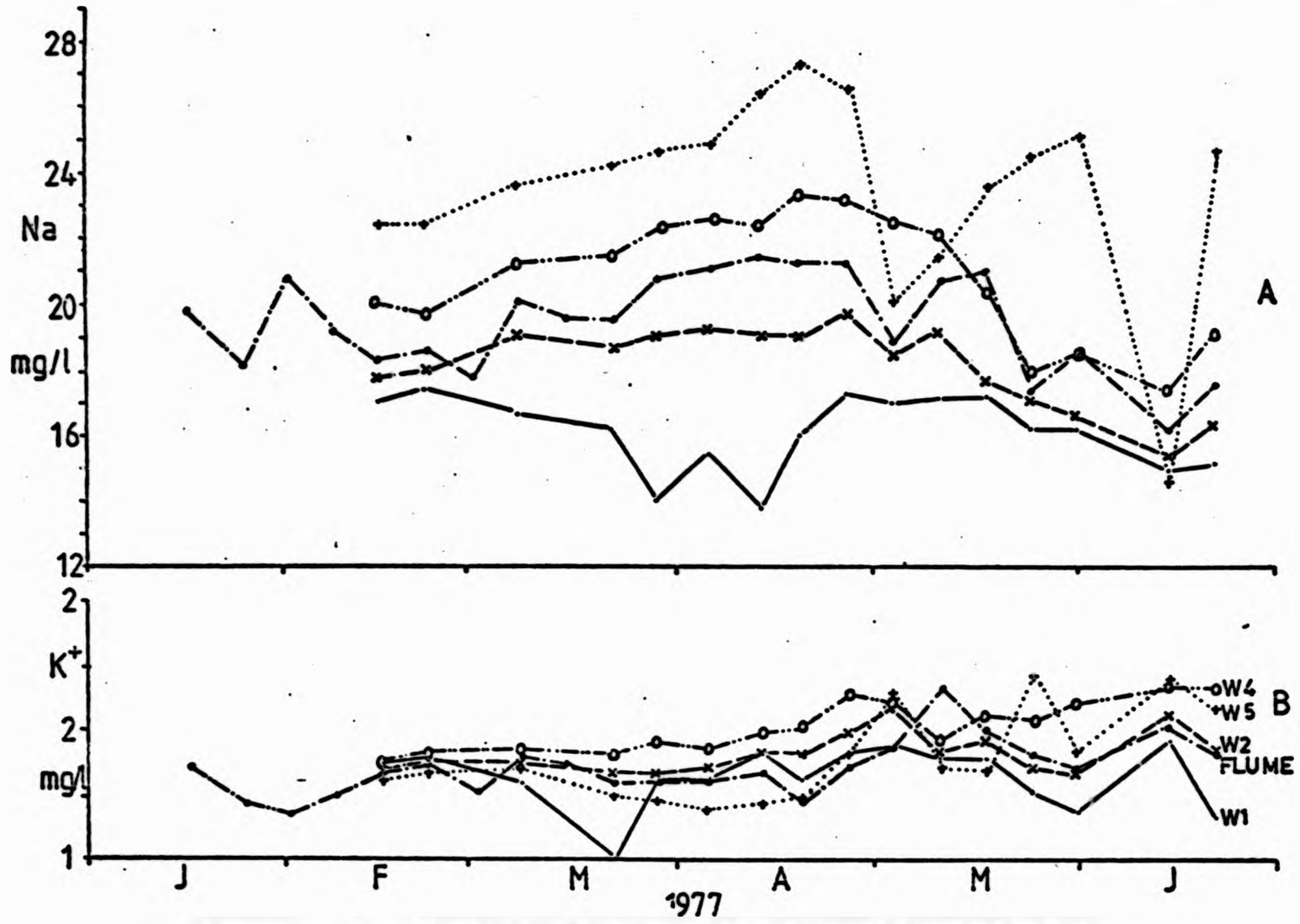

FIGURE 6.6: VARIATIONS OF SODIUM AND POTASSIUM CONCENTRATIONS IN STREAMFLOW, 1977

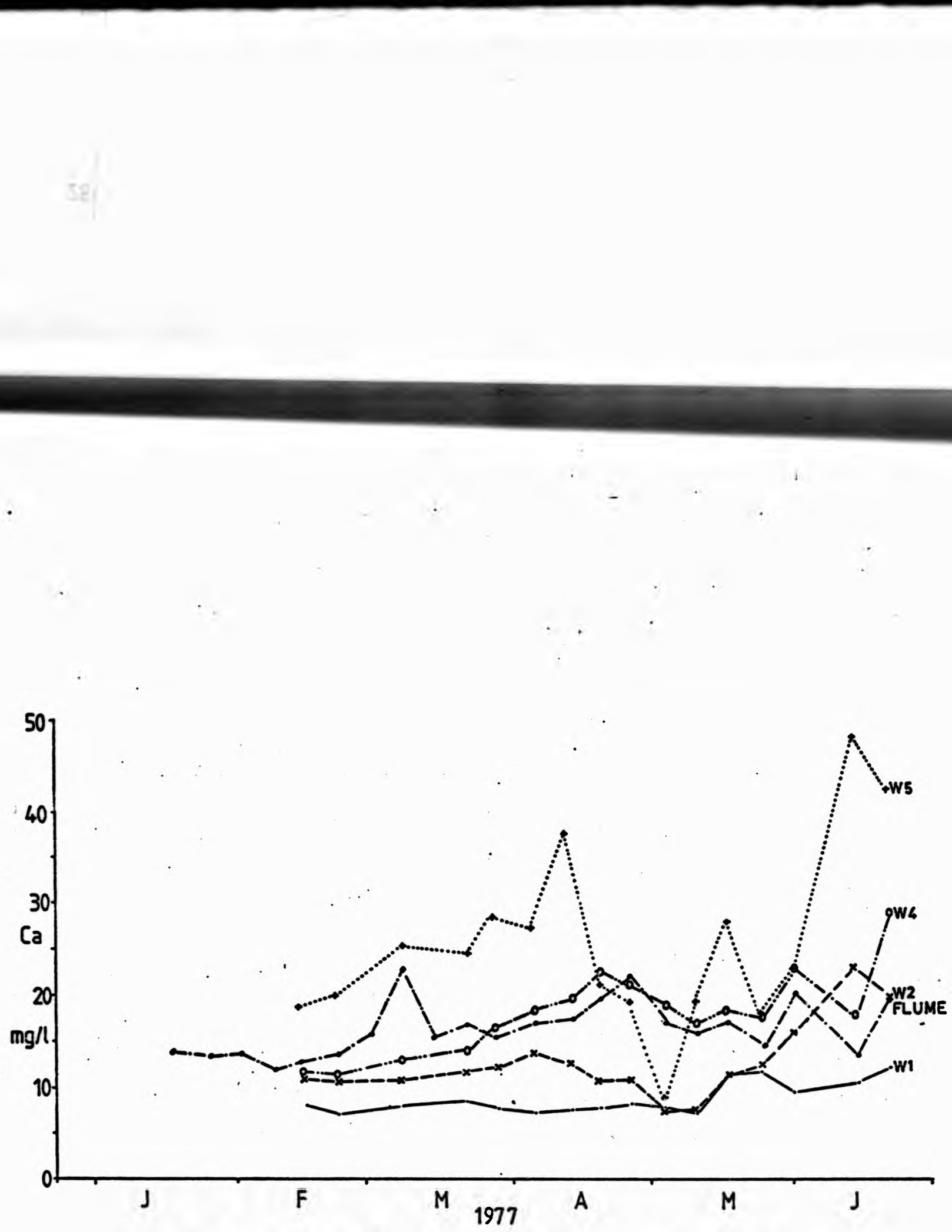

FIGURE 6.7: VARIATIONS OF CALCIUM CONCENTRATION IN STREAMFLOW, 1977

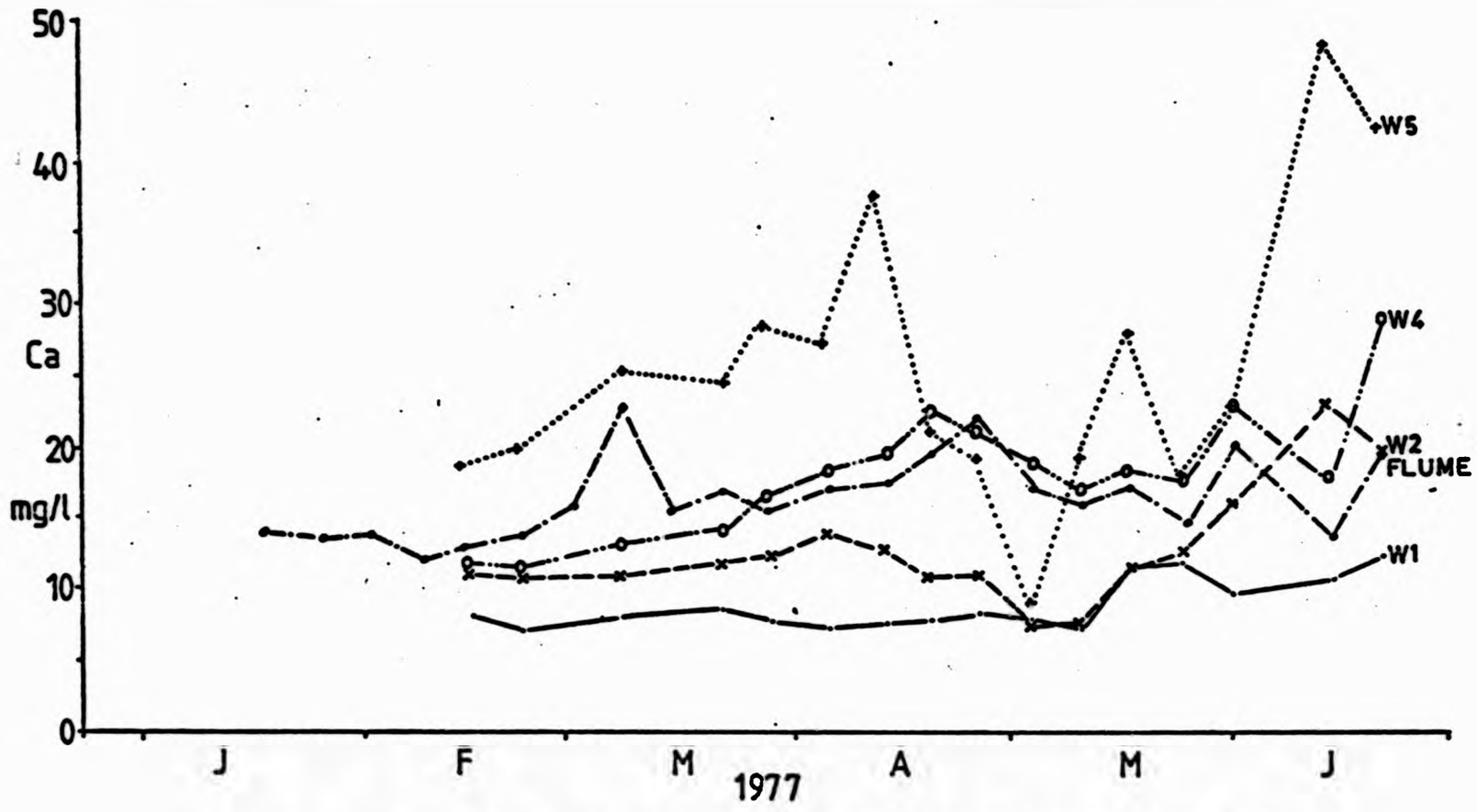

FIGURE 6.7: VARIATIONS OF CALCIUM CONCENTRATION IN STREAMFLOW, 1977

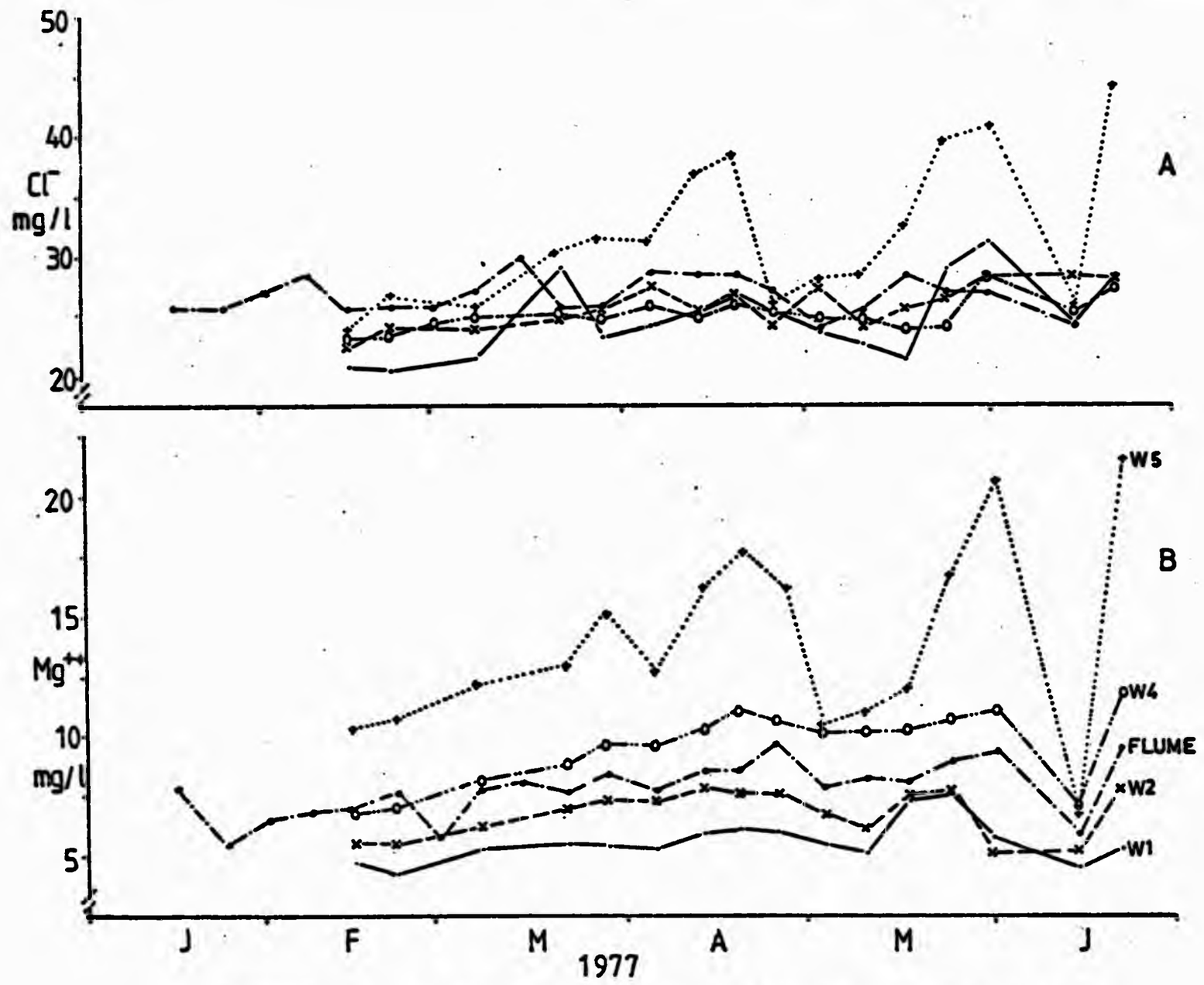

FIGURE 6.8: VARIATIONS OF CHLORIDE AND MAGNESIUM CONCENTRATIONS IN STREAMFLOW, 1977

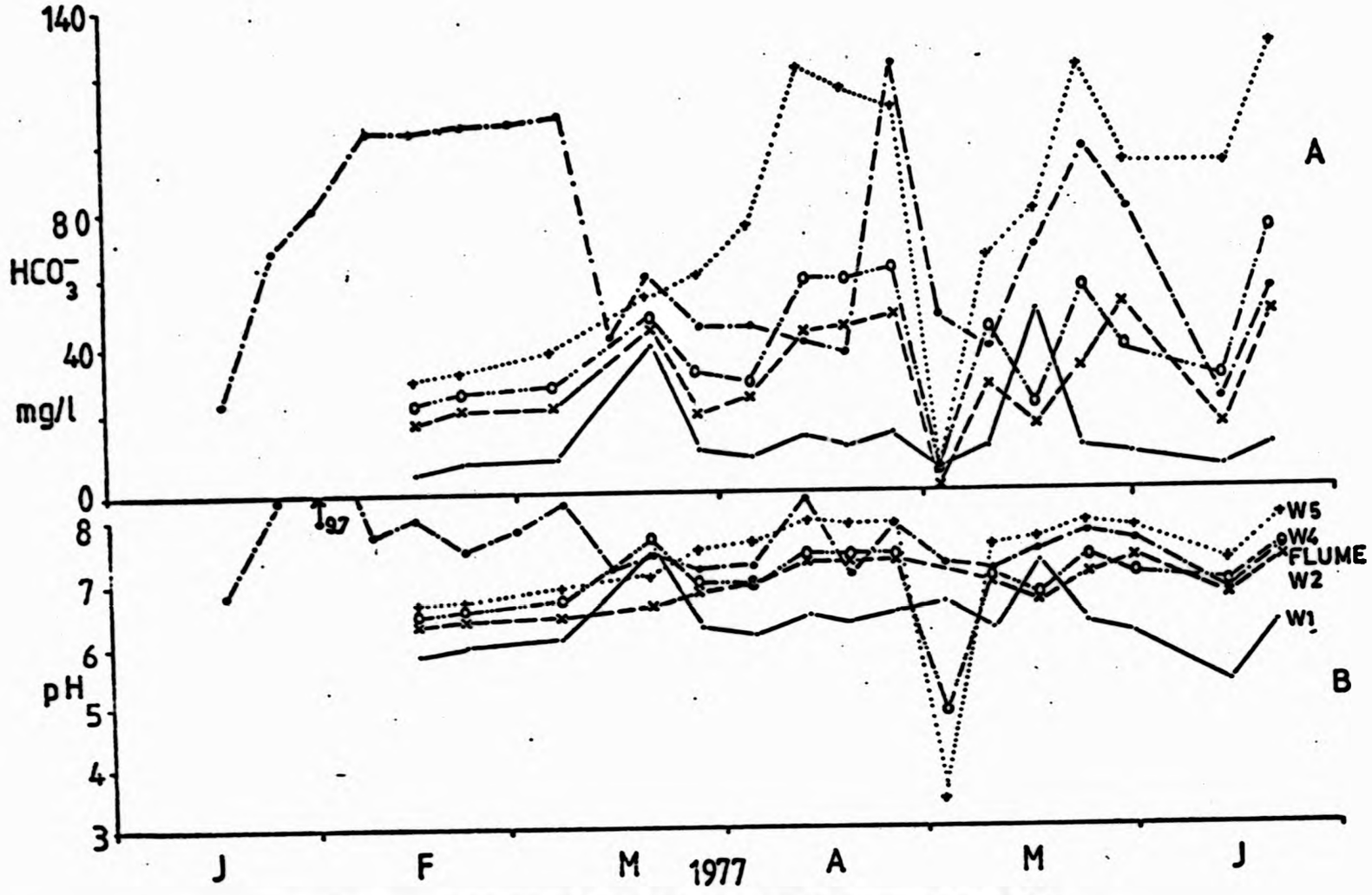

FIGURE 6.9: VARIATIONS OF BICARBONATE CONCENTRATION AND pH IN STREAMFLOW, 1977

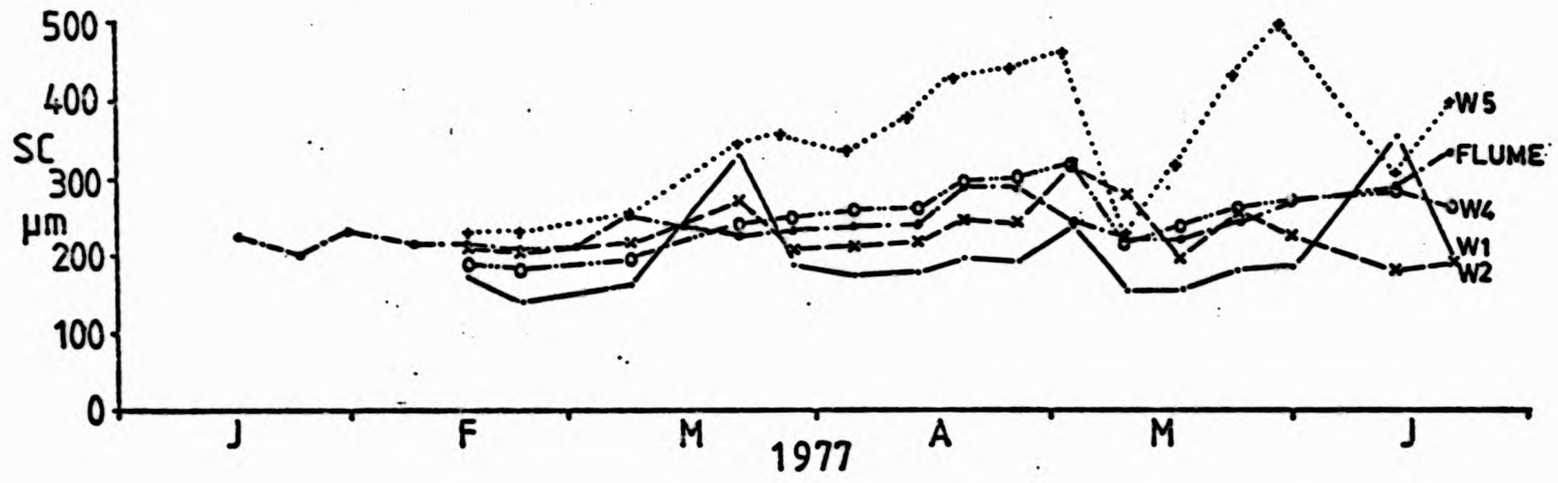

FIGURE 6.10: VARIATIONS OF SPECIFIC CONDUCTANCE IN STREAMFLOW, 1977

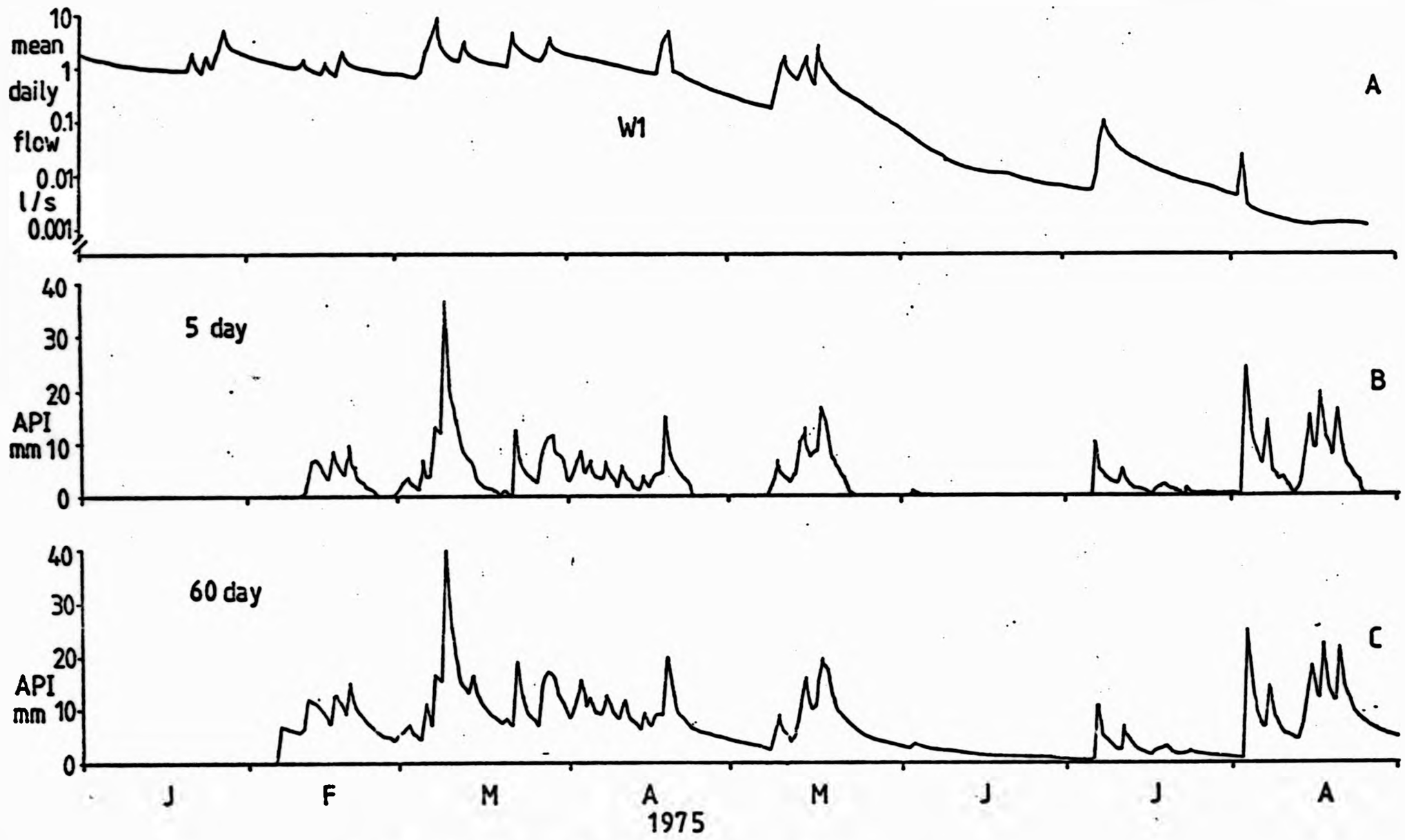

FIGURE 6.11: WEIR 1 DISCHARGE AND ANTECEDENT PRECIPITATION INDICES, 1975

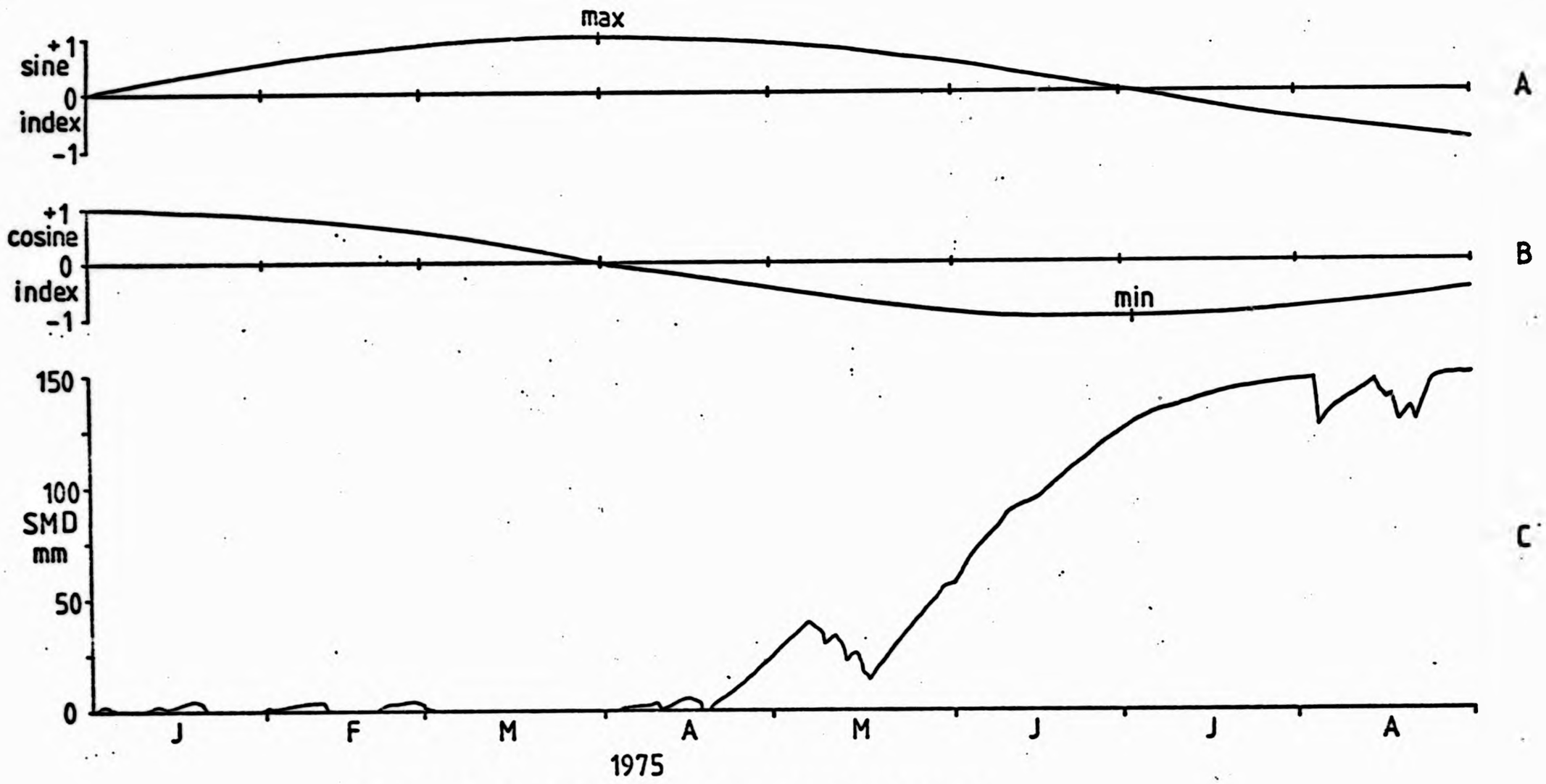

FIGURE 6.12: UNLAGGED SINE AND COSINE INDICES AND WEST WALK SOIL MOISTURE DEFICIT, 1975

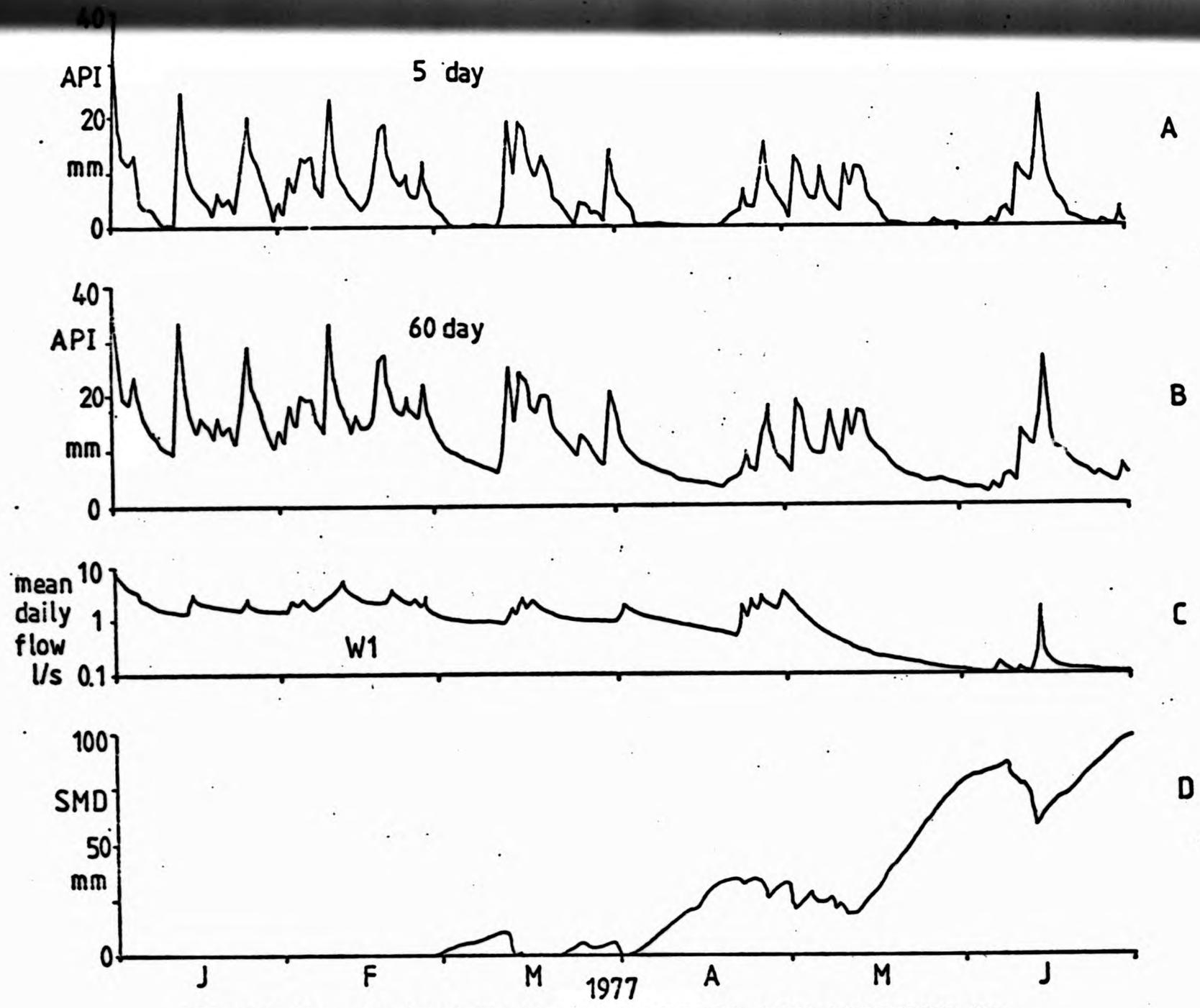

FIGURE 6.13: ANTECEDENT PRECIPITATION INDICES, WEIR 1 DISCHARGE AND WEST WALK SOIL MOISTURE DEFICIT, 1977

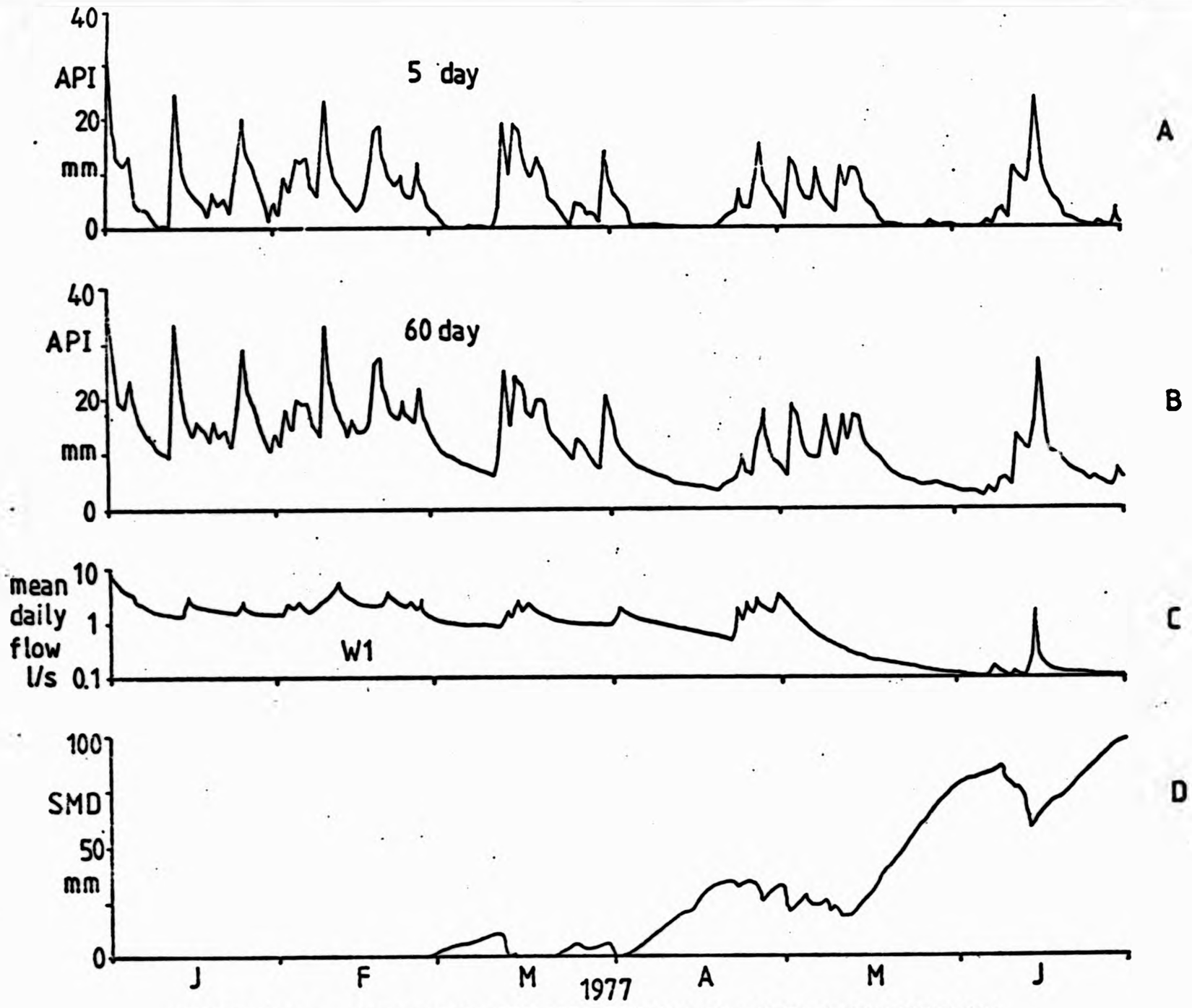

FIGURE 6.13: ANTECEDENT PRECIPITATION INDICES, WEIR 1 DISCHARGE AND WEST WALK SOIL MOISTURE DEFICIT, 1977

Normality was considered by calculating skewness and kurtosis for each variable in each catchment and testing for the significance of non-normality according to equations (6.2) and (6.3) (using the program MOMENTS 3 : Appendix 2). In addition to the untransformed data and the log-transformed data, reciprocal, square and square-root transforms were also used before computing skewness and kurtosis. The results are given in Tables 6.1 - 6.5 and show the probability levels for significance of skewness and kurtosis (i.e. non-normality).

First focussing attention upon the log-transformed data, since this corresponds with linear relationships, normality is achieved in only 16/75 cases when considering skewness and kurtosis together (5 % significance levels). A reciprocal transform was appropriate in 15/75 cases; square root transform in 2/75 cases; square transform in 1/75 cases; untransformed data was normal in 8/75 cases; leaving 33/75 variables where none of the considered transforms was appropriate. These results were surprising, since a logarithmic transform has been recommended for normalising hydrological data (Leopold, 1962). However, tests were carried out on the marginal distributions and thus represent only a very general guide to normality. Furthermore, "the robustness of regression analysis with respect to the assumption of normality and the fact there is greater need to satisfy such other assumptions as homoscedasticity and linearity, together have the result that transformations specifically for the purpose of imposing normality are infrequent" (Poole and O'Farrell, 1971, p.155). Henceforth, transformations for achieving linearity are given priority over transformations for normalising conditional and marginal distributions.

C. Preliminary Consideration of Solute Means and Standard Deviations for Sub-Catchments

(i) Solute Concentrations

Means, standard deviations and coefficients of variation were also output by the program MOMENTS 3 and are considered here because they form an introduction to subsequent work (Tables 6.6 and 6.7). Although the flume data is not strictly comparable with that from other subcatchments because of non-synchronous sampling times, concentrations increase downstream from W1, comparing well with similar results from the Eastern USA (Johnson, 1979). This is seen to be part of a process

TABLE 6.1 A W1 SKEWNESS: REGULARLY SAMPLED DATA Probability levels refer to significance of Skewness

		x	Sig.level	Log x	Sig.level	1/x	Sig.level	x^2	Sig.level	$\sqrt{x}$	Sig.level
K	mg/l x 1	- 0.15	NS	- 0.49	NS	+ 0.80	5 %	+ 0.22	NS	- 0.32	NS
Na	mg/l x 2	- 0.07	NS	- 0.25	NS	+ 0.42	NS	+ 0.10	NS	- 0.16	NS
Ca	mg/l x 3	+ 1.10	1 %	- 0.51	NS	- 0.02	NS	+ 1.83	1 %	+ 0.79	5 %
Mg	mg/l x 4	+ 0.70	5 %	+ 0.34	NS	+ 0.07	NS	+ 1.06	1 %	+ 0.52	NS
Cl	mg/l x 5	+ 0.25	NS	- 0.24	NS	+ 0.88	5 %	+ 0.63	5 %	+ 0.02	NS
pH	x 6	- 1.53	1 %	- 1.93	1 %	+ 2.27	1 %	- 1.12	1 %	- 1.74	1 %
HCO_3	mg/l x 7	+ 0.91	5 %	- 2.55	1 %	+ 3.75	1 %	+ 1.56	1 %	+ 0.17	NS
SC	umhos x 8	+ 0.71	5 %	+ 0.47	NS	- 0.18	NS	+ 0.96	1 %	+ 0.60	NS
Q	l/sec x 9	+ 3.55	1 %	- 0.81	5 %	+ 3.02	1 %	+ 5.40	1 %	+ 0.90	5 %
API 5	mm x 10	+ 3.06	1 %	+ 1.64	1 %	- 0.91	5 %	+ 4.53	1 %	+ 2.27	1 %
API 15	mm x 11	+ 2.93	1 %	+ 1.36	1 %	- 0.45	NS	+ 4.45	1 %	+ 2.08	1 %
API 30	mm x 12	+ 2.85	1 %	+ 1.24	1 %	- 0.23	NS	+ 4.40	1 %	+ 1.99	1 %
API 60	mm x 13	+ 2.32	1 %	+ 1.03	1 %	- 0.19	NS	+ 3.77	1 %	+ 1.61	1 %
SMD	mm x 14	+ 0.71	5 %	+ 0.22	NS	+ 0.25	NS	+ 1.10	1 %	+ 0.47	NS
Sine Index	x 15	- 0.66	5 %	- 0.66	5 %	- 0.66	5 %	- 0.66	5 %	- 0.66	5 %

Probability	$\sqrt{b_1}$	(N = 33, N^1 = 34
1 %	0.93	
5 %	0.63	

TABLE 6.1 B W1 KURTOSIS: REGULARLY SAMPLED DATA Probability levels refer to significance of Kurtosis

	x	Sig.level	Log x	Sig.level	1/x	Sig.level	x^2	Sig.level	$\sqrt{x}$	Sig.level
x 1	0.8360	NS	0.8325	NS	0.8236	NS	0.8290	NS	0.8362	NS
x 2	0.8367	NS	0.8345	NS	0.8326	NS	0.8389	NS	0.8351	NS
x 3	0.8226	NS	0.8597	5 %	0.8670	5 %	0.7489	NS	0.8457	NS
x 4	0.8500	10 %	0.8652	5 %	0.8586	10 %	0.8216	NS	0.8602	5 %
x 5	0.7932	NS	0.7745	NS	0.7404	5 %	0.8006	NS	0.7852	NS
x 6	0.6764	1 %	0.6373	1 %	0.6072	1 %	0.7136	1 %	0.6570	1 %
x 7	0.8609	5 %	0.5882	1 %	0.4706	1 %	0.7964	NS	0.8325	NS
x 8	0.8791	1 %	0.8918	1 %	0.8888	1 %	0.8560	NS	0.8872	1 %
x 9	0.5856	1 %	0.8544	NS	0.6108	1 %	0.3704	1 %	0.7932	NS
x 10	0.6746	1 %	0.7932	NS	0.8549	NS	0.5149	1 %	0.7418	5 %
x 11	0.6529	1 %	0.7635	NS	0.8219	NS	0.5153	1 %	0.7148	5 %
x 12	0.6460	1 %	0.7563	NS	0.8143	NS	0.5188	1 %	0.7072	1 %
x 13	0.6937	1 %	0.7853	NS	0.8316	NS	0.5767	1 %	0.7429	5 %
x 14	0.8755	5 %	0.8754	5 %	0.8890	1 %	0.8398	10 %	0.8791	1 %
x 15	0.8596	5 %	0.8596	5 %	0.8596	5 %	0.8596	5 %	0.8596	5 %

Probability	Bounds a lower	a upper
1 %	0.7140	0.8790
5 %	0.7430	0.8590

($N = 33$, $N^1 = 34$)

Variables defined in Table 6.1A

TABLE 6.2 A W2 SKEWNESS: REGULARLY SAMPLED DATA Probability levels refer to significance of Skewness

	x	Sig.level	Log x	Sig.level	1/x	Sig.level	x^2	Sig.level	$\sqrt{x}$	Sig.level
x 1	+ 0.18	NS	- 0.12	NS	+ 0.45	NS	+ 0.45	NS	+ 0.04	NS
x 2	- 0.40	NS	- 0.62	NS	+ 0.84	5 %	- 0.19	NS	- 0.50	NS
x 3	+ 1.10	1 %	+ 0.47	NS	+ 0.37	NS	+ 1.60	1 %	+ 0.81	5 %
x 4	+ 1.73	1 %	+ 0.75	5 %	+ 0.29	NS	+ 2.80	1 %	+ 1.26	1 %
x 5	- 2.84	1 %	- 4.62	1 %	+ 0.54	NS	- 0.97	1 %	- 3.83	1 %
x 6	- 2.85	1 %	- 3.88	1 %	+ 0.47	NS	- 1.79	1 %	- 3.39	1 %
x 7	+ 1.10	1 %	- 4.33	1 %	+ 0.56	NS	+ 1.72	1 %	+ 0.10	NS
x 8	+ 0.10	NS	- 4.20	1 %	+ 0.56	NS	+ 1.18	1 %	- 1.56	1 %
x 9	+ 5.46	1 %	+ 0.07	NS	+ 0.37	NS	+ 5.57	1 %	+ 4.52	1 %
x 10	+ 3.33	1 %	+ 1.82	1 %	- 0.99	1 %	+ 4.71	1 %	+ 2.51	1 %
x 11	+ 2.95	1 %	+ 1.39	1 %	- 0.47	NS	+ 4.45	1 %	+ 2.11	1 %
x 12	+ 2.77	1 %	+ 1.18	1 %	- 0.22	NS	+ 4.34	1 %	+ 1.91	1 %
x 13	2.64	1 %	+ 1.09	1 %	- 0.15	NS	+ 4.23	1 %	+ 1.80	1 %
x 14	+ 0.71	5 %	+ 0.26	NS	+ 0.16	NS	+ 1.09	1 %	+ 0.49	NS
x 15	- 0.90	5 %	- 0.90	5 %	- 0.90	5 %	- 0.90	5 %	- 0.90	5 %

Probability	$\sqrt{b_1}$	(N = 33, N^1 = 34)
1 %	0.93	
5 %	0.63	

Variables defined in Table 6.1A

TABLE 6.2 B W2 KURTOSIS: REGULARLY SAMPLED DATA Probability levels refer to significance of Kurtosis

	x	Sig.level	Log x	Sig.level	1/x	Sig.level	x^2	Sig.level	$\sqrt{x}$	Sig.level
x 1	0.8024	NS	0.7910	NS	0.7724	NS	0.8082	NS	0.7973	NS
x 2	0.8149	NS	0.8014	NS	0.7844	NS	0.8239	NS	0.8087	NS
x 3	0.8108	NS	0.8175	NS	0.7878	NS	0.7739	NS	0.8203	NS
x 4	0.7162	5 %	0.7507	NS	0.7422	NS	0.6495	1 %	0.7375	5 %
x 5	0.5896	1 %	0.4412	1 %	0.3458	1 %	0.6954	1 %	0.5158	1 %
x 6	0.5707	1 %	0.5008	1 %	0.4369	1 %	0.6418	1 %	0.5345	1 %
x 7	0.7657	NS	0.4791	1 %	0.3379	1 %	0.7416	5 %	0.7290	5 %
x 8	0.7618	NS	0.4609	1 %	0.3377	1 %	0.7862	NS	0.6667	1 %
x 9	0.3606	1 %	0.7474	NS	0.5577	1 %	0.3379	1 %	0.4558	1 %
x 10	0.6446	1 %	0.7760	NS	0.8402	NS	0.4890	1 %	0.7170	5 %
x 11	0.6449	1 %	0.7557	NS	0.8166	NS	0.5177	1 %	0.7062	1 %
x 12	0.6605	1 %	0.7746	NS	0.8205	NS	0.5250	1 %	0.7263	5 %
x 13	0.6683	1 %	0.7778	NS	0.8288	NS	0.5354	1 %	0.7295	5 %
x 14	0.8803	1 %	0.8891	1 %	0.9000	1 %	0.8413	NS	0.8857	1 %
x 15	0.8193	NS	0.8193	NS	0.8193	NS	0.8193	NS	0.8193	NS

Probability	Bounds a lower	a upper
1 %	0.7140	0.8790
5 %	0.7430	0.8590

($N = 33$, $N^1 = 34$)

Variables defined in Table 6.1A

TABLE 6.3 A FLUME SKEWNESS: REGULARLY SAMPLED DATA Probability levels refer to significance of Skewness

	x	Sig.level	Log x	Sig.level	1/x	Sig.level	x^2	Sig.level	$\sqrt{x}$	Sig.level
x 1	+ 1.64	1 %	+ 1.14	1 %	- 0.64	5 %	+ 2.12	1 %	+ 1.39	1 %
x 2	- 0.05	NS	- 0.22	NS	+ 0.40	NS	+ 0.12	NS	- 0.13	NS
x 3	+ 0.85	5 %	+ 0.47	NS	- 0.07	NS	+ 1.18	1 %	+ 0.66	5 %
x 4	+ 0.34	NS	- 1.85	1 %	+ 4.45	1 %	+ 1.16	1 %	- 0.52	NS
x 5	- 0.34	NS	- 0.97	1 %	+ 1.71	1 %	+ 0.16	NS	- 0.63	5 %
x 6	+ 5.00	1 %	+ 4.34	1 %	+ 3.16	1 %	+ 5.23	1 %	+ 4.34	1 %
x 7	+ 0.38	NS	- 0.71	5 %	+ 2.62	1 %	+ 1.01	1 %	- 0.07	NS
x 8	- 0.46	NS	- 3.32	1 %	+ 5.08	1 %	+ 0.60	NS	- 1.71	1 %
x 9	+ 0.38	NS	- 1.05	1 %	+ 3.09	1 %	+ 1.34	1 %	- 0.28	NS
x 10	+ 4.98	1 %	+ 2.94	1 %	- 1.00	1 %	+ 5.28	1 %	+ 4.25	1 %
x 11	+ 5.22	1 %	+ 3.24	1 %	- 0.36	NS	+ 5.29	1 %	+ 4.78	1 %
x 12	+ 1.04	1 %	+ 0.35	NS	+ 0.14	NS	+ 1.90	1 %	+ 0.66	5 %
x 13	+ 0.88	5 %	+ 0.21	NS	+ 0.26	NS	+ 1.73	1 %	+ 0.52	NS
x 14	+ 0.76	5 %	+ 0.31	NS	+ 0.07	NS	+ 1.15	1 %	+ 0.53	NS
x 15	- 0.53	NS	- 0.53	NS	- 0.53	NS	- 0.53	NS	- 0.53	NS

Probability	$\sqrt{b_1}$
1 %	0.93
5 %	0.63

(N = 33, N^1 = 34)

Variables defined in Table 6.1A

TABLE 6.3 B FLUME KURTOSIS: REGULARLY SAMPLED DATA Probability levels refer to significance of Kurtosis

	x	Sig.level	Log x	Sig.level	1/x	Sig.level	x^2	Sig.level	$\sqrt{x}$	Sig.level
x 1	0.7166	5 %	0.7437	NS	0.7567	NS	0.6882	1 %	0.7312	5 %
x 2	0.8494	NS	0.8448	NS	0.8374	NS	0.8507	NS	0.8475	NS
x 3	0.8205	NS	0.8499	NS	0.8564	NS	0.7939	NS	0.8376	NS
x 4	0.7645	NS	0.6458	1 %	0.4546	1 %	0.7870	NS	0.7216	5 %
x 5	0.7753	NS	0.7483	NS	0.7045	1 %	0.7869	NS	0.7639	NS
x 6	0.3889	1 %	0.4813	1 %	0.5964	1 %	0.3590	1 %	0.4292	1 %
x 7	0.8654	5 %	0.8200	NS	0.6617	1 %	0.8195	NS	0.8554	NS
x 8	0.7836	NS	0.5556	NS	0.3584	1 %	0.8481	10 %	0.6931	1 %
x 9	0.8410	NS	0.8297	NS	0.5826	1 %	0.7814	NS	0.8630	5 %
x 10	0.4111	1 %	0.6534	1 %	0.8357	NS	0.3530	1 %	0.5143	1 %
x 11	0.3500	1 %	0.6114	1 %	0.8525	NS	0.3534	1 %	0.4214	1 %
x 12	0.8178	NS	0.8606	NS	0.8781	5 %	0.7403	5 %	0.8404	NS
x 13	0.8324	NS	0.8674	NS	0.8797	1 %	0.7569	NS	0.8544	NS
x 14	0.8801	1 %	0.8924	1 %	0.9177	1 %	0.8357	NS	0.8909	1 %
x 15	0.8426	NS	0.8426	NS	0.8426	NS	0.8426	NS	0.8426	NS

Probability	Bounds a lower	a upper
1 %	0.7130	0.8800
5 %	0.7450	0.8600

(N = 32, N^1 = 33)

Variables defined in Table 6.1A

TABLE 6.4 A W4 SKEWNESS: REGULARLY SAMPLED DATA Probability levels refer to significance of Skewness

	X	Sig.level	Log x	Sig.level	1/x	Sig.level	x^2	Sig.level	$\sqrt{x}$	Sig.level
x 1	- 0.16	NS	- 0.42	NS	+ 0.68	5 %	+ 0.09	NS	- 0.30	NS
x 2	- 0.05	NS	- 0.40	NS	+ 0.87	5 %	+ 0.23	NS	- 0.22	NS
x 3	+ 0.47	NS	+ 0.20	NS	+ 0.13	NS	+ 0.71	5 %	+ 0.34	NS
x 4	+ 0.26	NS	- 0.61	NS	+ 1.63	1 %	+ 0.94	1 %	- 0.15	NS
x 5	+ 1.05	1 %	+ 0.66	5 %	- 0.25	NS	+ 1.44	1 %	+ 0.86	5 %
x 6	- 3.95	1 %	- 4.37	1 %	+ 4.71	1 %	- 3.48	1 %	- 4.17	1 %
x 7	- 0.19	NS	- 3.34	1 %	+ 5.19	1 %	+ 1.33	1 %	- 1.62	1 %
x 8	- 3.04	1 %	- 5.13	1 %	+ 5.55	1 %	- 0.89	5 %	- 4.30	1 %
x 9	+ 5.40	1 %	+ 0.22	NS	+ 3.38	1 %	+ 5.57	1 %	+ 5.11	1 %
x 10	+ 2.98	1 %	+ 1.56	1 %	- 0.82	5 %	+ 4.46	1 %	+ 2.19	1 %
x 11	+ 2.57	1 %	+ 1.45	1 %	- 0.51	NS	+ 3.33	1 %	+ 2.03	1 %
x 12	+ 2.77	1 %	+ 1.12	1 %	- 0.10	NS	+ 4.36	1 %	+ 1.88	1 %
x 13	+ 3.66	1 %	+ 1.83	1 %	- .038	NS	+ 4.79	1 %	+ 2.78	1 %
x 14	+ 2.10	1 %	+ 0.46	NS	+ 0.23	NS	+ 4.25	1 %	+ 1.11	1 %
x 15	- 0.88	5 %	+ 0.88	5 %	- 0.88	5 %	- 0.88	5 %	- 0.88	5 %

Probability	$\sqrt{b_1}$
1 %	0.93
5 %	0.63

(N = 33, N^1 = 34)

Variables defined in Table 6.1A

TABLE 6.4 B W4 KURTOSIS: REGULARLY SAMPLED DATA Probability levels refer to significance of Kurtosis

	x	Sig.level	Log x	Sig.level	1/x	Sig.level	x^2	Sig.level	$\sqrt{x}$	Sig.level
x 1	0.7792	NS	0.7698	NS	0.7631	NS	0.7848	NS	0.7742	NS
x 2	0.8260	NS	0.8112	NS	0.7871	NS	0.8317	NS	0.8198	NS
x 3	0.8882	1 %	0.8816	1 %	0.8691	5 %	0.8775	5 %	0.8880	1 %
x 4	0.7316	5 %	0.7072	1 %	0.6627	1 %	0.7320	5 %	0.7229	5 %
x 5	0.7693	NS	0.7797	NS	0.7828	NS	0.7527	NS	0.7748	NS
x 6	0.5336	1 %	0.4895	1 %	0.4470	1 %	0.5779	1 %	0.5112	1 %
x 7	0.7630	NS	0.5290	1 %	0.3950	1 %	0.7503	NS	0.6906	1 %
x 8	0.5860	1 %	0.3830	1 %	0.3376	1 %	0.7208	5 %	0.4767	1 %
x 9	0.3602	1 %	0.7135	1 %	0.5366	1 %	0.3379	1 %	0.5137	1 %
x 10	0.6762	1 %	0.7983	NS	0.8613	5 %	0.5183	1 %	0.7461	NS
x 11	0.6514	1 %	0.7439	NS	0.8056	NS	0.5485	1 %	0.6997	1 %
x 12	0.6524	1 %	0.7685	NS	0.8175	NS	0.5189	1 %	0.7183	5 %
x 13	0.5488	1 %	0.7059	1 %	0.8037	NS	0.4264	1 %	0.6308	1 %
x 14	0.7519	NS	0.8539	10 %	0.8875	1 %	0.5468	1 %	0.8246	NS
x 15	0.8356	NS	0.8356	NS	0.8356	NS	0.8356	NS	0.8356	NS

Probability	Bounds a lower	a upper
1 %	0.7140	0.8790
5 %	0.7430	0.8590

(N = 33, N^1 = 34)

Variables defined in Table 6.1A

TABLE 6.5 A W5 SKEWNESS: REGULARLY SAMPLED DATA (Probability levels refer to significance of Skewness

	x	Sig.level	Log x	Sig.level	1/x	Sig.level	x^2	Sig.level	$\sqrt{x}$	Sig.level
x 1	- 0.71	5 %	- 0.78	5 %	+ 0.84	5 %	+ 0.18	5 %	- 0.74	5 %
x 2	- 0.86	5 %	- 1.07	1 %	+ 1.19	1 %	+ 0.58	NS	- 0.98	1 %
x 3	+ 0.40	NS	- 0.49	NS	+ 0.99	1 %	+ 1.32	1 %	- 0.07	NS
x 4	- 0.29	NS	- 0.71	5 %	+ 0.99	1 %	+ 0.22	NS	- 0.52	NS
x 5	- 0.58	NS	- 0.85	5 %	+ 1.00	1 %	- 0.19	NS	- 0.73	5 %
x 6	+ 3.67	1 %	+ 1.37	1 %	+ 0.37	NS	+ 4.93	1 %	+ 2.59	1 %
x 7	+ 0.83	5 %	- 0.29	NS	+ 0.83	5 %	+ 2.14	1 %	+ 0.20	NS
x 8	- 0.28	NS	- 0.82	5 %	+ 0.99	1 %	+ 0.61	NS	- 0.63	5 %
x 9	+ 3.96	1 %	+ 3.32	1 %	- 2.37	1 %	+ 4.45	1 %	+ 3.72	1 %
x 10	+ 3.51	1 %	+ 2.10	1 %	- 1.27	1 %	+ 4.76	1 %	+ 2.76	1 %
x 11	+ 3.64	1 %	+ 2.18	1 %	- 0.94	1 %	+ 4.61	1 %	+ 2.93	1 %
x 12	+ 5.31	1 %	+ 3.27	1 %	- 0.82	5 %	+ 5.56	1 %	+ 4.64	1 %
x 13	+ 2.96	1 %	+ 1.35	1 %	- 0.34	NS	+ 4.44	1 %	+ 2.10	1 %
x 14	+ 0.60	NS	+ 0.20	NS	+ 0.17	NS	+ 0.93	1 %	+ 0.40	NS
x 15	- 0.68	5 %	- 0.68	5 %	- 0.68	5 %	- 0.68	5 %	- 0.68	5 %

Probability	$\sqrt{b_1}$
1 %	0.93
5 %	0.63

(N = 33, N^1 = 34)

Variables defined in Table 6.1A

TABLE 6.5 B W5 KURTOSIS: REGULARLY SAMPLED DATA (Probability levels refer to significance of Kurtosis

	x	Sig.level	Log x	Sig.level	1/x	Sig.level	x^2	Sig.level	$\sqrt{x}$	Sig.level
x 1	0.8151	NS	0.8144	NS	0.8135	NS	0.8162	NS	0.8145	NS
x 2	0.8559	NS	0.8810	1 %	0.8403	NS	0.8701	5 %	0.8421	NS
x 3	0.7806	NS	0.8327	NS	0.8381	NS	0.7636	NS	0.8065	NS
x 4	0.8197	NS	0.8388	NS	0.8379	NS	0.8075	NS	0.8312	NS
x 5	0.8817	1 %	0.8773	5 %	0.8767	5 %	0.8616	5 %	0.8805	1 %
x 6	0.4670	1 %	0.6037	1 %	0.7627	NS	0.4266	1 %	0.4995	1 %
x 7	0.8163	NS	0.9045	1 %	0.8788	5 %	0.7118	1 %	0.8703	5 %
x 8	0.8627	5 %	0.9056	1 %	0.8921	1 %	0.7909	NS	0.9010	1 %
x 9	0.4637	1 %	0.5566	1 %	0.6588	1 %	0.4415	1 %	0.4921	1 %
x 10	0.6114	1 %	0.7335	5 %	0.8134	NS	0.4792	1 %	0.6771	1 %
x 11	0.5398	1 %	0.6794	1 %	0.7924	NS	0.4445	1 %	0.6051	1 %
x 12	0.3791	1 %	0.5911	1 %	0.7732	NS	0.3397	1 %	0.4628	1 %
x 13	0.6345	1 %	0.7607	NS	0.8193	NS	0.4991	1 %	0.7024	1 %
x 14	0.8977	1 %	0.9039	1 %	0.9212	1 %	0.8644	5 %	0.9058	1 %
x 15	0.8370	NS	0.8370	NS	0.8370	NS	0.8370	NS	0.8370	NS

Probability	Bounds a lower	a upper
1 %	0.7140	0.8790
5 %	0.7430	0.8690

(N = 33, N^1 = 34)

Variables defined in Table 6.1A

of neutralisation of acids derived primarily from organic materials within the soil, but also from atmospheric sources. Neutralisation is effected by chemical weathering reactions with the gain of bases en route downstream. Within West Walk there is a tendency for higher hydrogen ion concentration (lower pH) to be associated with areas of podsols, notably within SC1. The slightly yellow-coloured water at W1 suggests the presence of organic acids, which are probably derived from humic deposits on the side slopes and valley bottom.

High concentrations recorded at W4 may be related to deforestation and replanting in the lower part of the subcatchment during 1973. The associated soil disturbance is likely to have increased solute availability for some time after deforestation, especially since slow growing oaks were planted and ground flora was suppressed by herbicides (c.f. Likens et al, 1970). The 'flashy' response of SC4 (noted in Chapter 4.4 B,) probably acccunts for higher solute levels, notably potassium. The high levels of Na^+ and Cl^- may represent the contribution of rainfall, especially since throughfall and stemflow processes are unlikely to be significant. High concentrations of Ca^{2+}, Mg^{2+} and high pH at W5 seem more likely to be the result of evapotranspiration than storm runoff, under the control of mature Western Hemlock woodland.

Means and standard deviations for Fe, Si and SO_4 (Table 6.7) are compiled from smaller samples and only give a general indication of solute levels. Mean Si levels are high compared with those recently found in Dartmoor drainage waters (Ternan and Williams, 1979) but compare favourably with the median value of 6.54 mg/l Si for USA streams (Davis, 1964). Silicon is probably derived from hydrous aluminium silicates in the London Clay, notably montmorillonite (Gilkes, 1968). It also seems likely that a higher proportion of fine colloidal silica (SiO_2) would be present in London Clay drainage waters than in those derived from granite rocks.

Whilst Si concentrations are poorly related to pH, Fe solubility appears to increase rapidly below pH 4.8 (Figure 6.14). J D Hem (1970) also noted that above a pH of 4.8, the solubility of ferric species was low (less than 0.01 mg/l Fe). This probably corresponds to an increase in organic acid concentration with subsequent reduction of

TABLE 6.6 MEANS, STANDARD DEVIATIONS AND COEFFICIENTS OF VARIATION FOR REGULARLY SAMPLED DATA

Data untransformed: N = 34 for W1 - W5; N = 33 for Flume

Variables defined in Table 6.1A

TABLE 6.6 A : W1

	Mean	S.D.	CV %
x 1	1.45	0.32	21.8
x 2	15.37	1.62	10.5
x 3	10.63	3.87	36.4
x 4	6.78	1.76	25.9
x 5	24.67	3.32	13.5
x 6	6.45	0.87	13.5
x 7	21.80	18.96	86.9
x 8	227	60	26.5
x 9	1.24	1.73	139.9
x 10	14.10	6.93	49.2
x 11	15.25	6.88	45.1
x 12	16.27	6.97	42.8
x 13	17.91	7.59	42.4
x 14	79.34	49.66	62.6
x 15	0.541	0.414	76.6

TABLE 6.6 B : W 2

	Mean	S.D.	CV %
x 1	1.76	0.26	14.9
x 2	17.3	1.73	10.0
x 3	16.07	6.76	42.09
x 4	9.17	3.76	40.5
x 5	27.07	4.44	16.4
x 6	7.29	0.76	10.5
x 7	61.74	41.55	67.3
x 8	239	86	35.9
x 9	9.74	40.43	414.0
x 10	14.10	6.93	49.7
x 11	15.25	6.88	45.1
x 12	16.27	6.97	42.8
x 13	17.91	7.59	42.4
x 14	79.34	49.66	62.6
x 15	0.541	0.414	76.6

TABLE 6.6 C : Flume

	Mean	S.D.	CV %
x 1	1.78	0.41	23.0
x 2	19.62	1.55	7.9
x 3	19.24	5.87	30.5
x 4	8.88	2.95	33.2
x 5	27.7	3.15	11.38
x 6	8.41	3.33	39.6
x 7	83.61	44.77	53.5
x 8	260	72	27.5
x 9	6.16	4.87	74.0
x 10	18.64	26.33	141.0
x 11	17.26	61.94	277.0
x 12	17.16	6.22	36.3
x 13	18.72	6.90	36.8
x 14	76.40	50.85	66.6
x 15	0.495	0.408	82.0

TABLE 6.6 D : W4

	Mean	S.D.	CV %
x 1	1.91	0.21	10.9
x 2	19.74	2.21	11.2
x 3	21.64	5.92	27.4
x 4	10.36	1.86	17.9
x 5	30.70	4.48	14.50
x 6	7.18	0.44	6.12
x 7	47.99	19.68	41.0
x 8	266	52	19.4
x 9	1.59	4.47	281.3
x 10	14.10	6.93	49.2
x 11	15.25	6.88	45.1
x 12	16.27	6.97	42.8
x 13	17.91	7.59	42.4
x 14	79.34	49.66	62.6
x 15	0.541	0.414	76.6

Variables defined in Table 6.1A

TABLE 6.6 E : W5

	Mean	S.D.	CV %
x 1	1.28	0.09	6.8
x 2	17.46	6.60	37.8
x 3	42.1	12.92	30.7
x 4	10.94	3.79	34.6
x 5	23.8	11.02	46.3
x 6	8.32	4.93	59.3
x 7	55.2	44.55	80.7
x 8	239	166	69.6
x 9	0.56	1.51	269.1
x 10	14.1	6.93	49.2
x 11	15.25	6.88	45.1
x 12	16.27	6.97	42.8
x 13	17.91	7.59	42.4
x 14	79.34	49.66	62.6
x 15	0.541	0.414	76.6

Variables defined in Table 6.1A

TABLE 6.7 MOMENTS FOR REGULARLY SAMPLED DATA (untransformed)

SILICON, IRON AND SULPHATE

Concentrations (mg/l)

6.7 A : W1

	Mean	S.D.	CV %	N
Si	4.66	1.02	22.0	12
Fe	0.115	0.013	11.5	5
SO_4	17.20	1.74	10.1	5

6.7 B : W2

	Mean	S.D.	CV %	N
Si	6.98	0.58	8.3	12
Fe	0.190	0.21	112.0	5
SO_4	15.25	0.60	3.9	5

6.7 C : FLUME

	Mean	S.D.	CV %	N
Si	5.27	2.07	39.3	15
Fe	0.108	0.049	44.9	5
SO_4	16.50	1.04	6.3	5

6.7 D : W4

	Mean	S.D.	CV %	N
Si	7.98	2.78	34.8	12
Fe	0.131	0.053	40.0	5
SO_4	14.10	0.54	3.8	5

6.7 E : W5

	Mean	S.D.	CV %	N
Si	5.63	2.07	36.9	12
Fe	0.109	0.107	98.0	5
SO_4	15.10	1.41	9.3	5

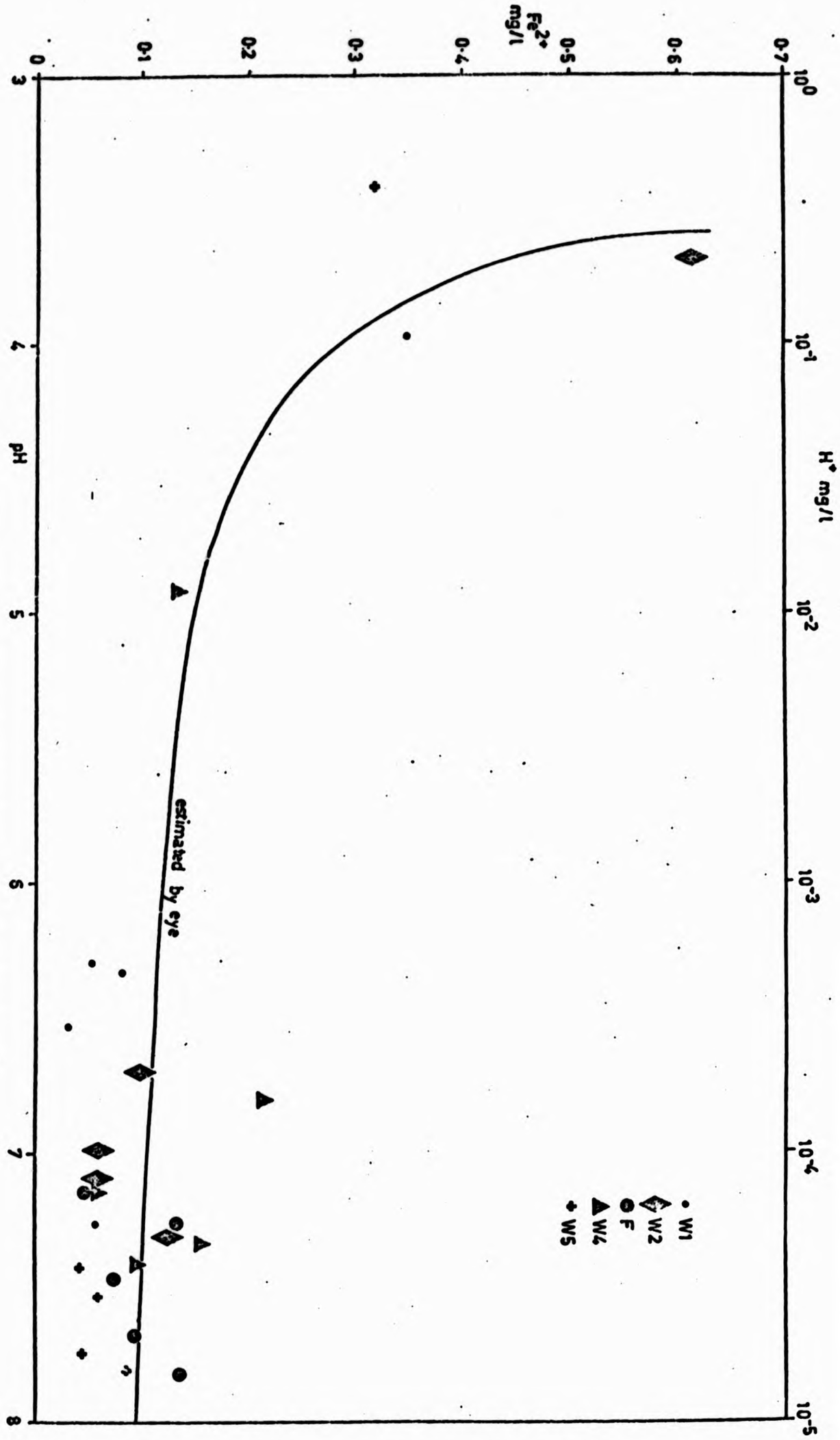

FIGURE 6.14: IRON/pH RELATIONSHIP FOR SIMULATION AT WEST WALK

iron from the ferric (Fe^{3+}) to ferrous (Fe^{2+}) form by chelation. The reverse process has also been observed at West Walk (see Figure 4.5) colloidal iron precipitating in slow moving waters as the organic acid supply diminishes and pH rises during baseflow recession.

(ii) Solute Loads

Mean solute loadings for the sub-catchments give an overall check on data accuracy (i.e. only in exceptional circumstances should dissolved loads decrease downstream) and illustrate temporal and spatial variability in sub-catchment contributions to total load (Tables 6.8 and 6.9). The results appear reasonable with the exception of Mg^{2+} loads at W1 and W4, which add to more than the load at W2. The error may lie in low flow calculations for W4, where calibration was not carried out. The alternative explanation, that the area of catchment between W1 and W2, excluding SC4, contributes little or no solutes to streamflow, seems likely.

Solute loads per unit area (Tables 6.8C and 6.9C) confirm the importance of SC4 as the area of most intensive solute production within West Walk, possibly due in part to the disturbance caused by deforestation and replanting, as noted earlier.

A preliminary view of temporal and spatial patterns has been obtained by schematically plotting the change of TDS loads for each sub-catchment through the 1977 sampling period (Figure 6.15). Proportions of the total catchment load are also shown for each gauging station. It is shown that, over the period 28th March to 14th June 1977, as flow decreases and SMD increases, the proportion of total solute load contributed by the more remote sub-catchments diminishes. For example, at 28th March 1977 the catchment area between W2. W5 and the flume (23 %) of total catchment area) was contributing 14 % of the total solute load. By 31st May 1977 this had increased to 57 %. During and after storm rainfall, e.g. 3rd May 1977, the remote areas again contribute significantly to total catchment load (although there may be some disparity in the data during high discharge due to 10 - 15 minute differences in the times manual samples were taken). These TDS results demonstrate the operation of a dynamic contributing area within West Walk, the downstream areas delivering a high proportion of the

TABLE 6.8 MEAN SOLUTE DISCHARGES FOR 1977 REGULARLY SAMPLED DATA

6.8 A MEAN CONCENTRATIONS (mg/l) (N = 15)

	W1	W2	Flume	W4	W5
K	1.68	1.83	1.78	2.08	1.84
Na	15.68	18.10	19.60	20.87	23.46
Ca	9.20	12.42	17.25	19.62	26.74
Mg	5.78	6.94	8.32	10.09	14.83
Cl	25.47	16.55	16.83	29.12	33.05
pH	6.12	6.79	7.42	6.99	7.25
HCO_3	11.14	34.16	58	41.2	82.40
SC (um)	197	231	248	259	377
Q (l/s)	1.22	2.52	5.46	0.99	0.40

6.8 B MEAN SOLUTE DISCHARGES (milligrams/sec) ($H^+ \times 10^{-5}$)

	W1	W2	Flume	W4	W5
K	2.04	4.61	9.74	2.04	0.73
Na	19.26	45.60	106.99	20.56	9.36
Ca	11.18	31.33	94.90	19.32	10.67
Mg	7.02	17.52	45.44	11.07	5.92
Cl	30.97	66.95	146.50	28.69	13.19
H	91.39	40.92	20.95	10.08	2.23
HCO_3	13.55	86.18	316.70	40.60	32.90
*TDS	186	422	949	176	80

* Using measured TDS

6.8 C MEAN SOLUTE DISCHARGES PER UNIT CATCHMENT AREA
(mg/sec/km^2) ($H^+ \times 10^{-5}$)

	W1	W2	Flume	W4	W5
K	12.36	11.78	16.26	27.14	10.05
Na	116.73	116.70	178.70	273.0	128.30
Ca	67.76	80.10	157.30	256.50	146.30
Mg	42.55	44.77	75.9	147.0	81.1
Cl	187.7	171.0	244.6	381.0	180.8
H	554.9	105.0	85.0	134	31.0
HCO_3	82.12	220.0	529.0	539	451.0
*TDS	922	1078	1585	2337	1096

* Using measured TDS

TABLE 6.9 MEAN SOLUTE DISCHARGES FOR 1977

REGULARLY SAMPLED DATA: SILICON, IRON AND SULPHATE

6.9 A MEAN CONCENTRATIONS (mg/l) (N = 5)

		W1	W2	FLUME	W4	W5
	Si	4.77	6.81	4.52	7.68	5.52
	Fe	0.115	0.190	0.108	0.131	0.109
	SO_4	17.20	15.25	16.50	14.10	15.10
for Si/	$\bar{Q}$ (l/s)	1.70	3.37	6.78	1.42	0.67
for FE/SO_4	$\bar{Q}$ (l/s)	1.27	2.8	5.83	1.0	0.51

6.9 B MEAN SOLUTE DISCHARGES (milligrams/sec)

	W1	W2	FLUME	W4	W5
Si	8.08	23.0	30.67	10.91	3.69
Fe	0.146	0.532	0.629	0.131	0.056
SO_4	21.84	42.70	96.20	14.10	7.70

6.9 C MEAN SOLUTE DISCHARGES PER UNIT CATCHMENT AREA (mg/sec/km^2)

	W1	W2	FLUME	W4	W5
Si	49	59	51	145	51
Fe	0.89	1.36	1.1	1.74	0.77
SO_4	132	109	161	187	106

FIGURE 6.15 TDS LOADS COMPUTED FROM REGULARLY SAMPLED DATA IN WEST WALK (1977)

Actual load (mg/sec) computed from measured TDS and discharge. Figures in brackets are proportions of load at Flume

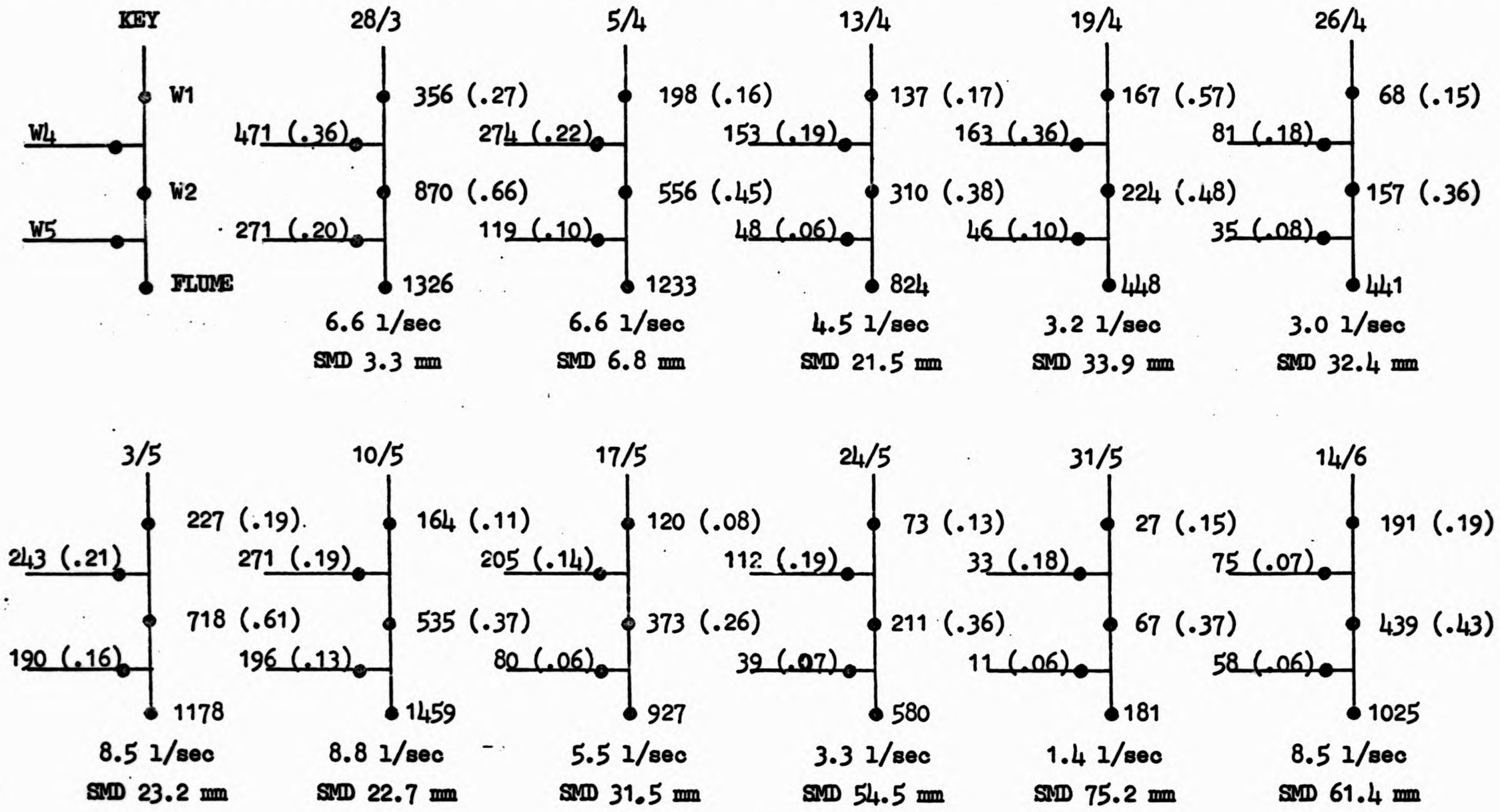

FIGURE 6.16 . IRON, SILICON AND SULPHATE LOADS COMPUTED FROM REGULARLY SAMPLED DATA IN WEST WALK (1977)

(Values in mg/sec)

FIGURE 6.16 A IRON (Values in brackets are pH)

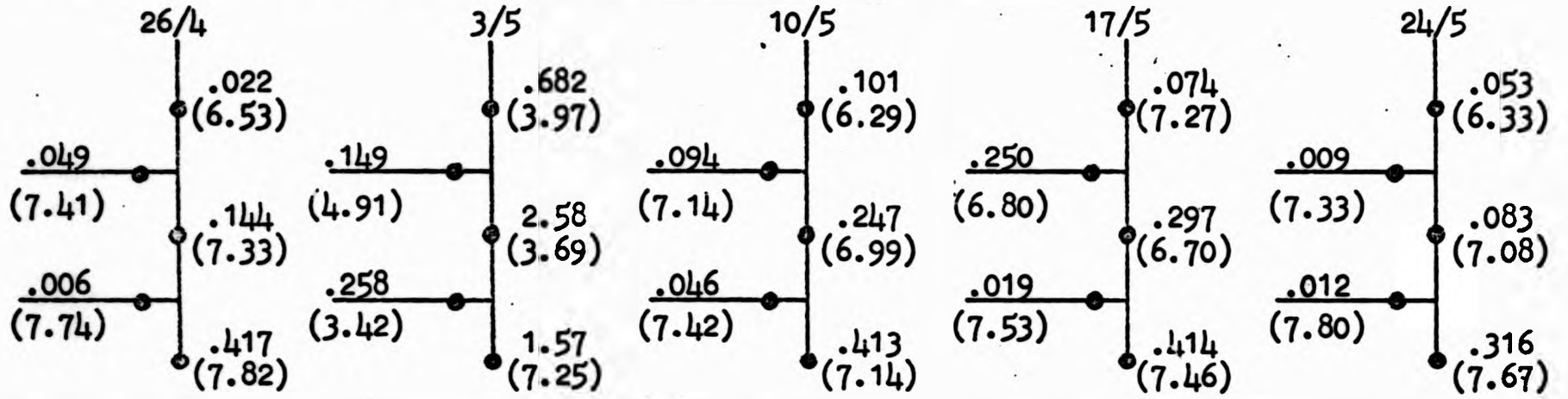

See 6.12 for Discharge and SMD

FIGURE 6.16 B SILICON (Values in brackets are proportions of load at the Flume)

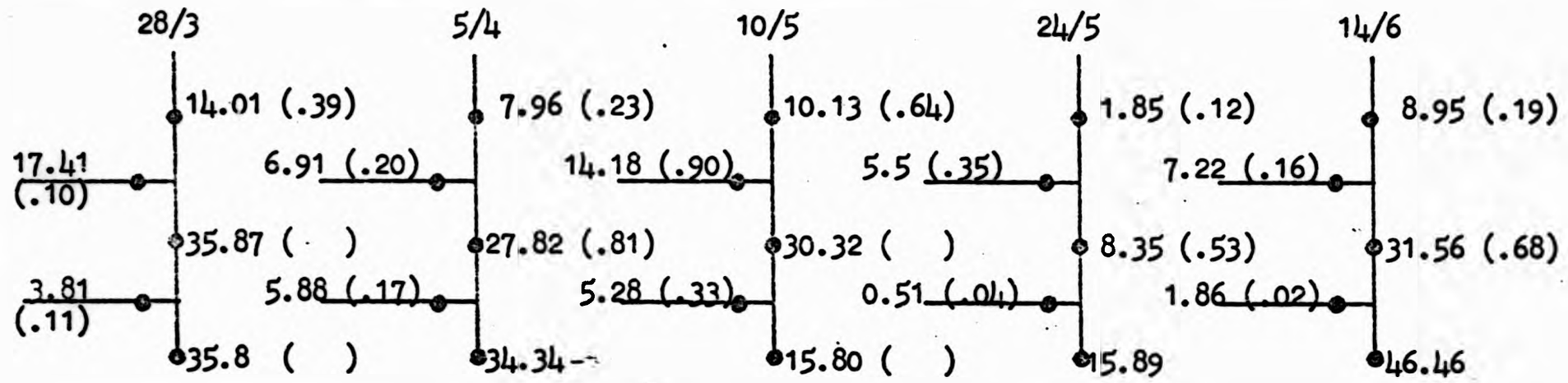

FIGURE 6.16 (Continued)

FIGURE 6.16 C **SULPHATE** (Values in brackets are proportions of load at the Flume)

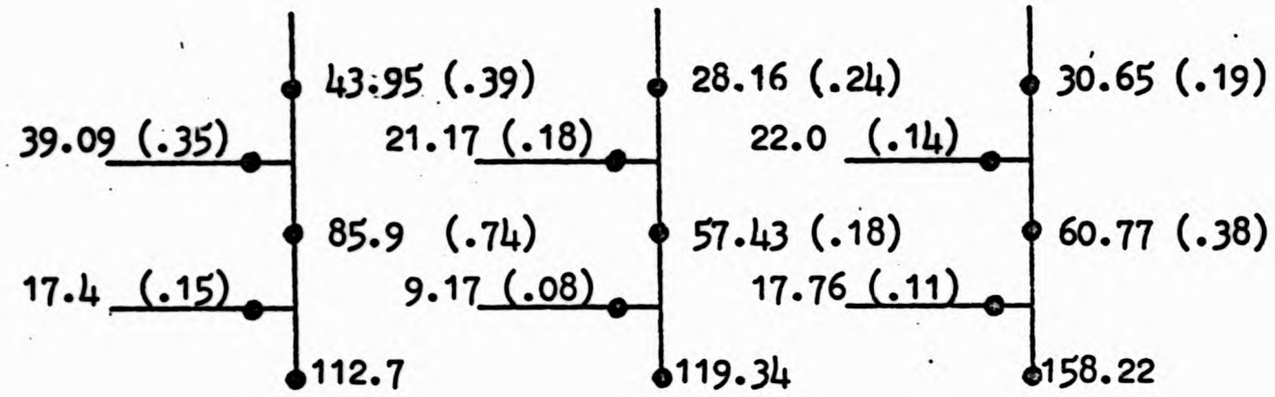

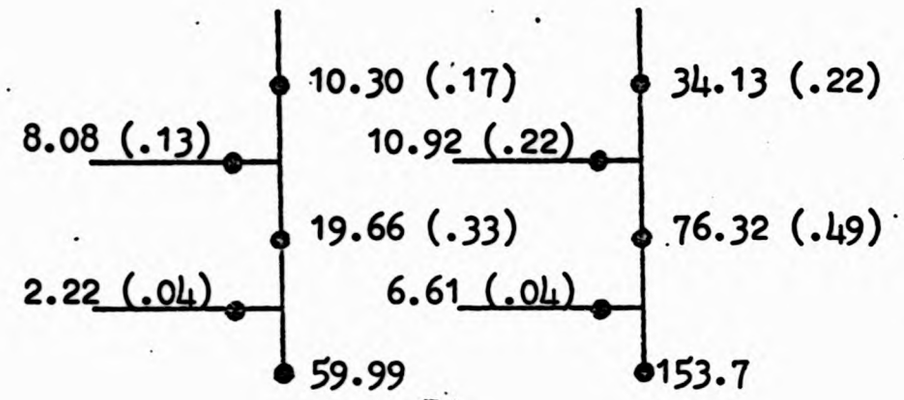

solutes during low flows, the remote areas becoming significant contributors during high flows. An examination of the discharge components used to compute loads gives similar results.

Iron, silicon and sulphate loads are presented in a similar way in Figure 6.16, since they will not be given detailed treatment elsewhere. The anomalously low iron load at the flume on 3rd May 1977 can be explained by the relationship with pH noted earlier. As pH rises near the flume (probably due to acid neutralisation by bases) dissolved iron (Fe^{2+}) becomes unstable and precipitates, forming a colloidal gel. Black discolouration of bed pebbles above and below the flume suggests that some of this iron is re-deposited. This is a common problem in hydrogeology, where underground mixing of waters can cause iron encrustation of well screens and thus reduce well yield. Colloidal material, however, could be lost during filtration and therefore remain unmeasured.

Silicon loads generally increase downstream, although anomalies are present. Why loads (and concentrations; see Table 6.9) are lower at the flume than upstream is not clear, because silica solubility usually increases with increasing pH and temperature (R A Freeze and J A Cherry, 1979).

Sulphate loads increase downstream, mainly due to increasing discharge, because SO_4 concentrations vary little within West Walk (Table 6.9).

D. Maxima and Minima in Solute Concentration and Discharge Data using the Sine Index

The optimised solute and discharge/Sine Index relationships are summarised in Table 6.10. The fact that only the first eight months of 1975 and 1977 are represented in Table 6.10 makes interpretation of the results tentative. Discharge maxima occur during April/May in all except SC5, where maximum discharge occurs in late January. Examination of the significant solute/SI relationships suggests that concentration minima occur at the times of discharge maxima, a general indication of a dilution effect. Conversely, maximum concentration and minimum discharge occur at about the same time. Potassium and discharge

TABLE 6.10

ANNUAL MAXIMA AND MINIMA IN WEST WALK: REGULARLY SAMPLED DATA

(Log. concentration and discharge)

Computed from 1975 and 1977 regularly sampled data; L = number of days before 31st March when maxima or minima occurred; r = best fit correlation coefficient; N = 34 for W1, W2, W4, W5; 33 for Flume

6.10 A : W1

	L	r	MAX	MIN	% Sig. r
K	156	- 0.72	27/04	26/10	0.1
Na	61	0.07	29/01	31/07	NS
Ca	156	0.85	26/10	27/04	0.1
Mg	161	0.63	21/10	22/04	0.1
Cl	146	0.67	05/11	07/05	0.1
pH	126	0.34	25/11	27/05	10.0
HCO_3	111	0.27	20/11	11/06	10.0
SC	151	0.78	31/10	01/05	0.1
Q	151	- 0.76	01/05	31/10	0.1

6.10 B : W2

	L	r	MAX	MIN	% Sig. r
K	186	0.31	26/09	28/03	10.0
Na	36	0.22	23/02	25/08	NS
Ca	176	0.84	06/10	07/04	0.1
Mg	181	0.71	01/10	02/04	0.1
Cl	156	0.39	26/10	27/04	5.0
pH	6	- 0.38	24/09	25/03	5.0
HCO_3	11	- 0.39	30/08	20/03	5.0
SC	31	0.23	28/02	30/08	NS
Q	156	- 0.79	27/04	26/10	0.1

6.10 C : FLUME

	L	r	MAX	MIN	% Sig. r
K	151	0.60	31/10	01/05	0.1
Na	31	0.22	28/02	30/08	NS
Ca	156	0.74	26/10	27/04	0.1
Mg	91	0.70	31/12	01/07	0.1
Cl	101	0.58	20/12	21/06	0.1
pH	26	- 0.53	04/09	05/03	1.0
HCO_3	161	0.38	21/10	22/04	5.0
SC	76	0.57	14/01	16/07	0.1
Q	151	- 0.79	01/05	31/10	0.1

6.10 D : W4

	L	r	MAX	MIN	% Sig. r
K	36	0.20	23/02	25/08	NS
Na	121	0.28	30/11	01/06	NS
Ca	166	0.82	16/10	17/04	0.1
Mg	176	0.61	06/10	07/04	0.1
Cl	171	0.78	11/10	12/04	0.1
pH	181	0.28	01/10	03/04	NS
HCO_3	96	0.26	25/01	26/06	NS
SC	46	0.56	13/02	15/08	0.1
Q	131	- 0.67	21/05	20/11	0.1

6.10 E : W5

	L	r	MAX	MIN	% Sig. r
K	166	- 0.69	17/04	16/10	0.7
Na	176	- 0.80	07/04	06/10	0.1
Ca	6	0.67	25/03	24/09	0.1
Mg	181	- 0.69	02/04	01/10	0.1
Cl	186	- 0.80	28/03	28/09	0.1
pH	126	- 0.66	27/05	25/11	0.1
HCO_3	11	0.71	20/03	19/09	0.1
SC	6	0.81	25/03	24/09	0.1
Q	66	0.66	24/01	26/07	0.1

minima and maxima respectively, occur at approximately the same time, a general indication of a concentration effect for K^+.

Contrasting with other subcatchments, SC5 shows a direct, although lagged, concentration response to discharge, with all solute maxima occurring two to four months after maximum discharge. It is also to be noted that the data for SC5 produce a consistently high set of correlation coefficients, suggesting a stronger seasonal fluctuation than in other subcatchments.

E. Bivariate Correlation and Regression Analysis on the Regularly Sampled Data

This section discusses the results of the log-linear bivariate model $Y = aX^{\pm b}$, discussed at length in Chapter 2.3 for solute/discharge relationships. Here, the model is used to determine correlation between all variables with a correlation matrix approach. The results are used, firstly, to examine factors tentatively influencing solute levels and, secondly, to help select variables for multiple regression analysis (Section 6.3F).

A program was written to produce correlation matrices using the fifteen variables for each subcatchment outlined earlier (CORMAT 4: Appendix 2). Outputs from the program in matrix form were:

(i) correlation coefficients, r;

(ii) student's t values for testing the significance of r;

(iii) the b coefficients for power functions;

(iv) the a coefficients for power functions;

(v) standard errors of the estimates of dependent variables.

Regressions of Y on X and X on Y were computed using the program, as this gave the information necessary for calculation of the RMA regression line (Till, 1973). Having averaged the b coefficients the intercept, a, can be re-calculated from:

$$\bar{a} = \bar{Y} / \bar{X}^{\bar{b}} \qquad (6.8)$$

where $\bar{b} = \tan \left\{(90 - \arctan|b_{xy}| + \arctan|b_{yx}|)/2\right\}$

$\bar{Y}$ can be obtained from

$$\bar{Y} = \text{EXP} \left\{\frac{\log_e a_{yx} \cdot b_{xy} + b_{yx}}{1 - \log_e a_{yx} \cdot \log_e a_{xy}}\right\}$$

and $\bar{X}$ from

$$\bar{X} = a\bar{Y}^{b}$$

The results for each subcatchment are given in Tables 6.11 - 6.15 and are discussed for each solute in turn below. Standard errors are not listed but are quoted in the text where necessary. The % of variance in Y explained by variance in X (r^2 %) is quoted in preference to r because it indicates how good the regression is for prediction. Significance levels are accepted if better than 5 %.

I. (i) Potassium/Discharge

Only at W1 is there a strong, significant, positive correlation between K^+ and discharge (r^2 = 77 %), conforming to the often reported direct relationship (e.g. Walling and Foster, 1975; Foster, 1978). This may be due to rapid leaching from upper soil horizons with the aid of organic acids derived from surface humus; average pH for W1 water is the lowest in West Walk (6.45 pH units). The soils in SC1 are also acid - see Chapter 3 and Appendix 1. The next best significant correlation occurs at the flume (r^2 = 21 %), implying a weak inverse association. The b coefficients were not statistically significant (using a t test, R J Johnston, 1978, p.48) and an interpretation of the rates of concentration change with discharge not attempted.

I. (ii) Potassium/API

Again, the correlations are strongest and most significant for W1, r^2 increasing from 33 % (API 5) to 55 % (API 30 and API 60). This

suggests that rain which fell 30 - 60 days before sampling had a significant effect on concentration. The positive relationship for API/K^+ agrees with that for Q/K^+; this is logical since the API's and Q show significant positive correlation (r^2 = 25 % - 53 %). Weaker significant positive correlations exist for W2, with maximum correlation at API.5, diminishing to a minimum at API.60. This suggests that K^+ concentration is strongly influenced by rainfall over the five days prior to sampling. For W5. API.60 shows the strongest correlation with K^+ (r^2 = 27 %), perhaps due to a longer residence time of water in SC 5. The relationships between API and K^+ for W4 and the flume are not significant.

I. (iii) Potassium/SMD

Significant correlations exist at W1, W5 and the flume (r^2 = 33% 24%, and 23 % respectively); there are negative relationships for W1 and W5, but a positive relationship for the flume. These results agree with the K^+/discharge relationships noted above (as the SMD increases, discharge decreases). K^+ concentration responds more quickly to an SMD change in SC1 than in SC5 (b coefficients and their differences significant at the 1.0 % level). This agrees with the slower hydrological response times for SC5 noted in Chapter 4.4.

The flume shows a consistently opposite response to the other subcatchments for significant relationships. As an example, when discharge increases, K^+ increases at W1 but decreases at the flume. This may be due to the comparatively low pH of water at W1 (i.e. W1 pH : 6.45; flume pH : 8.41), which reflects soil and drainage water acidity. The implication is that the catchment area below W2 and W5 is an abundant source of bases for neutralisation of acid water from upstream. K^+ leaching in this area is probably reduced due to lower concentrations of organic acids in drainage waters, assisting K^+ dilution at the flume.

II. (i) Sodium/Discharge

There are no strong correlations between Na^+ and discharge at any of the gauging stations. Significant, low, negative correlations occurred at W4 and the flume (r^2 = 15 % for both) suggesting a slight dilution effect.

II. (ii) Sodium/API

As with discharge, correlations are weak and mostly insignificant The negative correlations between Na^+ and API.30 at W4 and API.15 at the flume confirm the slight dilution effect.

II. (iii) Sodium/SMD

Only at W4 and W5 are the Na^+/SMD correlations significant (r^2 = 15 % and 23 % respectively). However, the relationships are positive and negative respectively, which means that for an increasing SMD in both catchments, Na^+ concentration would increase in SC4 but decrease in SC5. The positive relationship for W4 agrees with slight dilution effect noted above. It may be tentatively suggested that the decreasing Na^+ concentration with increasing SMD for SC5 is due to uptake of water and solutes from deeper storage by the dominant cover of mature Western Hemlock. Evidence from Thetford Forest, Norfolk, suggests that mature tree stands can exert strong negative pressure (tension) at depths of several metres into the unsaturated zone (D A Fourt, pers. comm. 1976; J D Cooper, 1980). It is interesting to note that SC5 is the only subcatchment where all the solute/SMD correlations are negative implying that a similar mechanism acts upon all solutes.

III. (i) Calcium/Discharge

There are significant, strong correlations between Ca^{2+} and discharge for W1, W2, the flume and W4 (r^2 = 59 %, 52 %, 73 % and 37 % respectively). No significant correlation exists at W5. The direction of the relationships is also consistent, all showing a dilution effect. The b coefficients (all significant with the exception of W5, at the 0.1 % level) indicate that Ca^{2+} concentration change is sensitive to discharge change in the order: flume = W2 > W4 > W1. Only the differences between the flume/W2 and W1 coefficients are significantly different (0.1 % level), suggesting differences in catchment solute response above and below W1.

III. (ii) Calcium/API

As with Ca^{2+}/discharge, the Ca^{2+}/API relationships show significant correlations for W1, W2, the flume and W4; W5 is again the

exception. The best correlations are achieved for API.60 at W1, W2 and the flume (r^2 = 45 %, 44 % and 62 % respectively) and for API.30 at W4 (r^2 = 29 %), suggesting the importance of throughflow waters with long residence times in controlling solute concentration during the periods of sampling.

III. (iii) Calcium/SMD

Ca^{2+} concentration increases as SMD increases at W1, W2, the flume and W4 (r^2 = 49 %, 38 %, 46 % and 59 % respectively). At W5 there is a weak negative correlation between Ca^{2+} and SMD. All correlations are significant, and concur with the Ca^{2+}/discharge dilution effect. The sensitivity of Ca^{2+} concentration change to SMD change is in reverse order compared with Ca^{2+}/discharge: W1 ≃ W2 > W4 > flume (b coefficients significant at the 0.1 % level). Interpretation of these results is difficult although the influential mechanisms may be evapotranspiration and soil drainage, whose rates of operation and relative importance vary spatially.

IV. (i) Magnesium/Discharge

Mg^{2+} concentration shows significant inverse correlation with discharge at W1, W2, the flume and W4 (r^2 = 61 %, 53 %, 52 % and 21 % respectively). The correlation coefficient for W5 is low, positive and insignificant. Mg^{2+} behaves in a similar way to Ca^{2+} in that it dilutes with increasing discharge. All the b coefficients are significant at the 0.1 % level with the exception of those for W4 and W5. These indicate that Mg^{2+} change is sensitive to change in discharge in the order, flume > W2 > W1, which is similar to that for Ca^{2+}. This reflects the rapid response of the lower catchment areas and hence faster dilution.

IV. (ii) Magnesium and API

The correlation coefficients between Mg^{2+} and API are significant in all cases. For W1 and W2 there is an inverse relationship with API.60 (r^2 = 45 % for both); at W5 a weak positive relationship exists with API.60 (r^2 = 8 %); for the flume an inverse correlation exists with API.15 (r^2 = 76 %); for W4 an inverse correlation exists with API.30 (r^2 = 30 %). The different APIs suggest varying rates of

throughflow, longer above W2 than below, again concurring with the hydrological response rates noted in Chapter 4.4.

IV. (iii) Magnesium and SMD

These results are very similar to those obtained for Ca^{2+}. Mg^{2+} concentration increases with increasing SMD at W1, W2, the flume and W4 (r^2 = 26 %. 24 %, 48 % and 45 % respectively). A weak negative correlation exists at W5 (r^2 = 12 %). All correlation coefficients are significant. The b coefficients (all signficant at the 5 % level) show increasing sensitivity of Mg^{2+} change to change in SMD in the order, flume > W2 > W1 > W4. This contradicts the order for Ca^{2+} and SMD, but agrees with that for Ca^{2+} and discharge.

V. (i) Chloride and Discharge

Chloride correlates inversely with discharge at W1, W2, the flume and W4 (r^2 = 21 %, 19 %, 46 % and 28 % respectively). All are significant at or above the 1.0 % level. Rainfall appears to make an insignificant contribution to streamflow chloride, in direct contrast to results from upland Britain (e.g. Cryer, 1976), although the data used for these regressions were not specifically obtained during storm hydrographs. Correlation is absent at W5. Comparison of the regression slopes is invalidated by their statistical insignificance.

V. (ii) Chloride and API

Negative correlations exist between Cl^- and API in all catchments, implying that concentration increases during catchment drying phases. There is little difference in the strength of correlation coefficients between the different API for W1 or W2 (r^2 = 42 % and 49 % respectively). At the flume the strongest correlation exists for API.15 (r^2 = 62 %) and at W4 for API.30 (r^2 = 31 %). There is a weak positive correlation between API.60 and Cl^- at W5 (r^2 = 16 %).

V. (iii) Chloride and SMD

The relationships between Cl^- and SMD are positive and significant at W1, W2, W4 and the flume (r^2 = 49 %, 17 %, 34 % and 61 % respectively), confirming the implication that concentration increases during catchment drying. For W5, however, there is a weak but

significant negative relationship (r^2 = 18 %), agreeing with the Cl^-/API.60 correlation noted above. It was suggested earlier that the decrease in solute concentrations for W5 may be partly due to reversal of soil moisture potential under the influence of evapotranspiration. Under such conditions, solutes might be taken up by the tree or accumulate at the root-soil interface. Chloride is not required by plants in such large quantities as potassium, calcium and magnesium (Sutcliffe and Baker, 1974) and thus would form larger accumulations in the soil.

VI. (i) <u>pH and Discharge</u>

An inverse relationship exists between acidity and discharge at all sites with the exception of W5. The strength of the correlation decreases downstream from W1 (r^2 = 28 %), to W2 (r^2 = 13 %), to the flume (r^2 < 1.0 %); at W4, r^2 = 13 %. The lower pH of waters flowing from SC1 was noted earlier, and the negative relationship with discharge accounted for by increased leaching of organic acids during higher flows. The downstream decrease in the strength of correlation implies a mixing of waters from different origins and simultaneous partial neutralisation of acidity.

At W5 acidity increases significantly with decreasing discharge (r^2 = 61 %) suggesting that SC5 is an important supplier of bases at higher flows. The mixing of waters from SC5 and above W2 would thus be an important factor in reducing acidity and weakening the pH/discharge relationship at the flume. The rate of pH decrease with increasing discharge is in the order W1 > W2 > W4, although only the W2 b coefficient is significant (o.1 % level). Conversely, pH increases more rapidly with rising discharge at W5 (b significant at the 0.1 % level).

VI. (ii) <u>pH and API</u>

A significant negative relationship occurs between API and pH at W1 (for all API : r^2 = 36 %) agreeing well with the trend noted for pH and discharge. A much weaker negative correlation also exists at W2 (r^2 = 7 %). The strong positive correlation with API 15 at the flume (r^2 = 56 %) is strong evidence for the dominance of lower catchment water in neutralising acid from upper areas at higher flows.

As the API 15 decreases, pH decreases, which seems incongruous; however, between 15 and 30 days the relationship becomes negative, suggesting that 'older' water has exchanged H^+ ions for cations during throughflow. The interpretation of pH/API relationships for W4 and W5 (API 30 : r^2 = 10 % and 16 % respectively) agrees with that for pH/discharge.

VI. (iii) pH and SMD

Relationships are weak and insignificant for W1, W2 W4 and the flume. A negative correlation at W5 (r^2 = 18 %) implies that as SMD decreases acidity also decreases, which agrees with the pH/discharge relationship.

VII. (i) Bicarbonate and Discharge

There are low negative correlations between HCO_3^- and discharge at W1, W2, the flume and W4 (r^2 = 20 %, 13 %, 27 % and 34 % respectively) at W5 the negative correlation was not significant. These results suggest a straightforward dilution effect with increasing discharge, although this might be more correctly termed acidification, as pH decreases with increasing discharge.

The rate of HCO_3^- dilution occurs in the order W4 > W1 > W2 > W5 > flume (all b coefficients significant at the 0.1 % level).

VII. (ii) Bicarbonate and API

Correlations between HCO_3 and API are low and negative, but significant with the exception of W5. There is no particular pattern to correlations with separate API's, except for the flume, where 5 and 15 day indices are most strongly correlated. The direction of correlation agrees with that for discharge.

VII. (iii) Bicarbonate and SMD

The HCO_3^- /SMD correlations are low and, with the exception of the flume, insignificant.

VIII. (i) Specific Conductance and Discharge

With one exception all the correlations are significant and

negative, suggesting a dilution of total dissolved matter with increasing discharge. The best correlations are for W1 (r^2 = 67 %), W4 (r^2 = 45 %) and the flume (r^2 = 30 %). For W5 the correlation is not significant, suggesting that factors other than discharge dominate concentration.

VIII. (ii) Specific Conductance and API

High negative correlations between SC, API 10 and API 15 are obtained for the flume (r^2 = 87 % and 76 % respectively) agreeing with the dilution effect noted above. At W1 and W4 similar, weaker relationships are noted with API 60, which at W5 the correlation with API 60 is positive, suggesting that concentration increases as the API, and hence flow, increase.

VIII. (iii) Specific Conductivity and SMD

Only at W1 and the flume are there significant positive correlations (r^2 = 49 % and 34 % respectively) implying that concentrations increase as the soil moisture store is depleted. The significant negative relationship for W5 (r^2 = 20 %) agrees with most other results for the subcatchment, implying a decrease in concentration with loss of water by evapotranspiration.

Residuals from the regressions were tested for homoscedasticity and serial correlation. Two programs were written for this purpose: 'DURBIN' (Appendix 2) calculated the Durbin and Watson statistic for Serial Correlation; 'RESID1' (Appendix 2) calculated squared residuals from the regression and plotted these against X_i. For serial correlation to be significant at the 5 % level the d statistic had to be less than 1.39 (n = 34); if d > 1.51 no significant serial correlation existed at the 5 % level. Serial correlation was found to be present in only a few regressions of Y on X. Only 24 out of a total of 805 regressions exhibited serial correlation significant at the 5 % level.

Homoscedasticity was assessed by visual inspection of the X_i against $(Y_i - \hat{Y}_i)^2$ plots. Selected regressions from each subcatchment were plotted to save computer time. These indicated that homoscedasticity was likely to occur in only about 18 % of the

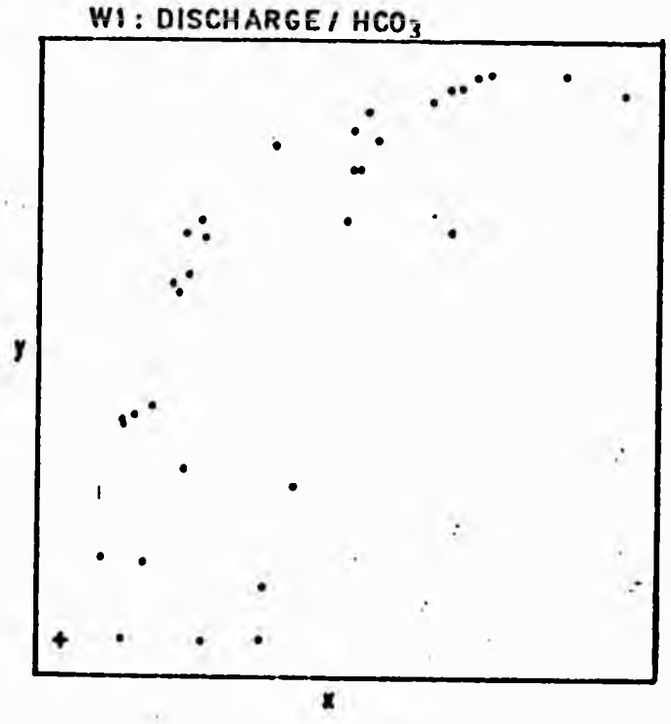

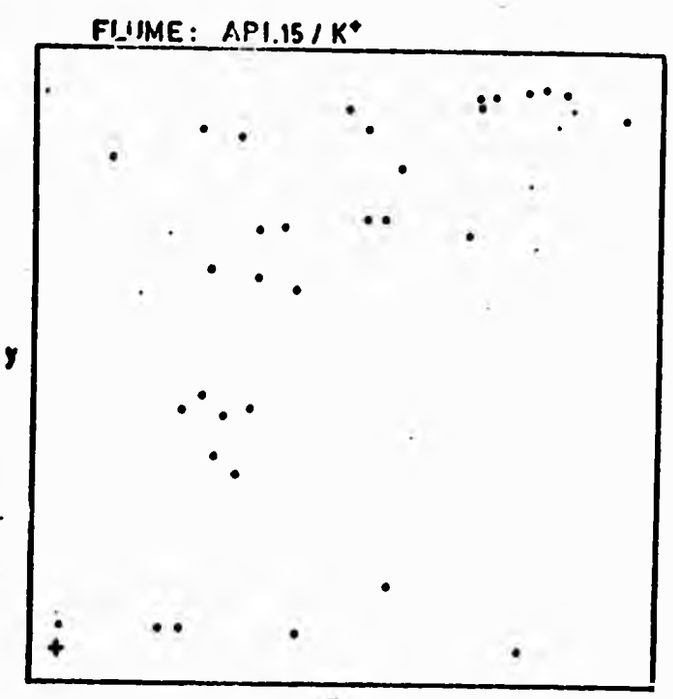

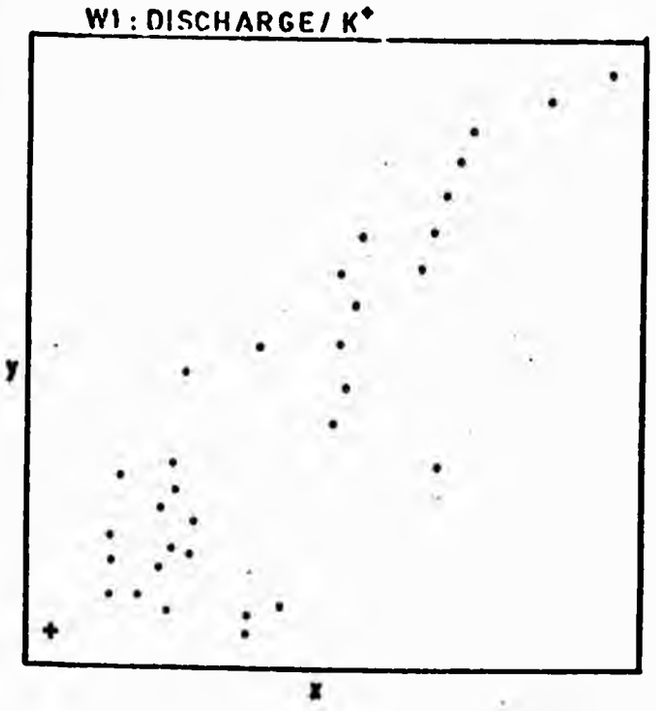

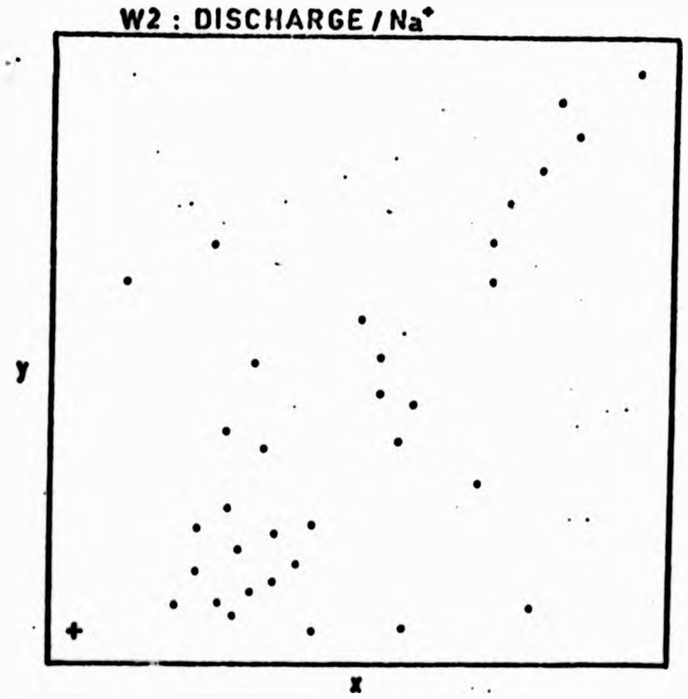

REDRAWN FROM COMPUTER PRINTOUT
+ = x AND y MINIMA
x = RESIDUAL SQUARED
y = INDEPENDENT VARIABLE

FIGURE 6.17: EXAMPLES OF RESIDUALS $(Y_i - \hat{Y}_i)^2$ PLOTTED AGAINST INDEPENDENT VARIABLES (X_i) FOR ASSESSING HOMOSCEDASTICITY

regressions, with heteroscedasticity prevalent in individual solute/discharge relationships. Some examples of these plots are shown in Figure 6.17. The implications of this analysis are that estimates of the regression coefficients are biased and valid inference is impossible.(Poole and O'Farrell, ibid). This places doubt upon conclusions regarding rates of solute change with discharge and SMD. Furthermore, it suggests that multiple regression coefficients might also have bias (although separate analysis of these coefficients is required), possibly ruling out this technique for everything except prediction of solute concentration.

F. Multiple Regression on the Regularly Sampled Data

Since predictive models were required for synthesis of solute concentration and solute loads in the subcatchments, an attempt was made to improve upon the % variance explanation of bivariate models by using multiple regression. This is only essential for W4 and W5, because no storm sampling was undertaken at these points to increase the range of conditions described. However, multiple regression was applied to all five regularly sampled data sets in order to assess any general improvement in % variance explanation by including hydrometeorological variables other than discharge.

Usually a stepwise procedure is employed in order to build up the multiple regression equations one variable at a time, and then assess the significance of the additional variance explained using an F statistic. Stepwise multiple regression was not available on the WANG 2200 B computer and, although a program could have been written for this purpose, the stepwise procedure was hand-calculated. Only four independent variables were involved, which made the method described by L J King (1969) relatively easy to apply.

I. First enter the independent variable with the highest correlation coefficient from the bivariate correlation matrix.

II. Secondly, compute first-order partial correlation coefficients between Y and the remaining independent variables, holding constant the one already in the equation. These are computed by:

TABLE 6.11A W1: CORRELATION MATRIX FOR BIVARIATE REGRESSION : REGULARLY SAMPLED DATA (LOG DATA EXCEPT SINE INDEX)

	x 1	x 2	x 3	x 4	x 5	x 6	x 7	x 8	x 9	x 10	x 11	x 12	x 13	x 14	x 15
x 1	*	-	-	-	-	-	-	-	0.88	0.57	0.67	0.74	0.74	-0.57	-0.72
x 2	-	*	-	-	-	-	-	-	-0.02	-0.17	-0.12	-0.11	-0.22	0.13	0.07
x 3	-	-	*	-	-	-	-	-	-0.77	-0.45	-0.52	-0.56	-0.61	0.70	0.85
x 4	-	-	-	*	-	-	-	-	-0.78	-0.49	-0.58	-0.61	-0.67	0.51	0.63
x 5	-	-	-	-	*	-	-	-	-0.46	-0.59	-0.63	-0.65	-0.68	0.70	0.61
x 6	-	-	-	-	-	*	-	-	-0.53	-0.56	-0.61	-0.58	-0.61	0.21	0.34
x 7	-	-	-	-	-	-	*	-	-0.45	-0.36	-0.42	-0.39	-0.42	0.09	0.27
x 8	-	-	-	-	-	-	-	*	-0.82	-0.33	-0.42	-0.51	-0.57	0.70	0.78
x 9	0.1	NS	0.1	0.1	1.0	1.0	1.0	0.1	*	0.50	0.61	0.69	0.73	-0.66	-0.75
x 10	0.1	NS	1.0	1.0	0.1	0.1	5.0	5.0	1.0	*	0.94	0.91	0.92	-0.58	-0.41
x 11	0.1	NS	1.0	0.1	0.1	0.1	1.0	1.0	0.1	0.1	*	0.98	0.94	-0.60	-0.46
x 12	0.1	NS	0.1	0.1	0.1	0.1	5.0	1.0	0.1	0.1	0.1	*	0.94	-0.66	-0.54
x 13	0.1	NS	0.1	0.1	0.1	0.1	1.0	0.1	0.1	0.1	0.1	0.1	*	-0.68	-0.60
x 14	0.1	NS	0.1	1.0	0.1	NS	NS	0.1	0.1	0.1	0.1	0.1	0.1	*	0.86
x 15	0.1	NS	0.1	1.0	0.1	5.0	NS	0.1	0.1	1.0	1.0	1.0	0.1	0.1	*

Significance levels using a t test shown in bottom half of table . Constants added: x10, x11, x12, x13 + 10
x14 +1.0

Variables defined in Table 6.1A

TABLE 6.11B W1: B COEFFICIENTS FOR BIVARIATE REGRESSION : REGULARLY SAMPLED DATA (LOG DATA EXCEPT SINE INDEX)

	x 1	x 2	x 3	x 4	x 5	x 6	x 7	x 8	x 9	x 10	x 11	x 12	x 13	x 14	x 15
x 1	1	-	-	-	-	-	-	-	8.42	0.86	0.98	1.05	1.09	-4.19	-1.68
x 2	-	1	-	-	-	-	-	-	-0.39	-0.57	-0.39	-0.33	-0.70	2.02	0.36
x 3	-	-	1	-	-	-	-	-	-5.08	-0.47	-0.52	-0.55	-0.69	3.55	1.38
x 4	-	-	-	1	-	-	-	-	-6.90	-0.68	-0.79	-0.81	-0.92	3.50	1.30
x 5	-	-	-	-	1	-	-	-	-7.62	-1.54	-1.57	-1.58	-1.72	8.70	2.91
x 6	-	-	-	-	-	1	-	-	-7.55	-1.26	-1.33	-1.23	-1.33	2.30	1.42
x 7	-	-	-	-	-	-	1	-	-0.504	-0.064	-0.073	-0.065	-0.075	-0.081	-0.095
x 8	-	-	-	-	-	-	-	1	-7.19	-0.473	-0.558	-0.671	-0.778	4.69	1.74
x 9	0.092	$\frac{-9.2}{x10-4}$	-0.117	-0.088	-0.029	-0.038	-0.394	-0.041	1	0.079	0.094	0.103	0.114	-0.512	-0.185
x 10	0.372	-0.052	-0.428	-0.346	-0.230	-0.247	-1.97	-0.244	3.13	1	0.91	0.85	0.90	-2.78	-0.630
x 11	0.458	-0.038	-0.511	-0.430	-0.254	-0.281	-2.42	-0.310	3.98	0.98	1	0.95	0.95	-2.99	-0.730
x 12	0.519	-0.835	-0.572	-0.464	-0.269	-0.275	-2.29	-0.394	4.62	0.97	1.01	1	0.98	-3.43	-0.900
x 13	0.499	-0.067	-0.656	-0.488	-0.272	-0.275	-2.42	-0.422	4.71	0.94	0.93	0.90	1	-3.39	-0.940
x 14	-0.077	0.008	0.130	0.075	0.055	0.019	0.106	0.103	-0.86	-0.11	-0.12	-0.13	-0.14	1	0.270
x 15	-0.310	0.014	0.534	0.305	0.155	0.079	0.783	0.346	-0.31	-0.27	-0.29	-0.33	-0.38	2.7	1

Variables defined in Table 6.1A

TABLE 6.11C W1: A COEFFICIENTS FOR BIVARIATE REGRESSION : REGULARLY SAMPLED DATA (LOG DATA EXCEPT SINE INDEX)

	x 1	x 2	x 3	x 4	x 5	x 6	x 7	x 8	x 9	x 10	x 11	x 12	x 13	x 14	x 15
x 1	0	-	-	-	-	-	-	-	0.019	9.72	10.18	10.64	11.51	84.44	1.26
x 2	-	0	-	-	-	-	-	-	0.997	61.73	40.82	37.66	111.95	0.081	0.640
x 3	-	-	0	-	-	-	-	-	4.2E4	38.82	47.38	54.56	81.33	0.006	0.030
x 4	-	-	-	0	-	-	-	-	1.5E5	47.89	63.46	69.99	95.13	0.027	0.058
x 5	-	-	-	-	0	-	-	-	1.3E10	1794	2178	2392	4150	1.7E-11	7.1E-5
x 6	-	-	-	-	-	0	-	-	4.1E5	135.7	168.6	150.0	198.5	0.281	0.069
x 7	-	-	-	-	-	-	0	-	1.11	15.20	16.91	17.80	19.96	16.56	0.90
x 8	-	-	-	-	-	-	-	0	2.3E16	168.1	288.8	570.2	1110	2.0E-10	6.3E-5
x 9	1.56	15.27	8.83	5.98	23.69	6.13	6.82	198.6	0	14.24	15.77	17.07	18.94	11.53	0.58
x 10	0.54	17.48	30.18	16.02	44.14	12.03	1667	411.3	1.0E-4	0	1.38	1.73	1.68	2.6E4	3.60
x 11	0.42	16.92	38.95	20.62	47.95	13.46	6480	500.8	8.7E-6	0.97	0	1.21	1.33	5.7E4	4.94
x 12	0.34	16.80	47.72	23.26	50.95	13.50	5389	643.9	1.2E-6	0.94	0.91	0	1.17	2.3E5	8.24
x 13	0.35	18.48	63.74	26.06	52.55	13.85	9449	722.1	5.9E-7	0.92	1.03	1.20	0	2.8E5	10.02
x 14	1.78	14.92	6.63	5.25	20.69	6.02	7.58	161.3	4.52	18.68	20.34	22.45	25.30	0	0.31
x 15	1.27	15.16	12.03	7.40	25.41	6.40	9.47	243.7	0.12	11.93	12.92	13.62	14.72	50.86	0

Variables defined in Table 6.1A

TABLE 6.12A W2: CORRELATION MATRIX FOR BIVARIATE REGRESSION : REGULARLY SAMPLED DATA (LOG DATA EXCEPT SINE INDEX)

	x 1	x 2	x 3	x 4	x 5	x 6	x 7	x 8	x 9	x 10	x 11	x 12	x 13	x 14	x 15
x 1	*	-	-	-	-	-	-	-	-0.16	0.38	0.37	0.34	0.29	0.13	0.31
x 2	-	*	-	-	-	-	-	-	-0.19	-0.24	-0.23	-0.26	-0.23	0.19	0.22
x 3	-	-	*	-	-	-	-	-	-0.72	-0.46	-0.53	-0.61	-0.66	0.62	0.84
x 4	-	-	-	*	-	-	-	-	-0.73	-0.49	-0.55	-0.61	-0.67	0.49	0.71
x 5	-	-	-	-	*	-	-	-	-0.43	-0.70	-0.68	-0.69	-0.70	0.41	0.39
x 6	-	-	-	-	-	*	-	-	-0.36	-0.15	-0.24	-0.25	-0.27	0.15	-0.38
x 7	-	-	-	-	-	-	*	-	-0.36	-0.29	-0.37	-0.37	-0.39	0.17	-0.39
x 8	-	-	-	-	-	-	-	*	-0.12	-0.09	-0.13	-0.11	-0.07	0.07	0.23
x 9	NS	NS	0.1	0.1	1.0	5.0	5.0	NS	*	0.48	0.56	0.60	0.65	-0.68	-0.70
x 10	5.0	NS	1.0	1.0	0.1	NS	5.0	NS	1.0	*	0.96	0.94	0.92	-0.56	0.28
x 11	5.0	NS	1.0	1.0	0.1	NS	5.0	NS	0.1	0.1	*	0.98	0.97	-0.56	-0.37
x 12	5.0	NS	0.1	0.1	0.1	NS	5.0	NS	0.1	0.1	0.1	*	0.99	-0.64	-0.44
x 13	5.0	NS	0.1	0.1	0.1	NS	5.0	NS	0.1	0.1	0.1	0.1	*	-0.66	-0.54
x 14	NS	NS	0.1	1.0	1.0	NS	NS	NS	0.1	0.1	1.0	0.1	0.1	*	0.57
x 15	5.0	NS	0.1	0.1	5.0	5.0	5.0	NS	0.1	0.1	1.0	1.0	1.0	0.1	*

Significance levels using a t test shown in bottom half of table. Constants as for Table 6.11.

Variables defined in Table 6.1A

TABLE 6.12B W2: B COEFFICIENTS FOR BIVARIATE REGRESSION : REGULARLY SAMPLED DATA (LOG DATA EXCEPT SINE INDEX)

	x 1	x 2	x 3	x 4	x 5	x 6	x 7	x 8	x 9	x 10	x 11	x 12	x 13	x 14	x 15
x 1	1	-	-	-	-	-	-	-	-1.94	0.860	0.841	0.761	0.621	1.57	0.771
x 2	-	1	-	-	-	-	-	-	-3.41	-0.779	-0.748	-0.830	-0.730	3.12	0.724
x 3	-	-	1	-	-	-	-	-	-3.37	-0.410	-0.467	-0.529	-0.559	2.84	0.944
x 4	-	-	-	1	-	-	-	-	-3.79	0.480	-0.540	-0.589	-0.628	2.50	0.832
x 5	-	-	-	-	1	-	-	-	-2.86	-0.879	-0.849	-0.855	-0.840	2.70	0.806
x 6	-	-	-	-	-	1	-	-	-5.08	-0.415	-0.619	-0.629	-0.677	2.02	-1.06
x 7	-	-	-	-	-	-	1	-	-0.414	-0.064	-0.079	-0.078	-0.081	0.198	-0.084
x 8	-	-	-	-	-	-	-	1	-0.283	-0.043	-0.056	-0.047	-0.033	0.163	0.098
x 9	-0.013	-0.011	-0.153	-0.139	-0.064	-0.027	-0.310	-0.049	1	0.091	0.105	0.110	0.116	-0.668	-0.145
x 10	0.166	-0.071	-0.523	-0.494	-0.551	-0.061	-1.35	-0.209	2.56	1	0.951	0.913	0.875	-2.90	-0.312
x 11	0.166	-0.070	-0.607	-0.567	-0.542	-0.093	-1.69	-0.280	3.020	0.968	1	0.968	0.935	-2.96	-0.408
x 12	0.155	-0.080	-0.707	-0.635	-0.561	-0.097	-1.73	-0.240	2.234	0.957	0.996	1	0.967	-3.398	-0.503
x 13	0.133	-0.074	-0.785	-0.712	-0.579	-0.109	-1.88	-0.177	3.588	0.963	1.010	1.016	1	-3.60	-0.622
x 14	0.091	0.011	0.133	0.095	0.062	-0.011	0.153	0.029	-0.691	-0.107	-0.107	-0.119	-0.120	1	0.121
x 15	0.122	0.067	0.739	0.607	0.190	-0.137	-1.76	0.530	-3.333	-0.255	-0.328	-0.392	-0.462	2.684	1

Variables defined in Table 6.1A

TABLE 6.12C W2: A COEFFICIENTS FOR BIVARIATE REGRESSION : REGULARLY SAMPLED DATA (LOG DATA EXCEPT SINE INDEX)

	x 1	x 2	x 3	x 4	x 5	x 6	x 7	x 8	x 9	x 10	x 11	x 12	x 13	x 14	x 15
x 1	0	-	-	-	-	-	-	-	3.758	8.050	8.944	10.085	11.76	7.47	0.361
x 2	-	0	-	-	-	-	-	-	2.1E+4	119	120	163	132	2.1E-3	0.247
x 3	-	-	0	-	-	-	-	-	1.2E+4	39.07	50.21	63.93	74.87	8.2E-3	0.046
x 4	-	-	-	0	-	-	-	-	4484	36.20	45.43	54.39	63.93	8.2E-2	0.095
x 5	-	-	-	-	0	-	-	-	1.5E+5	229	229	252	259	2.6E-3	0.049
x 6	-	-	-	-	-	0	-	-	3.0E+5	29.33	48.35	53.24	63.25	0.329	15.02
x 7	-	-	-	-	-	-	0	-	6.00	16.37	19.07	20.52	22.39	8.50	2.56
x 8	-	-	-	-	-	-	-	0	5.835	16.22	19.22	19.70	19.74	7.43	1.153
x 9	1.74	17.26	15.45	8.89	26.82	7.28	45.46	211	0	12.62	13.85	14.92	16.08	21.02	0.573
x 10	1.13	20.66	56.68	30.38	108	8.45	1283	355	1.863	0	1.250	1.48	1.77	29764	1.23
x 11	1.12	20.71	74.43	38.64	111	9.24	3690	437	4.24	0.988	0	1.17	1.39	46071	1.63
x 12	1.14	21.38	103	48.65	122	9.42	4960	401	$\frac{1.88}{x10^{-4}}$	0.946	0.936	0	1.18	$\frac{1.9}{x10^{5}}$	2.18
x 13	1.20	21.16	134	63.38	134	9.83	8055	342	$\frac{5.44}{x10^{-5}}$	0.864	0.834	0.897	0	4.30E+5	3.16
x 14	1.68	16.69	10.13	6.54	22.07	7.01	2646	191	9.39	17.54	19.33	21.61	23.39	0	0.391
x 15	1.86	16.47	22.04	12.10	28.31	7.86	124.2	146	0.178	11.10	11.71	12.15	12.59	87.22	0

Variables defined in Table 6.1A

TABLE 6.13A FLUME: CORRELATION MATRIX FOR BIVARIATE REGRESSION-REGULARLY SAMPLED DATA (LOG DATA EXCEPT SINE INDEX)

	x 1	x 2	x 3	x 4	x 5	x 6	x 7	x 8	x 9	x 10	x 11	x 12	x 13	x 14	x 15
x 1	*	-	-	-	-	-	-	-	-0.46	-0.09	-0.11	-0.10	-0.18	0.48	0.60
x 2	-	*	-	-	-	-	-	-	-0.39	-0.31	-0.33	-0.27	-0.26	0.18	0.22
x 3	-	-	*	-	-	-	-	-	-0.85	-0.10	-0.14	-0.74	-0.79	0.68	0.74
x 4	-	-	-	*	-	-	-	-	-0.72	-0.81	-0.87	-0.33	-0.30	0.69	0.70
x 5	-	-	-	-	*	-	-	-	-0.68	-0.74	-0.79	-0.36	-0.34	0.58	0.58
x 6	-	-	-	-	-	*	-	-	-0.05	0.71	0.75	-0.32	-0.38	-0.20	-0.53
x 7	-	-	-	-	-	-	*	-	-0.53	-0.59	-0.59	-0.21	-0.21	0.35	0.38
x 8	-	-	-	-	-	-	-	*	-0.55	-0.87	-0.93	-0.18	-0.14	0.58	0.57
x 9	1.0	5.0	0.1	0.1	0.1	NS	1.0	1.0	*	0.39	0.45	0.71	0.74	-0.78	-0.85
x 10	NS	5.0	NS	0.1	0.1	0.1	0.1	1.0	5.0	*	0.98	0.32	0.25	-0.53	-0.28
x 11	NS	5.0	NS	0.1	0.1	0.1	0.1	1.0	1.0	0.1	*	0.29	0.23	-0.57	-0.32
x 12	NS	NS	0.1	5.0	5.0	5.0	NS	NS	0.1	5.0	NS	*	0.99	-0.67	-0.60
x 13	NS	NS	0.1	5.0	5.0	5.0	NS	NS	0.1	NS	NS	0.1	*	-0.68	-0.66
x 14	1.0	NS	0.1	0.1	0.1	NS	5.0	1.0	0.1	1.0	1.0	0.1	0.1	*	0.86
x 15	0.1	NS	0.1	0.1	0.1	1.0	5.0	1.0	0.1	NS	NS	1.0	0.1	0.1	*

Significance levels using a t test are shown in bottom half of table. Constants as for Table 6.12.
Variables defined in Table 6.1A

TABLE 6.13B FLUME: B COEFFICIENTS FOR BIVARIATE REGRESSION : REGULARLY SAMPLED DATA (LOG DATA EXCEPT SINE INDEX)

	x 1	x 2	x 3	x 4	x 5	x 6	x 7	x 8	x 9	x 10	x 11	x 12	x 13	x 14	x 15
x 1	1	-	-	-	-	-	-	-	-3.68	-0.235	-0.345	-0.175	-0.319	4.54	1.72
x 2	-	1	-	-	-	-	-	-	-7.88	-2.09	-2.71	-1.16	-1.17	4.35	1.23
x 3	-	-	1	-	-	-	-	-	-4.75	-0.191	-0.323	-0.883	-0.911	4.53	1.43
x 4	-	-	-	1	-	-	-	-	-2.86	-1.08	-1.41	-0.276	-0.271	3.27	1.28
x 5	-	-	-	-	1	-	-	-	-9.15	-3.35	-4.37	-1.03	-1.01	9.33	3.67
x 6	-	-	-	-	-	1	-	-	-0.345	1.67	2.16	-0.475	-0.594	-1.65	-0.966
x 7	-	-	-	-	-	-	1	-	-1.33	-0.502	-0.605	-0.109	-0.118	1.03	0.306
x 8	-	-	-	-	-	-	-	1	-2.07	-1.11	-1.44	-0.144	-0.115	2.59	0.941
x 9	-0.059	-0.019	-0.152	-0.181	-0.030	-7.0E-3	-0.211	-0.143	1	0.131	0.183	0.150	0.164	-0.920	-0.309
x 10	-0.033	-0.045	-0.054	-0.605	-0.163	0.299	-0.703	-0.682	1.15	1	1.19	0.201	0.165	-1.84	-0.308
x 11	-0.033	-0.039	-0.062	-0.534	-0.143	0.262	-0.572	-0.595	1.091	0.803	1	0.152	0.122	-1.64	-0.283
x 12	-0.062	-0.063	-0.626	-0.389	-0.126	-0.214	-0.385	-0.222	3.34	0.506	0.565	1	1.03	-3.75	-1.031
x 13	-0.104	-0.059	-0.636	-0.353	-0.114	-0.247	-0.385	-0.163	3.37	0.383	0.422	0.952	1	-3.67	-1.085
x 14	0.052	7.5E-3	0.103	0.147	0.036	-0.024	0.116	0.127	-0.654	-0.148	-0.195	-0.120	-0.127	1	0.263
x 15	0.206	0.041	0.383	0.382	0.092	-0.294	0.460	0.350	-2.33	-0.263	-0.358	-0.350	-0.399	2.79	1

Variables defined in Table 6.1A

TABLE 6.13C FLUME: A COEFFICIENTS FOR BIVARIATE REGRESSION : REGULARLY SAMPLED DATA (LOG DATA EXCEPT SINE INDEX)

	x 1	x 2	x 3	x 4	x 5	x 6	x 7	x 8	x 9	x 10	x 11	x 12	x 13	x 14	x 15
x 1	0	-	-	-	-	-	-	-	22.98	16.26	20.18	17.82	20.98	1.17	0.279
x 2	-	0	-	-	-	-	-	-	4.4E+10	7155	5.4E+4	502	570	3.6E-5	0.043
x 3	-	-	0	-	-	-	-	-	3.0E+6	24.88	42.74	212	297	2.8E-5	0.011
x 4	-	-	-	0	-	-	-	-	1255	140	331	28.97	31.18	0.015	0.082
x 5	-	-	-	-	0	-	-	-	4.4E+13	9.6E+5	3.3E+7	496	502	6.5E-13	5.9E-6
x 6	-	-	-	-	-	0	-	-	6.12	0.436	0.181	43.62	60.89	465	12.84
x 7	-	-	-	-	-	-	0	-	840	120	218	25.70	29.02	0.187	0.185
x 8	-	-	-	-	-	-	-	0	2.7E+5	6546	4.6E+4	35.69	33.01	9.6E-6	7.8E-3
x 9	1.86	19.97	21.74	10.12	29.06	8.16	88.25	286	0	12.37	13.65	13.73	14.69	39.94	1.02
x 10	1.90	22.04	21.27	41.46	42.39	3.66	454	1499	0.139	0	0.705	9.48	11.33	1947	1.64
x 11	1.91	21.84	21.92	37.34	41.16	3.88	351	1303	0.138	1.49	0	10.55	12.44	1466	1.60
x 12	2.07	23.28	105	24.53	39.09	14.69	205	454	2.78E-4	3.49	3.45	0	0.997	5.1E+5	12.76
x 13	2.36	23.13	114	22.86	38.15	16.46	211	391	1.96E-4	4.76	4.98	1.06	0	5.5E+5	16.25
x 14	1.52	19.17	14.0	5.59	24.95	8.63	51.39	174	17.19	21.33	28.14	22.31	24.71	0	0.358
x 15	1.86	19.14	21.14	7.69	27.23	9.47	83.91	219	1040	13.11	14.85	14.44	15.44	36.02	0

Variables defined in Table 6.1A

TABLE 6.14A W4: CORRELATION MATRIX FOR BIVARIATE REGRESSION : REGULARLY SAMPLED DATA (LOG DATA EXCEPT SINE INDEX)

	x 1	x 2	x 3	x 4	x 5	x 6	x 7	x 8	x 9	x 10	x 11	x 12	x 13	x 14	x 15
x 1	*	-	-	-	-	-	-	-	0.08	0.21	0.15	0.26	0.09	0.04	0.20
x 2	-	*	-	-	-	-	-	-	-0.39	-0.28	-0.31	-0.36	-0.32	0.39	0.28
x 3	-	-	*	-	-	-	-	-	-0.61	-0.29	-0.29	-0.54	-0.34	0.77	0.82
x 4	-	-	-	*	-	-	-	-	-0.46	-0.32	-0.28	-0.55	-0.25	0.67	0.61
x 5	-	-	-	-	*	-	-	-	-0.53	-0.33	-0.27	-0.56	-0.27	0.78	0.78
x 6	-	-	-	-	-	*	-	-	-0.36	-0.26	-0.31	-0.32	-0.29	0.13	0.28
x 7	-	-	-	-	-	-	*	-	-0.58	-0.35	-0.51	-0.30	-0.56	-0.03	0.26
x 8	-	-	-	-	-	-	-	*	-0.67	-0.33	-0.57	-0.15	-0.71	-0.13	0.56
x 9	NS	5.0	0.1	1.0	1.0	5.0	0.1	0.1	*	0.51	0.69	0.56	0.79	-0.37	-0.22
x 10	NS	NS	5.0	5.0	5.0	NS	5.0	5.0	1.0	*	0.94	0.91	0.85	-0.43	-0.33
x 11	NS	5.0	5.0	NS	NS	5.0	1.0	0.1	0.1	0.1	*	0.87	0.97	-0.32	-0.38
x 12	NS	5.0	1.0	1.0	0.1	5.0	5.0	NS	0.1	0.1	0.1	*	0.79	-0.60	-0.15
x 13	NS	5.0	5.0	NS	NS	5.0	0.1	0.1	0.1	0.1	0.1	0.1	*	-0.31	-0.42
x 14	NS	5.0	0.1	0.1	0.1	NS	NS	NS	5.0	1.0	5.0	0.1	5.0	*	0.20
x 15	NS	NS	0.1	0.1	0.1	NS	NS	0.1	NS	5.0	5.0	NS	1.0	NS	*

Significance levels using a t test showin in bottom half of table. Constants as for Table 6.13.

Variables defined in Table 6.1A

TABLE 6.14B W4: B COEFFICIENTS FOR BIVARIATE REGRESSION : REGULARLY SAMPLED DATA (LOG DATA EXCEPT SINE INDEX)

	x 1	x 2	x 3	x 4	x 5	x 6	x 7	x 8	x 9	x 10	x 11	x 12	x 13	x 14	x 15
x 1	0	-	-	-	-	-	-	-	0.825	0.651	0.515	0.767	0.351	0.655	0.678
x 2	-	0	-	-	-	-	-	-	-3.96	-0.861	-1.05	-1.03	-1.16	6.10	1.61
x 3	-	-	0	-	-	-	-	-	-2.62	-0.382	-0.418	-0.660	-0.538	5.19	1.41
x 4	-	-	-	0	-	-	-	-	-2.90	-0.613	-0.590	-0.972	-0.564	6.48	1.35
x 5	-	-	-	-	0	-	-	-	-4.43	-0.829	-0.769	-1.322	-0.828	10.09	2.46
x 6	-	-	-	-	-	0	-	-	-5.95	-1.28	-1.70	-1.49	-1.74	3.40	1.53
x 7	-	-	-	-	-	-	0	-	-0.655	-0.121	-0.194	-0.096	-0.229	-0.050	0.165
x 8	-	-	-	-	-	-	-	0	-0.673	-0.329	-0.567	-0.150	-0.709	-0.134	0.560
x 9	7.6E-3	-0.038	-0.140	-0.074	-0.063	-0.022	-0.507	-0.269	0	0.154	0.232	0.159	0.287	-0.578	-0.135
x 10	0.065	-0.009	-0.221	-0.169	-0.128	-0.051	-1.018	-0.433	1.68	0	1.04	0.847	1.02	-2.19	-0.49
x 11	0.042	-0.089	-0.197	-0.132	-0.097	-0.055	-1.33	-0.674	2.05	0.844	0	0.730	1.04	-1.47	-0.492
x 12	0.088	-0.125	-0.441	-0.309	-0.235	-0.060	-0.928	-0.212	1.99	0.979	10.4	0	1.01	-3.30	-0.346
x 13	0.025	-0.085	-0.219	-0.109	-0.090	-0.049	-1.36	-0.783	2.19	0.717	0.891	0.616	0	-1.31	-0.522
x 14	0.003	0.025	0.116	0.069	0.060	5.3E-3	-0.016	-0.035	-0.242	-0.085	-0.069	-0.110	-0.072	0	0.093
x 15	0.058	0.050	0.473	0.274	0.246	0.051	0.414	0.605	-0.988	-0.331	-0.406	-0.202	-0.499	1.62	0

Variables defined in Table 6.1A

TABLE 6.14C W4: A COEFFICIENTS FOR BIVARIATE REGRESSION : REGULARLY SAMPLED DATA (LOG DATA EXCEPT SINE INDEX)

	x 1	x 2	x 3	x 4	x 5	x 6	x 7	x 8	x 9	x 10	x 11	x 12	x 13	x 14	x 15
x 1	0	-	-	-	-	-	-	-	0.376	8.73	10.69	9.52	14.02	12.70	1.26
x 2	-	0	-	-	-	-	-	-	8.3E+4	172	333	334	552	2.6E-7	8.2E-3
x 3	-	-	0	-	-	-	-	-	1821	42.32	52.85	116	90.08	2.8E-6	8.5E-3
x 4	-	-	-	0	-	-	-	-	629	54.99	58.43	148	64.98	5.6E-6	0.025
x 5	-	-	-	-	0	-	-	-	2.4E+6	224	206	1422	297	2.1E-14	1.4E-4
x 6	-	-	-	-	-	0	-	-	7.7E+4	164	418	294	536	0.024	0.028
x 7	-	-	-	-	-	-	0	-	6.91	20.61	30.08	22.05	40.44	23.18	0.717
x 8	-	-	-	-	-	-	-	0	6901	52.70	206	27.93	606	337	0.108
x 9	1.91	19.28	19.59	9.85	29.55	7.09	30.28	222	0	14.21	16.50	16.73	19.97	14.89	1.78
x 10	1.61	24.75	36.93	15.75	42.28	8.18	529	769	8.6E-3	0	1.03	1.74	1.26	5572	6.76
x 11	1.70	24.96	35.49	14.56	39.46	8.32	1363	1548	2.5E-3	1.36	0	2.17	1.06	1016	7.16
x 12	1.49	27.61	69.94	23.79	58.00	8.66	487	449	2.7E-3	0.902	0.867	0	1.09	1.68E+5	4.91
x 13	1.77	25.05	39.10	13.93	39.32	8.24	1856	2365	1.2E-3	1.70	1.13	2.66	0	826	8.47
x 14	1.88	18.24	14.81	8.31	25.46	7.04	39.92	278	1.31	17.03	18.26	21.59	21.70	0	1.44
x 15	1.83	19.63	26.15	11.85	34.53	7.37	34.07	170	1.20	16.39	19.29	17.72	24.15	6.86	0

Variables defined in Table 6.1A

TABLE 6.15A W5: CORRELATION MATRIX FOR BIVARIATE REGRESSION : REGULARLY SAMPLED DATA (LOG DATA EXCEPT SINE INDEX)

	x 1	x 2	x 3	x 4	x 5	x 6	x 7	x 8	x 9	x 10	x 11	x 12	x 13	x 14	x 15
x 1	*	-	-	-	-	-	-	-	0.3	0.3	0.36	0.36	0.52	-0.49	-0.69
x 2	-	*	-	-	-	-	-	-	0.16	0.13	0.22	0.25	0.38	-0.48	-0.80
x 3	-	-	*	-	-	-	-	-	0.03	0.07	0.14	0.15	0.31	-0.30	0.67
x 4	-	-	-	*	-	-	-	-	0.23	0.02	0.13	0.16	0.29	-0.34	-0.69
x 5	-	-	-	-	*	-	-	-	-0.03	-0.08	-0.02	-0.04	0.40	-0.45	-0.80
x 6	-	-	-	-	-	*	-	-	0.78	0.10	0.30	0.40	0.30	-0.42	-0.66
x 7	-	-	-	-	-	-	*	-	-0.25	-0.02	-0.01	-0.01	0.16	-0.19	0.71
x 8	-	-	-	-	-	-	-	*	-0.24	0.21	0.08	0.03	0.45	-0.45	0.81
x 9	5.0	NS	NS	NS	NS	0.1	NS	NS	*	0.03	0.22	0.29	0.17	-0.20	0.08
x 10	5.0	NS	NS	NS	NS	NS	NS	NS	NS	*	0.81	0.65	0.83	-0.55	0.20
x 11	5.0	NS	NS	NS	NS	5.0	NS	NS	NS	0.1	*	0.96	0.58	-0.48	0.08
x 12	5.0	NS	NS	NS	NS	1.0	NS	NS	5.0	0.1	0.1	*	0.39	-0.45	0.03
x 13	1.0	5.0	5.0	5.0	1.0	5.0	NS	1.0	NS	0.1	0.1	5.0	*	-0.67	0.48
x 14	1.0	1.0	5.0	5.0	1.0	1.0	NS	1.0	NS	0.1	1.0	1.0	0.1	*	-0.50
x 15	0.1	0.1	0.1	0.1	0.1	0.1	0.1	0.1	NS	NS	NS	NS	1.0	0.1	*

Significance levels using a t test shown in bottom half of table. Constants added: x 1 - x 13 + 10; x 14 + 1.0

Variables defined in Table 6.1A

TABLE 6.15B W5: B COEFFICIENTS FOR BIVARIATE REGRESSION : REGULARLY SAMPLED DATA (LOG DATA EXCEPT SINE INDEX)

	x 1	x 2	x 3	x 4	x 5	x 6	x 7	x 8	x 9	x 10	x 11	x 12	x 13	x 14	x 15
x 1	1	-	-	-	-	-	-	-	3.69	1.42	2.20	2.88	2.38	-12.06	-5.10
x 2	-	1	-	-	-	-	-	-	0.277	0.086	0.186	0.278	0.240	-1.64	0.717
x 3	-	-	1	-	-	-	-	-	0.039	0.040	0.102	0.140	0.163	-0.848	0.437
x 4	-	-	-	1	-	-	-	-	0.490	0.020	0.140	0.229	0.235	-1.44	-0.73
x 5	-	-	-	-	1	-	-	-	-0.044	-0.041	-0.014	-0.034	0.201	-1.22	-0.50
x 6	-	-	-	-	-	1	-	-	1.71	0.084	0.323	0.572	0.240	-1.84	-1.20
x 7	-	-	-	-	-	-	1	-	-0.218	-5.1E-3	-6.0E-3	-5.5E-3	0.052	-0.324	0.261
x 8	-	-	-	-	-	-	-	1	-0.130	0.044	0.021	0.012	0.090	-0.487	0.200
x 9	0.024	-0.096	-0.019	-0.105	-0.024	-0.351	-0.292	-0.430	1	0.012	0.107	0.109	0.064	-0.400	-0.126
x 10	0.063	0.204	0.133	0.029	0.151	0.117	-0.047	1.00	0.080	1	1.053	1.104	0.798	-2.867	-0.547
x 111	0.058	0.261	0.199	0.121	-0.031	0.270	-0.033	0.280	0.438	0.627	1	1.258	0.432	-1.927	-0.378
x 12	0.044	0.227	0.157	0.115	-0.043	0.277	-0.018	0.096	0.447	0.381	0.730	1	0.221	-1.35	-0.280
x 13	0.113	0.609	0.574	0.368	0.801	0.362	0.512	2.19	0.471	0.857	0.780	0.689	1	-3.59	-0.961
x 14	-0.020	-0.145	-0.104	-0.079	-0.169	-0.097	-0.112	-0.412	-0.102	-0.107	-0.121	-0.146	-0.124	1	0.245
x 15	-0.092	-0.899	1.041	-0.646	-1.27	-0.365	1.91	3.27	-0.352	-0.223	-0.260	-0.372	-0.367	2.68	1

Variables defined in Table 6.1A

TABLE 6.15C W5: A COEFFICIENTS FOR BIVARIATE REGRESSION - REGULARLY SAMPLED DATA (LOG DATA EXCEPT SINE INDEX)

	x 1	x 2	x 3	x 4	x 5	x 6	x 7	x 8	x 9	x 10	x 11	x 12	x 13	x 14	x 15
x 1	0	-	-	-	-	-	-	-	1.8E-3	0.401	0.069	0.015	0.050	9.5E+13	1.5E+5
x 2	-	0	-	-	-	-	-	-	5.64	9.50	7.86	6.58	7.30	3812	6.21
x 3	-	-	0	-	-	-	-	-	12.03	10.98	10.23	10.18	9.27	314	0.409
x 4	-	-	-	0	-	-	-	-	3.19	11.80	9.41	8.15	7.84	1432	5.32
x 5	-	-	-	-	0	-	-	-	15.84	10.93	14.93	17.96	8.03	1175	3.16
x 6	-	-	-	-	-	0	-	-	0.112	9.91	5.74	3.22	8.02	3466	27.24
x 7	-	-	-	-	-	-	0	-	30.92	12.77	14.57	16.39	12.97	56.63	0.65
x 8	-	-	-	-	-	-	-	0	25.54	10.13	12.89	15.14	10.21	205	0.651
x 9	10.57	19.20	24.82	14.80	30.41	6.63	91.33	374	0	12.15	10.15	9.78	13.32	56.38	0.923
x 10	9.60	14.71	18.64	18.07	19.51	12.35	47.81	963	11.17	0	0.994	0.985	2.09	2.8E+4	2.65
x 11	9.65	12.32	15.39	14.10	31.04	8.11	46.34	57.70	4.28	2.37	0	0.566	5.00	3304	1.82
x 12	9.96	13.12	16.79	14 14	32.20	7.69	44.57	93.12	3.95	4.35	1.88	0	8.51	846	1.44
x 13	8.25	4.59	5.35	7.05	3.14	6.12	10.35	0.289	3.74	1.18	1.66	2.40	0	3.9E+5	9.40
x 14	11.94	38.03	35.62	24.62	47.37	22.16	59.24	415	18.57	17.25	20.45	24.86	22.87	0	0.320
x 15	10.84	16.14	15.04	14.11	14.79	16.24	14.97	21.48	11.85	11.43	12.80	4.02	13.56	59.34	0

Variables defined in Table 6.1A

$$r_{01.2} = \frac{r_{01} - (r_{02})\,(r_{12})}{(1 - r_{02}^{2})^{\frac{1}{2}}\,(1 - r_{12}^{2})^{\frac{1}{2}}} \qquad (6.9)$$

where r_{01} = correlation coefficient between Y and X_1
r_{02} = correlation coefficient between Y and X_2 etc

III. Thirdly, select the largest of these partial correlation coefficients and add the relevant independent variable to the multiple regression equation. The latter now includes two independent variables.

IV. Fourthly, compute the second-order partial correlation coefficients, $r_{02.13}$ etc., from an extension of equation (6.9). Again select the highest and include the independent variable in the regression.

The procedure continues in this way until all the independent variables are included. Although collinearity is possibly not a serious problem, where a correlation coefficient between two independent variables exceeds 0.80 the one less correlated with the dependent variable was excluded from the stepwise procedure (Huang, 1970).

Multiple regression equations were fitted by least squares using the program MULTREG 2 (Appendix 2). The coefficients for each stage of the procedure are shown in Tables 6.16 - 6.20, together with the % variance explained by each equation (R^2 %). A variance ratio test was used to determine whether the additional variance explained by a new variable contributed significantly to the overall value of R^2 % (Brownlee, 1965). F was computed from:

$$\frac{SSR_{123} - SSR_{12}}{RMS_{123}} \qquad (6.10)$$

where SSR = sum of squares of the regression
RMS = residual mean squares
1,2,3, = independent variables included

and the 5 % significance level set as the limit for acceptance or rejection of an additional independent variable.

There are several points to note from the results.

(i) Discharge is not always the variable most highly correlated with concentration - seasonal or soil moisture conditions may control solute variation (this also emerged from the correlation matrices).

(ii) It is rarely worthwhile including more than two independent variables in a multiple regression model for predicting solute concentration, because the extra variables do not significantly improve the variance explanation. A comparison was made between actual and predicted solute concentrations for the best and worst multiple regression models from W4 and W5 (chosen by R^2 %). These are shown in Figure 6.18. The worst predictive model is for K^+ at W4.

$$K^+ \text{ conc.(mg/l)} = \text{EXP}\,(0.337 + 0.095 \log_e(\text{API } 5{+}10) + 0.086\ \text{SI}) \quad (R^2 = 12.1\ \%) \tag{6.11}$$

The best predictive model is also at W4:

$$\text{SC } (\mu\text{mhos}) = \text{EXP}\,(10.69 + 0.071 \log_e(\text{API } 60{+}10) - 2.222 \log_e(Q + 10)) \quad (R^2 = 96.0\ \%) \tag{6.12}$$

The bivariate model predictions are also plotted in Figure 6.18. These are:

$$K^+ \text{ conc. (mg/l)} = 1.91\ Q^{0.0076} \quad (R^2 = 4.4\ \%) \tag{6.13}$$

$$\text{and SC (umhos)} = 222\ Q^{-0.269} \quad (R^2 = 50.4\ \%) \tag{6.14}$$

The multiple regression model accurately predicts specific conductivity while the power function slightly under-estimates most of the time and grossly over-estimates during the months of June, July and August. The API and discharge appear to describe total dissolved solids concentration more accurately during a general stream recession phase than does stream discharge alone. Standard errors of the

estimates for each model underline the advantages of using the multiple regression, i.e. 0.098 for multiple regression and 0.16 for bivariate regression.

Neither the multiple (using API 5 and the Sine Index) nor the bivariate regression (using discharge) are capable of accurately predicting the fluctuation in K^+ concentration from April - August 1975 nor the increase in concentration during May and June 1977. The standard errors are similar for multiple and bivariate regressions (0.11 and 0.14 respectively).

(iii) Thirdly, in several cases the signs of the b coefficients change as a new independent variable is included, suggesting that significant collinearity may be present. Although other coefficients are uni-directional some exhibit large changes after their initial inclusion, as much as 40 % in some cases. These problems, together with possible heteroscedasticity noted earlier limit the use of the b coefficients for interpretation.

A summary of the ranges and means of variance explanation is given for each solute in Tables 6.21 A and B.

Although multiple regression gives improved levels of variance explanation over bivariate regression most are still low for a good predictive model, i.e. $R^2 > 90$ %. One possible cause of low variance explanation is omission of significant independent variables from the multiple regression procedure. Since the RSD includes late winter high flows in addition to flow recession phases, it seems likely that independent variables pertinent to the former (e.g. flood intensity) might improve explanation. This is difficult for weekly sampling times because much of the detailed solute variation is missing and an appraisal of the significant solute controls is not possible. (c.f. Walling, 1975).

6.4 SUMMARY AND CONCLUSIONS

(i) There is a spatial variation of solute levels within West Walk, shown by subcatchment means of the regularly sampled data. This spatial variation has developed under the influence of soil and

TABLE 6.16 W1 MULTIPLE REGRESSION FOR REGULARLY SAMPLED DATA
(LOG DATA EXCEPT SINE INDEX)

Discharge (x 9) in l/sec; API 5 - 60 (x 10 - x 13) in mm;
Sine Index (x 15); Concentration in mg/l

6.16 A : W1 POTASSIUM CONCENTRATION

	A	B1	B2	B3	B4	R^2 %	SigR %	F *	SigF %
x 9	0.445	0.092	-	-	-	77.4	0.1	-	-
x12+10	-0.053	0.075	0.175	-	-	81.1	0.1	11.35	0.1
x14+1	-0.066	0.067	0.171	-0.044	-	81.6	0.1	0.67	NS
x 15	Collinear : excluded								

6.16 B : W1 SODIUM CONCENTRATION

	A	B1	B2	B3	B4	R^2 %	SigR %	F	SigF %
x13+10	4.16	-0.067	-	-	-	4.8	NS	-	-
x 9	3.46	-0.079	0.009	-	-	8.4	NS	3.76	5.0
x14+1	3.45	-0.075	0.009	0.002	-	8.5	NS	1.2	NS
x 15	Collinear : excluded								

6.16 C : W1 CALCIUM CONCENTRATION

	A	B1	B2	B3	B4	R^2 %	SigR %	F	SigF %
x 15	2.49	0.530	-	-	-	72.3	0.1	-	-
x 9	2.39	0.390	-0.045	-	-	76.6	0.1	5.69	1.0
x13+10	2.88	0.378	-0.028	-0.167	-	77.9	0.1	1.28	0.1
x 14	Collinear : excluded								

6.16 D : W1 MAGNESIUM CONCENTRATION

	A	B1	B2	B3	B4	R^2 %	SigR %	F	SigF %
x 9	1.79	-0.088	-	-	-	60.8	0.1	-	-
x13+10	2.25	-0.070	-0.158	-	-	63.0	0.1	12.71	0.1
x 15	2.42	-0.071	-0.206	-0.065	-	64.5	0.1	1.26	NS
x 14	Collinear : excluded								

* for inclusion of independent variable

Variables defined in Table 6.1A

6.16 E : W1 CHLORIDE CONCENTRATION

	A	B1	B2	B3	B4	R^2 %	SigR %	F	SigF %
x14+1	3.030	0.055	-	-	-	49.0	0.1	-	-
x13+10	3.533	0.034	-0.156	-	-	56.6	0.1	20.17	0.1
x 9	3.674	0.040	-0.205	-0.015	-	59.1	0.1	1.7	NS
x 15	Collinear : excluded								

6.16 F : W1 pH VALUES

	A	B1	B2	B3	B4	R^2 %	SigR %	F	SigF %
x11+10	2.6	-0.281	-	-	-	37.2	0.1	-	-
x 9	2.393	-0.210	-0.018	-	-	41.5	0.1	2.18	NS
x 15	2.402	-0.217	-0.075	-0.037	-	42.6	0.1	0.63	NS
x14+1	Collinear : excluded								

6.16 G : W1 BICARBONATE CONCENTRATION

	A	B1	B2	B3	B4	R^2 %	SigR %	F	SigF %
x 9	1.92	-0.394	-	-	-	20.3	1.0	-	-
x11+10	5.670	-0.267	-1.360	-	-	23.4	1.0	1.25	NS
x 15	5.845	-0.317	-1.434	-0.274	-	23.8	1.0	0.18	NS
x14+1	Collinear : excluded								

6.16 H : W1 SC, µmhos

	A	B1	B2	B3	B4	R^2 %	SigR %	F	SigF %
x 9	5.29	-0.041	-	-	-	67.2	0.1	-	-
x13+10	5.373	-0.063	0.161	-	-	73.2	0.1	6.86	1.0
x 15	5.139	-0.071	0.168	0.081	-	73.8	0.1	0.63	NS
x14+1	Collinear : excluded								

Variables defined in Table 6.1A

TABLE 6.17 W2 MULTIPLE REGRESSION FOR REGULARLY SAMPLED DATA
(LOG DATA EXCEPT SINE INDEX)

6.17 A : W2 POTASSIUM CONCENTRATION

	A	B1	B2	B3	B4	R^2 %	SigR %	F	SigF %
x10+10	0.126	0.166	-	-	-	14.4	5.0	-	-
x 15	0.090	0.222	0.179	-	-	32.8	1.0	8.5	0.1
x 9	-0.012	0.251	0.127	-0.018	-	34.8	1.0	1.58	NS
x14+1	-0.192	0.289	0.103	-0.009	0.023	36.2	1.0	0.88	NS

6.17 B : W2 SODIUM CONCENTRATION

	A	B1	B2	B3	B4	R^2 %	SigR %	F	SigF %
x12+10	3.063	-0.080	-	-	-	6.8	NS	-	-
x 15	3.012	-0.076	0.063	-	-	10.86	NS	1.41	NS
x 9	2.977	-0.063	0.063	-0.004	-	11.17	NS	0.64	NS
x14+1	3.071	-0.089	0.092	-0.011	-0.014	13.08	NS	0.10	NS

6.17 C : W2 CALCIUM CONCENTRATION

	A	B1	B2	B3	B4	R^2 %	SigR %	F	SigF %
x 15	3.093	0.739	-	-	-	70.6	0.1	-	-
x13+10	3.940	0.395	-0.177	-	-	78.3	0.1	10.89	0.1
x 9	3.862	0.363	-0.155	-0.132	-	78.6	0.1	0.5	0.1
x 14	4.020	0.390	-0.188	-0.016	-0.019	79.4	0.1	0.46	0.1

6.17 D : W2 MAGNESIUM CONCENTRATION

	A	B1	B2	B3	B4	R^2 %	SigR %	F	SigF %
x 9	2.186	-0.139	-	-	-	53.3	0.1	-	-
x 15	2.358	-0.084	0.330	-	-	59.50	0.1	4.75	5.0
x13+10	3.201	-0.056	0.281	-0.312	-	64.36	0.1	4.11	5.0
x14+1	3.689	-0.071	0.348	-0.415	-0.056	67.86	0.1	3.18	5.0

Variables defined in Table 6.1A

6.17 E : W2 CHLORIDE CONCENTRATION

	A	B1	B2	B3	B4	R^2 %	SigR %	F	SigF %
x10+10	4.682	-0.551	-	-	-	49.0	0.1	-	-
x 9	4.571	-0.506	-0.018	-	-	49.5	0.1	0.33	NS
x14+1	4.631	-0.579	-0.022	-0.009	-	49.7	0.1	0.07	NS
x 15	4.942	-0.571	0.001	-0.049	0.185	51.8	0.1	0.95	NS

6.17 F : W2 pH VALUES

	A	B1	B2	B3	B4	R^2 %	SigR %	F	SigF %
x 15	2.061	-0.137	-	-	-	14.4	5.0	-	-
x 9	2.036	-0.089	-0.015	-	-	16.8	5.0	0.9	NS
x14+1	2.090	-0.097	0.024	-0.016	-	19.4	5.0	0.96	NS
x13+10	2.237	-0.092	-0.021	-0.197	-0.050	20.1	5.0	0.27	NS

6.17 G : W2 BICARBONATE CONCENTRATION

	A	B1	B2	B3	B4	R^2 %	SigR %	F	SigF %
x13+10	8.995	-1.880	-	-	-	15.2	5.0	-	-
x 9	7.45	-1.315	-0.158	-	-	17.19	5.0	0.74	NS
x 15	7.656	-1.157	-0.053	-1.083	-	20.70	5.0	1.3	NS
x14+1	9.659	-1.642	-0.160	-1.003	-0.231	23.84	5.0	1.19	NS

6.17 H : W2 SC µmhos

	A	B1	B2	B3	B4	R^2 %	SigR %	F	SigF %
x 15	4.984	0.530	-	-	-	5.3	NS	-	-
x11+10	5.754	0.536	-0.291	-	-	6.90	NS	0.53	NS
x 9	5.393	0.563	-0.158	-0.044	-	7.64	NS	0.25	NS
x 14	5.997	0.776	-0.306	-0.111	-0.117	10.51	NS	0.89	NS

Variables defined in Table 6.1A

TABLE 6.18 FLUME MULTIPLE REGRESSION FOR REGULARLY SAMPLED DATA
(LOG DATA EXCEPT FOR SINE INDEX)

6.18 A FLUME POTASSIUM CONCENTRATIONS

	A	B1	B2	B3	B4	R^2 %	SigR %	F	SigF %
x 9	0.62	-0.059	-	-	-	21.2	5.0	-	-
x13+10	2.391	-0.015	0.032	-	-	28.94	1.0	3.28	5.0
x14+1	2.334	-0.011	0.044	0.007	-	35.74	1.0	3.05	5.0
x 15	Collinear : excluded								

6.18 B FLUME SODIUM CONCENTRATION

	A	B1	B2	B3	B4	R^2 %	SigR %	F	SigF %
x 9	2.994	-0.019	-	-	-	15.2	5.0	-	-
x14+1	3.442	-0.240	-0.117	-	-	23.7	1.0	3.36	5.0
x11+10	3.529	-0.234	-0.163	-0.027	-	30.57	1.0	8.63	0.1
x 15	Collinear : excluded								

6.18 C FLUME CALCIUM CONCENTRATION

	A	B1	B2	B3	B4	R^2 %	SigR %	F	SigF %
x 9	3.079	-0.152	-	-	-	72.3	0.1	-	-
x13+10	3.880	-0.102	-0.297	-	-	76.8	0.1	5.86	1.0
x14+1	3.870	-0.101	-0.293	0.002	-	76.8	0.1	0.01	NS
x 15	Collinear : excluded								

6.18 D FLUME MAGNESIUM CONCENTRATION

	A	B1	B2	B3	B4	R^2 %	SigR %	F	SigF %
x11+10	3.62	-0.534	-	-	-	75.7	0.1	-	-
x 9	3.424	-0.423	-0.103	-	-	89.1	0.1	35.9	0.1
x 14	3.435	-0.425	-0.104	-0.002	-	89.1	0.1	0.01	NS
x 15	Collinear : excluded								

Variables defined in Table 6.1A

6.18 E FLUME CHLORIDE CONCENTRATION

	A	B1	B2	B3	B4	R^2 %	SigR %	F	SigF %
x11+10	3.118	0.143	-	-	-	62.4	0.1	-	-
x 9	3.663	-0.112	-0.029	-	-	75.4	0.1	15.88	0.1
x14+1	3.717	-0.120	-0.036	-0.089	-	76.2	0.1	0.99	NS
x 15	Collinear : excluded								

6.18 F FLUME pH VALUES

	A	B1	B2	B3	B4	R^2 %	SigR %	F	SigF %
x11+10	1.356	0.262	-	-	-	56.3	0.1	-	-
x 9	2.392	0.196	0.036	-	-	78.1	0.1	29.8	0.1
x 14	2.397	0.195	-0.037	-0.008	-	78.1	0.1	<0.1	NS
x 15	Collinear : excluded								

6.18 G FLUME BICARBONATE CONCENTRATIONS

	A	B1	B2	B3	B4	R^2 %	SigR %	F	SigF %
x11+10	5.861	-0.572	-	-	-	34.8	0.1	-	-
x 9	5.564	-0.419	-0.137	-	-	43.3	0.1	4.47	5.0
x 14	6.163	-0.412	-0.225	-0.129	-	50.2	0.1	4.01	1.0
x 15	Collinear : excluded								

6.18 H FLUME SC umhos

	A	B1	B2	B3	B4	R^2 %	SigR %	F	SigF %
x1+10	7.172	-0.595	-	-	-	86.5	1.0	-	-
x14+1	7.024	-0.560	0.023	-	-	86.8	1.0	3.44	5.0
x 9	7.117	-0.557	0.001	-0.037	-	86.9	1.0	1.89	NS
x 15	Collinear : excluded								

Variables defined in Table 6.1A

TABLE 6.19 W4 MULTIPLE REGRESSION FOR REGULARLY SAMPLED DATA
(LOG DATA EXCEPT FOR SINE INDEX)

6.19 A W4 POTASSIUM CONCENTRATION

	A	B1	B2	B3	B4	R^2 %	SigR %	F	SigF %
x10+10	0.476	0.065	-	-	-	4.4	NS	-	-
x 15	0.337	0.095	0.086	-	-	12.1	5.0	7.4	1.0
x 9	0.568	0.110	0.060	-0.104	-	14.8	5.0	1.5	NS
x14+1	0.567	0.151	0.041	-0.162	0.016	19.1	5.0	0.98	NS

6.19 B W4 SODIUM CONCENTRATION

	A	B1	B2	B3	B4	R^2 %	SigR %	F	SigF %
x 9	2.904	0.025	-	-	-	15.2	5.0	-	-
x14+1	3.17	-0.112	0.026	-	-	19.4	5.0	14.95	0.1
x 15	3.82	-0.248	0.057	-0.126	-	33.0	0.1	6.13	0.1
x12+10	3.806	-0.260	+0.059	-0.131	0.013	33.2	1.0	0.07	NS

6.19 C W4 CALCIUM CONCENTRATION

	A	B1	B2	B3	B4	R^2 %	SigR %	F	SigF %
x 15	3.26	0.473	-	-	-	67.2	0.1	-	-
x14+1	3.04	0.317	0.051	-	-	71.3	0.1	11.32	0.1
x 9	3.10	0.310	0.053	-0.028	-	71.3	0.1	0.41	NS
x12+10	3.24	0.313	0.044	0.003	0.070	71.7	0.1	0.05	NS

6.19 D W4 MAGNESIUM CONCENTRATION

	A	B1	B2	B3	B4	R^2 %	SigR %	F	SigF %
x14+1	2.117	0.069	-	-	-	44.9	0.1	-	-
x 15	2.24	0.049	0.121	-	-	48.1	0.1	11.26	0.1
x12+10	2.61	0.036	-.116	-0.122	-	51.5	0.1	1.84	NS
x 9	2.44	0.030	0.124	-0.157	0.121	52.8	0.1	1.03	NS

Variables defined in Table 6.1A

6.19 E W4 CHLORIDE CONCENTRATION

	A	B1	B2	B3	B4	R^2 %	SigR %	F	SigF %
x 15	3.542	0.246	-	-	-	60.8	0.1	-	-
x14+1	3.390	0.141	0.034	-	-	68.9	0.1	77.6	0.1
x12+10	3.540	0.139	0.029	-0.050	-	69.9	0.1	0.09	NS
x 9	3.420	0.150	0.023	-0.073	-0.083	71.2	0.1	0.01	NS

6.19 F W4 pH VALUES

	A	B1	B2	B3	B4	R^2 %	SigR %	F	SigF %
x 9	1.959	-0.022	-	-	-	13.00	5.0	-	-
x12+10	2.209	-0.025	-0.066	-	-	13.90	5.0	8.74	0.1
x 15	2.203	-0.035	-0.047	0.036	-	13.93	5.0	1.10	NS
x14+1	2.284	-0.020	-0.074	0.059	-0.011	14.20	5.0	1.10	NS

6.19 G W4 BICARBONATE CONCENTRATION

	A	B1	B2	B3	B4	R^2 %	SigR %	F	SigF %
x 9	3.411	-0.507	-	-	-	33.6	0.1	-	-
x13+10	9.890	-1.802	-0.663	-	-	37.3	0.1	10.22	0.1
x 15	10.40	-1.79	-0.832	-0.177	-	38.1	0.1	0.39	NS
x14+1	10.13	-1.60	-0.875	-0.104	-0.029	38.2	0.1	0.02	NS

6.19 H W4 SC μmhos

	A	B1	B2	B3	B4	R^2 %	SigR %	F	SigF %
x13+10	7.769	-0.783	-	-	-	50.4	0.1	-	-
x 9	10.69	0.071	-2.222	-	-	96.0	0.1	191.3	0.1
x 15	10.49	0.088	-2.177	0.063	-	92.6	0.1	1.92	NS
x 14	10.39	0.047	-2.078	0.089	0.012	96.3	0.1	0.74	NS

Variables defined in Table 6.1A

TABLE 6.20 W5 MULTIPLE REGRESSION FOR REGULARLY SAMPLED DATA
(LOG DATA EXCEPT SINE INDEX)

6.20 A W5 POTASSIUM CONCENTRATION (K^+ + 10.0)

	A	B1	B2	B3	B4	R^2 %	SigR %	F	SigF %
x 15	2.383	-0.092	-	-	-	47.6	0.1	-	-
x14+1	2.351	-0.113	0.0079	-	-	48.3	0.1	12.45	0.1
x12+10	2.252	-0.119	0.013	0.029	-	52.6	0.1	2.74	NS
x9+10	2.239	-0.116	0.013	0.025	0 0095	54.0	0.1	0.82	NS

6.20 B W5 SODIUM CONCENTRATION (Na^+ + 10.0)

	A	B1	B2	B3	B4	R^2 %	SigR %	F	SigF %
x 15	2.781	-0.899	-	-	-	64.0	0.1	-	-
x14+1	2.558	-1.040	0.052	-	-	65.9	0.1	12.80	0.1
x13+10	2.812	-0.051	0.044	-0.084	-	66.1	0.1	1.0	NS
x9+10	2.657	-1.063	0.051	-0.100	0.065	67.2	0.1	0.14	NS

6.20 C W5 CALCIUM CONCENTRATION (Ca^{2+} + 10.0)

	A	B1	B2	B3	B4	R^2 %	SigR %	F	SigF %
x 15	2.711	1.041	-	-	-	44.9	0.1	-	-
x13+10	2.837	1.061	-0.050	-	-	45.5	0.1	12.21	0.1
x14+1	2.617	1.079	0.0064	0.019	-	45.6	0.1	0.53	NS
x9+10	2.455	1.123	-0.021	0.028	0.072	46.6	0.1	0.08	NS

6.20 D W5 MAGNESIUM CONCENTRATION (Mg^{2+} + 10.0)

	A	B1	B2	B3	B4	R^2 %	SigR %	F	SigF %
x 15	2.647	-0.646	-	-	-	47.6	0.1	—	-
x14+1	2.467	-0.755	0.042	-	-	49.1	0.1	12.10	0.1
x9+10	2.098	-0.792	0.060	0.114	-	54.9	0.1	3.83	5.0
x13+10	2.352	-0.806	0.051	0.116	-0.087	55.1	0.1	0.17	NS

Variables defined in Table 6.1A

6.20 E W5 CHLORIDE CONCENTRATION (Cl^- + 10.0)

	A	B1	B2	B3	B4	R^2 %	SigR %	F	SigF %
x 15	2.694	-1.270	-	-	-	63.0	0.1	-	-
x14+1	2.728	-1.249	-0.008	-	-	63.2	0.1	14.2	0.1
x13+10	2.848	-1.255	-0.012	-0.040	-	63.2	0.1	0.02	NS
x9+10	2.856	-1.253	-0.013	-0.039	-0.004	63.2	0.1	0.002	NS

6.20 F W5 pH VALUES (pH + 10.0)

	A	B1	B2	B3	B4	R^2 %	SigR %	F	SigF %
x9+10	1.892	0.351	-	-	-	60.8	0.1	-	-
x 15	2.093	0.273	-0.222	-	-	73.3	0.1	15.47	0.1
x14+1	1.815	0.207	-0.566	0.140	-	77.5	0.1	5.68	1.0
x13+10	1.720	0.204	0.558	0.142	0.035	77.7	0.1	0.24	NS

6.20 G W5 BICARBONATE CONCENTRATION (HCO_3 + 10.0)

	A	B1	B2	B3	B4	R^2 %	SigR %	F	SigF %
x 15	2.706	1.91	-	-	-	50.4	0.1	-	-
x9+10	3.16	1.85	-0.159	-	-	51.6	0.1	12.4	0.1
x14+1	3.01	1.90	-0.144	0.028	-	51.8	0.1	0.81	NS
x13+10	4.45	2.0	-0.126	-0.025	-0.503	52.1	0.1	0.11	NS

6.20 H W5 SC μmhos (SC + 10.0)

	A	B1	B2	B3	B4	R^2 %	SigR %	F	SigF %
x 15	3.067	3.27	-	-	-	65.6	0.1	-	-
x14+1	3.29	3.15	-0.055	-	-	65.7	0.1	0.05	NS
x9+10	4.543	2.954	-0.115	-0.369	-	69.4	0.1	3.69	5.0
x13+10	3.340	2.879	-0.073	-0.381	0.417	69.8	0.1	0.35	NS

Variables defined in Table 6.1A

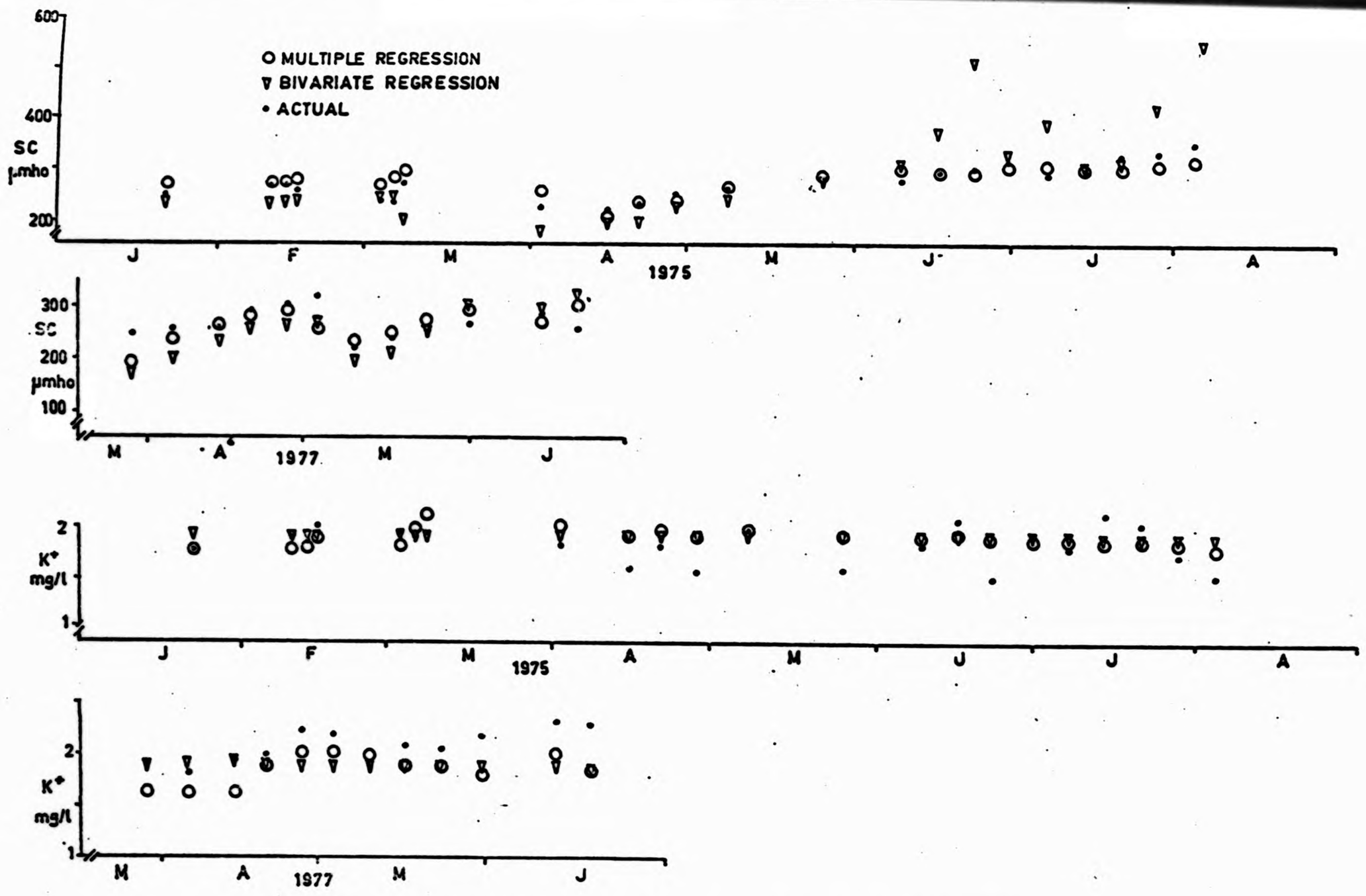

FIGURE 6.18: COMPARISON BETWEEN ACTUAL AND PREDICTED POTASSIUM CONCENTRATIONS AND SPECIFIC CONDUCTANCE USING BIVARIATE AND MULTIVARIATE REGRESSION MODELS

TABLE 6.21 :

A Summary of the Ranges and Means of Variance Explanation using Bivariate and Multiple Regression Models

A. Bivariate Models

	Range R^2 %	Mean R^2 %
K^+	4.4 - 77.4	33.0
Na^+	4.8 - 64.0	21.2
Ca^{2+}	44.9 - 72.3	65.5
Mg^{2+}	44.9 - 75.7	56.6
Cl^-	49.0 - 63.0	57.0
pH	13.0 - 60.8	36.3
HCO_3^-	15.2 - 50.4	31.0
SC	5.3 - 86.5	55.0

B. Multivariate Models

	Range R^2 %	Mean R^2 %	Increase over bivariate %
K^+	12.1 - 81.1	42.0	+ 9.0
Na^+	6.8 - 65.9	35.5	+ 14.3
Ca^{2+}	45.5 - 78.3	70.0	+ 4.5
Mg^{2+}	48.1 - 89.1	64.6	+ 8.1
Cl^-	56.6 - 75.4	62.7	+ 5.7
pH	13.9 - 77.5	44.2	+ 7.9
HCO_3^-	15.2 - 51.6	34.9	+ 3.9
SC	5.3 - 96.0	66.1	+ 11.1

vegetation controls. In particular solute levels increase downstream as pH increases, which agrees with the findings of Johnson (1979). The waters flowing from subcatchment 1, with its acid podsols developed on Bagshot Sand and Plateau Gravel, have a low pH and relatively low solute content. The low pH is thought primarily due to the presence of organic acids derived from humic deposits on the sideslopes and valley bottom.

The higher base-exchange capacity of soils developed on London Clay provides for partial neutralisation of acid waters from upstream. One of the interesting effects of this pH variation is the leaching of iron by acid waters and precipitation as the pH rises above about 4.5 further downstream. The lower part of subcatchment 4 was replanted in 1973, and it is interesting to note that there the highest solute concentrations were recorded. Mean solute loads per unit area emphasise the relatively high solute yield of this subcatchment.

Study of weekly loads from the subcatchments for the first months of 1977 points to the operation of a dynamic contributing area within West Walk, the downstream areas delivering a high proportion of solutes during low flows, the remote areas becoming significant contributors during high flows.

(ii) Solute concentrations for West Walk have been modelled using two different types of approach. Bivariate and multivariate regression analyses on the regularly sampled data has shown that catchment moisture conditions, in addition to discharge, are important in determining solute concentration. Some interesting relationships were demonstrated using correlation matrices which included discharge, antecedent rainfall, soil moisture deficit and a season index. These were considered in detail in an earlier section and are given here in summary form.

The K^+/discharge regression changed from strongly positive at W1 to weakly negative at the flume, emphasising spatial variation in solute response. Strong correlations between Na^+/discharge did not exist, implying that neither dilution nor concentration dominate the response of any one subcatchment. A general dilution effect was

demonstrated for Ca^{2+}, Mg^{2+} and Cl^{-} with the exception of SC5, where correlations were weakly positive for Ca^{2+} and Mg^{2+}, but very weakly negative for Cl^{-}. The acidity of water increased as discharge increased at all sites except W5. This is due to a combination of the hydrogen ion content of storm rainfall and organic acids leached from humic soil horizons, particularly in SC1. The inverse correlation with acidity for SC5 implies that this subcatchment is capable of supplying bases to the main channel at higher flows. Operation of an overall dilution effect for West Walk and its subcatchments was demonstrated by the inverse SC/discharge relationship, although this disguises the variable response of individual solutes.

The relationships between individual solutes and other hydrometeorological variables also produced some interesting results. For example, considering a single solute, the API.T was better correlated for some lengths of T (the memory length of the API) than others. Ca^{2+} and K^{+} were most highly correlated with 30 and 60 day API's, tentatively suggesting the influence of "older" rainfall and a longer throughflow period. Direct correlations between SMD and concentration, e.g. Cl^{-}, suggest that concentrations increase as moisture is lost through evapotranspiration. The reverse is true in SC5, possibly due to uptake of water and solutes by the vegetation. However, it is difficult to reconcile one process producing opposite results in separate catchments, pointing to the need for detailed field study of the actual mechanisms.

Statistical analysis of the regression residuals points out the dangers of placing too much emphasis upon interpretation of the regression coefficients. Thus multiple regression analysis was employed primarily to improve upon bivariate model prediction. This was successful in 33/40 cases, although in 23/33 the use of only one additional variable proved significant.

Chapter 7 examines the data collected during storms between 1975 and 1977 in order to elucidate some important solute controls and improve model prediction.

CHAPTER 7

AN ANALYSIS OF SURFACE WATER SOLUTE DYNAMICS IN WEST WALK CATCHMENT: II: THE STORM SAMPLE DATA (SSD)

7.1 INTRODUCTION

This chapter introduces data samples from W1, W2 and the flume during storms. Firstly, they are combined with RSD in assessing the ability of regression models to model over a wide range of flow conditions. Bivariate solute/discharge regressions are also performed with the separate autumn and non-autumn data to assess the influence of seasonal effects such as solute flushing on variance explanation. Polynomial regression is used in an attempt to describe non-linearity remaining after taking logarithms of the basic data. Secondly, an analysis of individual storms is undertaken to identify the important factors controlling the 'flushing effect' and non-synchronous hydrograph and chemograph peaks. Potassium is used as a specific sample.

Samples were collected at intervals ranging from 15 - 120 minutes during the autumns and winters of 1975 and 1976. It should be pointed out at this stage that the 1975 - 1976 drought badly disrupted the original sampling program, which had aimed to place emphasis on the 1975 autumn and winter for storm sampling of streamflow and then to concentrate upon the examination of hillslope water and solutes during the autumn and winter of 1976. Figure 4.11 shows that there were very few storms for sampling in late 1975 or early 1976. Hence, much of the storm sampling was done after the end of the drought, from September 1976 onwards. This created two problems.

Firstly, the total rainfall in the months September to December 1976 was 159 % of the 1916 - 1950 average (Southsea Common), storms were very frequent and the hydrological effects overlapped from one to the next. Secondly, sampling streamflow and soil water together created field work logistical problems and a large backlog of samples awaiting laboratory analysis.

7.2 BIVARIATE CORRELATION AND REGRESSION ANALYSIS

In an attempt to produce a set of simple relationships capable of predicting solute concentration over a wide range of conditions, the storm data set was combined with the regularly sampled data set at W1, W2 and the flume, and bivariate regression performed. The solute/discharge data are plotted in Figures 7.1 - 7.5. Table 7.1 A - C gives the results of these regressions for W1, W2 and the flume (using the program GEOREG 2, see Appendix 2). Correlation coefficients are all significant with the exception of pH, HCO_3^- and SC for W2, pH and SC for the flume. With the exception of Na^+, variance explanation is almost invariably much worse than for the RSD data regressions. An explanation for the improvement in Na^+ variance explanation can only be tentative from 'black box' modelling. It appears that with Na^+ the dilution effect only becomes dominant during storms; during periods of flow recession there is no single dominant process.

The 'break' of the 1975 - 1976 drought signalled a large flush of solutes from West Walk, as in many other British catchments (e.g. Foster and Walling, 1978; Walling and Foster, 1978). Over this drought period the 'normal' dilution changed to concentration for some solutes during individual storms. Such inter-storm response variability was thought to be a reason for the decrease in variance explanation using the total sampled data (TSD) set. This suggested that solute concentration during 'autumn' (arbitrarily defined as September, October and November, according to the time when significant flushing occurs) should be modelled separately. As a first step autumn samples were removed and the complementary data set subjected to bivariate regression.

The results are shown in Table 7.2 A and B for W1 and the flume, W2 regressions returning to the RSD set. There is no overall consistency to the results. In six regressions R^2 % progressively decreases from the RSD to the TSD: Ca^{2+} at W1 and the flume; K^+ at W1; SC at W1; and pH at the flume. The K^+/discharge relationship is interesting in that it changes direction, from positive for the RSD and TSD without autumn samples, to negative for the TSD. Inspection of the rating plots shows that this is due to high concentrations at low discharges during individual autumn storms. K^+ response is treated in detail later in this chapter.

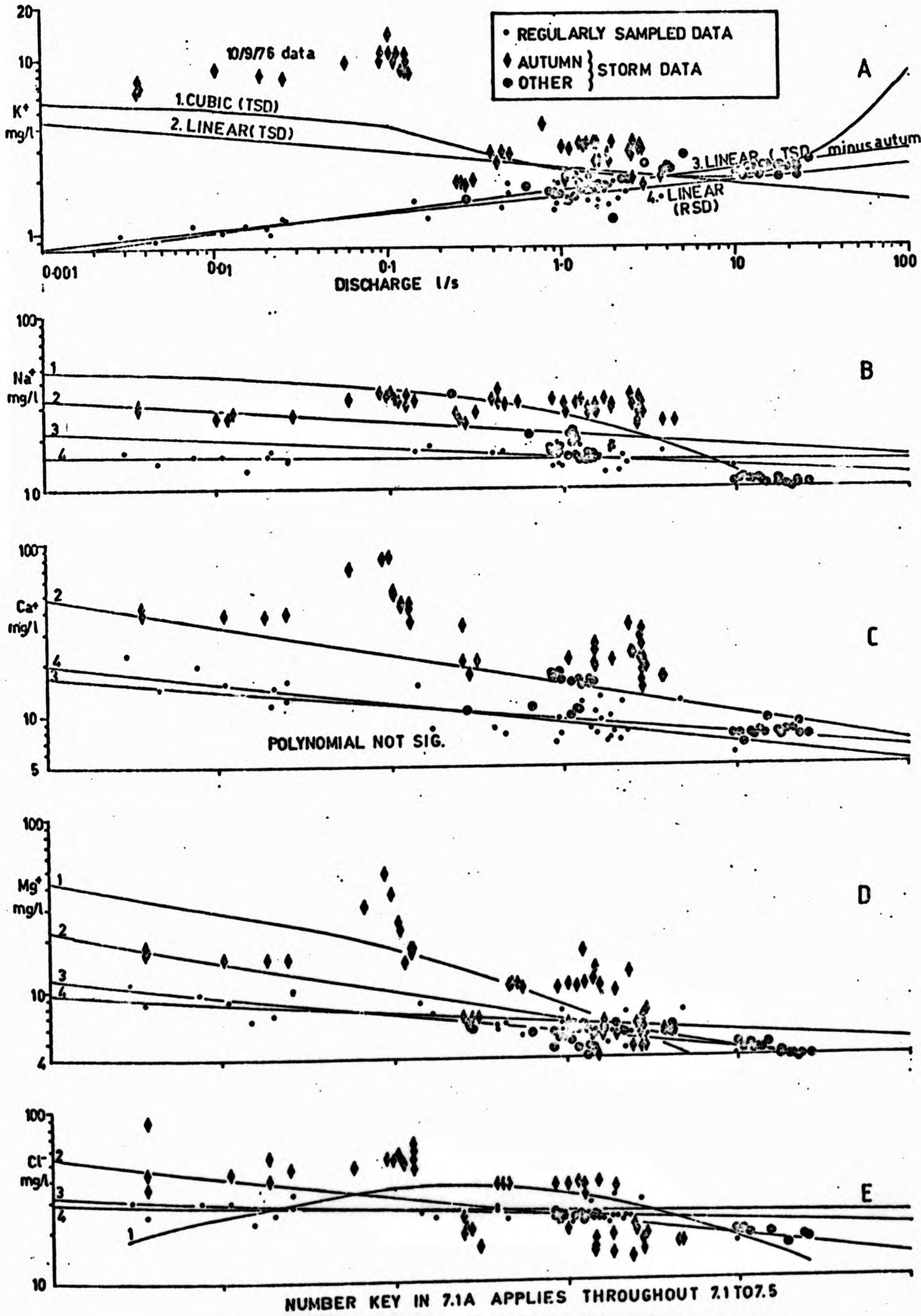

FIGURE 7.1: SOLUTE DISCHARGE RATINGS FOR WEIR 1

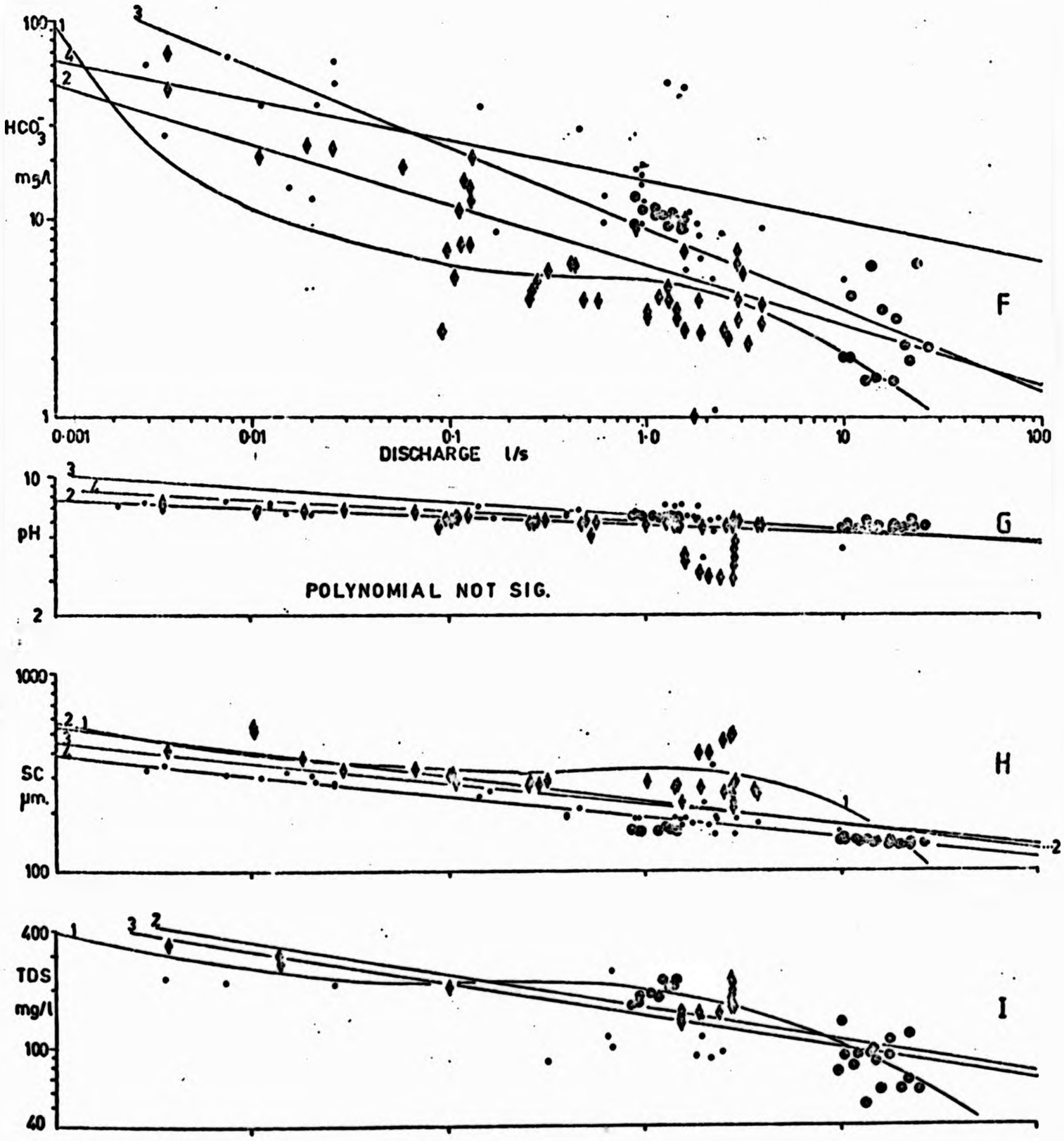

FIGURE 7.1 (cont'd):

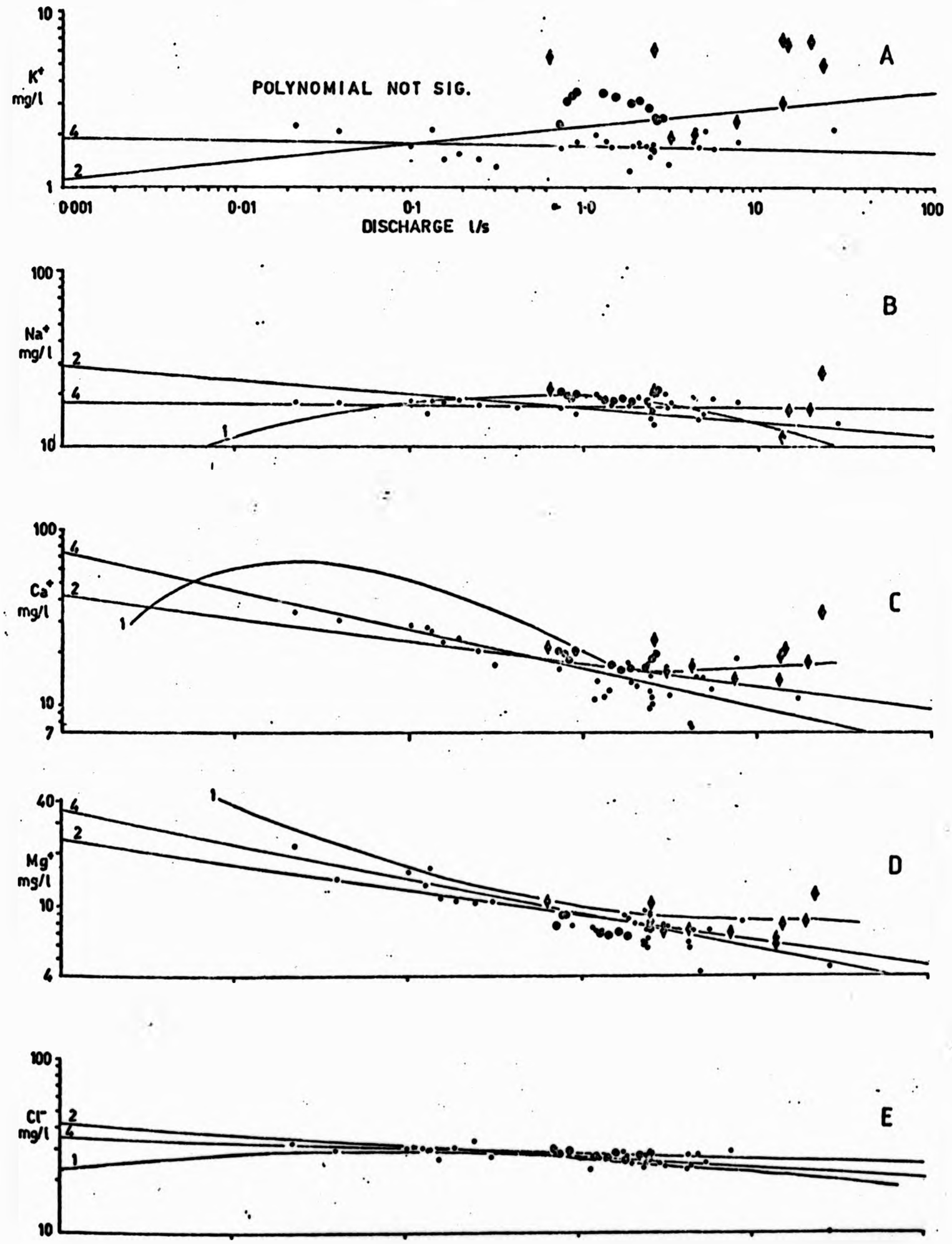

FIGURE 7.2: SOLUTE DISCHARGE RATINGS FOR WEIR 2

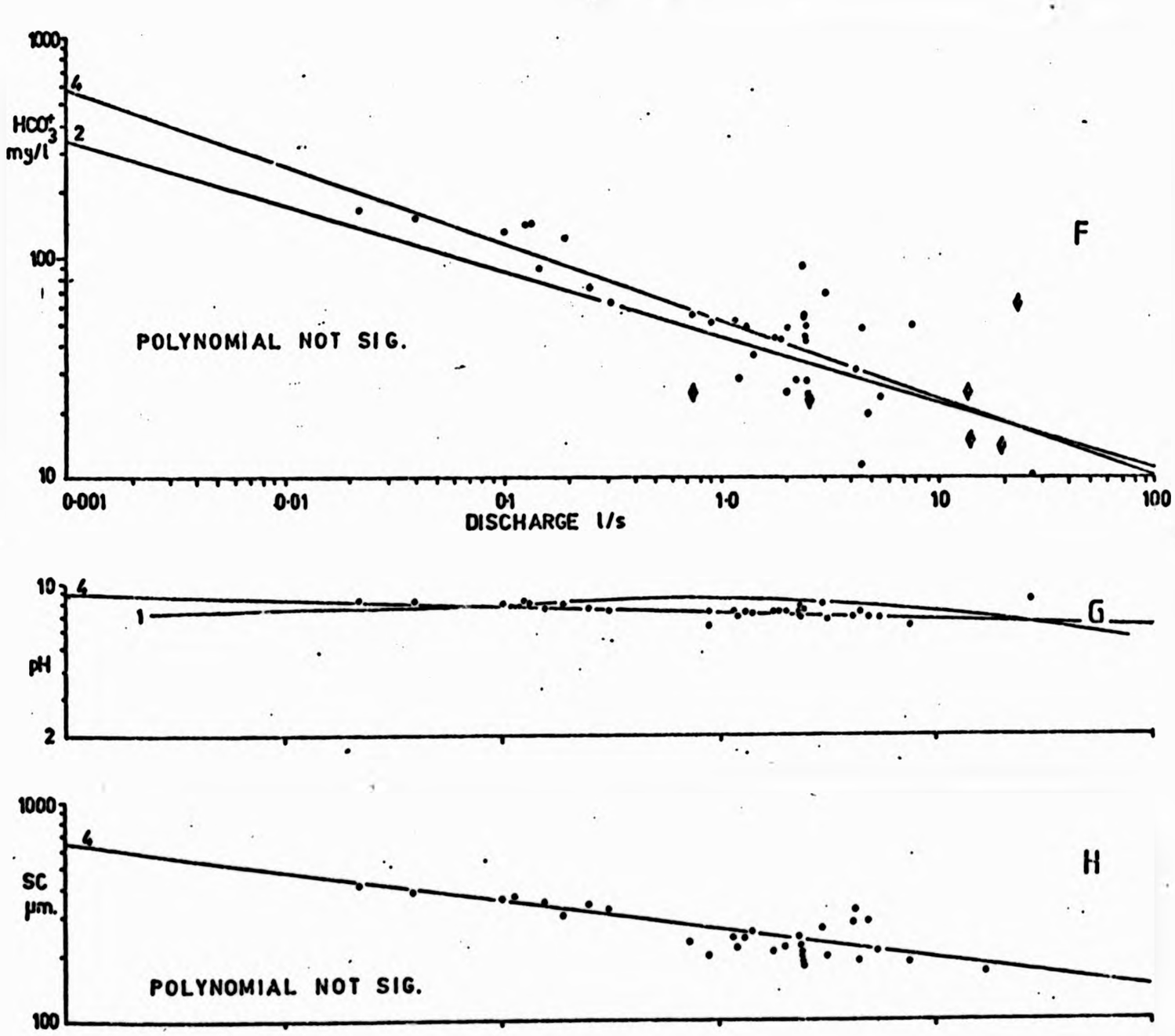

FIGURE 7.2 (cont'd):

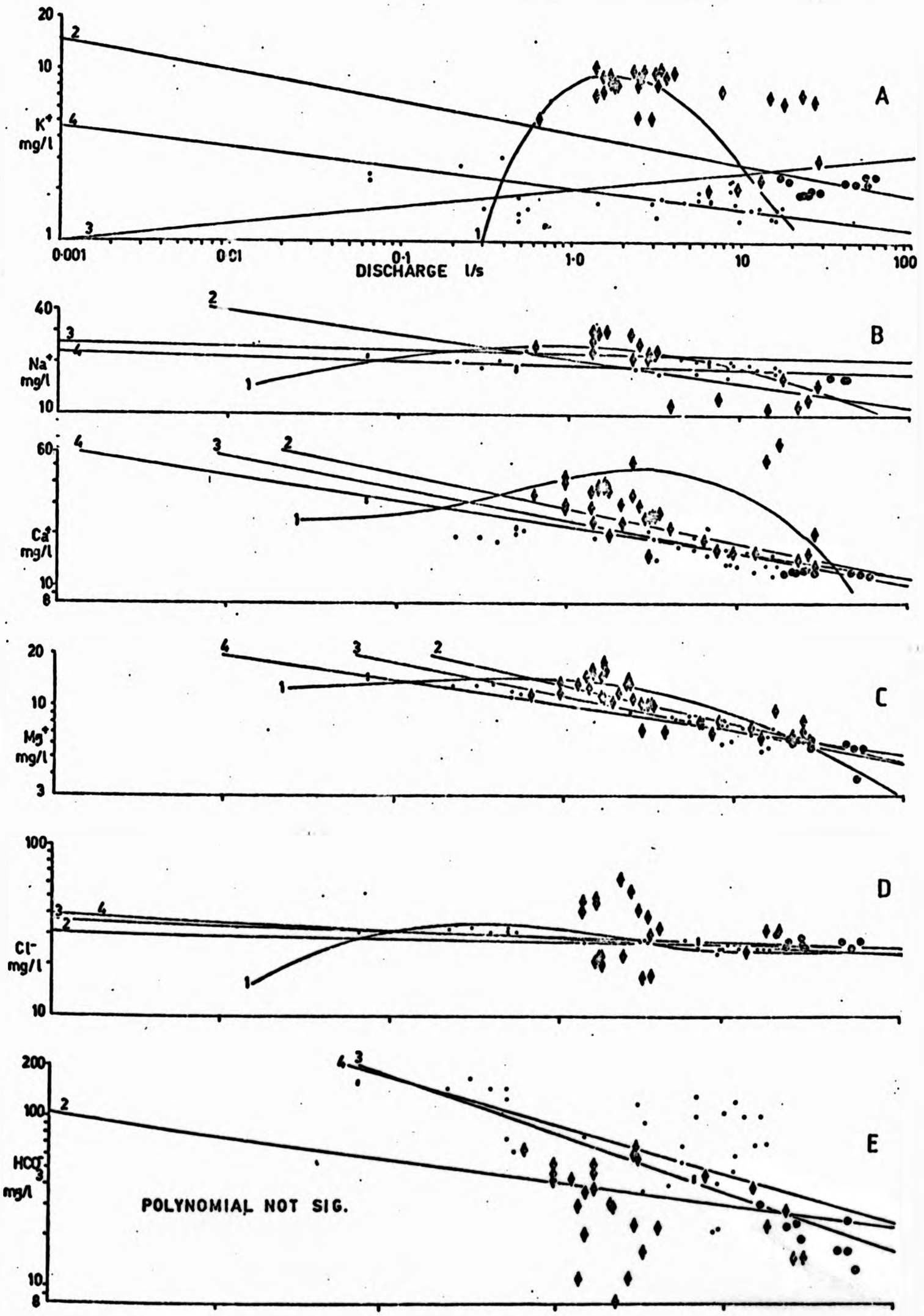

FIGURE 7.3: SOLUTE DISCHARGE RATINGS FOR THE FLUME

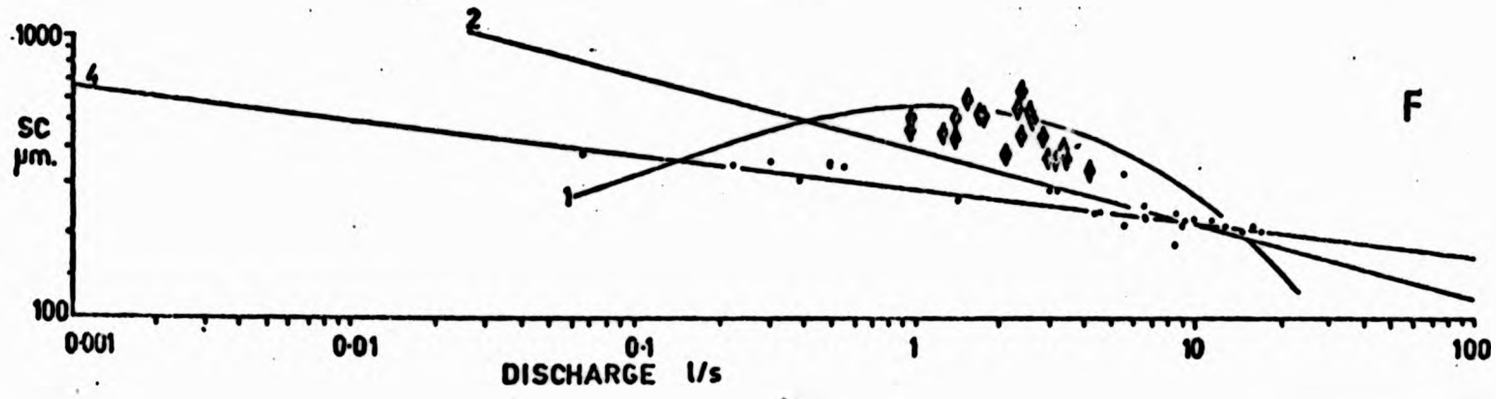

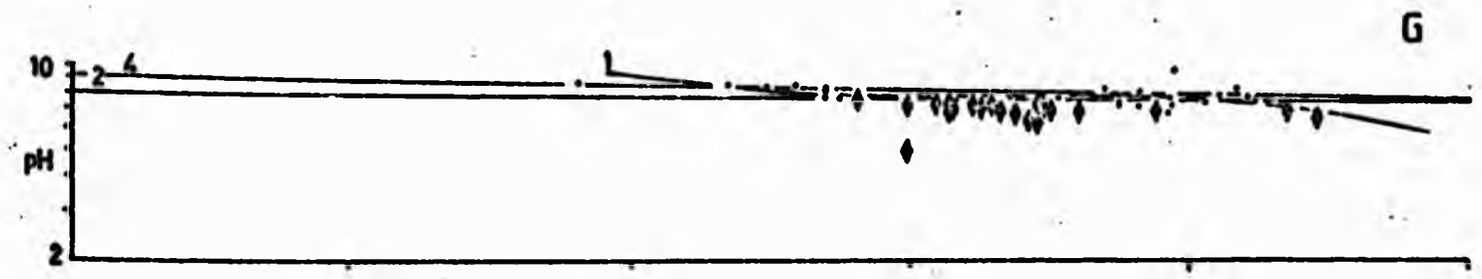

FIGURE 7.3 (cont'd):

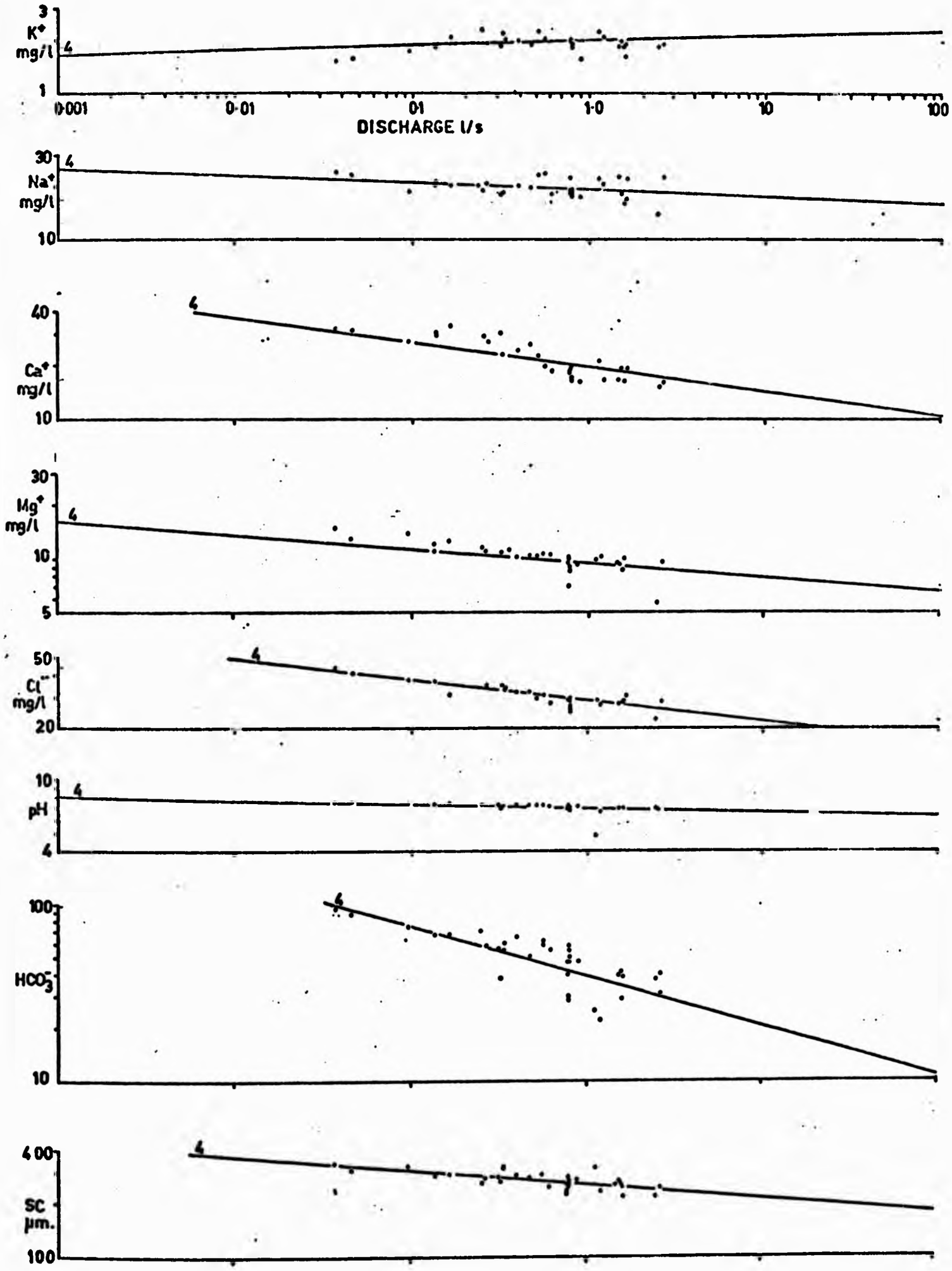

FIGURE 7.4: SOLUTE DISCHARGE RATINGS FOR WEIR 4

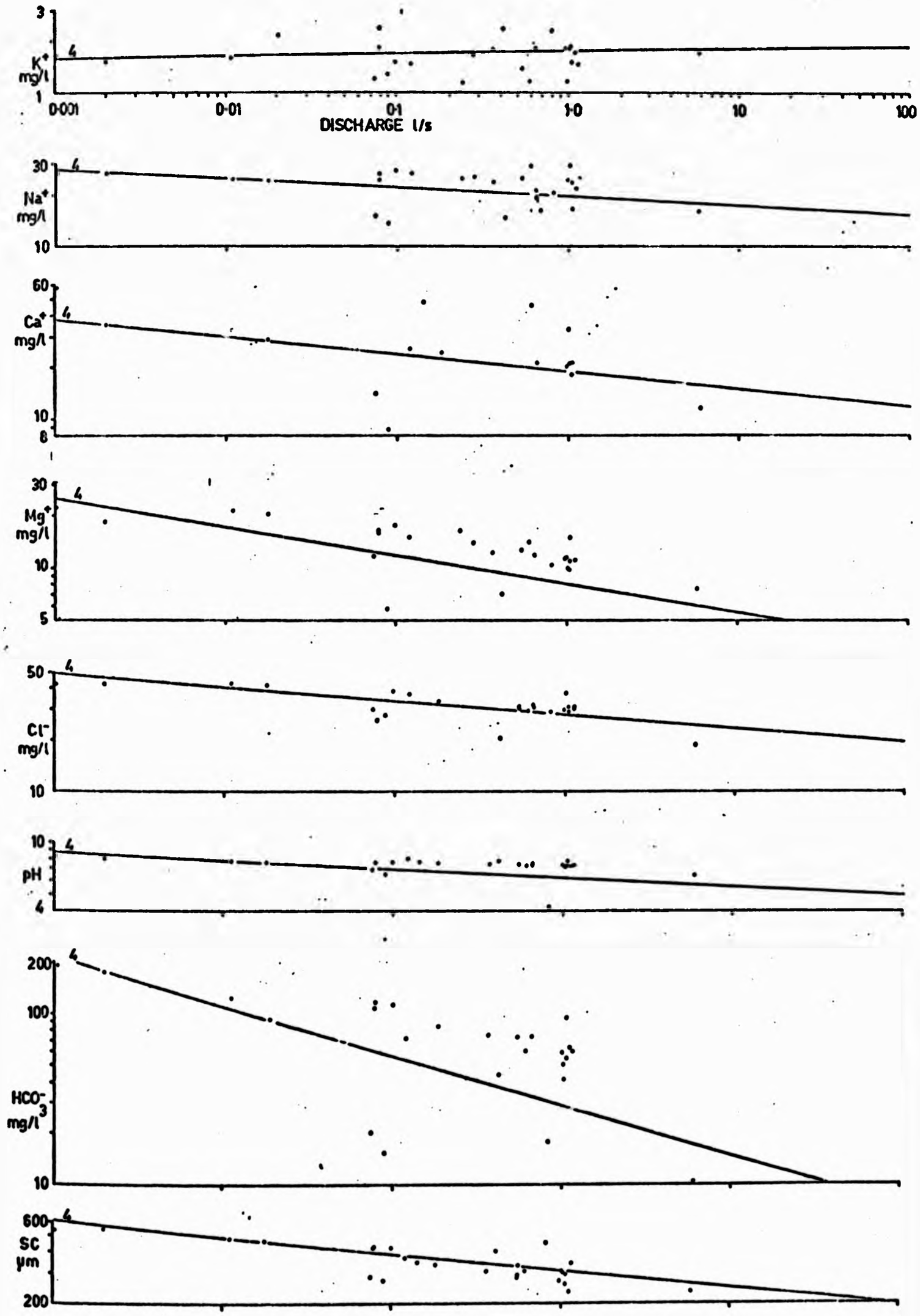

FIGURE 7.5: SOLUTE DISCHARGE RATINGS FOR WEIR 5

For five regressions the R^2 % is higher than for either the TSD or the RSD; Na^+ at W1; Mg^{2+} at W1 and the flume; and pH at W1. In three regressions the TSD without autumn samples provide the worst variance explanation.

The overall conclusion from this analysis is that autumn storm samples add to unexplained variance in the bivariate regressions, but with several inconsistencies evident from Tables 7.1 and 7.2.

Separate regressions were also fitted to autumn storm data (Tables 7.2 C and D). For W1 variance explanation is good with the exception of Na^+, while at the flume variance explanation is poor with the exception of Mg^{2+}. There are changes in the direction of correlation between autumn storm data and the TSD without autumn samples, which is most marked for the case of K^+. Reference to the rating plot (Figure 7.1 A) shows that the negative relationship for autumn storm data is due to direct correlations during a succession of autumn storms. Intercepts decrease through time, the net result being an inverse relationship.

For Na^+, Ca^{2+}, SC and TDS at W1 the intercepts increase (the pH intercept decreases) and for K^+, Na^+, Ca^{2+} and SC at the flume, the intercepts increase (the pH intercept decreases) when compared with regressions excluding autumn samples. Where regression slopes remain stable, this indicates a general rise in solute concentration in these parameters during the months of September, October and November.

7.3 POLYNOMIAL REGRESSION ON THE TOTAL SAMPLED DATA (i.e. RSD + SSD)

Polynomial regression was employed in a further attempt to model the TSD using a single independent variable (i.e. discharge). A polynomial is a special form of the multiple regression equation (2.8), with discharge raised to successively higher powers replacing the independent variables. It was thought that a quadratic or cubic function might describe non-linearity remaining after taking logarithms of the basic data. The program NTHOREG 1 (Appendix 2) was used to fit the regressions by least squares and equation 6.10 used to determine the significance of each additional term to the regression. It was found that terms higher than cubic did not contribute

TABLE 7.1: RESULTS OF BIVARIATE REGRESSIONS (RMA) FITTED TO THE TOTAL SAMPLED DATA AND DISCHARGE

Discharge in cumecs . log data

7.1 A : W1

Units	Variables	r	b	a	Sig. r %	SE	N*	r_1^2 %	r^2 %
mg/l	K	- 0.32	- 0.096	1.18	0.1	0.55	146	77.4	10.2
mg/l	Na	- 0.34	- 0.067	12.84	0.1	0.37	135	4.8	11.6
mg/l	Ca	- 0.52	- 0.170	4.54	0.1	0.56	148	72.3	27.0
mg/l	Mg	- 0.69	- 0.174	2.06	0.1	0.36	148	60.8	47.6
mg/l	Cl	- 0.58	- 0.119	10.49	0.1	0.33	105	49.0	33.6
pH units	pH	- 0.39	- 0.038	4.43	0.1	0.17	112	37.2	15.2
mg/l	HCO_3	- 0.64	- 0.303	0.733	0.1	0.71	98	20.3	41.0
µmhos	SC	- 0.53	- 0.120	98.59	0.1	0.30	73	67.2	28.1
mg/l	TDS	- 0.54	- 0.168	50.15	0.1	0.32	59	-	29.2

* major cause of unequal sample sizes is the variable quantity of water taken by NHE vacuum samplers

r_1^2 % : RSD variance explanation

r^2 % : TSD variance explanation

TABLE 7.1: RESULTS OF BIVARIATE REGRESSIONS (RMA) FITTED TO THE TOTAL SAMPLED DATA AND DISCHARGE

Discharge in cumecs . log data

7.1 A : W1

Units	Variables	r	b	a	Sig. r %	SE	N*	r_1^2 %	r^2 %
mg/l	K	- 0.32	- 0.096	1.18	0.1	0.55	146	77.4	10.2
mg/l	Na	- 0.34	- 0.067	12.84	0.1	0.37	135	4.8	11.6
mg/l	Ca	- 0.52	- 0.170	4.54	0.1	0.56	148	72.3	27.0
mg/l	Mg	- 0.69	- 0.174	2.06	0.1	0.36	148	60.8	47.6
mg/l	Cl	- 0.58	- 0.119	10.49	0.1	0.33	105	49.0	33.6
pH units	pH	- 0.39	- 0.038	4.43	0.1	0.17	112	37.2	15.2
mg/l	HCO_3	- 0.64	- 0.303	0.733	0.1	0.71	98	20.3	41.0
µmhos	SC	- 0.53	- 0.120	98.59	0.1	0.30	73	67.2	28.1
mg/l	TDS	- 0.54	- 0.168	50.15	0.1	0.32	59	-	29.2

* major cause of unequal sample sizes is the variable quantity of water taken by NHE vacuum samplers

r_1^2 % : RSD variance explanation

r^2 % : TSD variance explanation

7.1 B: W2

	r	b	a	%Sig r	SE	N	r_1^2%	r^2%
K	0.29	0.099	4.45	5.0	0.46	54	14.4	8.4
Na	- 0.45	- 0.078	9.92	0.1	0.23	51	6.8	20.3
Ca	- 0.56	- 0.125	7.32	0.1	0.29	53	70.6	31.4
Mg	- 0.75	- 0.146	3.21	0.1	0.20	56	53.3	56.3
Cl	- 0.71	- 0.059	18.13	0.1	0.09	45	49.0	50.4
pH	0.15	0.023	7.99	NS	0.16	53	14.4	2.3
HCO_3	- 0.14	- 0.221	6.81	NS	1.66	53	15.2	2.0
SC	0.09	0.021	259.6	NS	0.17	53	5.3	0.8

r_1^2 %, r^2 % as in 7.1 A

7.1 C: FLUME

	r	b	a	%Sig r	SE	N	r_1^2%	r^2%
K	- 0.30	- 0.176	1.31	1.0	0.69	89	21.2	9.0
Na	- 0.42	- 0.136	8.33	0.1	0.37	62	15.2	17.6
Ca	- 0.60	- 0.198	7.45	0.1	0.37	101	72.3	36.0
Mg	- 0.80	- 0.221	2.82	0.1	0.23	101	75.7	64.0
Cl	- 0.29	- 0.051	22.25	5.0	0.24	74	62.4	8.4
pH	0.09	- 0.007	7.32	NS	0.07	70	56.4	0.8
HCO_3	- 0.17	- 0.131	16.78	NS	0.83	77	34.8	2.9
SC	- 0.88	- 0.408	32.85	0.1	0.19	69	86.5	77.4

r_1^2 %, r^2 % as in 7.1 A

7.1 B: W2

	r	b	a	%Sig r	SE	N	r_1^2%	r^2%
K	0.29	0.099	4.45	5.0	0.46	54	14.4	8.4
Na	- 0.45	- 0.078	9.92	0.1	0.23	51	6.8	20.3
Ca	- 0.56	- 0.125	7.32	0.1	0.29	53	70.6	31.4
Mg	- 0.75	- 0.146	3.21	0.1	0.20	56	53.3	56.3
Cl	- 0.71	- 0.059	18.13	0.1	0.09	45	49.0	50.4
pH	0.15	0.023	7.99	NS	0.16	53	14.4	2.3
HCO_3	- 0.14	- 0.221	6.81	NS	1.66	53	15.2	2.0
SC	0.09	0.021	259.6	NS	0.17	53	5.3	0.8

r_1^2 %, r^2 % as in 7.1 A

7.1 C: FLUME

	r	b	a	%Sig r	SE	N	r_1^2%	r^2%
K	- 0.30	- 0.176	1.31	1.0	0.69	89	21.2	9.0
Na	- 0.42	- 0.136	8.33	0.1	0.37	62	15.2	17.6
Ca	- 0.60	- 0.198	7.45	0.1	0.37	101	72.3	36.0
Mg	- 0.80	- 0.221	2.82	0.1	0.23	101	75.7	64.0
Cl	- 0.29	- 0.051	22.25	5.0	0.24	74	62.4	8.4
pH	0.09	- 0.007	7.32	NS	0.07	70	56.4	0.8
HCO_3	- 0.17	- 0.131	16.78	NS	0.83	77	34.8	2.9
SC	- 0.88	- 0.408	32.85	0.1	0.19	69	86.5	77.4

r_1^2 %, r^2 % as in 7.1 A

TABLE 7.2: RESULTS OF BIVARIATE REGRESSIONS (RMA) FITTED TO SEPARATE AUTUMN AND NON-AUTUMN SAMPLES

(Autumn defined as the months of September, October and November. Discharge in cumecs; log data)

7.2 A: W1 Autumn data excluded

	r	b	a	% Sig r	SE	N	r_1^2%	r^2%	r_2^2%
K	0.87	0.138	4.37	0.1	0.13	79	77.4	75.7	10.2
Na	- 0.46	- 0.143	10.25	0.1	0.21	68	4.8	21.2	11.6
Ca	- 0.69	- 0.240	2.70	0.1	0.20	81	72.3	47.6	27.0
Mg	- 0.85	- 0.114	2.49	0.1	0.12	81	60.8	72.3	47.6
Cl	- 0.46	- 0.039	18.24	0.1	0.14	54	49.0	21.2	33.6
pH	- 0.65	- 0.069	3.91	0.1	0.071	45	37.2	42.3	16.2
HCO_3	- 0.59	- 0.408	0.541	0.1	0.79	43	20.3	34.8	41.0
SC	- 0.66	- 0.052	118.4	0.1	0.09	38	67.2	43.6	28.1
TDS	- 0.60	- 0.165	46.53	0.1	0.34	39	-	36.0	29.2

r_1^2 % : RSD variance explanation

r^2 % : TSD except autumn storm data, variance explanation

r_2^2 % : TSD variance explanation

7.2 B: FLUME Autumn data excluded

	r	b	a	% Sig r	SE	N	r_1^2%	r^2%	r_2^2%
K	0.28	0.108	4.27	5.0	0.51	65	21.2	7.8	9.0
Na	- 0.39	- 0.019	19.97	5.0	1.08	34	15.2	15.2	17.6
Ca	- 0.84	- 0.187	6.72	0.1	0.18	68	72.3	70.6	36.0
Mg	- 0.88	- 0.193	2.98	0.1	0.16	68	75.7	77.4	64.0
Cl	- 0.55	- 0.030	23.92	0.1	0.072	53	62.4	30.3	8.4
pH	0.16	0.014	7.76	NS	0.073	38	56.3	2.6	0.8
HCO_3	- 0.14	- 0.095	21.56	NS	0.81	45	34.8	2.0	2.9
SC	- 0.55	- 0.143	286	1.0	0.99	34	86.5	30.3	77.4

r_1^2 %, r^2 %, r_2^2 % as in 7.2 A

7.2 C: W1 Autumn data only

	r	b	a	%Sig r	SE	N	r^2 %
K	- 0.80	- 0.291	0.36	0.1	0.41	67	63.2
Na	- 0.26	- 0.016	26.10	5.0	0.11	67	6.8
Ca	- 0.70	- 0.158	8.47	0.1	0.30	67	49.0
Mg	- 0.76	- 0.241	1.54	0.1	0.38	67	57.5
Cl	- 0.74	- 0.202	5.90	0.1	0.37	51	54.5
pH	- 0.58	- 0.069	3.312	0.1	0.18	67	33.5
HCO_3	- 0.76	- 0.365	0.354	0.1	0.59	54	58.4
SC	- 0.52	- 0.105	137.7	1.0	0.24	35	27.3
TDS	0.63	- 0.353	1442	1.0	0.11	20	40.2

7.2 D: FLUME Autumn data only

	r	b	a	%Sig r	SE	N	r^2 %
K	- 0.23	- 0.045	6.26	NS	0.18	24	5.4
Na	- 0.19	- 0.111	22.4	NS	0.56	28	3.6
Ca	- 0.23	- 0.099	18.63	NS	0.40	33	5.3
Mg	- 0.81	- 0.279	2.46	0.1	0.20	33	65.0
Cl	- 0.27	- 0.355	3.74	NS	0.42	21	7.5
pH	- 0.07	- 0.004	6.73	NS	0.058	32	0.4
HCO_3	- 0.28	- 0.261	7.27	NS	0.88	32	7.7
SC	- 0.36	- 0.142	295	5.0	1.21	35	12.9

significantly to the regression, and these were discontinued after initial trials. The results are summarised in Tables 7.3 - 7.5.

In some cases, both quadratic and cubic terms improve R^2 %, e.g. Mg^{2+} at W1, while in others either quadratic or cubic terms alone are significant, e.g. Cl^- at W2 and K^+ at the flume, respectively. In several instances the additional variance explained by the polynomial over the bivariate model is large, e.g. TDS at W2, where a cubic function increases R^2 by 31 %. The results imply that the addition of storm data (particularly from autumn storms) to the regularly sampled data creates non-linearity in the bivariate solute/discharge models. Analysis for heteroscedasticity was not undertaken, but an examination of the rating plots suggests that there is unlikely to be improvement over heteroscedasticity found in the RSD. This is because the considerable variance introduced by autumn data is unequally distributed along the regression line, e.g. Figure 7.1A.

Polynomial models improve the variance explanation over bivariate models, partly returning R^2 % values to those obtained for the RSD regressions. For Na^{2+} the cubic functions give the best overall variance explanation at W1, W2 and the flume, the only solute in which this occurs.

7.4 AN ASSESSMENT OF THE BIVARIATE AND MULTIVARIATE MODELS FOR PREDICTION OF STORM SOLUTE CONCENTRATION

The main reasons for studying detailed solute dynamics are, firstly, to gain an understanding of the controlling processes and, secondly, to build models capable of predicting solute concentration during storms at different periods in the year. Simple bivariate models, involving concentration and discharge (e.g. Steele, 1976) have been criticised on the grounds of inadequacy in predicting concentration during individual storms (Foster, 1978).

Figures 7.6 and 7.7 show actual and predicted K^+ and TDS concentration for storms in October 1976 and April 1977. The equations used for synthesising solute concentration were derived from the foregoing analysis. These are as follows: solute concentration in mg/l; SC in μmhos, converted to TDS using equation 5.3 (SC < 400 μmhos)

significantly to the regression, and these were discontinued after initial trials. The results are summarised in Tables 7.3 - 7.5.

In some cases, both quadratic and cubic terms improve R^2 %, e.g. Mg^{2+} at W1, while in others either quadratic or cubic terms alone are significant, e.g. Cl^- at W2 and K^+ at the flume, respectively. In several instances the additional variance explained by the polynomial over the bivariate model is large, e.g. TDS at W2, where a cubic function increases R^2 by 31 %. The results imply that the addition of storm data (particularly from autumn storms) to the regularly sampled data creates non-linearity in the bivariate solute/discharge models. Analysis for heteroscedasticity was not undertaken, but an examination of the rating plots suggests that there is unlikely to be improvement over heteroscedasticity found in the RSD. This is because the considerable variance introduced by autumn data is unequally distributed along the regression line, e.g. Figure 7.1A.

Polynomial models improve the variance explanation over bivariate models, partly returning R^2 % values to those obtained for the RSD regressions. For Na^{2+} the cubic functions give the best overall variance explanation at W1, W2 and the flume, the only solute in which this occurs.

7.4 AN ASSESSMENT OF THE BIVARIATE AND MULTIVARIATE MODELS FOR PREDICTION OF STORM SOLUTE CONCENTRATION

The main reasons for studying detailed solute dynamics are, firstly, to gain an understanding of the controlling processes and, secondly, to build models capable of predicting solute concentration during storms at different periods in the year. Simple bivariate models, involving concentration and discharge (e.g. Steele, 1976) have been criticised on the grounds of inadequacy in predicting concentration during individual storms (Foster, 1978).

Figures 7.6 and 7.7 show actual and predicted K^+ and TDS concentration for storms in October 1976 and April 1977. The equations used for synthesising solute concentration were derived from the foregoing analysis. These are as follows: solute concentration in mg/l; SC in μmhos, converted to TDS using equation 5.3 (SC < 400 μmhos)

TABLE 7.3 W1: POLYNOMIALS FITTED TO THE TOTAL SAMPLED DATA AND DISCHARGE

(Concentration in mg/l; discharge in cumecs)

7.3 A POTASSIUM CONCENTRATION (N = 146)

	log A	B1	B2	B3	B4	R^2 %	SigR %	F	SigF %
log Q	0.166	-0.196	-	-	-	10.24	0.1	-	-
$\log Q^2$	0.745	0.062	0.010	-	-	10.91	0.1	1.08	NS
$\log Q^3$	5.581	2.163	0.296	0.012	-	17.92	0.1	12.14	0.1

7.3 B SODIUM CONCENTRATION
(4TH TERM EXCLUDED FROM FURTHER REGRESSION) (N = 135)

	log A	B1	B2	B3	R^2 %	SigR %	F	SigF %
log Q	2.553	-0.067	-	-	11.60	0.1	-	-
$\log Q^2$	0.747	-0.560	-0.031	-	30.30	0.1	35.17	0.1
$\log Q^3$	-1.056	-1.347	-0.138	-0.005	32.50	0.1	4.26	5.0

7.3 C CALCIUM CONCENTRATION (N = 148)

	log A	B1	B2	B3	R^2 %	SigR %	F	SigF %
log Q	1.513	-0.170	-	-	31.36	0.1	-	-
$\log Q^2$	0.421	-0.466	-1.864	-	31.37	0.1	0.01	NS
$\log Q^3$	2.110	0.262	0.080	0.004	31.76	0.1	1.39	NS

7.3 D MAGNESIUM CONCENTRATION (N = 148)

	log A	B1	B2	B3	R^2 %	SigR %	F	SigF %
log Q	1.513	-0.170	-	-	27.04	0.1	-	-
$\log Q^2$	0.123	-0.338	-0.010	-	48.9	0.1	62.1	0.1
$\log Q^3$	3.392	1.071	0.180	0.008	53.3	0.1	13.5	0.1

7.3 E CHLORIDE CONCENTRATION (N = 105)

	log A	B1	B2	B3	R^2 %	SigR %	F	SigF %
log Q	2.350	-0.119	-	-	33.64	0.1	-	-
$\log Q^2$	0.839	-0.489	-2.122	-	39.15	0.1	9.23	0.1
$\log Q^3$	4.657	0.960	0.155	0.007	42.37	0.1	5.65	1.0

7.3 F pH VALUES (N = 112)

	log A	B1	B2	B3	R^2 %	SigR %	F	SigF %
log Q	1.488	-0.038	-	-	15.21	0.1	-	-
$\log Q^2$	1.632	0.003	0.003	-	16.96	0.1	2.30	NS
$\log Q^3$	2.390	0.337	0.048	0.002	18.84	0.1	2.46	NS

7.3 G BICARBONATE CONCENTRATION (N = 98)

	log A	B1	B2	B3	R^2 %	SigR %	F	SigF %
log Q	-0.311	-0.303	-	-	40.96	0.1	-	-
$\log Q^2$	0.122	-0.180	0.008	-	41.19	0.1	0.37	NS
$\log Q^3$	-5.152	-2.499	-0.308	-0.013	44.89	0.1	6.31	0.1

7.3 H SC μmhos (N = 73)

	log A	B1	B2	B3	R^2 %	SigR %	F	SigF %
log Q	4.591	-0.120	-	-	27.56	0.1	-	-
$\log Q^2$	4.736	-0.074	0.003	-	27.68	0.1	0.120	NS
$\log Q^3$	-0.416	-2.519	-0.358	-0.167	41.01	0.1	15.52	0.1

7.3 I TDS CONCENTRATION (N = 59)

	log A	B1	B2	B3	R^2 %	SigR %	F	SigF %
log Q	3.915	-0.168	-	-	29.16	0.1	-	-
$\log Q^2$	0.424	-1.427	-0.108	-	59.60	0.1	49.27	0.1
$\log Q^3$	3.012	-0.066	0.120	0.012	60.08	0.1	0.65	NS

TABLE 7.4 W2: POLYNOMIALS FITTED TO THE TOTAL SAMPLED DATA AND DISCHARGE

(Concentration in mg/l; discharge in cumecs)

7.4 A POTASSIUM CONCENTRATION (N = 54)

	log A	B1	B2	B3	R^2 %	SigR %	F	SigF %
log Q	1.493	-0.099	-	-	8.41	5.0	-	-
$\log Q^2$	1.776	0.193	0.007	-	8.40	5.0	<0	NS
$\log Q^3$	7.593	3.189	0.499	0.026	11.52	5.0	1.76	NS

7.4 B SODIUM CONCENTRATION (N = 51)

	log A	B1	B2	B3	R^2 %	SigR %	F	SigF %
log Q	2.295	-0.078	-	-	20.25	0.1	-	-
$\log Q^2$	0.767	-0.568	-0.037	-	38.2	0.1	13.96	0.1
$\log Q^3$	-0.867	-1.383	-0.166	-0.007	39.78	0.1	1.22	NS

7.4 C CALCIUM CONCENTRATION (N = 53)

	Log A	B1	B2	B3	R^2 %	SigR %	F	SigF %
log Q	1.991	-0.125	-	-	31.36	0.1	-	-
$\log Q^2$	4.021	0.491	0.044	-	39.78	0.1	14.43	0.1
$\log Q^3$	10.29	3.411	0.477	0.020	46.73	0.1	14.80	0.1

7.4 D MAGNESIUM CONCENTRATION (N = 56)

	log A	B1	B2	B3	R^2 %	SigR %	F	SigF %
Log Q	1.166	-0.146	-	-	56.25	0.1	-	-
$\log Q^2$	2.643	0.259	0.030	-	67.75	0.1	18.6	0.1
$\log Q^3$	2.247	0.154	0.014	-0.001	67.78	0.1	<0.1	NS

7.4 E CHLORIDE CONCENTRATION (N = 45)

	log A	B1	B2	B3	R^2 %	SigR %	F	SigF %
log Q	2.898	-0.059	-	-	50.41	0.1	-	-
$\log Q^2$	2.442	-0.192	-0.010	-	55.59	0.1	4.91	1.0
$\log Q^3$	1.79	-0.489	-0.053	-0.002	56.62	0.1	0.99	NS

7.4 F pH VALUES (N = 53)

	log A	B1	B2	B3	R^2 %	SigR %	F	SigF %
log Q	2.078	0.023	-	-	2.25	NS	-	-
$\log Q^2$	4.03	0.763	0.067	-	25.89	0.1	6.1	0.1
$\log Q^3$	6.183	2.04	0.313	0.015	26.95	0.1	0.23	NS

7.4 G BICARBONATE CONCENTRATION (N = 53

	log A	B1	B2	B3	R^2 %	SigR %	F	SigF %
logQ	1.918	-0.221	-	-	1.96	NS	-	-
$\log Q^2$	11.287	3.227	0.307	-	5.63	NS	0.89	NS
$\log Q^3$	41.20	20.05	3.387	0.184	6.90	NS	0.31	NS

7.4 H SC µhmos (N = 53)

	log A	B1	B2	B3	R^2 %	SigR %	F	SigF %
log Q	5.559	0.021	-	-	0.81	NS	-	-
$\log Q^2$	3.043	-0.805	-0.067	-	2.77	NS	0.18	NS
$\log Q^3$	-24.31	-14.07	-2.20	-0.114	4.60	NS	0.15	NS

TABLE 7.5 FLUME: POLYNOMIALS FITTED TO THE TOTAL SAMPLED DATA AND DISCHARGE

(Concentration in mg/l; discharge in cumecs)

7.5 A POTASSIUM CONCENTRATION (N = 89)

	log A	B1	B2	B3	R^2 %	SigR %	F	SigF %
log Q	0.027	-0.176	-	-	9.0	1.0	-	-
$\log Q^2$	-1.369	-0.815	-0.059	-	11.90	1.0	2.83	NS
$\log Q^3$	15.132	9.042	1.806	0.112	33.70	0.1	27.96	0.1

7.5 B SODIUM CONCENTRATION (N = 62)

	log A	B1	B2	B3	R^2 %	SigR %	F	SigF %
log Q	2.120	-0.136	-	-	17.6	0.1	-	-
$\log Q^2$	-0.661	-1.084	-0.077	-	33.91	0.1	14.61	0.1
$\log Q^3$	-5.987	-3.802	-0.033	-0.011	38.89	0.1	4.76	1.0

7.5 C CALCIUM CONCENTRATION (N = 101)

	log A	B1	B2	B3	R^2 %	SigR %	F	SigF %
log Q	2.008	-0.148	-	-	36.0	0.1	-	-
$\log Q^2$	1.025	-0.557	-0.031	-	39.13	0.1	5.07	1.0
$\log Q^3$	3.237	0.660	0.179	-0.011	41.0	0.1	3.064	5.0

7.5 D MAGNESIUM CONCENTRATION

	log A	B1	B2	B3	R^2 %	SigR %	F	SigF %
log Q	1.037	-0.221	-	-	64.0	0.1	-	-
$\log Q^2$	0.185	-0.533	-0.027	-	68.0	0.1	12.40	0.1
$\log Q^3$	3.093	1.067	0.249	0.015	72.68	0.1	16.54	0.1

7.5 E CHLORIDE CONCENTRATION (N = 74)

	log A	B1	B2	B3	R^2 %	SigR %	F	SigF %
log Q	3.102	-0.051	-	-	8.4	5.0	-	-
$\log Q^2$	2.905	-0.122	-0.006	-	8.94	5.0	0.41	NS
$\log Q^3$	4.634	0.842	0.162	0.009	13.38	5.0	3.58	5.0

7.5 F pH VALUES (N = 70)

	log A	B1	B2	B3	R^2 %	SigR %	F	SigF %
log Q	1.991	-0.007	-	-	0.8	NS	-	-
$\log Q^2$	-0.110	-1.332	-0.117	-	6.75	5.0	4.72	5.0
$\log Q^3$	-1.309	-2.105	-0.275	-0.010	6.79	5.0	0.1	NS

7.5 G BICARBONATE CONCENTRATION (N = 77)

	log A	B1	B2	B3	R^2 %	SigR %	F	SigF %
log Q	2.820	-0.131	-	-	2.9	NS	-	-
$\log Q^2$	1.501	-0.178	-0.017	-	6.69	5.0	2.69	NS
$\log Q^3$	-0.458	-1.313	-0.231	-0.013	9.93	5.0	2.35	NS

7.5 H SC VALUES µmhos (N = 69)

	log A	B1	B2	B3	R^2 %	SigR %	F	SigF %
log Q	3.492	-0.408	-	-	77.4	0.1	-	-
$\log Q^2$	3.742	-0.318	0.008	-	76.85	0.1	1.56	NS
$\log Q^3$	35.72	17.41	3.235	0.193	84.40	0.1	31.3	0.1

or TDS = 0.48 SC + 44.36 (SC 400 umhos); Q in l/sec.

I. Bivariate Regression for RSD

(i) K^+ conc. = $1.56\ Q^{0.092}$

(ii) SC = $198.6\ Q^{-0.041}$

II. Multiple Regression for RSD

(i) K^+ conc. =

$$\text{EXP}\ (0.075 \log_e(Q) + 0.175 \log_e(\text{API } 30 + 10) - 0.053)$$

(ii) SC =

$$\text{EXP}\ (5.373 - 0.063 \log_e(Q) + 0.161 \log_e(\text{API } 60 + 10))$$

III. Bivariate Regression for TSD

(i) K^+ conc. = $1.18\ (Q/1000)^{-0.096}$

(ii) TDS conc. = $50.15\ (Q/1000)^{-0.168}$

IV. Bivariate Regression for TSD Minus Autumn Storm Data

(i) K^+ conc. = $4.37\ (Q/1000)^{0.138}$

(ii) TDS conc. = $46.53\ (Q/1000)^{-0.165}$

V. Bivariate Regression for Autumn Storm Data

(i) K^+ conc. = $0.36\ (Q/1000)^{-0.291}$

(ii) TDS conc. = $1442\ (Q/1000)^{0.353}$

VI. Polynomial Regression for TSD

(i) K^+ conc. =

$$\text{EXP}\ (5.581 + 2.163 \log_e(Q/1000) + 0.296\left[\log_e(Q/1000)\right]^2 + 0.012\left[\log_e(Q/1000)\right]^3)$$

(ii) TDS conc. =

$$\text{EXP}\ (3.012 - 0.066 \log_e(Q/1000) + 0.120\left[\log_e(Q/1000)\right]^2 + 0.012\left[\log_e(Q/1000)\right]^3)$$

A. Storm 1: 26/27 April 1977 (30 minute storm sampling interval)

This was a storm of 9 mm rainfall which began with the SMD at 37.6 mm and API 15 at 3.7 mm.

(a) K^+ concentration actually behaves as other ions behave during autumn flushing, initially diluting, then increasing and diluting again before returning towards pre-storm concentration. This response is atypical for West Walk: K^+ concentration usually increases with discharge. None of the regression models are capable of predicting pre-storm concentration, the intra-storm concentration or timing of peaks and troughs, or the post storm concentration.

(b) TDS concentration shows a straightforward dilution, with minor increases on the descending limb. The concentration trough lags the peak by about eight hours. None of the regression models correctly predict the pre-storm or post-storm concentrations and the lag effect is not accounted for. If the data were lagged by about eight hours and increased by about 25 umhos, then the bivariate regression for TSD would approximate the actual chemograph form.

B. Storm 2: 14/15 October 1976 (30 minute storm sampling interval)

This was a storm of 21.5 mm rainfall which began with an SMD of 24.3 mm and an API 15 of 11.6 mm.

(a) K^+ concentration shows a marked flush with the initial discharge rise, a decrease, and then a second peak, followed by a rapid decrease, then a gradual return towards pre-storm concentration. The detailed K^+ behaviour is poorly modelled by the regressions, although general solute level prediction is good.

(b) TDS concentration shows an initial decline, a small increase, then a rapid, peaked flush coinciding with a rapid rise in discharge; this was followed by a decrease, and then increase to above pre-storm concentrations. The multiple regression model using RSD predicts the general solute level well, although other models under-estimate the autumn TDS concentration and fail to give accurate intra-storm detail.

The general conclusion here is that the regression models are poor

A. Storm 1: 26/27 April 1977 (30 minute storm sampling interval)

This was a storm of 9 mm rainfall which began with the SMD at 37.6 mm and API 15 at 3.7 mm.

(a) K^+ concentration actually behaves as other ions behave during autumn flushing, initially diluting, then increasing and diluting again before returning towards pre-storm concentration. This response is atypical for West Walk: K^+ concentration usually increases with discharge. None of the regression models are capable of predicting pre-storm concentration, the intra-storm concentration or timing of peaks and troughs, or the post storm concentration.

(b) TDS concentration shows a straightforward dilution, with minor increases on the descending limb. The concentration trough lags the peak by about eight hours. None of the regression models correctly predict the pre-storm or post-storm concentrations and the lag effect is not accounted for. If the data were lagged by about eight hours and increased by about 25 umhos, then the bivariate regression for TSD would approximate the actual chemograph form.

B. Storm 2: 14/15 October 1976 (30 minute storm sampling interval)

This was a storm of 21.5 mm rainfall which began with an SMD of 24.3 mm and an API 15 of 11.6 mm.

(a) K^+ concentration shows a marked flush with the initial discharge rise, a decrease, and then a second peak, followed by a rapid decrease, then a gradual return towards pre-storm concentration. The detailed K^+ behaviour is poorly modelled by the regressions, although general solute level prediction is good.

(b) TDS concentration shows an initial decline, a small increase, then a rapid, peaked flush coinciding with a rapid rise in discharge; this was followed by a decrease, and then increase to above pre-storm concentrations. The multiple regression model using RSD predicts the general solute level well, although other models under-estimate the autumn TDS concentration and fail to give accurate intra-storm detail.

The general conclusion here is that the regression models are poor

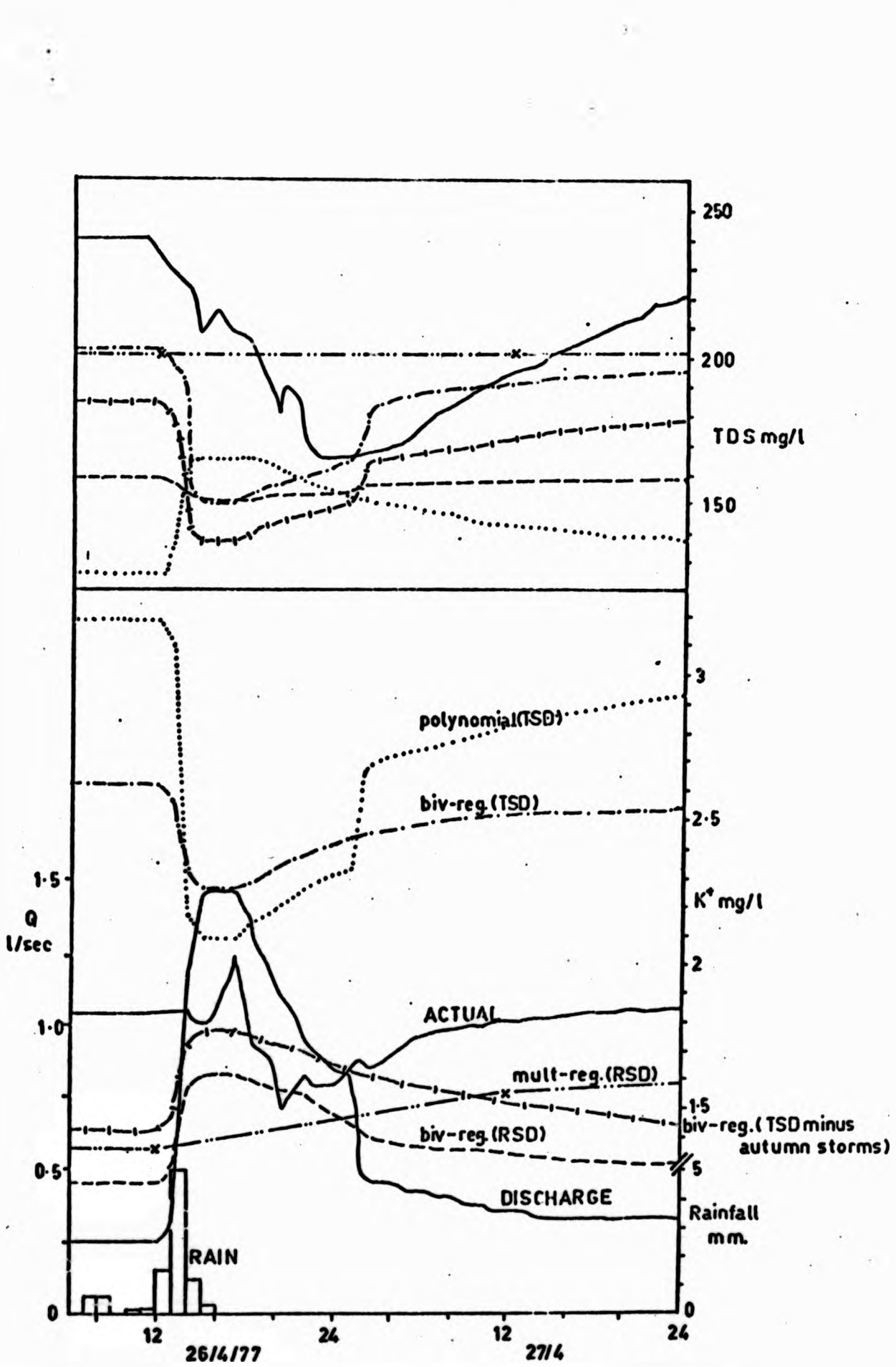

FIGURE 7.6: COMPARISON OF ACTUAL AND PREDICTED POTASSIUM AND TDS CONCENTRATIONS FOR A SINGLE APRIL STORM USING BIVARIATE AND MULTIVARIATE REGRESSION ON SEVERAL DATA SETS

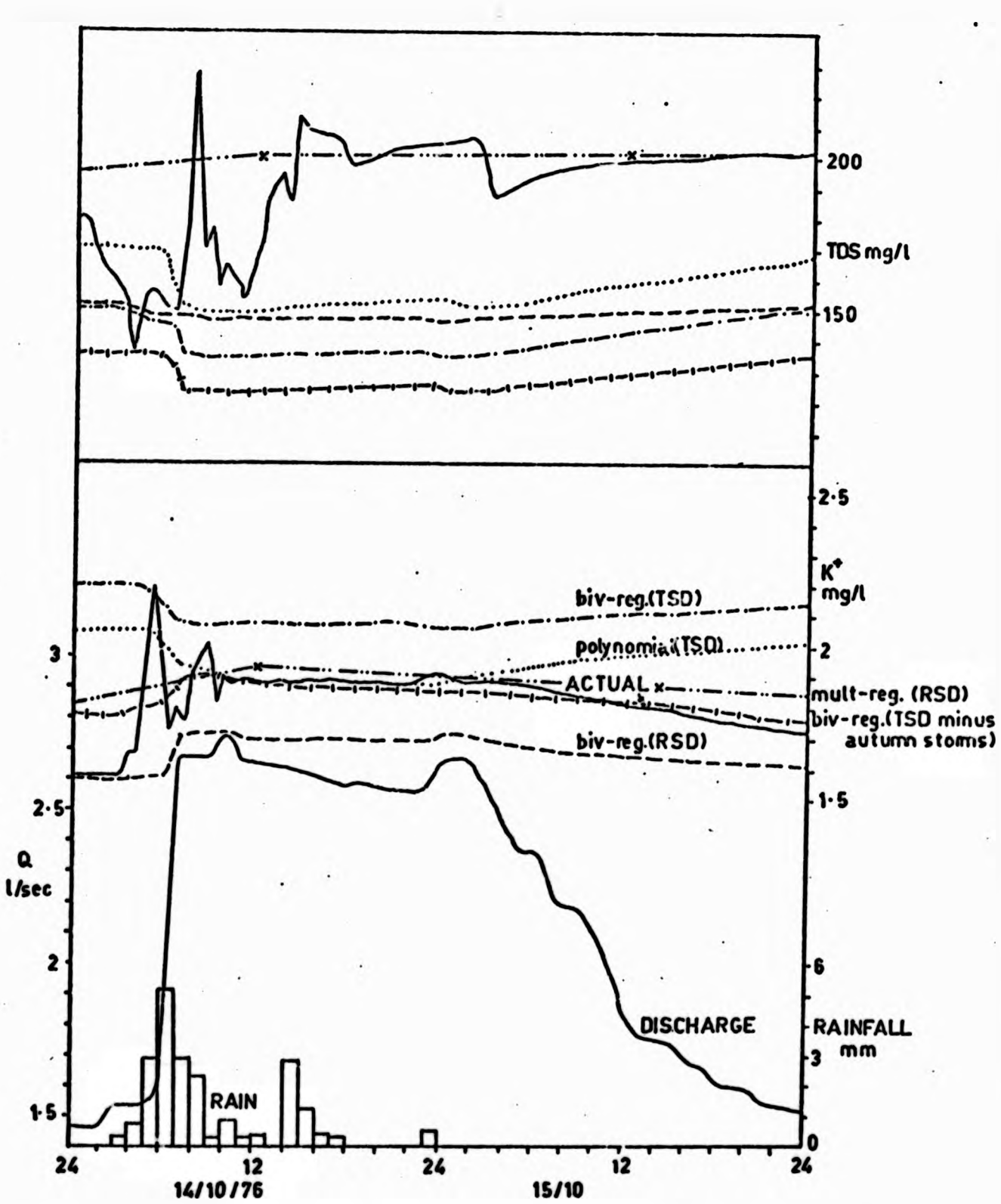

FIGURE 7.7: COMPARISON OF ACTUAL AND PREDICTED POTASSIUM AND TDS CONCENTRATIONS FOR A SINGLE OCTOBER STORM USING BIVARIATE AND MULTIVARIATE REGRESSION ON SEVERAL DATA SETS

predictors of detailed solute response under different catchment conditions (this also applies to other solutes not illustrated). The multiple regression model based upon RSD provides an encouraging estimate of general solute levels (re-affirming the conclusion of 6.2F), pointing to the importance of considering hydrometeorological variables in addition to discharge.

7.5 ANALYSIS OF INDIVIDUAL STORM SAMPLES

A. Introduction

The features of storm solute variation requiring detailed study were identified as:

(i) the generally high level of solute concentration during autumn storms and the 'flushing effect' (e.g. Walling and Foster, 1975);

(ii) the non-synchronous hydrograph and chemograph peaks, i.e. the 'lag and lead effect' (e.g. Glover and Johnson, 1974).

Problems encountered in the sampling program were discussed earlier, and as a result only 18 storm data sets were available for analysis; nine for W1, six for the flume and three for W2. From these storms, eight represent conditions during autumn 1976.

Several authors have reported unusually high solute levels during the post drought period (e.g. Foster and Walling, 1978; Walling and Foster, 1978; Anderson and Burt, 1978). Figure 7.8 shows the variation in five solute parameters between August and November 1976 at W1 (hydrological features of the drought were discussed in chapter 4). There had been little or no flow at W1 for six weeks before 29th August, when 29 mm rain fell, and a small rise in streamflow was accompanied by large rises in solute concentration. Above average solute levels were maintained until a further storm on 10th September, when further flushing occurred. Figures 7.9 A and B show this storm in detail and its effects on solute response at W1 and the flume. Both are plotted at the same scale, although the sampling interval at the flume (one hour) smooths detail in comparison with W1 (0.5 hour).

Considering W1, for K^+, the normal concentration effect occurs,

although the peak concentration was higher than average. However, for Na^+, Ca^{2+} and Mg^{2+} the normal dilution effect was almost completely overwhelmed by massive flushing. Cl^- concentration reacted very quickly to rainfall and may represent a direct input from the atmosphere to the channel (c.f. Weyman, 1974, for the effect of 'channel precipitation') or indirect input of Cl^- which had accumulated in channel-side interception storage. It is interesting to note that K^+ exhibited an initial concentration rise at the same time as Cl^-, since bracken has been found to contribute significant amounts of K^+ in throughfall (Carlisle et al, 1967). pH showed a normal dilution effect, the minimum value coinciding with flushing peaks of the other solutes, possibly due to the presence of dissolved organic acids. Fluctuation of solute levels continued after the maximum or minimum was reached, in this and other storms sampled, and may represent the arrival of solute pulses from relatively remote areas.

At the flume the response was different, which may be due to a variable spatial response within West Walk, and to the less frequent sampling interval. Hydrological response also varied, the hydrograph peaking earlier in response to the initial maximum rainfall intensity. Pre- and post storm solute levels were similar at both stations, but at the flume dilution replaced flushing.

After this storm high solute levels were maintained until the SMD had reduced to about 110 mm, when heavy rainfall caused an increase in streamflow, a rapid decrease in the SMD and a gradual decline in solute concentrations. Later storms caused reduced flushing effects as the available solute supply became exhausted.

Figure 7.10 shows solute response in late November 1976. By way of contrast with the earlier period described, dilution is now the dominant feature, with much smaller flushes of K^+, Ca^+, TDS (and SC) and an increase in pH, all during the hydrograph rise. Fluctuation of all solutes occurs during hydrograph recession.

Comparison of 1976 solute levels with average conditions is not possible because the early study period was also dry (i.e. summer - autumn 1975). However, mean concentrations for the RSD are plotted in Figure 7.8 and show the abnormally high September 1976 concentrations

although the peak concentration was higher than average. However, for Na^+, Ca^{2+} and Mg^{2+} the normal dilution effect was almost completely overwhelmed by massive flushing. Cl^- concentration reacted very quickly to rainfall and may represent a direct input from the atmosphere to the channel (c.f. Weyman, 1974, for the effect of 'channel precipitation') or indirect input of Cl^- which had accumulated in channel-side interception storage. It is interesting to note that K^+ exhibited an initial concentration rise at the same time as Cl^-, since bracken has been found to contribute significant amounts of K^+ in throughfall (Carlisle et al, 1967). pH showed a normal dilution effect, the minimum value coinciding with flushing peaks of the other solutes, possibly due to the presence of dissolved organic acids. Fluctuation of solute levels continued after the maximum or minimum was reached, in this and other storms sampled, and may represent the arrival of solute pulses from relatively remote areas.

At the flume the response was different, which may be due to a variable spatial response within West Walk, and to the less frequent sampling interval. Hydrological response also varied, the hydrograph peaking earlier in response to the initial maximum rainfall intensity. Pre- and post storm solute levels were similar at both stations, but at the flume dilution replaced flushing.

After this storm high solute levels were maintained until the SMD had reduced to about 110 mm, when heavy rainfall caused an increase in streamflow, a rapid decrease in the SMD and a gradual decline in solute concentrations. Later storms caused reduced flushing effects as the available solute supply became exhausted.

Figure 7.10 shows solute response in late November 1976. By way of contrast with the earlier period described, dilution is now the dominant feature, with much smaller flushes of K^+, Ca^+, TDS (and SC) and an increase in pH, all during the hydrograph rise. Fluctuation of all solutes occurs during hydrograph recession.

Comparison of 1976 solute levels with average conditions is not possible because the early study period was also dry (i.e. summer - autumn 1975). However, mean concentrations for the RSD are plotted in Figure 7.8 and show the abnormally high September 1976 concentrations

followed by the return to 'average' concentrations.

A further example of solute response is provided by a storm in April 1977 (Figures 7.11 A and B). Dilution dominates the response at W1, a feature well shown by SC and TDS. The exceptions to this trend are Na^{+}, Ca^{2+}, Mg^{2+} and pH which all exhibit a late flush during flow recession. Samples analysed for silicon, expressed as Si^{4+}, show an increase with discharge at W1 and the flume, which may reflect the contribution of colloidal material (< 0.5 µm) not excluded during the filtration process. On this occasion the flume exhibited a far more varied solute response. Although the overall reaction was one of dilution, flushing of Na^{+}, Ca^{2+}, Mg^{2+}, Cl^{-} (possibly rainfall) and TDS (with SC) occurred. These examples serve to emphasise:

(i) the complexity of detailed stream solute response;

(ii) the variable spatial response; and

(iii) solute flushing in West Walk can occur at any time of the year.

The latter phenomenon varies according to catchment moisture status, autumn lying at one end of a spectrum of conditions.

B. Analysis of Regression Coefficients for Individual Storms

Earlier regression analysis identified separate regressions for autumn and non-autumn data. In general this showed that the a coefficient (intercept) representing solute concentration at infinitely low flow, was higher for autumn than for non-autumn data. The effect was particularly pronounced for potassium concentration (e.g. Figure 7.1 A) where the individual storm intercepts began high in September and decreased as autumn progressed. This suggested that a regression model similar to that described by J O Ledbetter and E F Gloyna (1964) with variable coefficients, could be developed. It was decided to undertake detailed work using K^{+} concentration at W1 and the flume. This is presented as a case study.

Regression equations were fitted to the 15 individual storms to obtain a and b coefficients (Table 7.6). Using a t test, five of the

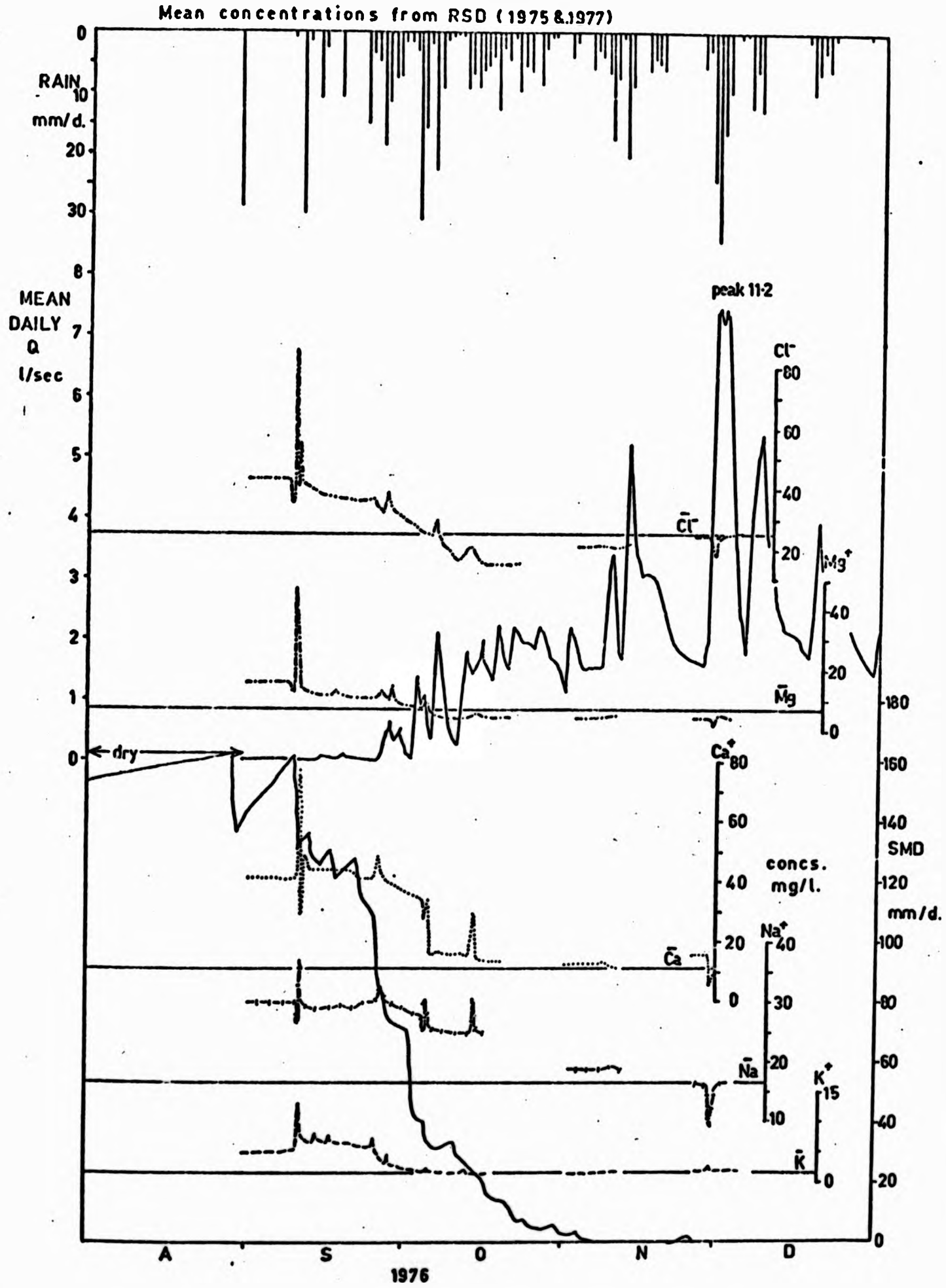

FIGURE 7.8: THE VARIATION OF POTASSIUM, SODIUM, MAGNESIUM, CALCIUM AND CHLORIDE AT WEIR 1 BETWEEN AUGUST AND NOVEMBER 1976

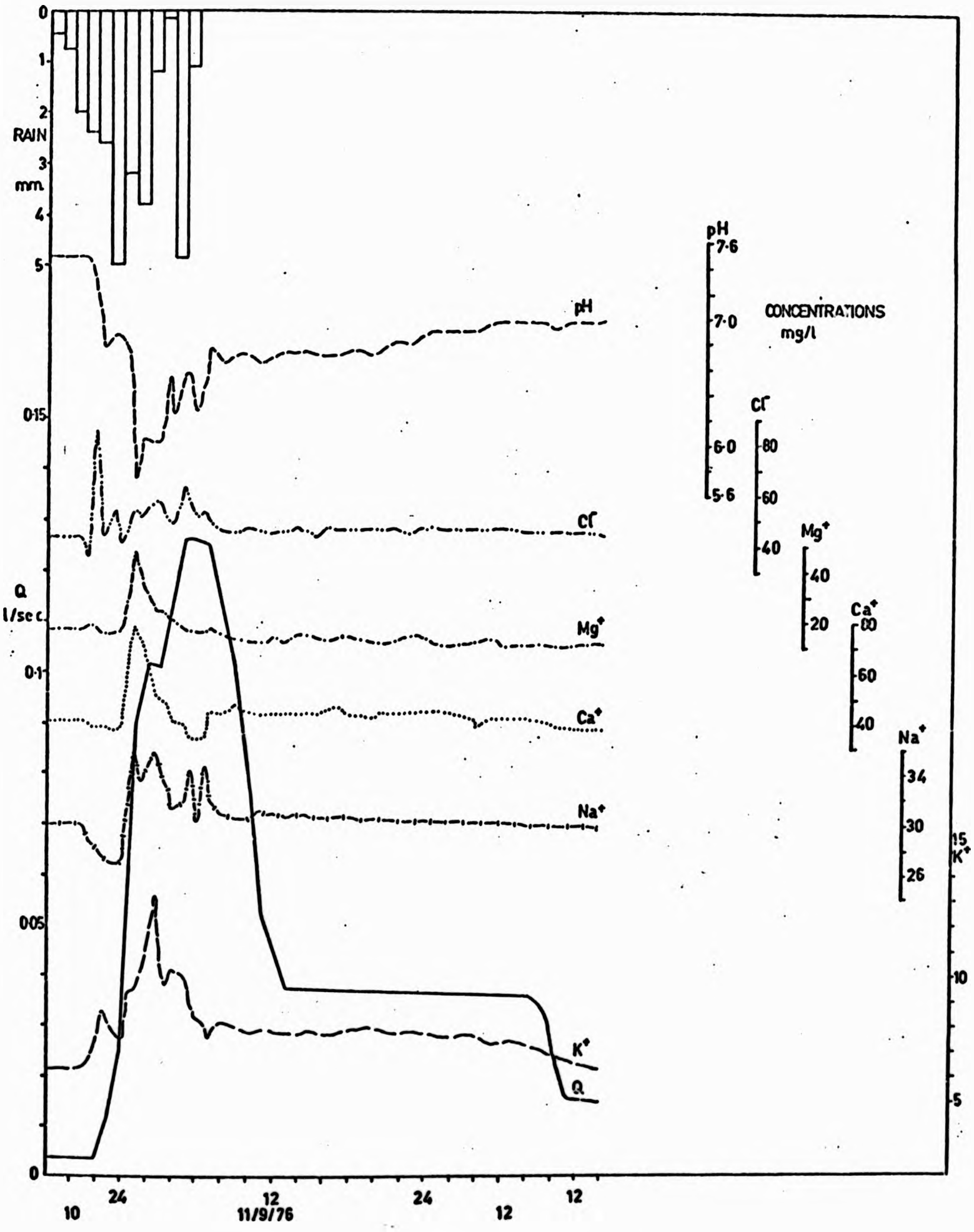

FIGURE 7.9 A: SOLUTE RESPONSE AT WEIR 1:
10 - 11 SEPTEMBER 1976

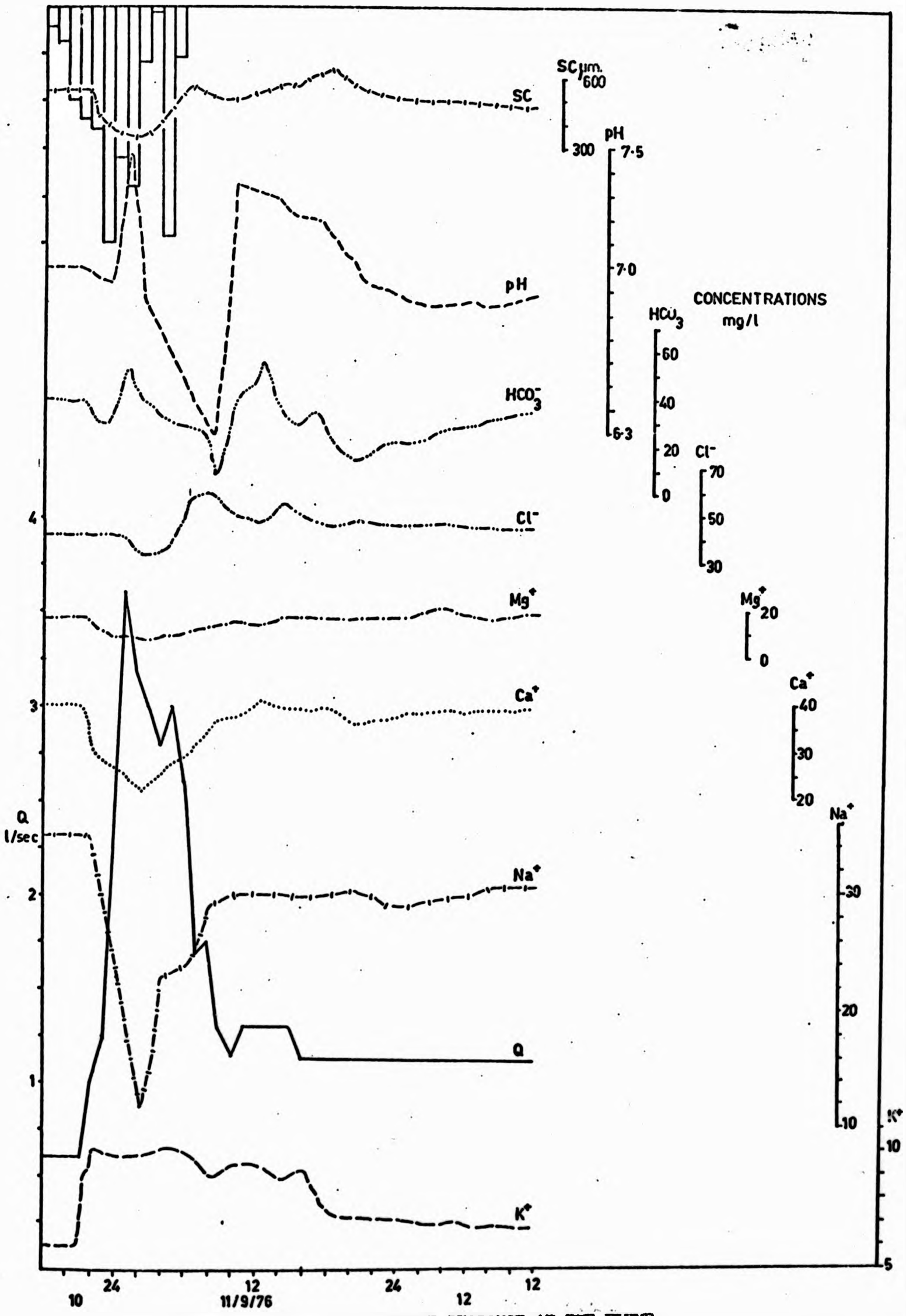

FIGURE 7.9 B: SOLUTE RESPONSE AT THE FLUME: 10 - 11 SEPTEMBER 1976

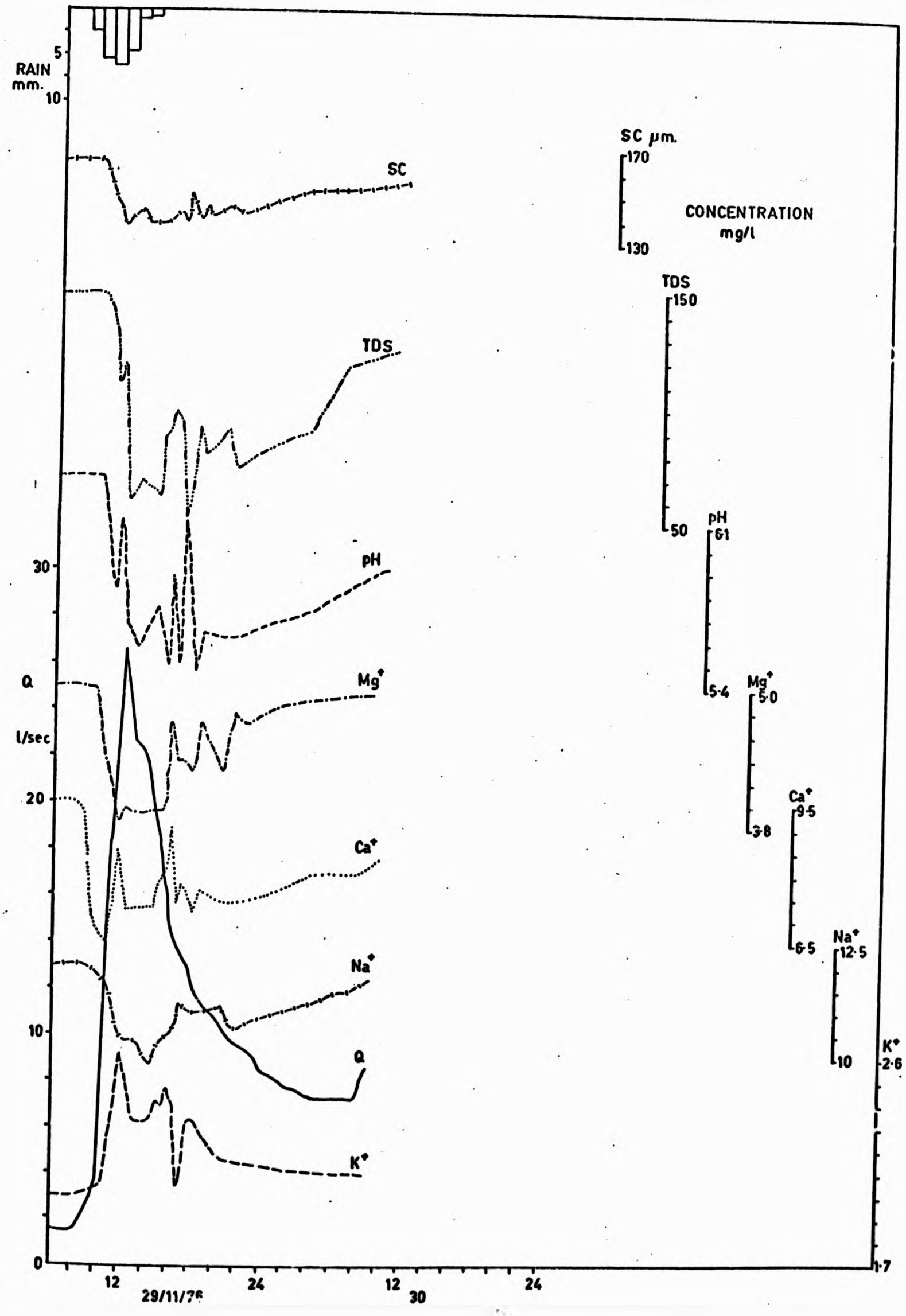

FIGURE 7.10: SOLUTE RESPONSE AT WEIR 1:
29 - 30 NOVEMBER 1976

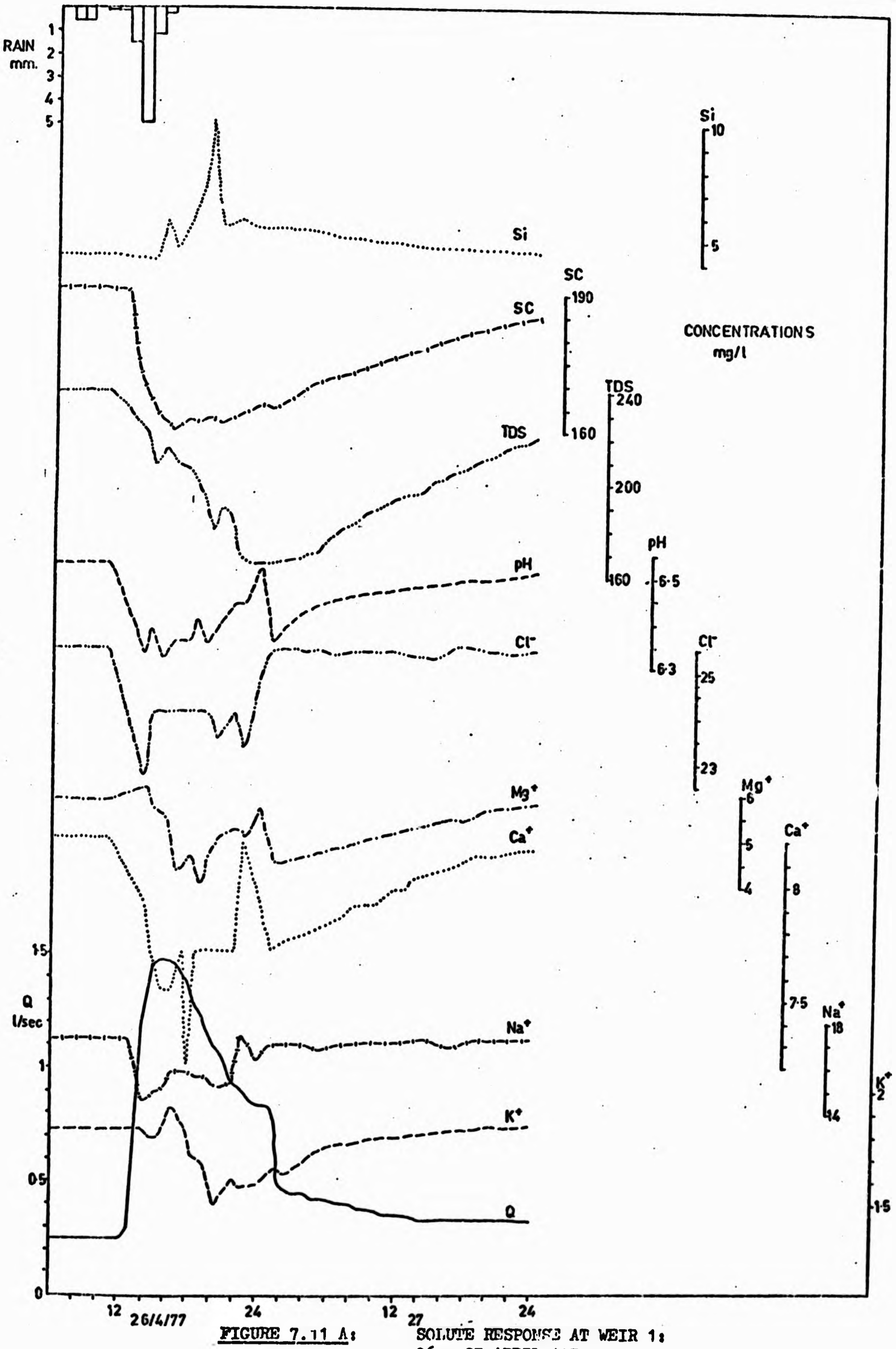

FIGURE 7.11 A: SOLUTE RESPONSE AT WEIR 1: 26 - 27 APRIL 1977

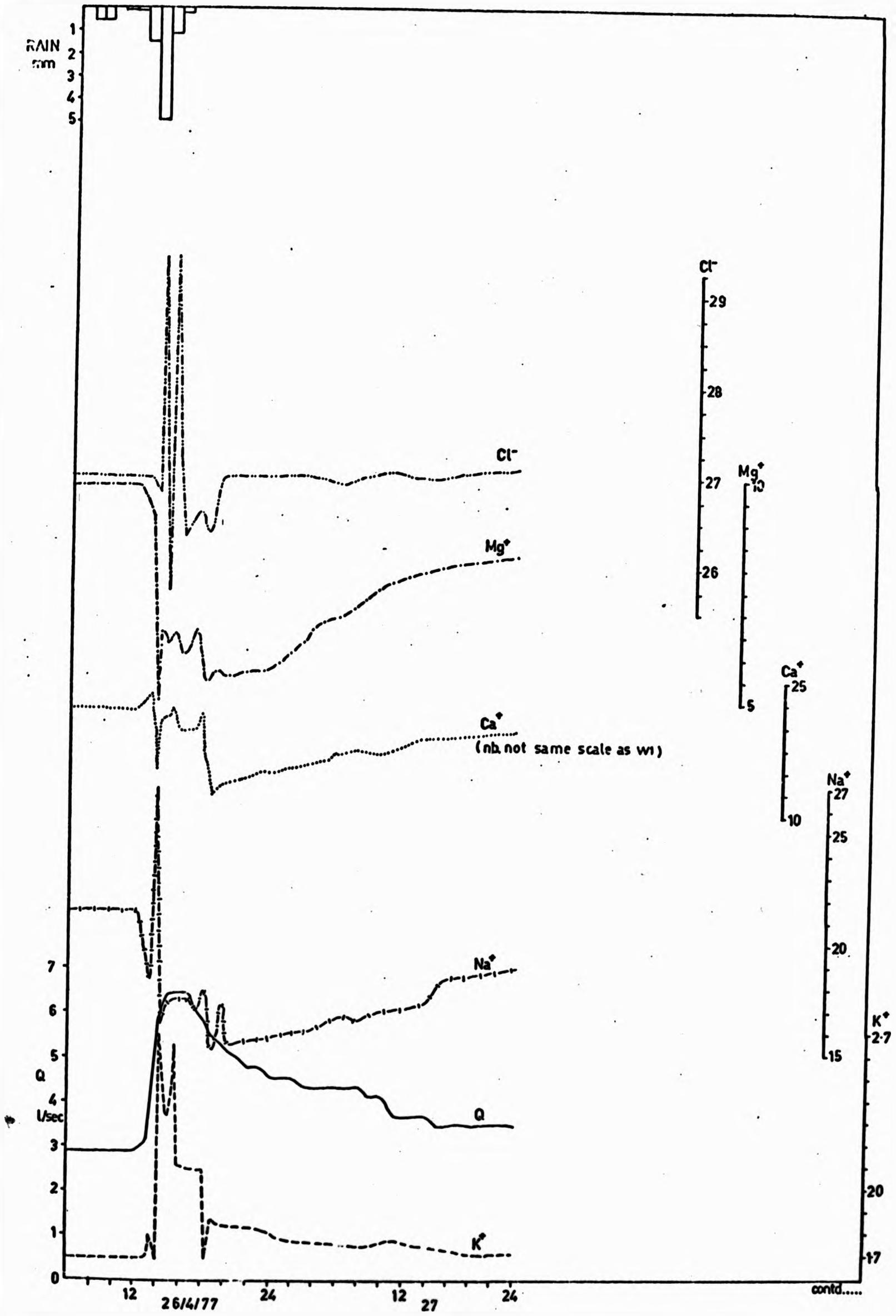

FIGURE 7.11 B: SOLUTE RESPONSE AT THE FLUME: 26 - 27 APRIL 1977

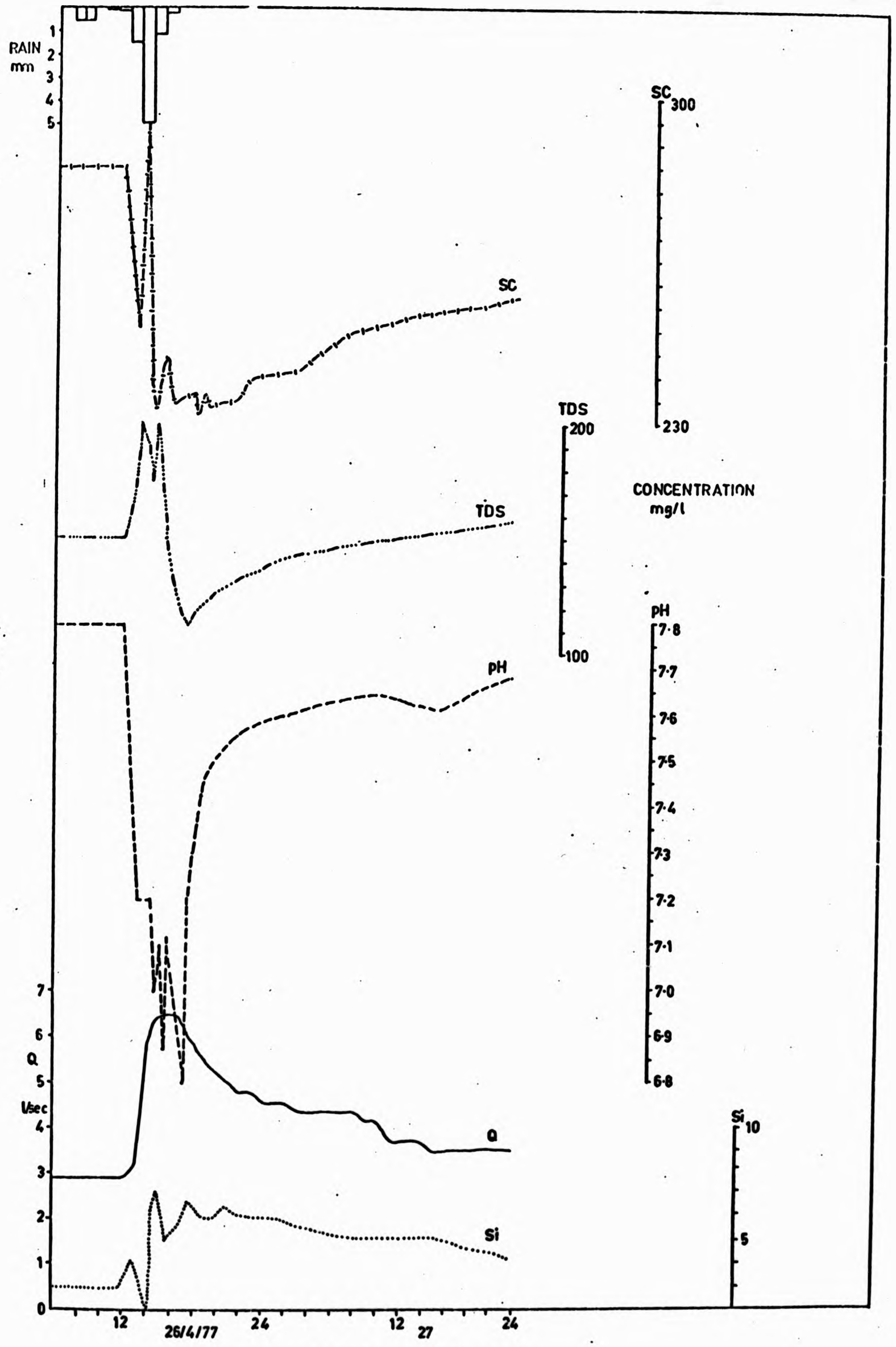

FIGURE 7.11 B (cont'd):

correlation coefficients were found to be insignificant at the 5.0 % level. Standard errors were computed for a from:

$$SE_a = V_x \left(\frac{1}{n} + \frac{\bar{x}}{\sum (x_i - x)^2} \right) \qquad \text{(Brownlee, 1965)} \qquad (7.1)$$

where V_x = residual mean squares from the regression

and b from:

$$SE_b = SE_y / S_x \sqrt{N - 2} \qquad \text{(Johnston, 1978)} \qquad (7.2)$$

where SE_y = standard error of Y
S_x = standard deviation of X

Significance levels for a and b were calculated from a 't' test.

$$t = a / SE_a \qquad (7.3)$$

$$t = b / SE_b \qquad (7.4)$$

Despite the insignificance of some coefficients, all were included in the analysis, primarily due to the small number of storms actually sampled.

Intuitively, it was thought that 'a' should be strongly related to the level of flow preceding the storm, Q_p. Other indices representing soil moisture status could have been used, e.g. SMD or an API, but Q_p had appeared to be important from visual inspection of the solute discharge ratings and was readily available from flow records. For W1 it was found that:

$$a = 1.567 \; Q_p^{-0.325} \qquad (7.5)$$

$r = -0.965$; $r^2 = 93.1\%$; $N = 9$; sig. level = 0.1 %;
$SE_{\hat{a}} = 0.183$. Q_p in litres/sec. a in mg/l

Slight non-linearity in this relationship can be described by a cubic function:

TABLE 7.6: POTASSIUM - INDIVIDUAL STORM REGRESSIONS WITH DISCHARGE (l/sec) (RMA line used; log data)

7.6 A: W1

Date	a	SE_a	Sig a %	b	SE_b	Sig b %	SE_y	r	Sig r %	N
28/11/75	1.471	0.001	0.1	0.392	0.019	0.1	0.04	0.98	1.0	5
01/12/75	1.618	0.005	0.1	0.233	0.004	0.1	0.008	0.99	0.1	8
12/03/76	1.966	0.038	0.1	0.210	0.037	0.1	0.03	0.96	0.1	9
10/09/76	11.435	0.180	0.1	0.090	0.680	NS	0.14	0.68	1.0	19
27/09/76	2.954	0.054	0.1	0.064	0.046	NS	0.11	0.37	NS	15
05/10/76	1.916	0.015	0.1	0.015	0.009	NS	0.04	0.42	NS	12
14/10/76	1.669	0.053	0.1	0.123	0.033	1.0	0.07	0.4	NS	19
29/11/76	1.484	0.018	0.1	0.162	0.003	0.1	0.05	0.7	1.0	15
26/04/76	1.711	0.079	0.1	0.046	0.081	NS	0.08	0.22	NS	13

7.6 B: FLUME

Date	a	SE_a	Sig a %	b	SE_b	Sig b %	SE_y	r	Sig r %	N
13/09/75	5.348	0.031	0.1	0.089	0.003	0.1	0.09	0.82	1.0	9
01/12/76	1.526	0.031	0.1	0.109	0.002	0.1	0.10	0.46	NS	12
28/11/76	1.159	0.019	0.1	0.287	0.003	0.1	0.03	0.99	5.0	4
10/09/76	8.200	0.061	0.1	0.168	0.038	1.0	0.10	0.54	1.0	12
14/09/76	7.795	0.026	0.1	0.124	0.016	0.1	0.03	0.71	0.1	12
26/04/76	0.994	0.085	0.1	0.426	0.038	0.1	0.12	0.64	5.0	12

NOTE: Coefficients are from equation $Y = aX^b$

$$a = \text{EXP}\,(0.381 + 0.062 \log_e Q_p + 0.287 \log_e Q_p^{\,2} + 0.038 \log_e Q_p^{\,3}) \qquad (7.6)$$

$r = -0.997$; $r^2 = 99.4\,\%$; $N = 9$; Sig. level $= 0.1\,\%$;
$SE_{\hat{a}} = 0.066$

F for inclusion of $Q_p^{\,2} = 11.5$, sig. level $= 0.1\,\%$
F for inclusion of $Q_p^{\,3} = 13.5$, sig. level $= 0.1\,\%$

For the flume it was found that:

$$a = 2.261\, Q_p^{-0.433} \qquad (7.7)$$

$r = -0.867$; $r^2 = 75.1\%$; $N = 6$; Sig. level $= 5.0\,\%$;
$SE_a = 0.867$

This relationship was not significantly improved by the addition of higher order terms.

Both regressions exhibit high variance explanation and the negative correlation suggests that the lower the pre-storm discharge the higher will be the model intercept. Furthermore, for any single pre-storm discharge, the intercept will be higher at the flume than at W1, which agrees with general catchment solute levels noted earlier (6.3 C).

Ledbetter and Gloyna (ibid) and Walling (1974) related the b coefficient to discharge. However, before attempting to correlate b with hydrometeorological factors, a variance ratio test was used to determine whether a significant difference existed between individual coefficients, b_i, and a mean coefficient, $\bar{b}$. If there was no significant difference then b could be used in the regression model. The variance ratio , F, was computed from:

$$F(K - 1,\ N - 2K) = S_2^{\,2} / S_1^{\,2} \qquad (7.8)$$

where $S_1^{\,2}$ = variance about individual regression lines
$S_2^{\,2}$ = variance about individual slopes

i...k = number of separate regressions

v...n_i = sample size for regression i

$$S_1^2 = \sum_i^k \sum_v^{n_i} (y_{iv} - \bar{y})^2 - \sum_i^k \left\{ \frac{\left(\sum_v^{n_i} (x_{iv} - \bar{x}_i)(y_{iv} - \bar{y}_i) \right)^2}{\sum_v^{n_i} (x_{iv} - \bar{x}_i)^2} \right\} \quad Df = (N - 2k) \qquad (7.9)$$

y = solute concentration, mg/l

x = discharge, l/sec

$$S_2^2 = \sum_i^k (b_i - \bar{b})^2 \sum_v^{n_i} (x_{iv} - \bar{x}_i)^2 \quad Df = (k - 1) \qquad (7.10)$$

This test was programmed in BASIC (Appendix 2 : ANACOVAR). For W1 and the flume, considering significant coefficients only, $F(5, 92) = 21.48$ and $F(4, 39) = 11.83$ respectively. The F values increased when all the b coefficients were included. Thus, at the 0.1 % level, significant differences in $\bar{b}$ and b_i existed.

Recognition of the factor controlling b coefficients was not as easy as with the intercepts. Therefore, eight possible factors were identified and included in a correlation matrix procedure, similar to that used earlier. The independent variables were as follows:

(i) Pre-storm discharge (Q_p), l/sec

(ii) Sine Index (SI)

This was included to identify any seasonal variation in b. SI was optimised in the same way as for RSD (6.3 Aiv).

The remaining six variables described hydrometeorological conditions during each storm.

(iii) Time of hydrograph rise. (T_r), minutes

This is the time from the start of the hydrograph to peak flow.

(iv) Hydrograph rise (H_r) l/sec

This represents peak storm discharge minus preceding flow level (Q_p).

(v) Flood Intensity (FI) l/sec/hour

This is computed from H_r / T_r.

(vi) Total Storm Rainfall (R), mm

(vii) Maximum Rainfall Intensity (IMAX), mm/hour

(viii) Mean Rainfall Intensity (IMEAN), mm/hour

Correlation matrices for W1 and the flume are shown in Tables 7.7 A and B. The insignificance of correlation coefficients is strongly influenced by the small sample size. However, the b coefficient is strongly correlated with SI at W1 and the flume, although the relationships are positive and negative respectively. They imply that the highest rate of solute change with discharge occurs in January at W1 and March at the flume; minimum rates occur in July and September respectively. At W1 the b coefficient shows significant negative correlation with IMAX but a positive correlation with IMEAN. Furthermore, the SI is positively correlated with IMAX and negatively correlated with IMEAN. These relationships imply that in July, for example, high IMAX would correspond with a low b coefficient. The occurrence of greatest IMAX in July is logical since it is during summer that heavy convectional rain often falls. The correspondingly low b value is difficult to interpret without knowledge of the physical processes, but it may be due to the longer time required for water to infiltrate dry soils and hence leach K^+.

It was noted in Chapter 2.3 that differences in the times of hydrograph and chemograph peaks (i.e. lag or lead) increased hysteresis in bivariate solute/discharge relationships. In the present case, it was thought that the elimination of lag and lead effects would improve the significance of individual storm correlations and their regression coefficients. This was achieved by cross-correlating series of interpolated hourly discharges and solute concentrations for each storm

TABLE 7.7: CORRELATION MATRIX FOR b COEFFICIENTS FROM INDIVIDUAL POTASSIUM/DISCHARGE REGRESSIONS
(Log data except sine index)

7.7 A: W1

	b	Qp	SI*	Tr	Hr	FI	R	I MAX	I MEAN
b	1	- 0.20	- 0.67	0.31	0.20	0.12	0.45	- 0.81	0.70
Qp	NS	1	0.07	0.60	0.62	0.50	0.46	0.50	- 0.30
SI*	5.0	NS	1	- 0.38	- 0.69	- 0.65	- 0.84	0.87	- 0.97
Tr	NS	NS	NS	1	0.50	0.24	0.73	- 0.15	0.28
Hr	NS	NS	5.0	NS	1	0.96	0.90	- 0.25	0.48
FI	NS	NS	NS	NS	0.1	1	0.78	- 0.23	0.45
R	NS	NS	1.0	5.0	0.1	5.0	1	- 0.51	0.70
I MAX	1.0	NS	1.0	NS	NS	NS	NS	1	- 0.96
I MEAN	5.0	NS	0.1	NS	NS	NS	5.0	0.1	1

* SI = SINE (RAD) (2 (D - 100) / 365), D = day of year, numbered from 1st January
Lower half of the table shows % significance levels from t tests.
N = 9

7.7 B: FLUME

	b	Qp	SI*	Tr	Hr	FI	R	I MAX	I MEAN
b	1	0.52	0.79	- 0.23	- 0.34	- 0.25	- 0.73	0.16	- 0.63
Qp	NS	1	0.50	0.45	0.38	0.33	- 0.50	- 0.48	- 0.19
SI*	5.0	NS	1	- 0.25	- 0.29	- 0.24	- 0.70	0.33	- 0.57
Tr	NS	NS	NS	1	0.85	0.59	0.50	- 0.17	0.65
Hr	NS	NS	NS	1.0	1	0.92	0.59	- 0.28	0.83
FI	NS	NS	NS	NS	0.1	1	0.48	- 0.38	0.76
R	NS	NS	NS	NS	NS	NS	1	0.23	0.93
I MAX	NS	NS	NS	NS	NS	NS	NS	1	0.06
I MEAN	NS	NS	NS	NS	5.0	NS	1.0	NS	1

* SI = SINE (RAD) (2 (D - 361) / 365)
N = 6

using the program LAG (Appendix 2). There was a significant improvement in correlation coefficients for lagged over unlagged regressions (Table 7.8 A and B).

Using the intercepts from lagged regressions it was found that the relationships were little different from equations 7.5 - 7.7 with no improvement in r^2 %. Correlation matrices for lagged b coefficients and independent variables are given in Tables 7.9 A and B. None of the correlation coefficients between b and independent variables for W1 are significant. Only the correlations with rainfall variables are significant for the flume. Although lagging the individual storms improves solute/discharge correlations, it worsens the relationships between b coefficients and independent variables. The unlagged data were therefore preferred to lagged data.

Consideration was given to developing multiple regression equations for explaining and predicting b values. The best bivariate relationship for W1 was:

$$b = 0.611\ IMAX^{-0.60} \qquad (7.11)$$

$r = -0.81$; $r^2 = 65.6\ \%$; $N = 9$; Sig. level $= 1.0\ \%$;
$SE_{\hat{b}} = 0.296$

Collinearity reduced the number of variables which could be included in a multiple regression model although the variables R and T_r did not significantly improve the variance explanation. The final predictive model for K^+ at W1 is therefore:

$$K^+ \text{ conc. (mg/l)} = \text{EXP}\ (0.381 + 0.062 \log_e Q_p + 0.287 \log_e Q_p^{\,2} + 0.038 \log_e Q_p^{\,3})\ Q^{(0.611\ IMAX^{-0.60})} \qquad (7.12)$$

where Q = discharge, l/sec
$IMAX$ = maximum storm rainfall intensity, mm/hour
Q_p = discharge prior to storm, l/sec

TABLE 7.8: POTASSIUM : INDIVIDUAL STORM REGRESSIONS WITH LAGGED DISCHARGE (l/sec)
(RMA line used; log data)

7.8 A: W1

Date	a	SE_a	Sig a %	b	SE_b	Sig b %	SE_y	r	Sig r %	N	L
28/11/75	1.450	0.001	0.1	0.403	0.025	1.0	0.051	0.97	1.0	5	0
01/12/76	1.640	0.007	0.1	0.217	0.007	0.1	0.018	0.98	0.1	8	1.0
12/03/76	1.950	0.039	0.1	0.186	0.012	0.1	0.032	0.96	0.1	9	0.25
10/09/76	16.87	0.201	0.1	0.270	0.553	NS	0.114	0.77	0.1	19	3.0
27/09/76	2.960	0.050	0.1	0.064		NS	0.098	0.40	NS	15	- 0.25
05/10/76	1.910	0.020	0.1	0.018		NS	0.039	0.50	NS	12	2.0
14/10/76	1.360	0.032	0.1	0.344	0.024	0.1	0.050	0.74	0.1	19	2.0
29/11/76	1.580	0.017	0.1	0.162	0.003	0.1	0.044	0.70	0.1	15	0
26/04/76	1.65	0.082	0.1	0.306	0.037	0.1	0.037	0.88	0.1	13	1.0

L = lag or lead (hours) of chemograph compared with hydrograph, giving maximum correlation.

7.8 B: **FLUME**

Date	a	SE_a	Sig a %	b	SE_b	Sig b %	SE_y	r	Sig r %	N
13/09/75	4.770	0.028	0.1	0.130	0.002	0.1	0.042	0.79	5.0	9
01/12/76	1.060	0.019	0.1	0.216	0.001	0.1	0.042	0.94	0.1	12
28/11/76	1.510	0.021	0.1	0.204	0.006	0.1	0.063	0.93	5.0	4
10/09/76	7.900	0.060	0.1	0.223	0.033	0.1	0.085	0.72	1.0	12
14/09/76	6.450	0.031	0.1	0.252	0.019	0.1	0.034	0.78	1.0	12
26/04/75	1.310	0.101	0.1	1.308	0.003	0.1	0.103	0.67	1.0	12

TABLE 7.9: CORRELATION MATRIX FOR b COEFFICIENTS FROM INDIVIDUAL POTASSIUM/LAGGED DISCHARGE REGRESSIONS (Log data except sine index)

7.9 A: W1

	b	Qp	SI*	Tr	Hr	FI	R	I MAX	I MEAN
b	1	0.12	- 0.60	- 0.14	- 0.38	- 0.10	- 0.32	- 0.03	- 0.49
Qp	NS	1	- 0.78	0.65	0.68	0.07	0.48	0.59	- 0.13
SI*	NS	1.0	1	- 0.87	- 0.76	0.30	- 0.50	- 0.71	- 0.32
Tr	NS	NS	0.1	1	0.63	- 0.42	0.58	0.57	0.43
Hr	NS	5.0	1.0	NS	1	0.34	0.87	0.22	0.56
FI	NS	NS	NS	NS	NS	1	0.45	- 0.63	0.08
R	NS	NS	NS	NS	0.1	NS	1	- 0.17	0.71
I MAX	NS	NS	5.0	NS	NS	NS	NS	1	- 0.27
I MEAN	NS	NS	NS	NS	NS	NS	5.0	NS	1

* SI = SINE (RAD) (2 (D - 61) / 365), D = day of year, numbered from 1st January.
Lower half of table shows % significance levels for t tests.
N = 9 .

7.9 B: **FLUME**

	b	Qp	SI*	Tr	Hr	FI	R	I MAX	I MEAN
b	1	0.29	0.18	- 0.11	- 0.52	- 0.64	- 0.77	- 0.45	- 0.96
Qp	NS	1	0.97	0.63	0.60	0.54	- 0.36	- 0.81	0.34
SI*	NS	0.1	1	0.77	0.72	0.61	- 0.16	- 0.64	- 0.17
Tr	NS	NS	5.0	1	0.84	0.54	0.43	- 0.12	0.14
Hr	NS	NS	NS	1.0	1	0.90	0.49	- 0.18	0.47
FI	NS	NS	NS	NS	0.1	1	0.34	- 0.27	0.58
R	5.0	NS	NS	NS	NS	NS	1	0.74	0.81
I MAX	NS	1.0	NS	NS	NS	NS	NS	1	0.60
I MEAN	0.1	NS	NS	NS	NS	NS	1.0	NS	1

* SI = SINE (RAD) (2 (D + 30) / 365)
N = 6

The best bivariate relationship for the flume was:

$$b = 0.552.EXP\ (0.664\ SI) \qquad (7.13)$$

$r = 0.79$; $r^2 = 62.4\ \%$; $N = 6$; Sig. level $= 5.0\ \%$;
$SE_{\hat{b}} = 0.418$

Collinearity was not such a problem as with W1 data and stepwise multiple regression using the procedure described earlier was applied. However, no additional variable significantly added to r^2 % and the final predictive at the flume is therefore:

$$K^+ \text{conc. (mg/l)} = (2.261\ Q_p^{-0.433})\ Q^{(0.552.EXP\ (0.664\ SI)} \qquad (7.14)$$

Q = discharge, l/sec

In Figures 7.12 A, B and C predicted K^+ concentrations at W1 using the equation (7.12) are compared with actual data (A and B are directly comparable with Figures 7.6 and 7.7). Predicted K^+ concentration using storm regression coefficients from Table 7.6 is also plotted.

(i) Storm: 26th April 1977

There is good agreement for pre-storm and post-storm concentrations, but a failure to predict the maximum storm concentration and subsequent dilution effect.

(ii) Storm: 14th October 1976

Pre-storm concentration is slightly over-predicted, while intra-storm predictions are about 6 % too low. There is also a failure to model the initial peak of 2.2 mg/l.

(iii) Storm: 10th September 1976

Concentrations are consistently under-predicted. Again, the sharp peak of 13.2 mg/l is estimated as only 8 mg/l.

Figures 7.13 A and B plot measured and predicted K^+ concentration for the flume using equation (7.14).

(i) Storm: 10th September 1976

The model greatly under-estimates concentrations, primarily due to a low intercept.

(ii) Storm: 1st December 1975

K^+ concentrations are over-predicted, largely due to poor estimation of the regression coefficients.

There are several conclusions to this particular case study.

Firstly, the variable coefficient model fails accurately to describe detailed storm solute variation over the full range of conditions recorded at West Walk. It therefore has no distinct advantage over other regression models developed in this chapter with the possible exception of bivariate and polynomial regression using the total sampled data.

Secondly, the individual storm 'a' coefficients are clearly dependent upon catchment wetness preceding the storm. The 'b' coefficients are significantly correlated with maximum rainfall intensity at W1 and the sine index at the flume. It is the errors incurred in the regressions which combine to reduce the advantage of the variable coefficient models over bivariate and multivariate approaches.

Thirdly, all the models developed so far fail to predict flushing of elements, as Figure 7.13 C shows. The next section attempts to elucidate the factors controlling these flushes.

C. Analysis of Solute Flushing during Storms

Eight storms from W1 were chosen for quantification of the flushing effect in Na^+, Ca^{2+} and Mg^{2+}. These solutes, usually showing a dilution effect, exhibited pronounced increases in concentration during autumn 1976 storms. K^+ is excluded from this analysis because concentration increase is a normal response.

It was noted earlier that the physical processes causing solute flushing are poorly understood. In an attempt to highlight primary

A.

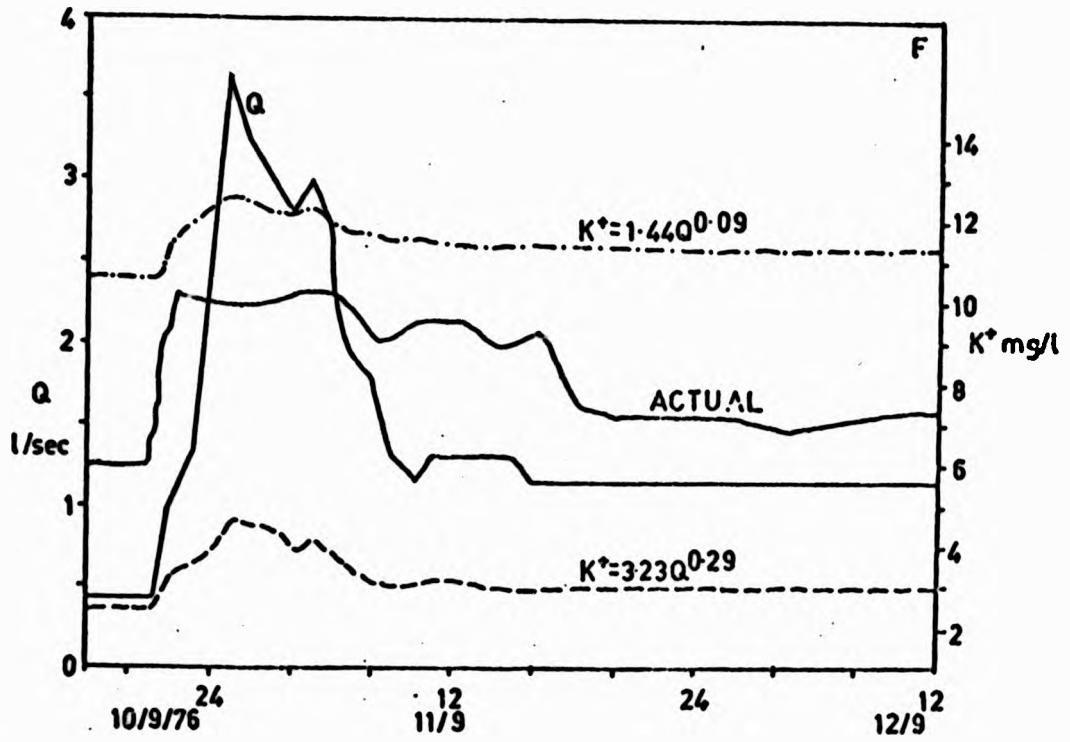

B.

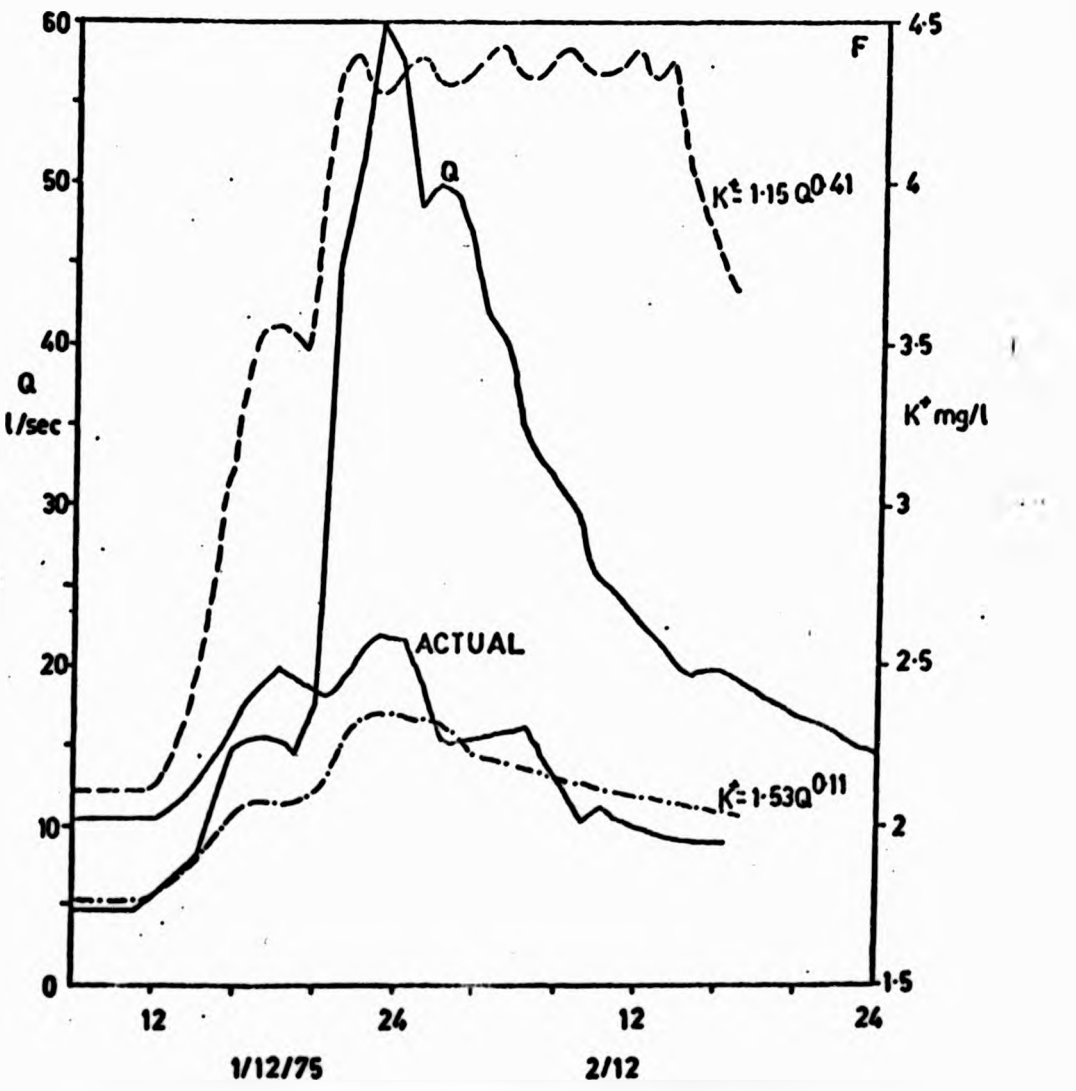

FIGURE 7.12: COMPARISON OF ACTUAL AND PREDICTED POTASSIUM CONCENTRATIONS FOR THREE STORMS AT WEIR 1 USING THE VARIABLE COEFFICIENT MODEL

A.

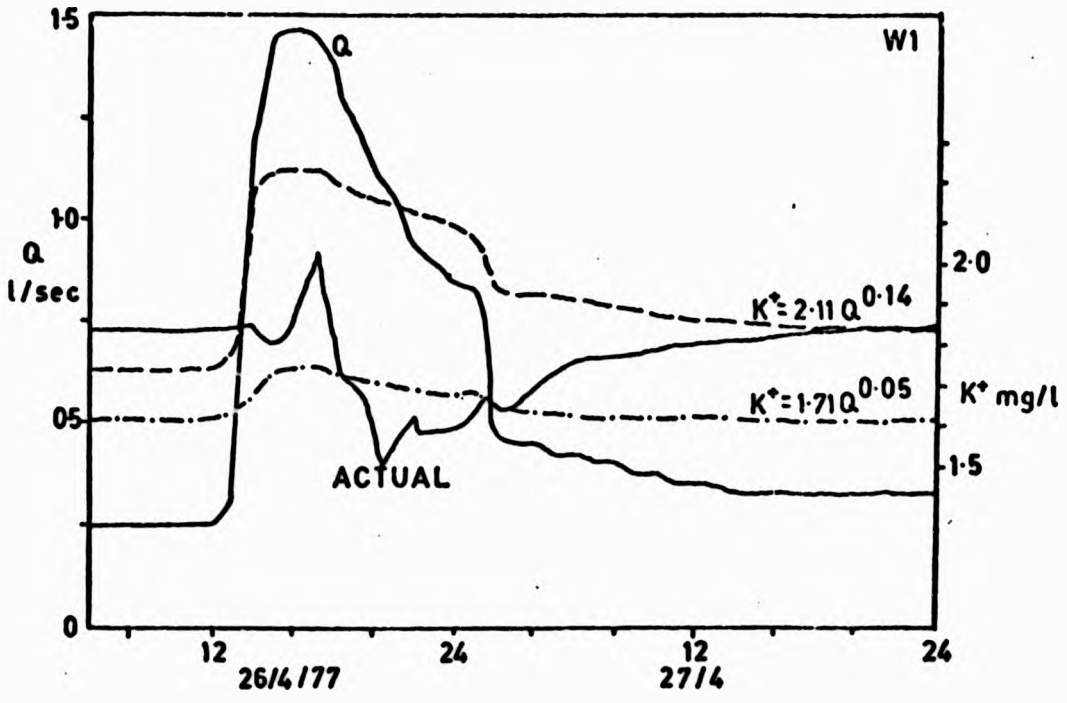

B.

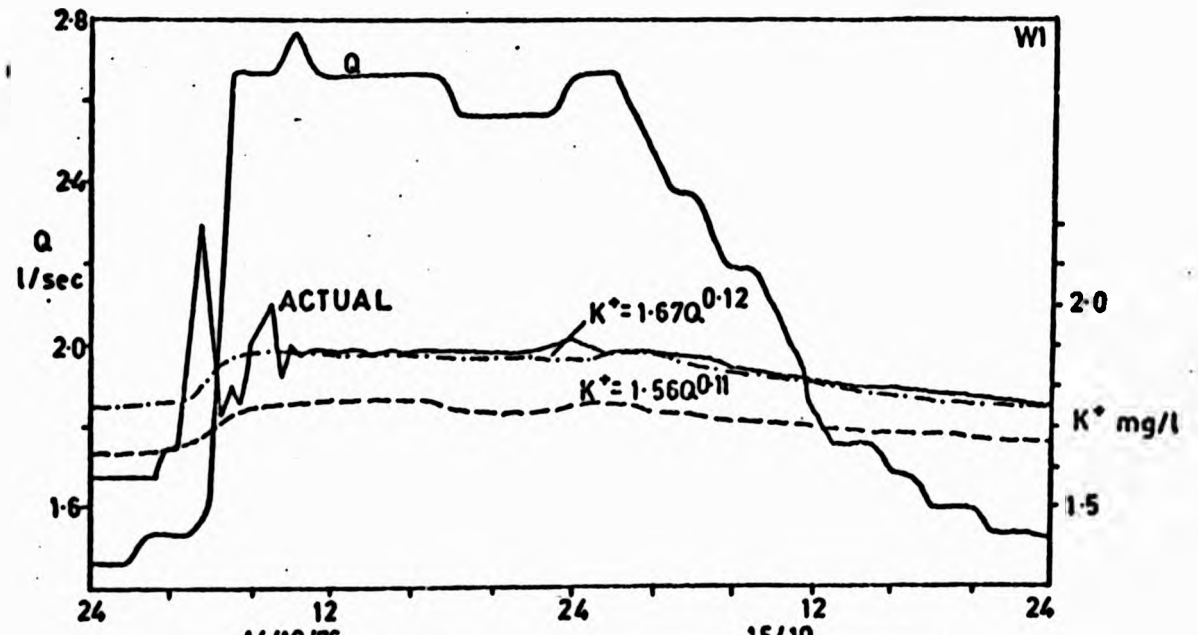

C.

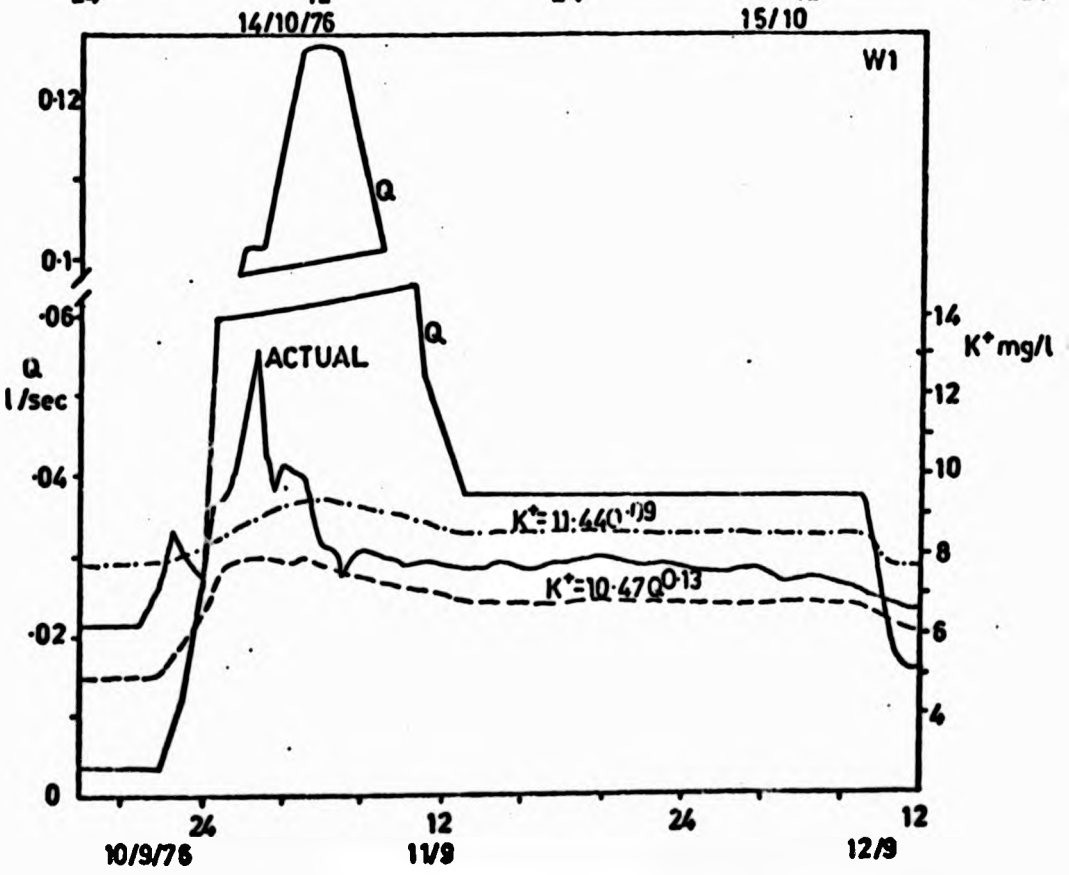

FIGURE 7.13: COMPARISON OF ACTUAL AND PREDICTED POTASSIUM CONCENTRATIONS FOR TWO STORMS AT THE FLUME USING THE VARIABLE COEFFICIENT MODEL

controlling factors, the eight hydrometeorological variables used in 6.5 A were, with the addition of SMD, included in a correlation matrix with the magnitude of Na^{+}, Ca^{2+} and Mg^{2+} flushes. Flush magnitude was taken as the peak concentration minus the concentration halfway between the start and end of the flush. The complex fluctuation during some storms presented problems in identifying individual flushes, and probably lead to error. Where two or more flushes occurred the largest was taken.

Few of the correlations are significant, partly due to the small sample size (Table 7.10 A). The SI is significantly correlated with the Ca^{2+} and Mg^{2+} flushes (R^2 = 84.6 % and 46.2 % respectively). The optimisation procedure used earlier for SI showed that flushing was at its peak in September. None of the other variables were significant, although FI and SMD gave consistently high correlations. Multiple regression was used in an attempt to improve variance explanation in flush magnitude. The selection procedure was that used in 6.3 F. For Mg^{2+} the bivariate regression gave:

$$Mg^{2+} \text{ flush magnitude, mg/l} = (10.59.EXP(-\ 1.10\ SI))/10 \qquad (7.15)$$

$r = -0.68$; $r^2 = 46.2\ \%$; N = 8; Sig. level = 5.0 %
SE = 0.985

The addition of only one extra variable, FI, was significant, giving:

$$Mg^{2+} \text{ flush magnitude, mg/l} = (EXP(2.026 - 1.18\ SI - 0.569\ \log_e FI))/10 \qquad (7.16)$$

$r = 0.91$; $r^2 = 82.8\ \%$; N = 8; Sig. level = 1.0 %;
SE = 0.421

F for inclusion of FI = 11.92 (significant at 5.0 % level)

For Ca^{2+}, the bivariate regression gave:

$$Ca^{2+} \text{ flush magnitude, mg/l} = (16.44.EXP(-\ 1.98\ SI))/10 \qquad (7.17)$$

$r = 0.92$; $r^2 = 84.6\ \%$: N = 8; Sig.level = 0.1 %; SE = 0.392

TABLE 7.10: CORRELATION MATRIX FOR BIVARIATE REGRESSION AT W1: MAGNITUDE OF SOLUTE FLUSH
(Log data except sine index)

7.10 A: CONCENTRATIONS (Mg^{2+}, Ca^{2+}, Na^{+} in mg/l)

	Mg^{2+}	Ca^{2+}	Na^{+}	Qp	SI*	Tr	Hr	FI	R	I MAX	I MEAN	SMD
Mg^{2+}	1	-	-	- 0.38	- 0.68	- 0.09	0.12	- 0.66	0.40	0.44	- 0.12	0.62
Ca^{2+}	-	1	-	- 0.46	- 0.92	0.58	- 0.23	- 0.46	0.41	0.35	- 0.14	0.55
Na^{+}	-	-	1	- 0.47	- 0.55	0.50	- 0.49	- 0.65	- 0.47	0.20	- 0.11	0.54
Qp	NS	NS	-	1	0.19	0.63	0.60	0.54	- 0.36	- 0.81	0.34	- 0.28
SI	5.0	0.1	NS	NS	1	0.24	- 0.57	0.11	- 0.40	- 0.22	- 0.80	0.32
Tr	NS	NS	NS	NS	NS	1	0.63	- 0.42	0.58	0.57	0.43	0.35
Hr	NS	NS	NS	NS	NS	NS	1	0.34	0.87	0.22	0.56	0.63
FI	NS	NS	NS	NS	NS	NS	NS	1	0.45	- 0.63	0.08	0.01
R	NS	NS	NS	NS	NS	NS	0.1	NS	1	- 0.17	0.71	0.08
I MAX	NS	NS	NS	1.0	NS	NS	NS	NS	NS	1	- 0.27	0.51
I MEAN	NS	NS	NS	NS	1.0	NS	NS	NS	5.0	NS	1	0.25
SMD	NS	NS	NS	NS	NS	NS	NS	NS	NS	NS	NS	1

* SI = SIN (RADIANS) (2 (D - 0) / 365 , D = Day of year, numbered from 1st January.
Lower half of table shows % significance levels for t tests
N = 7 for sodium; N = 8 for calcium and magnesium

7.10 B: LOADS (Mg^{2+}, Ca^{2+}, Na^{+} in mg/l)

	Mg^{2+}	Ca^{2+}	Na^{+}	Qp	SI**	Tr	Hr	FI	R	I MAX	I MEAN	SMD
Mg^{2+}	1	-	-	- 0.21	- 0.58	0.32	0.24	0.12	0.31	0.33	0.03	0.18
Ca^{2+}	-	1	-	0.07	- 0.83	0.30	0.20	0.20	0.33	0.21	- 0.09	0.40
Na^{+}	-	-	1	- 0.27	- 0.54	0.50	- 0.47	- 0.51	0.12	0.15	- 0.10	0.52
Qp	NS	NS	NS	1	*	*	*	*	*	*	*	*
SI	NS	1.0	NS	*	1	*	*	*	*	*	*	*
Tr	NS	NS	NS	*	*	1	*	*	*	*	*	*
Hr	NS	NS	NS	*	*	*	1	*	*	*	*	*
FI	NS	NS	NS	*	*	*	*	1	*	*	*	*
R	NS	NS	NS	*	*	*	*	*	1	*	*	*
I MAX	NS	NS	NS	*	*	*	*	*	*	1	*	*
I MEAN	NS	NS	NS	*	*	*	*	*	*	*	1	*
SMD	NS	NS	NS	*	*	*	*	*	*	*	*	1

* As in 7.10 A

** SI as in 7.10 A

This variance explanation was not significantly improved by the addition of other variables. For Na^+ the bivariate regression gave:

$$Na^+ \text{ flush magnitude, mg/l} = (75.2\ FI^{-1.6})/1000 \qquad (7.18)$$

$r = -0.65$; $r^2 = 42.3\ \%$; $N = 7$; not significant at 5 % level; SE = 1.120

The addition of SI gave:

$$Na^+ \text{ flush magnitude, mg/l} = (EXP(37.15 - 1.46 \log_e FI - 2.27\ SI))/1000 \qquad (7.19)$$

$r = -0.80$; $r^2 = 64.0\ \%$; $N = 7$; not significant at 5 % level; SE = 0.720

F for inclusion of SI = 5.96 (significant at 5 % level)

The sine index does not aid explanation of the physical processes contributing to flushing but it does point to a significant seasonal cycle, the maximum flush occurring in September, and minimum in March. These times correlate approximately with the water year, when flows are at minima and maxima respectively. The significant additional variance explanation by FI indicates the importance of storm characteristics. The negative coefficients, indicating greater flushing at lower FI, are difficult to explain in terms of physical processes. They could indicate the importance of longer infiltration times in early autumn when the SMD is still high, and water is able to dissolve a greater quantity of accumulated solutes than under wetter conditions.

A further correlation matrix was computed in an attempt to obtain predictive equations for the actual loads carried by flushing events. It was thought that, if quantified, the solute load due to flushing alone could be added to that predicted with a bivariate or multivariate model, giving more accurate computation of loads during autumn. This required precise definition of flushing duration and integration of the area between the normal dilution response and that due to flushing on the load/time curve. The results showed that only the Ca^{2+}/SI relationship was significant probably due to the error involved in

computing the solute loads (Table 7.10 B). The addition of other variables in multiple regression relationships was not significant.

It may be concluded that, although the analysis points to a significant annual variation in solute flushing, it does not clarify the factors controlling the phenomenon. This can be attributed to:

(i) the difficulty and probable error involved in defining solute flushes during complex fluctuation of concentration; and

(ii) the small sample size.

D. Chemograph Lag and Lead

It was noted in Chapter 2.3 that lead and lag effects introduce hysteresis into simple ratings between concentration and discharge. This was illustrated for K^+ at W1 (Tables 7.6 and 7.8), in that, by eliminating lag and lead, individual storm rating correlation coefficients were considerably improved. Walling and Foster (1975) suggested that the lag effect was related to processes operating over the entire catchment. Lag, defined by them as the time difference between streamflow peak and solute minimum, was found to be inversely related to Q_p and directly related to SMD. They also found a seasonal variation in lag with a peak in July/August.

An attempt was made to confirm these results for the K^+ lags and leads determined earlier, with the same independent variables used in the previous section. K^+ was used because peaks were relatively easy to define compared with other solutes where the dilution response was complicated by flushing.

K^+ concentration leads discharge in most of the storms sampled. The highest (and only significant) correlation was with flood intensity (Table 7.11). This suggests that the greater the FI, the smaller is the K^+ lead over discharge. Time of rise, T_r, and hydrograph rise, H_r, although insignificantly correlated with lead, both agree with the direction of the lead/FI relationship. The SI is poorly correlated with lead even after optimisation. This also applies to the cosine index (lagged by one month) used by Walling and Foster (1975).

TABLE 7.11: CORRELATION BETWEEN LAG/LEAD AND INDEPENDENT HYDROLOGICAL VARIABLES FOR POTASSIUM AT W1

	Qp	SI*	Tr	Hr	FI	R	I MAX	I MEAN	SMD	CI ≠
r	- 0.47	- 0.39	0.64	- 0.50	- 0.76	0.30	- 0.13	- 0.20	0.27	- 0.34
% Sig level	NS	NS	NS	NS	5.0	NS	NS	NS	NS	NS

N = 8

* SI = SINE (RAD) 2 π (D - 0) / 365

≠ COSINE INDEX used by Walling and Foster (1975) CI = COS (RAD) 2 π (D - 31) / 365

These results suggest that, not only does K^+ behave differently to other solutes by concentrating with increasing discharge, it also exhibits a lead effect, completely opposite to that found by Walling a and Foster (ibid) for specific conductivity in a South Devon catchment. They attribute the lag effect to flushing into the stream of readily soluble material, which has accumulated on the ground surface and in upper soil horizons, thus maintaining solute concentration until after the hydrograph peak. K^+ may be precipitated closer to the soil surface or stream bank than other solutes, or it may represent preferential washout from interception storage or the atmosphere. The exact mechanisms may be better understood by field experiment.

7.6 SUMMARY AND CONCLUSIONS

(i) It was found that by including storm data with the regularly sampled data, bivariate correlation coefficients were, in general, reduced. Separate regressions were performed upon the total sampled data excluding autumn samples, and the autumn samples alone, generally improving levels of variance explanation over those for the total sampled data, but rarely above those for the regularly sampled data. Na^+ proved an exception, however, with the total sampled data giving better levels of r^2 % than for the regularly sampled data at W1, W2 and the flume. The use of polynomial regression also improved variance explanation for the total sampled data, partly describing non-linearity introduced by the storm data. For Na^+ cubic functions gave the best overall variance explanation at W1, W2 and the flume, the only solute for which this was the case.

(ii) Close examination of the storm data shows unusually high solute levels during autumn 1976, according with results from other UK catchments (e.g. Foster and Walling, 1978). Solute response during this period, although exhibiting some general trends, e.g. diminution of flushing through time, was complex and highly variable, both spatially and temporally. The high solute levels associated with end of summer and early autumn conditions suggested that a variable intercept model, similar to that suggested by Ledbetter and Gloyna, (1964), could be employed. It was found that K^+ intercepts from individual storms were highly correlated with the preceding flow level, indirectly stressing the significance of soil water storage in

determining storm K^+ concentration. The rate of K^+ concentration change with discharge was found to vary significantly with maximum rainfall intensity at W1 and the time of year at the flume. The models incorporating these variable coefficients improve the general prediction of storm solute level but fail to accurately predict the detailed K^+ response within storms.

(iii) The magnitude of the flushing effect for Ca^{2+}, Mg^{2+} and Na^+ was found to vary with the time of year, maximum flushing occurring in autumn. Flood intensity was also identified as a significant influence. Bivariate and multivariate models were formulated for predicting Ca^{2+} and Mg^{2+} flush magnitudes respectively, both with high explanation of variance. The models for Na^+ were not significant. Similar models for predicting flush loads were not significant, possibly due to the error involved in estimating loads for individual storms.

(iv) Potassium concentration lead over discharge was found to be inversely correlated with flood intensity at W1. This exactly mirrors the findings of Glover and Johnson (1974) and Walling and Foster (1975) who both found that a chemograph lag for specific conductance was directly correlated with hydrograph rise.

If the requirement were to be a model capable of predicting specific conductance at no less than weekly intervals, excluding the months of September, October and November, then multiple regression models employing instantaneous values of discharge, a 60 day API, a Sine Index and the Soil Moisture Deficit, would give reasonable approximations at all the subcatchments within West Walk.

However, use of the bivariate models developed in this chapter gives only approximately correct levels. They do not accurately synthesise intra-storm solute variability, including maxima and minima. Furthermore, insight into the processes controlling solute variability is restricted by using such a 'black box' modelling approach. The second half of this thesis describes a field experiment to monitor solute and water movement in the hillslope soil of Subcatchment 1.

A detailed chemical analysis of the soil is also undertaken, to identify potential solute sources. An attempt to model the processes is made and the results used to assess the future of spatially distributed modelling of catchment solute response.

Firstly, however, tentative budgets are computed for West Walk and its subcatchments.

CHAPTER 8
THE SOLUTE BUDGET

8.1 INTRODUCTION

In this chapter the best predictive models developed in chapter 6 are used to compute solutional output from West Walk catchment and its subcatchments. Bulk precipitation is also considered and the net solutional loss estimated.

8.2 SOLUTE INPUTS IN PRECIPITATION AND DRY FALLOUT

In this study the main objective in obtaining solute input data was the computation of net solute budgets. Thus, only brief consideration is given to chemical sources, temporal variability, rainfall acidity, stemflow and throughfall.

A. Concentrations in Bulk Precipitation Samples

West Walk samples include atmospheric dust in addition to the dissolved constituents of rainfall. The dust may be derived from either inside or outside the catchment boundaries, which could lead to errors when computing gross catchment budgets (and net outputs). Finlayson (1976) found that more particulate matter was received in precipitation than left East Twin Brook (Mendips, UK) in streamflow. He attributed this to windblown material originating within the catchment boundary. The re-cycling process is thought to have increased concentrations in West Walk bulk samples during the months of May to August 1976, when dust deposits were visible on the sampling funnel. The problem was accentuated by sand extraction within the catchment and the consequent traffic of heavy lorries within about 100 metres of the sampling site. Since this was the only wide, open area it was not possible to re-locate the sampling device without interference from vegetation.

Temporal variations in the concentrations of K^+, Na^+, Ca^{2+}, Mg^{2+}, Cl^-, TDS and pH in bulk precipitation are given in Figures 8.1 A - G and the data summarised in Tables 8.1 A - C. Arithmetic and volume-weighted means are included in Table 8.1, because they can be compared to show whether concentration increases or decreases with increased

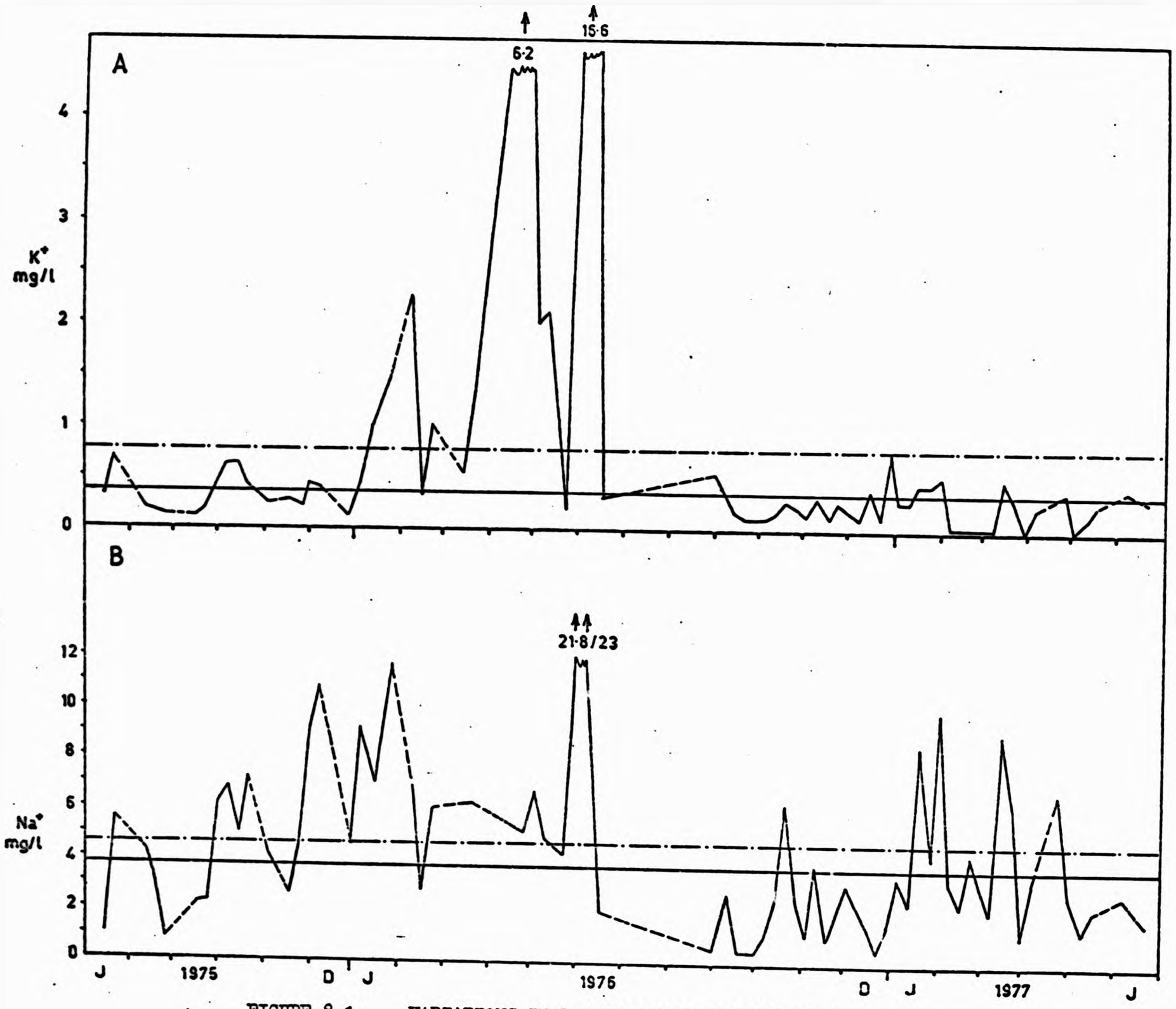

FIGURE 8.1: VARIATIONS IN RAINFALL SOLUTE CONCENTRATION, 1975/1976 - 1976/1977

A: POTASSIUM B: SODIUM

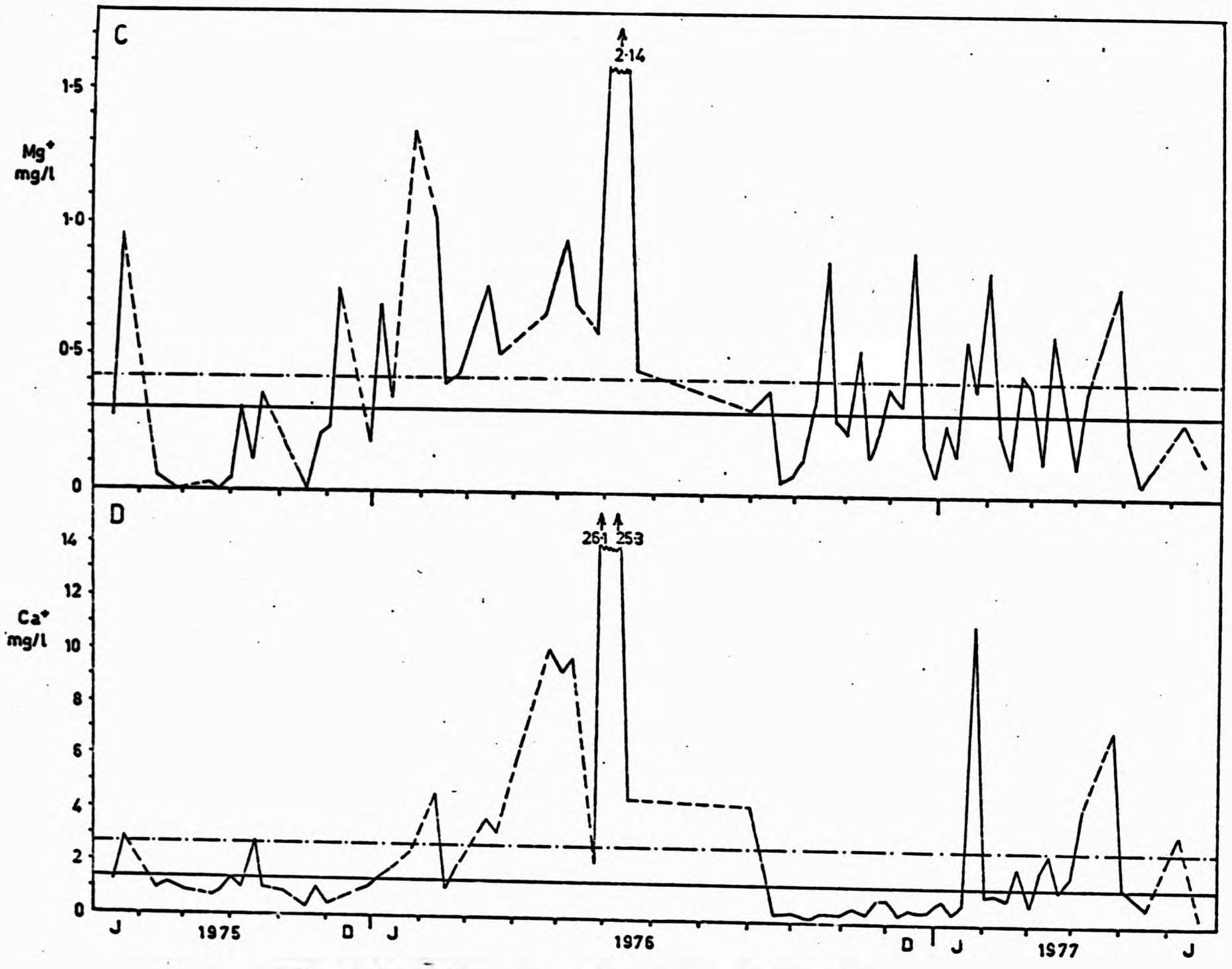

FIGURE 8.1 (cont'd): E: pH F: CHLORIDE

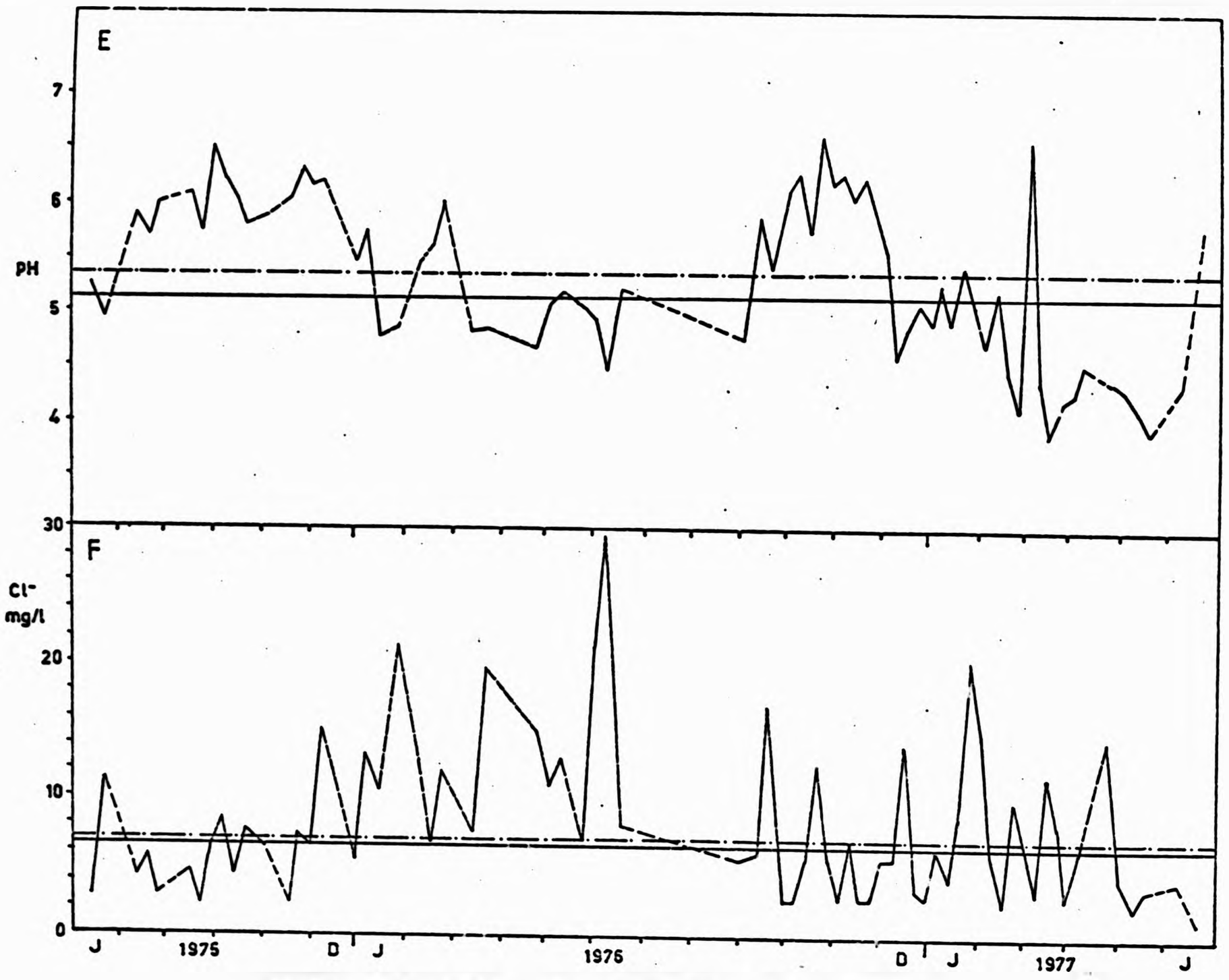

FIGURE 8.1 (cont'd): C: MAGNESIUM D: CALCIUM

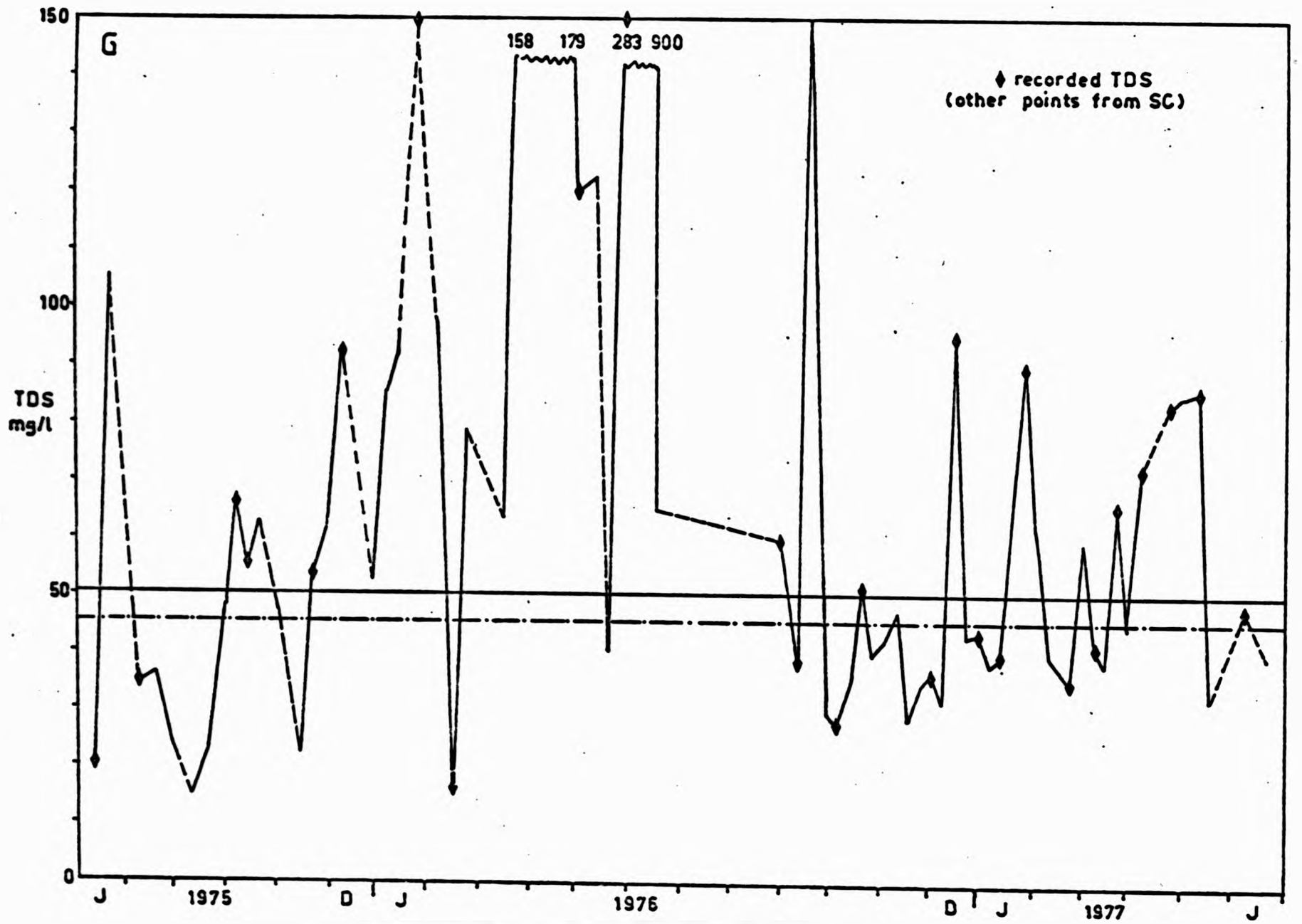

FIGURE 8.1 (cont'd): G: TOTAL DISSOLVED SOLIDS

TABLE 8.1: BULK PRECIPITATION CHEMISTRY FOR WEST WALK
(concentrations in mg/l)

8.1 A: 1975/1976

	N	Mean	Range	Vol.Wt.Mean
K^+	32	1.39	0.2 - 16.63	0.45
Na^+	32	6.44	1.13 - 23.0	4.93
Ca^{2+}	32	5.22	0.32 - 26.10	1.65
Mg^{2+}	32	0.52	0.02 - 2.13	0.28
Cl^-	32	7.46	2.32 - 21.26	6.32
TDS	32	42.78	15.0 - 900	46.83
pH	32	5.56	4.47 - 6.50	5.57

8.1 B: 1976/1977

	N	Mean	Range	Vol.Wt.Mean
K^+	37	0.25	0.02 - 0.75	0.20
Na^+	37	3.19	0.50 - 9.96	3.17
Ca^{2+}	37	0.50	0.15 - 7.3	1.14
Mg^{2+}	37	0.33	0.05 - 0.92	0.31
Cl^-	35	6.82	1.45 - 20.55	6.56
TDS	36	48.42	29.0 - 95.5	54.38
pH	36	5.15	3.91 - 6.61	4.69

8.1 C: 1975/1977 (two year period)

	N	Mean	Range	Vol.Wt Mean	Streamflow *	Streamflow ≠
K^+	69	0.78	0.02 - 16.63	0.29	1.78	1.45
Na^+	69	4.69	0.5 - 23.00	3.78	19.62	15.37
Ca^{2+}	69	2.69	0.15 - 26.10	1.32	19.24	10.63
Mg^{2+}	69	0.42	0.02 - 2.13	0.3	8.88	6.78
Cl^-	67	7.06	1.46 - 21.26	6.48	27.70	24.67
TDS	68	45.56	15.0 - 900	50.61	81.4	62.8
pH	68	5.35	3.91 - 6.61	5.13	8.41	6.45

* Means of RSD for Flume (Table 6.6 C)

≠ Means of RSD for W1 (Table 6.6 A)

rainfall amount (Cryer, 1976). The volume-weighted mean was computed by summing weekly products of rainfall (mm) and concentration (mg/l) over each year and dividing by the annual precipitation total. With the exception of TDS and pH for 1975/1976, all solute concentrations tend to decrease with increasing rainfall amount (i.e. arithmetic means > volume weighted means), which agrees with the results of Cryer (1976), Gorham (1958) and Douglas (1968). TDS concentrations are subject to the errors involved in estimation using specific conductivity because the small sample size often made it impossible to obtain a direct TDS measurement. Thus the low pH could increase the specific conductivity value and hence the estimation of TDS. Closer examination of the data does not support this hypothesis because, although low pH values in May - June 1976 correspond with high TDS, even lower pH values in March - May 1977 correspond with about average TDS concentrations. The other possibility is that solutes not determined by chemical analyses contribute significantly to TDS. These could include SO_4^{2-} and NO_3^- in rainfall and Fe^{3+}, Si^{4+} and other mineral elements from particulate matter.

Mean concentrations of individual solutes may be compared with results from a selection of other published sources (Table 8.2). There is good agreement with other near-coastal sites in the UK, Penglais, West Central Wales (Cryer, 1976) and Newton Abbot, South Devon (Stevenson, 1968). Mean chloride concentration for West Walk agrees exactly with a value interpolated from Stevenson (1968); i.e. 7.0 mg/l. The mean pH of bulk precipitation at West Walk acidity also ties in with values interpolated from Oden's maps of pH over Western Europe (5.5 - 5.75) (Oden, 1976). Furthermore, at West Walk, there does not appear to be the problem with acid rainfall encountered in Eastern USA and industrial Europe, i.e. $pH \simeq 4.0$.

Proximity to the sea usually increases the concentration of rainwater, especially that of Na^+ and Cl^-, the major constituents of seawater. Comparison of the ratios of solutes in rain and seawater can give an indication of how important a source the sea is in comparison with land sources, e.g. windblown dust. The 1975-1977 Cl/Na ratio for West Walk (1.72) is close to the value of 1.8 for seawater (Erikkson, 1960), emphasising the importance of coastal location on rainfall chemistry (Table 8.3). The 1975/1976 ratio is lower which may point to

TABLE 8.2: BULK PRECIPITATION CHEMISTRY FOR OTHER LOCATIONS WITHIN THE NORTHERN HEMISPHERE

Mean values in mg/l. * = volume weighted mean; ≠ = arithmetic mean; ** = median

Locality	K^+	Na^+	Ca^{2+}	Mg^{2+}	Cl^-	pH	TDS	Source	Sampling Period	
Theoretical for pure rain in equilibrium with CO_2 at 25°C	-		-	-	-	5.65	-	Reuss (1976)		
U.K.: Plynlimon, C. Wales	0.14	2.27	1.65	0.37	4.18	4.90	11.1	Cryer (1976)	1971/3	≠
Penglais, coast W. Wales	1.05	5.69	2.76	0.85	10.24	6.54	22.5	Cryer (1976)	1971/3	≠
East Twin, Mendips	0.26	1.84	0.59	0.57	3.94	4.13	-	Waylen (1976)	1972/3	≠
Rothamsted	0.3	1.8	1.4	0.3	3.1	-	-	Stevenson (1968)	1962	**
Newton Abbott	0.7	5.5	1.5	0.6	6.3	-	-	Stevenson (1968)	1962	**
Edinburgh	0.3	3.8	1.8	0.3	3.0	-	-	Stevenson (1968)	1962	**
South Hampshire (interpolated)		-	1.6	-	7.0	-	-	Stevenson (1968)	1962	**
N. Europe - 62 station mean	0.35	2.05	1.42	0.39	3.47	5.47	-	Carroll (1962)	pre 1955	≠
South Hampshire (interpolated)		-	-	-	-	5.75	-	Oden (1976)	1956	≠
South Hampshire (interpolated)		-	-	-	-	5.5	-	Oden (1976)	1966	≠
USA: Hubbard Bk, N. Hants	0.07	0.12	0.16	0.04	0.47	4.14	-	Likens et al (1976)	1963/4	*
Hubbard Bk, N. Hants	0.07	0.07	0.24	0.05	0.15	4.05	-	Cogbill & Likens (1974)	1972/3	*
West Walk: S. Hants, UK	0.78	4.69	2.69	0.42	7.06	5.35	45.56	Spraggs	1975/7	*
West Walk: S. Hants, UK	0.29	3.78	1.32	0.3	6.48	5.13	50.61	Spraggs	1975/7	*

the contribution of Na^+ in dust from land sources during the drought. The Cl/Ca ratio is considerably lower than that for seawater, implying that most (90 %) Ca^{2+} is land derived, agreeing with the suggestion by Allen et al (1968) that Ca^{2+} is essentially of terrestrial origin. It is also interesting to note that the M.27 road construction near Portsmouth was generating Chalk dust locally and regionally (due to quarrying and transportation) during 1975/1976. A land source also seems likely for about 45 % of K^+ in bulk precipitation. The Cl/Mg ratio is lower for bulk rainfall than seawater which implies either incomplete pick up of oceanic Mg^{2+} or early preferential deposition, because Cl^- is essentially derived by advection and evaporation from the seawater surface.

The temporal variation in rainfall solute concentration (Figures 8.1 A - G) shows above average values during the drought, particularly in May - July 1976. An annual cycle can be detected for pH, with higher acidity during the first five months of the year. Streamflow pH minima also occur in the first five months of the year for West Walk subcatchments.

With the exception of pH all mean rainfall solute concentrations are lower than those in streamflow. This is most pronounced for Mg^{2+} the mean streamflow solute concentration being sixteen times greater than that in rainfall.

B. Solute Loads in Bulk Precipitation Samples

Solute concentrations can be combined with rainfall quantity to compute the weights of each solute input to West Walk over the study period. These are shown in Table 8.4 A as kg, and 8.4 B as kg/ha/year. Clearly there is a very large difference in solute inputs between the two years. About twice as much Cl^-, Mg^{2+} and TDS entered West Walk in 1976/1977 as in 1975/1976; sixteen times as much hydrogen; 1.35 times as much Ca^{2+}, and 1.3 times as much Na^+. However, there was little difference in K^+ inputs between the two years. The fact that TDS is almost four times greater than the sum of individual solutes again points to the likely over-estimation of TDS. The input differences between 1975/1976 and 1976/1977 strongly reflect low rainfall during the 1975/1976 drought and above average rainfall in autumn 1976 with its associated solute washout effect.

TABLE 8.3: COMPARISON OF SOLUTE RATIOS IN PRECIPITATION WITH THOSE IN SEAWATER (row/column)

A. RATIOS IN SEAWATER (from Erikkson, 1960)

	Cl	Ca	Mg	Na	K
Cl	1	47.6	14.9	1.8	48.9
Ca		1	0.31	0.04	1.0
Mg			1	0.12	3.3
Na				1	27.2
K					1

B. RATIOS IN WEST WALK - BULK PRECIPITATION 1975/1976 AND 1976/1977
(Upper half of table 1975/1976; lower half 1976/1977)

	Cl	Ca	Mg	Na	K
Cl	1	4.19	22.97	1.28	14.0
Ca	5.75	1	6.01	0.35	3.66
Mg	20.95	3.65	1	0.06	0.61
Na	2.08	0.36	0.10	1	10.94
K	14.54	5.62	1.54	15.51	1

C. RATIOS IN WEST WALK - BULK PRECIPITATION 1975/1977

	Cl	Ca	Mg	Na	K
Cl	1	4.92	21.59	1.72	22.49
Ca		1	4.39	0.35	4.57
Mg			1	0.08	1.04
Na				1	13.11
K					1

TABLE 8.4: SOLUTE INPUTS TO WEST WALK
(Input, kg = concentration, mg/l,
x rainfall, mm, x catchment area, km^2)

A. Weights of Solutes Input to West Walk (kg)

	K^+	Na^+	Ca^{2+}	Mg^{2+}	Cl^-	H^+	TDS
1975/6	141.78	1505.50	524.88	82.75	2077.1	0.811	15695
1976/7	130.70	1961.30	710.50	194.10	4038.2	12.648	29134
1975/7	272.48	3466.80	1235.38	276.85	6115.30	13.459	44829

B. Weights of Solutes Input to West Walk
(kg/ha/yr) (Table 7.4 A ÷ 59.8874 ha)

	K^+	Na^+	Ca^{2+}	Mg^{2+}	Cl^-	H^+	TDS
1975/6	2.37	25.14	8.77	1.38	34.68	0.014	262.1
1976/7	2.18	32.75	11.86	3.24	67.43	0.211	486.5
1975/7	2.28	28.95	10.32	2.31	51.06	0.113	374.3

Table 8.5 lists a selection of reported precipitation solute loadings for Britain and other parts of the world. The nearest locations to West Walk are Bedgebury (Kent) and East Twin (Avon), although neither of these are coastal sites. Thus Na^+ snd Cl^- inputs are higher at West Walk than both these sites (except Cl^- at Bedgebury: no data). Norwich, further inland again, gives even lower loads of Na^+ and Cl^-. At the other extreme Lerwick (Shetland Isles) receives very high loads of Na^+, K^+ and Mg^{2+} due to its exposed coastal location. Data from Israel also illustrates the important influence maritime location exerts upon rain solute load, with a fourfold decrease in K^+ and threefold decreases in Na^+ and Ca^{2+}, over a distance of 96 km from the coast. It is difficult to compare West Walk with other near coastal locations because all of these are in northern or western Britain, at much higher altitudes. However, the West Walk figures (excluding TDS which may be over-estimated) are the same order of magnitude as those recorded at other UK locations.

C. Throughfall and Stemflow Concentrations

Throughfall and stemflow were not sampled during the study period. The concentrations of solutes in these components are known to be higher than concentrations in rainfall and could contribute to the stream chemograph. However, within West Walk the species and age of vegetation is so variable that any attempt to quantify the significance of stemflow and throughfall were considered beyond the scope of the project.

However, measurements of stemflow and throughfall chemistry were made at one site in West Walk during the months of February and March 1978 (Vidler, 1978). Samples were taken beneath a 40 year old Quercus petraea in the area of catchment between SC5 and the flume (other details: canopy area - 45 m^2; height - 30 m; girth - 1.0 m). Results showed that stemflow contained appreciably greater solute concentrations especially of K^+, than incident rainfall (Table 8.6). Throughfall concentrations were also greater than those in incident rainfall. Incident rainfall pH decreased during stemflow and throughfall, probably as a result of the uptake of basic salts.

These data confirm findings in the literature (Chapter 2.2(E)). The uptake of solutes by stemflow is particularly high and provides

TABLE 8.5: RAINFALL SOLUTE LOADS FOR OTHER AREAS (kg/ha/year)

Locality	K^+	Na^+	Ca^{2+}	Mg^{2+}	Cl^-	H^+	TDS	Source	Sampling Period
East Twin, Mendips, UK	2.77	19.80	6.40	6.10	42.45	0.810	-	Waylen (1976)	1972/73
Maesnant, C. Wales	1.60	27.2	25.1	4.4	45.8	0.104	139	Cryer (1976)	1971/73
Moor House, Westmorland, UK	2.27	32.14	9.53	4.48	-	-	-	Gore (1968)	1959/65
Lerwick, Shetland Isles	5.62	133.00	6.70	19.2	-	-	-	Egner and Erikkson (1958/60)	1958/59
N. Lancs, UK	2.96	35.34	7.30	4.63	-	-	-	Carlisle et al (1966)	1963/64
Kent, UK	2.80	19.30	10.70	4.20	-	-	-	Madgwick and Ovington (1959)	1955/57
Rough Sike, West'd, UK	3.07	21.55	8.98	-	-	-	-	Crisp (1966)	1962/63
Lake District, UK	1.91	19.67	11.40	2.96	18.51	-	-	White et al (1971)	1969/70
Norwich, UK	3.0	17.0	17.0	2.0	38.0			Edwards (1973b)	1970
Cynon, S. Wales	9.0	40.6	21.0	6.3	-	-	-	Hughes & Edwards (1977)	1972
Duddon, L.District, UK	5.4	47.7	7.7	-	-	-	-	Sutcliffe and Carrick (1973)	1970
Oesling, Luxembourg	1.86	6.6	5.92	1.12	23.46	0.178	75.62		
Israel (0.1 km inland)	4.0	73.0	73.0	-	-	-	-	Yaalon (1964)	-
Israel (96 km inland)	1.0	24.0	23.0	-	-	-	-	Yaalon (1964)	-
Tennessee, USA	18.0	16.0	24.0	11.0	44.0	-	270	Betson (1978)	1971
Dalen, Telemark, Norway	1.65	2.40	7.59	0.66	3.40	0.967	-	Lag (1968)	1957/62
Hubbard Brook, USA	1.40	1.5	2.6	0.7	-	-	-	Bormann & Likens (1969)	1964/67
Taita, New Zealand	4.05	45.68	4.16	4.53	93.98	-	-	Claridge (1975)	1969/73
WEST WALK, S. Hants, UK	2.28	28.95	10.32	2.31	51.06	0.113	374.3	Spraggs	1975/77

TABLE 8.6: RATIOS OF STEMFLOW AND THROUGHFALL SOLUTE CONCENTRATIONS TO INCIDENT RAINFALL CONCENTRATIONS - WEST WALK FEBRUARY/MARCH 1978 (Data from Vidler, 1978)

	Stemflow			Throughfall		
	Mean*	SD	CV %	Mean*	SD	CV %
K^+	21.94	7.69	35.0	2.44	0.28	11.6
Na^+	4.25	1.81	42.6	1.37	0.47	34.4
Ca^{2+}	14.62	4.92	33.7	3.22	1.77	55.1
Mg^{2+}	7.49	3.24	43.3	1.57	0.14	8.8
pH	0.9	0.16	17.9	0.78	0.10	12.7
SC	3.34	1.9	57.0	1.28	1.13	88.0
TDS	4.8	2.9	60.0	1.74	1.32	76.0

* Means of 5 weekly bulk samples

considerable quantities of dissolved matter at point locations within the catchment. It should also be noted that stemflow and throughfall increase the pH of incident rainfall finally reaching the ground surface, which must affect leaching processes within the soil.

8.3 SOLUTE OUTPUTS IN STREAMFLOW

The best predictive equations developed in Chapters 6 & 7 were used to compute daily loads of each solute leaving each subcatchment during the period 1975 - 1977. The predictive models used are summarised in Table 8.7. Some of these are inadequate in terms of the percentage variance explained in concentration by one or more independent variables, but they represent the best predictors available.

Careful consideration was given to the method for computing solute loads in West Walk. Walling (1978) reviewed some of the methods available and emphasised the need to take account of the degree of reliability of load measurements used in geomorphological studies. Very little difference in the percentage error terms was found between use of hourly and daily mean flow series with rating models based upon instantaneous data. The differences between total dissolved loads using an instantaneous rating and daily mean flow series, and a continuous record based upon specific conductivity were also small (3.7 % in 1974- 1975 for the River Creedy, South Devon). Differences for individual ions were greater, - 29.9 % being recorded for NO_3 loads in the River Dart during 1976 - 1977. It was also shown that little difference in error magnitude existed between the use of a weekly sampling scheme and daily mean flows with a rating model to compute loads.

It was thought that the use of an hourly flow record with instantaneous rating models would gain very little in accuracy, and use a disproportionate amount of computer time. Furthermore, such an approach would not have been compatible with the multiple regression models for W4 and W5, which required daily inputs of SMD, API and a Sine Index. Therefore, a daily mean flow series was used in combination with the instantaneous rating models given in Table 8.7. Although conceptually simple this involved logistical problems in programming and processing using the WANG 2200 B computer. Daily mean flows were

TABLE 8.7: MODELS EMPLOYED FOR COMPUTING WEST WALK SOLUTE LOADS

A. SC 1 : W1 Discharge in cumecs; concentration in mg/l
("Autumn" = September, October and November)

POTASSIUM

Non-autumn data: K^+ mg/l = $4.37\ Q^{0.138}$

Autumn data: K^+ mg/l = $0.36\ Q^{-0.291}$

SODIUM

All data: Na^+ mg/l =

$$\text{EXP}(-1.056 - 1.347 \log_e Q - 0.138[\log_e Q]^2 - 0.005[\log_e Q]^3)$$

CALCIUM

Non-autumn data: Ca^{2+} mg/l = $2.70\ Q^{-0.140}$

Autumn data: Ca^{2+} mg/l = $8.47\ Q^{-0.158}$

MAGNESIUM

Non-autumn data: Mg^{2+} mg/l = $2.49\ Q^{-0.114}$

Autumn data: Mg^{2+} mg/l = $1.54\ Q^{-0.241}$

CHLORIDE

Non-autumn data: Cl^- mg/l = $18.24\ Q^{-0.039}$

Autumn data: Cl^- mg/l = $5.90\ Q^{-0.202}$

pH

Non-autumn data: pH = $3.91\ Q^{-0.069}$

Autumn data: pH = $3.31\ Q^{-0.069}$

BICARBONATE

Non-autumn data: HCO_3^- mg/l = $0.541\ Q^{-0.408}$

Autumn data: HCO_3^- mg/l = $0.354\ Q^{-0.365}$

SPECIFIC CONDUCTIVITY

All data: SC μmhos =

$$\text{EXP}(0.424 - 1.427 \log_e Q - 0.108[\log_e Q]^2)$$

TABLE 8.7: (cont'd)

B. SC 2 : W2 Discharge in cumecs; concentration in mg/l

POTASSIUM

K^+ mg/l = $4.45\ Q^{-0.099}$

SODIUM

Na^+ mg/l = $EXP(0.767 - 0.568 \log_e Q - 0.037[\log_e Q]^2)$

CALCIUM

Ca^{2+} mg/l = $EXP(10.29 + 3.411 \log_e Q + 0.477[\log_e Q]^2 + 0.020[\log_e Q]^3)$

MAGNESIUM

Mg^{2+} mg/l = $EXP(2.643 + 0.259 \log_e Q + 0.030[\log_e Q]^2)$

CHLORIDE

Cl^- mg/l = $EXP(2.442 - 0.192 \log_e Q - 0.010[\log_e Q]^2)$

pH

pH = $EXP(4.03 + 0.763 \log_e Q + 0.067[\log_e Q]^2)$

BICARBONATE

HCO_3^- mg/l = $6.81\ Q^{-0.221}$

SPECIFIC CONDUCTIVITY

SC μmhos = $259.6\ Q^{0.021}$

TABLE 8.7: (cont'd)

C. WEST WALK : FLUME Discharge in cumecs; concentration in mg/l

POTASSIUM

K^+ mg/l = $EXP(15.132 + 9.042 \log_e Q + 1.806 [\log_e Q]^2 + 0.112 [\log_e Q]^3)$

SODIUM

Na^+ mg/l = $EXP(- 5.987 - 3.802 \log_e Q - 0.033 [\log_e Q]^2 - 0.011 [\log_e Q]^3)$

CALCIUM

Non-autumn data: Ca^{2+} mg/l = $6.72\ Q^{-0.187}$

Autumn data: Ca^{2+} mg/l = $18.63\ Q^{-0.090}$

MAGNESIUM

Non-autumn data: Mg^{2+} mg/l = $2.98\ Q^{-0.193}$

Autumn data: Mg^{2+} mg/l = $2.46\ Q^{-0.279}$

CHLORIDE

Non-autumn data: Cl^- mg/l = $23.92\ Q^{-0.030}$

Autumn data: Cl^- mg/l = $3.74\ Q^{-0.355}$

pH

pH = $EXP(- 0.110 - 1.332 \log_e Q - 0.117 [\log_e Q]^2)$

BICARBONATE

HCO_3^- mg/l = $16.78\ Q^{-0.131}$

SPECIFIC CONDUCTIVITY

SC, μmhos = $EXP(35.72 + 17.41 \log_e Q + 3.235 [\log_e Q]^2 + 0.193 [\log_e Q]^3)$

TABLE 8.7: (cont'd)

D. SC 4 : W4 Discharge in l/sec; API in mm;
Sine Index (SI) in radians; concentration in mg/l

POTASSIUM

K^+ mg/l =

$EXP(0.337 + 0.095 \log_e (API\ 5 + 10) + 0.086\ SIN.I)$

SODIUM

Na^+ mg/l =

$EXP(3.82 - 0.248 \log_e Q + 0.057 \log_e (SMD + 1) - 0.126\ SIN.I)$

CALCIUM

Ca^{2+} mg/l =

$EXP(3.04 + 0.317\ SIN.I + 0.051 \log_e (SMD + 1))$

MAGNESIUM

Mg^{2+} mg/l =

$EXP(2.24 + 0.049 \log_e (SMD + 1) + 0.121\ SIN.I)$

CHLORIDE

Cl^- mg/l =

$EXP(3.39 + 0.141\ SIN.I + 0.034 \log_e (SMD + 1))$

pH

pH =

$EXP(2.209 - 0.025 \log_e Q - 0.066 \log_e (API\ 30 + 10))$

BICARBONATE

HCO_3^- mg/l =

$EXP(9.89 - 1.802 \log_e Q - 0.663 \log_e (API\ 60 + 10))$

SPECIFIC CONDUCTIVITY

SC μmhos =

$EXP(10.69 - 0.071 \log_e (API\ 60 + 10) - 2.222 \log_e Q)$

TABLE 8.7: (cont'd)

E. SC 5 ; W5 Discharge in l/sec; API in mm;
Sine Index (SI) in radians; concentration in mg/l

POTASSIUM

K^+ mg/l =

$[EXP(2.351 - 0.113\ SIN.I + 0.008\ \log_e\ (SMD + 1))] - 10$

SODIUM

Na^+ mg/l =

$[EXP(2.558 - 1.040\ SIN.I + 0.052\ \log_e\ (SMD + 1))] - 10$

CALCIUM

Ca^+ mg/l =

$[EXP(2.837 + 1.061\ SIN.I - 0.050\ \log_e\ (API\ 60 - 10))] - 10$

MAGNESIUM

Mg^+ mg/l =

$[EXP(2.098 - 0.792\ SIN.I + 0.060\ \log_e(SMD + 1) + 0.114\ \log_e(Q + 10))] - 10$

CHLORIDE

Cl^- mg/l =

$[EXP(2.728 - 1.249\ SIN.I - 0.008\ \log_e\ (SMD + 1))] - 10$

pH

ph =

$[EXP(1.815 + 0.207\ \log_e(Q + 10) - 0.566\ SIN.I + 0.140\log_e(SMD + 1))] - 10$

BICARBONATE

HCO_3^- mg/l =

$[EXP(3.160 + 1.850\ SIN.I - 0.159\ \log_e\ (Q + 10))] - 10$

SPECIFIC CONDUCTIVITY

SC μmhos =

$[EXP(4.543 + 2954\ SIN.I - 0.115\ \log_e(SMD + 1) - 0.369\log_e(Q + 10))] - 10$

computed from the hourly flow sequences stored on magnetic tape for each subcatchment using the programs FLOWS (for weirs) and GLOWS (for the flume) - see Appendix 2 ix, xii. At the same time data streams were input from disc storage containing daily SMD and API values. The input data were accepted by simple sub-routines attached to 'FLOWS' and 'GLOWS', containing the relevant rating equations. The procedure is summarised in Table 8.8.

The data output, in milligrams per day and week, are used in several ways. Firstly to present gross solute outputs from various parts of West Walk, 1975 - 1977. Secondly in combination with bulk precipitation inputs, to compute net solute budgets for 1975 - 1977. Thirdly, to examine the detailed temporal response of each solute load during 1975 - 1977. Fourthly, to map the spatial variability of a selected solute load during 1975 - 1977.

(A) Gross Solute Output

Table 8.9 shows gross solute outputs from various parts of West Walk for 1975 - 1976 and 1976 - 1977, in kg. The loads for sub areas between W2, W5 and the flume ('SC 7'), and between W1, W4 and W2 ('SC 6') are computed by subtraction. Clearly this is hazardous, because it may involve a combination of error terms. For this reason, K^+ loads have not been computed, as the estimated totals for SC 2 and SC 5 appear excessive.

The overall picture is one of small loss of solutes during 1975 - 1976 but a huge increase during 1976 - 1977. This reflects the low discharges recorded during the drought and the heavy rainfall and much higher flows of autumn 1976. For the twelve month period July 1976 to June 1977 individual solute losses amounted to between 78.7 and 81.9 % of the total in the 24 month period 1975 - 1977. G E Likens et al (1967) found similar patterns of gross solute loss over the wet year 1963 - 1964 and the drought year 1964 - 1965 for Hubbard Brook, U.S.A.

Gross solute load is better expressed in kg/ha/year, because this allows comparison between subcatchments, and with work from other areas (Table 8.10). Again solute yields for West Walk are greater during 1976- 1977 than during 1975 - 1976, considerably so for K^+, probably due to the increased leaching by heavy rain during autumn 1976. The most

TABLE 8.8: PROCEDURE FOR COMPUTING DAILY AND WEEKLY SOLUTE LOADS

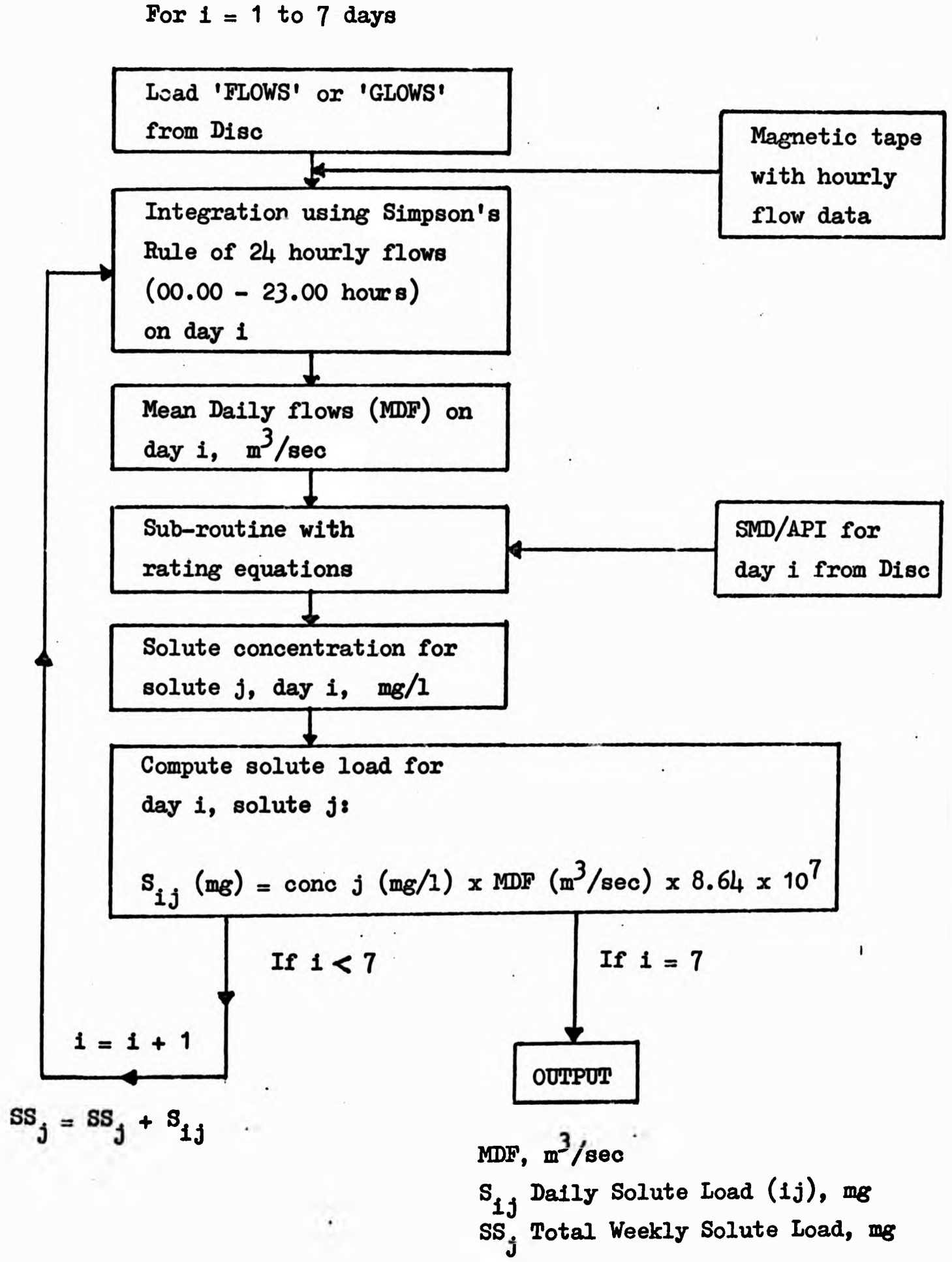

TABLE 8.9: WEST WALK : GROSS SOLUTE LOADS 1975 - 1977 (Values in kg)

1975 - 1976	K^+	Na^+	Ca^{2+}	Mg^{2+}	Cl^-	H^+	HCO_3^-	TDS
SC 1	18.78	191.00	114.70	75.08	295.5	.00904	101.9	1923.7
SC 4	13.09	135.80	148.90	69.44	212.6	.00046	361.8	1349.3
SC 5	58.98	106.90	138.23	82.50	170.3	? 4.27	577.4	1647.0
SC 6	-	125.10	150.40	82.4	175.3	-	282.2	957.0
SC 7	-	227.5	287.8	77.3	272.3	-	210.7	1579.4
Total West Walk	91.2	786.3	840.0	86.7	1126.0	.00301	1534.0	7496.0
% 1975 - 1977 Gross Load - West Walk	14.1	16.4	20.3	21.3	16.4	21.6	18.1	18.0

NOTE: SC 6 = SC 2 - SC 1 - SC 4 (area = 15.11 ha)

SC 7 = WW - SC 2 - SC 5 (area = 13.46 ha)

TABLE 8.9: (cont'd)

1976 - 1977	K^+	Na^+	Ca^{2+}	Mg^{2+}	Cl^-	H^+	HCO_3^-	TDS
SC 1	106.3	847.7	415.4	291.2	1275.8	.08719	246.7	8528
SC 4	72.41	710.0	679.6	354.6	1102.4	.00433	878.8	5914
SC 5	346	663	781	506	918.4	? 1.175	2326	7349
SC 6	-	770.8	544.9	25.7	912.2	-	1466	5521
SC 7	-	1009.5	881.1	319.5	1526	-	2009	6760
Total West Walk	555	4001	3302	1497	5734	.01094	6926	34072
% 1975 - 1977 Gross Load - West Walk	85.9	83.6	79.8	78.7	83.6	78.4	81.9	82.0

1975 - 1977	K^+	Na^+	Ca^{2+}	Mg^{2+}	Cl^-	H^+	HCO_3^-	TDS
SC 1	125.1	1038.7	530.1	295.7	1571.3	.09620	348.6	10452
SC 4	85.5	845.8	828.5	424.1	1315	.00479	1241	7263
SC 5	405	770	919	589	1089	5.45	2903	8996
SC 6	-	895.9	695.3	108.1	1087.5	-	1747.4	6518
SC 7	-	1237	1169	3396.8	1798.3	-	2219.7	14857
Total West Walk	646.2	4787	4142	1813.7	6860	.01395	8460	41568

intensive solute yield (TDS) is from SC 5, followed closely by SC 4. Individual solutes show variations on this pattern. Na^+ is most intensively yielded from SC 4, followed closely by SC 5 and SC 6. It is interesting to note that SC 4 provides the highest yield even during 1975 - 1976, with SC 7 (the lowest part of West Walk) also important in accordance with the diminished contributing area noted in Chapter 6. This pattern is even more pronounced for Ca^{2+} yield during 1975 - 1976 with SC 7 the highest yielding area. During 1976 - 1977, SC 5 and SC 4 dominate losses of Ca^{2+}. SC 5 yielded the highest amount of Mg^{2+}, again closely followed by SC 4. Cl^- yield is highest for SC 4 and SC 5 closely followed by SC 7. If most Cl^- is supplied by the atmosphere, then these differences in yield relate to differences in interception storage, soil water storage and possibly ground water or interflow movement between subcatchments. H^+ losses cannot be computed for SC 6 and SC 7 because this ion diminishes downstream as noted in Chapter 6. The high yields for SC 5 appear anomalous if compared with the mean pH of 8.32 noted earlier and may represent poor estimation of pH at higher flows, outside the range of the sampled data. A similar note of caution applies to all solutes sampled at W4 and W5. The highest HCO_3^- yield is from SC 5 (which naturally contradicts the H^+ results), fitting in well with the neutralisation of acid waters from SC 1 en route to the flume, and the high yields of other basic solues (Na^+, Ca^{2+} and Mg^{2+}).

These results represent spatial and temporal variability in solute loads. Walling and Webb (1975, 1978) and Webb and Walling (1974) found that spatial variation in solute load was significantly related to geology in the River Exe catchment, South Devon. Much of the spatial variability of West Walk can be explained by the solid geology underlying each subcatchment. Yield is found to increase with the proportion of London Clay underlying each catchment (Figures 8.2 A and B) and therefore decrease with the proportion of Bagshot Sand (ignoring superficial deposits). This suggests that London Clay is an important source of solutes in West Walk and the Tertiary rocks of the Hampshire Basin. The incomplete soil survey and complexity of vegetation make it difficult to elucidate the effects of floristic and edaphic factors in a similar way.

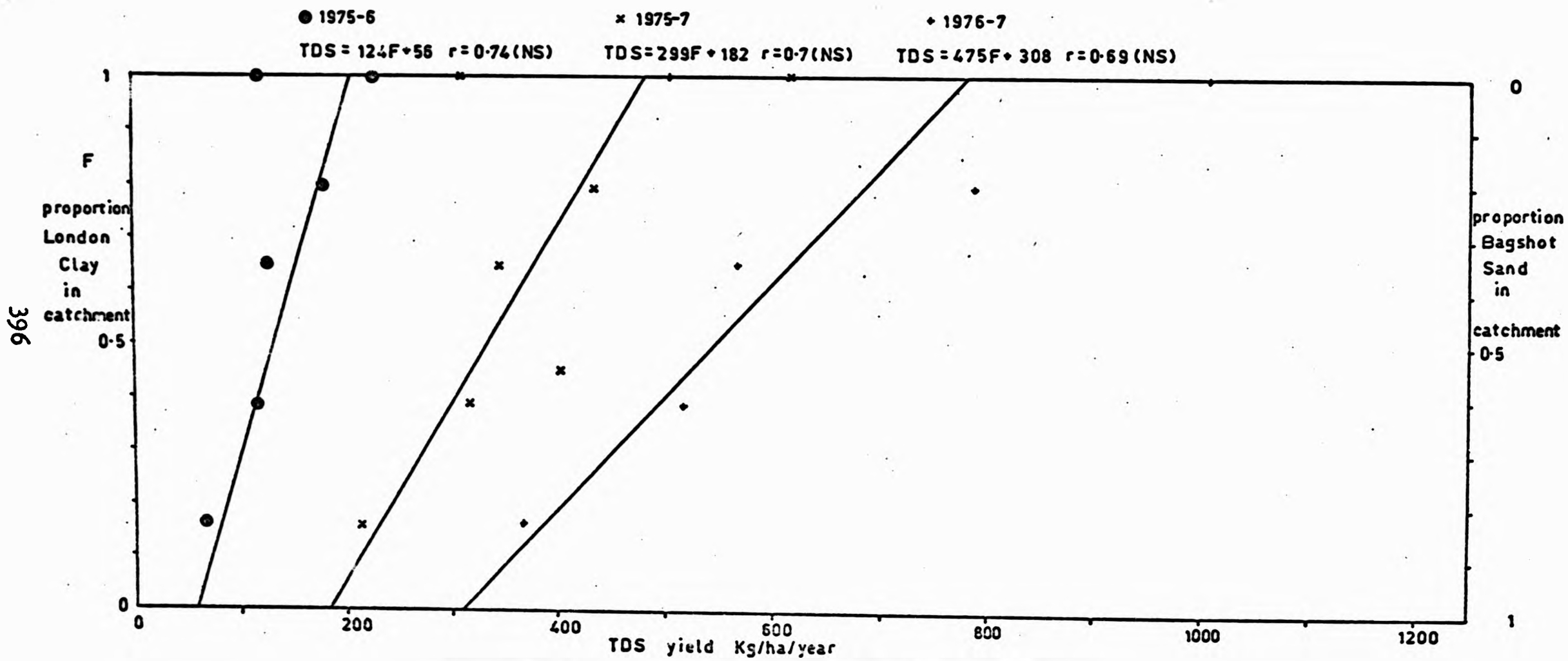

FIGURE 8.2 A: THE RELATIONSHIP BETWEEN TDS YIELD AND SOLID GEOLOGY AT WEST WALK

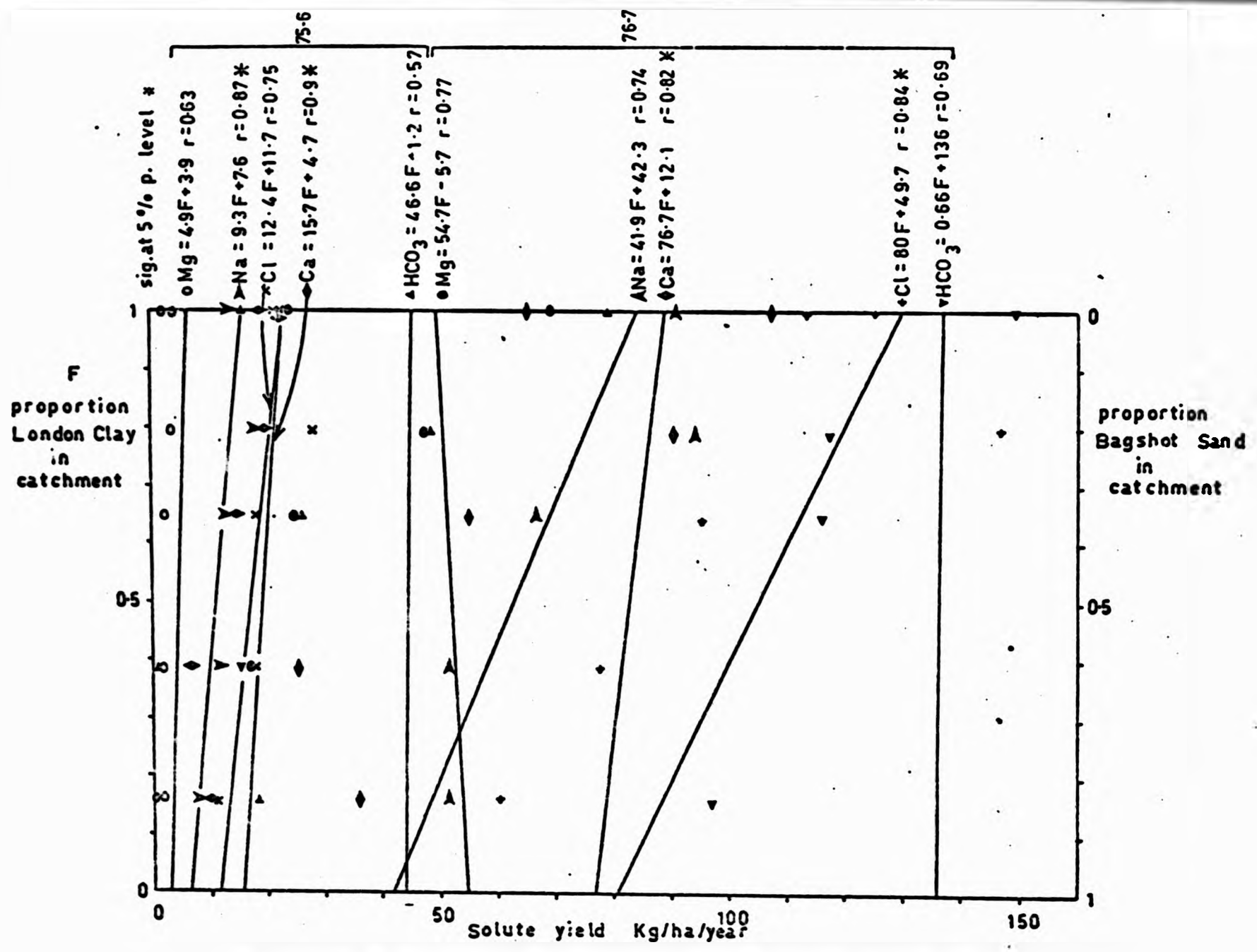

FIGURE 8.2 B: THE RELATIONSHIP BETWEEN SOLUTE YIELDS AND SOLID GEOLOGY AT WEST WALK

TABLE 8.10: WEST WALK : GROSS SOLUTE LOADS 1975 - 1977 kg/ha/year

1975 - 1976	K^+	Na^+	Ca^{2+}	Mg^{2+}	Cl^-	H^+	HCO_3^-	TDS
SC 1	1.14	11.58	6.95	4.55	17.91	.00055	6.18	116.59
SC 4	1.74	18.03	19.77	9.22	28.22	.00061	48.04	179.16
SC 5	8.22	14.66	18.95	11.31	23.35	0.586	79.16	225.81
SC 6	-	8.28	9.95	5.46	11.6	-	18.68	65.96
SC 7	-	16.90	21.38	5.74	20.23	-	15.65	117.34
Total West Walk	1.52	13.13	14.03	6.46	18.80	.00005	25.62	125.2

NOTE: SC 6 = SC 2 - SC 1 - SC 4 (area = 15.11 ha)

SC 7 = WW - SC 2 - SC 5 (area = 13.46 ha)

TABLE 8.10: (cont'd)

1976 - 1977	K^+	Na^+	Ca^{2+}	Mg^{2+}	Cl^-	H^+	HCO_3^-	TDS
SC 1	6.44	51.40	25.18	17.65	77.32	.0053	14.95	516.85
SC 4	9.62	94.27	90.24	47.08	146.38	.00058	116.69	785.26
SC 5	47.44	90.9	107.08	69.37	125.92	0.161	318.90	1007.57
SC 6	-	51.1	36.1	1.7	60.4	-	97.0	365.4
SC 7	-	66.8	65.5	23.74	113.3	-	149.3	502.2
Total West Walk	9.27	66.81	55.14	25.00	95.75	.00018	115.65	568.93
% increase over 1975/76	610.0	5.1	3.9	3.9	5.1	3.6	4.5	4.5

1975 - 1977	K^+	Na^+	Ca^{2+}	Mg^{2+}	Cl^-	H^+	HCO_3^-	TDS
SC 1	3.79	31.48	16.06	8.96	47.62	.00202	10.56	316.7
SC 4	5.68	56.15	55.00	28.16	87.30	.00032	82.39	482.2
SC 5	27.76	52.78	63.00	40.38	74.63	.3733	199.0	616.69
SC 6	-	29.7	23.0	3.58	36.0	-	57.8	215.7
SC 7	-	41.9	43.44	14.74	66.8	-	82.5	309.8
Total West Walk	5.40	39.97	34.58	44.78	52.27	.00012	70.63	347.05

Table 8.11 presents selected gross solute yields for different parts of the U.K., Europe, U.S.A. and New Zealand. There are no data from Tertiary rocks in Southern England for comparison. However, the data are the same order of magnitude as those measured at East Twin Brook, Mendips (Waylen, 1976; 1979). Na^+ is less than at East Twin although in general agreement with other localities in the U.K. Ca^{2+} and Mg^{2+} losses are both much greater than at East Twin, but Ca^{2+} is much less than in Chalk catchment (Edwards, 1973b; Williams, 1971). Cl^- output agrees well with East Twin, Maesnant (Cryer, 1976), River Tud (Edwards, 1973b), Wet Sledale (White et al, 1971). HCO_3^- losses are much less than in Chalk catchments, but close to those at East Twin and Haarts, Luxembourg (Verstraten, 1977).

(B) Net Solute Outputs

The data can also be expressed in the form of a solute balance, considering net losses or gains to be the difference between bulk precipitation solutes and streamflow solutes (Table 8.12). The effect of the drought is clearly seen during the first year as net gains to West Walk for all but Ca^{2+}, Mg^{2+} and HCO_3^-. It seems likely that inputs, although low, were retained in soil storage until the second year when they were flushed into the streams. Cl^- and Na^+ which are both high in precipitation, show large net gains for 1975 - 1976. However, it appears that outputs decreased much more under the influence of the drought than inputs, as solutes became fixed in the soil under the influence of evapotranspiration. Outputs for 1976 - 1977 outweigh the gains of the previous year, probably due to a combination of high autumn rainfall and flushing of accumulated soluble material. H^+ shows a net gain to the catchment for both years because this is exchanged for other solutes in weathering processes. The net gain to West Walk was much less in 1975 - 1976 than in 1976 - 1977 which, in combination with the reduced solute losses during the first year, implies that weathering was reduced during the drought. Net gains and losses also vary spatially, although these merely reflect gross solute losses, assuming inputs are spatially uniform.

Table 8.13 (from Feller and Kimmins, 1979) lists nutrient budget calculations for other watersheds elsewhere in humid temperate regions. Figures for West Walk (1975/1976) are about average for Na^+, but higher

TABLE 8.11: ANNUAL GROSS SOLUTE OUTPUTS REPORTED IN THE LITERATURE (kg/ha/year)

Locality	Lithology	Vegetation	K^+	Na^+	Ca^{2+}	Mg^{2+}	Cl^-	H^+	HCO_3^-	TDS	Source
East Twin Brook, Mendip, UK	Old Red Sandstone	Grass/heather	6.2	25.6	11.6	15.5	43.6	0.000	57.1	-	Wayler, 1976, 1979
Maesnant, Plynlimon, Wales	Peat over Ordovician greywackes	Grass/heather	1.0	43.7	11.2	9.2	75.0	0.280	-	406	Cryer, 1976
River Yare, Norfolk, UK	Calcareous (Chalk)	Arable agric/urban	9.0	73.0	302.0	12.0	102.0	-	678.0	-	Edwards, 1973b
River Tud, Norfolk, UK	Calcareous (Chalk)	Arable agric/urban	9.0	44.0	204.0	8.0	69.0	-	498.0	-	Edwards, 1973b
Saxmundham, Suffolk, UK	Calcareous (Chalk)	Grassland	2.9	34.5	307.0	13.0	85.5	-	-	-	Williams, 1971
Rough Sike, Westmorland, UK	Peat over limestone	Grassland	5.7	45.2	53.8	-	-	-	-	-	Crisp, 1966
R. Cynon, S. Wales, UK	ORS/Limestone/ Millstone Grit	Moorland/grass/ urban (10334 ha)	27.0	231.0	98.7	67.4	-	-	-	-	Hughes and Edwards, 1977
R.Cynon, S. Wales, UK	ORS/Limestone/ Millstone Grit	Moorland/grass/ urban (207 ha)	1.8	12.2	92.4	5.7	-	-	-	-	Hughes and Edwards, 1977 (subcatchment)
River Duddon, UK	Volcanics	N/A	5.2	76.5	74	-	-	-	-	-	Sutcliffe and Carrick, 1973
Wetsledale, Lake Distr. UK	Andesite/granite	Grassland/heather moor	5.8	40.2	38.3	14.4	41.9	-	-	-	White et al, 1971
Hartvikov, Czech.	Quartzitic Gneiss	Forest	—	43.0	30.0	-	15.0	-	-	-	Balek et al, 1979
Vooadlo, Czech.	Quartzitic Gneiss	Grassland/ agriculture	-	95.0	238.0	-	239.0	-	-	-	Balek et al, 1979
Vucksi, Finland	N/A	N/A	5.4	6.0	12.2	3.9	-	-	-	-	Viro, 1953 (from Görham, 1961)
Haarts, Luxembourg	Shales/Quartzites	Forest	2.0	15.6	14.6	16.9	23.7	tr	55.5	220.4	Verstraten, 1977

TABLE 8.11: (cont'd)

Locality	Lithology	Vegetation	K^+	Na^+	Ca^{2+}	Mg^{2+}	Cl^-	H^+	HCO_3^-	TDS	Source
Haney B.C., Canada	Quartz-diorite	Forest	1.3	10.8	13.8	2.8	9.5	-	-	-	Feller and Kimmins, 1979
Coweeta, Carolina, USA	Mica Gneiss and dolomite	Weeds	6.0	10.9	10.4	6.3	-	-	-	-	Johnson and Swank, 1973
Coweeta, Carolina, USA	Mica Gneiss and dolomite	Young pine forest	3.6	6.1	4.1	1.7	-	-	-	-	Johnson and Swank, 1973
Coweeta, Carolina, USA	Mica Gneiss and dolomite	Mature hardwood forest	5.2	9.7	6.9	3.1	-	-	-	-	Johnson and Swank, 1973
Pond Branch, Maryland, USA	Schist	N/A	2.0	3.5	3.0	1.8	4.4	-	16.7	-	Cleaves et al, 1970
Hubbard Brook, USA			1.5	6.6	9.85	2.8	4.7	-	2.0	-	Likens et al, 1967, 1977
Taita, New Zealand	Mesozoic Greywackes	Forest	2.8	30.5	2.8	2.7	56.1	-	-	-	Claridge, 1975, 1970
Hutt Valley, New Zealand	N/A		6.0	76.0	26.0	22.0					
West Walk, UK	Sandstone/clay/ gravel	Forest	5.4	40.0	34.6	44.8	52.3	0.000	70.6	347.1	Spraggs
West Walk, SC 1, UK	Sandstone/clay	Forest	3.8	31.5	16.1	9.0	47.6	0.003	10.6	316.7	Spraggs
West Walk, SC 5, UK	Clay	Forest	27.8	52.8	63.0	40.4	74.6	-	199.0	616.7	Spraggs

TABLE 8.12: WEST WALK: THE SOLUTE BALANCE - 1975 - 1977

Values in kg, computed from Inputs (Table 8.4A) minus Outputs (Table 8.9)
Subcatchment inputs taken as proportions of total catchment area.
Positive figures represent net gains, negative figures net losses.

1975 - 1976	K^+	Na^+	Ca^{2+}	Mg^{2+}	Cl^-	H^+	HCO_3^-	TDS
SC 1	+ 20.2	+ 223.8	+ 29.9	- 52.3	+ 276.8	+ 0.214	- 101.9	+ 2400.5
SC 4	+ 4.7	+ 53.5	- 82.9	- 59.0	+ 48.6	+ 0.102	- 362.8	+ 624.5
SC 5	- 41.7	+ 76.5	- 74.3	- 72.4	+ 82.7	- 4.171	- 577.4	+ 264.5
SC 6	-	+ 254.7	- 18.0	- 61.5	+ 348.6	-	- 282.2	+ 3002.0
SC 7	-	+ 110.8	- 169.9	- 58.7	+ 194.4	-	- 210.7	+ 1947.1
Total West Walk	+ 50.5	+ 719.2	- 315.1	- 303.9	+ 951.1	+ 0.808	- 1534.0	+ 8199.0

TABLE 8.12: (cont'd)

1976 - 1977	K^+	Na^+	Ca^{2+}	Mg^{2+}	Cl^-	H^+	HCO_3^-	TDS
SC 1	- 70.3	- 307.3	- 219,7	- 237.7	- 163.2	+ 3.398	- 246.7	- 501.1
SC 4	- 55.9	- 463.4	- 590.2	- 330.2	- 594.6	+ 1.586	- 878.8	- 2250
SC 5	- 330.0	- 424.1	- 694.5	- 419.5	- 426.6	+ 0.365	-2326	- 3801
SC 6	-	- 737.8	- 365.7	+ 23.3	+ 106.4	-	-1466	+ 1827
SC 7	-	- 568.8	- 721.5	- 275.9	- 618.7	-	-2009	- 213.9
Total West Walk	- 424.3	-2039.7	-2591.5	-1302.9	-1695.8	+12.64	-6926	- 4938.0

1975 - 1977	K^+	Na^+	Ca^{2+}	Mg^{2+}	Cl^-	H^+	HCO_3^-	TDS
SC 1	- 50.0	- 83.5	- 189.7	- 219.4	+ 113.6	+ 3.612	- 348.6	+ 1899
SC 4	- 51.2	- 409.8	- 673.1	- 389.3	- 545.9	+ 1.688	-1241	- 1625
SC 5	- 371.8	- 347.8	- 768.5	- 555.3	- 344.2	- 3.81	-2903	- 3536
SC 6	-	- 21.4	- 383.7	- 38.2	- 455.0	-	-1747	+ 4790
SC 7	-	- 458.0	- 891.4	- 334.6	- 424.3	-	-2219	- 4784
Total West Walk	- 373.7	-1320.2	-2906.6	-1536.9	- 744.7	+13.45	-8460	- 3261

TABLE 8.13: ANNUAL SOLUTE BUDGETS OF RELATIVELY UNDISTURBED FOREST WATERSHED ECOSYSTEMS IN HUMID TEMPERATE REGIONS

(From Feller and Kimmins, 1979) kg/ha/year

Locality	K^+	Na^+	Mg^{2+}	Ca^{2+}	Cl^-	Source *
Haney, British Colombia, Canada	- 1.2	- 9.1	- 3.3	- 15.8	- 2.9	Feller and Kimmins, 1979
Jamieson Creek, Vancouver, Canada	- 1.7	- 12.4	- 6.6	- 34.4	- 15.0	Zeman, 1973
Carnation Creek, Vancouver, Canada	- 2.3	- 27.4	- 7.4	- 5.4	- 33.1	Scrivener, 1975
Rawson Lake, Ontario, Canada	- 0.1	- 2.1	- 1.5	- 2.2	+ 1.4	Schindler et al, 1976
Hubbard Brook, N. Hampshire , USA	- 1.5	- 5.9	- 2.7	- 11.7	+ 1.6	Likens et al, 1977
Cowesta, N. Carolina, USA	- 3.4	- 6.4	- 3.6	- 4.0	- 1.5	Swank and Douglas, 1975
Oak Ridge, Tennessee, USA	+ 1.6	+ 1.1	- 46.7	- 58.6	-	Swank and Elwood, 1971
Maryland, USA	- 0.3	- 1.4	- 0.7	+ 0.2	+ 1.9	Cleaves et al, 1970
H J Andrews Exp. Forest, Oregon, USA	- 1.6	- 28.0	- 11.6	- 47.0	-	Frederiksen, 1972
Vucksi Streem, Finland	- 2.1	- 3.6	- 3.0	- 10.0	+ 0.2	Viro, 1953
Birkenes, Norway	+ 2.1	+ 1.1	- 1.2	- 9.6	0.0	Gjessing et al, 1976
Fyresdal/Nissedal, Norway	- 0.2	+ 0.9	+ 1.1	- 3.8	0.0	Gjessing et al, 1976
Kamigamo Exp. Forest, Japan	+ 0.4	-	- 1.0	+ 3.8	+ 4.9	Iwatsubo and Tsutsumi, 1968
Lake Birra, Japan	- 5.7	- 55.4	- 1.9	- 12.6	-	Nishimura, 1973
Hutt Valley, New Zealand	+ 1.0	- 8.0	- 10.0	- 17.0	0	Miller, 1968
Taita, New Zealand	+ 1.3	+ 15.1	+ 1.3	+ 1.3	+ 37.9	Claridge, 1970, 1975
Stewarts Creek, Australia	+ 2.1	- 1.9	- 2.2	+ 1.1	-	Guthrie, 1978
Average	- 0.7	- 8.8	- 5.9	- 11.9	- 0.7	
WEST WALK, 1975/1976	+ 0.90	+ 12.0	- 5.1	- 5.3	+ 15.9	)
WEST WALK, 1976/1977	- 7.1	- 34.1	- 43.3	- 21.8	- 28.3	} Spraggs
WEST WALK, 1975/1977	- 3.1	- 11.0	- 12.8	- 24.3	- 6.2	)

* For details of sources, see Feller and Kimmins, 1979

than average for K^+, Mg^{2+}, Ca^{2+} and Cl^-. Whether the extreme climatological conditions between 1975 and 1977 influenced these figures is impossible to say without data from an average year. Similarly, recent deforestation and replanting in West Walk may have increased solute loads, although no data are available prior to disturbance.

Denudation rates are often computed from solute yield data and expressed as mm/1000 years. This is not possible for West Walk because:

(i) TDS estimates are subject to the errors noted in Chapter 5,

and (ii) information on the total non-denudation component is not available (i.e. organics, nitrates, sulphates, etc., lost in streamflow and nutrients taken up by vegetation, in addition to bulk precipitation solutes).

(C) Temporal Variation in Loads for West Walk

Solute inputs and outputs for the whole catchment are plotted in Figures 8.3 A - G for the period 1975 - 1977. Bulk precipitation load (kg) is plotted at the mid point of the period in which it falls, while output (kg) is plotted weekly. Both strongly reflect the pattern of rainfall and streamflow for the period and emphasise the point made earlier that 1975 - 1976 is a year of small net gain while 1976 - 1977 is a year of larger net loss. For K^+ April to September 1976 is a period of net loss to the catchment. Similarly, more marked periods of net gain and loss occur for Ca^{2+} and Mg^{2+}. The pattern is less distinct for Na^+ and Cl^- due to their larger precipitation inputs. The net Cl^- gain for 1975 - 1976 was 750 kg less than the net loss for 1976 - 1977 which means that Cl^- stored before the drought was released from storage. There appears to be a washout of Cl^- at the end of the drought, September - October 1976. These seasonal trends are very similar to those found at Hubbard Brook (Likens et al, 1977) and Haney Watershed (Feller and Kimmins, 1979).

Hydrogen loads are not directly comparable and are therefore on different scales. H^+ shows the largest precipitation contrast between 1975 - 1976 and 1976 - 1977 for any ion plotted, the influx of being greatest in February, March and May 1977.

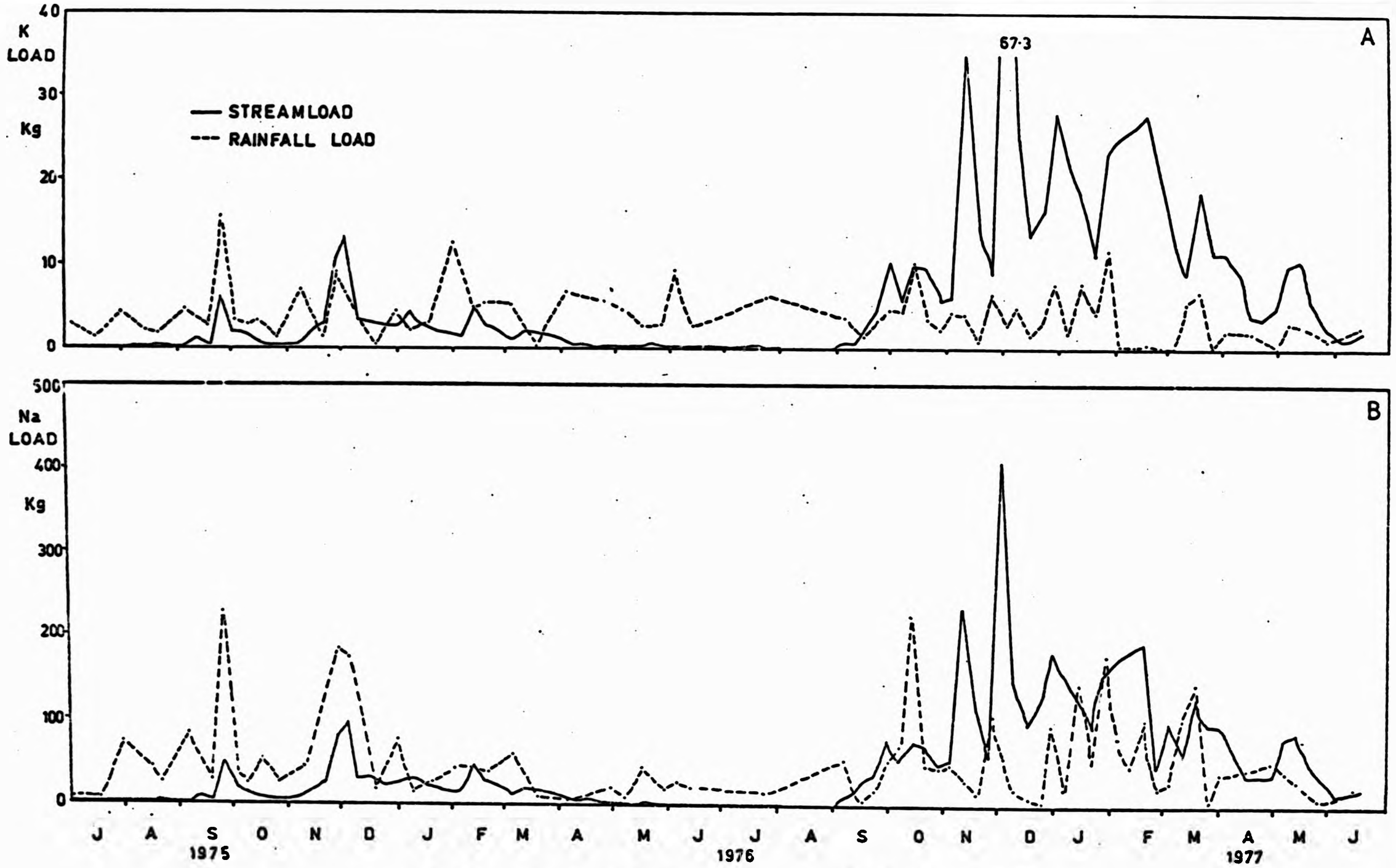

FIGURE 8.2: INPUT AND OUTPUT LOADS FOR WEST WALK, 1975 - 1977

A: POTASSIUM B: SODIUM

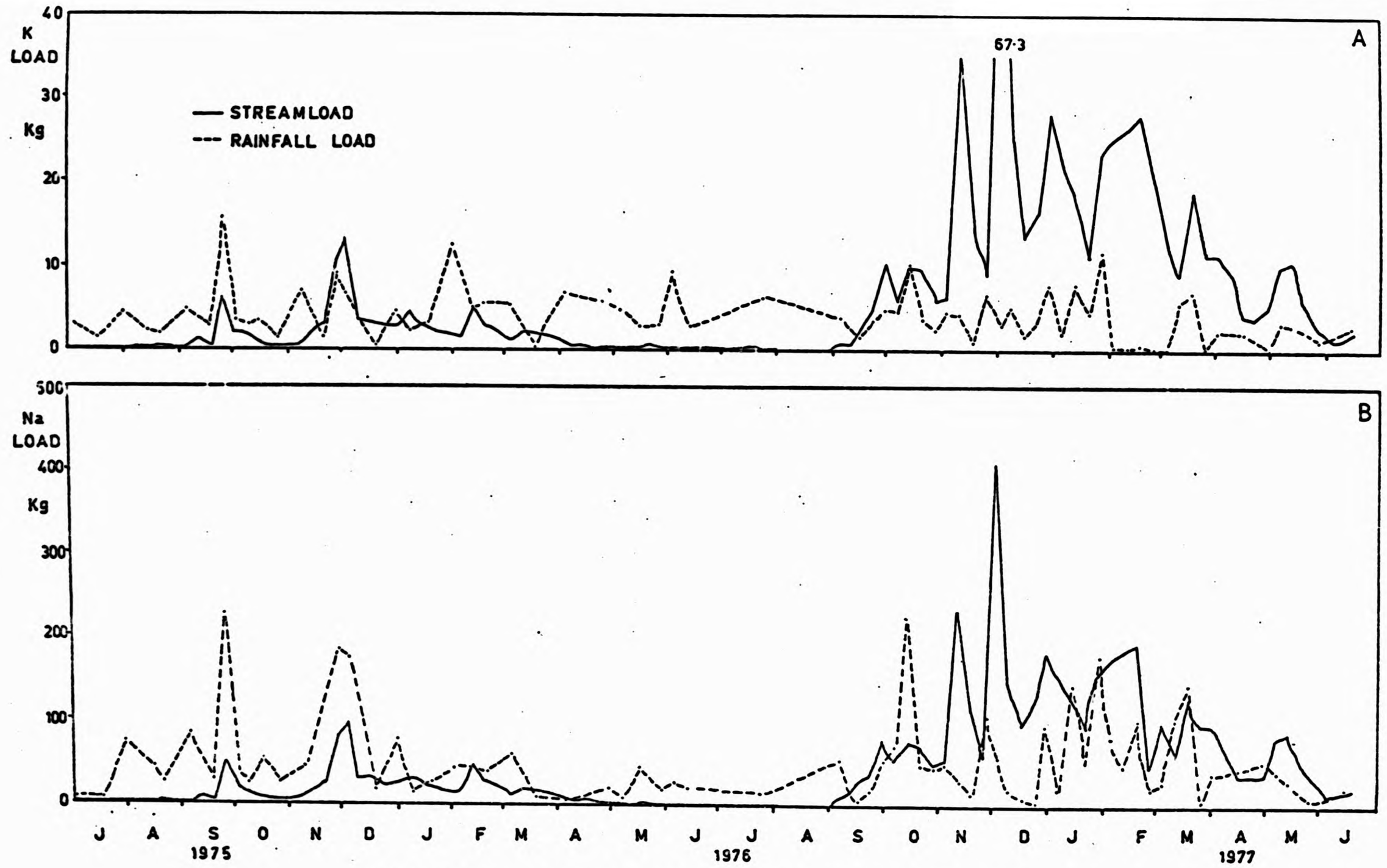

FIGURE 8.3: INPUT AND OUTPUT LOADS FOR WEST WALK, 1975 - 1977

A: POTASSIUM B: SODIUM

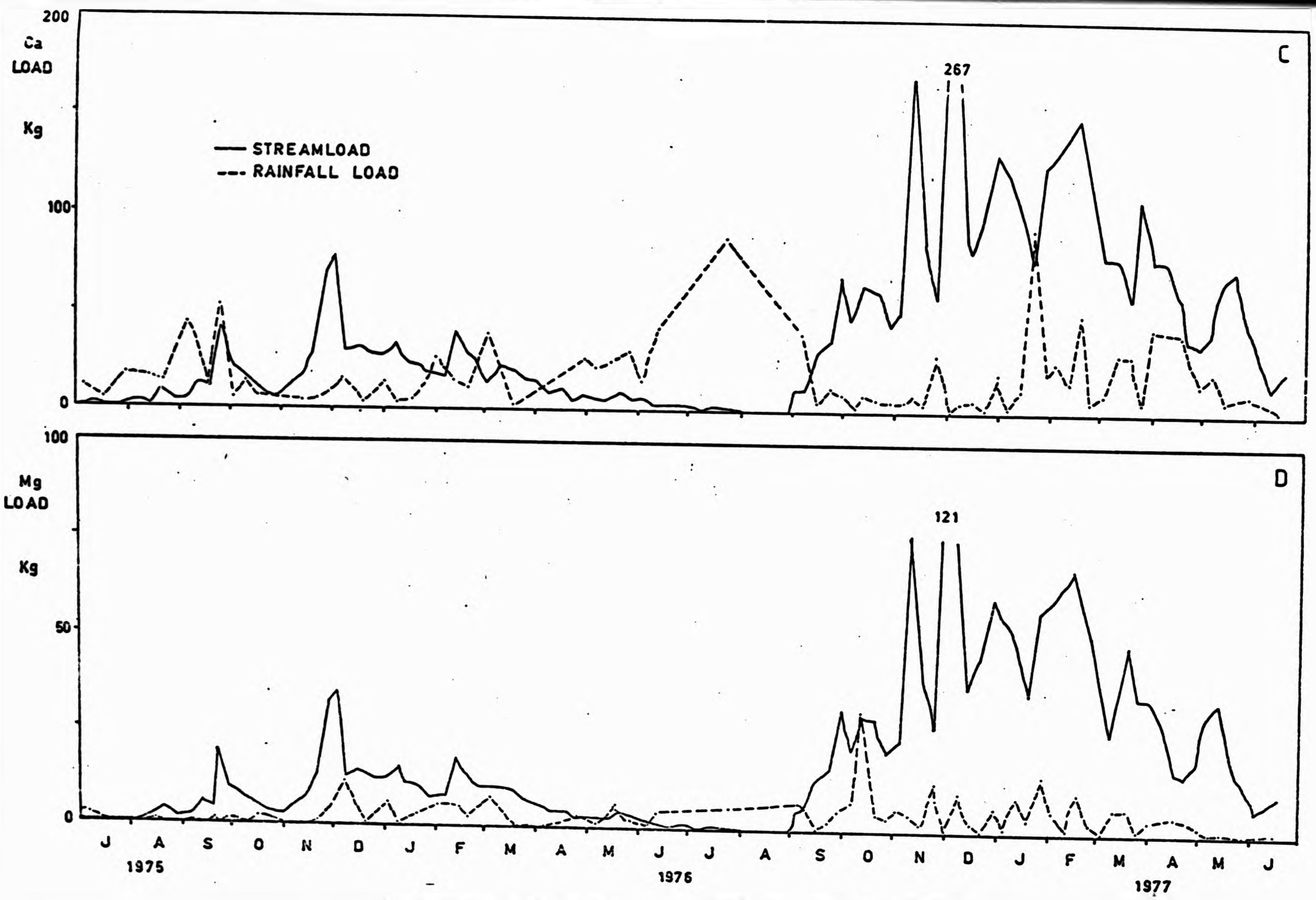

FIGURE 8.3 (cont'd): C: CALCIUM D: MAGNESIUM

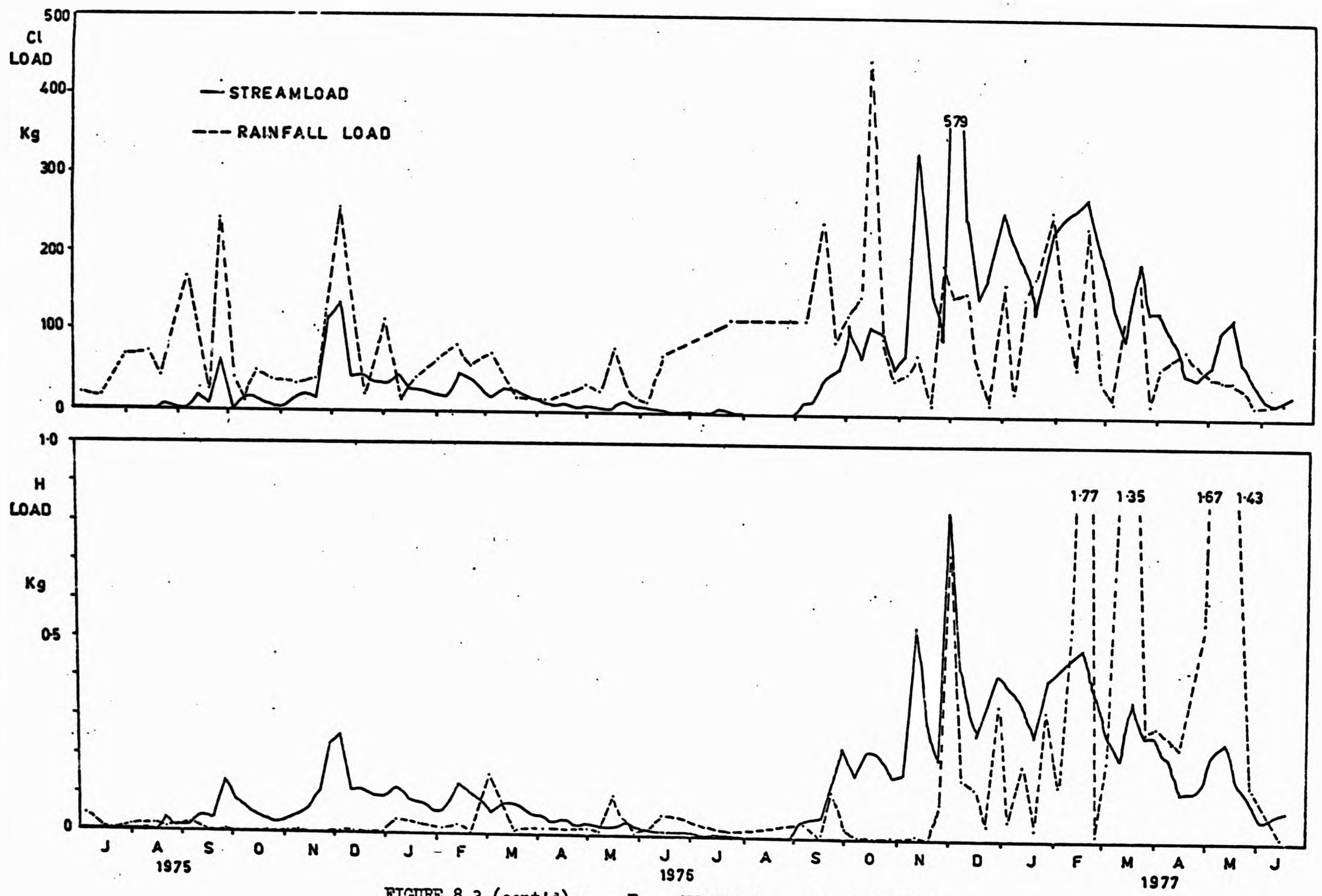

FIGURE 8.3 (cont'd): E: CHLORIDE F: HYDROGEN

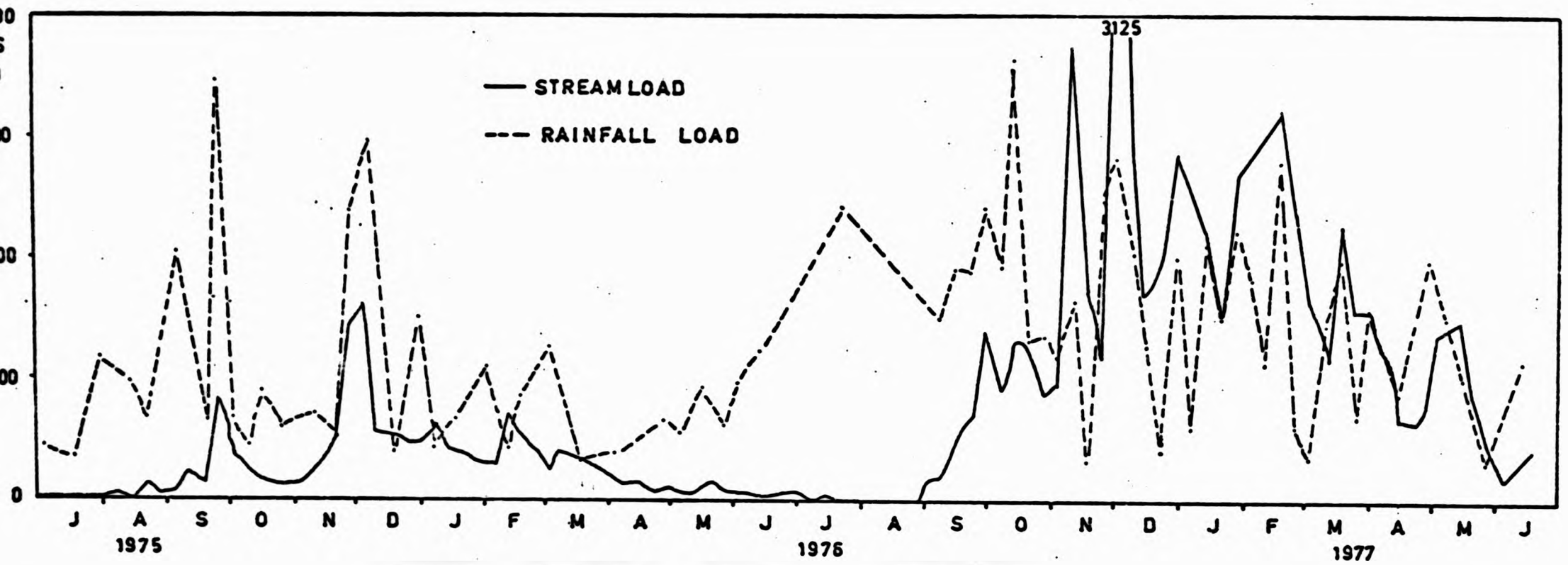

FIGURE 8.3 (cont'd): G: TOTAL DISSOLVED SOLIDS

(D) Spatial Variations within West Walk

Spatial variation in solute load has been noted by many authors in the literature (e.g. Walling and Webb, 1975; 1978; Webb and Walling, 1974; Miller, 1961) and thought to correspond with geological and vegetation variation in non-urban areas. Figure 8.4 represents an attempt to display temporal and spatial variation in Na^+ load at approximately bi-monthly intervals throughout the study period. This identifies the lower part of West Walk as the area yielding the most Na^+, SC 1 yielding the least Na^+, contrasts being most marked during periods of high flow (e.g. 3rd January to 9th January 1977). During periods of lower flow and flow recessions SC 4 and SC 7 (the lower part of West Walk) continue to provide the highest yields of Na^+. TDS loads were not portrayed because it was found that errors in weekly values of TDS estimated from SC gave a distorted picture. Other solutes give a similar pattern. The basic spatial pattern of solute load appears to be related to geology, with temporal variation controlled by hydrology and vegetation.

8.4 SUMMARY AND CONCLUSIONS

This Chapter has discussed input and output of solutes to West Walk and computed the net solute losses or gains. The 1975 - 1976 drought was a period of net solute accumulation in the catchment due to diminishing streamflow (the exporting agent) and above average evapotranspiration. Solutes supplied in bulk precipitation were probably maintained in the upper parts of the soil until flushed into the stream by heavy rain in autumn 1976. The subsequent year was a period of net solute loss from the catchment. Gross precipitation and streamflow loads have been compared with those computed for other areas of Britain, Europe, the U.S.A. and New Zealand. Although there are differences, results fall within the same order of magnitude. Unfortunately, there are no comparable data for an area in Lowland Britain of a similar lithology to West Walk.

Some detailed comments have been made upon bulk precipitation inputs. With the possible exception of TDS, which may be in error, and H^+, all solutes dilute with increasing rainfall, probably as the high concentration matter is initially flushed from the atmosphere. The pH of rainfall is not as acid as has been reported in some industrial areas

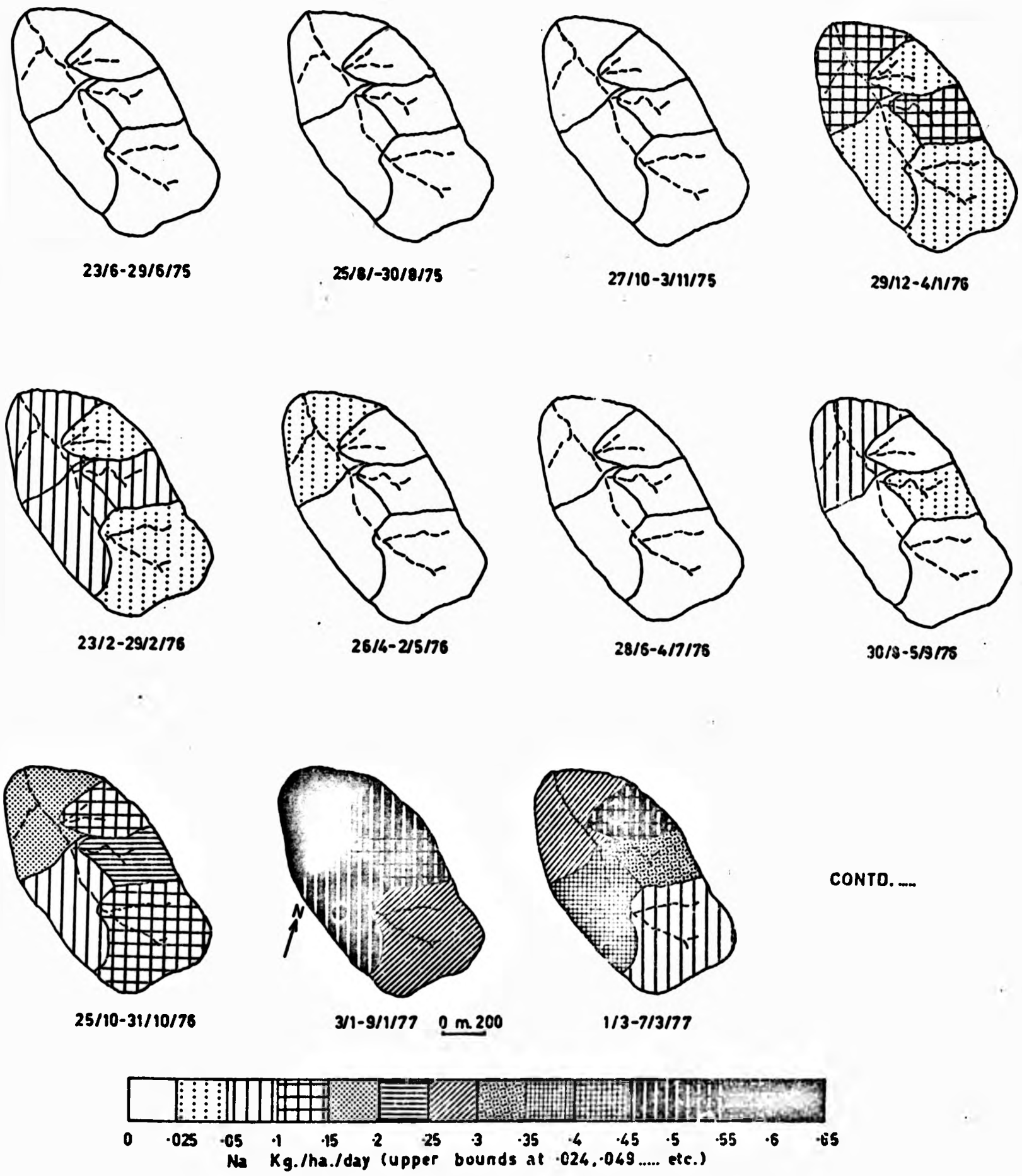

CONTD. .....

FIGURE 8.4: TEMPORAL AND SPATIAL VARIATION OF SODIUM LOADS IN WEST WALK, 1975 - 1977

19/4 - 25/4/77

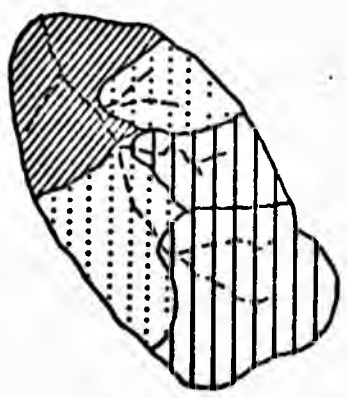

26/4 - 2/5/77

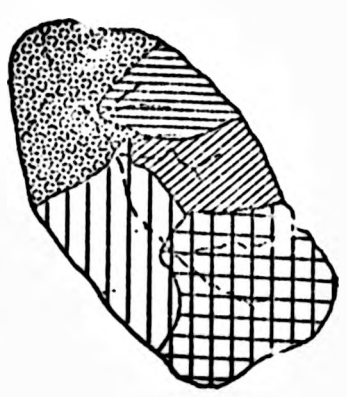

3/5 - 9/5/77

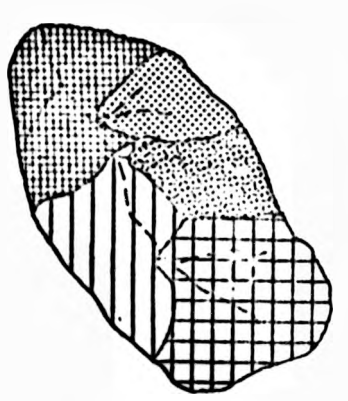

10/5 - 16/5/77

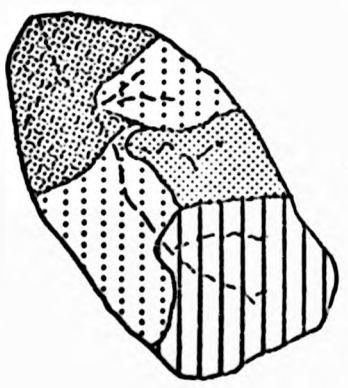

17/5 - 23/5/77

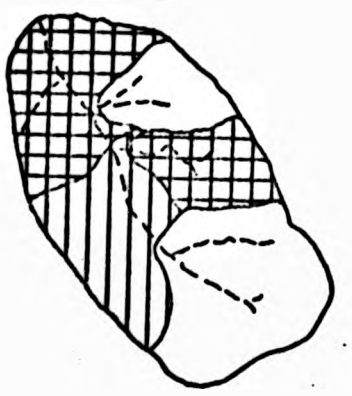

24/5 - 30/5/77

31/5 - 6/6/77

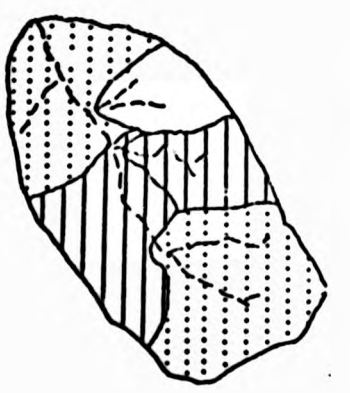

7/6 - 13/6/77

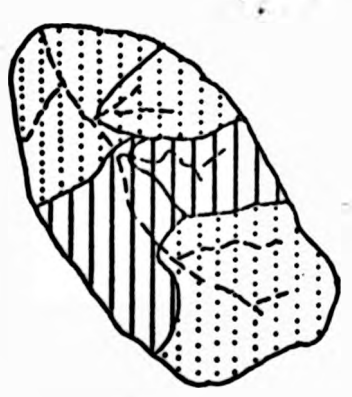

14/6 - 20/6/77

N

0 m 200

FIGURE 8.4 (cont'd):

of Western Europe and Eastern U.S.A. and does not represent an ecological problem. Due to its near coastal location, West Walk receives more solutes in bulk precipitation than would an inland catchment, a factor which is important in minimising net losses. This is principally due to high Na^+ and Cl^- loads, K^+ and Ca^{2+} being obtained mainly from land sources. Solute content of water increases dramatically during stemflow and throughfall, and research into solute dynamics of this sub-system would help elucidate its significance for stream solute response.

The basic pattern of solute yield is strongly related to the proportion of London Clay within the subcatchments. Soils which have developed upon London Clay have higher base exchange capacities than those on the more acid Bagshot Sand. Variable contributing areas and seasonal changes in vegetation probably influence temporal and spatial fluctuation of solute loads.

Both concentration and load frequency duration curves can be plotted for each solute on a daily basis (e.g. Hembree et al, 1964). The load curve can be used to estimate total annual load (e.g. Piest, 1964) while the concentration curve has potentially more application in water quality studies. The 95 % value has been stated as the concentration which is expected to be achieved for 95 % of the time on a river (N.W.C., 1978). Perhaps more important in ecological terms is the degree of persistence achieved by some specified concentration, and different concentration duration curves could be drawn for varying degrees of persistence (e.g. 1, 5, 10, 30 days). With particularly sensitive species hourly periods might be more appropriate. This highlights the problem of modelling detailed storm solute response, which is investigated in more specific manner in Section II.

I

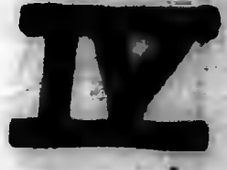

D 37788/81

SPRAGGS . GE

Vol II

pp

375

Total Pages 813

VOL 2.

ASPECTS OF SURFACE AND SUBSURFACE SOLUTE DYNAMICS IN A SMALL CATCHMENT : WEST WALK, SOUTH HAMPSHIRE

Gerald Edward Spraggs, B.A., Dip. Hydrol.

Thesis submitted as part of the requirement for the degree, Doctor of Philosophy, of the Council for National Academic Awards.

September 1980

The work was carried out while a Research Assistant in the Geography Department, Portsmouth Polytechnic, with the collaboration of Southern Water Authority.

VOLUME II

Chapters 9 - 13

References

Appendices

SECTION 3

SUBSURFACE SOLUTE DYNAMICS IN A HILLSLOPE SOIL AT WEST WALK: - TOWARDS A PHYSICALLY BASED, SPATIALLY DISTRIBUTED MODEL OF CATCHMENT SOLUTE RESPONSE

CHAPTER 9

MODELLING STRATEGIES AND AN INTRODUCTION TO WATER AND CHEMICAL MOVEMENT IN HILLSLOPE SOILS

9.1 INTRODUCTION

It was found in Chapters 6 and 7 that bivariate and multivariate regression approaches were not capable of modelling detailed storm solute response over the full range of hydrometeorological conditions. In some cases the addition of variables describing seasonality and moisture status improved the prediction of weekly solute levels, but gave very little indication of the physical processes actually operating. Such an approach treats the processes which convert rainfall into run off (both quantity and quality) as a 'black box'. Results from West Walk, together with research from other areas (e.g. Walling and Webb, 1975; 1980), also point to considerable spatial variation in solute production. This may be due to a combination of geology, soil and vegetation variability, which in the case of West Walk was reflected in downstream chemical changes and a more complex outflow chemograph. In larger catchments channel routing effects are also likely to influence chemograph response (Glover and Johnson, 1974).

Thus there appears to be need for a spatially distributed model of catchment solute response, which takes account of a variable contributing area and is capable of routing solute loads from subcatchment sources to produce an outflow chemograph. Model construction is dependent upon a good knowledge of solute transport processes operating within the 'black box' mentioned above.

Section III of this thesis describes the design, setting up and results of a hillslope experiment within SC1 at West Walk, with the principal aim of elucidating the mechanisms of one part of this black box - the transport of solutes by water through valley-side soils. In greater detail the project aims were:

(i) To gain a better understanding of the processes of water movement within a hillslope at West Walk.

(ii) To gain a detailed understanding of solute transport within the hillslope.

(iii) To use the data collected in (i) and (ii) to route water and solutes from rainfall to stream channel using a flux approach and to compute internal parameters such as hydraulic conductivity and solute dispersivity.

(iv) To compare the computed slope-base discharge and solute concentration with that actually measured.

(v) Using the results, assess the future of spatially distributed modelling of catchment solute response.

9.2 MODELLING CATCHMENT HYDROLOGY: PROGRESS TOWARDS A SPATIALLY DISTRIBUTED MODEL

Clarke (1973) has usefully grouped catchment run off models by technique rather than objective. Four main groups were identified.

(i) Stochastic-conceptual

(ii) Stochastic-empirical

(iii) Deterministic-conceptual

(iv) Deterministic-empirical

Stochasticity refers to the time-dependent probability distributions of the model variables.

Determinism states that the model is free from random variation, and follows laws of certainty.

Conceptualisation refers to a model comprising known physical processes, taken from a body of theory.

Empiricism suggests that the postulated model follows an observed relationship, the internal processes being either known or unknown.

Any of these models (i) to (iv) may be either linear or non-linear, and either (a) lumped; (b) probability-distributed; or (c) geometrically-distributed.

A lumped model 'takes no account of spatial distribution in the input variable, nor of the spatial variation in parameters characterising the physical processes acting upon input'.

A probability-distributed model describes the spatial vaiability of input variables of model parameters without reference to their geometrical distribution over space, i.e. a probability distribution over the catchment is assumed.

A geometrically-distributed model expresses spatial variability in terms of the orientation of the network of points one to another, and their distances apart. Such models are commonplace in ground water hydrology (e.g. Oakes and Pontin, 1976; Oakes, 1979).

Models developed in Chapters 6 and 7 could best be classified as linear, lumped, stochastic-empirical. They are linear in satisfying one assumption of the general linear model; lumped in that they do not model any spatial distribution within the catchment; stochastic in that they have a residual error (although admittedly this was often found to be related to an input variable); empirical in that the model optimised an observed relationship.

Recently there has been a change in direction in attempts to model catchment hydrology (Beven and Kirkby, 1979). Lumped parameter models (e.g. Anglian Water Authority, 1980b) are being challenged by an approach which explicitly considers the dynamic spatial variation in discharge source areas (Beven, 1977b; Beven and Kirkby, 1979). The approach has been developed from field evidence gathered over the last 20 years.

Much of this field research has questioned the general applicability of Horton's overland flow model (Horton, 1945). This postulates that when rainfall intensity exceeds infiltration capacity, overland flow results all over the basin. It has become

clear that the model "represents only a specialised end-member of a series of models ... the throughflow model being the other member. On most slopes both types occur although with markedly different frequencies," (Kirkby and Chorley, 1967).

The importance of throughflow in contributing to the storm hydrograph was a feature of discussion in early research. Hewlett (1961) and Hewlett and Hibbert (1963) concluded from laboratory experiments that unsaturated throughflow provided a means of sustaining base flow in steep mountain watersheds. A recent duplication of Hewlett and Hibbert's experiment (Anderson and Burt, 1977a) revealed that tension gradients and hydraulic conductivities in unsaturated soil failed to explain observed discharge. The latter was well correlated with water table slope and saturated area. Similar results were found from a field experiment by Weyman (1970; 1973). He measured throughflow from three soil horizons on a 12° slope with impermeable bedrock. Baseflow came from the 45 - 75 cm horizon and was supplied by slow unsaturated flow from the whole soil mass to a small fairly constant saturated zone. However, peak discharge was produced mainly by rapid flow from headwater zones of the catchment and not by flow from the 10 - 45 cm horizon of the experimental plot.

In contrast, Whipkey (1965; 1969) has recorded substantial stormflow from a forested slope under simulated rainstorms. As in Weyman's experiment flow took place above horizons of reduced permeability. More recently, Anderson and Burt (1977b; 1978a; 1978b) monitored soil moisture conditions in a hillslope spur and hollow to demonstrate the significant control of topography on water movement and the resulting streamflow response. From the storm event examined and the month-long recession which followed, the hillslope hollow was shown to be significant in both generating a throughflow peak in stream discharge and in maintaining baseflow. In this case the disparity between throughflow contributing to stormflow or baseflow is explained in terms of catchment topography.

The detailed monitoring of soil water movement over a range of conditions at East Twin Brook (Weyman, 1973) provided valuable information upon the hydraulics of subsurface hillslope flow. A spectrum of possible subsurface flow processes was derived from

theoretical considerations of unsaturated flow on hillslopes (Figure 9.1). These ranged from

(i) vertical water movement (horizontal equipotentials), to

(ii) lateral water movement (equipotentials orthogonal to the slope).

Between these two can be expected

(iii) a combination of vertical infiltration and lateral flow during a storm (equipotentials rotate from horizontal to orthogonal), and

(iv) a potential reversal from lateral flow to upward flow caused by evapotranspiration (equipotentials rotate from orthogonal to horizontal near the surface).

This was an idealised picture of hillslope water movement, but a useful framework within which to work. Weyman's empirical data fitted into this framework but included the expansion and contraction of a saturated wedge from adjacent to the channel upwards during and after storms (Figure 9.2). Four stages were identified:

(i) lateral unsaturated flow dominated before the rainstorm, with tension increasing up-profile;

(ii) during infiltration tension decreased from the wetting front to the soil surface giving vertical water movement in the upper part and lateral movement in the lower part of the profile;

(iii) moisture became vertically distributed and vertical flow caused a growth of the saturated wedge;

(iv) the extent of saturation was at a maximum at peak discharge, with lateral saturated flow equalling vertical and lateral saturated flow additions.

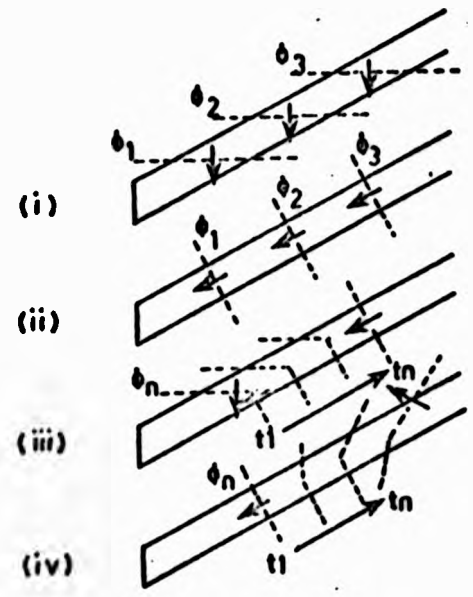

FIGURE 9.1: THEORETICAL CONSIDERATIONS OF UNSATURATED FLOW ON A HILLSLOPE (after Weyman, 1973)

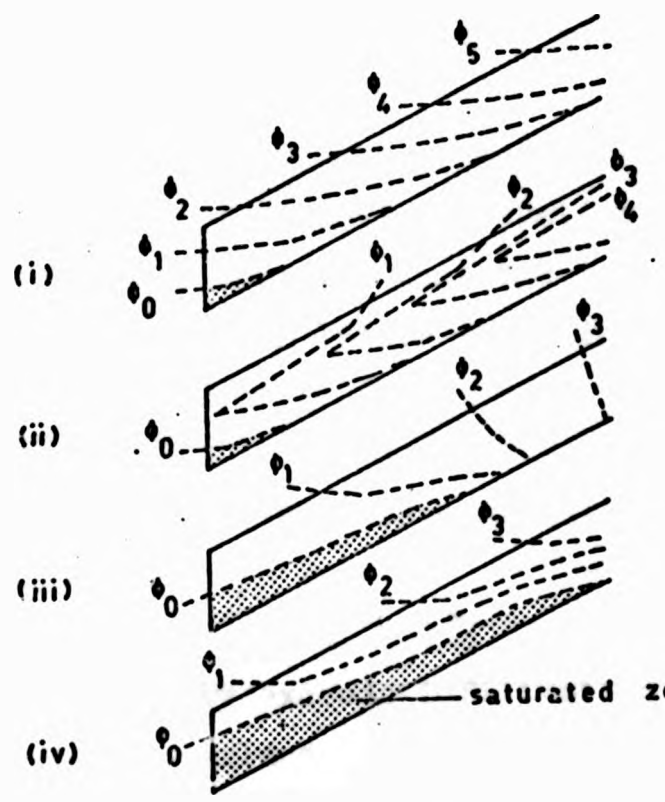

FIGURE 9.2: IDEALISED PATTERN OF WATER MOVEMENT IN A HILLSLOPE DURING AND FOLLOWING A STORM (after Weyman, 1973)

Following peak discharge the saturated wedge gradually shrinks back to its pre-storm dimensions. Weyman considered that the initiation of lateral saturated flow depended upon breaks in vertical soil permeability, in his case the base of the profile and the base of the B horizon, a conclusion reached by others (Whipkey, 1965; Knapp, 1970a).

Several authors have described pipeflow on hillslopes (Jones, 1971; Parker, 1963; Chamberlin, 1972). Knapp (1970b) suggested that subsurface pipeflow is a contributory factor to the flashy response of the upper Wye catchment, Plynlimon, Central Wales. He found that pipes originated in a zone of thinning peat in a region of large hydraulic gradients due to the steepness of the slopes. The Institute of Hydrology have carried out intensive research into pipeflow phenomena in the same area.

These patterns of water movement are likely to control solute transport within the soil, in particular relatively rapid flow to the channel as pipeflow or overland flow during storms. Slower, unsaturated flow might be more important in feeding the saturated zone during winter recession periods. Flow towards the soil surface is likely to be important when potential reversal occurs in response to evapotranspiration.

Field evidence of diurnal fluctuation in the specific conductance of throughflow water confirms that the latter process operates (Beven, 1979), but there has been little investigation of solute movement during storms.

Beven and Kirkby (1979) have classified the various mechanisms of run off production as

(a) Run off intensity exceeds infiltration or storage capacity resulting in overland flow all over the basin, i.e. the classical Horton model;

(b) Rainfall intensity exceeds infiltration or storage capacity on a variable area of near saturated soils. This provides the basis

for the 'partial area' model, when the spatially variable nature of infiltration capacities results in some areas of the basin being more likely to produce infiltration excess overland flow than others (Betson, 1964; Betson and Marius, 1969; Betson, Marius and Joyce, 1968; Ragan, 1968; TVA, 1965);

(c) Rain falling on stream channels and completely saturated soils. The saturated zone may build upwards from the bedrock or a relatively impermeable soil layer (Dunne and Black, 1970; Weyman, 1973);

(d) Downslope lateral flow of saturated or unsaturated soil water. This occurs essentially within the soil but may flow out, overland, where the soil storage capacity is exceeded (Dunne and Black, 1964; Nutter, 1973; Hewlett and Nutter, 1970; Nutter, 1969).

Beven and Kirkby (1979) conclude that in humid temperate basins mechanisms (b) and (c) are the important sources of stormflow, with subsurface flow establishing conditions within the soil before further rainfall occurs. If pipeflow is an important process then (d) could become significant, although the flow is non-Darcian.

Recently simulation models have appeared which incorporate the concept of dynamic contributing area and are useful for comparison with real processes. Freeze (1972a; 1972b) used finite difference models of two dimensional subsurface flow within convex and concave slopes for generating surface and subsurface run off hydrographs. One important conclusion, which supported field observation (Weyman, 1973), was that soils with low hydraulic conductivities were unlikely to contribute storm flow to the channel storm hydrograph, but could promote the up-profile extension of the saturated wedge enough to give overland flow.

Beven (1977a; 1977b) used a finite element model of two-dimensional, partially saturated flow within a hillslope soil mantle overlying an impermeable bedrock to investigate parameter variations and initial conditions on the hillslope hydrograph. Agreement with Weyman's findings were good although it was shown that the dominance of vertical over lateral flow throughout most of the

slope allowed the continued growth of the saturated zone upslope after the discharge peak. The importance of initial conditions, particularly in the unsaturated zone, in governing the timing and magnitude of the hydrograph peak was also demonstrated.

Work has been undertaken at the Institute of Hydrology to produce a distributed catchment model of the Wye and Severn headwater catchments at Plynlimon, Central Wales. The technique was to divide the catchment into slope and channel elements and to solve the appropriate surface and subsurface flow equations for each element in turn until the output hydrograph from the last (channel) element gave the catchment hydrograph (IoH, 1976; 1978). Beven (1977a) has pointed out that it is important to understand the working of this type of model before putting it to predictive use.

Soil water processes in the dynamic contributing area have been given detailed treatment here because it is thought that they could be of direct relevance to monitoring, understanding and finally modelling solute transport processes. The model formulated and tested by Beven and Kirkby (1979) could eventually form the basis of a spatially distributed model of catchment solute response, but only after sufficient field study of solute transport mechanisms. Their model aimed to combine the distributed effects of channel network topology and dynamic contributing area with the advantages of a simple lumped-parameter basin model. They aimed to produce a model capable of being applied operationally, and therefore developed a simpler model than those which were based upon finite element or finite difference approximations to the hillslope flow equations (e.g. Freeze, 1972a & b; Beven, 1977a & b).

It is claimed that the model structure requires only measurement of basin topography, infiltration rates, overland and channel flow velocities, a few discharge measurements and some simple measurements of the soil hydrological characteristics. It can then be used to predict run off in the ungauged basin, given rainfall and evaporation. Figure 9.3 illustrates the model structure for a subcatchment. The contributing area is modelled as a function of water storage in the saturated zone, S_3, the slope of the relationship between $\log_e$

discharge and relative catchment water storage, 1/M, and topography (contour length, a, and local slope angle, β). Rain falling on the computed contributing area, A_c, becomes overland flow. The surface interception store, S_1, has a maximum value, S_D, values in excess of which contribute to A_c or the infiltration store, S_2. Constant leakage is allowed from S_2 to S_3, and overland flow can occur by either infiltration excess overland flow (rainfall intensity > maximum infiltration intensity) or saturated excess overland flow (the near surface storage is exceeded). The subsurface saturated soil water store, S_3, provides delayed flow.

One sequence of stores represents the average response of soil water in a subcatchment and is therefore treated as a lumped system. The dominant source of surface run off is taken as the variable contributing area, the extent of which depends upon the storage level in S_3.

The present experiment concentrates upon the processes operating down a single slope, although it is acknowledged that spatial patterns are important.

9.3 WATER MOVEMENT IN HILLSLOPE SOILS

For hydraulically isotropic soils Darcy showed that the volume flux, or the volume of water crossing unit area per second, $\bar{F}$, is proportional to the gradient of hydraulic potential in the direction of flux, s. Thus Darcy's Law states (Rose, 1966):

$$\bar{F} = - K \frac{\partial \phi}{\partial s} \qquad (9.1)$$

where
- K = hydraulic conductivity, cm sec^{-1}
- ϕ = hydraulic potential, cm
- s = distance in direction of flux, cm
- $\bar{F}$ = flux of moisture per unit area, cm sec^{-1}

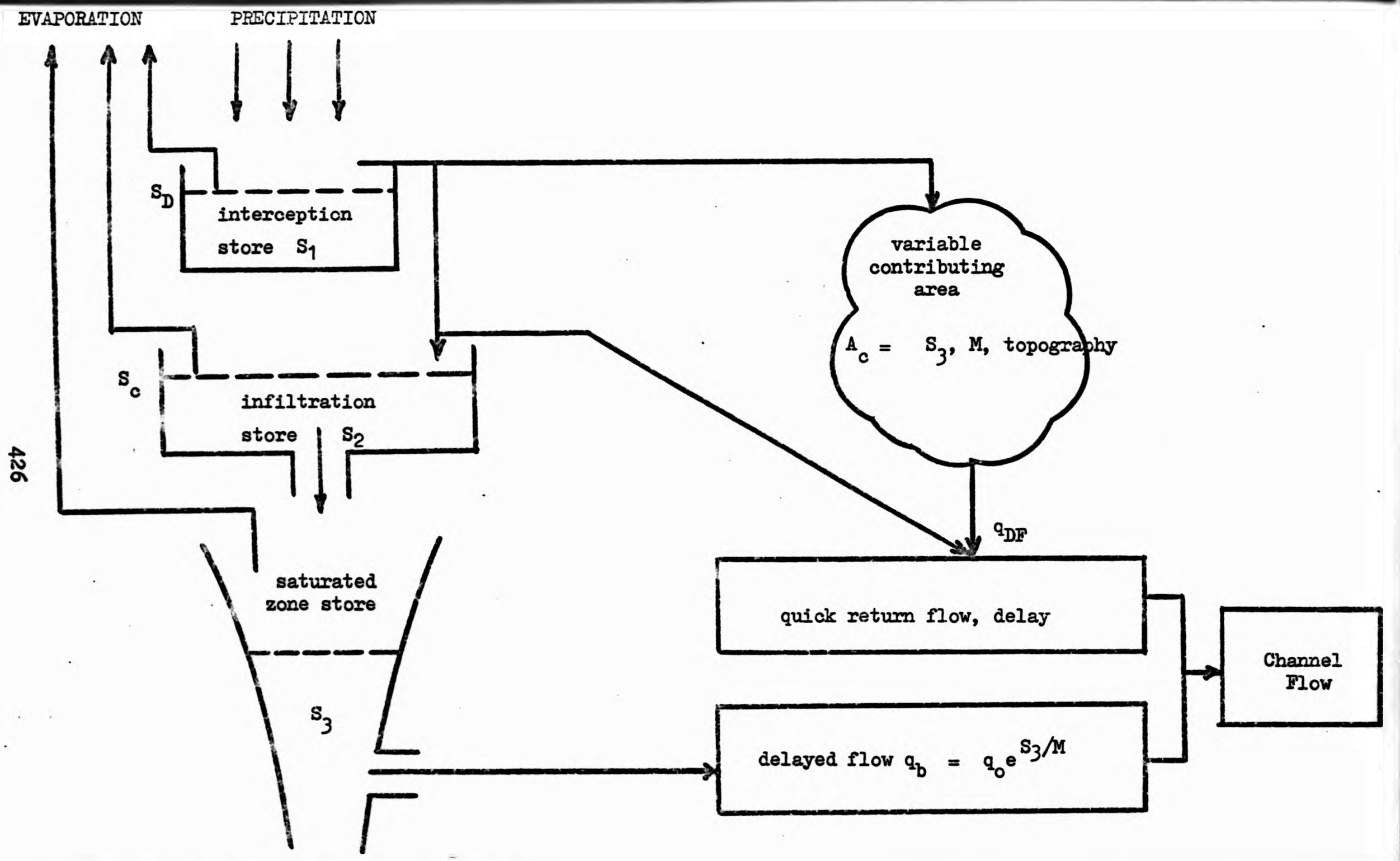

FIGURE 9.3 (After Beven and Kirkby, 1979)

SCHEMATIC REPRESENTATION OF BEVEN AND KIRKBY'S VARIABLE CONTRIBUTING AREA CATCHMENT MODEL

(A) Hydraulic Conductivity (K)

Hydraulic conductivity depends upon moisture content for any constant pore geometry or pedological structure; K increases with increasing moisture content and becomes approximately constant at saturation. The degree of hysteresis is the relationship at any point in time depends upon the previous history of wetting and drying. Childs (1969) gives the reasons for the variation of K with moisture content:-

Firstly, reduction in pore water content reduces the contribution of the flow path, i.e. effective porosity is reduced.

Secondly, the earlier stages of moisture reduction are more effective in reducing K, since this involves loss from larger pore spaces which make an important contribution to K.

Thirdly, a dry pore, full of air becomes an obstacle to water leading to a longer flow path for water particles. In addition this causes hysteresis on wetting.

Lastly, if the soil shrinks on drying, the reduction in pore space will cause a reduction in K. If inter-ped cracks widen during drying then they may dominate pores during wetting, increasing the value of K.

Soil structure is very important in determining hydraulic conductivity. Soil particles may align themselves parallel to the ground slope enhancing K in that direction. Alternatively, a higher K in the vertical axis may be due to the preferred orientation of inter-ped fractures. These are two examples of structural causes of anisotropy in soils, for which Darcy's Law as stated in 9.1 is not applicable. Childs (1969, p. 159 - 162) gives a more detailed discussion of the subject.

Hydraulic conductivity may be determined by either direct or indirect methods.

Indirect methods involve estimation using grain size analyses and porosity determinations. Freeze and Cherry (1979), reviewing the

relevant equations, consider that the Kozeny-Carmen equation gives good predictive results from grain size and porosity. However, Knapp (1970a) tried several methods of calculating K and found laboratory determined values to be 10^3 greater than those calculated from porosity.

Unsaturated or saturated K may be determined in the laboratory or in the field using direct methods. Laboratory methods require an undisturbed soil core, representative of the soil structure. For saturated conditions, the technique involves either a constant-head or a falling-head permeameter (e.g. Todd, 1959) but for unsaturated conditions the apparatus is more sophisticated, involving a controlled pressure chamber (e.g. Richards and Weeks, 1953; Youngs, 1964).

If saturated hydraulic conductivity alone is required, then this can be obtained in the field using the auger hole method (Bonell, 1972). Hydraulic conductivity can also be determined in the field over the entire range of water content whatever the nature of the soil profile using a vertical flux method (Rose et al, 1965). Average hydraulic conductivity over time interval T ($= t_2 - t_1$) is given by:

$$\bar{K}_z = \bar{F}_z / (\overline{\partial\psi / \partial z})_z \, T \qquad (\text{cm sec}^{-1}) \qquad (9.2)$$

where z = depth from soil surface, cm

ψ = pressure potential, cm

$\bar{F}_z$ = vertical flux of water at depth z (cm sec^{-1})

$$= \left\{ - \int_{t_1}^{t_2} \int_{0}^{z} \frac{\partial \theta}{\partial t} \, \partial z \, \partial t \right\} \qquad (9.3)$$

θ = volumetric water content $(\text{cm}^3 \ \text{cm}^{-3})$

An extension of this approach for two dimensional flow is given later.

(B) <u>Hydraulic Potential</u> (ϕ)

In equation (9.1), ϕ, the total hydraulic potential in the direction of flux, is the sum of gravitational and pressure potentials and is given by:

$$\phi = z + \psi \qquad (9.4)$$

(see Chapter 10, equation 10.1). The pressure potential is positive for points beneath the water table or negative for the unsaturated zone above the water table, and is measured by tensiometer, details of which are given in the next chapter.

In the present study the intension is to combine empirical and model approaches; that is, to test a defined model structure by processing data collected in the field. The two dimensional continuity equation used in modelling is:

$$\frac{\partial \theta}{\partial t} = \frac{\partial \bar{F}_z}{\partial x} + \frac{\partial \bar{F}_z}{\partial z} \qquad (9.5)$$

where $\frac{\partial \theta}{\partial t}$ = rate of moisture change in time t at a considered point

x and z = horizontal and vertical axes respectively

Substituting (9.1) in (9.5) gives:

$$\frac{\partial \theta}{\partial t} = K_x \frac{\partial^2 \phi}{\partial x^2} + K_z \frac{\partial^2 \phi}{\partial z^2} \qquad (9.6)$$

This is sometimes expressed as:

$$\frac{\partial \theta}{\partial t} = \frac{\partial}{\partial x}\left[D \frac{\partial \theta}{\partial x}\right] + \frac{\partial}{\partial z}\left[D \frac{\partial \theta}{\partial z}\right] \qquad (9.7)$$

where D = soil water diffusivity = $K\left[\frac{\partial \psi}{\partial \theta}\right]$

$\frac{\partial \psi}{\partial \theta}$ is the slope of the soil moisture characteristic (the relationship between matric pressure potential (ψ) and moisture content (θ)). Diffusivity is not the same as molecular diffusion, which is discussed later, although the water can be referred to as 'diffusing' through the soil (Childs, 1969). If the two dimensional hillslope profile is divided into a series of parallelograms

(hereafter 'elements') then (9.6) can be solved for each element in turn through (9.5) with certain assumptions (Figure 9.5) (Atkinson, 1978). Firstly, the soil is isotropic and homogenous in each element, with $K_{x_1} = K_{x_2} = K_{z_1} = K_{z_2}$. This assumption is not necessarily true, as previously stated, but is required as a first approximation for solution of (9.5). Secondly, there will be changes in the moisture content between the two ends of the element, which can only be minimised by making the length of the element as small as possible. Referring to Figure (9.4A) a flux equation analagous to (9.5) can be derived:

$$A(\theta_{t_2} - \theta_{t_1}) = (t_2 - t_1)\left\{H(\bar{F}_{x_2} - \bar{F}_{x_1}) + L(\bar{F}_{z_2} - \bar{F}_{z_1})\right\} \qquad (9.8)$$

where $A = H.L$ and θ_{t_1} and θ_{t_2} are the moisture contents in the element at times t_1 and t_2.

Re-arranging to the form of (9.5):

$$\frac{A\,(\theta_{t_2} - \theta_{t_1})}{t_2 - t_1} = H\,(\bar{F}_{x_2} - \bar{F}_{x_1}) + L\,(\bar{F}_{z_2} - \bar{F}_{z_1}) \qquad (9.9)$$

$\bar{F}_{z_1}$ is initially given the value of $\bar{F}_p$, the rainfall between t_1 and t_2; knowing this, the values of tension and moisture content within the element and tension on three sides of the element, the input and output fluxes for the element may be computed as follows:

$$\bar{F}_{x_1} = \bar{F}_{z_1} \frac{(\phi_5 - \phi_2)\,h_1}{(\phi_1 - \phi_2)\,l_1} \qquad (9.10)$$

$$\bar{F}_{x_2} = \bar{F}_{z_1} \frac{(\phi_2 - \phi_3)\,h_1}{(\phi_1 - \phi_2)\,l_2} \qquad (9.11)$$

$$\bar{F}_{z_2} = \bar{F}_{x_1} + \bar{F}_{z_1} - \bar{F}_{x_2} \pm \Delta s \qquad (9.12)$$

$\pm \Delta s$, storage change in time $t_2 - t_1$, $= A\,(\theta_{t_2} - \theta_{t_1})$.

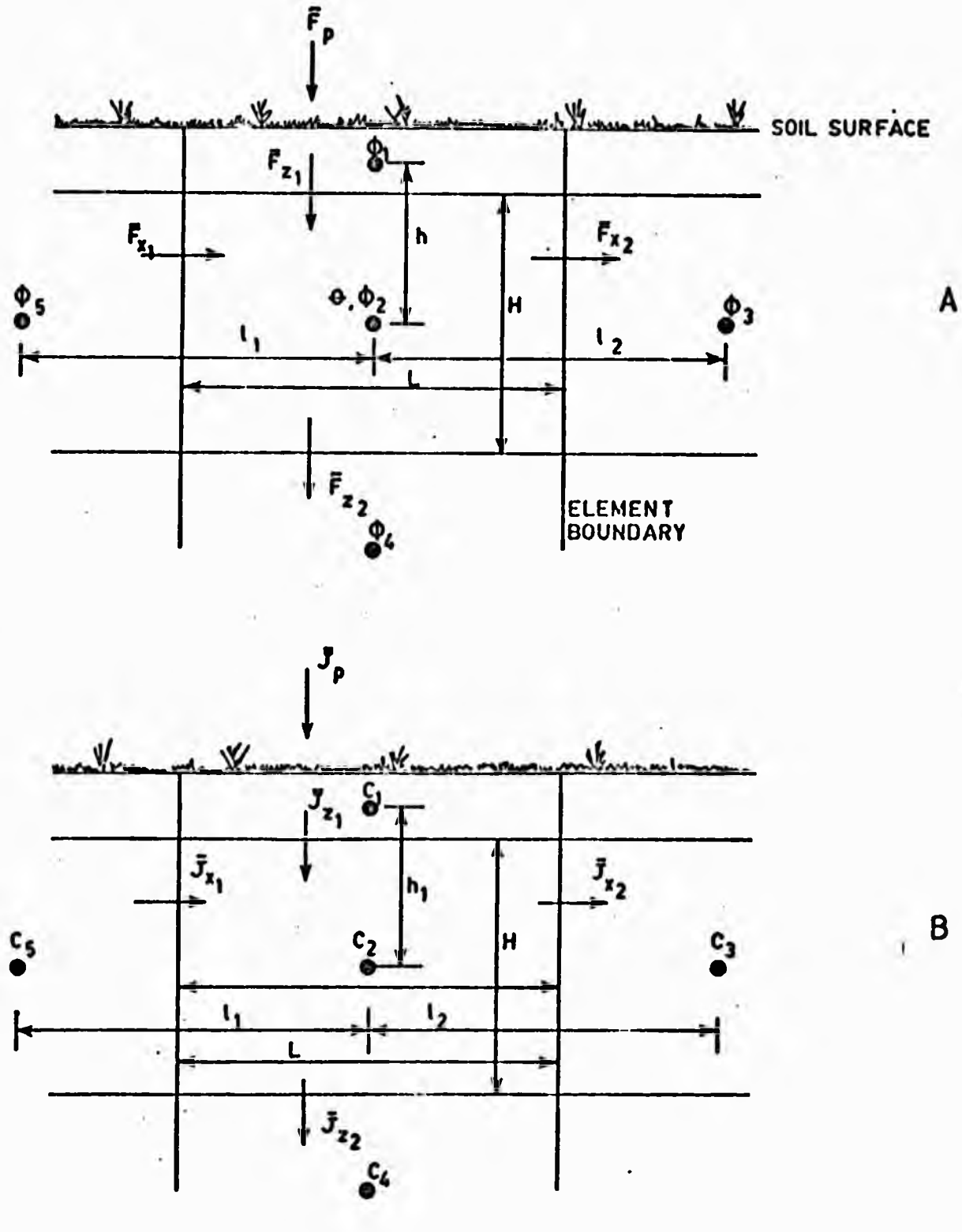

FIGURE 9.4: SINGLE HILLSLOPE ELEMENTS FOR COMPUTATION OF (A) WATER, AND (B) SOLUTE FLUX (see text for definition of terms)

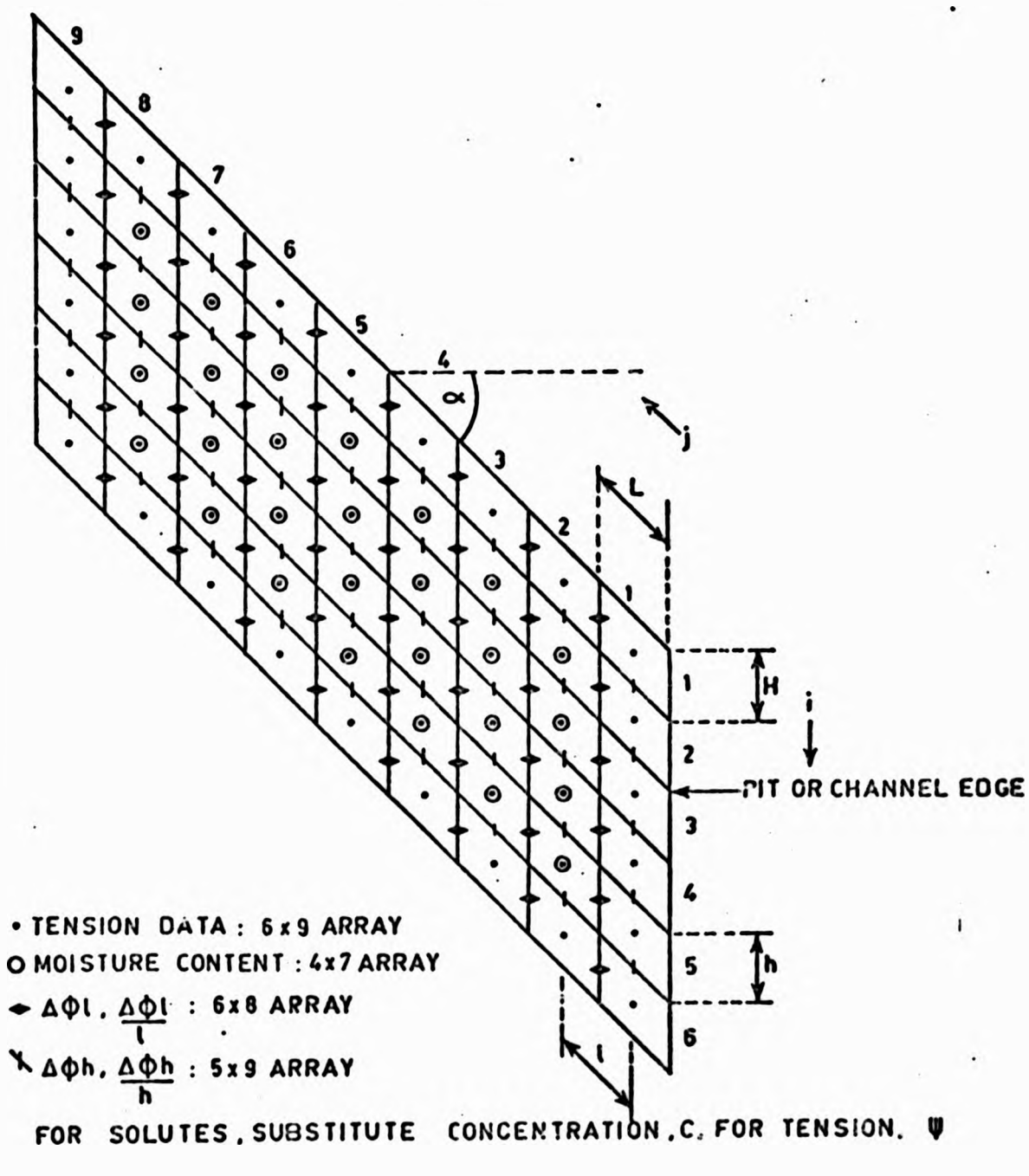

FIGURE 9.5: SCHEMATIC DIAGRAM OF A HILLSLOPE DIVIDED INTO ELEMENTS AND SUITABLE FOR FLUX COMPUTATION

Hydraulic potential, ϕ, is computed by equation (9.4) and averaged over the time period. Pore water velocity can then be computed from:

$$\bar{V}_{x_1} = \bar{F}_{x_1} / \theta \qquad (9.13)$$

$$\bar{V}_{z_1} = \bar{F}_{z_1} / \theta \qquad (9.14)$$

and hydraulic conductivity from:

$$K_{x_1} = \bar{F}_{x_1} \frac{\partial x}{\partial \phi} \qquad (9.15)$$

or,
$$K_{z_1} = \bar{F}_{z_1} \frac{\partial z}{\partial \phi} \qquad (9.16)$$

The procedure is repeated for each element at the first depth. Flux leaving the upslope element is made equal to that entering the downslope element by averaging and assigning excess to the downslope flux. Should this cause cumulative error then upslope and downslope fluxes might be converged by an iterative procedure. Computation proceeds through each row of elements, with $\bar{F}_{z_2}$ from the uppermost element being $\bar{F}_{z_1}$ for the down profile element. Discharge from the slope base is the sum of the separate discharges from the bottom column of elements, and may be compared with actually measured discharge to validate the model. Similar finite difference methods have been widely used in ground water hydrology (e.g. Taylor and Luthin, 1969).

9.4 SOLUTE MOVEMENT IN HILLSLOPE SOILS

One-dimensional transport of solutes in soil is both complex and incompletely understood, since the number of variable factors is much greater than with the flux of water. Most recent research in this context is being carried out by soil scientists, hydrogeologists and agricultural engineers, with a range of applications. In pedology and agricultural engineering, interest has focused upon measuring the change in water quality below the root zone stemming from applications of fertilisers, pesticides and other agrochemicals during crop production (e.g. Jury et al, 1976). Similarly, the pollution potential

of surface water and ground water has been examined by monitoring the solutes leached through the soil in the vicinity of industrial and municipal waste disposal (e.g. Naylor et al, 1978; Freeze and Cherry, 1979, Ch.9).

The movement of solutes in hillslope soils (i.e. two- and three-dimensional transport) and their contribution to the hillslope chemograph has been little studied in either the field, the laboratory or by computer simulation. The factors which have inhibited progress are firstly, the difficulty in accurately measuring physical processes under field conditions and secondly, the heterogeneity of field soils. In addition, solution of the continuity equations describing solute movement but neglecting adsorption and exchange processes is complex and has only been attempted for one-dimensional flow in soils (e.g. Biggar and Nielsen, 1976). A model including adsorption and exchange processes has been presented by H K Krupp et al (1972). This section presents the basic theoretical development of solute transport models and describes some of the complicating factors.

Considering the two-dimensional case of flow through an element, the continuity equation is:

$$\frac{\partial c}{\partial t} = \frac{\partial \bar{J}_x}{\partial x} + \frac{\partial \bar{J}_z}{\partial z} \qquad (9.17)$$

where c = solute concentration, mg cm^{-3}
$\bar{J}_x$ = solute flux in horizontal direction, mg cm^{-2} sec^{-1}
$\bar{J}_z$ = solute flux in vertical direction, mg cm^{-2} sec^{-1}

If the transport of solute is by diffusion only, then Fick's first law applies (Fick, 1855; see Freeze and Cherry, 1979, p.103):

$$\bar{J}_x = - D_x \frac{\partial c}{\partial x} \qquad (9.18)$$

$$\bar{J}_z = - D_z \frac{\partial c}{\partial z} \qquad (9.19)$$

where D = apparent diffusion coefficient, cm^2 sec^{-1}

Substituting (9.18) and (9.19) in (9.17) gives Fick's second law (Fick, 1855; see Freeze and Cherry, 1979, p.104).

$$\frac{\partial c}{\partial t} = D_x \frac{\partial c}{\partial x} + D_z \frac{\partial c}{\partial z} \qquad (9.20)$$

Diffusion results from a random motion of the ions or molecules and occurs preferentially in one direction or another depending on the activity gradients which provide the driving force (Biggar and Nielsen, 1967). Cations and anions can diffuse in the soil system, although there is an initial decrease in the apparent diffusivity of about a factor of two in a porous medium compared to that in aqueous solution (Graham-Bryce, 1965). This can be attributed primarily to the tortuosity of the diffusion pathway. Freeze and Cherry (1979) have calculated, using an analytical solution of (9.20) in only the x direction, that diffusion over a distance of 10 metres with $D_x = 5 \times 10^{-10}$ m^2/sec would take approximately 500 years. It is, therefore, a slow process if acting alone.

However, pure diffusion will not describe solute movement in a hillslope, and a mass transport term is introduced into (9.18) and (9.19). Combination of these two processes occurring simultaneously during transport suggests superposition of one upon the other to obtain a description of mixing, thus:

$$\bar{J}_x = - D_x^* \frac{\partial c}{\partial x} + \bar{F}_x \, c \qquad (9.21)$$

$$\bar{J}_z = - D_z^* \frac{\partial c}{\partial z} + \bar{F}_z \, c \qquad (9.22)$$

where D^* = dispersion coefficient, differing from the diffusion coefficient because water movement itself causes some dispersion of the solute; $\bar{F}$ = flux of water per unit area as defined earlier.

Substituting (9.21) and (9.22) in (9.17), gives for steady flow:

$$\frac{\partial c}{\partial t} = D_x^* \frac{\partial^2 c}{\partial x^2} - \bar{F}_x \frac{\partial c}{\partial x} + D_z^* \frac{\partial^2 c}{\partial z^2} - \bar{F}_z \frac{\partial c}{\partial z} \qquad (9.23)$$

(for unsteady flow the flux component, $\bar{F}$, should be included inside the differential). Other processes are likely to be operating in the soil, and these need to be represented in (9.23). They are:

(i) slow release of ions from non-exchangeable to exchangeable form;

(ii) adsorption-desorption reactions, possibly influenced by soil organic matter transformation;

(iii) degradation of organic solutes by chemical or microbial action (Nye and Tinker, 1977).

The total ionic strength of the soil solution depends upon the concentration of unadsorbed anions that it contains. Amongst these, chloride, nitrate and bicarbonate are not adsorbed by the negatively charged colloid surface unless it contains positively charged sites. Sulphate is not strongly adsorbed. Positively charged sites are often associated with iron or aluminium oxides at pH below 6. Substitution is enhanced in acid conditions which are supplied by acids in surface humus. Kerpen and Scharpenseel (1967) found that the mobility of Ca^{++} and Mg^{++} in laboratory leaching of basalt fragments was increased by more than ten times and that of Na^{+} and K^{+} by up to two when adding a humus layer over the basalt. The proportions in the soil solution of the different cations that balance the anions is determined by the ionic charge of the adsorbed cations, their properties on the exchange complex, their ionic size and the properties of the exchanger; further details of these processes are given in Nye and Tinker (1977). Although stable equilibrium is usually established within minutes between exchangeable cations and cations in solution, slower processes also operate. The reactions can be classified thus:

(a) Rapid reactions ($<$ 1 hour) occur when the exchangeable cation is held on the external surface of clay or humus particles, or in the interlayers of expanded clay minerals in which alumino-silicate sheets are separated by at least two and usually three molecular diameters of water molecules. Temporary disruption of equilibrium may be caused by plant uptake either from solution or

directly from the colloid surface. The balance is subsequently restored by movement into or from solution.

(b) Intermediate-rate reactions ($\simeq$ 1 day) for most cations are of little importance. However, for potassium the exchanging amount at intermediate rate is significant. In the presence of vermiculite, illite and other 2:1 type minerals, K^+ ions are adsorbed and may become "fixed" by soil colloids. Ions fit in between crystal units of these normally expanding days and become an integral part of the crystal. Potassium in this form cannot be replaced by ordinary exchange methods and is referred to as non-exchangeable potassium (Brady, 1974). This form is in equilibrium with the available forms and consequently acts as an extremely important reservoir of slowly available potassium.

(c) Slow-rate reactions ($\geqslant$ 1 week) come under the heading of mineral weathering, and are an important means by which exchangeable cations lost to drainage are replaced in the soil profile. They have low significance when considering short-term solute dynamics.

Inclusion of these processes in a model such as (9.23) is a formidable task, and one which has often been neglected as a means of simplifying analytical solutions (e.g. Biggar and Nielsen, 1976). M J Frissell (1972) has presented a model describing vertical transport of potassium in a soil, which includes mechanisms for cation exchange, fixation and release. The two equations describing homovalent exchange are:

$$\frac{K_{sol}}{Na_{sol}} = X_{Na,K} \frac{K_{ads}}{Na_{ads}} \qquad (9.24)$$

$$\frac{Mg_{sol}}{Ca_{sol}} = X_{Ca,Mg} \frac{Mg_{ads}}{Ca_{ads}} \qquad (9.25)$$

and for heterogenous exchange:

$$\frac{Ca_{sol}}{(Na_{sol})^2} = X_{Na,Ca} \frac{Ca_{ads}}{(Na_{ads})^2} \qquad (9.26)$$

where subscripts sol and ads refer to the dissolved and adsorbed ions respectively (concentrations in meq cm^{-3} bulk soil);
$X_{Na,K}$, $X_{Na,Ca}$ and $X_{Na,Ca}$ are the exchange constants.

Furthermore, the cation exchange capacity is found from:

$$Na_{ads} + K_{ads} + Ca_{ads} + Mg_{ads} = CEC \qquad (9.27)$$

If tot = ads + sol, and $X_1 = Na_{sol}/Na_{ads}$, (9.24 - 9.26) can be re-arranged and substituted in (9.27) giving:

$$CEC = \frac{Na_{tot}}{1 + X_1} + \frac{K_{tot}}{X_{Na,K}(1 + X_1)} + \frac{Ca_{tot}}{X_{Na,Ca}(1 + X_1^2} + \frac{Mg_{tot}}{X_{Na,Ca}.X_{Ca,Mg}(1 + X_1^2)}$$

(9.28)

Frissell solved (9.28) for X_1 by Newton-Rapshon iteration and substituted this in the preceding equations to give dissolved and adsorbed cations. K-fixation was regarded as an exchange with cations present on a particular part of the soil complex; this part of the soil complex is not part of the CEC. The amount fixed in the equilibrium situation, K_{eq}, is found from:

$$K_{eq} = F_{fr}\,(K_{fixed} = K_{ads} + K_{sol}) \qquad (9.29)$$

in which K_{fixed} is the amount actually fixed (meq cm^{-3} bulk soil) and F_{fr} is the fraction of K-ions per layer which can be fixed.
If $K_{eq} < K_{fixed}$, the release rate is found from:

$$R_{rate} = R_{rate}\,(K_{fixed} - K_{eq}) \qquad (9.30)$$

in which R_{rate} is the specific release rate.

Frissell used these equations in simulation experiments but without verification by real data. The method has the disadvantages that:

(i) the implicit assumption of immediate exchange could lead to errors under high mass flow rates;

(ii) the assumption that the exchange constant valid for a mixture of two species can also be used for more than two species is not verified by thermodynamics;

(iii) release and fixation are oversimplified as first order reactions; and

(iv) the assumption that the composition of the exchangeable ions for all exchange sites is identical is untrue, since K-ions show a preference for ions of a particular size.

If these processes are regarded as 'sources' and 'sinks' then a general descriptive term $f(C)_{x,z}$ may be added to (9.23) giving:

$$\frac{\partial c}{\partial t} = D_x^* \frac{\partial^2 c}{\partial x^2} - \bar{F}_x \frac{\partial c}{\partial x} + D_z^* \frac{\partial^2 c}{\partial z^2} - \bar{F}_z \frac{\partial c}{\partial z} + f(c)_{x,z} \qquad (9.31)$$

Solution of (9.31) is possible using an approach very similar to that for water flux. For the element shown in Figure 9.4B, (9.17) is equivalent to:

$$A(c_{2,t_2} - c_{2,t_1}) = (t_2 - t_1) \left\{ H (\bar{J}_{x_2} - \bar{J}_{x_1}) + L (\bar{J}_{z_2} - \bar{J}_{z_1}) \right\} \qquad (9.32)$$

where A = area of element = L.H, t = time.
This can be re-arranged to give:

$$\frac{A(c_{2,t_2} - C_{2,t_1})}{t_2 - t_1} = H (\bar{J}_{x_2} - \bar{J}_{x_1}) + L (\bar{J}_{z_2} - \bar{J}_{z_1}) \qquad (9.33)$$

To compute directional fluxes (9.21) and (9.22) can be used at times t_1 and t_2, assuming $D^*_{x_1} = D^*_{x_2} = D^*_{z_1} = D^*_{z_2}$, and knowing $\bar{J}_{z_1}$ (or $\bar{J}_p$),

the input flux of the solute by rainfall:

$$\bar{J}_{x_1} = \bar{J}_{z_1} \frac{(c_5 - c_2)\, h_1}{(c_1 - c_2)\, l_1} + \bar{F}_{x_1}\, c_2 \qquad (9.34)$$

$$\bar{J}_{x_2} = \bar{J}_{z_2} \frac{(c_2 - c_3)\, h_1}{(c_1 - c_2)\, l_2} + \bar{F}_{x_2}\, c_2 \qquad (9.35)$$

$$\bar{J}_{z_2} = \Delta S_c - \bar{J}_{x_2} + \bar{J}_{x_1} + \bar{J}_{z_1} \qquad (9.36)$$

where ΔS_c = storage change = $(\theta_{t_2}\, c_{2,t_2} - \theta_{t_1}\, c_{2,t_1})$ (9.37)

ΔS_c is assumed to include the term $f(c)_{x,z}$ lumping together ions stored in solution with those gained or lost by exchange reactions.

The apparent dispersion coefficient is calculated by:

$$D^*_{x_1} = \frac{\partial x_1}{\partial c}\, \bar{J}_{x_1} - \bar{F}_{x_1}\, c \qquad (9.38)$$

or $$D^*_{z_1} = \frac{\partial z_1}{\partial c}\, \bar{J}_{z_1} - \bar{F}_{z_1}\, c \qquad (9.39)$$

Little is known of the relative importance of the different terms in equation (9.31), and in particular whether D_* becomes insignificant at high velocities.

Biggar and Nielsen (1976) found the relationship between the apparent dispersion coefficient and velocity to be of the form:

$$D^* = D + \alpha \bar{v}^n \quad (\text{cm sec}^{-1}) \qquad (9.40)$$

where D is the molecular diffusion coefficient, $\bar{v}$ is mean velocity, α and n are constants. α is a characteristic property of the porous medium known as the dynamic dispersivity (m); and n is an empirically determined constant between 1.0 and 2.0, although $n \simeq 1.0$ for granular material (Freeze and Cherry, 1979).

Biggar and Nielsen (ibid) reported that most values of α and n in the literature were approximately 0.5 and 1.2 respectively for chloride transfer in unconsolidated porous materials composed of particles of uniform diameter. At a low velocity, diffusion is the important contributor to the dispersion, and therefore $D^* = D$. At a high velocity mechanical mixing is the dominant dispersive process, in which case $D^* = \alpha \bar{v}^n$. Larger dispersivity of the medium produces greater mixing of the solute front as it advances. T K Perkins and O C Johnson (1963) have established relationships between the influence of diffusion and mechanical dispersion as shown in Figure 9.6.

Nielsen et al (1973a) found pore water velocities of less than 0.01 cm min^{-1}, below which solute mixing is essentially governed by solute diffusion (Todd and Kemper, 1972; Kirda et al, 1973). Weyman (1973) found saturated throughflow velocities on a free-draining brown earth adjacent to the stream channel (slope angle $\triangleq 12^o$) varied from 0.01 cm min^{-1} to 0.3 cm min^{-1}. Substitution of assumed values of chloride concentration and distance downslope in (9.38) and (9.21) shows approximately that the $- D_x^* \frac{\partial c}{\partial x}$ term makes an increasing contribution to $\bar{J}_x$ with increasing velocity in the range of 0.01 to 0.3 cm min^{-1} (Weyman's values). This suggests that dispersion could be an important term in solute movement and should be included when modelling.

As with water flux, solute flux is computed for each hillslope element and the summed output at the slope base compared with the concentration in sampled water.

Recent advances in modelling solute transport processes have come from the field of hydrogeology and in particular ground water pollution. Freeze and Cherry (1979) have reviewed the various approaches to modelling the movement of ground water contaminants under a variety of geological conditions.

An analytical solution to the advection-dispersion equation (9.23) in three dimensions can be used to predict the movement of an instantaneous point source of contaminant (Figure 9.7). Viewed from above, the slug of tracer spreads out in all directions in the horizontal plane, the unchanged mass occupying an increasing volume of

the porous medium. The tracer develops an ellipse as it is transported through the system because the actual process of dispersion is anisotropic. Dispersion is stronger in the direction of flow than orthogonally to it. At low velocities molecular diffusion is the dominant dispersive mechanism, giving a circular tracer slug. This situation could be analagous to the movement of leachates in a hillslope soil, assuming an isolated source of exchangeable cations and a single infiltration pulse.

Due to the heterogeneous nature of soils and rocks flow is unlikely to be as simple as this. Thus solute movement may be concentrated along one or more layers of higher hydraulic conductivity. In fractured rocks and dry clay soils it may migrate in many directions along cracks, diffusing into the matrix as it proceeds. A subsequent influx of lower concentration water might cause diffusion back into the fissure system. Reactive constituents (generalised by the $f(c)_{x,z}$ term in equation (9.31)) show different transport patterns to those which are non-reactive. This is because movement of the concentration front is retarded by solute adsorption onto the porous medium, (Pickens and Lennox, 1976). The opposite effect, desorption, would accelerate the movement of the concentration front. The other reactions noted earlier will also influence solute release and movement.

9.5 SUMMARY AND CONCLUSIONS

The third section of this thesis represents a response to the need for improving the modelling of storm solute behaviour in small catchments. This chapter is an introduction to the concept of a physically-based, spatially distributed model of catchment hydrology and its potential as a general framework for progress towards an improved solute prediction model.

The progress achieved over the past 20 years in measuring and simulating surface and subsurface flow close to the channel has been briefly reviewed. Research has shown that 'saturation excess overland flow' is far more important than 'infiltration excess overland flow' in generating storm run off in humid temperate basins. Subsurface flow is an important mechanism in feeding a dynamic contributing area at the slope base between rainstorms. The first, relatively simple,

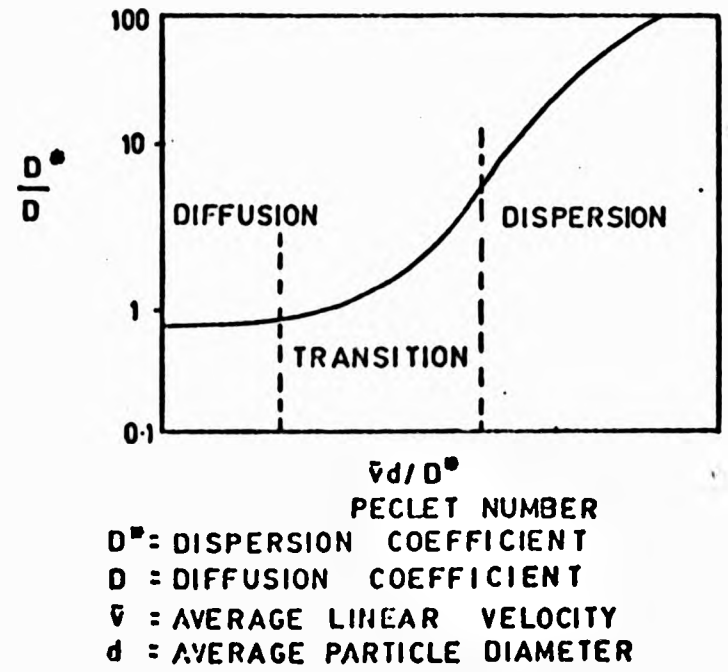

FIGURE 9.6: RELATIONSHIPS BETWEEN THE INFLUENCE OF DIFFUSION AND DISPERSION IN POROUS MEDIA

(after Perkins and Johnson, 1963)

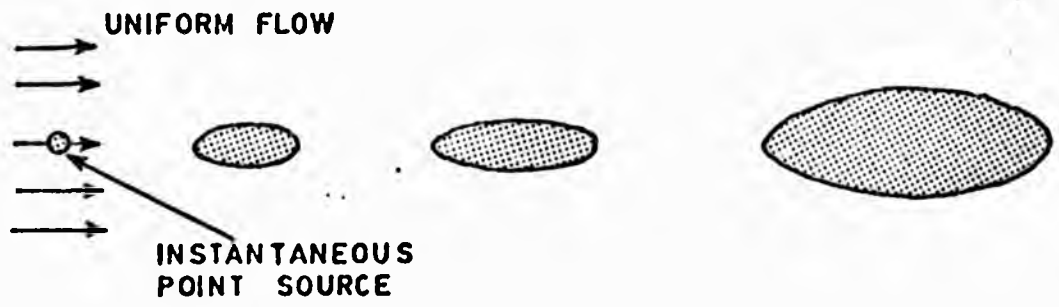

FIGURE 9.7: SPREADING OF A TRACER FROM AN INSTANTANEOUS POINT SOURCE IN A TWO-DIMENSIONAL, ISOTROPIC FLOW FIELD

(after Freeze and Cherry, 1979)

economically viable catchment hydrological model incorporating the dynamic contributing area concept has recently appeared (Beven and Kirkby, 1979). Before such a model can be adapted to the needs of solute prediction, the physical processes of solute transport from rainfall to streamflow must be studied.

Equations describing the movement of water and solutes in hillslope soils are set out. Examples from the field of ground water contamination are presented which suggest that these subsurface flow and convection-dispersion equations could be modified to model natural solute fluxes in soils. However, applied to soils the problem is far more challenging because of the greater complexity of chemical reactions, particularly under the influence of biotic factors. Recent work has focussed attention on weathering reactions in solute production at the catchment scale (e.g. Verstraten, 1977; Waylen, 1979). Here, emphasis is placed upon subsurface water and solute dynamics within one hillslope. A flux approach, based upon the flow equations presented, is described for use in moisture and solute accounting within soil elements of a hillslope segment. The design, installation and calibration of equipment for field data collection is described in the following chapter.

CHAPTER 10

AN EXPERIMENT TO MONITOR WATER AND CHEMICAL MOVEMENT IN A HILLSLOPE SOIL: DESIGN, INSTALLATION AND CALIBRATION OF EQUIPMENT

10.1 INTRODUCTION: THE EXPERIMENTAL SLOPE

In order to monitor in detail the processes of water and chemical movement within a hillslope soil an experiment was established within sub-catchment 1. A length of slope 2 metres wide at the base and 100 metres long from stream channel to divide was chosen for the study, (Figure 10.1). Because the slope is situated on the side of a spur, contour convexity above about 75 metres causes downslope divergence of water flow lines, and the slope width narrows. The actual contraction is small, however, and difficult to quantify from the available ground survey. From the channel, the slope is straight for the first 5.5 metres with a slope angle of only $2^{\circ}11'$; thereafter it steepens rapidly (max. angle = 12° 40'); the next 29.5 metres are concave with a minimum angle of only 2° 4', then becoming convex to the divide (max. angle = 8° 17').

Although the slope is underlain by London Clay, superficial deposits complicate the picture. The valley bottom has 40 - 50 cm of gravel, comprising angular flints and rounded pebbles, derived from the Plateau Gravel and Bagshot Sand respectively; London Clay is visible in the stream bed. The gravel deposit thickens upslope for about 14 metres reaching a maximum depth of about 80 cm, but then gradually thins, until it is almost non-existent at the divide. Occasional iron concretions and sand lenses confirm that the gravel deposit contains contributions from the Bagshot Sand in addition to the Plateau Gravel. The thickening of the gravel deposit corresponds with a pronounced convexity, followed by an upslope concavity. Preferential downslope orientation of stones was evident in a pit, dug 10 metres upslope, although no quantitative measurements were taken.

Unlike other experiments which have set out to monitor hillslope water flow (e.g. Weyman, 1973; Anderson and Burt, 1977a), the present slope has no completely impermeable bedrock and therefore no well defined boundary for vertical infiltration. The presence, however, of

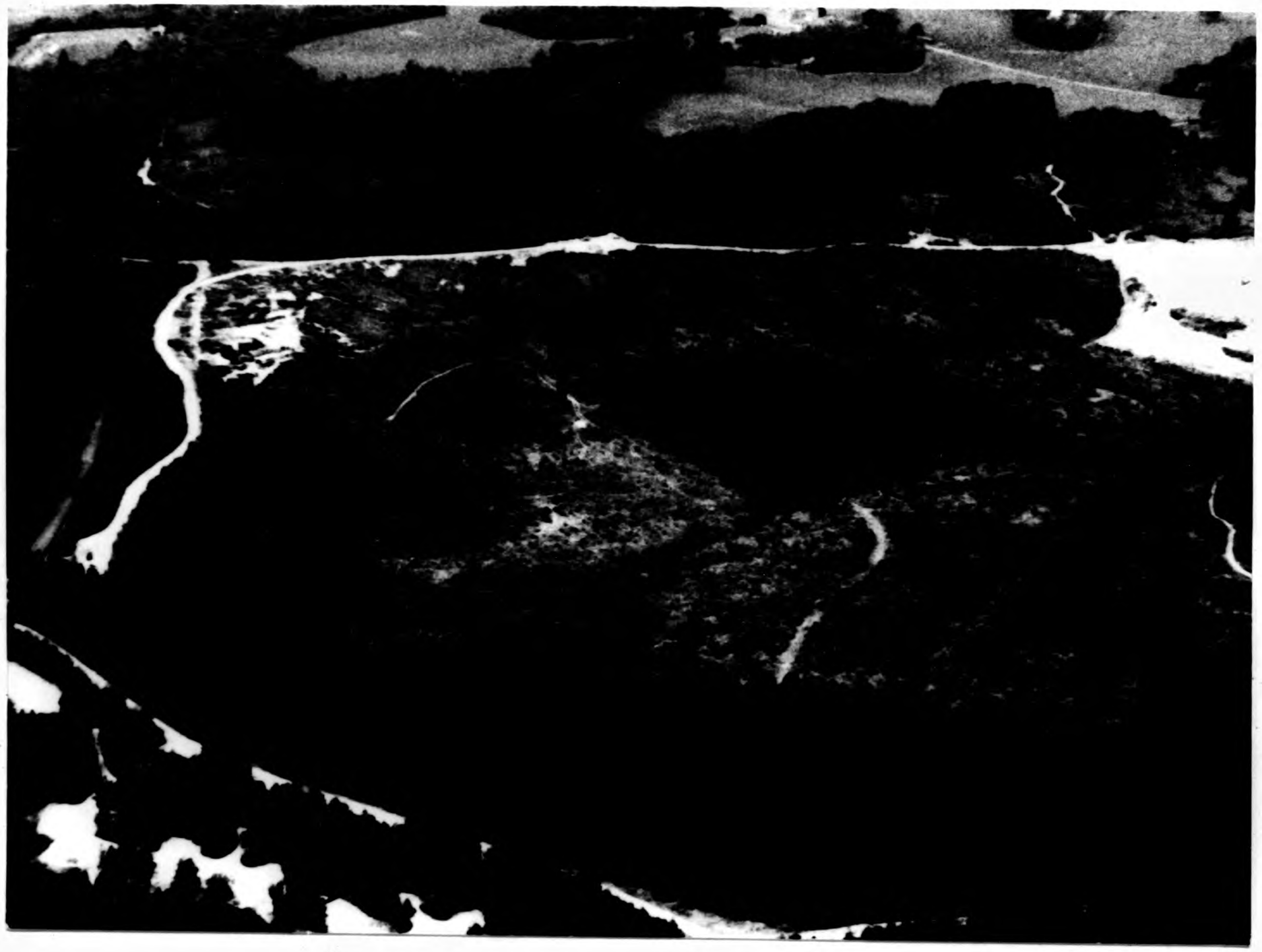

FIGURE 10.1: OBLIQUE AREAL VIEW OF THE EXPERIMENTAL SLOPE (dashed line)

FIGURE 10.1: OBLIQUE AREAL VIEW OF THE EXPERIMENTAL SLOPE (dashed line)

relatively impermeable London Clay at the profile base suggested that vertical losses might be minimal, at least during the winter when the clay was saturated or nearly saturated. During summer the clay could be expected to shrink on drying, allowing water loss via cracks and fissures.

The soil over most of the slope may be classified as the gravel phase of a clayey brown earth (Soil survey by members of Portsmouth Polytechnic Geography Department, Spring 1977). Figure 10.2 shows the soil profile in a pit, 10 metres upslope. Points to note are the thickness of the combined A and B horizons and depth to the C horizon. The B horizon is almost at its maximum thickness here, thinning very slightly downslope to 40 cm at the channel and gradually to zero at the divide. Particle size analysis of samples from the A and B/C horizons are given graphically in Figure 10.3. The A horizon contrasts strongly with the C horizon, the former containing 42.65 % gravel (i.e. > 2 mm fraction), the latter 36.7 % clay and 47.9 % silt. Soil adjacent to the channel may be classified as a ground water gley. A full chemical analysis of the slope soils is given in the following chapter.

The slope supports planted young Fagus sylvatica and Pinus sylvestris with occasional Quercus robur and Betula verrucosa and subordinate Pteridium aquilinum, Rubus species and various grasses. Figure 10.4 gives the areal distribution of these species on the slope. A detailed knowledge of vegetation distribution was thought to be necessary for possible explanations of water and solute movement during evapotranspiration.

Summarising, the chosen slope had four favourable attributes:

(i) A complete, 100 metres long, convex slope with a maximum angle of 12^{o} 40'.

(ii) A freely draining clayey brown earth soil situated upon the relatively impermeable London Clay.

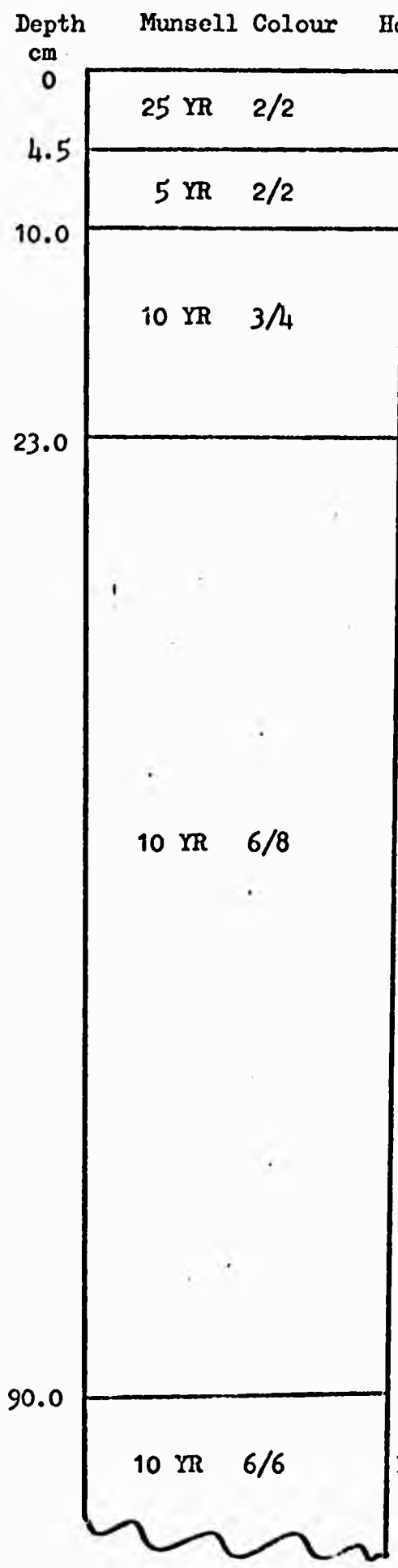

Horizon	pH	Organic Carbon %	Description
L	4.29	10.5	Litter; few roots; original structure maintained.
F	3.98	9.58	Partly decomposed litter; roots abundant; some of original plant structures visible.
A	4.14	2.07	Stony sand-loam; roots absent; 42.65 % > 2 mm.
B	4.33	1.43	Very stony sandy-loam; roots absent; stones large (6 - 20 cm long) and abundant (70 % total mass).
B/C	4.92	1.56	Silty-clay; roots absent; stones absent.

FIGURE 10.2 : Soil Profile located 10 metres upslope

(Nomenclature after Hodgson, 1974)

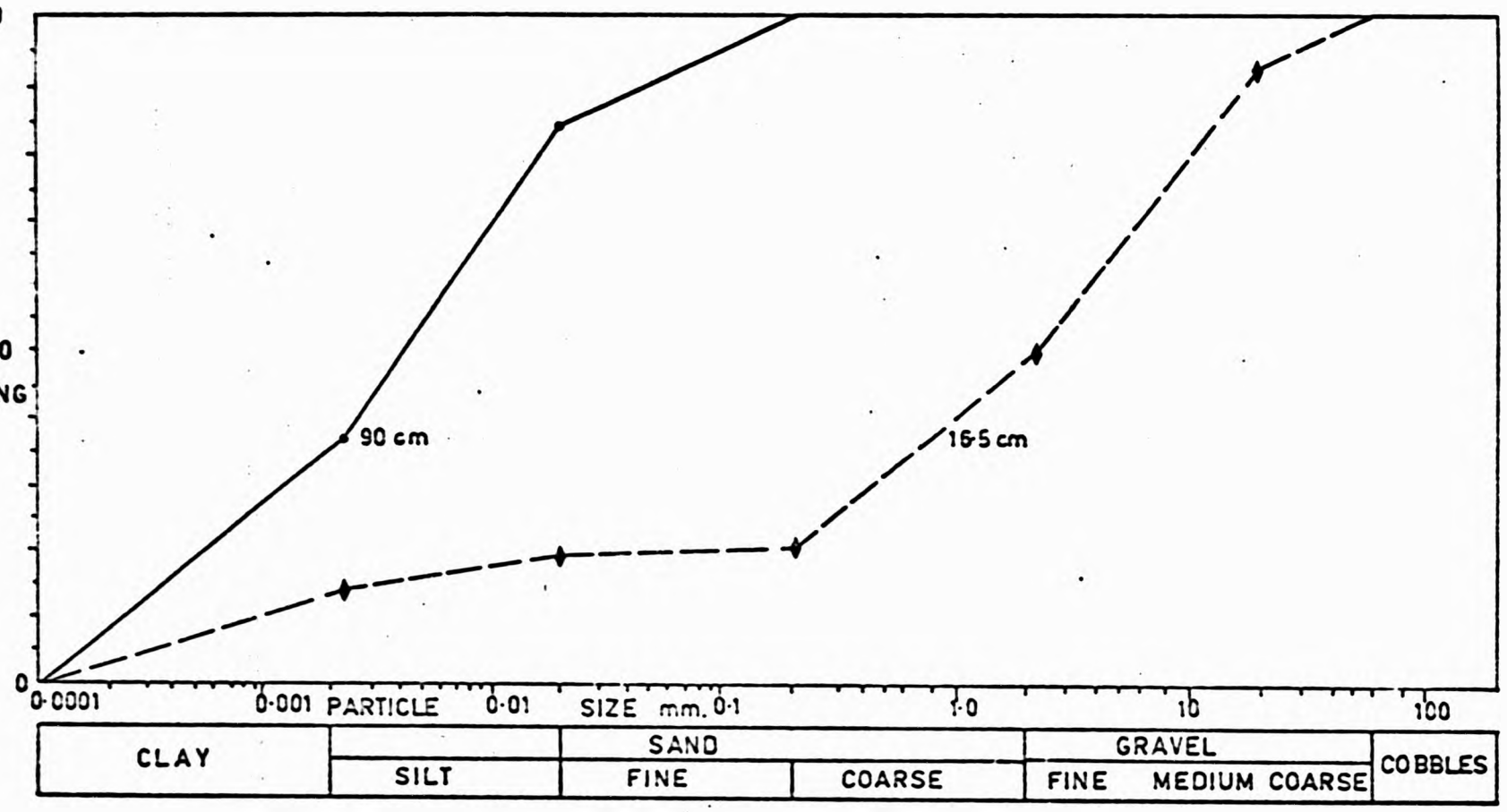

FIGURE 10.3: PARTICLE SIZE ANALYSIS FOR 16.5 CM AND 90.0 CM DEEP SAMPLES IN FIGURE 10.2

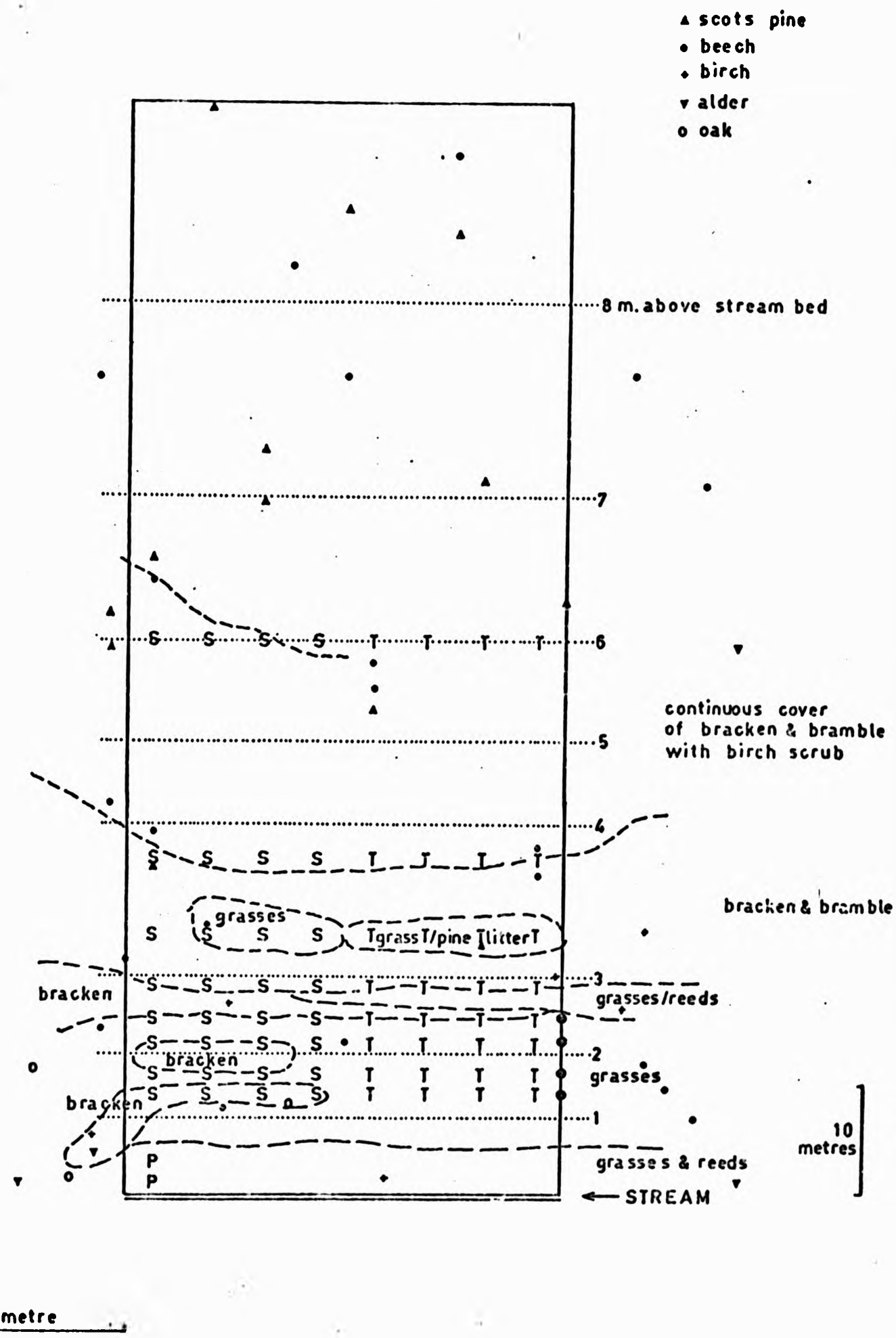

FIGURE 10.1: DETAILED DISTRIBUTION OF VEGETATION ON THE HILLSLOPE

(iii) Immature and open vegetation with a minimum of interception during autumn, winter and early spring, thus increasing hydrological response.

(iv) An established gauging station (W1) at the outlet to sub-catchment 1, 170 metres downstream from the slope base.

10.2 EXPERIMENTAL DESIGN

Four factors influenced the design of the slope experiment.

(i) Previous work (Weyman, 1973) suggested that a permanently saturated zone might exist adjacent to the channel and extend upslope and up-profile during storms. This view was reinforced by the observation of overland flow on the 2^{o} slope adjacent to channel during early 1976. This being the case, the area contributing to both hydrographs and chemographs would probably lie close to the channel and require a more intensive instrument network than further upslope.

(ii) Unsaturated flow was quite likely to dominate slope drainage (i.e. after storm hydrographs) particularly above and upslope of the saturated zone. This being the case tensiometers would be necessary to determine the pattern of soil water movement, and ceramic suction pots to sample the soil solution.

(iii) Streamflow and throughflow would be difficult to separate at the streambank because a well-defined impermeable horizon was absent, thus complicating boundary conditions and making collection and measurement of throughflow input to the stream very difficult.

(iv) Instruments should be as close together as possible for flux computations, striking a balance between accuracy and economy.

Taking these factors into consideration, instruments were located as is shown in Figure 10.5. Piezometers were situated 1.25 metres and 3.25 metres upslope from the channel centre with openings at depths of 40.8 and 50.4 centimetres respectively (i.e. level with the channel base). Shallow (10 cm) piezometers were also installed at each location.

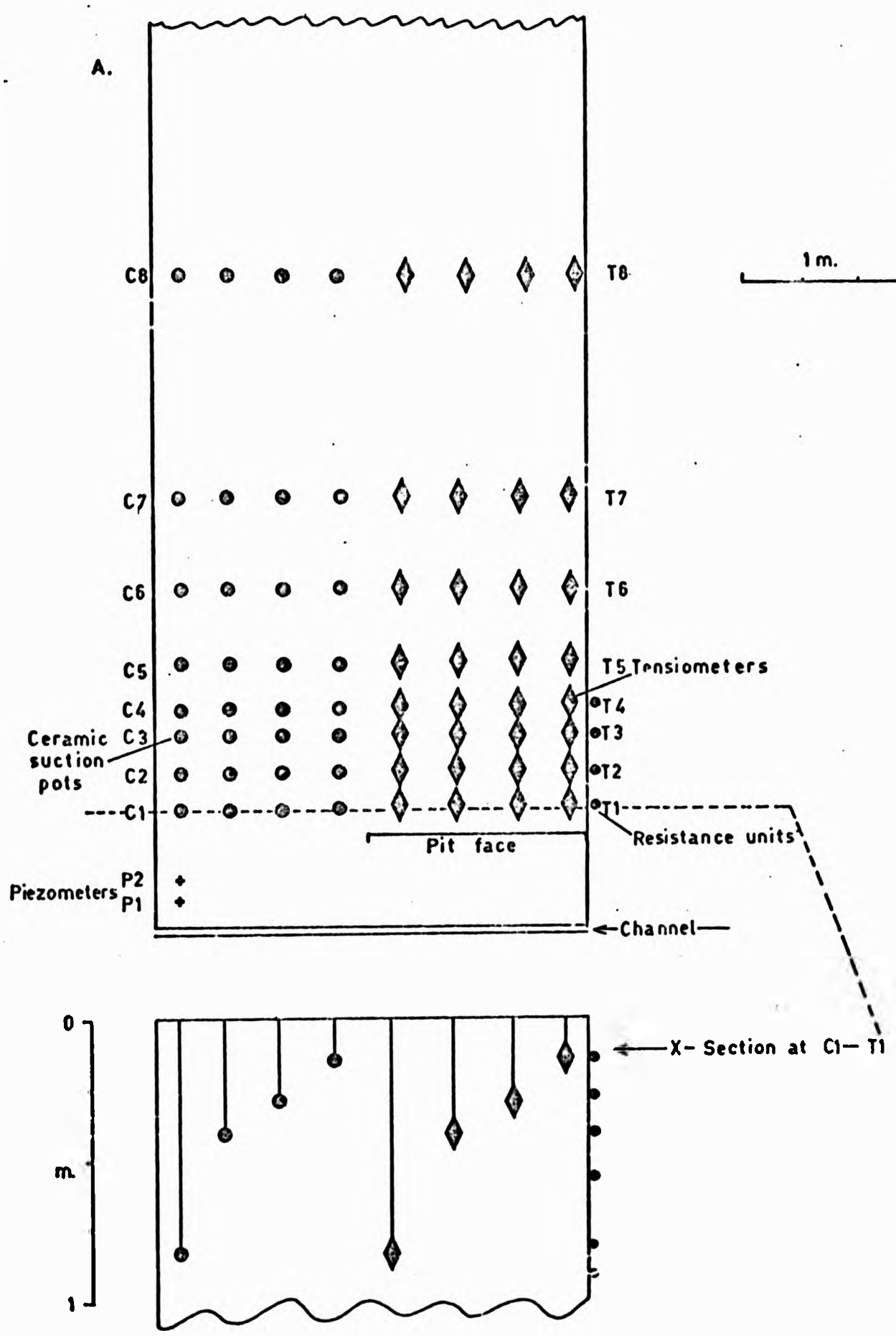

FIGURE 10.5: LOCATION OF INSTRUMENTS ON THE HILLSLOPE

Tensiometer location began 9.25 metres upslope, where the slope angle declined from 12° 40' to 6° 45'. From here it was decided to locate tensiometers with increasing incremental distances upslope in order to provide more intensive monitoring near the stream (see note (i) above). Eight tensiometer banks were located 9.25, 11.5, 13.9, 16.25, 19.3, 23.9, 31.0 and 50.5 metres upslope (Figure 10.5A). Ceramic suction cups were situated alongside the tensiometers at the same distances upslope. Figure 10.5B shows how the instruments were located through the soil profile. Tensiometers were at depths of 10 cm, 25 cm, 35 cm and 70 cm, depths being fixed since the instruments were borrowed from another experiment (see Webster, 1966). Ceramic suction cups were constructed to suit requirements and located at depths of 10 cm, 30 cm, 60 cm and 100 cm. With 25 cm between each instrument the data collected represented a slope two metres wide, across which it was assumed variations in water content, soil solution chemistry and soil characteristics were minimal when compared with downslope variation.

To support data from the tensiometers and for use in water and chemical flux computation, initially four sets of nylon stainless steel mesh electrical resistance units (later to be calibrated for moisture content) were situated 9.25, 11.5, 13.9 and 16.25 metres upslope (i.e. in parallel with the first four tensiometer banks); at each set units were located at depths of 10, 25, 35, 52, 70 and 90 cm. Thermistors were situated alongside the units at each depth to supply temperature correction data.

The problem of ceramic suction pot spacing and its effect upon the hydraulic gradient in the soil profile is analysed later in this chapter. As a result of this analysis the instruments were located as shown in Figure 10.5.

Direct measurement of throughflow input to the channel was required for calibration of a water and chemical flux model. However, this was not possible without large civil engineering works, due to the lack of an impermeable boundary between soil and bedrock. As an alternative a 1 metre wide pit was dug 7 metres upslope, that is, 2.25 metres below the first tensiometer bank. The pit base was 10 cm above the channel bed and lined with polythene to channel flow into a plastic

gutter. Discharge measurement was achieved using a volumetric cylinder and stopwatch. A 30 cm wide trench was dug from the pit to the channel to allow drainage.

The use of a pit in this way may have the disadvantage of distorting natural flow patterns and measured discharges (Knapp, 1973). Despite this drawback, some independent measurement of throughflow discharge was required, as noted earlier. A general view of the slope is given in Figure 10.6.

10.3 METHODS USED FOR IN SITU SOIL MOISTURE MEASUREMENT

There exists a considerable volume of literature on the various methods available for measuring soil moisture. Much of this information has been collated in literature surveys (e.g. Ballard, 1973; Curtis and Trudgill, 1974; Eastwell, 1953; Shaw, 1960). Therefore, no attempt will be made completely to cover the literature, only to assess the methods relevant to the likely experimental conditions. As with most scientific experiments cost plays an important role. While a balance should be obtained between economic and technical considerations, it is regrettable that, in the final choice, the former may outweigh the latter.

In the current experiment it was desirable to obtain data describing both energy conditions and volumetric water content within the soil body. In theory, field measurements can be made of one of these and the other obtained by laboratory calibration. In practice, however, this approach is not always viable, since the working range of an instrument may not completely cover field conditions. For example, the tensiometer used in measuring energy conditions has a working range of 0 - 750 cm water suction pressure, while that of an electrical resistance block is approximately 200 - 15,000 cm water (Curtis and Trudgill, 1974). By using both instruments, the range of measurement is considerably widened, while also giving independent assessment in the region of overlap. With these points in mind it was decided to employ instrumentation to measure independently volumetric moisture content and suction pressure within the soil on the experimental slope. At a later stage core samples were to be taken for the laboratory calibration of tension against moisture content.

FIGURE 10.6: GENERAL VIEW OF THE HILLSLOPE FROM THE STREAM: PIT WITH THROUGHFLOW COLLECTION GUTTER (foreground); TENSIOMETERS WITH INSULTATION PROTECTORS BEING REMOVED (background)

FIGURE 10.6: GENERAL VIEW OF THE HILLSLOPE FROM THE STREAM: PIT WITH THROUGHFLOW COLLECTION GUTTER (foreground); TENSIOMETERS WITH INSULTATION PROTECTORS BEING REMOVED (background)

In this section the instruments and techniques used for measuring soil water pressure, content and piezometric head are described.

A. Tensiometers

The soil water tension, or suction pressure, has been described as "the negative gauge pressure, relative to the external gas pressure on the soil water, to which a solution identical in composition with the soil solution must be subjected in order to be in equilibrium through a porous permeable wall with water in the soil" (I.S.S.S., 1963). The form of instrument commonly used to measure this negative soil water pressure in the field is generally called a 'tensiometer'. The most commonly used tensiometer employs a porous pot buried in the soil at the depth for which information concerning soil water is desired. This is connected to a mercury manometer (or other pressure sensing device) as shown in Figure 10.7. Thereafter, soil water, being usually at sub-atmospheric pressure, normally exercises a suction and water is drawn out of the pot until any elastic capacity in the system is taken up and the pot water is brought into hydraulic equilibrium with the soil water. As soil water is subsequently depleted by evapotranspiration or drainage, or replenished by rainfall, so the tensiometer will react accordingly, the mercury column rising for depletion and falling for replenishment.

Tension may then be calculated by:

$$\Psi = h_1 \cdot \rho_m - h_2 \text{ cm Hg} \qquad (10.1)$$

where ρ_m = density of mercury = 13.6 $gm^{-1}cm^3$
See Figure 10.7 for definition of h_1, h_2.

The selection of a suitable porous pot depends upon the range of tensions to be investigated; for tensions of up to about 150 or 200 cm of water, filter paper or sintered glass discs may be used; for tensions up to about 750 cm of water, porcelain is more suitable, although it reduces the sensitivity of the instrument.

A considerable number of tensiometer designs are reported in the literature. Most had to be discarded on the grounds of cost. The

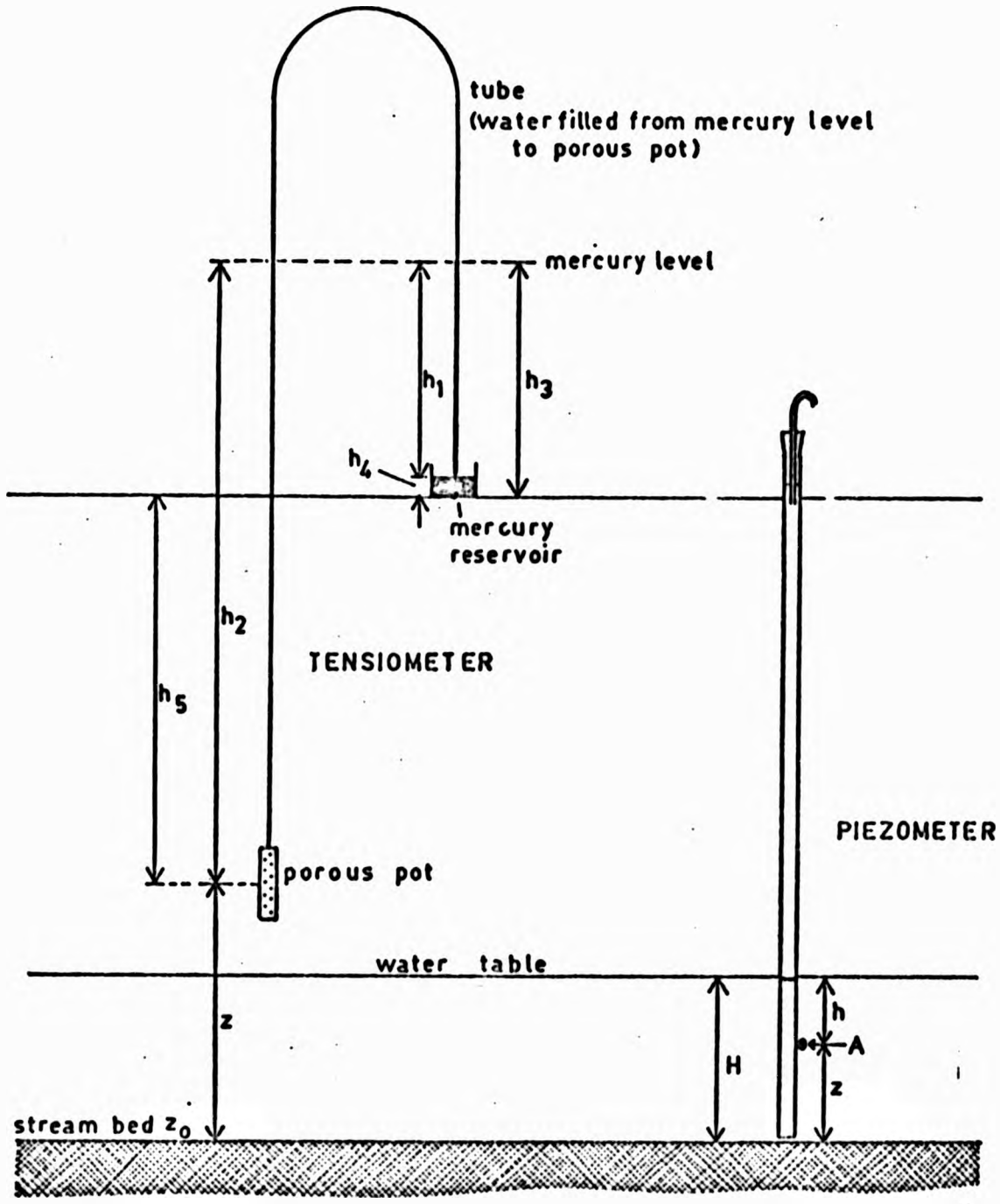

FIGURE 10.7: MEASUREMENTS REQUIRED TO CALCULATE SOIL WATER TENSION AND HYDRAULIC POTENTIAL

mercury manometer tensiometer described by Webster (1966) was considered suitable for the slope experiment, both on technical and economic grounds. This comprises a porous ceramic pot, 5.7 cm long x 0.95 cm external diameter, with a mean pore diameter of two microns, cemented to rigid nylon tube, 9.3 mm e.d. and 7.9 mm i.d., cut to length for insertion to the desired soil depth. A 'T' piece is cemented to the other end of the tube. Both joints are covered with a neoprene or polyolefin sleeve. Capillary tubing, 1.25 mm e.d. and 0.86 mm i.d., leads through a neoprene bung fitted to the side-arm of the 'T' piece, to the manometer. Tubes lead from four tensiometer cells to the manometer column, a 5 cm x 2.5 cm x 150 cm wooden stake with a recess for the mercury vessel and a groove for the tubes. A scale, graduated 0 - 80 cm, is fixed to the side and the front is covered by a strip of perspex.

The original tensiometer cells used by Webster were very kindly made available for the slope experiment (Figure 10.8). This had the disadvantage that cells were already made up and the lengths therefore predetermined. This left only the manometer assembly to be constructed, together with some repairs to the pot and 'T' piece joints. The stakes were located in 40 cm deep auger holes on the upstream edge of the slope, leaving the mercury reservoir about 10 cm above ground level. Using a 3.8 cm diameter helical auger, four holes, 25 cm apart, were drilled across the slope to depths of 10, 25, 35 and 70 cm. Problems were encountered augering the holes in 1976 due to the very hard, dry soil, and it was only possible to instal four sets before September. The soil was carefully stored on plastic sheeting in the order removed. A little soil from the bottom of the hole was crumbled, replaced and the tensiometer cell pushed gently into place. The soil removed was then replaced in reverse order and carefully tamped into place to ensure that water could not run down between tensiometer cell and soil. The top 5 cm of the hole was sealed with London Clay to preclude rapid infiltration around the cell. When the tensiometers were later removed, several were completely exposed in pits and found to be in very close contact with the soil along their total lengths.

The method of setting up the tensiometer bank is detailed by Webster (1966). Briefly, this involves filling each cell with air-free (i.e. cool, freshly boiled) distilled (a.f.d.) water and then, using a

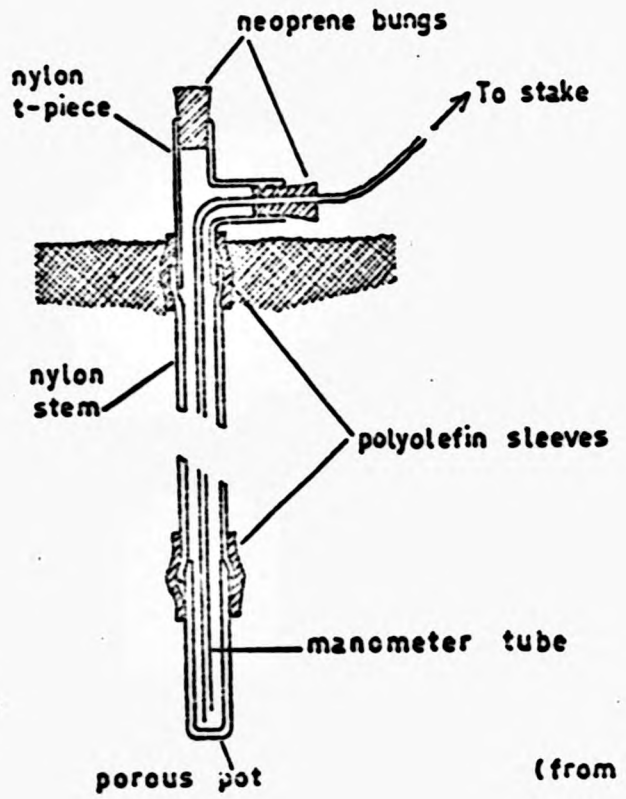

(from Webster,1955)

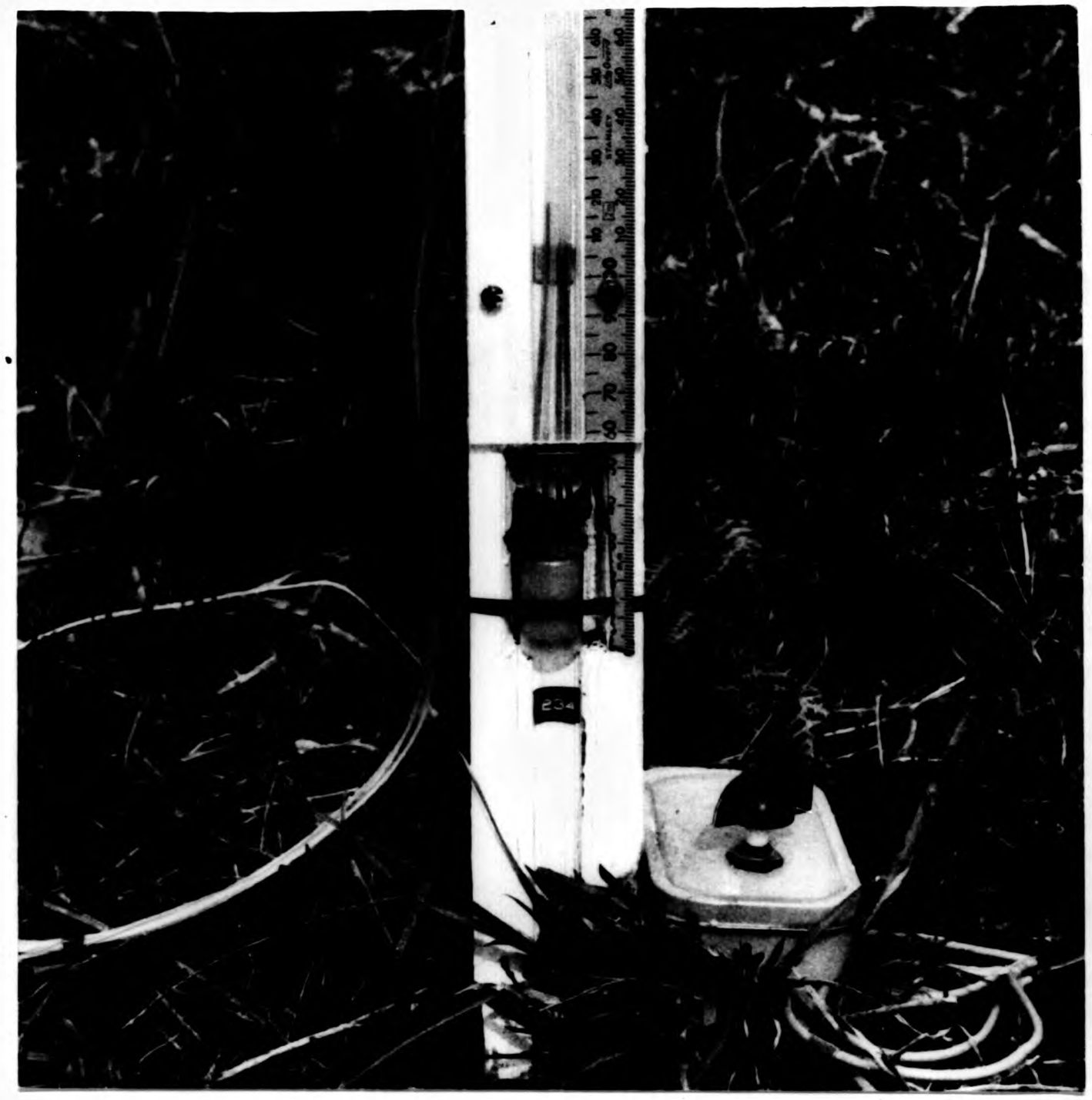

FIGURE 10.8: 'WEBSTER' MERCURY-MANOMETRIC TENSIOMETER USED IN THE STUDY (left) AND SURFACE MEASUREMENT OF TENSION (right)
(Attached to the base of the stake is a rotary switch for the nylon/stainless steel resistance units and thermistors)

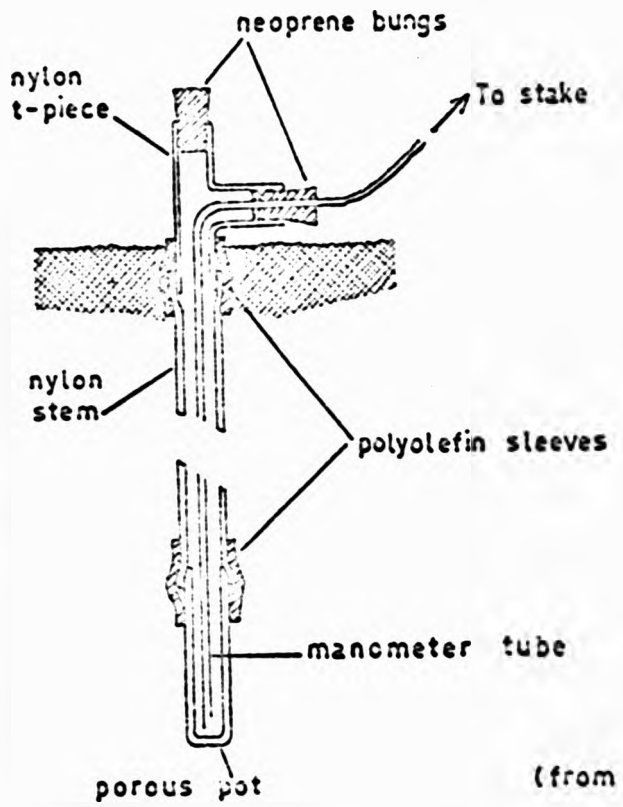

(from Webster,1955)

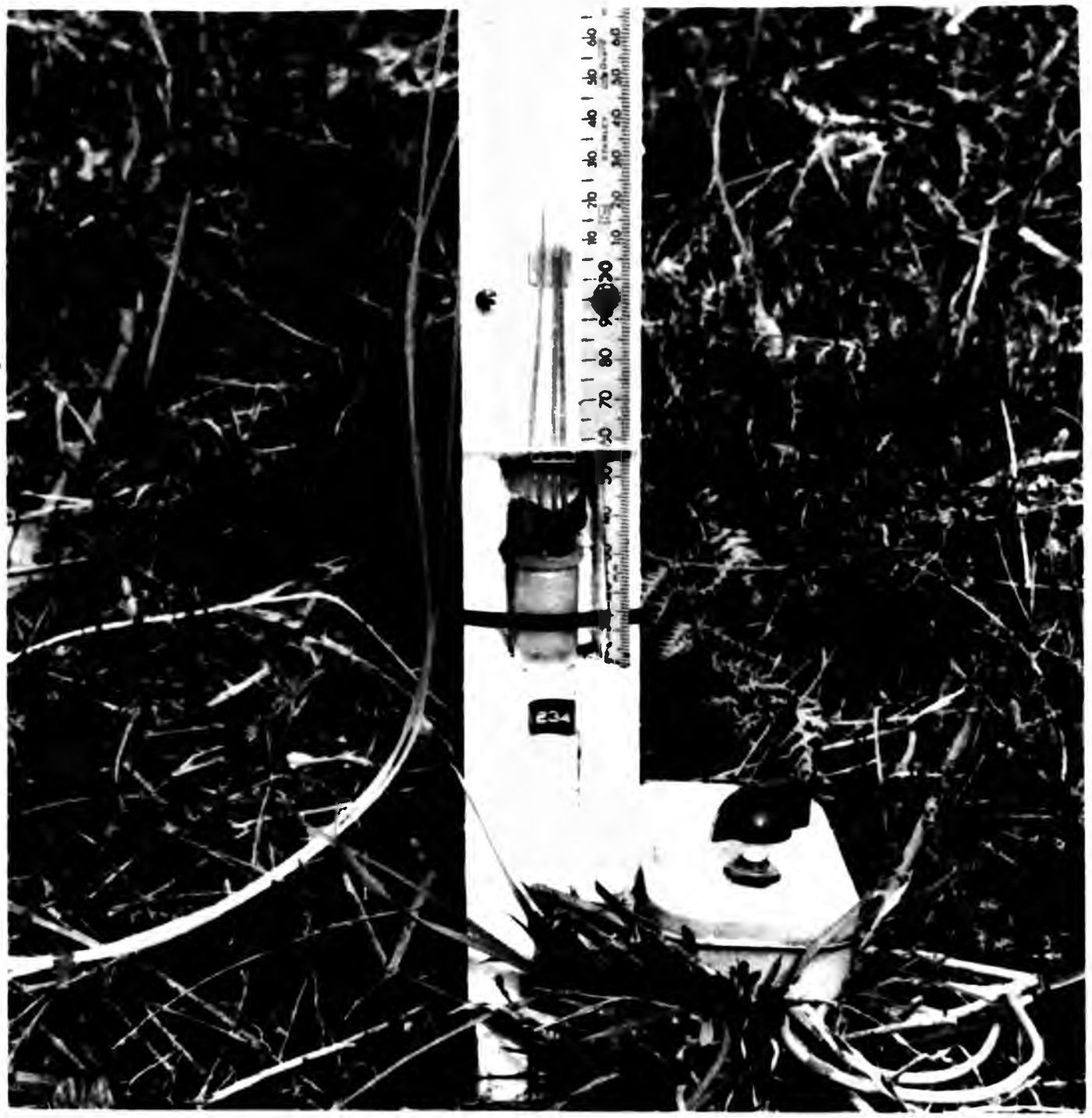

FIGURE 10.8: 'WEBSTER' MERCURY-MANOMETRIC TENSIOMETER USED IN THE STUDY (left) AND SURFACE MEASUREMENT OF TENSION (right)
(Attached to the base of the stake is a rotary switch for the nylon/stainless steel resistance units and thermistors)

syringe applied to the open top of the cell, forcing a.f.d. water through the manometer tubing until all the air is expelled. Several problems occurred during the experiment.

(i) Frost damaged the manometer and cell tubing. The remedy was to cover the manometer with a sheath made from old fire hose; this was in turn lagged with fibreglass roof insulation and then covered with polythene tubing, sealed at one end. The exposed tops of the cells and manometer tubing were protected by a polythene covered pad of fibreglass, held in position with 20 cm wide wire staples.

(ii) Severing of the manometer tubing by rodents. This problem was also remedied by the action taken under (i).

(iii) Collection of air in the top of the cell and air liberation in the manometer tubing. These problems were easily remedied by removing the top bung and flushing with a.f.d. water.

The 'Webster' tensiometer has four advantages over other models (Curtis and Trudgill, 1974).

(i) Maintenance is relatively easy. Leaks are easy to spot and repair in the field.

(ii) The narrow cup is easier to instal in stony soils; a point especially important in the slope experiment.

(iii) The tension data can be obtained without trampling the slope, because the stake is offset.

(iv) Small positive pressures can be measured in addition to tension.

From Equation (10.1), since

$$\psi = 13.6\, h_1 - h_2$$

where $h_1 = h_3 - h_4$

and $h_2 = h_3 + h_5$

then $$\psi = 13.6\ (h_3 - h_4) - (h_3 + h_5) \qquad (10.2)$$

(see Figure 10.7)

Because the manometer is filled with water, not air, then any difference in mercury level is equivalent to 12.6/13.6 of mercury tension in centimetres, and Equation (10.2) becomes:

$$\psi = 12.6\ h_3 - 13.6\ h_4 - h_5 \qquad (10.3)$$

where h_5 = a constant for each individual tensiometer cell.

This left five readings to be made at each tensiometer bank; h_4 and four values of h_3. For each point in time, readings were made by systematically working upslope and assuming that tension altered insignificantly during the ten minutes it took to complete the readings. This assumption seems reasonable considering that a porous pot's small pore size gives the system a relatively slow response to real changes in the soil. A computer program was developed to evaluate Equation (10.3) for each tensiometer (TENPLOT, Appendix 2). An example of the type of data output is shown in Figure 10.9. The signs of Equation (10.3) have been reversed in the program to give tension a negative prefix and pressure a positive prefix in the printout.

B. <u>The Measurement of Volumetric Water Content</u>

It was decided to instal profiles of electrical resistance units in parallel with the tensiometer banks. This would give the following advantages.

(i) The range of tension measured would be increased.

(ii) The 'Webster' tensiometer ceases to function efficiently in frosty conditions.

```
INPUT TIME,DAY,MONTH,YEAR
  INPUT A1,B1,C1,D1,E
  INPUT D2,C2,B2,A2,F
  INPUT B3,A3,C3,D3,Q
  INPUT C4,D4,A4,B4,R
  INPUT A5,B5,C5,D5,S
  INPUT D6,C6,B6,A6,T
  INPUT D7,C7,A7,B7,U
  INPUT D8,A8,B8,C8,V
  TIME DAY MONTH YEAR
  12.00 23    4    77
  WEST WALK SLOPE:PORE WATER PRESSURE(CM.WATER)

  VERTICAL SCALE:1INCH=2METRES(X50)
  HORIZONTAL SCALE:1INCH=5METRES(X20)
  SOIL DEPTH:1INCH=0.2METRES(X500)
```

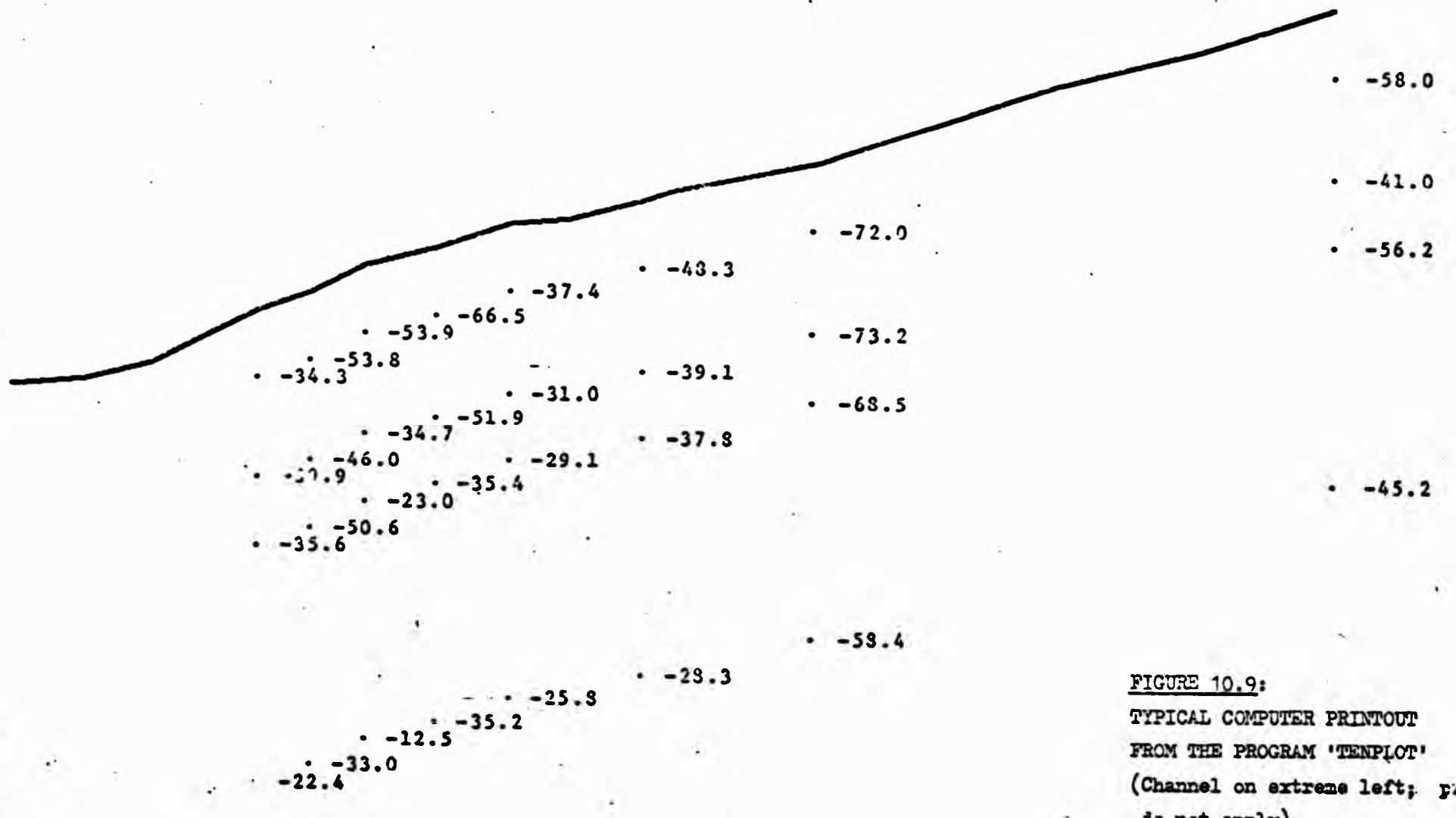

FIGURE 10.9:
TYPICAL COMPUTER PRINTOUT
FROM THE PROGRAM 'TENPLOT'
(Channel on extreme left; printed scales
do not apply)

(iii) Although the tensiometers were to be calibrated for moisture content in the laboratory, an independent field check seemed desirable due to probable hysteresis effects.

As with methods for the measurement of tension, the literature on moisture content determination is vast. Since a temporal series for one point in the soil was required, gravimetric and immersion methods were automatically ruled out. Equipment was not available for moisture determination by the neutron-scattering technique (Bell, 1973), leaving a range of electrical resistance units to be considered.

In principle, when an alternating current (this is used to avoid the electrolysis which occurs with D.C.) is passed from one electrode to another, through a material body, the resistance to transmission of the current through the body is inversely proportional to water content of the body. The method developed by Bouyoucos and Mick (1940, et seq) used two electrodes mounted in a plaster of paris block, and claimed an accuracy of $\pm$ 1 % of the total soil moisture, provided that the blocks were calibrated for the soil in which they were used and corrections applied for the temperature of the soil. Correction for temperature is important because it shows an inverse relationship with electrical resistance. If possible, ionic strength of the soil water should also be considered, since an increase accompanying drying will cause a drop in resistance.

Bouyoucos later produced a nylon resistance unit in which woven nylon separates wire mesh electrodes (Bouyoucos, 1949). He claimed the unit had the following advantages:

(i) It was sensitive from saturation almost to air dryness.

(ii) It was very durable and would last for a minimum of five years in very wet conditions.

(iii) It was easy to calibrate.

(iv) It was less sensitive to changes of solute content in the soil than materials such as fibreglass where there was a definite chemical reaction or ion exchange.

(v) 'The outer metal case of the unit acts as a shield and almost entirely eliminates electrical lines of force' (Bouyoucos, ibid). The confinement of the electrical field is certainly a very desirable feature.

Eastwell (1953) criticises the nylon unit on two grounds:

(i) It lacks the buffer action present when using plaster of paris blocks; the buffering is due to the presence of calcium sulphate solution dissolved from the block.

(ii) Imperfect contact between the absorbent and the electrode around which it is wrapped.

The range of moisture the nylon unit records is clearly an advantage as discussed earlier. The acid nature of the slope soils (pH 4.02 - 5.09) might severely reduce the life of a plaster of paris unit. Curtis and Trudgill (1974) state that gypsum blocks inserted in into the B horizon of an acid brown earth, pH 6.0 - 6.5, have shown complete solution after 12 - 18 months. While calibration is not difficult it is time-consuming since, for reliability, each block must be calibrated separately in the laboratory, with its own soil type. Lack of buffering is clearly a disadvantage of the nylon unit; even calibration of the unit in its own soil cannot guarantee to overcome the solute effect, since a change in solute concentration may reflect water and solute flux rather than a simple drying or wetting. Imperfect contact between nylon and electrode is a problem which can be overcome by greater compression of the outer casing.

It was considered that advantages of the nylon unit outweighed disadvantages and a decision made to manufacture a set for use on the slope. The electrodes were cut from a sheet of 1.5 mm mesh stainless steel gauze; the internal electrode was 18 mm x 44 mm and the external electrode 54 mm x 44 mm. Terylene webbing, available in a strip 60 cm wide, was cut into 40 mm pieces for use as the absorbent. Cable ends were woven into each electrode and then tinned to give rigidity. The terylene was folded around the inner electrode and the outer electrode bent around the terylene; the assembly was then tightly compressed in

a vice. The ends of the unit were impregnated with polyester resin to preclude any possibility of electrical short-circuiting. Two were made in this way and calibrated in the laboratory. This was carried out by embedding each unit in a loam soil contained in a 15 cm x 15 cm x 10 cm deep stainless steel mesh basket, saturating, and then taking resistance and weight readings during the drying cycle. Three cycles were completed for each unit and the results plotted as % moisture content against log resistance (corrected for temperature) for each unit. No problems occurred while using the units and replication over the three cycles appeared satisfactory. A further set of 22 was made for installation at the first four tensiometer sites on the slope. If operation was successful a further 24 would be made to complete the sampling scheme. Twenty-four thermistor probes were also constructed for installation alongside the resistance units. These were made from graphite resistors (TH1A supplied by R S Components Limited) and set in 6 cm long x 1.8 cm diameter columns of polyester resin after soldering to wire connectors. Although the resin shell reduced sensitivity, it was essential to give good electrical insulation. Thermistors were then pre-calibrated against resistance in the laboratory using a constant temperature bath for the temperature range 8° to 30°C and using a refrigerator for the range -10° to 4°C. With this temperature data unit resistance may be corrected to 20°C using the equation:

$$R_c = R_o^{1 + \alpha (T_o - T_c)} \qquad (10.4)$$

where R_o is the observed unit resistance
R_c is the corrected unit resistance
T_o is the observed unit temperature
T_c is the corrected unit temperature

α is taken as 0.00366 (Beckett and Webster, 1965).

Installation of these instruments was carried out in single profiles on the upstream edge of the slope. Using a 10 cm bucket auger a hole was drilled to a depth of 90 cm and the soil profile carefully laid out on polythene sheeting, the positions at 10, 25, 35, 52 and 70 cm being marked. This would ensure that the correct soil type surrounded the unit when it was replaced. Considerable problems

occurred in augering due to the presence of flints in the soil. Soil samples were taken from each of the depths at which units were to be installed, stored in polythene bags and labelled, later to be chemically analysed. The six depths for units represent those at which tensiometers were present, plus one intermediate between 35 and 70 cm, and the lowest at 90 cm where clay begins to dominate the particle size distribution. Units were placed on one side of the auger hole, broad edge down, with the thermistor parallel, 2 cm away. Cables were then led across the hole and up the opposite side, to the surface, the ends being clearly labelled with Dymo tape. A little soil from the correct horizon was then placed on top of the instruments and tamped down to provide intimate contact. Care was taken in compressing the soil to obtain approximately the same bulk density as occurred naturally.

Having completed the installation (Figure 10.10) and replaced the surface vegetation, cables were led to a junction box at the base of the tensiometer stake. To avoid continual connection and disconnection during measurements of resistance, a 'midget' 12-way wafer switch (supplied by R S Components Limited) was employed. Resistance measurements were made with a Doran Conductivity Bridge E3924 (range 0 - 10,000,000 ohms) loaned by the Military Engineering Experimental Establishment, Christchurch, Hampshire. This simply entailed connecting the bridge to the rotary switch and rotating the control for each unit and resistor in turn (12 per switch). Trials with the first 24 units during April, May and June 1976 were fraught with problems. The first of these was an inability to obtain needle balance on the conductivity bridge for six of the units, suggesting electrical shorting somewhere in the circuits. As there was a possibility of condensation inside the rotary switch covers, readings were taken without the switches. Recurrence of the problem suggested short-circuiting around the actual unit, although it was not clear why this did not show in the laboratory tests.

Inconsistent readings did little to inspire confidence in instrument reliability. This could have been due to soil shrinkage as drying proceeded, leading to very poor hydraulic continuity between soil and unit. Therefore, under certain conditions of rainfall infiltration it can be envisaged that the moisture content of the terylene fabric would not truly represent that of the surrounding soil.

A. 'Midget' 12-way rotary wafer switch

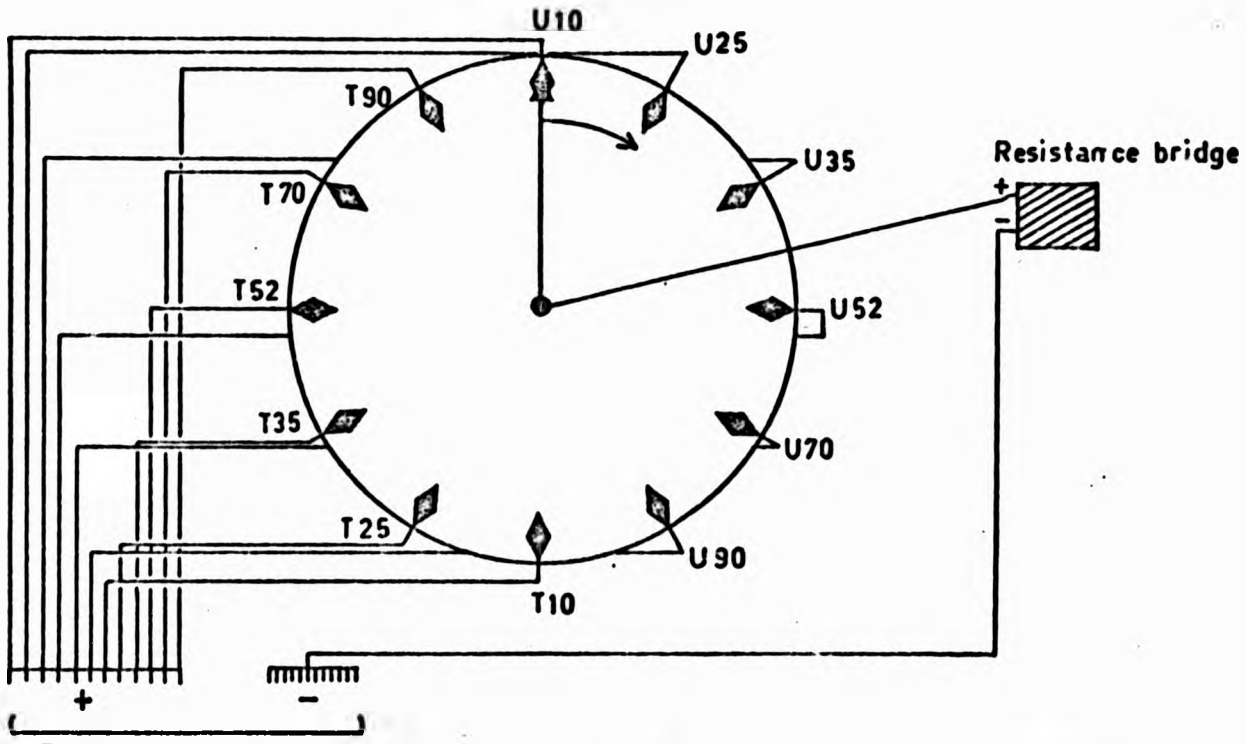

T= thermistor
U= electrical resistance unit } with depths cm.

B. Thermistor &. electrical resistance unit.

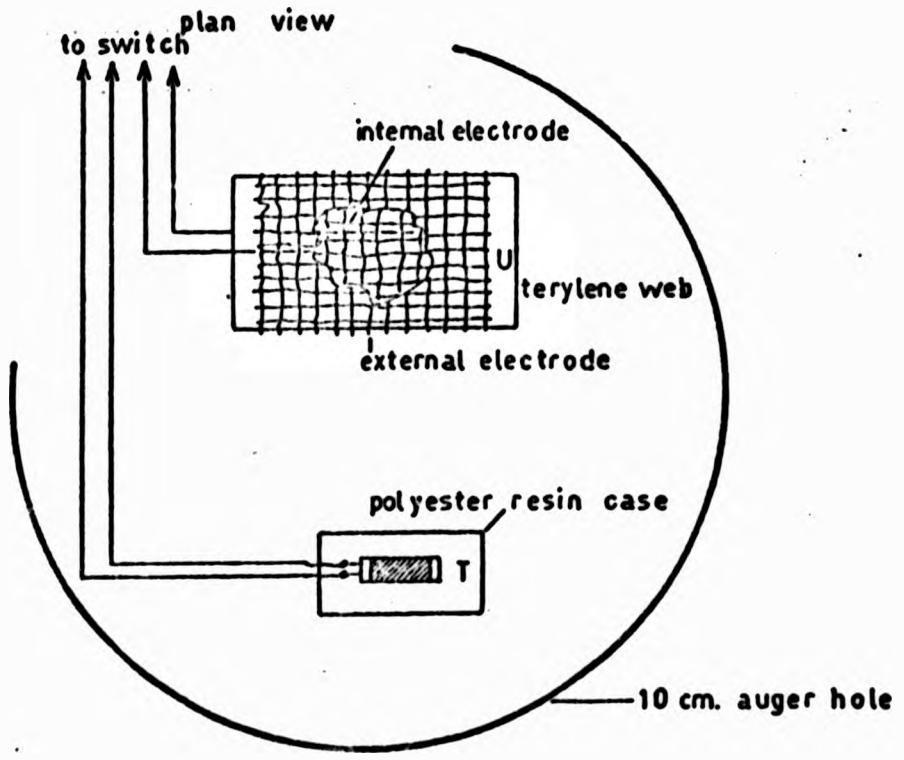

FIGURE 10.10: INSTALLATION DETAILS FOR THE ELECTRICAL RESISTANCE UNITS AND THERMISTORS

One profile of units was carefully excavated in early July 1976 when tension was above the operational range of the tensiometers. Gaps of 1 - 2 mm were found above three of the units (those at 10 cm, 25 cm and 35 cm), tending to confirm the suspicion of soil shrinkage. This was clearly a grave disadvantage with the units, especially since they were intended to increase the range of measurement.

Due to the unreliability of the terylene resistance units it was regrettably decided not to include them in the data collection but to rely entirely upon the tensiometers and their calibration for moisture content.

C. Piezometers

It has already been stated that a saturated zone was expected to occur adjacent to the channel and that piezometers were best suited for monitoring purposes.

Using a piezometer tube it is possible to obtain the hydraulic head defined by I.S.S.S. as 'the elevation with respect to a specified reference level at which water stands in a piezometer connected to the point in question in the soil' (I.S.S.S., 1973). In Figure 10.7, $H = z + h$, for the point labelled A, with pressure greater than atmospheric, where h is referred to as the piezometric head. By comparing H for point A with H for another point some distance away, it is possible to calculate a flow vector between the two points.

Piezometers were constructed using PVC tubing 17 mm i.d. and 22 mm e.d. Holes were drilled at one end and nylon curtain mesh bound around the tube at this point; (5 holes, diameter 6.4 mm, were drilled in one direction, with a spacing of 3 cm, and a further 5 were drilled at 90° to the first set). The bottom of the tube was sealed with epoxy resin and a cover made for the top, composed of a rubber bung with turned-over glass tube as air vent. To instal the piezometers, holes were dug in the gravel adjacent to the channel (augering was impossible), the piezometer inserted to the correct depth and the gravel replaced and firmly tamped. For head measurement a simple well dipper was constructed by taping two insulated cables to a graduated rod, exposed ends level with the rod end, and attaching the

loose cable ends to the Doran conductivity bridge. When the rod touched the water surface, the circuit was completed, deflecting the balance needle on the bridge.

10.4 THE METHODS OF SAMPLING SLOPE THROUGHFLOW FOR CHEMICAL ANALYSIS

Sampling throughflow for chemical analysis has largely been achieved by collecting water flowing into pits dug in the soil (e.g. Oxley, 1974). Knapp (1973) has shown that the use of flow data collected from pits can be inaccurate due to flow net distortion. Little is known about the effect of this flow net distortion upon solute concentrations. However, in situations where mass flow is dominant over diffusion, then unnatural concentrations might be recorded from pit samples. With this in mind consideration was given to the use of ceramic cups for the extraction of soil water, a technique previously used by soil scientists in leaching studies.

Samples were also taken from piezometers and pit throughflow.

A. The Use of Ceramic Suction Cups for Extracting Soil Water

(i) The Background

As long ago as 1904, L J Briggs and A G McCall suggested that ceramic cups be used as artificial roots to study soil water availability to plants as well as its composition. A ceramic cup was embedded in the soil, with a tube of sufficient length to extend to the soil surface, fastened to the cup with an air-tight seal. A vacuum applied to the top of the tube would draw in soil water, which was then removed from the cup through a small diameter tube extending to the bottom of the cup. In principle, little change has since been made to this basic design.

D W Cole (1958) described a 'tension lysimeter' which intercepted percolating water using an alundum filter disc. The leachate collected in a one gallon carboy situated in a trench below the filter disc and was weekly pumped to a surface receptacle. As much as 6.96 litres was collected using this method, and analysed for concentrations of NH_4, NO_3, K, Ca and Mg.

G H Wagner (1962) considerably refined Cole's technique. He used a porous ceramic cup assembly as shown in Figure 10.11A. The cup was inserted to the depth from which soil water was required and a suction inserted using a portable vacuum pump. For sample removal a capillary tube was pushed to the bottom of the cup and a vacuum exerted via an Erlenmeyer flask. Wagner found that only about half an hour was necessary for the ceramic cup to take in an 'adequate' sample of water using a suction of 1 atmosphere. When the soil water tension became greater than 1 atmosphere, sample removal became impossible.

R C Reeve and E J Doering (1965) improved Wagner's instrument by permanently installing a sample evacuation tube in the main sampling assembly. A vacuum was exerted via the sample receptacle, using a portable vacuum tank. Release of the air inlet clip allowed the sample to be drawn via the evacuation tubing to the sample bottles. They found that the time necessary for an adequate sample (25 ml) to be taken increased with the soil water tension. Accordingly, they varied the sampling time from ½ to 48 hours. A further important point made by Reeve and Doering is that much of the water sampled is that which is held at a relatively low suction in large pores.

R R Parizek and B E Lane (1970) modified the equipment to that shown in Figure 10.11B with vacuum extraction and sample outlet being given separate tubes. By applying pressure to the sampling tube water was forced into the sample bottle. This is not necessary for small sampling times where a suction is maintained since vacuum release automatically allows a re-distribution of pressure, and the sample bottle fills.

W W Wood (1973) used the same system for collecting water samples from as deep as 33 metres, but incorporated a check valve inside the ceramic cup, which opened at a pressure differential of 14.2 kg cm^{-2}. This had the advantage that it did not become gas-locked, nor could the sample be forced back through the cup into the formation from which it was derived (Figure 10.11C).

A R Harris and E A Hansen (1975) have recently described a miniature model that is particularly well suited to intensive sampling within small areas. It consisted of a small 6 mm by 65 mm porous

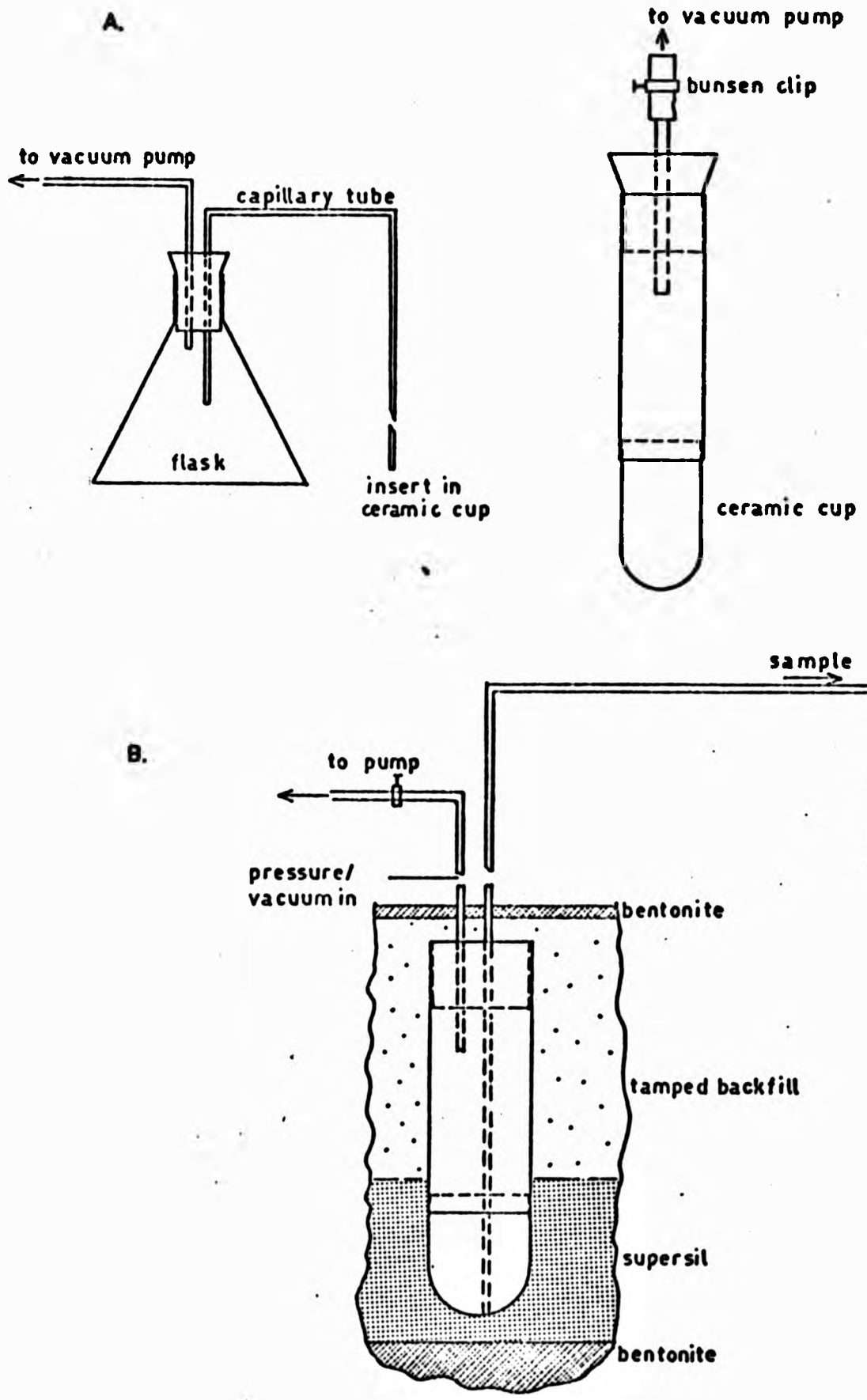

FIGURE 10.11: POROUS CERAMIC CUP ASSEMBLIES FOR SAMPLING SOIL WATER

A: After Wagner (1962)

B: After Parizek and Lane (1970)

C.

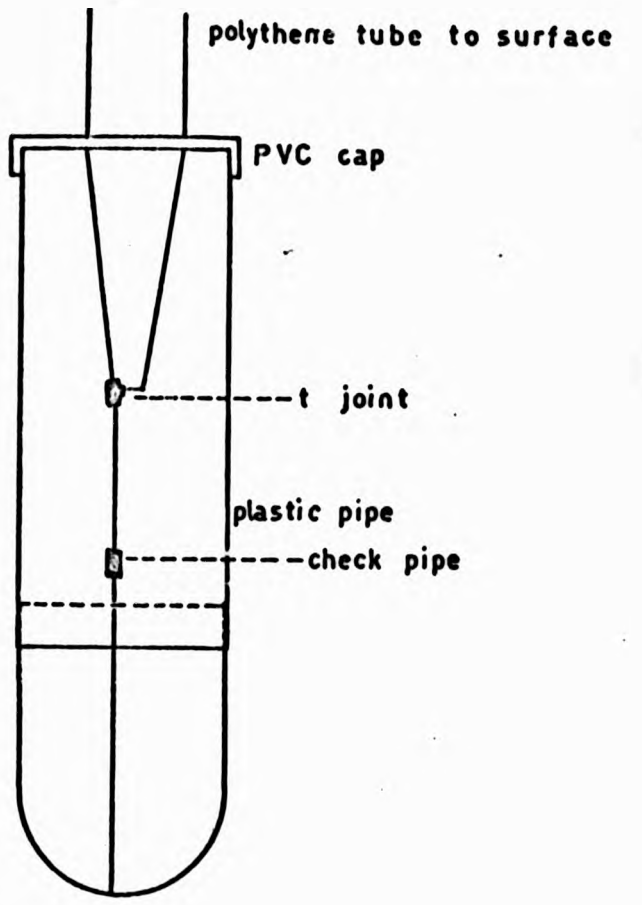

D.

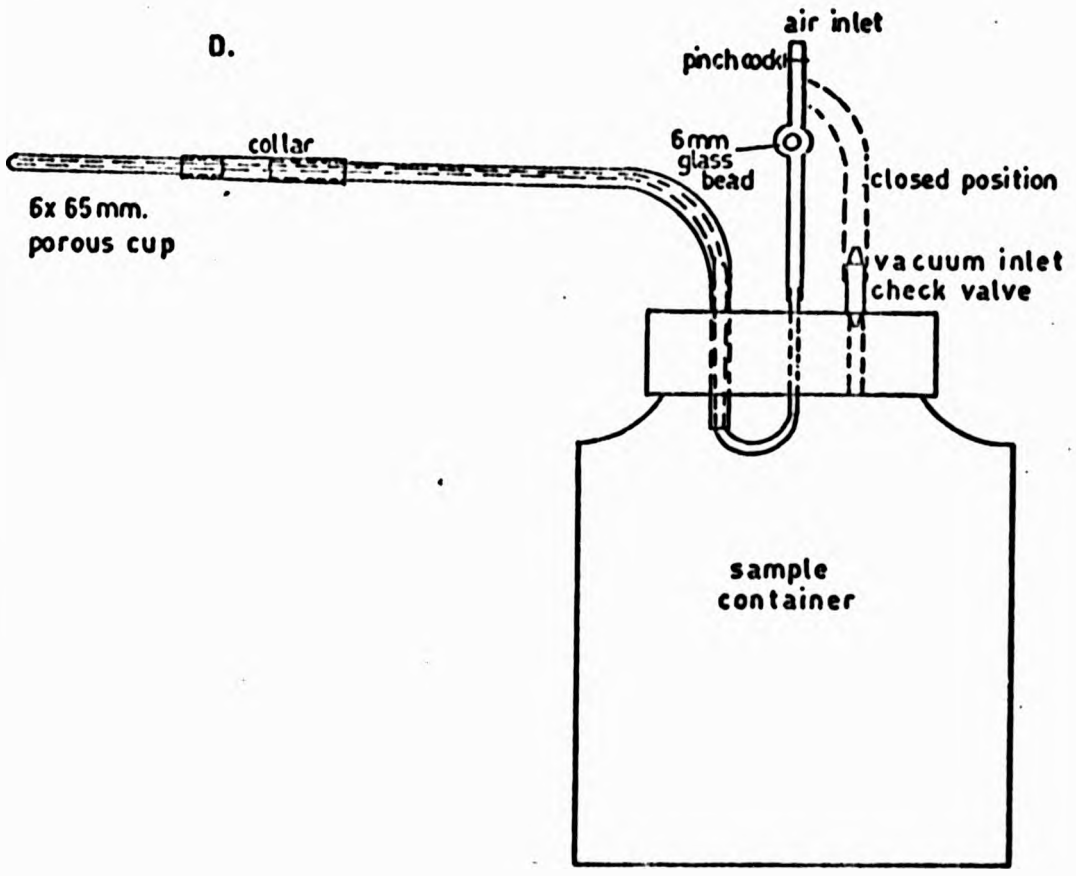

FIGURE 10.11 (cont'd): C: After Wood (1973)
D: After Harris and Hansen (1975)

ceramic cup attached to polyethylene tubing, containing a small internal evacuation tube, and a glass sample bottle with a rubber cap that held a glass bead pinchcock and a check valve. The system collected a 40 ml sample using a vacuum of 508 mm Hg. The use of a removable sample bottle eliminated the need to transfer the sample and reduced the possibility of contamination (Figure 10.11D).

(ii) Functional Considerations

Until recently little was known about how representative extracted samples were of the soil solution. Factors affecting the sample concentration may be either physical (i.e. sampler intake rate, plugging of cup pores, sampler depth, type of vacuum system and alteration of the natural tension gradient) or chemical (i.e. sorption, leaching, diffusion and screening of ions by the cup walls). Hansen and Harris (1975) have analysed the significance of these factors, and made six relevant recommendations.

Firstly, samplers should be selected with similar intake rates. Intake rate was found to vary considerably for the same sampler type, with the fastest rate more than six times that of the slowest. The intake rate is important for longer sampling times because the chemical concentration of soil water is continually changing. A multiple regression analysis of sample concentration against plugging, sampler depth and type of vacuum system (constant or falling) showed plugging and sampler depth to be important. Plugging affects the time distribution of sample intake, and corrections may be made by rating over the experimental period. A falling vacuum system causes an initially fast intake rate, which drops through time.

Secondly, a short sampling period is advised. This reduces sample concentration variability due to plugging and a falling vacuum system.

Thirdly, use a uniform sampler length.

Fourthly, use the same initial vacuum for each sample.

Fifthly, do not composite samples as this may obscure biases related to sampling technique and further distort results.

Sixthly, check the sampler bias for soils, ions and concentrations to be sampled.

New cup nutrient contents have been reported by both Hansen and Harris (1975) and Grover and Lamborn (1970). The latter suggest leaching with 1N HCL and rinsing with de-ionised water before use. This reduced Na and K leaching, although Ca contamination continued. Harris and Hansen reported considerable sorption of P by ceramic cups little of which was removed by subsequent leaching. Very little bias (3 %) could be accredited to sorption using small cups (6 x 65 mm) when sampling a solution containing 5.2 mg/litre P. Similar tests were not run for Ca, K, Na or Mg.

R R van der Ploeg and F Beese (1977) have simulated by computer the flow of moisture towards a suction unit, using the unsaturated moisture flow equation. This is compared with vertical flow under the same conditions, but without a suction unit in the soil. Results showed that the radius of influence of a suction unit, extracting water continuously over a period of 20 days, can be several metres. The flow system thus studied is then no longer representative of the actual processes occurring in the undisturbed soil, and chemical concentrations are not those which would have occurred at that point in the soil without sampling.

(iii) Instrument Construction

Careful consideration was given to the design of a set of samplers for the slope. Material specifications are shown in Table 10.1 and the finished sampler in Figure 10.12.

Only a small sample was required since analysis was to be carried out using atomic absorption spectrophotometry. Furthermore, alteration of the natural tension gradient should be minimised and sample concentration more representative. The design is thus a compromise between those of Harris and Hansen (1975) and Parizek and Lane (1970).

The end of the porous cup was coated with 'Araldite' epoxy resin and pushed into the PVC tube (softened first by heating). Construction of the other parts was straightforward although a long 'needle' was

TABLE 10.1

Ceramic Cup Samplers - Material Details

Item	Description	Supplier
Cups	No. 2132. 70 mm x 19 mm tapered porous cup. wall thickness 2.4 mm	Soil Moisture Equipment Corp. P O Box 30025 Santa Barbara, Calif. 93105, USA
Shafts	21 mm o.d. 17 mm i.d. rigid PVC tube	Local
Rubber bungs for above	No. 5	Jcncons Ltd, Hemel Hempstead, Herts, Engl.
Copper tube	8 mm o.d. 6 mm i.d.	Local
Polythene tube	1.52 mm o.d. 0.86 mm i.d.	Jencons Ltd
Rubber tube	Neoprene 8 mm o.d. 3 mm i.d.	Jencons Ltd
Bunsen clips	30 mm wide x 20 mm max. opening	Jencons Ltd
Glass Specimen tubes	25 mm o.d. x 50 mm deep + plastic caps (20 ml capacity)	Jencons Ltd
Rubber bungs for above	No. 23	Jencons Ltd
Suction pump	Hand operated, plastic 'trigger' type, max. suction 63.5 mm Hg	Jencons Ltd
Suction gauge	760 mm Hg max.	On loan
Pressure tube	19 mm o.d. 8 mm i.d.	Jencons Ltd
Tube connectors	4 cm long, 10 mm o.d. straight end, 10 mm to 6 mm tapered end	Jencons Ltd

FIGURE 10.12 A: POROUS CERAMIC CUP ASSEMBLY USED IN THIS STUDY
(50p gives scale)

FIGURE 10.12 A: POROUS CERAMIC CUP ASSEMBLY USED IN THIS STUDY
(50p gives scale)

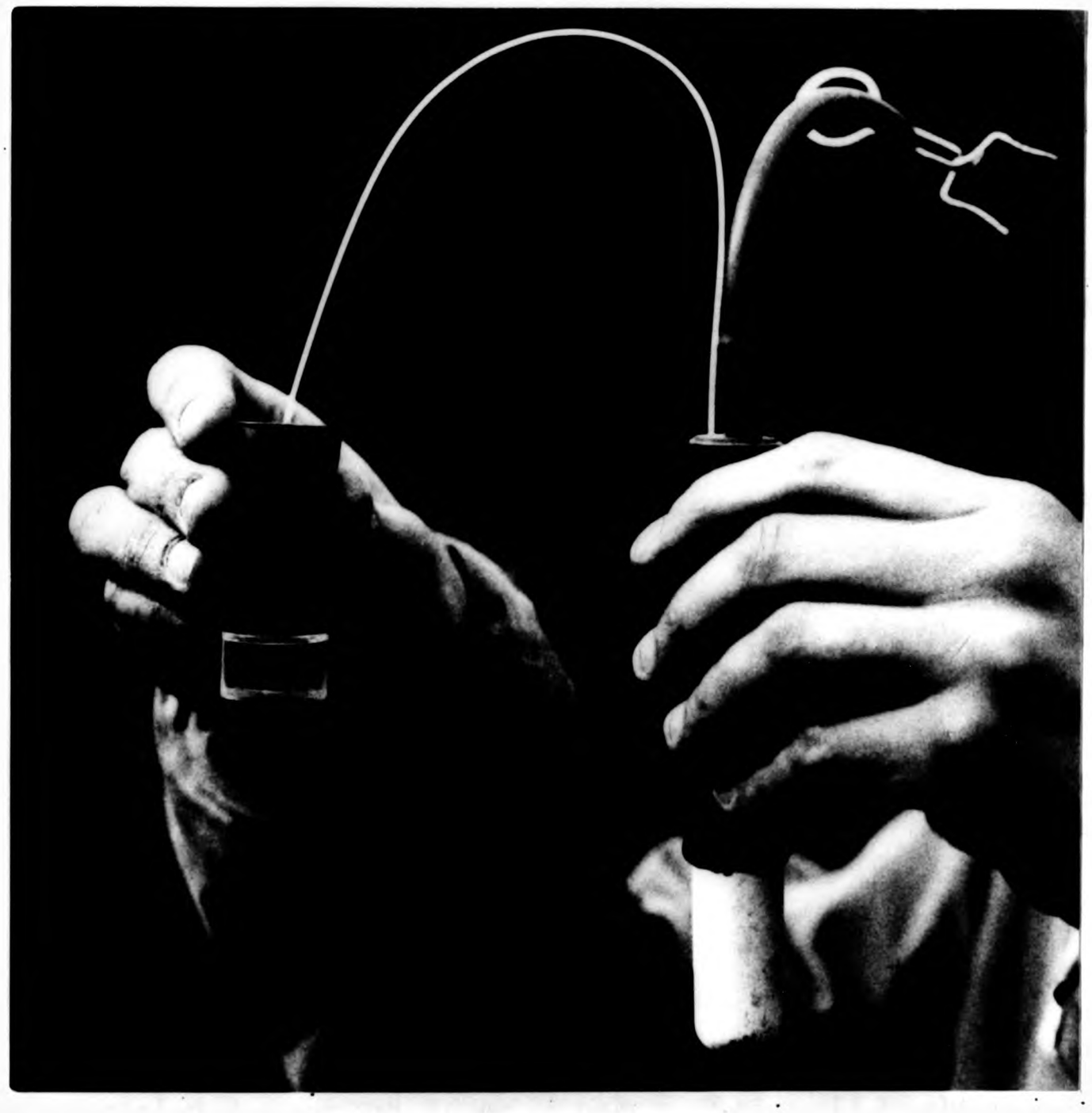

FIGURE 10.12 B: DETAILED VIEW OF THE POROUS CERAMIC CUP ASSEMBLY: SAMPLE RECEPTACLE (left); POROUS CUP (middle, bottom); VACUUM EXTRACTION TUBE (middle, top)

FIGURE 10.12 B: DETAILED VIEW OF THE POROUS CERAMIC CUP ASSEMBLY: SAMPLE RECEPTACLE (left); POROUS CUP (middle, bottom); VACUUM EXTRACTION TUBE (middle, top)

required to thread the flexible capillary tube to the bottom of the cup. The use of capillary tube has the advantage that samples of only a few ml can be withdrawn.

(iv) Pre-installation Tests and Treatments

As suggested by Grover and Lamborn (1970) each assembly was leached with 1N HCl followed by de-ionised water. This was achieved by standing in a beaker of the solution and exerting a suction of 64 cm Hg for 30 minutes. The treatment was carried out twice for HCl and twice for de-ionised water. No analysis of the leachates were made at this stage.

To check the sample representativeness solutions containing 5, 10, 20 mg/l of Ca^{++} and Mg^{++} and 5, 10, 20 mg/l of K^{+} and Na^{+} were separately sampled by 10 randomly chosen samplers, with intermediate flushing by de-ionised water, again using the same suction and sample time as before. Ionic concentrations were determined by atomic absorption spectrophotometry. No difference was found between the standard and sample concentrations for Na^{+}. Small changes were detected for K^{+} and Mg^{++} although these were both positive and negative, and were all less than 1 % of the standard concentration. Calcium showed mean increases of 5.1 %, 3.5 % and 2.26 % over the 5, 10 and 20 mg/l standards respectively. These results are consistent with those reported by Grover and Lamborn (1970) who suggest that small quantities of Ca^{++} may be contributed from the upper part of the cup covered by plastic, due to diffusion.

The same experiment enabled the determination of sample intake rates. Using a 30 minutes sampling time the vacuum was almost constant, falling by only 2 cm Hg. Intake rates ranged from 7 to 13 ml/hr. This suggested that a maximum volume of only 6.28 ml could be obtained in 30 minutes, limiting the number of cations which could be analysed by A.A.S. It was not desirable to increase the sampling time since this might mask changes in concentration due to throughflow.

Although the work of van der Ploeg and Beese studied soil tension changes around a cup over a period 960 times greater than was envisaged for the slope experiment, a similar analysis seemed desirable because of tensiometer proximity.

An experiment was set up under glass to simulate conditions around one set of suction cups and tensiometers installed as shown in Figure 10.13. This arrangement maximised the distance between suction cups and tensiometer cups and hopefully reduced the effect of water extraction on tension. Knowledge of the changes in tension around each suction cup and their effects upon the concentration of samples was also desirable. Two drainage cycles were monitored, the second with a series of water extractions. The pattern of natural drainage after application of 10 cm of rainfall as recorded by tensiometers 1 to 4 is given in Figure 10.14. The second drainage cycle, with soil suctions of 640 mm Hg exerted for 30 minutes before each reading on each suction cup, showed no significant differences from the first across the whole range of tension. This suggested that the tensiometers were outside the sphere of influence of the samplers and would accurately represent natural conditions.

To find out if the equipotential pattern around one suction cup changed significantly during extraction as shown by Figure 5 of van der Ploeg and Beese a third drainage cycle was monitored. This time a 4 hour suction was exacted only on cup 2 and readings taken from tensiometers 5 to 7 inclusive.

No preferential flow towards the suction cup could be detected from the equipotentials and the head distribution appeared very similar to drainage of cycle 1.

It was concluded that a constant sampling time of 30 minutes and suction of 640 mm Hg would not cause any major bias in the slope experiment.

B. Installation of Ceramic Suction Cups

Holes, each 4 cm diameter, were augered to depths of 10, 30, 60 and 100 cm. The soil removed was stored on polythene sheet and used in reverse order for packing around the inserted tube. The earth was carefully tamped to within about 4 cm of the surface to prevent water running down the side of the tube to the cup. The top 4 cm were filled with liquid polyester resin, which, when hard, formed an impermeable barrier to infiltrating water. No other heterogenous material was used for installation to reduce the possibility of sample contamination.

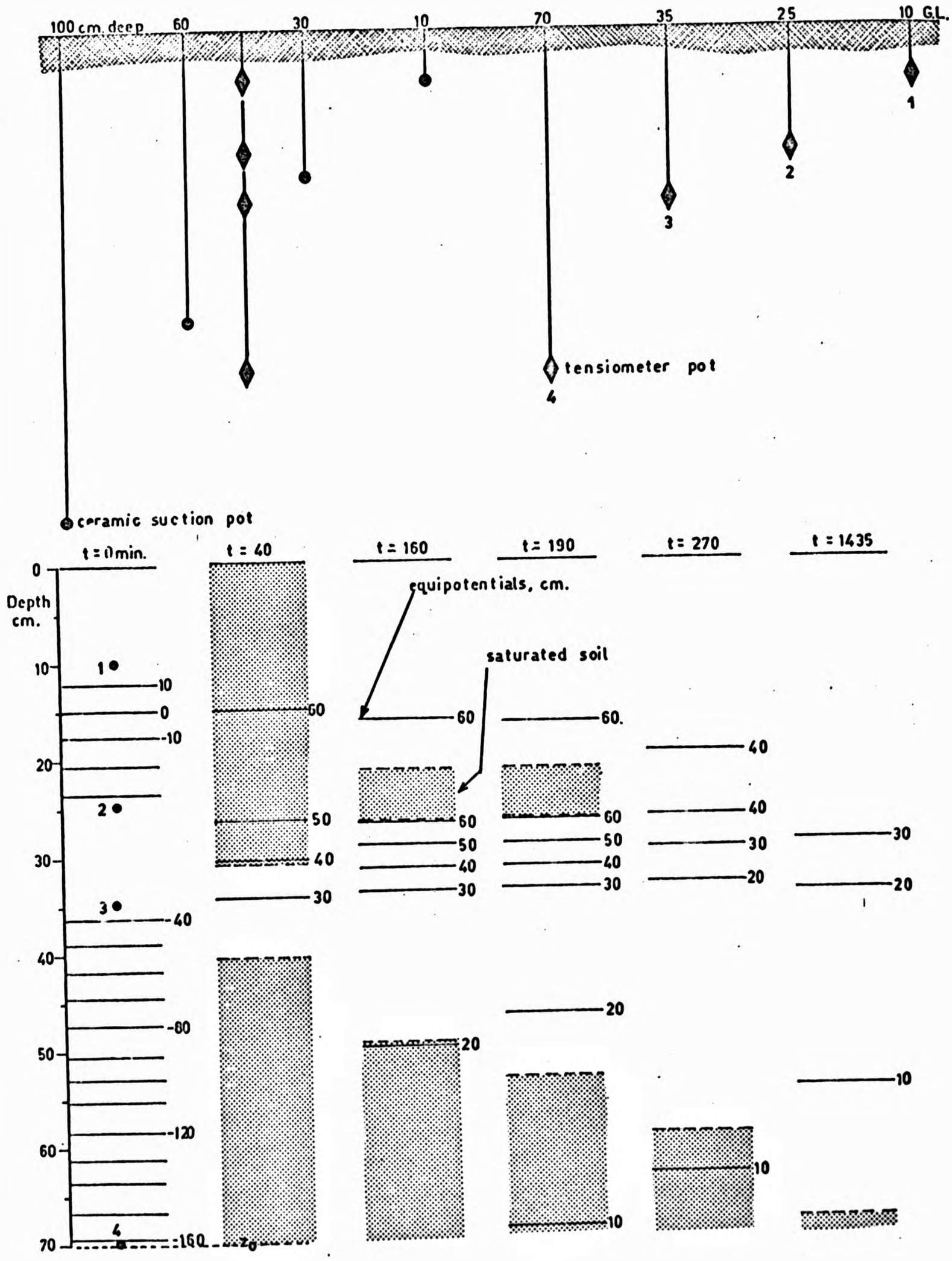

FIGURE 10.13: (top) LAYOUT OF AN EXPERIMENT TO DETERMINE THE EFFECT OF CERAMIC SAMPLING CUPS ON SOIL TENSION

FIGURE 10.14: (bottom) THE RESULTS OF TWO IDENTICAL INFILTRATION AND DRAINAGE CYCLES WITH AND WITHOUT SUCTION SAMPLING

C. Sampling Procedure

The pump was connected to the first series of 4 suction cups as shown in Figure 10.15. A suction of 640 mm Hg was exerted, the bunsen clips closed and the pump disconnected. This was repeated for each set of 4 suction cups, taking about 15 minutes overall. After 30 minutes had elapsed the vacuum was released on each suction cup, pressure re-distribution causing the samples to flow to the specimen tubes. These were removed and capped. Clean specimen tubes then replaced those collected and the bunsen clamps tightened to ensure atmospheric pressure did not reach the soil system. The equipment was then ready for the next set of samples to be extracted. The sampling time was taken as the mid-point of the 30 minutes extraction time.

D. Piezometer Sampling

Water from each piezometer was sampled using a syringe with 50 cm capillary tube extension. All water was first removed from the piezometer with the syringe before sampling. Samples were stored in 20 ml specimen tubes for transport to the laboratory.

10.5 TENSIOMETER CALIBRATION

Since values of moisture content were required for the experimental slope, 'scanning curves' (Childs, 1969, p.128, used this term to describe the relationship between water content and matric suction over a limited range, reserving the term 'soil moisture characteristic' for the major loop extending to high suction values) were prepared by laboratory calibration.

A pit was excavated at the position of each tensiometer, the tensiometer removed, and a soil core taken from the same depth as the pot. This was achieved by driving a 6 cm x 6 cm x 8 cm deep metal box into the pit face, removing with soil core, pushing into a plastic bag and wrapping tightly. Problems were encountered in sampling the very stony horizon, since these samples invariably crumbled. Thirty-two samples were removed, labelled and returned to the laboratory.

The standard calibration technique (Richards, 1941) uses a pressure apparatus, usually incorporating either a porous membrane or

FIGURE 10.15: SOIL WATER SAMPLING PROCEDURE
A SUCTION IS BEING EXERTED WITH THE STIRRUP PUMP;
VACUUM GAUGE (centre), SAMPLE CRATE (right)

FIGURE 10.15: SOIL WATER SAMPLING PROCEDURE
A SUCTION IS BEING EXERTED WITH THE STIRRUP PUMP;
VACUUM GAUGE (centre), SAMPLE CRATE (right)

ceramic filter. Suctions of over 100 atmospheres (> 7353 cm Hg) can be exerted using the apparatus. As this equipment was not available it was decided to calibrate with the 'Webster' tensiometers in the laboratory. 6 cm x 6 cm x 8 cm deep baskets were contructed from stainless steel wire mesh. Soil blocks were wrapped in muslin and inserted in the baskets (8 in one run). Using a hand drill 1 cm diameter holes were carefully drilled in the centre of each soil block to within 2 cm of the bottom and the tensiometer pot inserted. The top of the hole was sealed with clay. In cases where the sample had a high stone content, crumbling was unavoidable and the sample was compacted around the tensiometer by tamping.

The 8 baskets were saturated by immersing in water for 2 hours, linked to mercury manometers as described in an earlier section. Free air circulation around each basket was achieved by suspension from the edge of a bench. Readings of tension were taken between 0 and 60 cm Hg at intervals of approximately 5 cm Hg. At the same time, the complete basket was weighed on a balance without detaching from the manometer (it was found that there was no bias in weight reading so long as the capillary tubing was not 'pulling' on the basket). Three drying cycles were completed using this method giving about 36 points for plotting the 'scanning curve'.

Tensions in cm of water were calculated using Equation 10.3 water content, θ, in $cm^3 cm^{-3}$ was calculated by:

$$\theta = \frac{w_1 - w_2 - w_3}{v_1 - v_2} \qquad (10.5)$$

where w_1 = balance reading to nearest 0.01 g

w_2 = weight of water in tensiometer cell, assuming a density of 1 g cm^{-3}

w_3 = total weight after drying at $105^{o}C$ for 12 hours, g

v_1 = volume of soil sample (= 288 cm^3)

v_2 = volume occupied by tensiometer cell, cm^3

Figures 10.16 - 10.19 show the inverse relationships between θ and ψ as scanning curves. It is a well known fact that at any given

matric suction the water content of a soil will be greater on desorption than on adsorption, introducing hysteresis to the θ/ψ relationship. This hysteresis is very much a function of the distribution of pore space among pores of different sizes, as is very fully described by Childs (1969, Ch. 8). Equipment for empirical evaluation of an absorption (essentially a humidifying chamber) was not available and a single value relationship between θ/ψ was used in estimating θ. In fact, most tension data were collected during the course of slope drainage, probably reducing errors due to hysteresis over the range covered. For easy computer manipulation, cubic functions were fitted to each relationship between θ and ψ. These took the general form:

$$\theta = a - b\psi + c\psi^2 - d\psi^3 \qquad (10.6)$$

and are given in lines 80 - 390 of the computer program FLUX2 (Appendix 2). These equations cannot, of course, be used outside the range of the calibration data, which completely covers the range of tensions measured in the field.

10.6 SUMMARY

This Chapter has described the design of an experiment to monitor water and chemical movement in a hillslope soil above W1. Tensiometers and piezometers are used to obtain hydraulic potential and water content information, and ceramic suction cups to sample soil water for chemical analysis. The instrument layout is so designed to allow description, interpretation and modelling of processes operating within the soil. This analysis, together with a full soil chemical description, follows in Chapter 11.

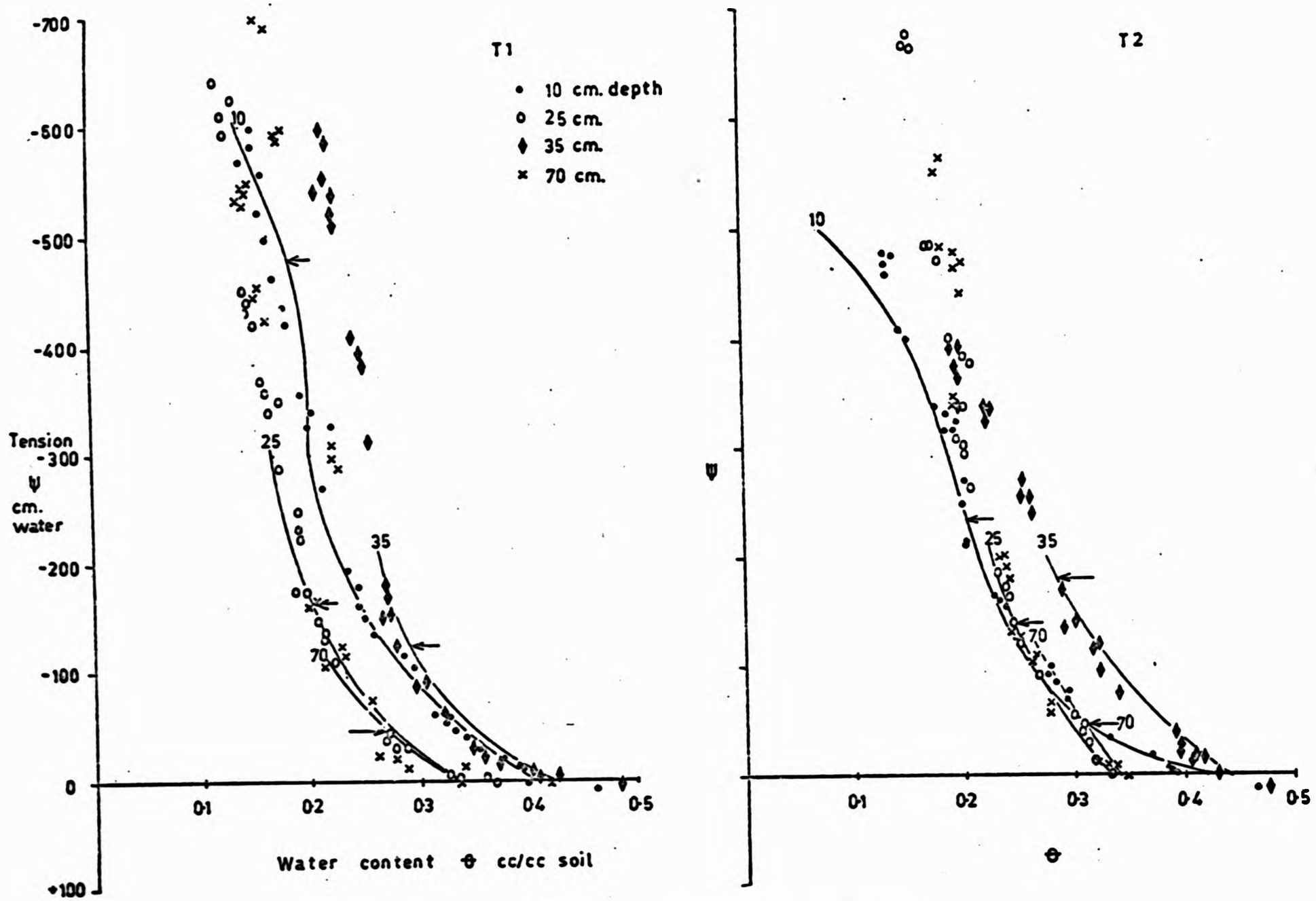

FIGURE 10.16: MOISTURE CONTENT/TENSION SCANNING CURVES AT TENSIOMETER BANKS 1 AND 2

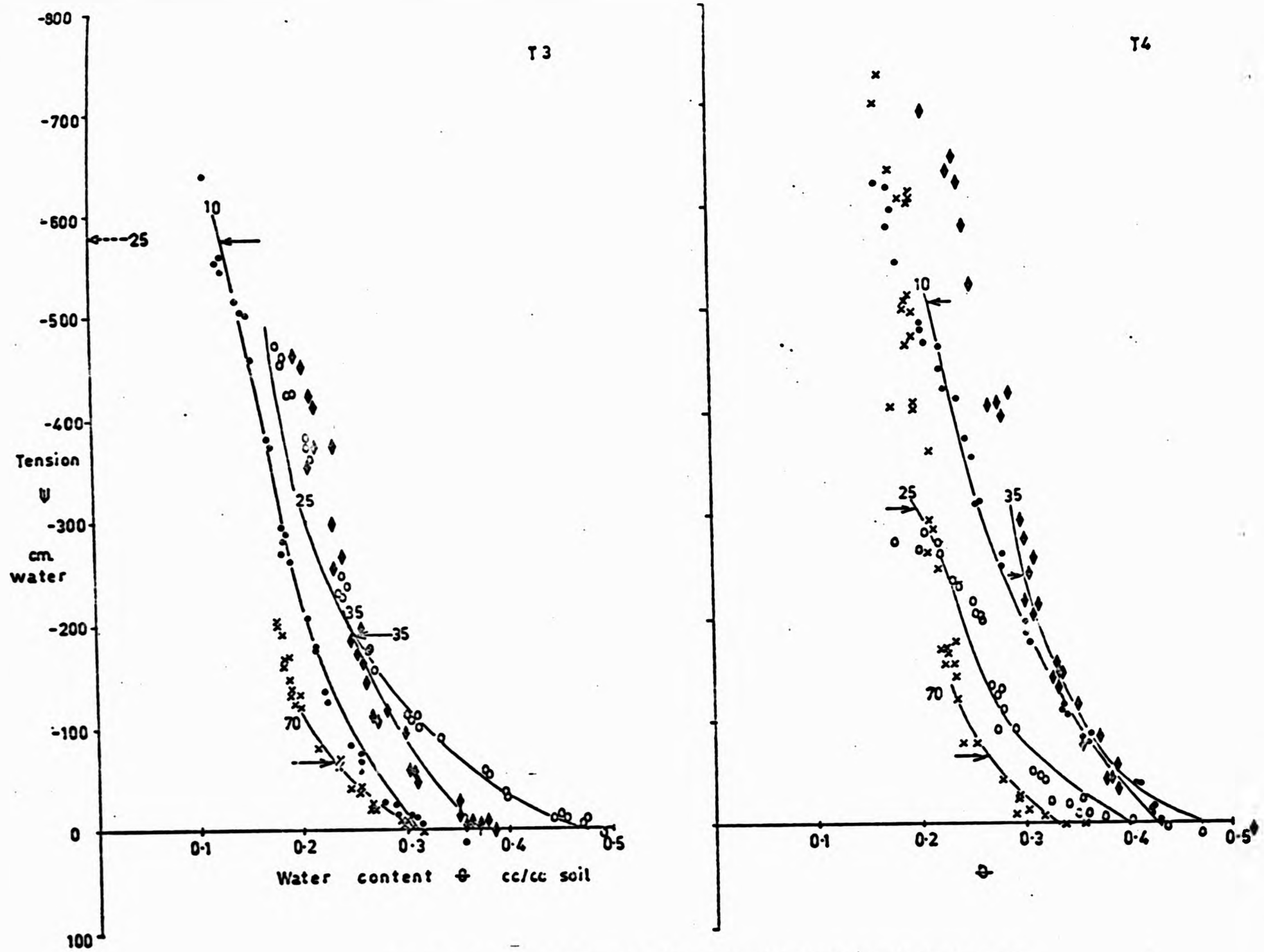

FIGURE 10.17: MOISTURE CONTENT/TENSION SCANNING CURVES AT TENSIOMETER BANKS 3 AND 4

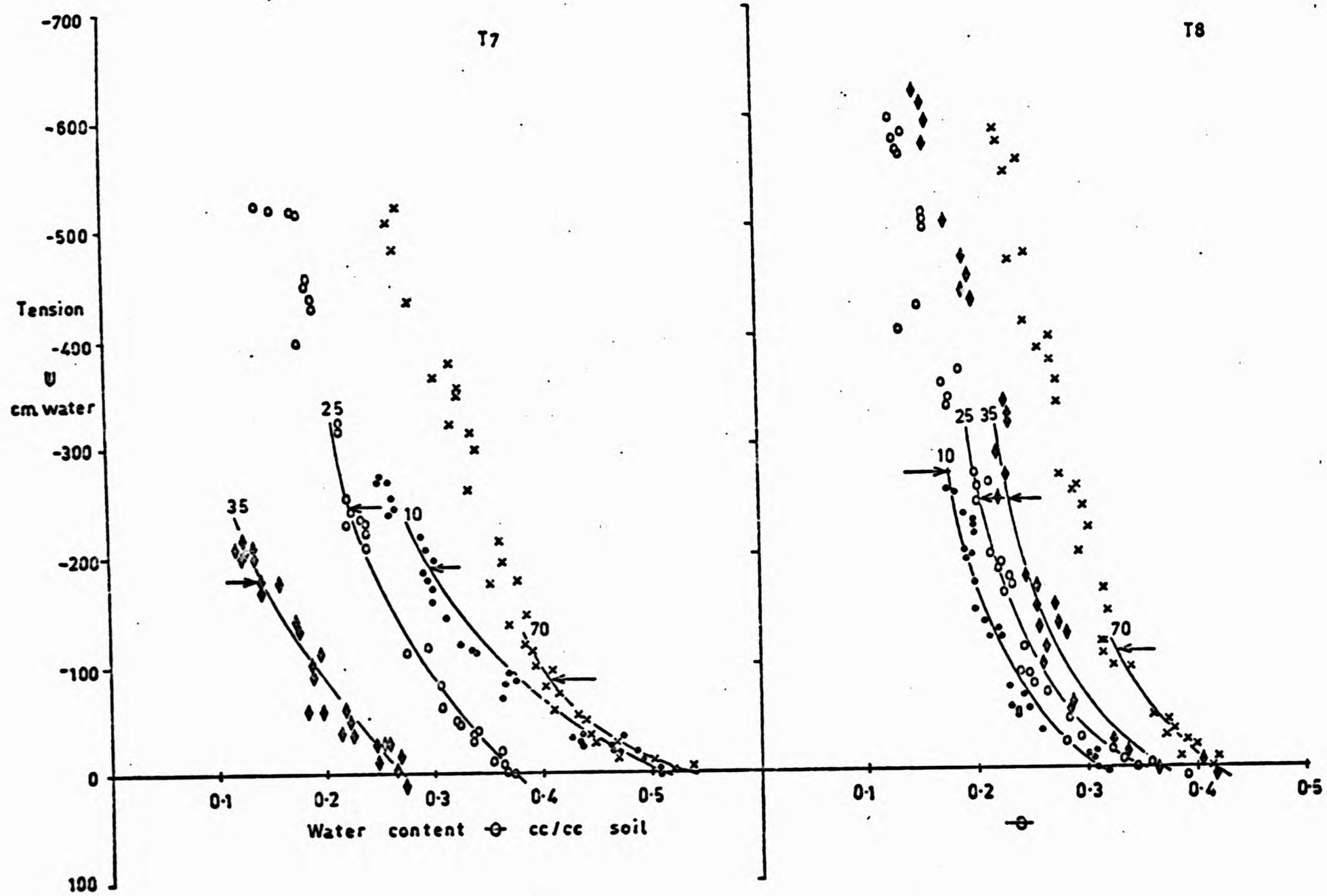

FIGURE 10.18: MOISTURE CONTENT/TENSION SCANNING CURVES AT TENSIOMETER BANKS 5 AND 6

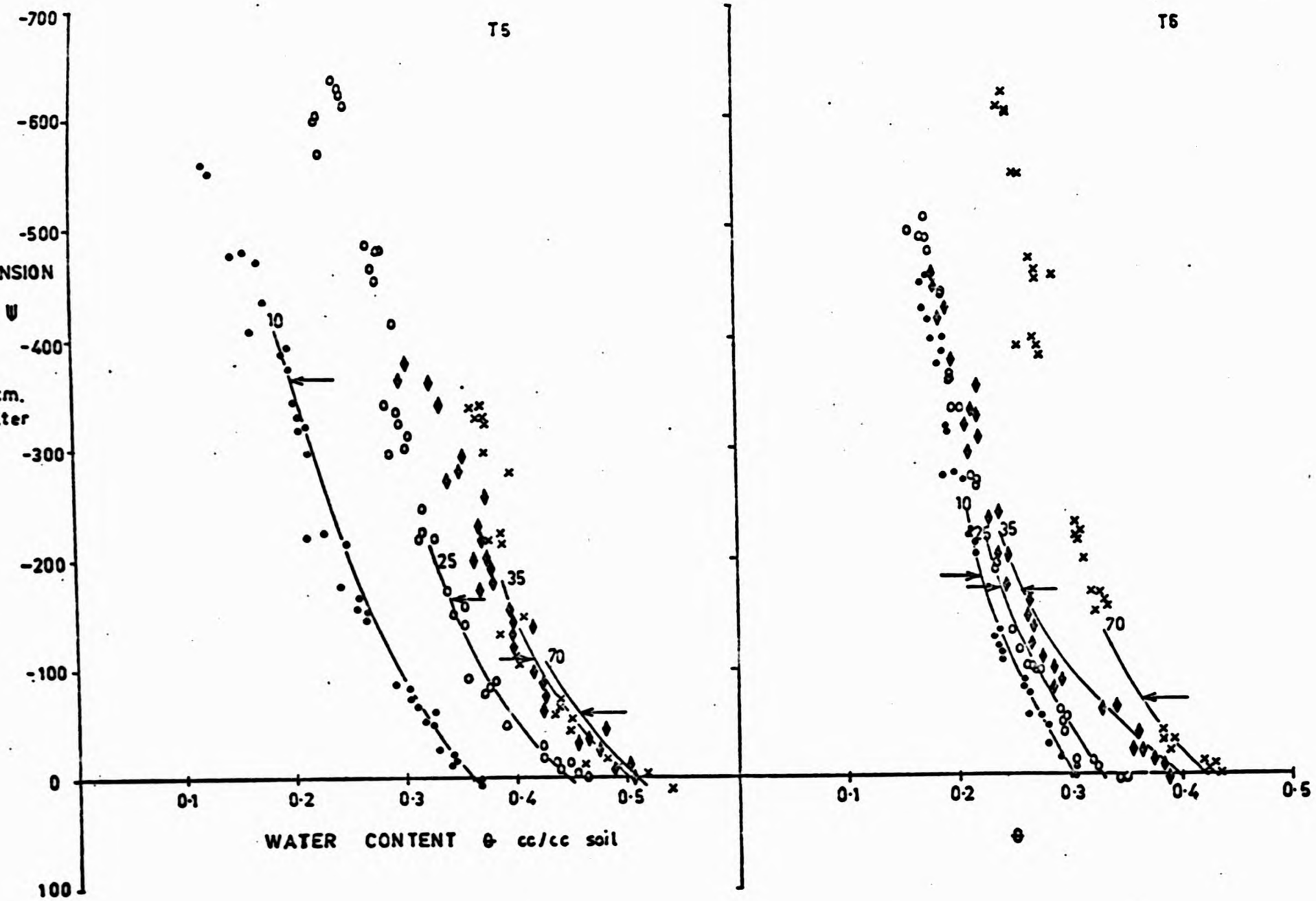

FIGURE 10.19: MOISTURE CONTENT/TENSION SCANNING CURVES AT TENSIOMETER BANKS 7 AND 8

CHAPTER 11:

AN ANALYSIS OF SUBSURFACE WATER AND SOLUTE DYNAMICS IN HILLSLOPE SOILS AT WEST WALK

11.1 INTRODUCTION

This chapter develops the results of data collected from tensiometers and ceramic suction cups. It was also thought that a good knowledge of the soil chemistry and hydraulic conductivity would provide a useful aid to analysis and interpretation of soil water hydrochemistry. Total element analyses were made to determine the total potential for chemical weathering, and exchangeable cation analyses to determine the capacity for relatively rapid cation exchange reactions. The latter is especially important for identifying potential sources of solutes contributing to the stream hydrograph. Percentage organic carbon content of the upper soil samples was also determined, because if present in sufficient quantity it may significantly increase the cation exchange capacity (Curtis et al, 1976). Saturated hydraulic conductivity measurements were made to assess soil anisotropy and the likelihood of infiltration excess overland flow occurring. These data are employed together with tension, hydraulic potential and soil water chemistry to describe subsurface solute dynamics, i.e. source areas, directions and rates of transport, under different hydrometeorological conditions. Basically, two types of condition are analysed: winter storm hydrographs and spring-early summer flow recession. Tension, hydraulic potential, hydraulic conductivity, total element contents, exchangeable cation contents and soil water cation contents are all contoured on a slope profile to make visual comparison possible. An attempt is made to relate processes operating on the slope with those in SC 1 and a schematic summary is made of water and solute response during storm hydrograph and low flow recession periods.

11.2 CHEMICAL CHARACTERISTICS OF THE HILLSLOPE SOILS

A detailed chemical analysis of the hillslope soils was undertaken as a basis for studying subsurface solute dynamics. Total element and exchangeable cation analyses were made, the first to determine the total potential amounts of each element available for weathering and removal

and the second to determine the capacity for relatively rapid cation exchange reactions. Neither analysis can be expected to show a uniform downslope chemical distribution, due to lithological, vegetation and organic matter and throughflow variability, and the past mass movement of soil. The distribution of exchangeable contents within the slope is of particular interest because this pinpoints potential sources of solutes for transport to the stream. A cation availability index (CAI), calculated as exchangeable contents/total contents, gives a further indication of potential source areas within the slope.

Soil sampling was carried out between January and March 1976 at the 55 locations shown in Figure 11.1A. Samples S1-3 were taken from the sidewall of the pit outflow trench; samples A1-4 from the pit face; samples B1-6, C1-6, D1-6 and E1-6 were taken from the nylon resistance unit calibration samples; samples F1-6, G1-8, H1-6 and J1-7 were obtained with a 4" bucket auger. The sampling line followed the upstream boundary of the slope experiment. Thus, as for soil water tension and solute content, soil chemical analysis placed priority upon the lower part of the hillslope. Two samples were taken at depths of two metres from the top and bottom of the slope to assess the total element contents of the less weathered subsoil.

Total analysis was completed for all the important elements expected in West Walk soil in order to:

(i) assess the accuracy of individual determinations (these should sum to the original weight of soil sample dissolved for analysis), and

(ii) indicate whether soil particles were translocated through the profile and re-deposited (in the form of aluminium, silicon, iron, etc.).

Details of analytical methods, together with the data reference pool are given in Appendix 3. Total element analysis was carried out for Si, Al, Fe, Ti, Mn, P, Ca, Mg, Na and K, all of which are expressed as oxide percentages in the sample, viz. SiO_2 %, Al_2O_3 %, Fe_2O_3 %, TiO_2 %, MnO %, P_2O_5 %, CaO %, MgO %, Na_2O % and K_2O %, the sum of which should be 100 %.

Organic carbon % was determined as part of the preparation process for the total element analysis. The mean error for the total element contents was + 1.22 %, which is good for the technique used. This disguises several high individual error terms, e.g. - 24.43 % (K4) possibly due to undissolved and thus unmeasured silica, and + 15.37 % (J7), possibly due to analytical error. Exchangeable cation analysis was undertaken for K, Na, Ca, Mg and Mn; pH was determined at approximately the same time. Precision of the techniquc for determining exchangeable cation content was regarded by Pye-Unicam to be low at ± 5 - 10 %.

In this chapter comments are made on the data presented as contours of chemical concentration through the slope. Reference is also made to one-dimensional plots of chemical contents against depth and distance upslope, although these are included in Appendix 3 to avoid overwhelming the text.

A. Potassium

(i) Total Contents as K_2O %

(range overslope: 800 - 3600 mg/100 gK)(Figures 11.1G, A3.2* and A3.12)

Potassium exhibits a tendency to decrease with soil depth over the lower 10 m of slope but to increase with depth over the upper 50 m. The section of soil between, corresponding to the convex slope noted in Chapter 10.1, shows an interesting pattern. Between 30 - 50 m upslope a zone of high K_2O exists at 80 - 90 cm depth. Downslope from this extends a 'tongue' of higher K_2O.

It seems likely that the 'tongue' represents mineral K_2O which has moved downslope, possible due to either soil mass movement or lateral translocation of silt and clay (cf. Huggett, 1976) from the upslope source area.

Both the deep samples and the lowest sample from the pit (A4) are relatively high in K_2O, indicating that the clay subsoil is a potential source for slow release of potassium.

* Note: Prefix A indicates Figure included in Appendix 3.

(ii) Exchangeable Cation Contents as K^+

(range over slope: 2 - 50 mg/100 g/K)(Figures 11.2A, 13.21 and A3.27)

Over most of the slope Ex.K^+ is high near the surface, decreases with depth, but shows a tendency to increase again at the profile base. This increase near the profile base accords with that noted for total K_2O, and probably represents a slow release from the clay mineral structure. The high Ex.K^+ near the soil surface appears strongly related to the presence of organic matter. The relationship between % organic carbon (% OC) and Ex.K^+(mg/100 g) is:

$$Ex.K^+ = 3.15\ \%\ OC + 12.94 \qquad (11.1)$$

$$r = +0.86; \quad N = 9; \quad \text{sig.level} = 1\ \%$$

The intercept (12.94 mg/100 g) represents the soil mineral component and the product (3.15 x % OC) the organic matter component of exchangeable potassium. Close similarity between the distribution of % OC and Ex.K^+ (Figures 11.1A and 11.2A) confirms this relationship. It is interesting to compare the results of J R Gosz et al (1972) who found potassium to be the third highest constituent of litter fall (after nitrogen and calcium) under deciduous woodland at Hubbard Brook, New Hampshire, USA.

It can also be noted that the near surface Ex.K^+ content is evenly distributed over the slope with the exception of the convex area where concentrations are lower. This also correlates with the presence of organic matter.

It is not possible to calculate the cation availability index (CAI) without first correcting total contents, because the total contents only includes soil mineral K and not organic matter K. Correction was achieved by computing the slope x % OC component of equation 11.1 and adding this to the total element contents before calculating the CAI. All the total element contents were re-calculated in this way. As expected the CAI shows that most potassium present is available near soil surface. The convex position of the slope exhibits a relatively low CAI as does the middle and lower soil profile at the slope base, the latter possibly as a result of leaching processes.

The CAI is also strongly correlated with % OC, thus:

$$CAI = 0.0023 \% OC + 0.005 \qquad (11.2)$$

$r = 0.86$; $N = 9$; sig.level = 1 %

This reaffirms the conclusion that organic matter is potentially a strong source of $Ex.K^+$.

In general the most likely sources of K for leaching and transport in soil water are the near surface horizons on the lower 10 m and upper 50 m of hillslope. The base of the profile over the lower 10 m might also provide a slowly-released source of K.

B. Sodium

(i) Total contents as Na_2O %

(range over slope: 100 - 850 mg/100 g Na) (Figures 11.1F; A3.4 and A3.11)

Sodium decreases with depth over the lower half of the slope but shows a gentle increase with depth over the upper half. As with K_2O there is a 'tongue' of higher Na_2O content extending downslope into the convex part of the slope. Both the deep samples are low at about 300 mg/100 g; the reason for this is uncertain because weathering reactions usually remove Na_2O selectively from upper soil horizons.

(ii) Exchangeable Cation Contents as Na^+

(range over slope: 10 - 150 mg/100 g Na) (Figures 11.2B, A3.22 and A3.28)

The distribution of $Ex.Na^+$ over the slope is more complex than for $Ex.K^+$ although the relatively low concentration in the convex part of the slope is again evident. There is a very high concentration of $Ex.Na^+$ in the near surface soil 2 - 3 m upslope, with a gradual decrease downprofile. This is represented by the peak concentration in Figure A3.28. A downprofile decrease in $Ex.Na^+$ is again found in the upper slope soil.

The relationship between $Ex.Na^+$ and % OC is:

$$Ex.Na^+ = 2.41\ \%\ OC + 33.6 \qquad (11.3)$$

$r = + 0.67$; $N = 6$; not significant

which makes it clear that the $Ex.Na^+$ is not as dependent upon the presence of organic matter as $Ex.K^+$.

The picture of sodium availability is complex (Figure 11.3B), but appears highest in the soil adjacent to the channel, decreasing downprofile. CAI decreases upslope, and also downprofile. The relationship between CAI and % OC is not significant:

$$CAI = 0.107 - 0.001\ \%\ OC \qquad (11.4)$$

$r = - 0.03$; $N = 9$; not significant

The major source area for $Ex.Na^+$ appears to be the bottom 10 m of slope, especially the 2 - 3 m adjacent to the channel. Here, due to the greater dependence upon soil minerals rather than organic matter, most of the soil profile appears important. $Ex.Na^+$ is also present in moderate quantities in the upper 50 m of slope.

C. Calcium

(i) Total Contents as CaO %

(range over slope: 0 - 285 mg/100 g) (Figures 11.1D; A3.3 and A3.13)

Calcium decreases with depth over most of the slope, except at 100 m upslope where a zone of high content occurs at 20 - 40 cm depth. The deep samples indicate that the CaO % increases in the less weathered subsoil.

(ii) Exchangeable Cation Contents as Ca^{2+}

(range over slope: 0 - 75 mg/100 g Ca^{2+}) (Figures 11.2D; A3.23 and A3.29)

$Ex.Ca^{2+}$ is particularly high in the bottom 10 m of slope soil, present in very low quantities in the middle slope soil, but again high

in the upper 20 cm of the higher slope. The picture adjacent to the stream is complex as Figure 11.2D shows. It depicts high $Ex.Ca^{2+}$ at the bottom of the profile next to the stream, decreasing up-profile for about 20 cm and then increasing again, reflecting the contribution of organic matter. Accordingly, the correlation between $Ex.Ca^{2+}$ and % OC is significant but not high:

$$Ex.Ca^{2+} = 3.88\ \%\ OC + 24.87 \qquad (11.5)$$

$r = +0.56$; $N = 9$; sig. at 0.1 % level

R J Gosz et al (1972) found Ca to be the second highest element in litter fall from deciduous woodland at Hubbard Brook, USA.

The pattern of the CAI is very similar to that for $Ex.Ca^{2+}$ (Figure 11.3C) showing dominance at the slope base, but the correlation with % OC is not significant.

$$CAI = 0.007\ \%\ OC + 0.32 \qquad (11.6)$$

$r = +0.12$; $N = 9$; not significant

As with Na^{+} the major source area for Ca^{2+} appears to be the bottom 10 m of slope soil. Here Ca^{2+} appears to be derived from both surface organic matter and clay minerals at the profile base.

D. Magnesium

(i) Total Contents as MgO %

(range over slope: 40 - 550 mg/100 g)(Figures 11.1E; A3.1 and A3.14)

In direct contrast with CaO, MgO consistently increases with soil depth, apart from the 2 - 3 m of slope nearest thc channel, where it decreases with depth. The convex area of slope again stands out due to its low MgO content. The deep samples are higher in MgO than any of the other samples, suggesting that this is a typical weathering profile (i.e. element increase vertically downprofile).

(ii) Exchangeable Cation Contents as Mg^{2+}

(range over slope: 0 - 75 mg/100 g) (Figures 11.2C; A3.24 and A3.30)

$Ex.Mg^{+}$ is present in significant quantities in the lower 12 m of slope soil. Above there is only a small quantity in the top 10 cm, at about 100 m upslope. The pattern of $Ex.Mg^{2+}$ at the base of the pit (Sample A4) closely resembles that for total MgO, suggesting that the clay subsoil at this point is an important potential source of Mg^{2+} in soil water. There also appears to be a contribution from soil organic matter in the top 10 cm, above the pit. However, the relationship between % OC and $Ex.Mg^{2+}$ is not significant.

$$Ex.Mg^{2+} = 29.33 - 0.79\ \%\ OC \qquad (11.7)$$

$r = 0.66$; $N = 7$; not significant

The CAI for Mg^{2+} indicates that virtually all is available at the bottom of the soil profile, at the slope base (Figure 11.3D). The relationship between this index and % OC is poor.

$$CAI = 0.104 - 0.003\ \%\ OC \qquad (11.8)$$

$r = -0.2$; $N = 8$; not significant

The bottom of the slope appears to be a major source of Mg^{2+} for soil water, and Figure A3.30 makes this very clear.

It is interesting to note that the soil pH (range over slope: 3.35 - 5.15, Figures 11.2F; A3.25 and A3.31) is highest at the profile base near the stream, which agrees with high values of $Ex.Ca^{2+}$, Mg^{2+} and Na^{+} for the same location. The soil becomes more acid up-profile over most of the slope, due to the influence of decaying organic matter. This provides a supply of dissolved organic compounds capable of chelating and transporting away major and minor (trace) metals. There is less pH variation over the upper half of the slope.

The other chemical constituents presented in Figures 11.1 and Appendix 3 are not of direct relevance to solutes within the hillslope,

but they are considered in brief here because they help to show the operation of soil physical processes, e.g. clay particle translocation.

E. Manganese

In general MnO content increases upslope (Figures 11.1B, A3.8 and A3.18). This pattern could result partly from reduction processes in the saturated zone adjacent to the stream. In acid water-logged soils manganese is reduced from manganic oxide (Mn^{4+}) to manganous oxide (Mn^{2+}), rendering it more soluble and liable to removal in throughflow water (Brady, 1974). The surface soil at the top of the slope represents a source of MnO, which can be traced downslope at depths between 20 - 40 cm. Interpretation of this is difficult. It may represent downslope transfer in throughflow or lateral translocation of clay and silt particles. It could also indicate fixation of Mn derived from surface organic material. R J Gosz et al (1972) found Mn to be the fourth highest constituent of litter fall after K, at Hubbard Brook, and the pattern of exchangeable Mn^{+} in the slope soils at West Walk suggests that this is mainly due to surface organic matter (Figure 11.2E). J D Hem (1970) also pointed out that Mn is an essential element in plant metabolism, while Slack and Feltz (1968) have shown that the Mn content of fallen leaves can significantly affect stream water quality. The CAI for Mn indicates that there is a much higher proportion in exchangeable form than for Ca, Mg, K and Na. Again, the CAI decreases with depth, emphasising the organic matter source.

F. Phosphorus

The content of P_2O_5 is high near the surface, decreases with profile depth to between 20 - 40 cm, and then gradually increases in the less weathered rock (Figures 11.1C, A3.10 and A3.19). Again, the high near surface content is probably due to organic matter.

G. Iron

Fe_2O_3 content decreases with depth over all the slope (Figures 11.1I, A3.6 and A3.17). The highest contents are to be found 5 - 15 m upslope, in the lower part of the slope convexity and this may reflect the iron content of material derived by mass movement from the Bagshot Sand.

In the 2 - 3 m adjacent to the stream channel the iron content is low, probably due to reduction in waterlogged, acid soil (i.e. from ferric to ferrous form) and removal in throughflow water. The lighter soil colour here (greyish-brown to white - see Table 11.1) is indicative of partially waterlogged conditions. The high Fe_2O_3 content upslope probably represents the source area for the higher concentrations of Fe^{2+} noted in Chapter 6.

H. Aluminium

Al_2O_3 increases with soil depth over most of the slope, except adjacent to the stream where it decreases (Figures 11.1H, A3.5 and A3.15). The increase with depth continues to about 60 cm, from where the Al_2O_3 content becomes fairly constant, as shown by the deep samples. This suggests that Al has been lost from upper soil horizons by vertical and lateral translocation of clay and silt particles or in solution. The latter process could be assisted by complexation due to strong organic acids derived from near the soil surface. The convex slope segment again shows a distinctive pattern, with a 'tongue' of higher Al_2O_3 content extending downslope. This feature lends support to the earlier suggestion that fine particulate material has moved downslope by lateral translocation. The decrease of Al_2O_3 with depth at the slope base agrees with all the other elements, except SiO_2, throughflow probably having been an important agent in Al removal.

J. Silicon

SiO_2 shows a rather different pattern to most of the other elements analysed (Figures 11.1J, A3.7 and A3.16). This is most apparent adjacent to the stream where % SiO_2 content is very high between 30 cm and the profile base (i.e. > 90 % SiO_2). This is a strong indication that other more soluble material has been removed from the soil by throughflow, leaving the less soluble SiO_2 as the major constituent of the matrix. In general, over the slope, SiO_2 decreases slightly with depth. SiO_2 falls from about 83.0 % at 7 cm depth to 75.0 % at 2 m depth, 3 m upslope, and from 90 % at 2 cm to 75 % at 2 m, 100 m upslope. This again implies that the more soluble material has been removed in preference to SiO_2 near the soil surface.

K. Titanium

Although Ti is one of the ten most abundant elements in the earth's crust, the Ti content of natural water is low due to its low solubility (Hem, 1970). Thus, it is often used as a standard to convert % by weight soil chemical analyses to % by volume, making the assumption that TiO_2 has not been dissolved or translocated. The pattern of TiO_2 in the hillslope is complex, and not that which would have been expected from complete TiO_2 immobility (Figures 11.1K, A3.9 and A3.20). In particular, % TiO_2 decreases with depth adjacent to the stream, implying that lateral translocation has occurred.

Before sampling, analysis and plotting of the data it was uncertain how useful the data would be in defining potential solute source areas within the hillslope soil. Field soils are characteristically heterogeneous, sometimes showing gradual spatial change, in other cases random variation (Hammond et al, 1958). However, soil changes are often greater and more uniform down a slope than across a slope. This 'catenary' variation may be attributed to soil water movement, differential transport of eroded material and the leaching, translocation and re-deposition of mobile chemical constituents (Curtis et al, 1976; e.g. Ballantyne, 1963). Such catenary variation emerges strongly from the West Walk hillslope soil analyses. Three points stand out. Firstly, the high concentrations of exchangeable cations present in the lowest 7 metres of slope. Secondly, the influence of organic matter to increase exchangeable cations in the near surface soil horizons. Thirdly, the possible effect of soil mass movement on total element and exchangeable cation contents between 30 - 50 m upslope. These points will be discussed further in relation with subsurface solute dynamics later in the chapter.

11.3 HYDRAULIC CONDUCTIVITY OF THE HILLSLOPE SOILS

Measurements of saturated hydraulic conductivity (K) were made on the slope soils for four main reasons.

(i) To assess the degree of soil anisotropy for the application of a flux approach to moisture and solute accounting based upon equation (9.1) and described in Chapter 9.3. Anisotropy is

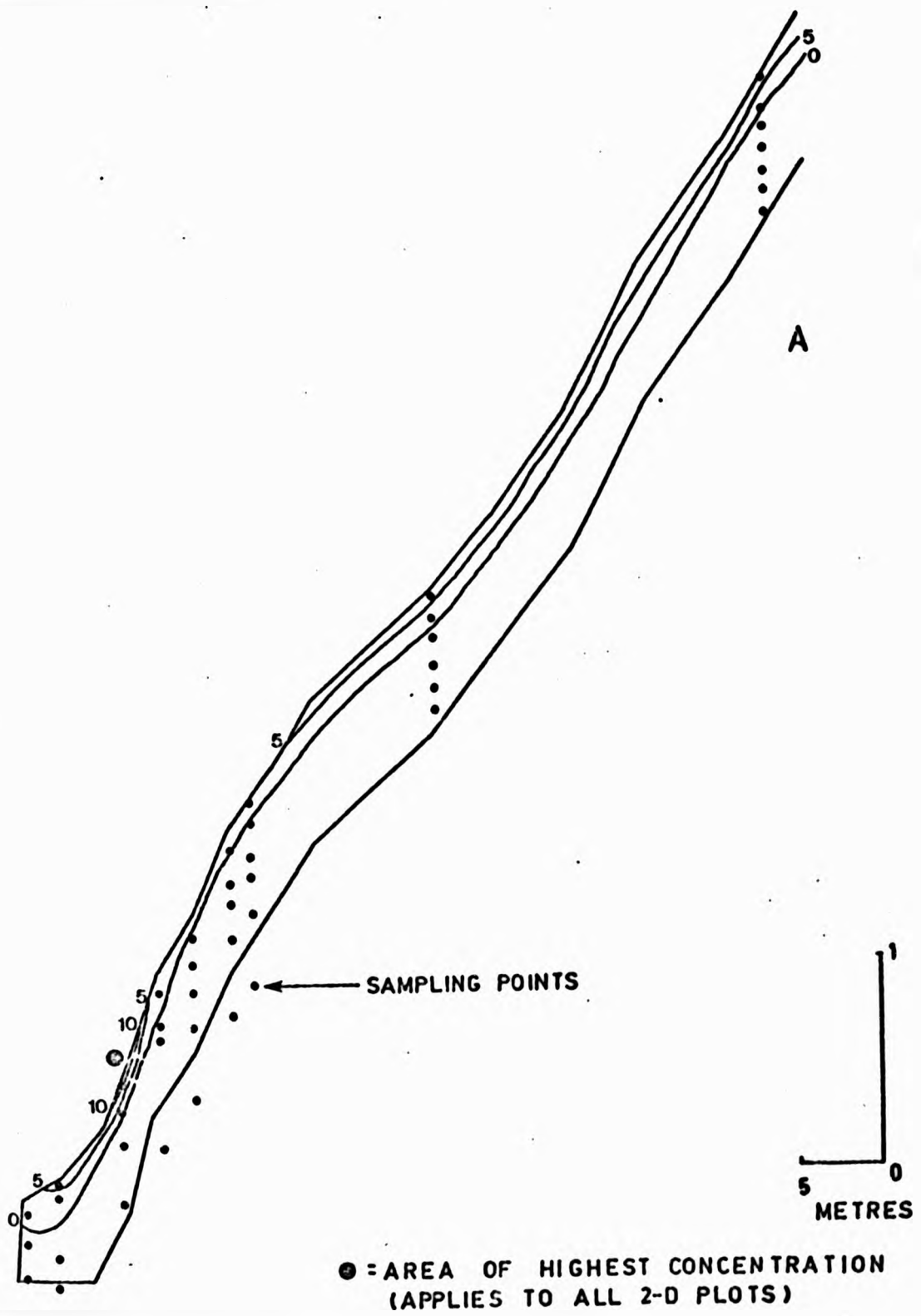

FIGURE 11.1 A: 2 - D PLOT THROUGH THE SLOPE OF % ORGANIC CARBON

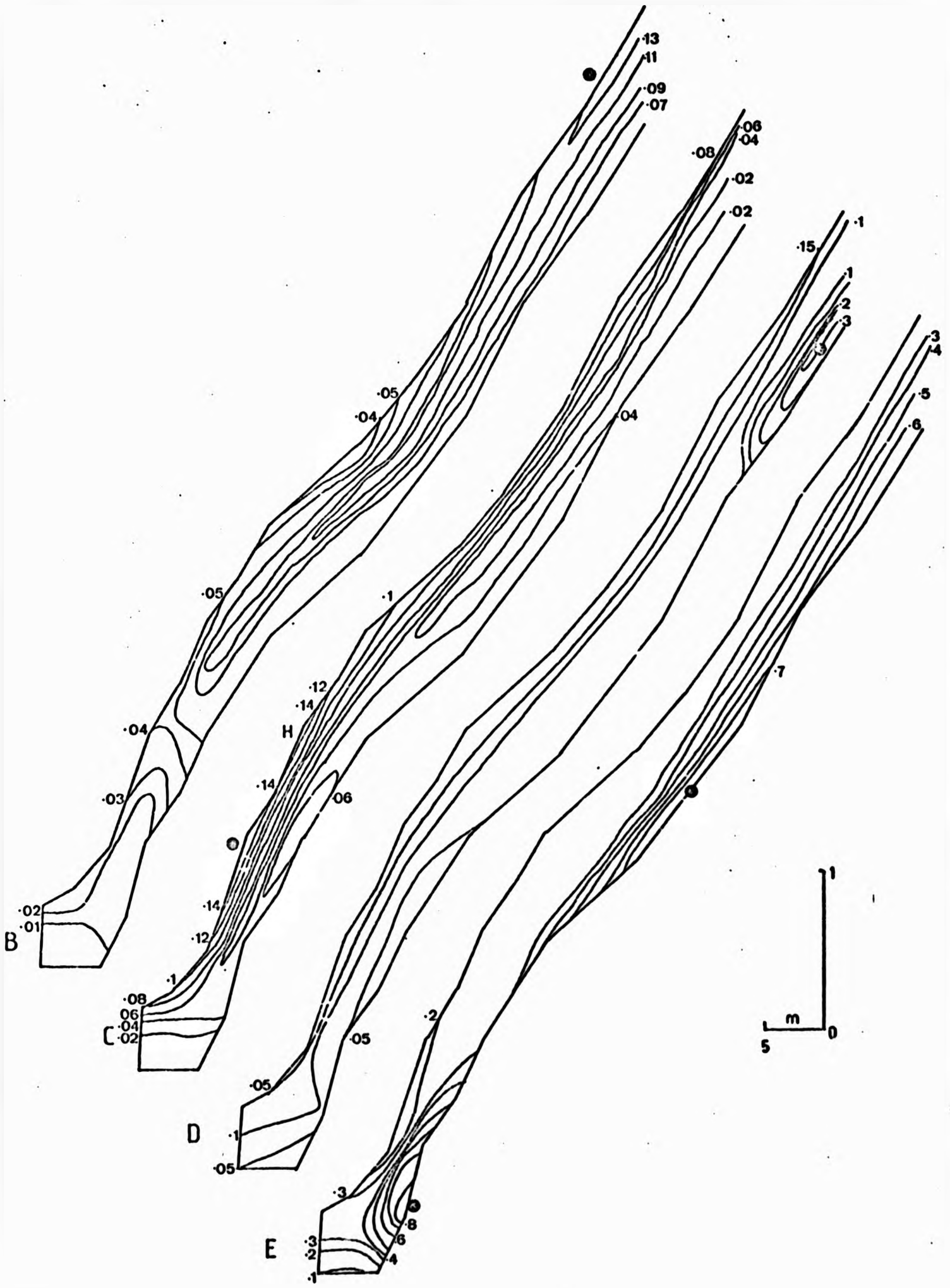

FIGURE 11.1 (cont'd): 2 - D PLOTS THROUGH THE SLOPE OF TOTAL OXIDE CONTENTS

B: % MnO C: % P_2O_5

D: % CaO E: % MgO

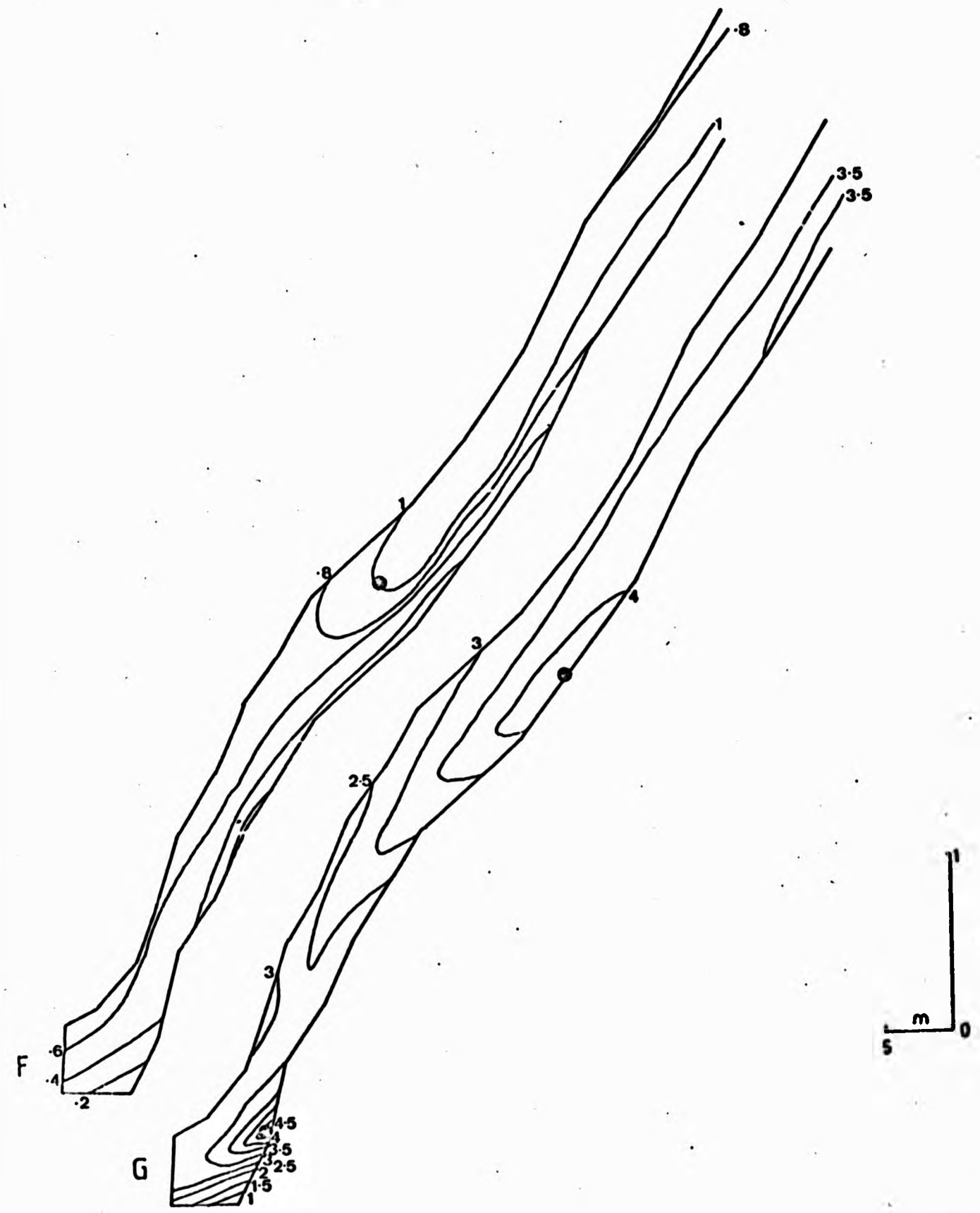

FIGURE 11.1 (cont'd): F: % Na_2O G: % K_2O

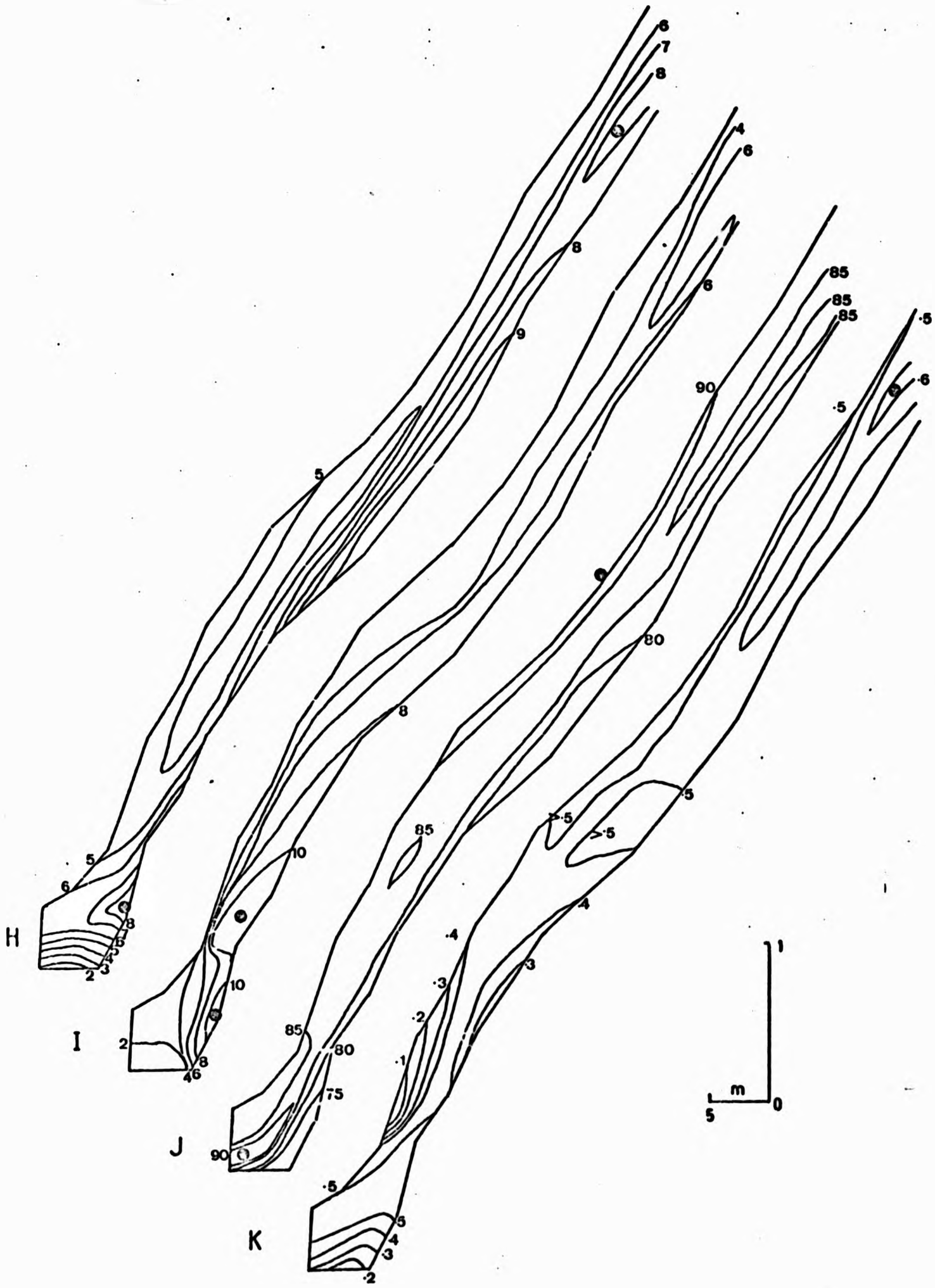

FIGURE 11.1 (cont'd): H: % Al_2O_3 I: % Fe_2O_3
J: % SiO_2 K: % TiO_2

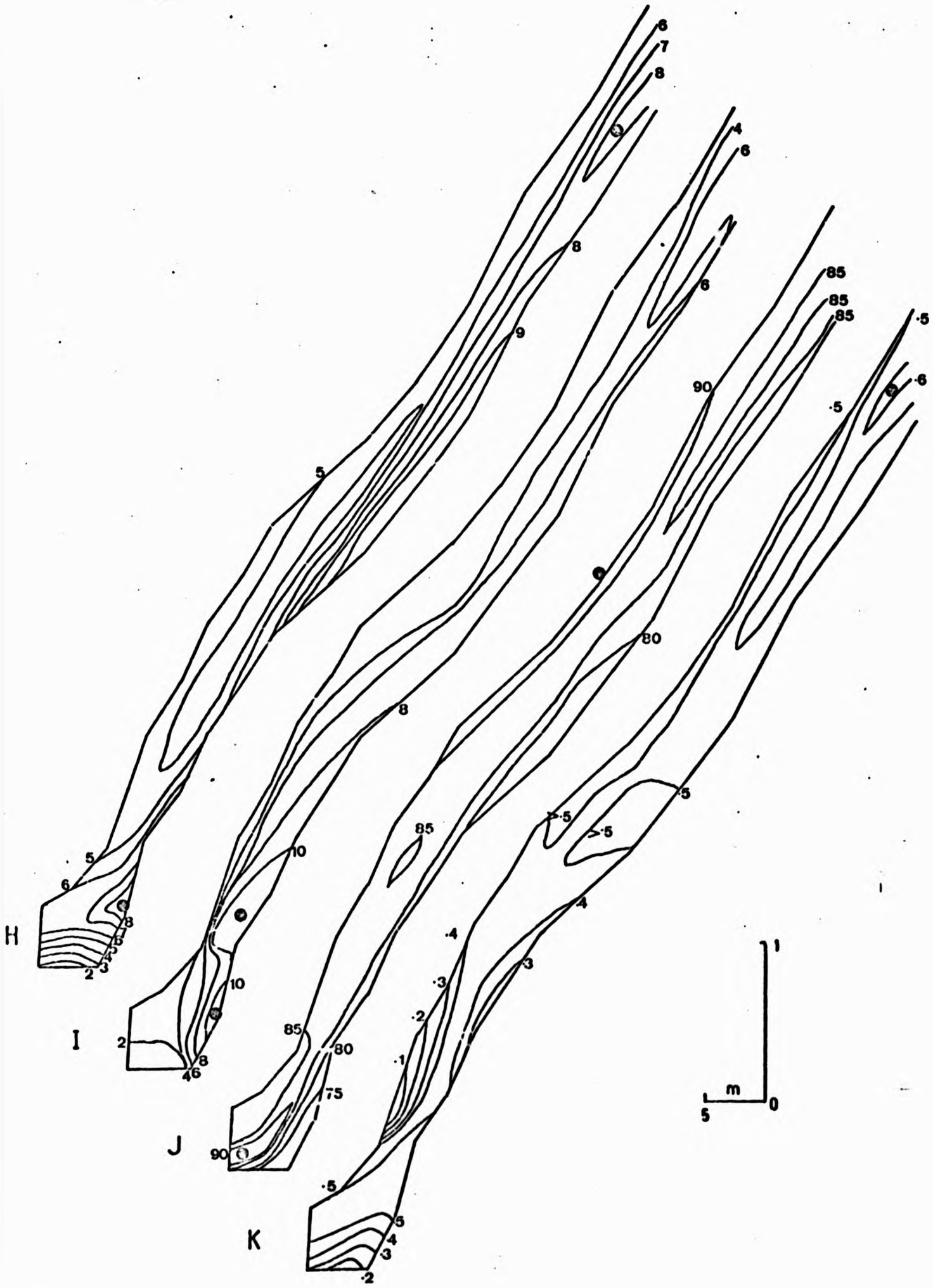

FIGURE 11.1 (cont'd): H: % Al_2O_3 I: % Fe_2O_3
J: % SiO_2 K: % TiO_2

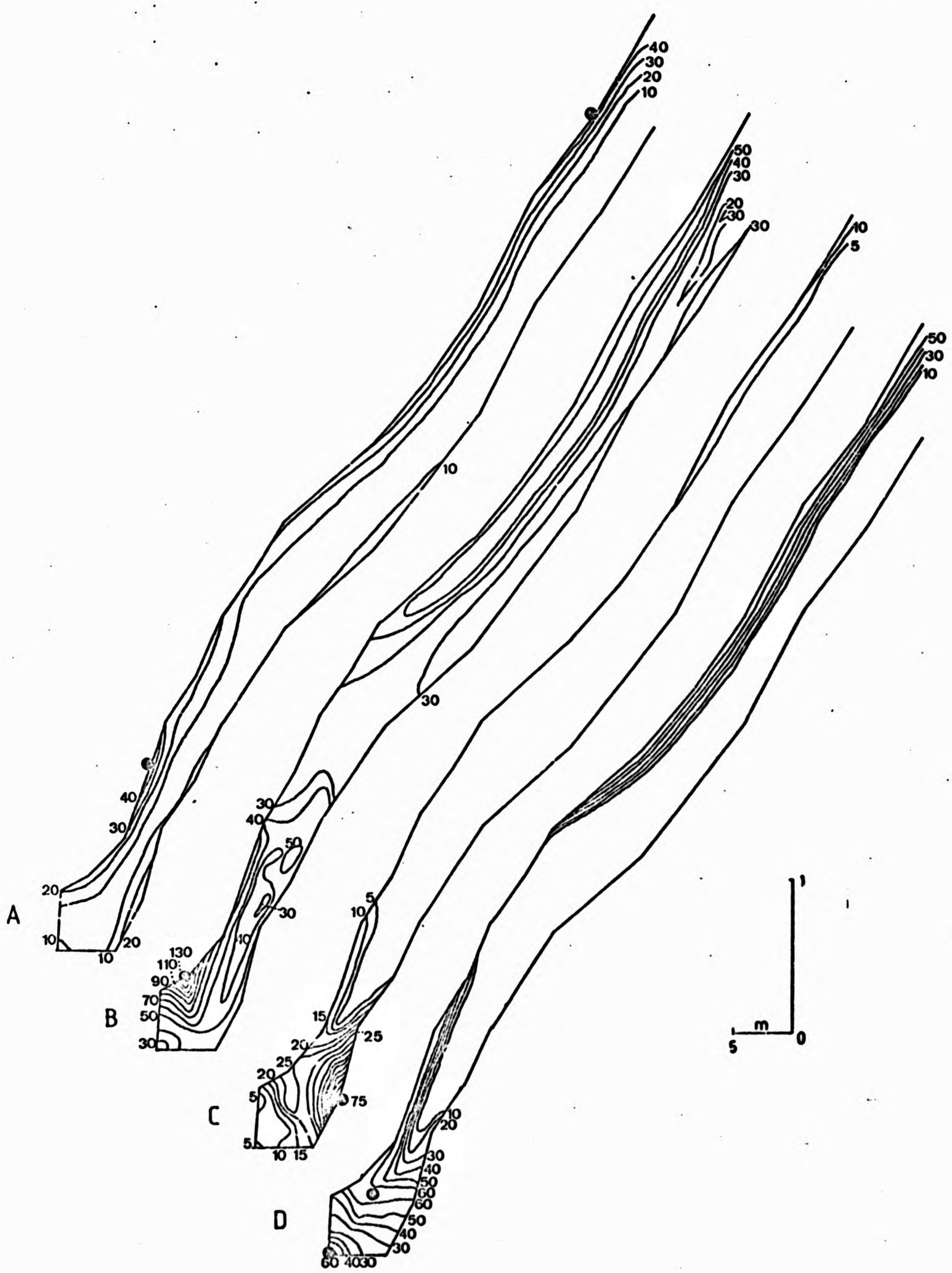

FIGURE 11.2: 2 - D PLOTS THROUGH THE SLOTE OF EXCHANGEABLE CATION CONTENTS (mg/100 g)

A: K^+ B: Na^+ C: Mg^{2+} D: Ca^{2+}

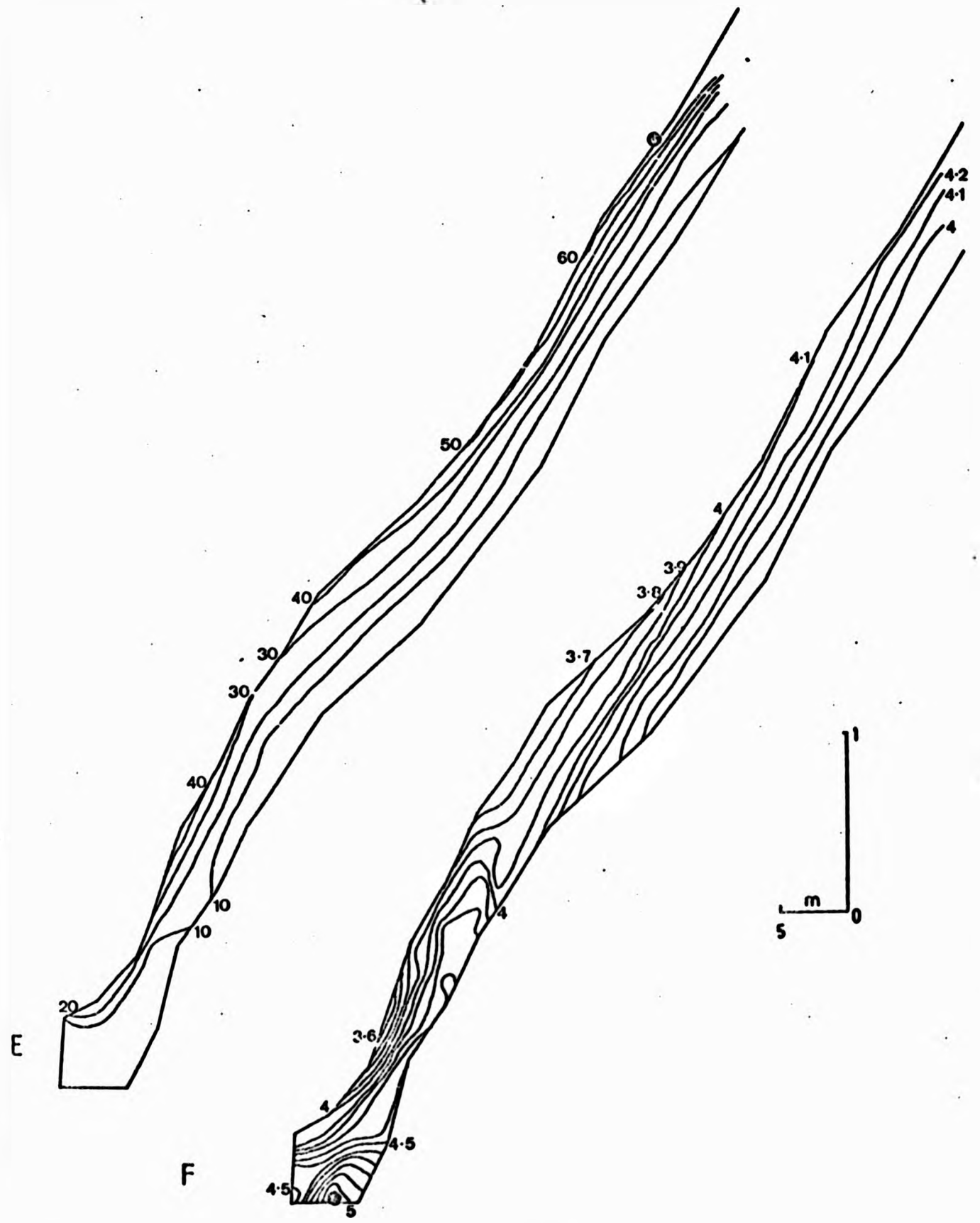

FIGURE 11.2 (cont'd): E: Mn^{+}; F: pH

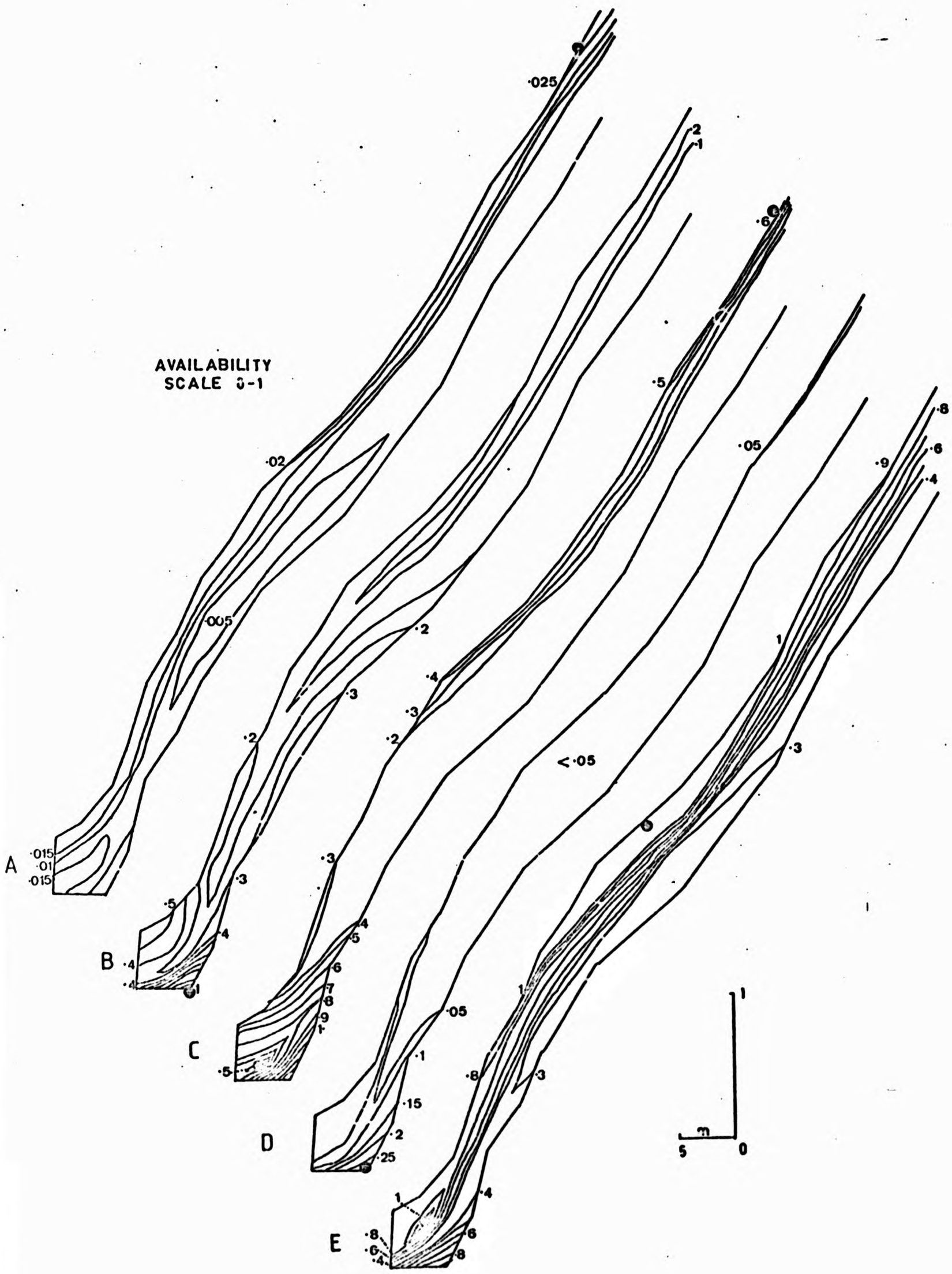

FIGURE 11.3: 2 - D PLOTS THROUGH THE SLOPE OF CATION AVAILABILITY (exchangeable/total contents)

A: Potassium B: Sodium E: Manganese

C: Calcium D: Magnesium

TABLE 11.1: COLOUR OF THE SOIL SAMPLES CHEMICALLY ANALYSED

Munsell colour codes and qualitative description, value in brackets after letter = distance upslope (m)

PROFILE	S (0)	K (2.8)	A (7.0)	B (9.25)	C (11.5)
Approximate Soil Depth, cm					
5					
10	10 YR, 3/2, v. dark greyish brown, slightly moist	10 YR, 3/2, v. dark greyish brown, slightly moist	10 YR, 2/2, v. dark brown, moist	7.5 YR, 3/2, dark brown, dry	7.5 YR, 4/4, brown/dark brown, dry
15					
20			10 YR, 3/4, dark brown, moist		
25	10 YR, 5/2, greyish brown, slightly moist	10 YR, 6/2, light brownish grey with 7.5 YR, 5/8 strong brown mottling around root tubes		7.5 YR, 4/4, brown/dark brown, moist	7.5 YR, 5/6, strong brown, moist
30					
35			10 YR, 5/8, yellowish brown, moist	7.5 YR, 5/6, strong/ brown, moist	7.5 YR, 5/6, strong brown, moist
40	7.5 YR, 5/6, strong brown with 10 YR, 7/1 mottles (light grey), moist	10 YR, 8/1, white, dry			
45					
50		10 YR, 6/8, brownish yellow and 10 YR, 8/2, white mottling		7.5 YR, 5/6, strong brown, moist	7.5 YR, 5/6, strong brown, moist
55					
60			7.5 YR, 5/8, strong brown, moist		
65					
70				7.5 YR, 5/8, strong brown, moist	7.5 YR, 5/8, strong brown, moist
75					
80					
85					
90				7.5 YR, 5/8, strong brown, moist	7.5 YR, 5/8, strong brown, moist

TABLE 11.1:(cont'd):

PROFILE	D (13.9)	E (16.25)	F (29.5)	G (53)	H (7.5)	J (100)
Approximate Soil Depth, cm						
0			10 YR, 2/2, v.dk.brown	10 YR, 2/2, v.dk.brown		10 YR, 3/2
5						
10	7.5 YR, 4/4, dark brown, dry	7.5 YR, 4/4, strong/ dark brown, dry	10 YR, 3/2, v. dark greyish brown	10 YR, 4/4. dark yellowish brown	10 YR, 3/2	10 YR, 3/2
15				10 YR, 4/4, dark yellowish brown	10 YR, 4/4	10 YR, 3/3
20			10 YR, 4/4, dark yellowish brown			
25	7.5 YR, 5/6, strong brown, moist	7.5 YR, 5/6, strong brown, moist		10 YR, 5/6	10 YR, 5/6	10 YR, 5/4
30						
35	7.5 YR, 5/6, strong brown, moist	7.5 YR, 5/6, strong brown, moist	10 YR, 6/6, brownish yellow	10 YR, 5/6	10 YR, 6/6	10 YR, 5/6
40						
45			10 YR, 5/8, yellowish brown	10 YR, 5/6	10 YR, 5/8	10 YR, 5/6
50						
55	7.5 YR, 5/6, strong brown, moist	7.5 YR, 5/6, strong brown, moist	7.5 YR, 5/6, strong brown	10 YR, 5/6	10 YR, 5/8	10 YR, 5/6
60						
65				10 YR, 5/6		
70	7.5 YR, 5/6, strong brown, moist	7.5 YR, 5/6, strong brown, moist				
75						
80						
85						
90	7.5 YR, 5/8, strong brown, moist	7.5 YR, 6/8, reddish yellow, moist				

also likely to affect the interpretation of hydraulic potential data when plotting flowlines.

(ii) As a means of assessing the likelihood of infiltration-excess overland flow occurring. This involves the use of downprofile K values for near-surface samples.

(iii) To give a quantitative assessment of the soil's ability to conduct water and solutes to the stream. When combined with cation exchange capacities K values should suggest potential sources and routeways.

(iv) In combination with hydraulic potential, soil water solute concentration and source zones, to give quantitative information on subsurface solute dynamics, i.e. source areas, directions and rates of transport.

A. Field and Laboratory Methods

Equipment availability restricted K determination to the saturated case. A laboratory method was preferred to the auger hole technique (e.g. Bonell, 1972) because it gave a network of point values in both horizontal (x) and vertical (z) directions.

Point values are susceptible to contouring and identification of high and low K zones within the soil, but the auger hole method gives only a single K value, averaged over the depth of the hole. A permeameter method (de Boodt, 1967) was employed. Soil cores were collected from the slope soils at the same time that the tensiometers were excavated. PVC tube, 5 cm diameter x 5 cm long, was driven into the soil adjacent to the tensiometer, the soil excavated around the tube and both tube and core removed. Two cores were taken at each tensiometer, one orientated vertically (z), the other orientated horizontally (x). In some cases it was found to be impossible to take cores due to impedance by stones or crumbling of the soil. A total of 40 cores were collected from piezometer 1 (P1) to tensiometer 7 (T7).

The laboratory equipment used in determining K is shown in Figure 11.21. Hydraulic conductivity was determined from:

$$K = \frac{V}{t_1 - t_0} \cdot \frac{L}{A} \cdot \frac{1}{(H_0 + H_1)/2} \quad \text{cm/hour} \qquad (11.9)$$

which is a re-arrangement of Darcy's Law. V, L, A, H_0 and H_1 are defined in Figure 11.4; t_0 and t_1 are times at the start and end of determination, in hours. Care was taken accurately to measure time (with a stopwatch), volume (with a 100 ml measuring cylinder) and head. More than one determination was made on each sample (usually 2 or 3), and good replication was obtained despite the comment by Freeze and Cherry (1979) that precise determination of the K for a given sample is not warranted due to excess variability.

The factors most likely to give incorrect determinations of K were:

(i) Gaps at the boundary of the sample and the plastic tube. It was thought that by saturating the sample for 2 - 3 hours before determination, small gaps would be closed by swelling. This would be especially true for samples with a high clay content.

(ii) Trapped air bubbles in the sample. Again, saturation for 2 - 3 hours should overcome this problem.

(iii) Compression of the sample surfaces during collection. The top and bottom of the sample were both removed to a depth of about 5 mm and the core pushed through, so that one side became flush with the end of the tube. This left 1 cm for a constant head to be maintained above the sample.

Where cracks or root tubes fully penetrated cores, then this may have given an excessively high K value, unrepresentative of the surrounding soil mass. Such phenomena were observed in two of the 40 samples, although the higher K values obtained did not appear excessive when compared to those from surrounding cores.

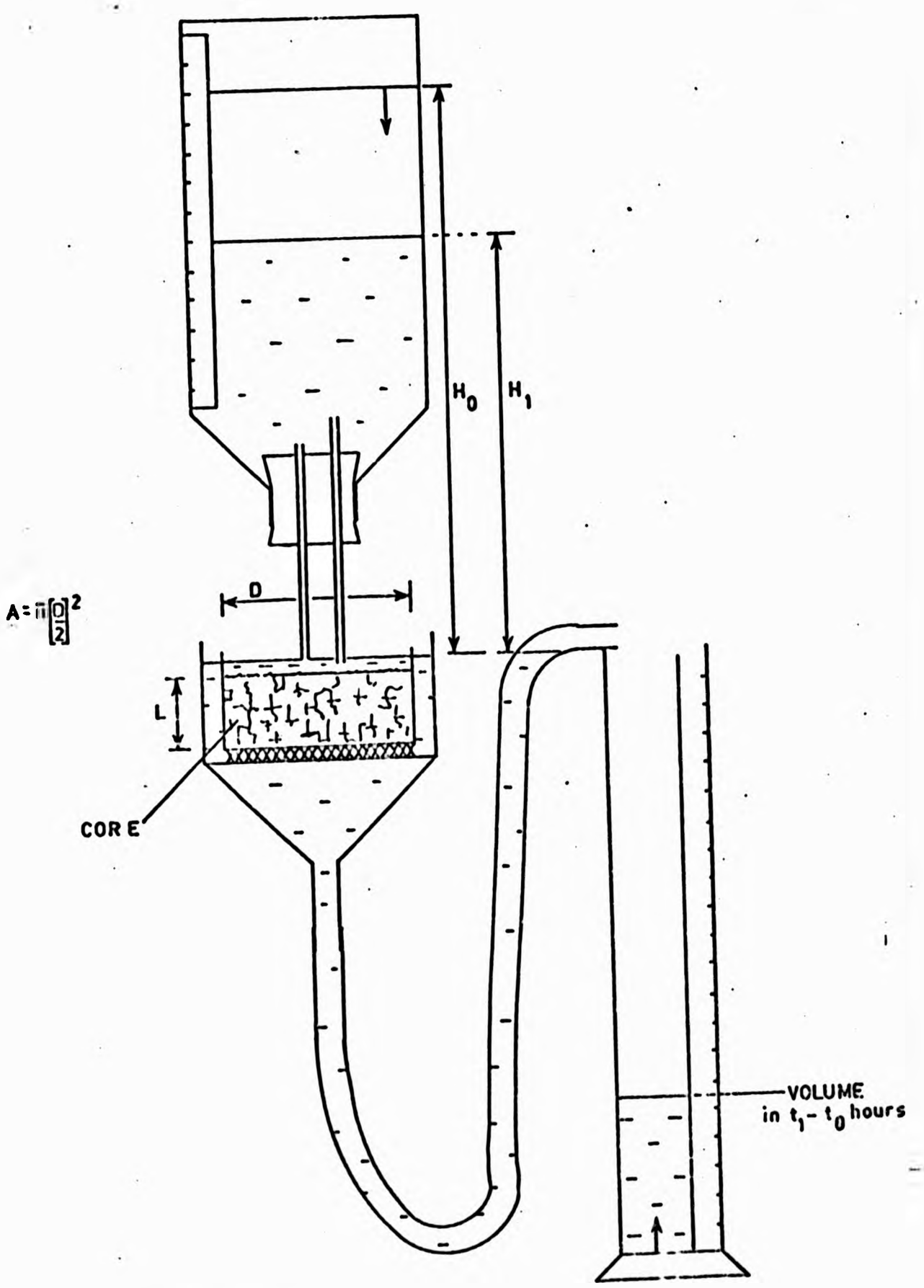

FIGURE 11.4: PERMEAMETER EQUIPMENT FOR LABORATORY DETERMINATION OF HYDRAULIC CONDUCTIVITY

(after de Boodt, 1967)

B. Interpretation and Discussion of Results -
The Problem of Anisotropy

The horizontal and vertical K values have been contoured over a cross section of slope in Figure 11.5.

The highest horizontal K occurs in the top 10 cm of soil at P1, adjacent to the stream (23 cm/hour). This decreases quite rapidly to 0.1 cm/hour at about 20 cm depth. The deepest sample at P1 had an observably high clay content and would not conduct water. The picture over the lowest 10 m of slope is similar. Horizontal K values generally decrease with soil depth and distance upslope. A further peak K value occurs at 10 cm depth, 10 metres upslope (10.5 cm/hour).

The highest vertical K also occurs 10 metres upslope (47 cm/hour). This is part of a zone of high K (i.e. > 10 cm/hour) extending from about 7 m to 11.5 m upslope, extending to a maximum depth of about 40 cm between 9 and 12 m upslope. Again, there is a tendency for K values to decrease with soil depth. By contrast with horizontal K, vertical K is quite low adjacent to the stream, at P1.

R A Freeze (1980) noted that saturated K can vary over 12 - 14 orders of magnitude, although for near surface soils the range is narrower, i.e. 0.036 - 36 cm/hour agreeing quite well with range of values found at West Walk.

Comparison of West Walk K values with those for various types of unconsolidated material (Freeze and Cherry, 1979) classifies them as permeable gravel deposits within the range .0028 - 47 cm/hour.

Gravel size material with little interstitial finer sediment covered the lowest 5 m of slope to a depth of 40 - 50 cm. Upslope, to about 14 m, the gravel comprised a smaller fraction of the soil matrix, extending to a maximum depth of about 80 cm. Thus, it is thought that the pattern of hydraulic conductivity is more than a simple function of gravel content, and that interstitial filling, soil shrinkage and root patterns are highly influential factors. The 2 - 3 m of slope soil adjacent to the stream is low in most total element contents, notably Fe_2O_3 and Al_2O_3, but high in SiO_2, which suggests that lateral

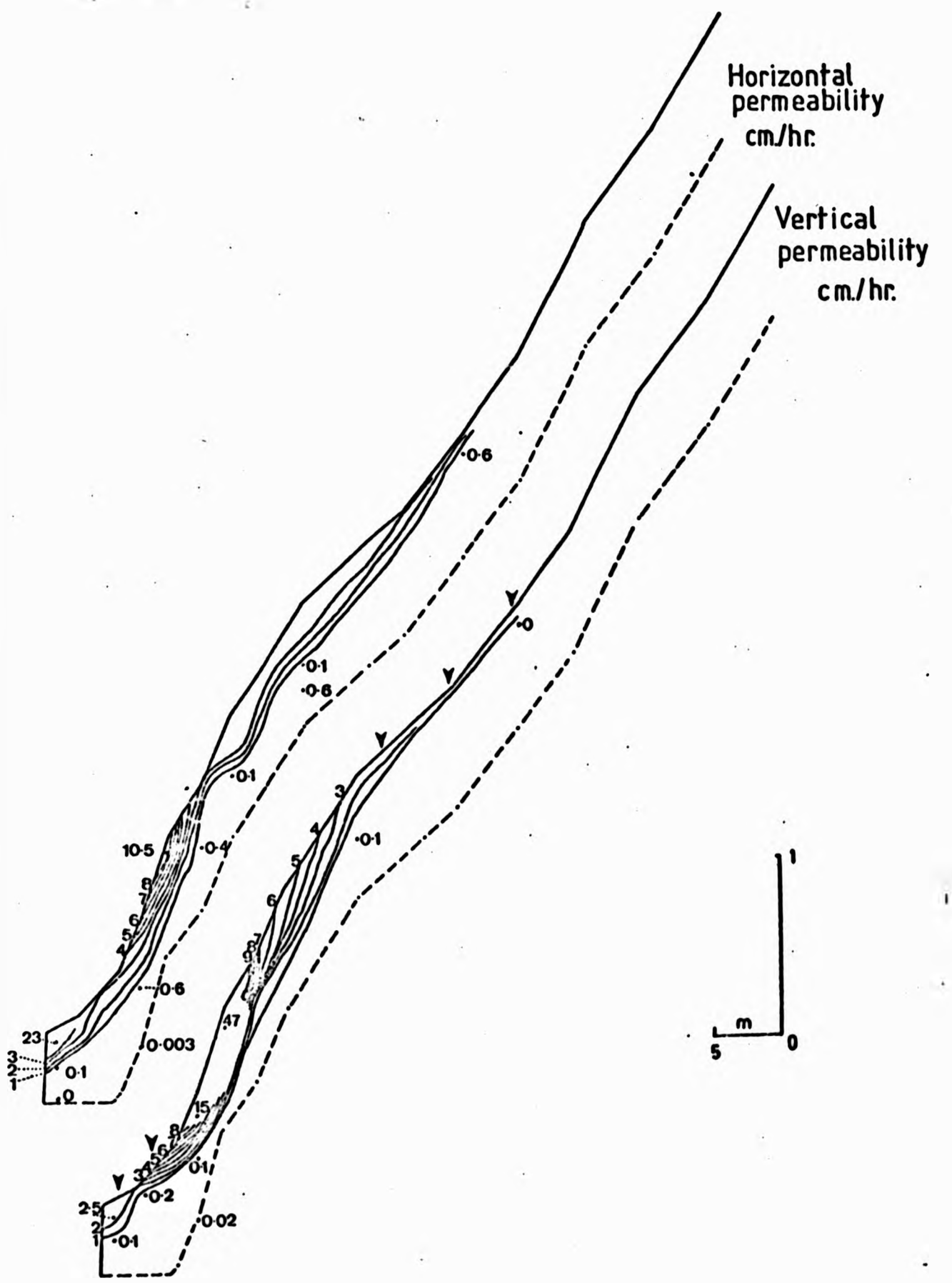

FIGURE 11.5: 2 - D PLOTS THROUGH THE SLOPE OF HYDRAULIC CONDUCTIVITY

translocation here may have removed more interstitial material than further upslope. Lateral translocation has probably been aided in this area by the more frequent expansion and contraction of the saturated wedge. This could help to account for the high K_x values. The situation is analgous to that of the higher K values found within the natural range of Chalk ground water levels, the annual fluctuation aiding solution processes in joints and fissures.

Near-surface hydraulic conductivity is higher, in part due to the effect of roots in helping to reduce bulk density. After a root dies, then the tube which remains increases K in one preferred direction. The ability of clay soils to shrink and crack whilst drying is an additional factor which increases K. This might be more pronounced in the topsoil where most water is lost. The orientation of the cracks increase K preferentially in one direction as noted in Chapter 9.3. These two factors could help to account for the high downprofile K values about 10 m upslope.

It is clear from the data obtained that the slope soil is heterogeneous and anisotropic.

Homogeneity implies that K is invariable at various points within the soil, while isotrophy implies that K is variable with the direction of measurement within the soil. If the soil is homogenous and isotropic then the two dimensional (x - z) continuity equation is simply (Eagleson, 1972):

$$K \nabla^2 \phi = 0 \qquad (11.10)$$

that is, $K_x = K_z = K$ (isotropy) and K_i are the same at all points (homogeneity).

However, if heterogenity exists, then $K_x \neq K_z \neq K$ and (11.10) becomes:

$$K_x \frac{\partial^2 \phi}{\partial x^2} + K_z \frac{\partial^2 \phi}{\partial z^2} = 0 \qquad (11.11)$$

(which is equivalent to equation 9.6).

If, additionally, the soil is anisotropic, then equation (11.11) further expands to:

$$K_x \frac{\partial^2 \phi}{\partial x^2} + K_z \frac{\partial^2 \phi}{\partial z^2} + \frac{\partial K_x \phi}{\partial x \partial x} + \frac{\partial K_z \phi}{\partial z \partial z} = 0 \qquad (11.12)$$

Equations (11.10) to (11.12) illustrate the increasing complexity caused by homogenity and anisotropy.

The flux approach to moisture accounting within the hillslope described in Chapter 9 uses an equivalent of equation (11.11) (i.e. including heterogeneity), but cannot cope with anisotropy as described by equation (11.12). This problem will be discussed later.

The effect of anisotropy on the magnitude and direction of downslope water flux has been described by D Zaslavsky and A S Rogowski (1969). They suggest that anisotropy would be promoted by a two layered soil, with the less permeable layer below. Streamlines would tend to become parallel to the soil surface as both slope angle, α, and anisotropy n (i.e. $K_{downslope}/K_{orthogonal\ to\ slope}$) increase.

This is not the situation for the West Walk hillslope, where the equivalent of n (K_x/K_z) is less than 1.0 over the steepest slope, implying that water would move preferentially downprofile. Nevertheless the zone of maximum slope angle maintains higher K_x values than all but the lowest 2 m of slope. The resulting picture is complex, although it could tentatively be explained by the combined downprofile influence of root tubes and shrinkage cracks exceeding that of downslope shrinkage cracks.

C. Comparison of near-surface K_z values with maximum rainfall intensity

In the absence of field determined infiltration rates for the hillslope, K_z values at 10 cm can be compared with maximum recorded rainfall intensity to assess the likelihood of infiltration excess overland flow occurring. Freeze (1980) noted that the saturated K of soil adjacent to a stream has a strong influence on the operation of

both infiltration excess and/or saturation excess overland flow. The maximum rainfall intensity recorded was 30 mm/hour on 5th August 1975; 24 mm/hour was recorded twice, on 21st August 1975 and 21st October 1976. Figure 11.5 shows that K_z varies upslope in the range < 0.01 mm/hour to 470 mm/hour. Arrows indicate the locations where K_z is exceeded by maximum rainfall intensity, notably adjacent to the stream, and above about 20 m upslope. Any overland flow from upslope is likely to be quickly absorbed into higher K soil downslope and subsequently deplete the SMD. Whether infiltration excess overland flow actually occurs adjacent to the stream is not clear because the top soil horizontal K is much higher than maximum infiltration capacity and might be capable of conducting infiltrating water, in addition to that arriving from upslope.

It is interesting to note that both the August 1975 storms gave flashy responses, high proportions of storm runoff/rainfall and a rapid return to pre-storm conditions.

D. Hydraulic Conductivity, Potential Solute Sources and Solute Routeways

Mapped hydraulic conductivity (Figure 11.5), % organic carbon (Figure 11.1A) and exchangeable cations (Figures 11.2A - F) can be compared to indicate the potential for rapid solute transport from a source to the stream.

The strongest visual correlation is between hydraulic conductivity and % organic carbon which implies that soluble organic matter could be transported quite rapidly downprofile and downslope. The flow pattern is likely to follow a rotational path downslope; essentially vertical over the steepest slope, 5 - 12 m from the stream, but gradually turning downslope as the higher K_z area thins, and then downslope over the final three metres of high K_x soil adjacent to the stream. Assuming the soil to be completely saturated then velocity (V) can be calculated from Darcy's law. The approximate maximum vertical and downslope velocities would be 47 cm/hour and 3.5 cm/hour respectively, at a point 9.25 m upslope (for downslope velocity, $V = K_{xz} \tan \alpha$, where K_{xz} is calculated as a vector, and α is the slope angle). These figures suggest that time is available for

complexation of metal ions by dissolved organic matter moving with the subsurface water (they can only approximate because dispersion has been ignored).

The highest values of $Ex.K^+$ also correlate well with K_x and K_z (Figure 11.2A). This suggests that surface, or near surface, $Ex.K^+$ could be rapidly transported to the stream, thus accounting for the direct relationship between K^+ and streamflow noted earlier. Increasing $Ex.K^+$ in the deeper soil horizons corresponds with lower K_x and K_z, and probably represents a supply of slowly available K^+.

High $Ex.Na^+$ concentrations also correlate well with K_x and K_z which makes it difficult to explain the dilution effect for Na^+ (Figure 11.2B). The implications are that either:

(i) Na^+ takes longer to equilibriate than K^+,

or (ii) K^+ is preferentially complexed by organic chelates,

or (iii) the high $Ex.Na^+$ distribution is unrepresentative of the pattern found within SC1 as a whole.

If (iii) is true, and soil $Ex.Na^+$ is variable, then this might account for the poor correlation between Na^+ and streamflow at W1.

The highest $Ex.Mg^{2+}$ concentrations are found in a zone of low K_x and K_z about 9 m upslope (Figure 11.2C), and would not be available for rapid solution and transport. Near-surface $Ex.Mg^{2+}$ is low in concentration. Thus storm runoff is likely to be low in Mg^{2+} and result in a stream dilution effect.

Near surface $Ex.Ca^{2+}$ is higher than at depth in the soil, especially 7 - 14 and 19 - 100 m upslope, although when dissolved, this is probably only important in supplying Ca^+ to the stream during hydrograph recessions, i.e. to aid the return to pre-storm concentrations (Figure 11.2D). $Ex.Ca^{2+}$ decreases towards the stream in the top 20 cm of soil and, in contrast with upslope areas, vertical concentration gradient is absent. This may account for the dilution effect noted in Chapters 6 and 7.

There is a strong similarity between the pattern of pH and K_x and K_z (Figure 11.2F). This implies that organic acids are available for rapid transport to the stream, and helps to account for decreasing pH with increasing discharge during hydrographs. Low pH (3.6 - 4.3) and high % organic carbon (5 - 10 %) coincide with a high % Fe_2O_3 (>10 %) content in the zone of high K_z about 9 m upslope. This supports the earlier suggestion that iron is complexed by organic compounds in the upper catchment soils, and subsequently transported downstream until a rise in pH causes precipitation. Complexation by mobile organics has recently been suggested as the major mechanism for iron transport in a New Jersey catchment (Swanson and Johnson, 1980).

This section has used hydraulic conductivity and soil chemistry, both essentially static, point descriptions of the slope soils, in discussing anisotropy, overland flow and solute sources and routeways. In the next section, collected hydraulic potential and soil water solute data are used to analyse the dynamics of subsurface from within the hillslope.

11.4 AN ANALYSIS OF SUBSURFACE WATER AND SOLUTE PROCESSES

This section presents an analysis of subsurface hillslope water and solute movement under rainfall infiltration and drainage conditions. Four main periods are considered.

A. 29th November - 7th December 1976: a period of heavy rainfall and infiltration followed by soil drainage.

B. 25th January - 10th February 1976: a period of intermittent lighter rainfall and infiltration.

C. 12th May - 1st June 1977: a period of slope drainage and steadily increasing SMD.

D. 12th March - 2nd May 1976: a period of slope drainage and steadily increasing SMD during the 1975/1976 drought, with rainfall and shallow infiltration at the beginning of the period.

These results, together with those from Sections 11.2 and 11.3 are discussed, and a summary made of the solute sources and transport processes operating.

Tension readings were converted from Hg to cm water using the program TENPLOT as described in Chapter 10. These were then stored on magnetic tape and used to produce a contour plot of tension with the program CONTEN 2 (Appendix 2). The most useful feature of these plots is the identification of a saturated zone within the soil (using piezometer readings, in addition to tension contours).

Hydraulic potential was also contoured using the stream as a reference datum, Z_0, (see equation 9.4). The program CONPOT (Appendix 2) was used for this purpose, producing "equipotentials" for water movement to the stream. If the soil is isotropic then the direction of flow is from high to low potential, perpendicular to the contours. However, measurements of hydraulic conductivity have already revealed that this condition is not met, at least for lateral flow in the upper soil horizons and vertical flow. It seems possible that tension readings could give matrix potential, implying movement perpendicular to the equipotentials (e.g. downslope), while in fact actual water movement could be in the direction of higher conductivity (e.g. downprofile). A simple analogy has already been made between water movement in fissured Chalk and a clay soil after a long dry period (Chapter 2.3), whereby recharge is slow and indirect through microfissures but faster and more direct through macrofissures (Young et al, 1976). Thus conclusions drawn from equipotentials must be treated with caution.

A. <u>Rainfall, infiltration and drainage:</u>
<u>29th November - 7th December 1976</u>

Tensiometer, piezometer, K^+ and Mg^{2+} solute data are available for this period. The catchment hydrological conditions are summarised in Figure 11.6. Between 28th November and 1st December, 84 mm rain fell at West Walk, giving the highest instantaneous discharge recorded at W1 in the study period (26.5 l/sec). The preceeding period of three months following the drought were wetter than average, so that by 28th November the SMD had fallen almost to zero.

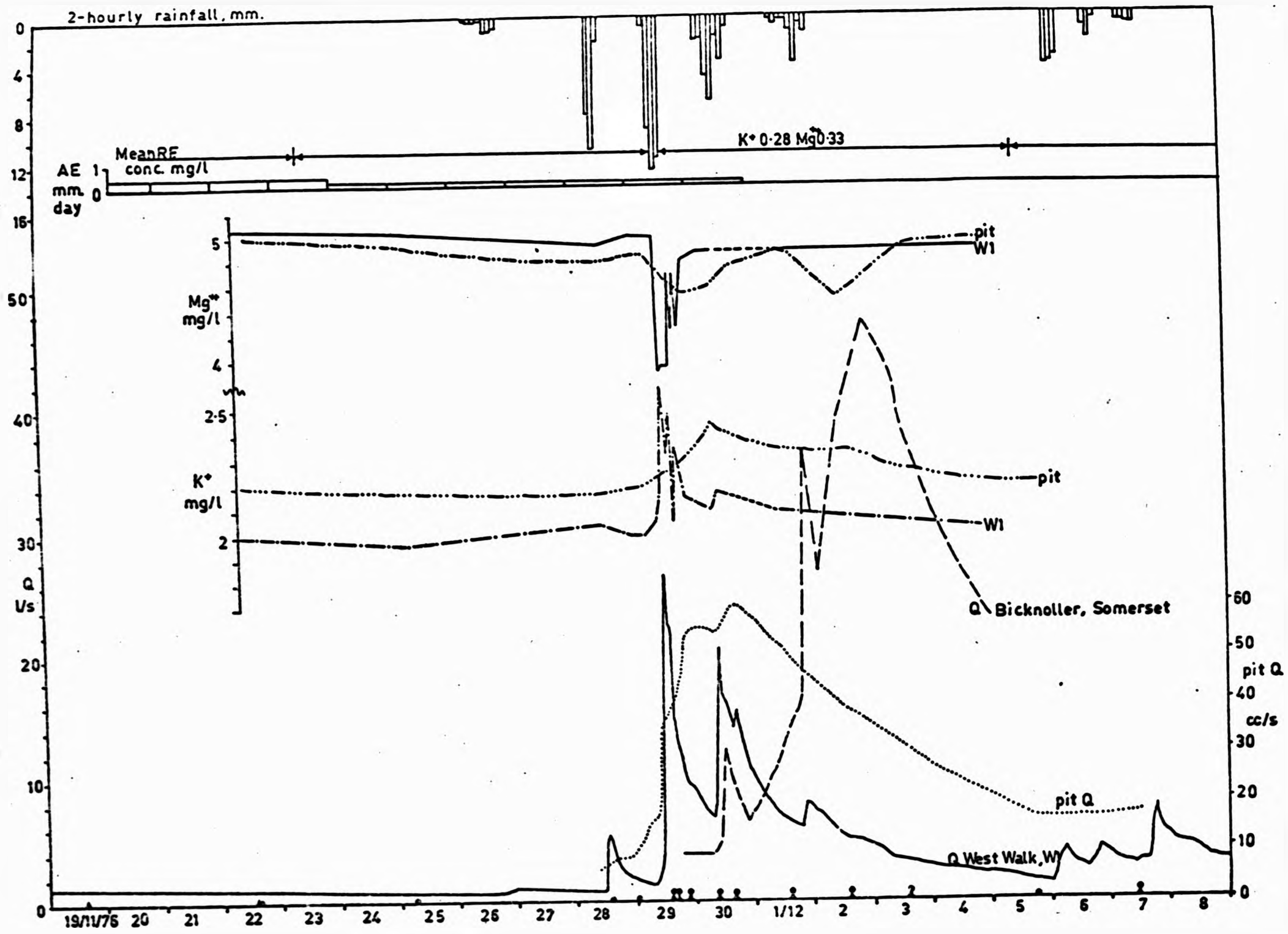

FIGURE 11.6: SUBCATCHMENT 1 AND SLOPE HYDROLOGY:
19 NOVEMBER - 8 DECEMBER 1976

(circles = pit sampling times;
triangles = tension sampling times)

I. Water Movement

(i) Prior to the rainfall of 28th/29th November 1976, a small saturated wedge existed adjacent to the stream (Figure 11.7), with tension increasing up-profile. Flow was essentially downslope, but with a downprofile component between 24 and 40 m upslope (Figure 11.8). The saturated zone was fed by lateral flow from upslope and vertical flow over the bottom 3 m.

(ii) The second picture of tension coincides with the hydrograph rise (1330, 29th November 1976), and shows saturated soil over most of the slope. The exceptions are the area of high conductivity just below the slope convexity, and 24 - 40 m above the slope convexity. Equipotentials suggest that flow direction was little changed for the upper slope, but became predominantly downprofile in the convex slope. Downslope flow was vertical in the area of high K_z, implying that the tensiometers gave true values in an integrated flow system. The pattern of flow agrees rather well with the directions suggested by the hydraulic conductivity (Figure 11.5). Over the last five metres, lateral flow to the stream dominates. The convex slope emerges as an area of resistance to downslope flow, promoting a higher water table. Above this the flow potential deflects into the slope, and then 're-appears' 10 m down, implying a rotational water movement under the convexity. The water table downslope of the convexity is also low, due to the reduced lateral supply. Although Figure 11.7 portrays a water table at the soil surface, overland flow was only noticed in the 2 - 3 metres adjacent to the stream. This was probably due to the higher hydraulic conductivity of the top soil, especially the organic layers. Overland flow was observed on footpaths and vehicle tracks leading to streams, and this is probably a further factor in determining stream hydro-and chemographs.

(iii) The third picture of tension and hydraulic potential (1600, 29th November 1976) shows little change, representing conditions immediately after rainfall, during hydrograph recession.

(iv) Seven and a half hours after rainfall, the water table had fallen over most of the slope except the lowest six metres. Flow appeared essentially downslope in the saturated zone, being fed by

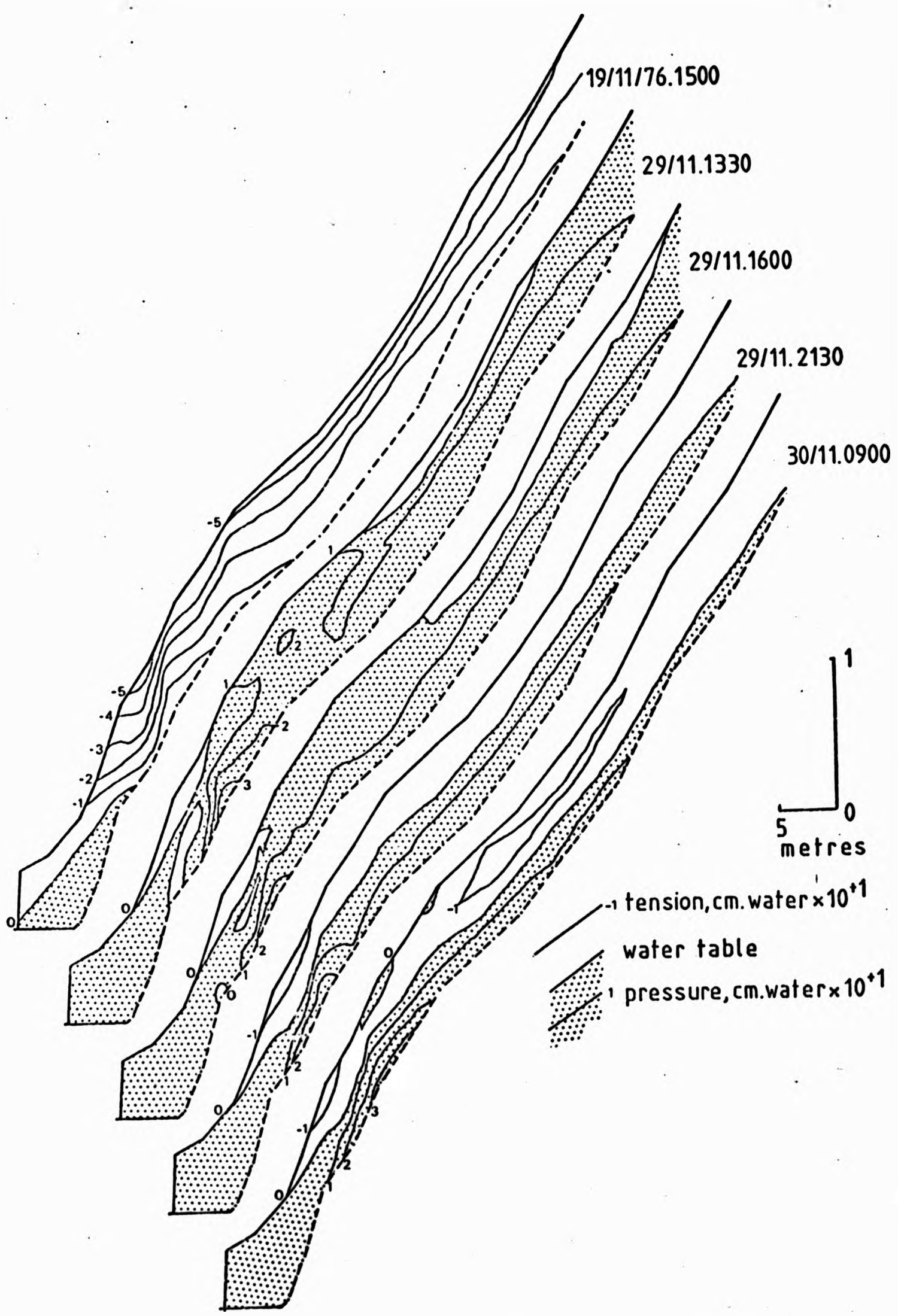

FIGURE 11.7: PATTERNS OF PORE WATER PRESSURE IN THE SLOPE 19 NOVEMBER - 7 DECEMBER 1976

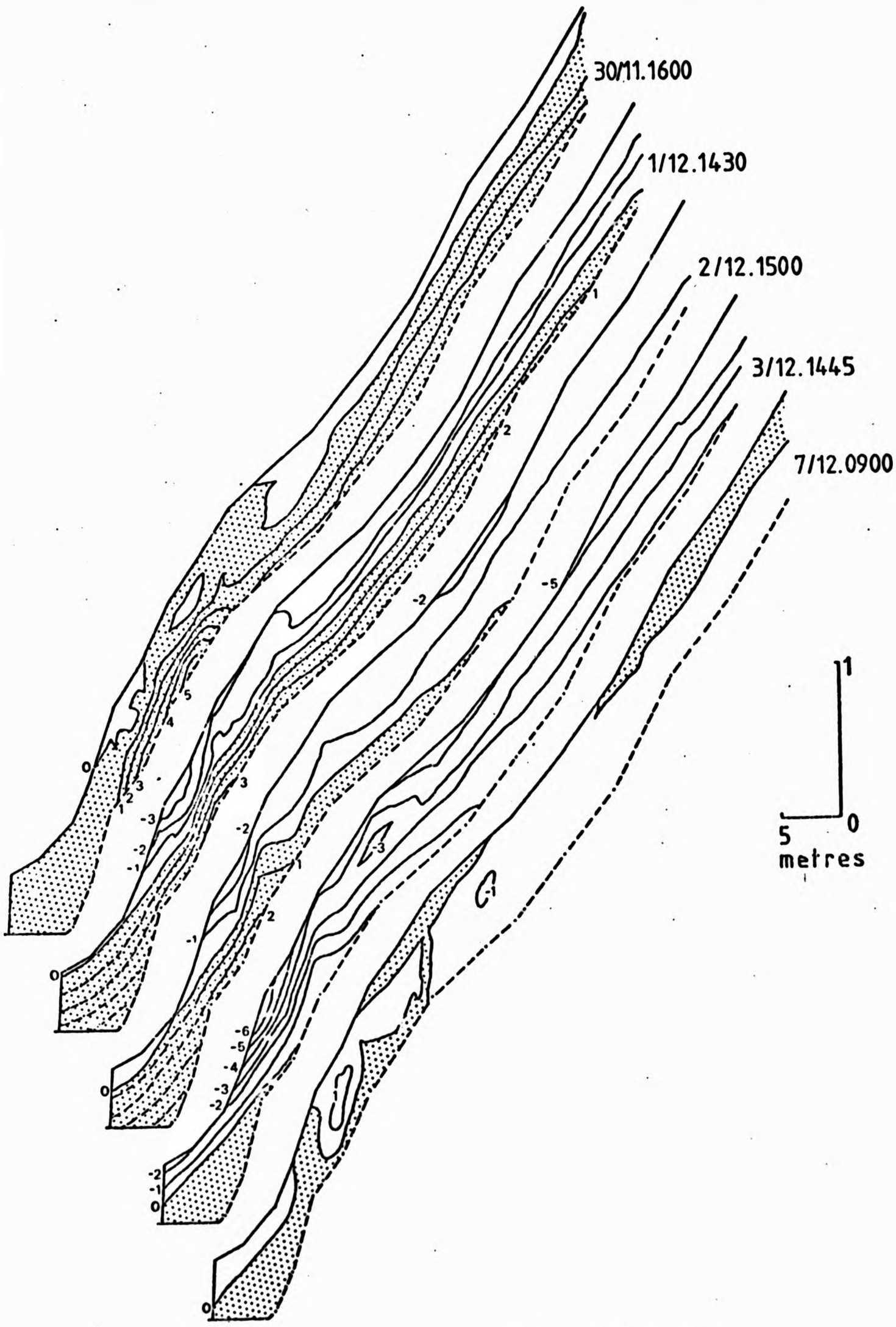

FIGURE 11.7 (cont'd):

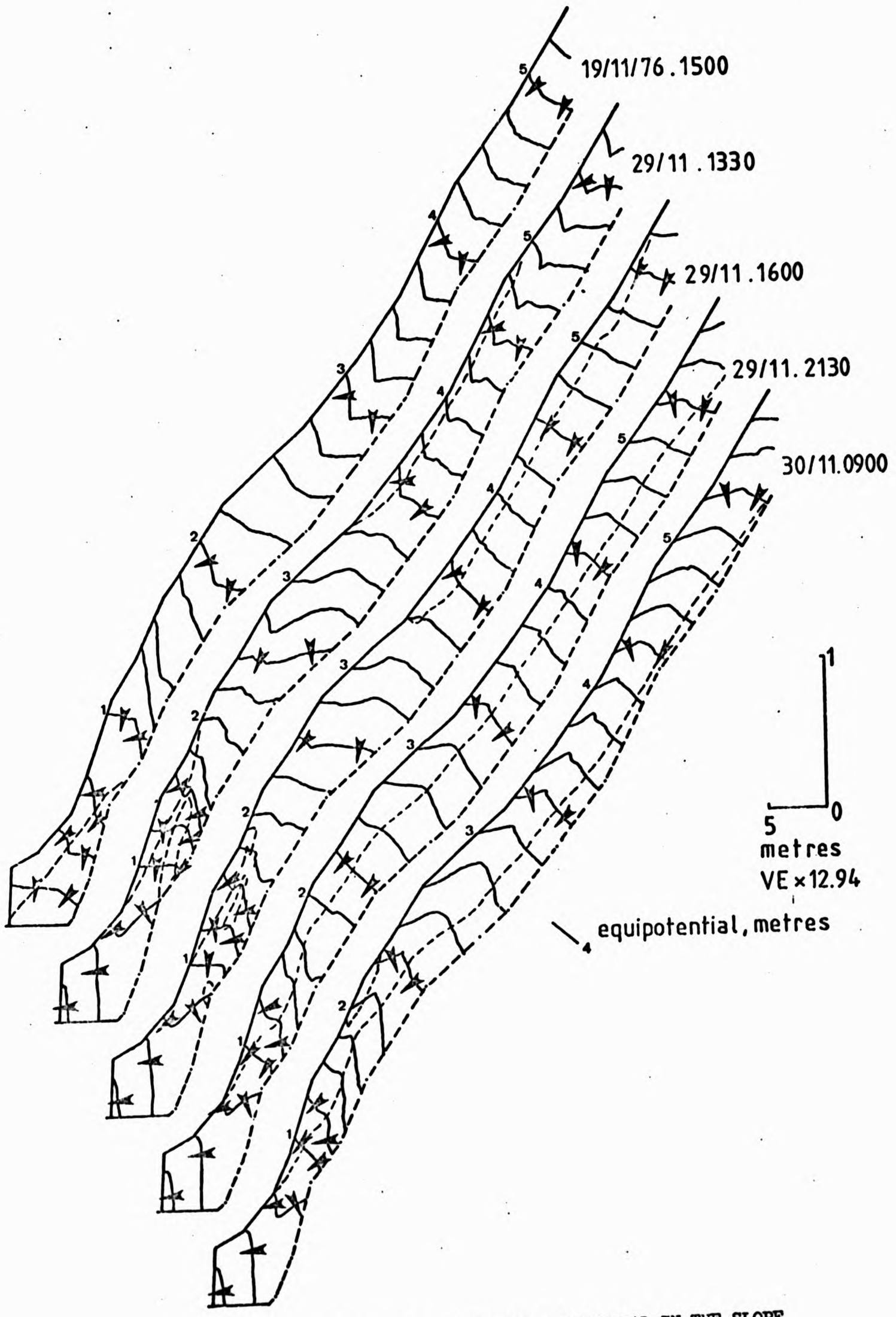

FIGURE 11.8: PATTERNS OF HYDRAULIC POTENTIAL IN THE SLOPE
19 NOVEMBER - 7 DECEMBER 1976
(arrow indicates direction of flow)

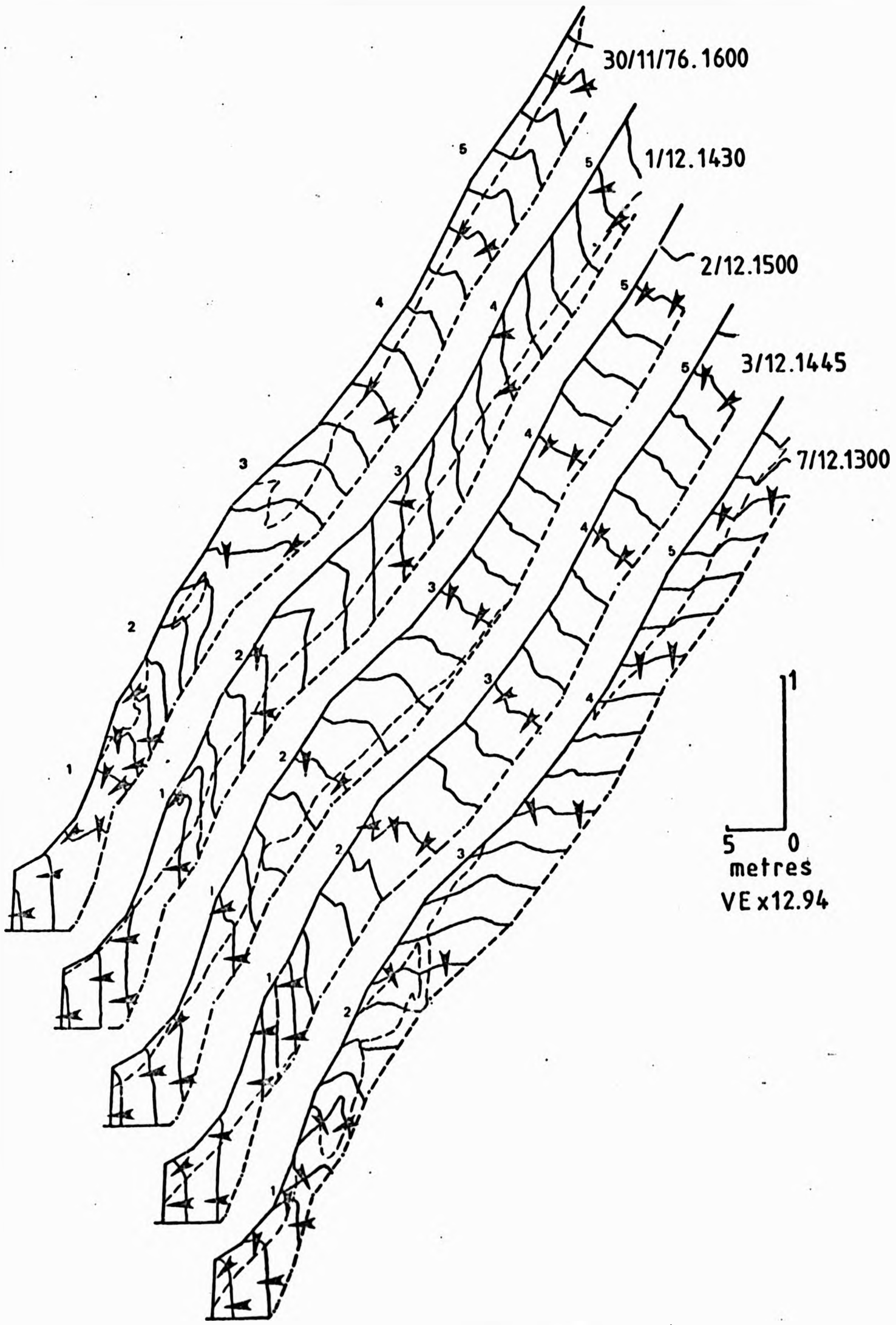

FIGURE 11.8 (cont'd)

vertical unsaturated flow upslope of the convexity. This agrees with the empirical findings of Weyman (1973) and simulations of Beven (1977a, 1977b). However, the disagreement with these and other published works lies in the upslope extent of the saturated zone. This effect is thought to be due to a relatively high resistance to downslope flow between 14 and 24 m upslope, and possibly to low subsoil hydraulic conductivities in the soil above about 40 m. These factors would also induce upward saturation from the profile base before upslope saturation due to movement of the saturated wedge.

(v) At 0900, 30th November 1976, rain was again falling. A wetting front, saturated in two parts, can be seen on its way downprofile. At this time it served to reinforce the vertical supply to the saturated zone below which, 19½ hours after the cessation of rainfall, still extended 50 m upslope.

(vi) By 1600, 30th November 1976, the water table had risen in response to a further 22.6 mm rainfall. Surface or near-surface saturation is again evident adjacent to the channel and below the slope convexity. In the latter case a pronounced 'pressure-hump' had built up at the profile base, possibly in response to convergence of vertical flow and 'rotational' flow from upslope.

(vii) Between 1st December and 6th December the picture is essentially one of drainage, the saturated zone gradually diminishing. The flow pattern does not alter significantly over this period.

(viii) By 0900, 7th December 1976, a further 16.8 mm rain had fallen, 12 mm the previous day. The pattern of infiltration as rain fell at 0900, 7th December 1976, is complex, showing the progress of a wetting front in three areas. The unusual 'strand' of saturated soil below the convexity may be due to a frost-affected reading. The saturated zone was again starting to build upslope.

II. Solute Movement

Samples taken from the soil during these storms were analysed by AAS for K^+ and Mg^{2+} concentrations using the techniques described in Chapter 5. The data were contoured using the program CONCHEM 2 (Appendix 2).

(a) Potassium concentration (Figure 11.9)

(i) Preceding the storm (1510, 19th November 1976) K^+ concentrations were highest 9 - 14 m upslope, decreasing downprofile. The slope convexity was an area of lower K^+ concentration. K^+ concentrations at the base of the saturated wedge were only slightly higher than that measured at W1. The dissolved K^+ distribution of the soil water can be seen broadly to agree with that which would be expected from the Ex.K^+ distribution of the soil (Figure 11.2A).

(ii) With the onset of rain (1230, 29th November 1976), near surface concentrations of K^+ had increased, probably due to the solution of Ex.K^+ suggested by Figure 11.2A. Again the convex slope has lower concentrations. The contour patterns suggest that some of the higher K^+ water from up profile is beginning to move downslope with lateral flow. K^+ concentrations in saturated soil near the slope base were particularly high, but decreased upslope and downprofile. This also correlates quite well with the Ex.K^+ distribution of Figure 11.2A and must represent the primary source of K^+ for increasing concentrations at W1 during the storm.

(iii) After the cessation of rainfall (1630, 29th November 1976), the high K^+ zone, formerly centred near the surface about 14 m upslope, had moved downprofile and downslope. The shape of the concentration cloud, attenuated downslope, was probably controlled by dispersion and hydraulic conductivity. Attenuation of upper slope concentrations was pronounced due to lateral flow. Adsorption was also likely to have affected concentrations and it is noticeable that the core concentration had decreased from 12 mg/l to 6 mg/l since 1230, 29th November 1976. The near channel surface concentration was still quite high, although subsurface concentrations had decreased slightly.

(iv) By 2300, 29th November 1976, the K^+ cloud had continued to progress downslope, but had then turned downprofile at the point where K_z was found to be high. A considerable re-distribution of K^+ contours had occurred upslope, either due to flow under the slope convexity or solute adsorption.

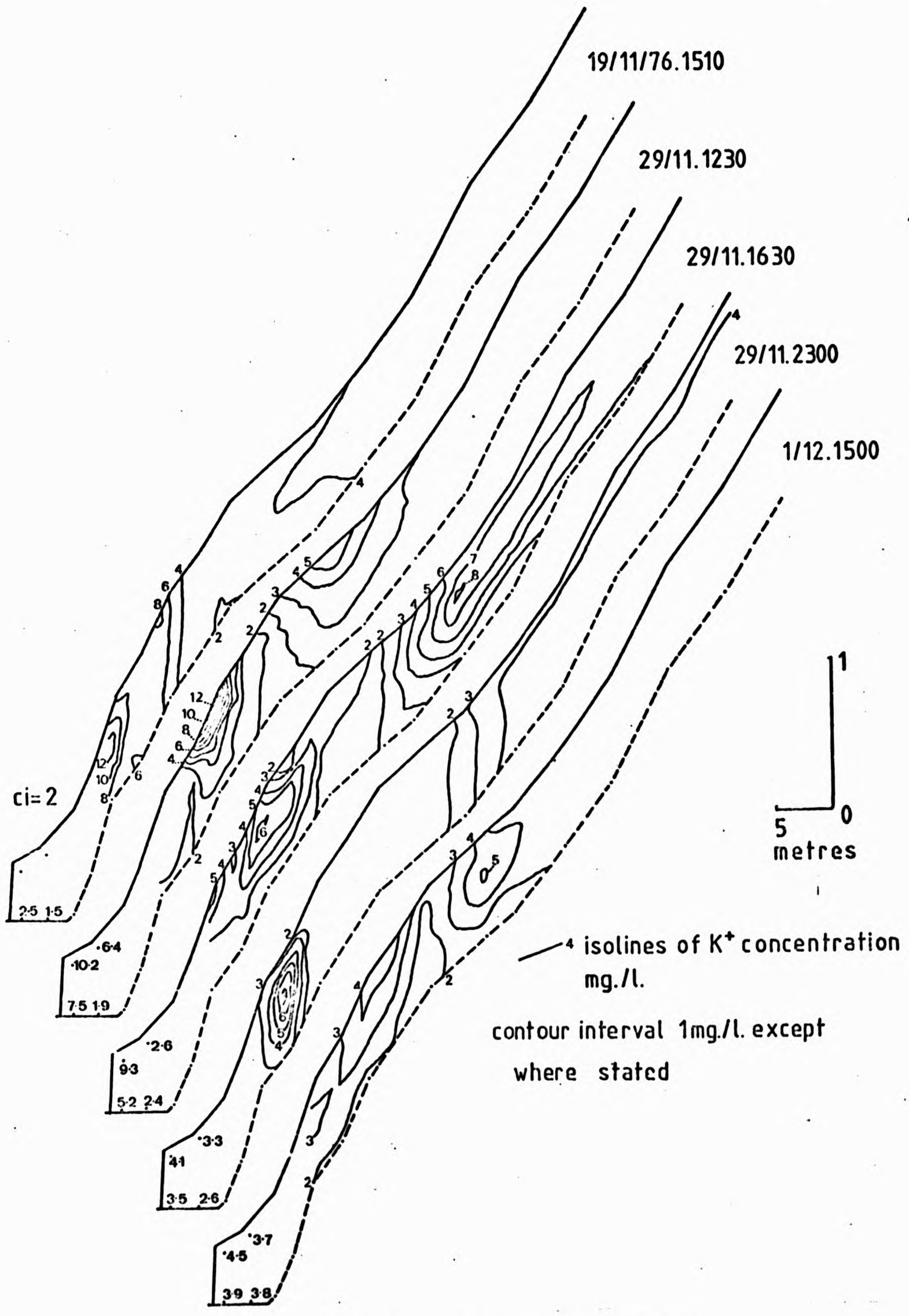

FIGURE 11.9: PATTERNS OF SOIL WATER POTASSIUM CONCENTRATION IN THE SLOPE, 19 NOVEMBER - 1 DECEMBER 1976

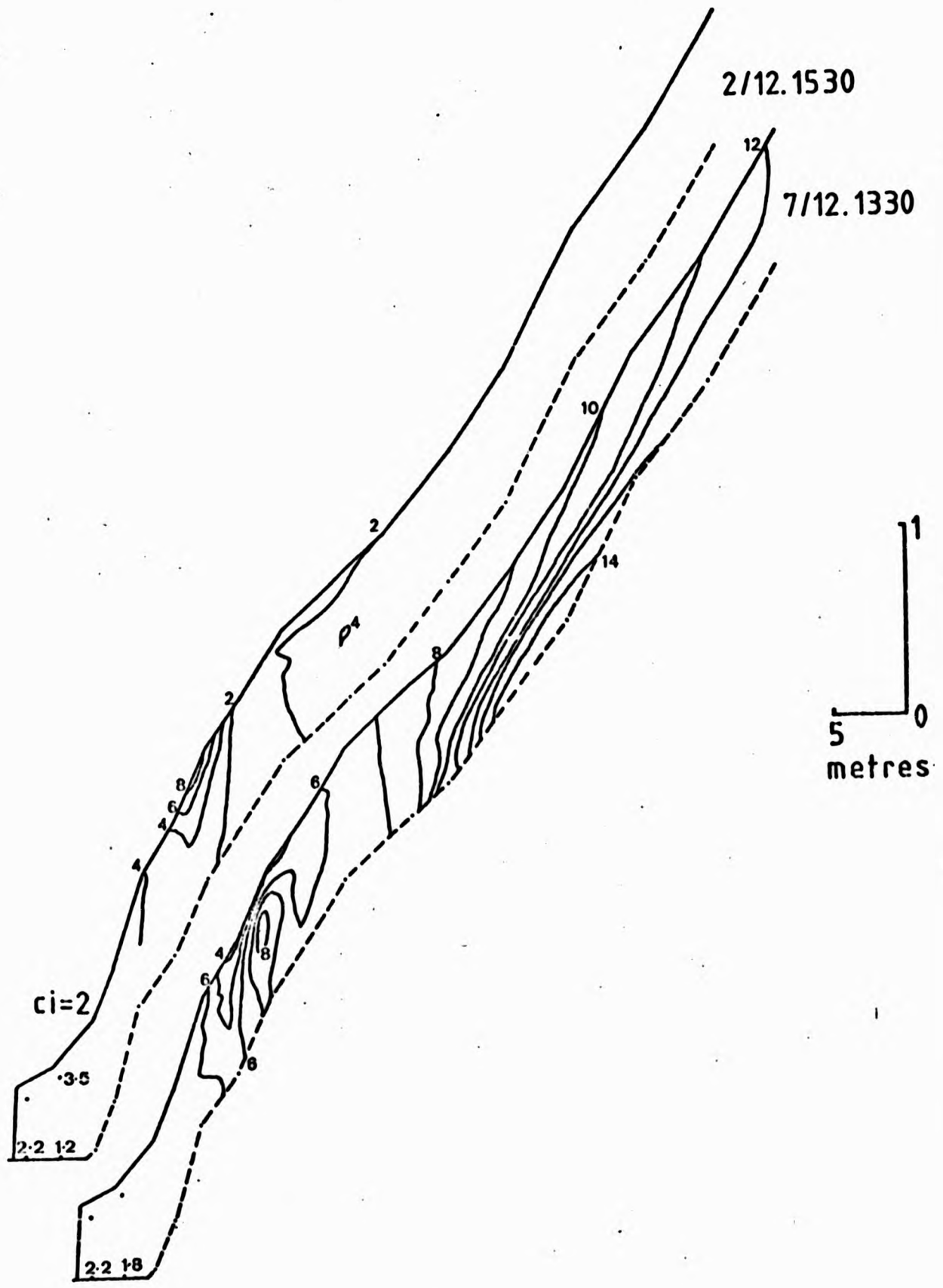

FIGURE 11.9 (cont'd)

(v) K^+ soil water concentrations were noticeably reduced after the storm due to leaching, transport and adsorption (1500, 1st December 1976). The return to high K^+ concentration at 1530, 2nd December 1976, may represent the sampling of high concentration residual water from smaller pores, since the soil was then unsaturated.

(vi) With the return of rainfall and infiltration, 1330, 7th December 1976, K^+ cloud movement is again evident. Upslope concentrations were also high, in better agreement with K^+ exchange capacities.

(b) Magnesium concentration (Figure 11.10)

Concentrations were 5 - 10 times higher than those in stream water and there is a poor visual correlation with the pattern of Ex.Mg^{2+} (Figure 11.2C). Concentration decreases in the saturated zone adjacent to the stream, possibly due to Mg^{2+} adsorption. It is not clear why high concentration zones appear and disappear over short periods of time; flow velocities are certainly not high enough to allow complete solute removal. Again, solute adsorption may provide the answer.

Thus, although some pattern similarities exist with the K^+ concentration diagrams due to possible inconsistencies in the data, it was decided not to attempt a detailed explanation of processes.

III. Discussion

Figure 11.6 shows the timing of flow and solute concentration over the period. The storm of 29th November 1976 produced a very rapid response at W1, typical dilution of Mg^{2+} and concentration of K^+. Both cations exhibited considerable fluctuation during the recession phase of the storm, which could be explained in terms of the arrival of solute pulses from upslope source areas.

Throughflow was also sampled at the pit during this storm, the hydrograph being shown in Figure 11.6. Flow slowly increased as a result of the 28th November 1976 storm, rose rapidly in response to the 29th November 1976 storm, but did not peak until about 14 hours after streamflow. Further rainfall on 30th November 1976 resulted in a less

(v) K^+ soil water concentrations were noticeably reduced after the storm due to leaching, transport and adsorption (1500, 1st December 1976). The return to high K^+ concentration at 1530, 2nd December 1976, may represent the sampling of high concentration residual water from smaller pores, since the soil was then unsaturated.

(vi) With the return of rainfall and infiltration, 1330, 7th December 1976, K^+ cloud movement is again evident. Upslope concentrations were also high, in better agreement with K^+ exchange capacities.

(b) Magnesium concentration (Figure 11.10)

Concentrations were 5 - 10 times higher than those in stream water and there is a poor visual correlation with the pattern of Ex.Mg^{2+} (Figure 11.2C). Concentration decreases in the saturated zone adjacent to the stream, possibly due to Mg^{2+} adsorption. It is not clear why high concentration zones appear and disappear over short periods of time; flow velocities are certainly not high enough to allow complete solute removal. Again, solute adsorption may provide the answer.

Thus, although some pattern similarities exist with the K^+ concentration diagrams due to possible inconsistencies in the data, it was decided not to attempt a detailed explanation of processes.

III. Discussion

Figure 11.6 shows the timing of flow and solute concentration over the period. The storm of 29th November 1976 produced a very rapid response at W1, typical dilution of Mg^{2+} and concentration of K^+. Both cations exhibited considerable fluctuation during the recession phase of the storm, which could be explained in terms of the arrival of solute pulses from upslope source areas.

Throughflow was also sampled at the pit during this storm, the hydrograph being shown in Figure 11.6. Flow slowly increased as a result of the 28th November 1976 storm, rose rapidly in response to the 29th November 1976 storm, but did not peak until about 14 hours after streamflow. Further rainfall on 30th November 1976 resulted in a less

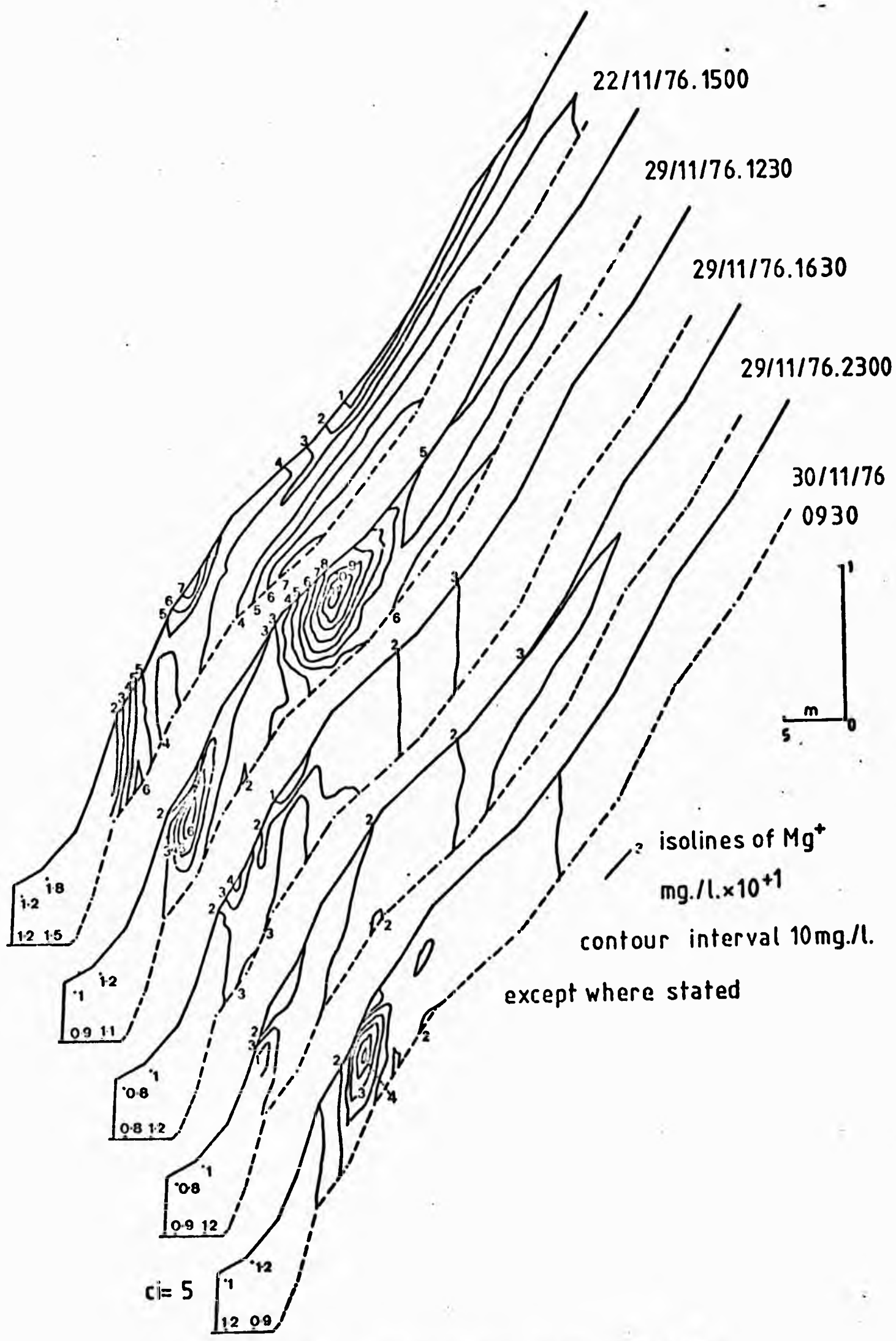

FIGURE 11.10: PATTERNS OF SOIL WATER MAGNESIUM CONCENTRATION IN THE SLOPE, 22 NOVEMBER - 7 DECEMBER 1976

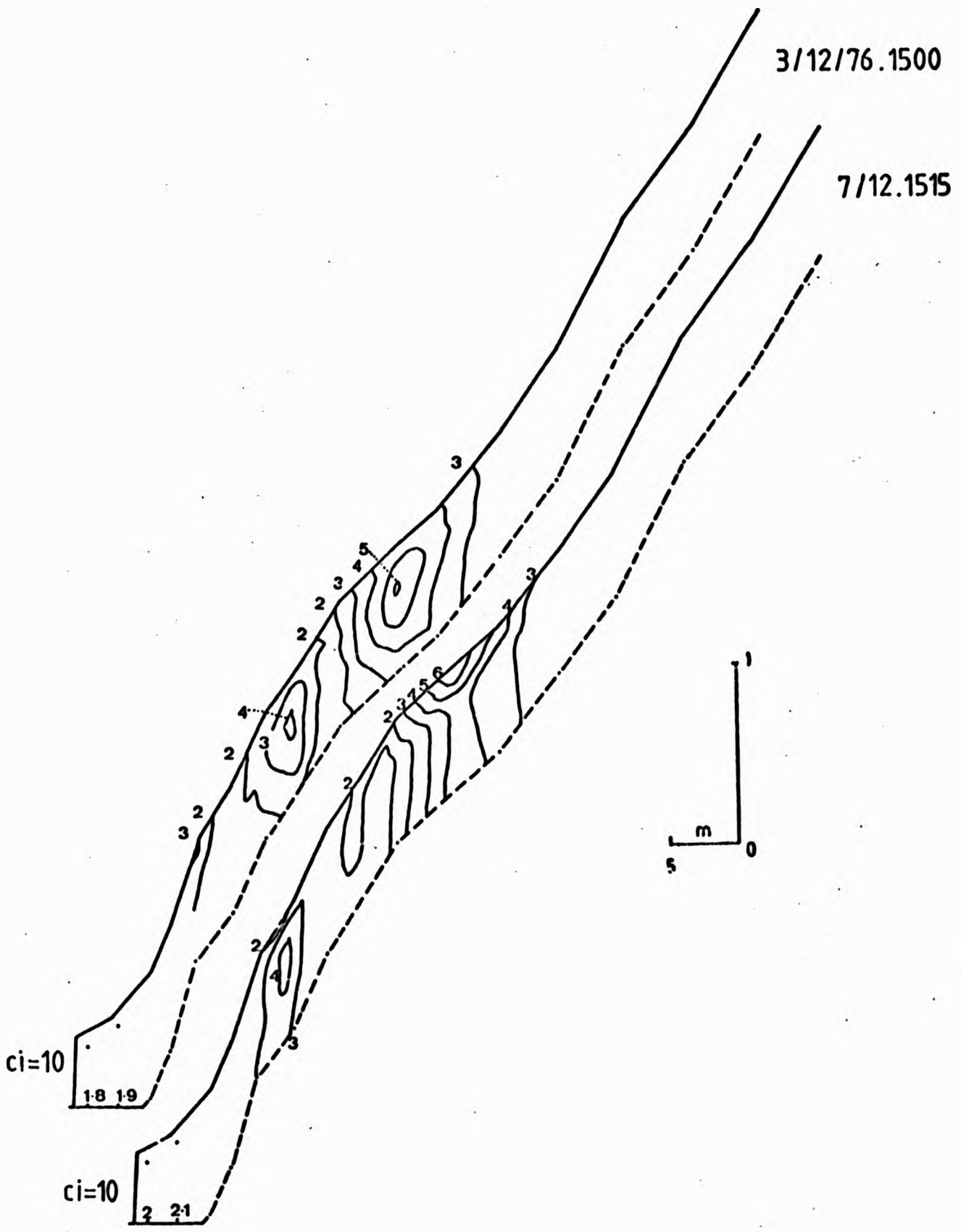

FIGURE 11.10 (cont'd)

peaked streamflow hydrograph, although this time the pit throughflow peak was higher and delayed by only seven hours, due to the already saturated soil. Overland flow was observed below but not above the pit. These results suggest that throughflow from upslope of 7 m can only contribute water and solutes to recession phases, (assuming it remains as throughflow), and that peak flow is primarily derived from surface and/or subsurface flow adjacent to the channel. A useful comparison can be made with the same hydrographs recorded in Bicknoller Combe, Somerset (Anderson and Burt, 1978)(Figure 11.6). There, a combination of soils and topography combined to produce a relatively small storm runoff peak but a large, delayed throughflow hydrograph, accentuated by further rainfall. D R Weyman (1974) obtained similar results for the same soil series (1 - 2 m deep, freely draining brown earths above Old Red Sandstone) on the nearby Mendip Hills. The throughflow delay at Bicknoller Combe was more pronounced due to the effect of side-slope hollows. Clearly the shallower West Walk soils with an absence of sideslope hollows are important in confining the upslope throughflow contribution to recession phases. The response of Mg^{2+} and K^{+} concentrations in pit throughflow showed dilution and concentration respectively, the peaks also being delayed with respect to streamflow.

There was a major recurring problem with throughflow discharge measured at the pit, in that it disagreed with saturated throughflow computed from Darcy's Law.

Saturated throughflow could be calculated from:

$$Q = W.\sin\theta \int_{Z=0}^{Z=h} K_{xz}.dz \qquad (11.13)$$

(Weyman, 1973) where w = slope width, m

θ = water table slope

Z = height above slope base, m

h = water table above Z_0, m

K_{xz} = saturated hydraulic conductivity, m/s,

calculated as a vector at the pit, but assumed horizontal at P1, adjacent to the stream.

Measured pit discharge is shown to be up to four orders of magnitude higher than that computed by equation 11.13 (Figure 11.11). This could be explained in either or both of two ways.

Firstly, as noted earlier, laboratory determinations of K could be unrepresentative of the soil mass, representing only flow through small pores and omitting the wider spaced cracks and root tubes. The major argument against this is that where samples including fissures and cracks were used the results fitted in well with the general pattern of conductivity (Figure 11.5). That is, the density of macropores was high enough to be described by the permeameter results.

Secondly, measured throughflow might have included water from diagonally above the pit, induced toward the pit by the artificial "drawdown" effect. Usually under such circumstances, the effect would be to reduce flow into the pit (Knapp, 1973) due to the artificial incursion of unsaturated conditions. Furthermore, at West Walk, an increase in saturated hydraulic gradients adjacent to the pit would have been more than offset by the downprofile decrease in measured K.

Close investigation of the pit face revealed the emergence of water from two macropores in the same way that water "bubbles" from underground springs. The emergence was from the bottom of the face, suggesting a piezometric surface just above the base of the pit. Under such conditions water could have been confined by the low conductivity clay, only able to emerge from local macropores, (which it would also tend to enlarge). Thus the measured pit discharge could not have represented true discharge from the one metre wide slope soil (see Figure 11.12). Although this explanation is only tentative it leads to the general conclusion that soil pits create more problems than they solve, an opinion shared by others working in the same field (e.g. Waylen, pers. comm. 1975).

Thus, the slope of the measured throughflow hydrograph with associated Mg^{2+} and K^{+} response, shown in Figures11.6 and 11.11 is probably more typical of deeper subsurface flow than it is of the soil profile. Computed throughflow hydrographs at the pit and P1 (1.25 m from the stream) show a more peaked response in time with the stream, although still contributing significantly to stream recession. The

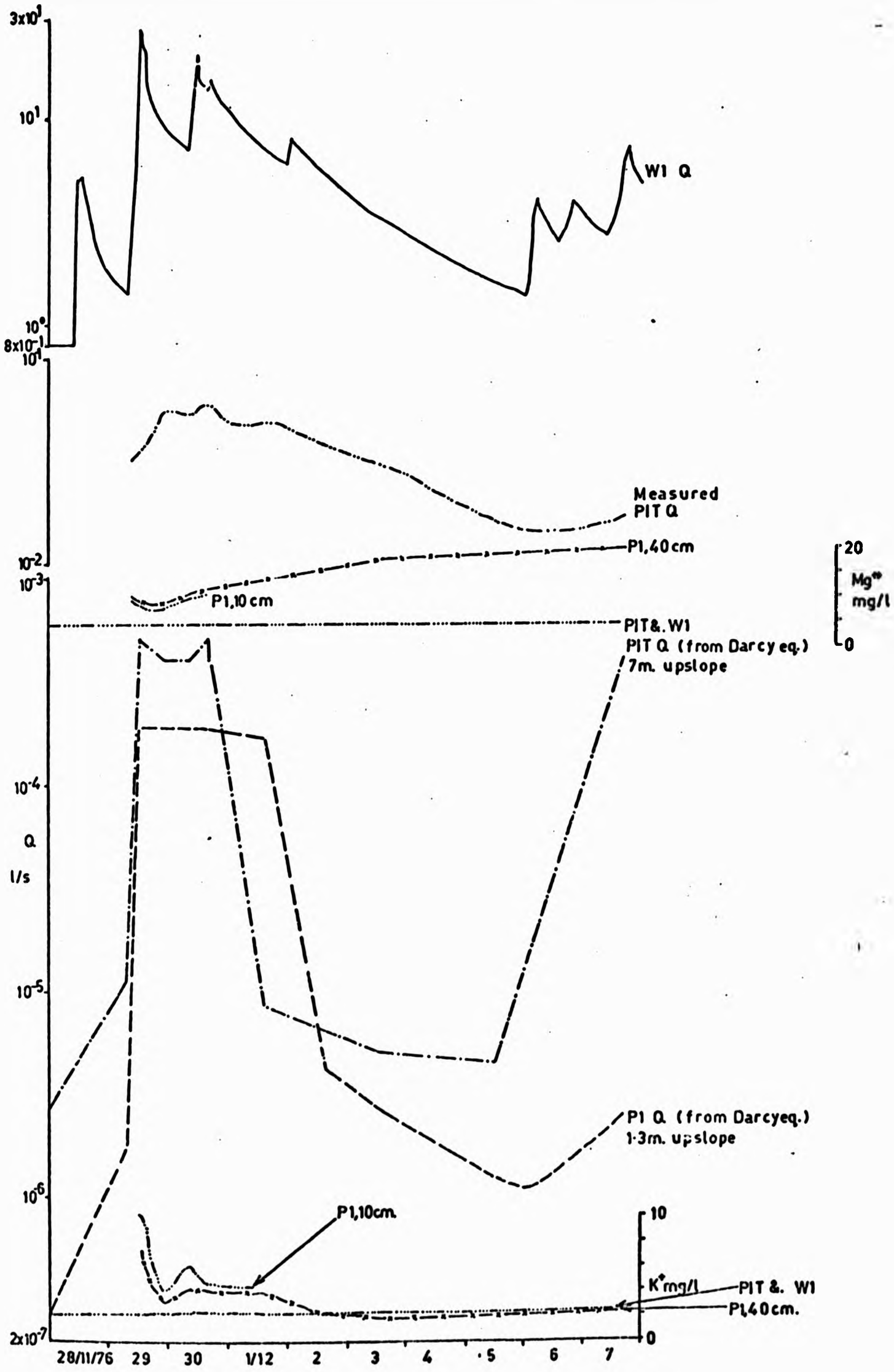

FIGURE 11.11: MEASURED AND COMPUTED SLOPE THROUGHFLOW AND CHEMICAL CONCENTRATIONS, 28 NOVEMBER - 7 DECEMBER 1976

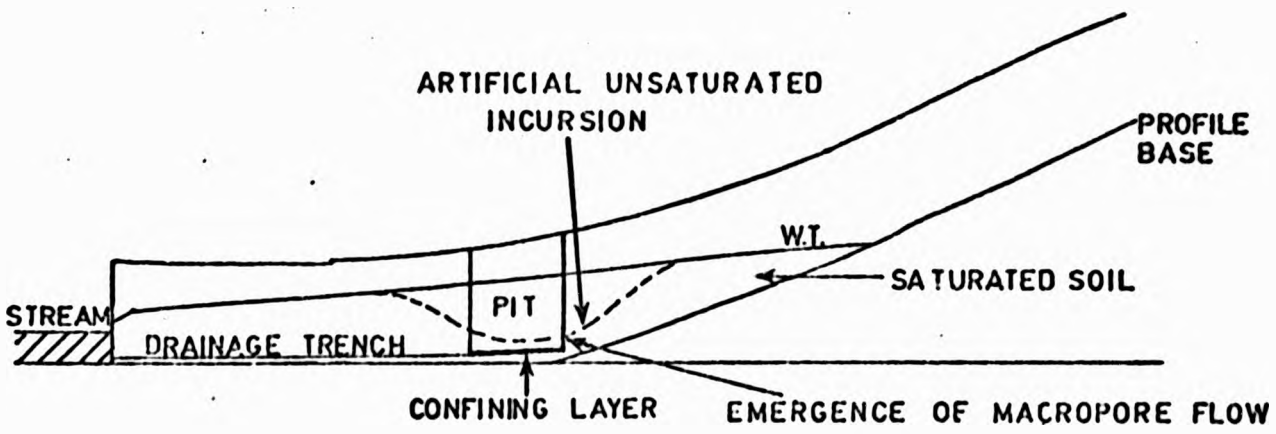

FIGURE 11.12: SIDE VIEW OF THE PIT, ILLUSTRATING DISTORTION OF THE NATURAL PIEZOMETRIC SURFACE AND EMERGENCE OF FLOW FROM LOCALISED MACROPORES

higher computed flow at the pit than at P1 could be purely coincidental or it could indicate the occurrence of saturation excess overland flow near the stream. K^+ concentrations were highest at P1, 10 cm, decreasing downprofile, and decreased from nearly 10 mg/l at the storm peak to about 2.5 mg/l during recession. Dilution of storm concentrations, possibly by overland flow, would have been required to produce the levels recorded at W1. However, it is clear that the direct relationship between K^+ and streamflow is primarily due to the leaching of potassium from near surface soil, particularly near to the channel, in concentrations too high to be diluted by weak solutions (e.g. overland flow or channel precipitation). Mg^{++} showed a slight dilution at P1, 10 cm and 40 cm during the storm, but a gradual rise to about 20 mg/l on 7th December 1976.

Tension or pressure, moisture contents and soil water solute concentrations can also be examined for single profiles to illustrate the processes operating during a storm (Figures 11.13, 11.14 and 11.15). During the pre-storm period tension gradients existed throughout each profile (t=1). The slope had already been affected by rainfall on 28th November 1976, but further rainfall on 29th November 1976 caused a reduction in the gradient, such that the soil was completely saturated 35 cm below the surface at profiles 9.25, 11.5 and 13.9 m upslope. The gradient steepened again during the days following the main storm, primarily due to profile drainage, i.e. tension increased in the upper soil as water moved downprofile and down slope, while pressure increased in the profile base due to the receipt of water from above. As time proceeded equilibrium was reached and the whole profile tended to drain uniformly, leading to a relatively constant tension gradient, moving to the right in Figures 11.13 A - C. This is remarkably similar to the process described by Weyman (1973).

Moisture content also increased with rainfall; the highest contents were in mid profile, decreasing with depth due to reduced porosity. Concentration gradients were rather more variable from profile to profile (this emerged strongly from the contour patterns discussed earlier). In general K^+ concentration tended to increase up profile, in a similar way to that of Ex.K in Figure A3.21. Changes of concentration through time do not follow such an easily recognisable trend as tension and are best viewed as a two-dimensional display to

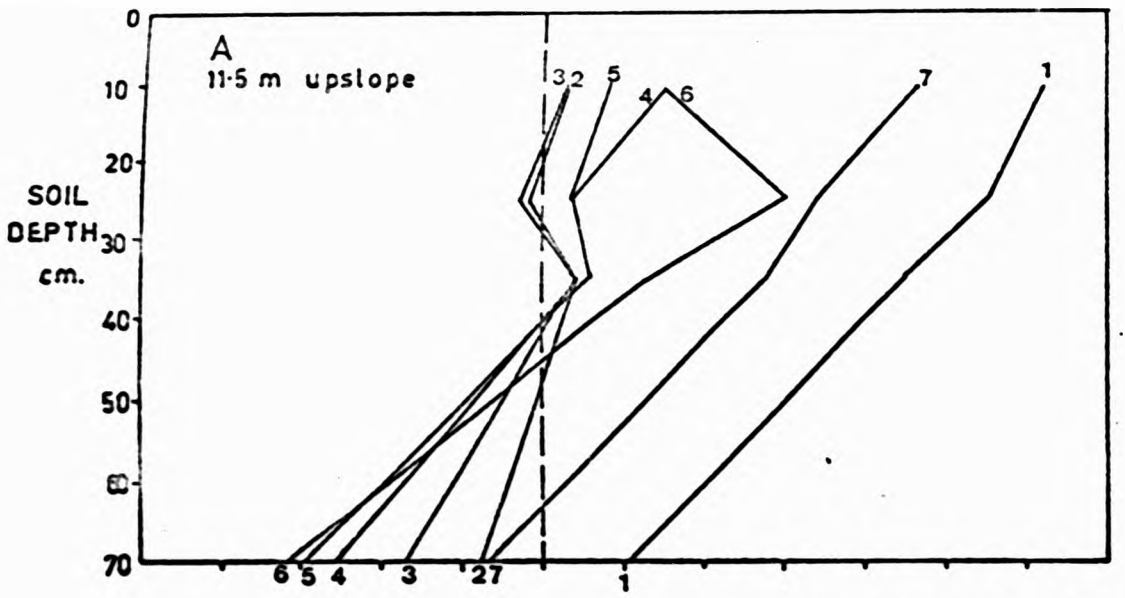

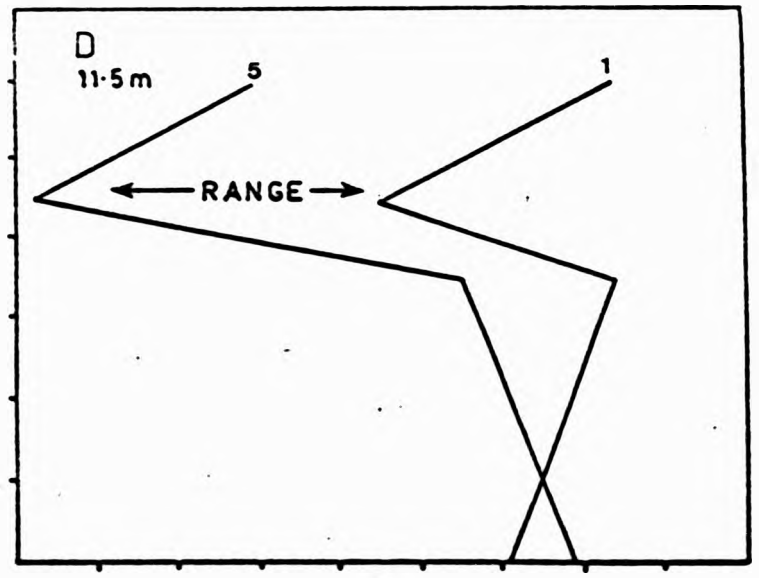

1 = 22/11/76 1420
2 = 29/11 1330
3 = 29/11 1600
4 = 29/11 2130
5 = 30/11 0900
6 = 1/12 1430
7 = 3/12 1445

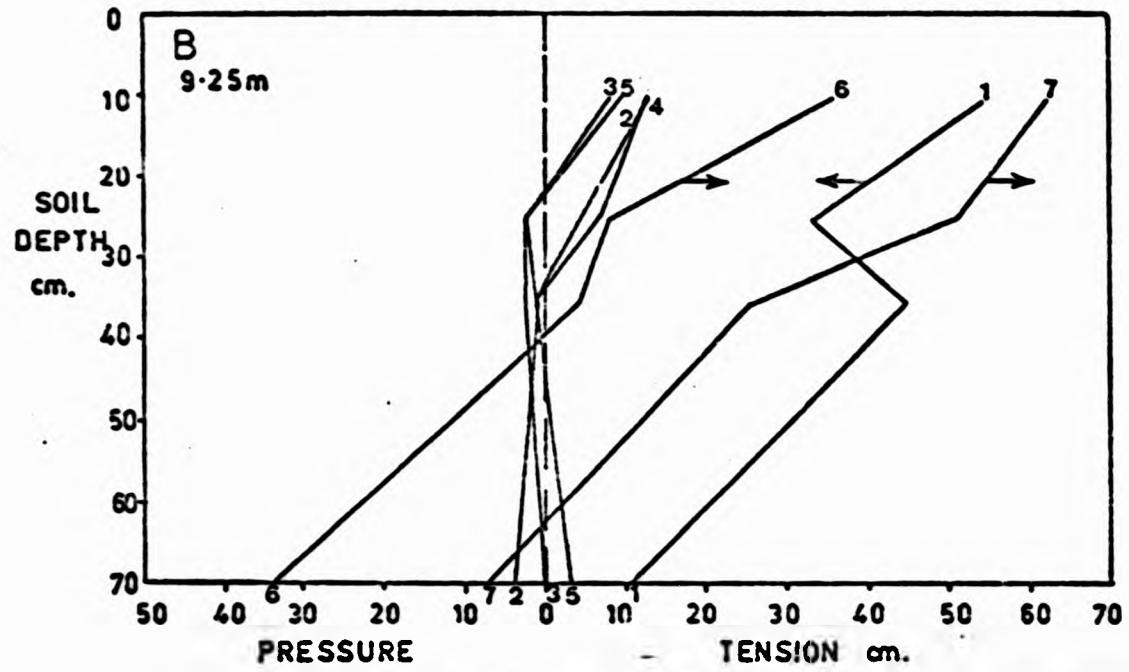

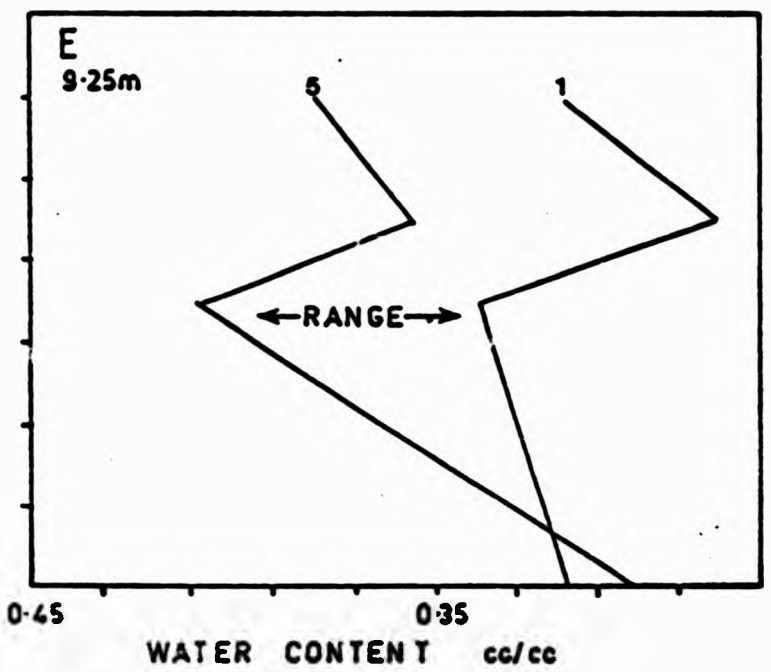

FIGURE 11.13: PORE WATER PRESSURE AND CONTENT FOR SELECTED PROFILES ON THE HILLSLOPE, 22 NOVEMBER - 3 DECEMBER 1976

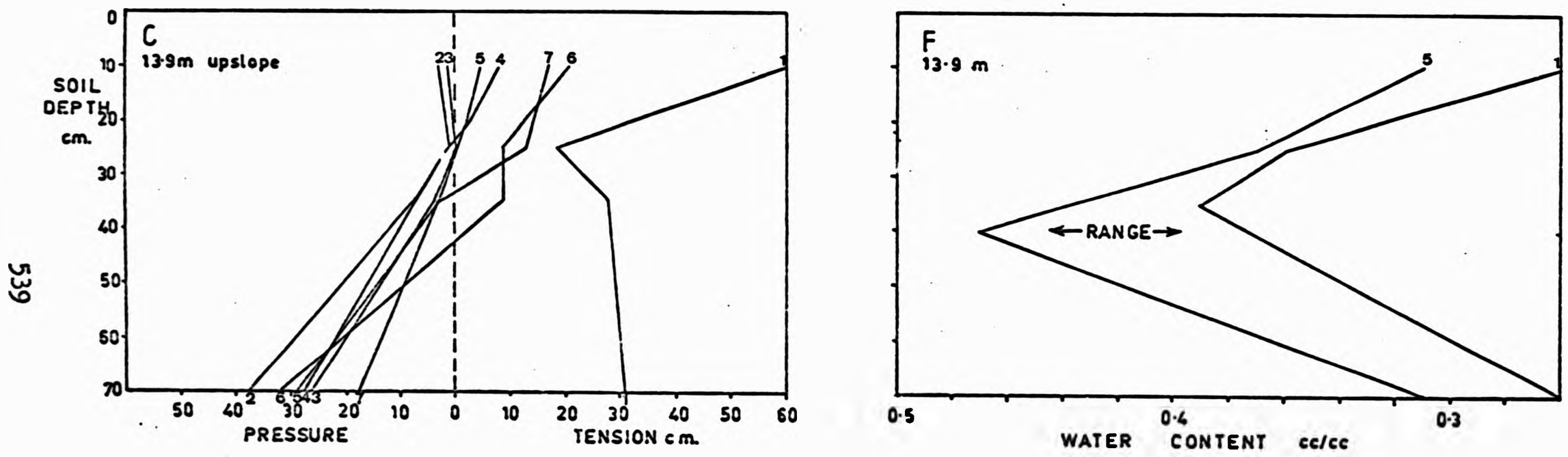

FIGURE 11.13 (cont'd):

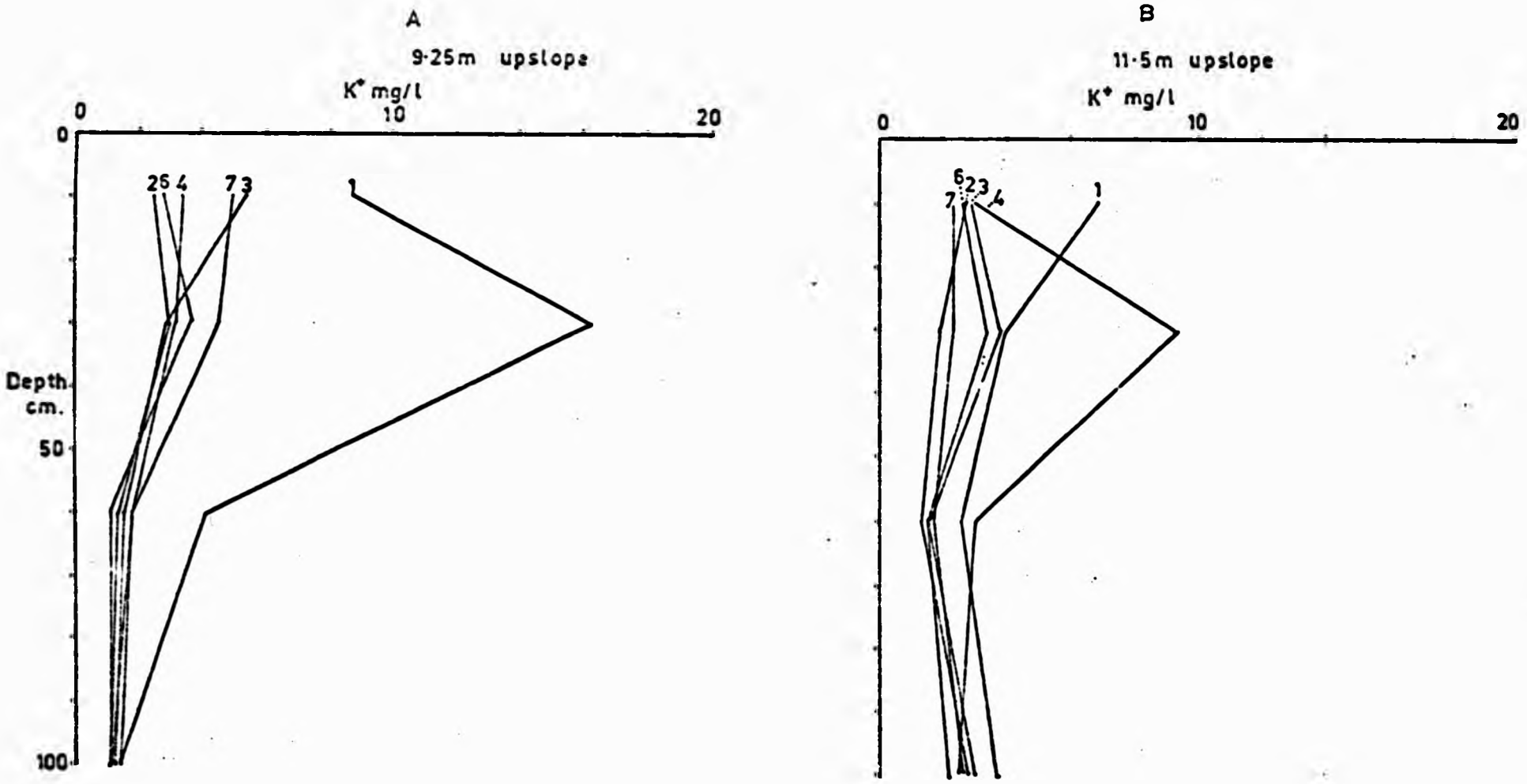

FIGURE 11.14: SOIL WATER POTASSIUM CONCENTRATION FOR SELECTED PROFILES ON THE HILLSLOPE, 22 NOVEMBER - 3 DECEMBER 1976

(for Key, see Figure 11.13)

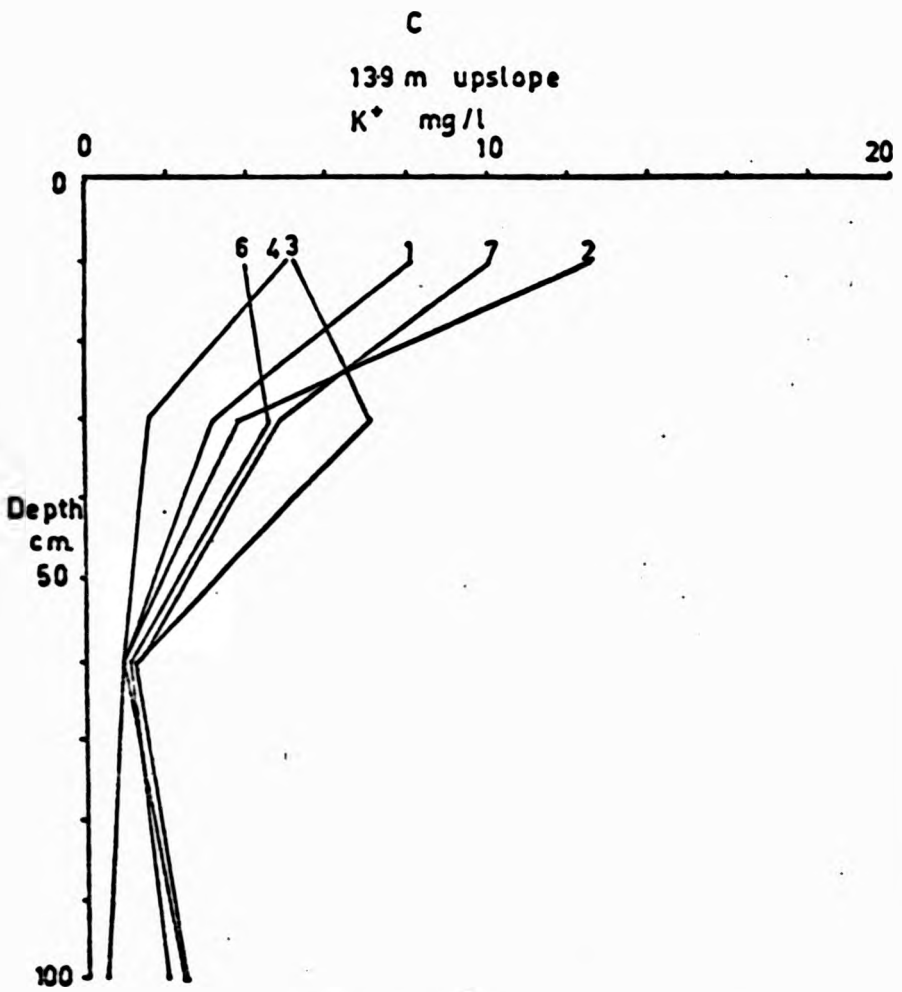

FIGURE 11.14 (cont'd):

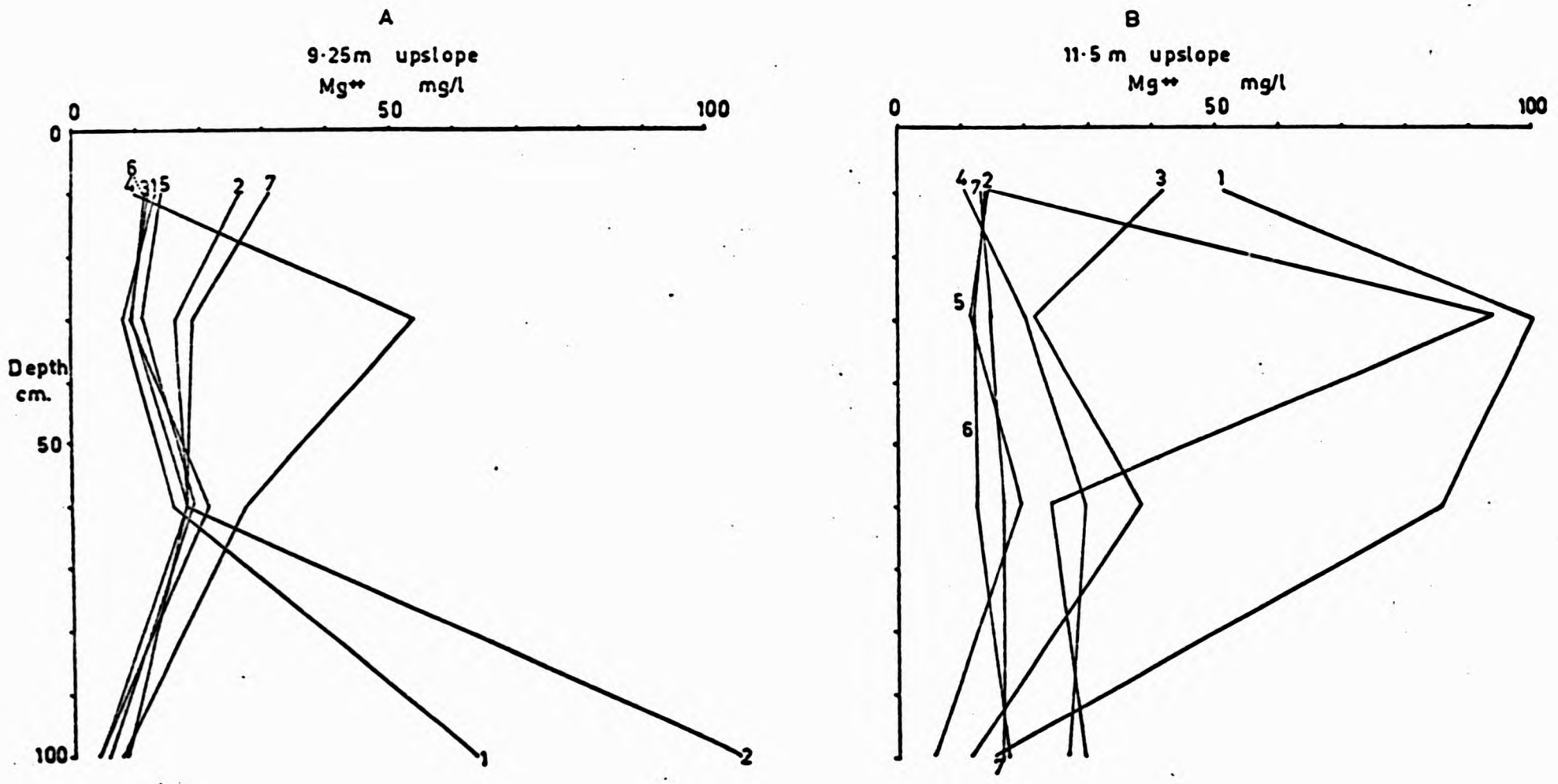

FIGURE 11.15: SOIL WATER MAGNESIUM CONCENTRATION FOR SELECTED PROFILES ON THE HILLSLOPE, 22 NOVEMBER - 3 DECEMBER 1976
(for Key, see Figure 11.13)

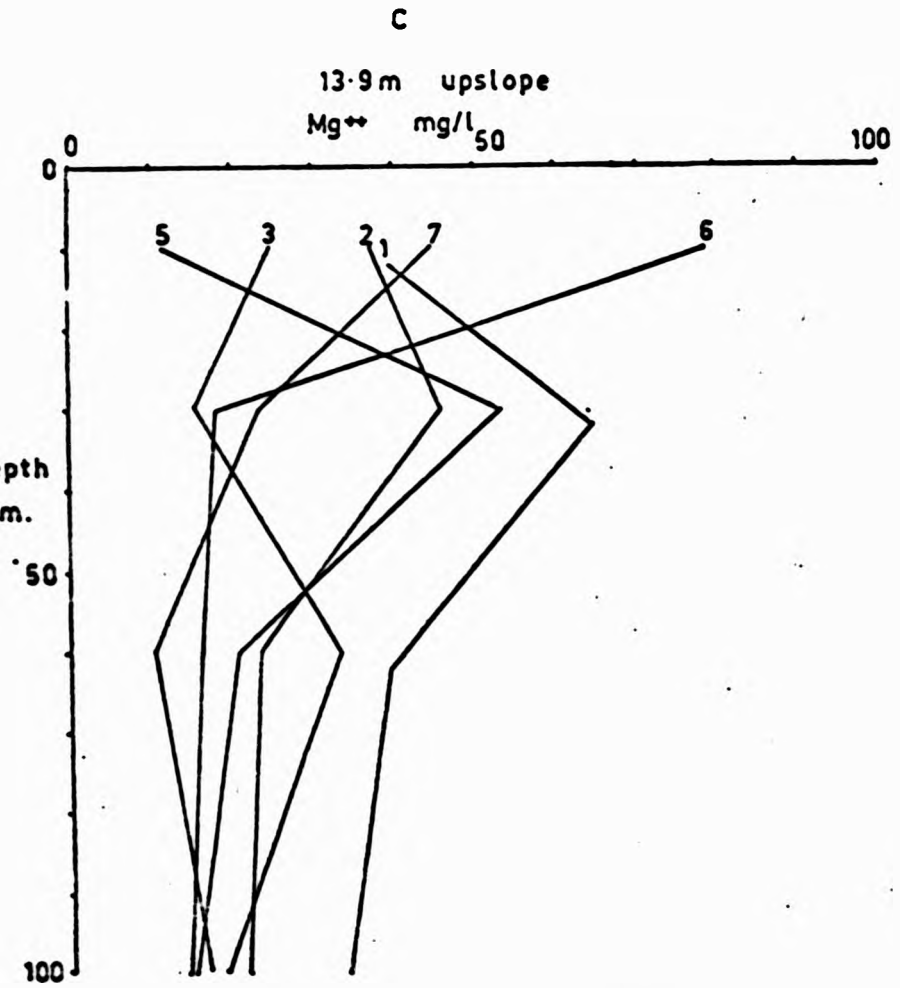

FIGURE 11.15 (cont'd):

identify processes. Figure 11.14 C suggests that leaching of K^+ occurs during rainfall, but that this is then transported from the profile, vertically (T2 to T3) and laterally (see Figure 11.9). Further K^+ can be leached by successive rainfall events. Mg^{++} concentration profiles also reflect exchangeable cation contents (Figure A3.24) particularly during pre-storm and early storm periods (T1 and T2 at 9.25 m upslope), but these are disrupted as flow re-distributes the water vertically and laterally (Figure 11.10).

The patterns on the hillslope of water and solute movement during a storm are summarised at the end of the Chapter.

B. Rainfall and Infiltration:
25th January - 10th February 1977

There were five small hydrographs during this period (Figure 11.16). The saturated wedge expanded upslope in response to the major rainfall inputs (26th January, 3rd February and 10th February 1977) although a curious dip in the pressure/tension contours existed throughout the period at 11.5 m upslope (tensiometer set T2). Closer inspection of all other contour plots shared a similar tendency and, since this is an area of high K_z, it seems likely that it represents relatively rapid vertical drainage.

The equipotentials show very similar features to the 29th November 1976 storm (Figure 11.18). Drainage is essentially lateral towards the stream in the saturated zone, with a supply from the unsaturated soil up-profile and upslope. Downprofile unsaturated flow dominates the convex slope for the whole period. Above this the equipotentials also indicate vertical, downprofile, unsaturated flow, except from 7th February to 10th February 1977 when there is evidence of downslope flow. This presumably occurs as a result of the additional rainfall overloading the vertical flow system.

Soil water samples were analysed for K^+ from 25th January to 29th January 1977 and Ca^{++} from 2nd February to 10th February 1977. The general patterns of K^+ are similar to those for the 29th December 1976 storm with high near surface concentrations, especially above and below the convexity, which again appears deficient

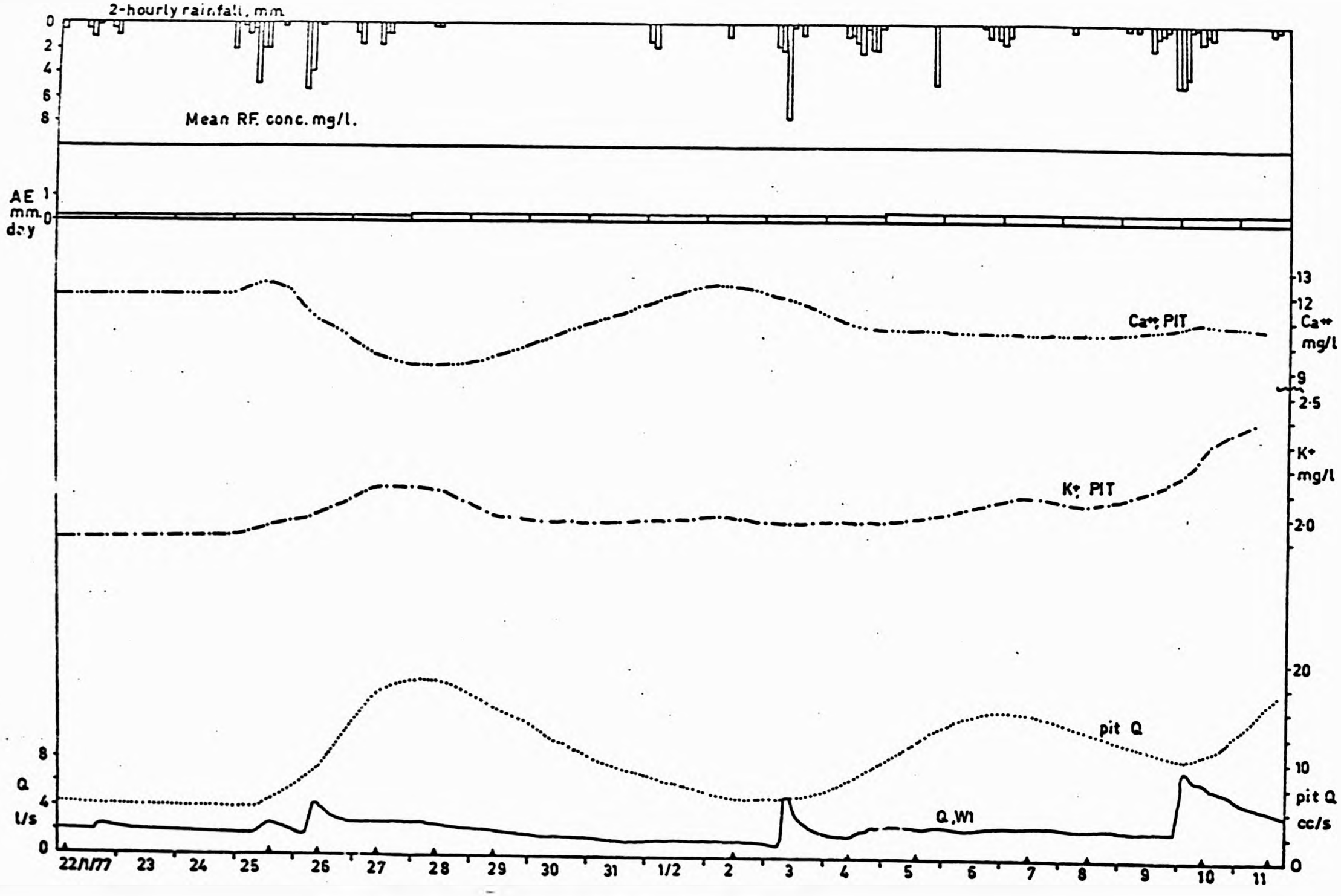

FIGURE 11.16: SUBCATCHMENT 1 AND SLOPE HYDROLOGY,
22 JANUARY - 11 FEBRUARY 1977
(triangles = pit and tension sampling times)

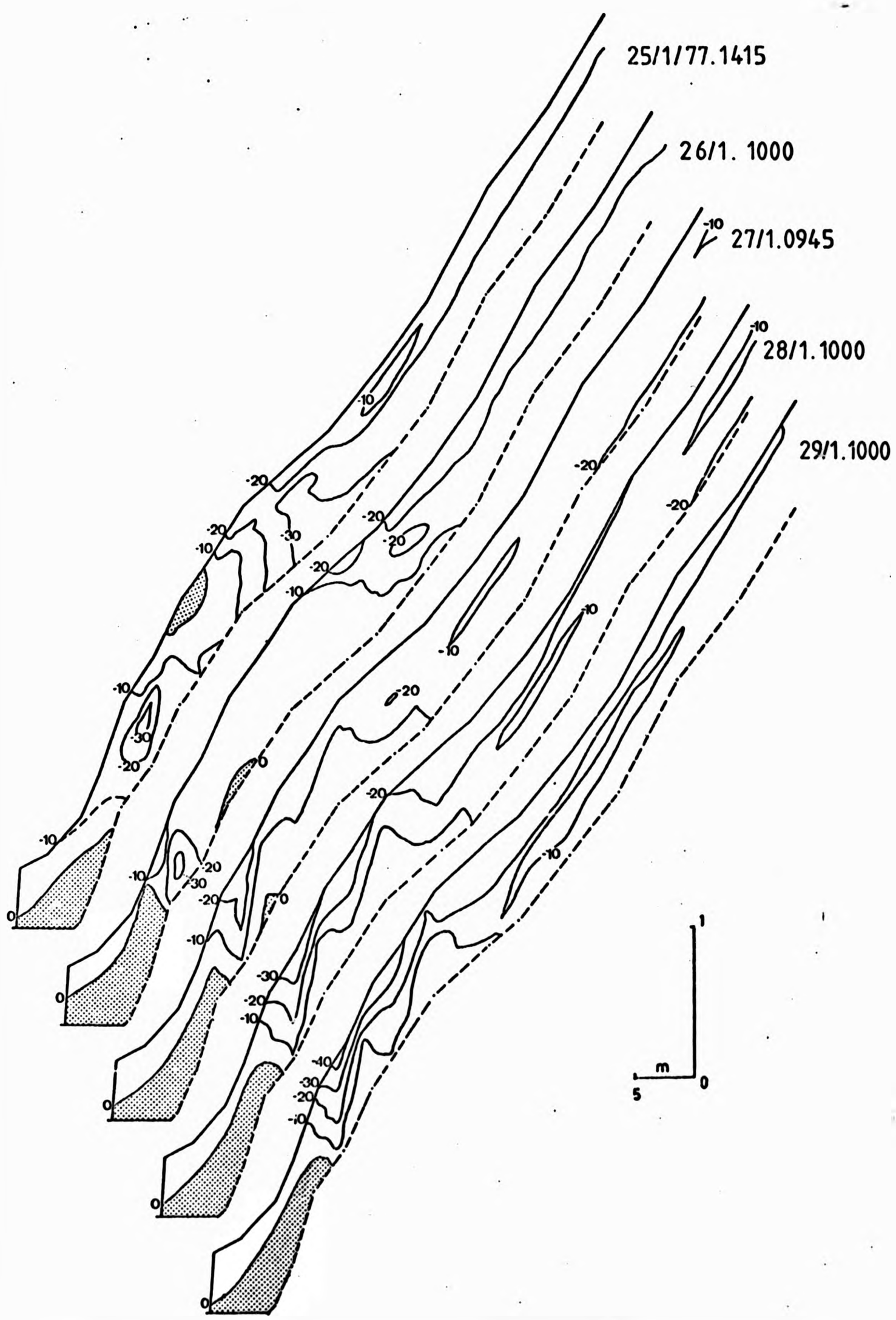

FIGURE 11.17: PATTERNS OF PORE WATER PRESSURE IN THE SLOPE, 25 JANUARY - 10 FEBRUARY 1977

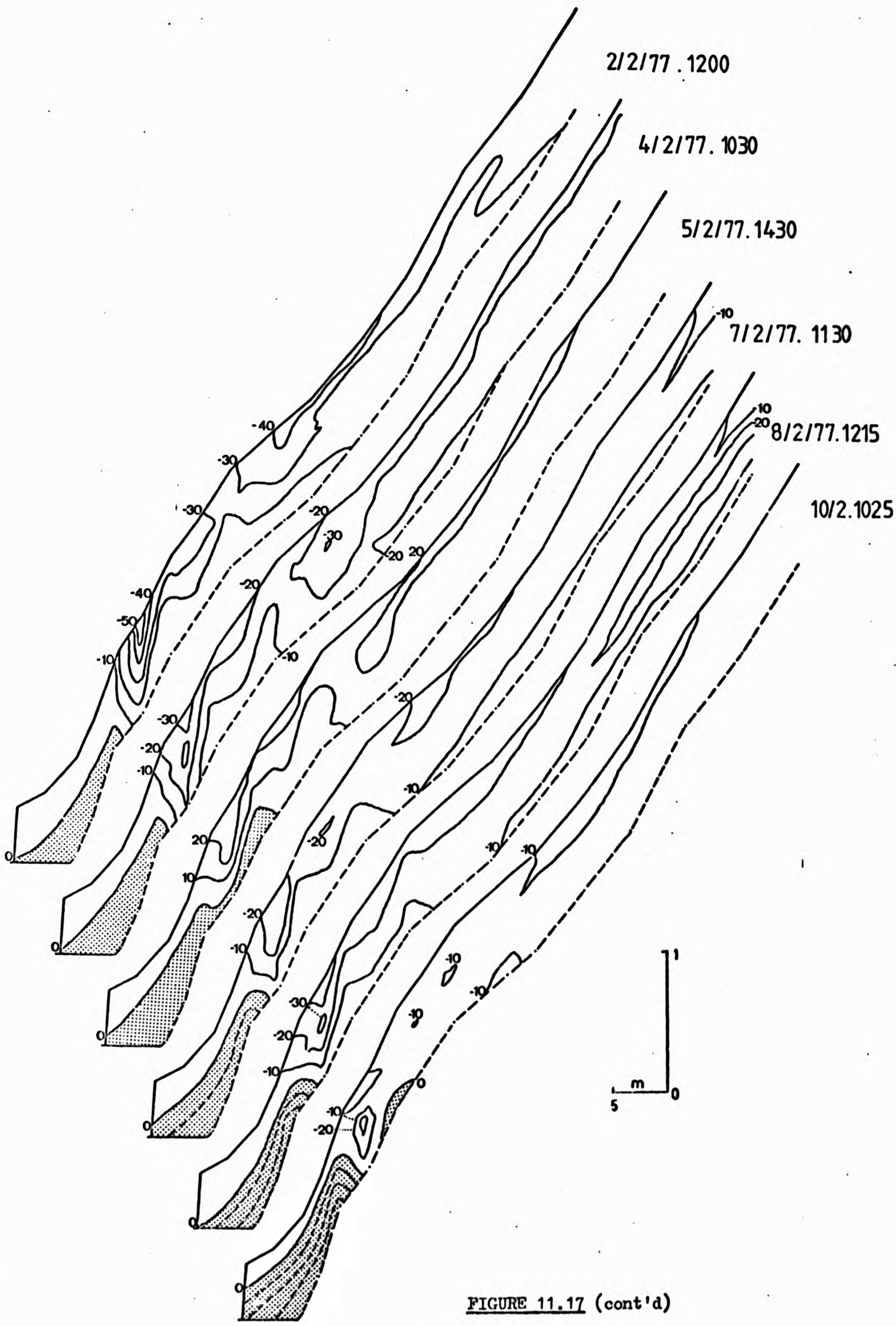

FIGURE 11.17 (cont'd)

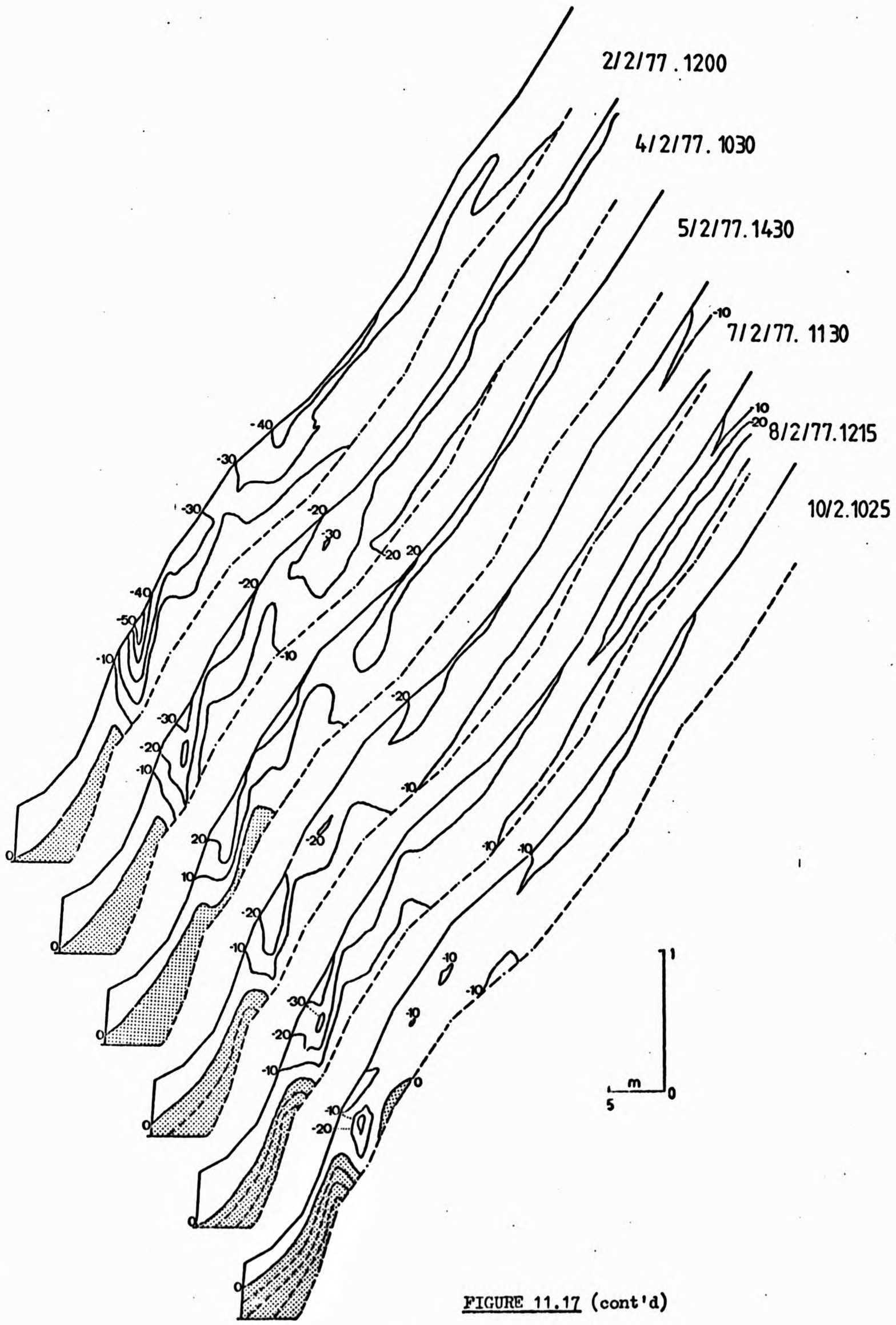

FIGURE 11.17 (cont'd)

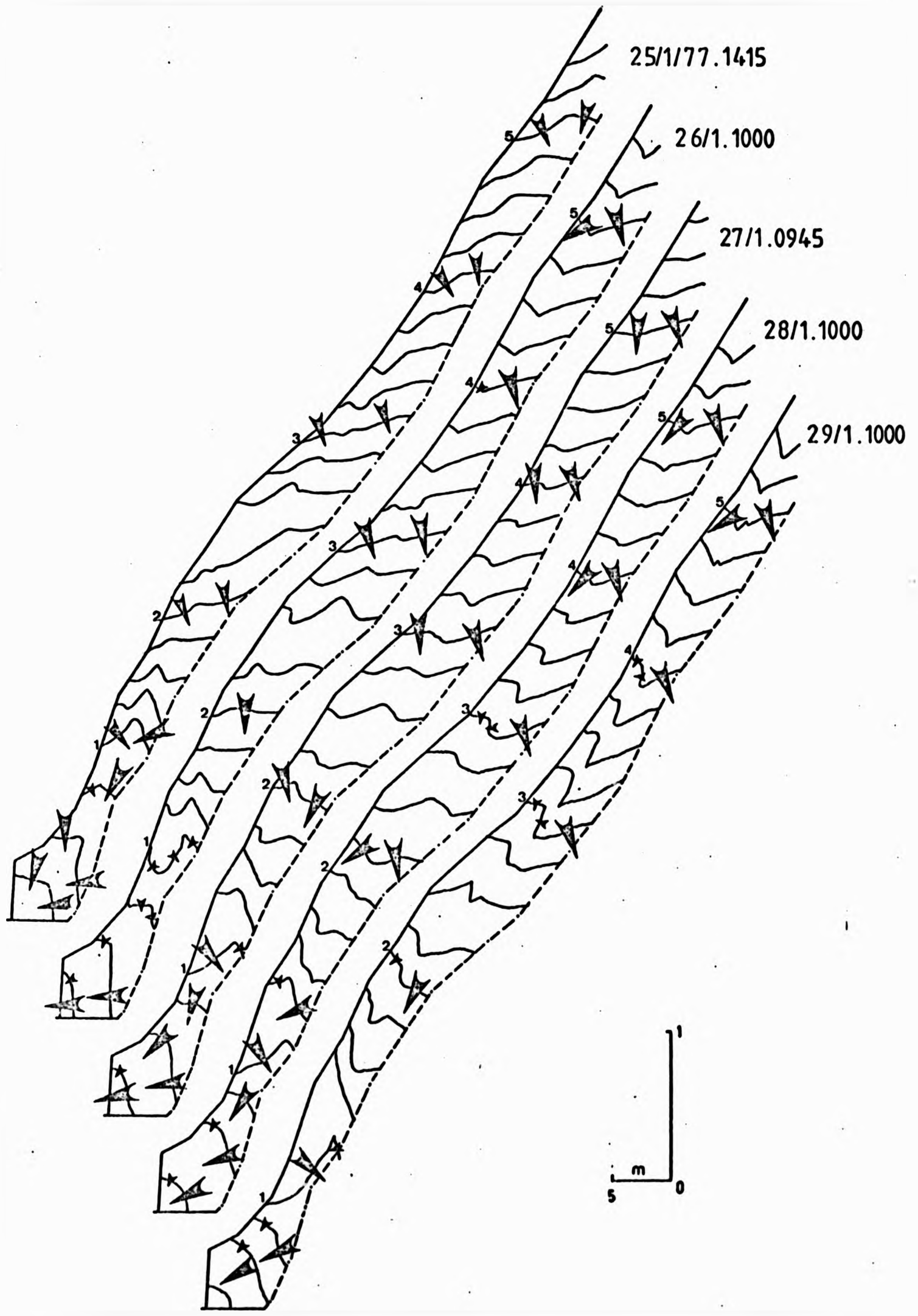

FIGURE 11.18: PATTERNS OF HYDRAULIC POTENTIAL IN THE SLOPE, 25 JANUARY - 10 FEBRUARY 1977

(arrow indicates direction of flow)

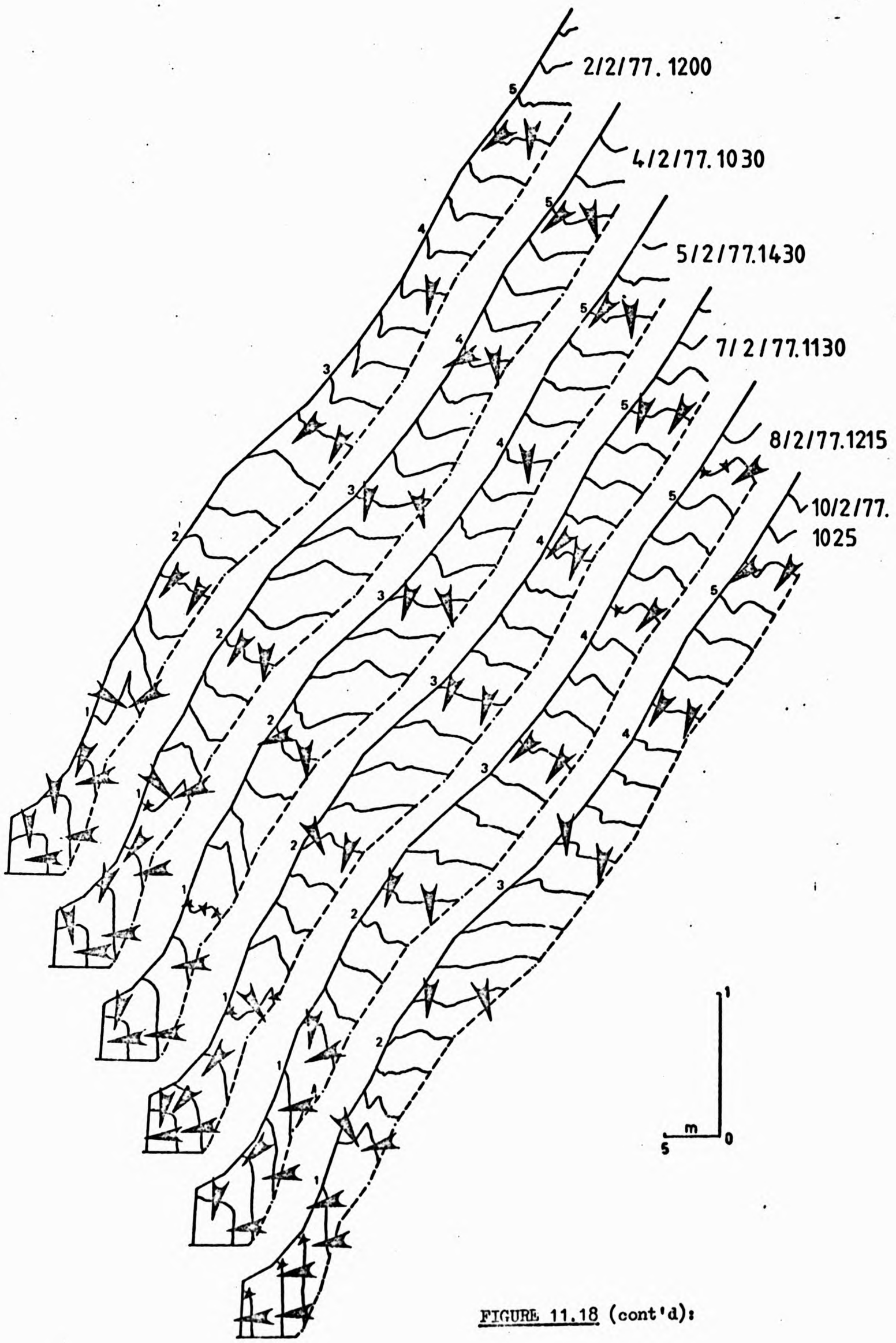

FIGURE 11.18 (cont'd):

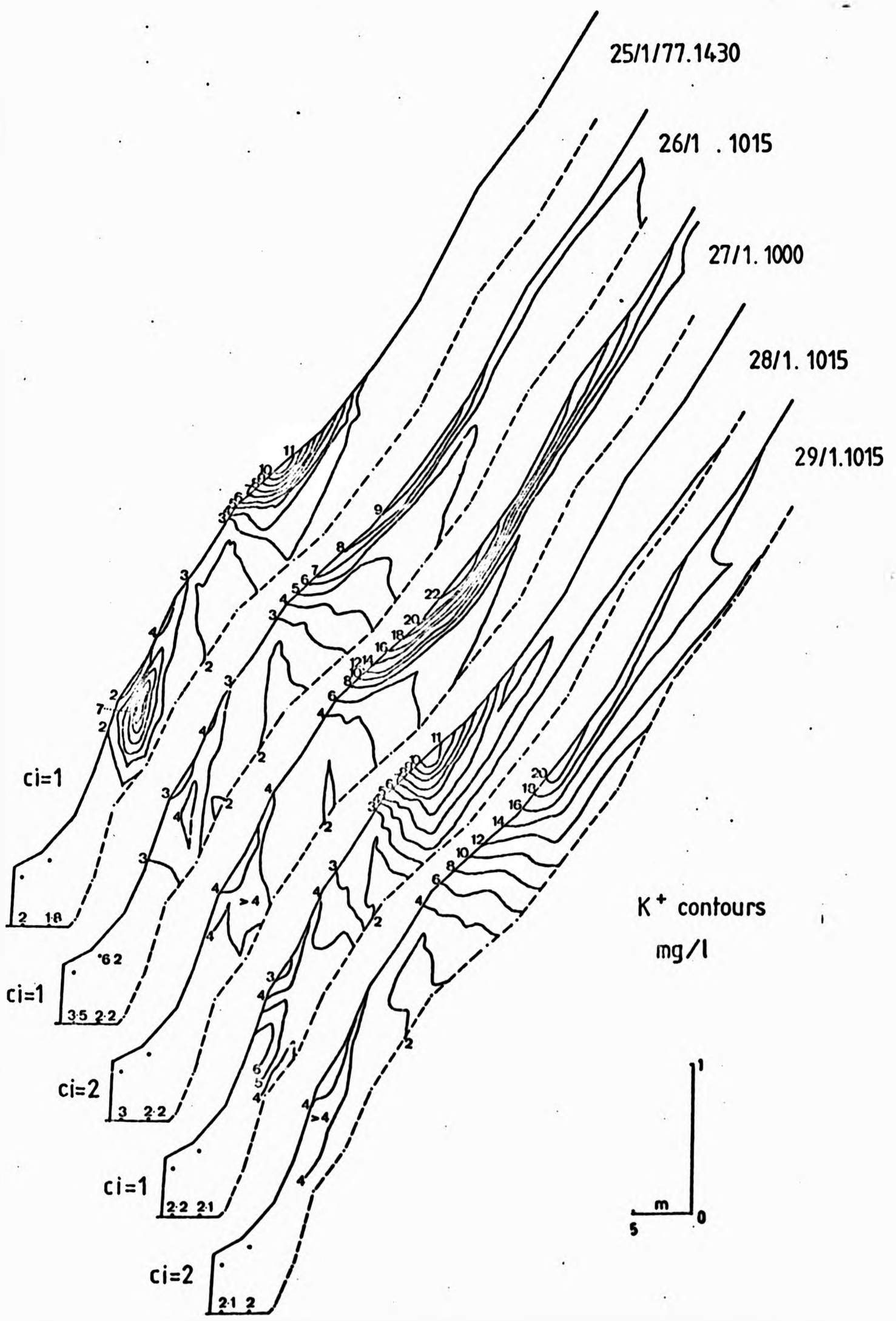

FIGURE 11.19: PATTERNS OF SOIL WATER POTASSIUM CONCENTRATION IN THE SLOPE, 25 JANUARY - 29 JANUARY 1977

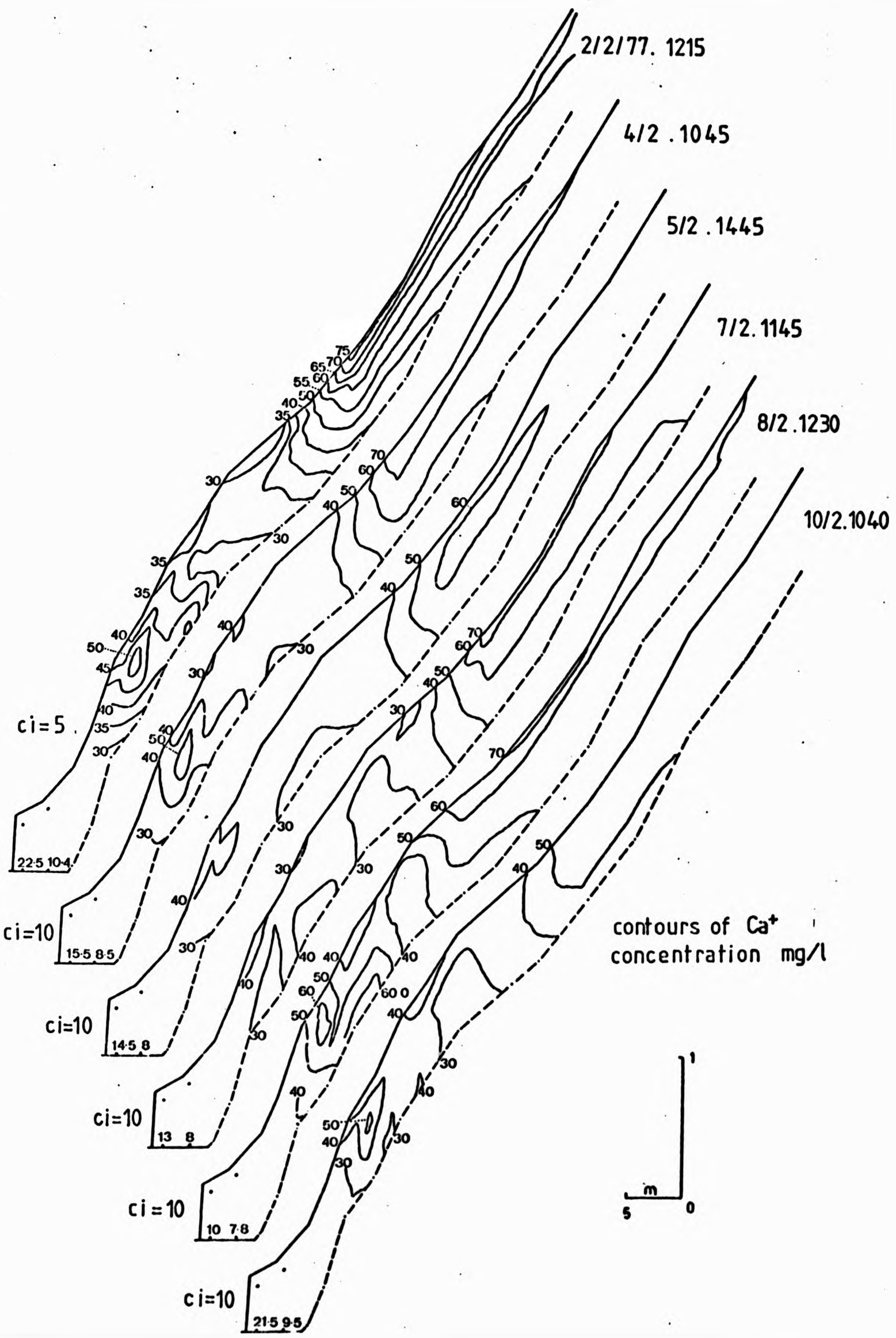

FIGURE 11.20: PATTERNS OF SOIL WATER CALCIUM CONCENTRATION IN THE SLOPE, 2 FEBRUARY - 10 FEBRUARY 1977

in K^+. A 'cloud' of high K^+ can be seen at 25th January although by the following day this has left the soil profile. K^+ from the upper slope is never seen to reach the convex area, indicating either quite rapid adsorption onto the matrix, or vertical transport into the soil with the dominant flow pattern. A noticeable vertical re-distribution of K^+ occurred by 28th and 29th January 1977 to support the latter hypothesis. Only one sample was possible from the 10 cm deep piezometers, showing a K^+ concentration of 6.2 mg/l during a rising water table after cessation of rainfall. K^+ concentration at P1 40 cm and P2 50 cm rose slightly in sympathy with the expansion of the saturated wedge. Ca^{++} contours again show the consistent cation deficiency of the convex slope, concentrations never rising above about 30 mg/l Ca^{++} (Figure 11.20). Zones high in Ca^{++} occur 11.5 m upslope at 20 cm depth and near the soil surface above 30 m upslope. The general pattern agrees well with that of $Ex.Ca^{++}$ (Figure 11.20).

C. Soil Drainage:

12th May - 1st June 1977

A 20 day recession period followed about 10 mm of rainfall on 11th May and 12th May 1977, (Figure 11.21). This presented an ideal opportunity to study moisture and solute movement within the soil during a period of drainage, with rainfall (actually, 0.7 mm fell on 26th May but this was absorbed by upward capillary flow, and therefore made no impact upon the saturated zone or streamflow). It was thought that in studying a lengthy period essentially dominated by evapotranspiration the mechanisms which set the catchment up for seasonal flushing effects might be identified. Such a period could not normally be monitored by tensiometers and suction sampling cups prior to autumn storms due to high values of soil tension beyond the range of the 'Webster' tensiometer.

I. Water Movement

(i) The rainfall of 11th and 12th May 1977 produced a small expansion of the saturated wedge, and distortion of vertical tension gradients, indicating downprofile movement of water through unsaturated soil (12th May and 13th May; Figures 11.22 and 11.23). However, flow in the saturated wedge was horizontal in the direction of the stream.

(ii) During the remaining period (16th May 1977 - 1st June 1977) water movement followed the theoretical pattern described by Weyman (1973), summarised in Chapter 9; that is, rotation of equipotentials from horizontal (vertical infiltration, (e.g. 13th May 1977) to orthogonal (lateral downslope flow, e.g. 16th May 1977) to nearly horizontal (vertical upward flow due to plant water demand, e.g. 1st June 1977). By the end of the period (1st June) flow was being drawn upwards from the saturated wedge and streamflow had actually ceased at the slope base. A low hydraulic potential still existed for lateral flow (see computed throughflow in Figure 11.21) but the water table appeared to have fallen below the streambed. This suggested that slow downstream subsurface seepage might be augmenting streamflow. It also pointed to a potential supply of solutes for autumn flushing, i.e. the residue remaining on and immediately below the streambed.

The distribution of equipotentials varied considerably downslope, with the highest tensions recorded near the surface, 9 - 14 m upslope (> 600 cm water, 1st June 1977). Above 24 m the down profile tension gradient was lower and confined to the soil 10 - 70 cm below ground level. This pattern can be explained by reference to the distribution of vegetation over the slope (Figure 9.4). Over the lower slope dominantly short rooted vegetation (i.e. grasses, bracken, reeds) produced a heavy near surface water demand, but on the upper slope dominant longer rooted species (i.e. birch, Scots pine and beech) drew water from depth.

II. Solute Movement

It was only possible to remove small volumes of soil water during this period due to difficulty in overcoming considerable natural tension. During the latter days less than 1 ml of solution was frequently available for analysis and in some instances no sample was obtained. Micropipetting was employed to handle these small volumes, but it meant that only a single cation concentration (K^+) could be determined to produce contour 'snapshots'.

The contour pattern for K^+ over the period of drainage was complex (Figure 11.24), but can be explained using the processes of water movement described earlier.

(i) Initially (12th May 1977) K^+ concentrations were low probably due to removal by post-rainstorm lateral flow, apart from near surface soil on the upper slope. The latter area shows some inconsistency in the contour 'snapshots' probably due to porous cup failure and the necessity to fill missing data points by interpolation. This was achieved by hand plotting of vertical and downslope profiles.

(ii) From 16th May 1977 onwards a pattern was established, at least over the lower slope. As equipotentials began rotating towards the horizontal a zone of higher K^+ concentration developed at the profile base (16th May - 25th May 1977). The K^+ contours lay parallel to the equipotentials, indicating a concentration gradient (K^+ decreasing) in the direction of upward flow. One possible explanation for this lies in the fact that the larger pores at depth, containing water of lower K^+ concentration, would be emptied preferentially, thus leaving higher concentration water in the smaller pores to be sampled.

(iii) As time proceeded water was drawn from the smaller pores at depth due to demand from the short rooted vegetation above, and the concentration gradient was reversed (e.g. 28th May and 1st June 1977). Higher K^+ concentration water moved upwards, the K^+ ions either being taken in by plants or accumulating at the soil root interface. Carlisle et al (1966) found that bracken played an important role in the woodland nutrient cycle, its litter and throughfall contributing 31.4 % of the total K falling from all sources. Thus bracken on the hillslope could be important in accumulating K during the growth period and returning it to the soil surface either as leaf exudant, dissolved by throughfall in the longer term or by chemical decomposition of bracken fronds.

The K^+ contour pattern during the latter days of the period bears a striking resemblance to that of Ex.K^+ (Figure 11.2A) with high concentrations in the upper and lower slope, but familiar low concentrations under the convex area. Thus upward flow appears to reinforce the pattern of Ex.K by solute accumulation in the upper soil, at the soil root interface and plant uptake and return either in throughfall or by longer term tissue decomposition.

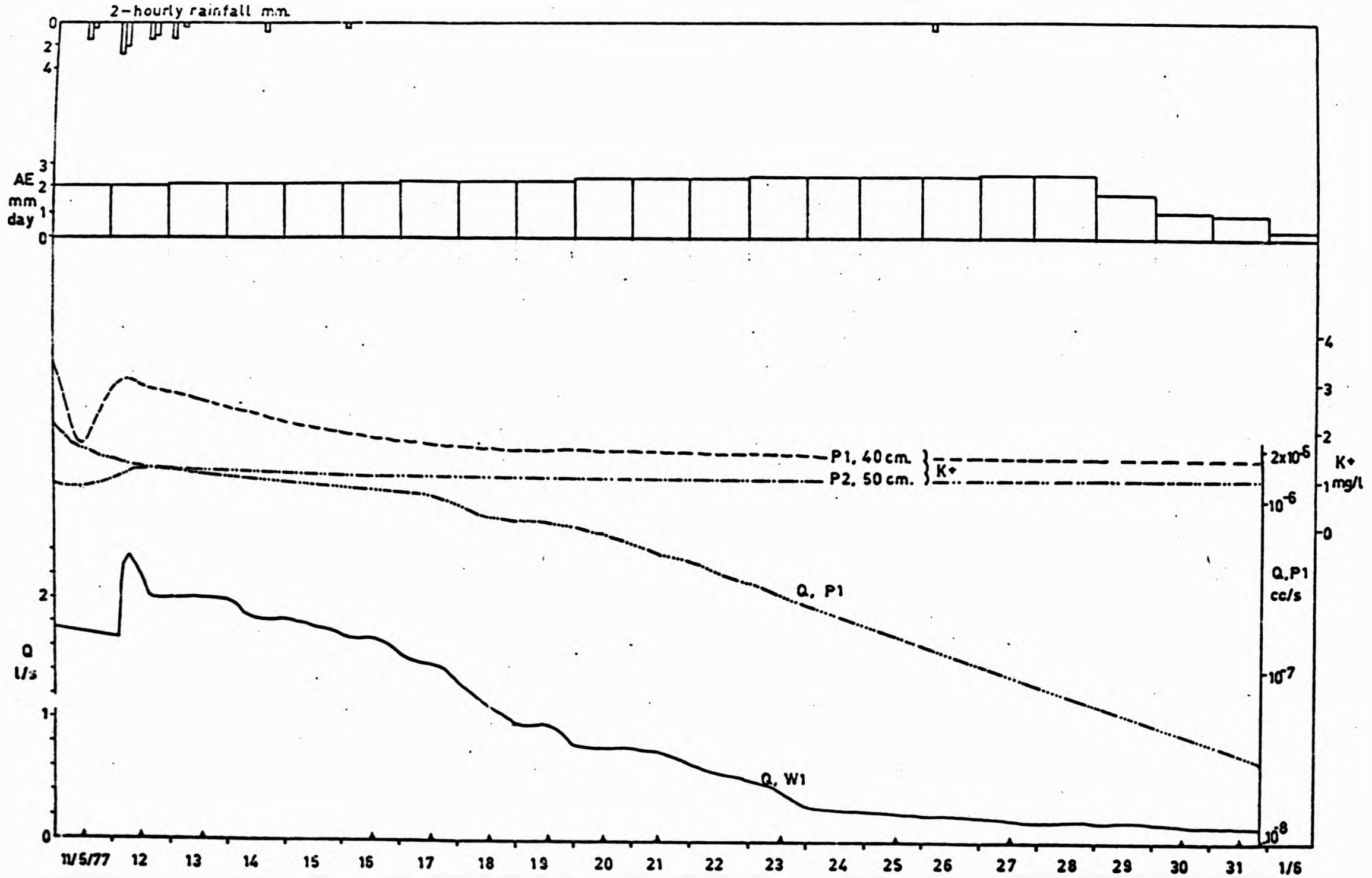

FIGURE 11.21: SUBCATCHMENT 1 AND SLOPE HYDROLOGY, 11 MAY - 1 JUNE 1977
(triangles = pit and tension sampling times)

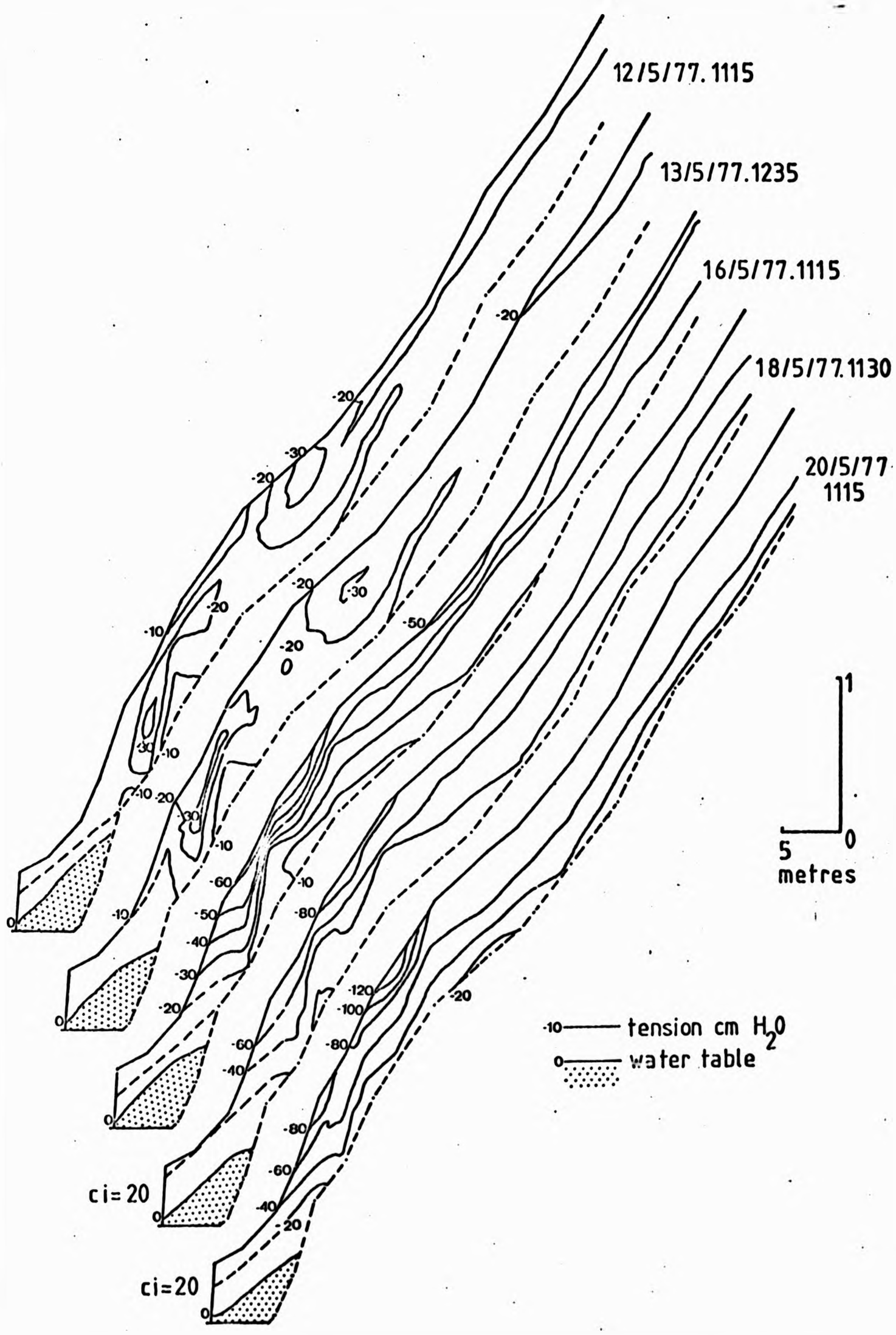

FIGURE 11.22: PATTERNS OF PORE WATER PRESSURE IN THE SLOPE, 12 MAY - 1 JUNE 1977

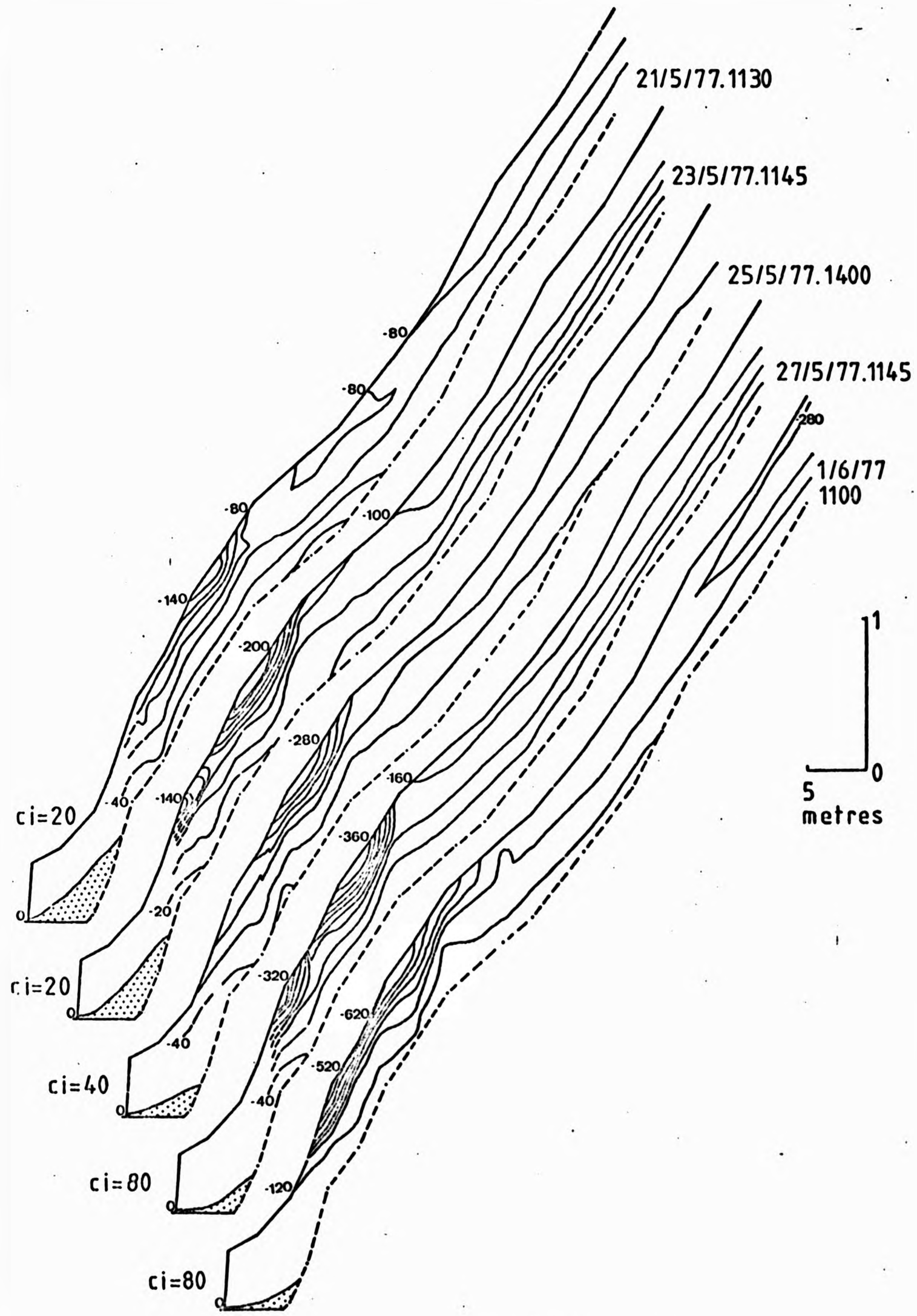

FIGURE 11.22 (cont'd)

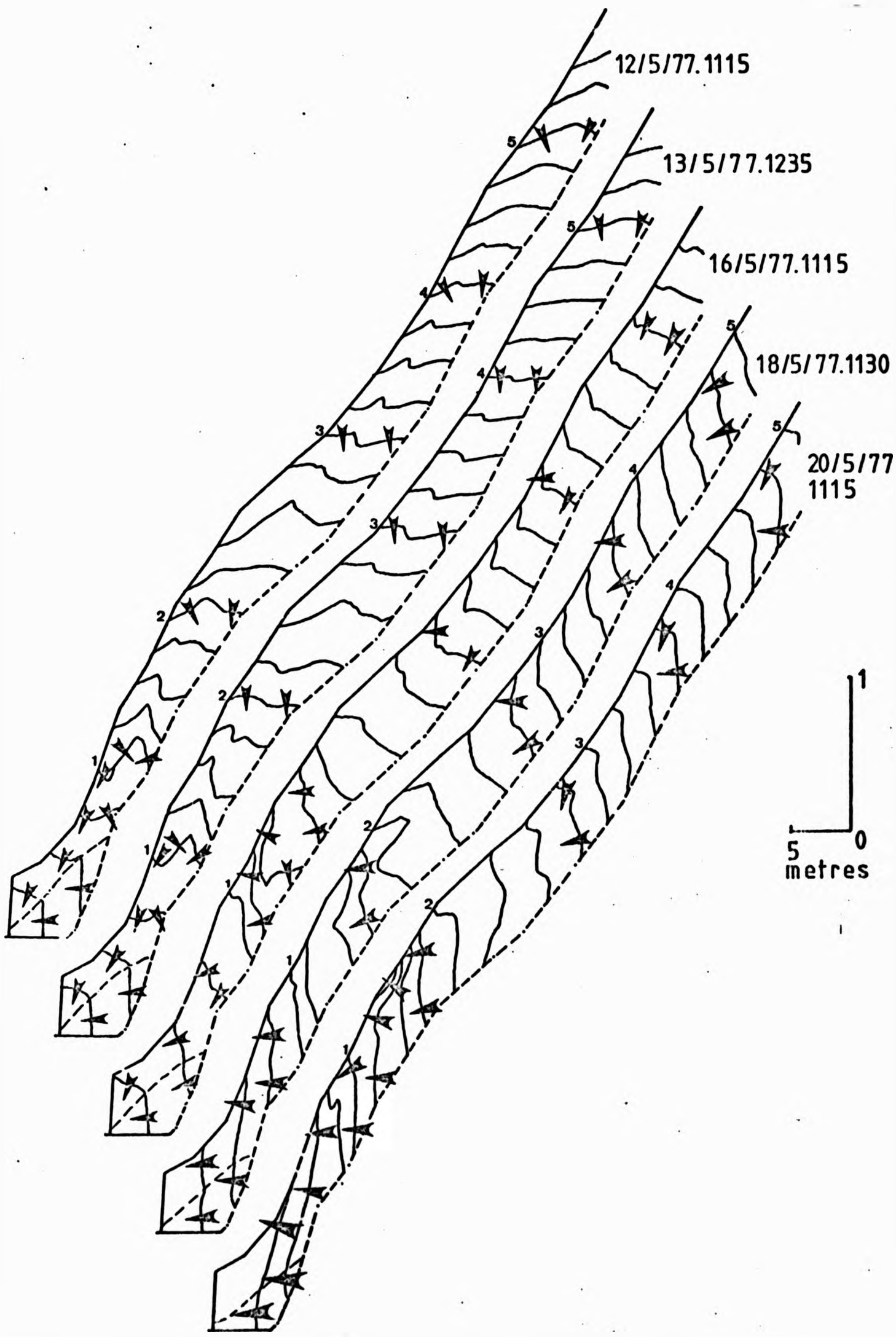

FIGURE 11.23: PATTERNS OF HYDRAULIC POTENTIAL IN THE SLOPE, 12 MAY - 1 JUNE 1977
(arrow indicates direction of flow)

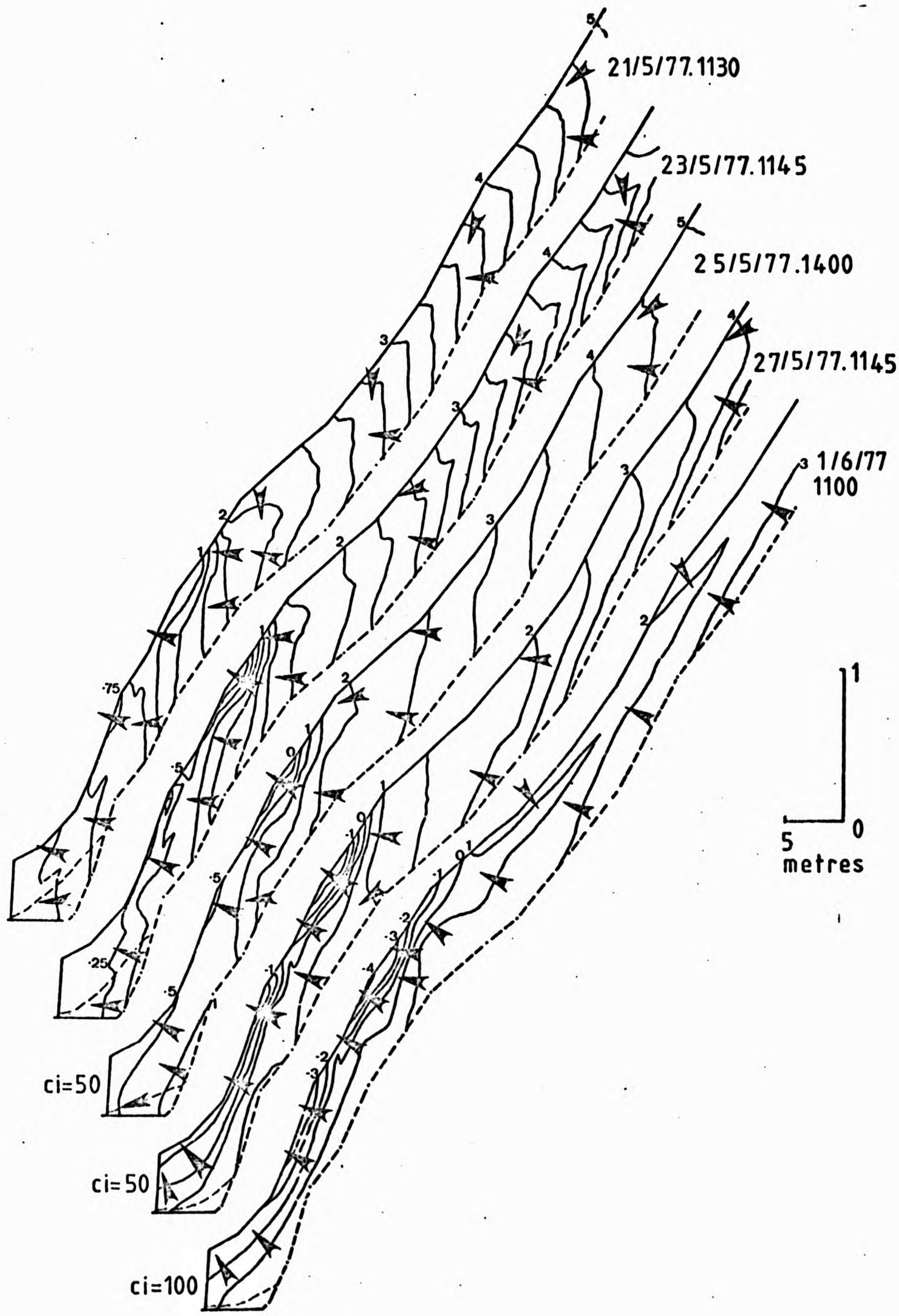

FIGURE 11.23 (cont'd)

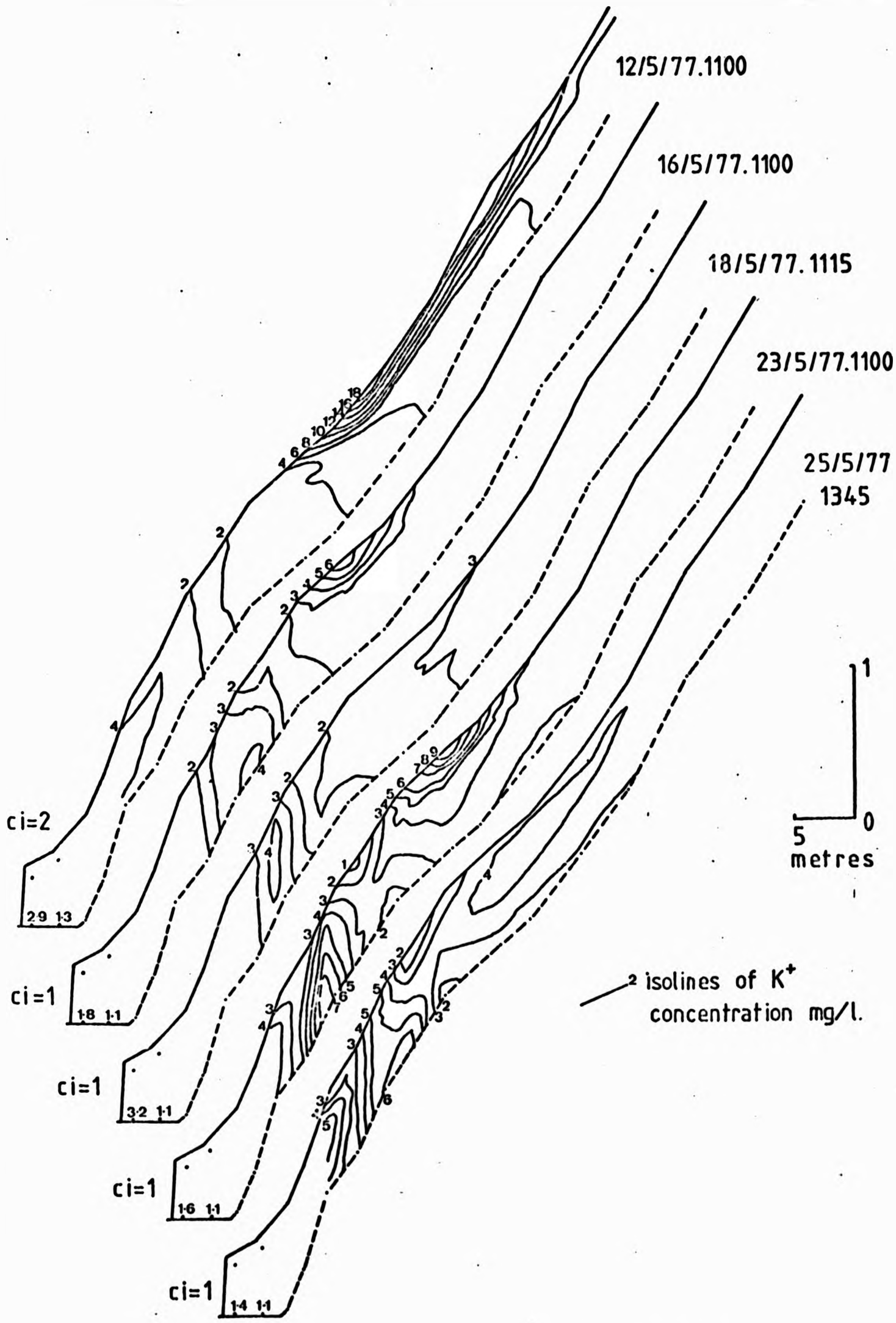

FIGURE 11.24: PATTERNS OF SOIL WATER POTASSIUM CONCENTRATION IN THE SLOPE, 12 MAY - 1 JUNE 1977

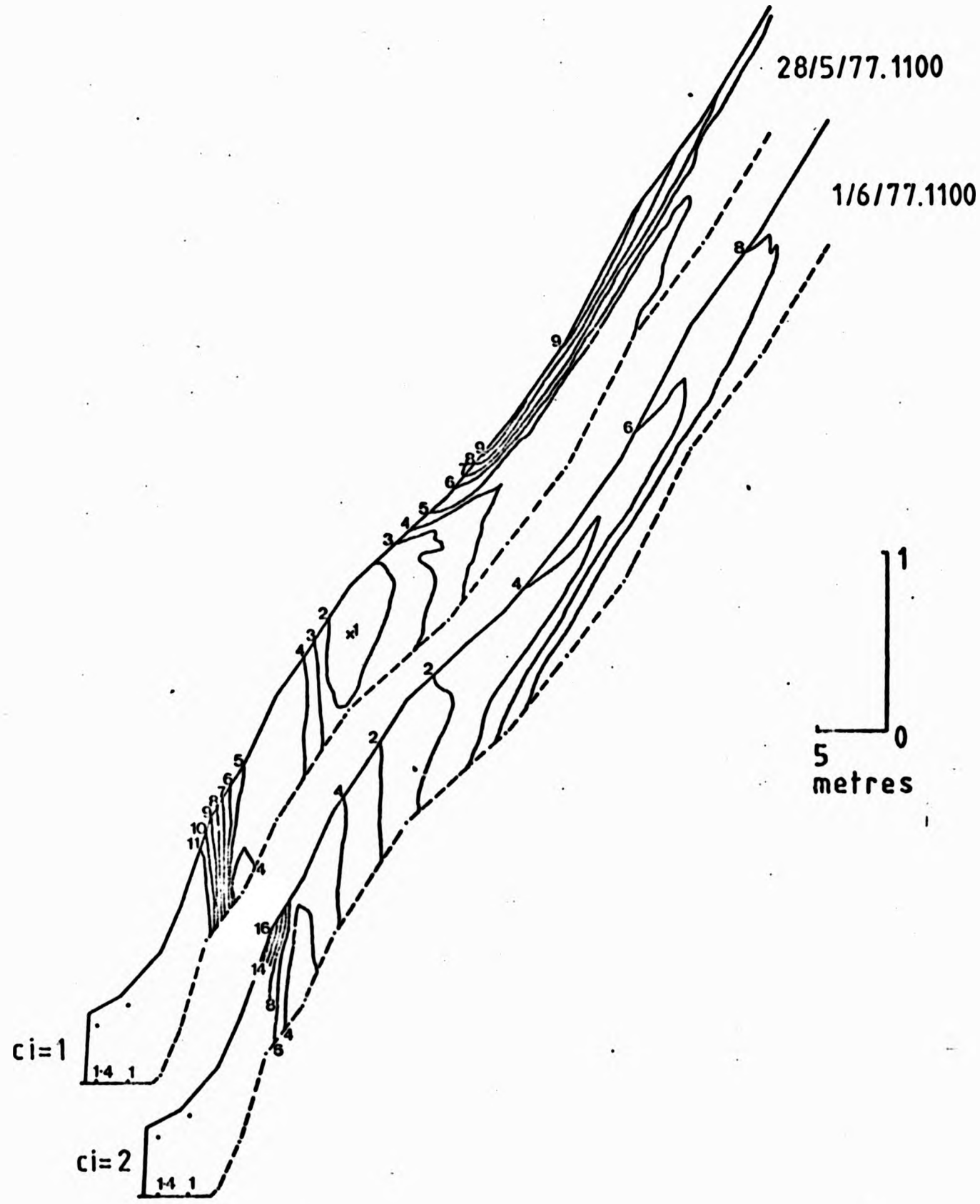

FIGURE 11.24 (cont'd):

Several samples were large enough for Ca^{++} and Mg^{++} determination over the period and these suggested that a similar process could be operating for these two ions.

It seems likely that the near surface cation accumulations could be significant contributors to the flushing effect noted in Section 2 of this thesis.

III. Further Discussion

Weyman (1973) found that tension (ψ) was linearly related to height above the slope base (z).

$$\psi = a' + b'z \qquad (11.14)$$

Slope base moisture content, a', and the upslope moisture gradient, b', were linear functions of time, t.

$$a' = q + pt \qquad (11.15)$$

$$b' = r + st \qquad (11.16)$$

The actual coefficients obtained for these relationships suggested to Weyman that the drainage rate did not increase rapidly with z and that the upslope moisture gradient was low at any point in time. Similar relationships were sought for the West Walk hillslope as a means of comparing flow regimes on two different soils with different vegetation covers; Weyman's bracken, bramble and grases on free draining brown earth, and West Walk's grasses, bracken, shrubs and trees on a gravelly, clayey, brown earth.

Equation (11.14) was fitted to data from 10 cm, 25cm, 35cm and 70 cm depth for each day over the period 12th May to 1st June 1977, but only at 70 cm were some significant linear correlations obtained (see Table 2 & Figure 11.25). This was due to the effect of upward flow on the lower slope, more pronounced at 10 cm than at 70 cm, and to a lesser extent the non-linearity of the moisture/tension relationship, notably at high tensions (Figures 10.6 - 10.19). Some success was achieved by treating the slope as two separate units: lower slope -

short rooted vegetation; upper slope - longer rooted vegetation, and fitting equation (11.14) to data from 25 cm and 35 cm (10 cm data was not susceptible to this division)(Table 11.3). Correlation coefficients increased but were not always significant, due to the reduced sample size. One interesting point here is that $\psi \geq z$ over much of the lower slope, which was primarily due to the influence of evapotranspiration and not gravity drainage, the principal mechanism suggested by Hewlett and Hibbert (1963).

Equations (11.15) and (11.16) were fitted to the coefficients in Tables 11.2 and 11.3, and the results are summarised in Table 11.4. The upslope moisture gradient is the same as that obtained by Weyman on the upper slope at 25 cm and 35 cm depths, but higher on the lower slope due to the effects of evapotranspiration. The gradient is much lower at 70 cm where the influence of upward water movement is subdued. The drainage rate, $d\alpha'/dt$, was stable for all but 35 cm deep readings on the upper slope (the latter possibly due to a faulty tensiometer) which also agrees with Weyman's results.

K^+ concentration has been plotted against height above the slope base (z) in the same way as tension (ψ)(Figure 11.26). The most marked feature, especially at 10 and 35 cm depths, is the zone of low K^+ between 16 and 19 m upslope. There are no clear linear relationships between K^+ concentration and z, as there were between ψ and z. Comparison of Figure 11.26 with Figure A3.27 (Ex.K^+) illustrates a general visual correlation between K^+ in sclution and exchangeable K^+, even over the wide range of tensions represented by the period 12th May to 1st June 1977. However, this correlation does not hold good statistically, using the average K^+ concentration of soil water for the drainage period.

$$K^+ \text{ conc. (mg/l)} = 4.36 + 0.067 \text{ Ex.}K^+ \text{ mg/l} \qquad (11.17)$$

$r = 0.14$; $N = 22$, not significant

For a single set of soil water samples (1100, 1st June 1977) the correlation improved but was still insignificant.

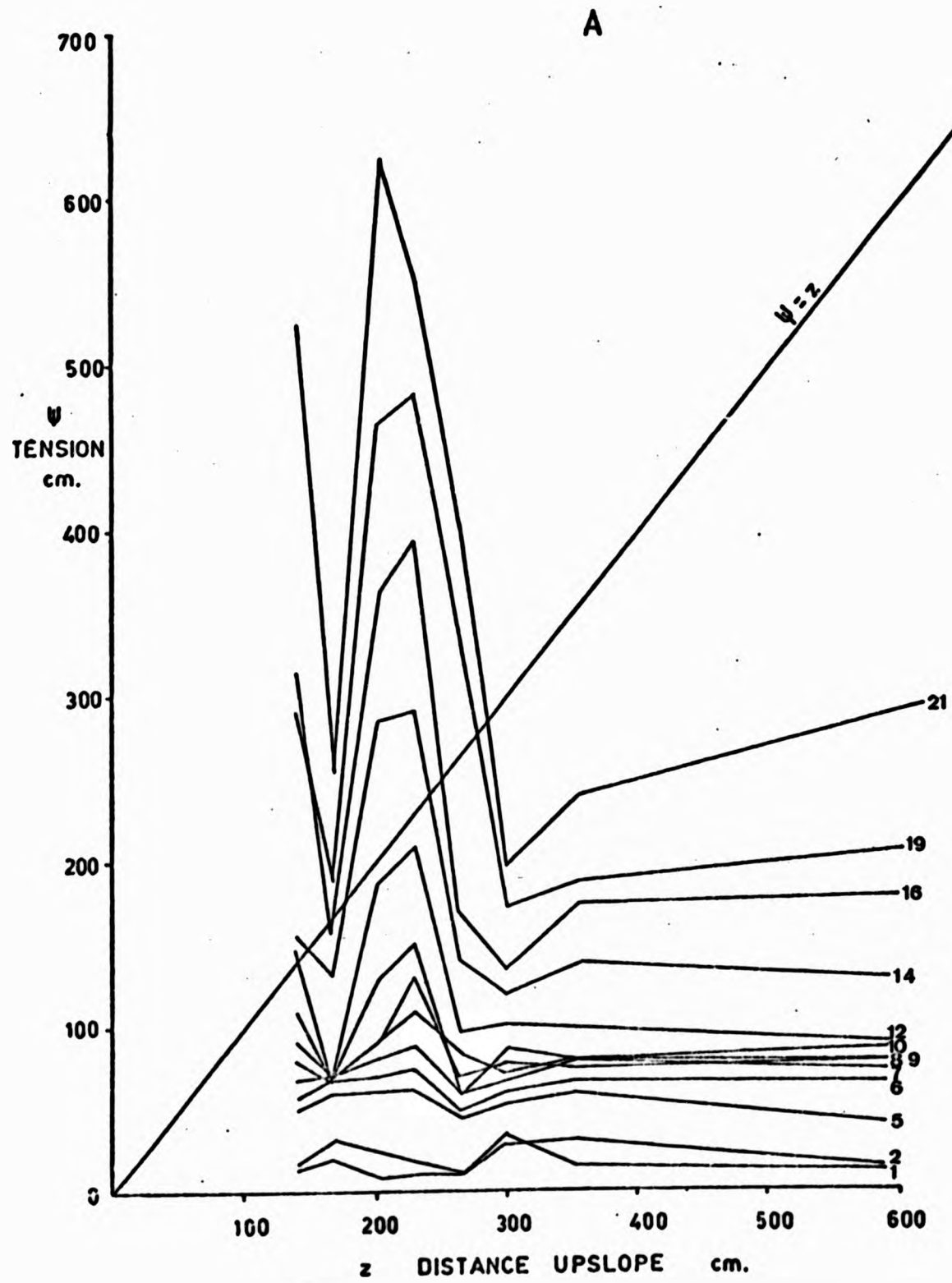

FIGURE 11.25: VARIATION OF TENSION WITH DISTANCE UPSLOPE DURING SLOPE DRAINAGE, 12 MAY (t = 1) - 1 JUNE 1977 (t = 21)

A: 10 CM DEPTH

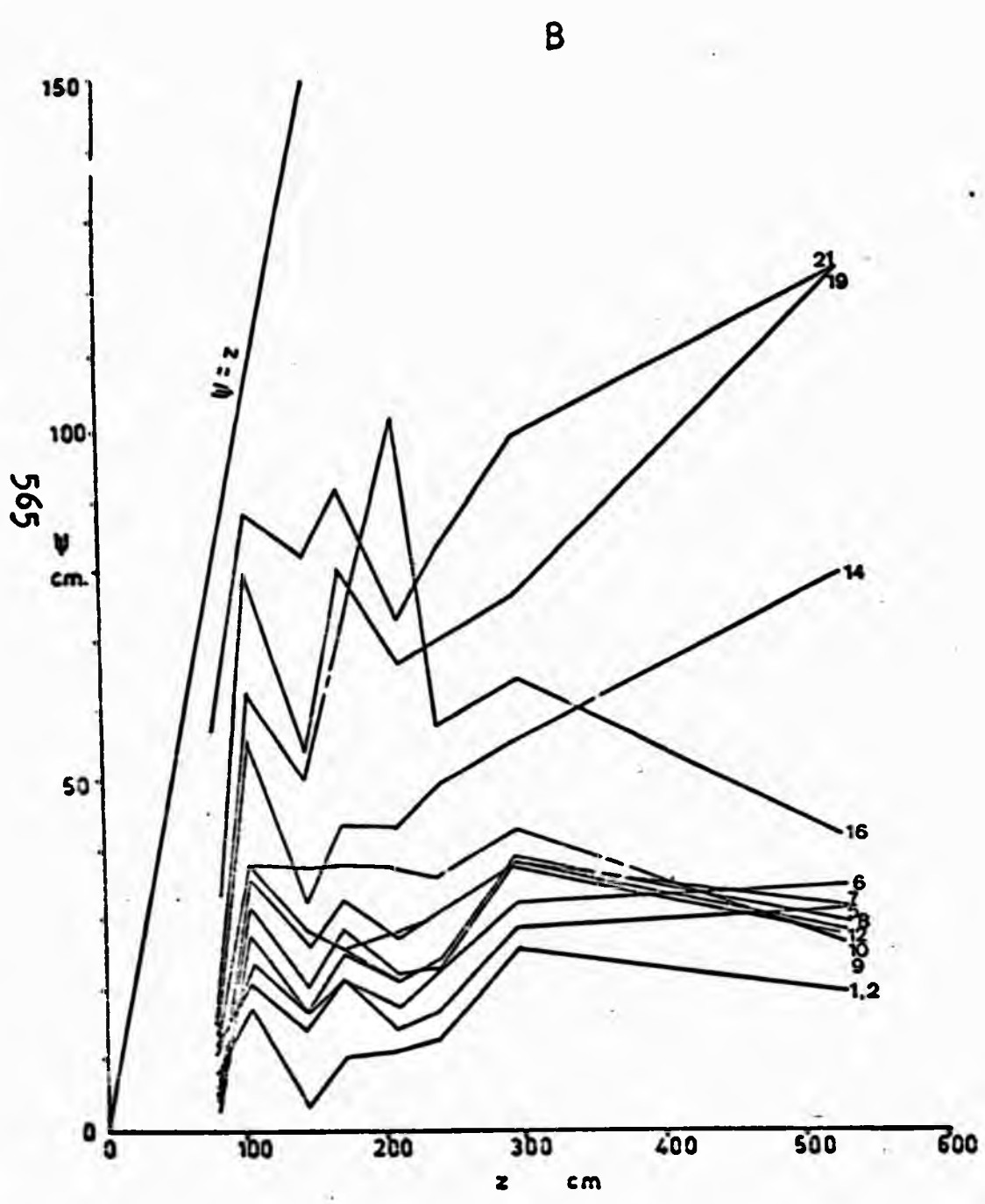

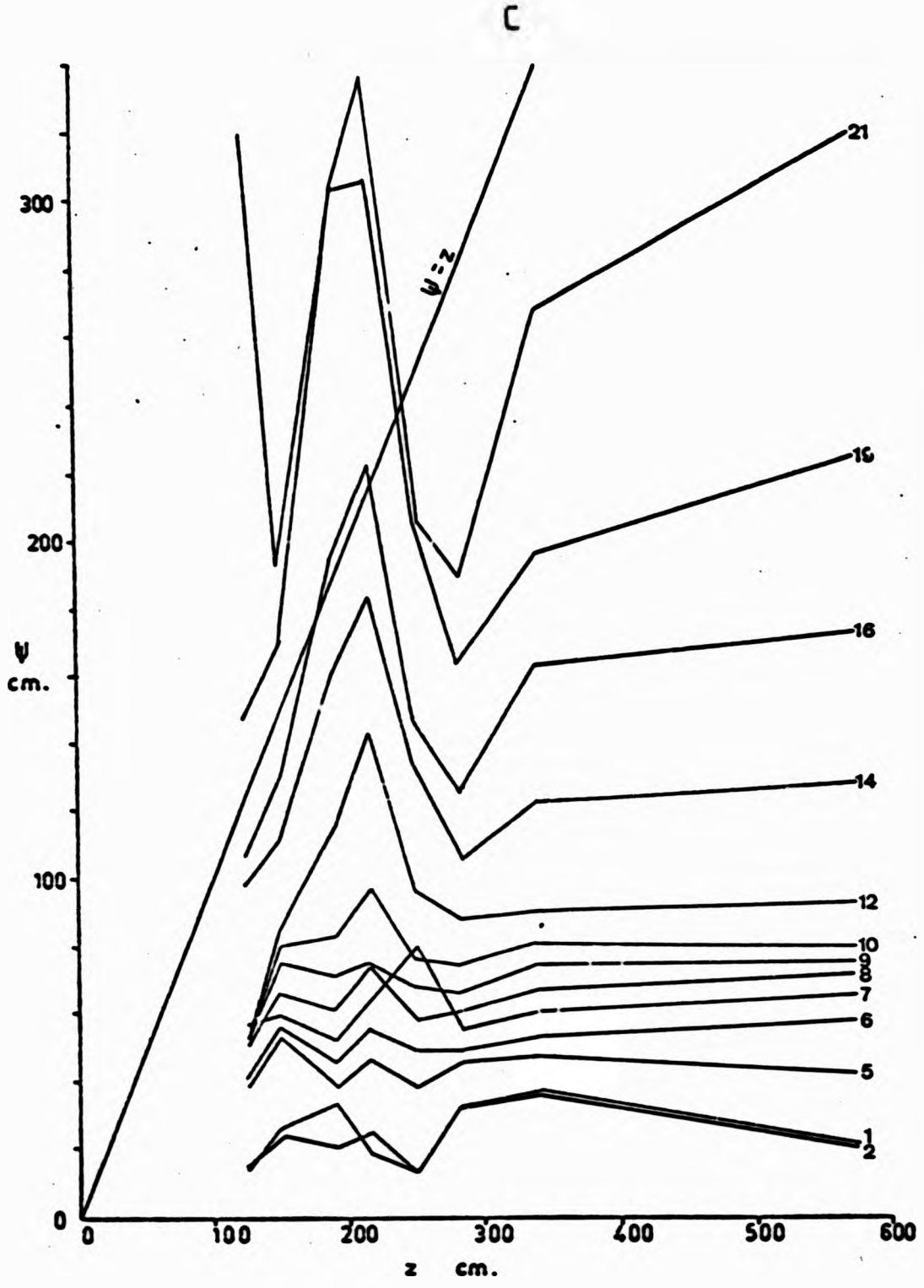

FIGURE 11.25 (cont'd): B: 25 CM DEPTH C: 70 CM DEPTH

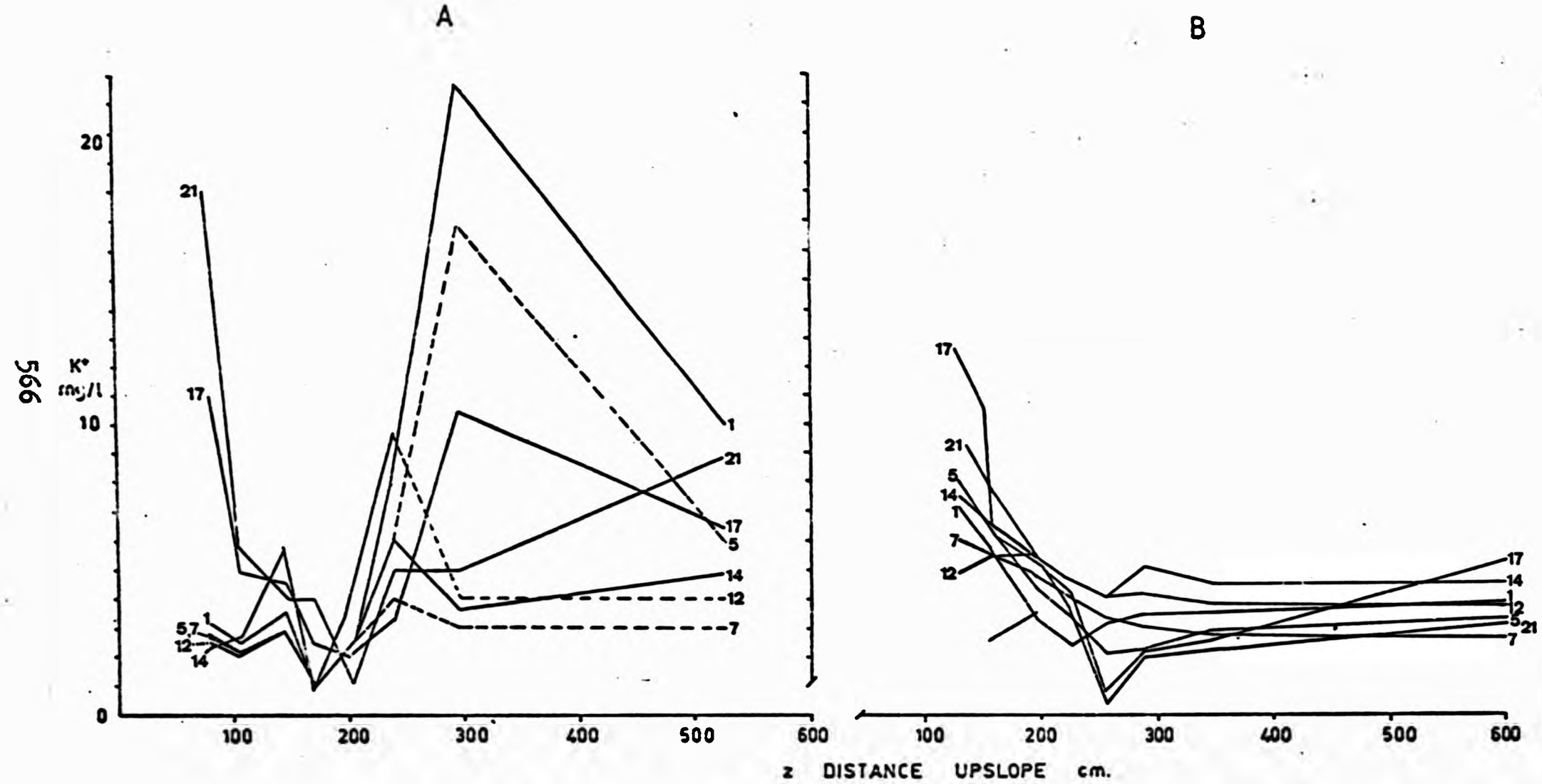

FIGURE 11.26: VARIATION OF SOIL WATER POTASSIUM CONCENTRATION WITH DISTANCE UPSLOPE DURING SLOPE DRAINAGE, 12 MAY (t = 1) - 1 JUNE 1977 (t = 21)

A: 10 CM DEPTH B: 25 CM DEPTH

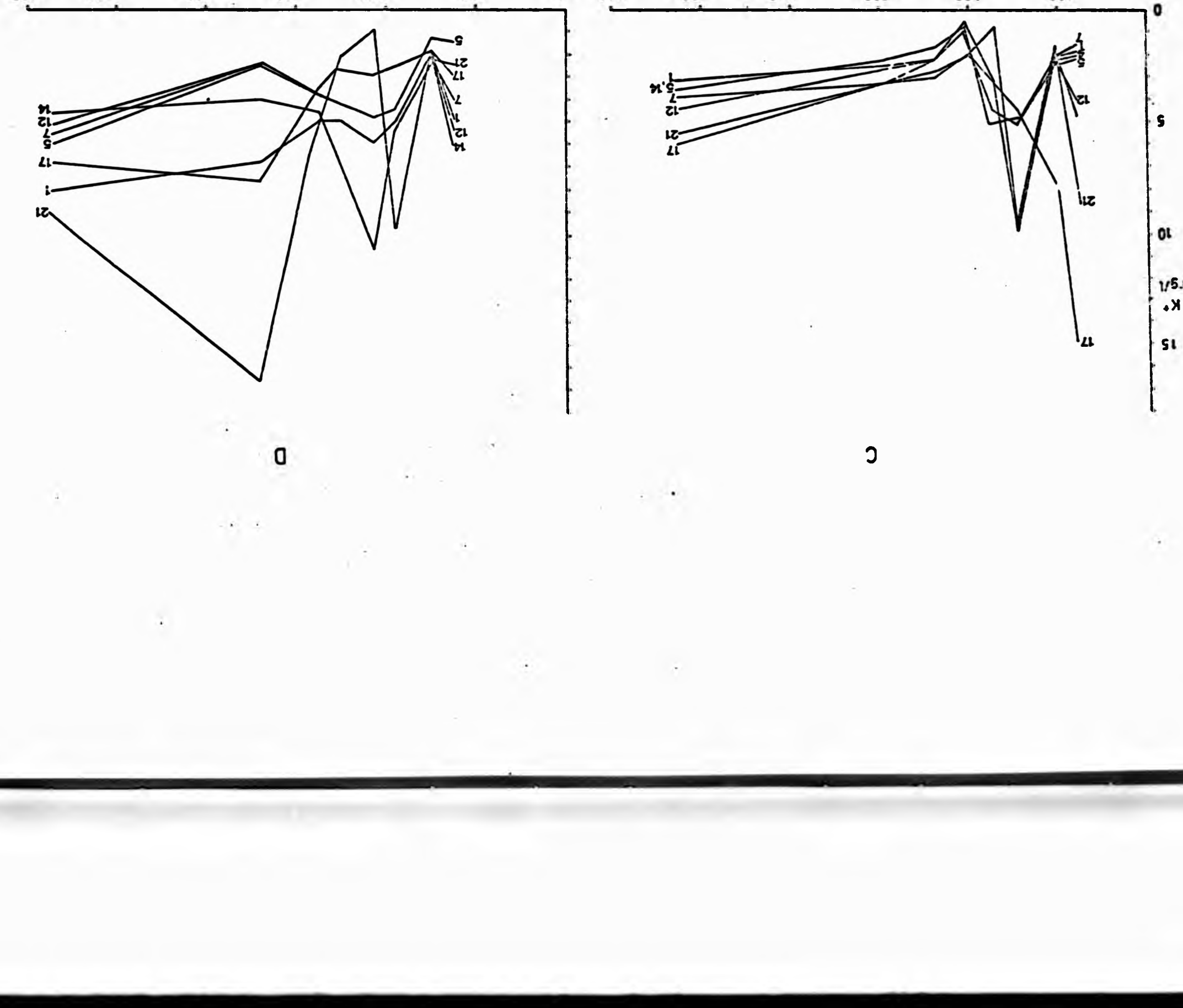

FIGURE 11.26 (cont'd): C: 35 CM DEPTH D: 70 CM DEPTH

TABLE 11.2: RELATIONSHIPS BETWEEN ψ AND z FOR THE 70 CM DEEP DATA: from 12th May to 1st June 1977

Time, t, since start of drainage (t = 1 = 12/5) days	Relationship	Correlation coefficient r	N	Significance Level r
1	ψ = 6.51 + 0.03 z	0.61	8	NS
2	ψ = 5.46 + 0.04 z	0.65	8	10 %
5	ψ = 10.41 + 0.042 z	0.80	8	5 %
6	ψ = 9.24 + 0.06 z	0.78	8	5 %
7	ψ = 14.26 + 0.04 z	0.62	8	NS
8	ψ = 17.57 + 0.03 z	0.45	8	NS
9	ψ = 22.84 + 0.02 z	0.32	8	NS
10	ψ = 24.96 + 0.02 z	0.26	8	NS
12	ψ = 32.50 + 0.01 z	0.07	8	NS
14	ψ = 22.07 + 0.11 z	0.83	8	5 %
16	ψ = 57.66 + 0.003 z	0.02	8	NS
19	ψ = 39.64 + 0.15 z	0.85	8	5 %
21	ψ = 61.84 + 0.12 z	0.85	8	5 %

TABLE 11.3 A: RELATIONSHIPS BETWEEN Ψ AND z FOR 25 CM DEEP DATA: from 19th May to 1st June 1977 *

Time, t, since start of drainage days	Relationship	Correlation coefficient r	N	Significance Level r
	Upper Slope			
8	$\Psi = 51.29 + 0.04\ z$	0.91	4	10 %
9	$\Psi = 62.12 + 0.02\ z$	0.78	4	NS
10	$\Psi = 73.11 + 0.01\ z$	0.62	4	NS
12	$\Psi = 92.08 - 0.001z$	0.03	4	NS
14	$\Psi = 114.4 + 0.02\ z$	0.26	4	NS
16	$\Psi = 113.2 + 0.11\ z$	0.75	4	NS
19	$\Psi = 153.0 + 0.12\ z$	0.69	4	NS
21	$\Psi = 108.8 + 0.38\ z$	0.92	4	10 %
	Lower Slope			
8	$\Psi = 30.65 + 0.19\ z$	0.80	4	10 %
9	$\Psi = 36.81 + 0.19\ z$	0.72	4	NS
10	$\Psi = 7.41 + 0.42\ z$	0.93	4	10 %
12	$\Psi = 0.94\ z - 59.23$	0.97	4	10 %
14	$\Psi = 0.98\ z - 28.94$	0.99	4	5 %
16	$\Psi = 1.34\ z - 62.60$	0.99	4	5 %
19	$\Psi = 2.0\ z - 107.67$	0.96	4	10 %
21	$\Psi = 189.27 + 0.585$	0.37	4	NS

* N.B. The early time data omitted due to low significance levels

TABLE 11.3 B: RELATIONSHIPS BETWEEN ψ AND z FOR 35 CM DEEP DATA: from 20th May to 1st June 1977 *

Time, t, since start of drainage days	Relationship	Correlation coefficient r	N	Significance Level r
	Upper Slope			
9	$\psi = 42.83 + 0.13\ z$	0.76	4	NS
10	$\psi = 53.05 + 0.07\ z$	0.54	4	NS
12	$\psi = 30.95 + 0.34\ z$	0.99	4	5 %
14	$\psi = 26.26 + 0.47\ z$	0.92	4	10 %
16	$\psi = 0.93\ z - 14.79$	0.99	4	5 %
19	$\psi = 1.22\ z - 33.26$	0.99	4	5 %
21	$\psi = 1.29\ z - 17.9\ z$	0.95	4	10 %
	Lower Slope			
9	$\psi = 44.87 + 0.05\ z$	0.92	4	10 %
10	$\psi = 56.13 + 0.03\ z$	0.65	4	NS
12	$\psi = 61.43 + 0.07\ z$	0.86	4	NS
14	$\psi = 67.26 + 0.10\ z$	0.91	4	10 %
16	$\psi = 84.42 + 0.15\ z$	0.90	4	10 %
19	$\psi = 87.10 + 0.22\ z$	0.84	4	NS
21	$\psi = 19.06 + 0.50\ z$	0.96	4	5 %

* N.B. The early time data omitted due to low significance levels

TABLE 11.4: RELATIONSHIPS BETWEEN DRAINAGE RATE, a', AND MOISTURE GRADIENT, b', WITH TIME SINCE START OF DRAINAGE, t

A. Slope Base Moisture Content. a'

Depth	Data Used	Relationship	Correlation coefficient r	N	Significance Level r
25 cm	upper slope t = 8 - 21	a' = 14.37 t + 5.99	0.86	8	0.1 %
	lower slope t = 8 - 19	a' = 131.85 t - 12.57	0.93	7	0.1 %
35 cm	upper slope t = 9 - 21	a' = 61.71 - 0.12 t	0.02	7	NS
	lower slope t = 9 - 21	a' = 112.84 - 6.96 t	0.93	7	0.1 %
70 cm	whole slope	a' = 2.43 - 1.63 t	0.94	12	0.1 %

B. Moisture Gradient. b'

25 cm	upper slope t = 8 - 21	b' = 0.021 - 0.20 t	0.80	8	1.0 %
	lower slope t = 9 - 19	b' = 0.164 - 1.20 t	0.99	7	0.1 %
35 cm	upper slope t = 9 - 21	b' = 0.03 t - 0.31	0.88	7	0.1 %
	lower slope t = 9 - 19	b' = 0.11 t - 0.96	0.98	7	0.1 %
70 cm	whole slope t = 1 - 19	b' = 2.09 t + 0.006	0.94	12	0.1 %

$$K^+ \text{ conc. (mg/l)} = 0.58\ \text{Ex.}K^+ - 2.86 \qquad (11.18)$$

$r = 0.52$; $N = 12$; not significant

The poor correlation could simply be the result of sampling or analytical error, or it could be due to actual physical and chemical processes. For example, at some stage in the procedure for determining $\text{Ex.}K^+$, potassium could have been freed from the clay mineral structure of the deep samples, and incorporated in the total exchangeable contents. Alternatively the reversed soil water potential might have reduced anion supply for exchange with K^+ at the deeper soil water sampling points. If the 100 cm data pairs are excluded (in these, high $\text{Ex.}K^+$ corresponds with low dissolved K^+) equation 11.18 improves considerably.

$$K^+ \text{ conc. (mg/l)} = 0.68\ \text{Ex.}K^+ - 1.79 \qquad (11.19)$$

$r = 0.93$; $N = 8$; sig. at 0.1 %

However, without more intensive research, isolation of the processes operating is not possible.

The relationships of K^+ concentration with tension, and hence moisture content, are poor (Figure 11.27). Only in the case of 70 cm data was a least-squares fit attempted, and this was not significant. These results suggest that during a soil drying phase the concentration of K^+ in solution is independent of moisture content and that, in general, an equilibrium is maintained between K^+ ions in solution and on exchange surfaces within the soil. However, this is a relatively crude assessment and the details are not fully understood. Weyman (1973) fitted an exponential function to the tension/time data.

$$\psi = ce^{ft} \qquad (11.20)$$

and discovered that the drainage rate, f, was significantly related to height above the profile base, y, but not height above the slope base, z, which confirmed the dominance of vertical over lateral flow during drainage. Equation (11.20) was successfully fitted to data from

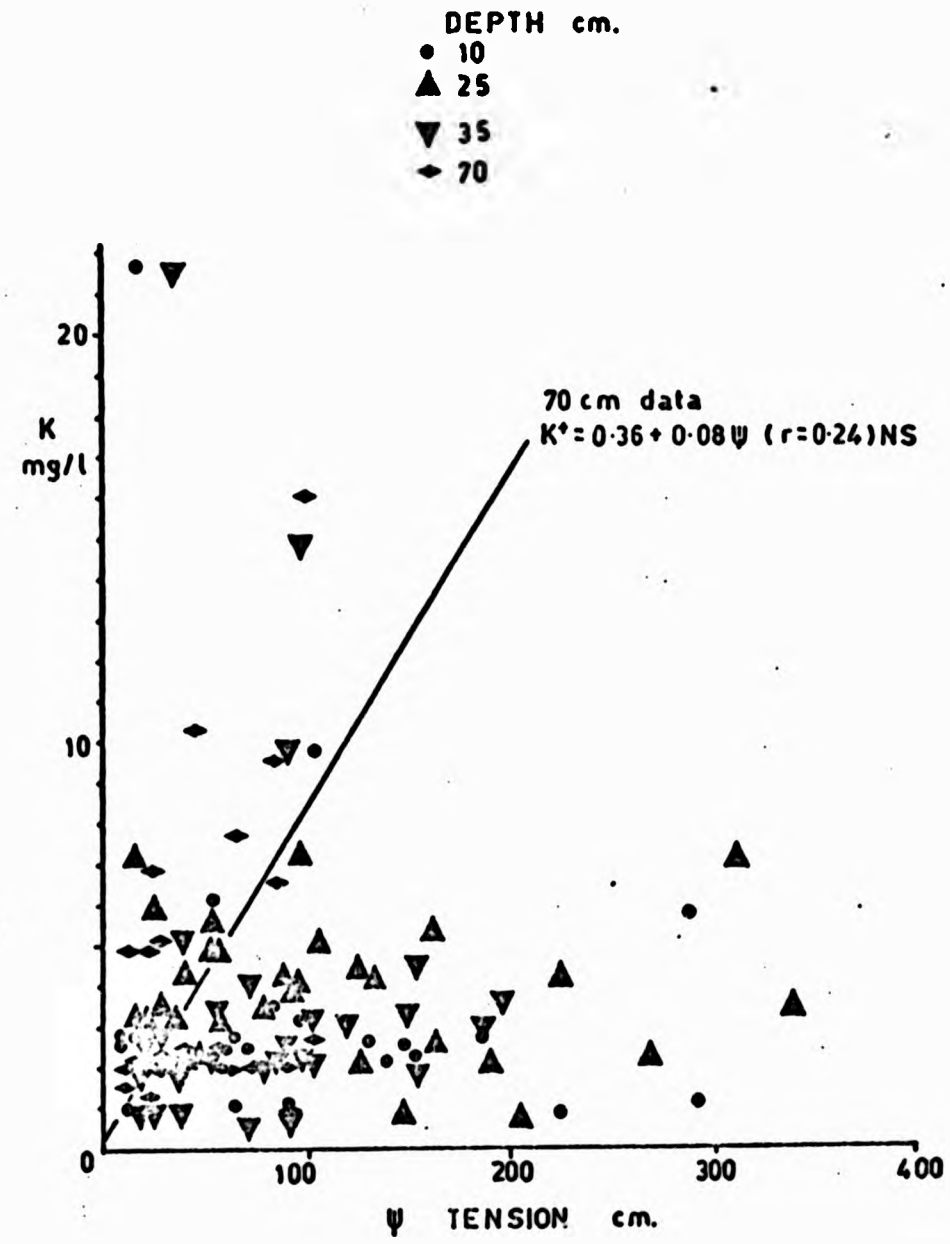

FIGURE 11.27: RELATIONSHIP BETWEEN TENSION AND SOIL WATER POTASSIUM CONTENT IN THE HILLSLOPE

12th May - 1st June 1977 (Figure 11.28; Table 11.5). No significant relationships were found between f and z (Table 11.6) although it is interesting to note that the highest correlation coefficient occurred for 70 cm data, implying some lateral seepage at this depth.

However, a significant linear relationship between f and y was obtained,

$$f = 0.09 + 8.2 \times 10^{-4} y \qquad (11.21)$$

$r = 0.58$; $N = 31$; Sig. level 0.1 %

confirming the dominance of vertical flow during drainage found by Weyman (1973) and noted earlier from the equipotential plots (Figure 11.23).

No simple consistent functional relationships existed between K^+ concentration and time, which tended to confirm the earlier suggestion that an equilibrium was maintained between soil and soil water K^+ concentrations. The exception to this might be in the upper layers of soil where K^+ could be held in solution at higher concentrations by organic chelates.

D. 12th March - 2nd May 1976:
A period of soil drainage with rainfall and infiltration during the 1975 - 1976 drought

During the period of tensiometer installation, tension data were collected from two storms of 10 mm and 7 mm and periodically during the 45 day recession which followed. Solute data was not available at this time, but a brief description of the flow pattern is included because it contains interesting features not present in periods A - C. Furthermore, it provides historical documentation of subsurface processes during the 1975 - 1976 drought. Figure 11.29 gives the hydrological background to this period; a period of low flow recession interrupted by two storm hydrographs; actual evaporation (calculated by the Met. Office with an estimated root constant of 50.8 mm for tree species < 10 years old) increased from 0.8 mm to 3.0 mm/day.

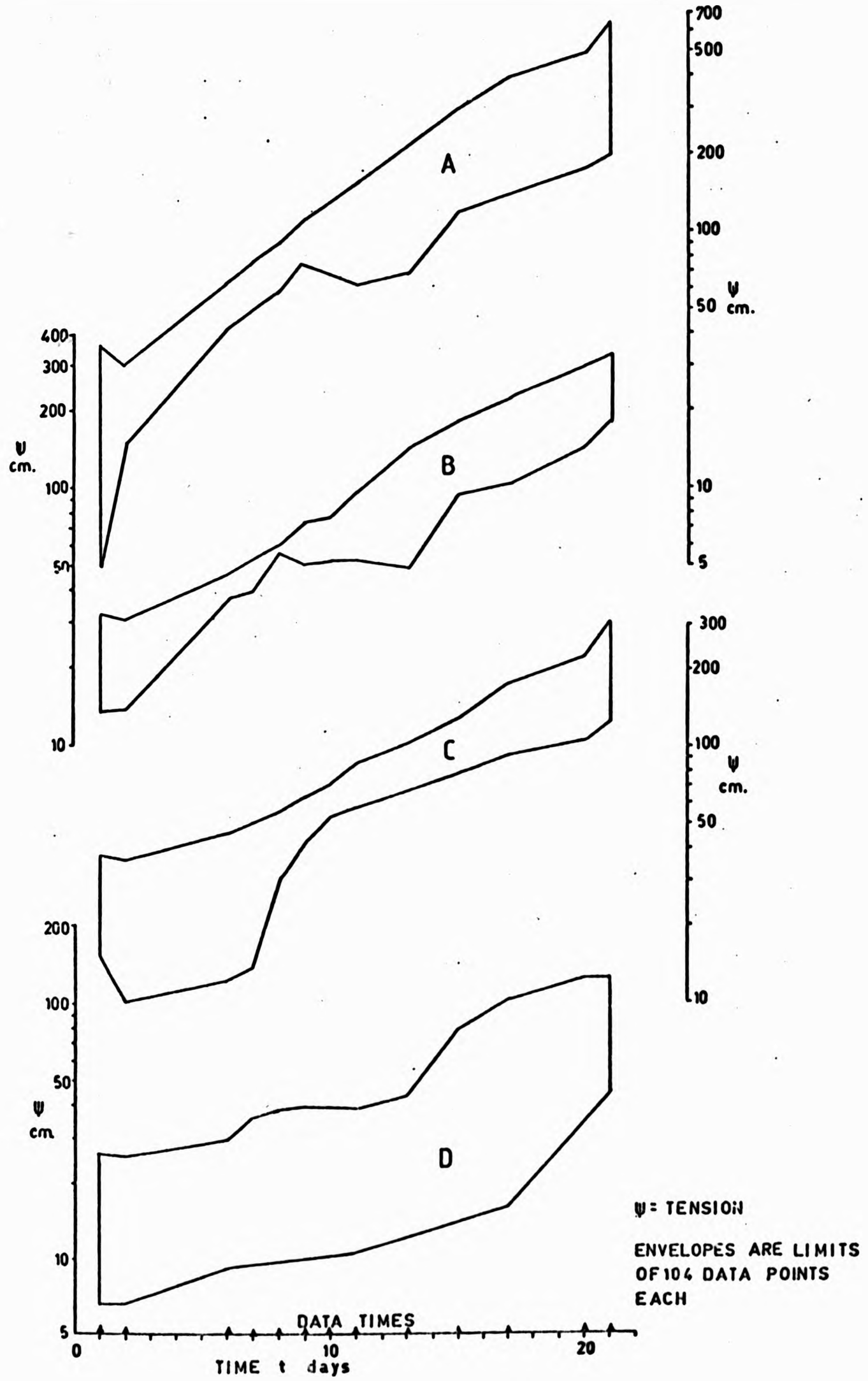

FIGURE 11.28: VARIATION OF TENSION WITH TIME, DURING SLOPE DRAINAGE 12 MAY (t = 1) - 1 JUNE 1977 (t = 21)

A: 10 CM DEPTH B: 25 CM DEPTH
C: 30 CM DEPTH D: 70 CM DEPTH

TABLE 11.5: EXPONENTIAL FUNCTIONS FITTED TO THE TENSION/TIME DATA from 12th May to 1st June 1977

Distance upslope m	Coefficients in Equation (11.20) c	f	Correlation coefficient r	N	Significance Level r %
		10 cm Depth			
9.25	15.64	0.166	0.98	13	0.1
11.50	24.28	0.108	0.96	13	0.1
13.90	14.38	0.190	0.97	13	0.1
16.25	16.75	0.184	0.97	13	0.1
19.30	10.63	0.176	0.95	13	0.1
23.90	30.64	0.090	0.99	13	0.1
31.00	24.11	0.114	0.96	13	0.1
50.50	18.22	0.134	0.97	13	0.1
		25 cm Depth			
9.25	14.1	0.130	0.96	13	0.1
11.50	25.58	0.099	0.99	13	0.1
13.90	19.30	0.134	0.99	13	0.1
16.25	19.50	0.142	0.99	13	0.1
19.30	16.05	0.134	0.96	13	0.1
23.90	27.45	0.090	0.99	13	0.1
31.00	23.72	0.111	0.99	13	0.1
50.50	19.52	0.129	0.99	13	0.1

TABLE 11.5 (cont'd)

Distance upslope m	Coefficients in Equation (11.20) c	f	Correlation coefficient r	N	Significance Level r %
		35 cm Depth			
9.25	15.56	0.107	0.98	13	0.1
11.50	30.25	0.097	0.99	13	0.1
13.90	8.93	0.158	0.94	13	0.1
16.25	17.77	0.129	0.99	13	0.1
19.30	13.11	0.124	0.96	13	0.1
23.90	22.13	0.100	0.99	13	0.1
31.00	19.22	0.110	0.98	13	0.1
50.50	21.63	0.118	0.99	13	0.1
		70 cm Depth			
9.25	2.87	0.108	0.79	13	0.1
11.50	14.48	0.085	0.99	11	0.1
13.90	7.88	0.107	0.97	11	0.1
16.25	9.44	0.110	0.99	13	0.1
19.30	9.36	0.106	0.96	11	0.1
23.90	10.87	0.096	0.99	13	0.1
31.00	21.05	0.066	0.98	13	0.1
50.50	16.12	0.083	0.85	13	0.1

TABLE 11.6: RELATIONSHIPS BETWEEN DRAINAGE RATE (f) AND HEIGHT ABOVE THE SLOPE BASE (z)

10 cm depth: $f = 0.167 - 7.9 \times 10^{-5} z$ r = 0.29; N = 8; Not sig.

25 cm depth: $f = 0.121 - 1.4 \times 10^{-6} z$ r = 0.01; N = 8; Not sig.

35 cm depth: $f = 0.112 - 1.3 \times 10^{-5} z$ r = 0.08; N = 8; Not sig.

70 cm depth: $f = 0.106 - 5.3 \times 10^{-5} z$ r = 0.45; N = 8; Not sig.

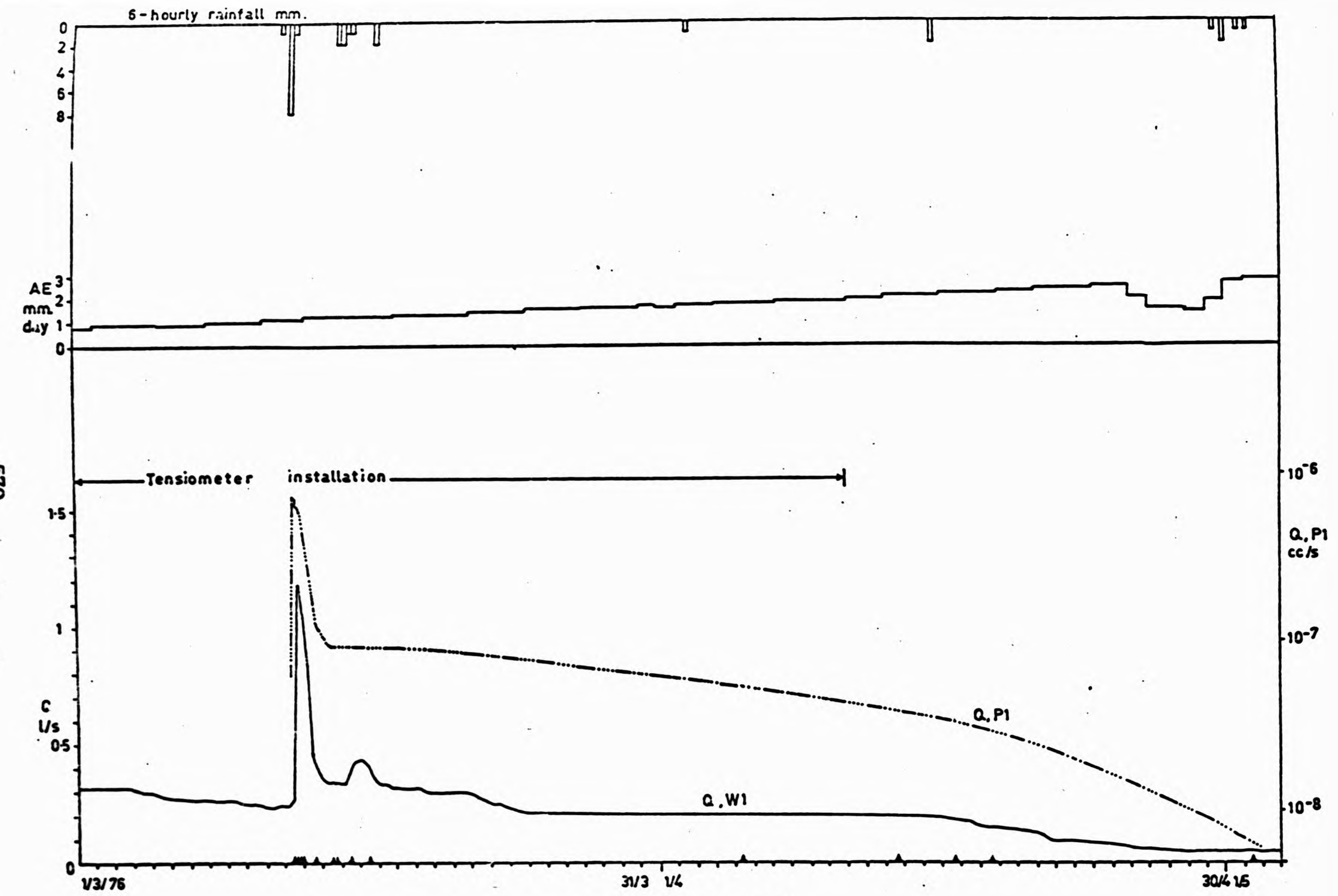

FIGURE 11.29: SUBCATCHMENT 1 AND SLOPE HYDROLOGY
1 MARCH - 30 APRIL 1976
(triangles indicate tension sampling times)

Prior to rain of 12th March 1976 equipotentials were rotating towards the surface under the influence of evapotranspiration. Rainfall produced a marked unsaturated wetting front which moved progressively down profile over the succeeding four days (dashed line, Figure 11.30). Initially progress was slow and uniform (to 1830, 12th March 1976) but by 1530, 13th March 1976 more rapid vertical flow was apparent on the lower slope, where higher hydraulic conductivity had been recorded. The saturated wedge responded quite rapidly to this rainfall input (Figure 11.31) and calculated saturated throughflow at P1 produced the peaked response shown in Figure 11.29. The striking synchroneity between this peak and the streamflow peak at W1 suggested that saturated throughflow from close to the channel was an important contributor to the streamflow hydrograph. The rapid throughflow response may have been asserted by shrinkage fissures within the soil due to drought conditions, increasing hydraulic conductivity, but the exact mechanisms are not fully understood. Thus the disjointed nature of the wetting front was in part due to variations in hydraulic conductivity (making the assumption that unsaturated K followed a similar pattern to saturated K, an assumption which might have been invalid due to further infiltrating rainfall on 15th March 1976 and 16th March 1976.

By 18th March 1976 equipotentials had begun to rotate back towards the surface under the influence of evapotranspiration, a trend which continued uninterrupted for the next 26 days. A transient 'zero flux plane' was apparent from the 18th March 1976 equipotential plot, dividing upward water fluxes in the upper part of the profile from downprofile and lateral drainage fluxes beneath (dotted line, Figure 11.32; 18th March 1976). The 'zero flux plane' (ZFP) has been identified as part of a detailed study of moisture fluxes in unsaturated soil under level ground at Thetford Forest (Cooper, 1980). ZFP depths showed considerable variability between instrument sets, but with reasonable consistency during the years 1974 - 1976. Interestingly, it was found that, in general, ZFP depths beneath grass were shallower than under trees. Under trees the maximum recorded ZFP depth was 3.2 m (1975) at which point the tensiometers all went off scale, but it was thought it may have reached the water table, some 10 m below the ground surface, the implication being that water flow was upward throughout the entire 10 m profile. Tensiometers at West

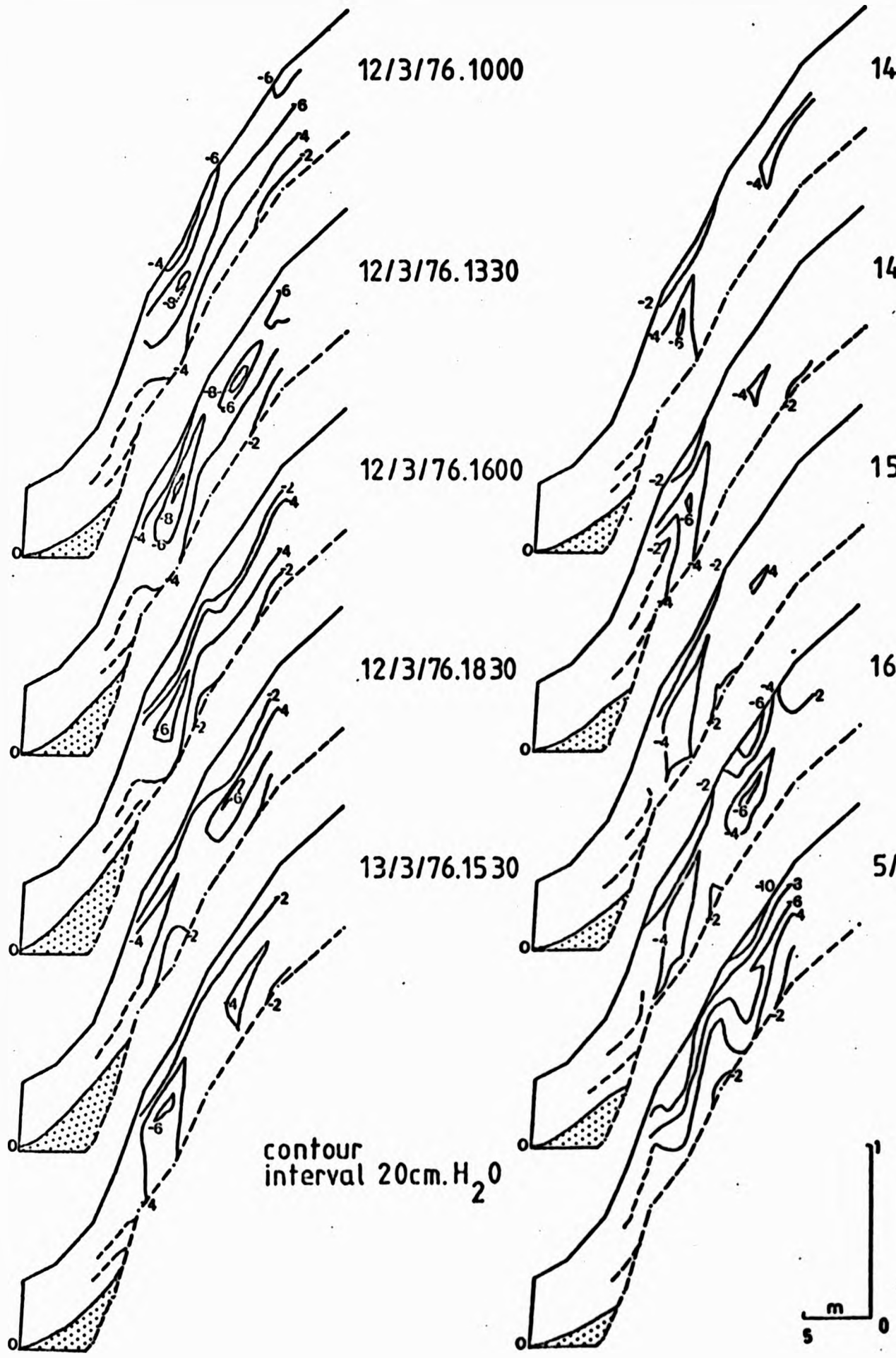

FIGURE 11.30: PATTERNS OF PORE WATER PRESSURE IN THE SLOPE 12 MARCH - 2 MAY 1976

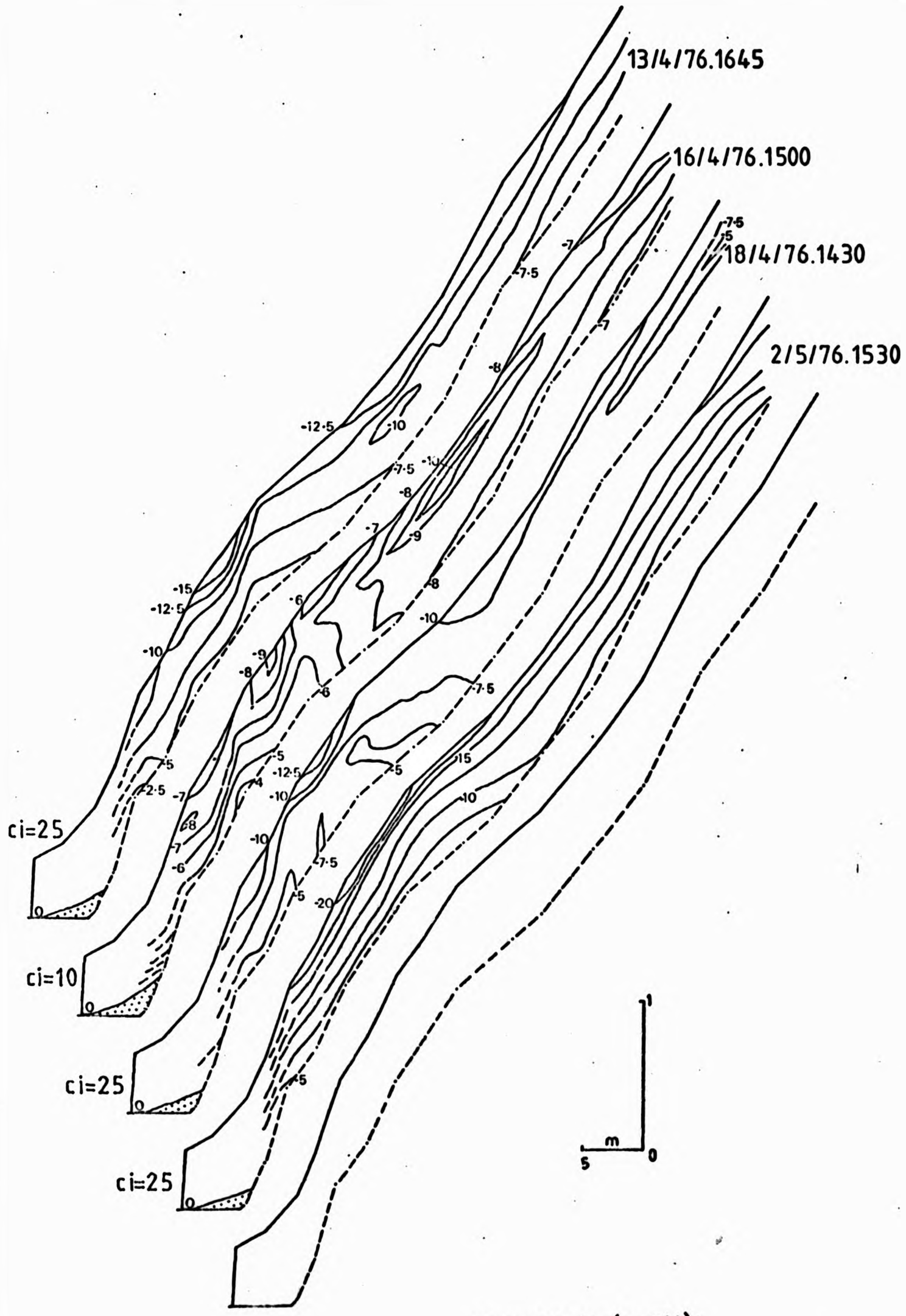

FIGURE 11.30 (cont'd):

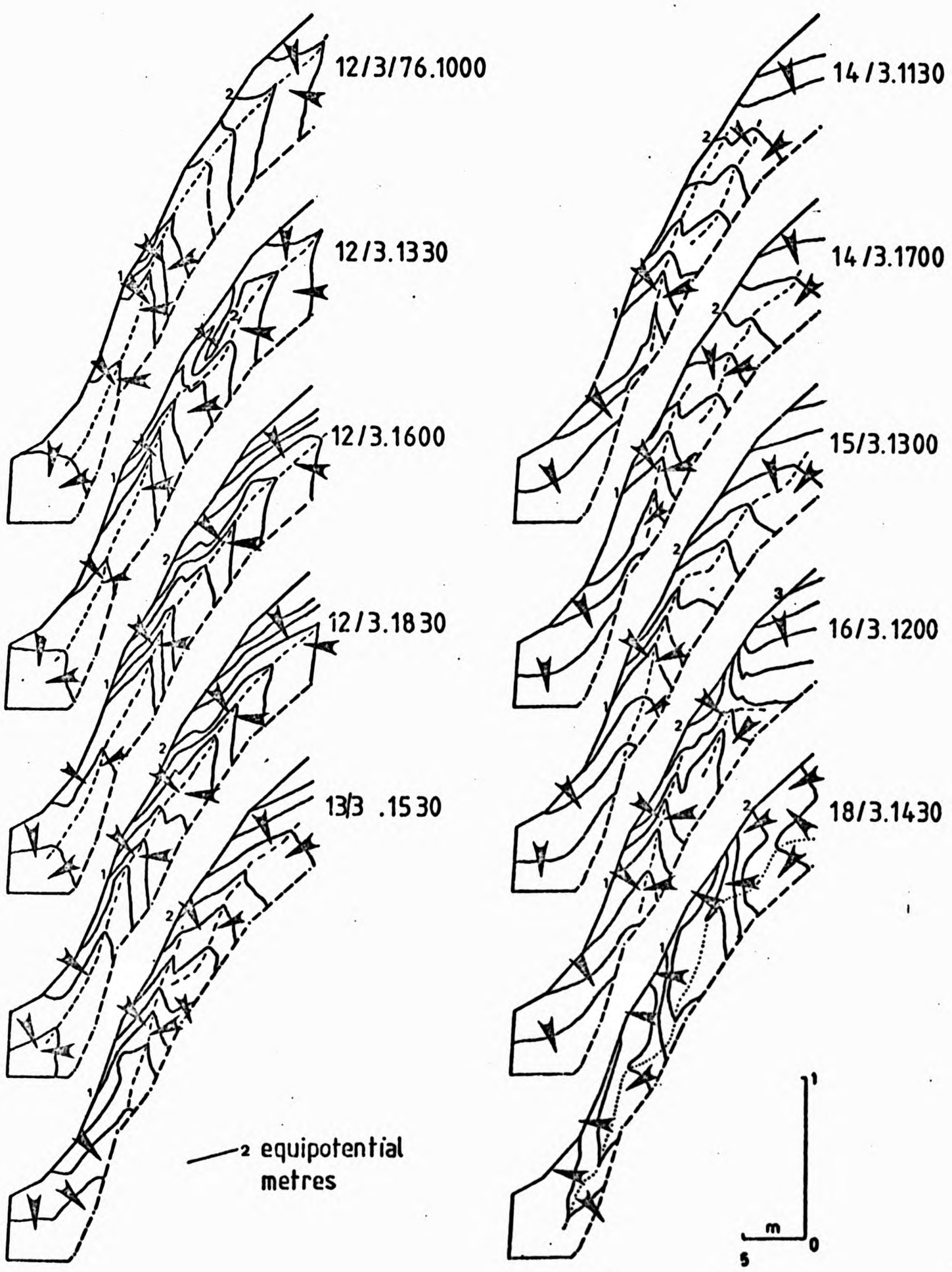

FIGURE 11.31: PATTERNS OF HYDRAULIC POTENTIAL IN THE SLOPE, 12 MARCH - 2 MAY 1976

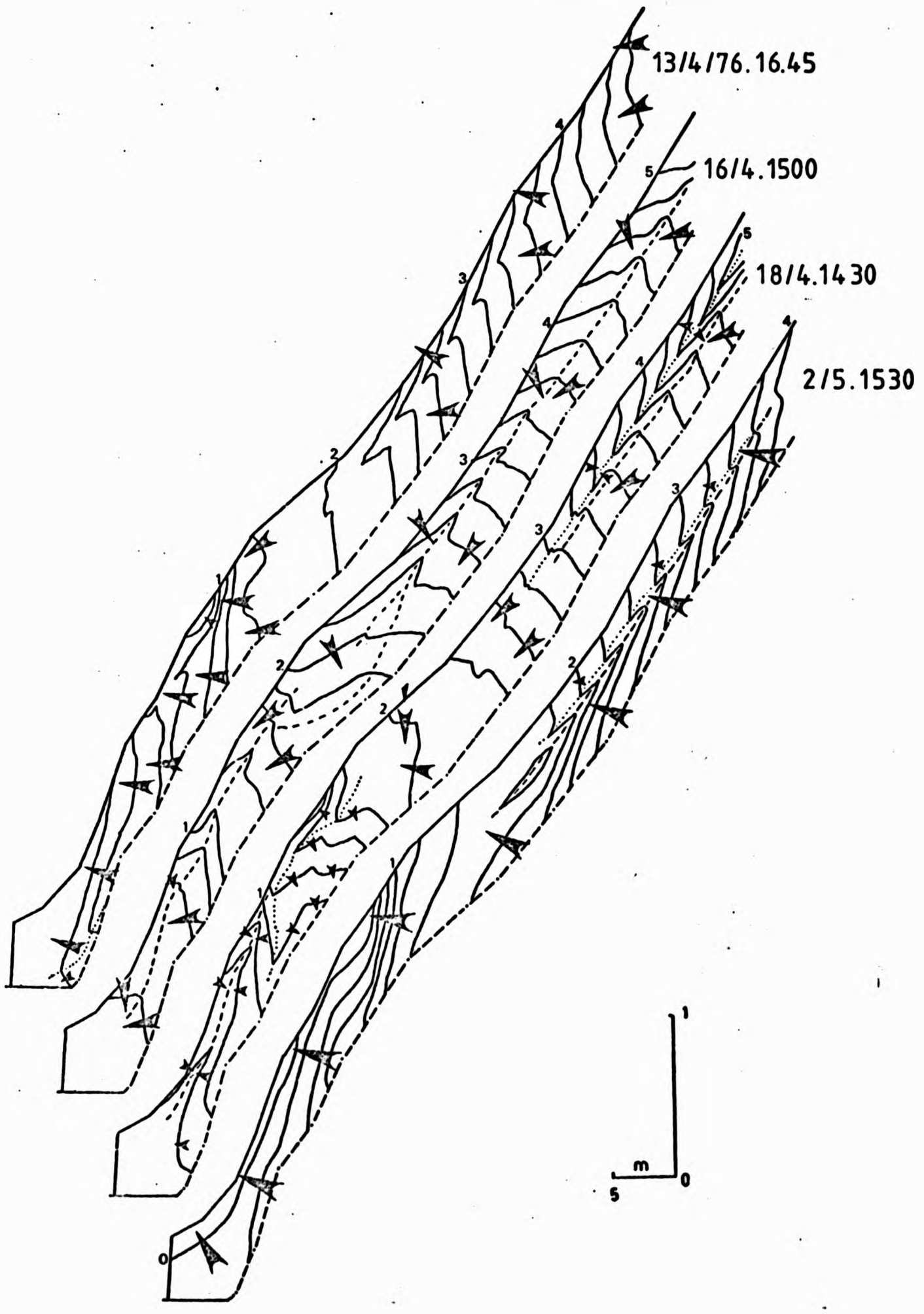

FIGURE 11.31 (cont'd)

Walk were only able to monitor ZFP depths to 70 cm below the surface, but it seems unlikely that upward flow extended to depths of 10 m due to the low hydraulic conductivity of the London Clay.

2 mm of rain during 15th April 1976 was adsorbed by upward flow and no increase in the size of the saturated wedge was recorded. Upwards flow was soon reinstated and continued for most of the 1976 summer.

11.5 DISCUSSION, SUMMARY AND CONCLUSIONS

In the final section of this chapter an attempt is made to summarise the results of water and solute movement with the hillslope and refer them to measurements at W1. This elevation of results from the slope to subcatchment scale takes no account of catchment spatial variation (Walling and Webb, 1980) but is a worthwhile step towards the physically based spatially distributed model discussed earlier.

A. Water Movement

Empirical relationships were found between height of the saturated zone (i.e. the water table) above the slope base and instantaneous stream discharge at W1 (Table 11.7 and Figure 11.32). There was a limited amount of data from upslope areas due to a reduced frequency of occurrence of saturated conditions, and this was partly responsible for non-significant correlations. The correlation is strongest near the channel, for piezometer 1 (1.25 m upslope) and piezometer 2 (4.5 m upslope), decreasing upslope, probably due to inaccuracies in the determination of the water table from tensiometer data. The relationship at P1 is almost linear for the data where $h \leqslant 30$ cm, validating the use of Darcy's Law for computing throughflow discharge and implying that recession flow was mainly supplied by the saturated wedge adjacent to the channel. Non-linearity is probably due to increases in saturated hydraulic conductivity near the soil surface noted earlier. Further slight non-linearity, not described by the power function, is also apparent at P1 and P2 above, about 30 cm, possibly due to the very marked increase in lateral K near the surface. The excellent correlation between the shape of the saturated wedge and streamflow confirms that this is the principal source of baseflow during recession periods and agrees well with research from other areas

TABLE 11.7: RELATIONSHIPS BETWEEN WATER TABLE HEIGHT ABOVE THE SLOPE BASE (h) cm, ON THE EXPERIMENTAL SLOPE AND STREAM DISCHARGE AT W1 (Q) l/s (RMA used)

Slope surface height above slope base z, cm	Distance upslope m	Relationship	Correlation coefficient r	N	Significance Level r, %
41	1.25	$Q = 0.38\ h^{0.74}$	0.97	28	0.1
50	4.50	$Q = 0.004h^{1.83}$	0.99	29	0.1
149	9.25	$Q = 2.34 \times 10^{-15} h^{7.53}$	0.73	21	0.1
176	11.5	$Q = 3.81 \times 10^{-24} h^{11.33}$	0.61	14	5 %
215	13.9	$Q = 7.31 \times 10^{-28} h^{12.38}$	0.80	10	0.1
240	16.25	$Q = 4.76 \times 10^{-30} h^{12.94}$	0.97	5	1.0
276	19.3	$Q = 5.62 \times 10^{-27} h^{11.36}$	0.93	4	NS
308	23.9	$Q = 5.71 \times 10^{-32} h^{13.20}$	0.73	5	NS
364	31.0	$Q = 7.84 \times 10^{-37} h^{14.72}$	0.77	7	5 %
597	50.5	$Q = 1.01 \times 10^{-47} h^{17.54}$	0.72	4	NS

TABLE 11.7: RELATIONSHIPS BETWEEN WATER TABLE HEIGHT ABOVE THE SLOPE BASE (h) cm, ON THE EXPERIMENTAL SLOPE AND STREAM DISCHARGE AT W1 (Q) l/s (RMA used)

Slope surface height above slope base z, cm	Distance upslope m	Relationship	Correlation coefficient r	N	Significance Level r, %
41	1.25	$Q = 0.38\ h^{0.74}$	0.97	28	0.1
50	4.50	$Q = 0.004h^{1.83}$	0.99	29	0.1
149	9.25	$Q = 2.34 \times 10^{-15}h^{7.53}$	0.73	21	0.1
176	11.5	$Q = 3.81 \times 10^{-24}h^{11.33}$	0.61	14	5 %
215	13.9	$Q = 7.31 \times 10^{-28}h^{12.38}$	0.80	10	0.1
240	16.25	$Q = 4.76 \times 10^{-30}h^{12.94}$	0.97	5	1.0
276	19.3	$Q = 5.62 \times 10^{-27}h^{11.36}$	0.93	4	NS
308	23.9	$Q = 5.71 \times 10^{-32}h^{13.20}$	0.73	5	NS
364	31.0	$Q = 7.84 \times 10^{-37}h^{14.72}$	0.77	7	5 %
597	50.5	$Q = 1.01 \times 10^{-47}h^{17.54}$	0.72	4	NS

(e.g. Weyman, 1973; Anderson and Burt, 1977b).

P1 and P2 hydraulic potential data was used with measured hydraulic conductivity to compute throughflow discharge 1.25 m upslope from equation (11.13). The relationship between W1 discharge (Q, l/s) and throughflow discharge (q, cc/s) is, as expected, of very similar form to that for water table height at P1,

$$Q = 9913\, q^{0.63} \quad (q < 5 \times 10^{-5}) \qquad (11.22)$$

$r = 0.99$; $N = 25$; Sig. level = 0.1 %

the data again exhibiting non-linearity (not included in equation 11.22) due to the rapid increase of hydraulic conductivity near the soil surface (Figure 11.33). In practice this means that high i intensity rain is required to fall upon a soil nearly saturated to the surface, before surface ponding can occur. Even then the rainfall must maintain this intensity for sufficient ponding to occur before overland flow can commence, ('ponding time', Freeze, 1980). Several authors found topography to be an important factor causing overland flow, particularly the presence of slope base concavity (e.g. Beven, 1977b) and hillside hollows, with convergent flow (e.g. Anderson and Burt, 1978). In the present case it has already been noted that concavity 5 - 6 m upslope may help cause surface seepage where the subsurface flow system is overloaded (see Figure 11.11, where computed flow at the pit is greater than computed flow at P1 when streamflow peaks). This feature, together with occasional seepage, was observed alongside the entire channel from the hillslope experiment to W1.

Two further points emerge from Figure 11.33. The first is that during hydrograph rise and recession periods the rate of water table rise decreases upslope. In particular the rapid rise at P1 and P2 is due to overloading of a thinning but highly conductive soil (at least near the surface) by lateral flow from upslope, in addition to rapid infiltration from above. The second point is that the fitted functions can be extrapolated to give minimum discharges at W1, for which saturation excess overland flow could occur on the hillslope ('minimum' due to the lack of precise information about the effect of high, near surface hydraulic conductivity). This discharge is shown by a dashed

line in Figure 11.33, and indicates that saturation excess overland flow is only likely to occur over the lowest 5 - 6 m of hillslope during conditions similar to those of November/December 1976.

B. Solute Movement

Solute data from the piezometer nearest to the channel (P1) are correlated with throughflow discharge over the same cross section (Figure 11.34). The relationships between throughflow discharge, q (cc/sec) and solute concentration (mg/l) are as follows (RMA given).

Potassium

$$K^+ \text{ conc.} = 0.66\ q^{0.82} \qquad (11.23)$$

r = 0.82; N = 22; sig. 0.1 % level

Sodium

$$Na^+ \text{ conc.} = 3.71\ q^{-0.10} \qquad (11.24)$$

r = - 0.81; N = 11; sig. 1.0 % level

Calcium

$$Ca^{++} \text{ conc.} = 3.65\ q^{-0.11} \qquad (11.25)$$

r = - 0.81; N = 11; Sig. 1.0 % level

Magnesium

$$Mg^{++} \text{ conc.} = 4.14\ q^{-0.10} \qquad (11.26)$$

r = - 0.86; N = 11; Sig, o.1 % level

The interesting point here is that they take the same general form as the discharge/concentration equations at W1. Although the sample sizes strictly limit detailed discussion, it is possible to detect perturbations of the general trends similar to those found during autumn 1976 storm data; these data however, were collected from late November 1976 to June 1977. Both calcium and potassium concentrations, for example, exhibit a rapid rise and fall in response to 8.4 mm of rainfall on 3rd May 1977, neither ion obeying the rating equation which describes the overall trend. Both peak concentrations were higher than those which occurred in streamflow at the same time, suggesting that the throughflow solute response was diluted by water from other sources,

found at West Walk, possibly due to the absence of a distinctly separate baseflow contributing aquifer.

The hillslope processes operating under conditions of storm rainfall and hydrograph recession which have been described in detail in this chapter are schematically summarised in Figures 11.35 and 11.36.

I. Storm Processes (Figure 11.35)

(i) Before start of rainfall (T = 0 hours)

Streamflow is maintained by lateral flow within a small saturated wedge. This is fed by mainly vertical unsaturated flow from up profile and lateral saturated and unsaturated flow from upslope. Over most of the slope flow is vertical and unsaturated. There is a tendency for lateral flow under the slope convexity and an indication that the saturated wedge extends deeper into the soil than was actually measured. Stream flow is relatively low in K^+ but higher in Ca^{++}, Mg^{++} and Na^+, primarily reflecting concentrations within the saturated wedge.

(ii) During intense rainfall (T = 1)

The saturated zone has extended up profile and upslope causing overland seepage about 6 m from the stream where the slope is concave. The zone from 6 - 12 m upslope is not saturated to the surface due to the higher vertical hydraulic conductivity, but between 12 - 24 m upslope is a zone of higher resistance to lateral throughflow causing a higher water table. Flow within the saturated zone is essentially downslope but turns down profile to overcome the lower hydraulic conductivity soil between 6 - 12 m. Equipotentials suggested that water flows under this zone (the 'convexity') to re-appear downslope. It appears that increases in K^+ concentration are due to leaching and transport of potassium from saturated upper soil horizons very close to the stream. Some of this K^+ may join overland seepage routes, leading to the familiar rise in K^+ concentration at W1. K^+ and Mg^{++} are also leached from near surface sources upslope and carried down into the saturated soil but is thought to be too far upslope to contribute to the stream chemograph. By contrast, the saturated wedge is higher in dissolved Ca^{++}, Mg^{++} and Na^+ than K^+, although it seems that additional amounts of these three cations are not leached from the upper soil

e.g. channel precipitation or overland flow from paths and tracks adjacent to the stream. It seems likely that these rapid increases in concentration result from the flushing of near surface cations accumulated in the soil 1 - 2 m from the stream by reverse potential flow under the influence of evapotranspiration. Subsurface water greater than 2 m away is unlikely to be transmitted rapidly enough to contribute to storm solute response. Whether the accumulated cations are in solution or adsorbed on particle surfaces is uncertain. However, in unsaturated soil, at the high tensions measured further upslope, it seems unlikely that dissolved cations could be flushed or diffuse from the small capillaries they occupy quickly enough to contribute to storm response. Under such conditions it is more likely that cations adsorbed onto the sides of the larger non-capillary cracks and root tubes would be re-dissolved and carried to the saturated zone. Vertical expansion of the saturated wedge adjacent to the stream will speed this process.

Surface organic matter has been identified as an important source of exchangeable cations, notably K^+ and Ca^+. This was likely to be a further source of cation supply adjacent to the stream, 10 cm piezometers exhibiting higher concentrations and visible organic colouring (as did suction pots further upslope).

T P Burt (1979) observed diurnal variations in the quantity and quality of stream discharge and throughflow in a Somerset catchment. He attributed flow reduction to evapotranspiration causing upward flow from the saturated wedge during the day, and flow increase to relaxation of plant water demand at night. At West Walk slight diurnal variations in streamflow at W1 were detected briefly on several occasions during spring flow recessions, at times when plant growth was probably at a maximum but not during extensive summer periods (e.g. the 1975 - 1976 drought). Detailed diurnal measurements of the saturated wedge were not made. Burt also explained the diurnal specific conductance variation of stream water by upward flow of high concentration soil water during the day, leaving low concentration ground water to sustain streamflow. The reverse flow of soil water at night led to an increase in the specific conductance of stream water. No measurable diurnal fluctuations in the SC of stream water at W1 were

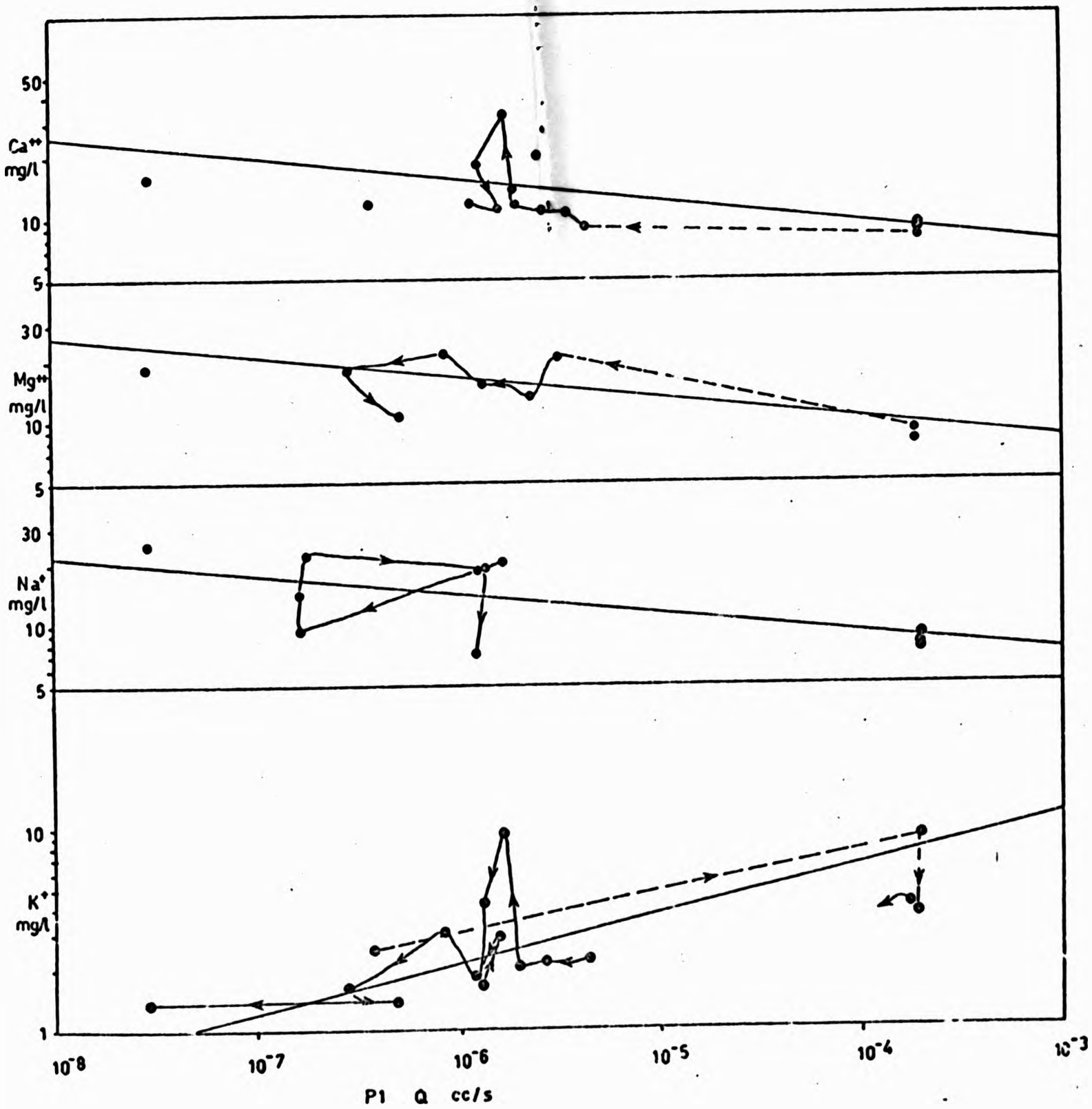

FIGURE 11.34: RELATIONSHIP BETWEEN SOIL WATER SOLUTE CONCENTRATIONS AND COMPUTED THROUGHFLOW AT PIEZOMETER 1

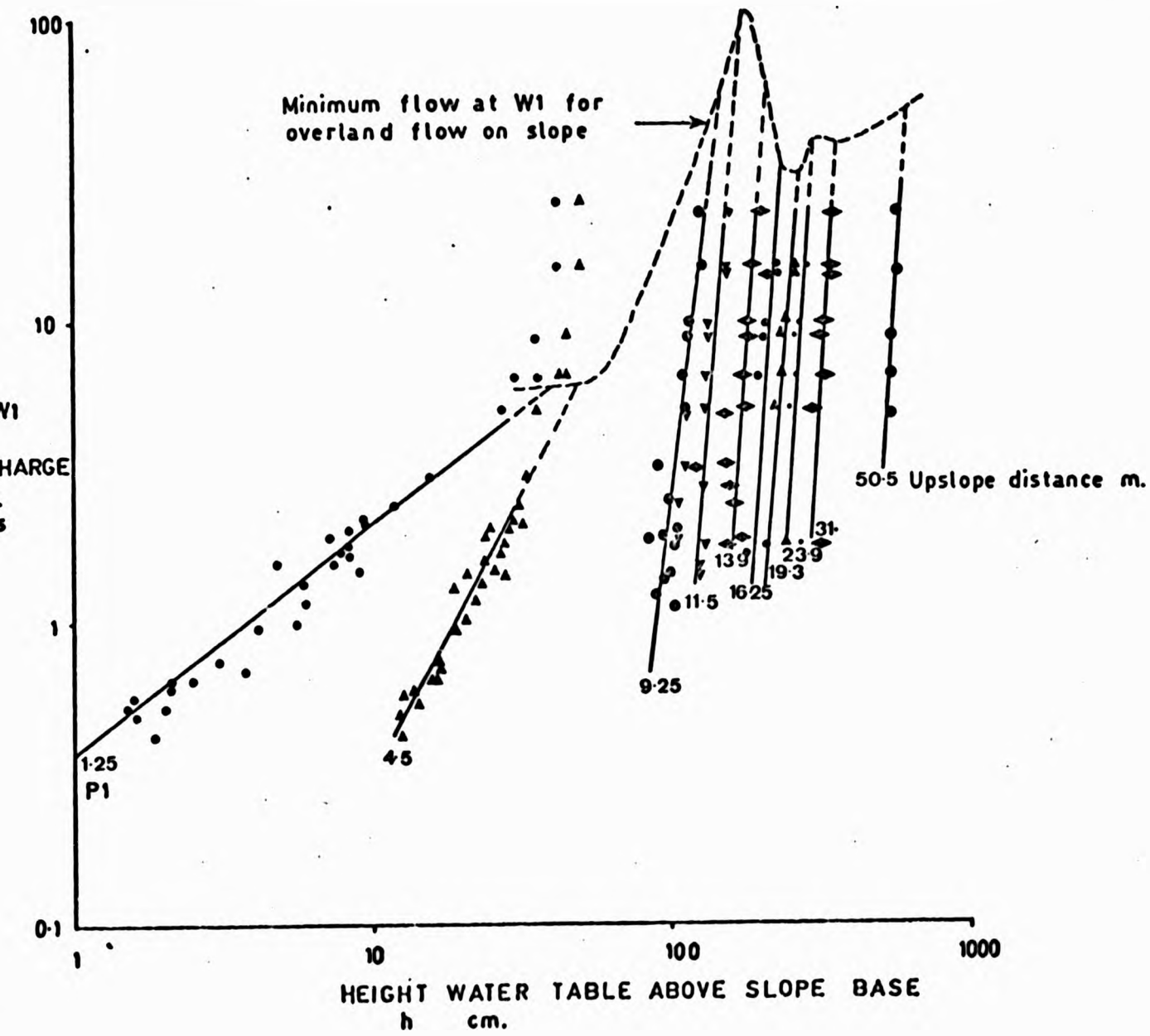

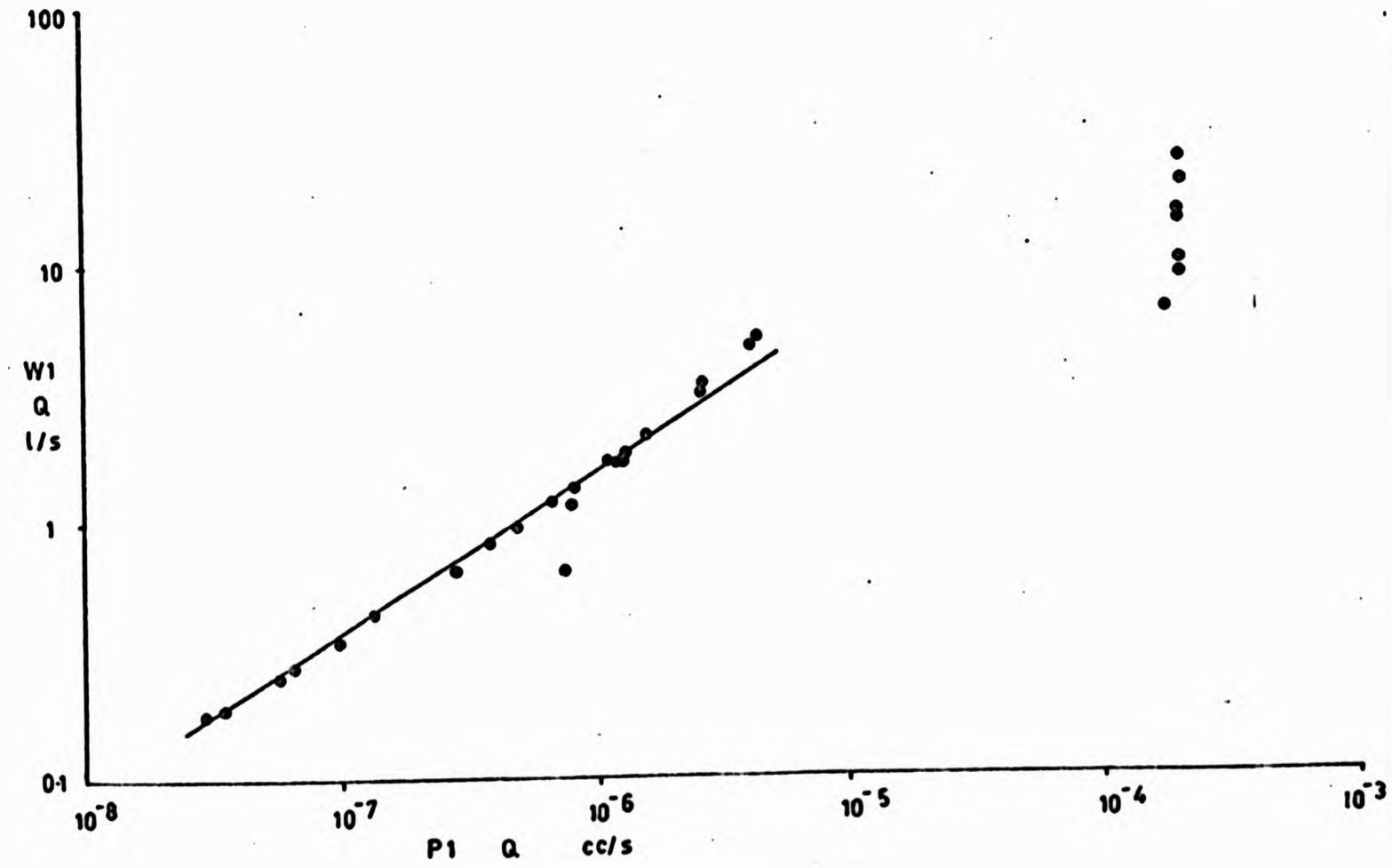

FIGURE 11.32: RELATIONSHIP BETWEEN WEIR 1 DISCHARGE AND HEIGHT OF THE WATER TABLE ON THE SLOPE (TOP)

FIGURE 11.33: RELATIONSHIP BETWEEN WEIR 1 DISCHARGE AND COMPUTED SLOPE BASE THROUGHFLOW (BOTTOM)

horizons in large enough quantities to overcome the dilution role of overland seepage and direct channel precipitation. Human and animal paths and tracks might also contribute significant (although unmeasured) quantities of infiltration excess overland flow, due to a reduction in hydraulic conductivity by trampling.

(iii) <u>After rainfall</u> (T = 6)

The water table is decreasing more rapidly upslope as lateral saturated dlow contributes to the saturated wedge. Vertical unsaturated flow contributes to the water table upslope. High concentration pulses of K^+ and Mg^{++} continue to move downslope in saturated soil and it is thought that these result in the quite common oscillation of solute concentrations during a normally smooth streamflow recession.

(iv) <u>Flow recession</u> (T = 12)

The saturated wedge continues to diminish and the processes are essentially the same as those described at T = 6. Overland seepage has stopped and solutes begin returns to pre-storm concentrations.

II. <u>Drainage</u> (Figure 11.36)

(i) <u>T = 0 days</u>

At the start of a recession period streamflow is maintained by a saturated wedge adjacent to the channel. At this stage the saturated wedge is fed by vertical unsaturated flow. Although the exact mechanisms of solute movement in the unsaturated soil are unclear, the saturated wedge is low in K^+ but higher in Ca^{++}, Mg^{++} and Na^{++}, accounting for the higher recession flow concentrations.

(ii) <u>T = 5 days</u>

After a period of increasing evapotranspiration rate, potential reversal occurs in slope soils, with flow towards the surface. This process dominates the lower slope due to the shorter rooted vegetation, while upslope potential reversal is more subdued and confined to the lower soil profile. Unsaturated flow is in both cases towards the surface, and carries solutes (although only K^+ was monitored) for plant uptake, adsorption onto soil particle surfaces or simple deposition.

(iii) T = 6 days

A small quantity of rainfall may reverse the upward unsaturated flow and although there is limited vertical progression of a wetting front, this is likely to cause vertical re-distribution of the surface accumulation of solutes, such that, near the stream, concentrations in the saturated zone may rise. This could be responsible for the cation 'flushing' phenomenon noted in Figure 11.35 and earlier chapters.

(iv) T = 7 days

If the rainfall and infiltration are sufficient to cause a rise in the water table near the stream, then this will speed the transfer of high cation concentrations to stream water. Moisture changes upslope are soon absorbed into the upwards flow system as evapotranspiration again begins to dominate.

(v) T = 20 days

A long period of upward flow without rainfall is likely to result in a considerable accumulation of cations near the soil surface, ready for autumn rainfall to reverse the pattern and carry solutes into stream water.

It was originally hoped that the slope experiment would help explain some of the complex features of stream flow solute variability within Subcatchment 1. Efforts have been made to link the two scales in this chapter, and a summary of the results seems desirable.

(a) The flushing of Ca^{2+}, Mg^{2+} and Na^{+}

Rapid increases in stream Ca^{2+}, Mg^{2+} and Na^{+} concentration, particularly during autumn storms, result from the flushing of near surface cations, accumulated in the soil close to the stream by upward flow during periods of evapotranspiration. Flushing could be reinforced by the piston displacement of water in the saturated wedge although the magnitude and timing of this process is not certain.

The recognition of a relationship between solute flushing and season in Chapter 7, together with results from the slope experiment, suggest that channel concentrations are the result of an interplay

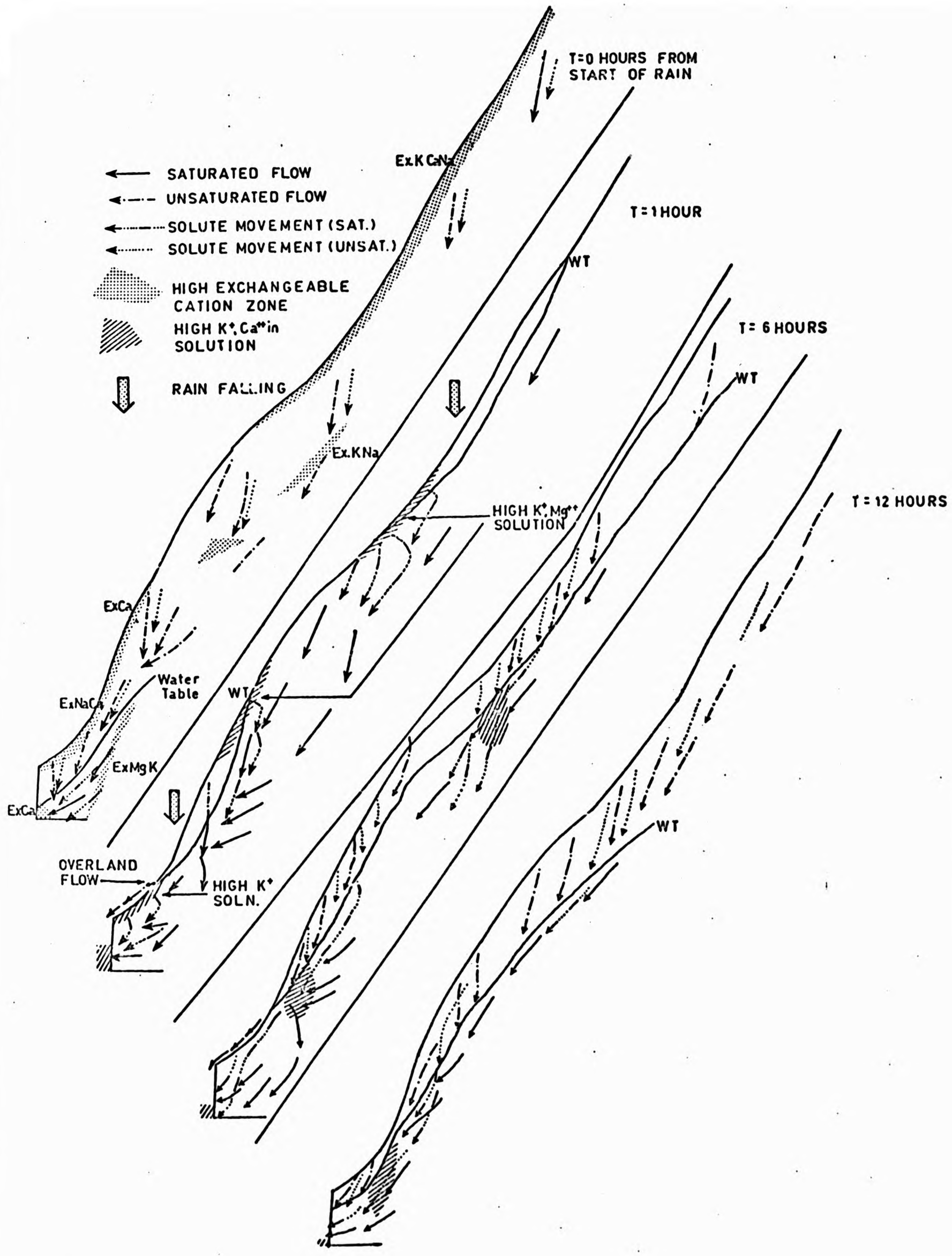

FIGURE 11.35: SCHEMATIC REPRESENTATION OF WATER AND SOLUTE PROCESSES IN THE HILLSLOPE DURING A WINTER STORM

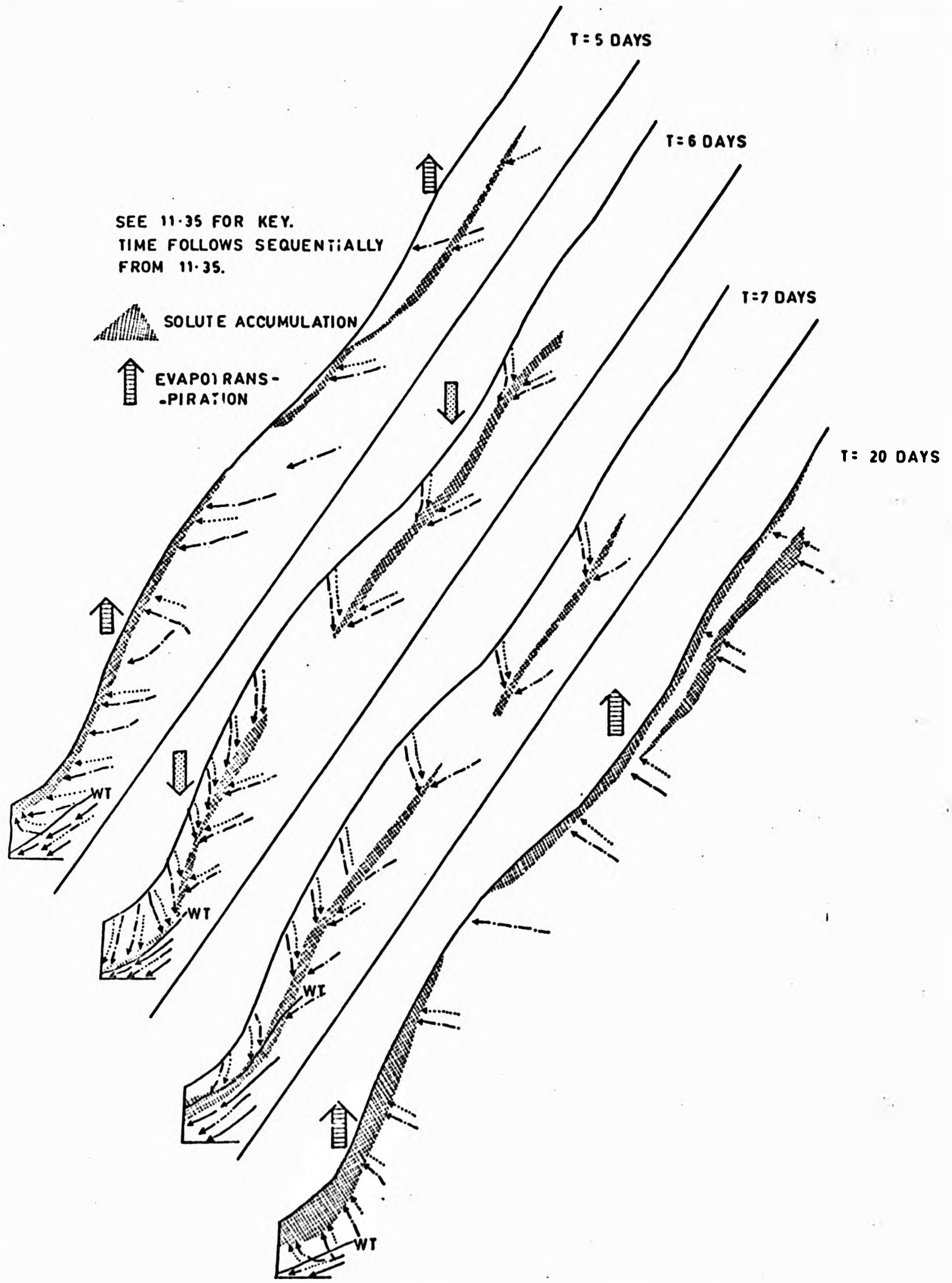

FIGURE 11.36: SCHEMATIC REPRESENTATION OF WATER AND SOLUTE PROCESSES IN THE HILLSLOPE DURING A DRAINAGE PERIOD

between different source areas. For example, the flushing effect seems to be enhanced during early autumn, partly due to limited dilution by overland flow. Stream flow sampling has shown a reduced flushing magnitude at other times of the year, possibly due in part to increased dilution by overland flow.

(b) K^+ and the lead effect

K^+ concentration in stream flow usually increases during storms due to the leaching of K^+ ions from near surface horizons adjacent to the stream. High lateral permeability in these horizons would allow rapid transport to the channel, the velocity controlling K^+ lead over discharge. It was shown that increased flood intensity, notably during summer months (see Figure 4.10) resulted in a smaller K^+ lead over discharge. From the available evidence this could be due to a reduction in unsaturated permeability at lower moisture contents, although it must outweigh the effect of inter-ped fissure enlargement as the soil dries. Conversely, during winter months the K^+ lead over discharge increases under the influence of higher lateral permeability and overland flow near the channel.

(c) Solute fluctuation during hydrograph recession

Fluctuations in solute concentration during early hydrograph recession phases are thought to be due to the arrival of high concentration solute pulses leached from upslope source areas. The spatial aspect of the processes operating requires further study. The arrival of K^+ at the stream would depend upon the length of subsurface travel involved, because this cation is preferentially adsorbed by clay minerals.

The net effect of upslope source areas during later recession periods seems to be one of solute supply (excluding K^+) to the saturated zone near the stream. This would account for the increase of Ca^{2+}, Mg^{2+} and Na^+, and decrease of K^+ in streamflow as flow recession proceeds.

In this study, the pattern of solute movement in the soil above 7 m upslope has been monitored using ceramic suction cups. Although there was some correlation between the cation concentration of soil water and exchangeable cation contents of the soil, no relationships existed with tension and hence moisture content. Cation concentration in soil water is a rather more complex function of exchange rates, adsorption and moisture flux according to the theoretical discussion of Chapter 9. The next Chapter develops a system of moisture and solute accounting based upon that theory.

CHAPTER 12

APPLICATION OF THE MODEL FOR WATER AND SOLUTE MOVEMENT IN THE HILLSLOPE SOIL AND A FRAMEWORK FOR MODELLING AT THE CATCHMENT SCALE

12.1 INTRODUCTION

Chapter 9 introduced continuity equations which are the basis of simulation models for water and solute movement in hillslope soils. K J Beven (1977a) noted that simulation models have two major aims. The first is to predict the behaviour of the real world system under a set of naturally occurring conditions. Model calibration is usually achieved by comparison of model and historical data, and where possible this should cover the magnitude frequency range anticipated in the simulation (e.g. A.W.A., 1980). The second is to explore the implications of making certain assumptions about the real world system. This approach has been used by Freeze (1972a and 1972b) and Beven (1977a and 1977b) to promote understanding of models' internal mechanisms.

In the present study elements of both aims are incorporated, as a defined model structure is tested by the processing of field data. Rainfall, soil water tension and chemical data are available, together with moisture/tension relationships for computation of water and solute fluxes within and at the base of the hillslope. Additional outputs from the model, which with these inputs is effectively a moisture - solute accounting method, are throughflow velocity, saturated - unsaturated hydraulic conductivity and solute dispersivity. Several factors can be varied to study their effect on outputs. Firstly, the anisotropy of soils with respect to hydraulic conductivity and dispersivity, and secondly the effect of interception on water and solute inputs.

At the end of the Chapter results from Section III of this thesis are reviewed in the context of a physically - based variable contributing area model of catchment solute response.

12.2 THE HILLSLOPE MODEL STRUCTURE

The computational technique employed in the model was introduced in Chapter 9. This is based upon a simple implicit finite difference

method (e.g. Atkinson, 1978; Freeze and Cherry, 1979) and extended to cover the case of solute movement. Such methods are commonly used in the field of ground water hydraulics (e.g. McWhorter and Sunada, 1977; Rushton and Redshaw, 1979) but were originally developed to solve heat flow problems in solid materials (e.g. Carslaw and Jaeger, 1959).

The selection of any particular technique depends upon the complexity of the problem, In the case of a homogenous, isotropic body, soil or aquifer, it might be adequate to employ an analytical solution to the relevant flux equations. The movement of pollutants in ground water has been modelled in this way (e.g. see the review by Freeze and Cherry, (1979), Ch. 9.2) Finite difference methods are versatile tools for the solution of more complex situations (Rushton and Redshaw, 1979) and can be very broadly divided into explicit or implicit solutions. Using the explicit method the value of hydraulic or chemical potential at any grid point is dependent only on potentials at the previous time step and not on concurrent values at adjacent grid points. With the implicit method, however, the potential at grid point (i, j) depends upon the value of potential at $t + \Delta t$ at the adjacent grid points, i.e. $(i + 1, j)$, $(i, j + 1)$, $(i - 1, j)$, $(i, j - 1)$. Solution using the latter approach is often achieved by an iterative technique (McWhorter and Sunada, 1977). In the present set of programs this has not been employed, although it might be a useful technique for converging element exit and entrance fluxes in further model development.

Whereas the finite difference technique requires a regular discretisation of the continuum that makes up the region of flow, the finite element technique allows the design of an irregular mesh that can be hand tailored to any specific application. Beven (1977a) gives the other advantages of this method as ability to deal with slope curvature, variable soil depth, complex boundary conditions, heterogeneity and anisotropy. Despite these advantages, development of this technique for processing of field data was beyond the scope of the present work. The finite difference technique used may be an over-simplification, but it was thought to be best to start at this level and introduce extra sophistication as necessary.

The method used continues from the outline in Chapter 9, but is detailed in Appendix 4 so as not to overburden the text. It has been

programmed in BASIC for use on the WANG 2200 B mini computer and is included in Appendix 2. Problems were encountered with the limited amount of storage space available and it was necessary to chain the program so that only one small section used computer storage at a time, the necessary common variables being carried across each chain. Thus there are 12 sections of program, seven for water flux computation and five for solute flux computation. A generalised flow chart is given in Table 12.1.

The dimensions of boundary elements are deliberately kept small in the model and the tension and solute concentration are estimated mathematically. Pit face tension is estimated by extrapolation from a linear equation fitted to the three upslope values of tension. This is a reasonable approximation judged from the work of the previous chapter, but could be misleading if the pit itself affects natural conditions. Near surface and profile base tensions (at 1.25 cm and 101.25 cm depths) are estimated by fitting cubic functions to the profile data. This technique has previously been used by Erh (1972) and Nielsen et al (1973). Similar methods are used for estimation of solute concentrations at the same points. There are dangers in extrapolating from fitted cubic functions because they can 'wander' and become poor estimators. In the absence of equipment for a more intensive sampling network they provided the best possible method for producing peripheral data.

Moisture content is estimated from tension with cubic functions which describe the ϕ / ψ scanning curves (see Appendix 2(x)(b) : FLUX 2, program lines 80 - 390). This represents a source of error because these curves do not take into consideration the hysteresis in soil wetting and drying. However, in the absence of actual moisture contents, they represent the best available method.

The approach described in Chapter 9 makes the assumption that the soil is homogenous and isotropic, although measurements of hydraulic conductivity showed that this was not the case. Therefore, in FLUX 5 an option is available for specifying the degree of anisotropy, R, present in each element, expressed as downslope K/downprofile K.

TABLE 12.1: GENERALISED FLOW CHART OF THE FLUX-CHEMFLUX MODEL

Start by loading FLUX 1 from disc; program will then continue to run, from FLUX 1 to CHEMFLUX 4, back to FLUX 1 etc., so long as there are data supplied from disc storage.

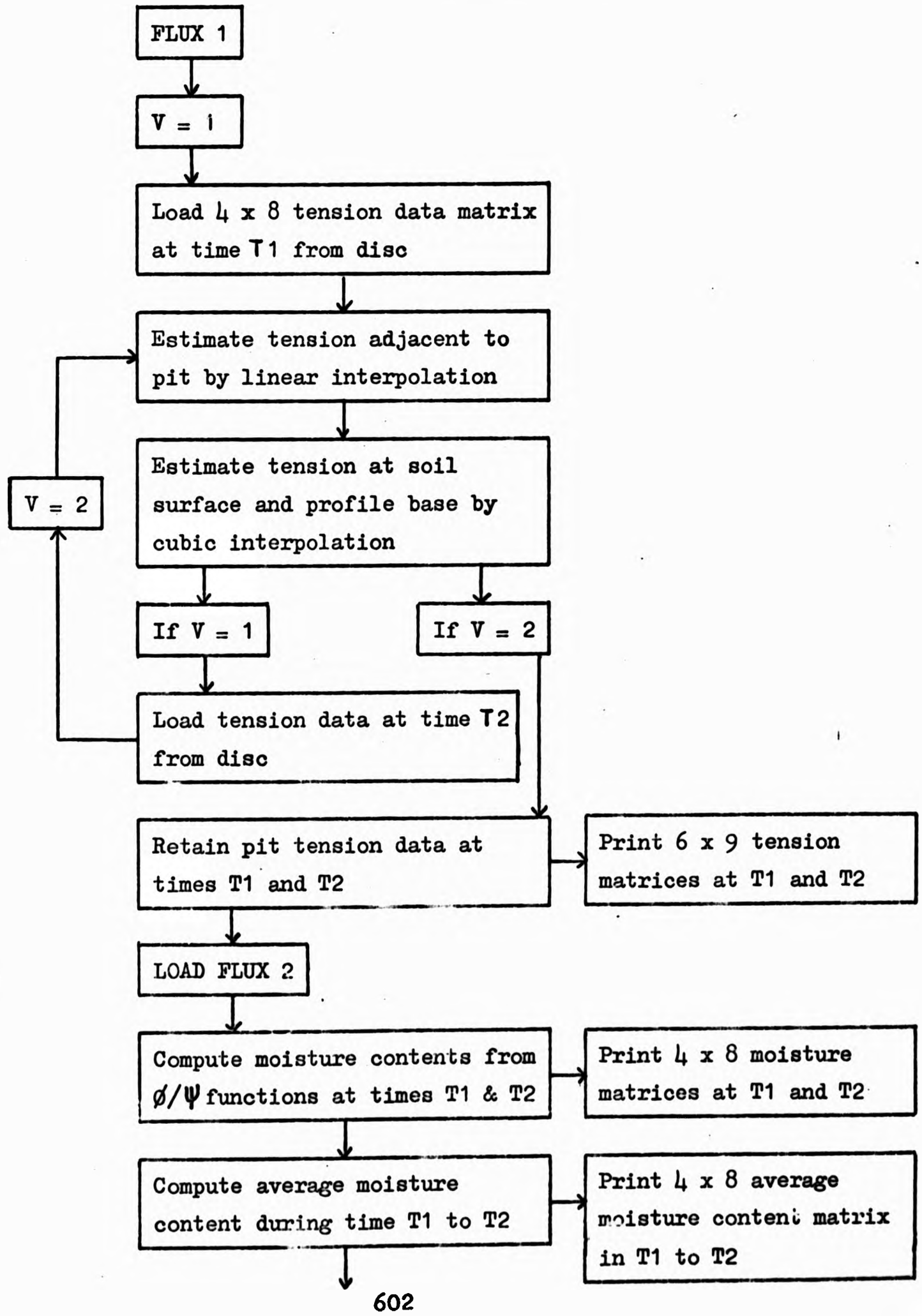

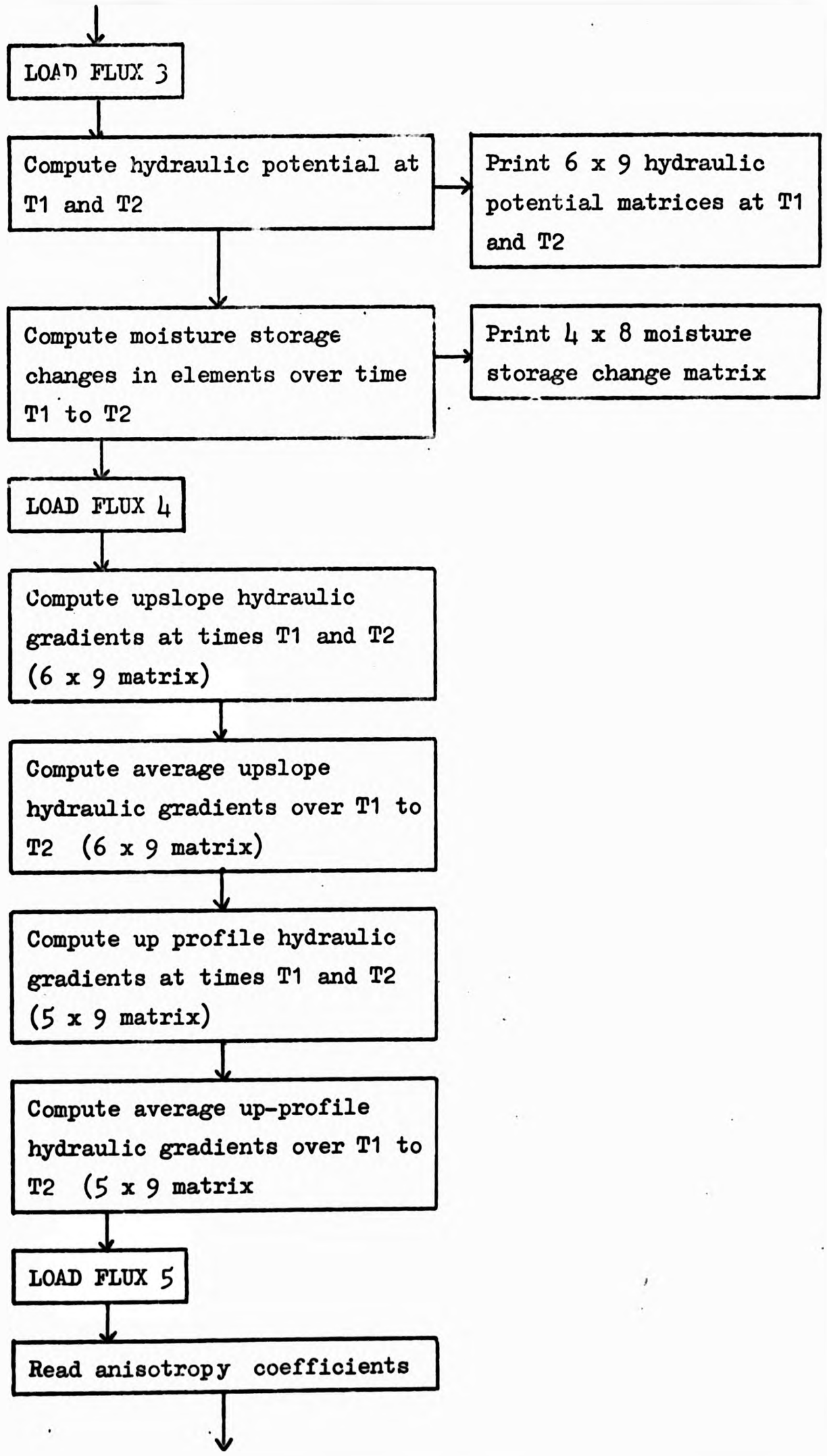
LOAD FLUX 3
Compute hydraulic potential at T1 and T2
Print 6 x 9 hydraulic potential matrices at T1 and T2
Compute moisture storage changes in elements over time T1 to T2
Print 4 x 8 moisture storage change matrix
LOAD FLUX 4
Compute upslope hydraulic gradients at times T1 and T2 (6 x 9 matrix)
Compute average upslope hydraulic gradients over T1 to T2 (6 x 9 matrix)
Compute up profile hydraulic gradients at times T1 and T2 (5 x 9 matrix)
Compute average up-profile hydraulic gradients over T1 to T2 (5 x 9 matrix
LOAD FLUX 5
Read anisotropy coefficients

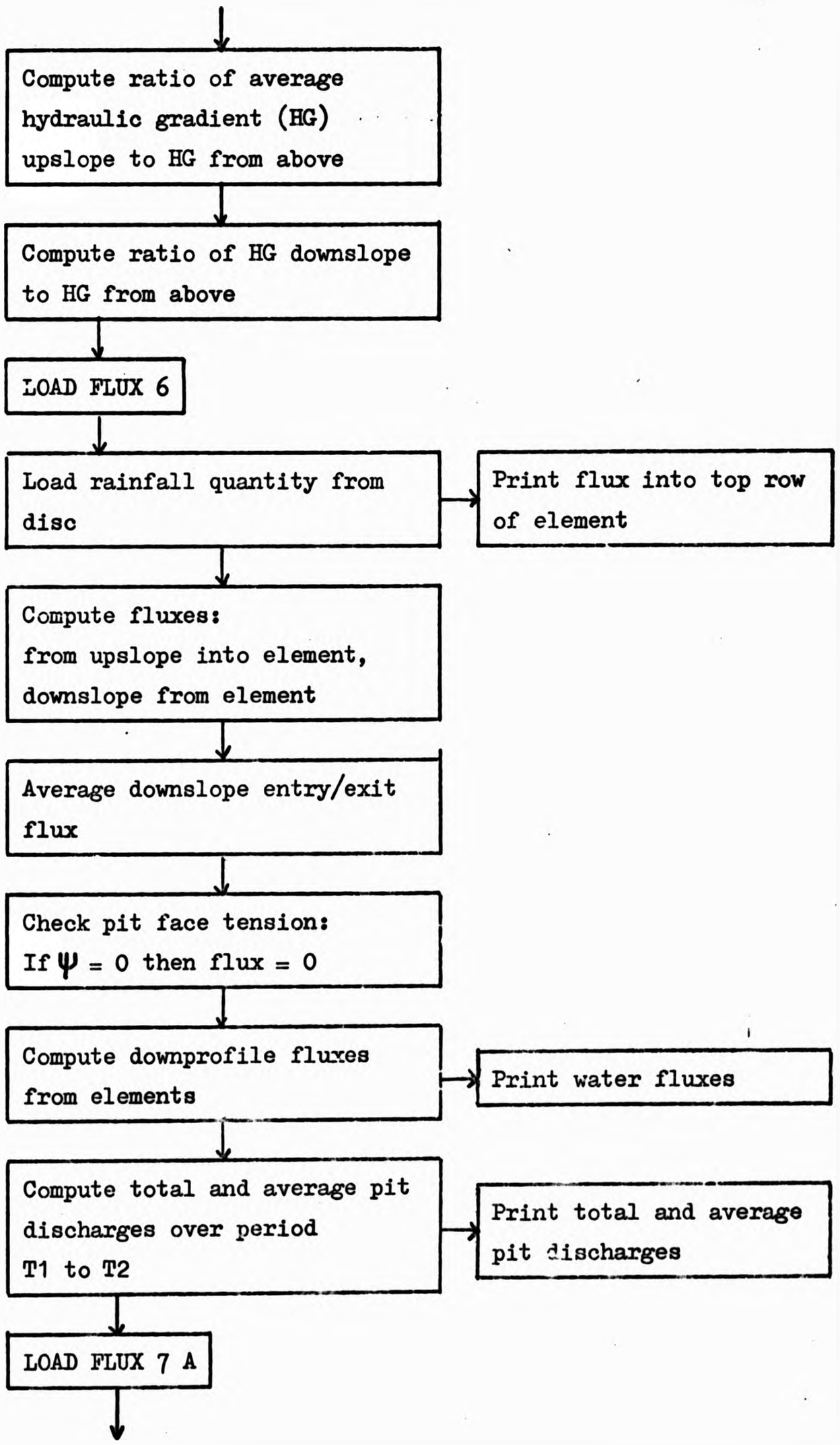
Compute ratio of average hydraulic gradient (HG) upslope to HG from above
Compute ratio of HG downslope to HG from above
LOAD FLUX 6
Load rainfall quantity from disc
Print flux into top row of element
Compute fluxes: from upslope into element, downslope from element
Average downslope entry/exit flux
Check pit face tension: If ψ = 0 then flux = 0
Compute downprofile fluxes from elements
Print water fluxes
Compute total and average pit discharges over period T1 to T2
Print total and average pit discharges
LOAD FLUX 7 A

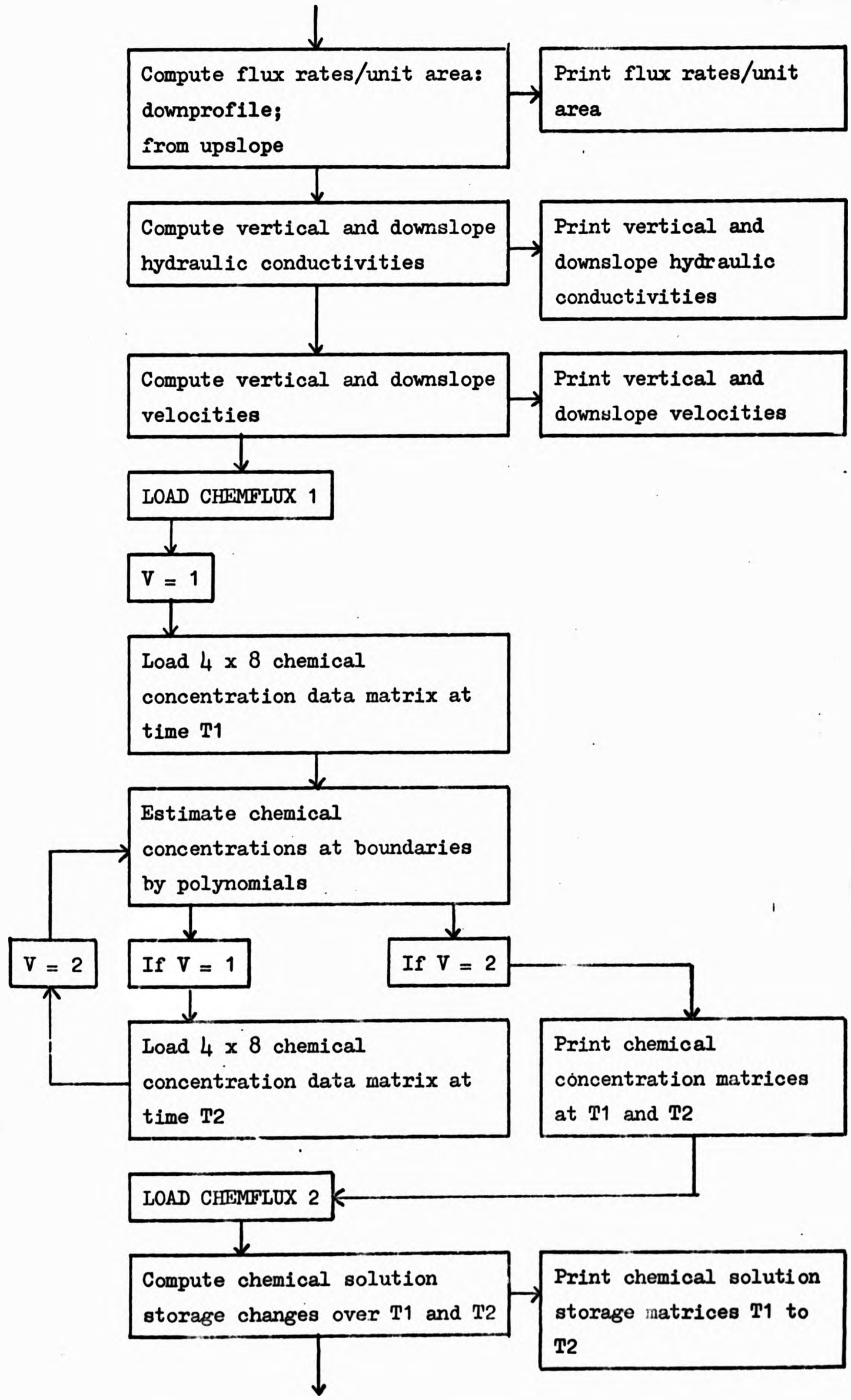
Compute flux rates/unit area: downprofile; from upslope
Print flux rates/unit area
Compute vertical and downslope hydraulic conductivities
Print vertical and downslope hydraulic conductivities
Compute vertical and downslope velocities
Print vertical and downslope velocities
LOAD CHEMFLUX 1
V = 1
Load 4 x 8 chemical concentration data matrix at time T1
Estimate chemical concentrations at boundaries by polynomials
V = 2
If V = 1
If V = 2
Load 4 x 8 chemical concentration data matrix at time T2
Print chemical concentration matrices at T1 and T2
LOAD CHEMFLUX 2
Compute chemical solution storage changes over T1 and T2
Print chemical solution storage matrices T1 to T2

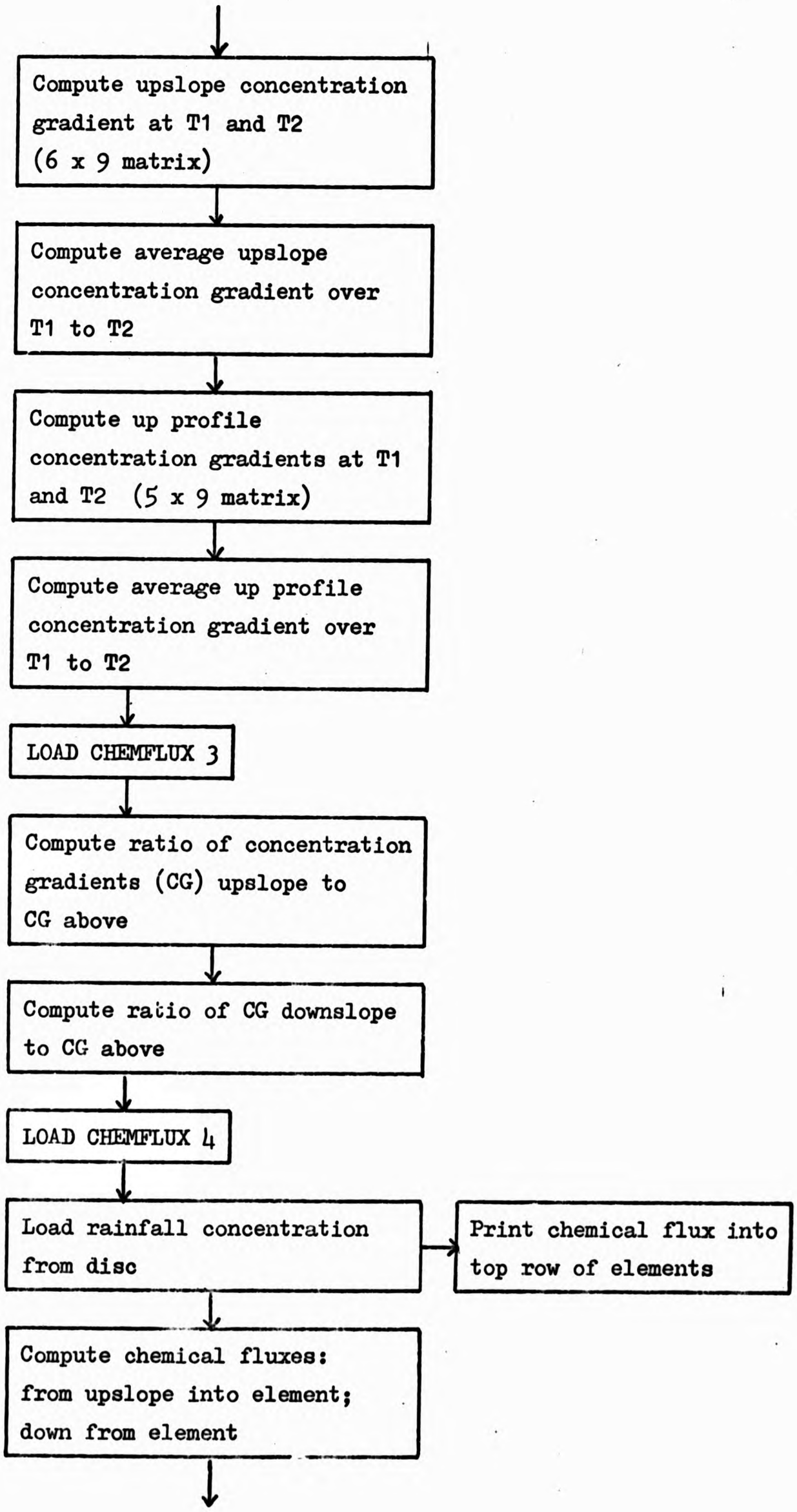
Compute upslope concentration gradient at T1 and T2 (6 x 9 matrix)
Compute average upslope concentration gradient over T1 to T2
Compute up profile concentration gradients at T1 and T2 (5 x 9 matrix)
Compute average up profile concentration gradient over T1 to T2
LOAD CHEMFLUX 3
Compute ratio of concentration gradients (CG) upslope to CG above
Compute ratio of CG downslope to CG above
LOAD CHEMFLUX 4
Load rainfall concentration from disc
Print chemical flux into top row of elements
Compute chemical fluxes: from upslope into element; down from element

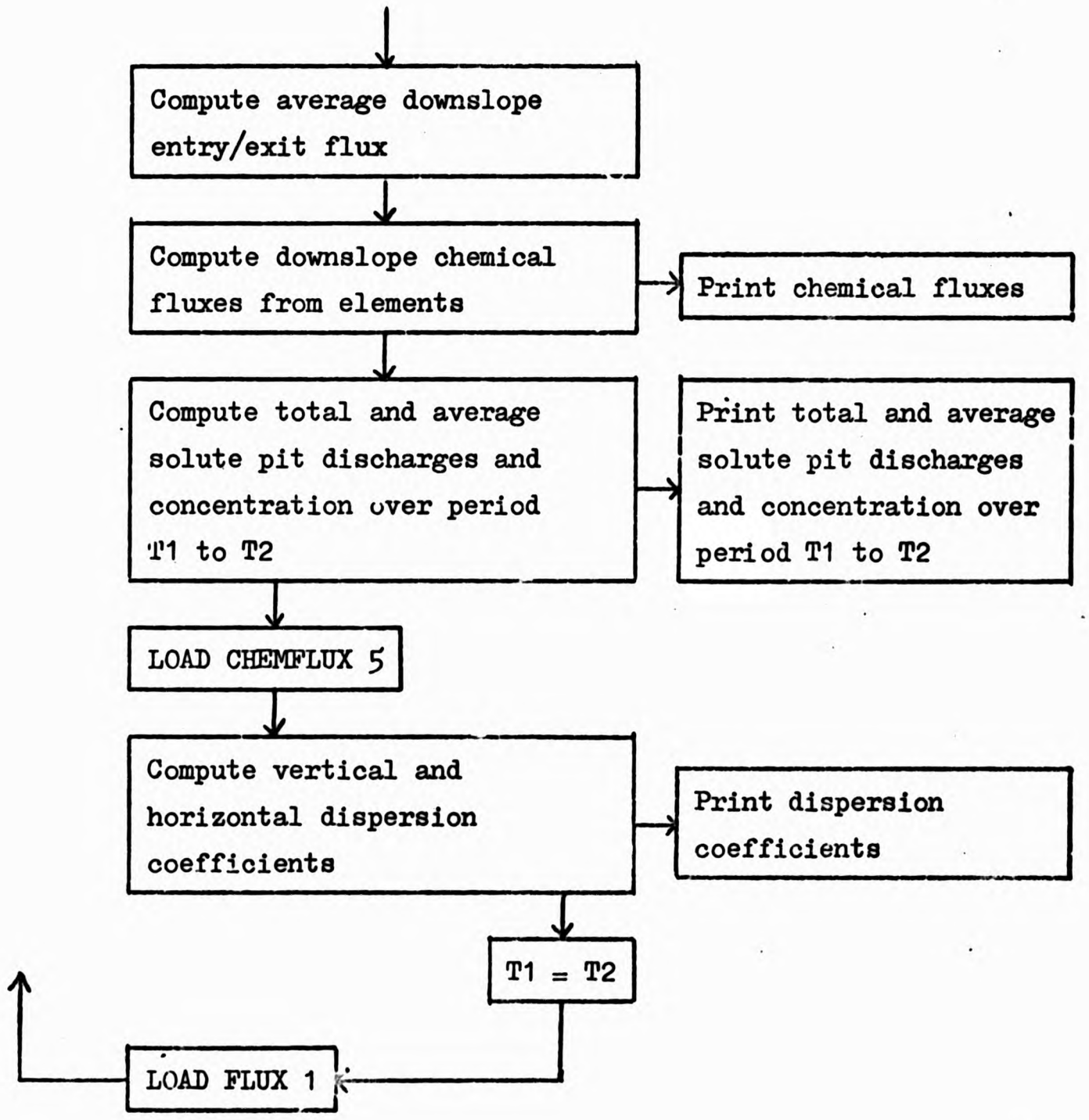
Compute average downslope entry/exit flux
Compute downslope chemical fluxes from elements
Print chemical fluxes
Compute total and average solute pit discharges and concentration over period T1 to T2
Print total and average solute pit discharges and concentration over period T1 to T2
LOAD CHEMFLUX 5
Compute vertical and horizontal dispersion coefficients
Print dispersion coefficients
T1 = T2
LOAD FLUX 1

Two sets of data were prepared for testing the model. The first was tension, rainfall, K^+ and Mg^{2+} concentrations from 1330, 29th November 1976 to 1330, 3rd December 1976, and prepared in four hour blocks by careful hand interpolation from the plotted data and stored on magnetic disc. The second was tension, actual evaporation (from the Met. Office) and K^+ concentration from 1200, 12th May 1976 to 1200, 1st June 1976, prepared as daily blocks by careful hand interpolation from the plotted data and stored on magnetic disc.

Actual evaporation was treated as a 'negative input' to the soil surface. The time resolutions might be too crude, e.g. in the latter case, not fully describing the diurnal cycle; but represent the best possible with the instrumentation available. Clearly, automatic monitoring of tension, e.g. Anderson and Burt, (1977), would give a more satisfactory data set without the necessity for interpolation.

Although the computer programs run as they stand it was not possible to carry out complete test runs with the data prepared, for the following reasons. Firstly, the WANG 2200 B computer was found to be very slow, one time increment taking 20 minutes to process the data and print the results. No other computer was available for the lengthy periods of debugging and experimentation necessary. Secondly, problems were encountered due to hardware errors with the WANG 2200 B system which prematurely curtailed work.

Two runs with the 29th November 1976 data were possible but restricted to moisture flux only, since this part of the program must operate satisfactorily before solute fluxes can be computed. The first part of a typical printout is shown in Figure 12.1.

Run 1

This was made with an anisotropy factor of R = 1, i.e. the soil was assumed to be isotropic. Two generalised results were considered first: average flux rate per unit area of soil profile at the pit face and average flux rate per unit area of the slope profile base (70 cm depth), taken as an average over the whole slope. The first gave the pit throughflow hydrograph while the second gave the hydrograph of vertical infiltration or loss from the slope soil. The data are

```
 TENSION TIME 1 CM
 - 37.6 - 17.9 -  1.2   7.1  18.7   8.8  20.0 - 14.1 -  0.2
 - 15.1 -  9.3 -  3.0   3.2  12.8  12.9  14.6 -  6.0   2.6
   3.1   2.2   2.7   1.0   5.9  23.0   9.4  10.2  13.3
 -  5.2   0.9 -  4.1   7.7   9.5  13.0   6.8  11.4   7.4
 - 25.4 -  3.0   8.2  37.6  27.0  17.2  11.6  26.2  10.2
   2.6 - 13.4  15.1  74.0  56.1   4.2  25.3  25.7 -  0.0
TENSION TIME 2
 - 20.6 - 17.1 -  4.1 -  6.7 -  1.5 -  2.4   8.0 - 12.3   1.1
 -12.5 -  8.7 -  6.7 -  1.7 -  0.5   0.0   4.2 -  7.5   0.5
   2.2   1.2   0.0 -  1.0   3.0   7.7   0.5   0.5 -  1.0
 -  6.7   2.8 -  4.5  13.5   5.5   6.0   2.5   5.7   1.5
 - 10.2 -  0.1  20.0  26.5  19.0  15.0  17.2  22.2   8.5
   1.1 -  8.9  37.6  39.5  31.6  17.9  42.2  34.6  21.3
MOISTURE CONTENT TIME 1 CC/CC
 .422 .425 .315 .427 .340 .292 .327 .307
 .331 .436 .472 .334 .426 .323 .356 .333
 .419 .332 .300 .455 .478 .383 .246 .350
 .336 .320 .253 .305 .471 .411 .435 .413
MOISTURE CONTENT TIME 2
 .421 .434 .320 .428 .359 .290 .531 .311
 .333 .442 .477 .391 .441 .331 .367 .352
 .417 .332 .354 .401 .495 .391 .254 .358
 .335 .310 .206 .312 .475 .406 .492 .413
AVERAGE MOISTURE CONTENT OVER PERIOD
 .421 .430 .318 .427 .352 .290 .529 .300
 .332 .440 .475 .368 .434 .327 .361 .343
 .418 .332 .357 .458 .430 .387 .250 .354
 .337 .321 .261 .390 .473 .409 .488 .413
HYDRAULIC POTENTIAL  TIME 1  CM
 61.3 129.7 172.9 220.8 257.4 283.6 326.7 348.6 595.4
 75.0 129.7 162.5 208.2 242.6 275.9 312.6 343.0 589.6
 78.4 126.2 153.2 191.0 220.9 274.0 292.4 349.2 535.3
 59.9 114.9 130.4 167.7 214.5 259.0 279.8 340.4 569.4
  4.8  76.0 113.7 182.6 197.0 223.2 249.6 320.2 537.2
  1.0  34.3  89.4 137.8 194.9 179.0 232.0 288.5 495.7
HYDRAULIC POTENTIAL  TIME 2
 72.3 130.5 170.0 207.0 237.2 272.3 314.7 350.3 596.9
 77.7 130.3 158.8 208.3 229.5 266.0 302.2 346.5 587.5
 77.4 125.2 150.5 189.0 218.0 258.7 283.5 339.5 571.0
 58.5 110.8 136.0 193.5 210.5 247.0 275.5 334.7 563.5
 19.9  78.9 125.5 171.5 189.0 221.0 255.2 316.2 535.5
  0.1  38.7 111.8 153.3 170.4 192.6 243.9 297.4 517.1
STORAGE CHANGE  FOR ELEMENT CC
 -  4.8  42.9  22.9   2.5  59.6  36.9  19.9
   3.0  10.2  12.7  21.8  44.0  23.0  31.5
 -  5.7   0.7 - 14.3  14.0  38.9  15.1  18.4
 - 61.0 -102.6 230.0 121.3  74.3 - 34.2 108.6
HILLSLOPE WATER FLUX.....PIT IS AT BOTTOM LEFT
OUTPUT FORMAT AS BELOW
**********************************************
DOWNPROFILE FLUX INTO TOP ELEMENT
**********************************
FLUX FROM UPSLOPE INTO ELEMENT
FLUX DOWNSLOPE FROM ELEMENT
DOWNPROFILE FLUX FROM ELEMENT
*****************************
FLUX IN CC.
***********
ROW 1
*************
   16.62    11.62    11.87    13.50    19.12    29.25    65.25
*************
    2.48     0.13     0.08     0.10     0.05     0.00     0.36
    0.00     2.48     0.13     0.08     0.10     0.06     0.00
   14.23    52.23    34.75    16.09    78.74    66.27    85.46
ROW 2
*********
    0.38     0.51     0.15     0.53     0.17     0.21     0.52
    0.40     0.38     0.51     0.15     0.53     0.17     0.21
   18.11    62.58    47.16    38.36   122.44    89.33   117.37
ROW 3
*********
    0.10     3.56     1.44     0.29     0.10     0.11     0.15
    0.00     0.10     3.56     1.44     0.29     0.10     0.11
   12.46    59.66    34.92    54.17   161.24   104.49   135.84
ROW 4
*********
    3.23     6.61     1.50     2.39     1.43     1.21     1.29
    0.00     3.23     6.61     1.50     2.39     1.43     1.21
   45.94    99.03   265.90   176.38   234.58    20.03   244.54
**********************************************************
TOTAL PIT DISCHARGE= 53.0039 469389 CC
AVERAGE PIT DISCHARGE= 2.11253038E-07 CC/SEC
**********************************************************
```

FIGURE 12.1: TYPICAL OUTPUT FROM THE HILLSLOPE WATER AND SOLUTE FLUX MODEL

```
FLUX RATE  PER UNIT AREA  CC/HOUR
DOWNPROFILE
INTO ELEMENT FROM UPSLOPE
*********
ROW 1
********
 0.010  0.056  0.036  0.014  0.051  0.028  0.016
 0.041  0.002  0.001  0.001  0.001  0.001  0.006
ROW 2
********
 0.013  0.067  0.050  0.035  0.080  0.038  0.022
 0.007  0.010  0.003  0.010  0.003  0.004  0.010
ROW 3
********
 0.009  0.064  0.037  0.059  0.105  0.044  0.026
 0.002  0.009  0.006  0.007  0.002  0.002  0.004
ROW 4
********
 0.035  0.103  0.282  0.164  0.153  0.008  0.047
 0.013  0.027  0.006  0.010  0.005  0.005  0.005



VERTICAL K,CM/HOUR
DOWNSLOPE K,CM/HOUR

ROW 1
*************************************************
0.0378 0.0967 0.0351 0.0134 0.1270 0.0219 0.0852
0.3062 0.0113 0.0116 0.0143 0.0140 0.0234 0.0437
ROW 2
*************************************************
0.0143 0.0434  0.0350 0.0514 0.0601 0.0371 0.0332
0.0074 0.0059 0.0243 0.0703 0.0744 0.0535 0.0352
ROW 3
*************************************************
0.0060 0.1366 0.0958 0.0906 0.1193 0.0621 0.0473
0.0287 y0.3906  0.3917 0.0558 0.0436 0.0352 0.0332
ROW 4
*************************************************
 0.0267  0.1780 1.3657 0.4972 0.1326 0.0226 0.0583
0.0723 0.1163 0.0033 0.1053 0.0909 0.0547 0.0473
*************************************************
WATER VELOCITIES
DO NPROFILE
DOWNSLOPE
CM/HOUR
**********
ROW 1
**********
0.0043 0.0244 0.0117 0.0064 0.0132 0.0084 0.0037
0.0177 0.0009 0.0004 0.0007 0.0003 0.0004 0.0032
ROW 2
**********
0.0043 0.0259 0.0238 0.0138 0.0348 0.0125 0.0081
0.0026 0.0046 0.0014 0.0041 0.0015 0.0013 0.0037
ROW 3
**********
0.0039 0.0215 0.0132 0.0231 0.0515 0.0173 0.0065
0.0010 y0.0218 y0.0130 0.0034 0.0012 0.0511 0.0010
ROW 4
**********
 0.0118  0.0347 0.0737 0.0507 0.0729 0.0035 0.0230
0.0043 0.0069 0.0010 0.0031 0.0028 0.0020 0.0026
```

FIGURE 12.1 (cont'd)

plotted in Figure 12.2 for comparison with streamflow, rainfall and measured pit throughflow. The salient features are as follows.

(i) Downprofile flux was generally greater than flux into the pit. There was an order of magnitude difference to begin with (29th November 1976), but a much smaller difference later in the simulation (1st December 1976).

(ii) Pit flux was low to begin with and then dropped to zero for sixteen hours (0130 - 1330, 30th December 1976). This was due to the control exerted by pit face tension (estimated by linear extrapolation), such that if $\psi \leq 0$ for any element the flux was set to zero. Thus, ostensibly, low pit flux could be seen as resulting from errors in mathematical estimation of ψ. However, since laboratory determined vertical hydraulic conductivity was high (higher than horizontal K) in this zone, preferential vertical flux might truly have increased tension in the upper horizons. Thus the pit flux would be low until such time as throughflow arrived from upslope and the vertical flow system became overloaded.

(iii) It is not possible to compare absolute rates of computed and measured pit discharge, because, as noted earlier, the latter does not represent flow under natural conditions. There was also a disparity in the timing of each hydrograph peak. Timing of the average downprofile flux rate compared well with the streamflow hydrograph. However, both downprofile and pit fluxes gave a second peak during stream recession. this could mean that both response times are lagged by 24 hours, but there are not enough data for confirmation.

(iv) It was decided not to undertake a detailed analysis of internal variables such as hydraulic conductivity or throughflow velocity until more experimentation had been achieved with the effects of anisotropy and rainfall interception change upon general flux rates.

Run 2

In this run anisotropy was set equal to that actually measured fr from laboratory soil cores (see Figure 11.5). Since vertical K was greater than horizontal K over most of the near surface soil above the

pit, the results, as anticipated, merely increased vertical losses from the slope at the expense of pit flux (Figure 12.2). The downward flux dominated between 7 and 30 m upslope, downslope flux 30 - 50 m upslope. These results do not completely agree with the flow patterns suggested by equipotential plots in the previous chapter. One reason for this could be that where the soil is anisotropic a simple linear interpolation technique does not give true equipotentials or flowlines, and more sophisticated analysis is required (e.g. Freeze and Cherry, 1979, p. 174 -8). The output hydraulic conductivities suggested that $K_z > K_x$, and that neither were greater than about 2 cm/hour, although these are average values for elements.

Although more work was desirable, particularly with respect to solutes, it was not possible for the reason stated earlier. It is suggested that a future project might be designed upon the following guidelines, incorporating both numerical simulation and processing of field data using the moisture and solute accounting model described previously.

(i) Choose a hillslope with relatively uniform vegetation and soils, and an impermeable bedrock. The vegetation should preferably be grass or other short-rooted vegetation to simplify modelling of throughfall processes. The slope could be convex or concave, or it might be desirable to choose a slope hollow, thus including the spatial dimension.

(ii) Set up a finite difference scheme for numerical simulation based upon the continuity equations of water and solute flux described in Chapter 9. This could follow either an explicit or implicit technique, the latter having the advantage of less dependence upon the time step (Δt) or mesh spacing (Δx) and therefore greater stability (Freeze, 1972a; Rushton and Redshaw, 1979). If a hillslope hollow were chosen this could be divided into a series of strips and each strip treated separately. Alternatively, 'sideways flow' between strips could be included in the model, which then becomes three-dimensional.

(iii) Design field instrumentation in accordance with the finite difference mesh. This should include at the centre of each element:

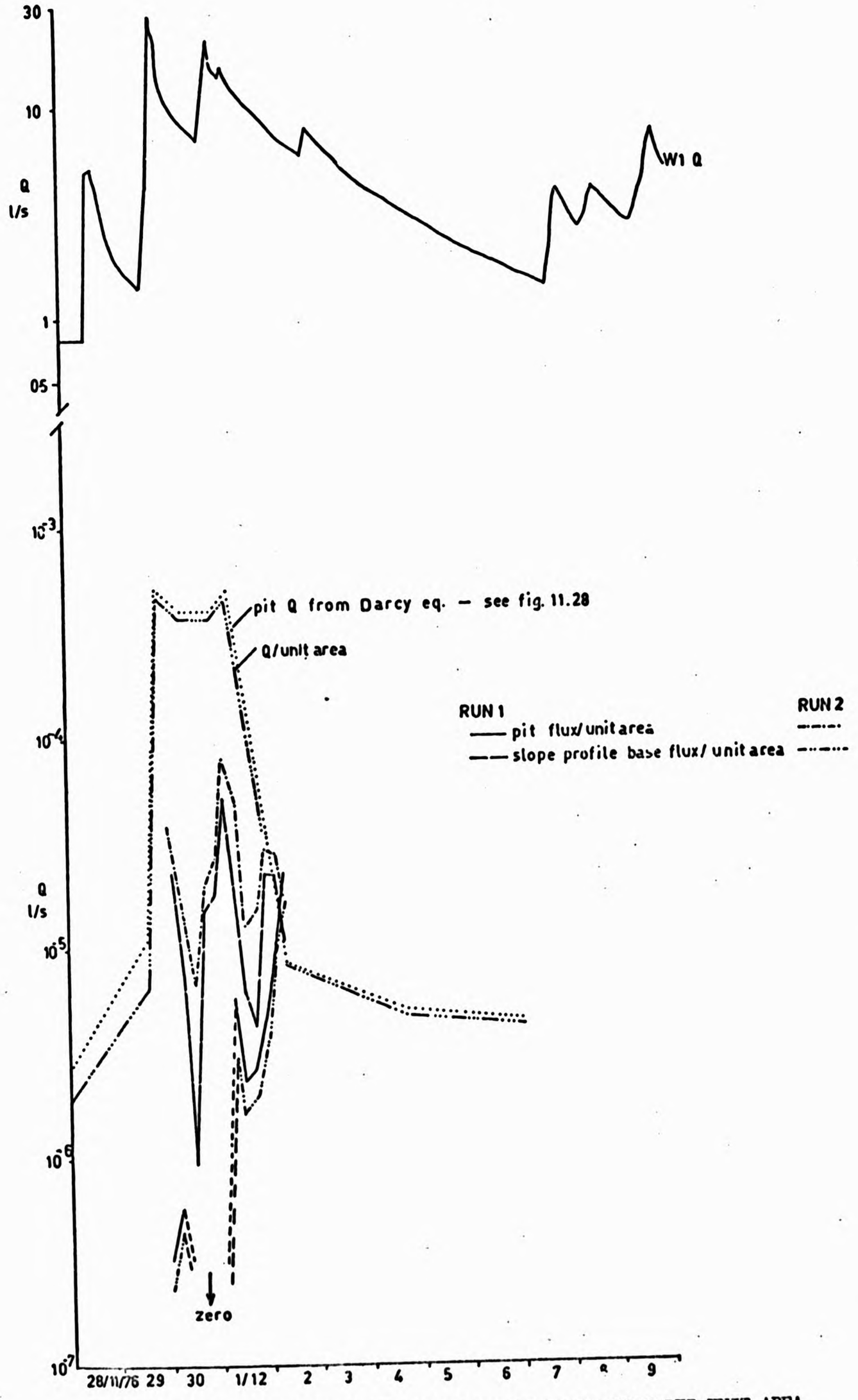

FIGURE 12.2: PIT AND SLOPE PROFILE BASE WATER FLUX PER UNIT AREA FOR TWO RUNS OF THE HILLSLOPE MODEL

a neutron-access tube (moisture content); tensiometers, piezometers and soil water suction pots at required nodal points. The location of tensiometers and suction pots at the same nodal point would be a problem and could be overcome by staggering location within a single profile, then using mathematical interpolation to standardise values at fixed nodal depths. As noted earlier, an automatically recording tensiometer system (recording at $\Delta t \leq 1$ hour) would be ideally suited for the experiment. Soil water sampling could also be partially automated by using an electrical vacuum pump for applying an instantaneous suction to all pots via a common tube delivery. Samples would still be collected in surface receptacles and would represent a uniform time period. It is thought that the ceramic suction pots, although reasonably successful in the present study, could be improved in the following ways.

(a) Increase the pot surface area to take a larger sample for more ion determination, e.g. increase the diameter from 21 mm to 50 mm.

(b) Determine sampling errors when sampling in saturated soil using a ceramic pot.

(c) Determine the possible effect of residual solutes in the pot pores from the previous sample.

Both (b) and (c) could be achieved in the laboratory.

If moisture content were recorded automatically by electrical resistance gauges, this would minimise soil trampling to collection of soil water samples. Stream flow upstream and downstream of the site should be gauged automatically by some suitable method, and automatic water samplers installed at each site. If possible slope base discharge and water quality should be monitored in several locations within the stream flow reach, as a check upon model results. Rainfall and rainfall chemistry should also be monitored in detail.

(iv) The field instrumentation phase would provide preliminary data for improving the simulation model. A power auger could be used to drill holes for the various tubes, and undisturbed soil cores

obtained. Using these it would be possible to determine, in the laboratory, hydraulic conductivity/tension curves over the complete saturated - unsaturated range at each node, for principal axes of flow. Dispersion coefficients could also be determined in the laboratory using variations of the analytical solutions described by Freeze and Cherry (1979), and the dispersivity /velocity function obtained. Initially, it might be prefereable to monitor chloride (or another relatively unreactive ion), since hydrochemical investigations have suggested that atmospheric Cl^- passes through the ecosystem with little loss or addition (e.g. Juang and Johnson, 1967). Reactive ions would require consideration of the myriad chemical and biochemical reactions that can control concentration: adsorption - desorption; acid - base; solution - precipitation; oxidation - reduction; ion-pairing or complexation and microbial cell synthesis (Freeze and Cherry, 1979). Modelling all these reactions would be a formidable task. Thus total and exchangeable analysis of the soil cores might point out those most likely to be important. A leaching and fixation model for K^+ was considered earlier (Frissel, 1972) and satisfactory models for agricultural nutrients based on short time periods are already being developed (de Wit and Van Keulen, 1972; Frissel and Reineger, 1974). Mathematical analogues of adsorption processes are also available (e.g. Helfferich, 1962). Complexation of metal ions by the organic compounds derived from decaying plant material is also likely to be important, although detailed modelling is itself highly complex (e.g. Schnitzer and Kahn, 1972).

(v) Incoming data from the slope experiment (soil and rainwater solute concentration, tension, moisture content and rainfall) would be processed by the finite difference model described in this section. Results computed from the latter, e.g. hydraulic conductivity and dispersivity, should provide feedback to improve the simulation approach. The ultimate test of both the simulation and moisture/solute accounting models would be their ability to predict slope-base discharge and solute concentration and, of course, the chemograph for the channel reach.

12.3 FRAMEWORK FOR A PHYSICALLY-BASED VARIABLE CONTRIBUTING AREA MODEL OF CATCHMENT SOLUTE RESPONSE WITH SUGGESTIONS FOR FURTHER WORK

In this last section an attempt is made to refer the findings of Section III of this study to the catchment scale and in particular Beven and Kirkby's variable contributing area model described in Chapter 9. This is done here only to produce a preliminary model framework. It is recognised that the final model structure can only be generalised after having carefully researched the detailed processes of solute transport within the catchment. Beven and Kirkby's model (itself a self-confessed prototype) represents the fruits of several years research into contributing areas by various workers from Betson (1964) to Anderson and Burt (1978). It is envisaged that a comparable solute model will progress by the same route, although hopefully at a faster rate.

The Beven and Kirkby model was used as the basis for a lumped - parameter, variable contributing area model of catchment solute response (Figure 12.3). The model would require that hydrological and chemical sections run together for computing mass flow transfers. Precipitation delivers solutes to an interception store (S 1) with water capacity S 2, such that S 2 - S_D = stemflow and throughfall. Little research into interception, throughfall and stemflow solutes has been undertaken. This is an area requiring the detailed study of solute leaching and absorption from leaves, branches and stems, retention by interception storage and transport to the soil or channel surfaces. Field and laboratory experiments should study processes over a range of vegetation (e.g. bracken to oak), with fine time resolution, to allow specification of functional relationships for the model.

Throughfall and stemflow solutes (C_{TS}) contributes to the infiltration store (S 2), the contributing area (A_c) or directly to channel flow. S 2 should be capable of specifying chemical processes in the upper soil horizons, e.g. leaching, complexation, adsorption, etc. Solutes can leave S 2 by a combination of four routes.

(i) as a constant downward leakage of solutes, C_o, to the saturated zone store (S 3) so long as the accompanying water leakage, i_o, is greater than potential evaporation, e_p, from S 3.

(ii) as the solute content of saturation - excess overland flow which occurs when the near surface storage capacity, S_c, is exceeded. Initially, this would be expected to leach organic compounds capable of complexing metal ions, from surface humus (e.g. K^+). Actual solute uptake by overland flow is not well understood and requires study.

(iii) as an independent subsurface flush of solutes, C_f, to the quick return flow. It might be possible to specify the proportion of water and solutes leaving S 2 by this route using a functional relationship between SMD or API and C_f.

(iv) as solute uptake by vegetation.

S 2 can receive solutes from the saturated store, S 3, if $e_p > i_o$, at a rate proportional to e_p. This represents a change from Beven and Kirkby's model by routing e_p through S 2 before it leaves the soil.

The background concentration of channel flow is provided from the saturated zone store, S 3. This receives solutes from two sources:

(i) as a constant downward leakage from S 2, C_o, so long as $i_o > e_p$.

(ii) during expansion and subsequent contraction of A_c according to specified mechanisms of solute supply. After preliminary soil chemical analysis over the subcatchment, it might be possible to obtain a functional relationship between exchangeable cations and A_c/A, such that as the contributing area expanded it 'captured' leachates from zones of high concentration.

This mechanism is postulated from the solute pulses monitored in the West Walk hillslope. Each pulse would require a time delay before reaching the channel as delayed flow, similar to that specified for overland flow,

$$T = \sum_{i=1}^{N} \frac{x_i}{SSFV \tan \beta_i}$$

where x_i is the length of the ith flow path segment of slope $\tan\beta_i$,

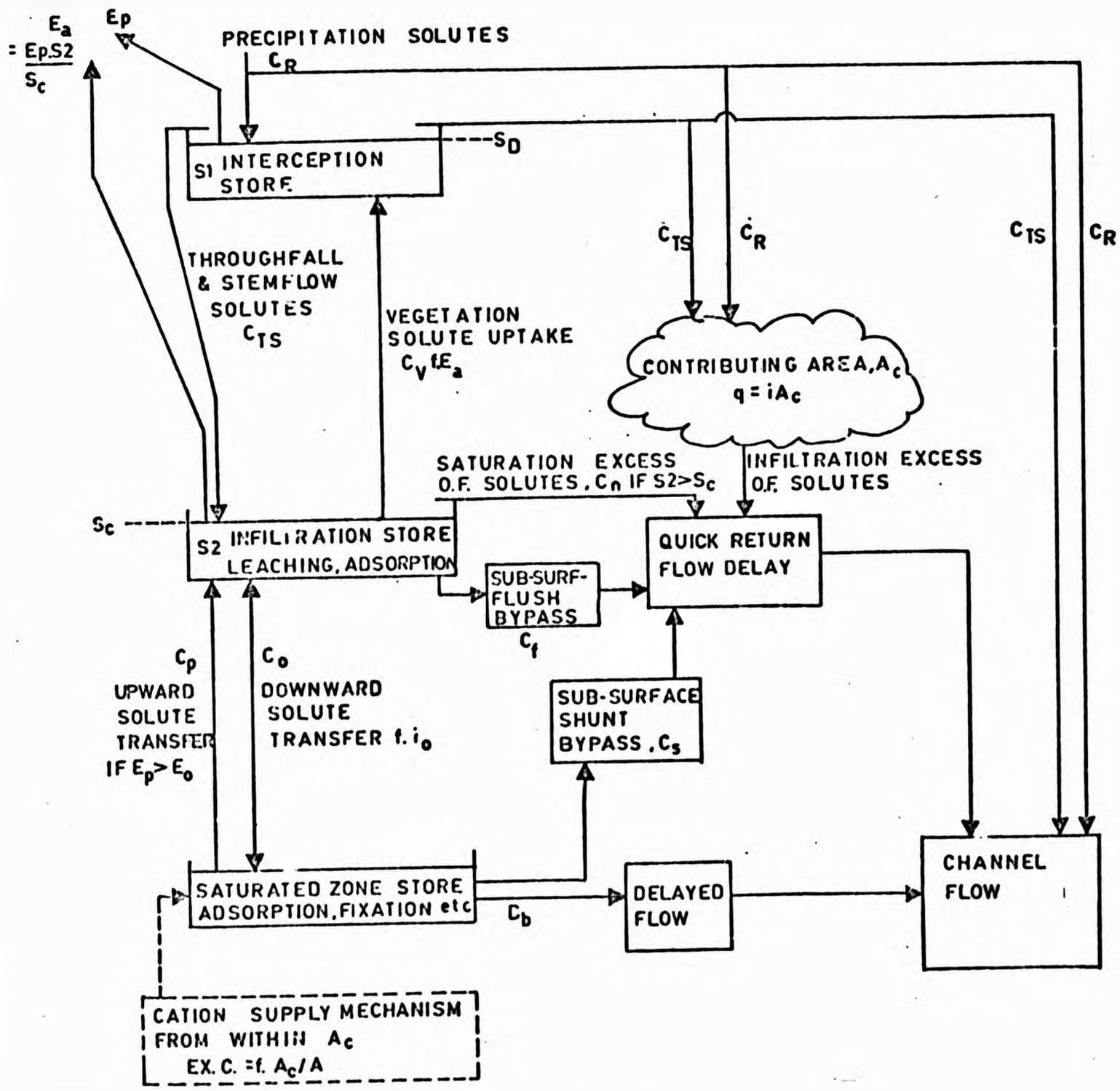

FIGURE 12.3: PRELIMINARY FRAMEWORK FOR A PHYSICALLY-BASED CONTRIBUTING AREA MODEL OF CATCHMENT SOLUTE RESPONSE

N is the number of segments between the point and the outflow, SSFV is subsurface flow velocity and T is time. During time T the solute concentration could be altered by chemical processes, i.e. adsorption, fixation, precipitation, etc., specified as part of the S 3 mechanisms.

A further loss from S 3 is postulated as a rapid subsurface 'shunt bypass' of near channel water to quick return flow. This mechanism has not been well documented in the present study but has been noted elsewhere (e.g. Trudgill, 1977), and could act as a cation flush mechanism. As with the solute flush from S 2 it might be necessary to relate the proportion of solutes lost in this way to SMD or API, or it may be found that overland flow volumes are sufficient to dilute high shunt concentrations during winter storms.

As with Beven and Kirkby's model one sequence of stores represents the average solute response of soil water in a subcatchment and is therefore a lumped system. However, some of the suggestions for this solute model are tentative and depend upon further field research.

By modification of a conceptual run off model, e.g. the Stamford Watershed Model (Crawford and Linsley, 1966), solute prediction would also be possible once knowledge of the processes was obtained, but this would not include the important distributed effects of variable contributing areas. It would also be very demanding on computer time, since the resulting highly complex model would require the optimisation of a large number of parameters.

12.4 SUMMARY AND CONCLUSIONS

This chapter has introduced a suite of BASIC computer programs for moisture - solute accounting on a real hillslope which incorporate the theoretical concepts introduced in Chapter 9. The method uses a simple implicit finite difference technique which is capable of modification for other localities. Some preliminary results for the West Walk hillslope model are discussed. It is suggested, with the benefit of hindsight, that a similar field experiment could run in parallel with numerical simulation. The experiment would help to validate the theoretical basis common to both approaches and provide feedback for improving the numerical simulation.

In the light of hillslope process studies at West Walk a tentative framework for a physically-based, variable contributing area model is outlined, based upon a previously published run off model. This is also useful in pointing out specific areas where further detailed research is needed. In addition, to further spatial monitoring of surface and subsurface soil water and solute transport, a study is required of storm precipitation solute dynamics, with special reference to processes of interception, throughfall and stemflow in different vegetation types.

The subsequent chapter is a synthesis of the main conclusions given in each previous chapter.

SECTION 4

CHAPTER 13
CONCLUSIONS

With reference to the original objective of this study, the most important conclusions from individual chapters are briefly reviewed and suggestions made for future progress in modelling the natural water quality of unpolluted streams (i.e. 'background' water quality).

The fundamental aim of this research was to improve modelling of background water quality. Gaining an understanding of the factors controlling solute dynamics was considered to be an important step in achieving the main objective.

A small catchment in South Hampshire was chosen as the outdoor laboratory for research towards this objective. A further division into subcatchments was made to help simplify the spatial diversity of geology, soils and vegetation, and thus their influence upon solute levels. Previous research in the same field had suggested that a more detailed knowledge of field processes would be beneficial in model development and improvement. Therefore, the study was aimed at two complementary scales; firstly the catchment scale, and secondly the hillslope scale.

(i) Catchment Scale

Considerable effort was put into the design, construction and installation of gauging stations; reliable, accurate stream flow data collection, processing and storage; and rain gauging. An assessment was made of the errors in stream flow gauging at the flume and V-notch weirs based upon British Standards criteria. It was considered that errors of 10 % or more could have occurred during the 1976 low flows, although this was a common problem in British catchments. Rainfall and stream flow data were checked for homogeneity using double mass curves and slight corrections made where necessary. A backcloth to the study period, which spanned the 1975 - 1976 drought, was painted using a water balance. Although the occurrence of the drought was of considerable hydrological interest its severity also delayed progress of the study due to reduced storm rainfall and difficulty installing instruments in hard soil. It appeared that actual evaporation was the

dominant loss process during 1975 - 1976. Spatial variation occurred within West Walk with highest storage losses and lowest run off losses from SC 5, with its relatively mature Western Hemlock flora and London Clay basement. 1976 - 1977 was a period of increased rainfall, higher interception and stream flow losses and soil moisture recharge. SC 4 exhibited the greatest surface run off for both periods with high evapotranspiration and relatively low interception losses, reflecting the London Clay basement and immature forest cover. A brief investigation of hydrograph response for the subcatchments showed that during a winter storm geology and soils were more influential than vegetation cover. By contrast, during the summer vegetation tended to dominate geology as a runoff control with greater replenishment of interception and soil water storage and loss by evapotranspiration. Overall, periods with a high SMD gave short, quick response hydrographs with a small percentage of direct run off, attributable to the replenishment of soil moisture storage over much of the 'dry' catchment with a relatively small contributing area adjacent to the channel.

Care was also taken in the collection of rainfall and stream flow samples for chemical analysis in the laboratory. The latter was achieved by a variety of techniques which were generally of high precision. An assessment of various methods of calculating TDS from specific conductance concluded that none was entirely satisfactory for West Walk data. Where waters have a high organic content and a low pH great care should be taken in both laboratory procedure and the final calculation of specific conductance (low pH samples contribute very strongly to specific conductance). These results support those by Waylen (1976). A quadratic equation was finally employed as the best means of predicting TDS from specific conductance.

Both hydrometric and water chemistry data were subsequently used to develop bivariate and multivariate regression models for prediction of solute levels in the subcatchments. Initially, statistical assumptions inherent in bivariate or multivariate regression methods were reviewed and it was noted that failure to satisfy the basic requirements placed limitations on the inferences or predictions made. Preliminary observations on subcatchment weekly data collected in 1975 and 1977 suggested a spatial variation of solute levels within West

Walk, strongly influenced by soil and vegetation. Solute levels and pH were both found to increase downstream, as ion rich waters from London Clay soils neutralised ion weak, acid waters from the Bagshot Sand.

Bivariate models using solute concentration and discharge showed considerable spatial variability. Potassium, for example, was strongly positively correlated with discharge at W1, but weakly negatively correlated at the flume, probably due to the mixing of waters arriving from areas with different response characteristics. A general dilution effect was demonstrated for calcium, magnesium and chloride with the exception of W5, where correlations were low and insignificant. Sodium/discharge correlations were consistently low, and of variable direction, implying that neither dilution nor concentration dominated the response of any one subcatchment.

Soil moisture conditions were also shown to influence solute levels. Direct correlations between soil moisture deficit and concentration, e.g. chloride, suggested that concentrations increased as moisture was lost through evapotranspiration. However, spatial variability was again influential with inverse relationships demonstrated at W5.

Incorporation of the soil moisture deficit, antecedent precipitation indices and season index in multivariate models improved the predictive power in 83 % of cases, although in 70 % of these the use of only one additional variable proved significant. Multivariate models were developed primarily to improve predictive accuracy, and no detailed interpretation was attempted due to the statistical limitations noted earlier.

Storm sample data were used to assess the ability of bivariate and polynomial regression to model concentration over a wider range of flow conditions. It was found that by including storm data with the 1975 and 1977 weekly data, bivariate correlation coefficients were, in general, reduced. This was primarily due to inadequacy of the bivariate model for autumn conditions. Subsequently, separate bivariate regressions were employed for autumn and non-autumn data with some degree of success. The use of either quadratic or cubic

functions also gave improved variance explanation over the bivariate model for the total data set, partly describing non-linearity introduced by the storm data. Cubic functions were the best of all models for predicting sodium concentration at W1, W2 and the flume, the only solute for which this was the case.

Variable solute response during autumn storms prompted a more detailed analysis of storm solute behaviour. During the post-drought period solute levels were unusually high and solute response was complex and highly variable, both spatially and temporally. These features agreed with reports from other British catchments in the same period. After examination of the potassium/discharge rating plots at W1 and the flume, variable coefficient models were developed, with the intercepts predicted by preceding flow level and the rates of concentration change predicted by maximum storm rainfall intensity (W1) and seasonality (flume). Although the model improved prediction of general storm solute levels it failed accurately to predict intra-storm response.

Thus, further detailed analysis was undertaken to determine the factors controlling solute flushing and chemograph lag and lead, features thought to be significant in creating model unexplained variance. The magnitudes of calcium, magnesium and sodium flushing were found to vary seasonally, with maxima in autumn. Bivariate and multivariate models were formulated for predicting calcium and magnesium flush magnitudes from season index and flood intensity. A strong potassium lead over discharge at W1 was found to be inversely correlated with flood intensity.

The main conclusion from this section was that both bivariate and multivariate models gave approximate solute levels during storm and recession flow periods but failed to reproduce intra-storm variability, including concentration maxima and minima. The importance of chemograph modelling was recognised in, for example, ecological studies where a certain species might only be able to tolerate a specific concentration for a limited period. Although some success had been achieved in identifying general controls on chemograph response it was thought that better progress towards chemograph modelling could be achieved by monitoring field processes, particularly soil water solute dynamics.

However, the best bivariate or multivariate models were used to compute gross and net solute losses from West Walk during the study period. The 1975 - 1976 drought was a period of net solute gain in the catchment (i.e. input exceeded output) due to diminishing stream flow and above average evapotranspiration, while the post-drought period was one of net solute loss. Temporal and spatial variation in solute loads was identified, with SC 4 and the lower catchment areas producing highest yields during periods of low flow. This basic pattern was maintained during higher flows, although the solute contributing area noticeably expanded to more remote parts of West Walk. Solute yield was strongly related to the proportion of London Clay within each subcatchment, probably due to higher base exchange capacities than for podsols on the Bagshot Sand.

The third section of this study represented a response to the need for improving the modelling of storm solute behaviour in small catchments. It was suggested that modelling should have a stronger physical basis and include dynamic spatial variation in solute and discharge source areas. Before an operational model can be developed much more research is required to study the actual processes of solute delivery to the channel system. These areas of research include interception, throughfall, stemflow, overland flow and subsurface solute dynamics, the last of which was investigated in Section III.

(ii) The Hillslope Soil Scale

A theoretical basis to solute and water movement in a slope soil was set out. The continuity equation for water flux was based upon Darcy's Law and for solute flux upon Fick's Laws of diffusion. Application of the approach to soils is far more challenging than in hydrogeology, because of the greater complexity of chemical reactions, particularly under the influence of biotic factors. The final model included components of dispersion, mass flow and solute loss or gain by reaction. One method of testing the validity of the model is to use actual field data in a numerical solution of the continuity equations. A system of moisture and solute accounting using an implicit finite difference technique was described to satisfy this requirement.

A hillslope within SC 1 was instrumented for the measurement of soil water. The latter involved ceramic suction pots, a technique little used in slope hydrology but with greater potential than soil pits due to reduced disturbance of the natural system . The instrument layout was so designed to allow description, interpretation and modelling of processes operating within the soil. Computer programs were developed for processing and storage of the field tension and water chemistry data and two-dimensional upslope plots of tension, hydraulic potential and water chemistry.

A comprehensive chemical analysis of the hillslope soils was undertaken. Total element analyses were made to determine the potential for chemical weathering, and exchangeable potassium, sodium, magnesium, calcium and manganese to identify potential source areas for solutes contributing to streamflow. Interesting catenary patterns emerged from the data obtained. Relatively high concentrations of exchangeable cations were noted in two areas: the lowest 7 metres of hillslope and the near surface soil horizons where the % organic carbon content was also high. Total element data together with particle size determination and slope angle measurement, suggested that downslope soil movement had occurred at some time in the past.*

Laboratory measurement of saturated hydraulic conductivity showed the soil to be anisotropic, and indicated zones of potentially rapid lateral water flow near the channel and vertical flow 10 m upslope.

Several periods of rainfall, infiltration and slope drainage were monitored, the results discussed in detail and later summarised. The processes of water movement within the hillslope during a storm were remarkably similar to those described by Weyman (1973). Streamflow was maintained by lateral flow within a small saturated wedge. This expanded upslope and up profile during a storm with saturation excess overland flow near the stream. The upslope extent of saturation was

* NOTE: Recent exposures (25th July 1980) on the opposite side of the catchment here revealed preferential stone orientation in plateau gravel which had moved downslope.

greater than reported by Weyman, probably as a result of lower hydraulic conductivity between 12 - 24 m, impeding downslope drainage. Increases in streamflow potassium concentration were probably due to the leaching and transport from saturated upper soil horizons near the stream. Potassium and magnesium were seen to be transported in pulse form by subsurface flow from upslope near surface horizons. Pulses from the nearer source areas probably reached the stream during early hydrograph recession. Ca^{2+}, Mg^{2+} and Na^{+} from the more distant source areas feed a diminishing saturated wedge during later flow recession, while K^{+} concentration decreases with distance transported due to preferential adsorption by clay minerals. It appeared that, although the saturated wedge contained quite high concentrations of calcium, magnesium and sodium, the quantities were not large enough to overcome dilution by overland flow and channel precipitation during winter storms.

During slope drainage, with a continuously increasing evapotranspiration rate, potential reversal was found to occur over the whole slope, with unsaturated flow towards the soil surface. Variations in the rate of upward flow were due to the type of vegetation, shorter rooted species creating the steepest near surface hydraulic potential gradients on the lower slope. Solutes were also transported towards the soil surface and either taken up by plants or possibly adsorbed onto soil particle surfaces. A short period of rainfall caused some downwards re-distribution of water and solutes. Near the channel vertical and lateral re-distribution could be responsible for cation flushing in streamflow, but upslope the downward movement is soon absorbed by upward movement as evapotranspiration again dominates. These results support the general findings of Chapters 6 and 7 that catchment moisture conditions influence solute levels in addition to stream discharge.

There was some correlation between cation concentration of soil water and exchangeable cation contents of the soil, but no relationships existed with tension and hence moisture content. This is because cation concentration in the soil water is a complex function of exchange rates, adsorption and moisture flux according to the theoretical equations previously set out.

A suite of BASIC computer programs incorporating these theoretical concepts was written for moisture - solute accounting on the hillslope. Field data (tension, rainfall, soil water and rainfall chemistry) provide the input to these programs, with the aim of validating the defined model structure. There is also facility for introducing anisotropy and the effect of throughfall and stemflow on rainfall quantity and quality. Some preliminary results working only with water flux were discussed, and it was suggested that a similar experiment might be expanded to cover spatial variation in a slope hollow and pure numerical simulation.

The tentative framework for a physically based, variable contributing area model was outlined, based upon a recent run off model but incorporating the important results from this study. Several areas were identified where future research into field processes could concentrate.

In this study progress has been made on the most important of these, subsurface soil water and solute dynamics in a small catchment.

REFERENCES

ABERG B & RODHE W, 1942 — Uber die Milieufactoren in einigen südsehwedischen Seen Symb Bot Upsala, 5,3 , 1-256

ACKERMANN W C, 1966 — Guidelines for Research on Hydrology of Small Watersheds US Dept Int OWRR, Washington DC, 26p

ACTON F S, 1959 — Analysis of Straight-Line Data Wiley, New York

ALLAN I, 1977 — Water Transfers - Will They Affect our Fisheries ? Water Space, Autumn, 19-21

A.P.H.A., 1969 — Standard Methods for the Examination of Water and Waste Water A.P.H.A., New York, 769p

ANDERSON M G & BURT T P, 1977a — A Laboratory Model to Investigate the Soil Moisture Conditions on a Draining Slope J Hydrol 33, 383-90

ANDERSON M G & BURT T P, 1977b — Automatic Monitoring of Soil Moisture Conditions in a Hillslope Spur and Hollow J Hydrol 33, 27-36

ANDERSON M G & BURT T P, 1978a — The Role of Topography in Controlling Throughflow Generation Earth Surface Processes, 3, 331-344

ANDERSON M G & BURT T P, 1978b — Toward More Detailed Field Monitoring of Variable Source Areas Water Resources Res., 14,6, 1123-1131

ANDERSON M G & BURT T P, 1978c — Analysis of Spatial Water Quality and Stream Networks in the Southern Cotswolds during and after the Drought of 1976 Earth Surface Processes, 3, 59-69

ANDERSON P W & GEORGE J R, 1966 — Water Quality Characteristics of New Jersey Streams
USGS Prof. Paper, 1819 G, 48p

A.W.A., 1980a — Allocation of Ground Water Resources in the Rhee and Cam Catchments
Unpublished Report, Anglian Water Authority, G.O.R.D., unpaginated

A.W.A., 1980b — The Development of a Simple Ground Water Model and its Application to the Southern Lincolnshire Limestone
A.W.A. Huntingdon, UK., unpaginated

ATKINSON T C, 1978 — Techniques for Measuring Subsurface Flow on Hillslopes, Chapter 3 in Hillslope Hydrology
Ed. M J Kirkby, 383p

ATKINSON T C & DREW D P, 1974 — Underground Drainage of Limestone Catchments in the Mendip Hills
p87-106 in Fluvial Processes in Instrumented Watersheds
IBG Spec Pub No 6
Ed. K J Gregory & D E Walling

ATKINSON T C & SMITH D I, 1974 — Rapid Ground Water Flow in Fissures in the Chalk: An Example from South Hampshire
Q J Eng Geol, 7, 197-205

ATLAS OF PORTSMOUTH, 1975 — Portsmouth Polytechnic, Department of Geography, 68p

ATTIWILL P M, 1966 — The Chemical Composition of Rainwater in relation to Cycling of Nutrients in Mature Eucalyptus Forest
Plant and Soil, 25, 3, 390-406

BAKER J, HOCKING D & NYBORG M, 1976 — Acidity of Open and Intercepted Precipitation in Forests and Effects on Forest Soils in Alberta
Proc.1st Int. Symp. Acid Precipitation and the Forest Ecosystem,
Ohio, 1975, 779-790

BALEK J, MOJDEN B, PACES T, SKOREPA J, 1978
Hydrological and Geochemical Mass Balance in Small Forested and Agricultural Basins
Internat. Assoc. Hydrol. Sci. Pub No 125, 50-58

BALLANTYNE A K, 1963
Recent Accumulation of Salts in the Soils of South-eastern Saskatchewan
Canadian Journ. Soil Sci. 43, 52-58

BALLARD L F, 1973
Instrumentation for Measurement of Moisture
Nat. Co-operative Highways Research Program, Report No 138, Washington, 60p

BARNES B S, 1939
The Structure of Discharge-Recession Curves
Trans Amer. Geophys Union, 20, 721-5

BARNES I, 1965
Geochemistry of Birch Creek, Inyo County, California: A Travertine Depositing Creek in an Arid Climate
Geochimica et Cosmochimica Acta, 29, 85-112

BARTLETT M S, 1949
Fitting a Straight Line when both Variables are subject to Error
Biometrics, 5, 207-212

BECKETT P H T & WEBSTER R, 1965
Field Trials of a Terrain Classification System - Organisation and Methods
Military Engineering Exper. Estab. Report No 873, Christchurch

BELL J P, 1973
Neutron Probe Practice
Institute of Hydrology, Report No 19, 12p

BETSON R P, 1964
What is Watershed Run-off ?
J. Geophysical Res. 69, 5, 1541-1552

BETSON R P, 1978
Bulk Precipitation and Streamflow Quality Relationships in an Urban Area
Water Resources Res. 14, 6, 1165-1169

BETSON R P & MARIUS J B, 1969
Source Areas of Storm Run-off
Water Resources Res. 5, 574-582

BETSON R P, MARIUS J B & JOYCE R T, 1968
Detection of Saturated Interflow in Soils with Piezometers
Proc.Soil Sci.Soc.Amer, 32 602-604

BEVEN K J, 1977a
Hillslope Hydrographs by the Finite Element Method
Earth Surface Processes, 2, 13-28

BEVEN K J, 1977b
Experiments with a Finite Element Model of Hillslope Hydrology - The Effect of Topography
Paper presented at the 3rd Internat. Hydrology Symp. Fort Collins, Colorado, 18p

BEVEN K J, 1977c
TOPMODEL - A Physically-based Variable Contributing Area Hydrologic Modelling Program
Working Paper No 183, School of Geography, Univ. of Leeds, 23p

BEVEN K J & KIRKBY M, 1979
A Physically-based Variable Contributing Area Model of Basin Hydrology
Hydrol. Sci. Bull. 24, 3, 43-69

BIGGAR J W & NIELSEN D R, 1967
Miscible Displacement and Leaching Phenomena, Chapter 14 in
Agronomy
Pub. Amer.Soc. Agronomy, Vol II

BIGGAR J W & NIELSEN D R, 1976
Spatial Variability of the Leaching of a Field Soil
Water Resources Res. 12,1 , 78-84

BIRTLES A B, 1978
Identification and Separation of Major Baseflow Components from a Stream Hydrograph
Water Resources Res. 14, 5, 791-803

BIRTLES A B & BROWN S R A, 1978
Computer Prediction of the Changes in River Quality Regimes following Large Scale Inter-basin Transfers
Internat. Assoc. Sci. Hydrol. Pub. No 125, 288-298

BLAKEMORE M, 1966
Seasonal Changes in the Amount of Phosphorus and Potassium dissolved from Soils by Dilute Calcium Chloride Solutions
J. Agric. Science, 66, 139-146

BONELL M, 1972
The Application of the Auger Hole Method in Holderness Glacial Drift
J. Hydrol. 16, 125-146

BORMANN F H & LIKENS G E, 1967
Nutrient Cycling
Science. 155, 424-429

BORMANN F H & LIKENS G E, 1969
The Watershed-Ecosystem Concept and Studies of Nutrient Cycles,
Chapter IV in
The Ecosystem Concept in Natural Resource Management
Ed. Van Dyne, 383p
Academic Press, New York

BORMANN F H & LIKENS G E, 1970
The Nutrient Cycles of an Ecosystem
Scientific American, October, 92-101

BORMANN F H, LIKENS G E, FISHER D W, PIERCE R S, 1967
Nutrient Loss Accelerated by Clear Cutting of a Forest Ecosystem
Science, 159, 882-884

BORMANN F H, LIKENS G E, SICCAMA T G, PIERCE R S, EATON J S, 1974
The Export of Nutrients and Recovery of Stable Conditions following Deforestation at Hubbard Brook
Ecological Monographs, 44, 255-277

BOUYOUCOS G J, 1949
Nylon Electrical Resistance Unit for Continuous Measurement of Soil Moisture in the Field
Soil Science, 67, 317-320

BOUYOUCOS G J & MICK H H, 1940
An Electrical Resistance Method for the Continuous Measurement of Soil Moisture under Field Conditions
Michigan Agric. Exper. Station Tech. Bulletin, 172p

BRADY N, 1974
The Nature and Property of Soils
Macmillan, New York, 639p

BRIGGS L J & McCALL A G, 1904 — An Artificial Root for inducing Capillary Movement of Soil Moisture. Science, 20, 566-569

BRITISH STANDARD INSTITUTION, 1965 — Measurement of Liquid Flow in Open Channels. BS 3680, Part 4A, Thin Plate Weirs and Venturi Flumes, 91

BRITISH STANDARD INSTITUTION, 1974 — Measurement of Liquid Flow in Open Channels. BS 3680, Parts 4 & 4C, Weirs and Flumes, 52

BROWN G W, GAHLER A R & MARSTON R B, 1973 — Nutrient Losses after Clear Cut Logging and Slash Burning in the Oregon Coast Range. Water Resources Res. 9, 5, 1450-1453

BROWNLEE K A, 1965 — Statistical Theory and Methodology in Science and Engineering. Wiley, New York, 590p

BURGESS D B & SMITH E J, 1979 — The Effects of Ground Water Development: The Case of the Southern Lincolnshire Limestone Aquifer, p 39-53 in Man's Impact on the Hydrological Cycle in the UK. Ed. G E Hollis

BURT T P, 1979 — The Relationship between Throughflow Generation and the Solute Concentration of Soil and Stream Water. Earth Surface Processes, 4, 257-266

BURT T P, & DAY M R, 1977 — Spatial Variations in Rainfall and Stream Water Quality around the Avonmouth Industrial Complex. Internat. J. Environ. Studies, 11, 205-209

CALDER I R, 1979 — Do Trees use more Water than Grass ? Water Services, 83, No 995, 11-14

CARLISLE A, BROWN A H F & WHITE E J, 1966
The Organic Matter and Nutrient Elements in the Precipitation Beneath a Sessile Oak (Quercus Petraea) Canopy
J. Ecol. 54, 89-98

CARLISLE A, BROWN A H F & WHITE E J, 1967
The Nutrient Content of Tree Stemflow and Ground Flora Litter and Leachates in a Sessile Oak (Quercus Petraea) Woodland
J. Ecol. 55, 615-627

CARROLL D, 1962
Rainwater as a Chemical Agent of Geologic Process - A Review
USGS Water Supply Paper, 1535-G

CARSLAW H S & JAEGAR J C, 1959
Conduction of Heat in Solids
O.U.P., London

CASEY H & NEWTON P V R, 1972
The Chemical Composition and Flow of the South Winterbourne in Dorset
Freshwater Biol. 2, 229-234

CASEY H & NEWTON P V R, 1973
The Chemical Compoistion and Flow of the River Frome and its Main Tributaries
Freshwater Biol. 3, 317-333

CENTRAL WATER PLANNING UNIT, 1976
The 1975 - 1976 Drought: A Hydrological Review
CWPU, Reading, 35p

CHAMBERLIN T W, 1972
Interflow in the Mountainous Forest Soils of Coastal British Columbia, Chapter 3.6 in
Mountain Geomorphology
Ed. O Slaymaker & H J McPherson

CHATWIN C P, 1960
The Hampshire Basin and Adjoining Areas
Inst. of Geol. Sci., Brit. Reg. Geol. Series, HMSO, London, 100p

CHILDS E C, 1969
An Introduction to the Physical Basis of Soil Water Phenomena
Wiley, London, 493p

CHOW VEN T, (Ed.), 1964 — Handbook of Applied Hydrology
New York

CLARKE G R, 1940 — Soil Survey of England and Wales Field Handbook
Clarendon Press, Oxford

CLARKE R T, 1973 — A Review of some Mathematical Models used in Hydrology, with Observations on their Calibration and Use
J. Hydrol. 19, 1-20

CLARIDGE G G C, 1970 — Studies in Element Balances in a Small Catchment at Taita, New Zealand
Internat. Assoc. Sci. Hydrol. Pub No 96, 523-540

CLARIDGE G G C, 1975 — Transit Time: A Factor affecting Element Balances in Small Catchments
N.Z. Journ. Sci. 18, 297-304

CLARKE R T & NEWSON M D, 1978 — Some Detailed Water Balance Studies of Research Catchments, p21-42 in Scientific Aspects of the 1975-1976 Drought in England and Wales
Proc. Roy. Soc. Lond. A, 363 (1712)

CLEAVES E T, GODFREY A E, & BRICK ER O P, 1970 — The Geochemical Balance of a Small Watershed and its Geomorphic Implications
Bull. Geol. Soc. Amer., 81, 3015-3032

COLE D W, 1958 — Alundum Tension Lysimeter
Soil Science, 85, 6, 293-296

COLLINGWOOD R W, 1977 — A survey of Eutrophication in Britain with particular Reference to its Effects on Water Supplies
Inst. Public Health Eng. Symp. on Eutrophication of Lakes and Reservoirs, 131-133

COGBILL C V & LIKENS G E, 1974 — Acid Precipitation in the North Eastern United States
Water Resources Res. 10, 6 , 1133-1137

COOKE G W & WILLIAMS R J B, 1970 — Losses of Nitrogen and Phosphorus from Agricultural Land. Wat.Treat.Exam. 19, 3 , 253 - 276

COOPER J D, 1980 — Measurement of Moisture Fluxes in Unsaturated Soil in Thetford Forest. Institute of Hydrology Report No. 66, 97p

CRAWFORD N H & LINSLEY R K, 1966 — The Stanford Watershed Model Mk. IV. Tech. Report 39, Dept. of Civil Eng. Stanford Univ.

CRISP D T, 1966 — Input and Output of Minerals for an Area of Pennine Moorland: the Importance of Precipitation, Drainage, Peat Erosion and Animals. J. Appl. Ecol., 3, 327-348

CRITCHFIELD A J, 1966 — General Climatology. Prentice Hall, New Jersey, 420p

CRYER R, 1976 — The Significance and Variation of Atmospheric Nutrient Inputs in a Small Catchment System. J. of Hydrol. 29, 121-137

CURTIS L F, COURTNEY F M, AND TRUDGILL S T, 1976 — Soils in the British Isles. Longman, London, 364

CURTIS L F & TRUDGILL S, 1974 — The Measurement of Soil Moisture. Technical Bulletin No 13, B.G.R.G., 70p

DAVIES A W, 1971 — Changes in River Quality associated with Storm Hydrographs. Unpub. MSc. Thesis, Univ. of Newcastle-upon-Tyne, 224p

DAVIES A W, 1978 — Pollution Problems arising from the 1975-1976 Drought. Proc.Roy. Soc. Lond.A, 363 (1712) 97-107

DAVIS S N, 1964 — Silica in Streams and Ground Water. Amer. Journ. Sci. 262, 870-891

DE BOODT M, 1967
Water Saturated Permeability Determination on Undisturbed Soil Samples
p 106-107 in West European Methods for Soil Structure Determination, Ed. M de Boodt, L de Leenheer, H Frese, A J Low and P K Peerlkamp State Faculty Agric. Sci., Ghent

DE WIT C T & VAN KEULEN H, 1972
Simulation of Transport Processes in Soils
Centre for Agricultural Publishing and Documentation, Wageringen, The Netherlands

DOUGLAS I, 1967
Man, Vegetation and the Sediment Yields of Rivers
Nature, 215, 925-928

DOUGLAS I, 1968
The Effects of Precipitation Chemistry and Catchment Area Lithology on the Quality of River Water in Selected Catchments in Eastern Australia
Earth Science Journal, 2,2 , 126-144

DUCE R A, WINCHESTER J W, VAN NAHL T W, 1965
Iodine, Bromide and Chloride in the Hawaiian Marine Atmosphere
J. Geophys.Res., 70,8 , 1777-1799

DUNK R, MOSTYN R A AND HOARE H C, 1967
The determination of Sulphate by Indirect Atomic Absorption Spectroscopy
Atomic Absorption Newsletter, 1, 26

DUNNE T & BLACK R D, 1970
An Experimental Investigation of Runoff Production in Permeable Soils
Water Resources Res. 6, 2 , 179-191

DURBIN J & WATSON G S, 1951
Testing for Serial Correlation in Least Squares Regression, II
Biometrika, 38, 159-178

DURUM W H, 1953
Relationships of the Mineral Constituents in Solution to Streamflow, Saline River, near Russell, Kansas
Trans.Amer. Geophysical Union, 34,3 , 435-442

DURUM W H, HEIDEL S G AND TISON L J, 1960
World-wide Runoff of Dissolved Solids
Internat. Assoc. Sci. Hydrol. Pub. 51, 618-628

EASTWELL B A, 1953
In Situ Methods of Measuring Soil Moisture Content - A Critical Resume
Technical Report W/T27, Electrical Research Association, 19p

EATON J S, LIKENS G E, AND BORMANN F H, 1973
Throughfall and Stemflow Chemistry in a Northern Hardwood Forest
J. Ecol., 61, 495-508

EDWARDS A M C, 1971
Aspects of the Chemistry of four East Anglian Rivers
Unpub. Ph.D. Thesis, University of East Anglia, 292p

EDWARDS A M C, 1973a
The Variation of Dissolved Constituents with Discharge in some Norfolk Rivers
J. of Hydrol., 18, 219-242

EDWARDS A M C, 1973b
Dissolved Load and Tentative Solute Budgets of some Norfolk Catchments
J. of Hydrol., 18, 201-217

EDWARDS A M C, 1974
Catchment Modelling of Water Quality
Paper presented to the B.G.R.G. Basin Sediment Systems Group, London, 9p

EDWARDS A M C & LISS P S, 1973
Evidence for Buffering of Dissolved Silicon in Fresh Water
Nature 243, 341-342

EDWARDS A M C & THORNES J B, 1973
Annual Cycle in River Water Quality: A Time Series Approach
Water Resources Res., 9,5 , 1286-1295

EGNER H & ERIKSSON E, 1955
Current Data on the Chemical Composition of Air Precipitation
Tellus, 11,1 , 134-139

ELLIS J B, 1977
The Characterisation of Particulate Solids and Quality of Water Discharged from an Urban Catchment
Internat. Assoc. Sci. Hydrol., Pub. No. 123, 283-291

ELLIS J B, 1979
The Nature and Sources of Urban Sediments and their Relation to Water Quality: A Case Study from North-West London
p. 199-216 in Man's Impact on the Hydrological Cycle in the UK
Ed. G E Hollis

ERH K T, 1972
Application of Spline Function to Soil Science
Soil Science, 114, 333-338

ERIKSSON E, 1955
Airborne Salts and the Chemical Composition of River Water
Tellus, 7,2 , 243-250

ERIKSSON E, 1959
The Yearly Circulation of Chloride and Sulphur in Nature: Meteorological, Geochemical and Pedological Implications, Part 1, I - III
Tellus, 11,4 , 377-403

ERIKSSON E, 1960
The Yearly Circulation of Chloride and Sulphur in Nature: Meteorological, Geochemical and Pedological Implications, Part 2, IV - X
Tellus, 12,1 , 61-109

FELLER M C, 1977
Nutrient Movement through Western Hemlock-Western Red Cedar Ecosystems in South West British Colombia
Ecology, 58, 1269-1283

FELLER M C & KIMMINS J P, 1979
Chemical Characteristics of Small Streams near Haney in South Western British Columbia
Water Resources Res., 15,2 , 247-258

FINLAYSON B L, 1976
Measurement of Geomorphic Processes in a Small Drainage Basin
Unpub. Ph.D. Thesis, University of Bristol

FISHER D W, GAMBELL A W, LIKENS G E & BORMANN F H, 1968
Atmospheric Contributions to Water Quality of Streams in the Hubbard Brook Experimental Forest, New Hampshire
Water Resources Res., 4,5 , 1115-1126

FOSTER I D L, 1977
Solute Dynamics in a Small Agricultural Catchment
Unpub. Ph.D. Thesis, University of Exeter, 509p

FOSTER I D L, 1978
A Multivariate Model of Storm Period Solute Behaviour
J. Hydrol., 39, 339-353

FOSTER I D L & WALLING D E, 1978
The Effects of the 1976 Drought and Autumn Rainfall on Stream Solute Levels
Earth Surface Processes, 3, 393-406

FOURT D, 1976
Forestry Commission Research Station, Alice Holt, Farnham
Private communication

FOYSTER A M, 1973
Application of the Grid Square Technique to the Mapping of Evapotranspiration
J. Hydrol., 19, 205-226

FREDRIKSEN R L, 1969
A Battery Powered Proportional Stream Water Sampler
Water Resources Res., 5, 1410-1413

FREEZE R A, 1972a
The Role of Subsurface Flow in the Generation of Surface Runoff, 1. Baseflow Contributions to Channel Flow
Water Resources Res., 8, 609-623

FREEZE R A, 1972b
The Role of Subsurface Flow in Generating Surface Runoff, 2. Upstream Source Areas
Water Resources Res., 8, 1272

FREEZE R A, 1980
A Stochastic Conceptual Analysis of Rainfall-Runoff Processes on a Hillslope
Water Resources Res., 16, 2, 391-408

FREEZE R A & CHERRY J A, 1979 — Groundwater
Prentice-Hall, New Jersey, 604p

FRISSELL M J, 1972 — Model Calculations on the Vertical Transport of Potassium Ions in Soil
Proc. 9th Colloq. Int. Potash Inst.
Landshut F R G, 157-170

FRISSELL M J & REINIGER P, 1974 — Simulation of Accumulation and Leaching in Soils
Centre for Agricultural Publishing and Documentation, Wageningen, The Netherlands

GALLOWAY J N & LIKENS G E, 1976 — Calibration of Collection Procedures for the Determination of Precipitation Chemistry
Proc. 1st Int. Symp. Acid Precip. and the Forest Ecosystem,
1975, 137-156

GAMBELL A W & FISHER D W, 1966 — Chemical Composition of Rainfall, Eastern North Carolina and South West Virginia
U.S.G.S. Water Supply Paper,
1535-K, 41 p

GARRELS R M & CHRIST C L, 1965 — Solutions, Minerals and Equilibria
Harper and Row, New York, 450p

GASH J H C & MORTON A J, 1978 — An Application of the Rutter Model to the Estimation of Interception Loss from Thetford Forest
J. Hydrol., 38, 49-58

GATZ D F & DINGLE A, 1971 — Trace Substances in Rain Water: Concentration Variation during Convective Rains and their Interpretation
Tellus, 23,1 , 14-27

GBUREK W J & HEALD W R, 1970 — Effects of Direct Runoff from Agricultural Land on the Water Quality of Small Streams
Proc. 1970 Cornell Agric. Waste Management Conf. 61-68

GEARY R C, 1936

Moments of the Ratio of the Mean Deviation to the Standard Deviation for normal Samples
Biometrika, 28, 295-307

GIBB O, PENMAN H L, PEREIRA C AND RATCLIFFE R A S (Eds), 1978

Scientific Aspects of the 1975-1976 Drought in England and Wales
Proc. Roy. Soc. Lond. A, 363 (1712), 133 p

GIBBS R J, 1972

Water Chemistry of the Amazon River
Geochim. Cosmochim. Acta, 36, 1062

GILKES R J, 1968

Clay Mineral Provinces in the Tertiary Sediments of the Hampshire Basin
Clay Minerals, 7, 351-360

GLANCY P A, VAN DENBURGH A S, AND BORN S M, 1972

Runoff, Erosion and Solutes in the Lower Truckee River, Nevada, during 1969
Water Resources Bull., 8,6 , 1157-1172

GLOVER B J & JOHNSON P, 1974

Variations in the Natural Chemical Concentration of River Water during Flood Flows and the Lag Effect
J. Hydrol., 22, 303-316

GOLTERMAN H L & CLYMO R S, 1969

Methods for the Chemical Analysis of Fresh Waters
IBP Handbook No 8, Blackwell, London 166p

GORE A J P, 1968

The Supply of Six Elements by Rain to an Upland Peat Area
J. Ecol., 56, 483-495

GORHAM E, 1958

The Influence and Importance of Daily Weather Conditions in the Supply of Chloride, Sulphate and other Ions to Fresh Waters from Atmospheric Precipitation
Proc. Roy. Soc. B., 241, 147-178

GORHAM E, 1961

Factors influencing the Supply of Major Ions to Inland Waters with Special Reference to the Atmosphere
Bull. Geol. Soc. Amer., 72, 795-840

GOSZ J R, LIKENS G E AND BORMANN F H, 1972

Nutrient Content of Litterfall on the Hubbard Brook Experimental Forest, New Hampshire
Ecology, 53, 769-784

GOSZ J R, LIKENS G E, EATON J S AND BORMANN F H, 1969

Leaching Losses from Leaves of Selected Tree Species
Bull. Ecol. Soc. Amer., 50, 72 (Abstract)

GOUDIE A, 1970

Input and Output Considerations in Estimating Rates of Chemical Denudation
Earth Science Journal, 4, 2 , 59-65

GRAHAM-BRYCE I J, 1965

Diffusion of Cations in Soils
p 42-56 in
Plant Nutrient Supply and Movement
Tech. Reports Series 48
Int. Atomic Energy Agency, Vienna

GREAT OUSE RIVER AUTHORITY, 1972

Great Ouse Ground Water Pilot Scheme - Final Report
Cambridge, 103 p

GREEN M J, 1969

Effects of Exposure on the Catch of Raingauges
Water Research Association
Tech. Pub. TP67, 67p,
Medmenham, England

GREGORY K J, 1974

Streamflow and Building Activity,
p 107-122 in
Fluvial Processes in Instrumented Watersheds
I.B.G. Spec. Pub. No 6
Ed. K J Gregory and D E Walling

GREGORY K J & WALLING D E, 1971

Field Measurements in the Drainage Basin
Geography, 56, 277-292

GREGORY K J & WALLING D E, 1973a — Drainage Basin: Form and Process
Arnold, London, 456p

GREGORY K J & WALLING D E, 1973b — Fluvial Processes in Small Instrumented Watersheds in the British Isles
Area. 5,4 , 297-302

GROVER B L & LAMBORN R E, 1970 — Preparation of Porous Ceramic Cups to be used for Extraction of Soil Water having Low Solute Concentrations
Proc. Soil Science Soc. America, 34, 706-708

GUNNERSON C G, 1967 — Streamflow and Quality in the Columbia River Basin
J. Sanit. Eng. Div. Proc. Amer. Soc. Civ. Eng., 93, 1-16

HALL F R, 1970 — Dissolved Solids - Discharge Relationships: 1. Mixing Models
Water Resources Res., 6,3 , 845-850

HALL F R, 1971 — Dissolved Solids - Discharge Relationships: 2. Applications to Field Data
Water Resources Res., 7,3 , 591-601

HAMLIN M J & WRIGHT C E, 1978 — The Effects of Drought on the River Systems
p 69-96 in
Scientific Aspects of the 1975-1976 Drought in England and Wales
Proc. Roy. Soc. Lond. A., 363,(1712)

HAMMOND L C, PRITCHETT W L AND CHEW V, 1958 — Soil Sampling in Relation to Soil Heterogeneity
Proc. Soil Science Soc. Amer., 22, 548-552

HANCOCK R S, 1977 — The Impact of Water Transfers and associated Regulation Reservoirs on the Fish Populations of the Tyne, Tees and Swale
Proc. 8th British Coarse Fish Conf. Liverpool, 137-158

HANSEN E A & HARRIS A R, 1975 — Validity of Soil Water Samples collected with Porous Ceramic Cups. Proc. Soil Science Soc. America, 39, 528-536

HARRIS A R & HANSEN E A, 1975 — A New Ceramic Cup Soil Water Sampler. Proc. Soil Science Soc. America, 39, 157-158

HARRISON S J, 1976 — Local Climates of the Portsmouth Area. p 51-65 in Portsmouth Geographical Essays Vol 2 Ed. D N Motterhead and R C Riley

HART F C, KING P H, TCHOBANOGLOUS G, 1964 — Predictive Techniques for Water Quality Inorganics - Discussion. J. Sanit. Eng. Div. Proc. A.S.C.E., SA 5, 63-64

HEADWORTH H G, 1970 — The Selection of Root Constants for the Calculation of Actual Evaporation and Infiltration for Chalk Catchments. J. Inst. Wat. Eng., 24,7 , 431-446

HEALY T V, McKAY H A C, PILBEAM A & SCARGILL D, 1970 — Ammonia and Ammonium Sulphate in the Troposphere over the UK. J. Geophysical Research, 75 12 , 2317-1321

HELFFERICH F, 1962 — Ion Exchange. McGraw-Hill, New York

HEM J D, 1970 — Study and Interpretation of the Chemical Characteristics of Natural Water. U.S.G.S. Water Supply Paper 1473 (2nd Ed), 363p

HEMBREE C H, KREIGER R A, AND JORDAN P R, 1964 — Chemical Quality of Surface Waters and Sedimentation in the Grand River Basin, North and South Dakota. U.S.G.S. Water Supply Paper 1769, 77p

HENDERSON G S, HARRIS W F, TODD D E & GRIZZARD J, 1977 — Quantity and Chemistry of Throughfall as Influenced by Forest Type and Season. J. Ecol., 65, 365-374

HANSEN E A & HARRIS A R, 1975
Validity of Soil Water Samples collected with Porous Ceramic Cups
Proc. Soil Science Soc. America, 39, 528-536

HARRIS A R & HANSEN E A, 1975
A New Ceramic Cup Soil Water Sampler
Proc. Soil Science Soc. America, 39, 157-158

HARRISON S J, 1976
Local Climates of the Portsmouth Area
p 51-65 in
Portsmouth Geographical Essays Vol 2
Ed. D N Motterhead and R C Riley

HART F C, KING P H, TCHOBANOGLOUS G, 1964
Predictive Techniques for Water Quality Inorganics - Discussion
J. Sanit. Eng. Div. Proc. A.S.C.E., SA 5, 63-64

HEADWORTH H G, 1970
The Selection of Root Constants for the Calculation of Actual Evaporation and Infiltration for Chalk Catchments
J. Inst. Wat. Eng., 24,7 , 431-446

HEALY T V, McKAY H A C, PILBEAM A & SCARGILL D, 1970
Ammonia and Ammonium Sulphate in the Troposphere over the UK
J. Geophysical Research, 75 12 , 2317-1321

HELFFERICH F, 1962
Ion Exchange
McGraw-Hill, New York

HEM J D, 1970
Study and Interpretation of the Chemical Characteristics of Natural Water
U.S.G.S. Water Supply Paper 1473 (2nd Ed), 363p

HEMBREE C H, KREIGER R A, AND JORDAN P R, 1964
Chemical Quality of Surface Waters and Sedimentation in the Grand River Basin, North and South Dakota
U.S.G.S. Water Supply Paper 1769, 77p

HENDERSON G S, HARRIS W F, TODD D E & GRIZZARD J, 1977
Quantity and Chemistry of Throughfall as Influenced by Forest Type and Season
J. Ecol., 65, 365-374

HENDRICKSON G E AND KREIGER R A, 1960
Relationship of Chemical Quality of Stream Water to Stream Discharge in Kentucky
Geochemical Cycles: Int. Geol. Congr. 21st Report, Pt 1, 66-75

HESSE P R, 1971
A Textbook of Soil Chemical Analysis
Murray, London, 520p

H.M.S.O., 1967
Wessex Rivers Hydrological Survey
H.M.S.O., 94p

HEWLETT J D, 1961
Soil Moisture as a Source of Baseflow from Steep Mountain Watersheds
USDA Forest Service, SE Forest Exper. Station Report 132

HEWLETT J D & HIBBERT A R, 1963
Moisture and Energy Conditions within a Sloping Mass during Drainage
J. Geophysical Research, 68, 1081-1087

HEWLETT J D & NUTTER W L, 1970
The Varying Source Area of Streamflow from Upland Basins
Amer. Soc. Div. Engineers, Proc. Symp. on Interdisciplinary Aspects of Watershed Management, 65-83

HIBBERT A R AND CUNNINGHAM G R, 1967
Streamflow Data Processing Opportunities and Application, p 725-736 in W E Soper and H W Lull (Eds) Int. Symp. on Forest Hydrology, Oxford

HOBBIE J E & LIKENS G E, 1973
Output of Phosphorus, Dissolved Organic Carbon and Fine Particulate Carbon from Hubbard Brook Watershed
Limnol. Oceanogr., 19, 734-742

HODGSON J M, 1974
Soil Survey Field Handbook
Tech. Monogr. Soil Survey G.B., 99p

HOLEMAN J N, 1968
The Sediment Yield of Major Rivers of the World
Water Resources Res., 4, 737-747

HOLLIS G E, 1974

The Effect of Urbanisation on Floods in the Canon's Brook, Harlow, Essex
p 123-139 in
Fluvial Processes in Instrumented Watersheds
IBG Spec. Pub. No 6
Eds. K J Gregory and D E Walling

HORNBECK J W, LIKENS G E, AND EATON J S, 1976

Seasonal Patterns in Acidity of Precipitation and their Implications for Forest Stream Ecosystems
Proc. 1st Int. Symp. Acid Precip. the Forest Ecosystem, Ohio, 1975
597-609

HORTON R E, 1945

Erosional Development of Streams and their Drainage Basins: Hydrophysical Approach to Quantitative Morphology
Bull. Geol. Soc. Amer., 56, 275-370

HUANG D J, 1970

Regression and Econometric Methods
Wiley, New York, 274p

HUGGETT R J, 1976

Lateral Translocation of Soil Plasma through a small Valley Basin in the Northam Great Wood, Hertfordshire
Earth Surface Processes, 1, 99-106

HUGHES B D & EDWARDS R W, 1977

Flows of Sodium, Potassium, Magnesium and Calcium in the River Cynon, South Wales
Water Research, 11, 563-566

INESON J, 1970

Development of Ground Water Resources in England and Wales
J. Inst. Water Eng., 24, 155-170

INESON J & DOWNING R A, 1964

The Ground Water Component of River Discharge and its Relationship to Hydrology
J. Inst. Wat. Eng., 18, 519-541

INSTITUTE OF HYDROLOGY, 1973

Institute of Hydrology Research Report 1972 - 1973
N.E.R.C., 66p

INSTITUTE OF HYDROLOGY, 1976

Institute of Hydrology Research Report 1974-1976
N.E.R.C., 107p

INSTITUTE OF HYDROLOGY, 1978
Institute of Hydrology Research Report, 1976-1978 N.E.R.C., 124p

IMESON A C, 1973
Solute Variations in Small Catchment Streams Trans. Inst. Brit. Geog. 60, 87-99

INTERNATIONAL SOCIETY OF SOIL SCIENCE, 1973
Soil Physical Terminology Bulletin No 22. 5p

JANDA R J, 1971
An Evaluation of Procedures used in Computing Chemical Denudation Rates Geol. Soc. Amer. Bull, 82, 67-80

JAWORSKA M, 1968
Erozja Chemiczna i Denudacja Zlewni Rzek Wieprza i Pilicy Prace Panstwowego Instytutu Hydrologiczno-Meteorologicznego, 95, 29 - 47

JOHNSON C M & NEEDHAM P R, 1966
Ionic Composition of Sagehen Creek, California, following a Forest Fire Ecology, 47, 4 , 636-639

JOHNSON N M, 1979
Acid Rain: Neutralisation within the Hubbard Brook Ecosystem and Regional Implications Science, 204, 497-499

JOHNSON N M, LIKENS G E, BORMANN F H, FISHER D W AND PIERCE R S, 1969
A Working Model for the Variation in Stream Water at the Hubbard Brook Experimental Forest, New Hampshire Water Resources Res., 5,6 , 1353-1363

JOHNSON N M, REYNOLDS F E AND LIKENS G E, 1972
Atmospheric Sulphur: Its Effect on the Chemical Weathering of New England Science, 177, 514-516

JOHNSON P L, & SWANK W T, 1973
Studies of Cation Budgets in the Southern Appalachians on Four Experimental Watersheds with Contrasting Vegetation Ecology, 54,1 , 70-80

JOHNSTON J, 1972 — Econometric Methods. Wiley, New York

JOHNSTON R J, 1978 — Multivariate Statistical Analysis in Geography. Longman, London, 280p

JONES A, 1971 — Soil Piping and Stream Channel Initiation. Water Resources Res., 7,3 , 602-610

JUANG F & JOHNSON N M, 1967 — Cycling of Chloride through a Forested Watershed in New England. J. Geophysical Research, 72, 5641-5647

JUNGE C E, 1956 — Recent Investigations in Air Chemistry. Tellus, 8, 127-139

JUNGE C E & WERBY R T, 1958 — The Concentration of Chloride, Sodium, Potassium, Calcium and Sulphate in Rain Water over the United States. J. of Meteorology, 15,5 , 417-425

JURY W A, GARDNER W R, SAFFIGNA P G & TANNER C B, 1976 — Model for Predicting Simultaneous Movement of Nitrate and Water through a Loamy Sand. Soil Sci., 122,i , 36-43

KAY F F, 1939 — A Soil Survey of the Strawberry District of South Hampshire. Bull. L.11, Dept. of Agric. Chem., University of Reading, 152p

KELLER H M, 1970 — Factors affecting Water Quality of Small Mountain Catchments. J. Hydrol., (N.Z.) 9,3 , 133-141

KELLER W D AND FREDERICKSON A F, 1952 — Role of Plants and Colloidal Acids in the Mechanism of Weathering. Amer. J. Sci., 250, 594-608

KENNEDY V C, 1964 — Base-exchange Capacity and Clay Mineralogy of some Modern Stream Sediments. Internat. Assoc. Sci. Hydrol. Pub. No 64, 95-105

KENNEDY V C, 1965
Mineralogy and Cation-exchange Capacity of Sediments from Selected Streams
USGS Prof. Paper 433-D, 27p

KENNEDY V C, 1971
Silica Variations in Streamwater with Time and Discharge
Advances in Chemistry Series 106, 94-130

KENNEDY V C, ZELLWEGER G W, AND AVANZINO R J, 1979
Variation of Rain Chemistry during Storms at two Sites in Northern California
Water Resources Res., 15,3 , 687-702

KERPEN W, AND SCHARPENSEEL H W, 1967
Movement of Ions and Colloids in Undisturbed Soil and Parent Rock Material Columns
Proc. Int. Atomic Energy Symp. Istanbul, 213-225

KING L J, 1969
Statistical Analysis in Geography
Prentice-Hall, New Jersey, 350p

KIRDA C, NIELSEN D R, AND BIGGAR J W, 1973
Simultaneous Transport of Chloride and Water During Infiltration
Soil Sci. Soc. Amer. Proc. 23,3 , 339-345

KIRKBY M J & CHORLEY R J, 1967
Throughflow, Overland Flow and Erosion
Bull. Int. Assoc. Sci. Hydrology 12,3 , 5-21

KNAPP B J, 1970a
Patterns of Soil Water Movement on a Steep Upland Hillside, Central Wales
Unpub. Ph.D. Thesis, University of Reading, 213p

KNAPP B J, 1970b
A Note on Throughflow and Overland Flow in Steep Mountain Watersheds
Reading Geographer, 1, 40-42

KNAPP B J, 1973
A System for the Field Measurement of Soil Water Movement
Tech. Bull. No 9, B.G.R.G., 26p

KRUPP H K, BIGGAR J W AND NIELSEN D R, 1972
Relative Flow Rates of Salt and Water in Soil
Soil Sci. Soc. Amer. Proc. 36, 412

KUNKLE G R, 1965
Computation of Ground Water Discharge to Streams during Floods or to Individual Reaches during Baseflow by Use of Specific Conductance
US Geol. Survey Prof. Paper, 525-D, 207-210

LAG J, 1968
Relationships between the Chemical Composition of the Precipitation and the Contents of Exchangeable Ions in the Humus Layer of Natural Soils
Acta Agriculturae Scandinavica, 18, 148-152

LAIDLAW I, SMART P AND TRUDGILL S T, 1974
Soil Water Residence Time and Solute Load of Soil Drainage Waters
Unpub. paper. Basin Sediment Systems Group of B.G.R.G., Exeter, 5p

LANE L J, MORTON H L, WALLACE D E, WILSON R E AND MARTIN R D, 1977
Non-Point Source Pollutants to Determine Run Off Volumes
Hydrol. & Water Resources in Arizona and the South West, 7, 89-102

LANGBEIN W B & DAWDY D R, 1963
Some General Comments on the Occurence of Dissolved Solids in the Surface Waters of the United States
US Geol. Survey Unpub. Report cited on p 77-78 in
L B Leopold, M G Wolman and J P Miller (Eds)
Fluvial Processes in Geomorphology, New York

LEDBETTER J O & GLOYNA E F, 1964
Predictive Techniques for Water Quality Inorganics
J. Sanit. Eng. Div. Proc. Amer. Soc. Civ. Eng., 89, 127-150

LEOPOLD L B, 1962
Rivers
Amer. Sci., 50, 511-537

LESTER W F & WOODWARD G M, 1972 — Water Quality Monitoring in the United Kingdom. Water Pollution Control, 71, 289-298

LEWIN R, CRYER R AND HARRISON D I, 1974 — Sources for Sediments and Solutes in Mid Wales. p 73-85 in Fluvial Processes in Instrumented Catchments. IBG Special Pub. No 6. Eds. K J Gregory and D E Walling

LEWIS L L, 1969 — Atomic Absorption Spectroscopy. ASTM Special Tech. Pub. 443, 47p

LI F H, 1976 — Baseflow - A Parameter for Ground Water Resource Evaluation. Unpub. M.Sc. Thesis, University of Birmingham, 41p

LIKENS G E & BORMANN F E, 1974 — Acid Rain: A Serious Regional Environmental Problem. Science, 184, 1176-1179

LIKENS G E, BORMANN F H, EATON J S, PIERCE R S AND JOHNSON N M, 1976 — Hydrogen Ion Input to the Hubbard Brook Experimental Forest, New Hampshire, during the Last Decade. Proc. 1st Int. Symp. Acid Precip. and the Forest Ecosystem, Ohio, 1975, 397-407

LIKENS G E, BORMANN F H AND JOHNSON N M, 1972 — Acid Rain. Environment, 14,2 , 33-40

LIKENS G E, BORMANN F H, JOHNSON N M & PIERCE R S, 1967 — The Calcium, Magnesium, Potassium and Sodium Budgets for a small Forested Ecosystem. Ecology, 48, 772-785

LIKENS G E, BORMANN F H, JOHNSON N M & PIERCE R S, 1977 — Biogeochemistry of a Forested Ecosystem. Springer, New York, 146p

LIKENS G E, JOHNSON N M, GALLOWAY J N AND BORMANN F H, 1976 — Acid Precipitation: Strong and Weak Acids. Science, 194, 643-645

LIKENS G E, BORMANN F H, JOHNSON N M, FISHER D W AND PIERCE R S, 1970
Effects of Forest Cutting and Herbicide Treatment on Nutrient Budgets in the Hubbard Brook Watershed Ecosystem
Ecol. Monog, 40, 23-47

LIVINGSTONE D A, 1963
Chemical Composition of Rivers and Lakes
US Geol. Survey Prof. Paper 440-G, 64p

MACKENZIE F T AND GARRELS R M, 1966
Chemical Mass Balance between Rivers and Oceans
Amer. J. Sci., 264, 507-525

MADGWICK A A I AND OVINGTON J D, 1959
The Chemical Composition of Precipitation in Adjacent Forest and Open Plots
Forestry, 32, 14-22

MAHLOCH J L, 1974
Multivariate Techniques for Water Quality Analysis
J. Environ. Eng. Div. Proc. A.S.C.E. EE 5, 100, 1119-1132

MATVEYEV A A AND BASHMAKOV O I, 1967
Chemical Composition of Atmospheric Precipitation in some Regions of the USSR
Soviet Hydrology, Issue 5, 480-491

McCARTHY L T AND KEIGHTON W B, 1964
Quality of Delaware River Water at Trenton, New Jersey
USGS Water Supply Paper, 1779-X, 50p

McWHORTER D B & SUNADA D K, 1977
Ground Water Hydrology and Hydraulics
Water Resources Pub., Fort Collins, Colorado, 359p

METEOROLOGICAL OFFICE (undated)
Rules for Rainfall Observers
HMSO, London

MILLER J P, 1961
Solutes in Small Streams Draining Single Rock Types, Sangre de Cristo, New Mexico
USGS Water Supply Paper, 1935 F, 23p

MORDY W A, 1953
A Note on the Chemical Composition of Rain Water
Tellus, 5, 470-474

MORE R J, 1969
The Basin Hydrological Cycle
p 27-35 in
Water, Earth and Man
Ed. R J Chorley, Methuen, London

NATIONAL WATER COUNCIL, 1978
Review of Consent Procedure
Unpaginated

N.E.R.C., 1975
Flood Studies Report
Vol I, Hydrological Studies, 389p

NAYLOR J A, ROWLAND C D AND YOUNG C P, 1978
The Investigation of Landfill Sites
WRC Tech. Report TR 91,
Medmenham, UK, 68p

NEWBURY R W, CHERRY J A AND COX R A, 1969
Ground Water Streamflow Systems in Wilson Creek Experimental Watershed, Manitoba
Canad. J. Earth Sci., 6, 613-623

NIELSEN D R, BIGGAR J W, AND ERH K T, 1973b
Spatial Variability of Field Measured Soil Water Properties
Hilgardia, 42, 7, 215-253

NIELSEN D R, STARR J L, KIRDA C & MISRA C, 1973a
Soil Water and Solute Movement Studies
Proc. Symp. on Isotopes and Radiation Techniques in Studies of Soil Physics, Irrigation and Drainage
Vienna, 117-133

NORDØ J, 1976
Long Range Transport of Air Pollutants in Europe and Acid Precipitation in Norway
Proc. 1st Int. Symp. Acid Precip. and the Forest Ecosystem,
Ohio, 1975, 87-103

NUTTER W L, 1969
Management Implications of Subsurface Stormflow and the variable Source Concept
Proc. Soc. Amer. Foresters, 69th Ann. Meeting, Miami Beach, Florida, 26p

NUTTER W L, 1973
The Role of Soil Water in the Hydrologic Behaviour of Upland Basins
Chapter 10 in
Field Soil Water Regime
Pub. Soil Sci. Soc. Amer., 181-193

NYE P H & TINKER P B, 1977
Solute Movement in the Soil Root System
Studies in Ecology, Vol. 4,
Blackwell, London, 342p

OAKES D B, 1979
A Model of Ground Water Flow in the Catchments of the Rivers Rhee and Cam
WRC Report LR 992, Medmenham, UK,
5p plus Figs.

OAKES D B & PONTIN J M A, 1976
Mathematical Modelling of a Chalk Aquifer: A Digital Computer Simulation of Ground Water Development to augment River Flow in the Lambourn Valley, Berkshire
WRC Tech. Report TR 24,
Medmenham, UK, 37p

ODEN S, 1976
The Acidity Problem An Outline of Concepts
Proc. 1st Int. Symp. Acid Precip. and the Forest Ecosystem
Ohio, 1975, 1-36

ODUM E P, 1971
Fundamentals of Ecology
Saunders, New York, 546p

OSBORN H B & LANE L, 1969
Precipitation-Run Off Relations for very Small Semi-Acid Rangeland Watersheds
Water Resources Res., 5,2 , 419-425

OWENS M & WOOD G, 1968
Some Aspects of the Eutrophication of Water
Water Research, 2, 151-159

OXLEY N C, 1974
Suspended Sediment Delivery Rates a and the Solute Concentration of Stream Discharge in two Welsh Catchments
p 141-145 in Fluvial Processes in Instrumented Watersheds
IBG Special Pub. No 6,
Eds. K J Gregory and D E Walling

PARIZEK R R & LANE B E, 1970 — Soil Water Sampling using Pan and Deep Pressure - Vacuum Lysimeters
J. of Hydrol., 11, 1-21

PARKER G G, 1963 — Piping: A Geomorphic Agent in Landform Development of the Drylands
Bull. Int. Assoc. Sci. Hydrol., Pub. No 65, 103-113

PATERSON M P & SCORER R S, 1975 — The Chemistry of Sea Salt Aerosol and its Measurement
Nature, 254, 491-495

PERKINS T K & JOHNSON O C, 1963 — A Review of Diffusion and Dispersion in Porous Media
J. Soc. Petrol. Eng., 3, 70-83

PICKENS J F & LENNOX W C, 1976 — Numerical Simulation of Waste Movement in Steady Ground Water Flow Systems
Water Resources Res., 12,2 , 171-180

PIEST R F, 1964 — Long Term Sediment Yields from small Watersheds
Intern. Assoc. Sci. Hydrol. Pub. No 65, 121-140

PILGRIM D H, HUFF D D AND STEELE T D, 1979 — Use of Specific Conductance and Contact Time Relations for Separating Flow Components in Storm Run Off
Water Resources Res., 15, 2, 329-339

PINDER G F & JONES J F, 1969 — Determination of the Ground Water Component of Peak Discharge from the Chemistry of Total Runoff
Water Resources Res., 5,2 , 438-445

PIONKE H B & NICKS A D, 1970 — The Effect of Selected Hydrological Variables on Stream Salinity
Internat. Assoc. Sci. Hydrol., Bull. 15 4 , 13-19

PLUMMER L N, JONES B J, AND TRUESDELL A H, 1976 — WATEQF: a FORTRAN IV Version of WATEQ, a Computer Program for calculating Chemical Equilibrium of Natural Waters
USGS Water Resources Investigations, 76-113

POOLE M A & O'FARRELL P N, 1971 — The Assumptions of the Linear Regression Model
Transactions Inst. British Geog., 52, 145-148

POWELL K E C, 1978 — Weed Growth - A Factor of Channel Roughness
p 327-352 in Hydrometry
Ed. R W Herschy, Wiley, Chichester

PRICE W J, 1972 — Analytical Atomic Absorption Spectrometry
Heyden and Son, London, 239p

PRICE W J & ROOS J T H, 1968 — The Determination of Silicon by Atomic Absorption Spectrophotometry with particular Reference to Steel, Cast Iron, Aluminium Alloys and Cement
Analyst, 93, 709-714

PYE-UNICAM, 1978 — Pye-Unicam Technical Manual for the SP 90
Pye-Unicam, unpaginated

RAGAN R M, 1967 — An Experimental Investigation of Partial Area Contributions
Internat. Assoc. Sci. Hydrol., Pub. No 76, 241-249

RAINWATER F H, 1962 — Stream Composition of the Conterminous United States
US Geol. Survey Hyd. Inv. Atlas HA6I

REEVE R C & DOERING E J, 1965 — Sampling the Soil Solution for Salinity Appraisal
Soil Science, 99, 5, 339-344

REUSS J O, 1976 — Chemical and Biological Relationships relevant to the Effect of Acid Rainfall on the Soil Plant System
Proc. 1st Int. Symp. Acid Precip. and the Forest Ecosystem
Ohio, 1975, 791-813

RICHARDS L A, 1941 — A Pressure Membrane Extraction Apparatus for Soil Solution
Soil Science, 51, 377

RICHARDS S J & WEEKS L V, 1953 — Capillary Conductivity Values from Moisture, Yield and Tension Measurements on Soil Columns. Soil Sci. Soc. Amer. Proc. 17, 206

ROBINSON R A & STOKES R H, 1965 — Electrolyte Solutions. Butterworth, London

RODDA J C, 1967 — The Rainfall Measurement Problem. Int. Assoc. Sci. Hydrol. Pub. No 78, 245

RODDA J C, DOWNING R A AND LAW F M, 1976 — Systematic Hydrology. Newnes-Butterworths, London, 399p

ROSE C W, 1966 — Agricultural Physics. Pergamon, Oxford, 230p

ROSE C W, STERN W R AND DRUMMOND J E, 1965 — Determination of the Hydraulic Conductivity as a Function of Depth and Water Content for Soil in situ. Austral. J. Soil Res., 3, 1

RUSHTON K R & REDSHAW S C, 1979 — Seepage and Ground Water Flow. Wiley Chichester, 339p

RUTTER A J, KERSHAW K A, ROBINS P C & MORTON A J, 1971 — A Predictive Model of Rainfall Interception in Forests. I. Derivation of the Model from Observations in a Plantation of Corsican Pine. Agric. Meteorol., 9, 367-384

RUTTER A J, MORTON A J AND ROBINS P C, 1975 — A Predictive Model of Rainfall Interception in Forests. II. Generalisation of the Model and Comparison with Observations in some Coniferous and Hardwood Stands. J. Appl. Ecol., 12, 367-380

SCHNITZER M & KAHN S V, 1972 — Humic Substances in the Environment. Marcel and Dekker, New York, 327p

SEARCY J K & HARDISON C H, 1960 — Double Mass Curves. USGS Water Supply Paper, 1541-B, 64p

SHAW M D, 1960

Analysis of Methods and Equipment for Measuring Soil Moisture
US Dept. Agric. 37p

SICCAMA T G, BORMANN F H AND LIKENS G E, 1970

The Hubbard Brook Ecosystem Study: Productivity, Nutrients and Phytosociology of the Herbaceous Layer
Ecol. Monog., 40, 389-402

SIEGEL S, 1956

Non-parametric Statistics for the Behavioural Sciences
McGraw-Hill, Tokyo, 312p

SJORS H, 1950

On the Relation between Vegetation and Electrolytes in North Swedish Mire Waters
Oikos, 2,2 , 241-247

SKAKALSKIY B G, 1966

Basic Geographical and Hydrochemical Characteristics of the Local Run Off of Natural Zones in the European Territory of the USSR
Trans. State Inst. (Trudy GGI), 137, 125-180

SLACK K V & FELTZ H R, 1968

Tree Leaf Control on Low Flow Water Quality in a small Virginia Stream
Environmental Science & Technol., 2, 126-131

SLACK K V & FISHER D W, 1965

Light Dependent Quality Changes in Stored Water Samples
USGS Prof. Paper, 525-C, 190-192

SPRAGGS G E, 1976

Solute Variations in a Local Catchment
The South Hampshire Geographer 8, 1-14, (see Appendix 5 of this Thesis)

SPRAGGS G E, 1979

Water Balance of the River Rhee Catchment, Cambridgeshire
Internal Report, A.W.A., G.O.R.D.30p

STEELE T D, 1968

Digital Computer Application in Chemical Quality Studies of Surface Water in a Small Watershed
Internat. Assoc. Sci. Hydrol., Pub. No 80, 203-214

STEELE T D, 1976
A Bivariate Regression Model for estimating Chemical Composition of Streamflow or Ground Water
Internat. Assoc. Sci. Hydrol., Bull. 21, 143-161

STEVENSON C M, 1968
An Analysis of the Chemical Composition of Rainfall and Air over the British Isles and Eire for the Years 1959-1964
Q.J.Roy. Met. Soc., 94, 56-70

STROBEL G & SILVESTRO F, 1970
Application of Remote Sensing to Water Quality Management
Proc. National Wat. Symp. on Data and Instrumentation for Water Quality Management, Wisconsin. Madison
W.R.Centre, USA, 137-144

SUTCLIFFE D W & CARRICK T R, 1973
Studies on Moutain Streams in the English Lake District.
II. Aspects of Water Chemistry in the River Duddon
Fresh. Biol., 3, 543-560

SUTCLIFFE J F & BAKER D A, 1974
Plants and Mineral Salts
Arnold, London, 60p

SWANSON K A & JOHNSON A H, 1980
Trace Metal Budgets for a Forested Watershed in the New Jersey Pine Barrens
Water Resources Res., 16, 2, 373-380

TAMM C O & COWLING E B, 1976
Acidic Precipitation and Forest Vegetation
Proc. 1st Int. Symp. Acid Precip. and the Forest Ecosystem, Ohio, 1975, 845-855

TANJII K K & BIGGAR J W, 1972
Specific Conductance Model for Natural Waters and Soil Solutions of Limited Salinity
Water Resources Res., 8,1 , 145-153

TAYLOR G S & LUTHIN J N, 1969
Computer Methods for Transient Analysis of Water Table Aquifers
Water Resources Res., 5,1 , 144-152

TENNESSEE VALLEY AUTHORITY, 1965 — Area Stream Factor Correlation: A Pilot Study in the Elk River Basin. Bull. Int. Assoc. Sci. Hydrol., 10, 22-37

TERNAN J L & WILLIAMS A G, 1979 — Hydrological Pathways and Granite Weathering on Dartmoor. p 5-30 in Geographical Approaches to Fluvial Processes. Ed. A F Pitty, Geobooks, Norwich, 300p

TILL R, 1973 — The Use of Linear Regression in Geomorphology. Area, 5,4 , 303-308

TODD D K, 1959 — Ground Water Hydrology. Wiley, New York, 336p

TODD R W & KEMPER W D, 1972 — Salt Dispersion Coefficients near an Evaporating Surface. Soil. Sci. Soc. Amer. Proc., 36,4 , 539-543

TOLER L G, 1965 — Relations between Chemical Quality and Water Discharge in Spring Creek, South Western Georgia. USGS Prof. Paper 525-C, 209-213

TRUDGILL S T, 1977 — Soil and Vegetation Systems. Clarendon Press, Oxford, 180p

TRUESDELL A H & JONES B F, 1974 — WATEQ, a Computer Program for Calculating Chemical Equilibria of Natural Waters. J. of Research. US Geol. Survey 2, 233-248

TURVEY N D, 1975 — Water Quality in a Tropical Rain Forested Catchment. J. Hydrol., 27, 111-125

U.S.D.A., 1976 — Proceedings of the 1st International Symposium on Acid Precipitation and the Forest Ecosystem. Ohio State University, 1975, 1074

VAN DENBURGH A S AND FETH J H, 1965
Solute Erosion and Chloride Balance in Selected River Basins in the Western Conterminous United States
Water Resources Res., 1, 537-541

VAN DER PLOEG R R AND BEESE F, 1977
Model Calculations for the Extraction of Soil Water by Ceramic Cups and Plates
J. Soil Sci. Soc. Amer., 41, 466-470

VERSTRATEN J M, 1977
Chemical Erosion in a Forested Watershed in the Oesling, Luxembourg
Earth Surface Processes, 2, 175-184

VIDLER A, 1978
The Variability of Chemical Content of Rainfall falling through a Tree Canopy
Unpub. B.Sc. Project,
Portsmouth Polytechnic, unpaginated

VIRO P J, 1953
Loss of Nutrients and the Nutrient Balance of the Soil in Finland
Inst. Forest. Fenniae Commun.,
42, 1, 51p

VOGEL A I, 1961
A Textbook of Quantitative Inorganic Analysis
Longmans, London, 1216p

WAGNER G H, 1962
Use of Porous Ceramic Cups to Sample Soil Water within the Profile
Soil Science, 94, 379-386

WALLING D E, 1974
Suspended Sediment and Solute Yields from a small Catchment prior to Urbanisation
p 169 - 192 in
Fluvial Processes in Instrumented Watersheds
IBG Spec. Pub. No 6
Ed. K J Gregory and D E Walling

WALLING D E, 1975
Solute Variation in Small Catchment Streams: Some Comments
Trans. Inst. Brit. Geog., 64, 141-147

WALLING D E, 1978
Reliability Considerations in the Evaluation and Analysis of River Loads
Zeit. für Geomorph., Suppl. Bd. 29, 29-42

WALLING D E & FOSTER I D L, 1975
Variations in the Natural Chemical Concentration of River Water during Flood Flows and the Lag Effect: Some Further Comments
J. Hydrol., 13, 315-337

WALLING D E & FOSTER I D L, 1978
The 1976 Drought and Nitrate Levels in the River Exe Basin
J. Inst. Water Eng. & Sci., 4, 341-352

WALLING D E & TEED A, 1971
A Simple Pumping Sampler for Research into Suspended Sediment Transport in Small Catchments
J. Hydrol., 13, 325-337

WALLING D E & TROAKE R P, 1973
The Natural History of Slapton Ley Nature Reserve VII
Field Studies, 3,5 , 719-740

WALLING D E & WEBB B W, 1975
Spatial Variation of River Water Quality: A Survey of the River Exe
Trans. Inst. Brit. Geog. 65, 155-171

WALLING D E & WEBB B W, 1978
Mapping Solute Loadings in an area of Devon, England
Earth Surface Processes, 3, 85-99

WALLING D E & WEBB B W, 1980
The Spatial Dimension in the Interpretation of Stream Solute Behaviour
J. Hydrol., 47, 1/2, 129-150

WANG W C & EVANS R C, 1969
Variation of Silica and Diatoms in a Stream
Limnol. and Oceanogr., 14,6 , 941-944

WARD R C, 1967
Principals of Hydrology
Methuen, London, 403p

WARD R C, 1978
Floods
Macmillan, London, 244p

WATER RESOURCES BOARD, 1973
Water Resources in England and Wales
H.M.S.O., 67p

WAYLEN M, 1976
Some Aspects of the Hydrochemistry of a small Drainage Basin
Unpub. Ph.D. Thesis,
University of Bristol, 386p

WAYLEN M J, 1979
Chemical Weathering in a Drainage Basin underlain by Old Red Sandstone
Earth Surface Processes, 4, 167-178

WEBB B W & WALLING D E, 1974
Local Variation in Background Water Quality
The Science of the Total Environment
3, 141-153

WEBSTER R, 1966
The Measurement of Soil Water Tension in the Field
New Phytologist, 62, 2, 249-258

WESTERLUND-HELMERSON W, 1966
The Determination of Chloride as Silver Chloride by Atomic Absorption Spectroscopy
Atomic Absorption Newsletter, 1, 97

WEYMAN D R, 1970
Throughflow on Hillslopes and its Relation to the Stream Hydrograph
Internat. Assoc. Sci. Hydrol.,
Bull. 15,3 , 25-33

WEYMAN D R, 1973
Measurements of the Downslope Flow of Water in a Soil
J. Hydrol., 20, 267-288

WEYMAN D R, 1974
Run Off Process, Contributing Areas and Streamflow in a small Upland Catchment
p 33-45 in
Fluvial Processes in Instrumented Watersheds
IBG Spec. Pub. No 6
Ed. K J Gregory and D E Walling

WHEATER H F, SHAW T L,
AND RUTHERFORD J C, 1978
An Analysis of Unit Hydrographs from the Gloucester Region
W.R.C. Tech. Report TR 96, 49p

WHIPKEY R Z, 1965

Subsurface Stormflow from Forested Slopes
Bull. Int. Assoc. Sci. Hydrol., 10, 74-85

WHIPKEY R Z, 1969

Storm Run Off from Forested Catchments by Subsurface Routes
Internat. Assoc. Sci. Hydrol., Pub. No 85, 773-779

WHITE E, STARKEY R S AND SAUNDERS M J, 1971

An Assessment of the Relative Importance of Several Chemical Sources to the Waters of a small Upland Catchment
J. Appl. Ecol., 8, 743-749

WHITEHEAD H C & FETH J H, 1964

Chemical Composition of Rain, Dry Fallout and Bulk Precipitation, California, 1957-1959
J. Geophys. Research, 19, 3319-3333

WIGLEY T M L, 1977

WATSPEC: a Computer Program for Determining the Equilibrium Speciation of Aqueous Solutions
B.G.R.G. Tech. Bull. No 20, 45p

WILLIAMS R J B, 1971

Results of the Rotation Experiment at Saxmundham, 1964-1969
Dept. of Rothamsted Exp. Stat., Part 2, 68-97

WINKLER E H, 1970

Errors in using Modern Stream Load Data to estimate Natural Rates of Denudation: Discussion
Geol. Soc. Amer. Bull., 81, 983-984

WOOD W W, 1973

A Technique using Porous Cups for Water Sampling at any Depth in the Unsaturated Zone
Water Resources Res., 9, 2, 486-488

WOODCOCK A H AND BLANCHARD D C, 1955

Tests of the Salt Nucleii Hypothesis of Rain Formation
Tellus, 7, 437-448

YAALON D H, 1964

Airborne Salts as an Active Agent in Pedogenic Processes
Trans. 8th Int. Soil Sci. Congress, Bucharest, 5, 997p

YOUNG A, 1969

The Present Rate of Land Erosion
Nature, 224, 851-852

YOUNG C P, HALL E S AND OAKES D B, 1976

Nitrate Ground Water - Studies on the Chalk near Winchester, Hampshire
WRC Tech. Report TR 31, Medmenham, UK, 67p

YOUNGS E G, 1964

An Infiltration Method of Measuring the Hydraulic Conductivity of Unsaturated Porous Materials
Soil Sci., 97, 307

YUE G K & MOHNEN V A, 1976

A Mechanism for Hydrochloric Acid Production in Cloud
Proc. 1st Int. Symp. Acid Precip. and the Forest Ecosystem, Ohio, 1975, 181-203

APPENDIX 1

A Selection of Soil Profiles Representing West Walk Soils

1. Profile HT

Horizon	1 L	2 H	3 Ea/A	4 Bh/B	5 B/C
Depth (cm)	-	-	-	-	-
Munsell colour	-	7.5YR3/2	10YR5/4	10YR5/3	10YR6/8
Particle density (g/cc)	-	-	3.664	4.860	-
% Clay	-	-	0.4	5.4	14.5
% Silt	-	-	1.0	0.6	1.0
% Fine Sand	-	-	17.0	55.0	83.2
% Coarse Sand	-	-	15.0	2.0	1.0
% Gravel	-	-	66.0	35.0	1.3
% Organic Carbon	-	26.430	1.190	3.050	0.896
Na (meq)	-	8.365	4.200	1.370	-
K (meq)	-	1.830	0.127	0.560	-
Ca (meq)	-	31.900	2.38	2.93	-
Mg (meq)	-	6.830	0.210	0.350	-
CEC (meq/100 g)	-	-	-	-	-
% Soil Moisture	18.65	60.02	12.10	20.09	25.6
pH	-	3.29	3.79	3.51	3.74

NOTES

(1) A dash denotes not measured

(2) The profile code, HT, corresponds to a location on Figure 3.4.

(3) Field and laboratory work was carried out by students of the pedology course at Portsmouth Polytehcnic and supervised by staff including the present writer.

2. Profile LB

Horizon	1 H	2 A	3 Ea	4 Bh	5 Bs
Depth (cm)	3-7	7-25	24-44	44-47	47-58
Munsell colour	2.5YR2/2	5YR5/2	10YR7/3	10YR3/3	10YR3/6
Particle density (g/cc)	-	1.96	3.20	2.63	2.79
% Clay	-	2.41	-	2.86	32.95
% Silt	-	7.42	-	4.87	9.50
% Fine Sand	-	3.40	-	3.91	18.30
% Coarse Sand	-	83.55	-	87.47	39.14
% Gravel	-	3.22	-	0.78	0.46
% Organic Carbon	37.8	4.5	1.2	0.058	0.058
Na (meq)	-	0.36	-	1.70	1.38
K (meq)	-	0.12	-	0.25	0.23
Ca (meq)	-	1.36	-	1.32	0.79
Mg (meq)	-	0.11	-	0.26	0.13
CEC (meq/100 g)	-	-	-	-	1
% Soil Moisture	62	10	7	15	5
pH	4.13	4.15	5.54	4.77	4.44

3. Profile PP

Horizon	1 L	2 A	3 Ea	4 B	5 C
Depth (cm)	0-1	1-4.5	4.5-11	11-21	21-50.5
Munsell colour	10YR3/2	10YR4/3	10YR4/4	10YR5/8	-
Particle density (g/cc)	-	3.332	3.065	2.555	-
% Clay	-	5.00	8.00	11.00	9.00
% Silt	-	27.25	2.05	1.00	0.50
% Fine Sand	-	51.25	54.95	1.00	0.55
% Coarse Sand	-	13.50	22.00	67.00	48.95
% Gravel	-	3.00	13.00	20.00	41.00
% Organic Carbon	-	2.40	1.40	0.70	0.30
Na (meq)	-	0.924	0.547	0.942	0.533
K (meq)	-	0.302	0.214	0.221	0.184
Ca (meq)	-	0.727	-	0.135	-
Mg (meq)	-	1.256	1.089	0.222	0.167
CEC (meq/100 g)	-	12.39	7.83	8.05	6.09
% Soil Moisture	-	14.28	10.25	7.24	7.80
pH	-	5.55	5.35	4.19	4.36

4. Profile NW

Horizon	1 L	2 F	3 H	4 A	5 Eb(A)	6 Eb(B)	7 Btg
Depth (cm)	0-3	3-5	5-7	7-9	9-14	14-38.5	38.5-70
Munsell colour	-	-	-	10YR2/2	7.5YR4/4	10YR5/4	10YR5/8
Particle density (g/cc)	-	-	-	2.816	2.664	2.567	2.206
% Clay	-	-	-	3.3	3.3	7.9	11.5
% Silt	-	-	-	5.0	5.9	11.6	4.9
% Fine Sand	-	-	-	29.7	32.7	49.9	36.8
% Coarse Sand	-	-	-	2.6	3.8	6.0	4.2
% Gravel	-	-	-	59.2	53.7	24.8	44.0
% Organic Carbon	-	-	-	5.096	1.011	0.496	0.565
Na (meq)	-	-	-	1.104	1.235	1.957	11.334
K (meq)	-	-	-	1.376	0.969	0.838	2.807
Ca (meq)	-	-	-	-	-	-	-
Mg (meq)	-	-	-	1.444	0.582	0.922	1.295
CEC (meq/100 g)	-	-	-	10.014	7.163	11.418	22.912
% Soil Moisture	-	-	-	26.71	22.1	14.5	13.1
pH	-	-	-	4.19	3.87	4.27	4.2

5. Profile GM

Horizon	1 H	2 A_1	3 A_2	4 B	5 Bg
Depth (cm)	0-2	2-3	3-4.8	4.8-14.8	14.8 +
Munsell colour	-	grey 5/1	greyish brown 5/2	V Dk brown 2/2	reddish yellow 6/8
Particle density (g/cc)	-	3.55	3.24	-	2.98
% Clay	-	13.86	8.76	-	14.23
% Silt	-	3.01	7.15	-	17.53
% Fine Sand	-	54.00	49.00	-	53.00
% Coarse Sand	-	28.00	34.00	-	15.0
% Gravel	-	0.00	0.00	-	-
% Organic Carbon	9.68	1.24	1.17	3.42	3.09
Na (meq)	-	0.773	0.771	0.445	0.460
K (meq)	-	0.599	0.580	0.732	0.985
Ca (meq)	-	1.532	0.772	1.372	0.598
Mg (meq)	-	0.535	0.648	2.355	0.607
CEC (meq/100 g)	-	2.843	6.055	11.668	27.59
% Soil Moisture	-	13.67	11.33	-	7.67
pH	8.52	8.8	7.82	7.9	4.84

6. Profile JA

Horizon	1 H	2 A	3 B_1	4 B_2	5 C
Depth (cm)	0-4.5	4.5-10	10-23	23-90	90 +
Munsell colour	2.5YR2/2	5YR2/2	5YR3/4	10YR6/8	10YR6/8
Particle density (g/cc)	-	-	-	-	-
% Clay	-	-	14.4	-	36.66
% Silt	-	-	5.19	-	47.91
% Fine Sand	-	-	0.739	-	15.41
% Coarse Sand	-	-	29.744	-	-
% Gravel	-	-	42.65	-	-
% Organic Carbon	10.5	9.58	2.07	1.43	1.560
Na (meq)	-	1.262	0.441	-	1.642
K (meq)	-	0.742	0.152	-	0.579
Ca (meq)	-	4.299	1.752	-	3.890
Mg (meq)	-	1.164	0.154	-	2.6
CEC (meq/100 g)	-	33.49	23.05	26.96	50.45
% Soil Moisture	55.46	31.08	19.90	9.69	23.83
pH	4.29	3.98	4.14	4.33	4.92

7. Profile SB

Horizon	1 H	2 A/B	3 B/Bt	4 Bt/C	5 C
Depth (cm)	0-1	1-18	18-30	30-38	38-74
Munsell colour	10YR3/2	10YR3/3	10YR4/3	10YR5/5	10YR6/6
Particle density (g/cc)	-	-	-	-	-
% Clay	-	28.14	37.85	2.24	-
% Silt	-	14.98	13.29	1.33	-
% Fine Sand	-	41.12	11.37	93.86	-
% Coarse Sand	-	15.74	37.51	1.56	-
% Gravel	-	0.00	0.00	0.00	-
% Organic Carbon	10.29	4.41	1.88	0.49	0.49
Na (meq)	1.24	-	0.65	-	0.60
K (meq)	1.93	-	0.52	-	0.30
Ca (meq)	5.74	-	1.40	-	0.48
Mg (meq)	1.90	-	0.58	-	0.68
CEC (meq/100 g)	64.3	-	21.78	-	27.70
% Soil Moisture	27.64	23.45	15.74	12.29	16.72
pH	4.29	4.21	4.05	4.39	4.31

8. Profile SC

Horizon	1 H	2 A_1	3 A_2	4 Bt	5 Bg
Depth (cm)	0-3	3-19	19-33	33-55	55-83 mottled
Munsell colour	-	7.5YR3/2	2.5YR4/4	10YR5/8	2.5Y5/4-10YR5/2
Particle density (g/cc)	-	1.79	2.169	-	2.477
% Clay	-	51.02	49.65	-	-
% Silt	-	25.71	29.83	-	-
% Fine Sand	-	19.42	17.2	-	-
% Coarse Sand	-	2.38	2.63	-	-
% Gravel	-	1.48	0.69	-	-
% Organic Carbon	-	1.405	0.346	-	1.028
Na (meq)	-	0.632	0.259	0.365	0.968
K (meq)	-	0.651	0.289	0.254	0.516
Ca (meq)	-	3.558	1.554	3.426	16.81
Mg (meq)	-	2.226	0.887	3.084	10.007
CEC (meq/100 g)	-	33.512	19.028	19.347	36.587
% Soil Moisture	-	1.84	1.42	1.64	3.4
pH	-	5.495	5.27	5.46	6.62

9. Profile MJ

Horizon	1 L	2 Ah/A	3 Ag	4 Bg
Depth (cm)	0-2	2-12	12-32	32-60 mottled
Munsell colour	-	7.5YR3/2	10YR5/3	7.5YR5/8 - 2.5Y6/2
Particle density (g/cc)	-	1.94	2.435	2.96
% Clay	-	58.77	54.68	82.13
% Silt	-	23.52	21.00	11.28
% Fine Sand	-	14.35	20.34	6.44
% Coarse Sand	-	1.52	1.96	0.16
% Gravel	-	1.85	1.99	-
% Organic Carbon	-	5.02	1.72	1.94
Na (meq)	-	0.79	0.393	1.133
K (meq)	-	0.549	0.173	0.761
Ca (meq)	-	3.822	0.499	1.021
Mg (meq)	-	0.969	0.618	2.601
CEC (meq/100 g)	-	22.48	11.55	19.71
% Soil Moisture	-	-	-	-
pH	-	5.26	4.9	4.885

APPENDIX 2

COMPUTER PROGRAMS

(i) ANACOVAR

(ii) APIPROG

(iii) CONCHEM 2

(iv) CONPOT

(v) CONTEN 2

(vi) CORMAT 4

(vii) DURBIN

(viii) FLUMQ

(ix) FLOWS

(x) FLUX/CHEMFLX

- (a) FLUX 1
- (b) FLUX 2
- (c) FLUX 3
- (d) FLUX 4
- (e) FLUX 5
- (f) FLUX 6
- (g) FLUX 7A
- (h) CHEMFLX 1
- (i) CHEMFLX 2
- (j) CHEMFLX 3
- (k) CHEMFLX 4
- (l) CHEMFLX 5

(xi) GEOREG 2

(xii) GLOWS

(xiii) MOMENTS 3

(xiv) MULTREG 2

(xv) NTHOREG 1

(xvi) PLOTS

(xvii) QUEZEDIG

(xviii) RESID 1

(xix) SINDAY

(xx) TENPLOT

(xxi) TRACES

(xxii) WATLOSW

(xxiii) WATQUAL

(xxiv) WEIRQ

(xxv) LAG

2. (i) **ANACOVAR**

Written by G.S.

```
10 REM ANACOVAR PROGRAM TO DETERMINE WHETHER SLOPES OF SEVERAL
11 REM REGRESSION LINES SIGNIFICANTLY DIFFERENT FROM MEAN SLOPE
12 DIM X(40),Y(40),B(40)
13SELECT PRINT 213
15 INPUT "NO. OF REGRESSION LINES",N
20 PRINT "INPUT SLOPES":FOR I=1 TO N:INPUT B(I): B1=B1+B(I):NEXT I
30B2=B1/N
40 FOR Z=1TO N:B(Z)=((B(Z)-B2)↑2)
50 PRINT "INPUT X,Y DATA FOR REGRESSION LINE";Z
80 INPUT "SAMPLE SIZE",Q
85 S1,S2,S3,S4=0
87 K=K+Q
90 FOR J=1TO Q
100 INPUT X(J),Y(J)
105X(J)=LOG(X(J)):Y(J)=LOG(Y(J))
110 S1=S1+X(J)
120 S2=S2+Y(J)
130 NEXT J
140 S1=S1/Q:S2=S2/Q
150 FOR P=1 TO Q
160 S3=S3+(((X(P)-S1)*(Y(P)-S2))↑2)
170 S4=S4+((X(P)-S1)↑2)
180 S5=S5+((Y(P)-S2)↑2)
190 NEXT P
200 S6=S6+(S3/S4)
210 S7=S7+(B(Z)*S4)
220NEXT Z
230 S9=S5-S6
240 F=(S5/(N-1))/(S9/(K-2*N))
245 PRINT "MEAN SLOPE=";B2
250PRINT "F=";F
255PRINT "F(";N-1;",";K-2*N;")"
260END
```


2

2. (ii) **APIPROG**

Written by G.S.

```
 2REM APIPROG
4 REM COMPUTES 5,10,15,20,25,30,60 DAY ANTECEDENT
5 REM PRECIPITATION INDICES
7 REM DATA IN MM.
8 REM ISTPOINT=8.12.1974
9 REM IST API'S =6.2.1975
10 DIM Z(6),Y(60)
15 X=2
17SELECT PRINT 213
18 PRINTUSING 19
19 %  DAY   RAIN  API5  API10 API15 API20 API25 API30 API60
20 R=0
25 FOR I=60 TO 1 STEP -1
30 READ P
35 Y(I)=P
37 NEXT I
38 RESTORE X
39 FOR I=1 TO 60
48 A=((1/I)*Y(I))
50 R=R+A
60 IF I=5 THEN 80
70 GOTO 90
80 Z(1)=R
90 IF I=10 THEN 110
100 GOTO 120
110 Z(2)=R
120 IF I=15 THEN 140
130 GOTO 150
140 Z(3)=R
150 IF I=20 THEN 170
160 GOTO 180
170 Z(4)=R
180 IF I=25 THEN 200
190 GOTO 202
200 Z(5)=R
202 IF I=30 THEN 206
204 GOTO 210
206 Z(6)=R
210 NEXT I
212 Z=I
220 Z2=Z+Z1
225 Z1=Z1+1
250 PRINTUSING 260,Z2;Y(1);Z(1);Z(2);Z(3);Z(4);Z(5);Z(6);R
260 %###.##
280 X=X+1
290 GOTO 20
```

```
300DATA 0,0,2,3,1,0,1,0,0
310DATA 0,1,0,4.5,1.5,5,5.5,17.5,13,1
320DATA 0,0,0,1,0,0,0,0,2,0
330DATA 2,0,0,0,0,0,1,0,0,0
340DATA 0,0,0,3,11,4,1,12,0,14
350DATA 13,3,1,7,0,0,0,0,0,0
360DATA 0,0,0,0,1,6,3,1,0,6
370 DATA 2,1,7,0,0,0,0,0,0,3
380 DATA 0,1,2,2,0,0,6,0,11,5
390 DATA 29,2,0,0,1,5,0,0,0,0
400 DATA 0,1,0,12,0,0,0,0,8,7
410 DATA 5,1,0,0,4,6,0,3,0,1
420 DATA 5,0,0,4,0,0,0,3,0,3
430 DATA 2,12,0,0,0,0,0,0,0,0
440 DATA 0,0,0,0,0,0,0,0,0,0
450 DATA 0,3,5,0,0,2,8,8,0,3
460 DATA 11,5,0,0,0,0,0,0,0,0
470 DATA 0,0,0,0,0,0,0,1,0,0
480 DATA 0,0,0,0,0,0,0,0,0,0
490 DATA 0,0,0,0,0,0,0,0,0,0
500 DATA 0,0,0,0,0,0,0,0,0,0
510 DATA 0,0,10,0,0,0,0,5,0,0
520 DATA 0,0,0,1,1,1,3,0,0,1
530 DATA 0,0,0,0,0,0,0,0,0,0
540 DATA 24,0,0,0,9,0,0,0,0,0
550 DATA 3,7,10,1,13,0,1,12,0,1
560 DATA 0,0,0,0,0,0,0,0,0,0
570 DATA 0,0,0,0,0,2,3,0,11,0
580 DATA 44,3,0,9,10,0,4,1,0,0
590 DATA 0,2,28,20,14,2,0,2,0,0
600 DATA 4,6,2,1,0,0,0,0,0,0
610 DATA 0,4,5,0,0,0,0,0,0,2
620 DATA 0,0,0,0,0,0,0,0,2,2
630 DATA 7,0,0,0,0,0,0,0,0,0
640 DATA 0,1,26,1,0,0,1,1,0,0
650 DATA 0,0,8,0,5,5,19,0,1,26
660 DATA 2,0,0,0,0,0,0,0,0,0
670 DATA 0,0,0,0,3,0,1,0,0,0
680 DATA 0,6,1,0,0,0,0,0,0,0
690 DATA 3,0,0,13,0,0,0,0,4,0
700 DATA 0,0,0,0,0,0,0,0,0,1
710 DATA 0,0,3,0,0,2,0,0,0,0
720 DATA 0,0,0,0,1,0,2,2,4,2
730 DATA 2,2,16,0,0,0,0,1,0,0
740 DATA 0,5,2,0,0,0,0,0,0,1
750 DATA 0,0,0,0,0,0,0,0,0,0
760 DATA 3,9,0,3,2,2,0,0,0,0
770 DATA 0,0,0,0,0,1,0,0,0,0
780 DATA 0,0,1,0,0,0,0,0,0,0
790 DATA 0,0,0,0,0,2,0,0,0,0
```

```
800 DATA 0,0,0,0,0,0,0,0,0,0
810 DATA 1,3,0,2,1,0,0,0,0,2
820 DATA 0,1,1,0,0,0,0,0,0,18
830 DATA 0,0,0,0,2,0,0,0,0,0
840 DATA 0,0,0,0,0,0,0,0,0,0
850 DATA 0,0,0,0,0,0,0,3,6,0,1
860 DATA 10,1,0,0,0,0,0,0,0,0
870 DATA 0,0,0,0,0,0,0,0,0,0,2
880 DATA 0,1,0,0,6,0,2,7,0,17,8,0,0,0
890 DATA 0,3,1,0,0,0,0,0,0,0,0
930 DATA 0,0,0,0,0,0,0,0,0,0
910 DATA 0,0,0,0,0,0,0,0,0,0
920 DATA 0,0,0,0,0,0,0,0,0,0,2
930 DATA 0,28,1,0,0,0,0,0,0,0
940 DATA 0,0,9,0,29,4,1,1,0,10,5,2,2,0,0
950 DATA 10,5,0,0,0,0,15,3,1,4,5,18,4,11,1
960 DATA 7,5,6,9,1,2,1,5,2,8,32,5,15,6,1,8,22,5,9
970 DATA 1,1,0,4,2,3,0,4,9,1,6,0,8,9,6,2,5,2,3,7
980DATA 12,6,2,5,4,4,0,8,9,4,5,6,6,2,0,2,8,2,2,6
990 DATA 0,4,0,4,0,0,3,8,1,2,0,0,1,5,9,2,8,4,1,5,6,17,1,7,2,0,5,20,2,8

1000 DATA 4,2,4,9,5,9,0,0,0,0,0,0,0
1010 DATA 5,5,2,5,23,9,33,8,16,2,9,8,0,0,2,0,1,11,7
1020 DATA 6,2,12,5,0,0,0,0,0,0,0,0
1030 DATA 1,1,9,9,6,3,2,7,6,0,3,0,0,0,0
1040 DATA 0,0,0,1,0,0,23,7,18,9,3,0,2,2
1050 DATA 8,2,0,0,1,0,8,0,0,0,4,0,24,6,1,4
1060 DATA 0,1,0,3,4,2,2,0,4,6,1,2,8,0,1,8,1
1070 DATA 15,2,8,2,6,1,0,0,3,4,0,6,7,8,1,7
1080 DATA 8,5 ,5,5,2,0,5,1,20,7,2,4,1,1,2,0
1090 DATA 3,7,1,3,2,5,5,2,13,2,9,4,1,8,0,5,1,9,6
1100 DATA 1,7,2,1,0,4,0,0,0,0,0,0,0
1110 DATA 0,0,5,0,0,0,0,0,7,17,2,0,12,2
1120 DATA 6,5,1,3,0,2,6,7,4,7,0,0,3,0,7,0,0
1130 DATA 3,9,2,0,0,0,13,4,2,5,0,0,0
1140 DATA 0,0,2,0,2,0,0,3,0,0,0,0,0
1150 DATA 0,0,0,0,2,2,1,1,1,2,1,3,5,4,0,3
1160 DATA 1,2,7,7,9,8,0,0,0,0,12,8,5,5,0
1170 DATA 0,1,1,9,3,1,1,0,8,4,1,2,7,2,4,6,0
1180 DATA 0,7,1,0,0,0,0,0,0,0,0
1190 DATA 0,0,7,0,0,0,0,0,0,0,0
1200 DATA 0,1,0,1,2,3,1,8,0,9,5,3,9,2,8,7,4
1210 DATA 16,2,2,1,0,0,1,1,1,1,0,2,0,0,0
1220 DATA 0,1,0,0,0,3,1,0,3,0,7,0,0
1230 DATA 0,0,0,0,0,0,1,6,0,0,0
1240 DATA 0,0,0,0,7,2,0,0,1,6,1,5,0
1250 DATA 0,2,4,3,8,0,0,0,0,0,0,0
1260 DATA 0,0,0,2,8,6,1,0,0,1,0,0,0
1270 DATA 0,3,1,2,2,0,13,3,0,6,0,4,9,4,0,0
1280 DATA 2,9,4,7,27,0,1,1,6,33,5,0,0,5,1,0
1290 DATA 2,9,5,5,0,0,0,3,0,2,3,4,0,0,0
1300 DATA 0,0,0,0,0,0,2,0,0,0,0
```

2. (iii) **CONCHEM 2**

Written by B Sprunt, modified by G.S.

```
    CONCHEM2
2 REM CONTOURS CHEMICAL DATA FOR HILLSLOPE
4 PRINT "INPUT LINE 60:DATA LOAD 'FILE NAME' THEN RUN8":STOP
8DIM B(4),C(7),D(7)
10 DIM T(5),X(5),Y(5),Z(5),R1(20),R2(20)
20 INPUT "ROWS,COLS,CONYOUR INT",M5,N5,H5
30 B(1)=50:B(2)=75:B(3)=100
32 C(1)=55:C(2)=100:C(3)=65:C(4)=90:C(5)=85:C(6)=140
34 D(1)=39:D(2)=40:D(3)=52:D(4)=54:D(5)=96:D(6)=124
36 B9=225:D9=405:C9=545
38 B(4)=0
60DATA LOAD "CHEMK6"
70 M1=0
80 M2=0
82X(1)=0:X(2),X(3)=1:X(4)=0:X(5)=0.5
84Y(1),Y(2)=0:Y(3),Y(4)=1:Y(5)=0.5
90 DATA LOAD R2()
92FOR J3=1TO M5-1
94 FOR J4=1TO N5:R1(J4)=R2(J4):NEXT J4
96 DATA LOAD R2()
102FOR I3=1TO N5-1
104T(1)=R2(I3):T(2)=R2(I3+1):T(3)=R1(I3+1)
105T(4)=R1(I3):T(5)=0.25*(T(1)+T(2)+T(3)+T(4))
108FOR I=1TO 4:Z(I)=T(I):NEXT I
110Z(5)=Z(1)
121FOR I=1TO 4
122IF Z(I)>Z(I+1)THEN 165
123NEXT I
124 PLOT <D(I3)-M1,C(I3)-M2,>:M1=0:M2=0
125NEXT I3
130 PLOT <-D9,0,>:PLOT <0,-C9-B(J3+1),>
131M1=0:M2=0
132NEXT J3
134 GOTO 930
165 C=INT(Z(I+1)/H5)*H5
166 C=C+H5
167 IF C<Z(I) THEN 198
168GOTO 123
198 N=2*I-1
200 J=INT(N/2+0.00001)+1
210 K=J+1
220 GOSUB '02(K)
230 K=J9
240 GOSUB '01(J,K,C)
```

2. (iv) **CONPOT**

Written by B Sprunt, modified by G.S.

```
05 REM CONPOT
6 REM CONTOURS HYDRAULIC POTENTIAL FOR HILLSLOPE
10PRINT "INPUT LINE 413: DATALOAD'...' , RUN50"
12 STOP
50DIM B(4),C(7),D(7)
90 DIM T(5),X(5),Y(5),Z(5),R1(23),R2(20)
130 INPUT "ROWS,COLS,CONYOUR INT",M5,N5,H5
170 B(1)=37:B(2)=25:B(3)=87
210 C(1)=65:C(2)=100:C(3)=65:C(4)=90:C(5)=85:C(6)=140:C(7)=585
250 D(1)=39:D(2)=42:D(3)=52:D(4)=54:D(5)=96:D(6)=124:D(7)=377
290B9=149:D9=782:C5=585
330 C9=545
370 B(4)=0
410DATA LOAD "T1"
450 M1=0
490 M2=0
530X(1)=0:X(2),X(3)=1:X(4)=0:X(5)=0.5
570Y(1),Y(2)=0:Y(3),Y(4)=1:Y(5)=0.5
610 DATA LOAD R2()
612 R2(1)=R2(1)+139:R2(2)=R2(2)+165.5:R2(3)=R2(3)+205:R2(4)=R2(4)+230
614 R2(5)=R2(5)+266:R2(6)=R2(6)+298:R2(7)=R2(7)+354:R2(8)=R2(8)+587
650FOR J3=1TO M5-1
690 FOR J4=1TO N5:R1(J4)=R2(J4):NEXT J4
730 DATA LOAD R2()
732 IF J3=1 THEN 738
734 IF J3=2 THEN 746
736 IF J3=3 THEN 754
738 R2(1)=R2(1)+124:R2(2)=R2(2)+150.5:R2(3)=R2(3)+190:R2(4)=R2(4)+215
740 R2(5)=R2(5)+251:R2(6)=R2(6)+283:R2(7)=R2(7)+339:R2(8)=R2(8)+572
744 GOTO 770
746 R2(1)=R2(1)+114:R2(2)=R2(2)+14[illegible].5:R2(3)=R2(3)+180:R2(4)=R2(4)+205
748 R2(5)=R2(5)+241:R2(6)=R2(6)+273:R2(7)=R2(7)+329:R2(8)=R2(8)+562
752 GOTO 770
754 R2(1)=R2(1)+79:R2(2)=R2(2)+105.5:R2(3)=R2(3)+145:R2(4)=R2(4)+170
756 R2(5)=R2(5)+206:R2(6)=R2(6)+238:R2(7)=R2(7)+294:R2(8)=R2(8)+527
770FOR I3=1TO N5-1
810T(1)=R2(I3):T(2)=R2(I3+1):T(3)=R1(I3+1)
850T(4)=R1(I3):T(5)=0.25*(T(1)+T(2)+T(3)+T(4))
890FOR I=1TO 4:Z(I)=T(I):NEXT I
930Z(5)=Z(1)
970FOR I=1TO 4
1010 IF Z(I)>Z(I+1)THEN 1330
1050NEXT I
1090 PLOT <D(I3)-M1,C(I3)-M2,>:M1=0:M2=0
1130NEXT I3
1170 PLOT <-D9,0,>:PLOT <0,-C9-B(J3+1),>:PLOT <0,-C5,>
1210M1=0:M2=0
1250NEXT J3
1290 GOTO 4090
```

2. (v) CONTEN 2

Written by B Sprunt, modified by G.S.

```
 1 REM CONTEN2
2 REM CONTOURS  TENSION  DATA FOR HILLSLOPE
4 PRINT "INPUT LINE 50:DATA LOAD 'FILE NAME' THEN RUN8":STOP
5 PRINT "INPUT LINE 20:DATASAVE OPEN'FILE NAME' THEN RUN 10"
6 STOP
8DIM B(4),C(7),D(7)
10 DIM T(5),X(5),Y(5),Z(5),R1(20),R2(20)
20 INPUT "ROWS,COLS,CONYOUR INT",M5,N5,H5
30 B(1)=37:B(2)=25:B(3)=87
32 C(1)=65:C(2)=100:C(3)=55:C(4)=90:C(5)=85:C(6)=140:C(7)=585
34 D(1)=39:D(2)=40:D(3)=52:D(4)=54:D(5)=96:D(6)=124:D(7)=377
36B9=149:D9=782:C5=585
37 C9=545
38 B(4)=0
40 FOR I=1 TO N
50 INPUT R(1),R(2),R(3),R(4),R(5),R(6),R(7),R(8)
60 DATA LOAD "TEN1"
70 M1=0
80 M2=0
82X(1)=0:X(2),X(3)=1:X(4)=0:X(5)=0.5
84Y(1),Y(2)=0:Y(3),Y(4)=1:Y(5)=0.5
90 DATA LOAD R2()
92FOR J3=1TO M5-1
94 FOR J4=1TO N5:R1(J4)=R2(J4):NEXT J4
96 DATA LOAD R2()
102FOR I3=1TO N5-1
104T(1)=R2(I3):T(2)=R2(I3+1):T(3)=R1(I3+1)
105T(4)=R1(I3):T(5)=0.25*(T(1)+T(2)+T(3)+T(4))
108FOR I=1TO 4:Z(I)=T(I):NEXT I
110Z(5)=Z(1)
121FOR I=1TO 4
122IF Z(I)>Z(I+1)THEN 165
123NEXT I
124 PLOT <D(I3)-M1,C(I3)-M2,>:M1=0:M2=0
125NEXT I3
130 PLOT <-D9,0,>:PLOT <0,-C9-B(J3+1),>:PLOT <0,-C5,>
131M1=0:M2=0
132NEXT J3
134 GOTO 930
165 C=INT(Z(I+1)/H5)*H5
166 C=C+H5
167 IF C<Z(I) THEN 198
168GOTO 123
198 N=2*I-1
200 J=INT(N/2+0.00001)+1
210 K=J+1
220 GOSUB '02(K)
230 K=J9
240 GOSUB '01(J,K,C)
```

```
260 GOSUB '36(P,Q)
270 IF T(5)>C THEN 520
280 J=INT(N/2+0.00001)+1
290 GOSUB '32(J)
300 J=J9
310 GOSUB '31(J,5,C)
330 GOSUB '36(P,Q)
340 N=N-1
350 IF N<>3 THEN 370
360 N=8
370 J=INT(N/2+0.00001)
380 IF T(J)>C THEN 470
390 K=J+1
400 GOSUB '32(K)
410 K=J9
420 GOSUB '31(K,J,C)
440 GOSUB '36(P,Q)
445 GOTO 166
470 GOSUB '31(J,5,C)
490 GOSUB '36(P,Q)
500N=N-2
510 GOTO 350
520 J=INT((N+3)/2+0.00001)
530 GOSUB '32(J)
540 J=J9
550 GOSUB '31(5,J,C)
570 GOSUB '36(P,Q)
580 N=N+1
590 J=INT(N/2+0.00001)+2
600 GOSUB '32(J)
610 J=J9
620 IF T(J)>C THEN 680
630 GOSUB '31(5,J,C)
650 GOSUB '36(P,Q)
660 N=N+2
670 GOTO 590
680 K=INT(N/2+0.00001)+1
690 GOSUB '32(K)
700 K=J9
710 GOSUB '31(J,K,C)
730 GOSUB '36(P,Q)
735 GOTO 166
760 DEFFN'36(P,Q)
770 K3=INT(P*D(I3)+0.5)
780 K4=INT(Q*B(J3)+P*C(I3)+0.5)
790PLOT <K3-M1,K4-M2,HEX(FB)>
800 M1=K3
810M2=K4
```

```
820 RETURN
830 DEFFN'02(J9)
840 IF J9>4 THEN 860
850 GOTO 870
860 J9=J9-4
870 RETURN
880 DEFFN'01(J1,J2,H)
890 D=(T(J1)-H)/(T(J1)-T(J2))
900 P=X(J1)+(X(J2)-X(J1))*D
910 Q=Y(J1)+(Y(J2)-Y(J1))*D
920 RETURN
930 PLOT <,149,HEX(0E)>
933 PLOT <,,HEX(2B)>
935 FOR J=1 TO N5
940 FOR I=1 TO M5-1: PLOT <0,-B(I),HEX(2B)>:NEXT I
945 IF J=N5 THEN 955
950 PLOT <D(J),B9+C(J),HEX(2B)>
955 NEXT J
970 END
```

2. (vi) CORMAT 4

WANG package program, modified by G.S.

```
 10REM CORMAT4
15 REM OUTPUTS MATRIX OF R,A,B,SE
16 REM DATA INPUT FROM TAPE
20 COM C(10,10),A(10),D(10,10)
30 DIM R(10,10),R2(10,10),E(10,10),B(10),X1(15)
40 DIM T(10,10)
50 INPUT "SAMPLE SIZE, NUMBER OF VARIABLES",N,M
60 INPUT "DAY OF YEAR INDEX LAG",L
70 INPUT "MATRIX COLUMN NUMBER OF SOLUTE",P
80 PRINT "INPUT LINE 90:DATALOAD<...>, 120:DATA TRANSFORMS"
82PRINT "700:EXPONENTIATES A FOR LOG/LOG,LOG/NORMAL
90DATA LOAD "FNS"
95FOR I=1TO 10:FOR J=1TO 10
96R(I,J),R2(I,J),E(I,J),T(I,J),C(I,J),D(I,J),B(I),A(I)=0
97NEXT J:NEXT I
100 FOR K=1TO N
110 DATA LOAD X1()
120X1(1)=X1(P):FOR Z=9TO 15:X1(Z-7)=X1(Z):NEXT Z
130 X1(1)=LOG(X1(1))
140X1(2)=LOG(X1(2))
150X1(3)=LOG(X1(3)+10)
160X1(4)=LOG(X1(4)+10)
170X1(5)=LOG(X1(5)+10)
180X1(6)=LOG(X1(6)+10)
190X1(8)=SIN((2*#PI*(X1(8)-L))/365)
200 X1(7)=LOG(X1(7)+1.0)
210FOR I=1TO M
220FOR J=1TO M
230R(I,J),R(J,I)=R(I,J)+X1(I)*X1(J)
240NEXT J
250A(I)=A(I)+X1(I)
260B(I)=B(I)+X1(I)↑2
270NEXT I
280NEXT K
290 M1=M:M=1:M2=1
300 FOR I=MTO M1 STEP M2:GOSUB 960
310 FOR J=I TO M1 STEP M2:GOSUB 980
320 R2(I,J)=(N*R(I,J)-A(I)*A(J))/SQR(S*(N*B(J)-A(J)↑2))
330IF R2(I,J)>=1.0 THEN 350
335IF R2(I,J)<=(-1.0) THEN 350
337IF SQR(1.0-ABS(R2(I,J)↑2))<=0 THEN 350
340T(I,J)=(ABS(R2(I,J))*SQR(N-2))/(SQR(1.0-ABS(R2(I,J)↑2)))
350 NEXT J
360 R2(I,I),C(I,I)=1:D(I,I),E(I,I)=0
370 NEXT I
380 IF M3=1 THEN 410
390 M=M1:M1=1:M3=1:M2=-1
400 GOTO 300
410SELECT PRINT 213
420PRINT
430 PRINT "CORRELATION MATRIX"
440 FOR I=1TO M
```

```
450 PRINT :PRINT
460 FOR J=1TO M
470 IF R2(I,J)<1 THEN 490
480R2(I,J)=1
490PRINT R2(I,J);
500 NEXT J:NEXT I
510PRINT :PRINT
520PRINT "STUDENTS T"
530 FOR I=1TO M
540 PRINT :PRINT
550 FOR J=1TO M
560PRINT T(I,J);
570 NEXT J:NEXT I
580PRINT :PRINT
590 PRINT "B COEFFICIENT"
600 FOR I=1TO M
610PRINT :PRINT
620 FOR J=1TO M
630PRINT C(I,J);
640 NEXT J:NEXT I
650PRINT :PRINT
660 PRINT "A COEFFICIENT"
670 FOR I=1TO M
680PRINT :PRINT
690 FOR J=1TO M
700PRINT EXP(D(I,J));
710 NEXT J:NEXT I
720PRINT :PRINT
730 PRINT "STANDARD ERRORS"
740 FOR I=1TO M
750PRINT :PRINT
760 FOR J=1TO M
770PRINT E(I,J);
780 NEXT J:NEXT I
785PRINT :PRINT
790SELECT PRINT 005
800PRINT "DO YOU REQUIRE DURBIN & WATSON STATISTIC FOR
810INPUT X
820IF X=0 THEN 840
830LOAD DC F"DURBIN"
840 END
850 REM SUBROUTINE 1
860 S=N*B(I)-A(I)↑2:RETURN
870 REM SUBROUTINE 2
880 C(I,J)=(N*R(I,J)-A(I)*A(J))/S
890 D(I,J)=(A(J)-(C(I,J)*A(I)))/N
900E(I,J)=SQR(ABS(((B(I)-(A(I)/N)-(C(I,J)*(R(I,J)-(A(J)*A(I)/N))))/N-2))
910 RETURN
```

2. (vii) **DURBIN**

Written by G.S.

```
5 REM DURBIN
10 REM DURBIN & WATSON STATISTIC FOR SERIAL CORRELATION IN
      BIVARIATE REGRESSION
12 REM Y ON X ONLY COMPUTED
15 COM C(10,10)
16 COM D(10,10)
17 COM A(10)
18 COM X3(40,8)
19 COM B(10)
21 COM G(16)
25 COM D1(10,10)
30 COM R(10,10),Z1(10,10),Z2(10,10),N(1),M(1),L(1)
40 INPUT "SAMPLE SIZE,NUMBER VARIABLES",N,M
50 M(1)=M:N(1)=N:L(1)=L
60 INPUT "DAY OF YEAR INDEX LAG",L
70 INPUT "MATRIX COLUMN NUMBER OF SOLUTE",P
75 PRINT "INPUT LINE 90:DATALOAD<...>,LINE  120:DATA TRANSFORMS
     AND RUN90":STOP
90DATA LOAD ""INS"
92 FOR I=1TO 10:FOR J=1TO 10
94 R(I,J),C(I,J),D(I,J),Z1(I,J),Z2(I,J)=0
96 NEXT J:NEXT I
100FOR K=1TO N
105 DATA LOAD G()
110 G(1)=G(P):FOR Z=9 TO 15:G(Z-7)=G(Z):NEXT Z
120 G(1)=LOG(G(1))
130 G(2)=LOG(G(2))
140 G(3)=LOG(G(3)+10)
150 G(4)=LOG(G(4)+10)
160 G(5)=LOG(G(5)+10)
170 G(6)=LOG(G(6)+10)
180 G(7)=LOG(G(7)+1)
190 G(8)=SIN((2*#PI*(G(8)-L))/365)
200 FOR I=1TO M
210 FOR J=1TO M
220 R(I,J)=R(I,J)+G(I)*G(J)
230 NEXT J
250 X3(K,I)=G(I)
260 A(I)=A(I)+G(I)
270 B(I)=B(I)+G(I)↑2
280 NEXT I
290 NEXT K
```

```
300 M1=M:M=1:M2=1
310 FOR I=MTO M1 STEP M2
320 S=N*B(I)-A(I)^2
330 FOR J=ITO M1 STEP M2
340 REM SLOPE
345 C(I,J)=(N*T(I,J)-A(I)*A(J))/S
350 REM INTERCEPT
355 D(I,J)=(A(J)-(C(I,J)*A(I)))/N
360 NEXT J
370 C(I,I),D(I,I)=1
375 NEXT I
405 FOR K=1TO N
410 FOR I=MTO M1 STEP M2
420 FOR J=ITO M1 STEP M2
430 Z1(I,J)=Z1(I,J)+(X3(K,J)-(A(J)/N)-(C(I,J)*(X3(K,I)-(A(I)/N))))^2
440REM FIRST DIFFERENCES
453 IF K=1 THEN 480
 460 Z2(I,J)=Z2(I,J)+((X3(K,J)-X3(K-1,J)*(C(I,J)*(X3(K,I)-X3(K-1,I)))))^2
480NEXT J
500NEXT I
550NEXT K
570 FOR I=M TO M1 STEP M2
580 FOR J=I TO M1 STEP M2
586 IF Z1(I,J)=0 THEN 595
590 D1(I,J)=Z2(I,J)/Z1(I,J)
594 GOTO 600
595 D1(I,J)=0
600 NEXT J
610 D1(I,I)=0
620 NEXT I
660SELECT PRINT 213
670PRINT "D  MATRIX"
675 M=M(1)
680FOR I=1TO M
682 PRINT :PRINT
685 FOR J=1TO M
700 PRINT D1(I,J);
710NEXT J:NEXT I
720 SELECT PRINT 005
730 PRINT "DO YOU REQUIRE PLOTS OF RESIDUALS AGAINST X, YES OR NO"
740 INPUT Z$
750 IF Z$="NO" THEN 770
760 LOAD DC F"RESID1"
770END
```

2. (viii) **FLUMQ**

Written by G.S.

```
1 REM FLUMQ
2 REM OUTPUTS HOURLY DISCHARGE DATA FOR FLUME
3 REM INPUT FROM MAG TAPE
4 PRINT "TOTAL NUMBER OF HOURS REQUIRED?":INPUT N
5 PRINT "INPUT START TIME,T,HOURS":INPUT T
7 PRINT "INPUTSTART DAY,MONTH,YEAR":INPUT D
20 PRINT "INPUT LINE 50 DATALOAD '........' THEN RUN 40"
30 STOP
40 DIM PS(200)11
50 DATA LOAD "09263477"
60 DATA LOAD PS()
70 CONVERT STR(PS(1),8,4) TO Y9
80 CONVERT STR(PS(2),8,4) TO Y8
90 Y9=(Y9+Y8)/2
92 SELECT PRINT 213
93 PRINT "WEST WALK FLUME"
94 PRINT "STARTING DATE=";D
95 PRINT "T(HOURS)          Q(CUMECS)"
100 FOR I= 3 TO N+3
107 T=T+1
109 IF T=25 THEN 113
111 GOTO 115
113 T=1
115 T2=(T-1)
120 CONVERT STR(PS(I),8,4) TO Y
124 IF Y<=0 THEN 290
130 REM CONVERTS TO STAGE IN METRES
135 IF (Y-Y9)<=0 THEN 270
140 H=(Y-Y9)*.3011
150 REM CONVERTS TO DISCHARGE IN CUMECS
160 A1=0.003
170 IF H<=A1 THEN 270
210 Q=(((H-0.003)/(H))↑1.5)*(H↑1.5)*0.7308
220 SELECT PRINT 213
230 IF T2=0 THEN 250
240 GOTO 260
250 PRINT " 24",Q
255 GOTO 280
260 PRINT T2,Q
265 GOTO 280
270 PRINT T2,"********ZERO FLOW********"
280 NEXT I
290 STOP
```

2. (ix) **FLOWS**

Written by G.S.

```
5 REM FLOWS
6 REM COMPUTES MEAN DAILY FLOWS FOR V-NOTCH WEIRS
7 REM DATA INPUT FROM TAPE
10 DIM Z(200),Q(200)
20 PRINT "INPUT LINE60 DATALOAD <******>"
25 PRINT "INPUT RATING EQUATIONS LINES 910,930,41,42.....RUN30":STOP
30 INPUT "RECORD START: HOUR-DAY-MONTH-YEAR",T1,T2,T3,T4
32 INPUT "RECORD END  :HOUR-DAY-MONTH-YEAR",T5,T6,T7,T8
33 Z9=T1:E=0:O=0
35 INPUT "DATUM,B,CENTIMETRES",B
37INPUT "WEIR NUMBER",W
40 GOSUB 960
41 REM LOW FLOW EQUATION USED BELOW H1,METRES
42 H1=0.05
45 FOR I=1TO 200:Q(I),Z(I)=0:NEXT I
50SELECT PRINT 01D
52 PRINT "WEIR";W
53 PRINT "DAY MONTH YEAR MDF"
54 SELECT PRINT 005
60DATA LOAD "12050176"
80 DATA LOAD Z()
90 IF T1<>24 THEN 110
100 GOTO 130
110 GOSUB 770
120 GOTO 260
130 P=24:N=P+24
140 O=0:E=0:V=0
150 FOR I=PTO N
160 IF (Z(I)*0.0254-B)<=0 THEN 180
170 GOTO 190
180 Q(I)=0:GOTO 240
190 H=(Z(I)*0.0254-B)*0.05
200 IF H<=H1 THEN 230
210 GOSUB 900
220 GOTO 240
230 GOSUB 930
240 NEXT I
250 GOSUB 610
260 A=(N-P+1)/2:C=INT((N-P+1)/2)
270 IF A=C THEN 295
280 N=N-1
290 REM INTEGRATION PROCEDURE
295 IF (N-1)-(P+1)<3 THEN 354
300 FOR J=P+1 TO N-1
310 IF J/2=INT(J/2) THEN 340
320 O=O+Q(J)
330 GOTO 350
340 E=E+Q(J)
350 NEXT J
```

```
352 GOTO 360
354 FOR K=PTO N:V=V+Q(K)*3600:NEXT K
356 IF A=C THEN 430
358 V=V+Q(N+1)*3600
360 IF A<>C THEN 390
370 V=1200*(Q(P)+4*E+2*O+Q(N))
384 GOTO 400
390 V=1200*(Q(P)+4*E+2*O+Q(N))+Q(N+1)*3600
400 IF A=C THEN 430
420 N=N+1
430 IF N>=T9 THEN 530
440 IF Z9<>24 THEN 460
442 Z9=24
450 GOTO 480
460 Q1=(V+V0)/86400
462 Z9=24
470 IF V0=0 THEN 472
471 GOTO 490
472 GOSUB 1400
473 GOTO 490
480 Q1=V/86400
490SELECT PRINT 31D
500 PRINT T2;T3;T4;Q1
510 SELECT PRINT 005
520 GOTO 540
530 V0=V:SELECT PRINT 01D:PRINT "V0=";V0:SELECT PRINT 0.5:GOTO 590
540 P=N:N=P+24
550 IF (T9-P)<24 THEN 570
560 GOTO 580
570 N=T9
580 GOTO 140
590 GOTO 20
600 END
610 REM SUBROUTINE TIMECOUNT
620 REM DAY
630 IF T2=F1 THEN 650
640 T2=T2+1:GOTO 660
650 T2=1
660 REM MONTH
670 IF T2=1 THEN 690
680 GOTO 700
690 T3=T3+1
700 REM YEAR
710 IF T2=1 THEN 730
720 GOTO 760
730 IF T3=13 THEN 750
740 GOTO 760
750 T4=T4+1:T3=1
760 RETURN
```

```
770 REM SUBROUTINE FIRSTHOURS
780 FOR I=1 TO 24-T1+1
790 IF (Z(I)*0.0254-B)<=0 THEN 810
800 GOTO 820
810 Q(I)=0:GOTO 870
820 H=(Z(I)*0.0254-B)*0.25
830 IF H<H1 THEN 860
840 GOSUB 900
850 GOTO 870
860 GOSUB 930
870 NEXT I
880P=1:N=24-T1+1
890 RETURN
900 REM SUBROUTINE FLOW RATING
910 Q(I)=((H+0.0009)↑2.5)*1.36545
920 RETURN
930 REM SUBROUTINE LOW FLOW RATING
940 Q(I)=3.0077*(H↑2.8138)
950 RETURN
960 REM SUBROUTINE TIMESORT
970 REM HOURS IN FIRST AND LAST DAYS
975 F1,F4,F5,F6=0
980 X1=(24-T1+1)+T5
990 M=T3
995 IF M =T7 THEN 1285
1000 IF M=1 THEN 1210
1010 IF M=2 THEN 1120
1020 IF M=3 THEN 1210
1030 IF M=4 THEN 1190
1040 IF M=5 THEN 1210
1050 IF M=6 THEN 1190
1060 IF M=7 THEN 1210
1070 IF M=8 THEN 1210
1080 IF M=9 THEN 1190
1090 IF M=10 THEN 1210
1100 IF M=11 THEN 1190
1110 IF M=12 THEN 1210
1120 PRINT HEX(07)
1130 INPUT "IS IT A LEAP YEAR,YES OR NO",Y$
1140 IF Y$="YES" THEN 1170
1150 F1=28
1160 GOTO 1230
1170 F1=29
1180 GOTO 1230
1190 F1=30
1200 GOTO 1230
1210 F1=31
1220 REM COMPLETE DAYS IN FIRST MONTH
1230 F4 =F1-T2
```

```
1240 REM HOURS IN COMPLETE DAYS OF FIRST MONTH
1250 F5=F4*24
1260 REM HOURS IN COMPLETE DAYS OF SECIND MONTH
1270 F6=(T6-1)*24
1280 REM TOTAL HOURS ON RECORD
1283 GOTO 1290
1285 F5=(T6-T2-1)*24
1287 IF F5<0 THEN 1289
1288 GOTO 1290
1289 F5=0:GOTO 1295
1290 T9=X1+F5+F6
1293 GOTO 1300
1295 T9=X1-1
1300 RETURN
1400 REM SUBROUTINE IF V0=0
1410 SELECT PRINT 01D
1420 PRINT "FIRST POINT IS MEAN OF LESS THEN 24 HOURS"
142501=V/((24-T1)*3600)
1430 RETURN
```

2. (x) FLUX/CHEMFLX (a) FLUX 1

Written by G.S.

```
1REM ************
2REM FLUX/CHEMFLUX
3REM ************
4REM A SERIES OF LINKED PROGRAMS TO TEST THE EQUATIONS
5REM OF WATER AND SOLUTE MOVEMENT IN HILLSLOPE
6REM SOILS.INPUTS ARE-RAINFALL OR EVAPORATION,PORE WATER
7REM PRESSURE AND VOLUMETRIC CONTENT,AND THE SOLUTE
8REM CONTENT OF SOIL WATER AND RAINFALL.COMPUTED OUTPUTS
9REM ARE-DOWNSLOPE AND DOWNPROFILE WATER AND SOLUTE
10REM FLUXES,DS AND DP HYDRAULIC CONDUCTIVITY AND SOLUTE
11REM DISPERSION COEFFICIENTS,STORAGE CHANGES,AND SLOPE-BASE
12REM WATER AND SOLUTE DISCHARGES.
13REM AT 22/8/79 THE PROGRAM USES A NON-ITERATIVE IMPLICIT
14 REM FINITE DIFFERENCE METHOD
16REM *****
17REM FLUX1
18REM *****
20COM Z(9),X(6),T(9),M(8),Z8(6),Z9(6)
22COM P(6,9),P1(6,9)
23 COM V1
26DIM A5(8),O(5,6),E(6)
30DIM R2(8)
31 REM Z=SOIL SURFACE HEIGHT ABOVE SLOPE BASE (CM)
32REM X=TENSIOMETER DEPTHS BELOW SURFACE(CM)
33REM T=TENSIOMETER INTERVALS SUB-PARALLEL TO SLOPE (CM)
34REM P1=TENSION TIME 0
35REM P=TENSION TIME 1
38REM H=ELEMENT HEIGHTS  L=ELEMENT LENGTHS(CM)
39REM M=ELEMENT SLOPE ANGLES(DEG)
40REM LOADS TENSION (CM WATER) AS A MATRIX
41 V=1
42FOR J=1TO 100:PRINT HEX(07):NEXT J
45 DATA LOAD DC OPEN F"SLOPDAT"
48 DSKIP V1
50FOR I=1TO 4
60 DATA LOAD DC X,R2()
80FOR J=2TO 9:P(I+1,J)=R2(J-1):NEXT J:NEXT I
100REM SLOPE ANGLES FOR EACH ELEMENT(DEG)
110 M(1)=9.71:M(2)=8.16:M(3)=7.79:M(4)=6.49:M(5)=5.1:M(6)=4.77:M(7)=6.66
111M(8)=5.55
120REM SOIL SURFACE HIEGHTS ABOVE SLOPE BASE (CM)
130Z(1)=100.25:Z(2)=149:Z(3)=175.5:Z(4)=215:Z(5)=240:ZI 6)=276:
:Z(7)=308:Z(8)=364:Z(9)=597
145REM TENSIOMETER DEPTHS BELOW SURFACE (CM)
150X(1)=1.25:X(2)=10:X(3)=25:X(4)=35:X(5)=70:X(6)=101.25
153REM TENSIOMETER INTERVALS SUB-PARALLEL TO SLOPE (CM)
155T(1)=2.5:T(2)=222.5:T(3)=225:T(4)=240:T(5)=235:TT(((6)=305:T
T(7)=463:T(8)=710:T(9)=1900
160REM TENSION ADJACENT PIT ESTIMATED BY LINEAR INTERPOLATION
```

```
170FOR I=2TO 5
180S1,S2,S3,S4,S5=0
185X=T(1)
190FOR J=2TO 4
200X=X+T(J)
210Y=P(I,J)
220S1=S1+X:S2=S2+Y:S3=S3+X↑2:S4=S4+Y↑2:S5=S5+X*Y
245NEXT J
250B=(3*S5-S2*S1)/(3*S3-S1↑2)
260A=(S2-B*S1)/3
270P(I,1)=A+B*T(1)
280NEXT I
290REM TENSION AT UPPER AND LOWER EDGES ESTIMATED
293REM BY A CUBIC FUNCTION
300M=3:N=4
332FOR J=1TO 9
334FOR K=2TO 2*M+1
335A5(K)=0:NEXT K
336FOR Q=1TO M+2:E(Q)=0:NEXT Q
338A1=N
310FOR I=2TO 5
312FOR K=2TO 2*M+1:A5(K)=A5(K)+(Z(J)-X(I))↑(K-1):NEXT K
315FOR K=1TO M+1:E(K),Q(K,M+2)=E(K)+(P(I,J))*(Z(J)-X(I))↑(K-1):NEXT K
320E(M+2)=E(M+2)+(P(I,J))↑2:NEXT I
325FOR I=1TO M+1:FOR K=1TO M+1:Q(I,K)=A5(I+K-1):NEXT K:NEXT I
330FOR S=1TO M+1
335FOR T=STO M+1:IF Q(T,S)<>0THEN 345:NEXT T
340PRINT "NO UNIQUE SOLUTION":STOP
345GOSUB 370
350C=1/Q(S,S):GOSUB 382
355FOR T=1TO M+1:IF T=STHEN 365
360C=-Q(T,S):GOSUB 384
365NEXT T:NEXT S:GOTO 386
370FOR K=1TO M+2
375B=Q(S,K):Q(S,K)=Q(T,K):Q(T,K)=B
380NEXT K:RETURN
382FOR K=1TO M+2:Q(S,K)=C*Q(S,K):NEXT K:RETURN
384FOR K=1TO M+2:Q(T,K)=Q(T,K)+C*Q(S,K):NEXT K:RETURN
386A=Q(1,M+2):B=Q(2,M+2):C=Q(3,M+2):D=Z(J)-X(1):F=Z(J)-X(6)
387E=Q(4,M+2)
390P(1,J)=A*D+B*D+C*D↑2+E*D↑3
395P(6,J)=A*F+B*F+C*F↑2+E*F↑3
400NEXT J
4[illegible]IF V=2THEN 45
43[illegible]FOR I=1TO 6:FOR J=1TO 9:P1(I,J)=P(I,J):NEXT J:NEXT I
435 FOR Z=1TO 100:PRINT HEX(07):NEXT Z
440 V1=V1+4:V=2:GOTO 45
448REM PIT FACE TENSION RETAINED FOR USE IN LATER PROGRAM
450 FOR I=1TO 6:Z8(I)=P1(I,1):Z9(I)=P(I,1):NEXT I:SELECT PRINT 213
451PRINT "TENSION TIME 1 CM"
452FOR I=1TO 6

454PRINTUSING 459,P1(I,1),P1(I,2),P1(I,3),P1(I,4),P1(I,5),P1(I,6)
,P1(I,7),P1(I,8),P1(I,9)
455NEXT I:PRINT "TENSION TIME 2"
456FOR I=1TO 6
457PRINTUSING 459,P(I,1),P(I,2),P(I,3),P(I,4),P(I,5),P(I,6),P(I, 7
),P(I,8),P(I,9)
458NEXT I
459% ###.# ###.# ###.# ###.# ###.# ###.# ###.# ###.# ###.# ###.#
470 REM FIRST CHAIN PROGRAM ENDS HERE
480LOAD DC F"FLUX2"
```

(b) FLUX 2

```
2REM *****
5REM FLUX2
7REM *****
10COM P(6,9),P1(6,9),B(4,8),B1(4,8),N(6,9),Z8(6),Z9(6)
12COM M(8)
13COM B2(4,8)
14 COM V1
15N=1
30REM B1=MOISTURE CONTENT TIME 0
40REM B=MOISTURE CONTENT TIME 1
60REM MOISTURE CONTENT COMPUTED (CC/CC SOIL)(4*7MATRIX)
65REM MOISTURE CHARACTERISTIC CURVES DESCRIBED BY CUBIC FUNCTIONS
66FOR I=1TO 6:FOR J=1TO 9:N(I,J)=P(I,J):NEXT J :NEXT I
70FOR I=1TO 6:FOR J=1TO 9:P(I,J)=P1(I,J):NEXT J :NEXT I:GOTO 80
75N=2
80D=P(2,2):B(1,1)=0.407-1.581E-3*D+4.071E-6*D↑2-3.642E-9*D↑3
90D=P(3,2):B(2,1)=0.335-1.373E-3*D+3.673E-6*D↑2-3.210E-9*D↑3
100D=P(4,2):B(3,1)=0.421-1.314E-3*D+5.333E-6*D↑2-4.973E-9*D↑3
110D=P(5,2):B(4,1)=0.335-1.324E-3*D+2.298E-6*D↑2-1.999E-9*D↑3
120D=P(2,3):B(1,2)=0.419-2.275E-3*D+7.887E-6*D↑2-9.477E-9*D↑3
130D=P(3,3):B(2,2)=0.442-1.335E-3*D+7.513E-6*D↑2-1.233E-8*D↑3
140D=P(4,3):B(3,2)=0.329-7.842E-4*D+1.683E-6*D↑2-1.252E-9*D↑3
150D=P(5,3):B(4,2)=0.334-9.264E-4*D+2.414E-6*D↑2-2.231E-9*D↑3
160D=P(2,4):B(1,3)=0.319-9.497E-4*D+2.157E-6*D↑2-1.869E-9*D↑3
170D=P(3,4):B(2,3)=0.475-2.219E-3*D+6.973E-6*D↑2-7.628E-9*D↑3
180D=P(4,4):B(3,3)=0.369-1.102E-3*D+2.415E-6*D↑2-1.625E-9*D↑3
190D=P(5,4):B(4,3)=0.314-2.317E-3*D+1.214E-5*D↑2-2.774E-8*D↑3
200D=P(2,5):B(1,4)=0.428-9.632E-4*D+1.734E-6*D↑2-1.398E-9*D↑3
210D=P(3,5):B(2,4)=0.400-2.785E-3*D+1.962E-5*D↑2-4.523E-8*D↑3
220D=P(4,5):B(3,4)=0.470-1.548E-3*D+3.863E-6*D↑2-3.164E-9*D↑3
230D=P(5,5):B(4,4)=  .332-1.  E-3*D+2.834E-6*D↑2-2.081E-9*D↑3
240D=P(2,6):B(1,5)=  .351-2.587E-4*D+2.182E-6*D↑2-2.272E-9*D↑3
250D=P(3,6):B(2,5)=  .457-1.173E-3*D+2.596E-6*D↑2-2.273E-9*D↑3
260D=P(4,6):B(3,5)=0.504-1.527E-3*D+6.611E-6*D↑2-1.385E-8*D↑3
270D=P(5,6):B(4,5)=0.512-2.687E-3*D+1.934E-5*D↑2-3.743E-8*D↑3
280D=P(2,7):B(1,6)=0.333-7.536E-4*D+1.893E-6*D↑2-1.984E-9*D↑3
290D=P(3,7):B(2,6)=0.332-9.186E-4*D+2.574E-6*D↑2-2.854E-9*D↑3
300D=P(4,7):B(3,6)=0.394-1.530E-3*D+4.536E-6*D↑2-4.910E-9*D↑3
310D=P(5,7):B(4,6)=0.423-9.965E-4*D+2.287E-6*D↑2-1.861E-9*D↑3
320D=P(2,8):B(1,7)=0.512-2.545E-3*D+1.329E-5*D↑2-1.648E-9*D↑3
330D=P(3,8):B(2,7)=0.368-1.142E-3*D+1.319E-6*D↑2-3.385E-9*D↑3
340D=P(4,8):B(3,7)=0.263-1.549E-3*D+1.883E-5*D↑2-3.213E-8*D↑3
350D=P(5,8):B(4,7)=0.533-1.974E-3*D+6.154E-6*D↑2-6.433E-9*D↑3
360D=P(2,9):B(1,8)=0.312-1.761E-3*D+1.083E-5*D↑2-2.581E-8*D↑3
370D=P(3,9):B(2,8)=0.351-1.336E-3*D+3.  5E-6*D↑2-3.717E-9*D↑3
380D=P(4,9):B(3,8)=0.361-1.402E-3*D+4.026E-6*D↑2-3.752E-9*D↑3
390D=P(5,9):B(4,8)=0.414-1.080E-4*D+2.882E-6*D↑2-2.732E-9*D↑3
410IF N=1THEN 430
420GOTO 473
430FOR I=1TO 4:FOR J=1TO 8
440B1(I,J)=B(I,J)
```

```
450NEXT J:NEXT I
472FOR I=1TO 6:FOR J=1TO 9:P(I,J)=N(I,J):NEXT J:NEXT I:GOTO 75
473SELECT PRINT 213
475PRINT "MOISTURE CONTENT TIME 1 CC/CC"
480FOR I=1TO 4
485PRINTUSING 530,B1(I,1),B1(I,2),B1(I,3),B1(I,4),B1(I,5),B1(I,
6),B1(I,7),B1(I,8)
490NEXT I:PRINT "MOISTURE CONTENT TIME 2"
500FOR I=1TO 4
505PRINTUSING 530,B(I,1),B(I,2),B(I,3),B(I,4),B(I,5),B(I,6),B(I
,7),B(I,8)
510NEXT I
512 FOR I=1TO 4:FOR J=1TO 8
514 B2(I,J)=(B1(I,J)+B(I,J))/2
516 NEXT J:NEXT I
518PRINT "AVERAGE MOISTURE CONTENT OVER PERIOD"
519FOR I=1TO 4
520 PRINTUSING 530,B2(I,1),B2(I,2),B2(I,3),B2(I,4),B2(I,5),B2(I
,6),B2(I,7),B2(I,8)
521NEXT I
530% .### .### .### .### .### .### .### .###
560REM SECOND CHAIN ENDS HERE
570LOAD DC F"FLUX3"
```

(c) FLUX 3

```
 2REM *****
5REM FLUX3
7REM *****
10COM Z(9),X(6),T(9),P(6,9),P1(6,9)
12COM H(4),L(7),M(8),Z8(6),Z9(6)
20COM B(4,8),B1(4,8),S(4,8)
21 COM V1
22COM B2(4,8)
25DIM S2(4,8)
120REM SOIL SURFACE HIEGHTS ABOVE SLOPE BASE (CM)
130 Z(1)=100.25:Z(2)=149:Z(3)=175.5:Z(4)=215:Z(5)=240:Z(6)=276:Z(7)=338
8:Z(8)=364:Z(9)=597
140REM TENSIOMETER DEPTHS BELOW SURFACE (CM)
150X(1)=1.25:X(2)=10:X(3)=25:X(4)=35:X(5)=70:X(6)=101.25
160REM TENSIOMETER INTERVALS SUB-PARALLEL TO SLOPE (CM)
170T(1)=2.5:T(2)=222.5:T(3)=225:T(4)=240:T(5)=235:T(6)=305:T(7)=460:T
T(8)=710:T(9)=1900
180FOR I=1TO 6
560FOR J=1TO 9
580REM TENSION CONVERTED TO POTENTIAL (6*9 MATRIX)
590P(I,J)=P(I,J)+(Z(J)-X(I))
600P1(I,J)=P1(I,J)+(Z(J)-X(I))
610NEXT J:NEXT I
620REM ELEMENT LENGTHS SUB-PARALLEL TO SLOPE
630L(1)=332.5:L(2)=232.5:L(3)=237.5:L(4)=270:L(5)=382.5:L(6)=535:L
(7)=1305
640REM ELEMENT HIEGHTS
650H(1)=15:H(2)=12.5:H(3)=10:H(4)=60
660REM STORAGE CHANGES PER ELEMENT COMPUTED
670SELECT D
680FOR I=1TO 4
690 FOR J=1TO 7
695 S2(I,J)=(B(I,J)-B1(I,J))
700S(I,J)=(S2(I,J))*(H(I)*(COS(M(J))*L(I))):NEXT J:NEXT I
705SELECT PRINT 213
707PRINT "HYDRAULIC POTENTIAL ,TIME 1 ,CM."
709FOR I=1TO 6
711PRINTUSING 730,P1(I,1),P1(I,2),P1(I,3),P1(I,4),P1(I,5),P1(I,6),
P1(I,7),P1(I,8),P1(I,9)
712NEXT I
714PRINT "HYDRAULIC POTENTIAL ,TIME 2"
716FOR I=1TO 6
718PRINTUSING 730,P(I,1),P(I,2),P(I,3),P(I,4),P(I,5),P(I,6),P(I,7),
 P(I,8),P(I,9)
720NEXT I
722PRINT "STORAGE CHANGES PER ELEMENT CC."
724FOR I=1TO 4
726PRINTUSING 735,S(I,1),S(I,2),S(I,3),S(I,4),S(I,5),S(I,6),S(I,7)

728NEXT I
730%###.# ###.# ###.# ###.# ###.# ###.# ###.# ###.# ###.#
735%###.# ###.# ###.# ###.# ###.# ###.# ###.# ###.#
740REM THIRD CHAIN PROGRAM ENDS HERE
750LOAD DC F"FLUX4"
EM CON
```

(d) FLUX 4

```
 5REM *****
10REM FLUX4
12REM *****
2% COM X(6),T(9),P(6,9),P1(6,9),B(4,3),B1(4,8),L(7),H(4),M(8),
,D(5,9),D1(6,8),Z8(6),Z9(6),S(4,8),Z(9)
25COM B2(4,3)
26 COM V1
30REM P1=POTENTIAL, TIME 0
32REM P=POTENTIAL , TIME 1
34REM AVERAGE VALUESOF HYDRAULIC GRADIENT UPSLOPE IN TIME
36REM INTERVAL COMPUTED (6*9 MATRIX)
5:FOR I=1TO 6:FOR J=1TO 8
60A9=(P(I,J+1)-P(I,J))/T(J+1)
70B9=(P1(I,J+1)-P1(I,J))/T(J+1)
80D1(I,J)=(A9+B9)/2
90NEXT J:NEXT I
100REM AVERAGE VALUES OF HYDRAULIC GRADIENT UPPROFILE IN TIME
102REM INTERVAL COMPUTED (5*9 MATRIX)
120FOR J=1TO 9:FOR I=1TO 5
130A8=(P(I,J)-P(I+1,J))/(X(I+1)-X(I))
140B8=(P1(I,J)-P1(I+1,J))/(X(I+1)-X(I))
150D(I,J)=(A8+B8)/2
155NEXT I:NEXT J
160REM FOURTH CHAIN PROGRAM ENDS HERE
170LOAD DC F"FLUX5"
```

(e) FLUX 5

```
 100 REM *****
120 REM FLUX5
140 REM *****
160 COM D1(6,8),D(5,9),S(4,8),Y(4,7),Y1(4,7),H(4),L(7),M(8),Z8(
 6),Z9(6),T(9)
180COM Z(9),X(6),B(4,8),B1(4,8)
200 COM R(4,7)
206 REM SPECIFY ANISTROPY
208 REM VALUE <1:0 IF DOWNSLOPE K< DOWNPROFILE K
220 REM COMPUTES RATIO OF HYDRAULIC GRADIENT UPSLOPE OF
230 REM TO HG FROM ABOVE (Y), AND HG DOWNSLOPE
240 REM TO HG FROM ABOVE (Y1)
280 FOR I=1TO 4:FOR J=1TO 7
290READ R
300 IF D(I,J+1)=0THEN 340
320 GOTO 380
340 Y(I,J),Y1(I,J)=0
360 GOTO 420
380 Y(I,J)=(D1(I+1,J+1)*R)/D(I,J+1)
400 Y1(I,J)=(D1(I+1,J)*R)/D(I,J+1)
420 NEXT J:NEXT I
430DATA 1,1,1,1,1,1,1,1
440DATA 1,1,1,1,1,1,1,1
450DATA 1,1,1,1,1,1,1,1
460DATA 1,1,1,1,1,1,1,1
480 REM FIFTH CHAIN PROGRAM END HERE
490 LOAD DC F"FLUX6"
```

(f) FLUX 6

```
5 REM *****
10 REM FLUX6
15REM *****
18 COM V1
20 COM S(4,8),Y(4,7),Y1(4,7),H(4),L(7),M(8),Z8(6),Z9(6),F(4,7)
,A(1)
22 COM G(1),T(4,7),T1(4,7)
23 COM B2(4,8)
25 COM B(4,8),B1(4,8),P2(9),T(9),Z(9),X(6),D(5,9),D1(6,8)
26 COM F1(4,7)
27 COM F3(4,7)
28SELECT PRINT 235:FOR I=1TO 100:PRINT HEX(07):NEXT I
29 DATA LOAD DC OPEN F"MAIN"
32 DSKIP (V1/4-1)
33 DATA LOAD DC X,P:P=P/10:A(1)=P
34 G(1)=4
35 SELECT PRINT 213
40 PRINT "HILLSLOPE WATER FLUX.....PIT IS AT BOTTOM LEFT"
42 PRINT "OUTPUT FORMAT AS BELOW"
50 PRINT "**************************************************"
60 PRINT "DOWNPROFILE FLUX INTO TOP ELEMENT"
65PRINT "**********************************"
70 PRINT "FLUX FROM UPSLOPE INTO ELEMENT"
80 PRINT "FLUX DOWNSLOPE FROM ELEMENT"
90 PRINT "DOWNPROFILE FLUX FROM ELEMENT"
100 PRINT "**************************"
110 PRINT "FLUX IN CC."
120 PRINT "***********"
121PRINT "ROW1"
122PRINT "*************"
125 FOR J=1TO 7:P2(J)=P*L(J):NEXT J:SELECT D
126 PRINTUSING 375,P2(1),P2(2),P2(3),P2(4),P2(5),P2(6),P2(7)
127 PRINT "*************"
130 FOR I=1TO 4:FOR J=1TO 7
140E9=(P2(J)*H(I)*((COS(M(J)))+(COS(M(J+1)))))/(2*L(J)*(COS(M(J))))
150 REM CALCULATES FLUX FROM UPSLOPE INTO EACH ELEMENT
160 F(I,J)=Y(I,J)*E9
170 REM CALCULATES FLUX DOWNSLOPE FROM EACH ELEMENT
180 F1(I,J)=Y1(I,J)*E9
190 NEXT J
200 REM EQUALIZES DOWNSLOPE ENTRY/EXIT FLUXES BETWEEN ELEMENTS
210 REM BY AVERAGING
215 FOR J=1 TO 6
220 IF F(I,J)<>F1(I,J+1)THEN 240
230 GOTO 260
240 F(I,J)=(F(I,J)+F1(I,J+1))/2
250 F1(I,J+1)=F(I,J)
260 NEXT J
270 REM CHECKS TENSION AT PIT FACE
```

```
280 IF Z8(I+1)<0 THEN 330
290 GOTO 330
300 IF Z9(I+1)<0 THEN 320
310 GOTO 330
320 F1(I,1)=0
330 REM CALCULATES DOWNWARD FLUX FROM EACH ELEMENT
340 FOR J=1 TO 7
350F3(I,J)=S(I,J)-F1(I,J)+F(I,J)+P2(J)
360 P2(J)=F3(I,J)
370 NEXT J:NEXT I
375%####.## ####.## ####.## ####.## ####.## ####.## ####.##
377%####.## ####.## ####.## ####.## ####.## ####.## ####.##
380 FOR I=1TO 4
400 PRINTUSING 377,F(I,1),F(I,2),F(I,3),F(I,4),F(I,5),F(I,6),F(I,7)

410 PRINTUSING 377,F1(I,1),F1(I,2),F1(I,3),F1(I,4),F1(I,5),F1(I,6)
,F1(I,7)
420 PRINTUSING 377,F3(I,1),F3(I,2),F3(I,3),F3(I,4),F3(I,5),F3(I,6)
),F3(I,7)
421 IF I=4 THEN 427
422 PRINT "ROW";I+1
423 PRINT "*********"
425NEXT I
427PRINT "**********************************************"
428Q4=F1(1,1)+F1(2,1)+F1(3,1)+F1(4,1)
430PRINT "TOTAL PIT DISCHARGE=";Q4*132;"CC"
433 PRINT "AVERAGE PIT DISCHARGE=";(Q4/132)/(G(1)*3600);"CC/SEC"
434PRINT "**********************************************"
436PRINT :PRINT
440 REM SIXTH CHAIN PROGRAM ENDS HERE
450LOAD DC F"FLUX7A"
```

(g) FLUX 7A

```
5 REM *****
10 REM FLUX7A
15 REM *****
18 COM V1
20 COM H(4),L(7),M(8),F(4,7),A(1),D1(6,8),D(5,9),K(4,7),K1(4,7)
25  COM F1(4,7),F3(4,7)
30 COM T(9),Z(9),X(6),B(4,8),B1(4,8)
32COM P2(9)
40COM S(4,8)
42 COM B2(4,8),F6(4,7),F7(4,7)
45 COM  (4,7),  1(4,7)
53COM G(1)
51DIM F4(4,7),F5(4,7)
52T1=G(1)
54 REM FLUX RATE/UNIT AREA COMPUTED
56 REM DOWNPROFILE
58 FOR I=1TO 4:FOR J=1TO 7
60 F4(I,J)=(F3(I,J)/(L(J)*COS(M(J))))/T1
62 NEXT J:NEXT I
66 FOR I=1TO 4:FOR J=1TO 7
68 REM INTO ELEMENT FROM UPSLOPE
70 F5(I,J)=((F(I,J)*2)/(H(I)*(COS(M(J+1))+COS(M(J)))))/(T1)
72NEXT J:NEXT I
74 PRINT "FLUX RATES PER UNIT AREA (CC/HOUR)"
75PRINT "DOWNPROFILE"
76PRINT "INTO ELEMENT FROM UPSLOPE"
77PRINT "**********"
78 FOR I=1TO 4
79 PRINT "ROW";I
80 PRINT "********"
82 PRINTUSING 275,F4(I,1),F4(I,2),F4(I,3),F4(I,4),F4(I,5),F4(I,6),F
F4(I,7)
83 PRINTUSING 275,F5(I,1),F5(I,2),F5(I,3),F5(I,4),F5(I,5),F5(I,6),
 F5(I,7)
85 NEXT I:PRINT :PRINT
95 REM COMPUTES HYDRAULIC CONDUCTIVITIES
100 FOR I=1TO 4:FOR J=1TO 7
110K(I,J)=F4(I,J)/D(I+1,J+1)
120K1(I,J)=F5(I,J)/D1(I+1,J+1)
130NEXT J:NEXT I
200 PRINT :PRINT :PRINT :SELECT PRINT 213
210 PRINT "VERTICAL K,CM/HOUR"
220 PRINT "DOWNSLOPE K,CM/HOUR"
230PRINT "(THE TWO SHOULD BE EQUAL IF SOIL ISOTROPIC)"
240 FOR I=1TO 4
242PRINT "ROW";I
245PRINT "*****************************************"
250 PRINTUSING 270,K(I,1),K(I,2),K(I,3),K(I,4),K(I,5),K(I,6),K(I,7)
260 PRINTUSING 270,K1(I,1),K1(I,2),K1(I,3),K1(I,4),K1(I,5),K1(I,
```

```
),K1(I,7)
270%#.#### #.#### #.#### #.#### #.#### #.#### #.#### #.####
275%##.### ##.### ##.### ##.### ##.### ##.### ##.### ##.###
280 NEXT I
285 PRINT "****************************************"
440 REM COMPUTES VELOCITIES
450 REM DOWNPROFILE
460FOR I=1TO 4:FOR J=1TO 7
470F6(I,J)=F4(I,J)*B2(I,J)
475 REM INTO ELEMENT FROM UPSLOPE
480 F7(I,J)=F5(I,J)*B2(I,J)
490 NEXT J:NEXT I
500 PRINT "WATER VELOCITIES"
510PRINT "DOWNPROFILE"
520PRINT "DOWNSLOPE"
540PRINT "CM/HOUR"
545PRINT "**********"
550FOR I=1TO 4
560PRINT "ROW";I
570PRINT "**********"
580PRINTUSING 270,F6(I,1),F6(I,2),F6(I,3),F6(I,4),F6(I,5),F6(I,6),F
6(I,7)
590PRINTUSING 270,F7(I,1),F7(I,2),F7(I,3),F7(I,4),F7(I,5),F7(I,6),
 F7(I,7)
600NEXT I
610PRINT :PRINT
620 LOAD DC F"FLUX1"
```

(h) CHEMFLX 1

```
5 REM "********"
10 REM CHEM FLX1
15REM "********"
17 COM V1
20 COM B(4,8),B1(4,8),C(6,9),C1(6,9),H(4),M(8),L(7),T(9),Z(9),X(6),
F(4,7),F1(4,7)
30 COM F3(4,7),C2(6,9),C3(6,9)
32 COM A(1)
35 DIM P2(8),V(12),Q(6,7),E(7)
50 REM LOADS CHEMICAL CONCENTRATION OF SOIL WATER AS MATRIX (MG/CC)
55 V=1
57 DATA LOAD DC OPEN F"CHEMDAT"
60 DSKIP (V1-4)
65 INPUT "FIRST OR SECOND SAMPLE",V
68 FOR I=1TO 4
70 DATA LOAD DC X,P2()
80 FOR J=2TO 9:C(I+1,J)=P2(J-1)/1000:NEXT J: NEXT I
97 REM CHEMICAL CONTENTS COMPUTED(MG/CC SOIL)
110 FOR I=2TO 4:FOR J=1TO 7
113 IF V=1 THEN 127
115 GOTO 140
127 C3(I+1,J+1)=B1(I,J)*C(I+1,J+1)
130 GOTO 150
140 C3(I+1,J+1)=B(I,J)*C(I+1,J+1)
150 NEXT J:NEXT I
280 REM BOUNDARY VALUES ESTIMATED BY POLYNOMIAL FUNCTION
290 REM VALUES AT BASE OF SLOPE
300 M=4:N=3
310 FOR I=2TO 5
320 GOSUB 500
325 D=T(1)
330 FOR J=2TO 4
340 D=D+T(J)
360 GOSUB 515
365 NEXT J
370 A=Q(1,M+2):B=Q(2,M+2):E=Q(4,M+2):D=T(1)
375 C=Q(3,M+2)
380 G=Q(5,M+2)
385 C3(I,1)=A*D+B*D+C*D↑2+E*D↑3+G*D↑4
390 NEXT I
410 REM UPPER AND LOWER EDGES NEXT
412 M=4:N=4
420 FOR J=1TO 9
425 GOSUB 500
445 FOR I=2TO 5
```

```
45% D=Z(J)-X(I)
455 GOSUB 515
457 NEXT I
460 A=Q(1,M+2):B=Q(2,M+2):C=Q(3,M+2):E=Q(4,M+2):D=Z(J)-X(1):F=Z(J)-X(5
6):G=Q(5,M+2)
470 C3(1,J)=A*D+B*D+C*D↑2+E*D↑3+G*D↑4
480 C3(6,J)=A*F+B*F+C*F↑2+E*F↑3+G*F↑4
490 NEXT J
500 FOR K=2 TO 2*M+1:W(K)=0:NEXT K
510 FOR Q=1TO M+2:E(Q)=0:NEXT Q:A1=N:RETURN
515 FOR K=2 TO 2*M+1:W(K)=W(K)+(Z(J)-X(I))↑(K-1):NEXT K
610 FOR K=1TO M+1:E(K),Q(K,M+2)=E(K)+C3(I,J)*D↑(K-1):NEXT K
620 E(M+2)=E(M+2)+((C3(I,J))↑2:NEXT I
630 FOR I=1TO M+1:FOR K=1TO M+1:Q(I,K-1)=W(I+K-1):NEXT K:NEXT I
640 FOR S=1TO M+1
650 FOR T=STO M+1:IF Q(T,S)<>0THEN 670:NEXT T
660 PRINT "NO UNIQUE SOLUTION":STOP
670 GOSUB 720
680 C=1/Q(S,S):GOSUB 750
690 FOR T=1TO M+1:IF T=S THEN 710
700 C=-Q(T,S):GOSUB 760
710 NEXT T:NEXT S:GOTO 770
720 FOR K=1TO M+2
730 B=Q(S,K):Q(S,K)=Q(T,K):Q(T,K)=B
740 NEXT K:RETURN
750 FOR K=1TO M+2:Q(S,K)=C*Q(S,K):NEXT K:RETURN
760 FOR K=1TO M+2:Q(T,K)=Q(T,K)+C*Q(S,K):NEXT K
770 RETURN
780 IF V=2THEN 825
810 FOR I=1TO 6:FOR J=1TO 9:C2(I,J)=C3(I,J):NEXT J:NEXT I
815 FOR I=1TO 4:FOR J=1TO 8:C1(I,J)=C(I,J):NEXT J:NEXT I
820 V1=V1+4:V=2:GOTO 57
825 SELECT PRINT 213
830 PRINT "CHEMICAL CONTENT AT TIME 1 MG/CC SOIL"
840 FOR I=1TO 6
850 PRINTUSING 900,C2(I,1),C2(I,2),C2(I,3),C2(I,4),C2(I,5),C2(I,6
  ,C2(I,7),C2(I,8),C2(I,9)
860 NEXT I
865 PRINT "CHEMICAL CONTENT AT TIME 2"
870 FOR I=1TO 6
875 PRINTUSING 900,C3(I,1),C3(I,2),C3(I,3),C3(I,4),C3(I,5),C3(I,6),
C3(I,7),C3(I,8),C3(I,9)
876 FOR J=1TO 8
877 C(I,J)=C(I,J)+C1(I,J)/2
878 NEXT J
880 NEXT I
882 FOR I=2TO 5:FOR J=2TO 9
884C(I,J)=(C(I,J)+C1(I,J))/2
886 NEXT J:NEXT I
900 %##.## ##.## ##.## ##.## ##.## ##.## ##.## ##.## ##.## ##.##
905 V1=V1-4
910 REM NINTH CHAIN PROGRAM ENDS HERE
920 LOAD DC F"CHEMFLX2"
```

```
 5 REM "********"
10 REM CHEMFLX2
15 REM "********"
17 COM V1
20 COM C(4,8),B(4,8),H(4),M(7),L(7),T(9),Z(9),X(6),F(4,7),F1(4,7)
25 COM F3(4,7),A(1),D(5,9),D1(6,8)
27 COM C2(6,9),C3(6,9),G(1)
30 REM CHEMICAL SOLUTION STORAGE CHANGES COMPUTED,MG/ELEMENT
35 SELECT PRINT 213
40 PRINT "CHEMICAL SOLUTION STORAGE STORAGE CHANGES MG/ELEMENT"
50 FOR I=1TO 4:FOR J=1TO 7
60 B(I,J)=(C3(I,J)-C2(I,J)*(H(I))*(H(I)*COS(M(J))*L(I)))
70 NEXT J
80 PRINTUSING 90,B(I,1),B(I,2),B(I,3),B(I,4),B(I,5),B(I,6),B(I,7)
90 %##.## ##.## ##.## ##.## ##.## ##.## ##.##
100 NEXT I
110REM AVERAGE VALUES OF CONTENT GRADIENT UPSLOPE IN TIME INTERVAL CO
OMPUTED (6X9 MATRIX)
130 FOR I=1TO 6:FOR J=1TO 8
140 A9=(C3(I,J+1)-C3(I,J))/T(J+1)
150 B9=(C2(I,J+1)-C2(I,J))/T(J+1)
160 D1(I,J)=(A9+B9)/2
170 NEXT J:NEXT I
180 REM AVERAGE VALUES OF CONTENT GRADIENT UP-PROFILE IN TIME INTERV
VAL COMPUTED (5X9 MATRIX)
200 FOR J=1TO 9:FOR I=1TO 5
210 A8=(C3(I,J)-C3(I+1,J))/(X(I+1)-X(I))
220 B8=(C2(I,J)-C2(I+1,J))/(X(I+1)-X(I))
230 D(I,J)=(A8+B8)/2
235 NEXT I:NEXT J
240 REM TENTH CHAIN PROGRAM ENDS HERE
250 LOAD DC F "CHEMFLX3"
```

(j) CHEMFLX 3

```
 10 REM CHEMFLX3
20 COM D1(6,8),D(5,9),B(4,8),Y(4,7),Y1(4,7),H(4),M(7),L(7),T(9),
 Z(9),V1
25 COM X(6),F(4,7),F1(4,7),A(1),C(4,8)
40 REM COMPUTES RATIO OF CONTENT GRADIENT UPSLOPE OF ELEMENT TOCG FR
OM ABOVE(Y) AND CG DOWNSLOPE TO CG FROM ABOVE(Y1)
70 FOR I=1TO 4:FOR J=1TO 7
80 Y(I,J)=D1(I+1,J+1)/D(I,J+1)
90 Y1(I,J)=D1(I+1,J)/D(I,J+1)
100 NEXT J:NEXT I
110 REM ELEVENTH CHAIN PROGRAM END HERE
120 LOAD DC F"CHEMFLX4"
```

(k) CHEMFLX 4

```
 5 REM ********
10 REM CHEMFLX4
15 REM ********
17 COM V1
20 COM B(4,8),Y(4,7),Y1(4,7),H(4),M(8),L(7),Z(9),X(6),F(4,7),F1(4,
7),F3(4,7)
30 COM  (1),C(6,9),J(4,7),J1(4,7)X,;U C2(6,9),C2(6,9)
32 SELECT PRINT 005:FOR I=1TO 100:PRINT HEX(07):NEXT I
44 C9=3.125
46 C9=C9/1000:C9(1)=C9
50 FOR J=1TO 7:P(J)=A(1)*C(9)*L(J):NEXT J
60 SELECT PRINT 213
70 PRINT "HILLSLOPE SOLUTE FLUX.....PIT AT BOTTOM LEFT"
80 PRINT "**************************************"
90 PRINT "OUTPUT FORMAT AS FO  WATER"
100 PRINT "**********"
110 PRINT "FLUX IN MG."
120 PRINT "**********"
130 SELECT D
132 PRINT "********"
133PRINT " ROW1"
134PRINT " ********"
135 PRINTUSING 390,P(1),P(2),P(3),P(4),P(5),P(6),P(7)
136PRINT " ********"
138 FOR I=1TO 4:FOR J=1TO 7
140 E9=(P(J)*H(I)*((COS(M(J)))+(COS(M(J+1)))))/(2*L(J)*COS(M(J)))
150 REM CALCULATES FLUX FROM UPSLOPE INTO EACH ELEMENT
160 J(I,J)=(Y(I,J)*E9)+(F(I,J)*C(I+1,J+2))
170 REM CALCULATES FLUX DOWNSLOPE FROM EACH ELEMENT
180 J1(I,J)=(Y1(I,J)*E9)+(F1(I,J)*C(I+1,J+1))
190 NEXT J
200 REM EQUALIZES DOWNSLOPE ENTRY/EXIT FLUXES BETWEEN ELEMENTS
210 REM BY AVERAGING
215 FOR J=1TO 6
220 IF J(I,J)<>J1(I,J+1)THEN 240
230 GOTO 260
240 J(I,J)=(J(I,J)+J1(I,J+1))/2
250 J1(I,J+1)=J(I,J)
260 NEXT J
330 REM CALCULATES DOWNWARD FLUX FROM EACH ELEMENT
340 FOR J=1TO 7
350 J3(I,J)=B(I,J)-J1(I,J)+J(I,J)+P(J)
360 P(J)=J3(I,J)
370 NEXT J:NEXT I
380 FOR I=1TO 4
390 %##.## ##.## ##.## ##.## ##.## ##.## ##.##
400 PRINTUSING 390,J(I,1),J(I,2),J(I,3),J(I,4),J(I,5),J(I,6),J(I,7)
)
410 PRINTUSING 390,J1(I,1),J1(I,2),J1(I,3),J1(I,4),J1(I,5),J1(I,6),
J1(I,7)
420 PRINTUSING 390,J3(I,1),J3(I,2),J3(I,3),J3(I,4),J3(I,5),J3(I,6),
J3(I,7)
430 Q9=J1(1,1)+J1(2,1)+J1(3,1)+J1(4,1)
435 PRINT "PIT DISCHARGE=";Q9;"MG."
440 R9=F1(1,1)+F1(2,1)+F1(3,1)+F1(4,1)
445 PRINT "PIT CONCENTRATION=";(Q9/R9)*1000;"MG/L"
450 PRINT "****************************"
460 REM TWELVTH CHAIN PROGRAM ENDS HERE""
470 LOAD DC F "CHEMFLX 5"
```

(1) CHEMFLX 5

```
 10 REM CHEMFLX5
17 COM V1
20 COM H(4),L(7),M(7),F(4,7),F1(4,7),F3(4,7),D1(6,8),D(5,9),D2(4,7
 ),D3(4,7)
30 COM T(9),Z(9),X(6),J(4,7),J1(4,7),J3(4,7)
80 INPUT "TIME INCREMENT IN HOURS AND MINUTES",T1,T2
90 T1=T1+T2/60
95 REM COMPUTES DISPERSION COEFFICIENTS
100 FOR I= 2TO 4
110 FOR J=1TO 7
120 D2(I,J)=(((J3(I,J)-(F3(I,J)*C(I,J)))/L(J)*H(I))/T1)/D(I+1,J+1)
130 NEXT J:NEXT I
140 FOR I=1TO 4
150 FOR J=1TO 7
160 K1(I,J)=(2*((J(I,J)-(F(I,J)*C(I,J)))/(H(I)*(COS(M(J+1))+COS(M(J)
)))))/T1)/D1(I+2,J+2)
170 NEXT J:NEXT I
180 PRINT :PRINT :PRINT :SELECT PRINT 213
190 PRINT "VERTICAL DISPERSION COEFFICIENT, SQCM/HR"
200 PRINT "DOWNSLOPE DISPERSION COEFFICIENT"
210 PRINT "*********************************"
220 FOR I=1TO 4
230 PRINTUSING 270,D(I,1),D(I,2),D(I,3),D(I,4),D(I,5),D(I,6),D(I,7)
240 PRINTUSING 270,D1(I,1),D1(I,2),D1(I,3),D1(I,4),D1(I,5),D1(I,6),
D1(I,7)
250 PRINT "*********************************************"
270 %##.## ##.## ##.## ##.## ##.## ##.## ##.##
280 REM LAST CHAIN PROGRAM ENDS HERE
290 LOAD DC F"FLUX1A"
```

2. (xi) GEOREG 2

WANG package program, modified by G.S.

```
1 REM GEOREG2
2SELECT PRINT 213
3 PRINT "TITLE? THEN INPUT LINE 455:PRINT'......'"
5 PRINT "INPUT LINES : 80 DATALOAD '........'
                       100 DATALOAD '........'"
6 PRINT "CHECK LINES 90,101,185,212"
7STOP
9 INPUT "NOS. IN X AND Y ARRAYS",P,N
10 DIM D1(10),D2(10)
12 DIM C1(10),C2(10)
13 DIM X(150),Y(150)
14J=0
15 FOR J=1 TO 50
20 PRINT "GIVE POSITIONS TO BE SKIPPED IN X ARRAY"
40INPUT D1(J),D2(J)
50 IF D1(J)<0 THEN 56
55NEXT J
56 FOR K=1 TO 50
57 PRINT "GIVE POSITIONS TO BE SKIPPED IN Y ARRAY"
58 INPUT C1(K),C2(K):IF C1(K)<0 THEN 60
59 NEXT K
60DIM Q(150)
70DIM K(150)
80DATA LOAD ""W1Q(I)"
90DATA LOAD Q()
100DATA LOAD ""W1K(I)"
101DATA LOAD K()
130J=1
131Z=0
132 K=1
133 W=0
135S1,S2,S3,S4,S5=0
140FOR I=1 TO P
150IF I=D1(J) THEN 180
170 GOTO 185
180I=D2(J):Z=Z+D2(J)-D1(J)+1:J=J+1
182 GOTO 190
185 X(I-Z)=Q(I)
190 NEXT I
202 FOR I=1 TO N
204 IF I=C1(K) THEN 208
206 GOTO 212
208 I=C2(K):W=W+C2(K)-C1(K)+1:K=K+1
210 GOTO 214
212 Y(I-W)=K(I)
214 NEXT I
220 FOR I= 1 TO (N-W)
225 X(I)=LOG(X(I))
```

```
227 Y(I)=LOG(Y(I))
310 S1=S1+Y(I)
315 S2=S2+Y(I)
320 S3=S3+(X(I))↑2
325 S4=S4+(Y(I))↑2
340 S5=S5+(X(I)*Y(I))
350 NEXT I
355 N=(N-W)
360 B=(N*S5-S2*S1)/(N*S3-S1↑2)
370 A=(S2-B*S1)/N
380 PRINT
390 PRINT "A=";EXP(A)
400 PRINT "B=";B
410 S1=B*(S5-S1*S2/N)
420 S4=S4-S2↑2/N
430 S2=S4-S1
450PRINT
455PRINT "W1K(I)"
460 PRINT
470 PRINT "                    REGRESSION TABLE"
480 PRINT
490 PRINT "SOURCE","SUM OF SQ.","DEG.FREEDOM","MEAN SQ."
500 PRINT "REGRESSION",S1,1,S1
510 PRINT "RESIDUAL",S2,N-2,S2/(N-2)
520 PRINT "TOTAL",S4,N-1
530 PRINT
540 PRINT "F=";S1/S2*(N-2)
550 PRINT
560 PRINT
570 S5=S1/S4
580 PRINT "COEFF. OF DETERMINATION=";S5
590 PRINT "COEFF. OF CORRELATION=";SQR(S5)
600 PRINT "STANDARD ERROR OF ESTIMATE=";SQR(S2/(N-2))
610 PRINT
620 PRINT
630 PRINT "DO YOU WISH TO ESTIMATE VALUES OF Y FROM "
640 PRINT "THE REGRESSION CURVE? (1=YES,0=NO)"
650 INPUT X
660 IF X=0 THEN 730
670 PRINT "INPUT X"
680 INPUT X
690 PRINT "Y=";EXP(A)*X↑B
700 PRINT
710 PRINT "ANOTHER POINT? (1=YES,0=NO)"
720 GOTO 650


730 END
```

2. (xii) **GLOWS**

Written by G.S.

```
 5 REM GLOWS
7 REM MEAN DAILY FLOWS FOR FLUME
8 REM DATA INPUT FROM MAG TAPE
13 DIM P$(200)11,Q(200)
20 PRINT "INPUT LINE60 DATALOAD <******>"
25 PRINT "RUN30":STOP
30 INPUT "RECORD START: HOUR-DAY-MONTH-YEAR",T1,T2,T3,T4
32 INPUT "RECORD END  :HOUR-DAY-MONTH-YEAR",T5,T6,T7,T8
33 Z9=T1:E=0:O=0
40 GOSUB 960
41 REM LOW FLOW EQUATION USED BELOW H1,METRES
42 H1=0.0
45 FOR I=1TO 200:Q(I)=0:NEXT I
 50 SELECT PRINT 01D
52 PRINT "WEST WALK FLUME"
53 PRINT "DAY MONTH YEAR MDF"
54 SELECT PRINT 005
60DATA LOAD "11050176"
65 DATA LOAD P$()
70 CONVERT STR(P$(1),8,4)TO Y9
72 CONVERT STR(P$(2),8,4) TO Y8
74 Y9=(Y9+Y8)/2
90 IF T1<>24 THEN 110
100 GOTO 130
110 GOSUB 770
120 GOTO 260
130 P=3:N=P+24
140 O=0:E=0:V=0
150 FOR I=PTO N
155 CONVERT STR(P$(I),8,4) TO Y
160 IF ((Y-Y9)*0.0011)<=0.003 THEN 180
170 GOTO 190
180 Q(I)=0:GOTO 240
190 H=(Y-Y9)*0.0011
200 IF H<=H1 THEN 230
210 GOSUB 930
220 GOTO 240
230 GOSUB 930
240 NEXT I
250 GOSUB 610
260 A=(N-P+1)/2:C=INT((N-P+1)/2)
270 IF A=C THEN 295
280 N=N-1
290 REM INTEGRATION PROCEDURE
295 IF (N-1)-(P+1)<3 THEN 354
300 FOR J=P+1 TO N-1
310 IF J/2=INT(J/2) THEN 340
320 O=O+Q(J)
330 GOTO 350
```

```
340 E=E+Q(J)
350 NEXT J
352 GOTO 360
354 FOR K=PTO N:V=V+Q(K)*3600:NEXT K
356 IF A=C THEN 400
358 V=V+Q(N+1)*3600
360 IF A<>C THEN 390
370 V=1200*(Q(P)+4*E+2*O+Q(N))
384 GOTO 400
390 V=1200*(Q(P)+4*E+2*O+Q(N))+Q(N+1)*3600
400 IF A=C THEN 430
420 N=N+1
430 IF N>=T9 THEN 530
440 IF Z9<>24 THEN 460
442 Z9=24
450 GOTO 480
460 Q1=(V+V0)/86400
462 Z9=24
470 IF V0=0 THEN 472
471 GOTO 490
472 GOSUB 1400
473 GOTO 490
480 Q1=V/86400
490 SELECT PRINT 01D
500 PRINT T2;T3;T4;Q1
510 SELECT PRINT 005
520 GOTO 540
530 V0=V:SELECT PRINT 01D:PRINT "V0=";V0:SELECT PRINT 005:GOTO 590
540 P=N:N=P+24
550 IF (T9-P)<24 THEN 570
560 GOTO 580
570 N=T9
580 GOTO 140
590 GOTO 20
600 END
610 REM SUBROUTINE TIMECOUNT
620 REM DAY
630 IF T2=F1 THEN 650
640 T2=T2+1:GOTO 660
650 T2=1
660 REM MONTH
670 IF T2=1 THEN 690
680 GOTO 700
690 T3=T3+1
700 REM YEAR
710 IF T2=1 THEN 730
720 GOTO 760
730 IF T3=13 THEN 750
740 GOTO 760
```

```
750 T4=T4+1:T3=1
760 RETURN
770 REM SUBROUTINE FIRSTHOURS
775 Q(I)=0.0
780 FOR I=3 TO 24-T1+1+2
785 CONVERT STR(P$(I),8,4) TO Y
790 IF ((Y-Y9)*0.0011)<=0.003 THEN 810
800 GOTO 820
810 Q(I)=[illegible]:GOTO 870
820 H=(Y-Y9)*0.[illegible]11
830 IF H<H1 THEN 860
840 GOSUB 900
850 GOTO 870
860 GOSUB 930
870 NEXT I
880 P=3:N=24-T1+1+2
890 RETURN
900 REM SUBROUTINE FLOW RATING
910 Q(I)=(((H-0.003)/(H))↑1.5)*(H↑1.5)*0.7308
920 RETURN
930 REM SUBROUTINE LOW FLOW RATING
940 Q(I)=0
950 RETURN
960 REM SUBROUTINE TIMESORT
970 REM HOURS IN FIRST AND LAST DAYS
975 F1,F4,F5,F6=0
980 X1=(24-T1+1)+T5
990 M=T3
995 IF M =T7 THEN 1285
1000 IF M=1 THEN 1210
1010 IF M=2 THEN 1120
1020 IF M=3 THEN 1210
1030 IF M=4 THEN 1190
1040 IF M=5 THEN 1210
1050 IF M=6 THEN 1190
1060 IF M=7 THEN 1210
1070 IF M=8 THEN 1210
1080 IF M=9 THEN 1190
1090 IF M=10 THEN 1210
1100 IF M=11 THEN 1190
1110 IF M=12 THEN 1210
1120 PRINT HEX(07)
1130 INPUT "IS IT A LEAP YEAR,YES OR NO",Y$
1140 IF Y$="YES" THEN 1170
1150 F1=28
1160 GOTO 1230
1170 F1=29
1180 GOTO 1230
```

```
1190 F1=30
1200 GOTO 1230
1210 F1=31
1220 REM COMPLETE DAYS IN FIRST MONTH
1230 F4 =F1-T2
1240 REM HOURS IN COMPLETE DAYS OF FIRST MONTH
1250 F5=F4*24
1260 REM HOURS IN COMPLETE DAYS OF SECIND MONTH
1270 F6=(T6-1)*24
1280 REM TOTAL HOURS ON RECORD
1283 GOTO 1290
1285 F5=(T6-T2-1)*24
1287 IF F5<0 THEN 1289
1288 GOTO 1290
1289 F5=0:GOTO 1295
1290 T9=X1+F5+F6
1293 GOTO 1300
1295 T9=X1-1
1300 RETURN
1400 REM SUBROUTINE IF V0=0
1410 SELECT PRINT 01D
1420 PRINT "FIRST POINT IS MEAN OF LESS THEN 24 HOURS"
142501=V/((24-T1)*3600)
1430 RETURN
```

2. (xiii) MOMENTS 3

Written by G.S.

```
5REM MOMENTS 3
10 REM CALCULATES MEAN,VARIANCE,CV%,SKEWNESS,KURTOSIS FROM
11 REM TAPE DATA
12 REM GEARY MOMENTS FROM GEARY,R.C.,BIOMETRIKA,1936
15 DIM X1(15),R(40,15),A(15),B(15),D(15),E(15)
16 DIM D1(15),E1(15)
17 Z=1
20 INPUT "INPUT SAMPLE SIZE,NUMBER VARIABLES",N,M
30 PRINT "INPUT LINE 40:DATALOAD<.....> CHANGE LINE 70 FOR
       DATA <=0 AND RUN40":STOP
40DATA LOAD "WINS"
42 SELECT PRINT 213
45 PRINT "UNTRANSFORMED DATA"
50 FOR K=1TO N
55 IF Z>1THEN 80
60 DATA LOAD X1()
70FOR J=1TO 13:X1(J)=X1(J)+10:NEXT J:X1(14)=X1(14)+30:X11(15)=SIN(2
2*#PI*(X1(15)/365))
80FOR J=1TO M
85 IF Z>1THEN 100
90 R(K,J)=X1(J)
100 A(J)=A(J)+R(K,J)
110 NEXT J
120 NEXT K
125 REM MEAN
130 FOR J=1TO M:A(J)=A(J)/N:NEXT J
140 FOR K=1TO N
150 FOR J=1TO M
155E1(J)=E1(J)+(R(K,J)-A(J))
160 B(J)=B(J)+(R(K,J)-A(J))↑2
170 D(J)=D(J)+(R(K,J)-A(J))↑3
180 E(J)=E(J)+(R(K,J)-A(J))↑4
185E1(J)=E1(J)+ABS(R(K,J)-A(J))
190 NEXT J
200 NEXT K
210 FOR J=1TO M
211 REM GEARY SKEWNESS
212 D1(J)=((SQR(N))*D(J))/B(J)↑1.5
213 REM GEARY KURTOSIS
214 E1(J)=E1(J)/SQR(N*B(J))
215 REM VARIANCE
220 B(J)=B(J)/N
225 REM SKEWNESS
230 D(J)=(D(J)/N)/B(J)↑1.5
235 REM KURTOSIS
240E(J)=(E(J)/N)/B(J)↑2
250 PRINT "******"
260 PRINT "*X";J;"*"
270 PRINT "******"
280 PRINT "MEAN=";A(J);"VARIANCE=";B(J);"S.DEV.=";SQR(B(J))
290 PRINT "CV%=";1[illegible]*(SQR(B(J)))/A(J);"N=";N
```

```
300 PRINT "SKEWNESS=";D(J);"KURTOSIS=";E(J)
302 PRINT "GEARY SKEWNESS=";D1(J)
303 PRINT "GEARY KURTOSIS=";E1(J)
310 NEXT J
315 PRINT :PRINT
320 IF Z=1 THEN 327
325 GOTO 350
327 PRINT "LOG TRANSFORM"
328 PRINT :PRINT
330 FOR K=1TO N:FOR J=1TO M-1:R(K,J)=LOG(R(K,J)):NEXT J:NEXT K
340 GOTO 480
350 IF Z=2THEN 365
360 GOTO 390
364PRINT :PRINT
365 PRINT "RECIPROCAL TRANSFORM"
366PRINT :PRINT
370 FOR K=1TO N:FOR J=1TO M-1:R(K,J)=1/(EXP(R(K,J))):NEXT J:NEXT K
380 GOTO 480
390 IF Z=3 THEN 410
400 GOTO 440
439PRINT :PRINT
410 PRINT "SQUARE TRANSFORM"
411PRINT :PRINT
420 FOR K=1TO N:FOR J=1TO M-1:R(K,J)=(1/R(K,J))↑2:NEXT J:NEXT K
430 GOTO 480
440 IF Z=4 THEN 460
450 GOTO 999
459PRINT :PRINT
460 PRINT "SQUARE ROOT TRANSFORM"
461PRINT :PRINT
470 FOR K=1TO N:FOR J=1TO M-1:R(K,J)=SQR(SQR(R(K,J))):NEXT J:NEXT K
480Z=Z+1
485 FOR J=1TO M:A(J),B(J),D(J),E(J),D1(J),E1(J)=0:NEXT J
490 GOTO 50
999 SELECT PRINT 005
1000END
```

2. (xiv) MULTREG 2

WANG Package program, modified by G.S.

```
 5 REM MULTREG2
6 REM DATA INPUT FROM TAPE
10 COM X(15),D(10),E(10),A(10,10),M,N
20 DIM X1(15)
30 PRINT "INPUT LINE 80 DATALOAD <:::::> RUN 50":STOP
40 PRINT "INPUT LINE 30 DATALOAD <::::::> AND RUN 50":STOP
50 INPUT "INPUT M,N",M,N
60 INPUT "MATRIX NO. OF API AND SOLUTE",R,T
65 G=9:O=14:H=15
70 INPUT "INPUT SINDAY LAG",L
80DATA LOAD "W5NS"
90 FOR I=1 TO M+2: FOR J=1 TO M+1: A(J,I)=0
100 NEXT J: D(I)=0: NEXT I
110 FOR K=1TO N
120 DATA LOAD X1()
130 A=LOG(X1(G)+10)
132 B=LOG(X1(R)+10)
134 C=LOG(X1(O)+1)
136 D=SIN(2*#PI*(X1(H)-L)/365)
138 E=LOG(X1(T)+10)
140X(1)=D
142X(2)=C
144X(3)=B
146X(4)=A
148X(5)=E
180 D(M+2)=D(M+2)+X(M+1)↑2: D(1),A(1,M+2)=A(1,M+2)+X(M+1)
190 FOR I=1 TO M: A(I+1,1),A(1,I+1)=A(1,I+1)+X(I)
200 D(I+1),A(I+1,M+2)=A(I+1,M+2)+X(I)*X(M+1)
210 FOR J=I TO M: A(I+1,J+1),A(J+1,I+1)=A(I+1,J+1)+X(I)*X(J)
220 NEXT J: NEXT I: NEXT K
230 A(1,1)=N
240 FOR I=2 TO M+1: E(I)=A(1,I): NEXT I
250 FOR S=1 TO M+1
260 FOR T=S TO M+1: IF A(T,S)<>0 THEN 280: NEXT T
270 PRINT "NO UNIQUE SOLUTION": GOTO 590
280 GOSUB 330
290 C=1/A(S,S): GOSUB 360
300 FOR T=1 TO M+1: IF T=S THEN 320
310 C=-A(T,S): GOSUB 370
320 NEXT T: NEXT S: GOTO 380
330 FOR J=1 TO M+2
340 B=A(S,J): A(S,J)=A(T,J): A(T,J)=B
350 NEXT J: RETURN
360 FOR J=1 TO M+2: A(S,J)=C*A(S,J): NEXT J: RETURN
370 FOR J=1 TO M+2: A(T,J)=A(T,J)+C*A(S,J): NEXT J: RETURN
380 PRINT
```

```
390 SELECT PRINT 213
400 FOR T=1 TO M+1: PRINT "B(";T-1;")=";A(T,M+2): NEXT T
410 S=0
420 FOR I=2 TO M+1: S=S+A(I,M+2)*(D(I)-E(I)*D(1)/N): NEXT I
430 T=D(M+2)-D(1)↑2/N: C=T-S
440 I=N-M-1: J=S/M: K=C/I
450 PRINT : PRINT
460 PRINT " "," REGRESSION TABLE": PRINT
470 PRINT "SOURCE","SUM OF SQ.","DEG.FREEDOM","MEAN SQ."
480 PRINT "REGRESSION",S,M,J
490 PRINT "RESIDUAL",C,I,K
500 PRINT "TOTAL",T,N-1: PRINT
510 PRINT "F=";J/K
520 PRINT : PRINT : J=S/T
530 PRINT "COEFF. OF DETERMINATION=";J
540 PRINT "COEFF. OF MULTIPLE CORRELATION=";SQR(J)
550 PRINT "STANDARD ERROR OF ESTIMATE=";SQR(C/I)
560 PRINT : PRINT
570 SELECT PRINT 005
580 BACKSPACE 1F
590 END
```

2. (xv) NTHOREG

WANG package program, modified by G.S.

```
 5 REM NTHOREG1 POLYNOMIAL REGRESSION FOR TAPE DATA
8 COM D1(20),D2(20),X(150),Y(150)
10 COM A(13),G(7,8),E(8),M,N,Q(150)
11DIM R(150)
12 PRINT "INPUT LINES 11,24,28,38,44 RUN13":STOP
13 INPUT "NUMBER IN X ARRAY P",P
14 INPUT "POLYNOMIAL ORDER M",M
15 J=0
16 FOR J=1TO 50
17 DIM Q(150),N(150)
18 INPUT "POSITIONS TO BE SKIPPED IN Y ARRAY,-1,-1 TO PROCEED",D1(J),D2(J
22 IF D1(J)<0 THEN 24
22 NEXT J
24DATA LOAD "W2Q(I)"
26 DATA LOAD Q()
28DATA LOAD "W2R(I)"
30DATA LOAD R()
32J=1:Z=0:K=1
34 FOR I=1TO P:IF I=D1(J) THEN 38
36 GOTO 42
38 I=D2(J):Z=Z+D2(J)-D1(J)+1:J=J+1
40 GOTO 46
42 X(K)=LOG(Q(I))
44Y(K)=LOG(R(I-Z))
45K=K+1
46 NEXT I
48 N=P-Z
60 FOR I=2 TO 2*M+1: A(I)=0: NEXT I
70 FOR I=1 TO M+2: E(I)=0: NEXT I
80 A(1)=N
90 FOR I=1TO N:X=X(I):Y=Y(I)
100 FOR J=2 TO 2*M+1: A(J)=A(J)+X↑(J-1): NEXT J
110 FOR J=1TO M+1:E(J),G(J,M+2)=E(J)+Y*X↑(J-1):NEXT J
120 E(M+2)=E(M+2)+Y↑2: NEXT I
130 FOR I= 1 TO M+1: FOR J=1 TO M+1:G(I,J)=A(I+J-1):NEXT J:NEXT I
140 FOR S=1 TO M+1
150 FOR T=S TO M+1:IF G(T,S)<>0 THEN 170: NEXT T
160 PRINT "NO UNIQUE SOLUTION": STOP
170 GOSUB 220
175 SELECT PRINT 213
180 C=1/G(S,S): GOSUB 250
190 FOR T=1 TO M+1: IF T=S THEN 210
200 C=-G(T,S): GOSUB 260
```

```
210 NEXT T: NEXT S: GOTO 270
220 FOR J=1 TO M+2
230 B=G(S,J):G(S,J)=G(T,J):G(T,J)=B
240 NEXT J: RETURN
250 FOR J=1TO M+2:G(S,J)=C*G(S,J):NEXT J:RETURN
260 FOR J=1TO M+2:G(T,J)=G(T,J)+C*G(S,J):NEXT J:RETURN
270 PRINT
280 FOR I=1TO M+1:PRINT I-1;"DEG. COEFF.=";G(I,M+2):NEXT I
300 S=0
310 FOR I=2TO M+1:S=S+G(I,M+2)*(E(I)-A(I)*E(1)/N):NEXT I
320 T=E(M+2)-E(1)↑2/N: C=T-S
330 I=N-M-1: J=S/M: K=C/I
340 PRINT : PRINT : PRINT "          REGRESSION TABLE": PRINT
350 PRINT "SOURCE","SUM OF SQ.","DEG. FREEDOM","MEAN SQ."
360 PRINT "REGRESSION",S,M,J
370 PRINT "RESIDUAL",C,I,K
380 PRINT "TOTAL",T,N-1: PRINT
390 PRINT "F=";J/K: PRINT : PRINT
400 J=S/T: PRINT "COEFF. OF DETERMINATION=";J
410 PRINT "COEFF. OF CORRELATION=";SQR(J)
420 PRINT "STANDARD ERROR OF ESTIMATE=";SQR(C/I): PRINT : PRINT
495 SELECT PRINT 005
510 INPUT "NEXT POLYNOMIAL ORDER,(0 IF NOT REQUIRED)",M
512 IF M=0 THEN 550:GOTO 60
550 END
```

2. (xvi) **PLOTS**

Written by B Sprunt

```
 1 REM PLOTS HYDROGRAPH ON SCREEN FROM TAPE DATA
2SELECT PRINT 405
5DIM PS(100)11
8DIM C$11
10DIM X1$32,X9$32,Y1$32,S$(4)64
12X1$=HEX(404142434445464748494A4B4C4D4E4F505152535455565758595A5B5C5D5
13X9$=HEX(202122232425262728292A2B2C2D2E2F303132333435363738393A3B3C3D3
14Y1$=HEX(606162636465666768696A6B6C6D6E6F707172737475767778797A7B7C7D7
15C$=HEX(07090A0D1B1D1F0C17)
19GOSUB '99:FOR I=1TO 150:NEXT I
20DATA LOAD "12230675"
21DATA LOAD PS()
30FOR I=1TO 100
32CONVERT STR(PS(I),4,4)TO X:CONVERT STR(PS(I),8,4)TO Y
34X=(X-1[illegible])/2:Y=(Y-23[illegible])/2
40IF STR(PS(I),2,1)="0"[illegible]11
41IF STR(PS(I),2,1)="1"THEN 82
49GOSUB '01(X,Y)
80NEXT I
81GOTO 21
82PRINT STR(C$,6,1);:GOSUB '01(X,Y):GOTO 80
110END
200DEFFN'01(X,Y)
210I9=INT(X/32)+1:I1=X-32*I9+33:J9=INT(Y/32)+1:J1=Y-32*J9+33
220PRINT STR(X9$,J9,1);STR(Y1$,J1,1);STR(X9$,I9,1);STR(X1$,I1,1);
225TRACE OFF
230RETURN
240DEFFN'02(X,Y)
250PRINT STR(C$,6,1);:GOSUB '01(X,Y):GOSUB '01(X,Y)
260RETURN
270DEFFN'99
280PRINT STR(C$,5,1);STR(C$,8,1);
290RETURN
```

2. (xvii) QUEZEDIG

Written by B Sprunt

```
 5 REM QUEZEDIG
6 REM DIGITISES HOURLY STAGE
7 REM FOR FLUME
8 REM DATA SAVED ON MAG TAPE
10DIM PS(100)11
20PRINT :PRINT :PRINT
30PRINT "DIGITISE ORIGIN ON SOURCE DOCUMENT"
40SELECT INPUT 65A
52INPUT W$
55PRINT HEX(07);
60IF STR(W$,2,1)="4"THEN 50
70INPUT P0
75PRINT HEX(07);
80X4=INT(P0/10000):Y4=P0-10000*INT(P0/10000)
90PRINT "COORDINATES OF YOUR CHOSEN ORIGIN ARE"
100PRINT "X0=";X4;"Y0=";Y4
110PRINT :PRINT :PRINT "LOAD MAG TAPE TO RECEIVE DATA POINTS"
120PRINT "NAME THE FILE BY ENTERING-DATASAVE OPEN <FILE NAME>"
130PRINT "THEN ENTER CONTINUE":STOP
140PRINT "1-START PT 2-END PT 3-INTERIOR PT 4 ENDFILE PT"
150PRINT "START DIGITISING NOW"
160I=0
170I=I+1:IF I=101THEN 230
180INPUT P$(I)
185PRINT HEX(07);
190IF STR(P$(I),2,1)="4"THEN 250
200CONVERT STR(P$(I),4,4)TO X
210CONVERT STR(P$(I),8,4)TO Y
220GOTO 170
230DATA SAVE P$()
240GOTO 160
250DATA SAVE P$():DATA SAVE END
```

2. (xviii) **RESID 1**

Written by G.S.

```
810REM RESID 1
20 REM PLOTS VARIANCE OF RESIDUALS AGAINST X
30 COM D(10,10),C(10,10),M(1),N(1),L(1),X3(40,8)
40 COM X1(15),Y(40),Y(40)
5  M=M(1):N=N(1)
60 M1=M:M=1:M2=1
70 FOR I=M TO M1-1 STEP M2
80 FOR J=I+1 TO M1 STEP M2
90 FOR K= 1TO N
100 X(K)=X3(K,I)
110 REM RESIDUAL VARIANCE
120Y(K)=X3(K,J)-((EXP(D(I,J))*X(K)+C(I,J)))^2
130 NEXT K
140 GOSUB 240
150 SELECT PRINT 005
160 PRINT "DO YOU REQURE LISTING OF RESIDUALS, YES OR NO?"
170INPUT Z$
180 IF Z$="NO" THEN 220
190 SELECT PRINT 213:PRINT :PRINT :PRINT :PRINT
200 FOR Q=1TO N:PRINT X(Q);Y(Q);"    ";:NEXT Q
210PRINT Q;:PRINT
220 NEXT J
230 NEXT I
240 REM SUBROUTINE PLOT
250 SELECT PRINT 005
260 PRINT "DO YOU WANT A PLOT OF X(";I;")/X(";J;"), YES OR NO?"
270 INPUT S$
280 IF S$="NO" THEN 690
290 GOTO 305
300 END
305 SELECT PRINT 213:PRINT :PRINT :PRINT :PRINT
310 X8,Y8=999999:X9,Y9=-999999
320 FOR Z=1TO N
330 IF X(Z)>=X8 THEN 350
340 X8=X(Z)
350 IF X(Z)<=X9 THEN 370
360 X9=X(Z)
370 IF Y(Z)>=Y8 THEN 390
380 Y8=Y(Z)
390 IF Y(Z)<=Y9 THEN 410
400 Y9=Y(Z)
410 NEXT Z
420 SELECT PRINT 213:PRINT
430 PRINT "X(";I;")";"X(";J;")"
440 PRINT "XMIN";X8;"XMAX";X9;"RESIDSQMIN";Y8;"RESIDSQMAX";Y9
450 H,W=4
```

```
460 PLOT <0,-500,>
470 PLOT <-25,-25,HEX(FB)>
480 PLOT 20*H+10<0,5,HEX(FB)>:PLOT 20*W+10<5,0,HEX(FB)>
490 PLOT 20*H+10<0,-5,HEX(FB)>:PLOT 20*W+10<-5,0,HEX(FB)>
500 PLOT <20,25,HEX(FB)>:PLOT <10,0,HEX(FB)>:PLOT <-5,5,HEX(FB)>
510 PLOT <,-10,HEX(FB)>:PLOT <0,5,HEX(FB)>
520 X7=X9-X8:Y7=Y9-Y8:X6=W*100:Y6=H*100
530 M4=0:M5=0
540 FOR Z=1TO N
550 P=(X(Z)-X8)/X7*X6:K3=INT(P+0.5)
560 Q=(Y(Z)-Y8)/Y7*Y6:K4=INT(Q+0.5)
570 PLOT <K3-M4,K4-M5,HEX(FB)>:M4=K3:M5=K4
580 NEXT Z
590 REM NOW MOVE BACK TO ORIGIN
600 IF M4>999 THEN 630
610 PLOT <-M4,0,>
620 IF M5>999 THEN 660
630 PLOT <0,-M5,>
640 GOTO 690
650 PLOT <,-100,>
660 PLOT <0,-999,>:M5=M5-999
670 GOTO 623
680 PLOT <-999,0,>:M4=M4-999
690 RETURN
```

2. (xix) **SINDAY**

Written by G.S.

```
 5REM SIN DAY OPTIMIZES SEASON INDEX TO CORRELATE WITH
6REM DEPENDENT VARIABLE. X&Y FROM TAPE
8 DIM X1(24),X2(44,15)
9PRINT "INPUT LINE 15:DATALOAD<....>
10INPUT "SAMPLE SIZE(N),P(-LAG),Q(+LEAD)",N,P,Q
15DATA LOAD ""5NS"
20FOR I=1TO N:DATA LOAD X;()
25FOR K=1TO 15:X2(I,K)=X1(K):NEXT K:NEXT I
30Z=1
35K9=0
40FOR I=PTO Q STEP 5
45 K1,K2,K3,K4,K5,S1,S2,S3,S4=0
46 B=0
50 FOR J=1 TO N
52Y=X2(J,Z)
53X=X2(J,15)
57Y=LOG(Y+10)
58 X=SIN((2*#PI*(X-I))/365)
70 K1=K1+X
80 K2=K2+Y
90 K3=K3+X↑2
100 K4=K4+Y↑2
110 K5=K5+X*Y
120 NEXT J
150 B=(N*K5-K2*K1)/(N*K3-K1↑2)
180 S1=B*(K5-K1*K2/N)
190 S4=K4-K2↑2/N
198 R=(SQR(S1/S4))
199PRINT I;R
200 IF R>K9 THEN 205
202 GOTO 210
205 K9=R:L=I
210 NEXT I
214SELECT PRINT 213
215PRINT "APPROX. BEST CORRELATION COEFF.=";K9;"APPROX.BEST LAG/LEAD=";L
217 K1,K2,K3,K4,K5,S1,S2,S3,S4=0
218 FOR J=1 TO N
219Y=X2(J,Z):Y=X2(J,15)
220 X=SIN((2*#PI*(X-L))/365)
230Y=LOG(Y+10)
240 K1=K1+Y
250 K2=K2+Y
260 K3=K3+Y↑2
270 K4=K4+Y↑2
280 K5=K5+X*Y
290 NEXT J
300 B=(N*K5-K2*K1)/(N*K3-K1↑2)
310 A=(K2-B*K2)/N
311SELECT PRINT 213
312 PRINT "A=";EXP(A)
315 PRINT "B=";B
320 S1=B*(K5-K1*K2/N)
330 S4=K4-K2↑2/N
340 S2=S4-S1
```

```
350PRINT :PRINT
360 PRINT "                    REGRESSION TABLE"
370 PRINT
380 PRINT "SOURCE","SUM OF SQ.","DEG.FREEDOM","MEAN SQ."
390 PRINT "REGRESSION",S1,1,S1
400 PRINT "RESIDUAL",S2,N-2,S2/(N-2)
410 PRINT "TOTAL",S4,N-1
420 PRINT
430 PRINT "F=";S1/S2*(N-2)
440 PRINT :PRINT
450 S5=S1/S4
460 PRINT "COEFF. OF DETERMINATION=";S5
470 PRINT "COEFF.OF CORRELATION=";SQR(S5)
480 PRINT "STANDARD ERROR OF ESTIMATE=";SQR(S2/(N-2))
500Z=Z+1
525SELECT PRINT 205
510IF Z>3THEN 999
530GOTO 35
999END
```

2. (xx) TENPLOT

Written by G.S.

```
 1 REM TENPLOT
2 REM PRELIM TREATMENT AND PLOT OF FIELD TENSION DATA
5 DIM W(32)
10 PRINT "INPUT TIME,DAY,MONTH,YEAR"
15 INPUT T2,T3,T4,T5
20 REM DATA INPUT ASPEAD IN THE FIELD
25 PRINT "INPUT A1,B1,C1,D1,N"
30 INPUT A1,B1,C1,D1,N
35 PRINT "INPUT D2,C2,B2,A2,P"
40 INPUT D2,C2,B2,A2,P
45 PRINT "INPUT B3,A3,C3,D3,Q"
50 INPUT B3,A3,C3,D3,Q
55 PRINT "INPUT C4,D4,A4,B4,R"
60 INPUT C4,D4,A4,B4,R
65 PRINT "INPUT A5,B5,C5,D5,S"
70 INPUT A5,B5,C5,D5,S
75 PRINT "INPUT D6,C6,B6,A6,T"
80 INPUT D6,C6,B6,A6,T
85 PRINT "INPUT D7,C7,A7,B7,U"
90 INPUT D7,C7,A7,B7,U
95 PRINT "INPUT D8,A8,B8,C8,V"
100 INPUT D8,A8,B8,C8,V
102 Z=13.6:Y =12.6
105 W(1)=22.7+Z*N-Y*A1
110 W(2)=38+Z*N-Y*B1
115 W(3)=48.1+Z*N-Y*C1
120 W(4)=85.7+Z*N-Y*D1
125 W(5)=26.5+Z*P-Y*A2
130 W(6)=43+Z*P-Y*B2
135 W(7)=51.2+Z*P-Y*C2
140 W(8)=35 +Z*P-Y*D2
145 W(9)=27.4+Z*Q-Y*A3
150 W(10)=46.6+Z*Q-Y*B3
155 W(11)=57.1+Z*Q-Y*C3
160 W(12)=90.8+Z*Q-Y*D3
165 W(13)=22.9+Z*R-Y*A4
170 W(14)=37.5+Z*R-Y*B4
175 W(15)=49.9+Z*R-Y*C4
180 W(16)=83.8+Z*R-Y*D4
185 W(17)=34.7+Z*S-Y*A5
190 W(18)=48.6+Z*S-Y*B5
195 W(19)=58.7+Z*S-Y*C5
200 W(20)=94.4+Z*S-Y*D5
205 W(21)=25+Z*T-Y*A6
210 W(22)=40+Z*T-Y*B6
215 W(23)=50+Z*T-Y*C6
220 W(24)=85+Z*T-Y*D6
225 W(25)=23.3+Z*U-Y*A7
230 W(26)=38.3+Z*U-Y*B7
```

```
235 W(27)=48.3+Z*U-Y*C7
240 W(28)=83.3+Z*U-Y*D7
245 W(29)=25.7+Z*V-Y*A8
250 W(30)=42.7+Z*V-Y*B8
255 W(31)=50.7+Z*V-Y*C8
260 W(32)=83.7+Z*V-Y*D8
265 SELECT PRINT 213: PRINT "TIME DAY MONTH YEAR"
270 PRINTUSING 275,T2,T3,T4,T5
275 %##.## ##   ##  ####
280 SELECT PLOT 413
285 PLOT <,,"WEST WALK SLOPE:PORE WATER PRESSURE(CM.WATER)">
290 PLOT <-450,,>,45<10,,HEX(5F)>,<-450,-25,>
295 SELECT PRINT 213
300 PRINT "VERTICAL SCALE:1INCH=2METRES(X50)"
305 PRINT "HORIZONTAL SCALE:1INCH=5METRES(X20)"
310 PRINT "SOIL DEPTH:1INCH=3.2METRES(X500)"
315 PLOT <,-300,>
320 READ A9,X
325 I=3
330 I=I+1
335 IF I=A9 THEN 320:IF A9=-1 THEN 360
340 PLOT X<1,,HEX(FB)>,<,1,>
345 GOTO 330
350 DATA 6,11,13,4,15,2,26,2,14,3,21,2,14,4,19,3,5,11
355 DATA 14,4,9,3,21,5,24,3,37,3,27,4,33,3,-1,0
360 PLOT <-963,-282,>
365 READ X9,Y9
370 IF X9=999THEN 430
375 PLOT <X9,Y9,HEX(FB)>
380 A=-75:B=-50:C=-175
385 PLOT <,A,HEX(FB)>,<,B,HEX(FB)>,<,C,HEX(FB)>
390 GOTO 365
395 DATA 131,6,39,313,43,327,52,313,54,318,96,317,124,328,377,417,999,3
400 PLOT <-963,68,>,<183,6,>
405 FOR I=1 TO 32
410 SELECT PRINT 213:PRINTUSING 415,W(I);
415 %-###.#
420 READ D,E
425 IF D=-999 THEN 465
430 PLOT <D,E,>
435 IF I=33 THEN 465
440 DATA -60,-75,-60,-50,-60,-175,-21,313,-60,-75,-60,-50,-60,-175
445 DATA -20,320,-60,-75,-60,-50,-60,-175,-9,313,-60,-75,-60,-50,-60,-13
450 DATA -6,318,-60,-75,-60,-50,-60,-175,38,317,-60,-75,-60,-50,-60,-175
 55 DATA 66,328,-60,-75,-60,-50,-60,-175,319,417,-60,-75,-60,-50,-60,-19
460 NEXT I
465 PLOT <-822,74,>
467 SELECT CO 305
470 END
```

2. (xxi) **TRACES**

Written by B Sprunt

```
5 REM TRACES
6 REM DIGITISES STAGE FOR V-NOTCH WEIRS
7 REM DATA STORED ON MAG TAPE
10DIM Z(28),A$11,B$11,C$11
15PRINT "DATA TAPE REQUIRED - SKIP TO NEXT AVAILABLE"
16PRINT "SPACE AND OPEN FILE BY ENTERING DATASAVE OPEN <FILENAME>"
18STOP
20PRINT "ADJUST BASE LINE TO GIVE EQUAL"
22PRINT "Y COORDS FOR DIGITISED END POINTS"
24PRINT "PROGRAM WILL CONTINUE WHEN DIGITISED POINTS HAVE SAME Y VALUE"
30PRINT :PRINT "DIGITISE START AND FINISH POINT OF BASE LINE"
40SELECT INPUT 65A:INPUT A$,B$
50CONVERT STR(A$,4,4) TO X8:CONVERT STR(A$,8,4)TO Y8
60CONVERT STR(B$,4,4)TO X9:CONVERT STR(B$,8,4) TO Y9
65IF Y9<>Y8THEN 40
70PRINT "COORDS OF START AND FINISH POINTS OF BASE LINE ARE"
72PRINT "START  X=  ";X8;"  Y=  ";Y8
74PRINT "FINISH  X=  ";X9;"  Y=  ";Y9
75SELECT INPUT 001
76PRINT :INPUT "ENTER BASE TIME - HOURS,MINS",H1,M1
78PRINT :INPUT "ENTER ELAPSED TIME - HOURS,MINS",H2,M2
79REM D IS INCREMENT PER HOUR
80D=(X9-X8)/(H2+M2/60)
81REM S9 IS COORD FOR NEXT HOUR RECORDING POINT
82S3=X9
83SELECT INPUT 65A
85PRINT "START TRACING CURVE"
86SELECT CO 65A:I=0
90FOR S9=X8+(60-M1)/60*DTO S3STEP D
92X1=INT(S9+.5)
110INPUT C$
120IF STR(C$,1,1)="+" THEN 140
130GOTO 110
140IF STR(C$,2,1)="4" THEN 300
150CONVERT STR(C$,4,4) TO X
160IF X=X1THEN 170
165GOTO 110
170PRINT HEX(07)
180I=I+1:IF I=29THEN 400
182CONVERT STR(C$,8,4)TO Y:Z(I)=Y
185Z(I)=Z(I)-Y8
190NEXT S9
192DATA SAVE Z():DATA SAVE END
300SELECT CO 005:SELECT INPUT 001
310PRINT "TAPE FILE CLOSED BUT TAPE NOT REWOUND"
350END
400PRINT HEX(07):PRINT HEX(07):PRINT HEX(07)
402DATA SAVE Z()
4041=0:GOTO 180
```

2. (xxii) **WATLOSW**

Written by G.S.

```
5 REM WATLOSW
6 REM COMPUTES VOLUME WATER LOST OVER 90 DEG. V-NOTCH
1%SELECT PRINT 213
24 PRINT "REMOVE PROGRAM TAPE AND ENTER DATATAPE"
25 INPUT "DATUM",B
26 INPUT "WEIR NUMBER",P
30 PRINT "INPUT LINE 70 :DATALOAD'........' THEN RUN 40":STOP
40 INPUT "DAY,MONTH,YEAR",T1
50 INPUT "NO. OF FIRST HOUR",A:INPUT "NO. OF LAST HOUR",N
60 DIM Z(230)
70DATA LOAD "11210775"
80 DATA LOAD Z()
120 Y=Z(A)
130 H=((Y*0.0254)-B)*3.05
140 IF H<=0 THEN 160
150 GOTO 170
160 Y1=0
161 GOTO 180
170 Y1=((H+0.3009)↑2.5)*1.36545*3600
180 L2=0
190 Z=(N-A+1)
200 S,T=0
210 IF Z/2=INT(Z/2) THEN 250
220 FOR I=A+1 TO N-1
230Y=Z(I)
240 GOTO 270
250 FOR J=A+1 TO N-2
260 Y=Z(J)
270 H=((Y*0.0254)-B)*3.05
280 IF H<=0 THEN 340
290 GOTO 320
300 L=0
310 GOTO 330
320 L=((H+0.0009)↑2.5)*1.36545*3600
330 D=1
340 IF Z/2=INT(Z/2) THEN 370
350 IF I/2=INT(I/2) THEN 400
360 GOTO 380
370 IF J/2=INT(J/2) THEN 400
380 S=S+L
390 GOTO 410
400 T=T+L
410 IF Z/2<>INT(Z/2) THEN 460
420 NEXT J
430 Y=Z(N)
440 H=((Y*0.0254)-B)*3.05
442 IF h<=0 THEN 444
443 GOTO 453
444 L2=0
446 GOTO 470
450 L2=((H+0.0009)↑2.5)*1.36545*3600
460 NEXT I
470 IF Z/2=INT(Z/2) THEN 500
```

```
480 Y=Z(N)
490 GOTO 510
500 Y=Z(N-1)
510 H=((Y*0.0254)-B)*0.05
511 IF H<=0 THEN 513
512 GOTO 520
513 Y2=0
516 GOTO 530
520 Y2=((H+0.0009)↑2.5)*1.36545*3600
530 PRINT "WEIR",P,T1,N-A+1;"HOURS DISCHARGE":PRINT "WATER LOSS IN CU M
535PRINT "**********************"
540 IF (A+3)/2=INT((A+3)/2) THEN 560
550 GOTO 580
560 PRINT D/3*(Y1+4*T+2*S+Y2)+L2
570 GOTO 590
580 PRINT D/3*(Y1+4*S+2*T+Y2)+L2
590PRINT "**********************"
595PRINT :PRINT :PRINT :PRINT
600END
```

2. (xxiii) **WATQUAL**

Written by G.S.

```
 1SELECT PRINT 213
5 DIM Z(12),K(12),D(12),Q(12)
6DIM J(12)
10REM PROGRAM TO CALCULATE IONIC STRENGTH AND TOTAL IONIC CONDUCTIVITY
Y OF AN AQUEOUS SOLUTION
20 PRINT "INPUT K,NA,CA,MG,CL,HCO3,SO4,SI(ALL PPM),PH,TEMP(DEG.CENT.),SC
32 INPUT J(1),J(2),J(3),J(4),J(5),J(6),J(7),J(8),J(9),J(10),J(11)
35 REM VALENCY
40 Z(1),Z(2),Z(5),Z(6),Z(9)=1
50 Z(3),Z(4),Z(7)=2
60 Z(8)=4
65 REM ATOMIC WEIGHT
70 K(1)=39.096:K(2)=22.997:K(3)=40.08:K(4)=24.32
80 K(5)=35.457:K(6)=61.018:K(7)=36.092:K(8)=23.96
90 J(9)=10↑(-J(9))
95 X=0
100 FOR P=1TO 9
110 X=X+J(P)
120 NEXT P
155 U=0
160 FOR N=1 TO 8
170 U=U+(J(N)/(K(N)*1000))*Z(N)
180 NEXT N
190 I=U/2
195 REM EFFECTIVE ION DIAMETER
200 D(1),D(5)=3
210 D(2),D(6),D(7)=4.25
220 D(3)=6:D(4)=8:D(9)=9
241 REM LIMIT IONIC CONDUCTANCE
242 Q(1)=73.5:Q(2)=50.1
244 Q(3)=59.5:Q(4)=53.1
246 Q(5)=76.4:Q(6)=44.5:Q(7)=80.2
250 A=0.4921-0.00379*(J(10)-5)
260 B=0.3249-0.00316*(J(10)-5)
265 L=0
270 FOR M=1 TO 7
280 G=(A*(Z(M)↑2)*SQR(I))/(1+D(M)*B*SQR(I))
290 H=(10↑(-G))*J(M)/(K(M)*1000)
300L=L+(H*Q(M)/0.031)
310 NEXT M
320 PRINT "IONIC STRENGTH=";I
330 PRINT "CALCULATED CONDUCTIVITY=";L+(J(9)*349800)
335 PRINT "MEASURED CONDUCTIVITY=";J(11)
338 PRINT "SUM OF IONS";X
340 GOTO 1
999 END
```

2. (xxiv) **WEIRQ**

Written by G.S.

```
1REM WEIRQ OUTPUTS DATA FOR 90 DEGREE V-NOTCH
2 PRINT "START TIME,T,HOURS?"
3 INPUT T
5 PRINT "DATUM,B,CENTIMETRES?"
6INPUT B
7PRINT "HOURS REQUIRED?"
8INPUT N
10 PRINT "INPUT LINE 40 DATALOAD'FILENAME' THEN RUN30"
20 STOP
30DIM Z(200)
40DATA LOAD "13201276"
50 DATA LOAD Z()
52 SELECT PRINT 213
53PRINT "201276"
54 PRINT "T(HOURS)          Q(CUMECS)"
55 FOR I= 1 TO N
56 T=T+1
57 IF T=25 THEN 59
58 GOTO 60
59T =1
60T2=(T-1)
62 IF (Z(I)*.0254-B)[=0 THEN 130
65 H=((Z(I)*.0254)-B)*.05
69 SELECT PRINT 213
70 IF T2 = 0 THEN 90
75 Q=((H+0.0009)12.5)*1.36545
80 GOTO 110
90 PRINT " 24",Q
100 GOTO 140
110PRINT T2,Q
120 GOTO 140
130PRINT T2,"**********ZERO FLOW**********"
140 NEXT I
400STOP
```

2. (xxv) LAG

Written by B. Sprunt, modified by G.S.

```
X1REM LAC CALCULATES CROSS CORRELATIONS AT VARIOUS LAGS & LEADS
5SELECT PRINT 213
10 DIM X1(100),X2(100)
20PRINT "GIVE NO OF ELEMENTS IN SERIES 1 THEN SERIES 2"
30 INPUT N1,N2:N=N1:IF N2<=N1THEN 50
40N=N2
50PRINT "GIVE ELEMENTS IN PAIRS,A1,B1-RETURN-A2,B2-RRETURN"
60PRINT "FILLOUT SHORTER SERIES WITH ZEROES"
70 FOR I=1TO N:INPUT X1(I),X2(I):X1(I)=LOG(X1(I))
71 IF X2(I)=0THEN 75:X2(I)=LOG(X2(I))
75 NEXT I
80N9=N1-N2+1:B1=1:B2=((N1-N2)/2)+1:L1=N2
85PRINT "  LAG          R              T              A              B          SE       N"
90FOR I=1TO N9
100S1,S2,S3,S4,S5=0
110FOR J=1TO L1:J1=B1+J-1:J2=B2+J-1
120S1=S1+X1(J1):S2=S2+X2(J2):S3=S3+X1(J1)*X2(J2)
130S4=S4+X1(J1)↑2:S5=S5+X2(J2)↑2
140NEXT J
145L3=B1-B2
150L1=L1
154 B=(A1*S3-S1*S2)/(A1*S4-S1↑2)
155 A=(S2-B*S1)/A1
157 S1=B*(S3-S1*S2/A1)
158 S4=S5-S2↑2/A1
159 S2=S4-S1:R=SQR(S1/S4)
170T=R*SQR((A1-2)/(1-R*R))
175 S9=SQR(S2/(A1-2))
179% ###   #.####   ###.###   ##.####   ##.####   ##.####   ###
181PRINTUSING 179,L3; R;T;EXP(A);B;S9;A1
190B1=B1+1
270NEXT I
275PRINT :PRINT :PRINT
280END
```

APPENDIX 3

ANALYTICAL METHODS USED FOR SOIL CHEMISTRY

I. Total Element Contents

The analysis of total SiO_2, Al_2O_3, Fe_2O_3, MnO, CaO, MgO, Na_2O and K_2O was performed by atomic absorption spectrophotometry; TiO_2 and P_2O_5 by visible spectrophotometry. Due to the time-consuming nature of total element analysis it was decided to select seven from the total of eleven profiles for analysis, again putting priority upon the lower part of the slope. The sample was totally digested in acid according to a Pye Unicam method for iron (P-U method Fe5).

(a) Sample Preparation

The soil sample was granulated in a PVC bowl with a PTFE rod. A small quantity (10 - 20 g) was placed in a crucible and heated in a furnace at 370°C for six hours to remove and determine organic matter by loss-on-ignition. This temperature was lower than that normally used for determining loss-on-ignition in order to reduce the loss of water from within the clay mineral structure (Hesse, 1971). % organic carbon was calculated using Ball's equation (Hesse, 1971):

$$\% \text{ O.C.} = 0.458 \,\% \text{ weight loss} - 0.4 \qquad (1)$$

0.25 g of the residue was weighed and placed in a 30 ml platinum dish. This was moistened with a few drops of water and 7.5 ml of HF (40 % w/w) 3.0 ml of HNO_3 (Sp.Gr. 1.42) and 3.0 ml of $HClO_4$ (60 % w/w) added. The dish was heated gently on a hotplate in a furnace cabinet until the fumes of perchloric acid were evolved; after a few minutes the dish was removed from the hotplate and allowed to cool. A further 3.0 ml of HF and 1.0 ml $HClO_4$ were added and the dish heated gently until fumes of perchloric acid were evolved. Fuming was allowed for five minutes, then the heat was increased and the mixture evaporated to dryness. After cooling 10 ml of 2M HCl was added and the dish warmed until the residue was partially dissolved. An equal volume of water was added and heating continued until complete dissolution of the residue. In one or two cases the silica did not dissolve completely and the addition of an extra 1 - 2 ml HF was necessary. The solution was transferred to a 100 ml volumetric flask, the dish washed thoroughly

APPENDIX 3

ANALYTICAL METHODS USED FOR SOIL CHEMISTRY

I. Total Element Contents

The analysis of total SiO_2, Al_2O_3, Fe_2O_3, MnO, CaO, MgO, Na_2O and K_2O was performed by atomic absorption spectrophotometry; TiO_2 and P_2O_5 by visible spectrophotometry. Due to the time-consuming nature of total element analysis it was decided to select seven from the total of eleven profiles for analysis, again putting priority upon the lower part of the slope. The sample was totally digested in acid according to a Pye Unicam method for iron (P-U method Fe5).

(a) Sample Preparation

The soil sample was granulated in a PVC bowl with a PTFE rod. A small quantity (10 - 20 g) was placed in a crucible and heated in a furnace at 370°C for six hours to remove and determine organic matter by loss-on-ignition. This temperature was lower than that normally used for determining loss-on-ignition in order to reduce the loss of water from within the clay mineral structure (Hesse, 1971). % organic carbon was calculated using Ball's equation (Hesse, 1971):

$$\% \text{ O.C.} = 0.458 \,\% \text{ weight loss} - 0.4 \qquad (1)$$

0.25 g of the residue was weighed and placed in a 30 ml platinum dish. This was moistened with a few drops of water and 7.5 ml of HF (40 % w/w) 3.0 ml of HNO_3 (Sp.Gr. 1.42) and 3.0 ml of $HClO_4$ (60 % w/w) added. The dish was heated gently on a hotplate in a furnace cabinet until the fumes of perchloric acid were evolved; after a few minutes the dish was removed from the hotplate and allowed to cool. A further 3.0 ml of HF and 1.0 ml $HClO_4$ were added and the dish heated gently until fumes of perchloric acid were evolved. Fuming was allowed for five minutes, then the heat was increased and the mixture evaporated to dryness. After cooling 10 ml of 2M HCl was added and the dish warmed until the residue was partially dissolved. An equal volume of water was added and heating continued until complete dissolution of the residue. In one or two cases the silica did not dissolve completely and the addition of an extra 1 - 2 ml HF was necessary. The solution was transferred to a 100 ml volumetric flask, the dish washed thoroughly

and the washings added to the solution. After cooling, water was added to 100 ml. This solution was used for the determination of all the aforementioned elements with the exception of Si. The details for each individual set of determinations are given below.

(b) Iron (Source of Method: P-U method Fe_9)

Instrument:	Pye Unicam SP90 AA Spectrophotometer
Wavelength:	248.3 nm
Slit Width:	0.1 mm
Scale Expansion:	x 2
Burner:	10 cm acetylene
Burner height:	1.0 cm
Fuel:	Acetylene pressure 0.7 kg/cm^2, flow 1400 cc/min
Air:	Pressure 2.1 kg/cm^2, flow 5 l/m

The undiluted solution was used for determination of ferric oxide contents of 0 - 1.60 %. For higher contents dilution was carried out according to Table 1.

Stock iron solution, equivalent to 1000 mg/l Fe (2859 mg/l Fe_2O_3), was available as $FeCl_3$, prepared in N HCl by BDH for AAS.

Table 1 Dilution for Determination of Ferric Oxide

% Fe_2O_3	Volume of Sample Solution	Volume of 2M HCl	Final Volume	Dilution Factor F
1.6 - 8.0	5.0	2.0	25	5
3.2 - 16.0	5.0	4.5	50	10

Standard iron solutions of 0, 5, 10, 25, 50 mg/l ferric oxide were made up from the stock solution. All solutions were stored in polythene screw top bottles. The calibration curve was a very shallow 'S' over the range 0 - 50 mg/l ferric oxide. Ferric oxide content was computed from:

$$\% Fe_2O_3 = \frac{(R - B) \times F}{W \times 100} \qquad (2)$$

where R = concentration in mg/l of ferric oxide in the sample solution

B = concentration in mg/l of ferric oxide in the blank solution

W = weight of sample dissolved, g

F = dilution factor (= 1 for sample solution)

(c) Aluminium (Source of Method: P-U method A12)

Instrument: Perkin Elmer AA Spectrophotometer
Wavelength: 309.3 nm
Slit Width: 0.1 mm
Burner: 5 cm nitrous oxide
Observation height: 1.0 cm
Fuel: Acetylene pressure 0.7 bar, flow 4000 cm^3/min
Nitrous Oxide: Pressure 2.1 bar, flow 5 l/m

Stock aluminium solution (500 mg/l Al_2O_3) was prepared by dissolving 0.2647 g of high purity aluminium foil in the minimum quantity of HCl (Sp.Gr. 1.18) and making up to 1.0 litre with water (Pye Unicam method Al2). Standard aluminium solutions of 0, 25.0, 50.0 and 75.0 mg/l Al_2O_3 were prepared. 0, 5, 10, 15 ml of stock Al solution was added to four volumetric flasks. 5 ml of HCl (Sp.Gr.1.16) and 10 ml of lanthanum chloride solution (5 % La^{3+}) were added to each volumetric flask and made up to the mark with water. Lanthanum chloride solution was added to overcome the suppression of aluminium absorption by silicate ions. The sample solutions were prepared in the same way, giving a dilution factor of F = 1.18. The calibration curve in the range 0 - 50 mg/l Al_2O_3 is effectively linear. Percentage Al_2O_3 is computed from equation 2 (units as before).

(d) Silicon (Source of Method: P-U method Si1)

Because the preparation of samples by heating in HF causes loss of silicon as volatile silicon tetrafluoride (W.J. Price and J.T.H. Roos, 1968) a different technique was used for silicon dissolution (Pye Unicam method Si1). 0.25 g of the prepared sample was placed in a 100 ml polythene beaker (these were used to prevent the uptake of impurities from glassware by HF). The sides of the beaker were washed down with about 10 ml of water. While stirring with a glass rod, 5 ml

of HCl (Sp.Gr. 1.18) was added, and gritty particles broken up. When the sample had dissolved, with the exception of any precipitated silica, the rod was rinsed down with water, removed from the beaker and 1.0 ml of HF (40 % w/w) added. If, after carefully swirling the mixture, silica grains failed to dissolve a further 1.0 ml of HF was added. Then 50 ml of boric acid solution (4 % w/v) was added to complex the hydrofluoric acid and thoroughly mixed. The solution was transferred to a 200 ml volumetric flask, 10 ml of lanthanum chloride solution (5 % La^{3+}) added and made up to the mark with water. $LaCl_2$ was added to all solutions in order to compensate for the enhancing effect of aluminium, iron and calcium ions on silicon absorption. A stock solution of SiO_2 (5000 mg/l SiO_2) was made by dissolving 8.823 g of pure sodium meta silicate, $Na_2SiO_35H_2O$ in water and diluted to 500 ml. No gravimetric standardisation was undertaken as very high precision was unnecessary. Standards corresponding to 0 %, 20 %, 40 %, 80 % and 100 % SiO_2 in the original sample were prepared by the addition of 0, 10, 20, 40 and 50 ml of the stock solution to five 100 ml volumetric flasks. 1.0 ml of HF, 2.5 ml of HCl, 5 ml of $LaCl_2$ and 25 ml of boric acid were added to each flask and these made up to the mark with water.

The instrument details for the Pye Unicam SP90 AAS were as follows:

Wavelength:	251.6 nm
Slit Width:	0.1 mm
Burner:	5 cm nitrous oxide
Observation height:	1.0 cm
Fuel:	Acetylene pressure 0.7 bar, flow 4500 cm^3/min
Nitrous Oxide:	Pressure 2.1 bar, flow 5 l/m

The calibration curve of percentage SiO_2 in the original sample against absorbance was slightly curved over the range 0 - 100 %. The incomplete dissolution of silica grains despite addition of extra HF was found to be a problem and may have contributed to error in the final value of percentage SiO_2.

(e) Titanium (Source of Method: Department of Geology, Portsmouth Polytechnic)

Titanium is usually determined for use in converting 'by weight' chemical analyses to 'by volume' chemical analyses, making the assumption that TiO_2 is totally insoluble in the form of ilmenite ($FeTiO_3$). The computation is not possible if significant amounts of TiO_2 have been translocated with the clay fraction of the soil. Titanium di-oxide was determined by visible spectrophotometry using a Unicam SP500 UV series 2 visible spectrophotometer. The TiO_2 stock solution was prepared as follows. 0.1 g of dried pure TiO_2 was weighed and put into a platinum crucible. 2 - 3 g of AnalaR $KHSO_4$ was added and heated over a low flame until the melt was clear. The crucible was allowed to cool and the residue put into a 250 ml glass beaker containing 100 ml of H_2SO_4 (25 % w/w). The cake was dissolved by heating on a hotplate, adding the washings of the crucible. The solution was allowed to cool, transferred to a 500 ml flask and made to the mark with H_2SO_4 (6 % w/w). This solution had a concentration of 200 mg/l TiO_2. 20 ml was then added to a 100 ml volumetric flask and made up to the mark with H_2SO_4 (10 % w/w), giving a dilute stock solution of 40 mg/l TiO_2. The Ti reagent was composed of 50 ml H_2SO_4 (50 % w/w), 50 ml ortho-phosphoric acid (25 % w/w) and 50 ml H_2O_2 (30 % w/w) diluted to 500 ml and stored in the dark. Standards of 0, 4, 8, 12, 16 and 20 mg/l were made up by adding 0, 5, 10, 15, 20 and 25 ml of 40 mg/l TiO_2 stock solution to 50 ml flasks, diluting to about 30 ml with water adding 15 ml of Ti reagent and diluting to the mark with water. Sample solutions were treated in the same way. Optical densities of calibration and sample solution were read at 400 nm. The calibration was very slightly curved in the range 0 - 20 mg/l TiO_2.

(f) Phosphorus (Source of Method: Department of Geology, Portsmouth Polytechnic)

P_2O_5 was also determined by visible spectrophotometry using the Unicam SP500. The P_2O_5 stock solution was prepared by drying a quantity of analaR KH_2PO_4 at 110°C and diluting 1.534 g to 500 ml in a volumetric flask (concentration 1600 mg/l P_2O_5). 25 ml was then diluted to 1 litre to make a working stock solution of 40 mg/l. The P reagent was prepared by dissolving 1.25 g ammonium metavanadate in 600 ml of HNO_3 (33 % v/v) and mixing with 50 g ammonium molybdate

diluted to 400 ml with water. Standards of 0, 4, 8, 12 and 16 mg/l TiO_2 were made by adding 0, 5, 10, 15 and 20 ml of dilute P_2O_5 stock solution to five volumetric flasks, diluting to 30 ml, adding 10 ml of P reagent by pipette, mixing and making up to 50 ml with water. After allowing to stand for 15 minutes optical densities of samples and standards were read at 430 nm. The calibration curve was found to be linear in the range 0 - 12 mg/l P_2O_5.

(g) Manganese (Source of Method: P-U method Mn5)

Instrument:	Perkin Elmer AA Spectrophotometer
Wavelength:	279.5 nm
Slit Width:	0.15 mm
Scale Expansion:	x 2
Burner:	10 cm acetylene
Burner Height:	0.8 cm
Fuel:	Acetylene pressure 0.7 kg/cm^2, flow 1500 cc/min
Air:	Pressure 2.1 kg/cm^2, flow 5 l/m

Stock manganese solution (250 mg/l MnO) was prepared by dissolving 0.1936 g of pure manganese metal in 10 ml of MCl (Sp.Gr. 1.16) and making up to 1 litre with water. A second stock solution (25 mg/l MnO) was prepared by pipetting 10 ml of 250 mg/l MnO solution into a 100 ml volumetric flask and making up to the mark with water. From this second stock solution standards of 0, 0.5, 1.0, 2.0, 3.0, 4.0 mg/l MnO were made by adding 0, 2.0, 4.0, 8.0, 12.0 and 16.0 ml to six 100 ml volumetric flasks and diluting to the mark with 0.2 M HCl. The calibration graph of MnO concentration against absorbance was very slightly curved. Percentage MnO was calculated using equation (2).

(h) Calcium (Source of Method: P-U method Ca3)

Instrument:	Pye Unicam AA Spectrophotometer
Wavelength:	422.7 nm
Burner:	10 cm acetylene
Slit Width:	0.08 mm
Scale Expansion:	x 3.5
Filter:	2
Burner:	10 cm acetylene
Burner Height:	1.0 cm

Fuel:	Acetylene pressure 0.7 kg/cm^2, flow 1500 cm^3/min
Air:	Pressure 2.1 kg/cm^2, flow 5 l/m

Stock calcium solution (100 mg/l Ca) was prepared by dissolving 0.2497 g of dry calcium carbonate in the minimum quantity of HCl (Sp.Gr. 1.18) and making up to 1 litre with water.

Standard calcium solutions of 0, 5, 10, 15 and 20 mg/l were prepared by adding 0, 5, 10, 15 and 20 ml of stock solution and 20 ml of $LaCl_2$ (5 % w/v) to each of five 100 ml volumetric flasks and diluting to the mark with water. $LaCl_2$ was also added to the sample solution in the same proportions (final dilution factor = 1.25). The calibration graph of Ca concentration against absorbance was linear in the range 0 - 10 mg/l Ca. Percentage CaO was calculated by equation (2) x 1.4.

(i) Magnesium (Source of Method: P-U method Mg4)

Instrument:	Pye-Unicam AA Spectrophotometer
Wavelength:	285.2 nm
Slit Width:	0.08 mm
Scale Expansion:	1.0
Burner:	10 cm acetylene
Burner Height:	1.0 cm
Fuel:	Acetylene pressure 0.7 kg/cm^2, flow 1500 cm^3/min
Air:	Pressure 2.1 kg/cm^2, flow 5 l/m

Stock magnesium solution (1oo mg/l Mg) was prepared by dissolving 0.10 g of oxide free magnesium ribbon in the minimum quantity of AnalaR HCl and made up to 1 litre with water. A second magnesium stock solution (10 mg/l Mg) was prepared by pipetting 25 ml of the first solution into a 250 ml volumetric flask and making up to the mark with water. Standard magnesium solutions of 0, 0.5, 1.0, 1.5 and 2.0 mg/l Mg were prepared by adding 0, 5, 10, 15 and 20 ml of stock solution II and 20 ml of $LaCl_2$ (5 % w/v) to each of five 100 ml volumetric flasks. The diluted sample solutions were prepared by adding 10 ml of the first sample solution, 20 ml of $LaCl_2$ (5 % w/v) to 100 ml volumetric flasks and making up to the mark with water. This gave a dilution factor of 10. The calibration graph of Mg concentration against absorbance was

found to be slightly curved. Percentage MgO was calculated by equation (2) x 1.66.

(j) Sodium (Source of Method: P-U method Na4)

Instrument:	Pye Unicam AA Spectrophotometer (flame emission mode)
Wavelength:	589 nm
Slit Width:	0.08 mm
Scale Expansion:	x 2
Burner:	Acetylene emission head
Burner Height:	1.8 cm
Fuel:	Acetylene pressure 0.7 kg/cm^2, flow 1000 cc/min
Air:	Pressure 2.1 kg/cm^2, flow 5 l/m

Stock sodium solution, equivalent to 100 mg/l Na_2O was prepared by dissolving 0.2290 g of AnalaR anhydrous sodium sulphate in water and diluting to 1 litre. Standard sodium solutions of 0, 1.0, 2.0, 3.0, 4.0 and 5.0 mg/l Na_2O were prepared by adding 0, 1.0, 2.0, 3.0, 4.0 and 5.0 ml of stock solution to six 100 ml volumetric flasks. Ammonium hydroxide-ammonium-carbonate solution was prepared by diluting 25 ml of AnalaR ammonia solution (Sp.Gr. 0.880) to 200 ml with water; dissolving 5.0 g of AnalaR ammonium carbonate in the solution, then transferring to a 500 ml volumetric flask and making up to the mark with water. 10 ml of this solution was then added to each of the six volumetric flasks, together with 1.0 ml of 2 M HCl and made up to the mark with water. The ammonium solution was added to suppress excessive flame ionisation. This was added to the sample solution in the same proportions giving a dilution factor of 1.11. The calibration curve of Na_2O concentration against percentage emission was slightly curved. Percentage Na_2O was calculated by equation (2).

(k) Potassium (Source of Method: P-U method K2)

Instrument:	Pye-Unicam AA Spectrophotometer (flame emission mode)
Wavelength:	766.5 nm
Slit Width:	0.1
Scale Expansion:	x 2
Burner:	Acetylene emission head

Burner Height: 1.8 cm

Fuel: Acetylene pressure 0.7 kg/cm^2, flow 1000 cc/min

Air: Pressure 2.1 kg/cm^2, flow 5 l/m

A stock K solution (100 mg/l K) was prepared by dissolving 0.1905 g of dry KCl in water and making up to 1 litre in a volumetric flask. Standards of 0, 1.5, 3, 5 and 10 mg/l were prepared by adding 0, 1.5, 3, 5 and 10 ml of stock solution and 10 ml of the ammonium solution used for determining Na_2O to each of five 100 ml volumetric flasks, and diluting to the mark with water. Again, the ammonium solution was added to suppress excessive flame ionisation. Samples were prepared by adding 5.0 ml of sample solution, 5.0 ml of ammonium solution to 100 ml volumetric flasks and making up to the mark with water. The dilution factor was 10.0. The calibration curve of K concentration against percentage emission was very slightly curved in the range 0 - 5 mg/l K, below which all samples fell. Percentage K_2O in the sample was calculated from equation (2) x 2.409.

The results of the analyses are compiled below

(1) Results of Total Element and Organic Carbon Analyses (expressed as oxides) (% by weight o.d. soil)

Profile K Distance upslope: 2.8 m

	K1	K2	K3	K4
Depth (cm)	8.00	22.5	36.5	52
% SiO_2	83.25	83.25	98.00	71.50*
% Al_2O_3	6.60	6.60	3.30	1.26
% Fe_2O_3	3.64	3.53	1.36	1.53
% TiO_2	0.538	0.508	0.340	0.138
% MnO	0.027 (21)$^{\emptyset}$	0.010 (7.7)	0.007 (54)	0.005 (3.9)
% P_2O_5	0.080	0.030	0.000	0.000
% CaO	0.132 (94)	0.101 (73)	0.087 (62)	0.035 (25)
% MgO	0.325 (196)	0.338 (204)	0.159 (96)	0.080 (48)
% Na_2O	0.718 (532)	0.556 (412)	0.380 (282)	0.129 (96)
% K_2O	3.16 (2624)	3.01 (2498)	2.390 (1984)	0.890 (733)
Total	98.47	97.93	106.2	75.57
% O/C	4.46	0.54	0.0	0.0

* Possibly too low due to non-dissolution of silica grains and higher sample viscosity due to extra addition of HF

ø Bracketted figures are quantities of elements (mg/100 g) for comparison with exchangeable contents Mg, Ca, K, Na, Mn

ND = not determined

Profile A Distance upslope: 6.0 m

	A1	A2	A3	A4
Depth (cm)	6.0	16.5	32.5	60
% SiO_2	87.69	82.5	85.25	75.5
% Al_2O_3	4.44	4.58	5.52	8.96
% Fe_2O_3	3.70	11.08	7.07	11.25
% TiO_2	0.056	0.420	0.510	0.552
% MnO	0.028 (22)	0.012 (9.3)	0.012 (9.3)	0.018 (13.9)
% P_2O_5	0.140	0.124	0.042	0.045
% CaO	0.175 (125)	0.066 (47)	0.066 (47)	0.099 (71)
% MgO	0.189 (114)	0.196 (118)	0.760 (458)	0.820 (495)
% Na_2O	0.586 (435)	0.536 (413)	0.454 (337)	0.390 (289)
% K_2O	2.990 (2485)	2.600 (2158)	3.04 (2524)	4.29 (3561)
Total	99.99	102.13	102.72	101.92
% O/C	10.73	0.51	0.0	0.0

Profile D Distance upslope: 13.9 m

	D1	D2	D3	D4	D5	D6
Depth (cm)	10	25	35	52	70	90
% SiO_2	82.00	85.25	85.25	81.75	85.75	77.00
% Al_2O_3	4.36	5.12	5.8	5.12	4.08	7.68
% Fe_2O_3	4.10	6.04	6.22	8.33	8.79	14.68
% TiO_2	0.424	0.452	0.48	0.372	0.248	0.398
% MnO	0.050	0.092	0.088	0.057	0.054	0.091
% P_2O_5	0.150	0.056	0.032	0.072	0.062	0.066
% CaO	0.164 (117)	0.088 (63)	0.066 (47)	0.022 (15.7)	0.000 (0)	0.000 (0)
% MgO	0.210 (127)	0.235 (142)	0.255 (154)	0.265 (160)	0.225 (136)	0.444 (268)
% Na_2O	0.641 (476)	0.781 (579)	0.597 (443)	0.403 (299)	0.170 (126)	0.287 (213)
% K_2O	2.380 (1976)	2.79 (2316)	2.89 (2399)	2.46 (2042)	1.810 (1503)	3.01 (2499)
Total	94.48	100.90	101.68	98.85	101.19	103.66
% O/C	0.0	0.0	0.0	0.0	ND	ND

Profile F Distance upslope: 29.5 m

	F1	F2	F3	F4	F5	F6
Depth (cm)	10	25	35	52	70	90
% SiO_2	95.00	86.25	87.75	86.50	81.00	78.75
% Al_2O_3	5.66	5.22	4.66	5.82	7.82	9.56
% Fe_2O_3	2.38	3.53	3.53	2.38	6.04	7.82
% TiO_2	0.584	0.516	0.466	0.532	0.564	0.506
% MnO	0.039	0.029	0.092	0.114	0.065	0.039
% P_2O_5	0.086	0.048	0.012	0.028	0.034	0.045
% CaO	0.197 (141)	0.110 (79)	0.088 (63)	0.099 (71)	0.099 (71)	0.077 (55)
% MgO	0.218 (131)	0.206 (124)	0.226 (136)	0.259 (156)	0.454 (274)	0.743 (448)
% Na_2O	1.041 (772	1.101 (817)	1.101 (817)	1.101 (817)	1.172 (870)	0.969 (719)
% K_2O	3.2 (2656)	3.420 (2839)	3.47 (2881)	3.42 (2839)	4.07 (3379)	4.24 (3520)
Total	108.41	100.43	101.40	100.25	101.32	102.75
% O/C	8.28	0.20	ND	ND	ND	ND

Profile G Distance upslope: 53 m

	G1	G2	G3	G4	G5	G6	G7	G8
Depth (cm)	1.5	7.5	16	25	35	45	55	65
% SiO_2	87.5	87.0	ND	85.75	79.25	79.50	89.00	83.00
% Al_2O_3	5.24	5.36	ND	6.66	7.96	8.54	7.96	7.54
% Fe_2O_3	3.24	4.10	ND	5.07	6.27	7.30	6.04	5.87
% TiO_2	0.494	0.556	ND	0.62	0.532	0.552	0.478	0.436
% MnO	0.115 (89)	0.141 (109)	ND	0.117 (91)	0.102 (79)	0.088 (68)	0.048 (37)	0.041 (32)
% P_2O_5	0.08	0.04	ND	0.025	0.016	0.034	0.023	0.037
% CaO	0.145 (106)	0.092 (62)	ND	0.057 (39)	0.081 (58)	0.302 (205)	0.066 (45)	0.110 (75)
% MgO	0.235 (284)	0.252 (304)	ND	0.332 (401)	0.527 (636)	0.647 (781)	0.647 (781)	0.444 (536)
% Na_2O	0.742 (551)	0.945 (701)	ND	0.885 (657)	1.005 (746)	1.071 (795)	0.945 (701)	0.945 (701)
% K_2O	3.180 (2639)	3.23 (2681)	ND	3.2 (2656)	3.59 (2980)	3.72 (3088)	3.45 (2864)	3.37 (2798)
Total	100.97	101.72	-	102.72	99.33	101.75	108.66	101.79
% O C	6.61	3.37	ND	ND	ND	ND	ND	ND

Profile H Distance upslope: 76.5 m

	H1	H2	H3	H4	H5	H6
Depth (cm)	5	15	25	35	45	55
% SiO_2	83.0	83.0	84.25	85.75	90.0	74.75
% Al_2O_3	5.52	5.66	5.24	4.94	9.40	10.24
% Fe_2O_3	3.99	4.10	3.87	3.87	6.84	8.67
% TiO_2	0.452	0.612	0.460	0.378	0.556	0.512
% MnO	0.076 (59)	0.159 (123)	0.130 (101)	0.101 (78)	0.070 (54)	0.039 (30)
% P_2O_5	0.04	0.047	0.00	0.008	0.025	0.034
% CaO	0.089 (64)	0.399 (285)	0.053 (38)	0.304 (217)	0.037 (26)	0.006 (4)
% MgO	0.265 (160)	0.279 (168)	0.252 (152)	0.259 (156)	0.620 (374)	0.809 (488)
% Na_2O	0.658 (488)	0.789 (585)	0.515 (382)	0.480 (356)	0.444 (329)	0.331 (246)
% K_2O	2.94 (2441)	3.04 (2524)	2.75 (2283)	2.60 (2158)	3.72 (3088)	3.72 (3088)
% O/C	0.0	2.26	ND	ND	ND	ND

Profile J Distance upslope: 100 m

	J1	J2	J3	J4	J5	J6	J7
Depth (cm)	1.5	6.5	15	25 b	35	45	55
% SiO_2	90.0	90.5	ND	98.0	80.25	84.00	85.0
% Al_2O_3	4.22	4.1	ND	4.96	8.80	10.26	10.84
% Fe_2O_3	2.38	2.38	ND	3.24	6.50	11.05	13.53
% TiO_2	0.452	0.494	ND	0.49	0.548	0.474	0.568
% MnO	0.090 (70)	0.076 (59)	ND	0.029 (23)	0.035 (27)	0.031 (24)	0.056 (43)
% P_2O_5	0.042	0.064	ND	0.03	0.047	0.096	0.056
% CaO	0.136 (97)	0.106 (76)	ND	0.183 (131)	0.020 (14)	0.141 (101)	0.011 (8)
% MgO	0.252 (152)	0.212 (128)	ND	0.259 (156)	0.822 (496)	0.842 (508)	0.922 (556)
% Na_2O	0.349 (259)	0.290 (215)	ND	0.331 (246)	0.290 (215)	0.320 (237)	0.290 (215)
% K_2O	2.79 (2316)	2.60 (2158)	ND	2.60 (2158)	3.59 (2986)	3.81 (3163)	4.10 (3404)
Total	100.71	100.82	-	110.12	100.90	111.05	115.37
% O C	3.89	1.85	ND	ND	ND	ND	ND

Deep Samples

	Z1		Z2	
Distance upslope (m)	6.0		100.0	
Depth (cm)	200		200.0	
% SiO_2	74.00		75.0	
% Al_2O_3	8.86		10.75	
% Fe_2O_3	11.65		13.03	
% TiO_2	0.632		0.644	
% MnO	0.027	(21)	0.030	(23)
% P_2O_5	0.43		0.060	
% CaO	0.417	(298)	0.32	(229)
% MgO	1.26	(760)	0.950	(573)
% Na_2O	0.430	(319)	0.390	(289)
% K_2O	4.43	(3677)	4.52	(3752)
Total	102.14		105.69	

II. Exchangeable Element Contents

Determination was made of the dominant exchangeable ions in the soil; these are calcium, magnesium, potassium, sodium and manganese. The method used was that developed by Pye-Unicam, in conjunction with S.E. Allen of the Nature Conservancy, for the SP1900 and SP1950 AA Spectrophotometers and published by Pye-Unicam as an AA Method Sheet.

(a) Reagent Preparation

Calcium stock solution (100 mg/l): 0.2497 g of dry calcium carbonate was dissolved in the minimum volume of HCl and made up to 1 litre in a volumetric flask.

Magnesium stock solution I (100 mg/l): 0.1000 g of oxide free magnesium ribbon was dissolved in the minimum quantity of dilute HCl and made up to 1 litre in a volumetric flask.

Magnesium stock solution II (5 mg/l): 5 ml of stock magnesium solution I was pipetted into a 100 ml volumetric flask and made up to the mark with water. This was prepared fresh daily.

Manganese stock solution (100 mg/l): 0.1000 g of oxide free manganese metal was dissolved in the minimum volume of dilute HCl and made up to 1 litre in a volumetric flask.

Potassium stock solution (100 mg/l): 0.1905 g of dry potassium chloride was dissolved in water and made up to 1 litre in a volumetric flask.

Lanthanum stock solution (0.4 % La^{3+}): 4.7 g of AA grade lanthanum oxide was weighed and transferred to a 500 ml beaker. 300 ml of water were added, followed by 25 ml of hydrochloric acid (Sp.Gr. 1.18). The beaker was heated and the mixture stirred until the salt had dissolved. The solution was cooled and filtered into a 1 litre volumetric flask and made up to the mark with water.

Ammonium acetate (4 M): 420 ml of ammonia solution (Sp.Gr.0.880) were added to 550 ml of glacial acetic acid and diluted to 1 litre with water. The pH was adjusted to 7.0 ± 0.1 with a pH meter by adding either ammonia or acetic acid.

Ammonium acetate (1 M): one volume of ammonium acetate (4 M) was diluted with three volumes of water.

Sulphuric acid (20 %): four volumes of water were added to one volume of sulphuric acid (Sp.Gr. 1.84).

(b) Calibration Solution Preparation

Manganese, potassium and sodium: 0, 2.5 and 5.0 ml of each manganese, potassium and sodium stock solutions was pipetted into three 100 ml volumetric flasks. 25 ml of ammonium acetate (4 M) was added and each made up to 100 ml. These solutions then contained 1, 2.5 and 5.0 mg/l of Mn, K and Na in the presence of 1 M ammonium acetate.

Calcium and magnesium: 0, 5.0 and 10.0 ml of calcium stock solution and 0, 5.0 and 10 ml of magnesium stock solution II were added to three 100 ml volumetric flasks. To each flask was added 20 ml of lanthanum stock solution, 5 ml of sulphuric acid (20 %) and 25 ml of ammonium acetate (4 M). These were then made up to the mark with water, finally containing 0, 5.0, 10.0 mg/l of Ca and 0, 0.25, 0.5 mg/l of Mg in the presence of 800 mg/l of lanthanum, 1 % sulphuric acid and 1 M ammonium acetate.

(c) Sample Solution Preparation

Soil samples were air dried (ad) at 40°C. The weights of ad soil were converted to oven dry (od) weights (115°C) before computing the element concentrations. 5.0 g of ad sample was transferred to a 250 ml polythene bottle and 125 ml of 1 M ammonium acetate added. A polythene screw cap was fitted and the bottle shaken in an end-to-end shaker for 1 hour. The mixture was filtered through a Whatman 44 filter paper and the filtrate retained. Samples were extracted in duplicate and blank extraction performed with each batch of samples (solution B). Solution A was used directly for the determination of manganese, potassium and sodium. The solution for calcium and magnesium was prepared by

pipetting 20 ml of solution A, 20 ml of lanthanum stock solution, 5 ml of sulphuric acid (20 %) and 20 ml of 4 M of ammonium acetate into a 100 ml flask and making up to the mark with water. Solution B was processed identically. Further dilution was required for the determination of calcium and magnesium in some samples, and this was achieved as shown in Table 2.

Potassium and sodium were determined by emission. The ammonium ions in solution had the effect of suppressing excessive flame ionisation and the addition of extra ammonium acetate was unnecessary.

The concentration of each metal in mg of extractable metal per 100 g of soil was calculated corrected tc od weight. For manganese, sodium and potassium:

$$\text{mg/100 g} = \frac{(C_S - C_B) \times 1.25 \times 10^3}{W_{40} \times (100 - L)} \qquad (3)$$

and for calcium and magnesium:

$$\text{mg/100 g} = \frac{(C_S - C_B) \times 1.25 \times 5 \times F \times 10^3}{W_{40} \times (100 - L)} \qquad (4)$$

where C_s = concentration of element in sample solution in mg/l (mean of duplicates)

C_B = concentration of element in extraction blank solution in mg/l

F = further dilution factor

W_{40} = weight of soil dried at 40°C (5.0 g approx.)

L = percentage loss at 105°C of soil previously dried at 40°C

Pye Unicam found the precision of the method to be low at ± 5 - 10 % which is attributable to the method of extraction. Other methods of extraction, e.g. the use of leaching columns, are relatively slow and the shaker method was used for this reason. Replicate samples were always within 5 % of one another.

TABLE 2

Calcium and Magnesium Dilutions

Dilution	Volume of Solution A or B	Volume of 4 M Ammonium Acetate	Volume of La^{3+}	Volume of 20 % H_2SO_4	Final Volume
2	10	22.5	20	5	100
4	5	24	20	5	100
10	2	25	20	5	100

(d) pH Determination

pH was determined using the Pye Unicam method described in Chapter 5.

A small quantity of the original sample was mixed to a paste with distilled de-ionised water in a 50 ml glass beaker. pH was then determined in exactly the same way as for water samples, although readings were only taken after meter drift had finished. The results of exchangeable cation and pH analyses are compiled below.

(e) Results of Exchangeable Cations and pH Analyses
(mg/100 g od soil)

Profile S Distance upslope: stream bank

	S1	S2	S3
Depth (cm)	7.0	22.0	37.5
pH	4.14	4.58	4.49
K	11.85	4.17	10.94
Na	70.31	44.13	125.00
Ca	31.88	22.19	64.38
Mg	3.00	7.50	4.53
Mn	4.33	2.76	4.01

Profile K Distance upslope: 2.8 m

	K1	K2	K3	K4
Depth (cm)	8.0	22.5	36.5	52.0
pH	4.12	4.40	5.09	5.13
K	21.47	7.50	2.99	4.14
Na	146.88	94.23	44.69	46.44
Ca	64.38	53.13	25.63	31.88
Mg	25.78	28.91	7.13	13.0
Mn	18.70	7.14	1.39	2.20

Profile A Distance upslope: 7.0 m

	A1	A2	A3	A4
Depth (cm)	6.0	16.5	32.5	60
pH	3.37	3.72	4.30	4.44
K	47.5	17.60	7.2	20.19
Na	58.75	35.31	34.75	51.88
Ca	51.88	10.94	20.63	61.25
Mg	14.69	2.63	23.91	73.75
Mn	35.94	5.25	1.90	3.70

Profile B Distance upslope: 9.25 m

	B1	B2	B3	B4	B5	B6
Depth (cm)	10	25	35	52	70	90
pH	3.90	3.84	4.02	4.18	4.40	4.46
K	27.19	16.19	8.66	7.88	9.73	19.69
Na	50.94	36.25	45.23	28.94	58.75	57.75
Ca	51.88	12.19	4.06	2.19	26.25	48.75
Mg	8.59	2.88	1.47	3.38	30.32	68.75
Mn	62.14	24.2	18.70	14.64	10.58	13.39

Profile C Distance upslope: 11.5 m

	C1	C2	C3	C4	C5	C6
Depth (cm)	10	25	35	52	70	90
pH	3.98	4.21	4.18	4.31	4.15	4.31
K	17.66	17.25	5.63	6.28	17.03	18.75
Na	27.50	37.82	45.94	54.38	40.94	34.69
Ca	3.13	0.0	0.0	0.0	5.63	30.31
Mg	2.09	1.03	0.72	0.84	5.0	46.25
Mn	13.39	34.45	11.83	16.20	10.95	9.86

PROFILE D Distance upslope: 13.9 m

	D1	D2	D3	D4	D5	D6
Depth (cm)	10	25	35	52	70	90
pH	3.83	4.01	4.06	4.24	4.17	4.1
K	17.71	5.5	10.67	4.7	5.5	16.75
Na	28.5	28.31	29.69	45	42.69	26.63
Ca	4.06	0.63	0.0	0.0	0.0	0.63
Mg	2.38	0.72	1.09	0.53	0.69	5.09
Mn	27.45	14.95	23.39	7.95	6.51	29.72

PROFILE E Distance upslope: 16.25 m

	E1	E2	E3	E4	E5	E6
Depth (cm)	10	25	35	52	70	90
pH	3.71	3.87	3.89	3.97	4.04	4.22
K	10.0	5.65	6.95	7.41	6.81	4.25
Na	26.25	24.75	26.44	27.5	27.19	25.0
Ca	3.44	0.0	0.0	0.0	0.0	0.0
Mg	1.78	0.94	1.06	0.9	0.56	0.31
Mn	33.08	12.33	10.45	5.08	4.2	4.2

PROFILE F Distance upslope: 29.5 m

	F1	F2	F3	F4	F5	F6
Depth (cm)	2.5	12.5	21.5	35	45	55
pH	3.82	3.88	4.14	4.17	4.05	3.9
K	29.38	14.06	8.41	6.48	6.40	10.67
Na	51.88	117.19	44.56	28.31	34.06	35.31
Ca	56.25	1.88	0.0	1.88	0.0	0.0
Mg	2.5	1.84	0.72	0.47	0.59	1.09
Mn	71.83	21.51	51.7	19.64	7.83	4.7

PROFILE G Distance upslope: 53 m

	G1	G2	G3	G4	G5	G6	G7	G8
Depth (cm)	1.5	7.5	16	25	35	45	55	65
pH	4.17	4.01	4.16	4.00	3.94	3.9	3.90	3.95
K	45.38	24.16	23.53	9.83	8.69	8.48	8.66	7.75
Na	57.5	24.1	13.88	33.31	19.66	36.56	32.25	30.31
Ca	68.13	9.06	11.25	00.0	1.25	3.13	5.31	0.0
Mg	10.0	3.41	2.09	0.79	1.13	1.03	0.97	1.09
Mn	241.2	134.3	131.8	37.76	32.33	15.58	8.45	9.70

PROFILE H Distance upslope: 76.5 m

	H1	H2	H3	H4	H5	H6
Depth (cm)	5	15	25	35	45	55
pH	3.79	3.87	3.91	3.88	3.82	3.81
K	17.35	11.66	14.69	10.69	3.55	4.19
Na	61.3	32.75	37.81	30	35.14	44.56
Ca	15.63	3.75	10.31	2.5	0.94	0.63
Mg	4.34	3.06	1.73	1.44	1.94	2.34
Mn	78.7	70.26	59.01	39.26	21.7	12.45

PROFILE J Distance upslope: 100 m

	J1	J2	J3	J4	J5	J6	J7
Depth (cm)	1.5	6.5	15	25	35	45	55
pH	4.01	4.1	3.97	3.83	3.77	3.76	3.81
K	21.41	18.53	17.56	11.15	17.03	25.16	22.66
Na	49.06	37.13	50.0	34.06	34.38	51.88	54.38
Ca	72.5	70.63	28.44	9.38	9.38	4.06	8.75
Mg	11.25	9.84	5.58	3.38	3.06	2.56	6.16
Mn	126.51	19.7	7.45	11.39	12.2	9.95	5.58

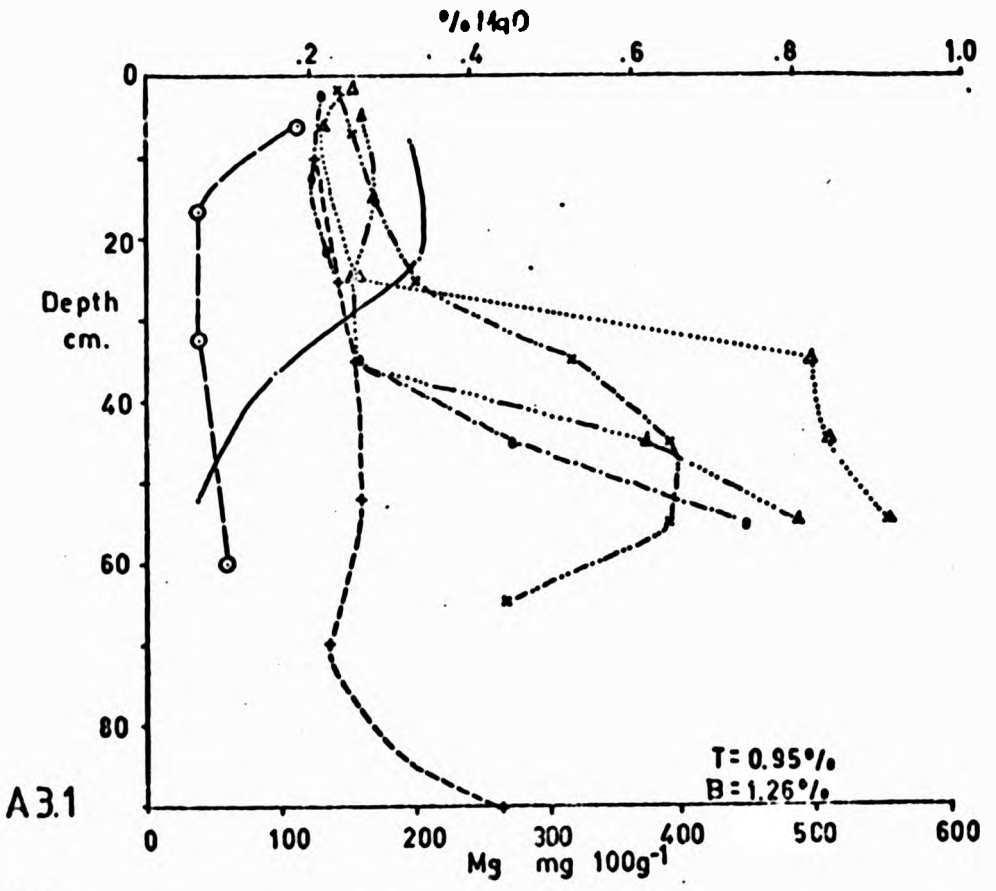
% Mg
0
.2
.4
.6
.8
1.0
20
Depth
cm.
40
60
80
T= 0.95%
B= 1.26%
0
100
200
300
400
500
600
Mg mg 100g-1

A3.1

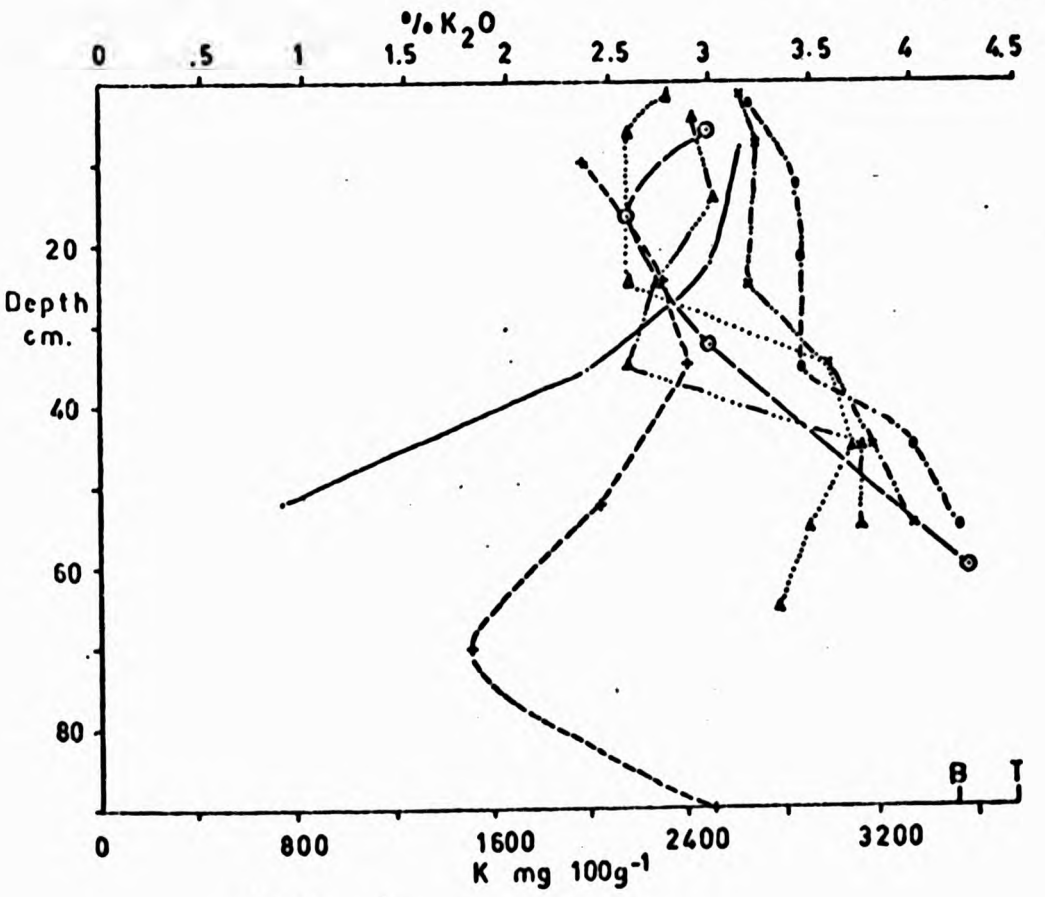
% K2O
0
.5
1
1.5
2
2.5
3
3.5
4
4.5
20
Depth
cm.
40
60
80
B
T
0
800
1600
2400
3200
K mg 100g-1

A3.2

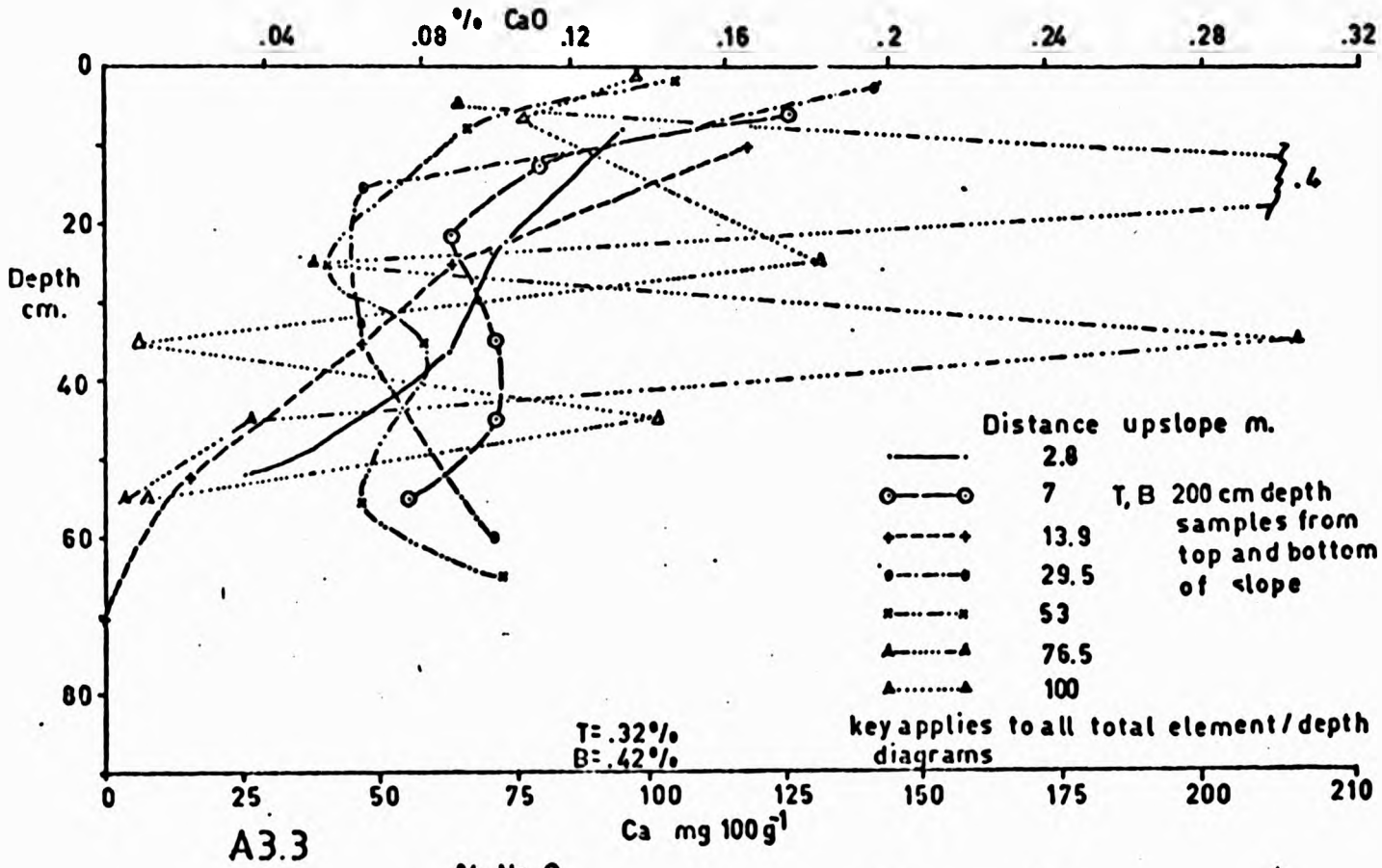
% CaO
.04
.08
.12
.16
.2
.24
.28
.32
0
20
40
60
80
Depth cm.
.4
Distance upslope m.
2.8
7
13.9
29.5
53
76.5
100
T, B 200 cm depth samples from top and bottom of slope
key applies to all total element/depth diagrams
T=.32%
B=.42%
0
25
50
75
100
125
150
175
200
210
Ca mg 100g-1

A3.3

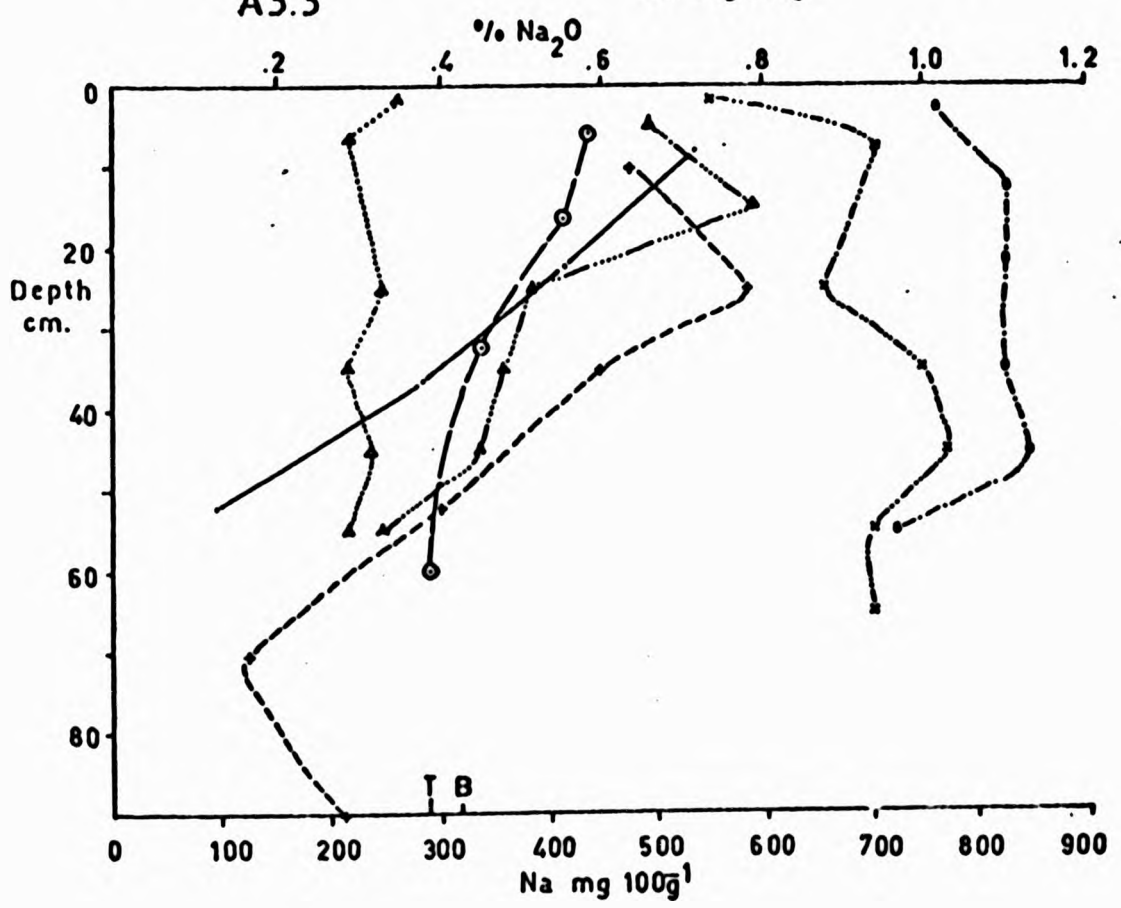
% Na2O
.2
.4
.6
.8
1.0
1.2
0
20
40
60
80
Depth cm.
T
B
0
100
200
300
400
500
600
700
800
900
Na mg 100g-1

A3.4

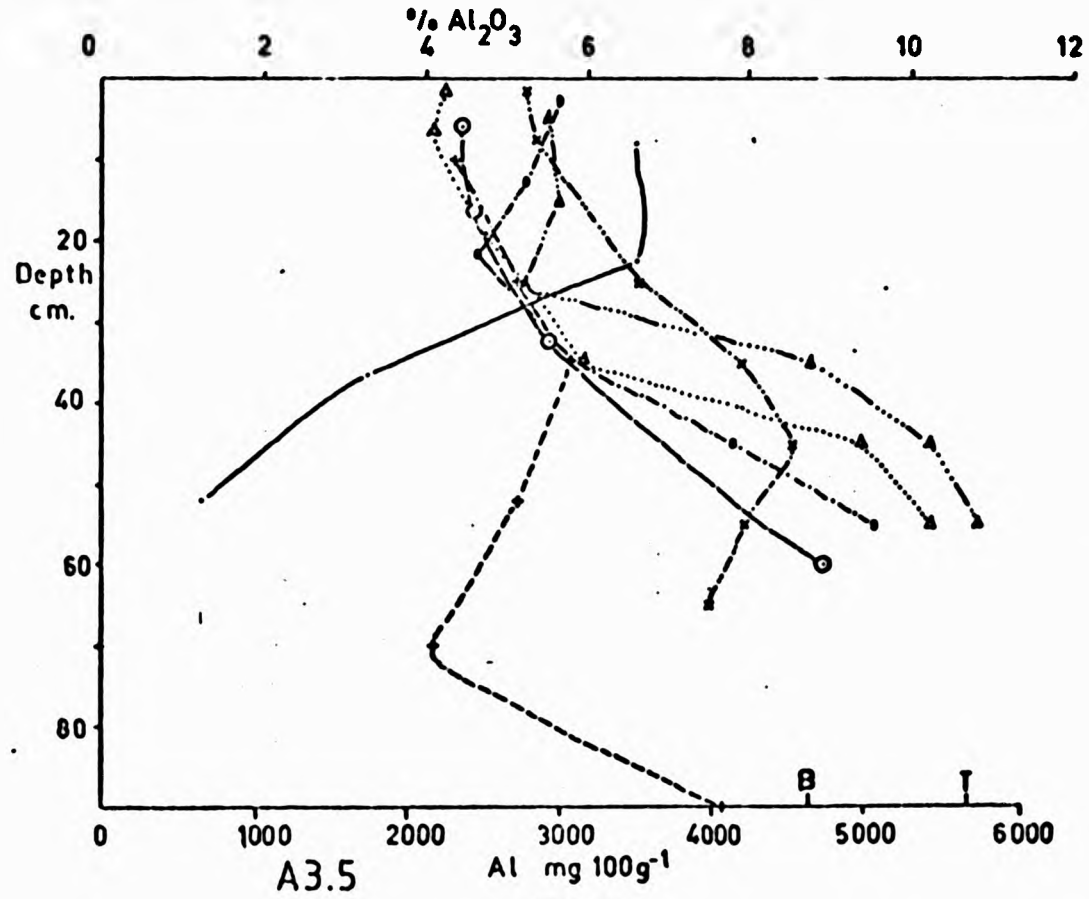
% Al_2O_3
0
2
4
6
8
10
12
20
Depth
cm.
40
60
80
B
I
0
1000
2000
3000
4000
5000
6000
Al mg $100g^{-1}$

A3.5

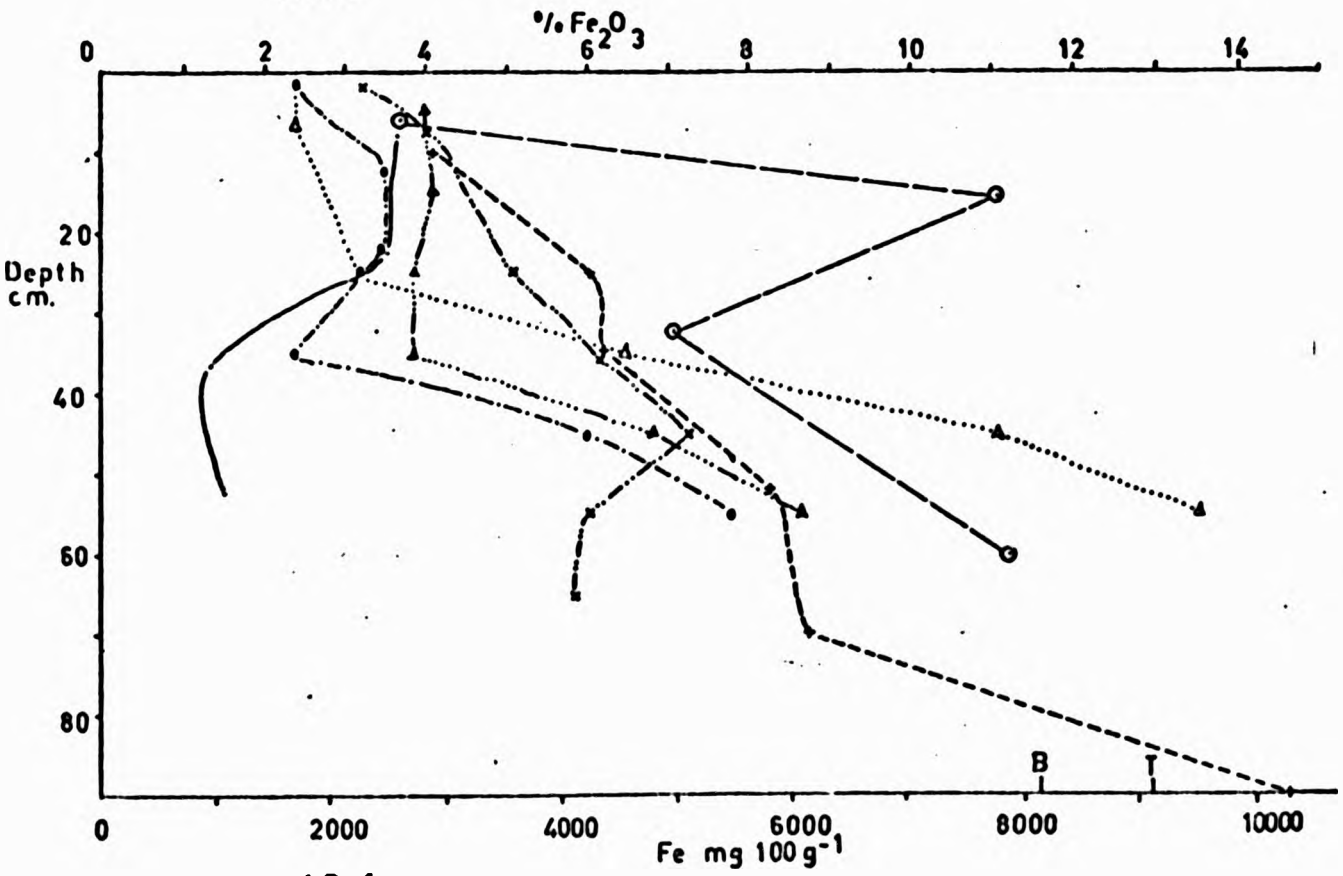
% Fe_2O_3
0
2
4
6
8
10
12
14
20
Depth
cm.
40
60
80
B
I
0
2000
4000
6000
8000
10000
Fe mg $100g^{-1}$

A3.6

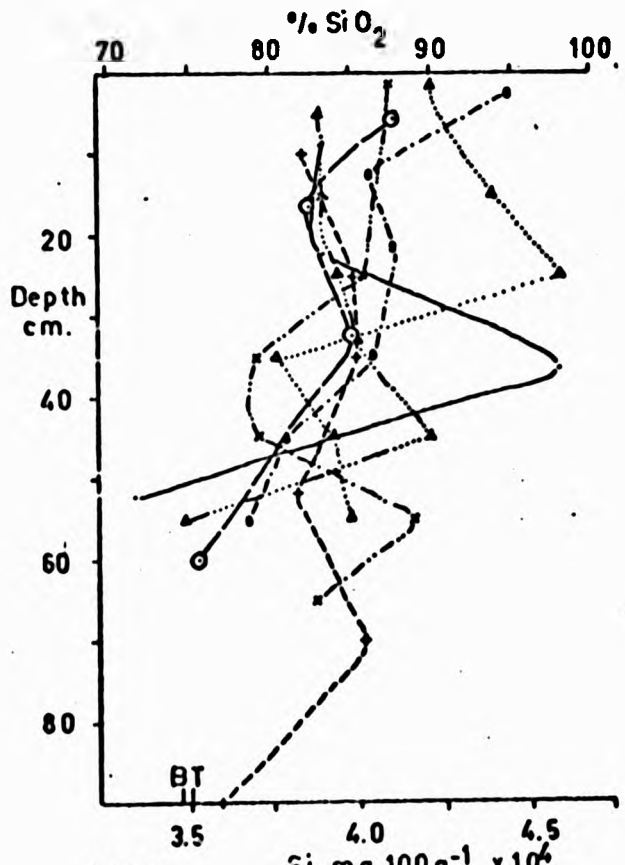
% Si O2
70
80
90
100
20
Depth
cm.
40
60
80
BT
3.5
4.0
4.5
Si mg 100g-1 x10-4

A3.7

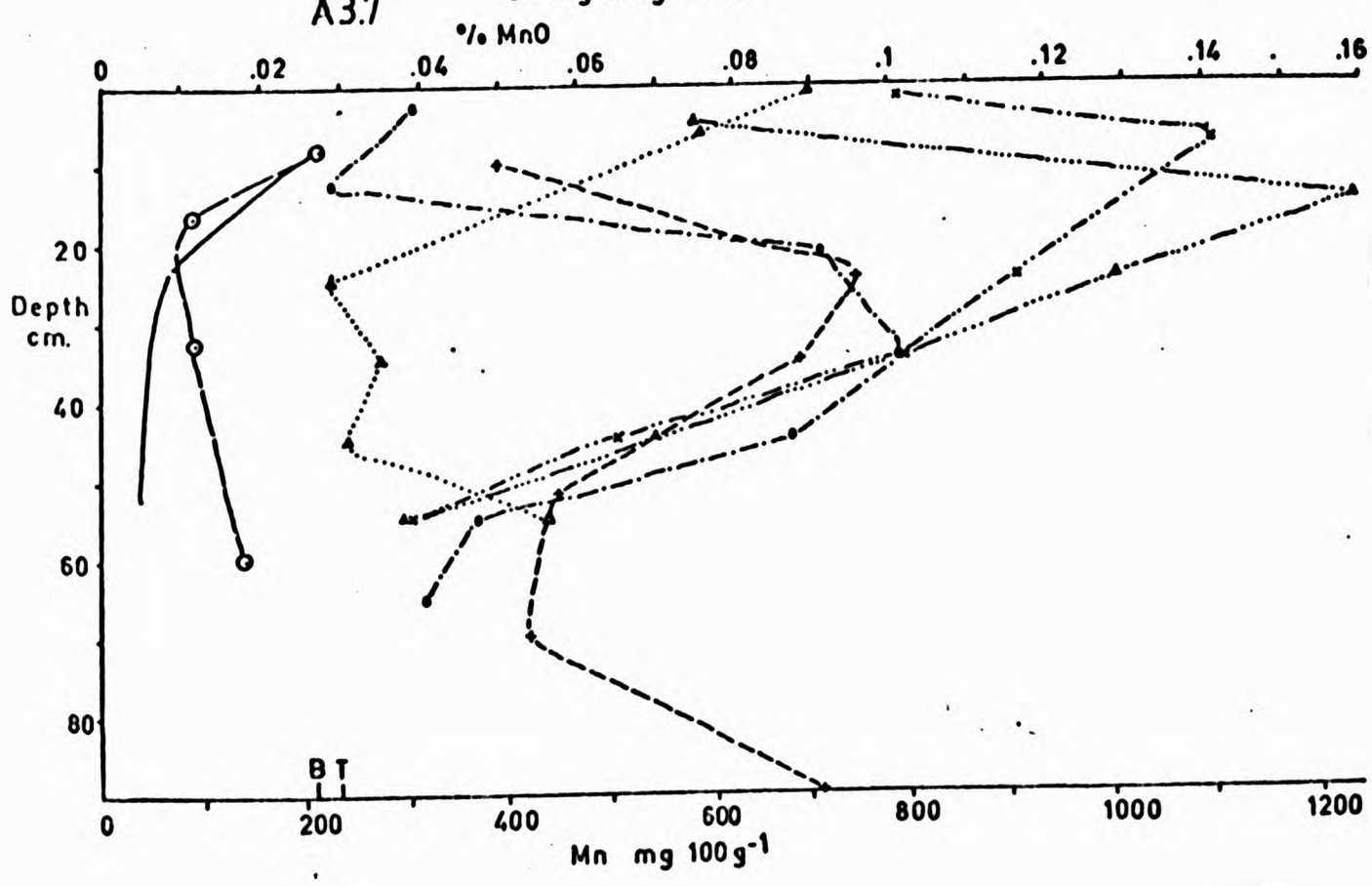
% MnO
0
.02
.04
.06
.08
.1
.12
.14
.16
20
Depth
cm.
40
60
80
BT
0
200
400
600
800
1000
1200
Mn mg 100g-1

A3.8

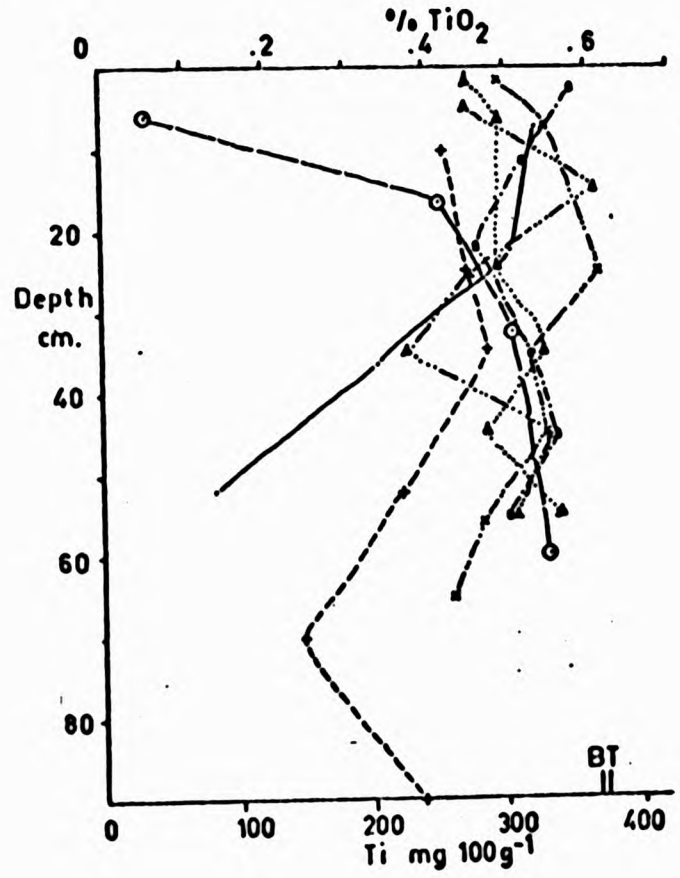
% TiO2
0
.2
.4
.6
20
Depth
cm.
40
60
80
BT
0
100
200
300
400
Ti mg 100g-1

A3.9

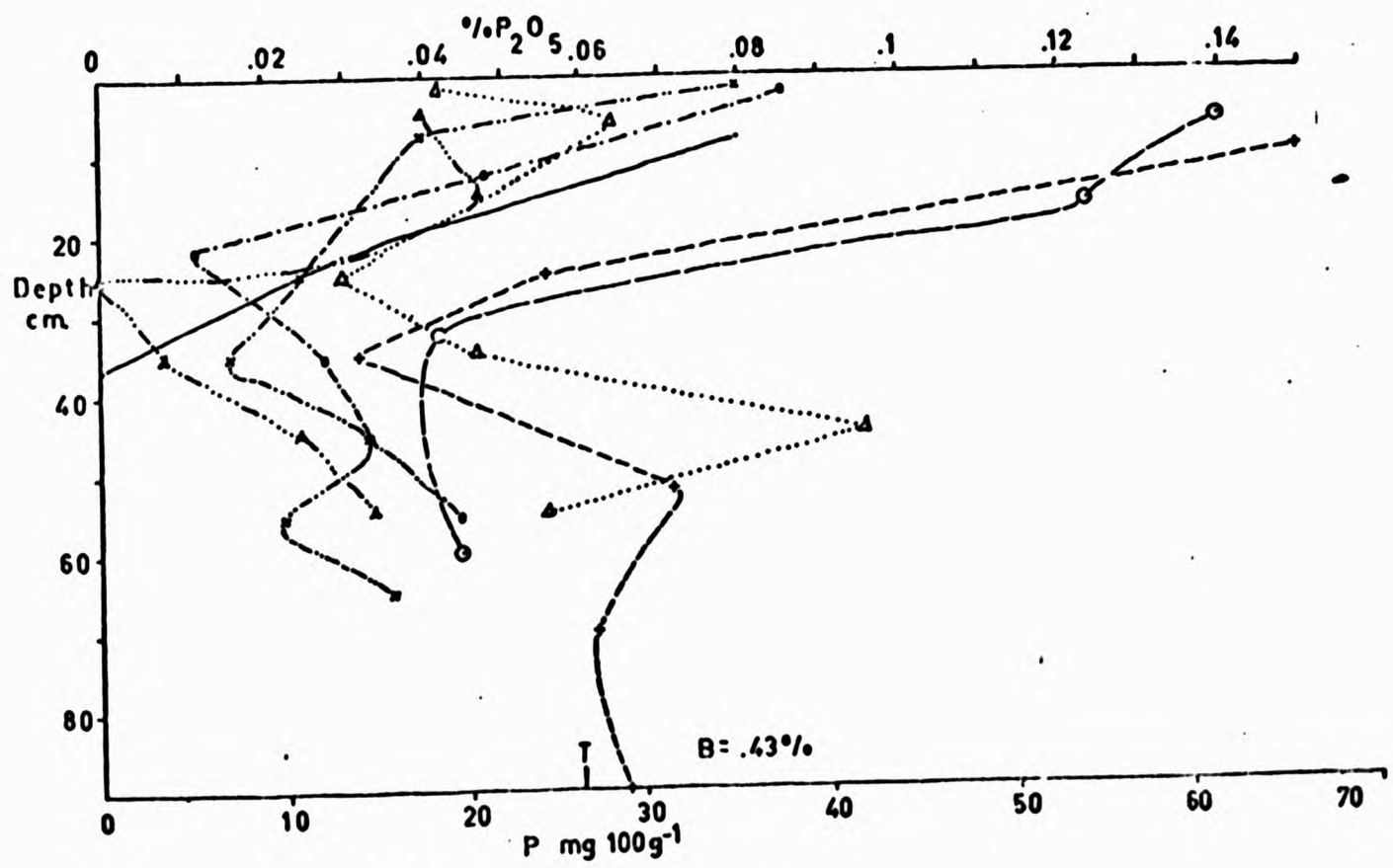
% P2O5
0
.02
.04
.06
.08
.1
.12
.14
20
Depth
cm.
40
60
80
T
B= .43%
0
10
20
30
40
50
60
70
P mg 100g-1

A3.10

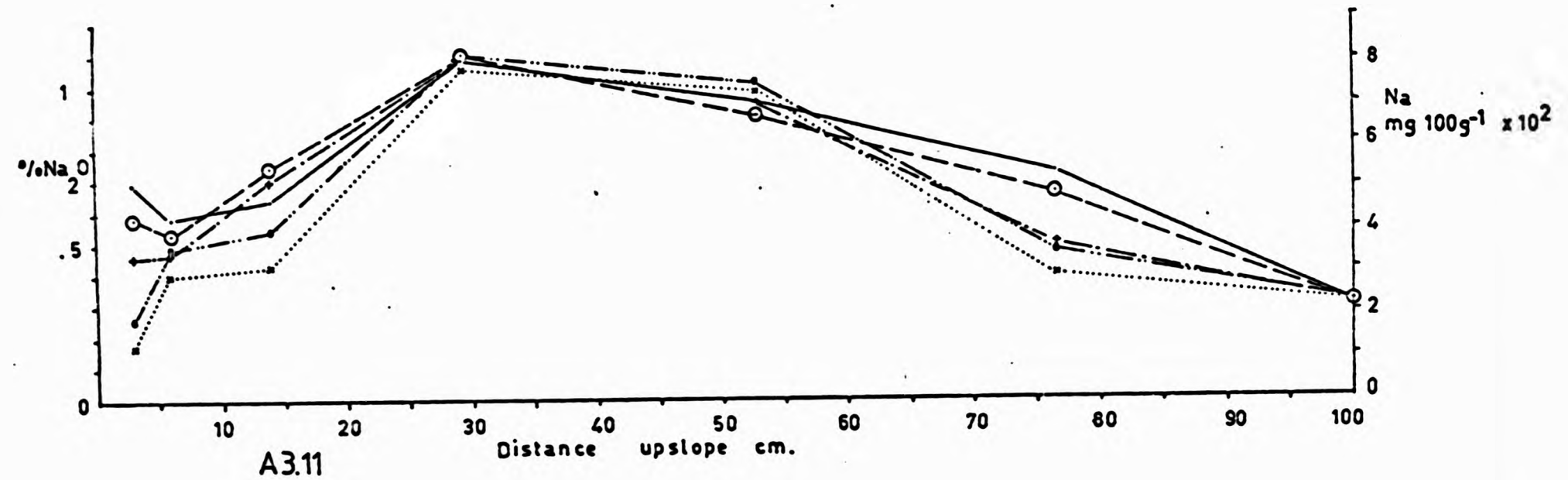
1
.5
0
%Na2O
8
6
4
2
0
Na
mg 100g-1 x10^2
10
20
30
40
50
60
70
80
90
100
Distance upslope cm.

A3.11

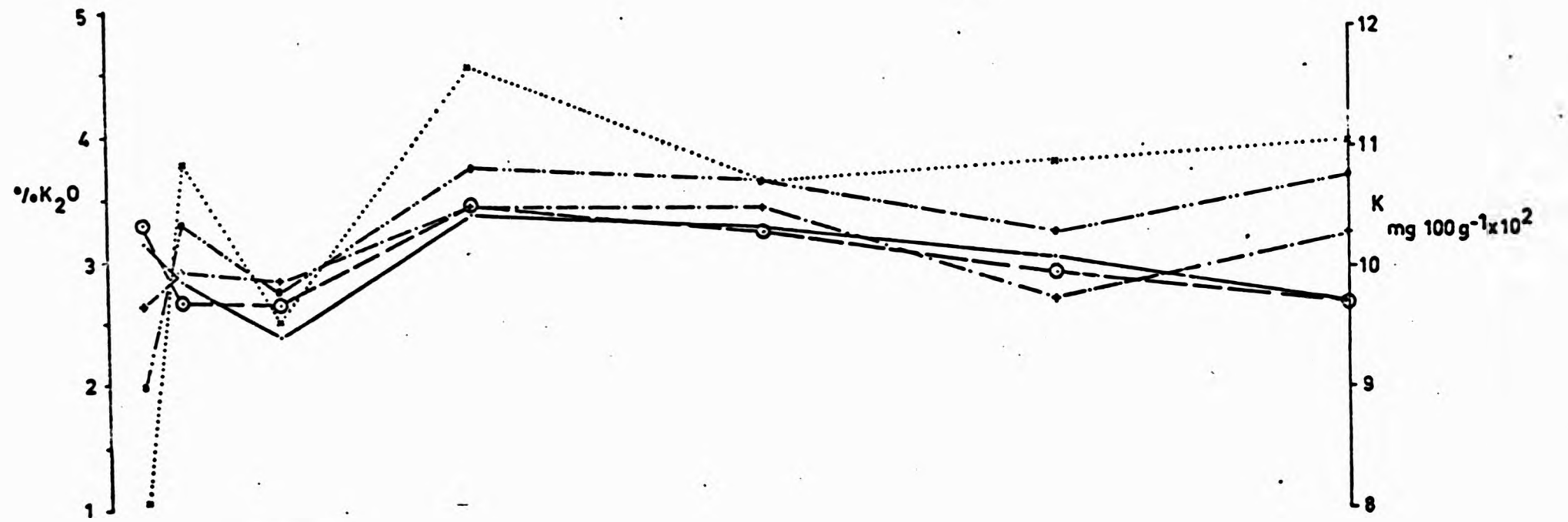
5
4
3
2
1
%K2O
12
11
10
9
8
K
mg 100g-1x10^2

A3.12

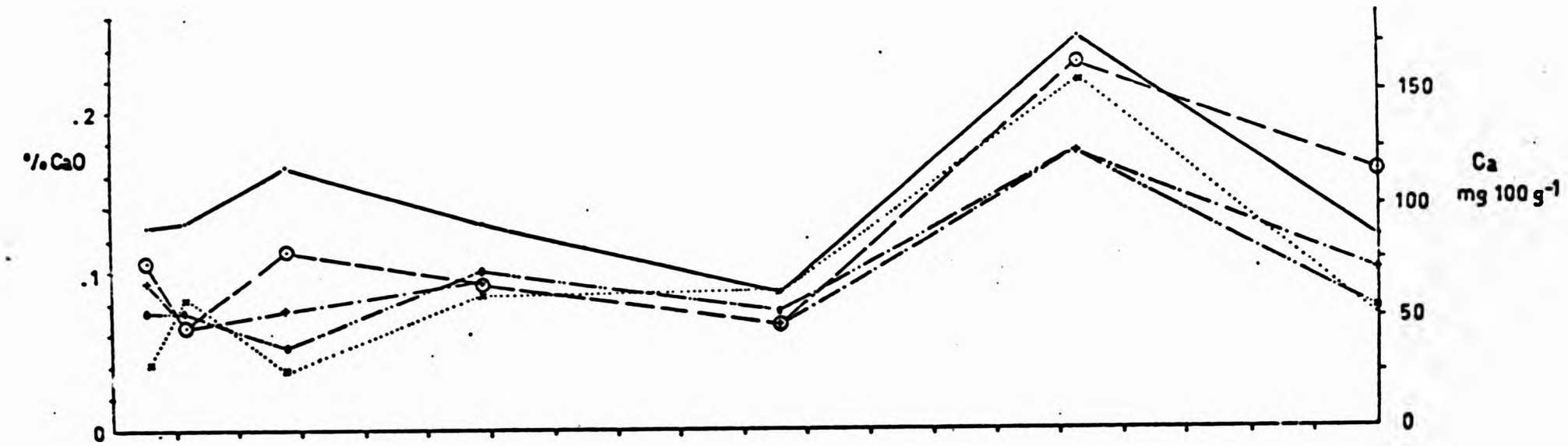
%CaO
.2
.1
0
150
100
50
0
Ca
mg 100 g⁻¹

A3.13

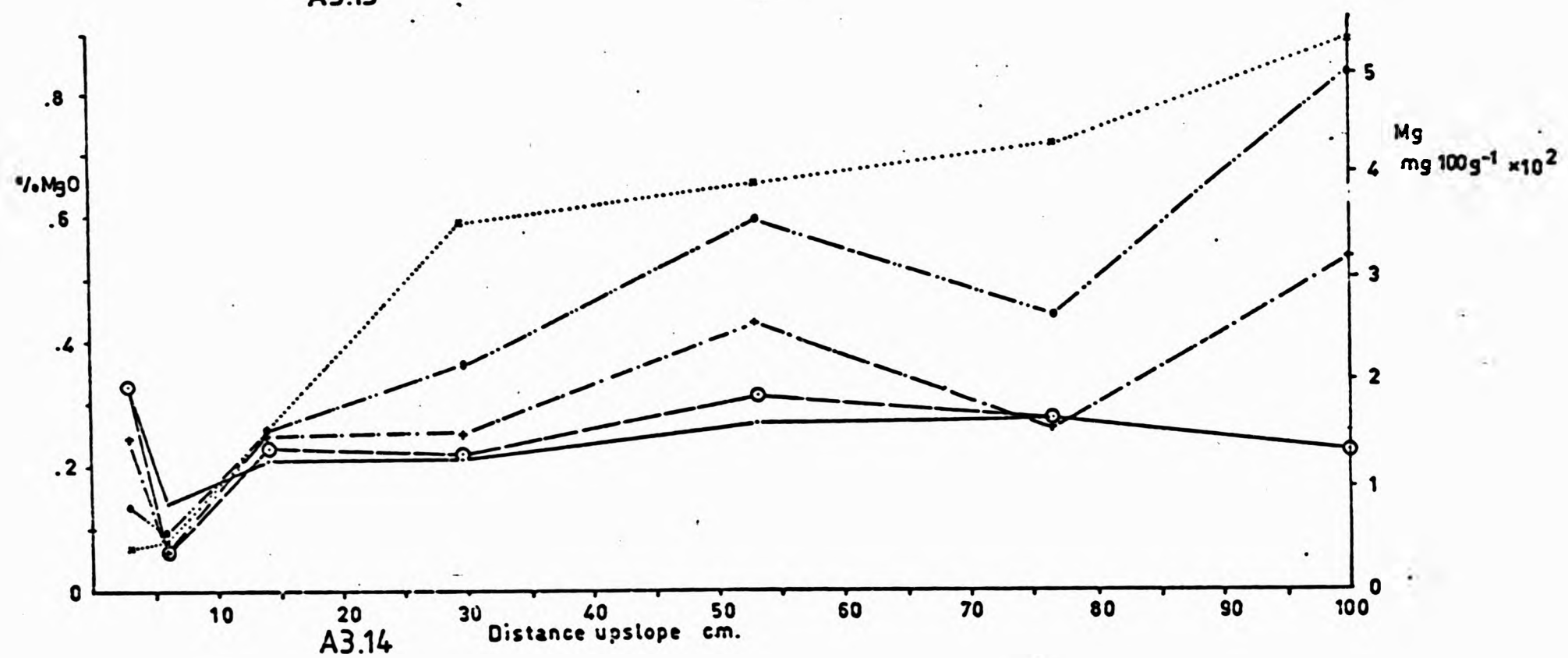
%MgO
.8
.6
.4
.2
0
5
4
3
2
1
0
Mg
mg 100g⁻¹ x10²
10
20
30
40
50
60
70
80
90
100
Distance upslope cm.

A3.14

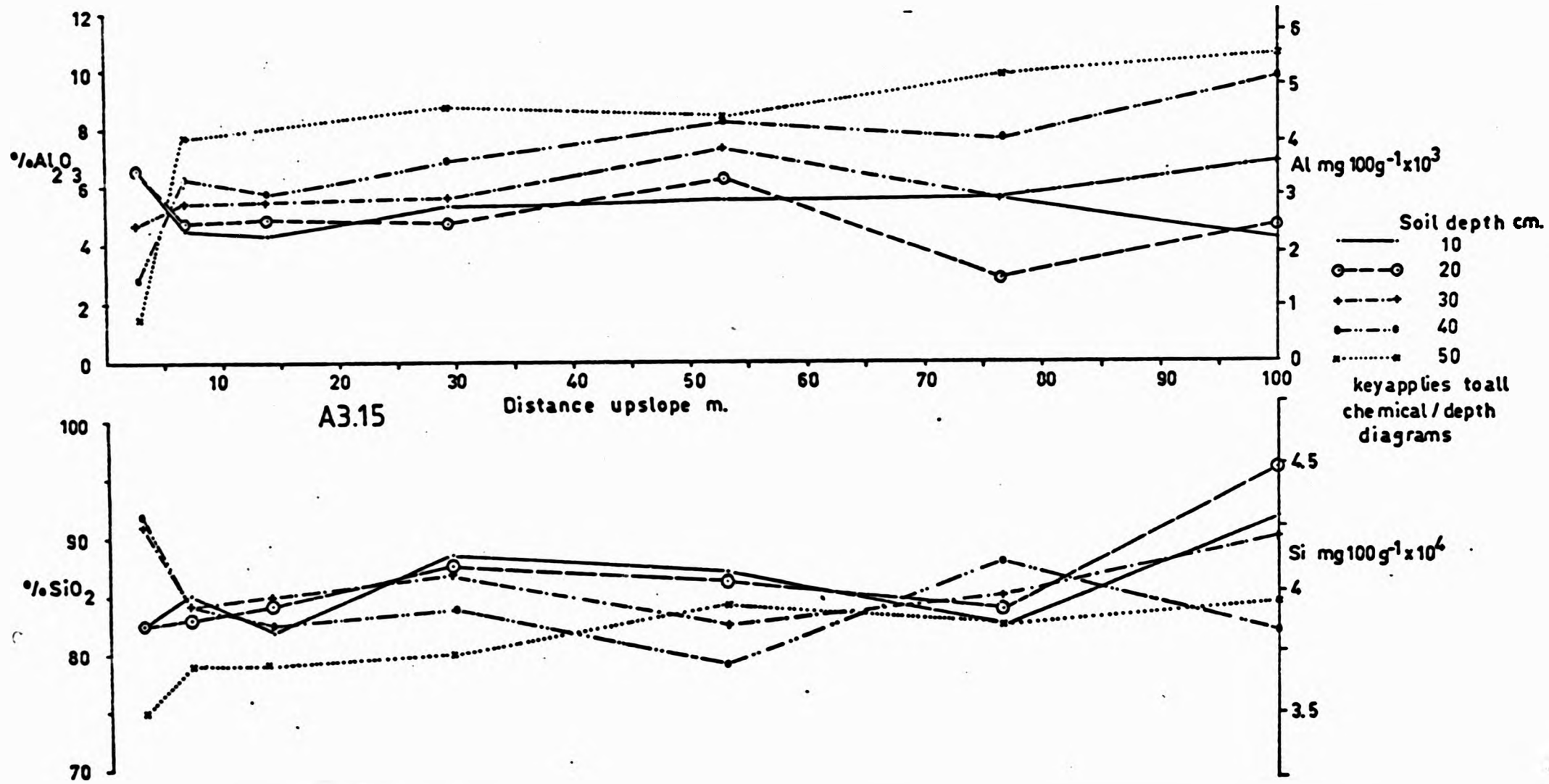
%Al2O3
Al mg 100g-1x10-3
Soil depth cm.
10
20
30
40
50
key applies to all chemical / depth diagrams
Distance upslope m.
A3.15
%SiO2
Si mg 100 g-1 x 10-4
A3.16

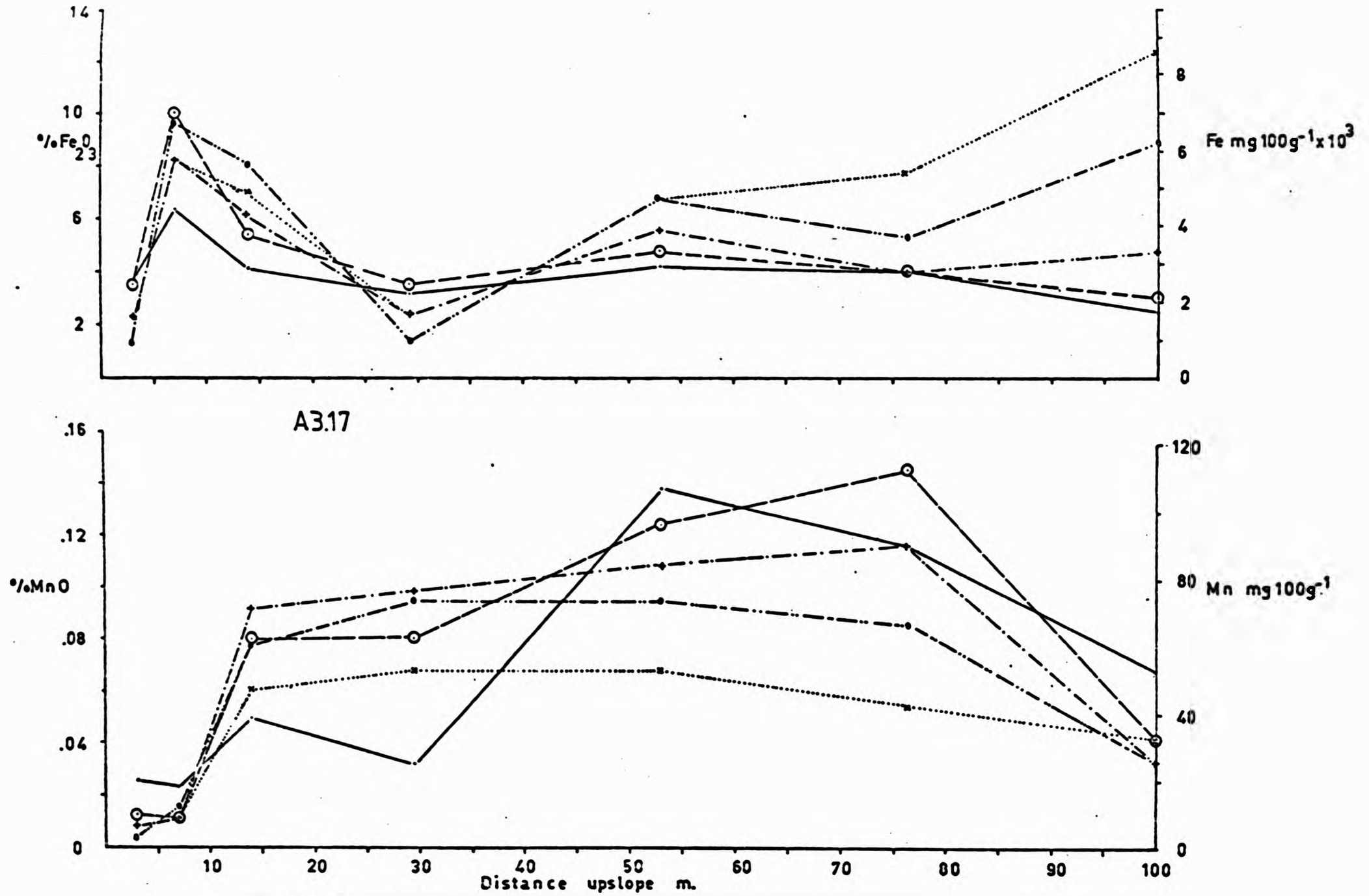
14
10
%Fe2O3
6
2
8
6
4
2
0
Fe mg 100g-1 x 10³
A3.17
.16
.12
%MnO
.08
.04
0
120
80
40
0
Mn mg 100g-1
10
20
30
40
50
60
70
80
90
100
Distance upslope m.
A3.18

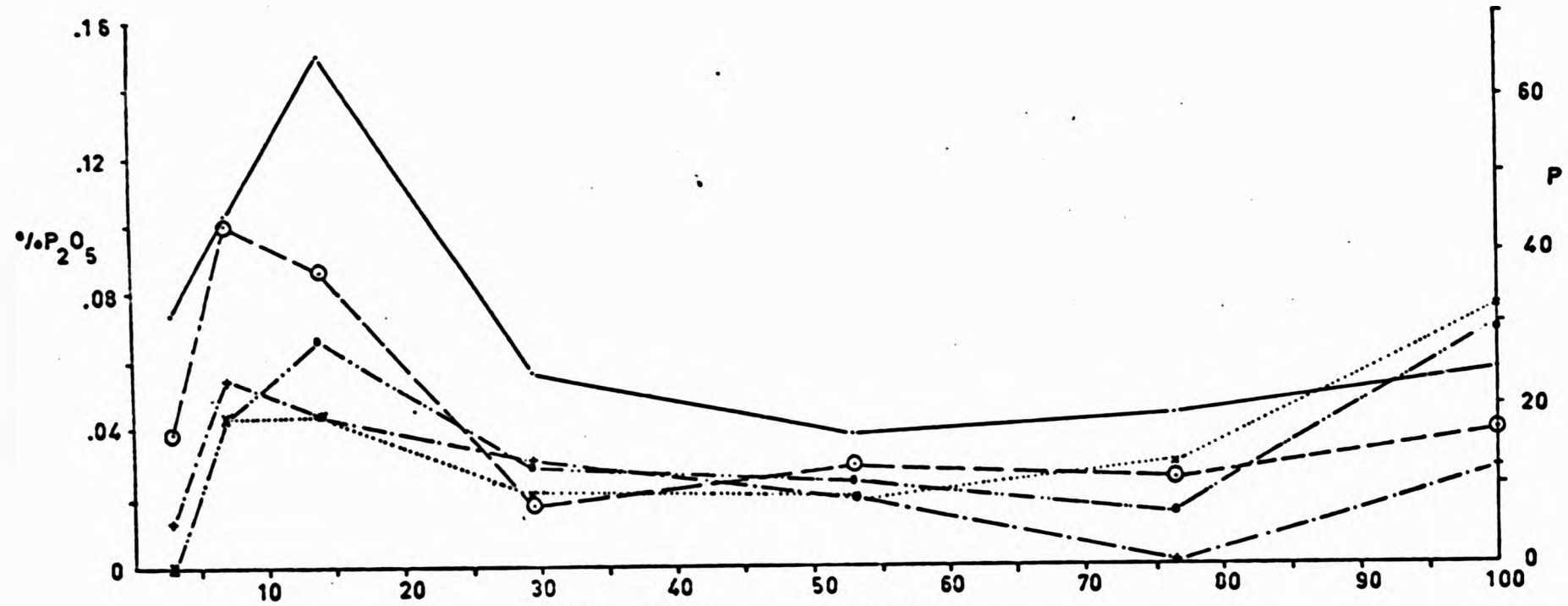

A3.19 Distance upslope m.

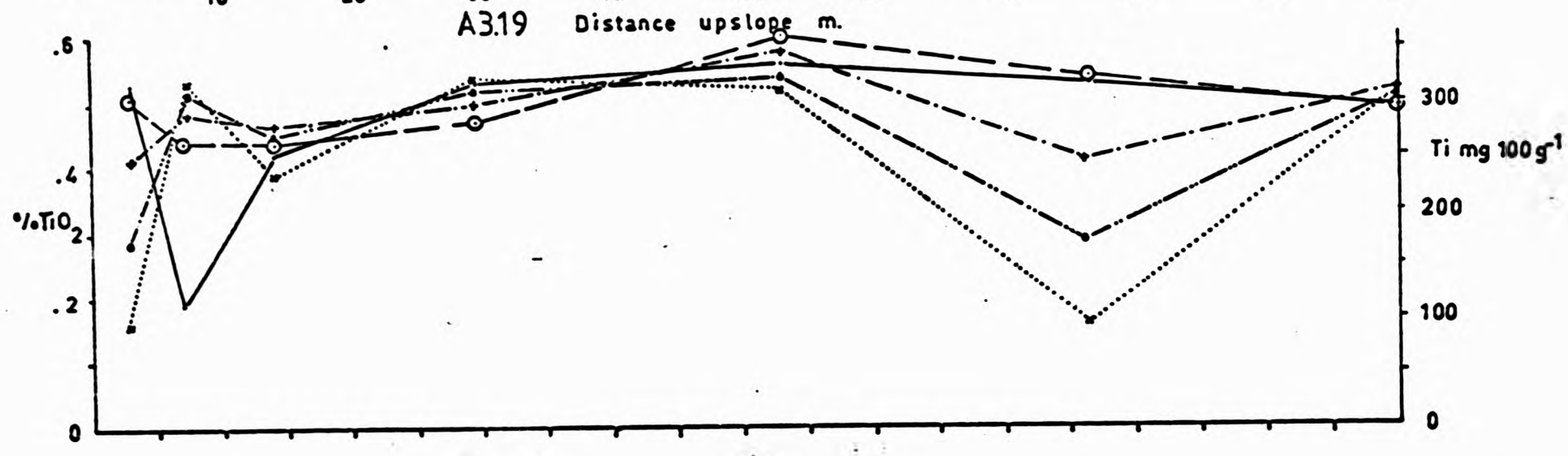

A3.20

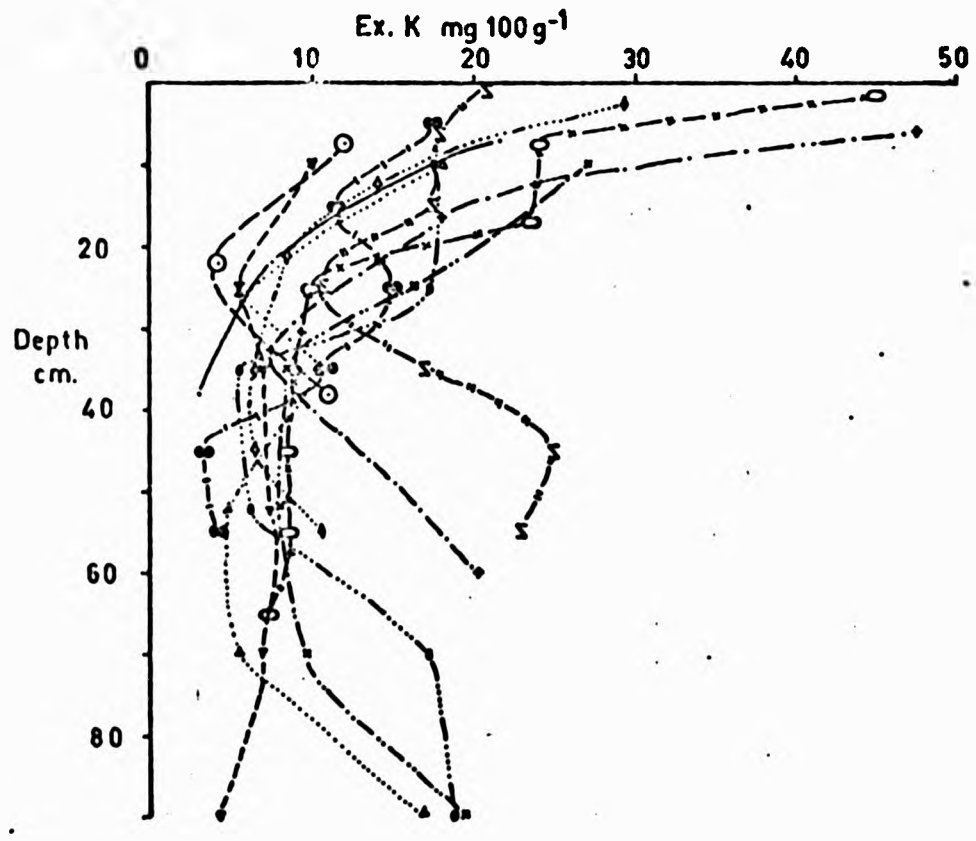
Ex. K mg 100 g-1
0
10
20
30
40
50
Depth
cm.
20
40
60
80

A3.21

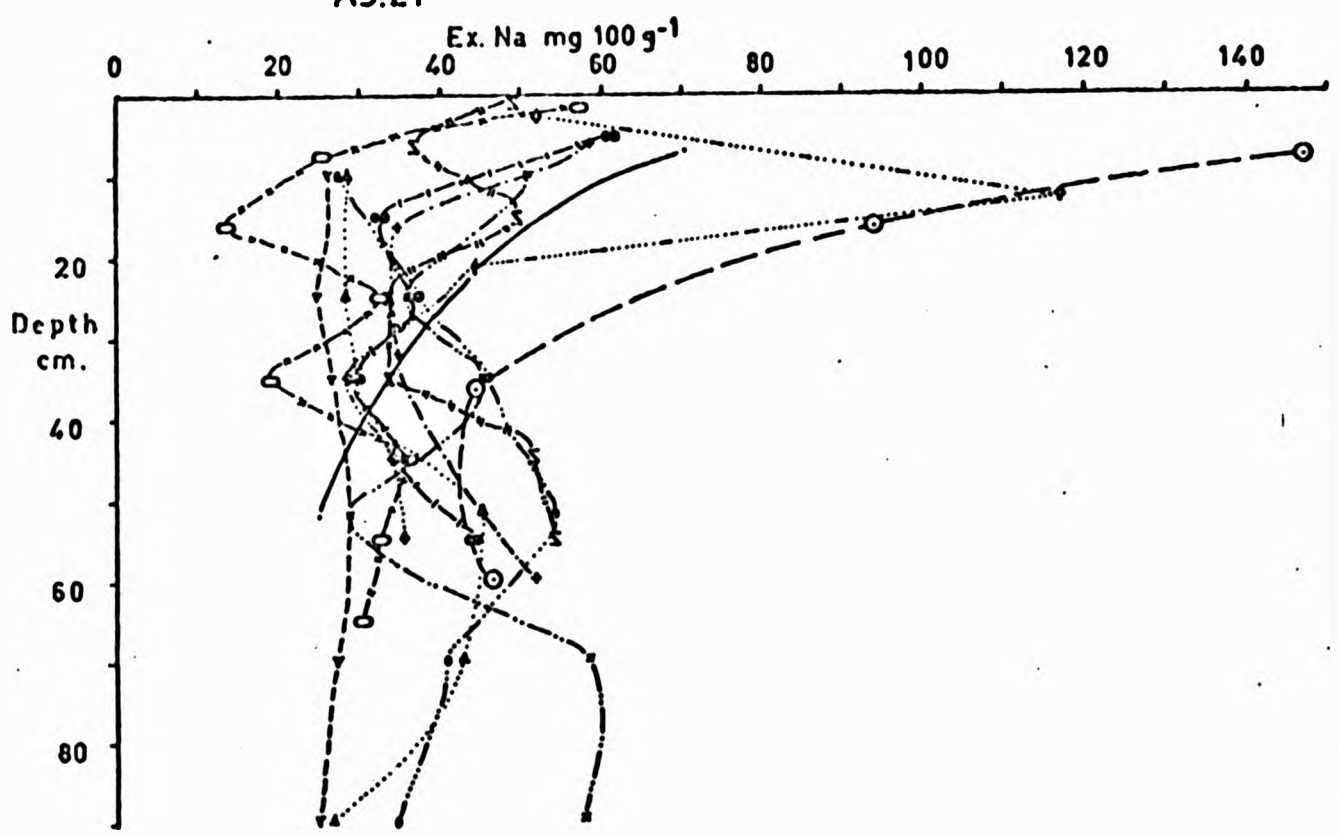
Ex. Na mg 100 g-1
0
20
40
60
80
100
120
140
Depth
cm.
20
40
60
80

A3.22

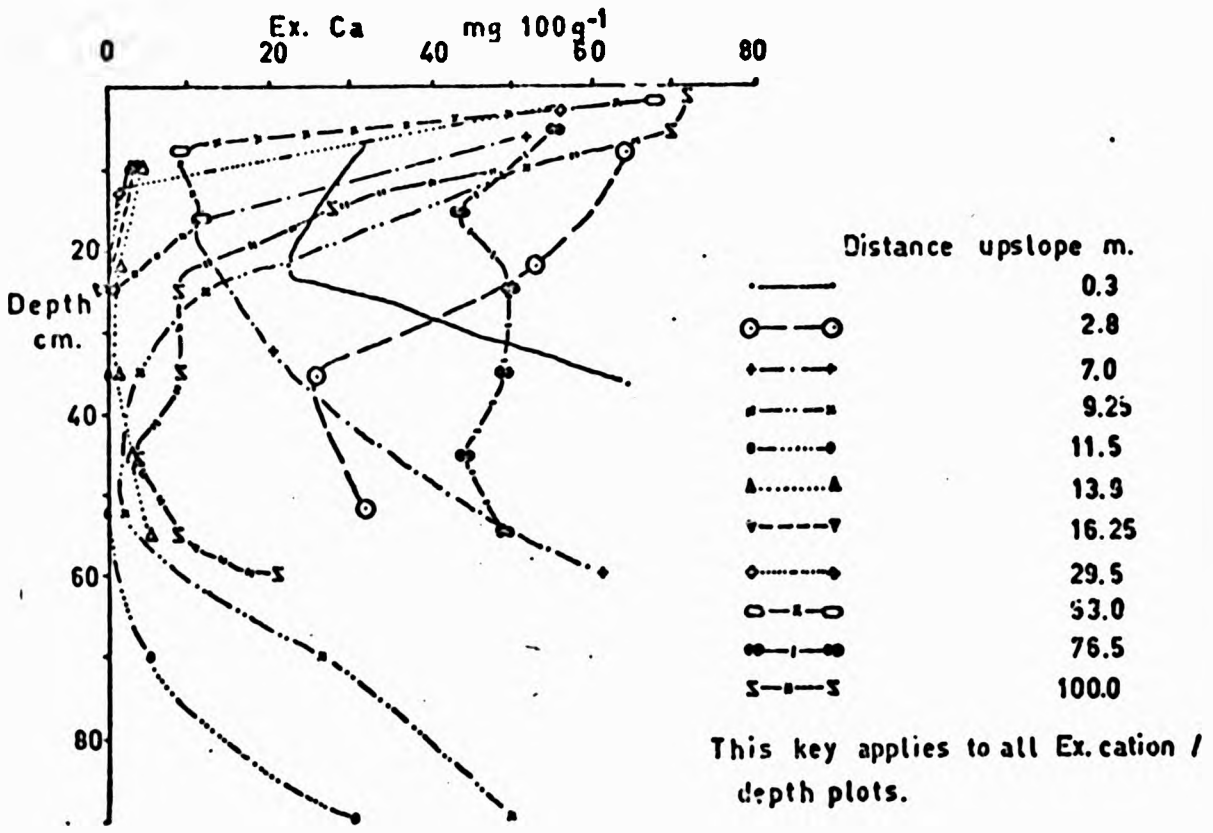
Ex. Ca mg 100g-1
0
20
40
60
80
Depth cm.
Distance upslope m.
0.3
2.8
7.0
9.25
11.5
13.9
16.25
29.5
53.0
76.5
100.0
This key applies to all Ex. cation / depth plots.

A3.23

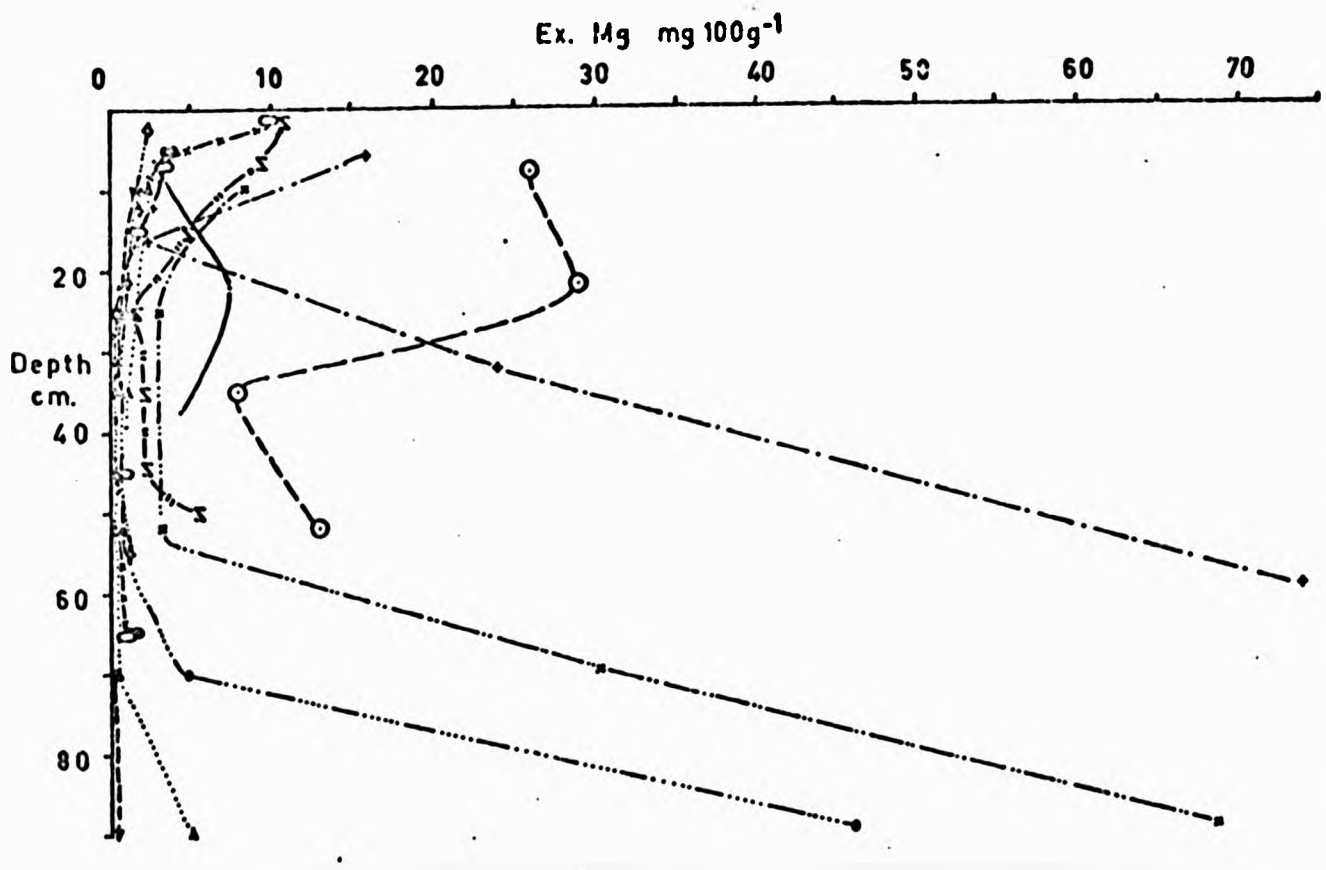
Ex. Mg mg 100g-1
0
10
20
30
40
50
60
70
Depth cm.
80

A3.24

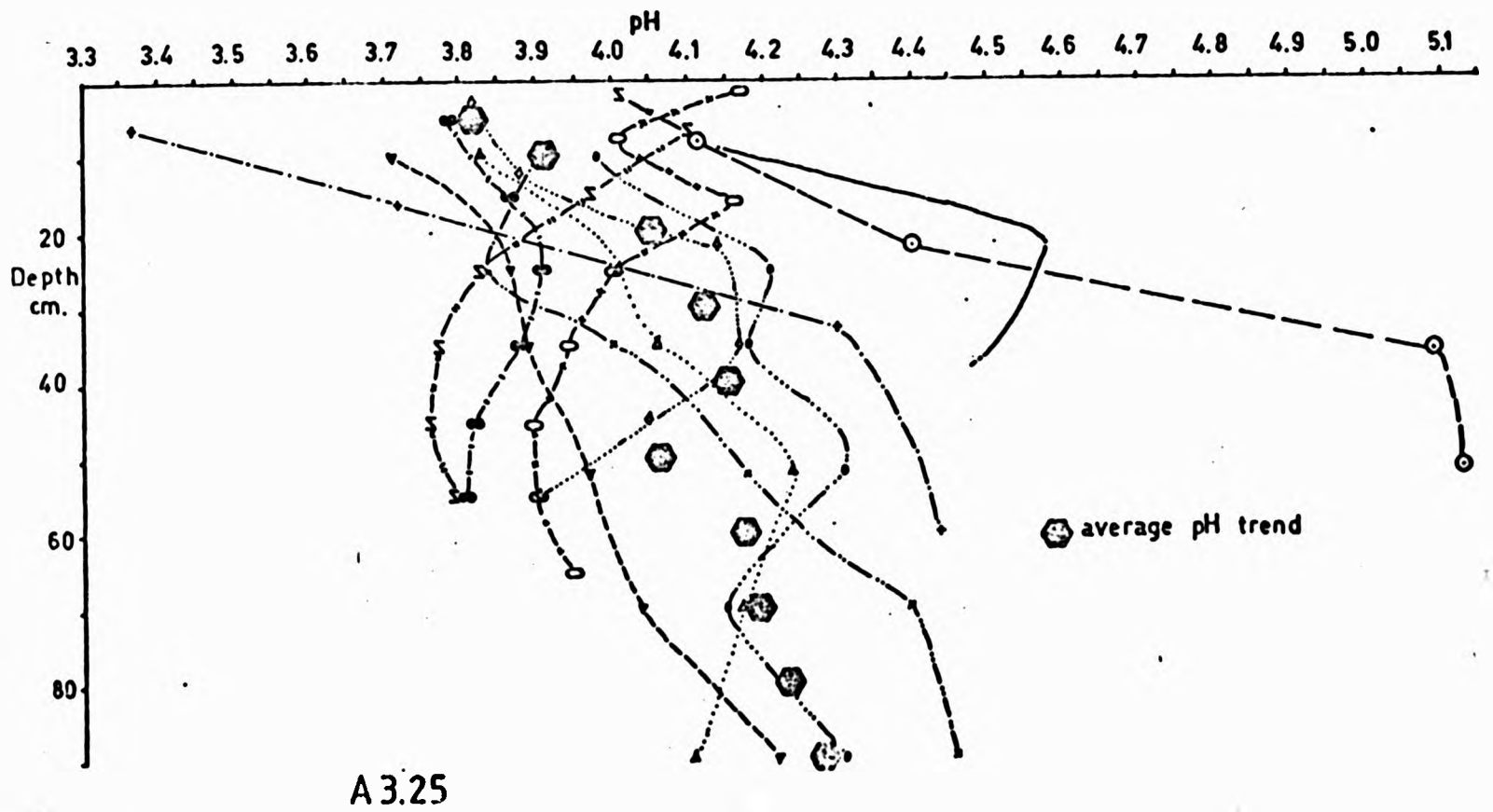
pH
3.3 3.4 3.5 3.6 3.7 3.8 3.9 4.0 4.1 4.2 4.3 4.4 4.5 4.6 4.7 4.8 4.9 5.0 5.1
Depth cm.
20
40
60
80
average pH trend

A 3.25

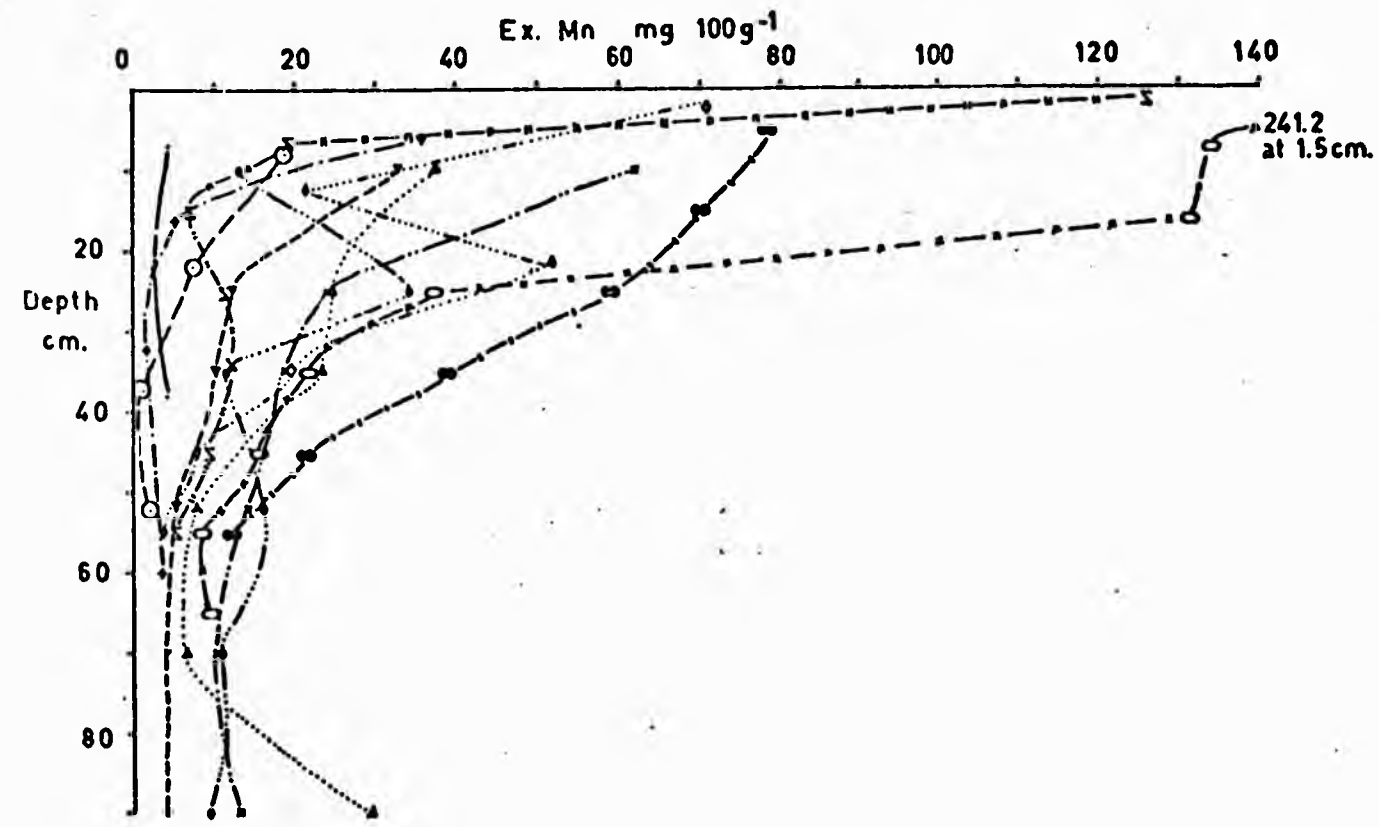
Ex. Mn mg 100g-1
0 20 40 60 80 100 120 140
241.2 at 1.5cm.
Depth cm.
20
40
60
80

A 3.26

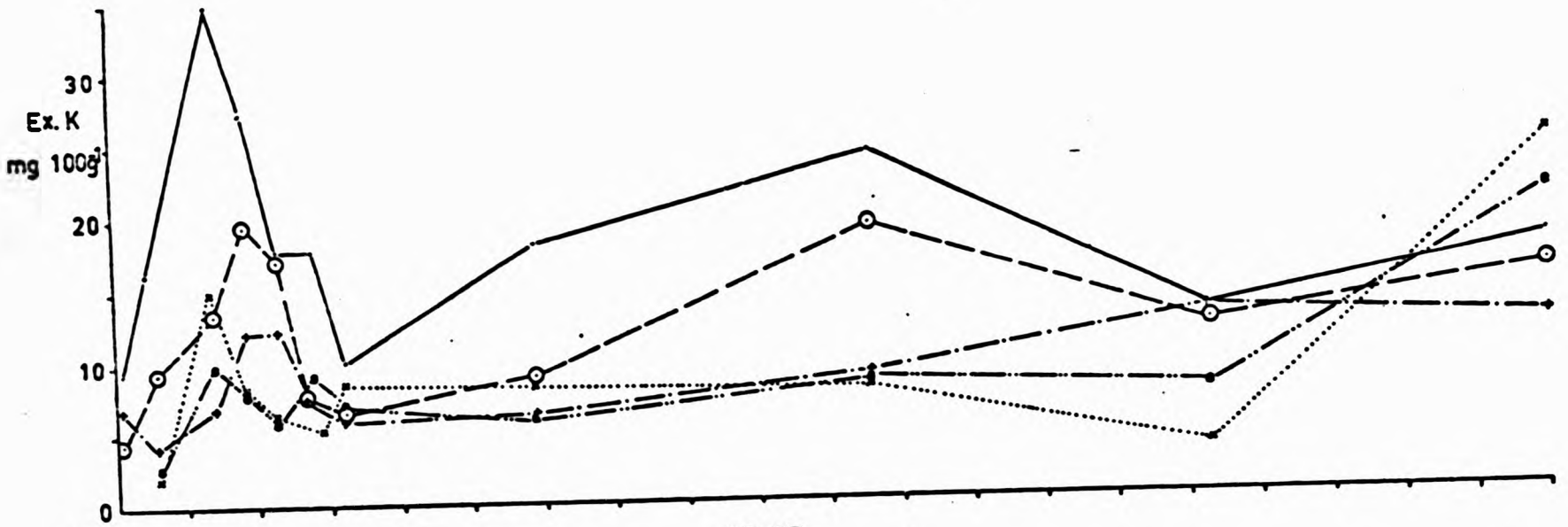
30
Ex. K
mg 100g⁻¹
20
10
0

A3.27

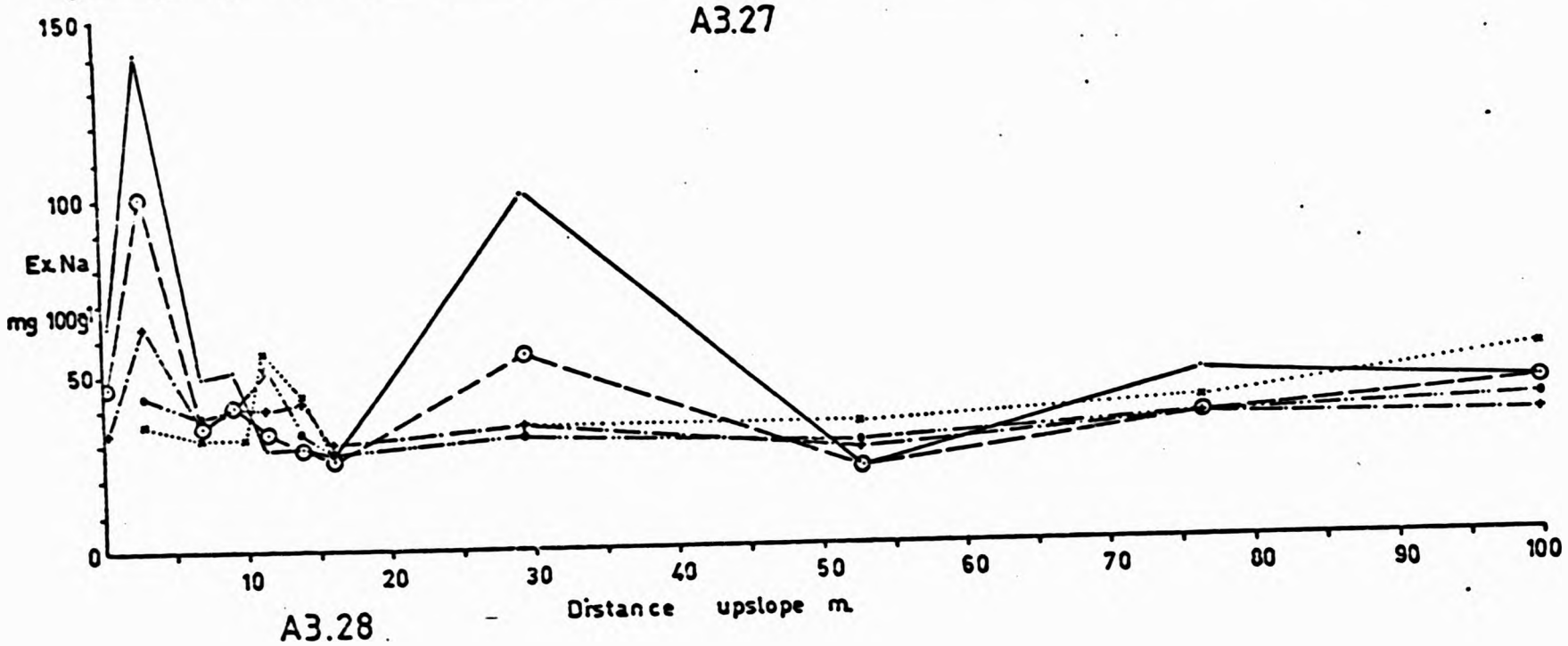
150
100
Ex. Na
mg 100g⁻¹
50
0
10
20
30
40
50
60
70
80
90
100
Distance upslope m.

A3.28

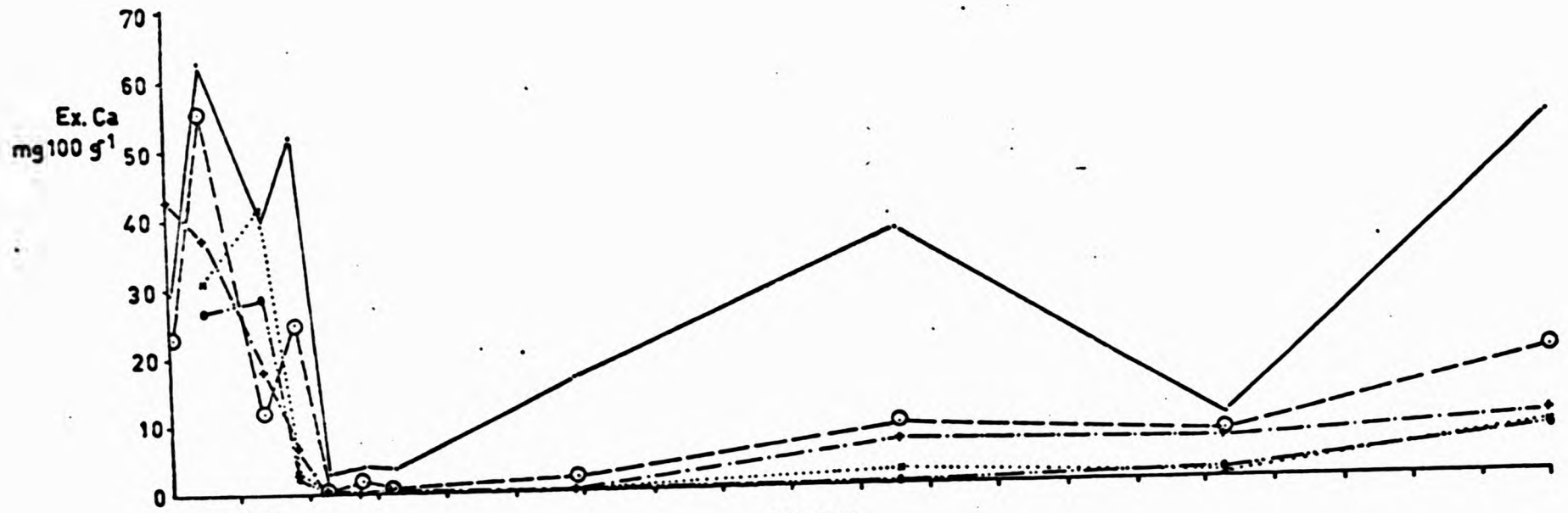
Ex. Ca
mg 100 g⁻¹
70
60
50
40
30
20
10
0

A3.29

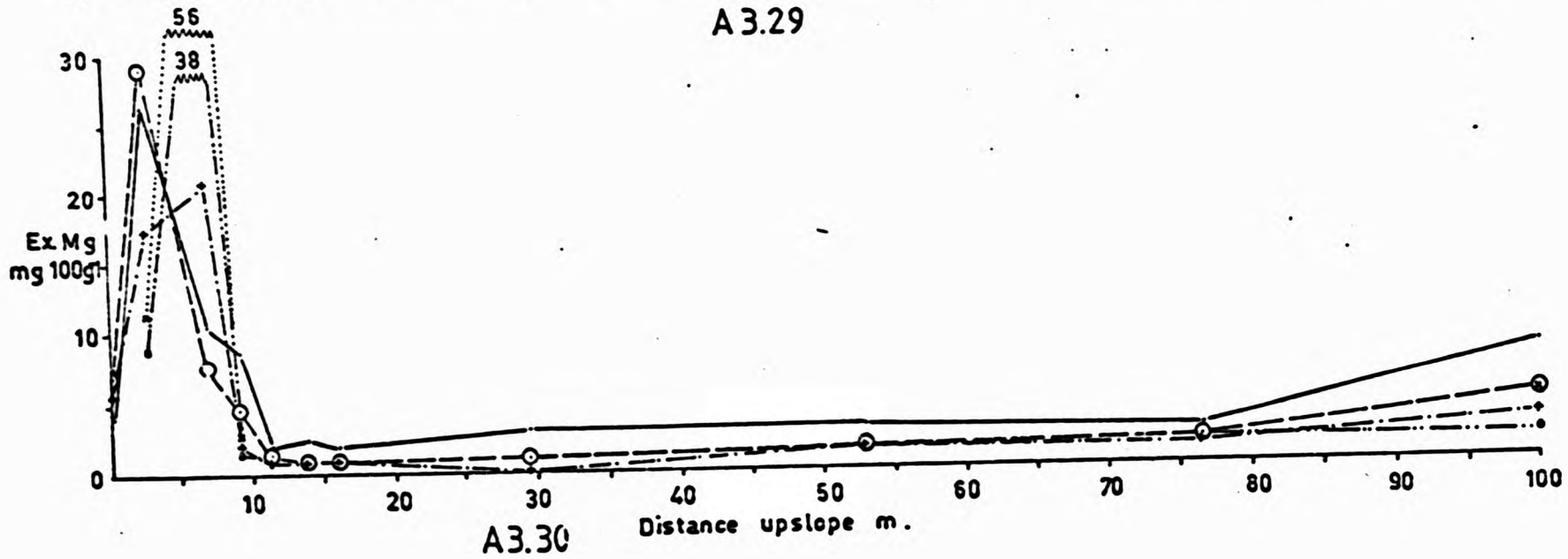
56
38
Ex Mg
mg 100g⁻¹
30
20
10
0
10
20
30
40
50
60
70
80
90
100
Distance upslope m.

A3.30

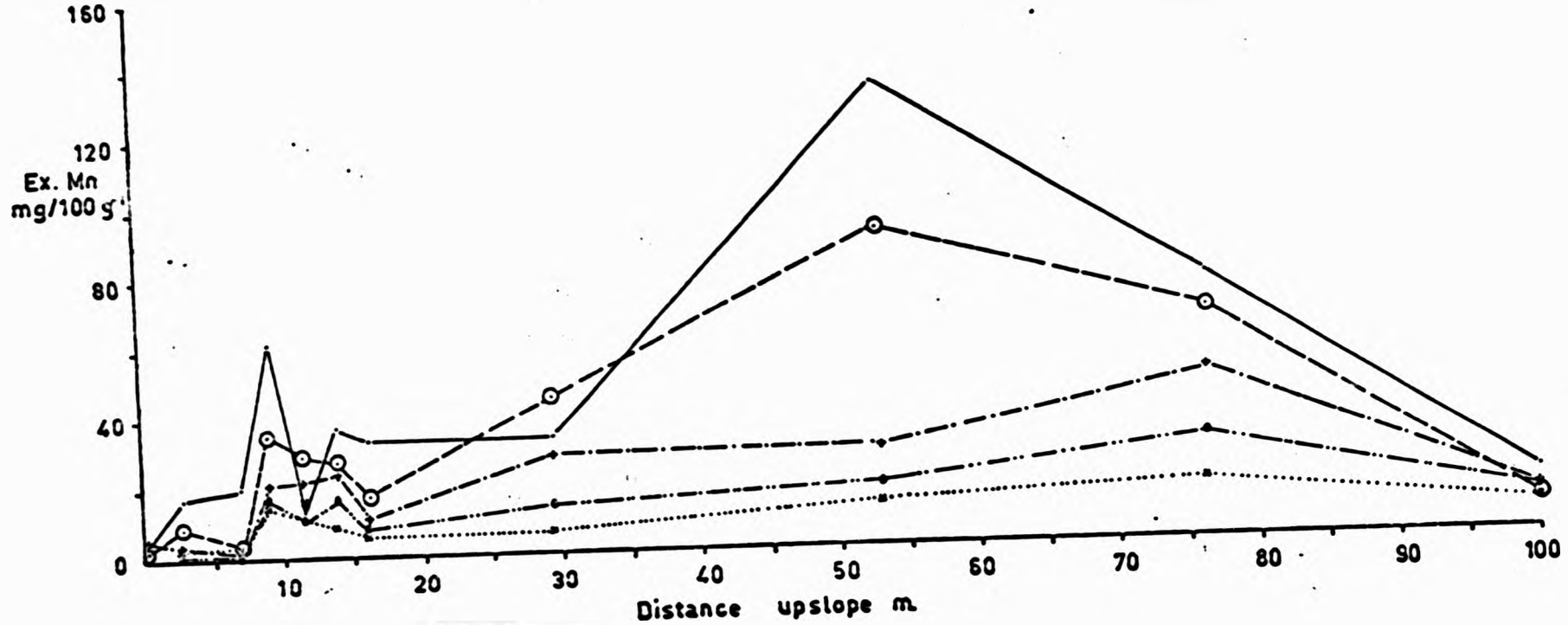
160
120
Ex. Mn
mg/100 g
80
40
0
10
20
30
40
50
60
70
80
90
100
Distance upslope m

A3.31

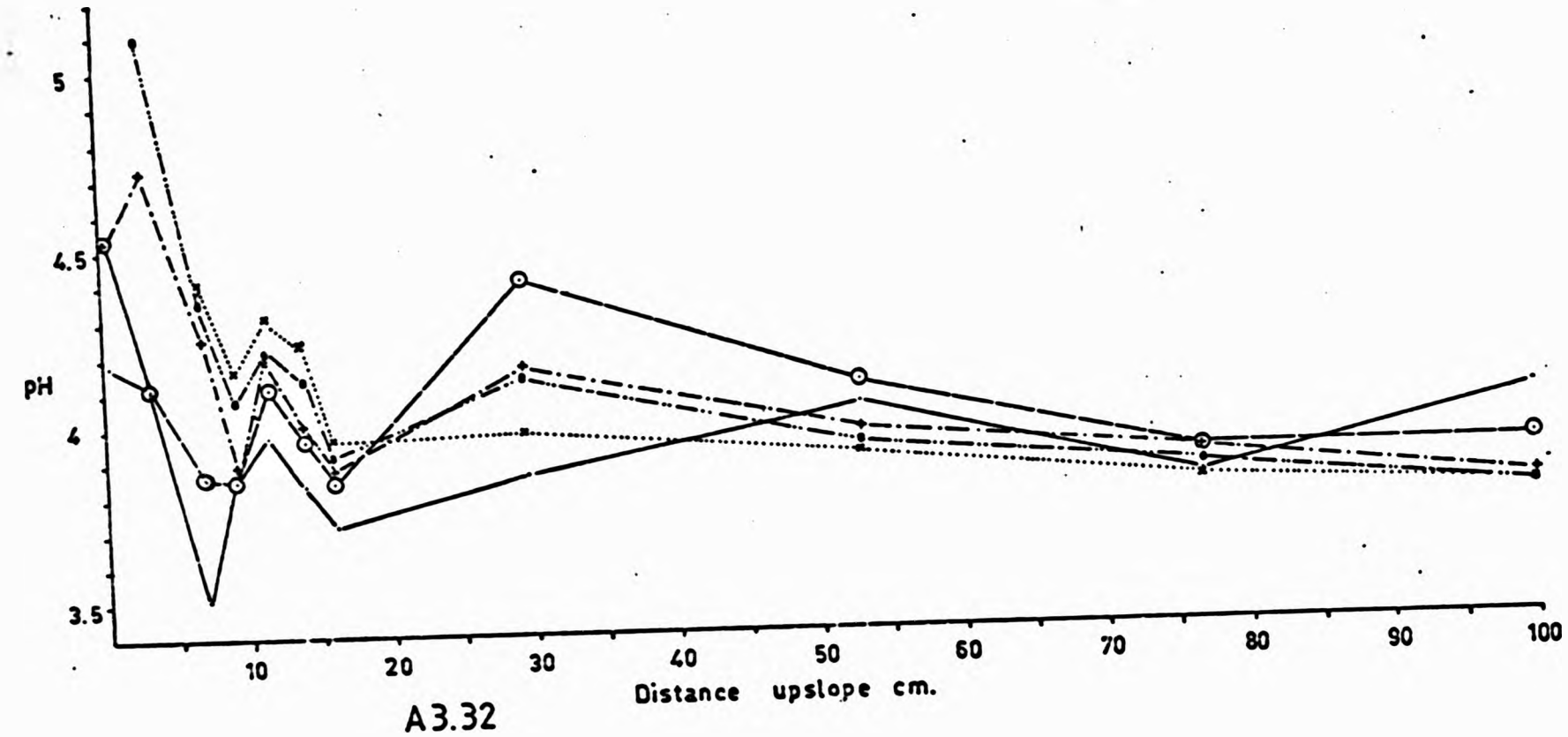

A3.32

APPENDIX 4:
DETAILS OF THE SCHEME FOR MOISTURE AND SOLUTE ACCOUNTING IN THE HILLSLOPE

The hillslope is divided into a series of boxes as shown in Figure 9.5 (repeated below), with the pit at the lowest box edge. Tension and solute concentration data is required for all boxes in the 6 x 9 array and moisture content for the inner 4 x 7 array. Additionally, the surface input fluxes, rainfall and the solute content of rainfall must also be known. The following symbols are used in outlining the method (see Figure 9.4 A, reproduced below):

A = element area, L^2

h = vertical distance between tensiometers, L

l = distance between tensiometers, sub-parallel to the slope, L

α = slope angle of upper element in each column, degrees

θ = soil moisture content at measurement point, L^3/L^3

H = height of vertical element boundary, L

L = length of element boundary sub-parallel to slope, L

Δt = time interval between readings $(t_2 - t_1)$, T

z = gravitational potential at measurement point, L

ψ = pressure potential at measurement point, L

ϕ = hydraulic potential at measurement point, L

$\bar{F}p$ = precipitation input to each element at the surface, L

$\bar{F}z_{1\Delta t}$ = down profile water flux into each element in Δt, $(= \bar{F}p$ for $i = 1)$, L^3/T

$\bar{F}x_{1\Delta t}$ = water flux from upslope into each element in Δt, L^3/T

$\bar{F}x_{2\Delta t}$ = water flux downslope from each element in Δt, L^3/T

$\bar{F}z_{2\Delta t}$ = water flux down profile from each element in Δt, L^3/T

$\bar{J}p$ = precipitation solute input to each element at the surface, W/L^3

$\bar{J}z_{1\Delta t}$ = down profile solute flux into each element in Δt, $W/L^2/T$

$\bar{J}x_{1\Delta t}$ = solute flux from upslope into each element in Δt, $W/L^2/T$

$\bar{J}x_{2\Delta t}$ = solute flux downslope from each element in Δt, $W/L^2/T$

$\bar{J}z_{2\Delta t}$ = solute flux down profile from each element in Δt, $W/L^2/T$

i = row notation

j = column notation

APPENDIX 4:

DETAILS OF THE SCHEME FOR MOISTURE AND SOLUTE ACCOUNTING IN THE HILLSLOPE

The hillslope is divided into a series of boxes as shown in Figure 9.5 (repeated below), with the pit at the lowest box edge. Tension and solute concentration data is required for all boxes in the 6 x 9 array and moisture content for the inner 4 x 7 array. Additionally, the surface input fluxes, rainfall and the solute content of rainfall must also be known. The following symbols are used in outlining the method (see Figure 9.4 A, reproduced below):

A = element area, L^2

h = vertical distance between tensiometers, L

l = distance between tensiometers, sub-parallel to the slope, L

α = slope angle of upper element in each column, degrees

θ = soil moisture content at measurement point, L^3/L^3

H = height of vertical element boundary, L

L = length of element boundary sub-parallel to slope, L

Δt = time interval between readings $(t_2 - t_1)$, T

z = gravitational potential at measurement point, L

ψ = pressure potential at measurement point, L

ϕ = hydraulic potential at measurement point, L

$\bar{F}p$ = precipitation input to each element at the surface, L

$\bar{F}z_1 \Delta t$ = down profile water flux into each element in Δt, $(= \bar{F}p$ for $i = 1)$, L^3/T

$\bar{F}x_1 \Delta t$ = water flux from upslope into each element in Δt, L^3/T

$\bar{F}x_2 \Delta t$ = water flux downslope from each element in Δt, L^3/T

$\bar{F}z_2 \Delta t$ = water flux down profile from each element in Δt, L^3/T

$\bar{J}p$ = precipitation solute input to each element at the surface, W/L^3

$\bar{J}z_1 \Delta t$ = down profile solute flux into each element in Δt, $W/L^2/T$

$\bar{J}x_1 \Delta t$ = solute flux from upslope into each element in Δt, $W/L^2/T$

$\bar{J}x_2 \Delta t$ = solute flux downslope from each element in Δt, $W/L^2/T$

$\bar{J}z_2 \Delta t$ = solute flux down profile from each element in Δt, $W/L^2/T$

i = row notation

j = column notation

Hydraulic potential for each element is:

$$\phi_{ij} = \psi_{ij} + z_{ij} \qquad (4\ i)$$

The water flux from upslope into each element is then:

$$\bar{F}x_{1,\ i+1,\ j+1}\Delta t = \Big\{\Big[\big((\phi_{i+1,\ j+2} - \phi_{i+1,\ j+1})/l_{i+1,\ j+1}\big)t_2 - \big((\phi_{i+1,\ j+2} - \phi_{i+1,\ j+1})/l_{i+1,\ j+1}\big)t_1\Big] \cdot \bar{F}z_{1\Delta t} \cdot H_{i+1} \cdot (\mathrm{Cos}\alpha_{j+1} - \mathrm{Cos}\alpha_{j+2})\Big\} \Big/ \Big\{\Big[\big((\phi_{i+1,\ j+1} - \phi_{i,\ j+1})/h_{i,\ j+1}\big)t_2 - \big((\phi_{i+1,\ j+1} - \phi_{i,\ j+1})/h_{i,\ j+1}\big)t_1\Big] \cdot 2 \cdot L_{j+1} \cdot \mathrm{Cos}\alpha_{j+1}\Big\} \qquad (4\ ii)$$

The flux downslope from each element is:

$$\bar{F}x_{2\ (i+1,\ j+1)}\Delta t = \Big\{\Big[\big((\phi_{i+1,\ j+1} - \phi_{i+1,\ j})/l_{i+1,\ j}\big)t_2 - \big((\phi_{i+1,\ j+1} - \phi_{i+1,\ j})/l_{i+1,\ j}\big)t_1\Big] \cdot \bar{F}z_{i,\ j+1\Delta t} \cdot H_i \cdot (\mathrm{Cos}\alpha_{j+1} - \mathrm{Cos}\alpha_{j+2})\Big\} \Big/ \Big\{\Big[\big((\phi_{i+1,\ j+1} - \phi_{i,\ j+1})/h_{i,\ j+1}\big)t_2 - \big((\phi_{i+1,\ j+1} - \phi_{i,\ j+1})/h_{i,\ j+1}\big)t_1\Big] \cdot 2 \cdot L_{j+1} \cdot \mathrm{Cos}\alpha_{j+1}\Big\} \qquad (4\ iii)$$

The flux down profile from each element is (from continuity):

$$\bar{F}z_{2\ i+1,\ j+1\Delta t} = \bar{F}x_{1\ i+1,\ j+1\ t} + \bar{F}x_{2\ i+1,\ j+1\Delta t} + \bar{F}z_{1\ i+1,\ j+1\Delta t}$$

$$- \left\{ \left(\theta_{i+1,\ j+1\ t_2} - \theta_{i+1,\ j+1\ t_1} \right) \right.$$

$$\left. \cdot\ H_{i+1} \cdot \mathrm{Cos}\alpha_{j+1} \cdot L_{i+1} \right\} \qquad (4\ \mathrm{iv})$$

Hydraulic conductivity for each element is:

$$K_{i+1,\ j+1\Delta t} = \bar{F}z_{i+1,\ j+1\Delta t} \Big/ L_{j+1} \cdot \mathrm{Cos}\alpha_{j+1} \cdot \Delta t$$

$$\cdot \left\{ \left[(\phi_{i+1,\ j+1} - \phi_{i,\ j+1}) \Big/ h_{i,\ j+1} \right]_{t_2} \right.$$

$$\left. - \left[(\phi_{i+1,\ j+1} - \phi_{i,\ j+1}) \Big/ h_{i,\ j+1} \right]_{t_1} \right\} \qquad (4\ \mathrm{v})$$

Downslope throughflow velocity is:

$$\bar{V}_{i+1,\ j+1\Delta t} = \bar{F}x_{2\ i+1,\ j+1\Delta t} \cdot 2 \ /\ H_{i+1,\ j+1}$$

$$\cdot\ (\mathrm{Cos}\alpha_{i+1,\ j+1} + \mathrm{Cos}\alpha_{i+1,\ j+1}) \cdot \Delta t \qquad (4\ \mathrm{vi})$$

Pit discharge is:

$$\bar{Q}_{\Delta t} = \left\{ \sum_{j=1}^{j=n} \sum_{i=2}^{i=2} Fx_{2ij\Delta t} \right\} / \Delta t \qquad (4\ \mathrm{vii})$$

The method for solute flux computation is the same but has an additional mass flow term. Thus, in equations (4 i - 4 iii) solute concentration, C, replaces hydraulic potential, ϕ, and solute flux from upslope into each element is:

The flux down profile from each element is (from continuity):

$$\bar{F}z_{2\ i+1,\ j+1\Delta t} = \bar{F}x_{1\ i+1,\ j+1\ t} + \bar{F}x_{2\ i+1,\ j+1\Delta t} + \bar{F}z_{1\ i+1,\ j+1\Delta t}$$

$$- \left\{\left(\theta_{i+1,\ j+1\ t_2} - \theta_{i+1,\ j+1\ t_1}\right)\right.$$

$$\left. \cdot\ H_{i+1} \cdot \mathrm{Cos}\alpha_{j+1} \cdot L_{i+1}\right\} \qquad (4\ \mathrm{iv})$$

Hydraulic conductivity for each element is:

$$K_{i+1,\ j+1\Delta t} = \bar{F}z_{i+1,\ j+1\Delta t} \Big/ L_{j+1} \cdot \mathrm{Cos}\alpha_{j+1} \cdot \Delta t$$

$$\cdot \left\{\left[(\phi_{i+1,\ j+1} - \phi_{i,\ j+1}) \Big/ h_{i,\ j+1}\right]_{t_2}\right.$$

$$\left. - \left[(\phi_{i+1,\ j+1} - \phi_{i,\ j+1}) \Big/ h_{i,\ j+1}\right]_{t_1}\right\} \qquad (4\ \mathrm{v})$$

Downslope throughflow velocity is:

$$\bar{V}_{i+1,\ j+1\Delta t} = \bar{F}x_{2\ i+1,\ j+1\Delta t} \cdot 2 \,/\, H_{i+1,\ j+1}$$

$$\cdot\ (\mathrm{Cos}\alpha_{i+1,\ j+1} + \mathrm{Cos}\alpha_{i+1,\ j+1}) \cdot \Delta t \qquad (4\ \mathrm{vi})$$

Pit discharge is:

$$\bar{Q}_{\Delta t} = \left\{ \sum_{j=1}^{i=n} \sum_{i=2} Fx_{2ij\Delta t} \right\} / \Delta t \qquad (4\ \mathrm{vii})$$

The method for solute flux computation is the same but has an additional mass flow term. Thus, in equations (4 i - 4 iii) solute concentration, C, replaces hydraulic potential, ϕ, and solute flux from upslope into each element is:

$$\bar{J}x_{1\ i+1,\ j+1\,\Delta t} = D_1 + \left\{\bar{F}x_{1\ i+1,\ j+1\,\Delta t} \cdot \left[\left(C_{i+1,\ j+1\ t_2} + C_{i+1,\ j+1\ t_1}\right)/2\right]\right\} \quad (4\ viii)$$

where D_1 is the RHS of equation (4 ii), but with C substituted for ϕ.

Solute flux downslope from each element is:

$$\bar{J}x_{2\ i+1,\ j+1\,\Delta t} = D_2 + \left\{\bar{F}x_{2\ i+1,\ j+1\,\Delta t} \cdot \left[\left(C_{i+1,\ j+1\ t_2} - C_{i+1,\ j+1\ t_1}\right)/2\right]\right\} \quad (4\ ix)$$

where D_2 is the RHS of equation (4 iii), but with C substituted for ϕ.

The down profile flux from each element is:

$$\bar{J}x_{2\ i+1,\ j+1\,\Delta t} = \bar{J}x_{1\ i+1,\ j+1\,\Delta t} + \bar{J}x_{2\ i+1,\ j+1\,\Delta t} + \bar{J}z_{1\ i+1,\ j+1\,\Delta t} - \left\{\left(C.\theta_{i+1,\ j+1\ t_2} - C.\theta_{i+1,\ j+1\ t_1}\right) \cdot H_{i+1} \cdot \cos\alpha_{j+1} \cdot L_{i+1}\right\} \quad (4\ x)$$

The dispersion coefficient is:

$$D^*_{i+1,\ j+1\,\Delta t} = \left\{\bar{J}x_{1\ i+1,\ j+1\,\Delta t} - \left[\bar{F}x_{1\ i+1,\ j+1\,\Delta t} \cdot \left((C_{i+1,\ j+1\ t_2} + C_{i+1,\ j+1\ t_1})/2\right)\right]\right\} \Big/ L_{i+1,\ j+1} \cdot \cos\alpha_{i+1,\ j+1} \cdot \Delta t \cdot \left\{\left((C_{i+1,\ j+1} - C_{i+1,\ j+1})/h_{i,\ j+1}\right) - \left((C_{i+1,\ j+1} - C_{i.\ j+1})/h_{i,\ j+1}\right)\right\} \quad (4\ xi)$$

Throughflow solute discharge to the pit is:

$$\bar{J}_{q\,\Delta t} = \left\{ j = 1 \sum_{i=2}^{i=n} \bar{J}x_{2ij\Delta t} \right\} \Big/ \Delta t \qquad (4\ \text{xii})$$

The concentration of this solution is:

$$\bar{C}_{\Delta t} = \bar{J}_{q\Delta t} \Big/ \bar{Q}_{\Delta t}$$

It is implicitly assumed that the "source-sink" term in equation (9.31), i.e. $f(c)_{x,\ z}$, is incorporated in the solute storage change term of equation (4 x), although in a pure simulation model this function would require specification.

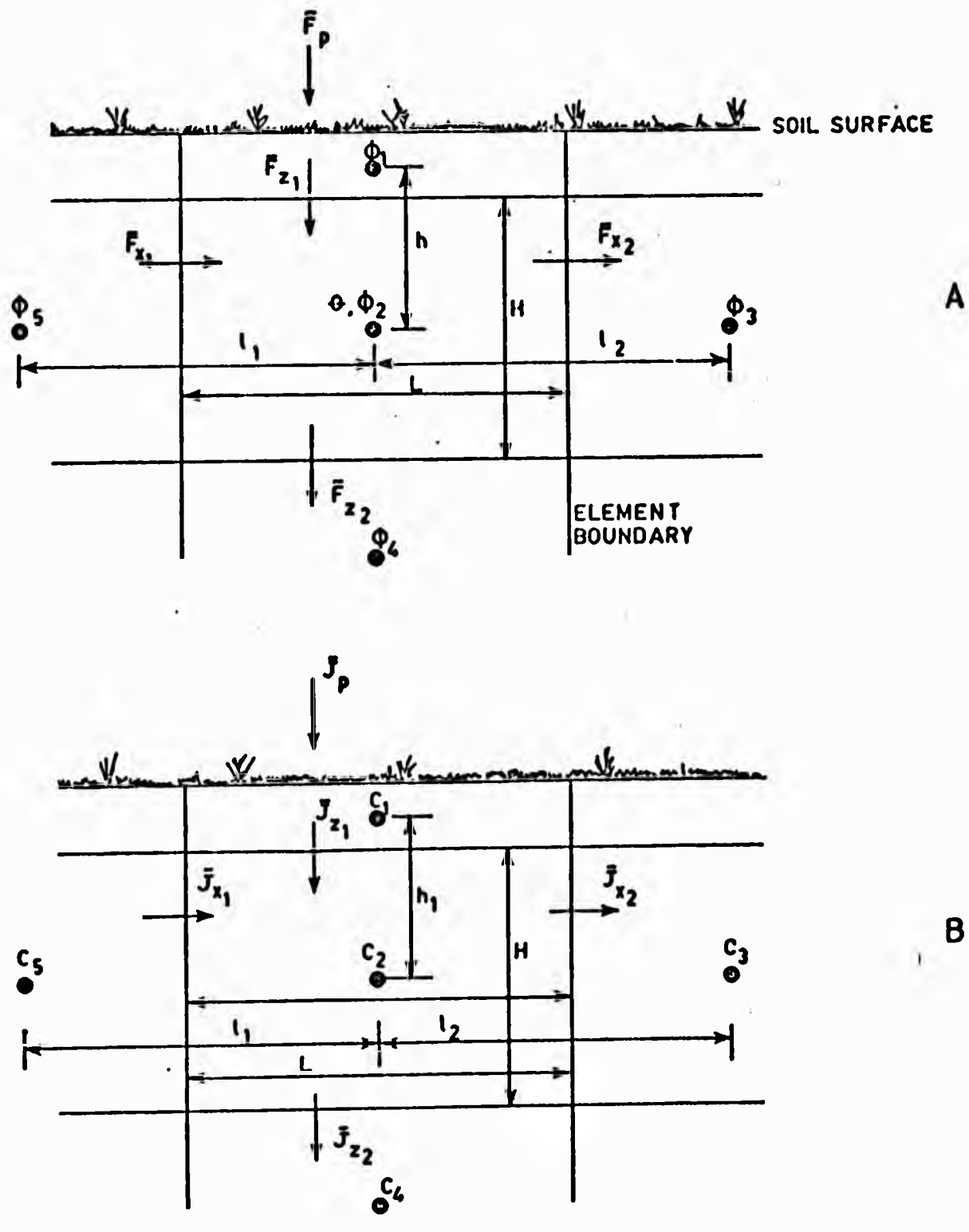

FIGURE 9.4: SINGLE HILLSLOPE ELEMENTS FOR COMPUTATION OF (A) WATER, AND (B) SOLUTE FLUX (see text for definition of terms)

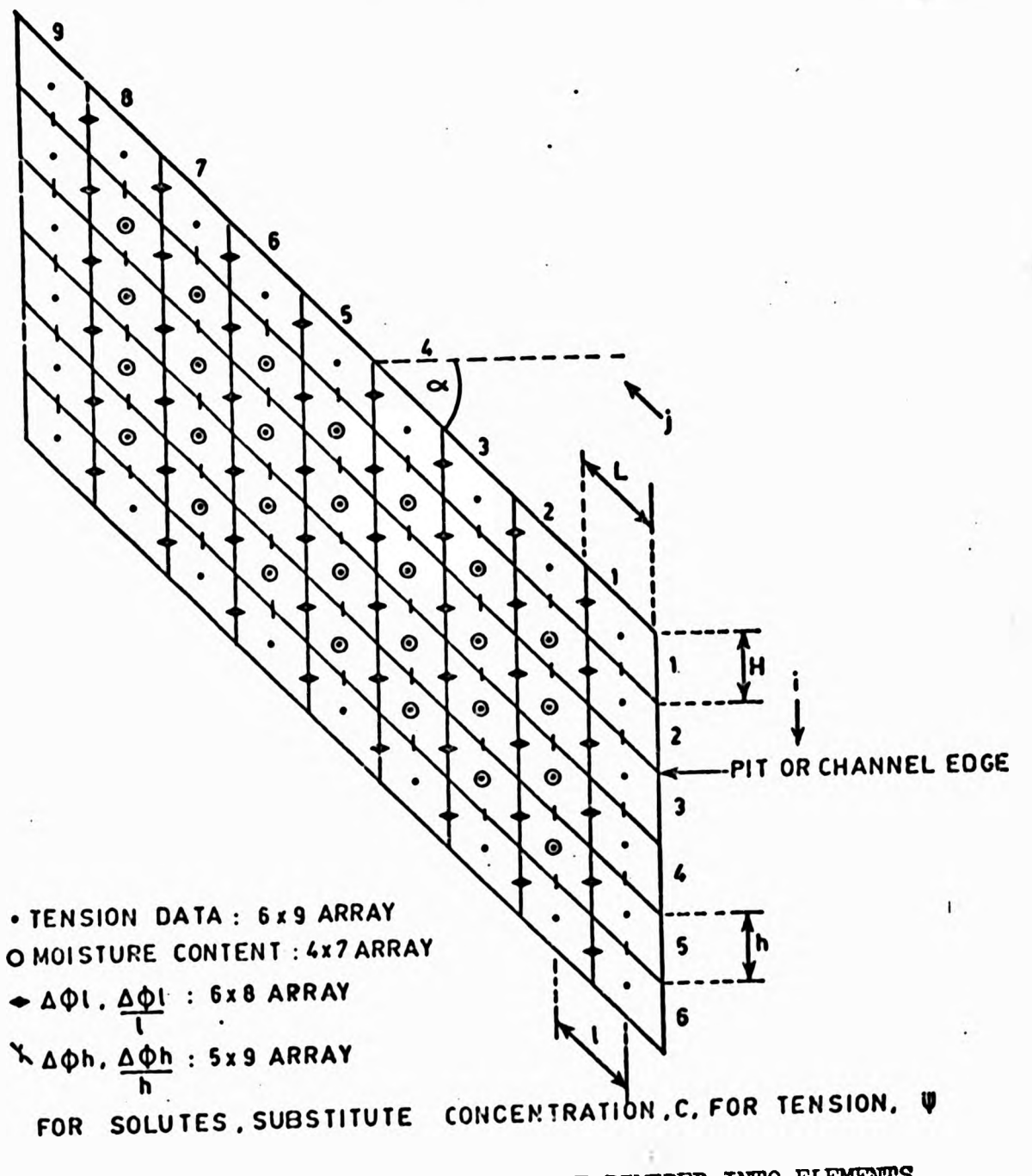

FIGURE 9.5: SCHEMATIC DIAGRAM OF A HILLSLOPE DIVIDED INTO ELEMENTS AND SUITABLE FOR FLUX COMPUTATION

APPENDIX 5:

PUBLISHED PAPER

TIGHTLY

BOUND

COPY

The
South Hampshire Geographer

Vol. 8 1976

The Journal of the Department of Geography
Portsmouth Polytechnic

SOLUTE VARIATIONS IN A LOCAL CATCHMENT

Gerald Spriggs B.A., Dip.Hydrol.

Introduction

The behaviour of the dissolved constituents occurring naturally in streamwater is studied for several reasons.

An understanding of the variation in 'background water quality' (Webb and Walling, 1974), i.e. the chemistry of streamwater uncontaminated by pollutants, is important in water resources planning. Inter-catchment transfer during periods of low flow, for example, implies the mixing of waters of different chemical content. The effects on freshwater ecology might be significant where a considerable dilution or concentration occurs.

Land management practices may have a significant effect on river water quality, especially in lowland Britain; for example, fertilizers applied to agricultural land during periods when the soil is at field capacity may enter and pollute streams during storms.

Separation of stream baseflow from storm runoff when establishing rainfall-runoff relationships is usually achieved by arbitrary procedures, for example, Hewlett and Hibbert (1967) project a line from the start of the hydrograph rise at a slope of 0.55 litres/hour/Km^2 to intersect the hydrograph recession limb. The area above the line is an estimation of the volume of rapid storm runoff or 'quickflow', while that below the line is the groundwater or 'delayed flow' contribution to the hydrograph. By studying the chemical variations in streamwater over a period of time and applying a mixing-model,

$$Q_{DF} = ((C_{TR} \cdot C_{QF}) / (C_{DF} - C_{QF}))\, Q_{TR} \qquad (1)$$

where $Q_{TR} = Q_{DF} + Q_{QF}$.

and Q_{TR} = total runoff, C_{TR} = Solute concentration of total runoff,
Q_{DF} = delayed flow, C_{DF} = Solute concentration of delayed flow
Q_{QF} = quickflow, C_{QF} = Solute concentration of quickflow,

both the delayed flow and quickflow components of the hydrograph can be determined (Pinder and Jones, 1969). To solve the mass-balance equation, it is necessary to estimate the chemical composition of the delayed flow and quickflow components. The solute concentration of delayed flow is determined from total runoff during baseflow; the chemical concentration of quickflow is estimated from samples of total runoff collected from selected locations in a catchment during peak discharge periods.

Recent work has shown that solutional loss may exceed sediment loss in the total denudation of many catchments, and points to the significance of water chemistry for the geomorphologist (Walling and Troake, 1973). In the present study emphasis is being placed upon the collection of water chemistry data for testing hydro-chemical models of slope erosion. Carson & Kirkby (1973 p 242) proposed the model where p is the amount of oxide present as a proportion (by substance) of the unweathered

$$\frac{-dp}{-dt} = k.\frac{dq_z}{dx}.p \qquad (2)$$

material, t is time elapsed, k is the solubility for the oxide, x is the distance downslope and qz is the water discharge through unit cross-section of the soil. This model is being

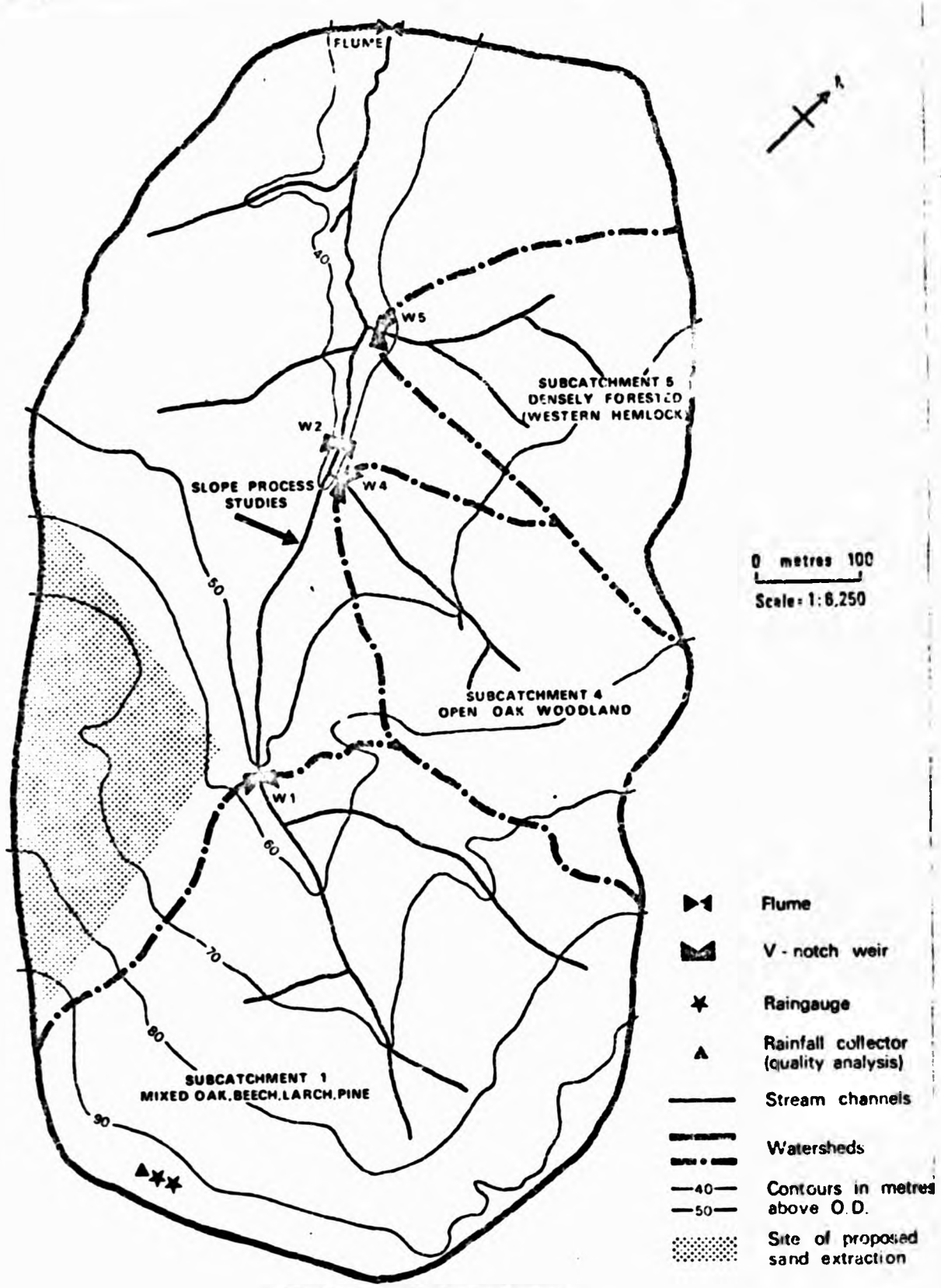

Fig. 1 West Walk Catchment

tested by, firstly, monitoring the composition of stream and soil waters and comparing them with the rocks from which they flow, and, secondly, by examining the evolution of parent materials into sub-soils by weathering.

The Catchment

Attention has been focussed on a small (0.61 Km^2) wooded catchment tributary to the R.Meon. The upper part of the catchment is composed of Bagshot Sands (40% total area) which provide a small aquifer and contribute baseflow. A transition takes place between Bagshot Sands and London Clay (60% total area) in the lower part of the basin. The sands form podzols of the Shirrell Heath Series (Kay, 1939) grading via soilwater gleys (Titchfield Series) into surface water gleys (Swanmore Series) on the London Clay. Geology and soils are significant in determining the hydrological and hydrochemical response of the catchment. Discharge from the relatively impervious clay is rapid while that from the sands is delayed due to the longer percolation time. The layout of instruments in the catchment is shown in Figure 1. Division into sub-catchments is on the basis of slope experiments and tree species and density (e.g. subcatchment 5 is vegetated by dense western Hemlock, while subcatchment 1 is young, open oak.).

Water Sampling and Analysis

Stream discharge is calculated for each gauging station using rating equations. Sampling interval is an important consideration since changes in solute are complex during storms (Walling, 1975). Water samples have been collected during individual storms at 30 minute intervals and weekly intervals during the period of summer baseflow. These were analysed initially for 6 ionic species: Ca^{+2}, Mg^{+2}, Na^{+1}, K^{+1}, HCO_3^{-1} and Cl^{-1}. Subsamples are stored under refridgeration for analysis as further techniques are developed. Emphasis has been placed upon the use of atomic absorption spectrometry for analysing Ca^{+2}, Mg^{+2}, Na^{+1} and K^{+1}, since this is a rapid method where a large number of samples were involved. HCO_3^{-1} was determined by titrating with HCl and Cl^{-1} using a mercuric nitrate titration (Golterman and Clymo, 1969). Further analysis is to be carried out by spectrometry for silicon, manganese and iron using direct methods and sulphate, phosphate and nitrate using indirect techniques.

Results and interpretation

Although sampling has to date been limited to a seven month period (March-September 1975) a complex picture of the behaviour of ions in streamwater is emerging. The details are best considered under 3 headings.

1 Response of ionic species

The inverse relationship between stream discharge and certain solute levels is well documented (e.g. Eden, 1970) and can be attributed to the dilution of ion-rich baseflow during high flows. Figure 2 shows this response for Ca^{+2}, Mg^{+2}, Na^{+1} and Cl^{-1} during a small winter storm of 11.0 mm rainfall, K^{+1} exhibits a positive relationship with discharge, a trend also demonstrated by Walling (1975). The concentration of K^{+1} ions in 'aqueous' solution decreases by a process of cation exchange as waters percolate through clay minerals to the stream. This tendency for absorption increases with increasing atomic number (thus absorption intensity $Na^{+1} < Mg^{+2} < K^{+1}$) and depends upon the type of clay mineral. Rapid throughflow or overland flow reduces the time available for exchange and allows K^{+1} in the upper soil horizons to be leached and carried into the stream. It is also interesting to note that for the storm

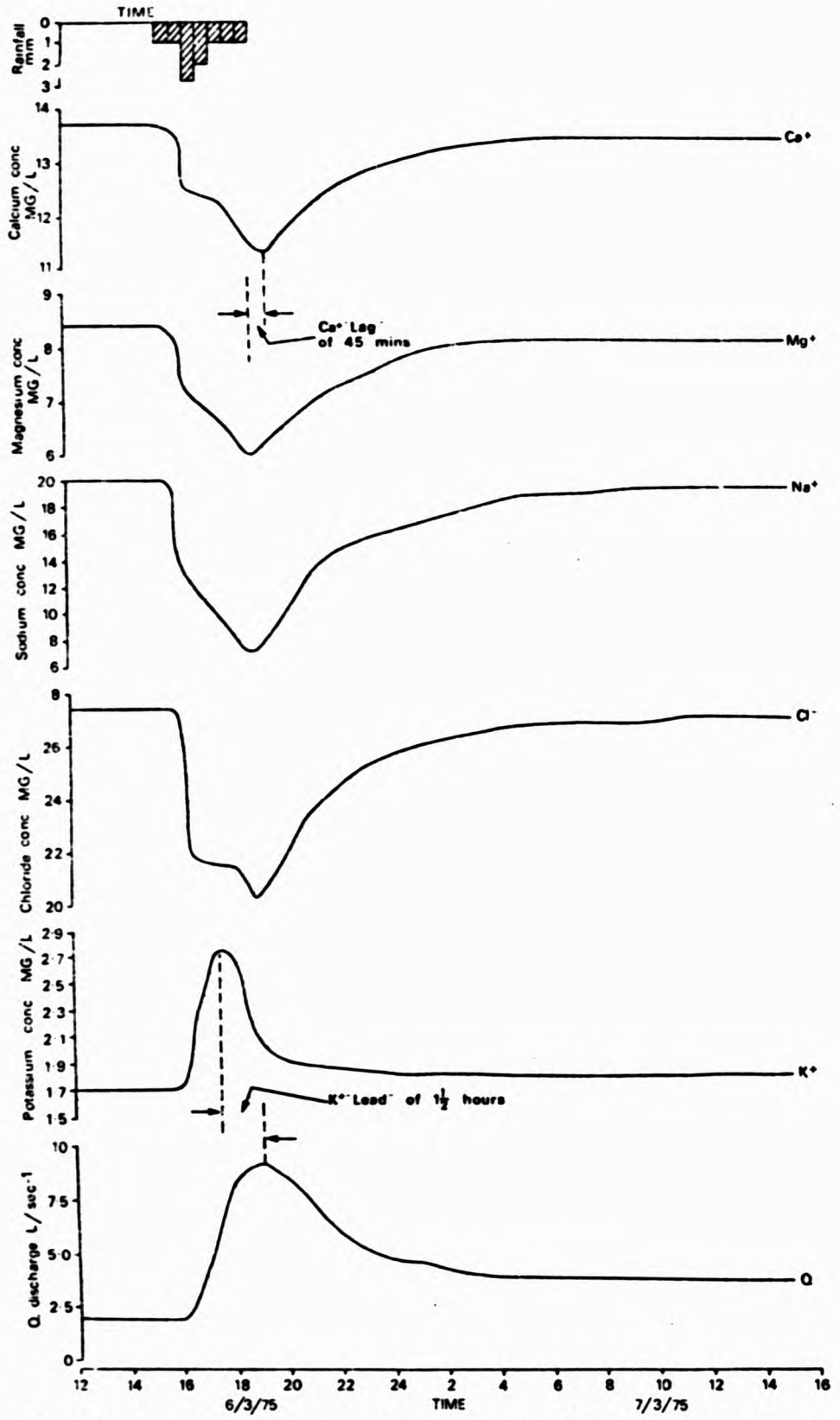

Fig. 2 The behaviour of calcium, magnesium, sodium, chloride and potassium during a small winter storm.

shown in Figure 2, changes in solute concentrations are more sensitive to changes in rainfall intensity than to variations of stream discharge.

2 Flushing effects

While those ionic species mentioned above exhibit consistent dilution trends for most of the year (concentration trend for K^{+1}) detailed sampling during autumn storms shows a marked increase in concentration at the beginning of the hydrograph as a result of the flushing of accumulated readily soluble material. The 'Chemograph' reaction for such an occasion follows the sequence:-

i initial fall in concentration coinciding with a rise in discharge,
ii sudden rise in concentration, followed by a fall to the preceding level,
iii gradual return to pre-storm concentrations,
iv dilution without or with a reduced flushing effect for any subsequent storms, suggesting a considerable depletion of the exchangeable ions by the first storm 'event'.

Figure 3 shows this sequence for data collected at Weir 2 and the flume for a storm during September 1975. Calcium shows an interesting reaction, with an initial dilution followed by two high magnitude flushes. There are two possibilities in explaining this dual flushing effect.

i At the catchment scale it may represent the arrival of separate Ca^{+2} pulses from areas with different water residence times. For example, because sub-catchment 5 is densely vegetated, water will take longer to reach the stream channel, although solute concentrations may be higher due to the longer residence time and leaching of accumulated nutrients on the forest floor. Automated sampling at all weirs would isolate sub-catchments with potentially different flow-through times and help locate the source of solutes.

ii By examining the changing nature of soil water flow during a stream and relating this to vertical variations of exchangeable ions in the soil profile it might be possible to explain the timing of solute flushes in streamwater. Figure 4 shows variations in the exchangeable cations Mg^{+2}, Ca^{+2}, Na^{+1} and K^{+1} with profile depth for a soil-water gley sampled during October 1974, the period of the year when flushing effects are most pronounced. High Ca^{+2} in the upper 10 cm is unusual but probably represents residual concentrations from the forest floor prior to de-forestation.

It is convenient at this point to consider a working model for the movement of water and chemicals in the soil. The three most important factors in formulating such a model are soil structure and chemistry and the behaviour of soil water. To simplify conditions in this particular case soil conditions are held constant and soil moisture movement is varied. Thus for a soil-water gley there are fissures between soil peds which expands and contract according to the moisture status; these will be considerably wider in summer than in winter. Individual peds contain micro-pores and root tubes surrounded by clay. Clearly the rate of flow through fissures $\gg$ micropores $\gg$ clay. This division can be visualized occurring through depth and an attempt made to superimpose patterns of water movement upon the structure (Figure 5). Assuming the soil is saturated in an upward direction according to Weyman's model (Weyman, 1973)

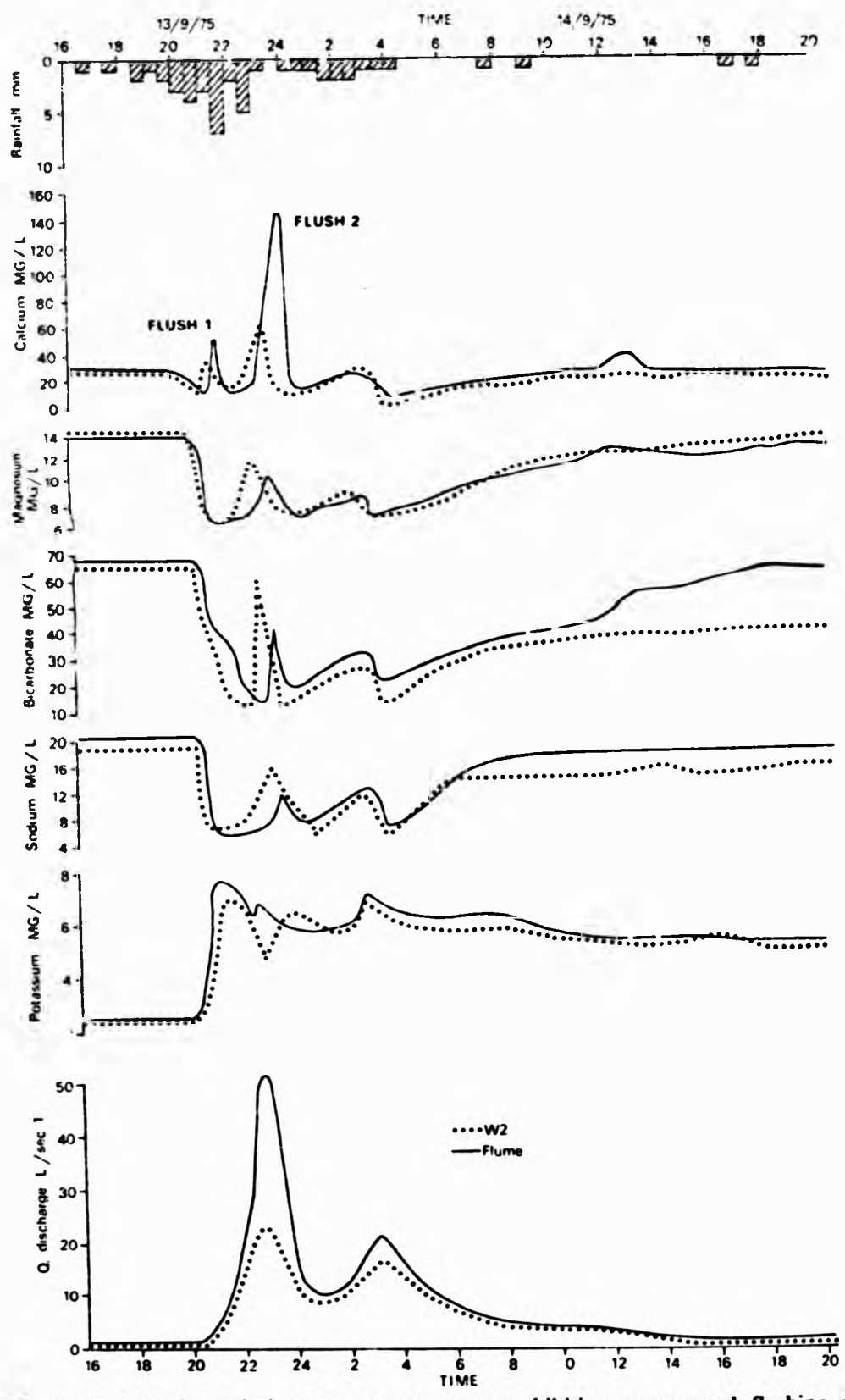

Fig. 3 Ionic behaviour during an autumn storm exhibiting pronounced flushing effects

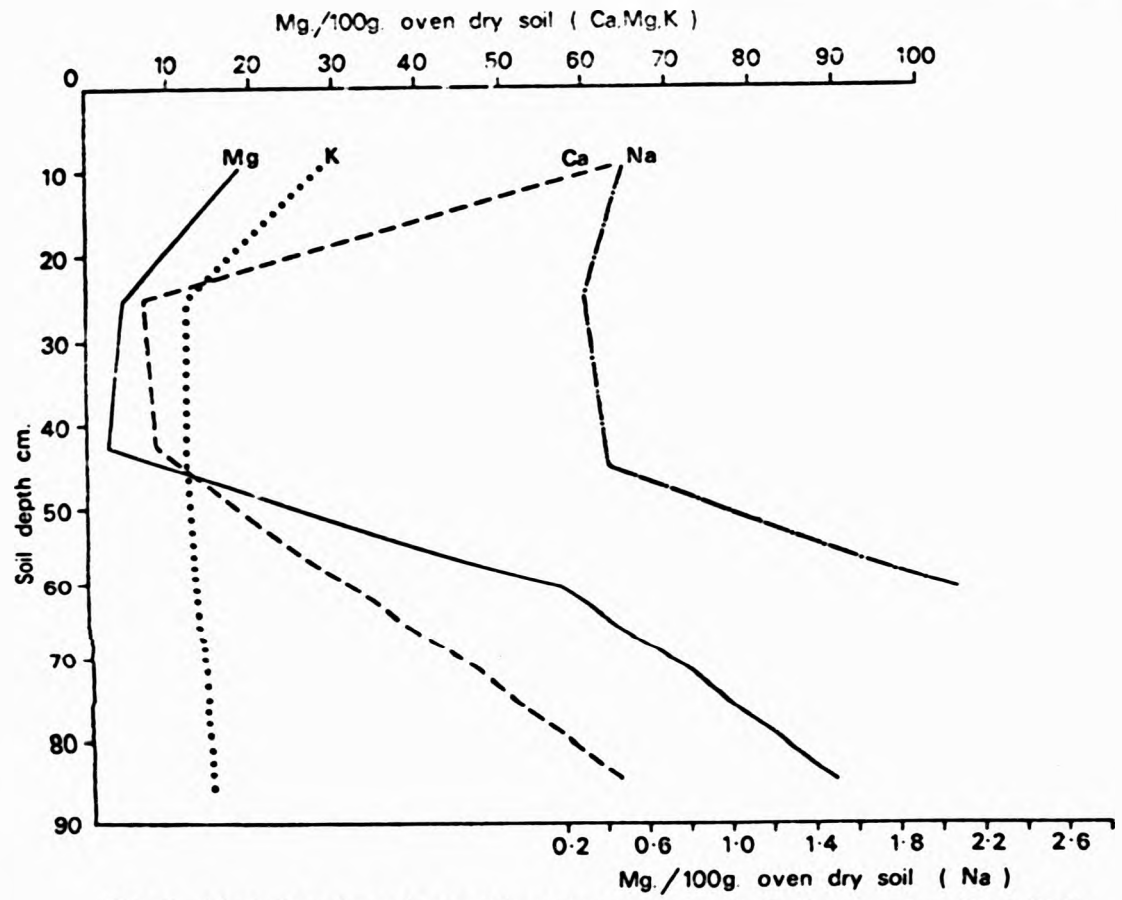

Fig. 4 Variations in exchangeable cations with depth. Soil water gley, West Walk

(this assumption seems justified since the surface infiltration capacity of the soil preceding the storm shown in Figure 3 was too high to permit the generation of infiltration - excess overland flow (Horton, 1945) under the observed rainfall conditions) then the sequence depicted in Figure 5 may be expected to occur as follows:-

i Rapid transmission of water to the base of the soil profile and stream channel via the fissure system. As the residence time is short and the available cations in the fissure system few, a dilution of streamflow occurs.

ii Water percolating more slowly through the intra-ped micropore system has a longer residence period which allows solution of available cations. Transfer of this water to the fissure system in the A horizon and flushing into the stream quickly follows. This explains the first flush of Ca^{+2} and K^{+1} in Figure 3.

iii As the storm proceeds the water table rises occupying all 3 systems and allowing ion-rich waters from the intro-ped micropores and clay to enter the fissure system. This gives the main flushes of Na^{+1}, Mg^{+2} and HCO_3^{-1} and the second flush of Ca^{+2}.

After the cessation of rainfall dilution by fissure flow is slowly replaced by a rise in concentration and domination of the intra-ped micropore and clay systems.

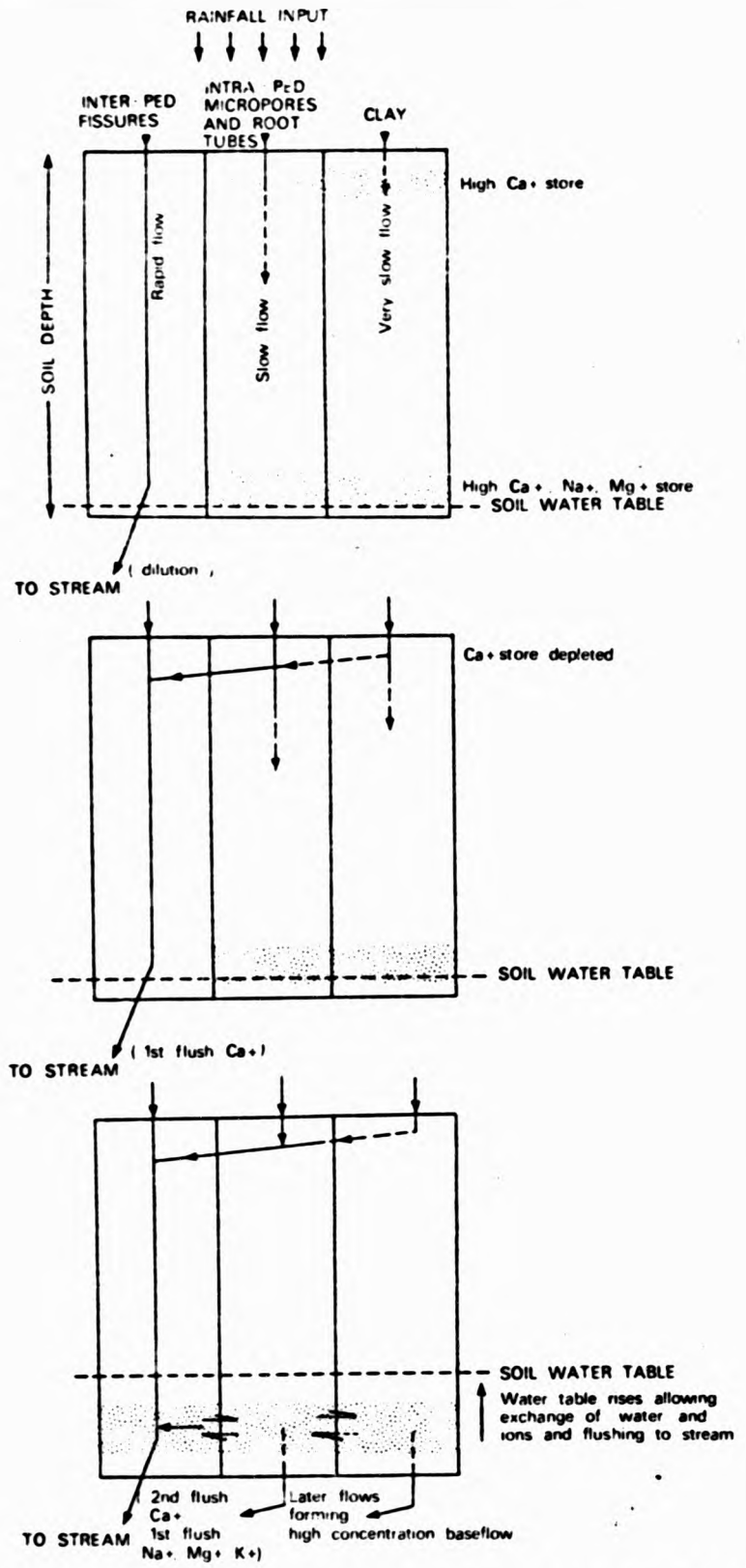

Fig. 5 A working model for the movements of water and chemicals in the soil

This model is dependent upon knowledge of the state of soil water within the system,a phenomenon requiring careful monitoring. Soil chemistry shows considerable spatial and probably temporal variation. The need for a closer study of these phenomena to test the model sequence is being met within the catchment by detailed slope instrumentation.

3 Lead and Lag effects

Close study of a number of hydrographs and their associated chemographs shows the dilution trough of the chemograph to lead, coincide with or lag behind the peak discharge. If the relationship between discharge and concentration is plotted on logarithmic scales then a concentration lead gives an anti-clockwise loop, concentration/discharge coincidence gives a straight line and a concentration lag gives a clockwise loop (Figure 6). Thus lead and lag effects, by creating hysteresis loops, introduce variance into the relationship between discharge and concentration.

Glover and Johnson (1974) have shown that the concentration lag-effect can be explained by kinematic wave theory. Because a flood wave travels at the wave velocity, which is greater than the mean water velocity, there is a lag in the arrival of dilute surface runoff water behind the rise in stage at the catchment outflow. This lag time is longer for small rises because their speed of travel down the channel is slower. Walling and Foster (1965) have shown by multiple regression techniques that the lag-effect is strongly influenced by seasonality and antecedent moisture conditions in addition to storm magnitude.

The lead effect is more difficult to interpret; it may represent the rapid input of low solute content overland flow as intense rain falls on a saturated soil or possibly the effect of channel precipitation. Lead and lag effects are also shown in Figure 2.

Solute - Discharge Relationships and their Applications

Relationships between chemical concentration and stream discharge and chemical load (the product of concentration and discharge) and discharge have been widely reported.

Steel (1968) in the U.S.A. and Edwards (1973a) in Britain both fitted a curve of the form

$$c = aQ^b$$

$$C = \text{concentration (mg/litre)}$$

$$Q = \text{discharge } (m^3/sec) \qquad (3)$$

$$a,b = \text{constants}$$

with varying degrees of success. Steele obtained consistent results with correlation coefficients ranging from -0.48 (SO_4^{-2}) to -0.97 (Na^{+1}). Edwards analysed 10 dissolved constituents in 3 Norfolk rivers and obtained correlation coefficients ranging from zero (Cl^{-1}) to +0.89 (NO_3^-). Results confirm that complex controls act upon individual ion concentrations and underline the need for a more realistic model incorporating seasonal (i.e. 'flushing', and variable lag and lead times) and antecedent effects (i.e. the pattern of preceding rainfall or runoff).

Leadbetter and Gloyna (1964) went part of the way toward this by building a model for

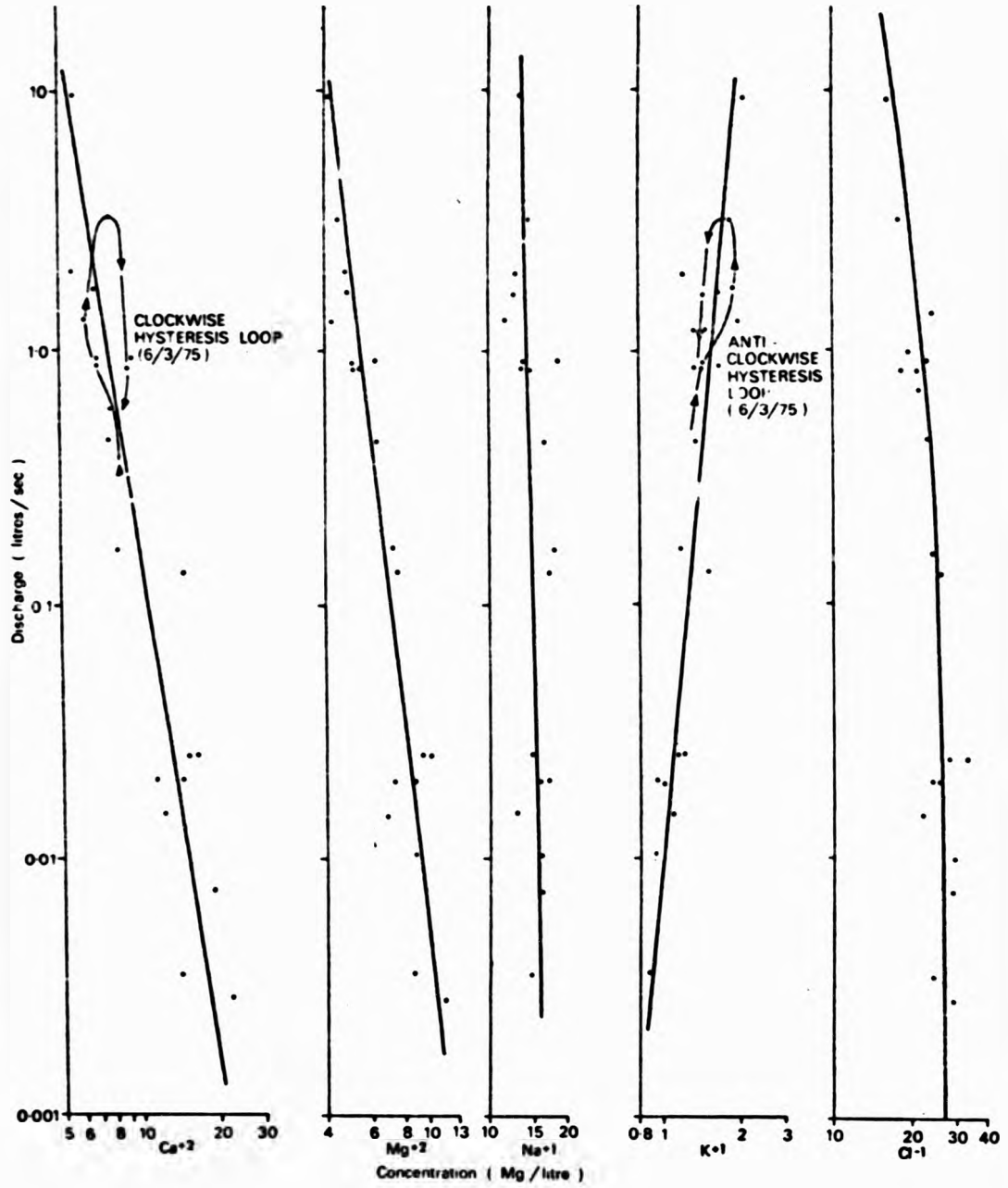

Fig. 6 Regression lines and hysteresis loops for concentration and discharge (Subcatchment 1).

predicting water quality from discharge data. Finding both 1st and 2nd order polynomials inadequate they fitted the relationship

$$C = aQ^{(f + g\log Aq + hQ^n)}$$

where Aq=30 day antecedent flow index $\sum_{k=1}^{i=30} Q_i/i$

a, f, g, h and n are constants, which resulted in an improved prediction of water quality.

Despite the small sample size, equation (3) was fitted to data for subcatchment 1. The results were presented graphically in Figure 6 and numerically in Table 1.

Table 1

Regression Equations and Correlation Coefficients for Concentration and Discharge

Ion	Equation	r	r^2	N	
Ca^{+2}	$C = 7.607Q^{-0.156}$	0.904	0.818	21	*
Mg^{+2}	$C = 5.441Q^{-0.111}$	0.921	0.847	20	*
Na^{+1}	$C = 14.091Q^{-0.017}$	0.327	0.107	20	
K^{+1}	$C = 1.519Q^{-0.097}$	0.874	0.763	19	*
Cl^{-1}	$\log C = \log 1.429 + 0.030 \log Q - 0.020 \log Q^2$	0.836	0.699	22	*

C=concentration (mg/litre); Q=discharge (litres/sec); L=Load (mg/sec); r=correlation coefficient; r^2=coefficient of determination; N=sample size; *= significant at the 0.1% level.

The plot of Cl^{-1} concentration against discharge is best fitted by a quadratic, the slope of the regression time decreasing with discharge. All constituents except Na^{+1} are significantly correlated with discharge, the value of r^2 giving the proportion of variance in concentration explained by variance in discharge. Hysteresis loops superimposed upon plots of Ca^{+2} and K^{+1} show how lag and lead effects introduce variance into the relationship. More pronounced scatter due to flushing effects is absent because of the lack of autumn samples for subcatchment 1. A comparison of correlation coefficients for data at Weir 2 shows the proportion of variance introduced by autumn flushing

effects. For the Ca^{+2} discharge relationship, including autumn samples, r=-0.606 (r^2=0.367); excluding autumn samples r=-0.975 (r^2=0.950). The poor fit of the geometric regression for Na^{+1} against discharge prompted an investigation of multiple regression techniques. It was thought that the introduction of an antecedent precipitation index (API) and a season index might help to explain variance due to the lag effect. A 30 day API was calculated by $API_{30} = \sum_{t=1}^{30} \frac{1}{t} P$, where P = precipitation on a day t before the point of calculation.

The season index was calculated by Sin Day (Radians) = (2IID)/365, where D = day of the year starting with January 1st. The multiple regression equation obtained was log C = log 1.263 - 0.003 log API_{30} + 0.168 Sin D - 0.076 log Q, with a coefficient of multiple correlation of 0.993. This result again points to the importance of other controls when formulating predictive models. Such a relationship, although significant at the 0.1% level, should be treated with caution because of the small sample size.

Edwards (1973b) used the relationship between load and discharge ($L=aQ^b$, where L = load in mg/sec) to estimate the amount of catchment erosion. In a forest ecosystem nutrient budgets may be calculated in a similar way by measuring meteorological inputs and hydrological outputs (Bormann and Likens, 1970). A sample balance sheet for subcatchment 1 is given in Table 2. This was compiled using the load-discharge equations of Table 3. The significance of the correlation coefficient should be treated with caution since Q occurs on both sides of the equation. Dissolved contents of rainfall were measured for bulk weekly samples taken from an exposed site at the catchment head. These probably underestimate the ground-level concentrations because further nutrients are dissolved as the water passes through the vegetation cover. Ca^{+2}, Mg^{+2}, Na^{+1} and K^{+1} all show a net loss for the period, reflecting the high base-exchange capacity of the soil.

Table 2

Sample Chemical Balance Sheet for Subcatchment 1, 3/3 - 10/3/1975 (Values in Grams)

Constituent	Input	Output	Net loss/Gain
Ca	756	1988	−1232
Mg	437	2087	−1650
Na	1310	4697	−3387
K	190	824	−634
Cl	14,351	7817	+6534

Table 3

Regression Equations and Correlation Coefficients for Load and Discharge

Ion	Equation	r	r^2	N	
Ca^{+2}	$L = 7.319Q^{0.832}$	0.996	0.991	21	*
Mg^{+2}	$L = 6.025Q^{0.900}$	0.994	0.988	20	*
Na^{+1}	$L = 12.51Q^{0.938}$	0.991	0.981	20	*
K^{+1}	$L = 1.483Q^{1.090}$	0.999	0.997	19	*
Cl^{-1}	$L = 21.206Q^{0.939}$	0.999	0.997	22	*

C = Concentration (mg/litre); Q = discharge (litres/sec); L = Load (mg/sec); r = correlation coefficient; r^2 = coefficient of determination; N = sample size; * = significant at the 0.1% level

The large net gain of Cl^{-1} can be accounted for by the near coastal location. It has been shown that sea salt is the principal source of both Cl^{-1} and Na^{+1} (Paterson and Scorer, 1975). If the ratio Cl^{-1}/Na^{+1} in seawater (1.80) were duplicated in precipitation, this would suggest a single source (i.e. the sea). For the period 3/3 – 10/3/1975 the ratio was 10.95, implying either an additional land source, e.g. local vegetation, or sample contamination. The ratio was always above 1.80, ranging from 2.6 (24/3 – 31/3/1975) to 24.82 (10/5 – 17/5/1975), showing an upward trend as summer progressed. This suggests that airborne dust becomes a more important constituent of rainfall during dry summer conditions.

The above discussion draws only upon a small portion of the data collected so far for two reasons. Firstly, sampling is still in progress to cover the complete range of seasonal controls influencing solute response in streamwater. Secondly, the modelling of solutes in streamwater using rating techniques treats the area between basin input and output as a 'black–box', ignoring processes operating in soil and groundwater. Work is in progress to study simultaneously these processes in the field with the aim of producing a physicaliy more realistic model of solute response. Such a model is essential for the solution of equations (1) and (2), discussed in the introduction.

Acknowledgements
I wish to thank Dr. D.N. Mottershead and Mr. B. Sprunt for reading the first draft of this paper, and Mrs. J. Brady for help with laboratory analysis.

References

Bormann F H & G E Likens (1970) 'The Nutrient Cycles of an Ecosystem', *Scientific American*, 92-101
Carson M A & M J Kirkby (1972) *Hillslope Form and Process*, C.U.P., 475
Edwards A M C (1973a) 'The Variation of Dissolved Constituents with Discharge in some Norfolk Rivers', *J. Hydrol*, 18, 219-242
Edwards A M C (1973b) 'Dissolved Load and Tentative Solute Budget of some Norfolk Catchments', *J. Hydrol* 18, 201-217
Glover B J & P Johnson (1974) 'Variations in the Natural Chemical Concentration of River Water during Flood Flows and the Lag Effect', *J. Hydrol* 22, 303-316

Golterman H & R S Clymo (Eds) (1969) *Methods for the Chemical Analysis of Freshwater*, IBP, handbook No. 8

Hem J D (1970) *Study and Interpretation of the Chemical Characteristics of Natural Water*, U.S. Geol Surv. Water Supply Paper 1973

Hewlett J D & A R Hibbert (1967) 'Factors Affecting the Response of Small Watersheds to Precipitation in Humid Areas', In: W E Sopper & H W Lull (Eds), *International Symposium on Forest Hydrology*, Pergamon, Oxford, 725-736

Horton R E (1945) 'Erosional Development of Streams and their Drainage Basins - Hydrophysical Approach to Quantitative Morphology', *Bull. Geol. Soc. Amer.* 56, 275-370

Kay F F (1939) *A Soil Survey of the Strawberry district of South Hampshire* Dept. of Agric. Chemist Univ. of Reading, Bulletin L11

Ledbetter J O & E F Gloyna (1964) 'Predictive Techniques for Water Quality Inorganics', *J. Sanit. Eng. Div. Proc. Amer. Soc. Civ. Engs.*, SA 1, 127-151

Paterson M P & R S Scorer (1975) 'The Chemistry of Sea Salt Aerosol and its Measurement', *Nature*, 254, 491-495

Pinder G F & J F Jones (1969) 'Determination of the Groundwater Component of Peak Discharge from the Chemistry of Total Run off', *Water Resources Res*, 5 (2), 438-445

Steel T D (1968) Digital Computer Application in Chemical-Quality Studies of Surface Water in a Small Watershed', *Int. Assoc. Sci. Hydrology* Pub. No. 80, 203-214

Walling D E (1975) 'Solute Variations in Small Catchment Streams: Some Comments', *Trans I.B.G.*, 64, 141-147

Walling D E & I D L Foster (1975) 'Variations in the Natural Chemical Concentration of River Water during Flood Flows, and the Lag Effect: Some Further Comments', *J. Hydro*, 26, 237-244

Walling D E & R P Troake (1973) 'The Natural History of Slapton Ley Nature Reserve. VII', *Field Studies*, 3 (5), 719-740

Webb B W & D E Walling (1974) 'Local Variation in Background Water Quality', *The Science of the Total Environment*, 3, 141-153

Weyman D R (1973) 'Measurements of the Downslope Flow of Water in a Soil', *J. Hydrol*, 20, 267-288

D37788'81

VOL 2

END